PROCEEDINGS OF THE THIRD CANADIAN CONFERENCE ON COMPUTER APPLICATIONS IN THE MINERAL INDUSTRY /MONTREAL /QUEBEC /22-25 OCTOBER 1995

COMPTES RENDUS DU TROISIÈME CONGRÈS CANADIEN SUR L'UTILISATION DE L'INFORMATIQUE DANS L'INDUSTRIE MINIÈRE /MONTRÉAL / QUÉBEC /22-25 OCTOBRE 1995

CAMI'95

Montréal, Canada, October 22-25, 1995

Computer Applications in the Mineral Industry

Utilisation de l'informatique dans l'industrie minière

Edited by / Édité par

HANI SABRI MITRI

Department of Mining and Metallurgical Engineering
McGill University, Montreal, Quebec, Canada

McGill

ÉCOLE POLYTECHNIQUE MONTRÉAL

génie sans frontières

CIM

PROCEEDINGS OF THE THIRD CANADIAN CONFERENCE ON COMPUTER APPLICATIONS IN THE MINERAL INDUSTRY /MONTREAL /QUEBEC /22-25 OCTOBER 1995

COMPTES RENDUS DU TROISIÈME CONGRÈS CANADIEN SUR L'UTILISATION DE L'INFORMATIQUE DANS L'INDUSTRIE MINIÈRE /MONTRÉAL / QUÉBEC /22-25 OCTOBRE 1995

The texts of the various papers in this volume were set individually by typists under the supervision of each of the authors concerned.

Organization of the conference /Organisation du congrès

Technical Program Committee / Comité du programme technique

Jackie Allison
Michel Aubertin
Michel Bilodeau
Robert Chapuis
Paul Cohen
Robert Corthésy
Laeeque Daneshmend
Jeff Davidson
Robert De L'Étoile
Roussos Dimitrikapoulos
Jorgen Elbrond
Jim Finch
Keyvan Fotoohi
Ferri Hassani
Ahmad Hemani
Hani Keira
André Laplante
Denis Marcotte
Bibhu Mohanty
Moe Momayez
Clotaire Moulounda
Malcolm Scoble
Xiaoli Tang
Zhenghe Xu
Lin Zhang

Local Organizating Committee / Comité organisateur

Ferri Hassani, Fund Raising
John Gaydos, Registration
Serge Lavoie, Treasurer
Pat MacLachlan, Publicity
Moe Momayez, Publicity
John Mossop, Technical Tours
Norma Procyshyn, Public Relations
Malcolm Scoble, Secretary
Michel Vachon, Social Program
Zhenghe Xu, Workshops

Preface

When awarded the honour to chair the Third Canadian Conference on Computer Applications in the Mineral Industry (CAMI'95), I was excited to organize such an important meeting that is held for the third time in Canada. However, as time passed, my excitement gradually subsided and nervousness began to grow. Deadlines came one after another and, at times, nothing seemed to be under control. I must admit that if it had not been for the dedication of Norma Procyshyn and for the continued support of the Organizing Committee, this conference would not have reached maturity.

This is the third of a series of conferences that began in 1988 in Quebec City and was organized then by Laval University. The second conference was held in 1991 in Vancouver and was organized by the University of British Columbia. The series aims to provide a forum for practitioners and researchers to share, discuss and exchange new ideas and innovations for the utilisation of modern computer technology to tackle a broad range of challenging problems that we are faced with in exploration, development, production and processing. It is hoped that the conference will stimulate further challenges and enhance collaborative projects in future. I personally hope that each one of us will return home with a new idea.

Over one hundred and fifty abstracts were submitted for consideration, from which the papers in this proceedings were selected. Divided into thirteen chapters, the papers cover the entire spectrum of our mineral industry from mineral exploration, mineral economics, ... to mineral processing and mine waste management.

I would like to express my sincere thanks to all the members of the Technical Program Committee and Session Chairs for their sincere help in making CAMI'95 a success.

Now that this Preface is written and another deadline has just been met, things finally seem to be under control!

Welcome to Montreal!

Hani Sabri Mitri
Chairman - CAMI'95

Préface

Quand on me conféra l'honneur de présider le troisième congrès canadien sur l'utilisation de l'informatique dans l'industrie minière, j'étais très enthousiaste à l'idée d'organiser une rencontre aussi importante qui se tiendrait pour la troisième fois au Canada. Cependant, comme le temps passait, mon enthousiasme fit graduellement place à une nervosité grandissante. Les délais venaient à échéance l'un après l'autre et, parfois, tout me semblait hors de contrôle. Je dois admettre que sans le dévouement de Norma Procyshyn et le support continu apporté par le Comité organisateur, ce congrès n'aurait pu voir le jour.

Ce congrès est le troisième d'une série qui a débuté en 1988 à Québec et qui était alors organisé par l'Université Laval. Le deuxième congrès a été tenu en 1991 à Vancouver et a été organisé par l'Université de Colombie Britannique. La série vise à constituer un forum pour les praticiens et les chercheurs afin d'apporter, échanger et discuter des nouvelles idées et des innovations aux fins de l'utilisation de la technologie moderne en informatique dans le but de relever les défis auxquels nous sommes confrontés en exploration, développement, production et traitement du minerai. Nous espérons que ce congrès saura favoriser d'autres défis et accroître la collaboration professionnelle dans l'avenir. J'espère personnellement que chacun de vous retournera chez lui avec de nouvelles idées.

Plus de cent cinquante résumés ont été soumis pour examen, parmi lesquels les articles contenus dans les comptes-rendus ont été choisis et divisés en treize sections. Ces articles couvrent le domaine entier de notre industrie minière, à partir de l'exploration, l'économie, ... jusqu'au traitement du minerai et l'aménagement des résidus miniers.

J'aimerais exprimer mes sincères remerciements aux membres du Comité du programme technique et aux Présidents de sessions pour leur coopération, afin de faire de CAMI'95 un succès.

Maintenant que cette préface est rédigée et que tous les délais ont été respectés, les choses semblent finalement sous contrôle!

Bienvenue à Montréal!

Hani Sabri Mitri
Président de CAMI'95

Table of contents / Table des matières

10. MINING AND PROCESS AUTOMATION

11. MINING INFRASTRUCTURE

13. MINE WASTE MANAGEMENT

1.

mineral exploration
exploration du minerai

Modélisation des gîtes d'or du district de Rouyn-Noranda (Abitibi): Des mesures structurales aux cartes paléobarométriques prévisionnelles

Michel Jébrak
Université du Québec à Montréal, Département des Sciences de la Terre, CP 8888, succ. Centre-ville, Montréal (QUE) H3C 3P8, Canada

Peter Holyland
Terra Sancta Inc. Perth, Western Australia, Australia

Alain Carrier
UQAM; presently INRS-Géoressources, 2700 Einstein, Ste-Foy (QUE) G1V 4C7, Canada

Jacques Angelier
Université Pierre et Marie Curie, Tectonique Quantitative, 4 place Jussieu, 75252 Paris 05, France

RÉSUMÉ:

La cartographie des conditions paléobarométriques fini-Archéennes permet de prédire la position des zones minéralisées en or de type mésothermal. Une étude microtectonique détaillée de la fracturation a été réalisée dans la tonalite de Powell, dans le district de Rouyn-Noranda, ceinture de l'Abitibi, Québec. A partir de plus de 2000 mesures, on peut reconstituer par inversion les principales étapes de la déformation cassante avant, pendant et après le dépôt des quartz minéralisés en or. La contrainte principale montre des variations importantes (N-S, NW-SE, puis NE-SW) associées à une collision oblique et à un processus d'inversion tectonique. Les contraintes ainsi déterminées servent ensuite à générer des cartes de paléopressions en utilisant un modèle en éléments distincts. La méthode permet de localiser avec précision la position de la mine Silidor. Elle souligne d'une part le rôle des failles ductiles de second ordre (faille Horne) dans la répartition des zones de basses et de haute pressions, et, d'autre part, le rôle des indentateurs tectoniques dans la localisation des minéralisations en or.

ABSTRACT:

Paleostress mapping of Archean terranes can be used to predict the location of mesothermal lode gold deposits. A detailed microtectonic study was carried out on the Powell tonalitic sill, Rouyn-Noranda district, Abitibi greenstone belt, Quebec. More than 2000 measurements allow reconstruction of the deformation, before, during or after the mineralising events, using a quantitative method. The reduced stress tensors display large variations of $\sigma 1$, trending successively N-S, NW-SE then NE-SW. Such variations could be related to an oblique collision mechanism and to stress inversion processes. These reduced stress tensors are used for the computation of paleostress maps, using a distinct elements' model. The position and timing of the Silidor Au-quartz mineralization appear on these paleostress maps, being related to an area of permanent low mean stress near the Horne fault. This study emphasises (i) the role of second-order faulting for the location of low and high pressure zones in the Archean crust, and (ii) the possible importance of tectonic indentator in the location of Au-mineralization.

INTRODUCTION

La distribution des gisements hydrothermaux est anisotrope: les gisements se regroupent en districts qui montrent une minéralogie, une association géochimique et un style structural similaire (Kerrich et al., 1987; Robert, 1991). Ce provincialisme est le reflet de zones percolées par des fluides hydrothermaux de composition homogène. Au sein d'un district, la distribution et les mouvements des fluides hydrothermaux dépend de plusieurs paramètres, dont les principaux sont la géométrie du réseau poreux et la répartition des pressions dans la croûte. Ces deux paramètres peuvent être reconstitués. Ainsi, dans les socles archéens, la géométrie du réseau poreux dépend principalement du système de fractures. La répartition des pressions est controlée principalement par la contrainte verticale, à caractère litho ou hydrostatique, et les pressions tectoniques horizontales reliées aux mouvements en limite des plaques (Bott et Kusnir, 1984). Il est donc théoriquement possible de rescontruire ces deux ensembles de paramètres pour des situations géologiques données. De telles reconstitutions devraient nous permettre de modéliser les circulations de fluides dans la croûte à différentes profondeurs, et de prévoir la position des zones hydrothermalisées. Les cratons archéens, et en particulier la sous-province de l'Abitibi, offrent des secteurs d'étude particulièrement favorables compte tenu des faibles déformations subséquentes et des nombreux travaux géologiques qui leur ont été consacrés.

Cette étude présente une modélisation des circulations hydrothermales responsables des dépôts de gisements d'or méasothermaux, mises en place à la fin de l'Archéen, basée sur l'étude du district de Powell, près de Rouyn-Noranda, dans la Province de Québec, Canada. Le rôle des contraintes tectoniques et leur incidence sur la géométrie des circulations hydrothermales et la propagation des fractures sera plus spécialement soulignée. Dans une première étape, nous reconstituerons les différentes étapes de l'évolution tectonique, en particulier au cours du processus de minéralisation. Ce travail a nécessité un grand nombre de mesures structurales sur le terrain et l'utilisation de méthodes de reconstitution des tenseurs de contraintes par inversion numérique. Dans une deuxième étape, les tenseurs de contraintes sont utilisées pour modéliser à deux dimensions la répartition des pressions au cours des différents évènements tectoniques. Les variations des conditions de pressions permettent alors de comprendre la logique des circulations hydrothermales, et leur incidence sur le développement du système de fractures. La combinaison de ces deux méthodes permet de prévoir la situation des zones potentielles de concentration en or.

GÉOLOGIE ET MINÉRALISATIONS

La Province du Lac Supérieur est composée d'un ensemble de microplaques volcaniques ou continentales archéennes mises en place dans un contexte de convergence (Card, 1990). Au Sud de cette province, dans la sous-province de l'Abitibi, le Groupe de Blake River est constitué de roches volcaniques mafiques et felsiques et de plutons appartenant à la série des tonalites-trondhjemites-granodiorites. Ce groupe se compose de plusieurs cycles volcaniques pouvant être associés au développement d'une caldeira sous-marine. Il serait contemporain du passage d'un régime d'extension (arrière arc) à un régime de compression. Le Groupe de Blake River est en contact tectonique au Sud avec le bloc de Pontiac, un ensemble de roches métasédimentaires composées de greywackes, métamorphisés au faciès des amphibolites. Ces roches correspondraient à un prisme d'accrétion sédimentaire associé à une subduction vers le Nord, le long de la zone tectonique de Cadillac - Larder Lake (Figure 1).

Vers 2680 Ma, les blocs de Blake River et de Pontiac rentrèrent en collision. Cet événement est marqué par la première déformation de l'orogénie kénoréenne, et est associée à un métamorphisme prograde, atteignant le faciès amphibolite au niveau des limites de bloc, mais limité à l'épizone au sein des volcanites de Blake River. Cette collision sans doute oblique évolua progressivement vers un régime décrochant en limite des blocs. Après 2665 Ma, les sédiments du Témiskaming se déposèrent dans des grabens de transtension le long de la zone de Cadillac - Larder Lake, en association avec un magmatisme alcalin. Ils sont affectés par un deuxième épisode de déformation, associé à un serrage oblique, avec un métamorphisme rétrograde. Enfin, un important événement thermique est enregistré autour de 2600 Ma dans tout le secteur, sans que l'on en connaisse encore exactement le contexte tectonique (Kerrich and Cassidy, 1994).

La région de Don-Rouyn - Silidor est située à 8 km au Nord de la zone tectonique Cadillac - Larder Lake, immédiatement à l'Ouest de la ville de Rouyn-Noranda (Figure 1). La pile volcanique du Groupe de Blake River comprend de nombreuses dome-coulées rhyolitiques qui marqueraient la marge méridionale de la caldeira de Noranda (Kerr and Gibson, 1993). Plus à l'Ouest, le pluton de Powell constitue un sill subhorizontal, à léger pendage vers l'Est, avec une épaisseur de l'ordre du kilomètre.. Il est composé de diorites précoces (unité de Héré), de trondhjémites blanches et roses, distinctes par l'abondance des minéraux ferro-magnésiens et celle des éléments alcalins. Il est recoupé par de nombreux dykes de composition dioritique et

rhyolitique, orientés E-W, ENE-WSW et NW-SE. Le pluton de Powell serait une apophyse du pluton de Flavrian, situé immédiatement au Nord, et daté à 2700 Ma (Corfu, 1993). Ces intrusions se seraient mises en place au cours de l'épanchement des laves volcaniques du Groupe de Blake River, sans doute lors d'un processus de caldeira résurgente. Les données géochimiques confirment que les laves et les plutons représentent des ensembles cogénétiques (Paradis et al., 1988).

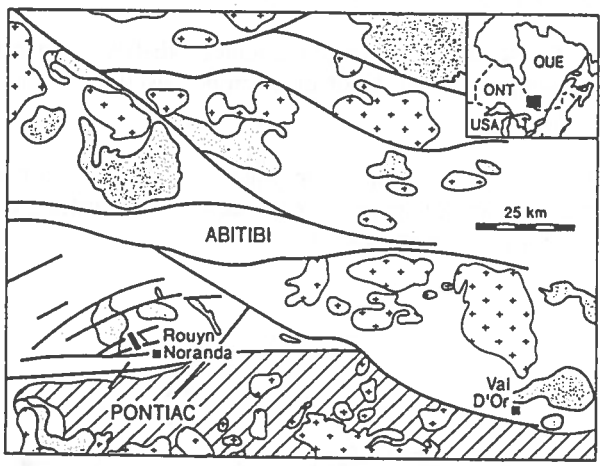

Figure 1: Situation de la zone étudiée, ceinture de l'Abitibi. *Location map, Abitibi greenstone belt.*

Les déformations tectoniques se sont principalement localisées en limite des blocs lithologiques. Ainsi, toutes les unités montrent une schistosité de fracture, associée à la première compression N-S de l'orogenèse Kénoréenne. Le pluton de Powell est limité par deux failles majeures, les failles de Horne au Sud, et de Beauchastel au Nord, qui montrent de multiples mouvements ductiles-cassants. Les mouvements les plus précoces sont marqués par des variations dans la stratigraphie volcanique de part et d'autre de ces failles (Kerr et Gibson, 1993). Mais ces failles recoupent et décalent les amas sulfurés volcanogènes, en particulier le gisement de Horne, et des dykes Protérozoiques, ce qui traduit des rejets très tardifs dont certains pourraient être associés à l'orogenèse Grenvilienne (Carrier, 1994).

Trois grands types de circulations hydrothermales ont percolées dans le pluton de Powell. Au cours de la mise en place du complexe volcanique de Blake River, le pluton a été recoupé par les circulations hydrothermales sous-marines responsables de la mise en place des amas sulfurés volcanogènes sus-jacents de Horne et de Quémont. Ces circulations ont été tracées par leur signature isotopique en oxygène (Cathles, 1993). Un deuxième événement hydrothermal correspond à la mise en place du porphyre à Cu-Mo de Don Rouyn. Enfin, cinq importants filons de quartz aurifères, orientés NW-SE, recoupent l'ensemble des structures antérieures et marquent un hydrothermalisme tardif.

Le porphyre de Don Rouyn a d'abord été développé comme un indice d'or (1925-1929), puis a été exploité en carrière comme source de fondant siliceux enrichi en cuivre, or et molybdène, pour la fonderie de Rouyn, entre 1957 et 1980. Ses ressources ont été estimées à 36 millions de tonnes à 0,15 % Cu (Goldie, 1976). La minéralisation y est associée à un système de fractures et de fentes d'extension, et à un ensemble de brèches hydrauliques et chimiques (Jébrak et al., 1995). Plusieurs épisodes d'altération peuvent être distingués, à chlorite, carbonates et épidote. Autour du porphyre se développe une altération à hématite qui suit des dykes mafiques précoces ou des structures orientés NW-SE et NE-SW. Ces minéralisations en Cu-Au-Mo se seraient déposées au cours, ou juste avant la première déformation kénoréenne, et donc entre 2700 et 2688 Ma.

Les filons aurifères ont été exploités depuis 1937. La dernière mine en exploitation est le filon de Silidor, découvert en 1985 par Noranda exploration, à partir d'une analyse statistique de l'orientation des veines de quartz dans la région et d'une interprétation des photographies aériennes. Le minerai produit et les réserves sont estimées à 2,63 Mt à 5,2 g/t Au. Le filon de Silidor est connu sur 900 m de long, 900 m de profondeur, et présente une puissance moyenne de 3,5 m. La minéralisation comprend plusieurs phases de dépôt de quartz, et s'accompagne d'une intense altération à hématite et carbonates le long de ses épontes (Picard, 1990; Carrier, 1994). L'altération et le remplissage minéralisé sont postérieurs au métamorphisme schiste vert, et donc à la déformation kénoréenne. Des datations par la méthode U-Pb sur la molybdénite suggèrent un âge de 2665± 4 Ma (Carignan and Gariepy, 1993).

DES MESURES TECTONIQUES A LA RECONSTITUTION DES CHAMPS DE CONTRAINTES

Méthodologie

Le pluton de Powell ne montre pas de grandes zones de déformation tectonique. Cependant, de très nombreuses fractures et fentes de tension indiquent que la région a été soumise à plusieurs phases de déformation cassantes. La reconstitution des tenseurs de contraintes est possible depuis les travaux de Carey et Brunier (1974), sur la base des relations entre contraintes et déformation décrites par Wallace (1951) et Bott (1959). Ces méthodes ont été progressivement améliorées en particulier par Angelier (1975, 1989) et Etchecopar et al. (1981). L'objectif de ces méthodes est de reconstituer le tenseur réduit des contraintes (directions et pendages des contraintes principales, et géométrie de l'ellipsoïde des contraintes), à partir de la détermination des mouvements de glissement sur les failles. Il s'agit donc d'un problème inverse: on mesure tout d'abord un grand nombre de failles, puis on recherche un tenseur réduit permettant de modéliser au mieux les données observées sur le terrain. Chaque épisode de déformation peut être distingué soit à partir de critères de terrain (recoupements, natures des altérations ou des remplissages associés), soit par des méthodes numériques automatisées basées sur la cohérence des tenseurs de contraintes calculés (Angelier et Marcoussis, 1980).

Des mesures systématiques dans le gisement filonien de Silidor et dans la carrière de Don Rouyn nous ont permis de recueillir plus de 2000 mesures. La distinction entre différentes familles de mouvements (inverse, normal, décrochant) a permis de distinguer les différents épisodes tectoniques, tandis que les relations de recoupement autorisaient l'établissement d'une chronologie relative. Un exemple de détermination des paléocontraintes dans la carrière de Don Rouyn est illustré sur la figure 2.

Reconstitution des contraintes

Huit régimes de contraintes, antérieures ou postérieures aux minéralisations ont été mis en évidence dans le pluton de Powell. Les détails sur chacune de ces déformations sont donnés dans Carrier (1994) et Angelier et al. (à paraître). Les trois premières phases sont les plus importantes pour l'évolution structurale et métallogénique de la région.

- D1 est une compression orientée N-S, responsable de la schistosité principale E-W, bien développée dans les dykes mafiques.

- D2 correspond à une compression orientée NW-SE à caractère ductile-cassant. Cette déformation est marquée par des veines à Cu-Au-Mo associées à l'altération à chlorite du porphyre de Don Rouyn (Goldie et al., 1979; Jébrak et al., 1995).

- D3 est une compression orientée NE-SW. Elle est contemporaine du dépôt de la minéralisation en or à Silidor.

Les autres événements tectoniques correspondent à des rejets postérieurs généralement sans minéralisation, en compression ou en extension.

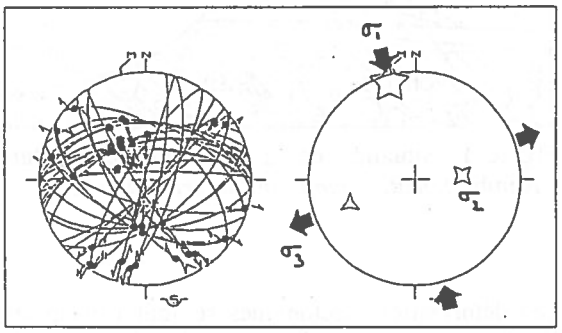

Figure 2: exemple de détermination des contraintes dans le secteur de Don Rouyn par inversion. *An example of inverse tectonic modeling in the Don Rouyn area.*

La variété de ces conditions tectoniques s'expliquent sans doute par différents mécanismes. Le passage de la compression D1 à la phase D2 pourrait correspondre à une rotation progressive dans le sens anti-horaire de la déformation associée à une rotation de bloc. Par contre, il ne semble pas y avoir de continuité ou de rotation progressive des contraintes entre les phases D2 et D3, ce qui traduit sans doute une évolution des contraintes par inversion ($\sigma 1$ et $\sigma 2$) dans un contexte d'ellipsoïde de déformation assez proche d'une sphère, et donc avec un différentiel des contraintes ($\sigma 3$ - $\sigma 1$) de faible amplitude.

DES PALÉOCONTRAINTES A LA PREVISION DES CHAMPS DE PRESSIONS

Méthodologie

Le dépôt des gisements aurifères mésothermaux est contrôlé par le mouvement des fluides hydrothermaux au sein de la croûte moyenne. L'hydrologie de ces circulations n'est pas accessible à une observation directe, mais les observations des systèmes fossiles, l'analyse des fluides et du métamorphisme, et l'analogie avec les migrations des systèmes pétroliers indiquent que le mouvement de ces fluides étaient principalement contrôlés par la répartition des pressions dans la croûte. A quelques kilomètres de profondeur, les pressions verticales sont généralement supérieures à la pression hydrostatique, et les fluides présenteront généralement un mouvement du bas vers le haut (Holyland et al., 1993). Les études détaillées du métamorphisme dans les Appalaches ont également montré que les fluides pouvaient avoir également un écoulement latéral sur des distances de plusieurs kilomètres, en suivant les unités stratigraphiques les plus perméables (Ferry, 1994).

Les fluides hydrothermaux s'accumuleront au voisinage de zones de faible perméabilité, jouant le rôle de barrières hydrologiques (anticlinaux, sills synvolcaniques par exemple), ou dans des zones de basses pressions. De telles zones peuvent être dues soit à une géométrie particulière des champs de contraintes et de déformations, soit à des variations rhéologiques, en particulier des contrastes de compétences (Ridley, 1993). Ce modèle permet de prévoir les zones d'accumulation potentielle des fluides hydrothermaux. Le calcul de cartes paléobarométriques, ou *Stress Mapping Technology* (STM™), a été développé depuis plusieurs années par Terra Sancta (Holyland, 1990). Ces cartes permettent d'étudier les variations de la contraintes et de la déformation dans des terrains hétérogènes sous l'action d'une contrainte régionale en deux dimensions.

Le calcul de cartes paléobarométriques nécessite: (i) la connaissance précise du contexte géologique, et en particulier la position et la géométrie des blocs lithologique et des grandes zones de discontinuités, et (ii) une estimation du champ de contrainte régional et des propriétés rhéologiques des roches et des failles au moment de la déformation.

La géologie de la zone étudiée est modélisée sous forme d'une mosaïque de blocs polygonaux de composition homogène, séparés par des contacts aux propriétés mécaniques diverses. Il est cependant nécessaire de reconstruire la géologie telle qu'elle était au moment des minéralisations. Dans le cas des minéralisations aurifères de l'Abitibi, on peut estimer que la région a relativement peu été déformée depuis le dépôt de veines de quartz aurifères, mise en place entre 2600 et 2680 Ma (Kerrich et Cassidy, 1994).

Les données sur les champs de contraintes proviennent de l'analyse tectonique quantitative. Toutefois, cette analyse doit être complétée par une estimation de la magnitude des contraintes principales, permettant de passer de tenseurs réduits des contraintes à des tenseurs complets. Cette estimation a été réalisée sur la base de comparaisons avec le bloc de Yirlgarn (Western Australia), avec des valeurs autour de 100 Mpa pour $\sigma 1$ et 70 Mpa pour $\sigma 3$, ce qui correspond approximativement à une profondeur de 4 à 8 km, pour une augmentation de 25 Mpa/km.

Les propriétés mécaniques des roches et des failles au cours des déformations archéennes doivent également être introduites dans la modélisation, et plus spécialement la résistance en tension et en compression, le module de Yong, la densité des unités, et les angles de friction et la fermeté (*stiffness*) des contacts. Dans la région de Rouyn-Noranda, la résistance décroît progressivement des intrusifs mafiques vers les basaltes, les granites, les roches ultramafiques, les sédiments grossiers et les zones de failles. Les contacts lithologiques présenteront des propriétés différentes selon qu'ils sont dans des zones de déformations modérées ou intenses. L'évaluation de ces paramètres (propriétés de Terra Sancta) est essentielle puisque les contacts jouent un rôle critique au cours de la déformation.

La modélisation est réalisée à deux dimensions à partir d'un code de calcul en éléments distincts (UDEC) sur un ordinateur de type compatible PC. Ce type de modélisation présente trois caractéristiques bien adaptées à la modélisation de milieux discontinues (Holyland, 1990). La méthode simule un assemblage de blocs homogènes en interaction sur leurs bordures et sur leurs coins. La méthode utilise un algorithme dynamique itératif qui permet des déplacements importants et des rotations, et un comportement mécanique non-linéaire de la matrice et des discontinuités. Quand une contrainte externe est appliquée au modèle, les blocs sont déformés jusqu'à ce qu'un équilibre soit atteint. Enfin, la modélisation permet de produire des cartes de contour, soit des déplacements, soit de la valeur de la contrainte moyenne ou minimale. La contrainte moyenne est une expression directe de la pression moyenne qui régnait au cours de la déformation.

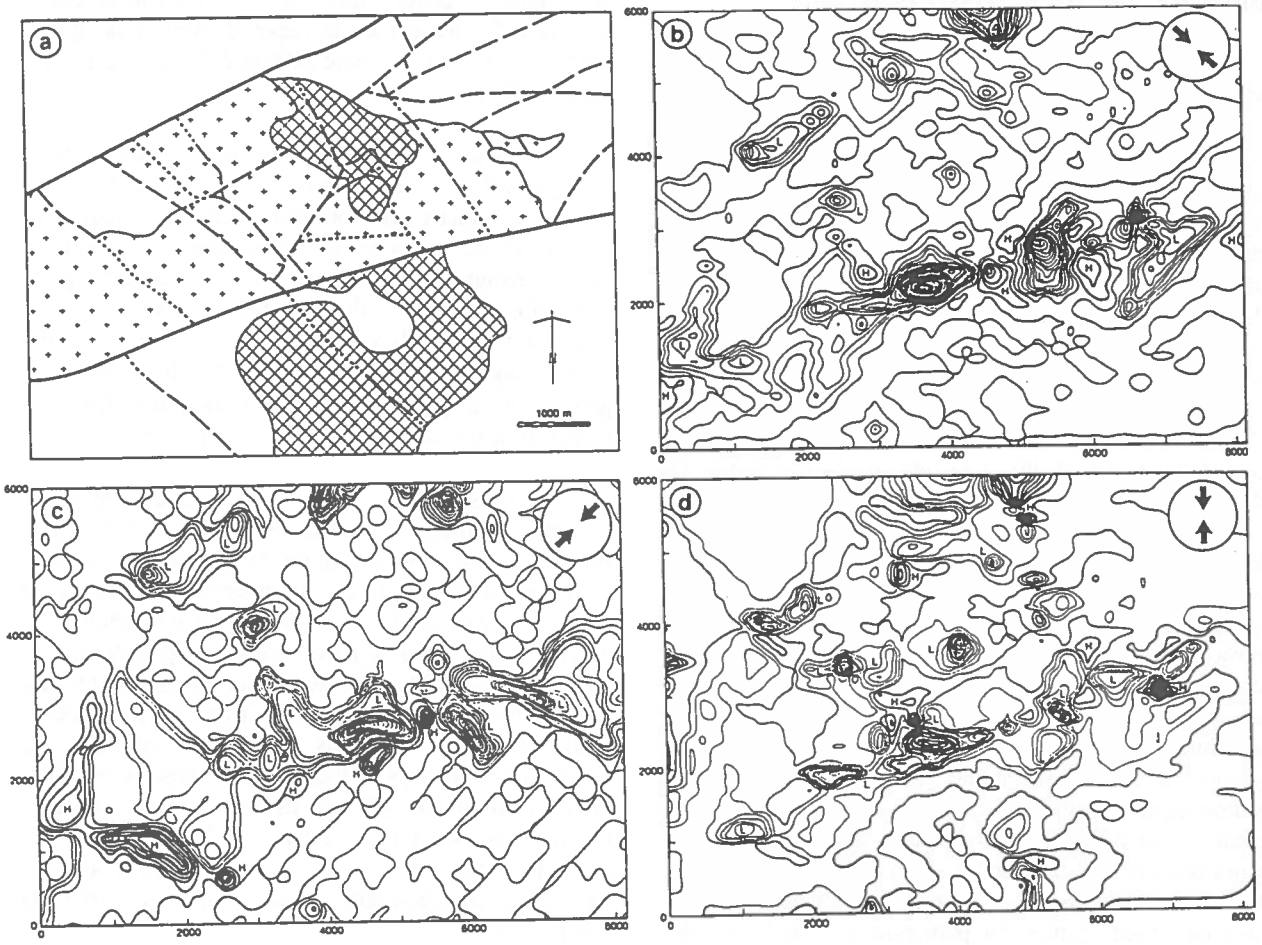

Figure 3: Carte géologique simplifiée (a) et résultats de la modélisation paléo-barométriques de la partie orientale du pluton de Powell lors de compressions NW-SE (b), NE-SW (c) et N-S (d). Le filon Silidor est représenté en noir sur les quatre cartes. Figure 2a: trait plein: failles majeures; trait tireté: failles mineures; trait pointillé : failles mineures supposées; hachuré : diorite; croix: pluton de Powell; blanc: roches volcaniques du Groupe de Blake River; H = xone de hautes pressions ; L =zone de basses pressions - *Simplified geological map (a) and results of paleostress modelling in the eastern part of the Powell pluton, using NW-SE (b), NE-SW (c) and (d) N-S compression. H = high pressures zone; L = Low pressure zone*

Résultats

Une carte très simplifiée de la terminaison orientale du pluton de Powell a été utilisée (Figure 3a). Trois types de roches ont seulement été considérés: le pluton de Powell, la diorite, et les roches volcaniques assimilées à des basaltes homogènes. Deux types de failles ont été définies, majeures, à faible résistance (failles de Beauchastel et de Horne), et mineures. Certaines failles ont été prolongées sur la base de l'analyse des photographies aériennes ou sur les cartes géophysiques afin de produire des blocs fermés. La carte a également été corrigée des phénomènes postérieurs à 2600 Ma (dykes protérozoiques, dépôts quaternaires). Trois états de contraintes, correspondant aux phases tectoniques déterminées régionalement ont été testés, avec un axe $\sigma 1$ orienté NW-SE, N-S et NE-SW.

Les cartes produites montrent que l'essentiel des zones de hautes et basses pression étaient situées le long de la faille Horne, et dans une moindre mesure, le long de la faille Beauchastel (Figure 3). Au cours de la compression NW-SE (Figure 3b), le modèle prédit une zone de basses pressions localisée à la rencontre de la structure portant le filon Silidor et la faille Horne. Une deuxième zone de basse pression apparaît dans les volcanites au Sud-Est de Don Rouyn. Des zones de basses pressions jalonnent la faille Horne à l'Ouest de son croisement avec la faille Mouilleuse. Lors de la compression NE-SW, une zone de basses pressions tectoniques s'allonge le long de la structure Silidor, au Sud-Est de Don Rouyn, et le long de la faille Mouilleuse (Figure 3c). Enfin, lors de la simulation d'une compression N-S, les zones de basses pressions et de hautes pressions sont plus diversement réparties, avec des zones de basses pressions supplémentaires apparaissant au Sud-Ouest du secteur étudié (région d'Évain), dans la région de Don Rouyn, dans celle de la mine Powell et au Nord de la mine New Marlon (Figure 3d).

DISCUSSION

La comparaison de ces trois cartes fait ressortir la permanence de zones de basses pressions au cours des différents épisodes tectoniques (Figure 4). Au cours des déformations fini-archéennes, la zone de rencontre entre la faille Silidor et la faille Horne semble avoir été le siège de zones de basses pressions permanentes, susceptibles de drainer d'une manière durable les fluides hydrothermaux.

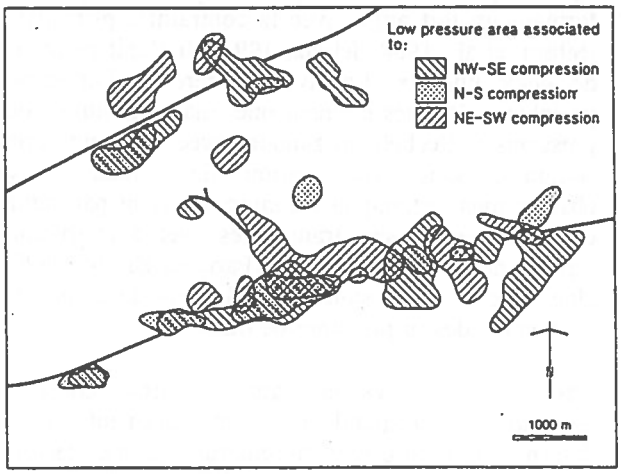

Figure 4: Situation des zones de basses pressions dans la partie orientale du pluton de Powell, Abitibi - *Location of the low pressure areas in the eastern part of the Powell pluton, Abitibi*

On observe également un comportement différentiel des failles de Horne et de Beauchastel, malgré une orientation et des rejeux tectoniques probablement similaires. La faille Horne semble contrôler d'une manière beaucoup plus efficace la distribution des zones de hautes et de basses pressions. Cette différence doit être mise en relation avec l'homogénéité qui a été supposée pour le bloc au Nord de la faille Beauchatel, et l'hétérogénéité du bloc au Sud de la faille Horne, Cette hétérogénéité est essentiellement due à la présence d'une masse dioritique résistante qui joue un rôle d'indentateur (Figure 5). Il est probable que l'utilisation de cartes plus précises nuancerait cette opposition. Toutefois, elle souligne l'importance que peut avoir la présence de masses résistantes au voisinage d'accidents majeurs dans la répartition des paléopressions, et donc dans la circulation des fluides hydrothermaux.

La position de la mine Silidor est remarquablement prédite par le modèle. La carte qui montre la meilleure coïncidence entre zone de basses pressions et zones minéralisées actuellement exploitées est celle correspondant à une contrainte orientée NE-SW. Le modèle est donc pleinement en accord avec les observations structurales qui associent le dépôt de la minéralisation en or avec une compression de ce type. Cette compression s'accompagne de mouvements inverse-décrochant le long de la structure minéralisée. Il peut sembler paradoxal d'associer des zones de basses pressions lithostatiques avec des zones de serrages tectoniques maximum où des surpressions de

fluides sont soulignées par la présence de brèches hydrauliques et le fonctionnement de cisaillements formant un fort angle avec la contraintes principales (Sibson et al., 1988; Jébrak, 1992). Il s'agit en réalité de deux niveaux d'analyses différents. Les cartes paléobarométriques donnent une image simplifiée des pressions à l'échelle régionale, avec des contraintes statiques, sans néoformation de fractures. Les observations tectoniques en mine montrent par contre des processus fugaces, transitoires, avec des variations rapides de la pression locale (Parry et Bruhn, 1990). Une zone en dépression régionale peut donc montrer localement des surpressions de fluides.

Enfin, si on considère que les trois contextes tectoniques correspondent à des incréments de la déformation kénoréenne, on remarque qu'une très forte rotation des contraintes ne modifie pas de manière drastique la situation des zones de hautes et de basses pressions dans le modèle considéré. Malgrè la rotation des contraintes, les fluides hydrothermaux auront tendance à se concentrer dans les mêmes sites tectoniques.

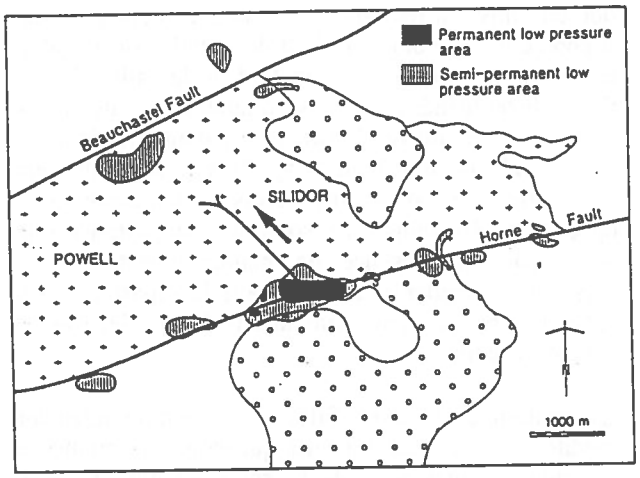

Figure 5: situation des zones de basses pressions lors des différentes phases tectoniques fini-Archéennes dans la partie orientale du pluton de Powell (+), et rôle d'indentateur de la diorite (o) située au Sud de la faille Horne - *Location of low pressure areas during the late-Archean tectonic episodes in the eastern part of the Powell pluton (+) and tectonic role of the diorite (o) south of the Horne fault.*

CONCLUSIONS

La modélisation des circulations hydrothermales responsables des dépôts de gisements d'or mésothermaux archéens constitue un défi auquel il est encore difficile de répondre avec précision. La méthodologie proposée ici repose sur la combinaison d'une analyse microtectonique détaillée et de levés de terrain d'une part, et de modélisations des axes de contrainte et de la répartition des paléopressions d'autre part. Malgrè d'importantes approximations, elle permet de prévoir la localisation des zones minéralisées dans les socles fracturés.

Dans un massif relativement homogène comme la tonalite de Powell, la localisation des zones minéralisées correspond à la combinaison de deux grands facteurs:

(i) la localisation des zones de déformation dans le pluton. Celle-ci est fortement contrôlée par le découpage en blocs lithologiques qui dépend de l'organisation volcano-plutonique et de la déformation précoce du bâti archéen. Sur ce découpage se superposent des fractures néoformées qui se développent généralement à partir des fractures préexistantes. La géométrie de ces fractures nécessite une analyse détaillée et une reconstitution des mécanismes de propagation (Renshaw et Pollard, 1994).

(ii) la migration des fluides hydrothermaux dans le réseaux de fractures. Elle s'effectue vers les zones de basses pressions relatives, correspondant à des zones de divergence de blocs sous contrainte. La localisation des zones de basses pressions dépend alors largement des lithologies qui environnent la zone étudiée. La méthode utilisée ici montre un remarquable pouvoir de prédiction des zones minéralisées. Des résultats comparables ont été obtenus dans le craton de Yilgarn pour des gisements de même nature dans des contextes géologiques sensiblement différents (Holyland, 1990). Toutefois, cette analyse reste limitée à des déplacements à deux dimensions et ignore donc les déplacements verticaux qui ont été mesurés dans tout le district. Elle ne tient pas compte par ailleurs de l'évolution de la géométrie du milieu en relation avec la déformation: rotation successive des blocs, apparition de nouvelles discontinuités, rôle de la pression de fluide dans la rhéologie des zones de contact. Ces différents paramètres devront être introduits dans les modèles à venir.

REFERENCES

ANGELIER, J., 1975
Sur l'analyse de mesures recueillies dans des sites faillés: l'utilité d'une confrontation entre les méthodes dynamiques et cinématiques. Comptes rendus des séances de l'Académie des sciences, série D, Vol. 281, pp. 1805-1808

ANGELIER, J., 1989
From orientation to magnitudes in paleostress determinations using fault slip data. Jour. struct. geol., Vol. 11, pp. 37-50

ANGELIER, J., et MANOUSSIS, S., 1980
Classification automatique et distinction des phases superposées en tectonique de failles. Comptes rendus des séances de l'Académie des sciences, série D, Vol. 290, pp. 651-654

BOTT, M.H.P., 1959
The mechanics of oblique slip faulting. Geol. Mag. Vol.. 96, pp. 109-117

BOTT, M.H.P., et KUSNIR, N.J. , 1984
The origin of stress in the lithosphere. Tectonophysics, Vol. 105, pp. 1-13

CARD, K.D., 1990
A review of the Superior Province of the Canadian Shield, a product of Archean accretion. Precambrian Research, Vol. 48, pp. 99-156

CAREY, E., et BRUNIER, B., 1974
Analyse théorique et numérique d'un modèle mécanique élémentaire appliqué à l'étude d'une population de failles. Comptes rendus des séances de l'Académie des sciences, série D, Vol. 279, pp. 891-894

CARIGNAN, J., et GARIEPY, C., 1993
Pb isotope geochemistry of the Silidor and Launay gold deposits, Abitibi Subprovince: Implications for the source of Archean Au. Economic Geology, Vol. 82, pp. 1931-1957

CARRIER, A., 1994
Evolution structurale et métallogénique du gisement aurifère Silidor, Abitibi, Québec. Thèse de M.Sc., UQAM, 272 p.

CATHLES, L.M., 1993
Oxygen Isotope alteration in the Noranda mining district, Abitibi greenstone belt, Quebec. Economic Geology, Vol. 88, pp. 1483-1511

CORFU, F., 1993
The evolution of the Southern Abitibi greenstone belt in light of precise U-Pb geochronology. Economic Geology, Vol. 88, pp. 1323-1340

ETCHECOPAR, A., VASSEUR, G., et DAIGNIERES, M., 1981
An inverse problem in microtectonics for the determination of stress tensors from fault striation analysis. Jour. struct. geol., Vol. 3, pp. 51-65

FERRY, J.M. ,1994
Overview of the petrologic record of fluid flow during regional metamorphism in northern New England. American Journal of Science, Vol. 294, pp. 905-988

GOLDIE, R.J., 1976
The Flavrian and Powell plutons, Noranda area, Québec. Ph.D. thesis, Queen's University, Kingston.

GOLDIE, R.J., KOTILA, B., et SEWARD, D., 1979
The Don Rouyn Mine: an Archean porphyry copper deposit near Noranda, Quebec. Economic Geology, Vol. 74, pp. 1680-1684

HOLYLAND, P.W., 1990
Targeting of epithermal ore deposits using stress mapping techniques. Proc. Pacific Rim Congr., Aus, I.M.M., Melbourne, Vol. III, pp. 337-341

HOLYLAND, P., RIDLEY, J.R., et VEARNCOMBE, J.R., 1993
Stress Mapping Technology (STM™). Geofluid 's 93. Conference abstract volume, Torquay England, May 1993, 4 p.

JÉBRAK, M., 1992
Les textures intra-filoniennes, marqueurs des conditions hydrauliques et tectoniques. Chronique de la Recherche Minière, Vol. 506, pp. 55-65

JÉBRAK, M., HARNOIS, L., CARRIER, A., et LAFRANCE, J. 1995
Don Rouyn. An Archean gold porphyry. Livret-guide de l'excursion du Congrès Precambrian '95

KERR, D.J., et GIBSON, H.L., 1993
Comparaison of the Horne volcanogenic massive sulfide deposit and intracauldron deposits of the mine sequence, Noranda, Quebec. Economic Geology, Vol. 88, pp. 1419-1442

KERRICH, R., FRYER, B.J., KING R., WILLMORE L.M., et VAN HEES E., 1987
Crustal outgassing and LILE enrichment in major lithosphere structures, Archean Abitibi greenstone belt : evidence on the source reservoir from strontium and carbon isotope tracers. Contribution Mineral. Petrol., Vol. 97, pp. 156-168

KERRICH, R., et CASSIDY, K.F., 1994
Temporal relationships of lode gold mineralization to accretion, magmatism, metamorphism and deformation - Archean to present: A review. Ore Geology Reviews, Vol. 9, pp. 263-310

PARADIS, S., LUDDEN, J., et GELINAS, L. , 1988
Evidence for contrasting compositional spectra in comagmatic intrusive and extrusive rocks of late Archean Blake River Group, Abitibi, Québec. Canadian Journal of Earth Sciences, Vol. 25, pp. 134-144

PARRY, W.T., et BRUHN, R.I. 1990
Fluid pressure transient on seismogenic normal fault. Tectonophysics, Vol. 179, pp. 335-344

PICARD, S., 1990
Le gisement Silidor. In: The Northwestern Quebec Polymetallic Belt, édité par M. Rive, P. Verpaelst, Y. Gagnon, J.M. Lulin, G. Riverin and A. Simard. The Canadian Institute of Mining and Metallurgy, Special Vol. 43, pp. 175-184

RENSHAW, C.E., et POLLARD, D.D., 1994
Numerical simulation of fracture set formation: A fracture mechanics model consistent with experimental observations. Journal of Geophysical Research, Vol. 99: B5, pp. 9359-9372

RIDLEY, J., 1993
The relations between mean rock stress and fluid flow in the crust: With reference to vein- and lode-style gold deposits. Ore geology reviews, Vol. 8, pp. 23-37

ROBERT, F., 1991
Gold metallogeny of greenstone belts: considerations from the Eastern Abitibi subprovince, Canada. Brazil Gold'91. The economics, geology, geochemistry and genesis of gold deposits. EA. Ladeira, 1991, pp. 83-86

SIBSON, R.H., ROBERT, F., et POULSEN, K.H., 1988
High-angle reverse faults, fluid pressure cycling and mesothermal gold-deposits. Geology, Vol. 16, pp. 551-555

WALLACE, R.E., 1951
Geometry of shearing stress and relation to faulting. Jour. Geol., Vol. 59, pp. 118-130

CAMI'95:3rd Canadian Conference on Computer Applications in the Mineral Industry
Montréal, Québec, Canada, October 22-25, 1995

A Computer Program for 2D Numerical Modelling of Thermal and Fluid Flow Fields Associated with Irregular Magmatic Intrusions Using Finite Difference Method Coupled with Body-Fitted Transformation Technique: Application to Localization of Ore Deposits

Guoxiang Chi* and Jayanta Guha
*Sciences de la Terre/Centre d'Etudes sur les Ressources Minérales, Université du Québec à Chicoutimi, Qc, Canada G7H 2B1 (*presently with GSC-Quebec Geoscience Centre, Ste-Foy, Québec)*

ABSTRACT

This program computes isotherms, isobars, stream lines and fluid flux vectors in a two dimensional domain surrounding an irregular magmatic intrusion. The finite difference method is used in conjunction with body-fitted transformation techniques to solve governing equations. Preliminary application of the program indicates that under reasonable assumption of boundary conditions and physical parameters, the computed results can be used to address heat and fluid flow related geological problems such as the localization of hydrothermal ore deposits.

RÉSUMÉ

Ce programme calcule les isothermes, isobares, lignes de courant et vecteurs d'écoulement des fluides dans un domaine à deux dimensions autour d'une intrusion magmatique irrégulière. La méthode de différence finie est couplée à des techniques de transformation conforme ajustée au corps physique pour résoudre les équations principales. L'application préliminaire de ce programme démontre qu'en portant de suppositions raisonnables sur des conditions limites et des paramètres physiques, les résultats calculés peuvent être utilisés pour résoudre des problems géologiques reliés à la chaleur et l'écoulements des fluides tel que la localisation des gîtes hydrothermaux.

INTRODUCTION

Numerical models of fluid flow and thermal fields around magmatic intrusions have been studied by a number of authors using finite difference methods since the 1970's. One of the difficulties frequently encountered in numerical modelling lies in the irregularities of the intrusion surface. A general approach to this problem is to approximate the intrusion body by a rectangular block, so that finite difference methods can be employed without the need of any interpolation between grid points at the boundaries (e.g. Norton and Knight, 1977; Norton and Cathles, 1979). This approach, however, may result in serious deviation from real physical systems, and cannot be applied to specific geologic conditions, in which the geometries of the intrusions are typically highly irregular. An improvement to this approach is to use step lines which are in accord with the grid system to approximate the irregular boundaries (Johnson and Norton, 1985). The accuracy of this method, however, depends on the multiplicity of the steps, which is proportional to the labour involved in the numerical procedures. An alternative approach is to use finite element methods (Sams and Thomas-Betts, 1988; Brikowski and Norton, 1989). The advantage of this method is, however, discounted by its complexity in programming, especially for beginners of numerical modelling.

The present program uses a body-fitted transformation technique (Thompson et al., 1985), which transforms a physical domain with irregular boundaries from the Cartesian coordinates to an "imaginary" computational domain where the space is rectangular, so that the boundaries coincide with grid lines. The conventional finite difference formulation can be carried out without the need of interpolation between grid points at the boundaries. Therefore, this program keeps the simplicity of finite difference methods, and has the same capacity as finite element methods to deal with irregular geometric boundaries.

GOVERNING EQUATIONS

The basic governing equations of fluid flow and heat transfer processes in porous media (2D) include the continuity equation, Darcy's law, and energy conservation equation.

Continuity (mass conservation) equation:

$$\partial u/\partial x + \partial v/\partial y = 0 \qquad (1)$$

Darcy's law:

$$u = - (k/\nu) (\partial P/\partial x) \quad (2)$$

$$v = - (k/\nu) (\partial P/\partial y + \rho g) \quad (3)$$

Energy conservation equation:

$$\rho_m (a + C_m) (\partial T/\partial t) + C_f [u (\partial T/\partial x) + v (\partial T/\partial y)] = K_m \nabla^2 T \quad (4)$$

where u and v are components of fluid flux vector (g cm^{-2} sec^{-1}) in x and y coordinates respectively; k is the permeability of the porous medium (cm^2); ν is kinematic viscosity of the fluid (cm^2 sec^{-1}); P is fluid pressure (dyne cm^{-2}); ρ is fluid density (g cm^{-3}); g is gravitational force vector (cm sec^{-2}); ρ_m is density of the medium (g cm^{-3}); a is heat generation rate (J g^{-1} $°C^{-1}$); C_m is the heat capacity of the medium (J g^{-1} $°C^{-1}$); T is temperature of the medium (°C); t is time (sec); C_f is the heat capacity of the fluid (J g^{-1} $°C^{-1}$); K_m is thermal conductivity of the medium (J cm^{-1} sec^{-1} $°C^{-1}$).

By introducing the Boussinesq approximation:

$$\rho = \rho_0 [1 - \beta (T - T_0)] \quad (5)$$

where ρ_0 and T_0 are initial fluid density and temperature respectively, and β is the coefficient of thermal expansion of the fluid ($°C^{-1}$), and by introducing the stream function (Ψ):

$$u = \partial\Psi/\partial y \quad (6)$$

$$v = - \partial\Psi/\partial x \quad (7)$$

Eqs. (1) - (3) can be combined to form the stream function equation and pressure equation:

$$\nabla^2\Psi = - (k/\nu) \rho_0 g \beta (\partial T/\partial x) \quad (8)$$

$$\nabla^2 P = \rho_0 g \beta (\partial T/\partial y) \quad (9)$$

Since Eqs. (1) - (3) have been implicitly included in Eqs. (8) and (9), the number of governing equations is reduced to three, i.e., the stream function equation (Eq.8), the pressure equation (Eq.9), and the energy conservation equation (Eq.4). The three dependent variables to be solved are the stream function, pressure, and temperature.

The non-dimensional forms of Eqs. (8), (9) and (4) are as follows:

$$\nabla^2\Psi = - Ra (\partial T/\partial x) \quad (10)$$

$$\nabla^2 P = Ra (\partial T/\partial y) \quad (11)$$

$$\partial T/\partial t + (\partial\Psi/\partial y) (\partial T/\partial x) - (\partial\Psi/\partial x) (\partial T/\partial y)] = \nabla^2 T \quad (12)$$

where

$$Ra = [\rho_0 g C_f \beta L_0 k (T_1 - T_0)]/(\nu K_m) \quad (13)$$

and L_0 is a reference length, T_1 is a reference high temperature, and T_0 is a reference low temperature.

The transformation relations between dimensional (*) and non-dimensional variables are as follows:

$$x = x^*/L_0$$

$$y = y^*/L_0$$

$$u = u^* (C_f L_0/K_m)$$

$$v = v^* (C_f L_0/K_m)$$

$$\Psi = \Psi^* (C_f/K_m)$$

$$P = P^* [(C_f k)/(\nu K_m)]$$

$$t = t^* K_m/[\rho_m (a + C_m) L_0^2]$$

$$T = (T^* - T_0)/(T_1 - T_0)$$

NUMERICAL SOLUTION

The numerical solution of the partial differential equations (10) - (12) using finite difference methods requires division of the physical domain into a grid network. Each grid point has three finite difference (algebraic) equations transformed from the partial differential equations. The algebraic equations at all the grid points are solved simultaneously to obtain the values of T, P and Ψ at each discrete grid point. The fluid flux vector can be calculated from Ψ according to the definition of the stream function (Eqs. 6 and 7).

In general, finite difference methods are less difficult to use for physical problems with simple geometric boundaries, when nodal points may be aligned on a regularly patterned grid. The most convenient grid network is composed of rectangles, and is most suitable for rectangular domains. To treat an irregular domain, however, interpolations have to be devised to overcome the difficulties encountered at the boundaries. When the interpolations between grid points do not fall exactly on the boundaries, the inaccuracy of the interpolation may significantly affect the numerical solution, especially for a system with large gradients in the vicinity of the boundaries.

A body-fitted transformation technique can be used to overcome the above problems. The principle of this technique is to transform the real irregular physical domain into a computational rectangular space, where the coordinate lines coincide with the boundaries of the domain. Consequently, the finite difference expressions at the boundaries only involve grid points on the intersections of coordinate lines without the need of any interpolation between grid points. The procedures of using this technique are described as follows.

Firstly, the boundaries of the physical domain on the Cartesian coordinates (x, y) are transformed onto the computational coordinates (ξ, η). The transformation equations used in this program are:

$$\nabla^2\xi = P(\xi, \eta) \qquad (14)$$

$$\nabla^2\eta = Q(\xi, \eta) \qquad (15)$$

In these two equations, the dependent variables are ξ and η, and the numerical solution has be to carried out on the x - y coordinates, which is difficult because of the irregular geometric boundaries as pointed out above. Therefore, Eqs. (14) and (15) have to be transformed so that the dependent variables are x and y, and the numerical solution can be carried out on the ξ - η coordinates, which is easier because of the rectangular geometry of the ξ - η space. The transformed form of Eqs. (14) and (15) are as follows:

$$g^{11}x_{\xi\xi} + 2g^{12}x_{\xi\eta} + g^{22}x_{\eta\eta} + P(\xi, \eta)\, x_\xi + Q(\xi, \eta)\, x_\eta = 0 \qquad (16)$$

$$g^{11}y_{\xi\xi} + 2g^{12}y_{\xi\eta} + g^{22}y_{\eta\eta} + P(\xi, \eta)\, y_\xi + Q(\xi, \eta)\, y_\eta = 0 \qquad (17)$$

where

$g^{11} = \xi_x^2 + \xi_y^2$ $\qquad$ $g^{11} = \xi_x \eta_x + \xi_y \eta_y$

$g^{22} = \eta_x^2 + \eta_y^2$ $\qquad$ $x_\xi = \partial x/\partial\xi$

$x_{\xi\xi} = \partial^2 x/\partial\xi^2$ $\qquad$ $x_{\xi\eta} = \partial^2 x/\partial\xi\partial\eta$

$\xi_x = \partial\xi/\partial x$ $\qquad$ etc.

and

$\xi_x = y_\eta/J$ $\qquad$ $\xi_y = -x_\eta/J$

$\eta_x = -y_\xi/J$ $\qquad$ $\eta_y = x_\xi/J$

$J = x_\xi y_\eta - x_\eta y_\xi$

With Dirichlet-type boundary conditions that specify physical coordinates for the end points of the curvilinear coordinate lines in the physical domain, the transformation equations (Eqs. 16 and 17) are amenable to numerical solution.

Secondly, a grid network is created in the domain on the computational coordinates. This grid network can be understood as an organized set of points formed by the intersections of the lines of a boundary-conforming curvilinear coordinate system. Since the domain is rectangular in the computational space, where the increments of the coordinates are arbitrarily defined in transformation from the Cartesian coordinates, a square grid is generally favoured.

Thirdly, the dependent variables Ψ, P and T in Eqs. (10) - (12) are transformed in accord with the computational coordinate system. Boundary conditions, which depend on specific physical problems, have to be transformed accordingly. The transformed Eqs. (10) - (12) take the following general form:

$$\partial(c\,\phi)/\partial t + \xi_t \partial(c\,\phi)/\partial\xi + \eta_t \partial(c\,\phi)/\partial\eta + \partial[c\,U\,\phi - (g^{11}\partial\phi/\partial\xi + g^{12}\partial\phi/\partial\eta)]/\partial\xi + \partial[c\,V\,\phi - (g^{22}\partial\phi/\partial\eta + g^{12}\partial\phi/\partial\xi)]/\partial\eta = S(\xi, \eta) \qquad (18)$$

where

$U = g\,\partial\Psi/\partial\eta$

$V = -g\,\partial\Psi/\partial\xi$

$g = \xi_x \eta_y - \xi_y \eta_x$

and other parameters are specified in Table 1.

Table 1. Variables and parameters in Eq. (18)

Equation	ϕ	c	$S(\xi, \eta)$
(10)	Ψ	0	$Ra\,(\xi_x\partial T/\partial\xi + \eta_x\partial T/\partial\eta)$
(11)	P	0	$-Ra\,(\xi_y\partial T/\partial\xi + \eta_y\partial T/\partial\eta)$
(12)	T	1	0

Finally, the transformed partial differential equations are discretized on the computational grid network. With the problem in the transformed space, only uniform square grids need be considered, hence the standard forms for finite difference representation of derivatives may be used. The finite difference representations of the transformed equation system (Eq. 18) are obtained by integrating Eq. (18) over all control volumes in the (ξ, η) plane. The nine-point difference scheme is adopted. A modified strongly implicit procedure (Patankar, 1980) is used to solve the finite difference equations for Ψ, P, and T. The fluid flux vectors (u and v) are calculated from Ψ.

PROGRAMMING

The program is written in FORTRAN, and can be run on most personal computers (80386 PC or better). A FORTRAN compiler is required. The program consists of a main program and 10 subroutines. The main program specifies variables and links subroutines. The functions of the subroutines are listed in Table 2.

Table 2. Functions of subroutines

Subroutine	Functions
INITIAL	Input parameters and initial conditions
USER-GRIDS	Input x - y coordinates of geometric boundaries
AUTO-GRIDS	Generate grids
COEFXY	Calculate transformation coefficients
TEMP	Solve the energy conservation equation
PSI	Solve the stream function equation
PRS	Solve the pressure equation
FLUX	Calculate fluid flux vectors
TDMA	Solve a triadiagonal matrix
OUTPUT	Output results

The inputs of the program include the x - y coordinates of the physical boundaries, grid numbers, and physical properties of the fluid and the solid medium. Boundary conditions of T, Ψ and P have to be specified in corresponding subroutines. The outputs of the program include x - y coordinates, T, Ψ, P, u and v for each grid points. These data can be used to construct isotherms, stream lines, isobars, and fluid flux vectors.

APPLICATION

The program has the potential in solving various heat and fluid flow related geological problems. The following is an example of the application of the program to characterize thermal fields around irregular magmatic intrusions and their control on localization of hydrothermal ore deposits.

The area of application is the Xinlu tin-polymetallic ore filed, Guangxi, southern China (Chi, 1992). The geology of the region is characterized by Devonian to Carboniferous carbonates which were deformed and intruded by granites in Mesozoic. Tin polymetallic deposits occur either in Devonian carbonates relatively far from the granites (distal deposits) or at the contact between granites and carbonates (proximal deposit) (Fig. 1).

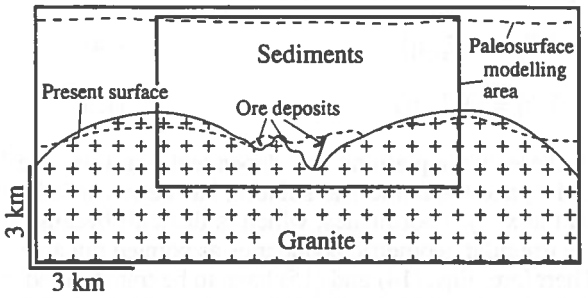

Figure 1. A schematic west-east geologic section of the Xinlu ore field.

Since the precipitation of cassiterite may be related to temperature drop of the ore-bearing fluids, the localization of the ore deposits is at least partly controlled by the the thermal field around the granite intrusions. Sams and Thomas-Betts (1988) noticed that the areas of greatest tin production in SW England are where the highest temperature gradient occurs. Demin and Zolotarev (1980) studied the heat conduction models for a polymetallic mineralization district associated with granite intrusions in the former USSR, and found out that 80% of the rare-metal deposits in the district are located in the zone where the thermal gradient was sharp and the temperature remained around 400°C for a relatively long time, and all the Pb-Zn deposits occur in the 240 - 320°C temperature-stable zone which had a sharp thermal gradient.

The mineralization in the Xinlu ore field is related to hydrothermal fluids derived from the granite intrusions. The ore-forming fluids were released after the emplacement of the intrusions, under the control of fluid pressure difference between the interior of the intrusions (lithostatic) and the fracture networks in the country rocks (hydrostatic) (Chi et al., 1993). Before the release of the ore-forming fluids, the country rocks around the granite intrusions had been heated, and thermal equilibrium may have been reached. The

thermal field established in this pre-ore stage provided the thermal background of ensuing ore-forming hydrothermal activities.

The pre-ore thermal field of the Xinlu ore field is numerically modelled by using the program described above, under specified boundary conditions as illustrated in Fig. 2. The top and bottom boundaries of the model are assumed to be heat and fluid flow insulators, with temperatures fixed at 20 and 750°C respectively (steady state model). The horizontal thermal gradient and fluid flux (u) on the two side boundaries are set at zero based on the symmetric geometry of the intrusion. The permeability (k) and heat conductivity (K_m) of the carbonates are 4.5 x 10^{-12} (cm^2) and 2.5 x 10^{-2} (J cm^{-1} sec^{-1} $°C^{-1}$) respectively. The initial (20°C) fluid density (ρ), heat capacity (C_f), kinematic viscosity (ν) and coefficient of thermal expansion (β) of the circulating underground water are 1.0 (g cm^{-3}), 7.0 (J g^{-1} $°C^{-1}$), 9.0 x 10^{-3} (cm^2 sec^{-1}) and 1.2 x 10^{-3} ($°C^{-1}$) respectively.

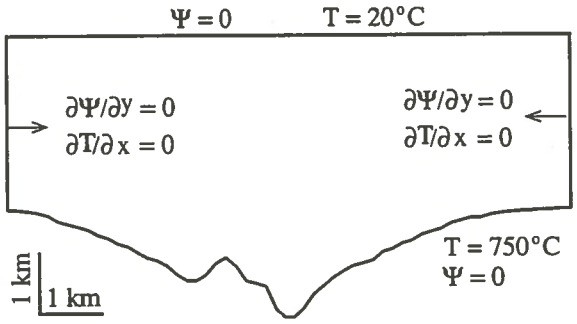

Figure 2. Physical model and boundary conditions.

The results of numerical modelling are illustrated in Figs. 3 and 4. The fluid flow patters shown in Fig. 3 represent the flow paths of underground water before mineralization, and are not indicative of the flow regime of the ore-forming fluids. The isotherms shown in Fig. 4 indicate the thermal background before mineralization. The temperature drop of the ore-forming fluids during their migration from the intrusion through the country rocks toward the surface was influenced by the pre-ore thermal field.

It is interesting to note that the sites of ore deposition coincide with the segments where temperature gradient is high (Fig. 4). The high temperature gradient is favorable for precipitation of ore minerals in a focussed area, a condition necessary for the formation of economic deposits. In segments where the top surface of the intrusion is sharply convex upward, thermal gradient is highest near the contact zone between the intrusion and the country rocks, thus favoring the formation of proximal deposits. In segments where the top surface of the intrusion is concave downward, thermal gradient is low near the contact zone, but tends to be relatively high in some distance above the contact. Such segments do not favor the formation of proximal deposits, but distal deposits may form under certain conditions.

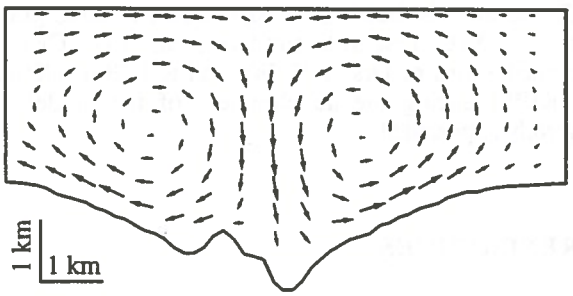

Figure 3. Fluid flux vectors showing the flow patterns of pre-ore underground water.

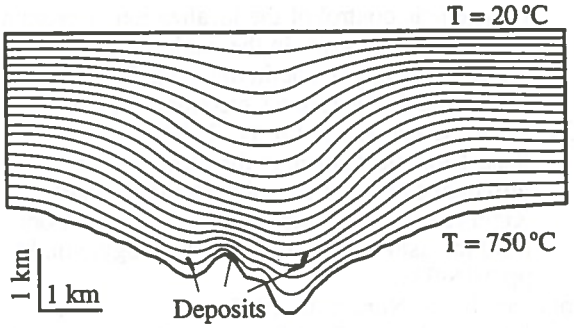

Figure 4. Isotherms showing the relationship between thermal gradients and localization of ore deposits in the Xinlu ore field.

CONCLUSIONS

Finite difference methods, when coupled with body-fitted transformation techniques, can be used to solve partial differential equations of heat transfer and fluid flow processes in irregular physical domains without the need of interpolation between grid points at the boundaries. The computer program described above keeps the simplicity of finite difference methods, and has the capacity of finite element methods to deal with irregular geometric boundaries, which are frequently

encountered in numerical modelling of geological processes. The program can be run on personal computers and is a handy tool for quick, first order evalution of heat and fluid flow related geological problems, and their effect on localization of ore deposits.

ACKNOWLEDGEMENTS

This project is financially supported by NSERC grants and UQAC research fundation to J.G. Critical contributions of Drs. Y.K. Wu and R.T. Bui (UQAC-GRIPS) during the development of the model are greatly appreciated.

REFERENCES

Brikowski, T. and Norton, D. 1989.
Consequences of magma chamber geometry on the thermal history of mid-ocean ridges. Earth and Planetary Science Letters, vol. 93, pp. 241-255.

Chi, G.-X. 1992.
Polygenetic control of the localization of proximal versus distal deposits in the Xinlu tin-polymetallic ore field, Guangxi, southern China. Ph.D. thesis, Université du Québec à Chicoutimi, 251 p.

Chi, G.-X., Guha, J. and Lu, H.-Z. 1993.
Separation mechanism in the formation of proximal and distal tin polymetallic deposits, Xinlu ore field, southern China - Evidence from fluid inclusion data. Economic Geology, vol. 88, pp. 916-933.

Johnson, J. and Norton, D. 1985.
State conditions, fluid flux, and solution-mineral equilibria during skarn formation in porphyry copper. Economic Geology, vol. 80, pp. 1797-1823.

Norton, D. and Cathles, L. M. 1979.
Thermal aspects of ore deposition. *In* Geochemistry of hydrothermal ore deposits (second edition). *Edited by* H. L. Barnes. John Wiley & Sons, New York, pp. 684-737.

Norton, D. and Knight, J. 1977.
Transport phenomena in hydrothermal systems: cooling plutons. American Journal of Science, vol. 277, pp. 937-981.

Patankar, S. V. 1980.
Numerical heat transfer and fluid flow. Hemisphere, Washington, DC.

Sams, M. S. and Thomas-Betts, A. 1988.
Models of convective fluid flow and mineralization in south-west England. Journal of Geological Society of London, vol. 145, pp. 809-817.

Thompson, J. F., Warsi, Z. U. A. and Mastin, C. W. 1985.
Numerical grid generation - foundations and applications. North-Holland, 483 p.

CAMI'95: 3rd Canadian Conference on Computer Applications in the Mineral Industry
Montréal, Québec, Canada, October 22-25, 1995

Power-Laws Versus Lognormal Models in Mineral Exploration

Frederik P. Agterberg
Geological Survey of Canada

ABSTRACT:

The high-value tails of the sizes and size-grade distributions for sets of mineral deposits of the same type can often be modelled as Pareto distributions plotting as straight lines on log-log paper. These power-law type relations may result from fractal and multifractal models. The multifractal model for size-grade distributions proposed here reflects self-similarity (approximate scale independence) of the underlying spatial distributions of the deposits. It predicts that the majority of deposits of the same type can be described by a lognormal distribution but the largest deposits in the tail are controlled by a hyperbolic instead of the lognormal law. One theoretical and three practical examples are presented for illustration. This topic is important because most ore comes from the relatively few, very large deposits in a population.

RÉSUMÉ:

Les valeurs extrèmes des distributions de tonnage-minerai et tonnage-métal pour des gisements d'un même type peuvent souvent être représentées par des modèles Pareto. Ce type de modèle, qui est révelé par une disposition linéaire des points expérimentaux lorsque portés sur un graphique à echelle logarithmique, peut être la manifestation d'un phénomène fractale ou multifractale. Le modèle multifractale proposé ici pour la distribution de tonnage-minerai est la conséquence de l'auto-similitude (indépendance d'echelle approximative) de la distribution spatiale des gisements. Il prédit que la majorité des gisements d'un même type pourrant être représentés par une distribution lognormale alors que les plus grands gisements, eux, seront représentés par une loi hyperbolique plutôt que lognormale. Un example théorique et trois examples pratiques sont présentés pour fin d'illustration. Ce sujet est pertinent à l'exploration minière car la plus grande production de minerai et de métal provient, en fait, d'un faible nombre de très grands gisements.

INTRODUCTION

The sizes and grades of minerals deposits are important for resource evaluation on a regional scale as well as for mineral exploration on a local scale. It is useful to distinguish between sets of mineral deposits on the basis of their type as well as their regional setting. If it is possible to define statistical populations for a mineral deposit type or for orebodies from the same geochemical environment, the next question is what type of size-grade frequency distribution model should be used. The answer to this question is relevant not only for the production of statistical summaries and graphical representation, but also for predictions related to unsampled parts of the environment.

In his book on the fractal geometry of nature, Mandelbrot (1983, p. 263) posed a challenge to the geoscience community by stating that oil and other natural resources have Pareto distributions, and this "finding disagrees with the dominant opinion, that the quantities in question are lognormally distributed. The difference is extremely significant, the reserves being much higher under the hyperbolic than under the lognormal law."

The book by Harris (1984) contains an excellent review of the various approaches which were taken in the past toward size-grade analysis of mineral deposits. As noted by Mandelbrot, the lognormal model has been most widely used. For example, the bivariate lognormal model often provides a good approximation for size-grade distributions of orebodies. Also, the element concentration values for blocks of equal size from

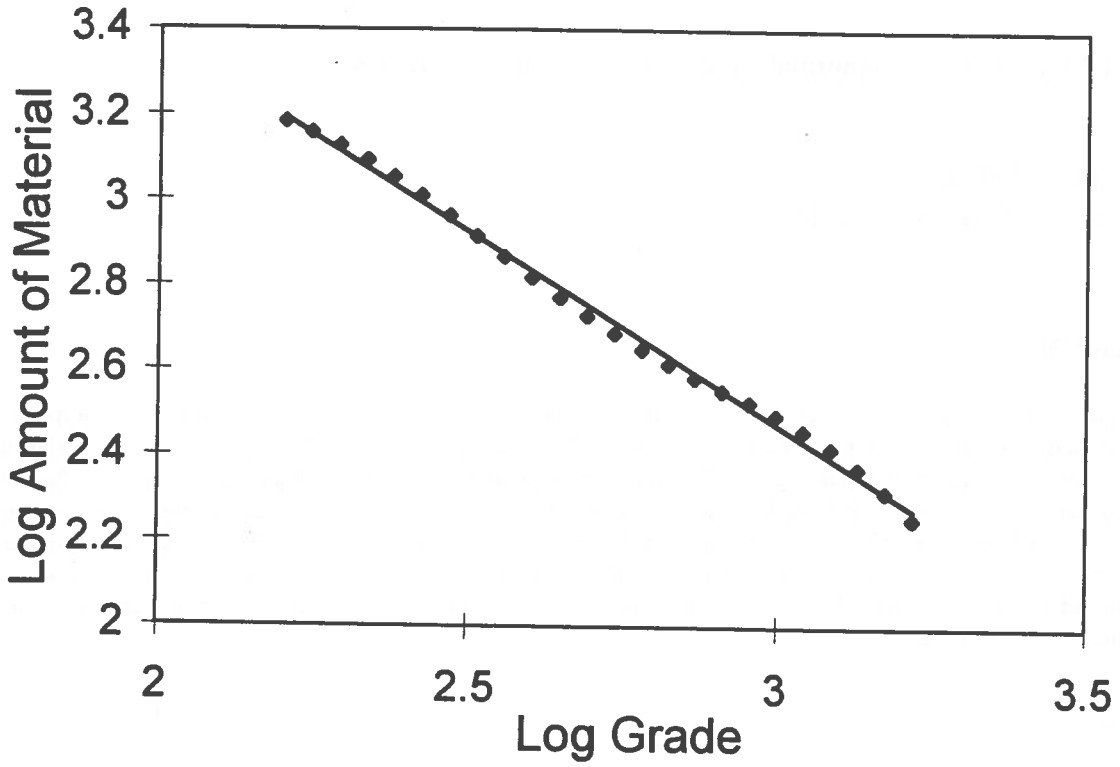

Figure 1. Probable worldwide uranium reserves according to de Wolde and Brinck (1971). Unit for amount of material is number of deposits of a given grade (in ppm U). The high-grade tail of the logbinomial model used for estimation can be approximated by a Pareto distribution plotting as a straight line on log-log paper (logarithms base 10).

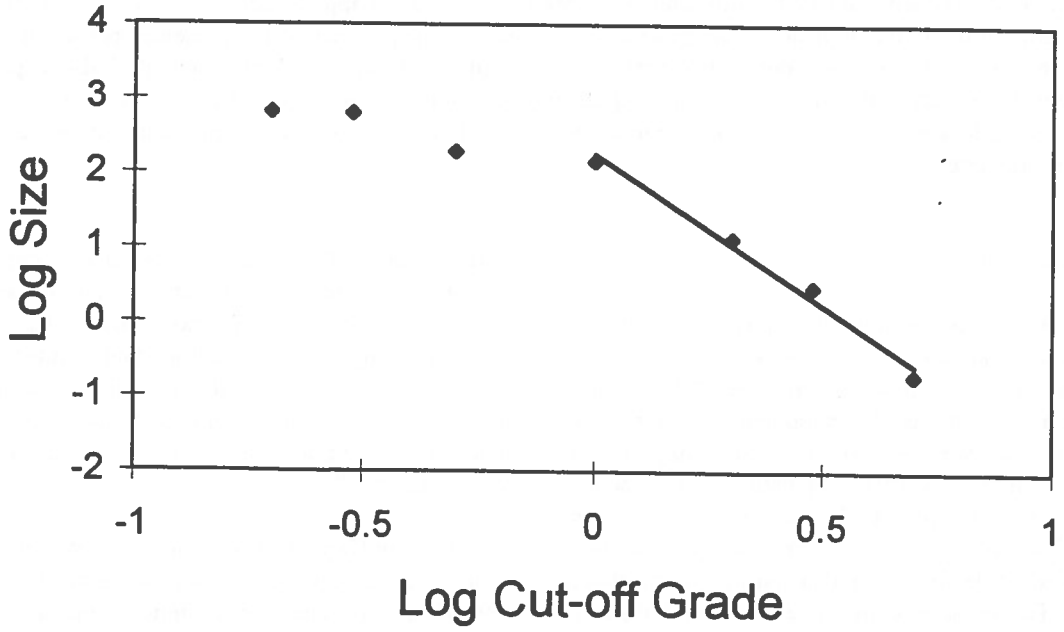

Figure 2. Tonnage of copper ore (unit = 10^6 tonnes) with grades exceeding the cut-off grade (in per cent Cu) in Canadian Appalachian Region on log-log paper (logarithms base 10). The straight line representing a Pareto distribution was fitted by least squares to the 4 data points with grades of 1.0 per cent Cu and higher (data from Agterberg and Divi, 1978).

within a mineral deposit or broader geochemical environment may satisfy lognormal distribution models. Power-law models have been preferred by relatively few scientists. However, the degrees of fit obtained in the high-value tails of the frequency distributions by means of power-law models are as good or better than those resulting from the lognormal model.

Frequencies are either numbers or quantities of items per class as those plotted in a histogram, or they are cumulative frequencies such as those plotted on logarithmic probability paper. In order to avoid confusion, the first type of frequencies will be referred to as histogram values or frequency densities when a statistical model is used. Otherwise, frequencies will mean cumulative frequencies which are modelled using frequency distribution curves.

HISTORICAL REVIEW

At an early date, Brinck (1967) proposed to use the logbinomial model for uranium resources in the earth's crust. The tail of this type of distribution can be approximated by a Pareto distribution which plots as a straight line on log-log paper. This is graphically illustrated in Figure 1 where Brinck's (1967) estimated frequencies for wordwide uranium resources are plotted against cut-off grade using logarithmic scales along both axes. The straight line was fitted by ordinary least squares to output values from the computer program "IRIS" of de Wolde and Brinck (1971, p. 22). The small deviations between the estimated logbinomial frequencies and the straight line in Figure 1 are mainly approximation errors introduced during numerical integration in IRIS. Theoretically, the logbinomial frequency curve should decrease monotonically with increasing grade.

Power-law relations were also observed between mean grade and cumulative ore tonnage of populations of mercury and copper deposits in the United States. The resulting straight lines on log-log paper were originally fitted by Cargill et al. (1981) and, later, Turcotte (1986) developed a fractal model to explain them.

In general, fractal models result in Pareto distributions. A drawback of using a fractal model for size and grade frequency density distributions is that it does not allow for maxima in the histograms as are commonly found in practice. The density curve of a Pareto distribution begins at a truncation value from where it decreases monotonically with increasing value. It is, of course, well known that the locations of maxima in histograms of size and grade values can be artificial. They are often the result of economic truncation related to cut-off values. Nevertheless, existence of a mean grade and a mean deposit size can be assumed in many types of applications and this would not be in agreement with the fractal model. It will be discussed in this paper that these types of cases can be modelled by a multifractal instead of a fractal model.

A specific type of multifractal model (multiplicative cascade model or model of de Wijs; cf. Agterberg, 1994) results in a logbinomial frequency distribution of the type illustrated in Figure 1. Although the Pareto distribution provides a good fit in the high-value tail of this distribution, it does not apply to lower values in the vicinity of the mean concentration value (= crustal abundance of uranium, outside of the range of grade values in Fig. 1).

Evertsz and Mandelbrot (1992) have pointed out that an important distinction between fractal and multifractal models is that fractal models apply to sets of objects and multifractal models to measures. In terms of spatial analysis, objects delineated by boundary surfaces in space can be modelled as binary (presence/absence) variables whereas measures assume (positive) real values at points in space inside or outside the objects. Metal concentration value (grade) is a measure requiring a multifractal approach but a set of objects of the same type with different shapes and sizes (e.g., orebodies) can be modelled as a fractal. Another fruitful area of application of fractal modelling is to sets of oil deposits with different sizes. The number of oil fields containing more than a given amount of oil can be modelled by means of a Pareto distribution as demonstrated by several authors including Drew et al. (1982) and Crovelli (1994).

According to the recently developed theory of multifractals, the sampling of self-similar environments may result in frequency distributions that are approximately lognormal except in their high-value and low-value tails where they tend to become hyperbolic (Pareto type). These tails plot as separate straight lines on log-log paper. Thus the concept of multifractality provides a new tool suggesting that, if there is self-similarity in natural situations, we can expect frequency distributions that are approximately lognormal except in their tails where power-law relations prevail.

Freiling (1967) made a direct comparison of lognormal and Pareto distributions showing that the tails of these

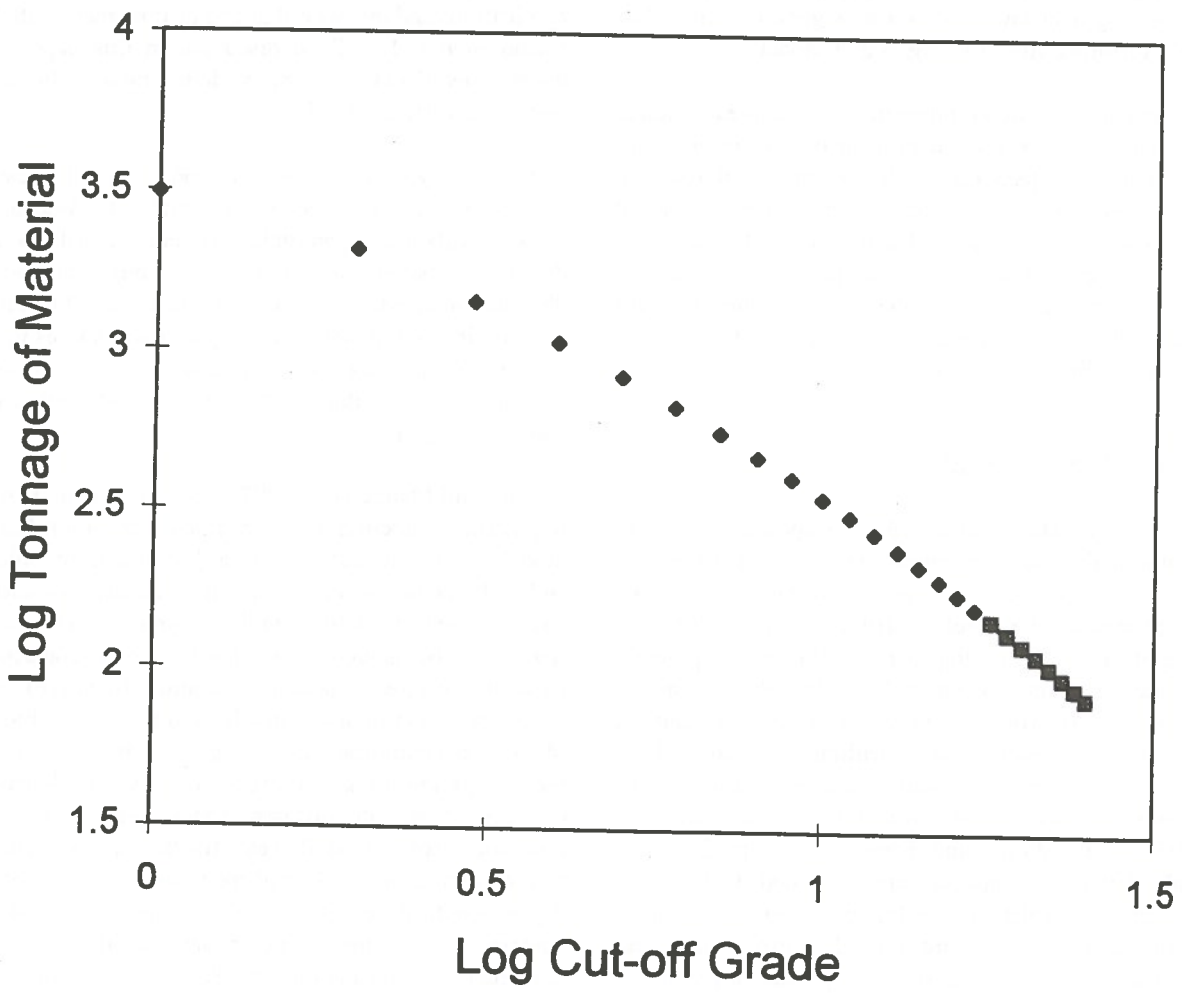

Figure 3. U.S. uranium resources (unit = 10^6 tons) versus cut-off grade (in per cent U_3O_8) from Harris (1984) on log-log paper (logarithms base 10). Last 8 values satisfy Pareto distribution model.

distributions are very different. However, extensive testing of the two models on mass-size distributions led him to the conclusion that available data were not sufficient to distinguish between lognormal and power-law distributions in practice.

The validity of the multifractal approach in mineral exploration was recently demonstrated by Cheng (1994) and Cheng et al. (1994) for gold and associated elements in altered volcanic rocks in the Mitchell-Sulphurets area, northwestern British Columbia. Plots of Au content in 1233 surface samples from altered and unaltered rocks using logarithmic probability paper suggest that the gold concentration values satisfy a single, positively skewed frequency distribution which is approximately lognormal. On the other hand, when geochemical isopleths are constructed (isolines or contours for concentration values ρ in ppb Au), and log-log paper is used to plot the cumulative area of rock with values exceeding ρ versus ρ, the altered and unaltered rocks show entirely different power-law relations.

Research on the topic of power-law ditributions is important because most ore for a metal tends to be concentrated in relatively few giant and supergiant deposits forming the tail of a size-frequency distribution. Two different types of approach of size-frequency analysis will be advocated in this paper. Firstly, it will be shown that the multifractal model leads to a power-law relation between a variable cut-off grade ρ and total amount of ore with grades exceeding ρ. This model will be applied to two examples of metal grade-tonnage relationships (copper in Canadian Appalachian region and uranium in U.S.A.) previously analyzed using other models. Secondly, the power-law relation resulting from a simple fractal model is used for the size-frequency of deposits which, like oil pools, can be modelled as a set of objects without consideration of grade during modelling. This model will be applied to gold tonnages in gold deposits in the Superior Province of the Canadian Shield.

SELF-SIMILARITY

The purpose of this section is to explain briefly the concept of self-similarity and how it is associated with the multifractal model. In two-dimensional space, a feature is scale-independent if, for two areas of the same shape but with different sizes, contouring it (e.g., by Kriging) produces identical results. This kind of reasoning was already applied by Krige (1978) to gold inch-dwt (inch x pennyweight) trend surfaces in Witwatersrand goldfields in the following way. Two-dimensional moving averages were computed by Krige (1978, Fig. 21) for two sections in the Klerksdorp goldfield with similar average grade x thickness values. Moving averages of 100 x 100 ft areas within a mined-out section of 500 x 500 ft were contoured. The resulting map is similar to another one based on moving averages of 2000 x 2000 ft areas within a mined-out section of 10 000 x 10 000 ft. Although the area of the second section is 400 times larger, the resulting patterns are similar, showing that, statistically, these gold values have the property of self-similarity. This suggests that they can be modelled as a multifractal. It is noted that different kinds of contour maps can be derived from actual data sets of grade and thickness. If all thicknesses were assumed to be the same, the contour map would represent variation in grade only, as in the case of gold concentration contours for the Mitchell-Sulphurets area (see before).

Feder (1988) introduces multifractals in a clear manner (also see Evertsz and Mandelbrot, 1992; Agterberg, 1994). Here, discussion is restricted to the following few comments. Suppose that a large square area in a goldfield is subdivided into n small (ϵ x ϵ) cells with, on average, $\mu_i(\epsilon)$ gram of gold per cell (i=1,2,...,n); ϵ denotes linear cell size. Then the partition function for the large square is defined as:

$$\chi_q(\epsilon) = \sum_{i=1}^{n} \mu_i{}^q(\epsilon) \qquad (1)$$

where q is a real number with $-\infty \leq q \leq \infty$. The multifractal model applies if for any value of q,

$$\chi_q(\epsilon) \propto \epsilon^{\tau(q)} \qquad (2)$$

It means that the partition function of order q and the mass exponent $\tau(q)$ have a power-law relation.

Korvin (1992) offers a heuristic exposition of the idea that self-similarity results in power-law type relations. Arguing along the same lines as Korvin, suppose that μ_1, μ_2, and μ_3 are the measures on a fractal set with "singularity" α (see later) in three cells with different sizes labelled ϵ_1, ϵ_2, and ϵ_3, respectively. Self-similarity would imply that the ratio of measures for two cells of different size depends on the ratio of the sizes only, or

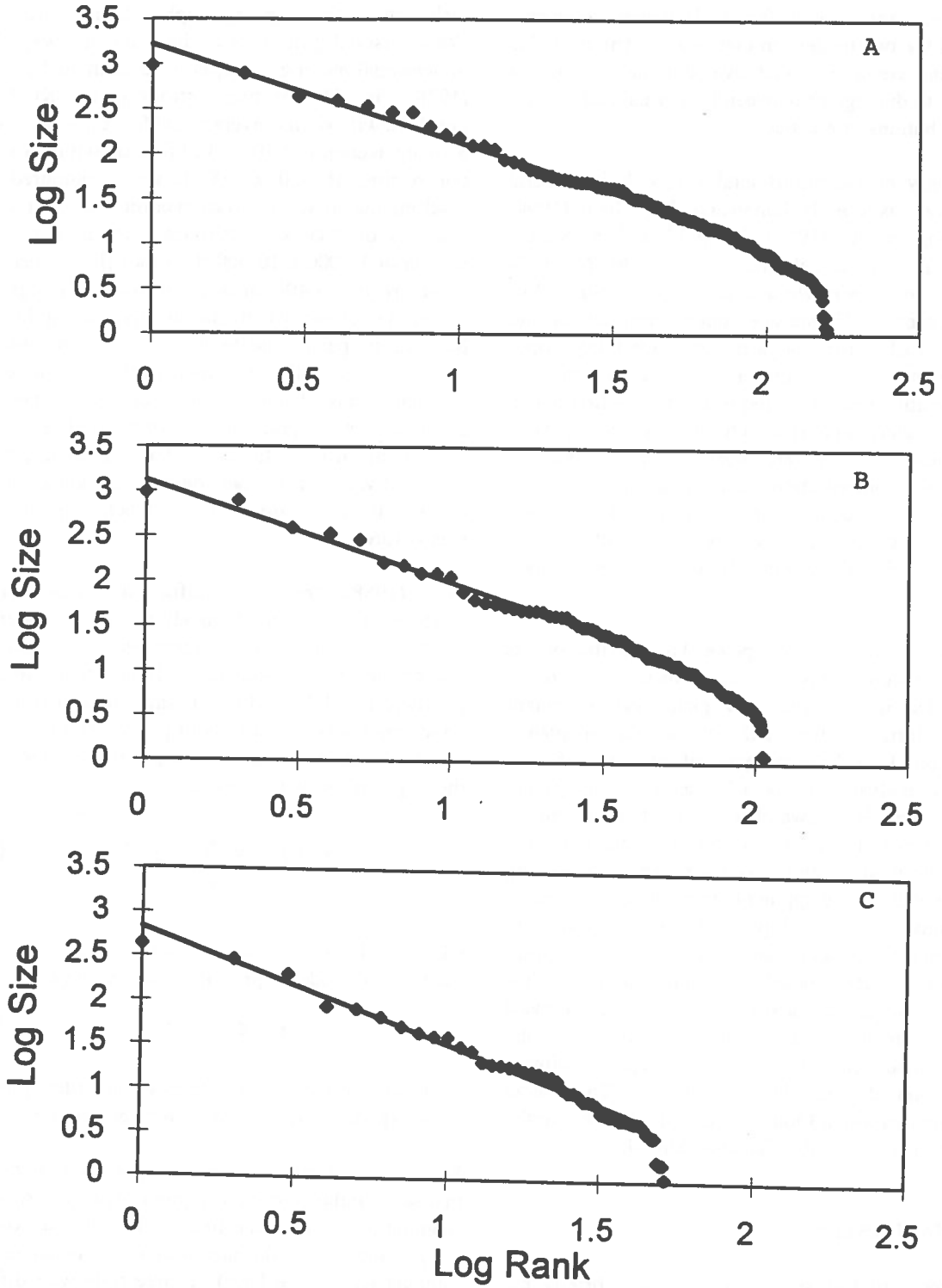

Figure 4. A: Production and reserves (in tonnes Au) of 160 lode gold deposits in Superior Province of Canadian Shield (data from Poulsen, 1995, personal information) ranked according to their size (largest deposit first). Best-fitting straight line on log-log paper represents Pareto distribution (logarithms base 10). B: Subset of lode gold deposits plotted in Figure 4A. These 107 deposits occur in the Abitibi Subprovince. C: Remaining 53 lode gold deposits from the Superior Province outside the Abitibi Volcanic Belt. The fitted Pareto distribution differs significantly from those in Figures 4A and 4B indicating that these deposits tend to be smaller.

$$\frac{\mu_1}{\mu_2} = f\left(\frac{\epsilon_1}{\epsilon_2}\right); \quad \frac{\mu_2}{\mu_3} = f\left(\frac{\epsilon_2}{\epsilon_3}\right); \quad \frac{\mu_1}{\mu_3} = f\left(\frac{\epsilon_1}{\epsilon_3}\right) \tag{3}$$

From this it is readily derived that

$$f\left(\frac{\epsilon_1}{\epsilon_3}\right) = f\left(\frac{\epsilon_1}{\epsilon_2}\right) f\left(\frac{\epsilon_2}{\epsilon_3}\right) \tag{4}$$

The function f is such that it satisfies a relation of the type f(ab) = f(a) f(b) where a and b are two constants. In the beginning of the last century the French mathematician Cauchy had already shown that this implies that f must be power-law type with $f(x) = x^p$ where p is a constant. It follows that for the measure on the fractal set

$$\mu_\alpha \propto \epsilon^\alpha \tag{5}$$

Suppose that μ_α is a subset of μ of approximately constant value (e.g., 2.9-3.1 grams of gold) in a relatively small cell of size ϵ, so that μ consists of many intertwined sets with different values of α. If μ_α occupies $N_\alpha(\epsilon)$ cells, replacement of μ by $N_\alpha(\epsilon)$ in Equation (3) results in

$$N_\alpha(\epsilon) \propto \epsilon^{f(\alpha)} \tag{6}$$

where $f(\alpha)$ represents the fractal dimension of the subset μ_α. Also, replacement of μ by $\chi_q(\epsilon)$ in Equation (3) results in Equation (2). Not only would fractals of different singularities be self-similar but patterns based on the entire measure would be self-similar as well. This type of reasoning is heuristic in the sense that it applies exactly to artificially constructed multifractals (e.g., model of de Wijs) but in practical applications, the measure μ_α and the partition function $\chi_q(\epsilon)$ must be regarded as mathematical expectations. It can be shown (Evertsz and Mandelbrot, 1992) that α is a function of q, or $\alpha=\alpha(q)$, and from Equations (2) and (5),

$$\alpha(q) = \frac{d\tau(q)}{dq} \tag{7}$$

Combination with Equation (6) results in the dimension spectrum $f(\alpha)$ with

$$f(\alpha) = q\alpha(q) - \tau(q) \tag{8}$$

If complete information is available, e.g. in the form of a map with estimates of $\mu(\epsilon)$ for a region, $f(\alpha)$ can be estimated. In the study of size-grade frequency distributions, less information is available. It usually consists of sizes and grades of mineral deposits or total amount of material $T(\rho > \rho_c)$ with grades ρ exceeding a variable cut-off grade ρ_c. In Appendix 1 it is shown that simple assumptions on existence of the multivariate dimension spectrum $f(\alpha)$ result in a power-law type relationship between volume of ore and cut-off grade. This can be extended to tonnages, so that

$$T(\rho > \rho_c) \propto \rho^{-\gamma} \tag{9}$$

where γ is a constant.

EXAMPLES

The first example is for copper in the Canadian Appalachian region. Agterberg and Divi (1978) developed a lognormal model for copper, lead and zinc using production and reserves estimates from all known sulphide deposits in this region. Their data for copper (Agterberg and Divi, 1978, Table 2, p. 111) are plotted on log-log paper in Figure 2. A straight line was fitted by least squares for copper grades of 0.01 and greater. It was shown in the earlier paper that these data are consistent with a lognormal distribution model with the mean set equal to the copper crustal abundance estimate. Figure 2 shows that the relationship for higher grades also can be approximated by a power-law relation.

The second example is for U.S. uranium resources (from Harris, 1984, Table 9.3, p. 228). Harris applied a lognormal model to these data (for an application of a fractal model to sizes and average grades, see Turcotte, 1986). The log-log plot in Figure 3 shows that as in Figure 2, a power-law relation can be used for the highest grades (straight line was fitted to the last 8 values only).

The final example (Fig. 4) is for lode gold deposits from the Superior Province in the Canadian Shield (data from Poulsen, 1995, personal communication; also see Poulsen, in press). This is an updated version of data previously used and discussed by Card et al. (1989).

Gold grade is not considered as a separate variable in this application. Each gold deposit tonnage plotted is representative of one or more gold mines with total production and reserves exceeding 1 tonne of gold. Most (two-thirds) deposits occur in the Abitibi Volcanic Belt of the Superior Province and the deposits from this subprovince were analyzed separately (Fig. 4B). The Abitibi Subprovince also contains the largest gold deposit consisting of three separate mines (Hollinger, McIntyre and Coniaurum).

In Figures 4 the log of size is plotted against the log of rank after ranking the deposits according to their size. A straight line was fitted by least squares using the majority of the deposits in each case. The observed data fall on a more or less continuous curve winding around the straight line that represents the power-law relation. The deviations from the straight line are largest on the left side because random fluctuations increase with decreasing sample size. The straight line provides an increasingly poor fit on the right side because information on smaller deposits becomes increasingly incomplete. The straight line for gold deposits outside the Abitibi Subprovince (Fig. 4C) has a smaller intercept and continues to stay below the other lines (Figs. 4A and 4B). This in in agreement with observations by Card et al. (1989, Table 1, p. 29) who concluded that degree of greenstone belt preservation (greatest in the Abitibi and Uchi Subprovinces) is an important factor in the present distribution of the lode gold deposits. Not only are these deposits relatively rare in the other subprovinces, they are also smaller on the average.

CONCLUSIONS

Power-law type relations can be used for the modelling of size-grade relations for populations of mineral deposits. These relations are easy to test because they correspond to straight lines on log-log plots of (a) size versus cut-off grade, and (b) size versus rank. It was shown (also see Appendix 1) that the first of these relations (a) can be the result of a multifractal model. The second type (b) has a fractal explanation. Both types of power-law relations may reflect self-similarity (scale independence) of the underlying, genetic processes. The data sets analyzed, for example, suggest validity of the fractal/multifractal approach. According to the multifractal model, the lognormal distribution provides a good fit to the majority of the deposits but the giants and supergiants would belong to tails controlled by power-law relations. More research is required to investigate the wider implications of this approach.

ACKOWLEDGEMENTS

Thanks are due to Dr. Howard Poulsen, Geological Survey of Canada, Ottawa, for allowing me to use his data base on Superior Province gold deposits and critical reading of the manuscript, and to Dr. Alexandre Desbarats, GSC, Ottawa, and Dr. Qiuming Cheng, Ottawa-Carleton Geoscience Centre, for suggestions.

REFERENCES

Agterberg, F.P., 1994
Fractals, multifractals, and change of support. In: R. Dimitrakopoulos (ed.), Geostatistics for the Next Century. Kluwer, Dordrecht, pp. 223-234.

Agterberg, F.P., and Divi, S.R., 1978
A statistical model for the distribution of copper, lead and zinc in the Canadian Appalachian Region. Economic Geol., vol. 73, pp. 230-245.

Brinck, J.W., 1967
The calculation of uranium resources in the earth's crust. Euratom Bull., vol. 6, no. 4, pp. 109-114.

Card, K.D., Poulsen, K.H., and Robert, F., 1989
The Archean Superior Province of the Canadian Shield and its lode deposits. Economic Geol., vol. 84, pp. 19-36.

Cargill, S.M., Root, D.H., and Bailey, E.H., 1981
Estimating usable resources from historical industry data. Economic Geol., vol. 76, pp. 1081-1095.

Cheng, Q., 1994
Multifractal Modelling and Spatial Analysis with GIS: Gold Potential Estimation in the Mitchell-Sulphurets Area, Northwestern British Columbia. Unpublished Ph.D. thesis, University of Ottawa, Ottawa, 268 p.

Cheng, Q., Agterberg, F.P., and Ballantyne, S.B., 1994
The separation of geochemical anomalies from

background by fractal models. Jour. Geochemical Exploration, vol. 51, pp. 109-130.

Crovelli, R.A., 1994
The generalized 20/80 law using probabilistic fractals applied to petroleum field size. Proceedings, International Association for Mathematical Geology Annual Conference, Mont Tremblant, Québec, Canada, October 1994, pp. 100-101.

de Wolde, H.I., and Brinck, J.W., 1971
The estimation of mineral resources by the computer program "IRIS". Commission of the European Communities Joint Nuclear Research Centre Report EUR 4607e, Ispra, Italy, 42 p.

Drew, L.J., Schuenemeyer, J.H., and Bawiec, W.J., 1982
Estimation of the future rates of oil and gas discoveries in the western Gulf of Mexico. U.S. Geological Survey Profess. Paper 1252, 26 p.

Evertsz, C.J.G. and Mandelbrot, B.B., 1992
Multifractal measures. Appendix B in: H.-O. Peitgen, H. Jurgens, and D. Saupe, Chaos and Fractals. Springer-Verlag, New York, pp. 922-953.

Feder, J., 1988
Fractals. Plenum Press, New York, 283 p.

Freiling, E.C., 1966
A comparison of the fallout mass-size distributions calculated by lognormal and power-law models. U.S. Naval Radiological Defense Laboratory Report TR-1105, San Francisco, 13 p.

Harris, D.P., 1984
Mineral Resources Appraisal. Clarendon Press, Oxford, 445 p.

Korvin, G., 1992
Fractal Models in the Earth Sciences. Elsevier, Amsterdam, 408 p.

Krige, D.G., 1978
Lognormal-de Wijsian Geostatistics for Ore Evaluation. South African Inst. Mining Metall., Johannesburg, 50 p.

Mandelbrot, B.B., 1983
The Fractal Geometry of Nature (updated and augmented edition). Freeman, New York, 486 p.

Poulsen, K.H., in press
Lode gold; in O.R. Eckstrand, W.D. Sinclair, and R.I. Thorpe, eds., Geology of Canadian Mineral Deposit Types. Geological Survey of Canada, Geology of Canada, No. 8, Ottawa, Canada (*also* Geological Society of America: The Geology of North America, vol. P-1).

Turcotte, D.L., 1986
A fractal approach to the relationship between ore and tonnage. Economic Geol., vol. 81, pp. 1528-1532.

Appendix 1

PROOF THAT MULTIFRACTALITY RESULTS IN POWER-LAW TYPE SIZE-GRADE DISTRIBUTION

It is assumed that the measure satisfies a multifractal model with continuous dimension spectrum $f(\alpha)$. The case to be considered is that α is relatively small and restricted to a narrow range $\alpha_0 < \alpha < \alpha_1$, where α_0 is equal to or slightly greater than α_{min} representing the minimum value of α. The volume of ore with measure from this restricted range is:

$$V(\alpha<\alpha_1) = \int_{\alpha_0}^{\alpha_1} C\,\epsilon^{-f(\alpha)+3}\,d\alpha$$

where C is a constant. If α is close to α_0, higher order terms can be neglected in the Taylor series expansion, and

$$\epsilon^{-f(\alpha)} \approx \epsilon^{-f(\alpha_0) - f'(\alpha_0)(\alpha-\alpha_0)}$$

This approximation is only valid if $f'(\alpha_0)$ exists. This is the reason for allowing $\alpha_0 > \alpha_{min}$ because $f'(\alpha_{min}) = \infty$ for some models including the binomial multiplicative cascade model. It follows that

$$V(\alpha<\alpha_1) \approx C\epsilon^{-f(\alpha_0)+3}\,\epsilon^{f'(\alpha_0)\alpha_0}\int_{\alpha_0}^{\alpha_1}\epsilon^{-f'(\alpha_0)\alpha}\,d\alpha$$

Consequently,

$$V(\alpha<\alpha_1) \approx \frac{C\epsilon^{-f(\alpha_0)+3}}{f'(\alpha_0)\ln\epsilon}\left[1-\epsilon^{f'(\alpha_0)(\alpha_0-\alpha_1)}\right]$$

If α_1 is close to α_0,

$$f'(\alpha_0) \approx \frac{f(\alpha_1)-f(\alpha_0)}{\alpha_1-\alpha_0}$$

and

$$V(\alpha<\alpha_1) \approx \frac{C\epsilon^3}{f'(\alpha_0)\ln\epsilon}\left[\epsilon^{-f(\alpha_0)}-\epsilon^{-f(\alpha_1)}\right]$$

Provided that the difference between $f(\alpha_0)$ and $f(\alpha_1)$ is small:

$$V(\alpha<\alpha_1) \approx \frac{C\epsilon^{-f(\alpha_0)+3}}{f'(\alpha_0)}\left[f(\alpha_1)-f(\alpha_0)\right]$$

Consequently,

$$V(\alpha<\alpha_1) \approx C\epsilon^{-f(\alpha_0)+3}(\alpha_1-\alpha_0)$$

Suppose that ρ denotes metal grade. The singularity α_0 corresponds to the highest grade considered which can be written as ρ_{max}. Suppose that α_1 corresponds to a variable cut-off grade $\rho_c<\rho<\rho_{max}$. These relations can be written as

$$\frac{\rho}{D} = \epsilon^{\alpha_1-3}; \quad \frac{\rho_{max}}{D} = \epsilon^{\alpha_0-3}$$

where D is a constant. It follows that

$$V(\rho>\rho_c) \approx \frac{C\epsilon^{-f(\alpha_0)+3}}{\ln\frac{1}{\epsilon}}\left[\ln\frac{\rho_{max}}{D}-\ln\frac{\rho}{D}\right]$$

and

$$V(\rho>\rho_c) \approx C\epsilon^{-f(\alpha_0)+3}(3-\alpha_0)\left[1-\frac{\ln\frac{\rho}{D}}{\ln\frac{\rho_{max}}{D}}\right]$$

For small values of x, ln (1+x) can be replaced by x. Therefore, log-transformation of both sides gives:

$$\ln V(\rho>\rho_c) \approx \ln\left[\epsilon^{-f(\alpha_0)+3}(3-\alpha_0)\right]-\frac{\ln\frac{\rho}{D}}{\ln\frac{\rho_{max}}{D}}$$

This is equivalent to

$$V(\rho>\rho_c) \propto \rho^{-\beta}; \quad \beta = \frac{1}{\ln\frac{\rho_{max}}{D}} = \frac{1}{(3-\alpha_0)\ln\frac{1}{\epsilon}}$$

A simple power-law relation between volume of ore and cut-off grade is indicated. Eq.(9) in the text follows after setting $\gamma = \beta+1$.

CAMI'95:3rd Canadian Conference on Computer Applications in the Mineral Industry
Montréal, Québec, Canada, October 22-25, 1995

A Spatial Analysis Method for Geochemical Anomaly Recognition

Qiuming Cheng, F.P. Agterberg and G.F. Bonham-Carter
Geological Survey of Canada

ABSTRACT:

One purpose of using statistical methods in exploration geochemistry is to assist exploration geologists in separating anomaly from background. This always involves two types of negatively associated errors of misclassification: type I errors occur when samples with background levels are rejected as background; and type II errors occur when samples with anomalous values are accepted as background. A new spatial statistical approach is proposed to minimize errors of total misclassification using a moving average technique with variable window radius. This method has been applied for geochemical anomaly enhancement and recognition as demonstrated by a case study of Au and Au-associated data for 698 stream sediment samples in the Iskut River area, northwestern British Columbia. Similar results were obtained by using the fractal concentration-area method on the same data. By employing spatial information in the analysis, the process of selecting anomalies becomes less subjective than in more traditional approaches.

RÉSUMÉ:

Des méthodes d'analyses statistiques spatiales permettent aux géochimistes d'exploration de différencier les anomalies des bruits de fond. Ce type de statistique est à la source de deux types d'erreurs de classification. Les erreurs de type 1 se produisent lorsque les valeurs anomaliques recherchées prises pour un bruit de fond, sont faussement rejetées. Dans le cas contraire, les erreurs de types deux, des bruits de fond sont pris pour des anomalies et faussement acceptés. Une analyse statistique spatiale fesant appel à une technique de "moving average" avec un "variable window radius" permet de minimiser les erreurs de classification. Cette méthode a été utilisée pour l'indentification des anomalies geochimiques comme démontré par l'étude de cas de l'Au et l'Au-relié de 698 échantillons de sediment de ruisseau dans la région de la rivière Iskut dans le nord-west de la colombie-britanique. Des résultats similaires ont été obtenus en utilisant la méthode fractale de concentration-spatiale sur les même échantillions. En utilisant l'information spatiale dans cette analyse le procédé de sélection des anomalies devient moins subjectif que dans les méthodes traditionnelles.

INTRODUCTION

Classification is widely used in applications of computer-based spatial analysis and geographic information systems (GIS) in different fields of mineral industry. In exploration geochemistry, for example, it is often required to classify geochemical samples into different classes to reflect various geochemical processes and environments. A basic task of this application is to recognize anomalies which are associated with mineralization of a certain type from background corresponding to regional geological processes. Statistical theory plays an important role in classification. Since more powerful computers and software such as GIS with capability of handling spatial data become available, more spatial analysis techniques are needed to aid geoscientists to incorporate spatial information for classification. In this paper, a spatial analysis method will be proposed for geochemical anomaly enhancement.

Methods that have been used for geochemical anomaly separation include statistical approaches such as

probability graphs and univariate and multivariate analysis methods; spatial statistical analysis using moving averages or Kriging (Garrett, 1989; Govett et al., 1975; Miesch, 1981; Sinclair, 1974, 1976, 1991; Stanley, 1988; Stanley and Sinclair, 1989), and fractal methods including the concentration-area fractal model (Cheng, Agterberg and Ballantyne, 1994). Various characteristics of geochemical data, samples and anomalies are considered in these method; for instance, (1) frequency distributions of element concentration values are employed in most statistical methods; (2) values and their spatial characteristics are considered in many spatial analysis methods such as Kriging, moving averaging and spatial factor techniques (Grunsky and Agterberg, 1988); and (3) these values, spatial correlation and the geometrical characteristics of the anomalous areas are used in fractal/multifractal methods (Cheng, Agterberg and Ballantyne, 1994). It has been shown that spatial characteristics of geological entities can provide useful information and this may improve the classification results significantly. In this paper, a spatial analysis method is developed on the basis of concentration values, spatial distributions and geometrical properties of anomalies and background. The effect of sampling density on the classification results will be clarified by applying this method. It is demonstrated by an artificial example, and an real data to separate geochemical anomalies from background for Au and the Au-associated element concentration values in stream sediment samples from the Iskut River map sheet, northwestern British Columbia.

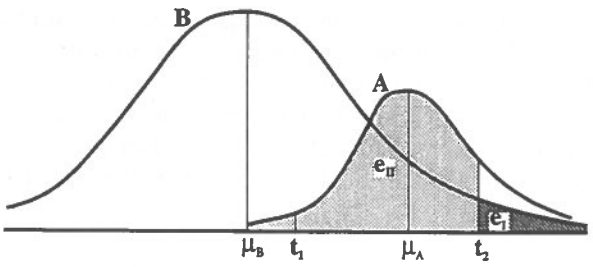

Fig. 1 Two populations: A: anomaly with mean μ_A. B: background with mean μ_B. t_1: lower limit of anomaly. t_2: upper limit of background. e_I and e_{II}: errors of types I and II with t_2 as threshold.

ANOMALY SEPARATION AND RISK ANALYSIS

Geochemical Anomaly Separation

The common purpose of various methods used for geochemical anomaly separation is summarized in Fig. 1 showing frequency distributions of concentration values (these might be estimated values resulting from moving averaging or Kriging); A (anomaly) and B (background) represent two populations with different spatial characteristics. One purpose of using spatial statistical methods is to define a threshold (t) so that samples can be classified according to their concentration values: samples with values greater than t are classified as anomalous and those less than t as background. There are different methods of defining the threshold t. Suppose that it is possible to set a lower limit for anomaly (t_1 in Fig. 1) and an upper limit for background (t_2). A sample with value less than t_1 may be grouped into the background category and, a sample with value greater than t_2 can be classified as anomalous. It is obvious that if the two populations (A and B) are overlapping to some extent, then t_1 and t_2 should be different with $t_1 < t_2$. This is because one is unable to classify the samples with values between t_1 and t_2, since they could belong to either anomaly or background. Two errors are always associated with classification: Type I (rejection error) occurs when a sample with background value is rejected as background, and Type II (acceptance error) when a sample with anomalous value is accepted as background. These two types of errors are negatively associated. If one type of error is made small by changing the threshold, the other will be large. In some cases, minimizing one type of error will be optimal and in other applications it is better to minimize the total error (Type I and Type II) (Stanley, 1988). In this paper, a new approach will be proposed for decreasing the total error (Type I and Type II) by incorporating spatial characteristics of the sample locations.

Risk Analysis

As mentioned in the previous section, there are two errors associated with geochemical anomaly separation. This concept can be described in terms of statistical inference as follows. Statistical inference can be used for testing a null hypothesis H_0 about the parameters of the frequency distribution of a population such as the mean and variance. Parametric statistical hypothesis testing usually consists of the following four steps: (1) assuming a group of distributions with unknown parameters θ and distribution functions $F(x, \theta)$ completely depending on the values of θ; for example, θ_A and θ_B may correspond to anomalous and background populations in geochemical exploration; (2)

creating a null hypothesis about the parameter θ, denoted as H_0: $\theta \in \Theta_0$; the total domain of θ, written as Θ, is called domain of admission for H_0 and H_1: $\theta \in \Theta - \Theta_0$ being the alternative hypothesis; for example, H_0 may be defined so that the sample belongs to background with the alternative hypothesis H_1 is for the sample belonging to an anomaly; (3) deriving samples $X_1,...,X_n$ from the same population to construct the statistics $U=U(x_1,...,x_n)$; (4) defining two subsets (W and W^-) for U, called rejection and acceptance regions, respectively. For the example in Fig. 1, W=(t, +∞) and W^-=(-∞, t). If the value of U belongs to W then the hypothesis (H_0) is rejected which means that the samples should not be accepted as background; in other words, they may be classified as anomaly; otherwise, if the value of U belongs to W^-, H_0 is accepted which means that the samples are classified as background. The two errors (rejection and acceptance) can be expressed in the following probability form:

$$e_I = P[U_{H_0} \in W]$$
$$e_{II} = P[U_{H_1} \in W^-] \qquad (1)$$

where U_{H0} indicates the value of U when H_0 is true, and U_{H1} is for the value of U when H_0 is false or H_1 is true. In the case of W=(t, +∞) and W^-=(-∞, t), these two errors can be expressed as

$$e_I = P[U_{H_0} \geq t]$$
$$e_{II} = P[U_{H_1} < t] \qquad (2)$$

Obviously, e_I increases and e_{II} decreases for decreasing t. Generally, e_I and e_{II} are negatively associated and depend on several factors such as the definition of W and W^- (value of threshold t), F distribution function, statistics (U) and sample size n.

Under the normal distribution (P), the statistics (U) can be grouped into two categories (Cheng, 1994): for one type, the two errors in Eq. 1 are approaching zero as the size of sample (n) increases with a proper threshold t;

$$\lim_{n\to\infty}(e_I + e_{II}) = 0 \qquad (3)$$

For the other type, however, the two errors will be not tend to zero no matter how large the sample size is, and

$$\lim_{n\to\infty}(e_I + e_{II}) > 0 \qquad (4)$$

For the first type of statistic, increasing the sample size (n) may greatly improve the testing results. It has been shown that U-, χ^2- and F-statistics belong to the first type and T-statistics belong to the second one (details more about proof of these properties is given in Cheng, 1994). Both errors (e_I and e_{II}) during the use of the U-, χ^2- and F-statistics are approaching zero as sample size increases infinitely, whereas the two errors for T-statistics approach a finite value not equal to zero. These properties of the statistics are to be considered in geochemical data analysis as shown in detail for U.

SPATIAL U*- STATISTICS

It has been shown (Cheng, 1994) that sample size may be the only factor which controls both errors (e_I and e_{II}). Therefore, in applications of a statistic, one usually gets better results by increasing the sample size. For geochemical exploration, the fact that a different sampling density may statistically affect the recognition of anomaly from background can be explained in terms of the classification errors (e_I and e_{II}) as follows. Suppose that two populations (A and B) have normal distributions with means of μ_A and μ_B, and variances σ^2_A and σ^2_B, respectively. Samples ($X_1,...,X_n$) are collected independently in order to distinguish between the populations A and B. A new random variable $U=(1/n)\Sigma X_i$ can be constructed (U-statistic) with the following properties: $E(U)=\mu_A$ and $\sigma^2(U)=(1/n)\sigma^2_A$ if all samples are from population A, and $EU=\mu_B$ and $\sigma^2(U)=1/n\sigma^2_B$ if all samples are from B. The distribution function for U is illustrated in Fig. 2. The means of U for samples from A or B are the same as the means of A or B, but the variances of U for A or B are different by the factor (1/n) which depends on sample size n.

More generally, instead of an arithmetic average, a weighted average U can be used with

$$U = \sum_{i=1}^{m} w_i X_i \qquad (5)$$

where $0 \leq w_i \leq 1$, $\Sigma w_i = 1$. Then, $E(U)=\mu_A$ and $\sigma^2(U)=\Sigma w^2_i \sigma^2_A$ if all samples are collected from population A, and $E(U)=\mu_B$, and $\sigma^2(U)=\Sigma w^2_i \sigma^2_B$ if all samples come from B. In general, $1/n \leq \Sigma w^2_i \leq 1$; $\Sigma w^2_i = 1$, if and only if i = k with $w_k=1$ (and $w_i=0$, when $i \neq k$) which implies that $U = X_k$; $\Sigma w^2_i = 1/n$, if and only if $w_i=1/n$, i=1,...,n, for the arithmetic average. Different types of weighting in Eq. 5 may result in a different

variance $\sigma^2(U)$ with another factor Σw^2_i but the smallest variance is reached for the arithmetic average.

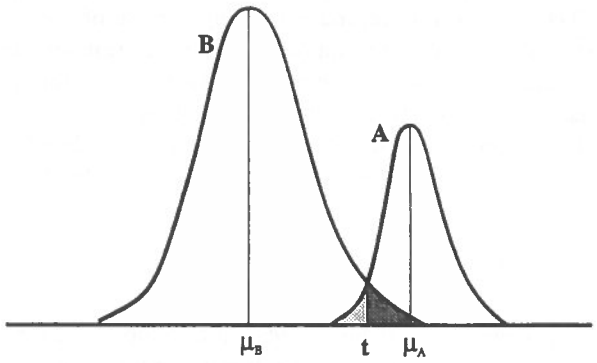

Fig. 2 Density function of random variable (statistics) U (see text for definition).

In the preceding discussion, all values were supposed to originate from a single population (A or B). In general, we do not know which population the values come from. However, by inspecting the geometrical characteristics of the geochemical anomalies, we may notice that anomalous samples often occur in groups which correspond to geographically distinct areas. Values of samples and the geometry of anomalous areas have been considered in anomaly separation (Sinclair, 1991; Cheng, Agterberg and Ballantyne, 1994). An experimental study of average values of samples was presented by Govett et al. (1975). These authors reported that for systematical sampling (grid sampling), averaging values of samples is useful for separation between populations. This idea can be generalized as follows.

Suppose that a given area consists of two subareas A and B (Fig. 3) representing anomaly and background, respectively. The area A could be circular, elliptical or belt-lake in shape. The mixture distribution for samples randomly collected from the area of Fig. 3 is assumed to be as illustrated in Fig. 1. Samples with values between the thresholds t_1 and t_2 in Fig. 1 can not be classified individually. If $t_1 << t_2$, only a small number of samples with values less than t_1 or greater than t_2 can be correctly classified. For this reason, a new statistic will be constructed:

Let α_i indicate the location of the i-th sample in the study area and X_i the value of this sample; choose any sample, say α_i, from the set of samples and create a circular neighbourhood around it denoted as $c(\alpha_i, r)$, with the radius r ($0 \le r \le r_{max}$). The value of r can be assigned in such a way that $c(\alpha_i, r) \subset A$ if $\alpha_i \in A$ or $c(\alpha_i, r) \subset B$ if $\alpha_i \in B$. A function for $c(\alpha_i, r)$ can be defined as follows:

$$\mu_{c(\alpha_i, r)}(\alpha_j) = \frac{r - d(\alpha_i, \alpha_j)}{r} \qquad (6)$$

where $d(\alpha_i, \alpha_j) \le r$ represents distance from sample location α_j to α_i. This function has the properties: $0 \le \mu_{c(\alpha i,r)}(\alpha_j) \le 1$; $\mu_{c(\alpha i,r)}(\alpha_j)=1$ if $\alpha_i=\alpha_j$; and $\mu_{c(\alpha i,r)}(\alpha_j)=0$ if $\alpha_j \notin c(\alpha_i, r)$, where $\notin$ indicates "does not belong to". A new value $U_i(r)$ for sample α_i can be defined as a linear combination of X_i:

$$U_i(r) = \frac{\overline{X}_i(r) - \mu}{S_i(r)} \qquad (7)$$

with

$$\overline{X}_i(r) = \sum_{j=1}^{n} w_j(r) X_j$$

$$S_i(r) = \sigma \sqrt{\sum_{j=1}^{n} w_j^2(r)} \qquad (8)$$

$$w_j(r) = \frac{\mu_{c(\alpha_i, r)}(\alpha_j)}{\sum_{j=1}^{n} \mu_{c(\alpha_i, r)}(\alpha_j)}$$

where μ and σ are the mean and standard deviation of X_i in the whole area. A new statistic $U^*_i = U_i(r_0)$ can be defined where r_0 is the value yielding

$$|U_i(r_0)| = \max_{0 \le r \le r_{max}} |U_i(r)| \qquad (9)$$

The value of U^*_i for sample α_i has the following normal distribution:
If $\alpha_i \in A$:

$$U_i^* \sim N\left(\frac{\mu_A - \mu}{S_i(r_0)}, \frac{\sigma_A}{\sigma}\right) \qquad (10)$$

and, if $\alpha_i \in B$:

$$U_i^* \sim N\left(\frac{\mu_B - \mu}{S_i(r_0)}, \frac{\sigma_B}{\sigma}\right) \qquad (11)$$

where $\mu_B \le \mu \le \mu_A$, so that $U^*_i(r_0)$ has mean $(\mu_A - \mu)/S_i(r_0) > (\mu_A - \mu)/\sigma > 0$ if α_i belongs to A, and $U^*_i(r_0)$ has mean $(\mu_B - \mu)/S_i(r_0) < (\mu_B - \mu)/\sigma < 0$ if α_i belongs to B. If α_i is located on the boundary between A and B, then r_0

should be close to zero and, therefore, $U^*_i(0)$ is reduced to $(X_i-\mu)/\sigma$ which is equal to the original standardized value of X_i. The value $U^*(r_0)$ can be easily classified. The value of $U^*_i(r_0)$ depends on the total number of samples within $c(\alpha_i, r)$. It is also associated with the location of α_i; e.g., if α_i is located near the boundary between A and B, there can only be relatively few samples in $c(\alpha_i, r)$ and the value of $U^*_i(r_0)$ will be close to the original standardized value of X_i. Of course, the value of $U^*_i(r_0)$ also depends on density of samples collected from the area and, statistically, the sampling density may influence the result of distinguishing between geochemical populations.

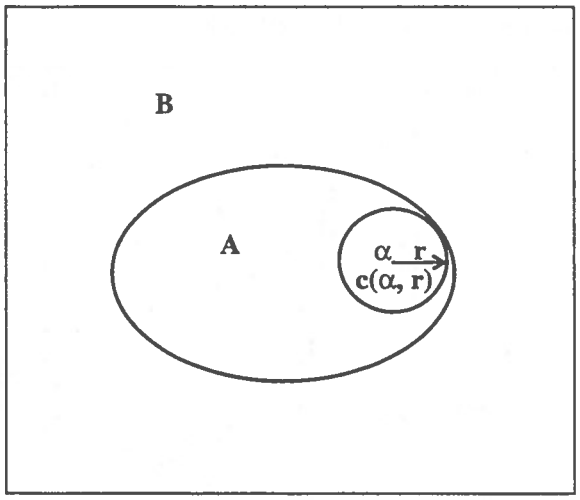

Fig. 3 Moving windows with varying radius. B: background. A: anomalous area. α: sample location. c(α, r): vicinity around a with a radius of r. Samples in c(α, r) are weighted and averaged.

APPLICATION EXAMPLES

An artificial example is given to demonstrate the method proposed in the previous section, before it will be used for separating Au-associated geochemical anomalies from background for stream sediment data in the Iskut River map sheet, northwestern British Columbia.

An Artificial Example

Suppose 2500 samples with sampling density of 1 sample per 1km^2 are regularly collected from a mineral district with total area of 2500 km^2 (Fig. 4), consisting of background B (2297 km^2) and anomalous areas A_1 (78 km^2) and A_2(125 km^2). In total, 203 samples are collected from A_1 and A_2, and 2297 samples from B with the anomalous samples accounting for 8.1% of all samples. The values for anomalous samples from A_1 belong to a normal distribution with mean of 25 (μ_{A1}) and standard deviation of 15 (s_{A1}). The values for anomalous samples from A_2 belong to a normal distribution with mean of 30 (μ_{A2}) and standard deviation of 10 (s_{A2}). Values for background samples from B belong to a normal distribution with mean of 10 (μ_B) and standard deviation of 20 (s_B). The distribution of mixed anomalous and background samples is shown in Fig. 5a. In order to separate anomalous samples from background using the frequency distribution, several thresholds are used; e.g.,

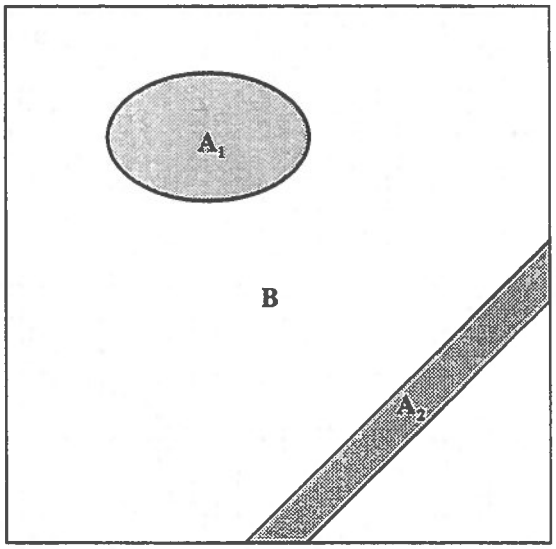

Fig. 4 Artificial example. A_1 and A_2: anomalous areas; B: background.

mean + c standard deviations (c = 1.0, 1.1, 1.5 and 2.0). The errors (e_I and e_{II}) of misclassification associated with these thresholds are estimated by means of the following formulae

e_I = {*number of samples from B classified into A*}/{*total number of samples in B*}

e_{II} = {*number of samples from A classified into B*}/{*total number of samples in A*}

The calculated results of e_I and e_{II} for various thresholds are shown in Table 1. It is shown that results obtained by these thresholds are not satisfactory because errors range from 0.8 to 0.97. The results for

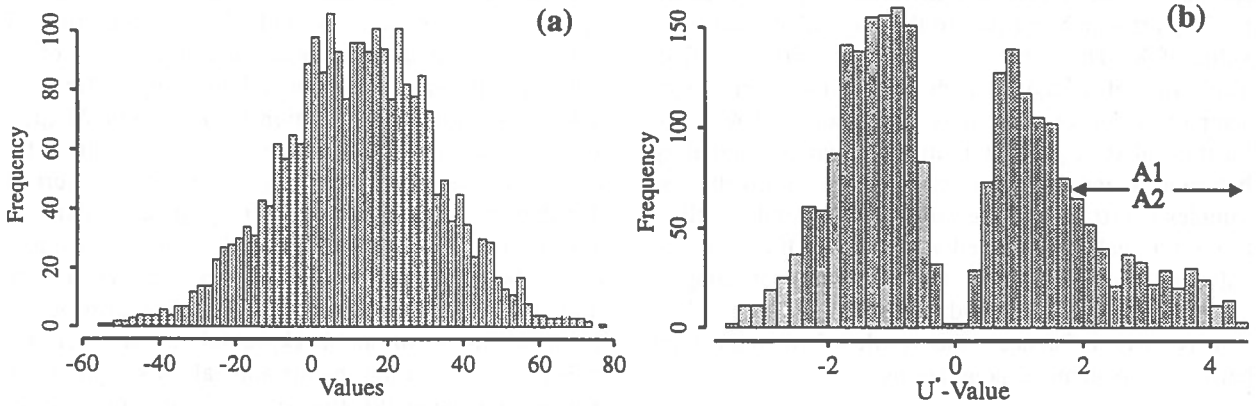

Fig. 5. Frequency distribution of mixed samples from background B and anomalies A_1 and A_2. (a) Original values; (b) U*-values. more than 92% of anomalous samples are located in the range indicated by A_1 and A_2 with value greater than 1.93.

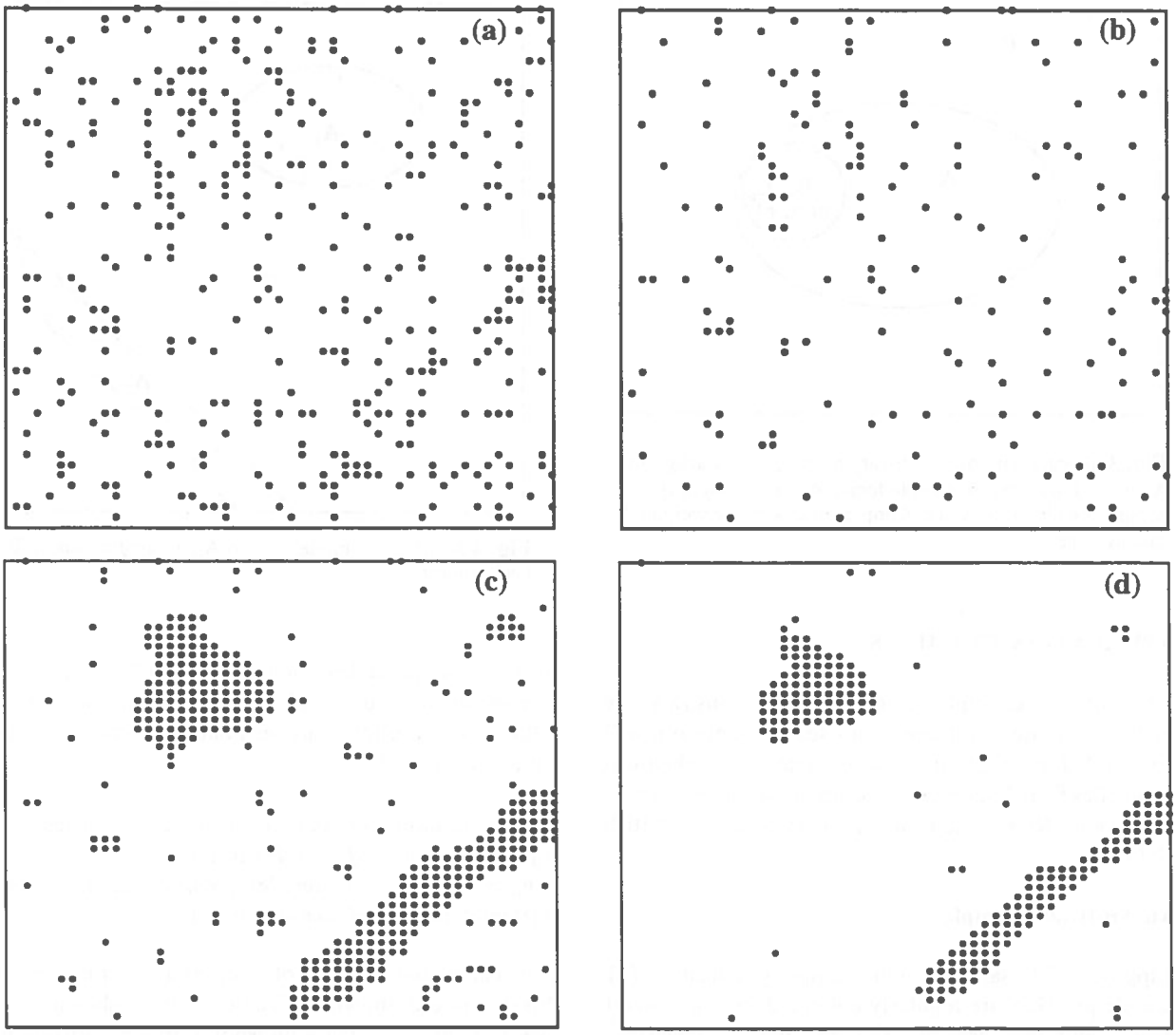

Fig. 6 Samples classified using different thresholds. (a) threshold of m+std based on values of Fig. 5a with total error $e_I + e_{II}$ =0.82; (b) threshold of m+1.5std based on values of Fig. 5a with e_I+e_{II}=0.91; (c) threshold of m+std based on U*-values with e_I+e_{II}=0.15; and (d) threshold of m+1.5std based on U*-values with e_I+e_{II}=0.15.

c=1 and 1.5 are shown in Fig. 6a and 6b, with total errors ($e_I + e_{II}$) 0.818 and 0.915, respectively.

Table 1 Errors of misclassification associated with original values

threshold	mean+ std	mean+ 1.1std	mean+ 1.5std	mean+ 2 std
e_I	0.134	0.118	0.058	0.019
e_{II}	0.684	0.724	0.857	0.95

Table 2 Errors of classification associated with the U*-statistics

threshold	mean+ std	mean+ 1.1 std	mean+ 1.5 std	mean+ 2 std
e_I	0.095	0.07	0.025	0.001
e_{II}	0.059	0.085	0.226	0.560

U*-statistics were obtained for the same artificial example. Calculations carried out for various distance parameters (r_{max}), including 15 km, 10 km and 5 km, essentially gave the same results. The results for r_{max}= 5 km are illustrated in Figs. 5b, 6c and 6d. The histogram in Fig. 5b shows two populations: the one for background B has values less than or close to zero, and the other for anomaly A has values greater than 1.93. More than 92% of anomalous samples are located in the right tail of the histogram with values greater than 1.93; only 7 % of background samples are misclassified in this area. The errors created by different thresholds (m+cs with c=1, 1.1, 1.5 and 2) are shown in Table 2. It can be seen that threshold U*=1.93 (c=1.1) provides good results with total error of 0.15, much smaller than 0.84 shown in Table 1. Figs. 6c and 6d illustrate the results for classifications by thresholds m + 1.1 standard deviation (U*=1.93) and mean + 1.5 standard deviation (U*=2.60). In Fig. 6c, 186 out of 203 anomalous samples (92%) are correctly classified and only 160 out of 2297 background samples (7%) are misclassified.

Stream Sediment Data from the Iskut River Map Sheet, Northwestern British Columbia

In total, 698 stream sediment samples were collected from the Iskut River area, northwestern British Columbia (Geological Survey of Canada, 1988, GSC Open file 1645). The samples are irregularly distributed in the area (Fig. 7). They were analyzed for many trace elements including Au, Ag, Cu, Mo, As, Sb and Pb. The element concentration values of Au, Ag, Cu, As and Sb are spatially associated with Au mineralization (Cheng, 1994). Gold concentration values of the 698 samples are shown in a Q-Q plot (Fig. 8a) and histogram (Fig. 8c), respectively. Purpose of the study is to delineate Au-associated anomalous areas based on these concentration values. The anomalous areas were delineated by means of fractal methods in previous work (Cheng et al., 1994; see next section).

The U*-statistics method was applied to the stream sediment data with maximum radius r_{max}=10 km. The results are illustrated in Figs. 8b, 8d and 9a. Fig. 8b shows two distinct distributions for values of U* of which one (with U*>0) is close to normal. The same results can be seen in Fig. 8d where background samples (506 samples) are located on the left side (U*<0) and anomalous samples (192) on the right (U*>0). The anomalous samples classified by threshold U*=0 are plotted in Fig. 9a. Similar results were obtained for Cu and As as shown in Figs. 9b and 9c. These anomalous areas obtained by means of U*-statistic will be compared with spatial distribution of Au mineral occurrences and with results obtained by the fractal method in next section.

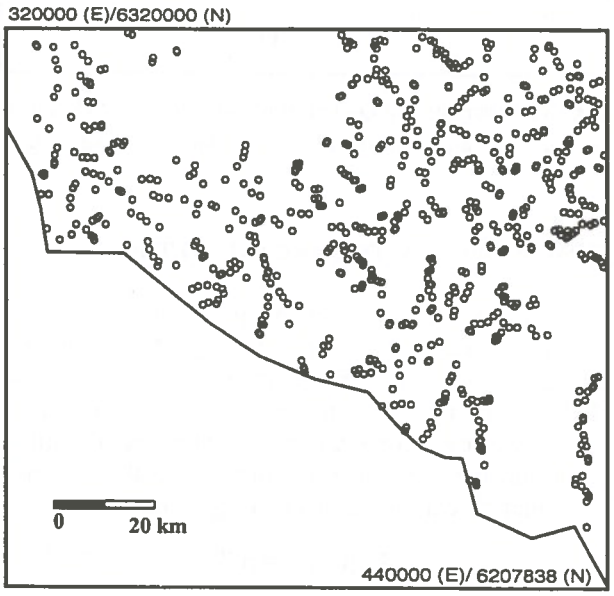

Fig. 7 698 stream sediment samples in Iskut River map sheet, northwestern British Columbia (N.G.R. data, GSC., 1988).

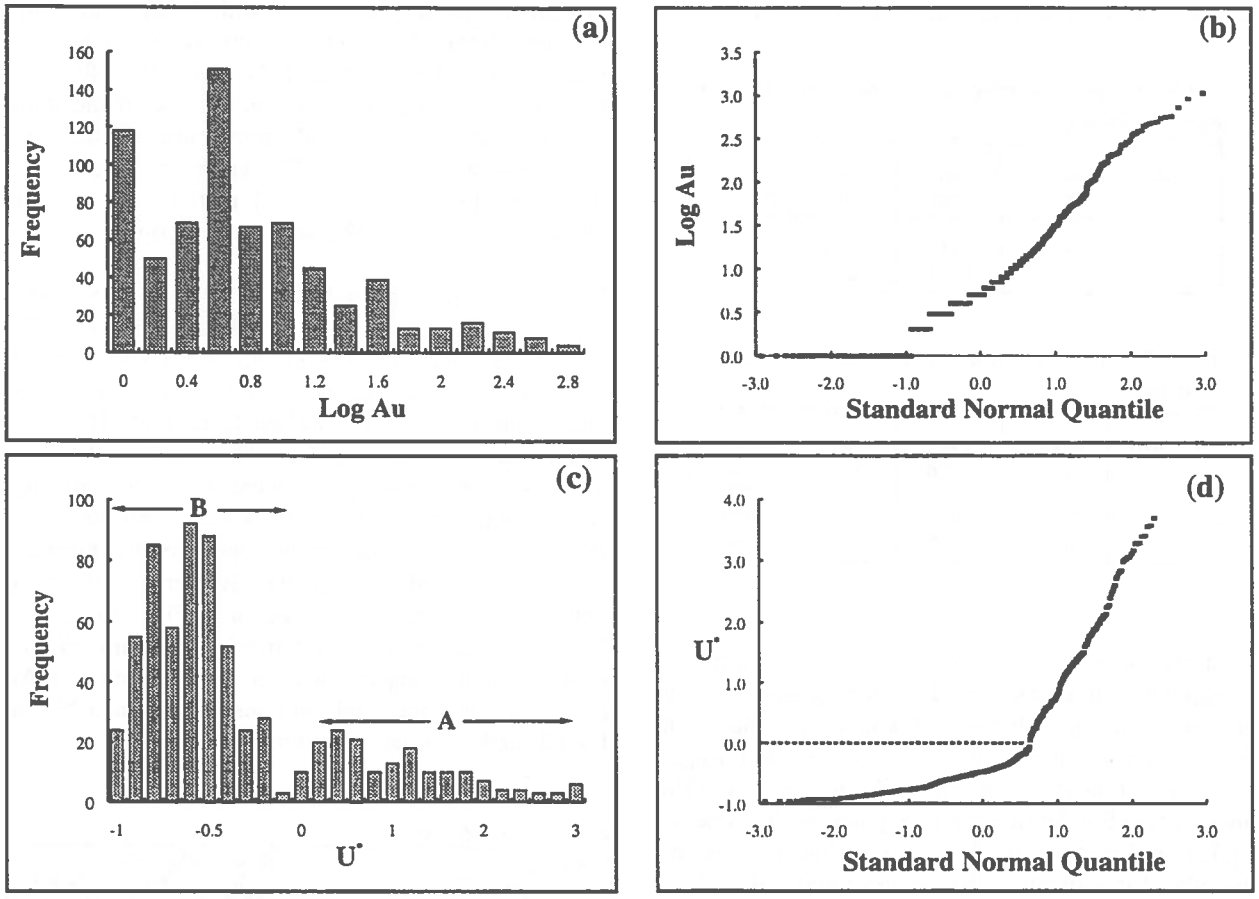

Fig. 8 Histograms and Q-Q plots of Au values for 698 samples. (a) histogram for base 10 transformed raw values; (b) Q-Q plot for values in (a); (c) histogram for U*-values. B: background and A: anomaly; and (d) Q-Q plot for U*-values in (c).

COMPARISON WITH FRACTAL METHOD

In order to use the concentration-area fractal method (C-A) for anomaly separation (Cheng, Agterberg and Ballantyne, 1994), contour maps were created by SPANS-GIS for Au, Cu and As values. The areas enclosed by each contour and the contour values satisfy the following power-law relations since these values have multifractal properties (Cheng et al., 1994):

$$A(\mu \geq \rho) \propto \rho^{-\alpha} \qquad (12)$$

where A represents the cumulative area enclosed by the contours with values greater than ρ. The relation of Eq. 12 can be fitted by constructing straight lines on log-log paper. Different slopes of the straight lines (-α) correspond to different sets of similarly shaped contours. The corresponding value separating these contours can be used as the threshold to separate anomalies from background. The calculated results for Au are shown as log-log plot (Fig. 10) in which two straight lines were fitted by least squares yielding a cutoff value of 30 ppb. The anomalous areas delineated by the threshold 30 ppb are shown in Fig. 11 together with Au mineral occurrences. Samples with Au values greater than 30 ppb are shown in Fig. 12. Comparison of Fig. 9a and Fig. 11 shows that these two methods (U*-statistic and C-A) provide similar anomalies which are associated with the spatial distribution of Au mineral occurrences. In addition, Figs. 9a and 12 show that more anomalous samples were correctly classified by the threshold U*=0 than samples with original values greater than 30 ppb are located within and fewer outside the anomalous areas delineated by the fractal method. This implies that the total error of classification for threshold U* =0 is smaller than that for the threshold of Au=30ppb.

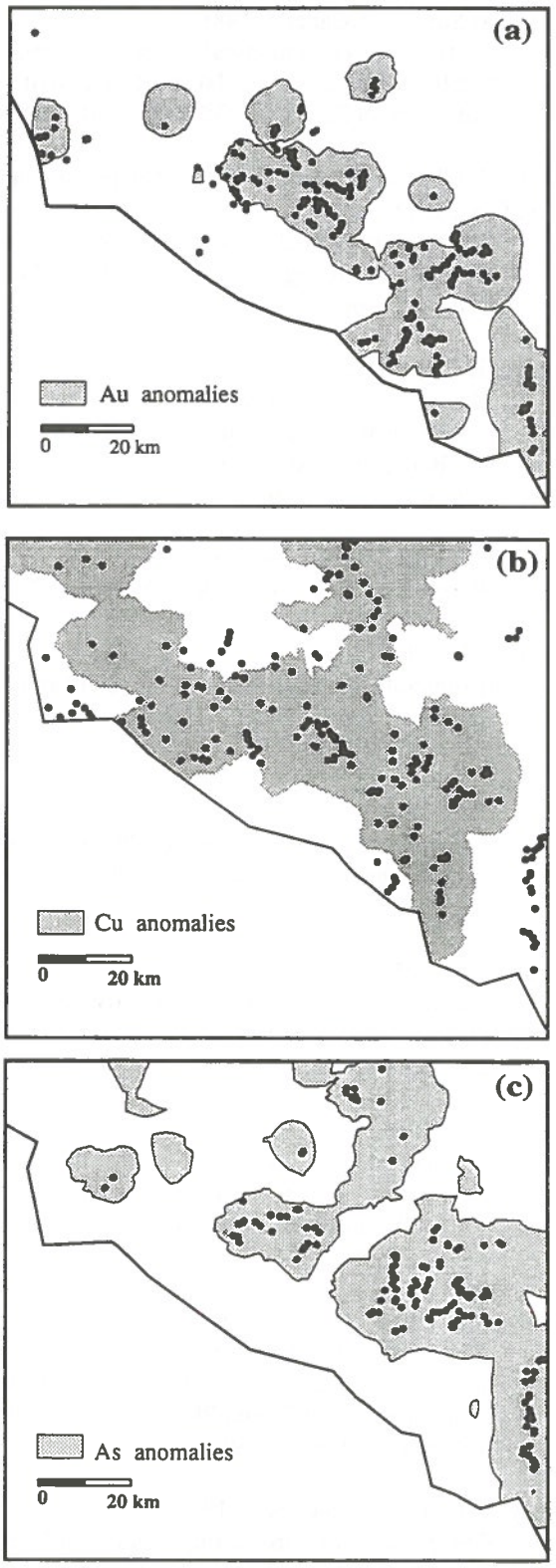

Fig. 9 Anomalies of stream sediment samples. Black dots represent anomalous samples obtained using U*-statistics and shaded areas are anomalies obtained by fractal method. (a) Au; (b) Cu; and (c) As.

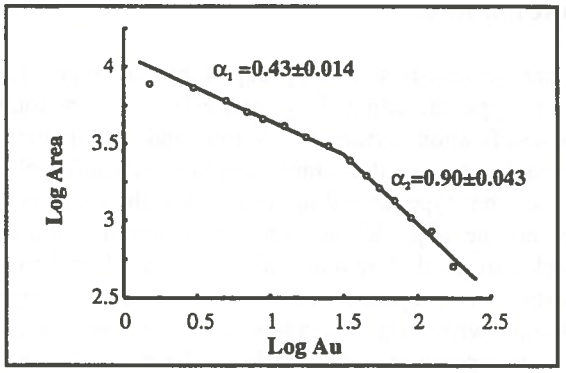

Fig. 10 Concentration-area model for Au. Values of areas were computed from a contour map created for Au values by using SPANS-GIS (Cheng et al., 1994).

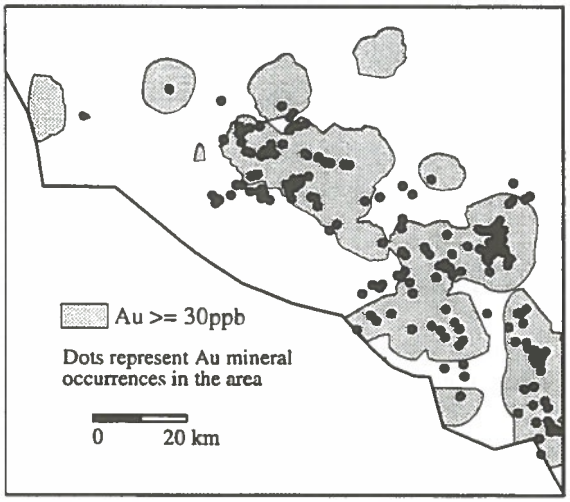

Fig. 11 Anomalies (Au) obtained using the fractal concentration -area method (Cheng et al., 1994). Shaded areas represent anomalous areas and dots for Au mineral occurrences.

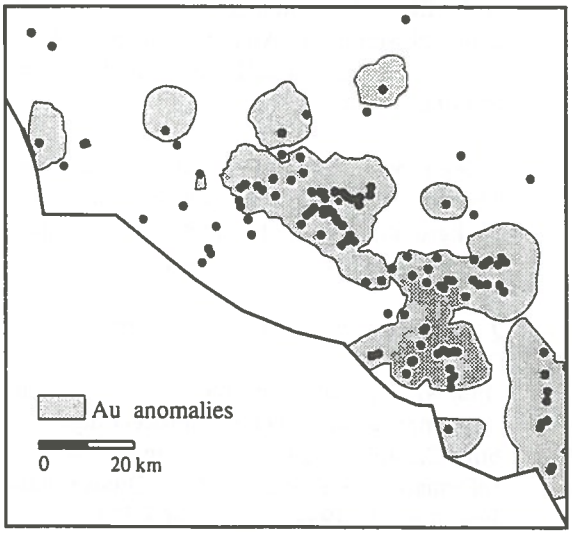

Fig. 12 Anomalous samples with Au values greater than 30 ppb (dots). Shaded areas represent anomalous areas obtained in Fig. 11.

CONCLUSIONS

Parametric statistics can be grouped into two types: for the first type, including U-, χ^2- and F-statistics, the total misclassification errors (rejection and acceptance) approaches zero as the sample size increases infinitely; for the other type, including T-statistics, the total error may not be approaching zero no matter how many samples are used. A spatial statistic U^* (based on the U-statistic) is proposed using the moving average technique with variable window radius for geochemical anomaly separation. It reduces the total misclassification errors by taking the spatial information of geochemical samples into account. This method was successfully used for Au-associated geochemical anomaly separation in stream sediment samples from the Iskut River map sheet, northwestern British Columbia. The results obtained by this method are similar to the results obtained by the fractal method. The anomalies of Au, Cu and As are spatially associated with the locations of Au mineral occurrences in the study area.

ACKNOWLEDGEMENTS

The authors would like to thank J-F. Tardif for translating the abstract from English into French.

REFERENCES

Cheng, Q., 1994
Multifractal Modelling and Spatial Analsys with GIS: Au Potential Estimation in the Mitchell-Sulphurets Area, northwestern British Columbia. Unpublished Ph.D. thesis, University of Ottawa, Ottawa, 268 p.

Cheng, Q., Agterberg, F.P. and Ballantyne, S.B., 1994
The separation of geochemical anomalies from background by fractal methods: Geochem. Explor., v.51, No. 2, pp. 109-130.

Cheng, Q., Bonham-Carter, G.F., Agterberg, F.P. and Wright, D.F., 1994
Fractal modelling in the geosciences and implementation with GIS: in Proceedings of the 6th Canadian Conference on Geographic Information Systems, held in Ottawa, Ont., June 4 to 10, 1994, v. 1, pp.565-577.

Garrett, R.G., 1989
A cry from the heart: Explore, v.66, pp.18-20.

Geological Survey of Canada, 1988
National Geochemical reconnaissance 1:250,000 map sheet, Iskut River, British Columbia (NTS 104B), GSC Open file 1645.

Govett, G.J.S., Goodfellow, W.D., Chapman, and Chork, C.Y., 1975
Exploration geochemistry distribution of elements and recognition of anomalies: Math. Geol. v. 7,. pp.415-446.

Grunsky, E.C. and Agterberg, F.P., 1988
Spatial and multivariate analysis of geochemical data from metavolcanic rocks in the Ben Nevis Area, Ontario; Math. Geol., v.20, n.7, pp. 825-861.

Intera Tydac Technologies Inc., 1993
Reference Manual of SPANS Version 5.2.

Miesch, A.T., 1981
Estimation of the geochemical threshold and its statistical significance. Geochem. Explor., v.16, pp. 49-76.

Sinclair, A.J., 1974
Selection of thresholds in geochemical data using probability graphs: Geochem. Explor., v.3, pp.129-149.

Sinclair, A.J., 1976
Application of probability graphs in mineral exploration: Association of Exploration Geochemists, Special Volume 4, 95p.

Sinclair, A.J., 1991
A fundamental approach to threshold estimation in exploration geochemistry, Probability plots revisited: Geochem. Explor., v.41, pp. 1-22.

Stanley, C.R., 1988
Comparison of data classification procedures in applied geochemistry using Monte Carlo simulation: Unpublished Ph.D. thesis in Univ. of British Columbia, 1988, 256p.

Stanley, C.R. and Sinclair, A.J., 1989
Comparison of probability plots and gap statistics in the selection of thresholds for exploration geochemistry data: Geochem. Explor., v. 32, pp. 355-357.

CAMI'95: 3rd Canadian Conference on Computer Applications in the Mineral Industry
Montréal, Québec, Canada, October 22-25, 1995

Fractal Lognormal Percentage Assessment of Porphyry Copper Resources

Robert A. Crovelli
Branch of Petroleum Geology
U.S. Geological Survey, Denver, Colorado, USA

Saul B. Suslick
Department of Mineral Resources Policy and Management
State University of Campinas, Campinas, Sao Paulo, Brazil

Donald A. Singer
Branch of Resource Analysis
U.S. Geological Survey, Menlo Park, California, USA

Richard H. Balay
Department of Mathematical and Computer Sciences
Metropolitan State College of Denver, Denver, Colorado, USA

ABSTRACT:

The 20/80 law is a heuristic law that has evolved over the years into the following rule of thumb for many populations: 20% of the population accounts for 80% of the total value. This law states quantitatively that often a relatively small portion of a population accounts for most of the total value of the population. This principle is certainly applicable in the case of mineral deposits where the few largest deposits have an overwhelming amount of the total resources. The general $p100/q100$ law in statistical form is defined with the statistic q as a function of p where p is the population proportion and q is the proportion of total value. The general $p100/q100$ law in probabilistic form is defined with the parameter q as a function of p for any probability distribution that models the population distribution. Using the lognormal distribution, the $p100/q100$ law in lognormal form is derived with the lognormal q being a fractal, where q unexpectedly possesses the scale invariance property. The $p100/q100$ law in lognormal form was applied to data on porphyry copper deposits to obtain "$p100\%$ of the porphyry copper deposits account for $q100\%$ of the total porphyry copper resources of the deposits." The theoretical percentages of total resources of porphyry copper using the lognormal q are extremely close to the empirical percentages from the porphyry copper data using the statistic q. For example, 20% of the 289 porphyry copper deposits account for 78.3% of the total porphyry copper resources of the deposits if we use the lognormal q, or for 78.1% if we use the statistic q.

RÉSUMÉ:

La loi 20/80 est la loi heuristique qui est utiliseé comme règle générale pour plusieurs populations: 20% de la population est responsable pour 80% de sa valeur totale. Cette loi determine, de facon quantitative que une petite partie de la population répondre pour la majorité de la valeur totale. Ce principle est surtout applicable pour le cas du dêpót minéral où les grands dêpóts existant concentre la plus grande partie des ressources totales. La loi general $p100/q100$ est, en sa forme statistique, définie avec le paramètre q comme une fonction de p, où p represénte la proportion de la population et q la proportion de la valeur totale. La loi general $p100/q100$ en sa forme probabilistique est défini comme le paramètre q comme fonction de p pour quelconque distribution de probabilité qui modèle la distribution de la population. En utilisant la distribution lognormal, la loi $p100/q100$ en sa forme lognormal est dérivée avec la lognormal q en soit un fractal, où q a une propriété de échelle invariable. La loi $p100/q100$ en sa forme lognormal est utilisée sur les donées des dêpóts de cuivre porphyrique. Cette loi est appliquée pour obtenir $p100\%$ de dêpóts de cuivre porphyrique que répond pour $q100\%$ du total des ressources de cuivre des dêpóts. En utilisant le lognormal q, la pourcentage théorique du total des ressources de cuivre s'approache de la pourcentage empirique des données de cuivre en utilisant le paramètre q. Par example, si nous prénons la lognormal q, 20% de 289 dêpóts de cuivre porphyrique répondent pour 78.3% du total des ressources de cuivre. Si on utilise le statistique q la pourcentage est de 78.1%.

INTRODUCTION

Vilfredo Pareto (1848-1923), an Italian engineer turned economist and sociologist, was a pioneer in econometrics, applying the statistical methods of the physical sciences to the social sciences. Pareto discovered that, generally, a relatively small portion of a population accounts for most of the total value of the population. That is, in any set of elements, the critical elements usually constitute a minority of the set (Douglass and Douglass, 1993). Pareto's principle is certainly applicable in the case of mineral deposits where the few largest deposits have an overwhelming amount of the total resources.

As originally proposed, Pareto's law (Pareto, 1897; Turla and Hawkins, 1983) was an empirical relation describing the distribution of income among the population of a country; viz.,

20 percent of the people in Italy owned 80 percent of the wealth.

From this principle, the heuristic "20/80 law" has evolved over the years into the following simple rule of thumb, which is applicable to many populations:

20% of the population accounts for 80% of the total value.

Numerous applications of this law exist in the management sciences. For example,

20% of the customers account for 80% of the sales;

20% of the employees account for 80% of the work; and,

20% of the components account for 80% of the cost.

The principle is observed in other disciplines as well. The objective of the present paper is to generalize "the 20/80 law" using the lognormal distribution and apply the generalization to data on porphyry copper deposits to obtain "p100% of the porphyry copper deposits account for q100% (q is a function of p) of the total porphyry copper resources of the deposits." Fractal lognormal percentage theory is developed first; the porphyry copper data is described next; and, finally, the theory is applied to the data.

FRACTAL LOGNORMAL PERCENTAGE THEORY

The p100/q100 Law in Statistical Form

Consider a population of N values for a random variable X arranged in increasing order of magnitude:

$$x_1, x_2, \ldots, x_N .$$

The total value of the population is:

$$\sum_{i=1}^{N} x_i .$$

Given a proportion p ($0 \le p \le 1$) of largest values of the population, the sum of the p100% of largest values of the population is:

$$\sum_{i=[(1-p)N]+1}^{N} x_i \quad ,$$

where $[\cdot]$ is the greatest integer value.

Let the proportion of the total value of the population accounted for by p100% of the population be given by q ($0 \le q \le 1$), where the statistic q is defined as:

$$q = \sum_{i=[(1-p)N]+1}^{N} x_i \Big/ \sum_{i=1}^{N} x_i .$$

An alternative form is:

$$q = \frac{p \sum_{i=[(1-p)N]+1}^{N} x_i \Big/ pN}{\sum_{i=1}^{N} x_i \Big/ N} .$$

Summarizing, p is a proportion (or fraction) of the population, and p100% is a percentage of the population; whereas, q is a proportion (or fraction) of the total value, q100% is a percentage of the total value, and p100% of the population accounts for q100% of the total value.

The p100/q100 Law in Probabilistic Form

Given a population of values of a random variable X having a probability distribution that models the population distribution, then p100% of the population values account for q100% of the total value, where the parameter q is called the proportion of total value and defined in terms of conditional expectation, $E(X|\cdot)$, as follows.

$$q = \frac{pE(X \mid X > x_p)}{E(X)}, \quad 0 \le p \le 1,$$

with $p = P(X > x_p)$ and x_p is called the $p100$th fractile.

Various probability distributions could be used as models for the population distribution. We will consider the lognormal probability distribution. The percentage theory based on the Pareto distribution has been developed and applied to petroleum field size data (Crovelli, in press).

The Lognormal Probability Distribution

The lognormal distribution is discussed in detail in Aitchison and Brown (1957), Johnson and Kotz (1970), and Crow and Shimizu (1988). A nonnegative random variable X has a lognormal distribution if the random variable $Y = \ln X$ has a normal distribution.

The lognormal probability density function of X is

$$f(x) = \frac{1}{\sqrt{2\pi}\,\sigma x} \exp \frac{-(\ln x - \mu)^2}{2\sigma^2}, \quad x > 0$$

where $\sigma > 0$ is a shape parameter and μ is a scale parameter.

The expected value or mean of X is

$$E(X) = e^{\mu + \sigma^2/2}$$

The variance of X is

$$V(X) = e^{2\mu + \sigma^2}(e^{\sigma^2} - 1)$$

The scale parameter μ and the shape parameter σ of the lognormal distribution are computed from the following formulas:

$$\mu = \frac{1}{N}\sum_{i=1}^{N} \ln x_i$$

and

$$\sigma = \left[\frac{N\sum_{i=1}^{N} (\ln x_i)^2 - \left(\sum_{i=1}^{N} \ln x_i \right)^2}{N^2} \right]^{1/2}.$$

The following notation will be used throughout the remainder of the paper:

$X \sim$ lognormal (shape parameter σ, scale parameter μ),

where the symbol ~ is read "is distributed as."

The Lognormal Distribution Has a Fractal Property

If $X \sim$ lognormal (shape parameter σ, scale parameter μ), let

$$X' = cX, \qquad c > 0.$$

The fractal property of X under a positive multiplicative constant results in:

$X' \sim$ lognormal (shape parameter σ, scale parameter $\mu + \ln c$).

Note that the distributions of X and X' are identical (with the same shape parameter) except for scale. A probabilistic fractal is a probability distribution that is invariant except for scale (scale invariant or self-similar) under a given transformation (Mandelbrot, 1983). Under a positive multiplicative constant, the lognormal distribution remains a lognormal distribution with fixed σ and changed μ.

The $p100/q100$ Law in Lognormal Form

Consider the $p100/q100$ law in probabilistic form when the population distribution is modeled as a lognormal distribution; i.e.,

$$q = \frac{pE(X \mid X > x_p)}{E(X)}, \quad 0 \le p \le 1,$$

when $X \sim$ lognormal (shape parameter σ, scale parameter μ).

Recall that the expected value of X is

$$E(X) = e^{\mu + \sigma^2/2}.$$

It can be shown that the conditional expectation is given by

$$E(X \mid X > x_p) = e^{\mu + \sigma^2/2} \frac{R((\ln x_p - \mu - \sigma^2)/\sigma)}{R((\ln x_p - \mu)/\sigma)}$$

where R denotes the complementary cumulative distribution function of a standard normal random variable Z, i.e., $R(z) \equiv P(Z > z)$.

Let us define the following notation:

$$R(z_p) = P(Z > z_p) = p$$

where z_p is called the p100th fractile of Z.
Since

$$R((\ln x_p - \mu)/\sigma) = R(z_p) = p$$

and

$$R((\ln x_p - \mu - \sigma^2)/\sigma) = R(z_p - \sigma)$$

we have

$$E(X \mid X > x_p) = e^{\mu+\sigma^2/2}\ \frac{R(z_p - \sigma)}{p}$$

Substituting into the general formula for q and simplifying, we get

$$q = R(z_p - \sigma), \quad 0 < p < 1$$

or

$$q = 1 - \Phi(z_p - \sigma), \quad 0 < p < 1$$

where Φ denotes the standard normal cumulative distribution function.

Observe that if $p \to 0$, then $q \to 0$, and if $p \to 1$, then $q \to 1$.Thus we define $q = 0$ if $p = 0$, and $q = 1$ if $p = 1$.The special case when $p = 0.5$ and $z_p = 0$ yields

$$q = R(-\sigma) = 1 - \Phi(-\sigma)$$

Note the surprising result that the parameter q has the very remarkable property of being scale-free; i.e., q does not depend upon the scale parameter μ. Since the parameter q is scale-free, q stays the same for all lognormal distributions with fixed σ and changed μ, as in the case of the fractal property of the lognormal distribution under a positive multiplicative constant. Because it is scale invariant, the proportion q can be considered to be a parametric fractal.

The proportion q of the $p100/q100$ law in statistical form is called the statistic q, in probabilistic form it is called the parameter q, and in lognormal form it is called the lognormal q.

PORPHYRY COPPER DATA

We examined the total premining contained copper metal (in metric tons) of 289 porphyry copper deposits. Data used in this study represent mineral deposits--not mineral occurrences or geochemically anomalous rocks. A mineral deposit is a mineral concentration of sufficient size and grade that it might, under the most favorable circumstances, be considered to have economic potential (Cox and others, 1986). Thus, these known deposits are from well-explored bodies that someone thought, at least in the exploration phase, might be economic to develop. Data used here are the same as those used by Singer (1995) where it was shown that porphyry copper deposits contain 57 percent of all discovered copper and dominate all other deposit types. These data include the information from older grade and tonnage models (Singer and others, 1986) and from an additional 79 deposits that have not been checked as carefully for thoroughness of exploration.

Because of the high correlation (r = 0.95) between tonnage of copper and tonnage of ore (both in logarithms), the results obtained using tonnage of metal also apply to tonnage of ore and probably to the areal extent of mineralization (via Singer and Mosier, 1981, where r = 0.66).

Data gathered for each deposit include average grades of each metal of possible economic interest and the associated tonnage based on the total production, reserves, and resources at the lowest possible cutoff grade. Where both reserves and geologic resource (geologic reserve) estimates are available, geologic resource estimates are used. These data represent estimates of the endowment of each known deposit in order to allow for the possibility of lower production costs or higher commodity prices.

APPLICATION OF THEORY

The fractal lognormal percentage theory will now be applied to the porphyry copper data. This new probabilistic methodology for percentage assessment lends itself as an ideal spreadsheet software application.

A frequency distribution of the 289 porphyry copper deposits (in metric tons Cu) is displayed in Figure 1. Because the plotted random variable is ln(metric tons Cu), the bell-shaped distribution suggests that the porphyry copper resources are approximately distributed as a lognormal distribution.

Spreadsheet software was used to make various calculations involving the porphyry copper data. For

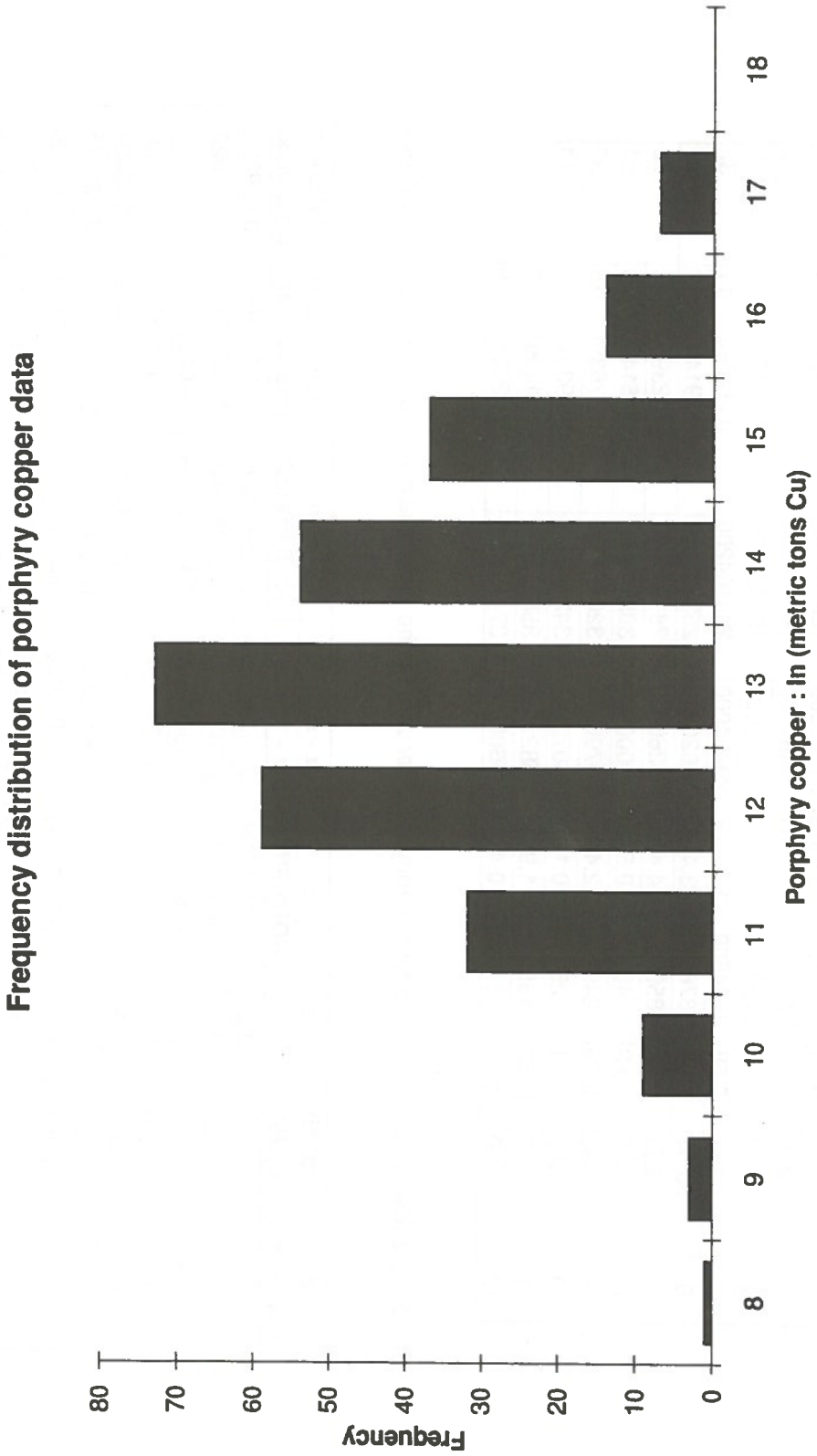

Figure 1. Frequency distribution of 289 porphyry copper deposits (in metric tons Cu).

TABLE 1. Spreadsheet of porphyry copper data and calculations for the statistic q (first 12 of 289 rows).

	Tonnes /			ln	Sorted	Partial sum	Statistic q		
n	10^6	Cu%	TonsCu	TonsCu	TonsCu	sorted	Partial/Total		
1	150	0.5	750000	13.5278	64768000	64768000	0.07440	Bin	Frequency
2	27.5	0.63	173250	12.0625	61385200	126153200	0.14491	8	1
3	800	0.6	4800000	15.3841	39467000	165620200	0.19024	9	3
4	1100	0.25	2750000	14.8271	30000000	195620200	0.22470	10	9
5	187	0.58	1084600	13.8967	29484000	225104200	0.25856	11	32
6	58.32	1.16	676512	13.4247	28620000	253724200	0.29144	12	59
7	250	0.74	1850000	14.4307	28260000	281984200	0.32390	13	73
8	20	0.2	40000	10.5966	24000000	305984200	0.35147	14	54
9	85	0.29	246500	12.4151	20790000	326774200	0.37535	15	37
10	2.5	1	25000	10.1266	16073640	342847840	0.39381	16	14
11	102	0.152	155040	11.9514	15827000	358674840	0.41199	17	7
12	20	0.17	34000	10.4341	15600000	374274840	0.42991	18	0

TABLE 2. Spreadsheet of calculations from porphyry copper data for the lognormal q as a function of various values of p.

p	(p)(N)	1 - p	z	z - sigma	1 - q	lognormal q	statistic q
Pop. Prop.	(p)(289)		NORMSINV	(z - 1.6245)	NORMSDIST	(theoretical)	(empirical)
0.1	28.9	0.9	1.281550794	-0.342949206	0.365818399	0.634181601	0.619027
0.2	57.8	0.8	0.841621386	-0.782878614	0.21684913	0.78315087	0.781022
0.3	86.7	0.7	0.524401003	-1.100098997	0.135644536	0.864355464	0.866005
0.4	115.6	0.6	0.25334657	-1.37115343	0.085163623	0.914836377	0.91633
0.5	144.5	0.5	0	-1.6245	0.052134561	0.947865439	0.948625
0.6	173.4	0.4	-0.25334657	-1.87784657	0.030201014	0.969798986	0.969334
0.7	202.3	0.3	-0.524401003	-2.148901003	0.015821067	0.984178933	0.983666
0.8	231.2	0.2	-0.841621386	-2.466121386	0.006829259	0.993170741	0.99267
0.9	260.1	0.1	-1.281550794	-2.906050794	0.001830177	0.998169823	0.997952
0.05	14.45	0.95	1.644853	0.020353	0.508119153	0.491880847	0.469028
0.025	7.225	0.975	1.959961082	0.335461082	0.631361288	0.368638712	0.33010325
0.01	2.89	0.99	2.326341928	0.701841928	0.7586112	0.2413888	0.1852537

illustrative purposes, Table 1 is just the first 12 rows of a spreadsheet with 289 rows. The data are listed and several calculations are made, including those necessary for the statistic q. The lognormal parameters were computed: scale parameter $\mu =$ 13.6247 and shape parameter $\sigma =$ 1.6245.

Table 2 is a spreadsheet of the calculations from the porphyry copper data that are necessary for the lognormal q as a function of various values of p. The formula for the lognormal q in the case of the porphyry copper data is the following:

$$q = R(z_p - 1.6245) = 1 - \Phi(z_p - 1.6245), \quad 0 < p < 1$$

Therefore, for any specified value of p, we can obtain "p100% of the porphyry copper deposits account for q100% of the total porphyry copper resources of the deposits."

The fractal lognormal percentage assessment of porphyry copper resources is summarized in Table 3. The corresponding graph of the summary is given in Figure 2. The theoretical percentages of total resources of porphyry copper using the lognormal q are extremely close to the empirical percentages from the porphyry copper data using the statistic q.

TABLE 3. Fractal lognormal percentage assessment of porphyry copper resources.

Percentage of porphyry copper deposits	Percentage of total porphyry copper resources q100%	
p100%	Theoretical (lognormal q)	Empirical (statistic q)
0	0	0
1	24.14	18.52
2.5	36.86	33.01
5	49.19	46.90
10	63.42	61.90
20	78.32	78.10
30	86.44	86.60
40	91.48	91.63
50	94.79	94.86
60	96.98	96.93
70	98.42	98.37
80	99.32	99.27
90	99.82	99.80
100	100	100

SUMMARY AND CONCLUSIONS

The results of the models and methods discussed in this paper are summarized below.

1. "The 20/80 law" is completely generalized as the $p100/q100$ law in probabilistic form for any probability distribution that models the population distribution. The parameter q is called the proportion of total value and defined in terms of the population proportion p and conditional expectation.

2. When the population distribution is modeled with the lognormal distribution, the $p100/q100$ law in probabilistic form produces the $p100/q100$ law in lognormal form. The proportion of total value is derived, and the parameter q is only a function of p and the shape parameter σ. Surprisingly, the parameter q is scale-free; i.e., it does not depend upon the lognormal scale parameter μ. Because it is scale invariant, the proportion q is a parametric fractal.

3. The $p100/q100$ law in lognormal form can be applied to porphyry copper data. The lognormal q is a function of p such that "p100% of the porphyry copper deposits account for q100% of the total porphyry copper resources of the deposits." The theoretical percentages of total porphyry copper resources using the lognormal q are extremely close to the empirical percentages from example data using the statistic q.

4. This new probabilistic methodology for percentage assessment can also be applied to other mineral resources, such as gold, silver, zinc, and lead. The methodology lends itself as an ideal spreadsheet software application.

REFERENCES

Aitchison, J. and Brown, J.A.C., 1957
The lognormal distribution. Cambridge University Press, Cambridge, 176p.

Cox, D.P., Barton, P.R. and Singer, D.A., 1986
Introduction, in Cox, D.P. and Singer, D.A., eds., Mineral deposit models. U.S. Geological Survey Bulletin 1693, pp. 1-10.

Crovelli, R.A., [in press]
The generalized 20/80 law using probabilistic fractals applied to petroleum field size. Nonrenewable Resources.

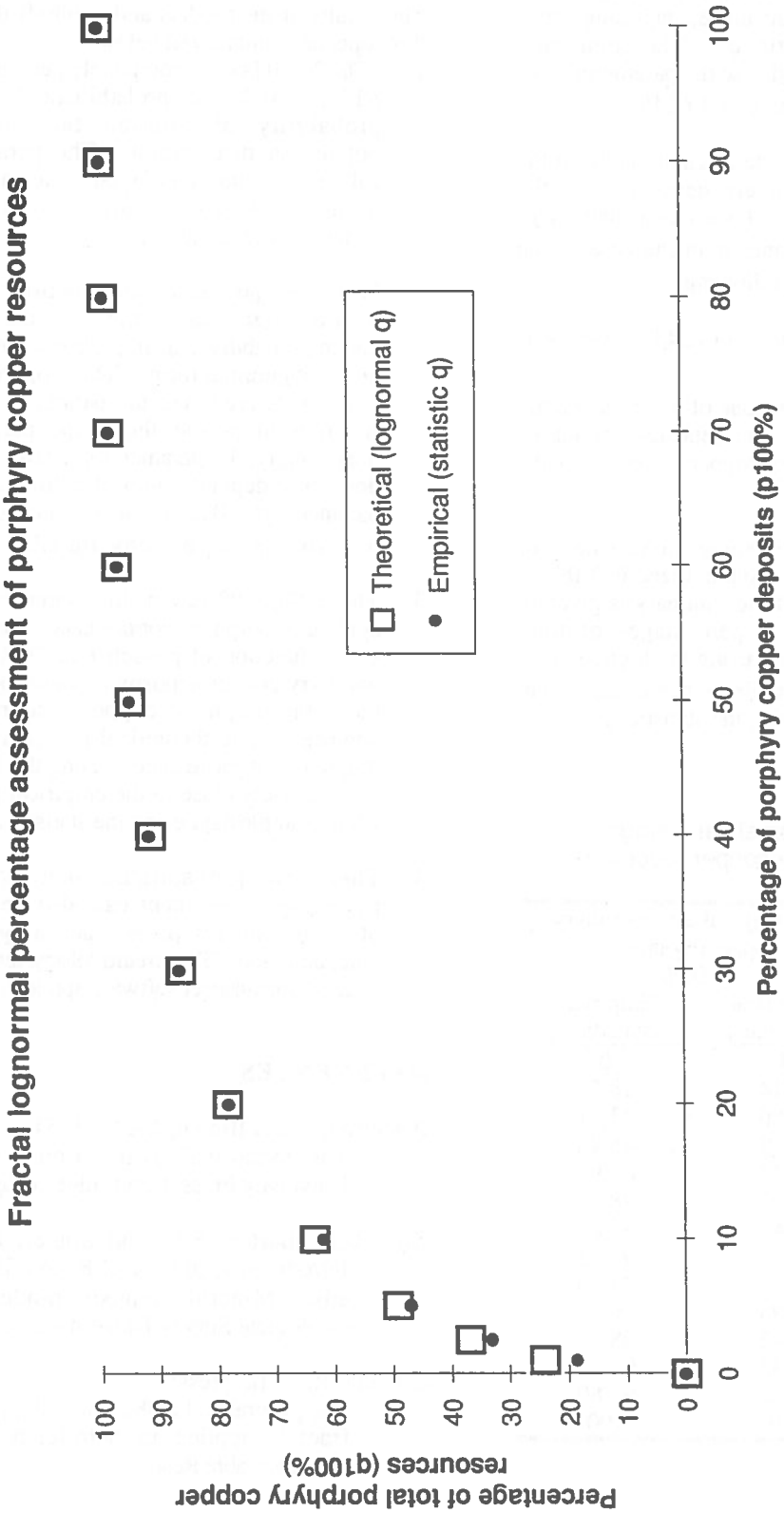

Figure 2. Theoretical percentage of total porphyry copper resources using the lognormal q as a function of the percentage of porphyry copper deposits, along with the corresponding empirical values using the statistic q.

Crow, E.L. and Shimizu, Kunio, eds., 1988
Lognormal distributions—Theory and applications. Marcel Dekker, Inc., New York and Basel, 387p.

Douglass, M.E. and Douglass, D.N., 1993
Manage your time your work yourself. AMACOM, New York, 194p.

Johnson, N.L. and Kotz, S., 1970
Distributions in statistics—Continuous univariate distributions-1. John Wiley & Sons, Inc., New York, 300p.

Mandelbrot, B.B., 1983
The fractal geometry of nature. W.H. Freeman and Co., San Francisco, 460p.

Pareto, V., 1897
Cours d'Economie Politique. Rouge and Cie, Lausanne and Paris.

Singer, D.A., 1995
World class base and precious metal deposits—a quantitative analysis. Economic Geology, v. 90, no. 1, p. --

Singer, D.A. and Mosier, D.L., 1981
The relation between exploration economics and the characteristics of mineral deposits, in Ramsey, J.B., ed., The Economics of Exploration for Energy Resources. JAI Press, New York, pp. 313-326.

Singer, D.A., Mosier, D.L. and Cox, D.P., 1986
Grade and tonnage model of porphyry copper deposits, in Cox, D.P. and Singer, D.A., eds., Mineral deposit models. U.S. Geological Survey Bulletin 1693, pp. 77-81.

Turla, P.A. and Hawkins, K.L., 1983
Time management made easy. E.P. Dutton, New York, 206p.

2.

mineral economics
évaluation minière

CAMI'95: 3rd Canadian Conference on Computer Applications in the Mineral Industry
Montréal, Québec, Canada, October 22-25, 1995

An Optimized 2D Model of Complex Mine Feasibility Studies using the DMV Method

Samuel Frimpong, Ph.D., P.Eng.
Department of Mining and Metallurgical Engineering
Technical University of Nova Scotia, Halifax, Canada

Jerry M. Whiting, Ph.D., P.Eng.
Department of Mining, Metallurgical & Petroleum Engineering
University of Alberta, Edmonton, Canada

ABSTRACT

Design and implementation of complex mine feasibility studies, in the most efficient manner, are essential to securing an edge in the competitive environment of the mining industry. Investors are exposed to a variety of risks and uncertainties in new mining projects. Thus, project managers must clearly understand and manage these risks and uncertainties, and the available options appropriately over a long period of time. In this study, a detailed mine feasibility study for a copper project has been modeled using the derivative mine valuation method. This model is solved using dynamic programming and the backward implicit algorithm for the appropriate combination of strategic decisions that maximizes the market value of the project. The results show that investors must use multiple-stage feasibility study and waiting options to maximize the project value. Further, it is shown that no feasibility study should be undertaken after stage 2 and that each stage duration should not exceed one year. Phase diagrams have also been provided to aid investors in making strategic decisions to maximize the project value.

RÉSUMÉ

La conception et l'exécution d'études de faisabilités minières, d'une manière efficace, sont essentielles dans le milieu compétitif de l'industrie minière. Les investisseurs sont exposés à de nombreuses risques et d'incertitudes dans un projet minier. Les directeurs de projets miniers doivent se rendre compte de ces risques et incertitudes. Ce document décrit une étude de faisabilité d'un projet pour l'exploration du cuivre en utilisant la méthode dérivatif d'évaluation minière. Ce modèle est évalué en utilisant la programmation dynamique ainsi q'un algorithme implicite rétrograde pour maximiser la valeur marchande du projet. Les résultats indiquent que les investisseurs doivent utiliser une étude de faisabilité d'étapes multiples ainsi que des options d'attentes pour maximiser le projet. Ce modèle indique qu'on ne devrais par entreprendre une étude de faisabilité après étape 2. La durée de chaque étape ne devrais pas dépasser un ans. Des diagrammes d'équilibre de phases sont présentés pour assister les investisseurs pour faire des décisions pour maximiser la valeur de leurs projets.

INTRODUCTION

Mine feasibility studies and investment valuation form a critical part in a successful mine development and operation chain. This involves the collection of information on a mineral deposit, and the experimental and analytical processing of such information to yield results that could help investors make informed decisions on this deposit. The cost of a feasibility study, in terms of dollars and time, may be high, but the cost of no feasibility study, or an inadequate one, could easily be higher. Thus, investors want to undertake a certain amount of feasibility study to reduce ore grade uncertainties, while minimizing cost. Valuation of mining projects requires rigorous analytical procedures to establish the project monetary value and associated risks and uncertainties. Conventional methods do not contain such procedures, and therefore are inefficient for analyzing the timing and management of mine feasibility studies, investment decision strategies, and mine operating options. Mine operating options include blending,

development and production scheduling, cut-off grade dynamics, temporary closure and maintenance, and abandonment of a mine during unfavourable conditions. The derivative mine valuation (DMV) method is a new and advanced method which overcomes these and other limitations of conventional methods [Frimpong, 1992].

The mining industry is extremely capital intensive, and mining ventures are characterized by possible early cost overruns which affect their economic viability. Long preproduction periods, coupled with inflation, high interest rates and volatile markets expose investors to a variety of risks and uncertainties prior to project start-up and during its economic life. Ore reserve grade and tonnage distributions, ore body dimensions and heterogeneity, and other geological and geomechanic characteristics of both the host rock and the ore body are still complex factors which call for decision-making based on thorough and rigorous analytical studies.

The main objective of this work is to determine the optimized mine value and the best policy for managing complex mine feasibility studies and investment decision strategies in a competitive market. The elements of this objective are to: (i) minimize the amount of information gathered in each feasibility study stage; (ii) determine the appropriate timing required before and during a feasibility study stage; (iii) minimize investment cost overruns resulting from under- and over-investment; (iv) generate phase diagrams for making strategic investment decisions; and (v) derive the optimized mine value under various conditions. This study is significant because it introduces an advanced method capable of handling the dynamics of complex mine feasibility studies and investment decisions. In using the DMV method to value mineral projects, critical problems, such as investment timing options, feasibility study management and mine operating options are dealt with thoroughly, to aid in decision making. Also, the difficult problem of determining the appropriate discount rate for a specific project is solved, by using as inputs, the discounting structures for claims to the project cash flows [Frimpong, 1992].

This study deals with a 2D model of a detailed mine feasibility study and investment decision strategies in a competitive market using the DMV method [Frimpong, 1992; Frimpong, Laughton and Whiting, 1991]. It combines the dynamic arbitrage arguments proposed by Black and Scholes (1973) and Merton (1973) for valuing derivative securities, stochastic control theory in a continuous-time framework [Cox and Ross,1976; Malliaris and Brock,1982] and the technical and operational framework of a typical mine [Buijtor and McMahon , 1983] to derive the value of a mine feasibility study. *This DMV method is based on a small set of propositions about the structure and information content of financial markets. The key proposition is that valuation is carried out in competitive markets that are free of transaction barriers. In such markets, different assets which produce the same cash flows have the same price. It is also possible to replicate the cash flows of a complex asset, such as a proposed or actual mine feasibility study project, by trading in portfolios of simpler assets, such as riskless bonds and metal futures contracts. Thus, the basic assets that provide information about risk discounting are those that have direct interaction with future macroeconomic variables [Brealey and Myers, 1988].* It is assumed that future volatility of metal price expectation, future price of risks of mineral commodity [Hull, 1989] and interest rates are known with certainty.

In this study, the authors describe the dynamics of the decision strategies and provide a mathematical model of the feasibility study and investment decision problem. A numerical example is provided with a case study in a proposed copper project. Analysis of the results is provided to show the significance of the study to similar projects.

DECISION STRATEGY DYNAMICS

For any particular investment opportunity with ongoing feasibility studies, there are many combinations of strategic decisions (e.g., waiting, feasibility study, investment) available to investors. The objective of investors in any such venture is to choose an appropriate combination of these strategic decisions to maximize the value of the project. The choice and implementation of one such combination are irreversible, and thus, must be based on a thorough and rigorous analysis of all available options. In Figure 1, WUi and IUi are the respective waiting and investment without any feasibility study at the ith stage. Fi is the feasibility study carried out at the ith stage. WCi and ICi are the respective waiting and investment after the ith feasibility study. F1|WU1 is the occurrence of F1 conditioned on WU1, and n is the feasibility study limit. After nodes IUi and ICi, the mine is opened, and no decision is made subsequently. After nodes Fi, each of the three subsequent decisions, Fi+1, ICi and WCi can be made at relatively lower level of uncertainty. After nodes WUi and WCi, each of three subsequent decisions to invest, wait and undertake a feasibility study can be made at the same level of uncertainty.

From the starting point, STRT in Figure 1, investors can choose any combination by tracing a route through arrows

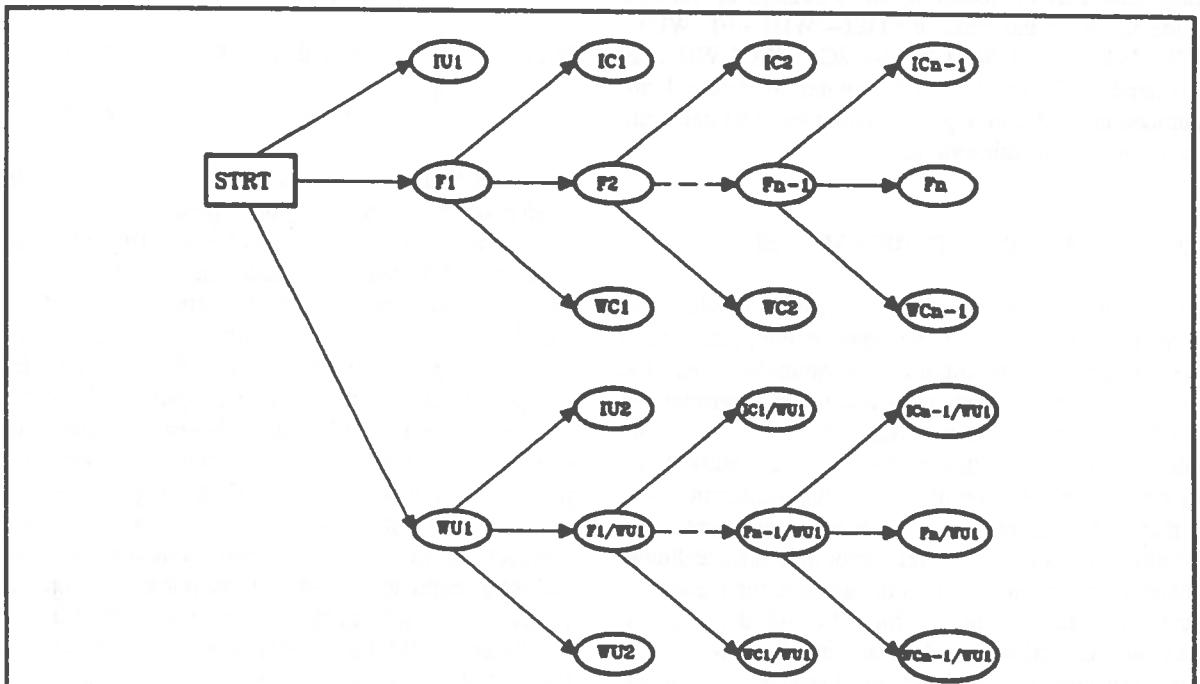

Figure 1 Mine Feasibility Study Decision Strategies

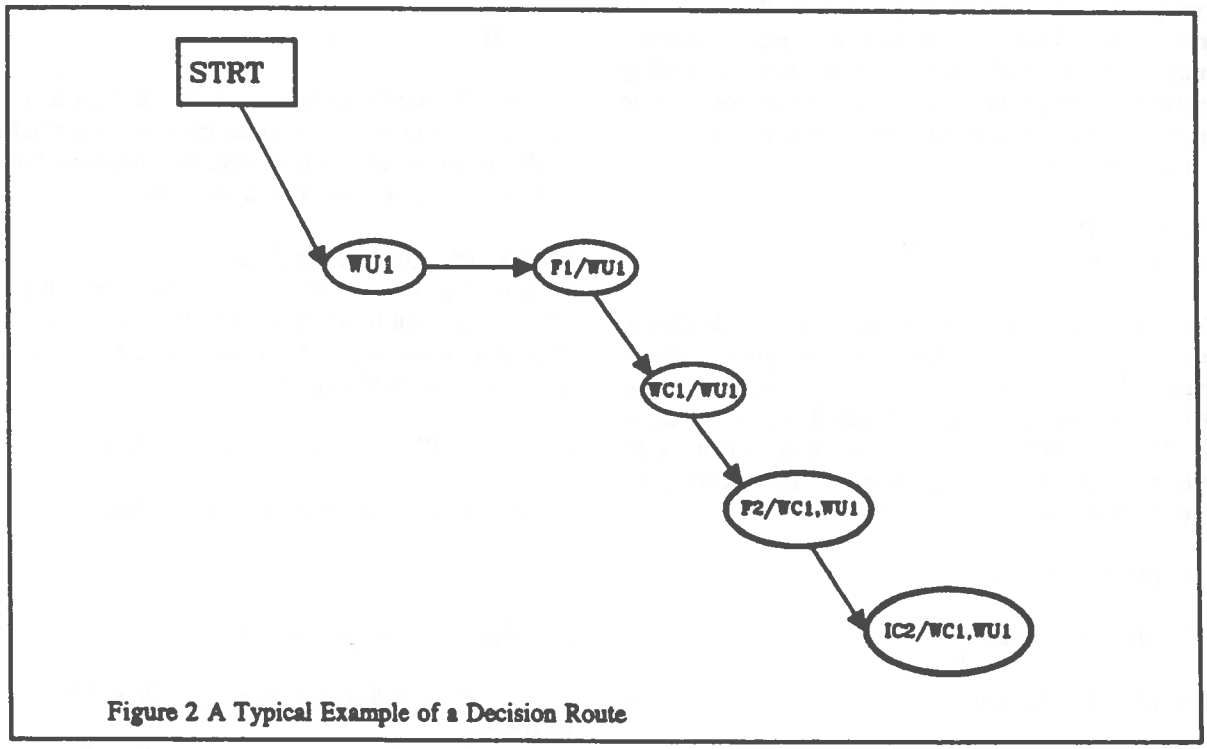

Figure 2 A Typical Example of a Decision Route

in the same direction. For example, if investors wait now, undertake the feasibility study at stage 1, wait after this study, undertake the feasibility study at stage 2, and then decide to invest, the route is: STRT→ WU1→ F1 | WU1→ WC1 | WU1→ F2 | WC1,WU1→ IC2 | WC1,WU1, as illustrated in Figure 2. All the routes in Figure 1 are examined using dynamic programming to select one route that maximizes the mine value.

MINE FEASIBILITY STUDIES MODEL

In this study, a feasibility study is used to reduce the uncertainty associated with the expected ore grade, and to help investors avoid assumptions and estimates under high levels of uncertainty and over- and under-investment of capital which lead to cost overruns and erratic results. The value of a mining project, at any time in a feasibility study, may depend on many variables including economic (such as, metal price, interest rates, indices of real capital and operating costs and the general rate of inflation), technical and operating variables (such as the grade of the ore and its distribution, mineralogical composition of the ore, ore reserve tonnage, stripping and extraction ratios, ore dilution factor and the physical and mechanical properties of the ore body and host rock) and the fiscal regime of the environment (such as corporate income tax and royalties, currency convertibility and import duties). The value also depends on strategic options, such as, waiting, feasibility study or investment available to investors in making decisions. The problem, then, is to choose a set of these strategic options that maximizes the project's market value, which is given by

$$V(t, *) = \text{Maximize } \{H(t, *, \phi)\}$$
$$\text{s.t.} \quad \phi \in \Phi(t, *) \qquad (1)$$

V(t, *) is the value of the project at any time in a feasibility study stage, t ($0 \le t \le T$); H(t, *, ϕ) is the project value if strategy, ϕ, is chosen from the set of possible strategies, Φ(t, *); (*) indicates that V, H, and Φ depend on many variables. The respective mine values with all options, H, with only the feasibility study option, HF, and with only the investment option, HI, are given by

$$H \equiv H(S, E, t; k(\phi), i) \qquad (2)$$

$$HF \equiv HF(S, E, t; k(\phi), i) \qquad (3)$$

$$HI \equiv HI(S, E, t; k(\phi), i) \qquad (4)$$

S is the metal price; E is the expected ore grade; k is a set of parameters that are used in the model as deterministic variables, and is given by

$$k(\phi) = \begin{cases} \{\sigma_S, \sigma_E, \rho, c, FCi\} & \phi \text{ is F} \\ \{q_o, Q_o, \beta, \rho, c, ICi, ri\} & \phi \text{ is I} \\ \{\sigma_S, \rho, c\} & \phi \text{ is W} \end{cases} \qquad (5)$$

Q_o, q_o and β are the respective proven ore reserves, annual production rate and the unit mine operating cost; σ_S and σ_E are the respective volatilities in metal price and expected ore grade; i is the feasibility study stage ($0 \le i \le n$); ρ is the risk-free interest rate; c is the convenience yield of metal; FCi is the feasibility study cost at stage i; ICi is the investment capital at stage i; ri is the ignorance factor associated with the ith investment capital; F, I and W are the respective feasibility study, investment and waiting decision strategies. Under no arbitrage conditions, the partial differential equation of the project value with ongoing feasibility study is derived from the futures contracts on the mineral commodity based on dynamic portfolio replication and the technical and operating variables that affect the mine [Frimpong, 1992; Frimpong, Laughton and Whiting, 1991; Black and Scholes, 1973; Hull, 1989]. This value is given by

$$(1/2)\,\sigma_S^2 S^2 H_{SS} + (1/2)\,\sigma_E^2 E^2 H_{EE} + S(\rho - c) H_S + Ht - FCi - \rho H = 0 \qquad (6)$$

H_{SS}, and H_{EE} are the respective second derivatives of the mine value with respect to metal price and expected ore grade. H_S and Ht are the respective first derivatives of the mine value with respect to metal price and time.

Mine Value in the Waiting Phase

In the waiting phase, a change in metal price or technology are the dominant factors that affect the mine value. It is assumed that technology is the same in this phase, and thus, the mine value, HW, is given by

$$(1/2)\,\sigma_S^2 S^2 HW_{SS} + S(\rho - c) HW_S - \rho HW = 0 \qquad (7)$$

The boundary conditions associated with equation (7) are:

$$HW(0; i) = 0 \qquad (8)$$

$$S^2 HW_{SS}(S; i) \to 0 \quad \text{as} \quad S \to \infty \qquad (9)$$

$$HW(S; i) \begin{cases} > H(S, E, t; k(\phi), i) & S < S^* \\ = H(S, E, t; k(\phi), i) & S \ge S^* \end{cases} \qquad (10)$$

Equation (8) is the zero metal price condition of the mine value. As the metal price approaches infinity, the second derivative term in equation (7) goes to zero as illustrated in equation (9). Below a certain critical metal price, S*, the value of waiting is greater than the mine value with a feasibility study and investment decision strategies and investors will wait. Above S*, the decision to either invest or undertake a study is made as in equation (10).

Mine Value in the Feasibility Phase

The stochastic variables that affect the mine value, in this study, are the metal price, the expected ore grade and time as illustrated in equation (6). The value of the mine with ongoing feasibility study, HF, is continuous in S because changes in this variable occur in any trading day. Mine feasibility study, however, is carried out in multiple discrete stages, and thus, HF is continuous in E only in a given feasibility study stage. Therefore, equation (6) is divided into two parts to solve for HF values at different conditions, as shown in equations (11) and (12), which illustrate the respective dynamics of HF with respect to S and E.

$$(1/2)\,\sigma_s^2 S^2 HF_{ss} + S(\rho - c)\,HF_s + HFt - \rho\,HF = 0 \qquad (11)$$

The mine value at the end of a feasibility study stage is also given by

$$HF(S, E, T; k(\phi), i) = \sum_{E'=Emin}^{Emax} \{H(S, E', t; k(\phi), i+1)^* dui(E'|E)\} \qquad (12)$$

Emax and Emin are the respective maximum and minimum expected ore grades. dui(E'|E) is the probability of the expected ore grade E' conditioned on the occurrence of the grade E. This distribution is assumed to be lognormal [Frimpong, 1992; Ang an Tang, 1975]. The expected ore grade and its variance can be obtained from kriging using the updated sample data base [Journel and Huijbregts, 1978]. The boundary conditions associated with equations (11) and (12) are:

$$HF(0, E, t; k(\phi), i) = 0 \qquad (13)$$

$$HF(S, 0, t; k(\phi), i) = 0 \qquad (14)$$

$$S^2 HF_{ss}(S, E, t; k(\phi), i) \to 0 \quad \text{as} \quad S \to \infty \qquad (15)$$

$$H(S, E, t; k(\phi), i) = \begin{cases} \max [HF'', HI] & i < n \\ HI & i = n \end{cases} \qquad (16)$$

$$HF'' = HF(S, E, 0; k(\phi), i) - FCi \qquad (17)$$

$$FCi = ki \quad (i = 0, n; k0 < k1 < k2 = \ldots = kn) \qquad (18)$$

The mine value with ongoing feasibility studies, at any stage, is zero when the metal price or expected ore grade is zero as in equations (13) and (14). As the metal price approaches infinity, the second derivative term in equation (11) goes to zero as in equation (15). The mine value, H, at the horizon at any stage before the feasibility study limit, is the maximum of the feasibility study and investment options. At the feasibility study limit, this value is equal to the investment option as in equation (16). The mine value at the beginning of a feasibility study is equal to the difference in the feasibility study option and the feasibility study cost at that stage, FCi, as in equation (17). It is assumed that FCi increases as the level of detail of the study increases as in equation (18).

Mine Value in the Investment Phase

The mine value in the investment phase, HI, at the end of any stage is also given by:

$$HI(S, E, t; i) = HO(S, E) - IC_i \qquad (19)$$

$$HO(S, E) = (S\,E\,q_o / c) * [1 - \exp(-c\,Q_o / q_o)] - (\beta\,q_o / \rho) * [1 - \exp(-\rho\,Q_o / q_o)] \qquad (20)$$

$$ICi = ri * IC_K \quad (ri \geq 1.0) \qquad (21)$$

HO and ICi are the respective open mine value and the investment capital at the end of the ith stage. ICi depends on the level of knowledge about the reserves, termed *ignorance factor*, ri, in Frimpong (1992). This factor is greatest at the beginning of the feasibility studies when uncertainty is high. It reduces as the uncertainty reduces as a result of feasibility studies. IC_K is the investment capital at the investment stage.

CASE STUDY: A COPPER PROJECT EXAMPLE

The DMV method is used to model the value of a copper project feasibility study. Four feasibility study stages are considered, each with one year duration. As investors progress through the feasibility study stages, the variance of the log of the expected ore grade is expected to reduce from 3.00 at stage 0 to 0.113 at stage 1, 0.026 at stage 2, 0.011

at stage 3, and finally 0.006 at stage 4. The cost of feasibility study ($M) are 0.05, 0.20 and 5, respectively for stages 0, 1 and 2 or latter stages. The expected ore reserve tonnage is 100 million tons and the expected investment capital at the investment stage is $405M. The ignorance factors in the investment capital are 1.358, 1.111, 1.049 and 1.025, respectively, at stages 0, 1, 2, and 3. The expected unit operating cost is $0.50/lb of copper. The preproduction period is 3 years, and the expected mine life is 20 years. Expected value of ore grade varies between 2 and 100 lb/ton of ore.

The market price of risk of copper, the extent to which investors require higher returns to compensate them for bearing the copper risks [Hull (1989)] is 0.40. The risk-free interest rate (in real terms) is 0.03, and the volatility in copper price is 0.20. The expected value of copper price ($/lb) could vary between 1.00 to 5.00. In this feasibility study program, investors have the option to wait on a decision to undertake any feasibility study or on investment. The option to undertake all the required study at stage 0 is also available.

ANALYSIS OF RESULTS

Fifteen possible decision strategies, derived from Figure 1 and typical of real-world situations, are used to examine the case study. The partial differential equations and associated boundary conditions are solved using dynamic programming and the backward implicit algorithms [Press et al.,1990; Lapidus and Pinder,1982] to obtain the maximum value characteristics of the copper project at various conditions. The study shows that a multiple-stage feasibility study program allows investors to maximize the project value. The appropriate combination of strategic decisions, derived from Figure 1 for this project, is : STRT→ WU1→ F1 | WU1→ WC1 | WU1→ F2 | WC1,WU1→ WC2 | WC1,WU1→ IC2 | WC2,WC1,WU1.

Phase Diagrams for Strategic Decisions

Phase diagrams illustrate the metal price boundaries and their corresponding expected ore grades at which strategic decisions must be made to maximize the market value of this project. Figures 3 and 4 illustrate this idea at the respective study stages 0 and 1. In these figures, the appropriate decisions are labeled as waiting, feasibility and investment phases. The feasibility phase is largest at stage 0 in Figure 3, compared to Figure 4. This is due to the fact that, at stage 0, ore grade uncertainty is higher, and the study cost is smaller. The project value could be maximized by using a feasibility study at this stage. Through the study stages, the feasibility phase decreases in area as a result of increasing level of knowledge about the ore grade and the relatively higher study costs as in Figure 4. The study also shows that after stage 2, no feasibility study should be undertaken and investors should wait to invest in the project.

Value of Waiting on a Strategic Decision

The option to wait on a strategic decision at any stage allows the investor to make the decision at the appropriate time to avoid the loss that would be incurred otherwise. The values of the option to wait on the feasibility studies at stage 2 and the investment stage, at various conditions, are illustrated in Figures 5 and 6 respectively. These are the differences in mine values of a multiple-stage study with and without waiting option. The first case, 10.00, illustrates the values for using a multiple-stage study with the option to wait on strategic decisions, at various copper prices, with an expected ore grade of 10 lb/ton of ore. The other cases, 30.00, 50.00 and 70.00 illustrate the same idea for these respective ore grades. The analysis shows that there is value for waiting on a strategic decision at all stages. This is partly due to the study cost of $5M at stake, and the expected ore grade and copper price uncertainties at stage 2 and the huge investment capital of $405M at the investment stage. Project investors must therefore use the waiting options to maximize their investments.

Value of Multiple Stage Feasibility Study Program

A multiple-stage program could be used to avoid unnecessary feasibility studies, and to enable investors to make appropriate decisions. Figures 7 and 8 illustrate the values of such a program for various expected ore grades at stages 0 and 1 respectively. These values are the differences between the mine value for using multiple-stage and single-stage programs. The first case, 0.50, is the value at a copper price of $0.50/lb. The other cases, 1.00, 1.50, 2.00 and 2.50 illustrate the same idea at these respective copper prices. The analysis shows that a multiple-stage program could increase the value of the project by about $180 million at a price of $2.50/lb and expected ore grade of 10 lb/ton at stage 0 as shown in Figure 7. This value reduces sharply to $18 million at stage 1 in Figure 8 as knowledge is gained about the ore grade. If all the feasibility studies are undertaken at stage 0, the investor forgoes the opportunity of being able to use future information to guide the program. Under conditions of high ore grade and metal price uncertainties and low to medium-high copper prices, multiple-stage program allows the investor to evaluate the mine after every stage and take advantage of available information to direct the next stage of the study.

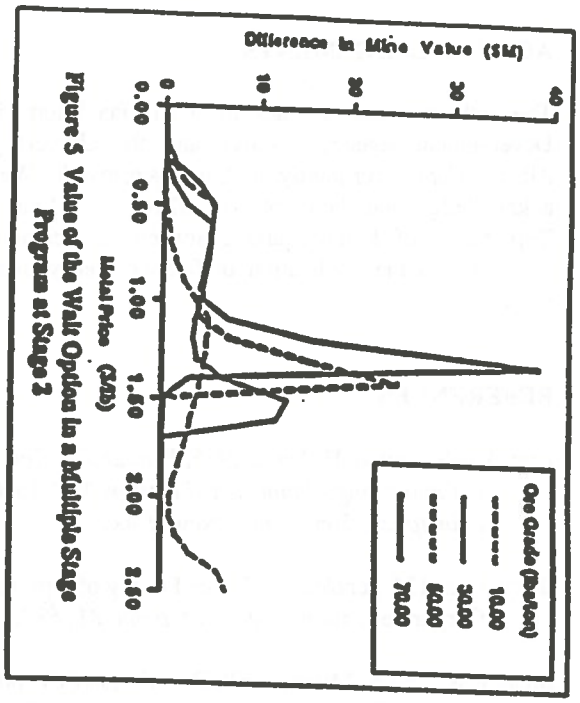

Figure 5 Value of the Wait Option in a Multiple Stage Program at Stage 2

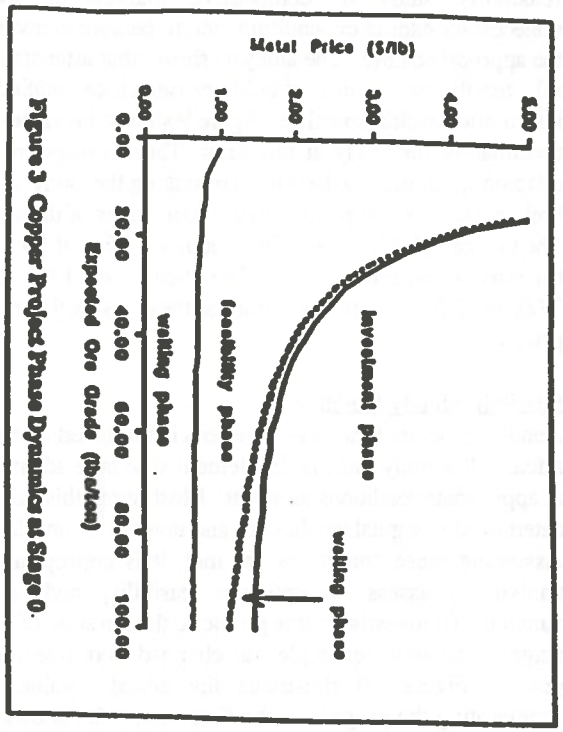

Figure 3 Copper Project Phase Dynamics at Stage 0.

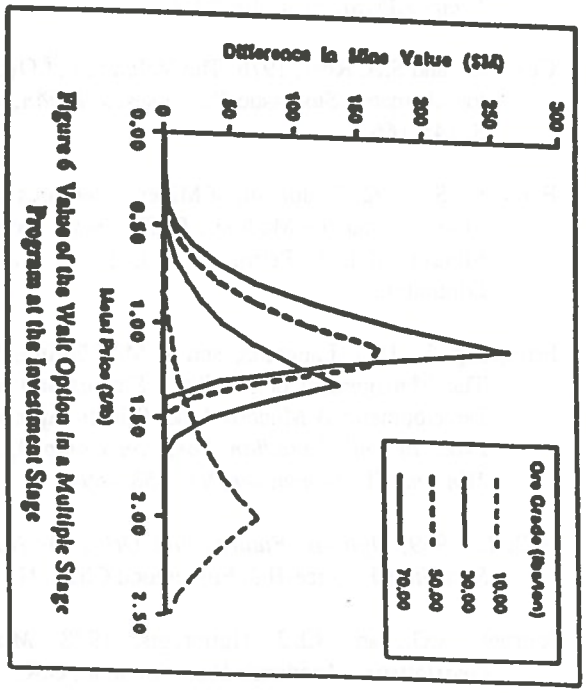

Figure 6 Value of the Wait Option in a Multiple Stage Program at the Investment Stage

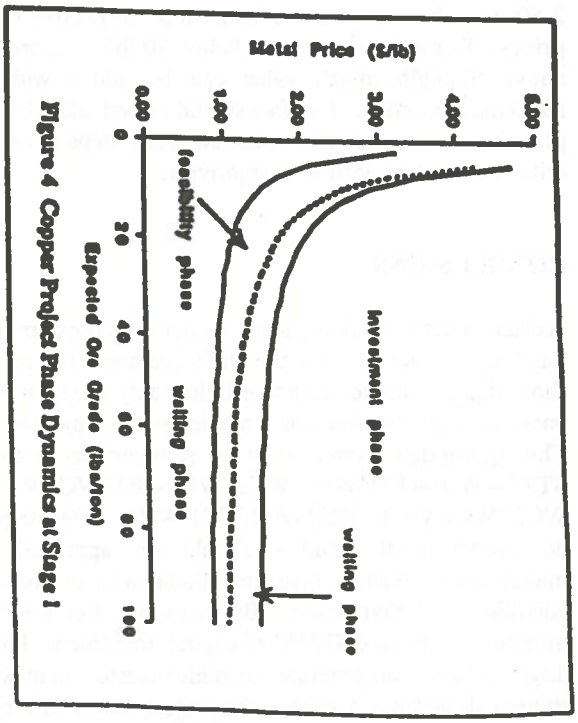

Figure 4 Copper Project Phase Dynamics at Stage 1

Value of Optimum Feasibility Study

Investors must strive to undertake only the required feasibility study in competitive markets to avoid unnecessary capital expenditure, and to be able to invest at the appropriate time. The analysis shows that after stage 2, all feasibility studies should cease since additional information yields no value. Figure 9 shows the values for terminating the study at this limit. These values are the differences in mine values for terminating the study at this limit and that for completing all the four stages of the study. The first case, 0.50, is the value at a metal price of $0.50/lb for various expected grades. The other cases, 1.00, 1.50, 2.00, and 2.50 show the same idea at these respective metal prices.

Feasibility Study Duration

Another problem that faces investors is the speed at which a feasibility study must be implemented to take advantage of appropriate conditions to invest. Most often, this may be determined by capital availability and investor's confidence. Assuming these conditions are met, it is appropriate to analytically assess the optimum feasibility study stage duration. To investigate this problem, the duration of each stage in the above example was changed from one to two years. Figure 10 illustrates the added values by accelerating the program. The first case, 0.50, shows the differences in mine values for using either durations at a price of $0.50/lb. The other cases, 1.00, 1.50, 2.00, and 2.50 also show the same idea at these respective metal prices. This study shows that, below 70 lb/ton of ore and above $1.00/lb, much value can be added with an accelerated program. This fact should be considered when planning environmental studies and other steps to secure critical and time-consuming approvals.

CONCLUSIONS

A detailed mine feasibility study model of a copper project has been developed using the DMV method. The results show that a multiple-stage feasibility study program with one-year stage duration would maximize the project value. The appropriate combination of strategic decisions is STRT→ WU1→ F1 | WU1→ WC1 | WU1→ F2 | WC1,WU1→ WC2 | WC1,WU1→ IC2 | WC2,WC1,WU1. After stage 2, no further costly studies should be approved by management. Rather, investors should wait or invest if conditions are favourable. By investing after stage 2, investors could save $125M of capital investment. Phase diagrams have been generated to guide investors in making strategic decisions to maximize the project value. This type of analytical study could be used to help investors model and evaluate any mine feasibility study problem in competitive markets.

ACKNOWLEDGEMENTS

The authors sincerely thank the Canadian International Development Agency (CIDA), and the University of Alberta, Canada for jointly funding this research. We also acknowledge the help of Dr. David G. Laughton, Department of Finance and Management Science for insights into the application of finance theory in mine valuation.

REFERENCES

Ang, A.H-S., and W.H. Tang, 1975, *Probability Concepts in Engineering Planning and Design, Vol. 1 (Basic Principles)*. John Wiley, New York.

Black, F., and M. Scholes, 1973, The Pricing of Option and Corporate Liabilities. *J. Polit. Econ.* **81**, *637*.

Brealey, R., and S. Myers, 1988, *Principles of Corporate Finance, 3rd Edition*. McGraw-Hill, New York.

Buijtor, G.J., and D.W. McMahon, 1983, Mineral Reserve Estimation for Project Development.*Proj. Dev. Symp*. AIMM, Australia, 23-34.

Cox, J.C., and S.A. Ross, 1976, The Valuation of Options for Alternative Stochastic Processes. *J. Finan.Econ.* **3**, 145-166.

Frimpong, S., 1992, Evaluation of Mineral Ventures using Modern Financial Methods. *Ph.D. Thesis*. Dept. of Mining, Met. & Petro. Eng., Univ. of Alberta, Edmonton.

Frimpong, S., D.G. Laughton, and J. M. Whiting,1991, The Management of Feasibilty Studies and Mine Development: A Modern Asset Pricing Approach. *Proc. of 2nd Canadian Conf. on Comp Applic. Min. Ind.* **II**., *Vancouver, B.C.*, 583-594.

Hull, J., 1989, *Options, Futures and Other Derivative Securities*.Prentice-Hal, Englewood Cliffs, NJ.

Journel, A.G., and Ch.J. Huijbregts, 1978, *Mining Geostatistics*. Academic Press, London, U.K.

Lapidus, L., and G.F. Pinder, 1982, *Numerical Solution of Partial Differential Equations in Science and*

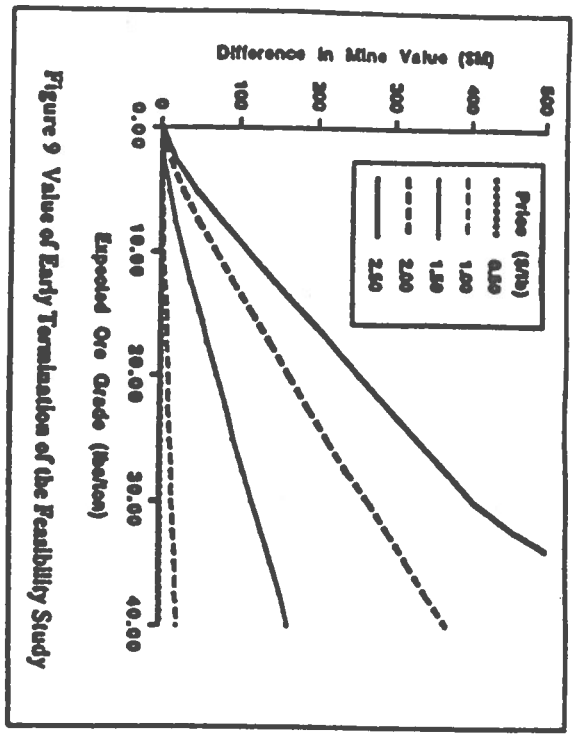

Figure 9 Value of Early Termination of the Feasibility Study

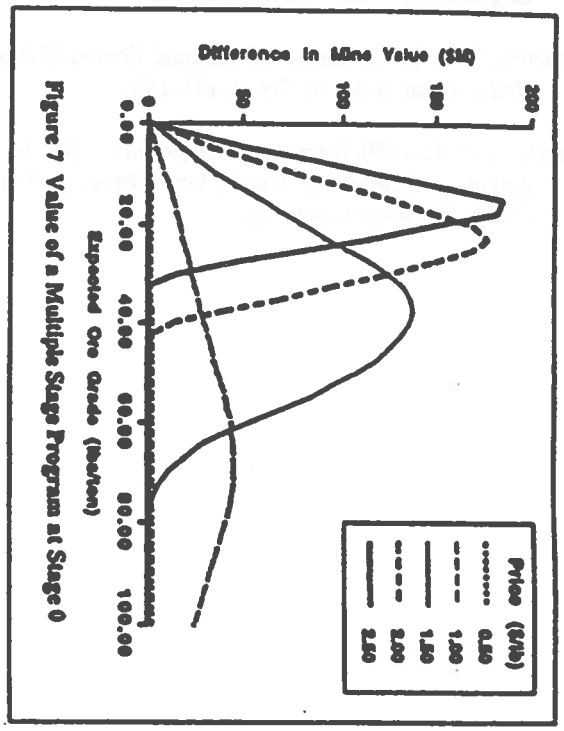

Figure 7 Value of a Multiple Stage Program at Stage 0

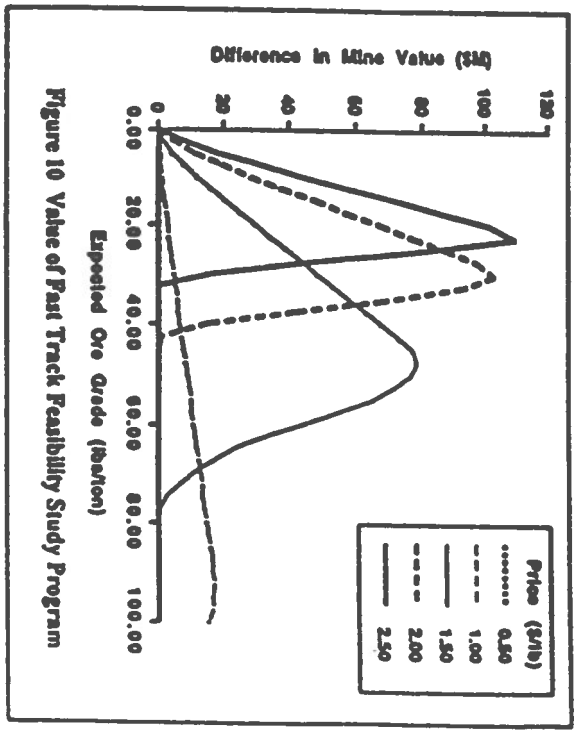

Figure 10 Value of Fast Track Feasibility Study Program

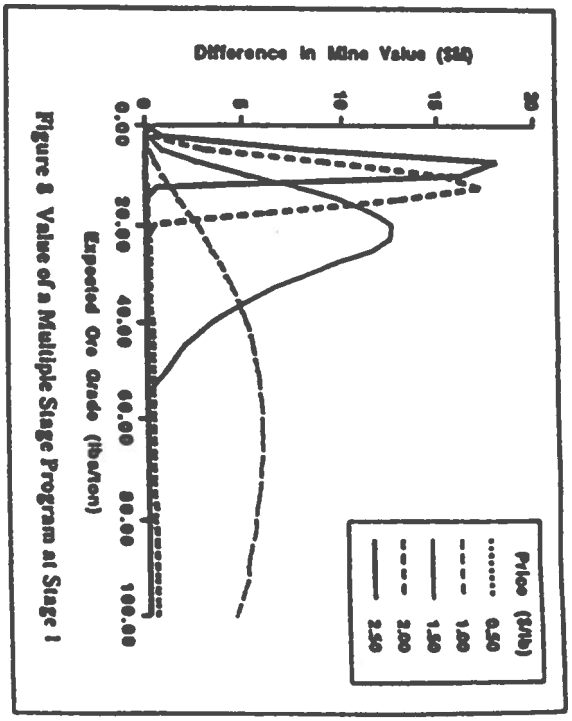

Figure 8 Value of a Multiple Stage Program at Stage 1

Engineering. John Wiley, New York.

Merton, R.C, 1973, Theory of Rational Option Pricing. *Bell J. Econ. & Mgmt. Sci.* **4**, 141-183.

Press, H., et al., 1990, *Numerical Recipes in C: The Art of Scientific Computing*. Camb. Univ. Press & Num. Recip. Software; Cambridge.

CAMI'95:3rd Canadian Conference on Computer Application in the Mineral Industry
Montreal, Quebec, Canada, October 22-25,1995

Simulation of Mine Accounting System

Xiaoli Tang
Department of Economics
University of Montreal
Montreal, Quebec

Jorgen Elbrond
Department of Mineral Engineering
Ecole Polytechnique, Montreal, Quebec

ABSTRACT:

A mixed physical-financial input-output model is build up to simulate the mine accounting system based on a gold mine in China. The model includes most of the economic, technical, production and management information. It can be used to: 1). quantitatively analyze how the changes in the economic, technical and geological factors affect the mine's production and management; 2). search for a series of bottle-neck components in the mine when the capacities of some components of the mine change; 3). calculate cut-off grades.

The mixed input-output table is edited in the same way as the statistical and accounting systems of the mine, it is therefore easy to use.

INTRODUCTION

In a mine accounting system, there are many information, which can be divided as geological information related to the nature of the ore body, technical information related to each productive activity and administrative information related to the management as well as the economical one related to the economical environment in which the mine is. Although the I-O analysis is not used as often in a micro economic system as in a macro one, we have found that it is a wonderful tool to simulate the mine accounting system by putting all the information data into a simple two dimensional table. Any too abstract discussion will be a trial, we use therefore a specific gold mine in China to illustrate our analysis.

In the mine there are five submines. The East, the West, Jiuqu and Dakaitou provide ore to feed Linglong mill plant and the Lingsan submine provides ore for Lingsan mill plant. The final product in Linlong system is gold together with two by-products, silver and S-concentrate; in the Lingsan system the final product is gold concentrate. The underground extraction process in each of the five submines consists of "drifting", " mining ", " drawing ", " hauling " and "hoisting". The output of each submine is " ore ". The yearly gold production as well as the yearly profit of the mine are stipulated by the upper administration. The gold is sold

to the Central Bank at a price which is kept stable over a certain time period. The materials needed for the production, however, are bought from the market where the prices vary according to demand and supply.

THE MIXED PHYSICAL-FINANCIAL INPUT-OUTPUT MODEL

All intermediate and final products, for the purpose of the mixed I-O model, are defined as **products.** Those produced by the production are defined as **internal products** and those used in the production of the internal products but not produced by the production are defined as **bought products.** Those items expressed by monetary values are called **value items.**

Because of the characteristics of mine production, the subsequent rules must be followed while developing a mixed I-O model for a mine:

1). The I-O table should be edited in the same manner as the statistical and accounting systems in the mine so that it is easy to adjust the information in the table while the practical production goes on;
2). It should depict the relationships among the main production activities.
3). It should be easy to understand and to use;
4). It should reflect the consumption of energy and materials in the mine's production;
5). The " product " should have an accurate technical and / or economic definition.

Based on the above rules and on the characteristics of the mine, the model for the mine includes 30 internal products, 2 final products, 34 bought products and 9 value terms (including 2 by-products expressed by monetary values). The definition of each product is shown in table 1.

The I-O table consists of 6 interactive parts. Part I is a 30 x 30 matrix, where $x_{(i,j)}$ represents the element at row i and column j. It represents the input amount of the i^{th} internal product to the production of the j^{th} internal product, it is also the amount of the direct consumption of product j to product i. So row i gives the distribution of product i into different product j's production and column j gives the direct consumption of product j to different product i.

Part II is a 30 x 3 matrix. Let $y_{(i)}$ be the amount of product i which becomes final product(i.e. not in the production but in stock or for sale, instead.); let $x_{(i)}$ be the total amount of product i, then the distribution equations of internal products are

$$\sum_{j=1}^{30} x_{(i,j)} + y_{(i)} = x_{(i)}, \ (i = 1, 2, \ldots, 30), \quad (1)$$

Part III is a 34 x 30 matrix, rows give 34 kind of bought materials, let $h_{(i,j)}$ be the amount of i^{th} bought material used in the production of product j.

Part IV is a 34 x 3 matrix. Let $f_{(i)}$ be the amount of i^{th} bought material which is out of the production in the given period and let $h_{(i)}$ be the total amount of the i^{th} bought material, the distribution equations of bought materials are

$$\sum_{j=1}^{30} h_{(i,j)} + f_{(i)} = h_{(i)}, \ (i = 1, 2, \ldots, 34), \quad (2)$$

Part V is a 9 x 30 matrix expressed by monetary value. The columns are the same as Part I and III, and the rows are all other information which is difficultly expressed by physical value. Let $m_{(i,j)}$ be the element at row i and column j and $m_{(i)}$ be the total amount of the i^{th} item, the distribution equations are

$$\sum_{j=1}^{30} m_{(i,j)} = m_{(i)}, \ (i = 1, 2, \ldots, 9), \quad (3)$$

Let $$a_{(i,j)} = x_{(i,j)} / x_{(j)}, \quad (4)$$

$$d_{(i,j)} = h_{(i,j)} / x_{(j)}, \quad (5)$$

where: $$e_{(i,j)} = m_{(i,j)} / x_{(j)}, \quad (6)$$

$a_{(i,j)}$, $d_{(i,j)}$ and $e_{(i,j)}$ are called the **direct consumption coefficients** of the j^{th} internal product to the i^{th} internal product, the i^{th} bought product, and to the i^{th} value term, respectively.

Let $b_{(i,j)}$ represent the **complete consumption coefficient,** which means the complete consumption of the i^{th} internal product in the production of one unit of the j^{th} final product, i.e.

$$B = (I - A)^{-1} - I. \quad (7)$$

Therefore the input-output equations can be rewritten as follows:

$$X = (I - A)^{-1} \times Y, \quad (8)$$

$$H = D \times (I - A)^{-1} \times Y + F, \quad (9)$$

$$M = E \times (I - A)^{-1} \times Y. \quad (10)$$

THE APPLICATIONS OF THE MIXED INPUT-OUTPUT MODEL

The model is used to analyze the economic and production structure of the mine. It is also used to analyze the impact of a various of factors on the mine's production and management.

1. Structure Analysis

With the help of the direct consumption coefficients and the complete consumption coefficients, it is convenient to analyze the relationships among all the production activities.

For example, the direct consumption coefficients of the " mining " to the "drifting" in the five submines respectively are: $a_{(1,5)} = 1.431$ (in the East), $a_{(2,6)} = 2.691$ (in the West), $a_{(3,7)} = 1.711$ (in Jiuqu), $a_{(4,8)} = 0.953$ (in Dakaitou) and $a_{(24,25)} = 0.524$ (in Lingsan). These coefficients indicate how many kilometres of the " drifting " in each submine should be prepared in order to mine 10,000 tons of the " ore ". These coefficients are also called the "ratio between mining and drifting", which are important indices in mine production. They reflect the overall mining conditions in each submine and form an important basis for the mining-drifting balance plan. On the other hand, because of the indirect consumption, the complete consumption coefficients are more suitable for determining the capacity of each activity than the direct coefficients. In the East submine, for example, the direct coefficient of the " ore " to the "hauling", $a_{(13,9)}$ is 1. However, the " ore " production must consume the " mining " and the " mining " must consume the "drifting ". Furthermore the waste from the "drifting" will also consume the "hauling". Thus the complete coefficient of the " ore " to the "hauling", $b_{(13,9)}$, becomes 1.793, where 0.793 is the indirect consumption. Therefore, when the planning is done for the " ore " production, the required " hauling " capacity should be calculated using the ratio of " ore : hauling " of 1 : 1.793 given by the complete consumption coefficient rather than the ratio of 1 : 1 as indicated by the direct consumption coefficient. The complete consumption of all the other activities by the "ore" production in the East submine will again be taken as an example. In order to ensure that the output of the " ore " is , say 10,000 t, the capacities of the "drifting", " mining ", "hauling" and " hoisting " should be 1,013 m, 7,080 t, 17,930 t and 17,930 t, respectively. Accurate knowledge of the relationships among the capacities of all the activities can help to carry out planning, forecasting and integral balancing of all activities as well as to find the best way of expanding the overall capacity of the mine. Furthermore, by comparing the complete consumption coefficients of the "ore" in different submines to the same kind of the internal product, say, the " drifting ", the differences among all the submines with respect to geological conditions, technological levels and management levels could easily be demonstrated.

2. Bottle-Neck Analysis

Normally the mine production should be developed rationally. When the demand for the final products increases, the capacity of each activity should increase correspondingly. In practical production, however, the capacity of each activity does not always maintain the initial ratio. For example, when the demand for the final products increases, it may not be necessary to increase the capacities of some activities because these are already sufficient to meet the increased demand. The capacities of other activities, however, may need increasing. This means that there exists one (or more) critical activity (ies). As long as the capacity of the critical activity increases, the output of the final products could increase. Such a critical activity is called a " bottle-neck". Finding the " bottle-neck " of a mine has a great significance on improving the economic results. By means of the input-output equations, it is easy to diagnose the "bottle-neck" and even a series of "bottle-necks".

From equations (8) and (9), if the basic system is described by the following equations:

$$X^{(0)} = (I - A)^{-1} \times Y^{(0)}, \quad (11)$$

$$H^{(0)} = D \times (I - A)^{-1} \times Y^{(0)} + F, \quad (12)$$

then, when the demand for the final products increases by ΔY, the system can be described by:

$$X^{(1)} = (I - A)^{-1} \times (Y^{(0)} + \Delta Y), \qquad (13)$$

$$H^{(1)} = D \times (I - A)^{-1} \times (Y^{(0)} + \Delta Y) + F, \qquad (14)$$

Assuming that the maximum capacities of the production of internal products and the supply of bought materials are X^{max} and H^{max}, respectively, let

$$q_{(i)} = [x_{(i)}^{(1)} - x_{(i)}^{(0)}] / [x_{(i)}^{max} - x_{(i)}^{(0)}], \qquad (15)$$

$$r_{(i)} = [h_{(i)}^{(1)} - h_{(i)}^{(0)}] / [h_{(i)}^{max} - h_{(i)}^{(0)}]. \qquad (16)$$

Those activities which result in $q_{(i)} >= 1$ and / or $r_{(i)} >= 1$ become weak and the most critical bottle-neck should be the i^{th} activity which meets

$$\text{MAX} \{\max [q_{(i)} | \ q_{(i)} >= 1], \max[r_{(i)} | r_{(i)} >= 1]\}, \qquad (17)$$
$$i=1$$

Relaxing the constraint of the bottle-neck, when the demand for the final products continues to increase a new bottle-neck can be found by (17).

Thus, the input-output analysis can help to identify a "bottle-neck" or a series of " bottle-necks " which could result as the demand for the final product increases. Presently in China the demand for gold increases yearly.It is therefore imperative to precisely identify any " bottle-necks " and eliminate them by appropriate measures so that as much gold as possible might be produced with as little input as possible.

3. Cost-Price Analysis

Based on the cost-price theory and the mixed input-output model, a cost-price model for all the products can be expressed by the following equations:

$$C_{1,n} = (R_{m,1}^{T} \times D_{m,n} + K_{1,s} \times E_{s,n}) \times (I_{n,n} - A_{n,n})^{-1} + M_{1,n} \times B_{n,n}, \qquad (18)$$

$$P_{1,n} = (R_{m,1}^{T} \times D_{m,n} + K_{1,s} \times E_{s,n} + M_{1,n}) \times (I_{n,n} - An_{\times} n)^{-1}, \qquad (19)$$

where:

$C_{1,n}$ is the unit cost vector of the internal products, n is the number of the internal products;
$P_{1,n}$ is the unit price vector of the internal products;
$R_{m,1}$ is the unit price vector of the bought products, m is the number of all the bought products;
$D_{m,n}$ is the direct consumption coefficient matrix of internal products to bought products (physical value);
$K_{1,s} = (1, ..., 1)$;
$E_{s,n}$ is the direct consumption coefficients matrix of internal products to value terms, i. e. wages, welfare, overheads, depletion, price differences of materials and so on, s is the number of all the items listed above;
$M_{1,n}$ is the unit profit vector of the internal products;
$I_{n,n}$ is a unit matrix;
$A_{n,n}$ is the direct consumption coefficients matrix of internal products;
$B_{n,n}$ is the complete consumption coefficients matrix of internal products.

Using the corresponding data to equations (18) and (19), the calculated unit costs of the two final products, " gold " in the Linglong System and " gold-concentrate" in the Lingsan System, are 3.035 and 4.340 (10^4 yuan/kg), respectively and the unit prices are 4.145 and 5.450 (10^4 yuan / kg), respectively.

Compared with the real sale price, 4.800 (10^4 yuan / kg) for the " gold " and 4.008 (10^4 yuan / kg) for the gold in the " gold-concentrate ", it is obvious that the "gold" is very profitable and the " gold-concentrate " is unprofitable. This result seems incorrect since the mine has proven to be profitable for many years. However, in the mine the costs are calculated in the following manner:

$$C_t = F_t / (A_g + A_c), \qquad (20)$$

$$C_g = P_g \times F_t / (A_g \times P_g + A_c \times P_c), \qquad (21)$$

$$C_c = P_c \times F_t / (N_g \times P_g + N_c \times P_c), \qquad (22)$$

where:

F_t is the total cost used in the mine for the total gold output (10^4 yuan / kg);
N_g is the output of the gold in the "gold" (kg);
N_c is the output of the "gold-concentrate" (kg);
P_g is the sale price of the " gold " (10^4 yuan / kg);
P_c is the sale price of the " gold-concentrate " (10^4 yuan / kg).

The results obtained by using the three equations presented above show that the final products are both profitable. However, equations (21) and (22) indicate that C_g and C_c are average costs based upon the input used to produce one unit of revenue, which can

not reflect the real consumption of the products. Hence the profit made with the " gold " covers the losses incurred in the production of the " gold-concentrate ".

The above analysis indicates that the decision-makers in the mine should take some particulary measures to change the consumption structure of the "gold-concentrate".

4. The Impact of Different Factors on the Unit Costs of the Products

1). The Impact of the prices of the Bought Products

Based on the equation (18) the following expression relates to the change in unit costs of products to the change in the prices of the bought products:

$$\Delta C = \Delta R^T \times D \times (I - A)^{-1}, \qquad (23)$$

where:

$\Delta R = (\Delta r_{(1)}, ..., \Delta r_{(m)})^T$, $\Delta r_{(i)}$ is the price change of the i^{th} bought product.

Equation (23) shows that the unit costs of internal-products vary lineally with a change in the prices of the bought materials and that the extent of the change is dependent upon the Leontif inverse, $(I - A)^{-1}$, as well as the direct consumption coefficients of the internal-products to the bought products, D.

In the mine the bought products include electricity and materials. Generally speaking, the prices of most materials change by a similar extent and the change in the price of electricity is independent of that of the materials. Figures 1 and 2 show how the changes in the prices of the electricity and materials influence the unit cost of the " gold " and of the " gold-concentrate ".

Figure 1 indicates that the fluctuation of the prices of the materials has a greater influence than that of the electricity on the unit cost of the " gold " . This means that the unit cost of the "gold" consists of more material consumption than electricity consumption. The unit cost of the " gold-concentrate " consists of almost the same proportion of the two kinds of consumption (see figure 2). The unit cost of the " gold " is more sensitive to the change of the electricity and materials than that of the " gold-concentrate ". For example, if both prices of the electricity and the materials increase by 50 %, the unit costs of the " gold " and " gold-concentrate " will increase 10.5 % and 7.8 %, respectively.

2) The Impact of the Geological Grades

The geological conditions in a mine are always uncertain, in particulary the geological grade of the deposit.

As a consequence of the change of the geological grade, the direct consumption coefficient matrix, A, and hence the complete coefficient matrix, B, of the internal products, will change. Let A_g and B_g represent the changed matrices A and B, then

$$\Delta C = (R^T \times D + K \times E) \times [(I - A_g)^{-1} - (I - A)^{-1}] + M \times (B_g - B). \qquad (24)$$

where: $A_g = (a'_{(i,j)})$ and $a'_{(i,j)} = a_{(i,j)}$ for all i and j except the following elements:

$$a'_{(i,21)} = x_{(i)} / \{ k_{1(i)} [\sum_{j=9}^{12} x_{(j)} / k_{1(j)} + h_{(1,21)}] \} \qquad (25)$$

where,

$x_{(i)}$ presents the original ore amount;

$k_{1(i)} = g'_{(i)} / g_{(i)}$, (i= 9, 10, 11, 12, 26) (26)

$g_{(i)}$ and $g'_{(i)}$ are the original and changed grades, respectively;

$h_{(1,21)}$ is the amount of the bought ore.

$$a'_{(22,23)} = [\sum_{j=9}^{12} x_{(j)} / k_{1(j)} + h_{(1,21)}] / [a_{(21,22)} x_{(23)}] \qquad (27)$$

$$a'_{(26,27)} = a_{(26,27)} / k_{1(26)} \qquad (28)$$

$$B_g = (I - A_g)^{-1} - I \qquad (29)$$

Figure 3 shows the relationship between the change of grade in Lingsan submine and the change of the unit cost of the "gold concentrate" in the Lingsan system. It is clear that the unit cost of the "gold concentrate " is very sensitive to the change of the geological grade. In particulary, it is more sensitive to a decrease in the grade of the deposit than an increase. Furthermore while the grade continues to increase the changes in the cost will trend to flatten out.

3) The Impact of Rock Dilutions

The first time rock dilution, $d^{(1)}$, incurs during the mining process and the second one, $d^{(2)}$, during the drawing, hauling and hoisting. Let d be the total dilution, then

$$d = d^{(1)} + d^{(2)} - d^{(1)} d^{(2)} \qquad (30)$$

The change of the first-time dilution will influence four type of coefficients, which are:

(1). The direct consumption of " mining " to "drifting ", $a_{(i-8,\, i-4)}$ (i= 9, 10 , 11, 12) and $a_{(24,25)}$;

(2). The direct consumption of " mining " to the bought materials, $d_{(f,\, i-4)}$) (i= 9, 10, 11, 12) and $d_{(f,25)}$, where f = 9, ..., 17 represent different kind of bought materials in the I- O table;

(3). The direct consumption of " ore dressing " to the " ore " from the submines in the Linglong system and the " gold-concentrate " to the "ore" in the Lingsan system, $a_{(i,21)}$ (i = 9, 10, 11, 12) and $a_{(26,\, 27)}$;

(4). The direct consumption of " gold "("smelting") to the " mineral-concentrating ", $a_{(22,23)}$.

The change of the second-time dilution will just affects the third and fourth type of coefficients above.

Let $k_{2(i)} = (1 - d'^{(1)}_{(i)}) / (1 - d^{(1)}_{(i)})$, (i = 9, 10, 11, 12, 26) (31)

$k_{3(i)} = (1 - d'^{(2)}_{(i)}) / (1 - d^{(2)}_{(i)})$, (i = 9, 10, 11, 12, 26) (32)

then, due to the rock dilutions,

$$a'_{(i-8,\, i-4)} = k_{2(i)}\, a_{(i-8,\, i-4)} \qquad (33)$$

$$a'_{(24,\, 25)} = k_{2(26)}\, a_{(24,\, 25)} \qquad (34)$$

$$d'_{(f,\, i-4)} = k_{2(i)}\, d_{(f,\, i-4)} \qquad (35)$$

$$d'_{(f,25)} = k_{2(26)}\, d_{(f,\, 25)} \qquad (36)$$

$$a'_{(i,21)} = x_{(i)} / \{ k_{2(i)} k_{3(i)} [\sum_{j=9}^{12} x_{(j)} / (k_{2(j)}\, k_{3(j)}) + h_{(1,21)}] \}, \qquad (37)$$

$$a'_{(22,23)} = \{ \sum_{j=9}^{12} x_{(j)} / [k_{2(j)} k_{3(j)}] + h_{(1,21)} \} / [a_{(21,22)} x_{(23)}] \qquad (38)$$

$$a'_{(26,27)} = a_{(26,27)} / [\, k_{3(26)}\, k_{2(26)}] \qquad (39)$$

So due to the changes of rock dilutions, the unit cost of all products will become:

$$C' = (R^T \times D' + K \times E) (I - A')^{-1} \qquad (40)$$

Figure 4 shows the relationship between the change of the unit cost of gold and the changes of first-time and second-time rock dilutions in the Linglong system.

4) The impact of Ore Loss

The ore loss r will affect the relationship between " mining " and " drifting ", i.e. $a_{(i,i+4)}$ (i= 1, 2, 3, 4, respectively representing the four submines in the Linglong system) and $a_{(24,25)}$ (Lingsan),

$a'_{(i,\, i+4)} = a_{(i,\, i+4)} / k_{4(i)}$ (i = 1, 2, 3, 4), (41)

$a'_{(24,\, 25)} = a_{(24,\, 25)} / k_{4(24)}$ (42)

where,

$k_{4(i)} = [\, 1 - r'_{(i)}] / [\, 1 - r_{(i)}]$, i = 1, 2, 3, 4, 24) (43)

Figure 5 shows the relationship between the change of the ore loss and the unit cost of gold concentrate in the Lingsan system. We can see that the effect is very small. This is because that the ore loss itself in the mine is in fact very low.

5. Calculation of Cut-off Grades

We define "mining cut-off grade" g_m as the lowest mining grade in each mining block; " Drawing cut-off grade" g_d as the lowest drawing grade at each drawing piont and " ore-dressing cut-off grade" g_o as the grade to distinguish the ore, which goes to the mill plant, and the waste, which goes to the waste dump.

Let $\delta = \beta\varepsilon_2(p_1 + p_2) + p_3 - (1 + \theta)(10\, \beta\varepsilon_2 Z_g + Z_c)$, then

$$g_m = \beta(1 + \theta)[(1- d_2) Z_m + (1- r_2)(Z_o + Z_{ha} + Z_{ho} + Z_{od})] / [\delta (1-r_2)(1-d_1)(1-d_2)\varepsilon_1] \qquad (44)$$

$$g_d = \beta(1+\theta)(Z_o + Z_{ha} + Z_{ho} + Z_{od}) / [\delta(1-d_2)\varepsilon_1], \qquad (45)$$

$$g_o = \beta(1 + \theta) Z_{od} / (\delta\, \varepsilon_1) \qquad (46)$$

where:

d_1: first-time rock dilution, %;
d_2: second-time rock dilution, %;
r_2: second-time ore loss, %;
ε_1: recovery rate in ore-dressing, %;
ε_2: recovery rate in mineral-concentrating, %;
β: grade of concentrate, g/t;
p_1: sale price of the gold, yuan / g ;
p_2: sale price of the silver, yuan / g ;
p_3: sale price of the S-concentrate, yuan / t;

Z_m, Z_o, Z_{ha}, Z_{ho}, Z_{od}, Z_g and Z_c are the direct variable unit costs of "mining", "ore", "Hauling","hoisting", "ore-dressing","gold" and "gold concentrate", respectively, which can be calculated directly from the I-O table.

From the formula we can see that $g_m > g_o > g_{od}$

CONCLUSION

Applying input-output analysis to simulate mine accounting system is a new approach. Its use in a gold mine in China has proven it to be quite successful. How to increase the degree of precision of the model requires further research work.

REFERENCES

Li, B., 1989
Input-output Technique and the Modernization of Enterprise Management, (Beijing, Science Press)

Wu, J. and Zhang, S., 1984
The Applications of the Input-Output Technique in China (Shanxi People Press).

Tang, X., 1993
Input-Output Analysis and Decision-Making Methodology on Production and Management of Gold Mine Enterprises Ph.D. Thesis (University of Science and Technology Beijing).

Gols, A.G. ,1974
The Use of Input-Output Analysis in Industrial Planning, in: K. Polenske and J. Skolka (eds.) Advances of Input-Output Analysis, (Ballinger Publishing Company).

No.	Name	Unit	Definitions
1.	drifting(5)#	km	driving of drifts and raises for preparing mining blocks, serving "mining".
2.	mining(5)	10^4t	drilling and blasting for making the mineralized materials collapse, serving "ore".
3.	ore(5)	10^4t	mined materials drawing from each block, serving "ore dressing".
4.	hauling(5)	10^4t	main auxiliary activity, serving "ore" and "drifting"
5.	hoisting(5)	10^4t	main auxiliary activity, serving "ore" and "drifting"
6.	ore dressing(5)	10^4t	cleaning of the ore by the removal of certain valueless portion, serving for "concentrating"(in Linglong).
7.	concentrating(1)	10^4t	further cleaning of the concentrate from "ore dressing", serving for "gold"
8.	gold(1)	kg	one of the main final products, including smelting, gold-silver separation.
9.	gold-concentrate(1)	kg	including ore dressing in Lingshan.
10.	ventilation(1)	km^3	serving underground production in Lingshan.
11.	bought materials(34)		all materials, water and electricity bought from markets
12.	by-products(2)	10^4¥	silver and sulphur-concentrate
13.	labour wage and welfare(2)	10^4¥	wage and welfare of workers in direct production.
14.	WJF(1)	10^4¥	charge according to ore amount from each submine.
15.	overheads(3)	10^4¥	overheads in three levels of workshops, submines and the mine.
16.	depreciation(1)	10^4¥	depreciation of equipment.

#: number of the same kind of products.

Table 1. Definitions of Products

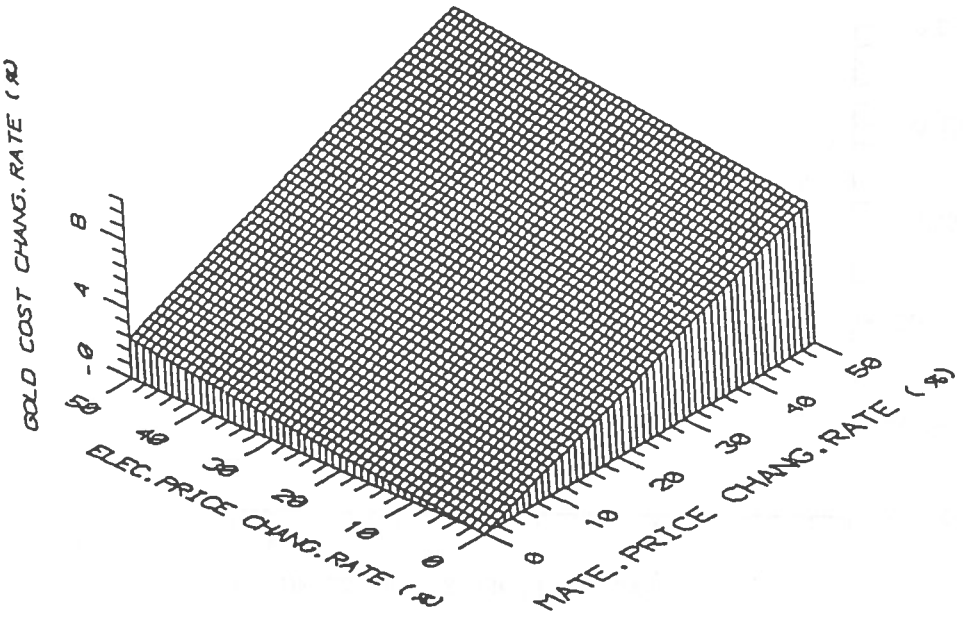

Fig.1 The Impact of the Changes of the Prices of Electricity and Materials on the Unit Cost of the Gold(Linglong)

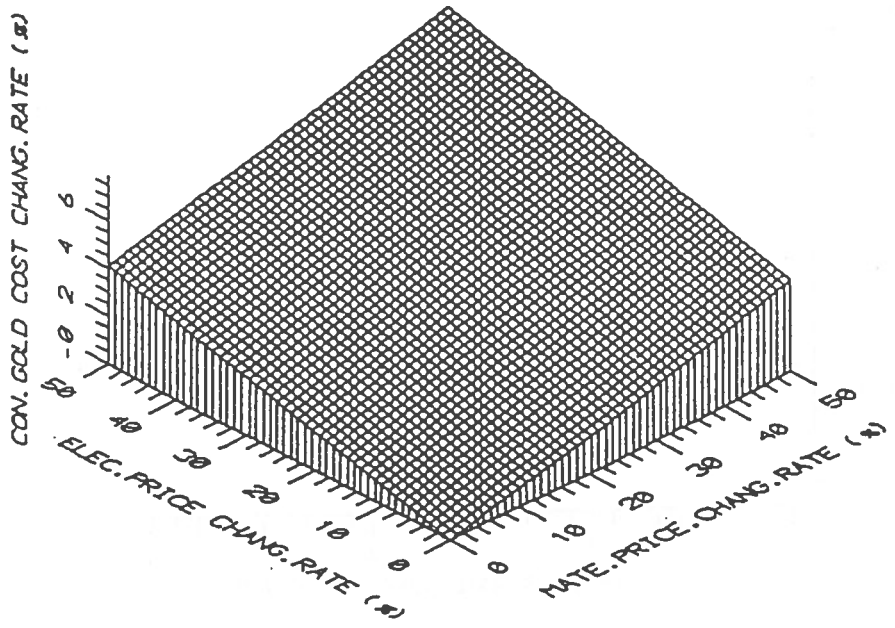

Fig.2 The Impact of the Changes of the Prices of Electricity and Materials on the Unit Cost of the Gold Concentrate(Lingsan)

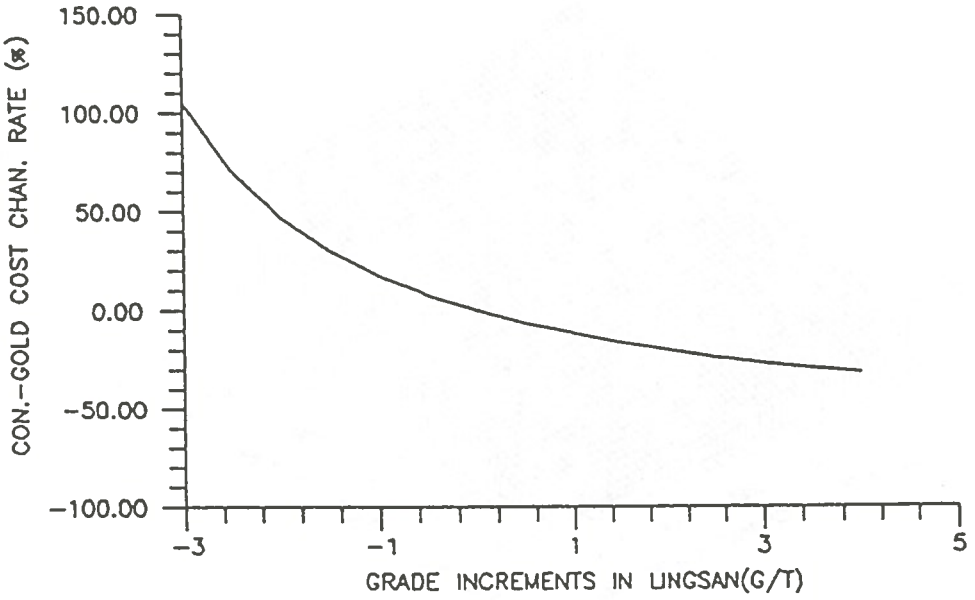

Fig.3 The Impact of the Changes of Grade on the Unit Cost of the Gold Concentrate(Lingsan)

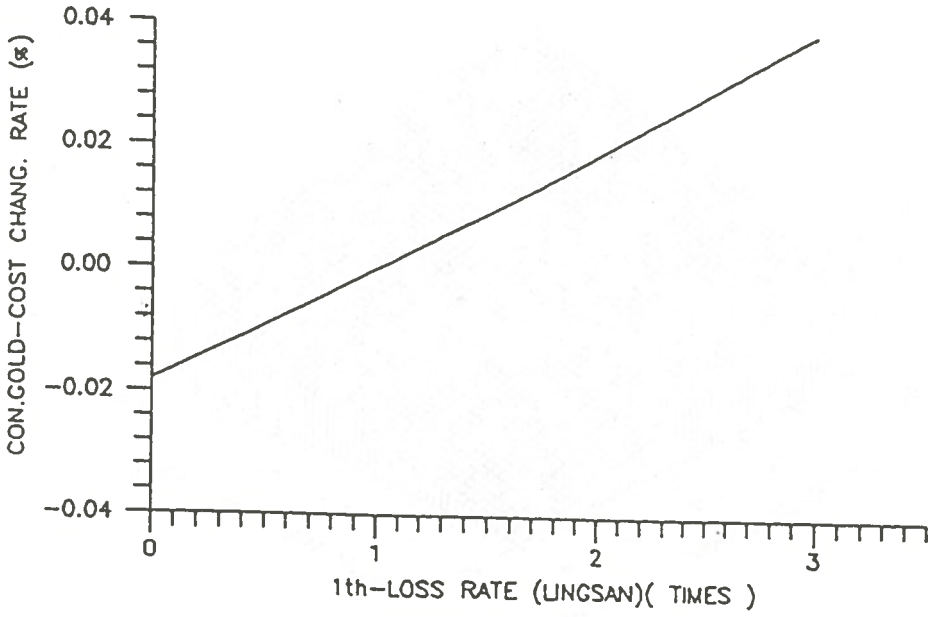

Fig.5 The Impact of the Changes of Ore Loss on the Unit Cost of the Gold Concentrate(Lingsan)

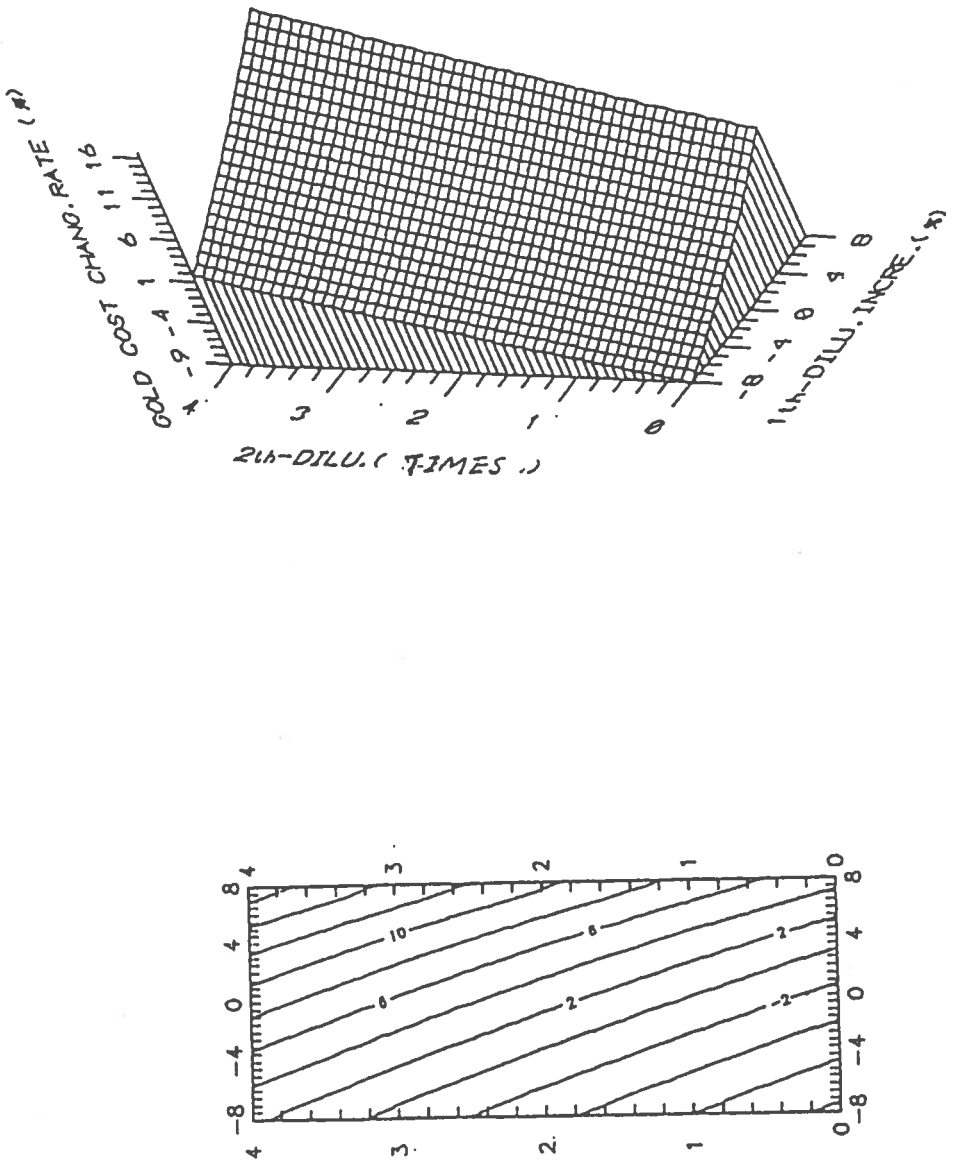

Fig.4 The Impact of the Changes of Rock Dilutions (1th and 2nd) on the Unit Cost of the Gold(Linglong)

CAMI'95: 3rd Canadian Conference on Computer Applications in the Mineral Industry
Montréal, Québec, Canada, October 22-25, 1995

'The Mine Manager' -- An Application of Computer Gaming To Mineral Project Decision Making

Jacqueline E. Allison, Michel L. Bilodeau, Roussos G. Dimitrakopoulos
Department of Mining and Metallurgical Engineering
McGill University, Montreal, Quebec

ABSTRACT

The Mine Manager is an interactive microcomputer-based game in which the user assumes the role of mine management in the exploitation of a mineral deposit. The game is based on a model of the sequence of decisions required for mine development and production. At the development stage, the selection of project specifications concerns the mining method and capacity installation. Decisions on cut-off grade and/or cut-off value, capacity utilization, the sequence of extraction, stockpiling and expansion are made during the production stage. Decision making must comply with rules which ensure that only feasible decisions are made.

As a basis for decision-making, the user receives limited information on the geology of a simulated massive sulphide deposit, the historical prices of its elements of economic interest, typical costs of mine development and production, and other relevant data. Decisions are based on estimates of parameters whereas the cash flows of the project are determined from the actual values prevailing in each year.

This paper describes the user interface, and illustrates the operation of the game by using a sample run and presenting some of the information displays which it creates. The game provides a framework for experimentation, testing of operating policies and training in mine economics.

RÉSUMÉ

'Mine Manager' est un logiciel interactif avec lequel l'usager assume le rôle d'opérateur dans l'exploitation d'un gîte minéral. Ce 'jeu' de type recherche opérationnelle se base sur la séquence des décisions qui sont prises lors des activités de développement et d'extraction du gisement. Le choix d'une méthode d'extraction et le dimensionnement des installations doivent être fait en premier lieu, au début de la période de développement. Viennent ensuite des décisions relatives à la teneur de coupure et/ou valeur de coupure, au taux ainsi qu'à la séquence d'extraction, au stockage du minerai de plus faible teneur et à l'expansion de la capacité d'extraction pendant la période de production. Toutes ces décisions doivent respecter des règles qui assurent un déroulement logique et ordonné des activités minières.

Tout d'abord, l'usager reçoit des renseignements sur la géologie d'un gîte de sulfures massifs hypothétique qui a été simulé pour les besoins de la cause, sur le cours du marché des éléments d'intérêt économique, sur des coûts typiques de développement et d'opération d'un projet minier de ce genre, et sur certains autres paramètres d'intérêt secondaire. Les décisions qu'il doit prendre par la suite se basent sur la prévision des paramètres d'intérêt, tandis que les conséquences économiques de ces décisions dépendent des valeurs actuelles des paramètres réalisées au fil des années.

Ce texte décrit les composantes du logiciel et illustre le déroulement du jeu à l'aide de figures et de tableaux montrant les intrants fournis par l'usager ainsi que les résultats produits par le logiciel. En plus d'offrir un environnement tout désigné pour étudier l'efficacité de certaines stratégies et tactiques opérationnelles d'une exploitation minière, ce logiciel est un outil éducationnel très utile en économie minière.

INTRODUCTION

The mine environment is defined by geological and economic parameters. The geological parameters are those which refer to the deposit, that is, the quantity and grade of mineralized material, and other physical features. The economic parameters are external to the deposit, and are in effect during the period in which decisions are made with respect to mine development and production. Economic parameters include commodity prices, capital and operating costs, inflation and currency exchange rates.

The combined effect of the uncertainties associated with the various geological and economic parameters is a high level of risk in mineral project investment. It is likely that mine management will alter its planning decisions as its database improves and uncertainty is resolved during the life of the mine. The difficulties which are encountered in decision making with respect to mine development and production point to a need for systems which enhance the process by which decisions are made. These should take into account the sequential nature of the decision process and the dynamic features of the mine environment.

The profitable exploitation of a mineral deposit requires astute decisions concerning mine development and production. At the development stage, the selection of project specifications is made, that is, the mining and processing methods and the capacity of the plant are chosen. The latter refers to the installed mining and milling capacities which determine the initial requirements of capital expenditure. Future operations are constrained by the capacity installations based on the initial planning decisions.

At the production stage, decisions are made concerning operating variables and the expansion of existing capacity. The level of capacity utilization is influenced by economic and technical parameters. Short-term shutdown is an extreme form of capacity underutilization, and may be a favourable alternative to operating at a loss when the mining operation is facing economic problems. Permanent plant closure is warranted when the ore reserves are exhausted. Premature closure may become necessary for economic or technical reasons.

The cut-off grade, a specific concentration of an element of economic interest, dictates the amount of mineralized material that will be targeted for recovery. The cut-off value refers to a monetary amount which is based on a combination of grade, price and various parameters of extraction and processing. The cut-off value may also be used to distinguish between ore and waste, and the partitioning of mineralized material may be based on a series of cut-off values.

Unless the grade is uniform in all parts of the deposit, financial performance will be affected by the order of extraction of the mineable units. In many deposits, grades display a zonal pattern and a firm will select a sequence of mining according to its operating policy. The sequence of mining may be reconsidered many times during the production phase. Stockpiles may be created; stockpiling decisions determine the number, size and grade of stockpiles, defined here as an inventory of mined material at the minesite.

An expansion of the installed capacity may be considered advantageous if ore reserves increase or if market conditions are favourable. An additional capital expenditure will be associated with an expansion of the installed capacity, and a change in unit operating costs may result. Deepening of the shaft in an underground mine may be required during the operating stage.

The incorporation of uncertainty adds a new dimension to mine decision making. It increases the need for more complex tools capable of representing not only the intricate interrelationships in the mine system, but also the actual mode of decision making.

MINE MANAGEMENT GAMING

Gaming refers to the playing of games that simulate actual conditions, especially for training or testing purposes (Webster's Ninth New Collegiate Dictionary, 1990). A game is a simplified representation of a real situation in which participants or players implement decisions by making simultaneous or sequential 'moves'. In a mining game, the 'moves' which a player makes reflect the decisions of mine management; a sequence of such decisions could lead to the eventual depletion of the ore reserves. The sequential nature of the decisions on capacity, and cut-off grade and/or value, is an important aspect of mine decision making and should be included so as to increase realism.

In the mineral industry, few computer-based models have been developed for training or educational purposes, and more specifically, in the form of games. The existing mining games (Carlson and Misshauk,

1972; Mutmansky and Kim, 1973; Bodle, 1976; and O'Neil, 1994) provide the means for assessing alternative approaches to some of the problems faced by mine planners and operators. They allow the participant to gain management experience in specific functional areas such as marketing, production scheduling and transportation. There is, however, scope for a game which is based on a more comprehensive mining system rather than on the limited spectrum of issues addressed in existing games. Advances in computer technologies have made it possible to improve the interactive nature of games, thereby eliminating long lags in the output of feedback and reducing the need for expert game administrators or instructors.

By addressing these concerns, mining games could become more useful tools for mid- to upper-level management, both in terms of their understanding of the decision-making process and their appreciation of interests beyond their immediate area of expertise.

THE MINE MANAGER

The Mine Manager, also referred to as the Game, is based on a model which incorporates elements of geology, mining and management. It is a fully interactive computer-based game in which the mine environment and mine decision-making process over a period of time are simulated. The Mine Manager is most appropriately categorized as an operations research game in that it has the ultimate purpose of being an aid to decision making, planning and policy implementation. However, rather than focusing on a single real case, the deposit to be mined is a hypothetical one. The Mine Manager is also considered to be an educational game: it can be used to enhance a player's understanding of the relationships between key variables and the mining system as a whole, while also providing useful insights into the decision making process associated with the development and operation of a mine.

The Game allows for considerable flexibility in setting the installed capacity, level of capacity utilization and cut-off grade and/or value as events unfold over time. In this interactive system, the user is provided with preliminary geological information, typical cost functions and historical commodity prices, and must make a series of decisions which establish the operating environment. The input arising from these decisions is validated, and mining and milling are simulated. The results of these activities are available on the screen or in hard-copy format, and may be used to support subsequent decisions.

The geological information which is provided to the user pertains to a simulated mineral deposit. The behaviour of prices, costs and other production-related parameters, and the uncertainty associated with them, are also modelled. Decisions concerning the level of capacity utilization and cut-off grade and/or value call for the selection of mining units and their intermediate or final destination -- mill, stockpile or dump. Consideration is also given to the mining method, that is, underground or open-pit, installed capacity, sequence of mining, stockpiling, and temporary and permanent closure.

The model contains elements of a real-life situation, but the behaviour of these elements has been generalized and, therefore, cannot be ascribed to any specific system. The level of detail and realism in the model is sufficient to provide verisimilitude, but is less than that which would be required of a simulator intended for direct use as an aid to management decision making.

It is possible for several players to 'compete' against each other in independent runs of the Game. An assessment of the approach taken to the problems encountered, or a comparison of the resulting financial performance would determine the 'winner'. Project evaluation is based on the assumption that the mine/mill plant is part of an integrated company.

The model which has been developed, and its operation, are described using the terminology of games (Bowen, 1978, and Stahl, 1983). As depicted in Figure 1, the Game can be regarded as a model of the real world (the game-world) and a set of rules which

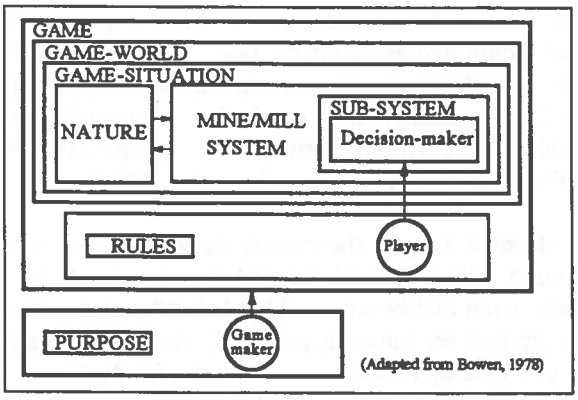

Figure 1. Representation of a Game

govern the behaviour of the player and thus, the mine/mill plant under the management of the player. The game-situation includes those elements of the game-world which impact directly on the mine/mill system and 'Nature'.

The Mine Manager is a 'rigid-rule' game in that the rules of play cannot be changed from those defined at the start of the game. There is one player, or a group of participants acting as one decision-maker, and the decisions of any others who might be assumed to exist in the particular scenario are regarded as exogenous variables. The Mine Manager is, therefore, referred to as a 'game against Nature'.

In the model of the real world, there are many factors which are external to the hypothetical mine/mill system, but which characterize the general operating environment. The mining firm is assumed to have access to, but no control over, capital and labour markets. The final products, mineral concentrates, are purchased from the firm at the market-dictated price as soon as they are produced. The firm operates in what is similar to a perfectly-competitive market except for the existence of uncertainty. The game-world is, however, described mainly in terms of the game-situation, that is, the parameters of the mine/mill system and the mine environment.

The Game-Situation

The focus of the simulated mining activity is a Noranda-type massive sulphide deposit containing copper, zinc and gold. The products of the mining and milling operations are copper and zinc concentrates, the former containing by-product gold. The mineral deposit is lense-shaped, and dips 45 degrees to the east as shown in Figure 2. The grades of copper, zinc and gold have been simulated on the basis of prespecified variograms and grade distributions which are typical of this type of deposit. The simulation was conditioned to produce a zoning pattern in which a copper-rich core is flanked by a zinc-rich envelope. Conditional simulation is described by Dimitrakopoulos (1990).

Sublevel stoping is the mining technique used underground. The vertical interval between levels is 75 metres and that between sublevels is 20 metres. There are up to three sublevels per level. Access to the mine is provided by a shaft; once in place, its depth can be increased in multiples of 75 metres. Development drifting, and primary and secondary stoping advance northwards from the shaft along strike of the deposit.

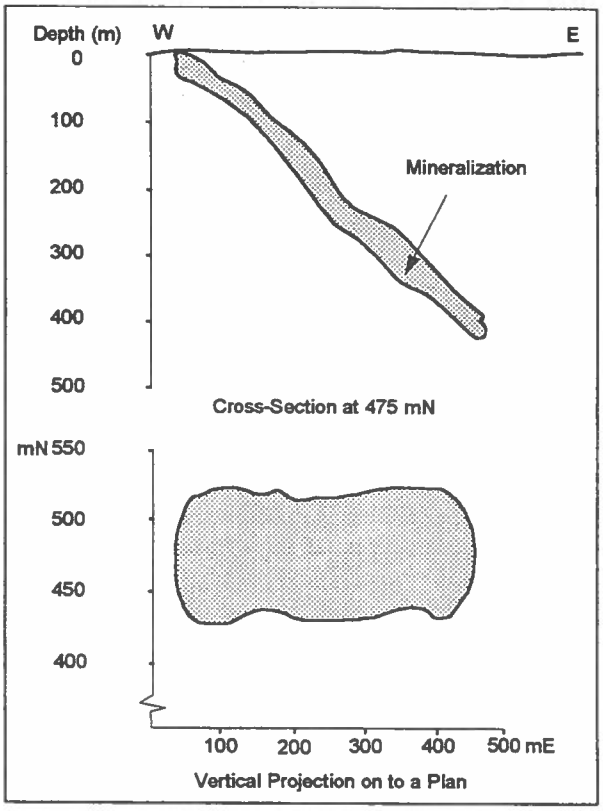

Figure 2. Shape and Orientation of the Mineral Deposit

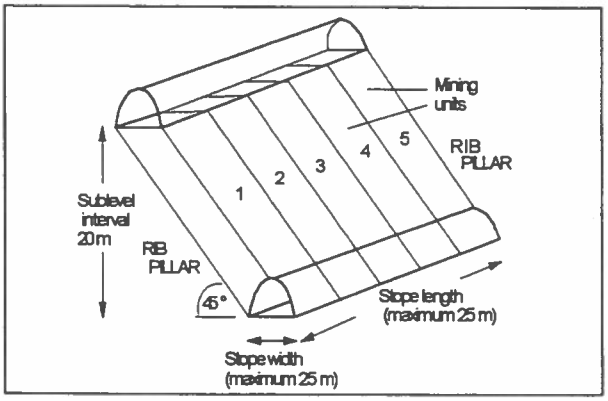

Figure 3. Parameters in Sublevel Stoping

Mining on a lower sublevel must be at least as advanced as on an upper sublevel.

Stopes dip 45 degrees to the east, paralleling the dip of the deposit. The deposit is to be mined in one cut from hangingwall to footwall. Figure 3 shows some of the parameters of the sublevel stoping technique. A mining unit has a length of 5 metres, a vertical height equal to the sublevel interval, and a width of up to 25

metres. The maximum length of stopes and the minimum length of intervening rib pillars is 25 metres.

A block of one or more mining units is selected by specification of its bounding coordinates. Upon validation of the coordinates, drilling of the block is simulated and grade estimates generated for each in situ mining unit. On the basis of these estimates, equivalent to those which would be produced from blasthole sample data, the player may decide to extract some or all of the selected mining units, or to leave the block in situ. Drilling of a mining unit which does not lead to extraction is considered to be exploratory; although not production-related, this activity consumes some of the resources which would otherwise be available for mine production. All of the material which is extracted is regarded as ore, and is either milled or stockpiled.

The amount of material mined during a particular year is a function of the average annual rates of dilution[1] and mine recovery, unknown to the player until mining operations have been completed for the year. The values of these parameters are simulated from probability distributions characterized by most-likely values of 15 percent for dilution and 87 percent for mine recovery. The amount and grade of material which is extracted is also a function of the proportions of mineralized material and host rock in the selected mining units and additional material associated with dilution.

Open-pit mining is an appropriate complement or alternative to sublevel stoping. The mining units are cubic blocks which have a length of 10 metres. The bench width is a multiple of 10 metres. A minimum mining width of 20 metres applies to mining on a new level. The maximum pit slope angle is 45 degrees.

Mining takes place in a pit which is roughly square or rectangular in plan. This shape, while uncommon in practice, reduces the complexity in the specification of pit increments by the user. There are four boundaries, each referring to a side of the pit; these may be straight or divided into segments which parallel the north-south or east-west axes. As shown in Figure 4, each boundary is defined by three coordinates which determine the outermost section of the pit along the boundary. On the pit level outlined, the northern and western boundaries are straight.

[1] Unless otherwise specified, the term 'dilution' refers to external dilution

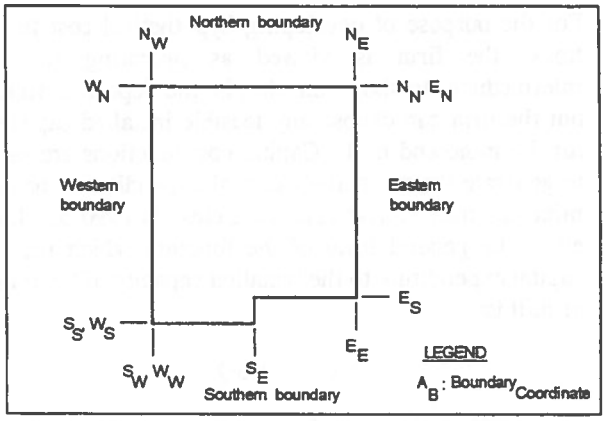

Figure 4. Boundaries of the Open-Pit

The limits of the open-pit are extended in two ways. In perpendicular extension, a block of one or more mining units is removed from a straight boundary. Parallel extension involves the removal of at least one block of mining units from a boundary which is not straight.

Grade estimates are generated for the mining units selected in the open-pit and can be used to support the decision concerning extraction. The amount of material mined in a given year is based on the assumption of full recovery and no dilution.

The range of technically acceptable installed annual capacities for the underground mine and mill is 75 000 to 675 000 tonnes; the range for the open-pit mine is 227 000 to 11.34 million tonnes. The maximum operating life is set at 45 years. Production rates up to 20 percent in excess of the stated installed capacity are attainable through the use of overtime. The player has the option to shut down the plant on a temporary basis, and to expand the installed capacity of the mine and/or mill during the production stage of the project.

The preproduction period, in years, is a function of the installed annual capacity:

$$\text{Preproduction period} = 0.84Q^{0.22}$$

where Q is the installed annual capacity in thousands of tonnes. If there is a difference in the values calculated on the basis of the installed annual capacities of the mine and mill, the preproduction period is the longer of the two. The commencement of preproduction work can be delayed for up to 15 years, thus providing the user with some flexibility in timing the start of production.

For the purpose of developing hypothetical cost functions, the firm is viewed as operating in the intermediate- to short-run, that is, the deposit is fixed, but the firm can choose any feasible installed capacity for the mine and mill. Capital cost functions are used to generate the most-likely capital expenditures for the mine and mill. These values are close to 1990 cost levels. The general form of the function which relates capital expenditure to the installed capacity of the mine or mill is:

$$CC = a + bQ^c$$

where CC is the capital expenditure in thousands of dollars, and Q is the installed annual capacity in thousands of tonnes; the values of the scaling constants a, b and c used in the capital cost functions appear in Table 1. The total capital expenditure is the sum of the amounts required for the mine and the mill. The capital expenditure for an underground mine which is developed while an open-pit is in operation is 70 percent of the amount otherwise required, as some of the costs of providing infrastructure have already been incurred.

Working capital is 25 percent of the expected annual operating expenses. The annual sustaining capital for the mine and mill is a function of the installed capacity. Capital expenditures are responsive to inflation; the most-likely rate of cost inflation is 4.7 percent.

A pricing model is used to generate series of copper, zinc and gold prices, in current U.S. money, with behaviour similar to that of prices on the London Metal Exchange. The model incorporates a trend, cyclicity and a random component, and simulation is designed so as to centralize prices. New price series are produced for each run of the Game.

TABLE 1. Constants in the capital cost functions

Capital Cost Function	Constant	Value
Underground mine	a	3226.3109
	b	233.31596
	c	0.7662613
Open-pit mine	a	475.40588
	b	132.44452
	c	0.6088922
Mill	a	5767.628
	b	229.91615
	c	0.7093054

Hypothetical intermediate- and short-run operating cost functions have been developed. The intermediate-run average cost curve for the mine and the short-run average cost curves for the mine and mill are generated using functions of the general form:

$$OC = aQ^2 - bQ + c + d/Q$$

where OC is the average operating cost in dollars per tonne, Q is the annual production rate in thousands of tonnes, and a, b, c and d are scaling constants. The intermediate-run average operating cost (IROC) function for the mill is:

$$IROC = a + bQ^{-c}$$

The values of the constants in the IROC and short-run operating cost (SROC) functions are given in Table 2. The functions yield values which are close to 1990 operating cost levels. In the short-run, the average cost is minimized by operating at a rate which is equal to the installed capacity. A premium is added to the minimum average cost if production is at over- or undercapacity. An increase in unit costs with depth arises because of the greater distance over which hoisting underground, or haulage in an open-pit, is required. Unit hoisting costs increase by 0.33 cents per metre below a depth of 170 metres. Unit haulage costs in the open-pit increase by 2 cents per bench.

The cost of permanent closure is included with the operating costs in the final year of the project. At this time, dismantling and severance costs exceed the proceeds from the sale of assets by about $2 million. The level of operating costs are influenced by the economic cycles which impact on metal prices. Operating expenses are also responsive to cost inflation.

The value of an extracted mining unit is a function of the grades of copper, zinc and gold, metal prices, the net smelter return and the mill recovery rate. The selected net smelter schedules are typical for the smelting of a copper concentrate with gold credits, and a zinc concentrate (Mackenzie, 1987; O'Hara, 1987; and Schumacher, 1988). Freight charges are incurred for transporting the concentrates to the nearest smelters.

TABLE 2. Constants in the intermediate-run and short-run average operating cost functions

Installation	Constant	Operating Cost Function IROC	SROC[1]
Underground mine	a	2.1279×10^{-4}	2.8693×10^{-4}
	b	0.1165666	0.1670942
	c	32.63499	39.934133
	d	1000	906
Open-pit mine	a	1.2453×10^{-7}	1.6710×10^{-7}
	b	7.5761×10^{-4}	1.0392×10^{-3}
	c	2.3318907	2.7997892
	d	700	693
Mill	a	2.0002226	2.5624×10^{-4}
	b	164.48033	0.1447459
	c	0.4085363	35.661884
	d	---	810

[1] For an installed annual capacity of 300 000 tonnes for the underground mine and mill, and 3.3 million tonnes for the open-pit mine

For concentrates of constant grade produced in a mill of a given design, the most-likely mill recoveries of copper and zinc from copper-zinc ore vary with the ore grade. The most-likely recoveries of copper and zinc are determined using O'Hara's (1987) functions; a recovery rate of 60 percent (Mackenzie, 1987) is considered to be most-likely for gold in a copper-zinc mill.

Cash flows associated with the mining project are calculated on an annual basis. The cash flow components are revenue, operating expenses, capital expenditures and taxes. Revenue is converted from U.S. to Canadian currency using an annual exchange rate with a most-likely value of 0.86 U.S. dollars per Canadian dollar. The annual operating expenses are related to the type of activities which have been carried out. If the mine or mill was closed on a temporary basis, the operating expenses comprise the cost of maintenance on a stand-by basis. Expenses associated with drifting underground and exploratory drilling may be incurred.

Tax allowances are based on the declining-balance depreciation method and an annual rate of 15 percent. An income tax rate of 30 percent applies to this project. The financial performance is measured using discounted cash flow criteria. The current money cash flows are first deflated using a series of general inflation rates based on the mean annual rate of change in the Consumer Price Index. The rate of return is determined, and the net present value at the start of the preproduction period is computed for discount rates varying from 5 to 25 percent.

The Sequence of Decisions

At the development stage, the player specifies the mining method, open-pit or underground, to be used, the capacities of the mine and mill, and the length of delay, if any, in the start-up of preproduction activities. If an open-pit mine is initially selected, a decision may subsequently be made to convert to an underground mine, for which the shaft site and depth must be specified.

At the production stage, blocks are selected for drilling and, possibly, extraction, and stockpiling operations may be carried out. It is through these mechanisms that the decisions on capacity utilization and cut-off grade and/or value are implemented. The sequence of decisions made during the open-pit mine life is displayed in flow chart format in Figure 5. The sequence of decisions during the underground mine life is similar except that blocks of material are selected on levels and sublevels, and there is no option to convert to a different mining method.

Rules of the Game

The rules have been set according to the scope of and degree of detail in the model upon which the Game is based. The rules pertain to the various types of decisions required of the user: development and expansion, open-pit mining, underground mining, stockpiling and milling, and permanent closure. Most of the rules relate to the constraints of the mining method.

SAMPLE RUN

The sample run leads to one of many possible outcomes in terms of financial performance and mine configuration. Several operating policies are implemented, and the deposit is mined using both open-pit and underground methods. Mine sequencing reflects the

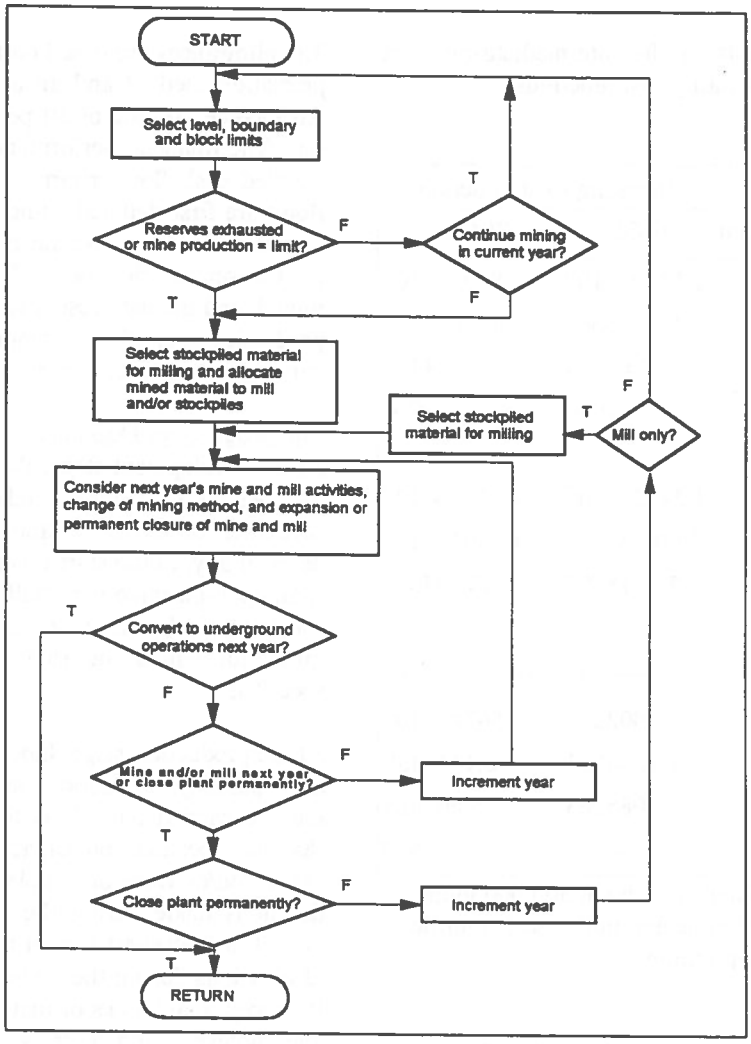

Figure 5. The Sequence of Decisions During the Open-Pit Mine Life

selected operating policies which are not necessarily optimal.

The plant capacity utilization policy is:

i) operate the plant at overcapacity if the price forecasts for at least two of the metals are higher than the normal level based on regression of historical prices.
ii) close the plant on a temporary basis if the price forecasts for all three metals are lower than normal.
iii) operate the plant at a rate equal to the installed annual capacity in all other cases.

All mining units having an estimated average value of less than the estimated mill unit operating costs are stockpiled. Up to two more stockpiles are created if necessary, that is, if the mill capacity is insufficient to accommodate the remaining mined material. If there is inadequate direct mill feed, stockpiled material is used as a supplement.

Open-pit mining seeks to minimize internal dilution and ensure adequate access to ore through advanced stripping. The grade policy implemented underground is one of blending in order to restrict the range of grades received by the mill.

The Game is started and the user is informed of the average annual metal prices during the 15-year period prior to the mine development decision. Preproduction activities are timed such that the start-up of production will coincide with a period of expected price recovery based on forecasts. Upon selection of the installed annual mine and mill capacities, a summary report of

construction parameters, as shown in Figure 6, is generated.

Following a three-year preproduction period -- Years 1 to 3 of the project -- open-pit extraction takes place over a four-year period, using a series of perpendicular extensions, after which underground mining is performed for six years. The underground mine is closed temporarily in Year 11 of the project.

In Year 4, the first operating year, open-pit mine production is 2 528 682 tonnes, the mill throughput is 163 542 tonnes, and the operations yield a net cash flow of about $9.5 million as shown in Figures 7 and 8. Mill expansion and underground mine construction are completed by the end of Year 7. The actual underground mining sequence is shown in Figure 9 which reveals the selectivity permitted by the use of the sublevel stoping technique. The rate of return associated with the project is 24 percent, and net present values range from $35 438 219 to -$683 900 at discount rates of 5 and 25 percent, respectively.

LIMITATIONS AND SUMMARY

The limitations of the Game include the lack of more complex geological features and the omission of technical problems such as slope failure and rockburst. The shape of the open-pit has been simplified, underground mining is restricted to one direction of advance, and the possibility of mixing of material in ore passes has not been taken into account. Operating periods of less than one year are not considered in the Mine Manager. The Game must be played from start to finish without interrupting the execution of the code.

In spite of these limitations, the Mine Manager is a practical tool for operations research and educational purposes. It is an interactive game based on a model of the sequence of decisions required for mine development and production. The Game reflects a compromise between simplicity and realism, but offers a high degree of flexibility in setting the values of decision variables. As a computerized mine management game, it has the potential for further development in various directions with far-reaching benefits.

```
SUMMARY OF CONSTRUCTION PARAMETERS AND ESTIMATED UNIT OPERATING COSTS
-----------------------------------------------------------------------

Installed open-pit mine capacity (tpa): 2200000
Installed mill capacity (tpa): 213900

Preproduction period (years): 3

Capital costs (thousand $):  30675.480
                      Mine:  14249.144
                      Mill:  16426.337

Estimated unit operating costs for
full capacity operations ($/tonne)
                             Mine:   1.71
                             Mill:  21.95

F1-Print screen and continue  <ENTER>-Continue
```

Figure 6. Summary of Construction Parameters and Estimated Unit Operating Costs for the Open-Pit Mine and Mill

```
SUMMARY OF OPERATIONS (OPEN-PIT MINE/MILL) -- YEAR 4
-----------------------------------------------------
Tonnes mined:              2528682
Tonnes milled:             163542
Milled grades:             1.76 %Cu
                           9.11 %Zn
                           8.64 g/t Au
Mill recovery:             Cu -- 92%
                           Zn -- 87%
                           Au -- 60%
Net smelter return:        Cu -- 71%
                           Zn -- 38%
                           Au -- 93%
Mine operating cost:       $1.79/tonne
Mill operating cost:       $27.38/tonne
No exploratory drilling was carried out.

F1-Print screen and continue  <ENTER>-Continue
```

Figure 7. Summary of Operations -- Year 4

```
CASH FLOW -- YEAR 4 (thou. $)
-----------------------------
Revenue                                :                21487.828
   Cu concentrate (US$0.89/lb Cu)      :   4865.500
   Au credits in Cu conc (US$416.95/oz Au):  11594.236
   Zn concentrate (US$0.48/lb Zn)      :   5828.092
Operating Costs                        :                 8991.195
   Mine                                :   4514.283
   Mill                                :   4476.992
   Permanent plant closure             :      0.000
Tax Allowances                         :                 3786.833
Taxable Income                         :                 8789.888
Taxes                                  :                 2636.948
Capital Expenditure                    :                    0.000
Annual Sustaining Capital              :                  198.873
   Mine                                :    140.272
   Mill                                :     58.601
Net Working Capital                    :                  101.283
-------------------------------------------------------------------
Cash Flow                              :                 9559.616

Annual Rates --
Exchange: 0.91 US$/Can$   Cost Inflation: 4.0%   Gen. Inflation: 5.4%

F1-Print screen and continue  <ENTER>-Continue
```

Figure 8. Cash Flow Statement -- Year 4

REFERENCES

Bodle, R., 1976
The development of the Colliery Game. OR 710/16/6, informal paper, Operational Research Executive, National Coal Board, Middlesex, U.K.

Bowen, K.C., 1978
Research Games – An Approach to the Study of Decision Processes. Taylor and Francis Ltd, 126p.

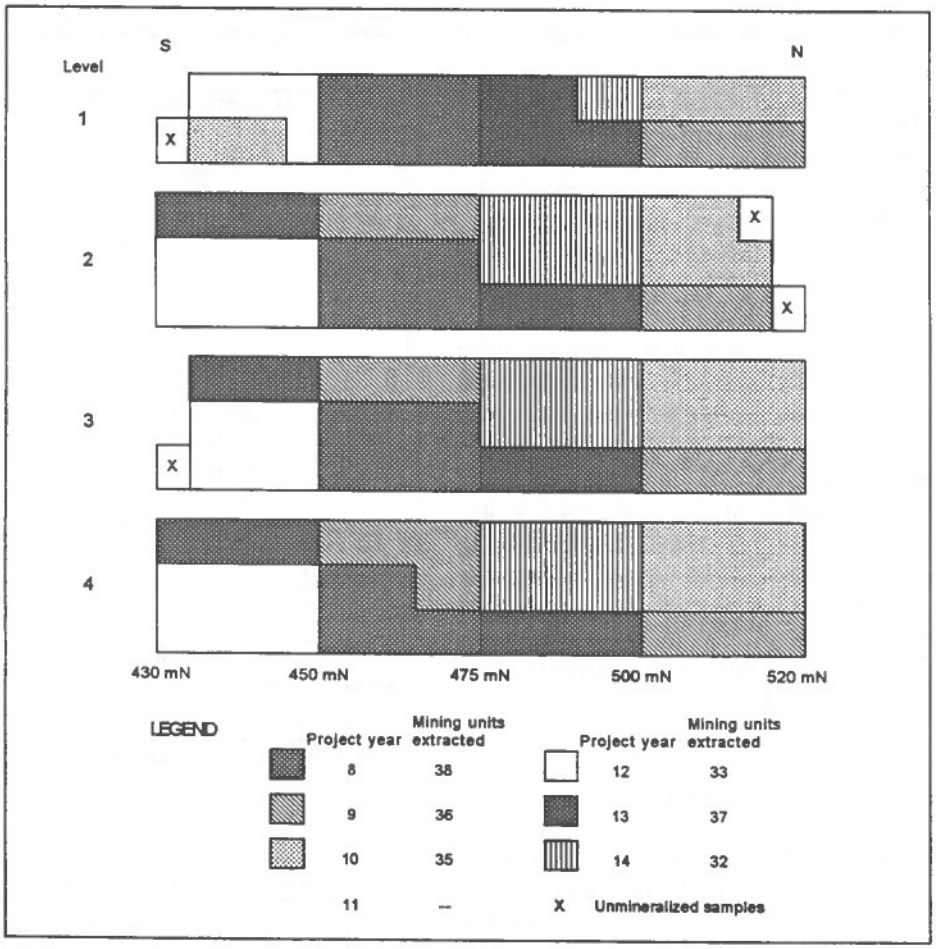

Figure 9. Horizontal Projection of Stopes on to a Longitudinal Section Showing the Underground Mining Sequence

Carlson, J.G.H. and Misshauk, M.J., 1972
Introduction to Gaming: Management Decision Simulations. Wiley, 184p.

Dimitrakopoulos, R.G., 1990
Conditional simulation of intrinsic random functions of order k. Mathematical Geology, Vol. 22, No. 3, pp. 361-380.

Mackenzie, B.W., 1987
Economic guidelines for exploration planning. Mineral project evaluation techniques and applications seminar notes, McGill University.

Mutmansky, J.M. and Kim, Y.C., 1973
The use of simulation gaming for evaluation of base metals marketing strategies. Proceedings, 11th Symposium on Computer Applications in the Minerals Industry, Tucson, April, pp. G66-G80.

O'Hara, T.A., 1987
Quick guides to mine operating costs and revenue. 89th Annual General Meeting of Canadian Institute of Mining, Metallurgy and Petroleum, Toronto, May.

O'Neil, T. (ed.), 1994
Mining Engineering, Vol. 46, No. 7, pp. 602.

Schumacher, O. (ed.), 1988
Mining Cost Service. Western Mine Engineering, Spokane, pp. 1-5.

Stahl, I., 1983
What is operational gaming? Operational Gaming – An International Approach. I. Stahl, ed., Frontiers of Operational Research and Applied Systems Analysis, Vol. 3, Pergamon Press, 330p.

CAMI'95: 3rd Canadian Conference on Computer Applications in the Mineral Industry
Montréal, Québec, Canada, October 22-25, 1995

An Option Pricing Analysis of the 1990 Capital Structure of East Rand Proprietary Mine

Michael R. Samis
University of British Columbia

ABSTRACT

East Rand Proprietary Mines (ERPM) is a South African limited liability mining company which owns a deep level gold mine approximately 40 kilometres east of Johannesburg, South Africa. A government commission was appointed during early 1990 to investigate the mine's future prospects when ERPM approached the government and its creditors for further financial assistance and the restructuring of its balance sheet. This paper uses option pricing techniques (OPT) to re-evaluate the government commission's analysis. OPT was able to show that the project's probability of success was much lower than expected by the government commission. Further, OPT was able to show how the conversion of debt to equity re-distributes value between project stakeholders and increases the project's chance of success.

RESUME

East Rand Proprietary Mines (ERPM) est une compagnie Limitée minière d'Afrique du Sud qui posséde une mine d'or profonde environ 40 kilomètres 1'est de Johannesburg, Afrique du Sud. Au début des années 1990, lorsque ERPM a approché le gouvernement et ses créditeurs pour une assistance financière supplémentaire et pour restructurer ses états financiers une commission gouvernementale a été appointée pour enquêter sur le potentiel future de la mine. Les resultats de l'analyse de cette commission est évaluer dans cette article par la technique du prix des options (TPO). La TPO a démontré que la probabilité de succés du project était plus basse que prévue par la commission gouvernementales. De plus, la TPO a montré que la conversion de dettes en actions redistribue la valeur entre les participants et accroie les chances de succés du project.

INTRODUCTION

East Rand Proprietary Mines (ERPM) is a South African limited liability gold mining company. It owns a deep level gold mine approximately 40 km east of Johannesburg, South Africa. During the mid-1980's, ERPM initiated a project to expand the Far East Vertical (FEV) Shaft complex. The objectives of the expansion were to:

a) increase the amount of long-term ore reserves;
b) improve the efficiency of the mine's infrastructure; and
c) improve the working conditions underground.

Initial project financing consisted of an equity issue and a loan provided by a South African banking consortium. It was envisaged that production in other areas would be able to provide sufficient funds to service the debt until the FEV shaft system was in operation. However, the mine incurred large working losses between 1983 and 1990 due to declining grades, rising costs, and seismic events which caused falling production. Additional financing, in the form of bridging finance and preference shares, was arranged to cover working losses.

During the first quarter of 1990, ERPM approached the government and its creditors for further financial assistance and restructuring. At this point, ERPM's long-term viability was questioned and a government commission, the Melamet Commission, was appointed on the 7th June 1990 to investigate the mine's future prospects

ERPM's future prospects were determined by consulting the stakeholders of the operation and industry experts. The project's ability to support outstanding financing was determined by developing a long-term plan which matched operating profits to debtor repayments. The conversion of debt into equity was not considered as previous conversion proposals had been rejected by the South African Receiver of Revenue, (Melamet, D. (1990), pp. 18).

The Melamet Commission recommended that State assistance should continue in the form of guarantees and loans. It estimated, by qualitative analysis, that the long range operating plan had a 50% chance of success[2]. It also noted that the success of the plan was highly dependent upon achieving the gold price and maintaining the grades outlined in the long-range plan. The recommendation was made after considering the socio-economic implications of mine failure and the substantial losses which would be incurred by various parties who had provided earlier financing.

This case study has two objectives:

a) Evaluate ERPM as it was at 01 January 1990 using option pricing theory (OPT); and
b) Re-examine select conclusions of the Melamet Commission in an option pricing framework to determine whether this framework could have provided additional insights.

OPTION PRICING EVALUATION

An option pricing framework was chosen to evaluate ERPM because it has the ability to evaluate non-linear payoffs. Non-linear cash flows are the result of management flexibility, such as expansion options or salvage opportunities, and the characteristics of project financing. OPT was originally developed to evaluate financial options and, as financial theory developed, was extended to project evaluation. It has the same theoretical foundation as the discounted cash flow method but differs in:

a) its approach to the calculation of project value;
b) the incorporation of cash flow uncertainty; and
c) certain assumptions about management's reaction to future events.

For an example of non-linear payoffs, consider a project that in one period may be either used to produce an uncertain cash flow, V, or sold for a certain salvage value, S. Management's payoff is dependent upon the final value of the underlying project cash flow. Management will operate the project and receive the cash flow if the cash flow value is greater than the salvage value. If the cash flow value is less than the project's salvage value, management abandons the project and receives the salvage value, S. Possible management payoffs are described by the 100% equity financed management payoff line in Figure 1. This payoff line is produced from the equation:

$$\text{Management payoff line} = \quad \text{Max}(V, S) \quad (1)$$

More complex non-linear cash flows are produced when the project is financed by a combination of debt and equity. Project value, as described by Equation 1, is distributed between equity and debt when debt is introduced into the capital structure. As an example, consider the project when its capital structure contains a discount debt issue which requires a payment, P, in one period. Assume that this payment is larger than the project's salvage value. Further assume that the project's tax rate is the same whether it is financed by equity alone or a combination of debt and equity.

If the cash flow is worth more than P, equity operates the project and repays the debtor. In this situation, the value of equity is V - P and the value of the debt is P. If the cash flow is worth less than P, equity abandons the project to the debtors and it has no value.

If the project is abandoned, the debtor's payoff is dependent upon whether the project's cash flow is greater than the project's salvage value and whether the debtors can operate the project (or sell the project to someone who can). If the project cash flow is worth less than S, the debtors salvage the project and receive S in compensation. If the cash flow is worth more than S and the debtors can operate the project, the debtors receive the cash flow value, V; otherwise, they receive the project's salvage value, S.

The payoff lines of both debt and equity are depicted in Figure 1 and can be calculated from the equations:

$$\text{Equity payoff} \quad = \quad \text{Max}(V-P, 0) \quad (2)$$

[2] MELAMET, D. (1990), *Report of the Commission of Inquiry into State Assistance to East Rand Proprietary Mines Ltd*, Pretoria: Government Press, pp. 38, 45.

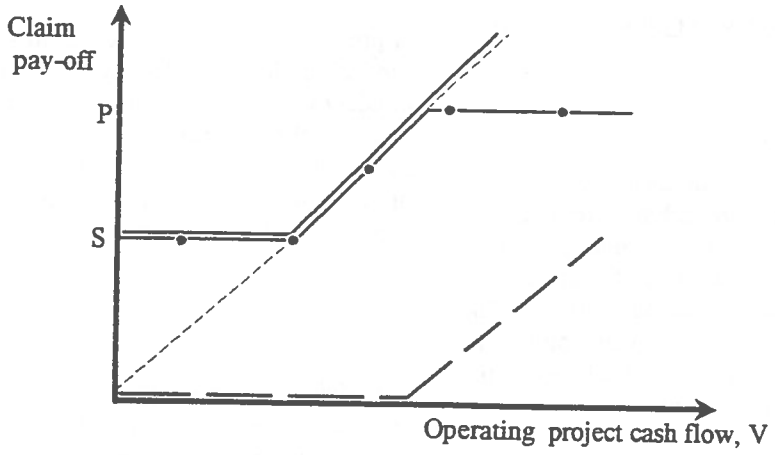

—•— Debt pay-off
— — Equity pay-off
——— 100% equity pay-off
------ Cash flow from an operating project

S = The salvage of the project
P = Debtor's principal repayment

FIGURE 1. Claimholder payoff lines for a simple project

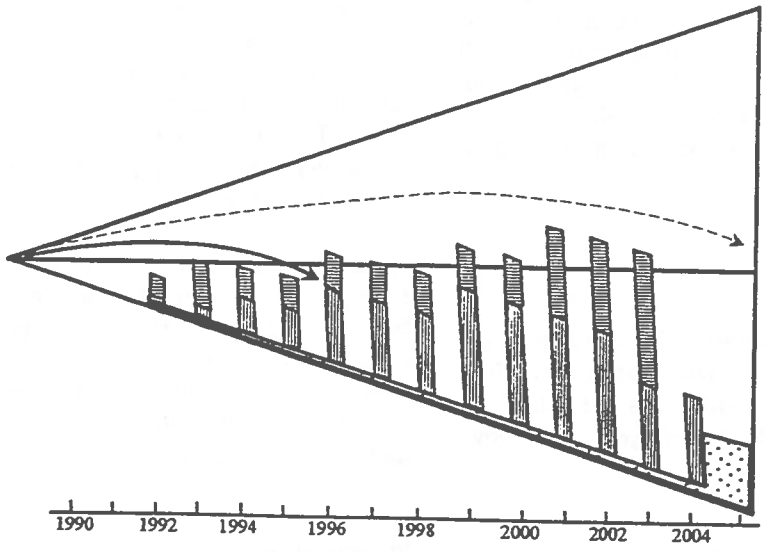

Area where ERPM is abandoned for salvage under 100% equity ownership
Area where ERPM is abandoned or refinanced due to a cashflow shortfall
Area where ERPM is abandoned due to lack of equity value
Path 1 : Debt servicing according to the Melamet Report.
Favourable operating and economic environment.
Path 2 : ERPM refinanced or abandoned due to debt servicing requirements

FIGURE 2. ERPM uncertainty envelop

$$\text{Debt payoff} = \text{Min}\left[P, \text{Max}(V, S)\right] \quad (3)$$

In this example, the presence of debt decreases the overall value of the project if the debtors are unable to operate the project. The loss of value occurs in abandonment situations where the project's cash flow is worth more than the project's salvage value. The debtors sell the project for its salvage value and incur an opportunity cost equal to the difference between the cash flow value and the project's salvage value.

THE FAR EAST VERTICAL SHAFT PROJECT

The original FEV shaft complex was sunk in the late 1950's and consisted of a single primary and secondary vertical shaft. This complex was never equipped and was used as a downcast ventilation shaft. The project entailed expanding and deepening the existing Far East Vertical Shaft facility into a twin primary and secondary shaft system. By the 31st December 1989, most of the FEV project had been completed and ore from this area was supplementing production from other areas of the mine.

Market Assumptions

The financial market is assumed to be frictionless and complete. The real riskless interest rate is 5%. The price of the financial asset, which has the same risk characteristics as the underlying project cash flow, follows a log-normal diffusion.

The Underlying Project and Cash Flow Value

The underlying operating cash flows were determined from the long-range plan presented by the Melamet Report and are equal to the difference between working revenues and working costs. The cash flows were first stated in nominal terms and then deflated using expected inflation indices. Using a real risk adjusted discount rate of 10%, the present value of the underlying cash flows was calculated to be R 309.9 million.

A proportional dividend process was used to model the project's cash flows. This type of process expresses the dividends or cash flows as a percentage of the present value of the remaining cash flows before the current cash flow is generated. The underlying cash flow present value is assumed to be log-normally distributed and has a volatility of 20%.

Capital Expenditure

The Melamet Commission Report indicates that capital expenditures are to be made in each year from 1990 to 2002. No details were provided regarding the nature of these expenditures. It is assumed that these outlays are used for the completion of the shaft complex and the replacement of equipment during the life of the project.

Mining Taxation

The South African gold mine tax regime is modelled as a portfolio of European call options written on the project's operating cash flow[3]. The tax rate was determined by applying the South African gold mining tax formula to the project's expected operating cash flows. The current management's tax rate is considered to be zero because there are large future interest payments, unredeemed capital expenditure and carried forward tax losses which may be applied against the operating cash flow. It is also assumed that the project's tax rate, when financed only by equity, is zero because of the unredeemed capital expenditure and carried forward tax losses. Third party management does not receive any tax relief because unredeemed capital expenditure and tax losses are not transferable under South African mining tax law.

Project Salvage Value

ERPM derives its salvage value either from the sale of its physical assets or as a going concern to a third party. The Melamet Report estimated that the salvage value of ERPM's physical assets was R66 million. This figure is used for the initial salvage value of the mine's assets on the 1st January 1990. Over the life of the project, this

[3] MAJD, S. (1984) *Applications of Option Pricing to Corporate Finance*, Unpublished Doctoral Dissertation, Massachusetts Institute of Technology, pp. 31.

figure changes due to additional capital expenditure and asset depreciation. It is assumed that capital expenditure increases the project's salvage value by 50% of the expenditure at the time the expenditure is made. The salvage value of the project's physical assets is also continuously depreciated at 13% per annum over time.

The project's value to a third party reflects the ability of the third party to default on capital expenditure and salvage the project's physical assets. It also incorporates the unique tax environment of the third party.

Project Financing

The project was financed by a combination of equity, preference shares, debt, government subsidies and government loan guarantees. As of 31st December 1989, the outstanding non-government components of ERPM's capital structure were:

a) A South African Bank Consortium loan of R220 million;
b) A First National Bank loan of R60 million;
c) Rand Mines Limited loan facility of R20 million drawn down to R17.3 million;
d) a overdraft facility;
e) 350 000 "B" Class Variable Rate Cumulative Redeemable Preference Shares; and
f) 16 632 000 common equity shares.

Further non-government financing was raised on the 1st January 1990 and included:

a) A further R2.7 million draw-down of the Rand Mines Limited loan facility of R20 million; and
b) A further Rand Mines Limited loan of R35 million.

ERPM also had a cash account in which a portion of the project's cash flow was deposited. Funds in this account were used to help cover debt servicing. If the project is abandoned, the funds in this account are combined with the project's salvage value and distributed between the project's claimholders.

The South African Government provided the following financing for the FEV project:

a) A loan guarantee for the principal, deferred interest and interest due to the South African Bank Consortium.
b) An interest subsidy of R22 million to be paid to the South African banking consortium on the 31st December of 1990, 1991 and 1992;
c) A pumping subsidy which is paid into the project on the 31st December in each year from 1990 to 1994; and
d) An interest-free pumping loan which provides funds on the 31st December of each year from 1989 through to 1992. Principal repayments are made on the 31st December of the years from 1993 to 1997.

The following covenants apply to ERPM's outstanding financial claims:

a) Contractual interest payments and principal repayments are due on the 31st December of each year. Loans will be called if interest payments and principal repayments are missed.
b) Principal repayments are made on the 1st January of each year and the loans are called if repayments are missed.
c) The seniority of the non-subsidy claims are:
   Rank 1: South African Bank Consortium loan of R 220 million.
   First National Bank loan of R60 million.
   Rand Mines Limited loan of R20 million.
   Rand Mines Limited loan of R35 million.
   Rank 2: Government pumping loan.
   Rank 3: Class B preference shares.
   Rank 4: Overdraft facility.
   Rank 5: Common equity shares.
d) If equity abandons the project, salvage value is distributed according to the seniority of the outstanding non-subsidy claims. The most senior claims are paid out first and any residual value is used to pay off the next most senior claims. This process continues until either the salvage value is totally distributed or the least senior claims are paid out. If the salvage value is insufficient to pay out all claims within a claimholder seniority category, salvage value is divided on a proportional basis. The proportion of salvage value a claim receives is determined by the ratio of value due to the claim upon abandonment to the total value due to the category. The claim's value in abandonment situations consists of the

outstanding principal, the currently due interest and outstanding deferred interest.

e) Initial debt funds are not payable in abandonment situations.
f) Both the Government interest subsidy and pumping subsidy are payable in abandonment situations.

The debtors are assumed to be unable to operate the project in abandonment situations.

Debtor Opportunity Costs

Equity abandons the project when either the project's cash flow is insufficient to cover the debt servicing requirements or the value of equity is less than the debt servicing requirements. The opportunity cost incurred in the former situation is called cash flow shortfall opportunity cost. The opportunity cost resulting from the latter reason is called financing opportunity cost.

Inherent Project Options

The project contains the following forms of management flexibility:

a) In the years 1990 to 2000, management may purchase the remaining project cash flows by making the required annual capital expenditure;
b) The project may be abandoned by management for its salvage value; and
c) Management may default on the debt servicing payments if the project cash flow is not sufficient to cover debt payments.

THE EVALUATION OF ERPM

The project and stakeholder claims were evaluated using the binomial option pricing technique. A computer program was developed using the Pascal programming language (version 7.0) to complete the calculations. Table 1 details the market value of each claim. The probability of the various project events occurring is presented in Table 2.

Figure 2[4] displays the possible project event outcomes. The triangular area outlines the possible project values and value paths that could occur over the life of the project. The vertical distance between the upper and lower sides of the triangle is indicative of the number of possible project values. As the project progresses, the uncertainty becomes greater and hence a larger number of project value outcomes are possible. The two arrows represent possible value paths which the project could follow. Many other value paths are also possible. Project events are represented by the shaded areas.

The vertical bars indicate areas where the project is abandoned due to debt servicing requirements. If the project value path crosses these bars, the current equity owners will be forced to either abandon the project to the debtors or restructure the current financing arrangements. There is a 78.7% chance of this occurring under the current financing arrangement.

The vertical bars are further sub-divided into two areas. The upper area represents the situation where the project cash flows are not large enough to pay for the debt servicing, yet the value of equity is greater than the debt servicing requirements. The probability of this occurring is 57.1%. This situation can be avoided by the current management providing a cash infusion.

The lower bar area represents the situation where project's value to the current management is less than the current debt servicing requirements. The project is abandoned to the debtors and the project's salvage value is equal to a maximum of either the project's value to a third party or the project's physical asset value.

Between the abandonment bars, the current management operates the project because there are no payments which will force the project to be abandoned. It is not in the current management's interest to abandon the project mid-year because the project's debtors receive all of the project's salvage value.

---

[4] Graphic representation from:
TRIGEORGIS, L. (1993), "The Nature of Options Interactions and the Valuation of Investments with Multiple Real Options," *Journal of Financial and Quantitative Analysis*, Vol. 2, No. 1, pp. 6 - 7.

TABLE 1. Market values of individual claims - current situation and refinancing scenario

Claim	Current claim values (Rand million)	Refinancing scenario - claim values (Rand million)
Equity in 100% equity financed project	210.6	210.6
Current equity claim	44.8	80.3
Cash account	9.6	2.2
Overdraft facility	-0.3	0.0
Government pumping loan	-20.2	-20.4
Government pumping subsidy	-18.6	-19.6
Government interest subsidy	-39.9	-39.9
Government loan guarantee	-78.9	-50.8
Consortium loan	228.1	227.3
First National Bank loan	36.6	0.0
Rand Mines Limited loan - R 20 million	9.4	0.0
Rand Mines Limited loan - R 35 million	-12.1	-7.8
Class B preference shares	1.8	8.8
Cash flow shortfall opportunity cost	33.7	26.0
Financing opportunity cost	16.5	4.5
Value of all current claims	210.5	210.6

TABLE 2. Project event probabilities - current situation and refinancing scenario

Project event	Current situation - probability of occurrence (%)	Refinancing scenario - probability of occurrence (%)
Abandonment under third party management	35.9	35.9
Abandonment if the project is 100% equity financed	13.8	13.8
Abandonment due to a cash flow shortfall	57.1	63.1
Abandonment due financing	21.6	7.3
Abandonment due to both a cash flow shortfall and financing	78.7	70.3

Comments

The option pricing framework has distributed project value between the stakeholders in a consistent manner. The maximum project value that can be distributed is the value generated under 100% equity financing because the project's tax schedule is the same whether it is financed by equity alone or a combination of equity and debt. In this case study, the existence of debt financing decreases the amount of distributable value and the value loss is accounted for as either cash flow shortfall opportunity cost or financing opportunity cost.

An additional benefit of the option pricing framework is its ability to value loan guarantees. Loan guarantees are traditionally difficult to evaluate because their value is based on the probability of payout. The government is shown to have incurred a significant liability by agreeing to guarantee the Consortium loan.

The probability of abandonment was determined by linking project events to the nodes of the underlying project value lattice. The probability of abandonment was determined to be 78.7%. This is much greater than the abandonment probability subjectively estimated by the Melamet Commission. The much smaller abandonment probabilities of the project under third party management and 100% equity financing suggest that the underlying project is viable.

REFINANCING ERPM

A possible strategy to improve the prospects for ERPM is to convert specific debt issues into equity. ERPM was re-evaluated with the First National Bank loan and Rand Mines Limited loan of R20 million converted into equity. The results are presented in Tables 1 and 2.

Comments

Financial restructuring re-distributes project value and changes the risk profile of each stakeholder. OPT is able to incorporate these aspects of financial restructuring into its assessment of the refinanced project. The proposed refinancing scheme decreases the probability of abandonment by an unremarkable 8.4%. It appears that a radical restructuring is necessary to decrease the abandonment probability to acceptable levels.

The decrease in pumping subsidy value and the increase in value of the Class B preference shares and the Rand Mines loan of R35 million reflects the increased chance of a full pay-out. The loan guarantee becomes a smaller liability because there is a smaller probability of pay-out. The decrease in value of debtor opportunity cost is also consistent with a decrease in abandonment probability.

Equity appears to have gained from the restructuring. However, a value loss of R6.2 million is apparent when the total current value of equity, the First National Bank loan and both Rand Mines Limited loans is compared to the value of equity in the refinanced scenario. This value loss is transferred to the remaining non-equity claims.

As structured, the refinancing scenario is not in the interest of equity, the First National Bank nor Rand Mines Limited. An equitable refinancing scenario can be determined by studying the value transfers. The non-equity claimholders remaining after the proposed refinancing (Class B preference shares, Government claims, the Consortium loan, and the overdraft facility) gain R33.4 million in value. This value originates from the reduction of debtor opportunity cost and the decrease in value of the cash account and the combined equity and converted debt claims (equity, Rand Mines Limited loans, and the First National Bank loan). The reduction of debtor opportunity cost and the decrease in the value of the cash account provides R27.1 million of the transferred value. This value may be freely transferred because the cash account claim is unable to contest the refinancing and the reduction of debtor opportunity cost is the result of a decrease in abandonment probability. The decrease in the combined value of equity and converted debt provides the remaining R6.2 million of transferred value. This transfer may be contested by these claims. Hence, the remaining non-equity claims may theoretically gain R27.1 million in value by converting select debt issues (the First National Bank loan and Rand Mines Limited loan) to equity and paying the new equity claim R 6.2 million.

CONCLUSION

Given the case study assumptions, option pricing theory was able to evaluate each component of ERPM's capital structure and explicitly incorporate the chance of project abandonment into the evaluation. Notably, option pricing theory was able to evaluate the government loan guarantee. This technique was further able to determine the probability of various project events occurring.

Both the Melamet Commission and the option pricing evaluation conclude that the underlying project is viable. However, the two analyses differ in their assessment of the project's future prospects with the current capital structure. The Melamet Commission subjectively estimated that the project had a 50% chance of success. The option pricing evaluation is a more rigorous approach and calculated the project's chance of success to be 21.3%. This discrepancy indicates that a more in-depth analysis of the project is required.

A refinancing scenario was proposed where the First National Bank loan and the Rand Mines Limited loan of R20 million was converted to equity. Option pricing the was able to determine the conversion's effect on the value of the remaining capital structure components. It also calculated that the debt conversion decreased the probability of project abandonment by an undramatic 8.4%. A more radical refinancing scheme is required to reduce the probability of abandonment to acceptable levels.

The refinancing scenario also revealed that the value of the government claims would be substantially increased by the proposed debt conversion. It appears that the South African tax authorities should reconsider their opposition to the conversion of debt into equity.

Though more research is required into such areas as taxation models and underlying asset price models, option pricing theory can provide valuable insights when used in conjunction with traditional project evaluation techniques. This case study is just one example of where option pricing theory can be usefully applied to mining evaluation problems.

REFERENCES

BLACK, F. and SCHOLES, M., 1973.
The Pricing of Options and Corporate Liabilites. *Journal of Political Economy*. Vol. 81, May - June, pp. 637 - 654.

COX, J., ROSS, S., and RUBENSTEIN, M., 1979.
Option Pricing: A Simplified Approach. *Journal of Financial Economics*. Vol. 7, October, pp. 229 - 263.

EAST RAND PROPRIETARY MINES LTD., 1980.
Long-Term Strategy: Physical and Financial Plans for the Mine and Proposed Increases in Borrowing Powers and Authorised Share Capital. *Circular to Members and Notice of General Meeting*. Johannesburg, 18 November 1985.

JONES, E. and MASON S., 1980.
Valuation of Loan Guarantees. *Journal of Banking and Finance*. Vol. 4, pp. 89 - 107.

MAJD, S., 1984.
Applications of Option Pricing to Corporate Finance. *Unpublished Doctoral Dissertation*. Massachusetts Institute of Technology.

MASON, S. and MERTON, R., 1985.
Contingent Claims Analysis in Corporate Finance. *Recent Advances in Corporate Finance*. Editors: E.I. Altman and M.G. Subrahmanyam, Homewood, IL., pp. 7 - 54.

MASON, S. and BALDWIN, C., 1988.
Evaluation of Government Subsidies into Large-Scale Energy Projects: A Contingent Claims Approach. *Advances in Futures and Options Research - Volume 3*. Editor: F.J. Fabozzi, JAI Press Inc, pp. 164 - 181.

MELAMET, D., 1990.
Report of the Commission of Inquiry into State Assistance to East Rand Proprietary Mines Ltd. Government Press, Pretoria, 70p.

MERTON, R., 1977.
On the Pricing of Contingent Claims and the Modigliani - Miller Theorem. *Journal of Financial Economics*. Vol. 5, No. 2, pp. 241 - 249.

MYERS, S. and Majd, S., 1990.
Abandonment Value and Project Life. *Advances in Futures and Options Research - Volume 4*. Editor: F.J. Fabozzi, JAI Press, pp. 1 - 21.

TRIGEORGIS, L., 1986.
Valuing Real Investment Opportunities: An Options Approach to Strategic Capital Budgeting, *Unpublished Doctoral Dissertation*. Harvard University.

TRIGEORGIS, L. 1993.
The Nature of Options Interactions and the Valuation of Investments with Multiple Real Options. *Journal of Financial and Quantitative Analysis*. Vol. 28, No. 1, pp. 1 - 20.

3.

geostatistics
géostatistiques

CAMI'95: 3rd Canadian Conference on Computer Applications in the Mineral Industry
Montréal, Québec, Canada, October 22-25, 1995

Random Kriging: A Useful Tool in the Case of Unsurveyed Drill Holes

George W. Verly
Placer Dome Inc.

ABSTRACT

Unsurveyed drill holes resulting in uncertain sample locations can be a significant problem for an ore reserve estimation. A slight modification of random kriging, however, can easily cope with this situation. In this paper, the theory and practice of random kriging is reviewed within the context of unsurveyed drill holes. The technique is then illustrated with a simple example. Results obtained from an actual orebody are also presented.

RÉSUMÉ

Une localisation imprécise d'échantillons appartenant à des sondages sans mesures de déviation peut être un obstacle de taille pour une estimation des réserves d'un gisement. Dans ce papier, la théorie et pratique du krigeage aléatoire est revue dans le contexte de sondages non arpentés. La méthode est ensuite illustrée au moyen d'un example simple et de résultats obtenus pour un gisement d'or.

INTRODUCTION

It occurs from time to time in geological exploration that holes are drilled without down hole surveys. There can be many reasons for this. For example, magnetite rocks hinders down hole survey measurements, or the priority during a particular exploration stage may be to get as many mineralized intercepts as possible at the expense of full down hole surveys.

If the prospect reaches the stage of pre-feasibility, these drill holes without down hole surveys (in short "unsurveyed drill holes") have to be dealt with. The usual solution is then to discard or to relocate them, or to do a combination of both. This, however, is not always satisfactory. Indeed, discarding drill holes is throwing away information that can be valuable. On the other hand, relocating drill holes amounts to creating false information because most of the estimation algorithms consider the sample locations as exact.

A better solution is to relocate the unsurveyed drill holes within zones of uncertainty and to use an estimation technique that can handle them.

One possible technique is random kriging, or a modified version of it. Random kriging has been available for quite a long time (Maréchal and Serra, 1970; David, 1977; Journel and Huijbregth, 1978). Its purpose was to speed up computations when computers were slow and expensive. The essence of random kriging is to consider that the samples are located randomly within a regular set of blocks. The size of the blocks must be so that not all of the sample spatial geometry is lost. Kriging is then based on the number of samples located within this regular configuration of blocks rather than on the exact sample locations. This greatly reduces the computer time required to search for samples and to build and solve the kriging systems.

In the last 15 years, however, computer power has increased and its cost decreased. As a consequence, techniques such as random kriging lost their appeal and sank into oblivion. This is unfortunate because, as will be seen in this paper, a slightly modified version of random kriging is a simple method to deal with unsurveyed drill holes.

Note that the problem of randomizing the location of uncertain data has been discussed by J.P. Chiles (1976), and has probably been used by several other people. It is, however, difficult if not impossible to find a clear description of the method in the case of unsurveyed drill holes. The objective of this paper is to describe the procedure in that particular situation and to illustrate it by means of an artificial and an actual dataset.

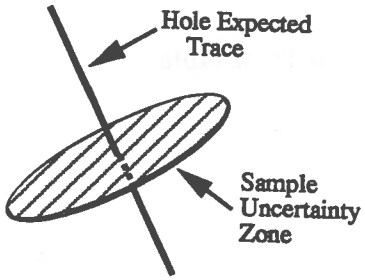

Figure 1: Illustration of expected hole trace and one sample uncertainty zone.

THEORY

The suggested procedure handles a mix of surveyed and unsurveyed drill holes. There are no conditions on the surveyed drill holes. There are, however, the following conditions on the unsurveyed drill holes (Figure 1):

- a best guess of the drill hole trace, called expected trace, is available;
- each drill hole sample is associated with a 2D uncertainty zone (that can be discretized);
- to each possible location of a sample within its uncertainty zone corresponds a probability.

The set of all sample uncertainty zones of a given hole form an irregular cylinder of uncertainty around its expected trace. How to get the uncertainty zones is discussed in the next section.

Geostatistics interprets the grade $z(x)$ (lower case) at location x as the realization of a random variable denoted $Z(x)$ (upper case). The set of random variables ($Z(x)$, x within the deposit) is a random function, also denoted $Z(x)$. Note that this does not mean that the deposit is random. On the contrary, there is one and only one deposit, but its characteristics are so complex, and the amount of available information is so limited that it cannot be known with certainty. Geostatistics is a tool to deal with that uncertainty.

Suppose that we want to estimate the grade of a block $Z_V(x_0)$ at location x_0, using the N surrounding sample grades $Z(x_i)$, $i=1$ to N, surveyed and/or unsurveyed. A linear estimate of the block is:

$$Z_V(x_0)^* = \sum_{i=1}^{N} w_i \times Z(x_i) \qquad (1)$$

where $(w_i;\ i = 1 \text{ to } N)$ are the weights applied to the available sample grades. The error of estimation is:

$$Er(x_0) = Z_V(x_0)^* - Z_V(x_0)$$

where $Z_V(x_0)^*$ is the random variable "estimated grade of block V at location x_0" and $Z_V(x_0)$ is the random variable "grade of block V at x_0". Er is the random variable of the error. The actual error e_r (realization of Er) is never known. Indeed, the estimated grade $z_V(x_0)^*$ (realization of $Z_V(x_0)^*$) is known if the surrounding sample grades $Z(x_i)$ are known, but the actual block grade $z_V(x_0)$ (realization of $Z_V(x_0)$) is not available. However, if the grade is considered stationary (quasi-intrinsic) over the deposit (Journel and Huijbregts, 1978, p. 57), the error is on average 0 if the sum of the weights is 1:

$$E\{Er(x_0)\}=0 \quad \text{if} \quad \sum_{i=1}^{N} w_i = 1$$

where $E\{\cdot\}$ denotes the expectation.

Ordinary Kriging

Note that so far, these equations are not different from those used by another method, say for example inverse square distance (ID^2): the estimate is a linear combination of the sample grades and the sum of the weights is 1. There is a difference, however, on the way the weights are chosen. ID^2 bases its choice on the euclidian distances between the samples and the centre of the block to be estimated whereas geostatistics tries to minimize the spread of possible errors. To achieve this, geostatistics first quantifies the spatial correlation of grade with the variogram $\gamma(h)$ where h represents the distance and angle between any 2 locations in the deposit (Journel and Huijbregts, 1978, p 31). It can then be shown that the variance of the error is (Journel and Huijbregts, 1978, p. 57):

$$Var\{Er(x_0)\} = 2\sum_{i=1}^{N} w_i \gamma(V,x_i) - \gamma(V,V) - \sum_{i=1}^{N}\sum_{j=1}^{N} w_i w_j \gamma(x_i,x_j) \qquad (2)$$

where:

- w_i is the estimation weight used for sample $Z(x_i)$, located at x_i;

- $\gamma(xi, xj)$ is the variogram value for the distance between the samples located at x_i and x_j (in short: variogram value between locations i and j)
- $\gamma(V,V)$ is the average of all variogram values between any two locations within block V;
- $\gamma(V,x_i)$ is the average of all the variogram values between any location in block V and sample location i;

All these (average) variogram values are easily computed from the variogram model and so is the variance if the weights are known. It is also possible to compute the weights such that the variance of the error is minimum, in other words to minimise the spread of the errors around the 0 expected value. This is called ordinary kriging (OK) if the sample locations are known, i.e. surveyed. The weights are obtained from the following system of equations (Journel and Huijbregts, 1978, p. 306) where the only new variable, μ, is necessary because there is a constraint on the weights (sum equals 1).

$$\begin{aligned} &w_1\gamma(x_1,x_1)+w_2\gamma(x_1,x_2)+\cdots+w_N\gamma(x_1,x_N)+\mu=\gamma(V,x_1)\\ &w_1\gamma(x_2,x_1)+w_2\gamma(x_2,x_2)+\cdots+w_N\gamma(x_2,x_N)+\mu=\gamma(V,x_2)\\ &\qquad\qquad\cdots\\ &w_1\gamma(x_N,x_1)+w_2\gamma(x_N,x_2)+\cdots+w_N\gamma(x_N,x_N)+\mu=\gamma(V,x_N)\\ &w_1\qquad+w_2\qquad+\cdots+w_N\qquad=1 \end{aligned} \qquad (3)$$

"Random" Kriging

The same equations (1, 2, 3) are used when the information is a mix of surveyed and unsurveyed drill hole samples. The (average) variogram values, however, are computed differently when an unsurveyed sample is involved. The possible cases are now discussed.

$\gamma(x_i, x_j)$

- If both samples $Z(x_i)$ and $Z(x_j)$ belong to surveyed drill holes, then $\gamma(x_i,x_j)$ is computed as for OK, i.e. is the variogram value between sample i and j locations.
- If both sample $Z(x_i)$ and $Z(x_j)$ belong to the SAME unsurveyed drill hole, their absolute locations are not known, but their locations relative to each other are assumed to be fixed as along the expected drill hole trace. Note that this assumes that, for a given unsurveyed hole, all the possible hole traces within its uncertainty envelope are parallel to the expected trace (at least, in the mineralized envelope of interest). $\gamma(x_i,x_j)$ is then computed as for OK, using the expected trace coordinates. Note that if $i=j$, then $\gamma(x_i,x_j) = \gamma(0) = 0$.
- If both samples $Z(x_i)$ and $Z(x_j)$ belong to two DIFFERENT unsurveyed drill holes, then $\gamma(x_i,x_j)$ is a weighted average of all the variogram values between any location of sample i and any location of sample j within their respective uncertainty zones:

$$\gamma(x_i,x_j)=\int_{U_i}\int_{U_j} p_i(u)p_j(v)\gamma(u,v)dudv \qquad (4)$$

where:

- U_i, U_j are the uncertainty zones of samples i and j;
- $p_i(u)$, $p_j(v)$ are the probability that the samples i and j are respectively located at locations u and v within U_i and U_j;
- $\gamma(u,v)$ is the variogram value of the distance between locations u and v.

- If one of the samples, say $Z(x_i)$, belongs to a surveyed hole whereas the other sample, $Z(x_j)$, belongs to an unsurveyed hole, then $\gamma(x_i,x_j)$ is the weighted average of all the variogram values between the fixed location i and any location of sample j within its uncertainty zone:

$$\gamma(x_i,x_j)=\int_{U_j} p_j(u)\gamma(x_i,u)du \qquad (5)$$

$\gamma(V, x_i)$

- The location of block V is always known;
- If sample $Z(x_i)$ belongs to an surveyed hole, then $\gamma(V,x_i)$ is computed as for OK, i.e. is the average of all the variogram values between the sample location i and any point within the block V;
- If sample $Z(x_i)$ belongs to a unsurveyed hole, then $\gamma(V,x_i)$ is a weighted average of all the variogram values between any location within block V and any location within the uncertainty zone U_i:

$$\gamma(V,x_i)=\frac{1}{V}\int_{V}\int_{U_i} p_i(v)\gamma(u,v)dudv \qquad (6)$$

$\gamma(V, V)$

- Since the location of the block V is always known, $\gamma(V, V)$ is the average of all the

variogram values between any two locations within the block.

Notes

- The procedure could be called semi-random kriging since only a fraction of the holes is unsurveyed. In addition, the distance between 2 samples within the same unsurveyed hole is fixed, and not randomized as if the 2 samples were from 2 different unsurveyed holes.
- All the average variogram values (i.e. the integrals) are easily computed once the various blocks and uncertainty zones are discretized.

PRACTICE

The practice of (semi) random kriging is very similar to any other type of geostatistical study. The following is based on a gold deposit that could be an underground mine. The deposit has been explored at an early stage with several unsurveyed (or partially surveyed) surface holes. Since then, many surface and underground holes have been drilled and fully surveyed.

Step #1 - Geology Model

This first step consists in building a geology model that indicates the main zones for the estimation, i.e the zones within which the characteristics of the mineralization remains relatively constant. This model is almost entirely based on geological interpretation. It is good practice, however, to confirm the significance of the zone boundaries via exploratory data analysis. For obvious reasons, only the surveyed drill holes should be used when defining the geology model. It is also important to realize that the geological model, even if very important, is not exact and must be considered so during the subsequent steps (especially when used to locate the expected traces of the unsurveyed drill holes)

Step #2 - Exploratory Data Analysis

This is a standard step in any geostatistical analysis and will not be discussed further. See for example Isaaks and Srivastava for more information (1989).

Step #3 - Structural Analysis

Again, this is a standard step (Isaaks and Srivastava, 1989). Only the surveyed drill holes samples should be used.

Step #4 - Unsurveyed Drill Hole Processing

If the surveyed drill holes provide a sufficient and consistent information, it might be possible to process statistically this information and define, for each unsurveyed hole, the "expected" deviations together with the possible uncertainty spread as a function of depth. It may also be possible to attach a weight to each possible location within the uncertainty zones around the expected deviations. If this is the case, go to the kriging step (Step 5).

Unfortunately, if the surveyed drill holes do provide information about deviations, it is not always in sufficient amount to allow a reliable statistical processing. It is then suggested to classify the unsurveyed holes as following:

1) possible to relocate with quasi certainty;
2) possible to relocate within zone of uncertainty;
3) impossible to relocate.

This classification is based on the geology model and the recorded surveyed drill hole deviations. There is some subjectivity attached to it and it is better to be conservative in order not to introduce "false" information in the data. In other word, it is better to classify a hole in Class 2 rather than in Class 1 if there is any doubt about its Class 1 classification. After relocation, there is no difference between the surveyed drill holes and those from Class 1. Holes belonging to Class 2 are those for which this random kriging procedure can be used. Holes from Class 3 are considered hopeless and discarded.

For each Class 2 hole, the expected trace must be defined together with the uncertainty zone. This step is a mix of manual and computer processing. Note that the manual work is not a daunting task since only the drill hole intercepts with the mineralized portion of the geology model are important. Commercial 3D visualization software are helpful to compute the expected traces, for example by getting the coordinates of the hole intercepts with the 3D geological envelope, and eventually by computing the coordinates of the samples between these intercepts. Simple rules can then be designed to automatically defined the uncertainty zones. The simplest one is to discretize a circular or elliptical uncertainty disk around each sample (Figure 1). The disk can be perpendicular to the expected drill hole trace, or parallel to the geological envelope at the hole

entry and/or exit points (again, 3D visualization software are most useful here). An orientation parallel to the envelope (instead of perpendicular to the hole) comes in handy if one wants to avoid sample uncertainty zones crossing geological boundaries. The size and/or the orientation of the uncertainty ellipses can be constant or gradually changing. Eventually, probabilities can be attached to the sample locations within their zones of uncertainty using, for example, the knowledge gained from similar drill holes which have been fully surveyed.

It is important to realize that the whole procedure, even if it is a reasonable one given the circumstances, is still subjective. As a consequence, one must be conservative as already mentioned. The results after kriging should also be checked to see that the unsurveyed drill hole information has been used as an "add-on" to the surveyed drill hole information and has not replaced it.

Step #5 - Kriging

This step is very similar to an ordinary kriging step with respect to the search, the minimum and maximum number of samples to be used per estimate, etc. The only difference is the number of points to use to discretize the sample uncertainty zone which are needed to compute the average variogram values (eqts 4, 5, 6). Although no test has been done, 16 to 25 points regularly located within each sample zone appears reasonable.

CASE STUDY #1

The objective of this case study is to illustrate the concept of random kriging and its impact on the estimation results. The following simplistic and not very realistic situation has been chosen (Figure 2a):

- the zone to be estimated is a 100x15 metre rectangle along the horizontal and vertical directions respectively;
- the blocks to be estimated within the rectangle are 5x1 metres;
- three vertical drill holes are available: two at the extremities of the rectangle, and the other (unsurveyed) somewhere in the middle;
- the drill hole samples are 1 metre long;
- the horizontal limits of the rectangle are "hard" boundaries, in other words, the blocks within the rectangle are estimated using the samples located in the rectangle only;
- the average grade increases linearly from 0.4 g/t Au (top) to 6 g/t Au (bottom) in each drill hole;
- the variogram is spherical with no nugget; the horizontal and vertical ranges are 50 and 5 metres respectively; the sill has been standardized to 1.

Four situations have been investigated with respect to the unsurveyed drill hole:

1) the hole is discarded;
2) the hole is relocated in the middle without uncertainty;
3) the hole is relocated in the middle within a 20 metre uncertainty zone;
4) same as 3, within a 60 metre uncertainty zone.

In both cases 3 and 4, the possible locations of the unsurveyed drill hole are considered to be uniformly distributed within the uncertainty zone. In other words, the weights (probabilities) attached to each possible location are constant.

Figures 2b to 2i show the estimated grades and the corresponding variances in each case. It is clear from the figures (2b, c) that Case No 1 does not achieve a proper estimation in the middle of the rectangle because the unsurveyed central hole has been discarded. Note the estimated grades close to the average and the high estimation variances. Case No 2, on the other hand, is over-optimistic. If the estimated grades appear to be reasonable (2d), the estimation variances in the middle of the rectangle are too low (2e) because no uncertainty about the middle drill hole location has been considered. This clearly is a problem if the variance is used to categorize the block estimates as "measured" or "indicated". Case No 3 (2f, g) appears to achieve a good trade-off: estimated grades that are reasonable, and estimation variances that are not too low. Of course, that trade-off is as good as the uncertainty zone limits are good. Note that the layering of the mineralization has been reproduced because the locations of the samples within the unsurveyed drill hole are not random with respect to each other. In other words, the low grade samples are always in the top layers of the uncertainty zone, whereas the higher grade samples are in the bottom layers. Case No 4 (2h, i) shows some degradation in the estimation caused by a dramatic increase of the uncertainty zone. Some improvement could have been obtained by attaching probabilities to the possible locations of the central holes, with increasing values from the limits to the centre. But this is roughly equivalent to reducing the extent of the drill hole uncertainty zone.

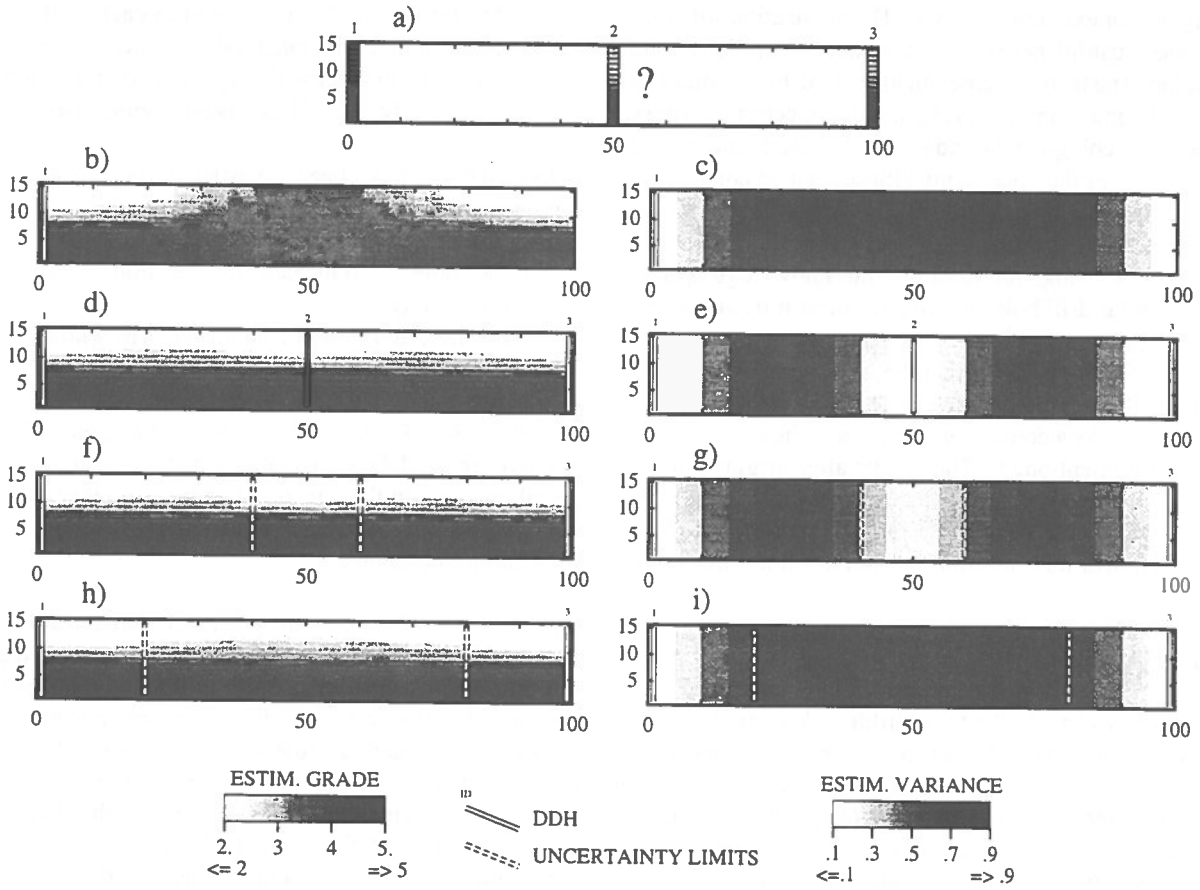

Figure 2: Case study # 1: random kriging results in some simple situations. The top figure (a) shows the 3 drill holes and their sample grades. The location of the central hole is uncertain. The other figures show the estimated grades (left) and variances (right) in 4 cases: central hole discarded (b,c), central hole relocated with no uncertainty (d,e), central hole relocated within 20 (f,g) or 60m (h,i) metre uncertainty zones.

CASE STUDY #2

Random kriging has been applied to a Au deposit located in NW Ontario. The deposit has been drilled from surface (180 holes) and underground (175 holes). 130 of the surface holes, completed during an early exploration stage, have been acid tested only, due to the magnetic host rocks hindering down hole surveys. Only the recent surface holes have down hole surveys (using a light log instrument). The underground holes are short and do not have down hole surveys. An analysis of the most recent holes indicates that the lateral surface hole deviations can be significant at the mineralization level: sometimes more than 20 metres. Only the underground holes and the surveyed surface holes were used to create the geology model and compute the variograms. It was decided, however, to use the unsurveyed surface holes for the estimation because some of them fill gaps within the drilling pattern. The unsurveyed drill holes were therefore classified by the geologist into 3 groups:

1) negligible deviations;
2) significant deviations;
3) deviations beyond reconciliation.

Group No 1 holes were relocated without uncertainty. Group No 2 holes were relocated and assigned uncertainty zones varying from 5 to 10 metres laterally from the expected traces. Group No 3 holes were discarded.

Several types of kriging were then completed on a test zone:

1) kriging using the underground holes only (which do not deviate significantly because of their short lengths);
2) kriging using all the holes without uncertainty;

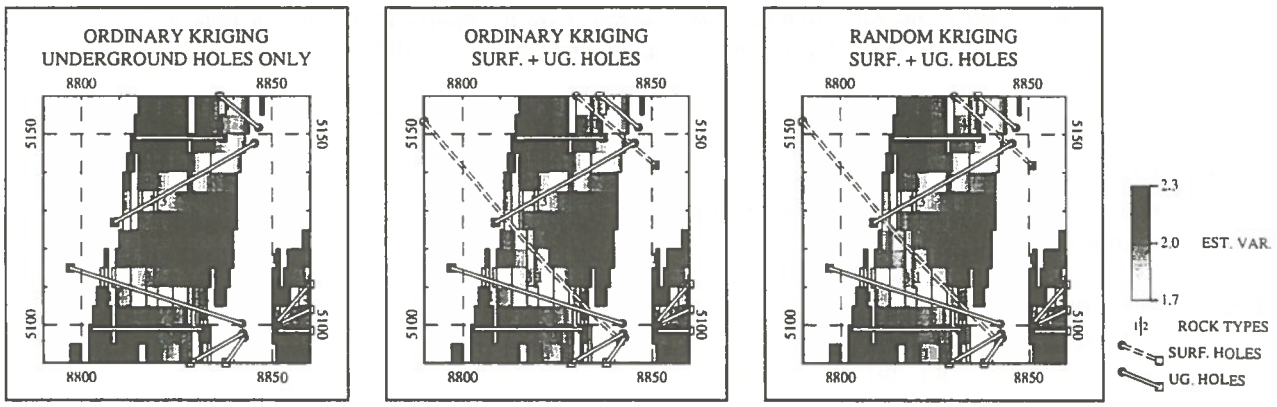

Figure 3: Case study # 2: random kriging results for an actual gold deposit. Only a typical section with the estimation variances is shown for three different cases: using underground holes only, i.e. a pessimistic case (left); using all the holes without uncertainty, i.e. an over optimistic case (middle); and using all the holes with their respective uncertainty, i.e the realistic case (right).

3) kriging using all the holes with their uncertainty if necessary, i.e. random kriging.

Figure 3 shows a typical section after kriging. Only the estimation variances are shown as they better illustrate the difference between the various options. It can be seen from Figure 3, Case No 3, that the random kriging estimation variances in the vicinity of the unsurveyed drill hole (dashed hollow line) are between the ordinary kriging variances obtained with the surveyed holes only (Case No 1) and all the holes without uncertainty (Case No 2). This reflects the fact that random kriging is using the additional unsurveyed information together with its associated uncertainty.

CONCLUSIONS

Unsurveyed drill holes have sometimes to be considered for an ore reserve estimation. The easiest solution is either to discard them as unreliable or to consider their most plausible locations as exact. Both solutions are unsatisfactory. The first one because it discards information that could be valuable; the second because it creates false information.

In this paper, a simple modification of random kriging has been suggested as a possible solution to the problem. The method consists of defining zones of uncertainty around the unsurveyed drill holes. These zones are then incorporated in the kriging solution by means of average variogram values that reflect the degrees of uncertainty.

The advantage of the method is its ability to handle both surveyed and unsurveyed drill holes consistently. The results are better and more realistic estimated grades and variances, especially in the unsurveyed drill hole vicinity. This in turn implies a better classification of the reserves if they are based on the estimation variance.

The method has been presented as an enhancement to ordinary kriging. Similar alternatives can be implemented for other types of kriging and for stochastic simulations.

ACKNOWLEDGEMENT

The author wishes to thank Placer Dome Inc. for permission to publish this paper. He is also grateful to Graham Barber and Marc Jutras for useful discussions and technical support.

REFERENCES

Chiles, J.P. (1976).
"How to adapt kriging to nonclassical problems", *Advanced Geostatistics in the Mining Industry*, Eds. Guarascio et al, D. Reidel Publ. Co. pp. 80-89.

David, M. (1977).
Geostatistical Ore Reserve Estimation, Elsevier Scientific Publising, Amsterdam, 364pp.

Journel, A.G. and Huijbregts, Ch.J. (1978).
Mining Geostatistics, 2nd printing (revised), Academic Press, London, 600pp.

Isaaks, E.H., Srivastava, R.M. (1989).
An Introduction to Applied geostatistics, Oxford University Press, Oxford, 561 pp.

Maréchal, A. and Serra, J. (1970).
"Random Kriging", Note No 188, CGMM Fontainebleau.

Unsmoothed Estimation with Dense Secondary Information Using Probability Field Technique.

Gilles Bourgault and André G. Journel
Geological and Environmental Sciences Department,
Stanford University, Stanford, CA

ABSTRACT

Cokriging allows estimating a primary variable taking into account linearly correlated secondary information. However, cokriging calls for a linear relationship between variables and produces smooth estimates. An algorithm is proposed for producing unique, unsmoothed accurate estimates of the primary variable using dense secondary information. The algorithm utilizes the probability field concept whereby uniform scores of the secondary values are used to sample the conditional probability distributions of the primary variable. The algorithm is shown to reproduce both the sample histogram and variogram of the primary variable whenever the two variables are related by any monotonic, possibly non-linear, statistical regression.

RÉSUMÉ

Le cokrigeage permet l'estimation d'une première variable en considérant une information plus dense provenant d'une seconde variable. Le cokrigeage est bien adapté aux situations où les variables sont en relation linéaire. Cependant, même si la seconde variable est densément échantillonnée, il produit un estimé lisse de la première variable. Une approche est proposée afin d'obtenir des estimés qui reproduisent toute la variabilité des valeurs mesurées. L'algorithme proposé est basé sur le concept de champs de probabilités, où la transformée uniforme des valeurs observées de la seconde variable sont utilisées pour echantillonner la distribution modélisant l'incertitude locale de la variable principale. L'approche proposée permet de reproduire l'histogramme des données ainsi que leur variogramme lorsque les variables sont en relation monotonique croissante.

INTRODUCTION

This paper presents a new approach to condition the estimation of a primary variable by information provided by a secondary variable known at every node of the estimation grid. This corresponds to the case of a phenomenon observed through sparse primary data and secondary data available on a much denser grid. For example in the mining industry, the attribute of primary interest could be a concentration of metal (e.g. gold, copper ...) whereas the secondary and exhaustive information could be geophysical, remote-sensing or any low cost data. The secondary information could also be a simulated realization of a densely but not exhaustively sampled variable.

The approach proposed is based on the probability field (*pf*) concept (Srivastava, 1992, Froideveaux, 1992) whereby simulated probability values, denoted $p_s(\mathbf{u})$, are used to sample local conditional probability distributions for the primary variable, one at each node of the simulation grid. These probability $p_s(\mathbf{u})$ are obtained by any non-conditional simulation allowing to reproduce the covariance of the uniform transform of the primary data. The local conditional probability distributions, modeling the local uncertainty, are obtained by any appropriate geostatistical algorithm (see Deutsch and Journel, 1992, p.72).

Instead of a non-conditional simulation, it is proposed here to use the uniform transform of the secondary data as a realization of the probability field of the primary variable. This yields a unique realization of the primary variable since the probability field value at each grid node is now unique as the realization of the secondary variable is unique. Multiple realizations are available only in cases of repetitive surveys of the secondary variable or if

that secondary information is itself provided by stochastic simulation.

This paper discusses the necessary conditions for using the uniform transform of a secondary variable as probability field for a primary variable. Examples and comparisons with cokriging are shown in using synthetic and actual data sets.

METHODOLOGY

In general, the relationship between two variables can be modeled as:

$$Z_1(\mathbf{u}) = f(Z_2(\mathbf{u})) + \varepsilon(\mathbf{u}) \qquad (1)$$

where $Z_1(\mathbf{u})$ is the primary variable, $Z_2(\mathbf{u})$ the secondary variable, $\varepsilon(\mathbf{u})$ a noise component and $f(\cdot)$ a regression function. Cokriging amounts to approximate the relationship $f(\cdot)$ by a linear one. In the earth sciences, however, non-linear relations are frequent. Thus, the motivation for a technique that does not call for linearity between the two variables. As illustrated by Bourgault and *al.* (1995), underlying a non-linear relationship in the original values there may be a linear relationship in their ranks. Indeed, if $f(\cdot)$ is monotonic increasing (or decreasing) the rank values of both variables are linearly related. The standardized rank of any datum $z(\mathbf{u})$[1] is defined as its uniform transform valued in [0,1]:

$$v(\mathbf{u}) = F_Z(z(\mathbf{u})) \qquad (2)$$

where $F_Z(z)$ is the stationary cumulative density function (*cdf*) of variable $Z(\mathbf{u})$. To any monotonic increasing relationship between variables $Z_1(\mathbf{u})$ and $Z_2(\mathbf{u})$ corresponds a linear relationship between their standardized ranks:

$$v_1(\mathbf{u}) = v_2(\mathbf{u}) + \eta(\mathbf{u}) \qquad (3)$$

where $\eta(\mathbf{u})$ is a noise of amplitude related to that of $\varepsilon(\mathbf{u})$ as defined in relation (1). If the magnitude of the noise $\eta(\mathbf{u})$ is deemed small, one may use the rank $v_2(\mathbf{u})$ value in lieu of the unknown rank value $v_1(\mathbf{u})$. In other words, the field of $v_2(\mathbf{u})$ values, which is better sampled than the field of $v_1(\mathbf{u})$ values, can be used as probability field for the primary variable. Aspects of the noise component, either in the z_2-data or in the v_2 values, can be filtered out by factorial kriging (Ma and Royer, 1988). Then, the uniform scores of the filtered secondary data can be used as probability field for the primary variable. Only the Z_2 spatial structures (components seen on its variogram) which are relevant to the estimation of Z_1 should be kept, all others structures should be filtered out (Deutsch and Journel, 1992, p.68). Note also that any (co)kriging technique already filters out the noise component.

[1] Capital letters denote variables whereas small letters denote an actual value.

Local Uncertainty Modeling.

The modeling of the uncertainty about an unsampled primary value can be done in multiple ways. The two most commonly used approaches consider either a multi-Gaussian model or an indicator kriging model (Deutsch and Journel, 1992, chap.V). In this paper the multi-Gaussian model is adopted: the local conditional cumulative distribution functions (*ccdf's*) of the normal score transform Y_1 of the primary variable Z_1 are assumed Gaussian with mean and variance given by a simple kriging of the y_1-data. The local Gaussian *ccdf* of the normal score transform $Y_1(\mathbf{u})$ at location $\mathbf{u}$ is denoted:

$$F_{Y_1}(\mathbf{u}; y_1) = Prob\{Y_1(\mathbf{u}) \leq y_1 \mid (n)\} \qquad (4)$$

where (n) represents conditioning by n neighboring primary normal scores data.

Sampling the Local Distributions.

The local *ccdf's* (4) are sampled in order to provide realizations of the variable Y_1 at the location $\mathbf{u}$. It is proposed here to use the observed uniform score of the secondary variable, $v_2(\mathbf{u})$ to sample the local Y_1 *ccdf*. More precisely, the uniform score of datum $z_2(\mathbf{u})$; i.e.

$$p_s(\mathbf{u}) = v_2(\mathbf{u}) = F_{Z_2}(z_2(\mathbf{u})) \qquad (5)$$

is used to draw the simulated y_1-value:

$$y_s(\mathbf{u}) = F_{Y_1}^{-1}(\mathbf{u}; p_s(\mathbf{u})) \qquad (6)$$

The $v_2(\mathbf{u})$ value acts as a probability field value to generate a simulated value of variable Y_1 at location $\mathbf{u}$. The simulated value $y_s(\mathbf{u})$ is unique since the $v_2(\mathbf{u})$ value is unique. The simulated values $y_s(\mathbf{u})$ are then backtransformed into the original z_1-data units. This backtransformation ensures reproduction of the z_1-histogram.

Pros and Cons.

Unlike a model of linear coregionalization (cokriging), the proposed approach does not require any assumption of regression linearity of the primary variable upon the secondary. The probability field approach does not require modeling of the variogram of the secondary variable and the cross-variogram between both variables. Cokriging capitalizes on the linear correlation between both variables whereas the probability field approach capitalizes on the linear relationship of their ranks. The latter calls for a monotonic increasing (or decreasing) regression function between both variables (see relation 1).

A disadvantage of the proposed approach is that reproduction of the Z_1-covariance (variogram) is not directly guaranteed. The simulated pattern of dependence of the Z_1-simulated values is borrowed from the Z_2-covariance, more precisely, from the covariance of the v_2 conditioning values, see equations (5) and (6). This is not a problem if the spatial structures seen in the secondary information are all relevant to the primary variable. In some cases, it may be necessary to filter out from Z_2 or V_2 some specific structures seen in the secondary information but not shared by the primary variable (Bourgault and *al.*, 1995).

CASES STUDY

The first case study uses the GSLIB synthetic data set (Deutsch and Journel, 1992, p.34). This allows comparing the results to a known truth. The second case study uses a soil salinity data set (Lesch and *al.*, 1995). Both cases can be assimilated to issues related to geochemical exploration in mining exploration. The methods used and conclusions are easily transferable.

The Synthetic Data Set.

The primary variable (Z_1) of the public-domain GSLIB data set used as reference (the truth) is shown in Figure 1a. A secondary variable (Z_2) is then built from that primary variable such as to generate a non-linear relationship between both variables. Figures 1 present grayscale maps and scattergram of the Z_1 and Z_2 reference values. The scattergram shows a non-linear and monotonic increasing relationship. The rank correlation between the two variables Z_1 and Z_2 is seen to be higher (0.7) than their linear coefficient of correlation (0.5).

Figures 2 give the grayscale map for the uniform scores v_1 and v_2, and their crossplot. Unlike the scattergram of the original values, z_1-z_2, the uniform scores scattergram shows a linear relationship. An interesting feature seen on that uniform scores scattergram is the lesser scattering of both low and high rank values. This means that the secondary variable is more informative about extreme Z_1 values than about its middle class values. Thus, uniform scores of the secondary variable could be used to detect Z_1 extreme values. Note also that similarities and differences between the spatial patterns of Z_1 and Z_2 appear clearer when looking at the uniform scores maps than when looking at the original values maps (compare Figures 1a, 1b with 2a, 2b). Because uniform score values are bounded between [0,1], they allow a more objective and unit-free comparison between primary and secondary information.

Using 25 data (see Figure 1c) randomly sampled from the 2500 primary values (Figure 1a), the probability field approach as previously described is applied. The secondary uniform scores values, once filtered of their nugget effect (noise component) by factorial kriging, were used to sample the local *ccdfs* of the primary variable, see Figure 2b. Because unreliable statistics might result from only 25 samples the exhaustive primary variable histogram (not shown) is used for the normal scores transform and backtransform. In real applications with very few primary data, such statistics might be imported from other areas better sampled and showing similar geological environment. The resulting estimated image (Figure 3a) is to be compared with the results of ordinary cokriging (Figure 4a). Cokriging was implemented using all 25 primary data and the 9 nearest neighbor secondary data (including the co-located) for each node. Exhaustive primary and secondary information were used to model the direct variograms and cross-variogram needed for that cokriging (not shown).

Even with so few primary data, using the uniform scores of the secondary variable as probability field values allows to reproduce very well the spatial patterns of the reference Z_1 variable (compare Figures 1a and 3a). This result highlights the importance of an exhaustively

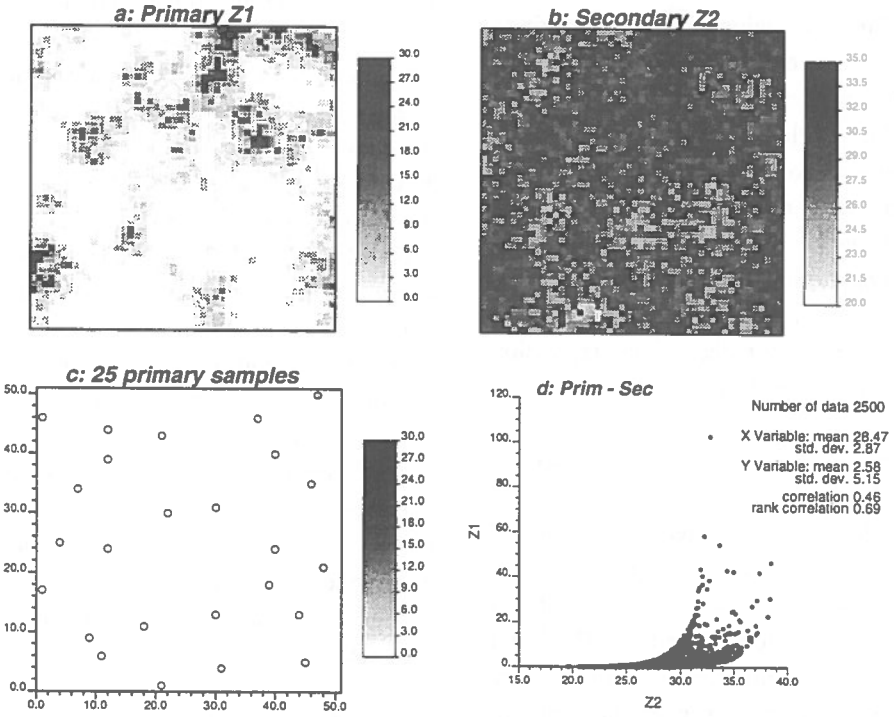

Figure 1: *Primary and secondary information map with their scattergram.*

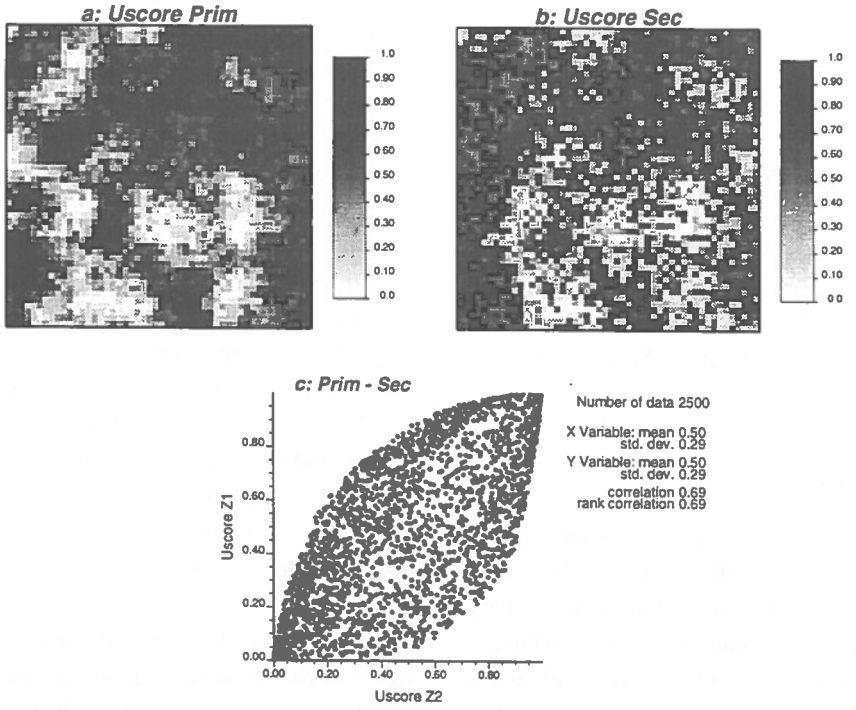

Figure 2: *Primary and secondary uniform scores map with their scattergram.*

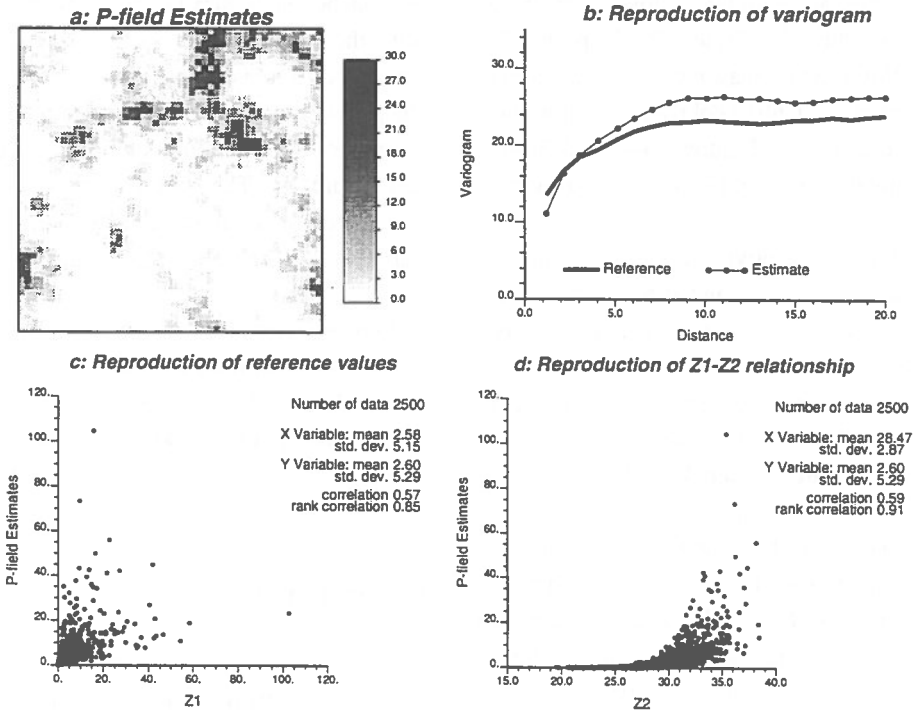

Figure 3: *Map, variogram and scattergrams of estimates from the p-field approach.*

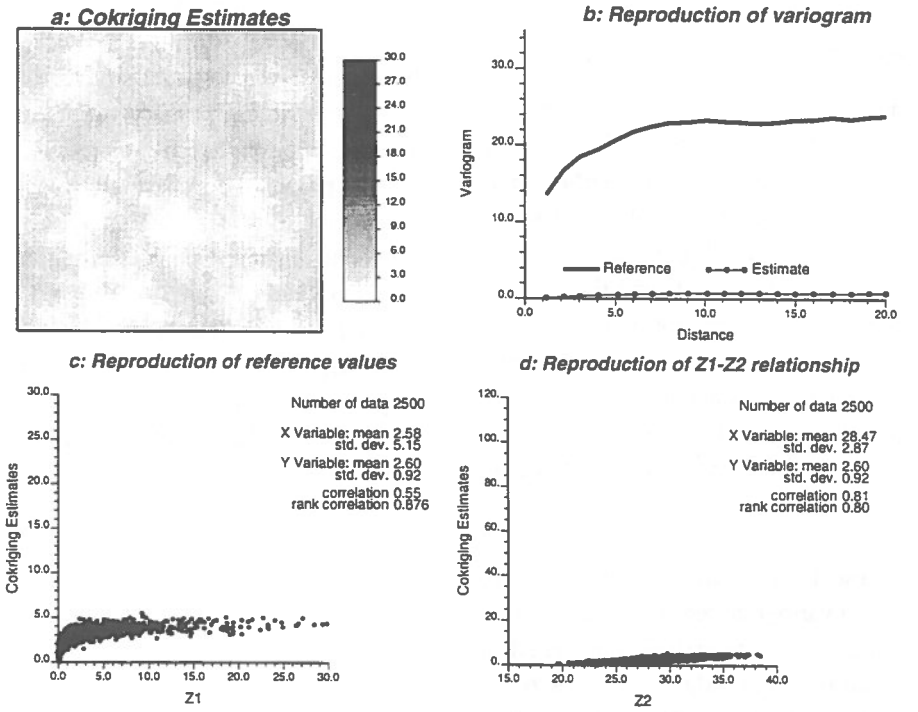

Figure 4: *Map, variogram and scattergrams of estimates from cokriging.*

sampled secondary information no matter its poor correlation with the primary variable as long as ranks are well correlated. As shown in Figure 3b, the probability field approach allows also a reasonable reproduction of the reference variogram. Unlike cokriging no smoothing effect is observed (compare Figures 3a-4a and 3b-4b), the cokriging estimates yield an almost zero variogram.

Because cokriging is a moving average process, its maximum estimated value is bounded by the maximum sampled value used for estimation. This has for consequence that all the true values higher than the maximum sampled value ($\approx$ 6.0) are underestimated. Such conditional bias is not observed with the proposed p-field approach (compare Figures 3c and 4c). The variance of the cokriging estimates is very low ($\approx$ 1.0) whereas that of the p-field reproduces well the variance of the reference values ($\approx$ 25.0). In addition, the p-field approach reproduce much better the non-linear relationship observed in the scattergram of the primary and secondary variables (compare Figures 1d, 3d and 4d). Cokriging tends to force a linear relationship between the estimates of the primary variable and the values of the secondary variable (Figure 4d).

A Soil Salinity Data Set.

This data set comprises 315 soil core measurements of electrical conductivity (EC, Figure 5a) and 2385 measurements of soil electromagnetic response (EM, Figure 5b). The regular 100m x 100m grid of EM data defines the extent of the study area. Figure 5c presents the scattergram for the 315 co-located EC and EM data. A non-linear monotonic increasing relationship is observed. The relationship of their uniform scores (ranks, see Figure 5d) is seen to be linear, with smaller scattering for the high uniform scores (high ranks). Thus, the secondary variable (EM) is more informative about high EC values than about low EC values.

Figures 6a-6b present the unique estimated EC map and the corresponding variogram reproduction when using the uniform scores of the EM variable (nugget effect is filtered) as probability field values. Figures 6c-6d present the results obtained using cokriging. In this case, simple cokriging was implemented using the 24 nearest primary data and the 25 nearest secondary data (including the co-located) for each node. The p-field and cokriging approaches yield similar maps, both reproduce reasonably the spatial patterns of the secondary information (compare Figures 6a-6c with 5b). The variograms of the p-field estimates are similar to the variograms of the secondary information, with no smoothing, as expected, see Figure 6b. The cokriging estimates although more noisy show less variance, as demonstrated by the lower variogram sills.

Figures 7 compare the histogram of p-field and cokriging estimates with the EC sample histogram. The p-field approach reproduces quite well the positively skewed sample histogram. Cokriging tends to yield estimates with a more symmetric and smoothed histogram.

CONCLUSIONS

A non-linear and unsmoothed approach is proposed to condition the estimation of a primary variable by dense secondary information. The resulting estimates are conditionally unbiased but tend to reproduce the spatial patterns of the secondary data. This emphasizes the importance of using correctly pre-processed secondary information. In some cases, it is necessary to filter out from the secondary data spatial structures or noises that are not relevant to the primary variable. When both variables present a high (rank) correlation in their high values, the proposed approach allows using the secondary information to detect locations of high primary values. Similar to a simulation, the proposed probability field approach yield estimates that reproduce well the entire sample histogram. The typical smoothing effect of kriging/cokriging is corrected, yet the estimates remain locally accurate as long as the secondary information has good rank correlation with the co-located primary variable.

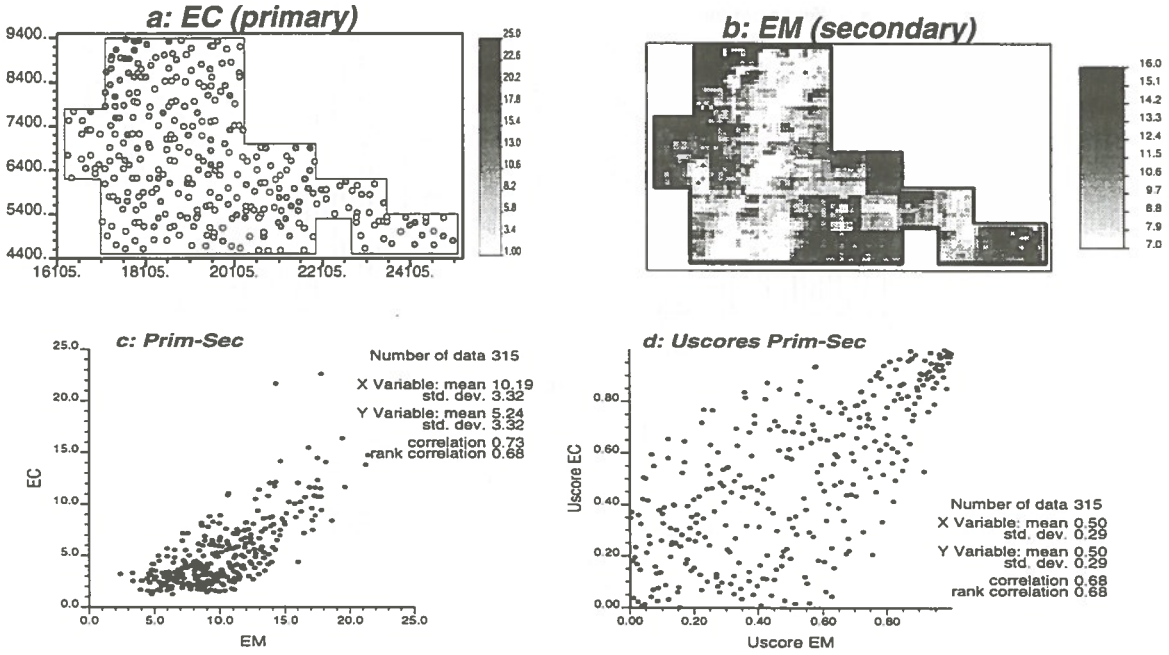

Figure 5: *Electrical conductivity and electromagnetic response maps with their original and uniform score values scattergrams.*

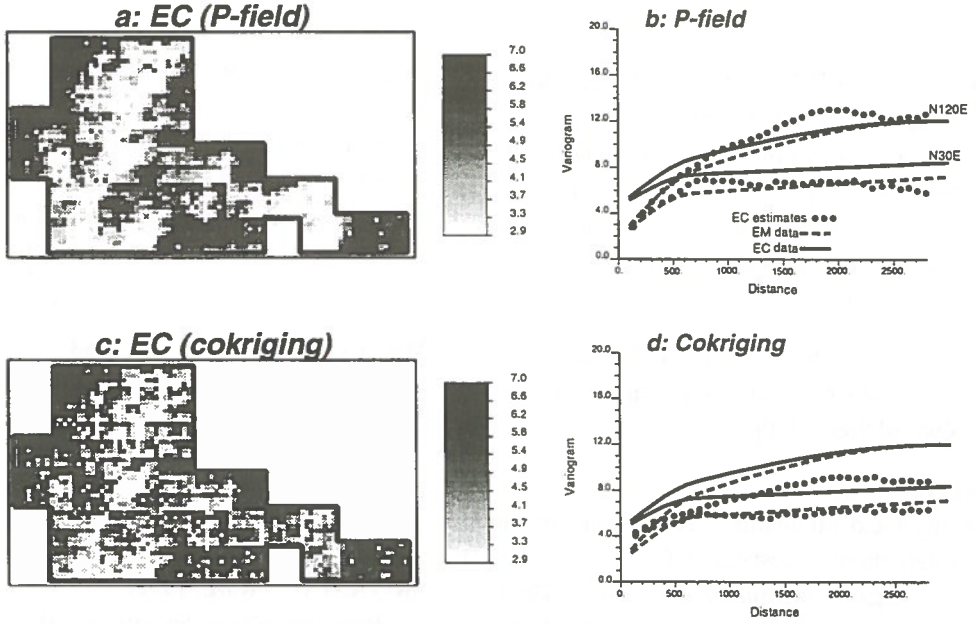

Figure 6: *Map of p-field and cokriging estimates with the corresponding variogram reproduction for the electrical conductivity.*

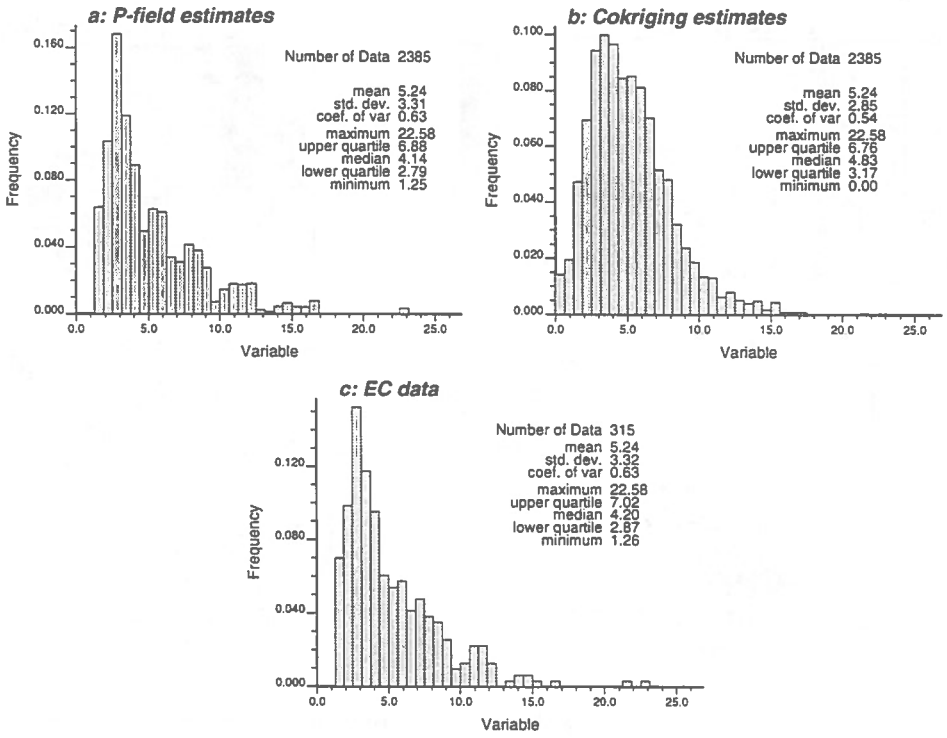

Figure 7: *Comparison of p-field and cokriging estimates histograms with the sample histogram.*

REFERENCES

BOURGAULT, G., JOURNEL, A.G., LESCH, S.M., RHOADES, J.D. and CORWIN, D.L., 1995.
Geostatistical Analysis of a Soil Salinity Data Set. Proceedings of the 1995 Bouyoucos Conference, Application of GIS to the Modeling of Non-Point Source Pollutants in the Vadose Zone, May 1-3 95, Riverside, California.

DEUTSCH, C.V. and JOURNEL, A. G., 1992.
GSLIB: Geostatistical Software Library and User's Guide, Oxford Press, 340p.

FROIDEVEAUX, R., 1992.
Probability Field Simulation. Proceedings of the Fourth International Geostatistics Congress, Soares A. (ed.), Geostatistics Tróia '92, Quantitative Geology and Geostatistics, Volume 1, Kluwer Academic Publishers, pp. 73-83.

LESCH, S.M., STRAUSS, D.J. and RHOADES, J.D., 1995.
Spatial prediction of soil salinity using electromagnetic induction techniques. 1. Statistical prediction models: A Comparison of multiple linear and cokriging., Water Resources Research, Vol. 31, No. 2, p. 373-386.

MA, Y.Z. and ROYER, J.J., 1988.
Local Geostatistical Filtering Application to Remote Sensing, in: Geomatematics and Geostatistics Analysis Applied to Space and Time Dependent Data, Sciences de la Terre, Série Informatique, Nancy, vol. 27, p. 17-36.

SRIVASTAVA, R.M., 1992.
Reservoir Characterization with Probability Field Simulation, SPE paper no. 24753, Soc. of Pet. Eng.

CAMI'95: 3rd Canadian Conference on Computer Applications in the Mineral Industry
Montréal, Québec, Canada, October 22-25, 1995

Geostatistical Modeling of El-Gidida Iron Ore Deposit

Mohamed A. Gouda, Mohamed R. Moharam
Mining and Petroleum Engineering Department, Faculty of Engineering
Al-Azhar University, Cairo, Egypt

Eileen Ashworth
Mining Engineering Department
South Dakota School of Mines & Technology, Rapid City, USA

ABSTRACT:

El-Gidida iron ore deposit is one of several deposits of the Bahariya Depression situated on the Western Desert of Egypt. The deposit is oval shaped with major normal faults displacing different blocks into one high central area surrounded by low areas. The present study aims to show the importance of considering these structural units by geostatistical modeling. Two cases have been considered; the deposit treated as one zone; the structural units treated as individual and separate zones. Standard statistical parameters are found to be similar for the two cases and different zones. However, horizontal and vertical variograms reveal that there is a significant difference. When treated as one zone, there is no directional anisotropy. The variogram parameters show both the presence of zonal inhomogeneity and directional anisotropy. In addition, the anisotropy shows a relationship with the direction of the major faults. Thus, the paper presents data which shows that, for this deposit, geostatistical modeling without considering the geological characteristics can lead to errors and would be an unsuitable base for mine planning.

RÉSUMÉ:

Le dépôt de mineral de fer El-Gidida est un de plusieurs dépôts de la Dépression Bahariya qui se trouve dans le Désert de l'Ouest en Egypte. Le dépôt est en forme d'ovale avec des des failles normales majeures qui déplacent des blocs divers dans une haute région centrale entourée par des régions basses. Cette étude montre l'importance de l'examen de ces éléments structuraux par modelage géostatistique. On a consideré deux cas: le dépôt considéré comme une zone; les unités structurelles considérées comme des zones individuelles et séparées. Les paramètres statistiques normaux sont semblables pour les deux cas et les zones différentes. Pourtant, les variogrammes verticaux et horizontaux montrent qu'il y a une différence considérable. Quand on la considère comme une seule zone, il n'y a pas d'anisotropic directionnelle. Les paramètres du variogramme montrent la présence de l'inhomogénéité zonale et de l'anisotropic direction-nelle tous les deux. En plus, l'anisotropic montre un rapport à la direction des failles majeures. Donc, cette étude présente des données qui montrent que, pour ce dépôt, le modelage géostatistique sans considération des caractéristiques géologiques peut produire des erreurs et ce modelage serait une base impropre pour les projets d'aménagement des mines.

INTRODUCTION

Geostatistical modelling through the construction of variograms, with the aid of a computerized database, plays an important role in studying the behaviour of the ore, for example, the continuity and nature of mineralization and its variation in grade over the deposit by considering the positions of the available samples within any deposit. When constructing variograms, the samples must belong to one zone to represent the spatial variability of that zone. These zones can be defined by studying the geology of the orebody including its structural, mineralogical, and chemical properties. The database is then created for a specific zone which has the same geological features and similar assay values.

Based on previous geological studies which were carried out on the El-Gidida iron ore deposit, it is clear that the orebody could be divided structurally into several zones. Major faults trending through different directions have displaced the orebody into two areas; a high central region and a lower surrounding region. This division might affect the mineralogical characteristics of the orebody and the ultimate ore reserve calculations. However, this could be investigated through geostatistical modeling of the orebody by considering two cases. In the first case, it is assumed that the structural geology has no effect on the mineralization of the orebody, and the whole area can be taken as one zone in constructing the variograms. In the second case, the geology of the orebody can be considered and variograms construct-ed for individual different zones. Also, statistical analysis can then be performed for the two cases to show if the statistical parameters reflect any differences between the two cases.

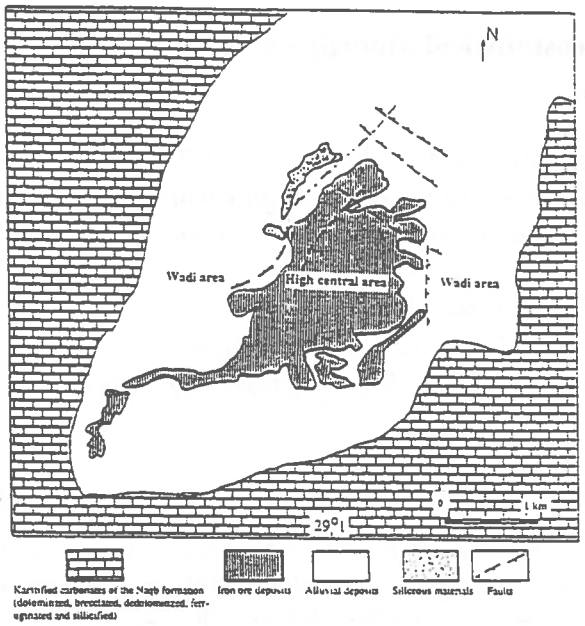

Figure 1. Geological map of El-Gidida area.
(Simplified after El-Aref and Lotfy, 1989)

GEOLOGY OF THE OREBODY

El-Gidida area is an oval-shaped depression, up to 15 km^2, and its main structural elements are a major anticline striking NE-SW and plunging to the NE, and normal faults, trending NE-SW, N-S and NW-SE, as shown in figure 1. The NE-SW fault intersects the orebody formation along the western scarp of the depression; the vertical displacements range between 3 and 25 m. These faults divide the orebody into two main areas; a high central area and a low wadi area which are both composed mainly of iron ore deposits. (El-Aerf and Lotfy, 1989).

The orebody occurs more or less as a horizontal bed with difference in elevation from the roof to foot of up to 76 m. It also includes lenses and lens-shaped intercalations, with thicknesses varying from 1 to 3 m, and slightly mineralized barren rocks represented mainly by ferruginous clays and rarely by sands (El-Akkad and Issawi, 1963). The orebody is characterized by wide variety of mineralogical composition and distribution of main ore-bearing and gangue minerals, both horizontally and vertically. The main minerals are hematite, geothite, hydrogeothite, quartz, halite and barite. The main mineral, hematite, may be crystalline in the form of tabular crystals or spheriods, which are formed either separately or in groups (Mahgoub and Amer, 1964).

Orebody Zones

According to the structural geology of the orebody, the major faults might divide the orebody into seven different zones with the central area including two zones; the mine (M) and central (C) zones and the wadi area includes five zones; the north west (NW) and north (N) zones, which are in the west of the central area, and south east (SE), east (E) and north east (NE) zones which are east of the central area, as shown in figure 2.

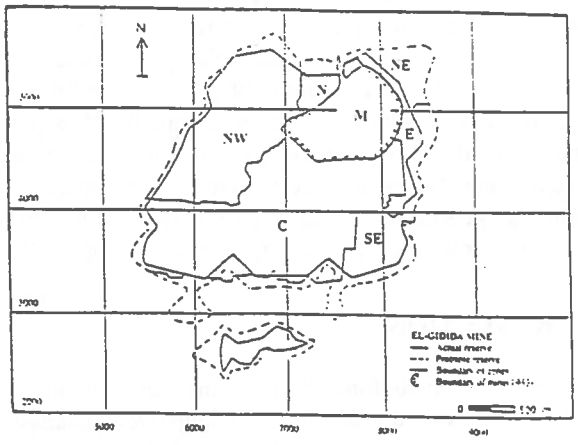

Figure 2. Zone divisions in El-Gidida area.

Preparation of data for computer entry

The present study is based on sampling information derived from 100 x 100 m test pits/drill-hole grid system comprising 82 test pits and 481 drill-holes. For each zone, a database has been established using only the drill-hole data which fall within each zone. Later, all the data bases were merged into one to represent the whole area. The drill hole data were prepared for files with individual drill-hole identification codes, and the collar northing, easting, and elevation. The data obtained by direct examination of core or cuttings were logged as a function of distance down the drill-hole from the collar. The attributes of the drill-hole have been measured in discrete intervals associated with from-to data field. Assay data for iron content were taken according to every logged interval. The intervals varied in size from 0.5 to 12.3 m.

STATISTICAL ANALYSIS

Statistical analysis gives standard parameters; mean, standard deviation, and coefficient of variation. It is obvious from table 1 that a difference is found in the average iron content between the two cases. The average iron content for the different zones ranges from 44.1% to 53.7%; that for the El-Gidida deposit is 49.8%. This reflects that the orebody contains, at least for some extent, poor and rich zones. This result could support the need to divide the orebody into different zones.

TABLE 1. Statistical parameters.

Zone	N	Mean	S.D.	COV
C	243	53.7	7.3	0.13
NW	114	44.1	5.4	0.12
M	63	48.8	6.3	0.13
E	57	48.2	5.7	0.12
SE	45	50.9	6.1	0.12
NE	21	44.6	6.6	0.15
N	20	47.2	6.7	0.14
El-Gidida	563	49.8	7.1	0.14

Although there are differences in the mean values, the coefficient of variation, which represents the variability of the orebody from a statistical point of view, did not give a clear difference between the two cases. It is 14% for the whole area (El-Gidida) and ranges from 12% to 15% for the different zones. This result might give an indication that the ore variabilty is the same within the different zones and there is little effect on the mineralization characteristics of the orebody.

Traditional statistical methods are based on the assumption that all sample values are equally representative of the properties of the deposit under study, and the physical positions of the samples with respect to each other are not taken into account (Rendu and Mathieson, 1990). This could be considered the reason that the coefficient of variation did not give any clear difference between the studied cases and reflect the insufficiency of traditional statistics in analysing the variability of the orebody. Geostatistical modeling, which allows the relative sample positions to be taken into account, can therefore be used to check this supposition.

CONSTRUCTION OF VARIOGRAMS

Computing an experimental variogram from a set of randomly spaced data involves finding pairs of data that are oriented in the required direction, determining the distance between the samples, then summing the squared differences of the grades and dividing by the number of pairs (Clark, 1979). Construction of variograms is an important step in any geostatistical modeling since it reflects the variability of the ore mineralization and could be used to differentiate between characteristics of the different zones of an orebody and as a base of the next steps in the geostatistical modeling, such as kriging. To achieve our goal in the present study and to compare the two cases to illustrate the effect of geology of the orebody, directional variograms have been constructed for the two cases to check the anistropy characteristics for each case and each zone of the second case.

MicroLynx software, which is a system designed to aid geologists and engineers in mine evaluation and mine planning, was used to construct the variograms. This software was developed by Lynx Geosystems Inc. of Canada. According to the data arrangement, the required parameters for constructing variograms were introduced to the programme. A lag interval of 100 m with a 10% tolerance was considered when constructing horizontal variograms and a lag of 1 m for the vertical variograms with a 0.3 m tolerance. When the directional variograms were constructed, the azimuth (bearing, clock-wise from North) was considered; 0° for N-S, 90° for E-W, and 45° and 135° for the diagonal directions NE-SW and NW-SE by considering a 20° tolerance on the direction.

Directional Anisotropy

The directional variograms reveal the changes in the variogram parameters as the direction changes. The directional variograms for the whole area are shown in figure 3. These demonstrate the absence of anistropy when the El-Gidida iron deposit is considered as one zone and the geological characteristics are neglected .

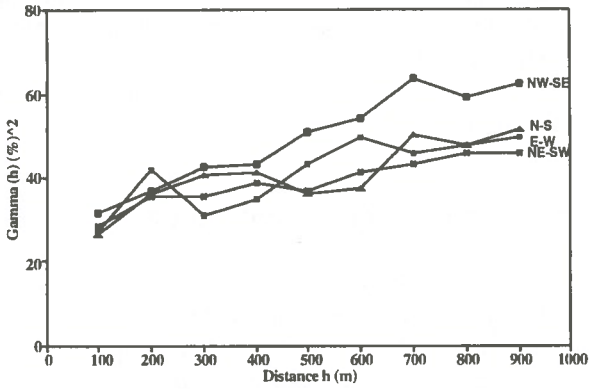

Figure 3. Directional variograms for El-Gidida area as one zone.

The variogram curves are sufficiently close to each other for the different directions and appear to be the same. Also, the fitted spherical models through the four directions, as shown in figure 4, and their parameters nugget effect (C_o), sill (C) and range of influence (a) do not show any clear differences. This information is also shown in table 2. The orebody of El-Gidida area, at this point, could be considered isotropic when neglecting the effect of its structural geology.

However, when considering the effect of the geology of the orebody, directional variograms for the different zones reflect the presence of anisotriopy in some zones, particularly the central zone (C) and the north west zone (NW). The directional variograms in the other zones have limited number of pairs, such that parts of the variograms do not meet the recommended 30 pairs of samples (David, 1977).

Figures 5 and 6 show that the variogram in the NE-SW direction in both of the two main zones reflect higher continuity than the other directions; anisotropy is definitely indicated. The variogram parameters, as deduced from the fitted spherical model, shown in

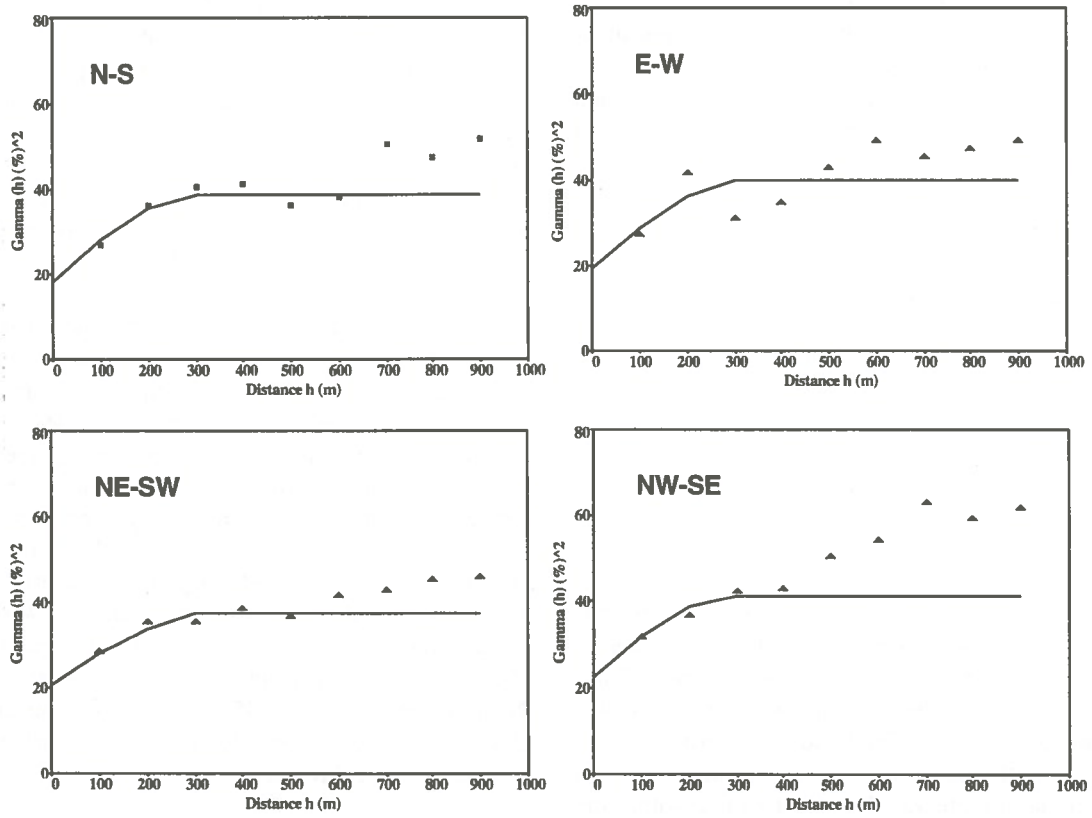

Figure 4. Fitted spherical models for the directional variograms of El-Gidida Area.

figures 7 and 8, support this result; they vary from one direction to another within wide ranges than those for the whole area. This indicates that some of the mineralization characteristics do not have the chance to appear in the first case. Treating the orebody as one zone caused the disappearance of the different mineralization behaviour. The direction NE-SW recorded the highest range of influence (400 m) and lowest sill (15.7) and tends to have the highest level of continuity than the other directions.

TABLE 2. Directional variogram parameters

Zone		N-S	E-W	NE-SW	NW-SE
El-Gidida	C_0	18.2	19.1	20.3	22.3
	C	38.5	39.7	37.2	41.2
	a	300	320	330	300
C	C_0	12.1	21.6	15.7	14.5
	C	41.4	30.8	25.7	42.3
	a	300	230	400	270
NW	C_0	11.6	13.0	10.5	21.8
	C	29.9	23.3	18.2	27.7
	a	300	225	400	300

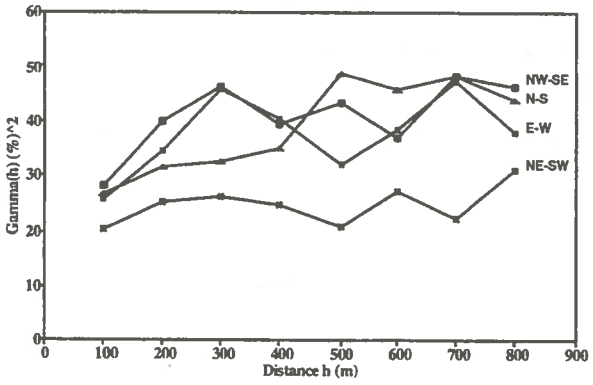

Figure 5. Directional variogram through zone C.

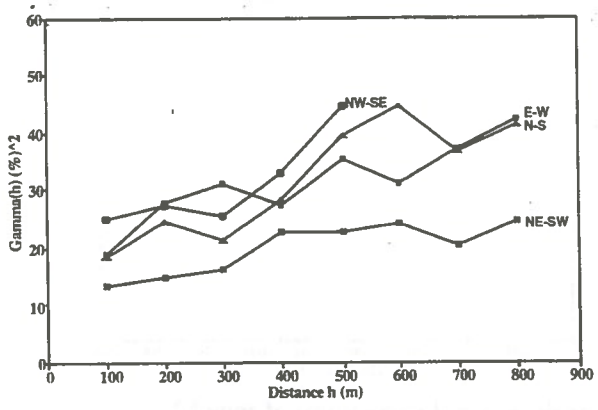

Figure 6. Directional variogram through zone NW.

It is observed that the direction of higher continuity is the same as the direction of the major fault trending NE-SW. This might reflect the effect of this structure on the mineralization of the orebody and make its variability smaller. The mineral distribution in that direction could then be considered more homogeneous. If this result is taken into account during the planning and production stages, the problems resulting from variation in the orebody mineralization, such as the presence of an unexpected poor mineralized zone or intercalations, could be avoided or decreased.

Zonal anistropy

The variogram behaviour can vary within the different zones of the orebody indicating the presence of zonal anisotropy. To prove the presence of zonal anisotropy within the El-Gidida iron ore deposit and to support the concept of dividing the orebody into zones according to its geology, global vertical and horizontal variograms have been constructed for the two cases, with results shown in figures 9 and 10 .

The horizontal variograms for the different zones illustrate that the variability of the orebody is not the same within them. As seen from figure 11, zone NW gives the highest vertical continuity and zone SE reflects the lowest continuity. These two zones are situated in the wadi area in the west and east side of the central part. The mineralization of the orebody could therefore be expected to have different characteristics within these different zones. The variogram for the El-Gidida area represents the orebody as one population and this could give misunderstanding about the mineralization characteristics of the orebody giving the impression that the orebody mineralogically is homogeneous. The vertical variograms show that zone C has the highest continuity and zone M has the lowest, where these two zones are located in the high central area.

The presence of zonal anisotropy can also be observed in the differences between the variogram curves and their parameters as shown in table 3 and figures 11 and 12. It is seen that the sill values vary from 29.5 $(\%)^2$ to 66.2 $(\%)^2$ horizontally and from 73.8 $(\%)^2$ to 135.4 $(\%)^2$ vertically which represent wide ranges. Also, the continuity is not the same within the different zones of the orebody. This shows that the mineralization behaviour can change vertically and horizontally from one zone to another. It is noticed that the faults have an obvious effect on mineralization of the orebody and different mineralized zones are found in El-Gidida area.

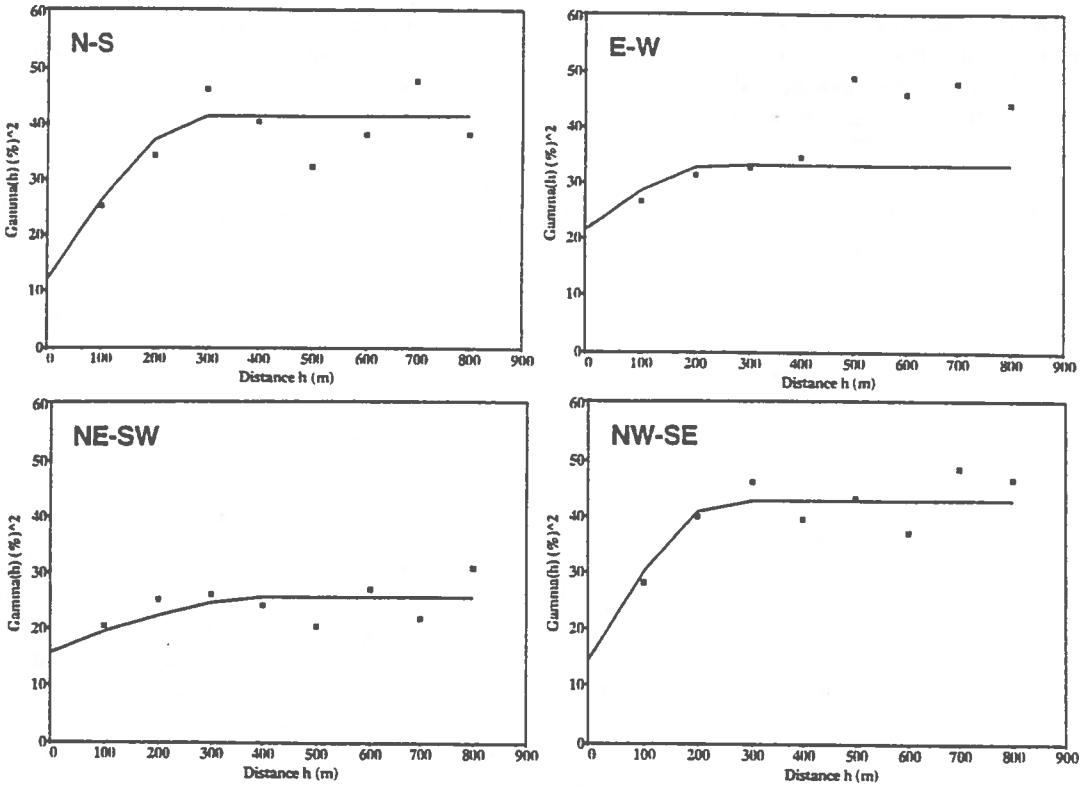

Figure 7. Fitted spherical models for the directional variograms of zone C.

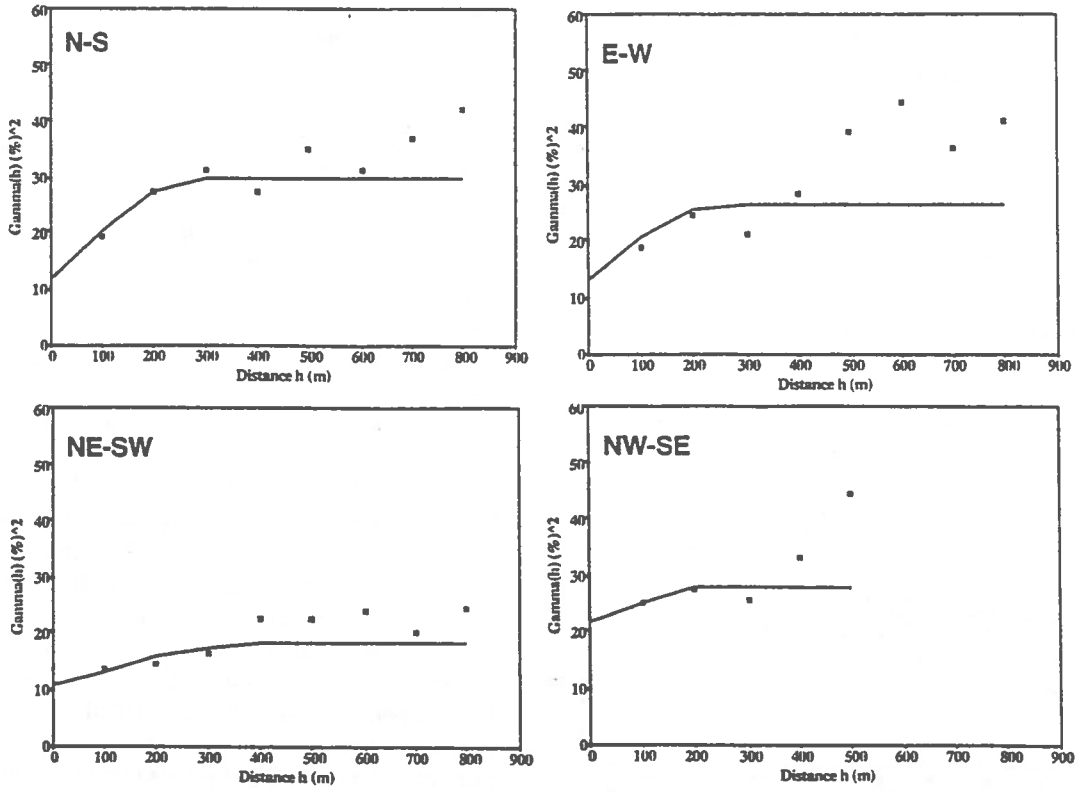

Figure 8. Fitted spherical models for the directional variograms of zone NW.

TABLE 3. Global variogram parameters.

Zone	Vertical			Horizontal		
	C_o	C	a	C_oC		a
C	21.9	73.8	3	22.7	36.8	300
NW	14.5	100.0	7	12.9	29.5	300
M	37.1	135.0	4	25.1	44.3	300
SE	18.9	92.4	3	51.3	66.2	300
E	19.4	90.8	4	26.9	47.3	300
El-Gidida	23.9	78.6	3	21.4	40.3	300

Both of the horizontal and vertical variability of the ore-body confirm the mineralogical studies which indicate the transition from one mineralogical element to another horizontally and vertically. Also, the intrusion of the ore strata or lenses with waste material, where El-Gidida iron ore deposit has intercalations of mineralized barren rocks represented mainly by ferruginous clays and rarely by sands. The thicknesses of these intercalations change from one part of the orebody to another within range 1-3 m.

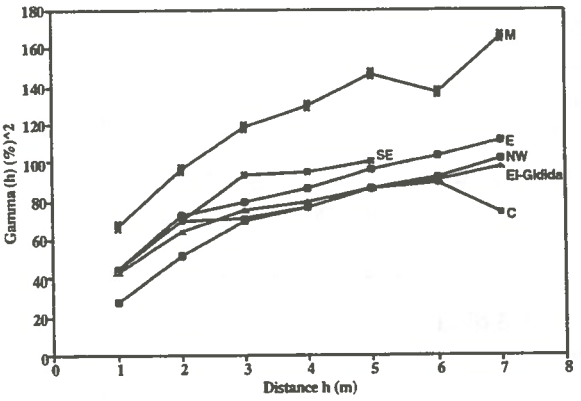

Figure 9. Vertical variograms for the whole area and the different zones.

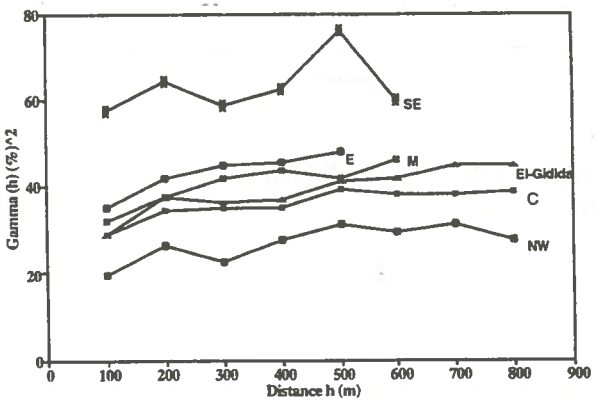

Figure 10. Horizontal variogram for the whole area and the different zones.

On the other hand, the clear differences in variability, as reflected by the variogram for each zone, indicate that, when considering the orebody as one zone and neglecting the differences, there will be a mixing between the different mineralization characteristics of the orebody. When followed by kriging, or any other geostatistical modeling techniques, significant error in the model is likely when the orebody considered as one zone.

The advantage of constructing variograms, which are based on the spatial distribution of a regionalized variable, has been clearly shown. When considering the whole orebody as one zone, the similarity in the grade values distribution, which comes from a specific zone within the orebody, is neglected. Zonal anistropy for El-Gidida iron orebody has been demonstrated, both horizontally and vertically. This result must be taken into account. In fact, this result is in agreement with most of the mineralogical studies which has explained the wide variety of mineralogical compositions of the orebody.

CONCLUSION

This study has shown that is important, when modeling an orebody, to begin with knowledge of its geology to define the parameters affecting the mineralization of the orebody. For the El-Gidida iron ore deposit, it is clear that considering it as one zone, that is neglecting the structural geology effects, will lead to lack of information in its mineralization characteristics.

The vertical and the horizontal variograms show that the orebody should not be considered as one population. Dividing the orebody into zones according to the faults showed the difference in the mineralization characteristics between them. Although the traditional statistical analysis illustrated that there are some differences in the mean iron content values of the different zones, the variability of its mineralization was not demonstrated. This is an indication that statistical analysis is not enough to show the differences in the mineralization characteristics of this orebody.

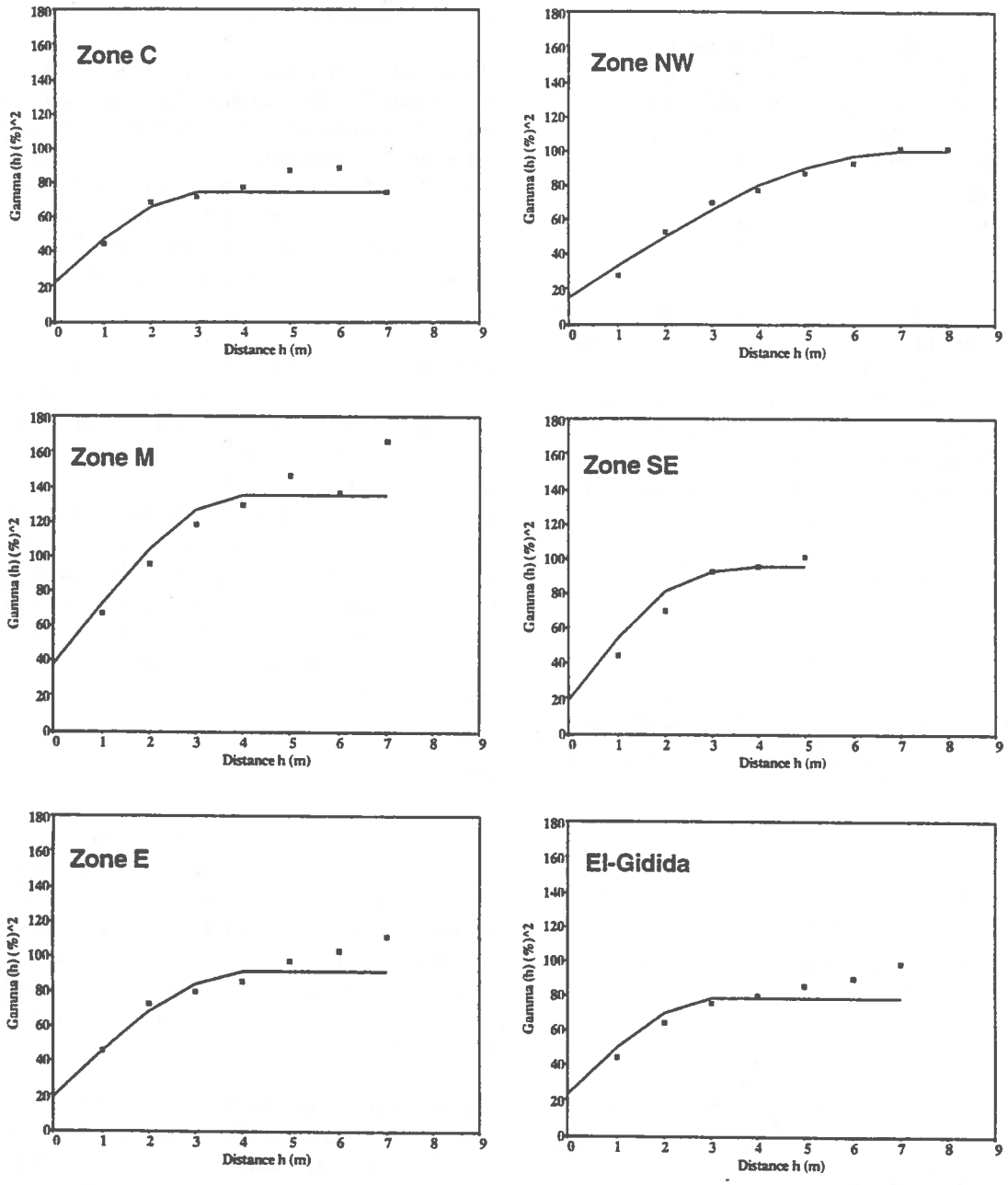

Figure 11. Fitted vertical spherical model for El-Gidida area and the different zones.

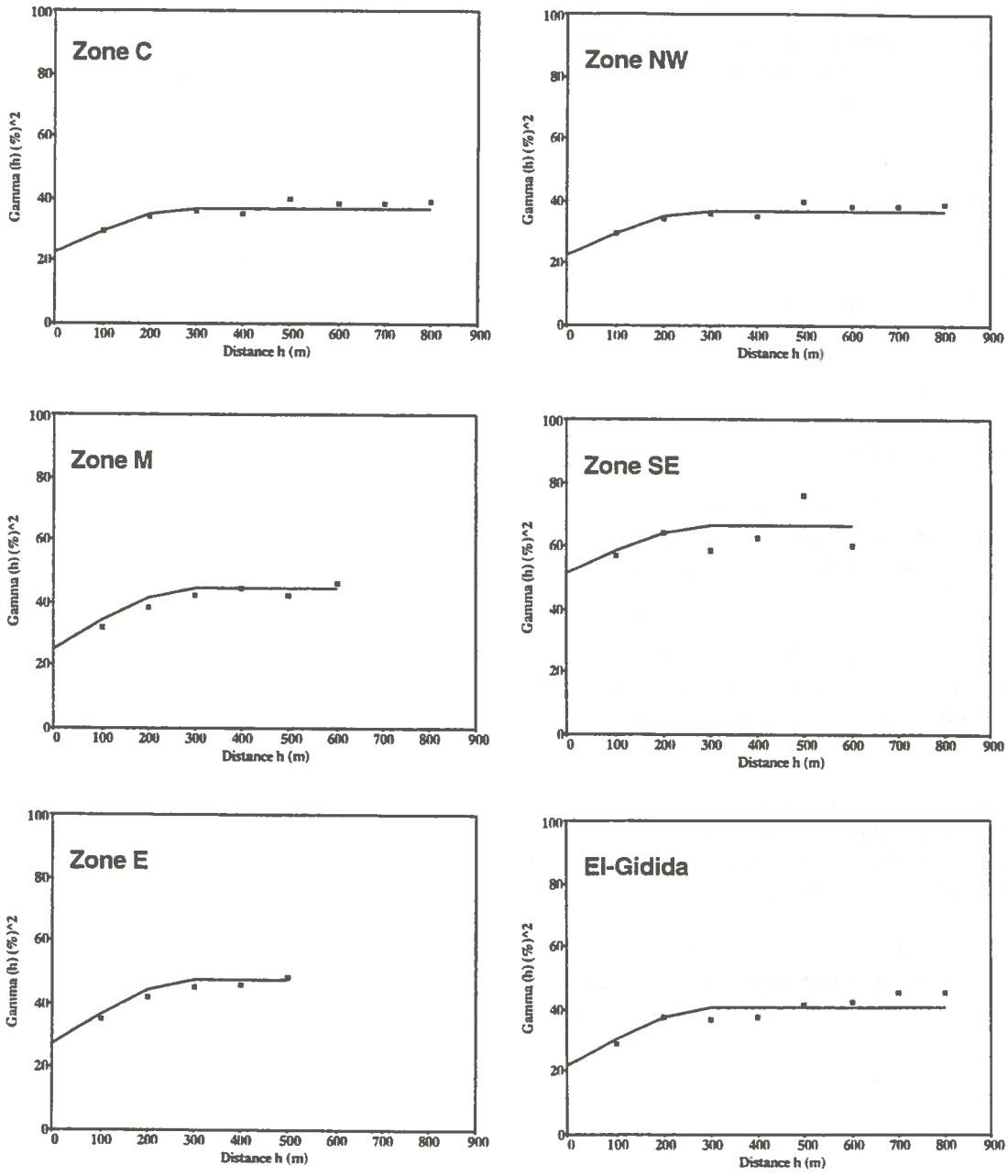

Figure 12. Fitted horizontal spherical model for El-Gidida area and the different zones.

Neglecting the effect of faults on the mineralization of the orebody caused the absence of anisotropy in the first case. However, the anisotropic effect is dramatically seen in the second case, particularly in the larger C and NW zones.

REFERENCES

CLARK, I., 1979.
Practical Geostatistics, Applied Science Publishers, London, 129 p.

DAVID, M., 1977.
Geostatistical Ore Reserve Estimation, Elsevier, Amsterdam , 364 p.

EL-AKKAD, S. and ISSAWI, B., 1963.
Geology and iron ore deposits of the Bahariya Oasis: Geological Survey of Egypt , Cairo, Vol.18, 301 p.

EL-AREF, M.M. and LOTFY, Z.H., 1989.
Genetic karst significance of the iron deposits of El-Bahariya Oasis Western Desert, Egypt: Geological Survey of Egypt, Vol. XV, 27 p.

MAHGOUB,O. and AMER, A.F., 1964.
Geology and evaluation of three iron ore occurances (Gebel Ghorabi, Nasser and El-Gidida), Geological Survey of Egypt, 229 p.

RENDU, J.M. and MATHIESON, G., 1990.
Statistical and Geostatistical Methods, Surface Mining, Kennedy, B. A. (editor), AIME-SME, pp 301-348.

CAMI'95:3rd Canadian Conference on Computer Applications in the Mineral Industry
Montréal, Québec, Canada, October 22-25, 1995

ORE BODY MODELING AT THE DIVRIGI IRON ORE DEPOSIT

Birol Elevli
Cumhuriyet University, Sivas, Turkey

Salih Yüksek
Cumhuriyet University, Sivas,Turkey

ABSTRACT

One of the most difficult problems frequently facing geologist and mining engineers is that of defining the ore body boundaries and estimating the ore reserves. A number of methods are available for the engineers to analyze the ore body. The ore body modeling of a deposit, which is also known as block model by the help of computer is most appreciated method to estimate ore reserve and to define the ore body boundaries. In this study, the block model of Divrigi-Iron Ore deposit is generated by the application of different drill hole interpolation methods such as polygon, inverse distance weighting and geostatistics. After generating the block models, ore reserves were estimated, and results were compared to each other.

RESUME

Un des plus importent probleme dont les ingenieurs des mines et aussi des géologies sont souvent face a face est de déterminer les frontieres du gisement et d'éstimer son reserve. Un nombre des méthodes est disponible pour les ingénieurs a analyser le gisement. Pour déterminer le réserve du gisement elson frontiere le procédé plus souvent employé estbien le modele du bloc en utilasant l'ordinateur. En cet étude, le modele du bloc est developpé a partir du gisement du fer de Divrigi, Sivas, Turquie, tenant compte different sondage effectués auissi que les procédés de Polygon, de L'inverse de distence et auissi de Géostatistique. Finalement, apres qu'engendrer les modeles du bloc, les reserves d'un gisement ont été éstimés et les resultats obtenues de certaines modeles ont été comparés.

INTRODUCTION

Divrigi Iron ore mine, owned and operated by the Turkish Iron and Steel Co. of Turkey, is the largest ore producers in Turkey, producing, 2,2 million ton per year, about 50% of domestic iron ore production and 25% of domestic iron ore demand. Located in the east part of mid-Anatolia, at the elevation of 1500m, 180km south-east of Sivas, Turkey (Figure 1), the ore is extracted by means of open pit mining. Extracted magnetite ore is first sent to the primary crushers, located on underground at the level of 1440, through in-pit shafts, then sent to the secondary crushers, located on surface at the level of 1100, via shafts, underground and surface conveyors. After secondary crushers, broken ore is transferred to benefication and pelletizing plants.

Although the mine has been in production since 1938, extensive investigation of the ore body was conducted from 1969 to 1988. During this period about 100

diamond drills have been done. After completing drills, ore reserves were calculated drawing maps by hand and applying the classical polygon method. Polygons were constructed for 12m height that is fixed bench height for mining. The top bench was 1536m above sea level and the bottom bench was 1104m above sea level (Karmali, 1988). After depletion of the upper levels by 1992, hand drown maps have become inadequate in terms of defining ore boundaries at the benches below 1500m. In addition to above problems, more diamond drills have been done in order to define ore body better. Therefore, it was decided to remodel (3-D block model) ore body by utilizing computers and different estimation methods.

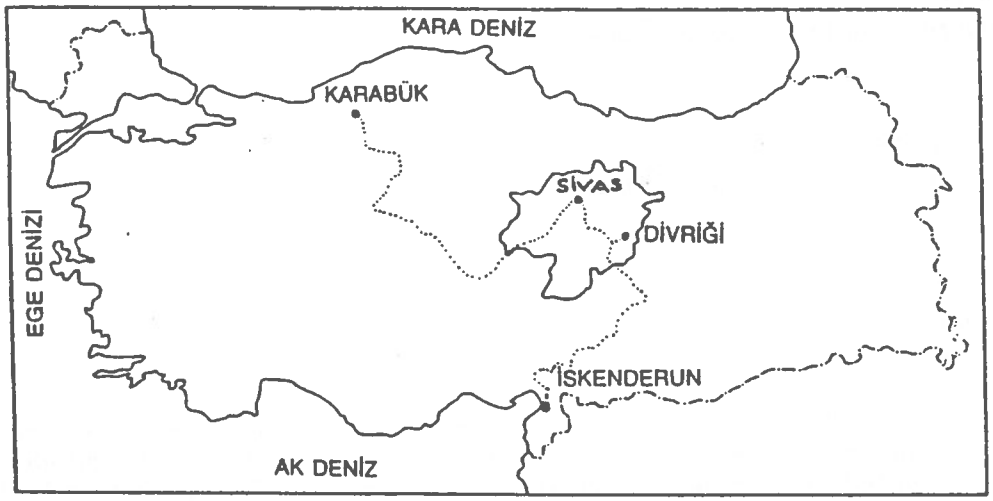

Figure 1: Location Map of Divrigi Iron ore Mine in Turkey.

In order to create 3-D block model of ore body, drill hole information was used to create a database. Each hole's coordinates(x,y,z) and assay values (Fe, SiO_2, S, Fe_2O_3) were recorded in the database. Since drillholes samples for assaying were unequal in length, they were regularized at 12m. Then, by using special programs, which utilize polygon, inverse distance weighting and geostatistics, 3-D block models were generated. The created block models are 25x25x12m in dimension, having 56x24 blocks in the plan with 36 benches. The top elevation of the block model is 1512. For this study, 97 of diamond drills were considered. The location of holes and physical limits of the block model are given in figure 2.

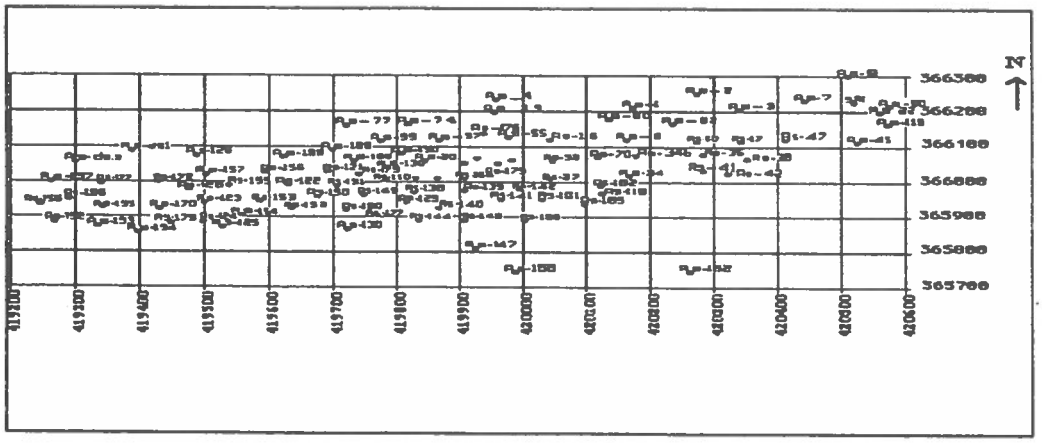

Figure 2. Boreholes location plan of Divrigi Iron Mine

Physical and Geological Setting of Deposit

The deposit subject to this study is situated in the triple contact of serpentine, siyenite and limestone. Ore body is head like in the upper levels, but pod-like in the lower levels (Kosal 1973). Mineralisation, 1500m long and 400m wide, is in the EW direction and dipping 40-45^{0} to south. Iron grades vary from about 30 to 65 %Fe as magnetite ore which is divided into two groups; high grade ore, which is over 45 %Fe and low grade ore which is between 35-45 %Fe.

BLOCK MODEL OF THE ORE BODY

The whole idea of block model is to divide an ore body into small blocks to which it is practical to assign grade, tonnage, and geologic values. Assignment of these values can be done with either or all of the drill hole interpolation methods; polygon, inverse distance weighting and geostatistics. Since computer programs for all of these methods are available, block model of the Divrigi iron ore body is generated with each method.

Polygon Method

The important parameter for the polygon method is the determination of radius of influence. After discussing with geologist and mining engineers, three radius of influence were established. These are 50m, 75m and 100m, and for each a block model is generated. By checking the results and comparing them with quantities of already mined out benches, block model generated using 75m radius of influence is selected for further studies. The ore reserves and average grades of each bench between the level of 1512 and 1404 are given in table 1. For reserve calculations, density of 3.82 ton/m^{3} for the grade of 35-45%Fe and 4.12 ton/m^{3} for the grade of >45%Fe are assumed.

It can be seen in table 1 that the quality and quantity of iron decreases with depth. This tendency is the result of geological structure given before.

TABLE 1. The Results of Polygon Method.

Bench	<% 45 Fe		>% 45 Fe	
	ton (x10^{3})	Grade %Fe	ton (x10^{3})	Grade %Fe
1512	716	36.1	2515	51.6
1500	1031	41.4	2635	60.2
1488	315	40.2	2620	60.4
1476	658	42.7	2215	60.5
1464	229	40.1	2416	58.2
1452	802	38.1	2933	56.7
1440	429	41.4	3413	56.1
1438	114	39.8	2124	58.0
1426	114	37.5	1307	55.0
1414	229	44.4	1816	53.6
TOT.	4637	40.1	23994	57.0

Inverse Distance Weighting Method

The assignment of grade, tonnage and geologic factors to a block by the inverse distance weighting method is not like polygon method. This method provides varying weighting factors which decreases in magnitude with increasing distance from the block under question. The important factors of inverse distance method are the values of exponent, exclusion angle and radius of influence (Hughes, et.al 1979). For the sake of this study, the following values of these factors were used for block modeling.

Radius	: 55m	Exclusion angle	: 10^{0}
Exponent	: 2	Max. Point	: 10

The results obtained from the inverse distance method were given in table 2.

TABLE 2. The Results of Inverse Distance Method.

Bench	<% 45 Fe		> % 45 Fe	
	ton (x10^{3})	Grade %Fe	ton (x10^{3})	Grade %Fe
1512	774	37.8	2251	52.9
1500	945	40.7	2443	57.3
1488	430	40.2	2520	57.3
1476	458	42.8	2308	56.9
1464	401	40.9	2565	55.7
1452	917	39.4	2765	56.1
1440	544	40.3	3057	55.8
1438	573	39.5	2623	58.1
1426	516	39.6	1689	54.3
1414	659	42.1	2482	53.4
TOT.	6217	40.3	24703	55.8

Geostatistics

Any geostatistical modeling begins with the statistical analysis of data and drawing of variograms. Variograms are used to define the geological properties, such as anisotropy, continuity and range (Journel 1978, David 1988). These parameters are used in the later stage of geostatistics that is kriging. The drawing of variogram is also known as structural analysis of raw data. For the Divrigi iron ore body, an average variogram is modeled using the following parameters (Figure 3) .

Type	: Spherical
Nugget(Co)	: 17
Sill (C)	: 101
Range (a)	: 85 m
Direction	: 20^{o}
Anisotropy (a/b)	: 1.3
Mean	: 49.6
Variance	: 120.82

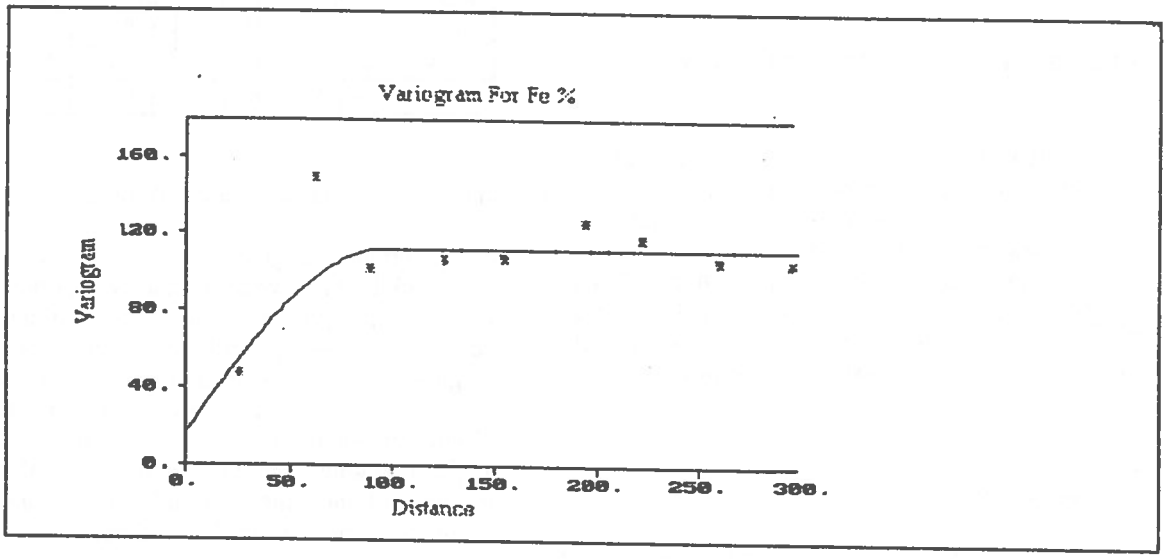

Figure 3: Experimental and Modeled Variogram

The grade values between 20% Fe and 71%Fe were used in variogram analysis. After completing the variogram analysis, next step is kriging. A simple kriging program was used to derive 25 meters square block estimates over the entire deposit. Using the variogram parameters obtained from the variogram analysis, %Fe values assigned to the blocks of each level. The ore reserves were calculated in the same way of polygon method. The reserves and mean grades of each benches is given in the Table 3.

TABLE 3. The results of Kriging

Bench	<%45Fe		> % 45 Fe	
	ton ($x10^3$)	Grade %Fe	ton ($x10^3$)	Grade %Fe
1512	1347	41.1	3060	56.7
1500	602	40.2	2635	57.6
1488	458	41.9	2620	56.2
1476	687	40.3	2215	54.8
1464	1347	39.6	2416	55.8
1452	688	40.4	2933	55.6
1440	888	39.1	3413	58.2
1438	573	39.6	2124	54.6
1426	1261	41.7	1307	53.8
1414	544	38.8	1816	53.4
TOT.	8394	40.3	30663	55.7

COMPARISON OF DIFFERENT METHODS

Ore reserves of Divrigi Iron Mine were calculated from the block models generated by applying polygon, inverse distance and simple kriging. The reserve of the ore body was previously estimated from the hand

drawn polygons with the help of planimeter. In addition to above, the benches of 1512, 1500 and 1488 were already mined out and amount of excavated ore from each bench is known. So, it was possible to compare actual mined out reserve and estimated reserves. The total mined out ore from the benches of 1512, 1500 and 1488 was approximately 8.9 mt. The estimated tonnages for those benches are 9.5 mt., 7.2 mt. and 7.7 mt. for kriging, inverse distance and polygon method respectively.

Figure 4 shows graphical comparison of reserves estimated with different methods. 'Kriging' represents reserves estimated by geostatistics, 'Id' represents reserves estimated by inverse distance, 'Poligon' represents reserves estimated by polygon, 'Divm' represents reserves estimated from hand drawn maps, and 'Divg' represents amount of ore mined out from the benches of 1512, 1500 and 1488. In this figure, reserves are only given for the grade above 45%Fe . Except benches of 1440 and 1428, kriging gave more reserves than that of other methods. However, the average grades are lower for kriging (Figure 5).

Figure 6,7 and 8 show the plan view of bench 1440 determined by polygon, inverse distance and geostatistics respectively.

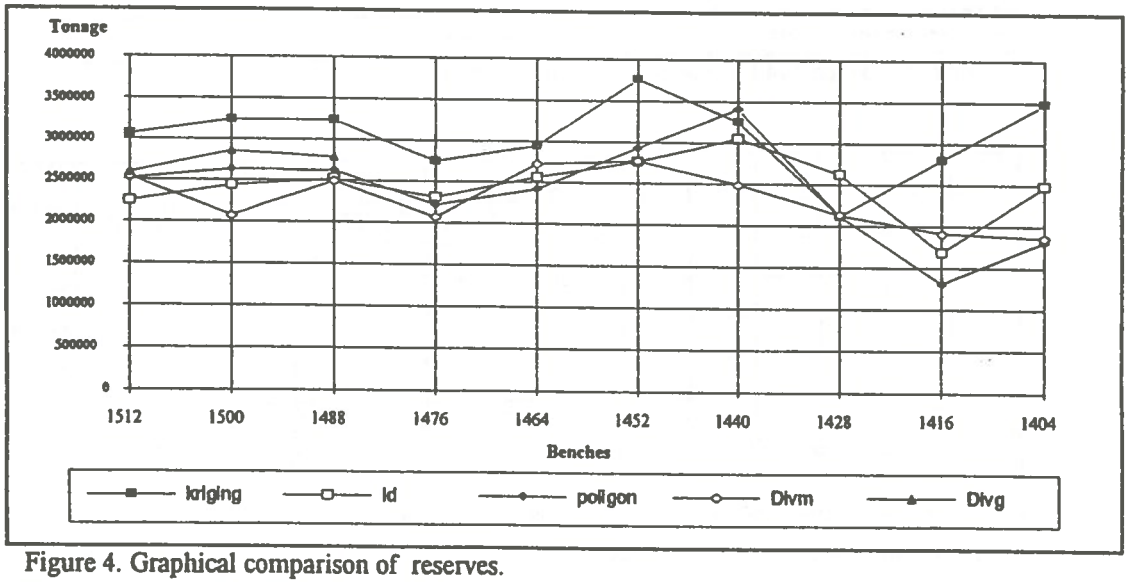

Figure 4. Graphical comparison of reserves.

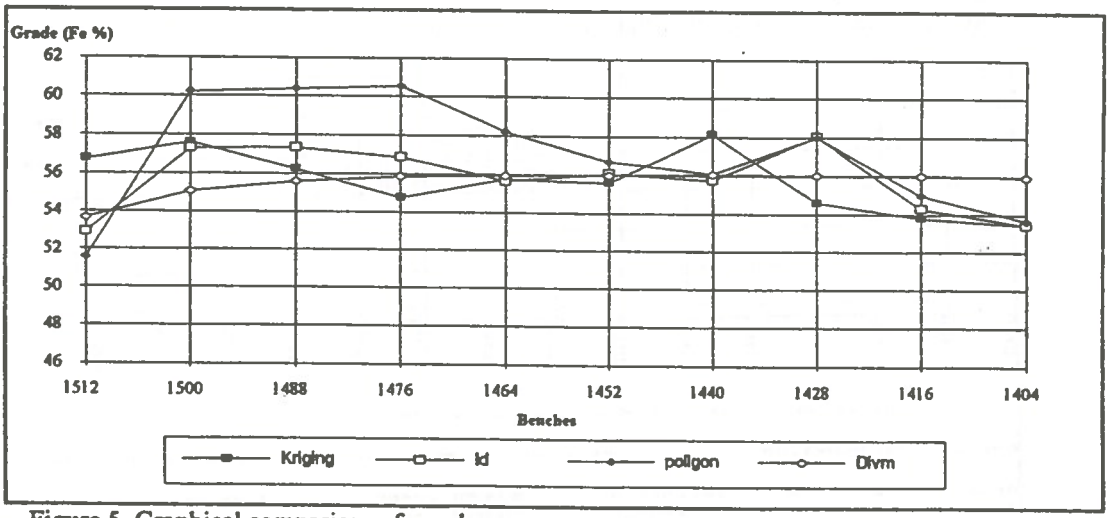

Figure 5. Graphical comparison of grades.

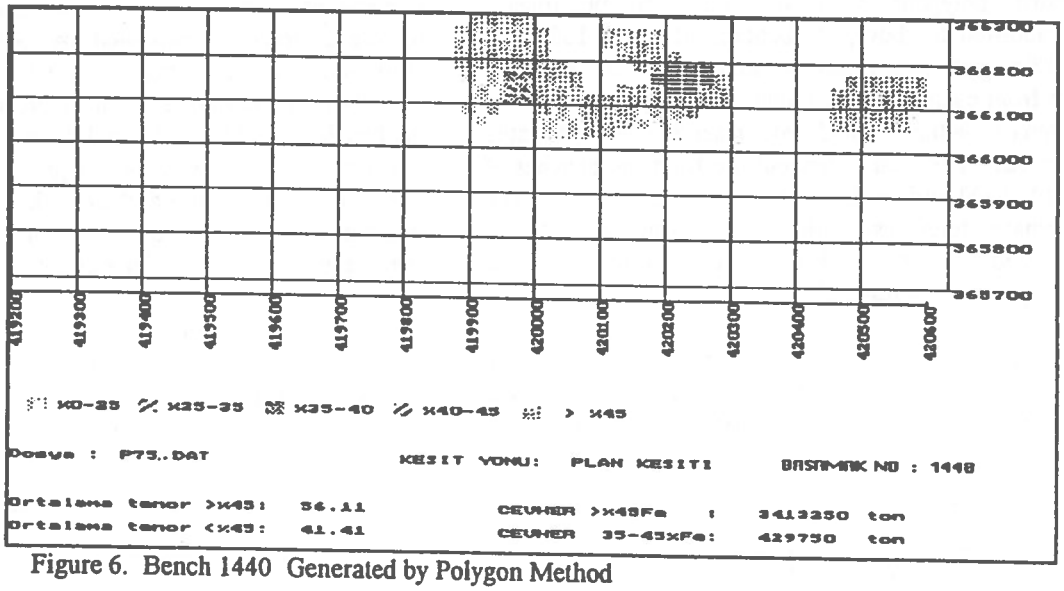

Figure 6. Bench 1440 Generated by Polygon Method

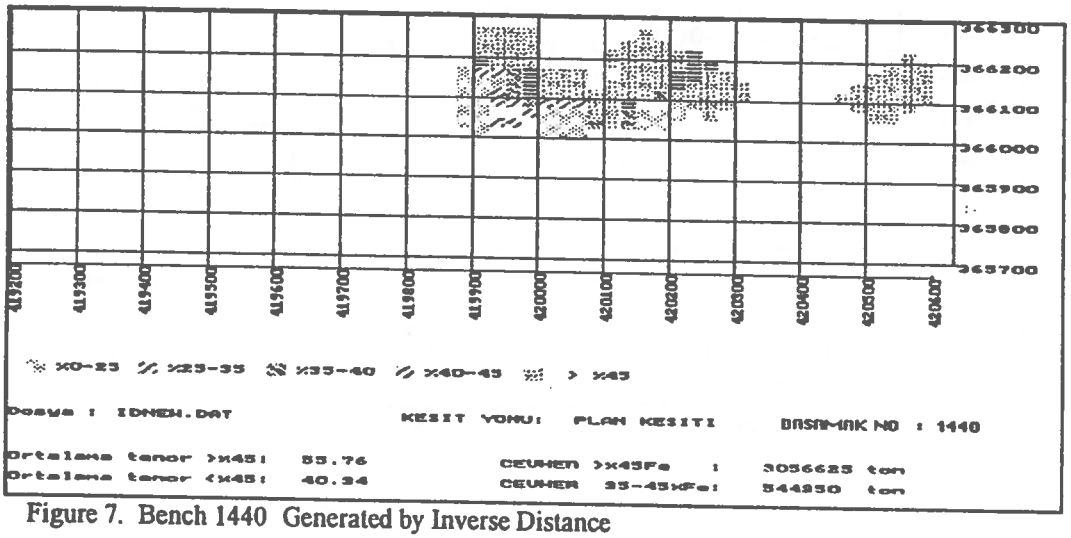

Figure 7. Bench 1440 Generated by Inverse Distance

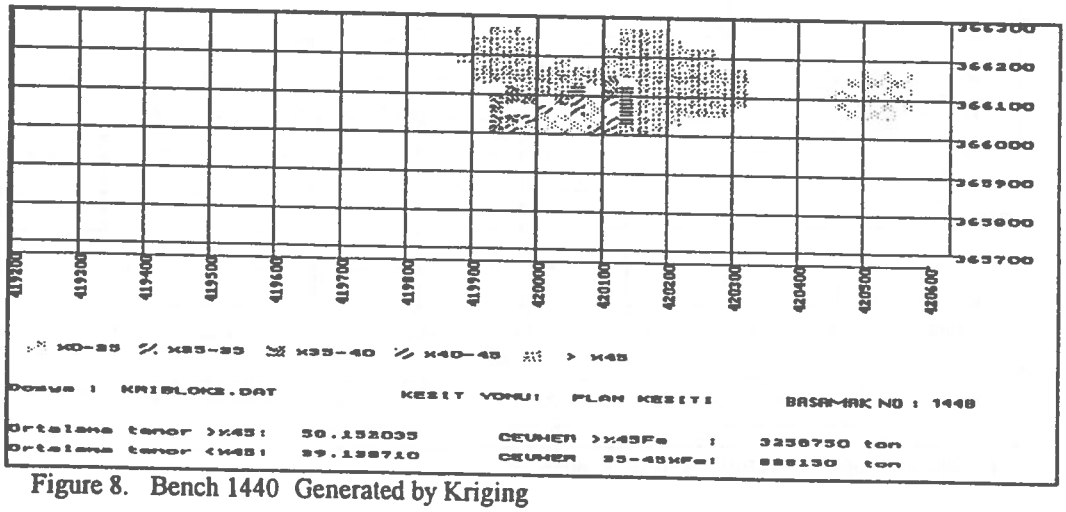

Figure 8. Bench 1440 Generated by Kriging

CONCLUSION

In this study, the ore body modeling of Divrigi iron ore body is carried out using polygon, inverse distance weighting and geostatistical methods. The ore body is divided into levels with 12m height and 25x25m wide blocks in order to obtain 3-D block model. Each block is assigned a %Fe grade.

It is found that kriging provides more ore reserves but the mean grade is lower. At least for the mined out benches, kriging gave the closest tonnage to the actual amount of ore. Each method proves that the ore body is pod-like at the lower levels. Radius of influence is effected by the major fault zones.

The final benefit of this study is that now computers can be used for better planning of ore production, and ore body can be examined visually with relative ease by the help of computer programs. These models can also be used to determine final pit limits of the ore body with computerized methods that is the next step of this project.

ACKNOWLEDGMENT

Author wishes to express his appreciation to Dr. R.Cameron who wrote most of the programs used in this study and special thanks to Divrigi Division of Turkish Iron&Steel Co. for providing boreholes data.

REFERENCES

DAVID, M., 1988. Handbook of Applied Advanced Geostatistical Ore Reserve Estimation. Elsevier, Amsterdam, 216p.

HUGHES, W.E., and DOWEY, K.R., 1979, "Drill Hole Interpolation: Mineralized Interpolation Techniques", AIME-SME Open Pit Mine and Design, Crawford &Hustrulid (ed.), pp.51-64

JOURNEL, A.G. and HUIJBREGTS, CH.J., 1978. Minin Geostatistics. Academic Press, New York, 594p.

KARMALI, M.R., ERKAN, S.R.,et.al. ,1989, "Divrigi Madenleri A-B Kafa Yataklari Rezerv Degerlendirme Raporu", TDCI Genel Mudurlugu, Hammadde Etud ve Daire Baskanligi.

KOSAL, C., 1973, "Divrigi A-B-C Demir Yataklarinin Jeolojisi ve Olusumu Uzerinde Calismalar", MTA Dergisi, sayi: 81

4.

operations research
recherche opérationnelle

CAMI'95: 3rd Canadian Conference on Computer Applications in the Mineral Industry
Montréal, Québec, Canada, October 22-25, 1995

Design and Simulation of an Underground Haulage System using SLAM II

Samuel Frimpong, Ph.D, P.Eng.
Department of Mining and Metallurgical Engineering
Technical University of Nova Scotia, Halifax, Nova Scotia

Jerry M. Whiting, Ph.D., P.Eng.
Department of Mining, Metallurgical & Petroleum Engineering
University of Alberta, Edmonton, Alberta

ABSTRACT

A practical application of computer simulation to the design of a mine production system in a constrained resource environment is presented in this paper. The management of a mining company wants to build a rail network to haul ore from a section of the mine to the central shaft. To meet the plant feed, this system should be capable of hauling a capacity between 1000 and 1500 tonnes per day. In this study, the authors build a simulation model to emulate the proposed system. Data from a similar project is used to validate this model. The technically feasible options are used in a batch simulation of the problem. Production and economic analyses of simulation results show that two of the feasible options can be used to build the actual system. Implementation of the recommended options could reduce the capital investments by 18%, in the short and medium-terms, and by 17%, in the long-term, of the original estimates.

RÉSUMÉ

Une application pratique qui utilise les ordinateurs pour la simulation d'un systéme de production minier dans un milieu de resources contraintes sont ici présentés. L'administration d'une compagnie minière veut bâtir un réseau ferroviaire pour transporter les minerais d'une partie de la mine jusqu'au puits de mine centrale. Pour fournir la quantité de minerais nécessaire pour le concentrateur il faut transporter à peu près 1000 à 1500 tonnes de roches par jours. Les auteurs présentent un modèle pour imiter ce système préposé. Des données d'autres projets semblables vont être utilisés pour vérifier ce modèle. Les options techniques qui sont réalisable sont utilisés dans une simulations par lots du problème. Les résultats des simulations d'analyses économiques est de production démontrent que deux options faisables peuvent être utilisés pour bâtir le système. La mise à exécution des options recommandés pourraient réduire les investissement capitaux par 18% a court terme et 17% a long terme comparer aux estimations originaux.

INTRODUCTION

Simulation modelling techniques have been used extensively by analysts to study the behaviour of complex systems in engineering and other fields [Pritsker, 1986]. In mining, simulation models have been used to study underground mine production [Beckett, Haycocks and Lucas, 1979; Lilke et al., 1993], surface mine production [Manular, Albert and Ramani, 1979; Ramani, 1990], and oil and gas production economics [Tortike and Frimpong, 1994]. Generally, simulation models are problem-specific, and extensive modifications are required to tackle other problems which can be very costly.

The management of an underground gold mining company wants to build a haulage system to haul ore from a section of the mine, through a distance of 4.5 km, to the loading bins at the central shaft. To meet the required daily plant feed of 5,500 tonnes, a daily target between 1,000 and 1,500 tonnes must be hauled from this section. An initial study has indicated that the most economic system, under the given constraints, is the rail haulage system. Management is constrained with respect to the number of resources (i.e., fleets of mine cars, bins, and chute systems) available for this haulage system. Based on proven and probable reserve estimates and production and development plans, it is estimated that the expected respective production

ratios in the stopes being served by chute system 1 to that being served by systems 2 and 3 are 4 : 1 : 1, in the short and medium terms. Also, chute system 2 can serve the production stopes served by system 3 in the short and medium-terms, but system 3 is required in the long-term.

The solution of this problem involves complex, but quantifiable steps in making irreversible capital-intensive investment decisions. In conventional methods, many of these steps are left to the judgement of analysts because of their simplistic analytical procedures [Borquez and Thompson, 1990; Gentry and O'Neil, 1984]. In particular, conventional methods have no built-in procedures for analyzing the complex functional relations, randomness of system variables and the response of system results to changes in mine design which are critical in this project. Computer simulation technique is a methodology being proposed to help management overcome these limitations. This methodology combines the power of SLAM II, stochastic modelling of system variables and alternate mine design concepts to abstract this problem for experimental analysis. *The novelty of this approach includes the incorporation of rigorous procedures in the simulation model for analyzing the system and its response to changes in mine design options which yield the technically feasible option at minimum cost. This study is significant because it combines simulation methodology with rigorous statistical and probabilistic analyses, in a capital rationing environment, to help a company make appropriate investment decisions.*

The main objectives of this study are: (i) to build a simulation model to emulate the haulage system; (ii) from (i) determine the optimum numbers of resource combinations that are feasible to achieve the target; and (iii) make recommendations on appropriate design option(s). In this study, the project background and a review of the proposed system are provided. Mathematical and simulation models of the system have been developed and validated using data from a similar project. Analysis of results has been provided with conclusions and recommendations. *Short and medium-terms are defined as periods ranging between one and three years and long-term as a period greater than three years.*

PROJECT BACKGROUND

This project was undertaken for the State Gold Mining Corporation (Ghana) Ltd., a company Dr. Frimpong, one of the authors, had previously worked for. It became necessary as a result of a policy adopted in November 1991 to ration capital over the company's many projects. Two Mining Engineers and the Director of Operations from this company participated in this study. The first project assignment began in June 1992 and the complete project report was presented to management in May 1993.

REVIEW OF PROPOSED HAULAGE SYSTEM

Figure 1 illustrates a schematic plan view of a section of the proposed rail network. It shows the location of the bin servers, the routes to various chute systems, a temporary parking route, and one fleet of diesel locomotive and eight mine cars, each with a capacity of 4.5 tonnes and a fill factor of 0.9. Traffic signs are located at various intersections to ensure traffic safety. At the beginning of a tramming shift, empty mine car fleets travel from loco stations located near the bins to various chute systems. At the 3-route intersection, A, the dispatch system routes the incoming fleets to the chute system with the shortest queue. A queue length is determined by the number of fleets waiting at a particular chute system, and those enroute to this system from point A. At the assigned chute system, this empty fleet either waits (if a fleet is already in the queue), or is loaded, after which it travels back to the bin to dump its load. With a 2-way radio communication system, empty fleet drivers clear off the main rail track onto temporary parking routes to allow loaded fleets to pass by before proceeding to the chute systems. A double lane rail system will be required to solve this delay problem, but the capital and maintenance costs requirements make it uneconomical.

HAULAGE SYSTEM MATHEMATICAL MODEL

The two important stochastic models in the haulage system design are the actual production and cycle time models.

Actual Production Model

The actual production, Pa, of the system is defined by:

$$P_a = k.\phi(\psi(N), \beta, \alpha, \mu, \xi, \epsilon; s_1) \quad (1)$$

$$k = \{n, c\} \quad (2)$$

The random number seed, s_1, in equation (1) reflects the system stochasticity through the error term $\varepsilon(s_1)$. $\varepsilon(s_1)$ is a random variable with a mean of zero and a variance of $\sigma^2(s_1)$. Thus, equation (1) becomes:

$$P_a = k.\phi(\psi(N), \beta, \alpha, \mu, \xi, \epsilon) + \varepsilon(s_1) \quad (3)$$

$$\psi(N) = 1/C_t(N) \quad (4)$$

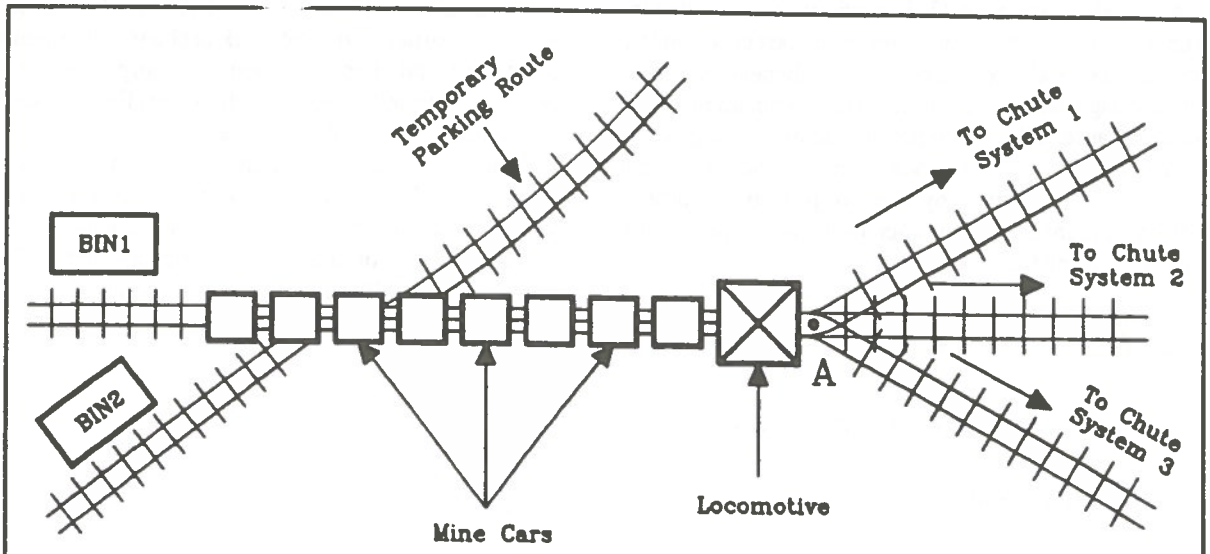

Figure 1 Schematic Plan View of a Section of the Ore Transportation System

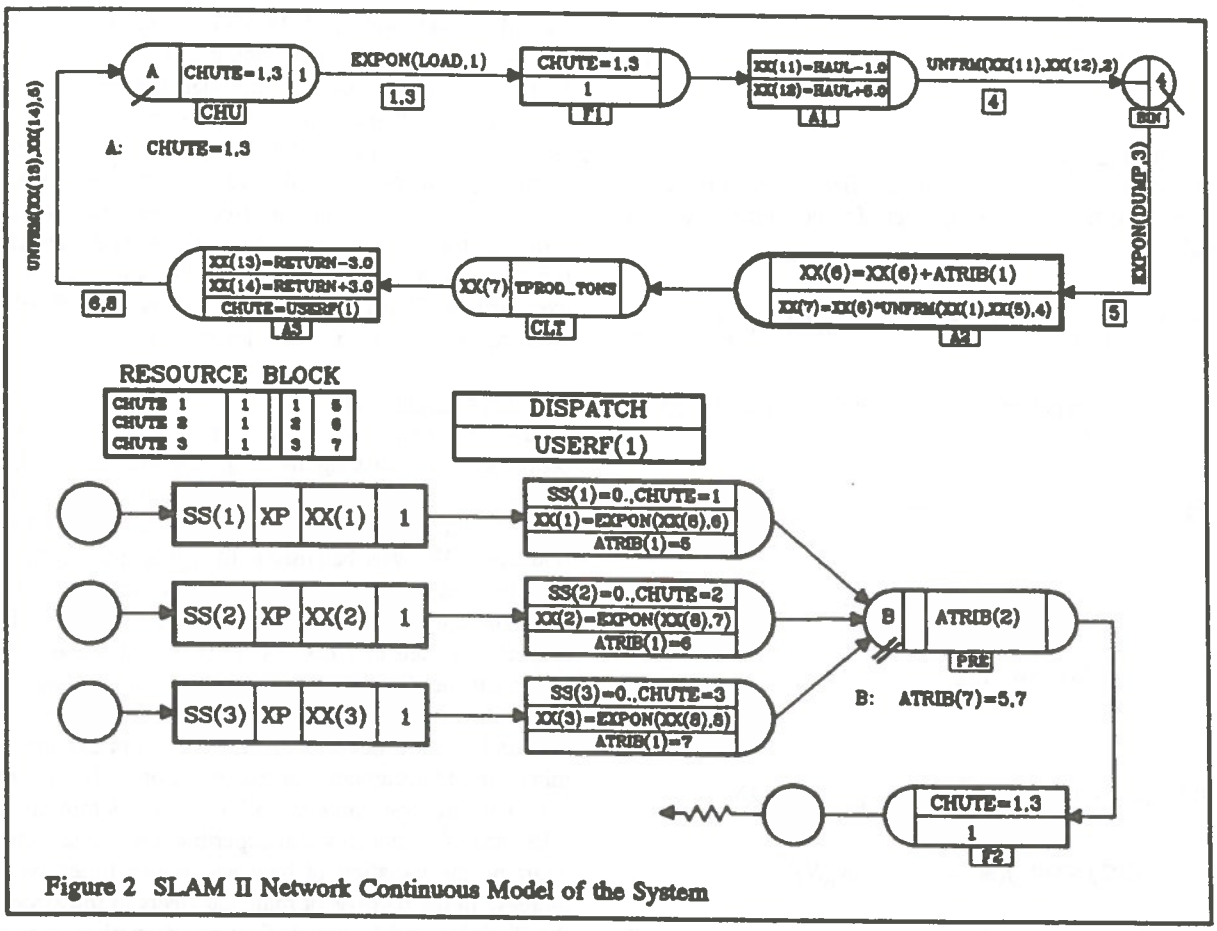

Figure 2 SLAM II Network Continuous Model of the System

It is assumed that equation (3) is continuous. Also, that the error term, $\varepsilon(s_1)$, represents a set of uncorrelated random variables, i.e., $COV[\varepsilon(s_1), \varepsilon(s_2)] = 0$, whenever $s_1 \neq s_2$. In order to design the system, it is important to obtain the mean and the variance of the actual production over a long period of time. Assuming that all the variables are random and that they can be described by known probability density functions, the mean and variance of the actual production can be determined as:

$$E[P_a] = k.\int_{-\infty}^{\infty}\cdots\cdots\int_{-\infty}^{\infty}\phi(\psi(N),\beta,\cdots\cdots,\epsilon)\cdot f(\psi(N),\beta,\cdots\cdots,\epsilon)\cdot d\psi\, d\beta \cdots\cdots d\epsilon + \int_{-\infty}^{\infty}\varepsilon(s_1)f(\varepsilon)\,d\varepsilon \quad (5)$$

$$VAR[P_a] = k^2.\int_{-\infty}^{\infty}\cdots\cdots\int_{-\infty}^{\infty}[\phi(\psi(N),\beta,\cdots\cdots,\epsilon) - E(P_a)]^2\cdot f(\psi(N),\beta,\cdots\cdots,\epsilon)\cdot d\psi\, d\beta\, d\epsilon \quad (6)$$

Cycle Time Model

The actual cycle time, Ct(N), of a fleet of locomotive and mine cars depends on the number of fleets in the system. It is also given by:

$$C_t(N) = \phi[m_t, \lambda_t, \tau_t(N), \delta_t, \tau_a(N), \omega_t(N)] + \varepsilon(s_2) \quad (7)$$

Under similar arguments, the mean and variance of equation (7) can be defined as:

$$E[C_t(N)] = \int_{-\infty}^{\infty}\cdots\cdots\int_{-\infty}^{\infty}\phi[m_t, \lambda_t, \cdots\cdots, \omega_t(N)]\cdot f(m_t, \lambda_t, \cdots\cdots, \omega_t(N))\cdot dm_t\, d\lambda_t \cdots\cdots d\omega_t + \int_{-\infty}^{\infty}\varepsilon(s_2)f(\varepsilon)\,d\varepsilon \quad (8)$$

$$VAR[C_t(N)] = \int_{-\infty}^{\infty}\cdots\cdots\int_{-\infty}^{\infty}[\phi(m_t, \lambda_t, \cdots\cdots, \omega_t(N)) - E(C_t(N))]^2\cdot f(m_t, \lambda_t, \cdots\cdots, \omega_t(N))\cdot dm_t\, d\lambda_t, \cdots\cdots, d\omega_t \quad (9)$$

Equations (5) and (8) and (6) and (9) are the respective means and variances of a network problem with queues at the loading and dumping points. Incorporated in this network is a dispatch system which assigns fleets to various chute systems. The problems reflected by these equations are best solved via a simulation model of the system with many runs. Due to limiting financial constraints and operating experience, the constraints in equations (10) to (13) are imposed on the system by management. These constraints yielded 18 design options, illustrated in Table 1, which are simulated in this study.

$$2 \leq N \leq 6 \quad (10)$$

$$2 \leq \sum cs \leq 3 \quad (11)$$

$$1 \leq \sum bs \leq 3 \quad (12)$$

$$N \geq \sum cs \quad (13)$$

HAULAGE SYSTEM SIMULATION MODEL

SLAM II, an advanced FORTRAN-based simulation language, was used for developing this simulation model. It is one of the most comprehensive and powerful simulation languages for mining systems, because it combines network, discrete event, and continuous modelling capabilities. It also incorporates advanced statistical tools that could be used to process simulation results for relevant decision making, an essential element of this study [Pritsker, 1986]. The ability to interface with user-written FORTRAN codes allowed the flexibility required to model such a complex system.

Analysis of Input Data

Data were collected, over a period of time, on the cycle time components, i.e., loading, hauling, dumping and returning. Waiting times at the bins and chute systems were included in the haul and return times. The BestFit software [Palisade, 1994] was then used to fit appropriate probability distributions to the data for each cycle time component. From the test results, the exponential distribution with the respective means of 10.00 and 15.00 minutes was used to represent the distribution of dumping and loading times data. The uniform distribution was also used to represent haul and return times data distributions. For example, the minimum and maximum haul and return times for five mine car fleets are, respectively, 25.33 and 31.78 minutes, and 19.34 and 24.77 minutes. An experiment was conducted to examine the variation of haul and return times with an increase in the number of mine car fleets in the system at the Training and Research Section of another company.

The results show that the haul and return times increase as the number of fleets in the system increases. This may be due partly to the waiting times at loading and dumping sites, and delays in hauling and returning of fleets.

SLAM II Network Continuous Model

Figure 2 is the SLAM II network continuous model of the system. The chute systems are modelled as resources, bin servers as queues, fleets of mine cars as entities flowing through the system, and cycle time components as service activities. The chute systems, represented by the RESOURCE BLOCK, have capacity of one each, and the corresponding AWAIT and PREEMPT file numbers. Entities or fleets of mine cars arriving at the AWAIT node CHU are routed by DISPATCH to the assigned chute system. If the assigned chute system is busy, this fleet is placed in the AWAIT file corresponding to the particular chute system. Loading an empty fleet takes EXPON(LOAD, 1) minutes, which is a random sample from an exponential distribution with a mean of LOAD. After loading, the chute system is freed by the FREE node F1 to begin loading the next fleet if any. The loaded fleet hauls the ore to the QUEUE node BIN. The ASSIGN node A1 sets XX(11) and XX(12) to the respective minimum and maximum haul times of the uniform distribution, i.e., UNFRM(XX(11), XX(12), 2).

Dumping a fleet load takes EXPON(DUMP, 3) minutes, which is a random sample from an exponential distribution with a mean of DUMP. After dumping, the ASSIGN node A2 updates the theoretical production, XX(6), multiplies it by the fleet availability and sets the product to XX(7), the actual production. Fleet availability is a random variable described by a uniform distribution with XX(4) and XX(5) as its respective minimum and maximum values, i.e., UNFRM(XX(4), XX(5), 5). The COLCT node CLT collects statistics on the total production. The ASSIGN node A3 sets XX(13) and XX(14) to the respective minimum and maximum return times of the uniform distribution for the empty fleet, i.e., UNFRM(XX(13), XX(14), 4). The fleet is then routed to the chute system with the shortest queue by the DISPATCH system. This DISPATCH system, a user-written function in FORTRAN 77, counts the remaining mine cars in a chute system queue to be loaded, and assigns an incoming empty fleet to a chute system with the shortest queue. In this model, seven attributes (i.e., ATRIB(I), I = 1, 7) define, respectively, ore tonnage, chute system, and loading, hauling, dumping and returning times of the mine car fleets.

The second portion of this model is the continuous part which accumulates the chute systems' operating hours, breakdowns and repairs. A STATE EVENT FORTRAN subroutine accumulates the operating hours of the chute systems, SS(I), I = 1, 3. The chute mean service time to failure is a random sample drawn from an exponential distribution with a mean of XX(8), i.e., EXPON(XX(8), S), S = 6, 8., and set to the global vectors XX(I), I = 1, 3, for the various chute systems. A DETECT node detects exactly when the accumulated operating hours of a particular chute system is greater than the mean service time to failure by a tolerance of 1 in the positive direction denoted by XP. Immediately this happens, the PREEMPT node, PRE, is activated and it pulls the particular chute system out for repairs, at the end of which it is introduced back into the system. Simulation of the model continues until the time limit set up in the control file, which is 23040 minutes. This time is equivalent to 48 working shifts, i.e., one-month period using two 8-hour shifts per day schedule.

Experimental Design and Experimentation

The number of runs used in this study to achieve variance stability and the desired tolerance [Scheaffer and Mcclave, 1994] is 500. This number was chosen from the experimental design process. Four design options were simulated for trial runs between 100 and 1000 with an increment of 100 runs. The variance of the outputs for each design option stabilized at 500 runs (i.e., increasing the runs from 500 did not affect the variance to any significant effect). The control file ORETRAMI.CON, network file ORETRAMI.NET, scenario file ORETRAMI.SCE, and fortran routines file ORETRAMI.FOR (I = 1, 18) for all the 18 design options are prepared and simulated in batch for 500 runs each.

ANALYSIS AND SELECTION OF OPTIONS

Based on past performance of the treatment plant, management requires that, within a year, the design option that is implemented should be able to achieve the lower production target (LPT) 70% of the time, and the upper production target (UPT) 30% of the time. A safety factor (SF) of 10% is added to these limits, in this study, to ensure that the selected option will be able to do the job, as illustrated in equations (14) and (15):

$$PROB(X = LPT) + SF \geq 0.80 \quad (14)$$

$$PROB(X = UPT) + SF \geq 0.40 \quad (15)$$

The probabilities for achieving LPT and UPT for each design option were calculated from the simulation results as follows:

$$PROB(X \geq LPT) = [SR(m \geq LPT)]/TSR \quad (16)$$

$$PROB(X \geq UPT) = [SR(m \geq UPT)]/TSR \quad (17)$$

Table 1 contains production statistics, and the probabilities of achieving LPT and UPT for each design option.

Selection Phase 1: Probabilities for Achieving Targets
Design options that meet the criteria defined in equations (4) and (5) are selected at this phase. Options 4, 5, 8, 9, 10, 13, 14, 16, 17, and 18 meet these criteria, and are highlighted in bold in Table 1.

Selection Phase 2: Fleet of Mine Cars Cost
The results from the selection phase 1 are considered in phase 2 and the selection criterion is the cost of a fleet of mine cars. Selection is based only on the probability of achieving UPT, because that for LPT, for all the options, is above the safety limit by over 10 %, and therefore not critical in this project. Comparison is made of options with the same number of resources, except mine car fleets. The first group consists of options 4 and 5. Probability of achieving UPT for these options are higher than the safety limit. Management can achieve UPT with a probability of 29.45% above the safety limit and reduce the capital investments in mine car fleets by about 16% by using option 4, and thus, this option is selected. Comparison is made of options 8, 9 and 10. Design option 9 is selected because the probability of achieving UPT for option 8 is too near and that for 10 is far above the safety limit. Thirdly, comparison is made of options 13 and 14. Option 13 is selected because it can achieve the UPT with less than 17% of capital investment requirements. Finally, comparison is made of 16, 17, and 18. Option 17 is selected because 16 is too near and 18 is too much above the safety limit. The selected options at this phase are marked with an asterisk (*) in Table 1.

Selection Phase 3: Cost of Chute System
The results from phase 2 are the input in the analysis at phase 3 and the criterion is the cost of constructing a chute system. Comparison is made of options with the same number of resource combinations except the number of chute systems. Comparison is made of options 4 and 13 and then of options 9 and 17. Options 4 and 9 are selected because the net value derived from addition of one chute system, in each case, is insignificant.

Selection Phase 4: Cost of a Bin Server
Comparison is made of options 4 and 9 based on the cost of building a bin server. Option 4 is selected with 1.3 % savings in investment capital to build the system in the short and medium-terms. Based on the composition of various design options, 13 is considered in the long-term since it preserves the technical features of option 4 while satisfying the long-term requirement of chute system 3.

Queuing Characteristics of Design Option 4
Preserving the static features of options and 4 and 13, 1000 simulation runs were carried out on these two options using @RISK [8]. The results are presented in Figures 3 and 4, respectively, for options 4 and 13. They are normally distributed with a mean of 40,439.92 and a standard deviation of 8,043.43 tonnes per month for option 4 and a mean of 40,874.75 and a standard deviation of 8,072.81 for option 13. The respective probabilities for achieving LPT and UPT are 97.86 and 71.17% for option 4 and that for option 13 are respectively 71.55 and 98.25%. The respective average utilization of chute systems 1 and 2, and the bin server are 78, 35 and 60% in the short- and medium-terms. The low utilization of chute system 2 is due to the low production tonnage served by this system, and hence the priority placed on chute system 1. The respective average waiting times in the chute systems 1 and 2, and the bin server queues are 3.00, 3.20, and 3.25 minutes per trip in the short and medium-terms.

ECONOMIC BENEFITS OF THE STUDY

Table 2 contains a summary of the capital requirements of the results of this study as compared to the original estimates made by engineers from the company. The original estimates resulted in a recommendation to construct 3 chute systems, 2 bin servers and to purchase 6 mine car fleets. The results and monetary values have been modified for the sake of confidentiality.

CONCLUSIONS AND RECOMMENDATIONS

A simulation model of an ore haulage system has been developed. From the technical and economic analyses of simulation results, the following conclusions and recommendation are drawn:

1. Design option 4 best meets the requirements of the system and minimize the capital investments, in the short and medium-terms. In the long term, however, the technical requirements necessitate the building of a third chute system, and thus, option13 is appropriate.

2. Probability of achieving UPT of 1500 tonnes per day exceeds the safety limit by 29% using option 4 and by 30% using option 13.

3. Implementation of these options will reduce the capital investments by 18% in the short- and medium-terms

TABLE 1 Production Statistics (*10^3 tonnes) and Probabilities for achieving LPT and UPT (%)

Deign Options	Chute Systems	Bin Servers	Mine Car Fleets	Average Tonnage	Standard Deviation	Probability LPT	Probability UPT
1	2	1	2	19.10	3.82	10.03	0.00
2	2	1	3	25.80	5.16	63.67	2.39
3	2	1	4	31.90	6.38	89.27	26.11
4*	**2**	**1**	**5**	**40.00**	**8.00**	**97.72**	**69.15**
5	**2**	**1**	**6**	**45.30**	**9.06**	**99.06**	**84.85**
6	2	2	2	19.60	3.92	13.14	0.00
7	2	2	3	27.30	5.46	27.43	5.59
8	**2**	**2**	**4**	**34.60**	**6.92**	**93.70**	**42.07**
9*	**2**	**2**	**5**	**41.60**	**8.32**	**98.30**	**74.86**
10	**2**	**2**	**6**	**48.30**	**9.66**	**99.41**	**89.80**
11	3	1	3	25.80	5.16	63.67	2.39
12	3	1	4	31.90	6.38	89.25	26.11
13*	**3**	**1**	**5**	**40.85**	**8.13**	**97.88**	**70.12**
14	**3**	**1**	**6**	**44.30**	**8.86**	**98.90**	**82.64**
15	3	2	3	27.30	5.46	27.43	5.59
16	**3**	**2**	**4**	**34.60**	**6.92**	**93.70**	**42.07**
17*	**3**	**2**	**5**	**42.20**	**8.44**	**98.46**	**76.73**
18	**3**	**2**	**6**	**48.30**	**9.66**	**99.41**	**89.80**

TABLE 2 Haulage System Capital Requirements

Design Option	Total Cost ($M)	%age Savings (%)
Original Estimates	3.475	0.00
4	2.850	18.00
13	2.875	17.27

and by 17% in the long-term compared to estimates obtained by the company under an earlier feasibility study.

4. It is therefore recommended that option 4 be used in the short- and medium-terms, and option 13 in the long-term, for building the actual system.

REFERENCES

Beckett, L.A., C. Haycocks and J.R. Lucas, 1979, "LHDSIM - A Load-Haul-Dump Simulator for Room-and-Pillar Mining Operations"; *Proc. of the 16th APCOM*, Tucson, AZ, pp 408.

Lilke, A.B., et al., 1993, "A Computer Model of

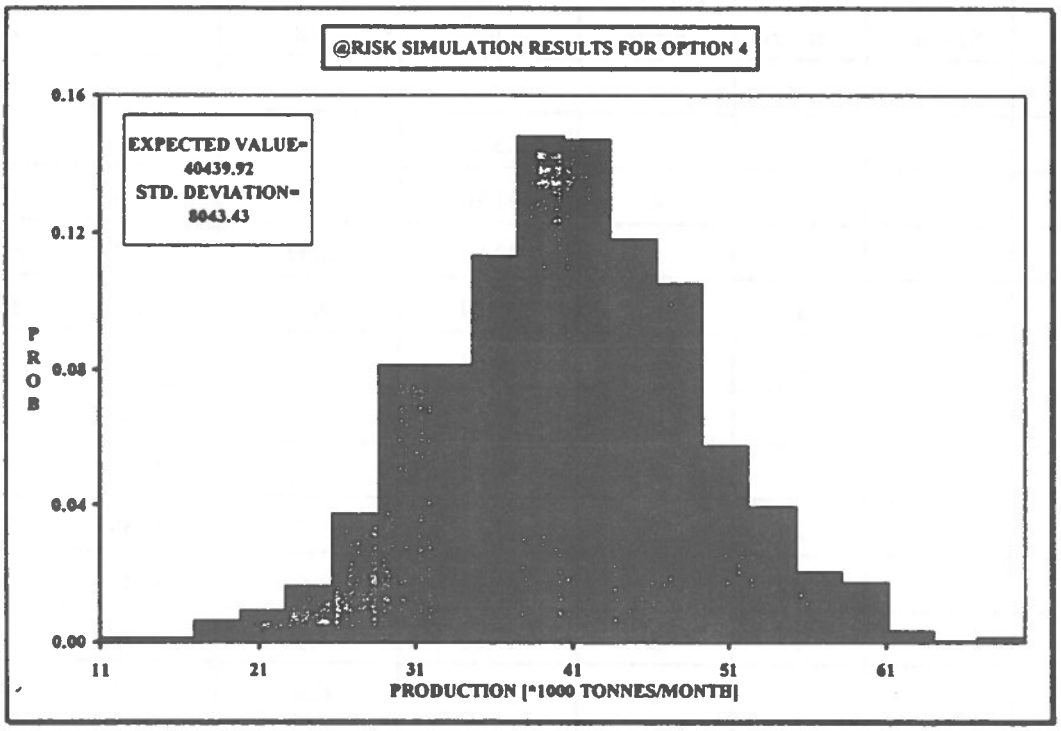

Figure 3 @RISK Simulation Results of Design Option 4

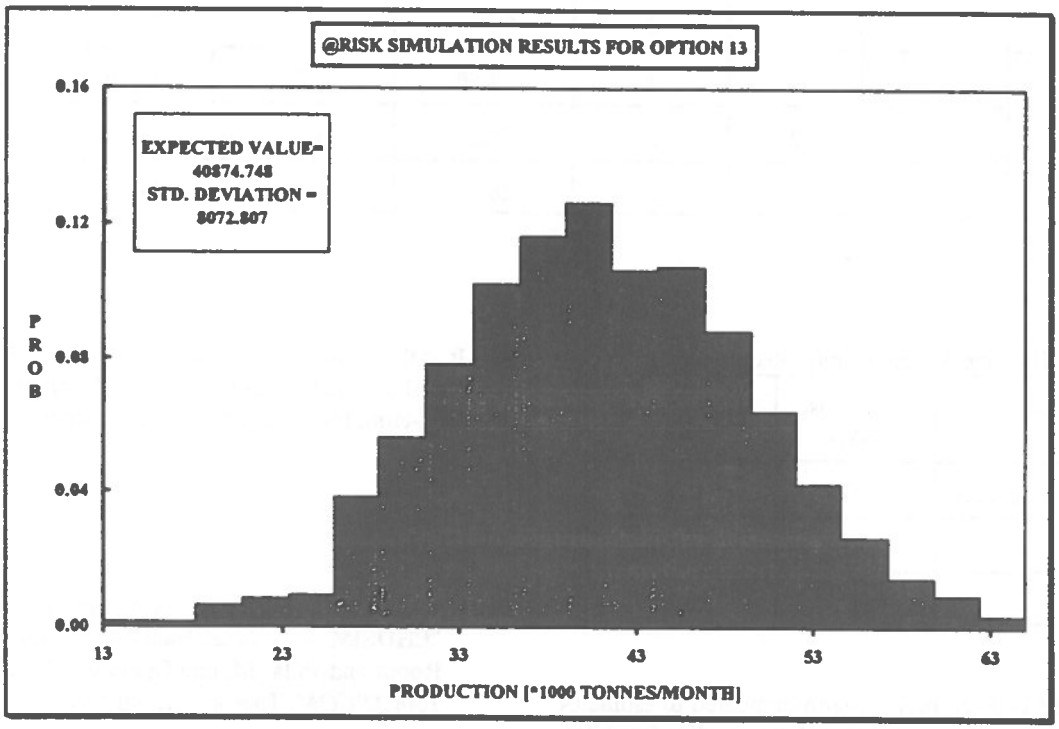

Figure 4 @RISK Simulation Results of Design Option 13

Underground Production Mining: A Tool for Benchmarking"; *Proc. of APCOM 93, Vol. 3*; Montreal, Quebec; pp 402-409.

Manular, C.B., E.K. Albert and R.V. Ramani, 1979, "A Simulation of a Surface Multi-Pit Surface Mining Operation"; *Proc. of the 16th APCOM*, Tucson, AZ, pp 384 -399.

Pritsker, A. Alan B., 1986, Introduction to Simulation and SLAM II, 3rd Edition; (c) by Systems Publishing Corp., W. Lafayette, IN.

Ramani, R.V., 1990, "Haulage Systems Simulation Analysis"; *in Surface Mining, 2nd Edition*, B. A. Kennedy (Editor); (c) by SME, Littleton, CO; pp 724 - 742.

Scheaffer, R.L. and J.T. Mcclave, 1994, Probability and Statistics for Engineers, 4th Edition; (c) by Wadworth.

Palisade Corporation, 1993, BestFit: The Automated Windows Solution to Finding the Best Distribution; (c) by Palisade Corporation, Newfield, NY.

Palisade Corporation, 1993, @RISK: Advanced Risk Analysis Software for Decision Makers; (c) by Palisade Corporation, Newfield, NY.

Tortike, W.S. and S. Frimpong, 1994, "Variance Simulation - A Practical Alternative to Monte Carlo Simulation and Sensitivity Analysis"; *Proc. of the 1994 SPE Petroleum Conference; Dallas, TX (August), pp 281-293.*

Borquez, G.V. and J.V. Thompson, 1990, "Feasibility Studies"; *in Surface Mining, 2nd Edition*, B. A. Kennedy (Editor); (c) by SME, Littleton, CO; *pp 396 - 423.*

Gentry, D.W. and T.J. O'Neil, 1984, Mine Investment Analysis; (c) by SME of the American Institute of Mining, Metallurgy and Petroleum Engineers, New York.

ACKNOWLEDGEMENT

The authors express sincere gratitude to the management and personnel of the State Gold Mining Corporation for their help in this study.

NOMENCLATURE

ϕ functional operator
N number of fleets in system
β measure of residue at car's bottom
α system availability
μ system utilization
ξ mine car fill factor
ϵ system operating efficiency
s_1, s_2 random number seeds
k constant
n number of cars in a fleet
c mine car capacity
ε error term
m_t maneuvering time
λ_t loading time
τ_l, τ_e loaded and empty travel times
δ_t dumping time
ω_t waiting time
cs available chute systems
bs available bin servers
SR(m ≥ LPT) number of simulation runs equal to or greater than LPT
SR(m ≥ UPT) number of simulation runs equal to or greater than UPT
TSR total simulation runs.

CAMI'95: 3rd Canadian Conference on Computer Applications in the Mineral Industry
Montréal, Québec, Canada, October 22-25, 1995

Economic Optimization of Stope Geometry Using Separable Programming with Special Branch and Bound Techniques

Jason Ovanic
Pea Ridge Iron Ore Company
Sullivan, Missouri, USA 63080

Dae S. Young
Department of Mining Engineering
Michigan Technological University
Houghton, Michigan, USA 49931

ABSTRACT:

Separable programming has lead to a new method of stope design, which uses a three-dimensional discretization of the ore zone. The block size, shape, and orientation are determined from a conceptual mining plan, and are not limited to regular shapes. An optimal economic stoping boundary is developed by optimizing the starting and ending locations for mining within each row of blocks. To determine these locations, two piecewise linear, cumulative functions are used for each row. The first function sums block values along the row for inclusion within the stope boundary, while the second function sums values for exclusion. The difference between the two functions is the sum of block values lying between the starting and ending locations. These positions are modelled by boundary location variables, which are used to build constraints associated with the mining plan. The stope boundary model is optimized by a mixed integer approach known as "special ordered sets". Restrictions are placed on ordered sets of discrete variables to create intervals in which the boundary locations must reside during each solution iteration. These restrictions force an efficient solution for the optimal boundary locations, and allow partial blocks at the boundary to be included.

RÉSUMÉ:

La programmation separée a mené une nouvelle méthode du dessin de stope qui utilise des valeurs discrets qui sont constitués des parties distincts; ces valeurs sont à trois dimensions du zone de minerai. La taille de bloc, de forme, et d'orientation est déterminée d'un projet minier conceptual, et ces tailles ne sont pas limitées aux formes regulières. Une limite optime de stope est déveeloppée par faire optime les emplacements au commencement et les emplacements à la fin pour l'explotation minière dans chaque rangée de bloc. Pour déterminer ces emplacements, deux fonctions-linéaires et cumulatives-sont utilisées pour chaque rangée. La première fonction ajoute des valeurs de bloc plar la rangée pour l'inclusion dans la limite de stope, tandis que la seconde ajoute de valeurs pour l'exclusion. La différence entre les deux fonctions est la somme de valeurs de bloc qui s'étend entre les emplacements au commenement et les emplacements à la fin. Ces positions sont modelées par des variantes limitées d'emplacement, qui sont utilisées à bâtir les constraits associés avec le projet minière. Le modèle est fait optime par une approche de numéro mêlé qui est connue comme "les séries arrangées spéciales." Les limitations sont mises sur de séries arrangées de variantes discrètes pour créer des intervalles dont les emplacements limitées doivent résider pendant chaque intération de solution. Ces limitations forcent une solution efficace pour les emplacements optimes et limitées et celles permettent des parties de bloc à la limite d'être incluies.

INTRODUCTION

A variety of algorithms for open pit optimization have revolutionized surface mine design (floating cone, Lerchs-Grossman, etc.). Melamud, and Young (1993) use a similar method of using special ordered sets to optimize pit geometry.

Compared to open pits, relatively little effort has been spent on underground mine optimization. Although less noted, some research into underground design optimization does exist (Tatiya, 1989; Tatiya, 1987; Nilsson,1986; Lizotte and Elbrond, 1985; Lawrence, 1984; and Riddle, 1977). Reasons for a lack of research include:

- Generality - It is difficult to develop an algorithm which is general to the various mining methods.
- Complexity - The geological, geotechnical, and economic data tend to be quite complex.
- Acceptability - Although CAD systems have automated the steps, underground mine design practitioners are loyal to traditional techniques of applying rules of thumb to plans and sections.

The purpose of this paper is to present a general approach for economic optimization of stope geometry. The approach is applicable to a wide variety of stoping situations and uses commercially available software for data reduction, optimization, and graphical presentation. This approach provides two major advantages over traditional stope layout methods:

1) It allows creative modelling of complex data without the offensive loss of control to a "black box".

2) The relatively quick solutions provide quantitative results for immediate comparisons between design scenarios.

THE STOPE LAYOUT MODELLING APPROACH

The Approach Description

There are four general requirements for stope layout modelling:

- A conceptual mine plan.
- A clear objective to be achieved by optimization .
- A block model (2 or 3-D) of data.
- The technical and economic constraints.

Before modelling begins the layout engineer must have a clear understanding of the overall mining system, and how the stoping layout fits into the mine plan. This understanding comes from a detailed conceptual plan, including mining method, mining direction, production rate and other pertinent details.

After the conceptual mine plan has been established, the optimization effort must be given direction. Direction is given through the development of a mathematical objective function. Objectives for stope layout might include:

- Maximum Net Present Value
- Maximum Resource Recovery
- Minimum Payback Period
- Minimum Cost

After the objective has been defined, the data to support optimization must be assembled. Remember that an optimal stope geometry is being sought. Therefore, any attribute used to support optimization must be spatially related. This data is best represented in a block model form. It will be shown later that, although convenient, the blocks are not required to be uniform or regularly shaped. Block geometry, however, should be consistent with the conceptual mine plane. Some block attributes that might be used to support optimization include:

- Block Tonnages
- Block Volumes
- Block Grades
- Block Total Costs
- Block Unit Cost

The last step before optimization is to develop the mathematical constraints that are the technical and economic restrictions to the stope layout model. Many of the technical constraints are straight forward and come from prior experience in similar ore zones. For example ground control considerations may dictate maximum stope dimensions, while equipment selection as a result of production rate may indicate minimum stope dimensions. Distances to geologic structures, and spatial relationships between adjacent stopes or development workings can also be modelled.

It can be seen from the above description, that the layout practitioners are in control of the optimization. There are no predefined objectives or constraints imposed. Therefore

the approach to optimization does not limit the creativity of designers, but provides quantifiable results to their creativity.

The Optimization Technique

A technique known as "Type-Two Special Ordered Sets" (SOS2) is used to optimize the stope layout model. "Type-two special ordered sets" is an operations research technique used to optimize piecewise linear functions. In general this type of technique is referred to as separable programming. The functions may be naturally piecewise linear, or they may be piecewise linear approximations of non-linear functions. An SOS2 is an ordered set of special variables for which the solution allows at most two variables to be nonzero. If two special variables are allowed in the solution, they must be adjacent. Creegan and Monforte (1990) present the following general example of an SOS2.

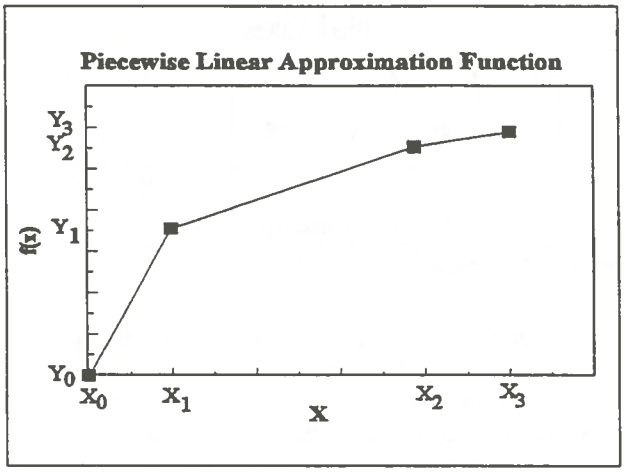

Figure 1: Typical Piecewise Linear Approximation Function

> "... a set of [special] variables [$\lambda_i's$] each of which is bounded between zero and one, the sum of the variables [λ_i] in the set is 1.0, and the variables are ordered so that some common attribute [reference value] is strictly increasing. From an abstract point of view, consider, in two dimensions, a nonlinear function ($y = f(x)$). This function is modeled by defining the model variables as points on the curve; [a piecewise linear approximation (see figure 1)] in this case the strictly increasing common attribute is the value of x. If the value of one of the variables[λ_i] is one, then all others equal zero, that is the point on the curve [$(x_i, f(x_i))$] represented by the variable [λ_i] is the solution. Otherwise two adjacent variables are nonzero and their values sum to one [$\lambda_i + \lambda_{i+1} = 1.0$], the remaining variables are zero, that is the solution is a midpoint on the straight line connecting the two points on the curve represented by the selected variables [$x_i\lambda_i + x_{i+1}\lambda_{i+1}, f(x_i\lambda_i + x_{i+1}\lambda_{i+1})$]."

An SOS2 is applied through mixed integer programming via a branch-and-bound algorithm. Branch-and-bound algorithms alone are not sufficient to solve even modest sized separable programming problems. However, the ordered structure of an SOS2 provides additional guidance to branching-and-bounding. Creegan and Monforte (1990, p.33) provide the following explanation of SOS2 logic.

> "The SOS2 set is dealt with as a whole by the branching algorithm instead of treating the variables within the set as individual discrete variables. The modeler assigns each variable a reference value, and the reference values are strictly increasing. The relaxed LP [linear programming] solution ignores the SOS2 requirements. When an SOS2 is selected for branching, the branching algorithm computes the sum of the variables in the set times [multiplied by] their reference values; the result is the amount of the reference attribute desired from this set. The subsequent branching step is set up using the computed value by considering two subsets: all variables from the beginning of the set up to the first variable whose reference is greater than the computed value; and all variables from the end of the set down to the first variable whose reference value is less than the computed value. Thus, the reference values are used to focus on the neighborhood of the desired solution in order to partition the solution space near the most likely optimal integer variable."

Stope Modelling

For convenience, refer to a typical row of blocks within a block model as a panel. Stope modelling is performed along a single panel or along several adjacent panels as dictated by the conceptual mine plans. Finding the stope outline which optimizes some attribute is the general objective of stope modelling. If the optimal starting and ending location for mining within each panel can be determined, then the optimal stoping boundary can be found.

A general method for constructing SOS2 sets has been shown. However, SOS2 sets must be incorporated into a mathematical model for stope optimization. To begin,

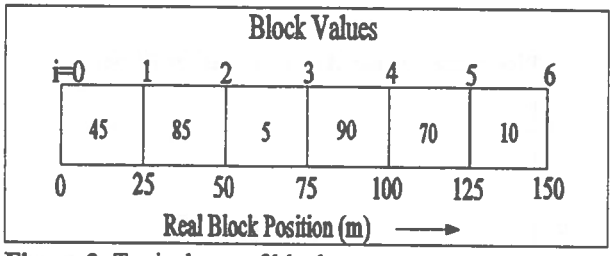

Figure 2: Typical row of blocks

assume the layout engineer is directed to find the optimal stope boundary which maximizes the block attributes from the panel shown in figure 2. Additional constraints for block referencing and stope size will be given.

SOS2 construction: Modelling begins by developing cumulative function for block values along each panel to be included in the stope. As a strictly increasing, piecewise linear function, a cumulative block value function is a natural candidate for construction of SOS2 sets. Figure 2 shows a typical row of blocks with their associated block values and block position. Figure 3 shows the cumulative block value function for the panel shown in figure 2. The block values can be any quantitative attributes which are cumulative in nature. The block position values serve as reference values for each special variable within the SOS2 sets.

Recall, special variables are bounded between zero and one, the sum of the variables in each set is 1.0, no more than two variables from each set can appear in any solution, and if two appear they must be adjacent. These properties are used to ensure the stope beginning and ending locations fall on discrete points on the block value cumulative function. In a case where only one special variable from any set appears in a solution, the solution lies at a breakpoint on the cumulative function (at the edge between two blocks). In a case where two special variables from any set appear in the solution, the solution occurs at a point between two breakpoints on the cumulative function (within a block).

Two SOS2 sets can be generated from Figures 2 and 3. Assume that mining will proceed from left to right somewhere within the panel. One SOS2 set will define where mining will begin, the second SOS2 set will define where mining will end. Let the first SOS2 set be identified by the special variables L_t (leading boundary) and the second set, by T_t (trailing boundary), where t ranges over the number of points on the cumulative block value function (number of blocks in the panel plus one). By using two cumulative functions as defined above, the difference between the two functions can be examined to optimize the sum of the values between the boundaries.

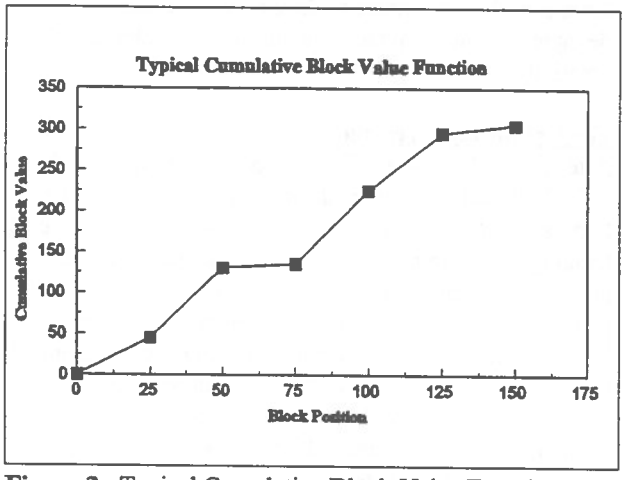

Figure 3: Typical Cumulative Block Value Function

An objective function can be developed using the two SOS2 sets and the difference between the two cumulative functions described above. In model form the objective function is:

$$\text{Maximize } \sum_{i=0}^{n} a_i L_i - \sum_{i=0}^{n} a_i T_i$$

where: a_i is the ith attribute value
L_i is the ith leading special variable
T_i is the ith trailing special variable
L_i and T_i are bounded between 0 and 1

To optimize the objective function, a relationship between the special variables in each set and the block positions must be established. This is accomplished using the reference values referred to earlier. A special set of constraints known as reference rows are written into the formulation to direct the optimization. In model form the reference rows are:

$$\left(\sum_{i=0}^{n} x_i L_i\right) - B_l = 0.0$$

$$\left(\sum_{i=0}^{n} x_i T_i\right) - B_t = 0.0$$

where: x_i is the ith block position (reference value)
L_i is the ith leading special variable
T_i is the ith trailing special variable
B_l is the leading boundary location variable
B_t is the trailing boundary location variable

In practice, the values of the boundary location variables

provide the meaningful results from the optimal solution to the objective function. When an optimal solution is found, B_l is the real position of the optimal leading stope boundary and B_t is the real position of the optimal trailing stope boundary. These positions are located from the zero position of the first block, or from some arbitrary datum (a mine grid system can be incorporated).

When modelling with SOS2 sets another special type of constraint is usually required. This constraint is referred to as the convexity row. A convexity row is required for each SOS2 set. The convexity rows are simple explicit statements requiring the sum of the special variables to equal one. In model form the convexity rows for this example are:

$$\sum_{i=0}^{n} L_i = 1.0$$

$$\sum_{i=0}^{n} T_i = 1.0$$

where: L_i is the ith leading special variable
T_i is the ith trailing special variable
L_i and T_i are bounded between 0 and 1

Any remaining constraints necessary to adequately model the stope are entirely constructed by the layout engineer. These types of constraints are typically referred to as structural constraints. For example, experience may show for similar mining conditions there may be some maximum stope length which should not be exceeded due to ground control concerns. There may also be some minimum stope length based on equipment requirements. In model form such constraints might be:

$$B_l - B_t \leq MaximumValue$$
$$B_l - B_t \geq MinimumValue$$

Notice that these constraints operate only on the boundary location variables representing the real location of the stope boundaries. However, there is virtually no limit to the types of constraints which might be developed.

Optimization and Results: After the stope model has been mathematically formulated with an objective function, reference and convexity rows, and all necessary structural constraints, the optimization follows. Several commercial, mathematical programming computer software packages provide special ordered set facilities. MPS and LINDO are two of the more popular packages.

To the author's knowledge all of the commercial packages use proprietary variants of the special ordered set facilities originally developed by Beale and Tomlin (1969) and Tomlin (1970). The MIPIII User's Manual (Ketron, 1993) describes the algorithm in the following way:

> "The SOS algorithm works by squeezing both end against the middle. For each [SOS2] set, MIPIII establishes a lower bound and an upper bound, ie., the sequential number of the first member of the set that can be nonzero and the number of the last member of the set that can be nonzero. MIPIII manipulates these bounds to force the nonzero member of the set to be selected from the subset of interest. Initially , the bounds are set on the first and last members of the set; thus permitting any member of the set to be nonzero [the relaxed solution]. The branch and bound algorithm systematically limits selection from a smaller and smaller subset until it forces an integer [discrete] solution. Because of this process and its demonstrated efficiency, you should properly order the members of the set relative to a significant reference value."

Suppose the layout engineer is given the data shown in figure 2, and is asked to design a stope which maximizes the block attributes, but the stope must be less than or equal to 33 1/3 meters long. The solution arrived at by modelling and mixed integer programming is the same solution which can be arrived at by inspection. The solution is shown in figure 4. The resulting solution indicates that there are two special variables corresponding to the leading stope boundary (L_4 and L_5). They are adjacent and their sum is equal to 1.0. The special variable corresponding to the trailing stope boundary is equal to 1.0. All other special variables are equal to zero. These values result in a stope begining 75 meters from the origin ($x_3\ T_3 = 75$) and ending 108.33 meters from the origin ($x_4\ L_4 + x_5\ L_5 = 108.33$).

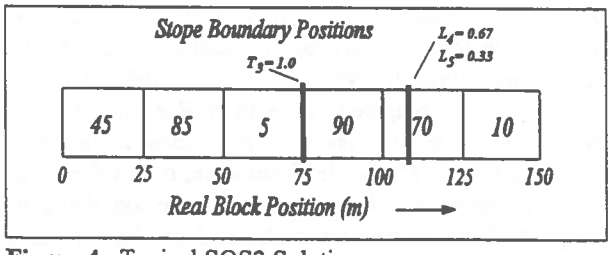

Figure 4: Typical SOS2 Solution

The solution shown in Figure 4 represents a stope boundary

that begins at block four, and continues 8.33 meters into block five. The stope is 33.33 meters long, containing 113.33 block attribute units.

It can be seen from figure 4 that it is not necessary to take complete blocks along the stope boundary as required by other optimization techniques which utilize block models. Also, the blocks are not required to be regularly or uniformly shaped. Because the models are built on cumulative functions, there are no restrictions on size or shape. This allows geologic interpretations to be overlaid on the block model to truncate blocks at discontinuities prior to optimization. Once optimized, the solution for the boundary location variables can be used to create coordinates which are (or can be) tied in to the mine grid coordinates. This facilitates automated plotting of the resulting optimal stope layout.

CONCLUSIONS

The example presented here is admittedly overly simplified for practical purposes. However, the example allows the reader to follow the general modelling approach to the same conclusion as found by inspection. In reality, when optimizing stope boundaries with a block model, the layout engineer is faced with tens of panels comprised of hundreds of blocks on several levels or layers. At this level of modelling there is no way of achieving a solution by inspection. The general modelling approach however, is the same. Two special ordered sets of variables defining the leading boundary and the trailing boundary are required for each panel of blocks to be included in the stope model. The associated reference rows and convexity rows are also required. The structural constraints are virtually entirely developed by the layout engineer, as dictated by the conceptual mine plan. As the model becomes more complex additional constraints may be required to constrain the amount of boundary offset between the ends of adjacent panels.

As models become large, computer memory and speed become factors in practical application of the general modelling approach. Moderate sized models have been optimized for stoping boundaries in the Pea Ridge iron ore body, near Sullivan, Missouri, USA. These models were optimized using MPS-MIPIII software, on a DOS based personal computer. The optimization were completed in a range of a few minutes to several hours depending on model complexity. The stope models have not yet been incorporated into the mining plans, therefore it is too early to determine if the modelling has been realistically successful. The general optimization method discussed here has proven to be an effective tool for stope modelling.

REFERENCES

BEALE, E.M.L., and TOMLIN, J.A., 1969.
Special Facilities in a General Mathematical Programming System for Non-Convex Problems Using Ordered Sets of Variables. Proceedings, 5th International Conference on Operational Research, John Wiley, New York, pp. 447-454.

CREEGAN, J.B., and MONFORTE, F.A., 1990.
Southern California Gas Company Uses Special Ordered Sets to Model Regulatory Guidelines. Interfaces, Vol. 20, No. 4, pp. 28-42.

KETRON MANAGEMENT SCIENCE. 1993.
MIPIII User's Manual, Ketron Management Science, Arlington, VA.

LAWRENCE, D. R., 1984.
The Optimization of Raise-Connection Spacing in Gold Mines. Journal of the South African Institute of Mining and Metallurgy, Vol. 84, No. 1, pp.10-20.

LIZOTTE, Y., and ELBROND, J., 1985.
Optimal Layout of Underground Mining Levels. Canadian Institute of Mining and Metallurgy Bulletin, Vol. 78, No. 873, pp. 41-48.

MELAMUD, A., and YOUNG, D.S., 1993.
A System for Optimizing the Interdependence of Operating Cost and Three Dimensional Pit Development. 24th APCOM Symposium, Montreal, Quebec, Canada, pp. 75-82.

NILSSON, D., 1986.
Optimum Stope Height and Blasthole Length at Luossavaara. Engineering and Mining Journal, June, pp. 52-57.

RIDDLE, J.M., 1977.
A Dynamic Programming Solution of a Block-Caving Mine Layout. 14th Symposium of the Application of Computers and Operations Research in the Minerals Industry. Society of Mining Engineers-American Institute of Mining, Metallurgy, and Petroleum Engineers, New York, pp.767-780.

TATIYA, R.R., and ALLEN, H.E.K., 1987.
An Approach to Modelling Stoping Boundaries by Use of Incremental Analysis. African Mining, The Institution of Mining and Metallurgy, pp. 365-374.

TATIYA, R.R., 1989.
Computer Assisted Stope Design. 21st Symposium of the Application of Computers and Operations Research in the Minerals Industry. Society of Mining Engineers, Littleton, CO, USA, pp.767-780.

TOMLIN, J.A., 1970.
Branch and Bound Methods for Integer and Non-Convex Programming. Integer and Non-Linear Programming, North-Holland, pp. 437-450.

Shave Off Grade in stead of Cut Off Grade

Jorgen Elbrond and Atef Hanna Harb
Department of Mining Engineering
École Polytechnique, Montreal, Canada

Nicolas Sisto
Department of Economics, University of the South Pacific, Suva, Fiji

Xiaoli Tang
Department of Economics, University of Montreal, Canada

ABSTRACT:

The numerical results of optimization of the cut off grade of underground mineral deposits show consistently larger amounts of ore at a higher grade, thus higher values of the deposits, than what is being obtained by the mining. There are many reasons for that. One of the reasons is that sometimes rich ore has to be left in situ because it is "*hidden*" behind poor ore and some poor ore has to be mined to gain access to rich ore behind. This problem cannot be solved by the conventional optimization procedure: cutting in a grade frequency function, but it can be captured by defining the mining constraints and proceeding with a contour optimization.

The result is a "*shave off*" of the grade frequency function, which generally results in a lower amount of ore of a lower grade and consequently a lower but more realistic value of the deposit.

RÉSUMÉ:

Les résultats numériques de l'optimisation de la teneur de coupure de gisements de minerai exploités en souterrain montrent le plus souvent des quantités de minerai plus grandes et de teneurs plus élevées donc des valeurs des gisements plus élevées, que ce qu'on obtiendra par le minage. Il y a plusieurs causes de cet état de chose. Une de ces causes est que quelques fois du minerai riche doit être laissé en place parce que "*caché*" derrière du minerai pauvre, et quelques fois du minerai pauvre doit être miné afin d'avoir accès à du minerai riche derrière le minerai pauvre. Ce problème ne peut être résolu par l'optimisation traditionnelle: couper dans une fonction de fréquence de teneur. Mais il peut être capturé en définissant les contraintes de minage et procéder avec une optimisation du contour.

Le résultat est un "*copeau*" de la fonction de fréquence de teneur, ce qui produirait des quantités moindre de teneur moindre et une valeur moindre mais plus réaliste du gisement.

INTRODUCTION

A general complaint by practical mining people about underground mine production plans, which have been elaborated on the basis of geostatistical and other geological estimation procedures, is that the cut off grade "optimization" of the mine value leaves "*a patchwork of blocks in the reserve with no relation to the mineability*" (Clow).

In open pit mines the maximization of the mine value is found by the final contour optimization. The constraints to mining a block on a lower level are that the 9 blocks on the level immediate above must have

been mined first and so on upwards.

In the underground mine there is a lot more flexibility of the mining sequences. The mining could even technically be done like by a mole. This should not leave, however, the impression that anything valuable could be mined, which of course conducted to the above mentioned complaint. The problem can be solved by using the technique of contour optimization by 1) defining the precedences (constraints) of blocks to be mined and then by 2) finding the maximal value of the mined blocks submitted to the prescribed mining constraints. These must be established by the mining operations engineer. The optimization procedure, which finds the maximal value, would then leave rich blocks, which could not pay for poor blocks ahead of them, unmined, and include poor blocks, which can be payed for by rich blocks behind them.

This concept can be called shave off grade optimization in stead of cut off grade optimization. It doesn't applied a clean vertical cut in the block grade (value) frequency curve, but shaves off blocks of various grades (values) in the frequency curve.

The mathematical technique used is the maximal flow in networks.

THE METHOD

This method, presented by Picard in his famous paper "*The maximal flow in networks*", lends itself very well to the underground mine production planning problem. On figure 1, the nodes O represent the mining blocks,

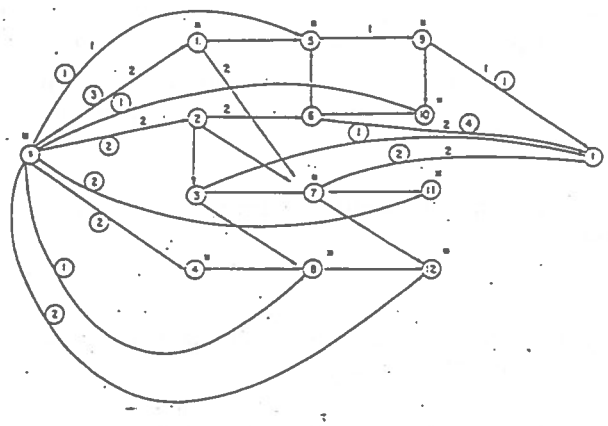

Figure 1. Network, Picard.

which have net values, negative and positive, derived from mineral contents and sales prices and costs of exploitation and treatment. The blocks are connected by arcs, which describe that a certain block has to be mined before the considered block can be mined. Picard's example is even directly applicable to a level of the underground mine and nothing prevents us to add other levels to simulate an underground mine. We can also add arcs, which describe the precedences of block of one level over blocks on a lower level. Safety precedences and mine lay out precedences can thus easily be illustrated. The solution procedure consists in joining all positive blocks with a source (s) and all negative blocks with a sink (t) by fictive arcs and assigning the value of the nodes as capacities of the fictive arcs and assigning infinite capacities to the original arcs and then search for the maximal flow by the Ford and Fulkerson procedure.

Picard also describes the transformation of the maximal flow problem to a 0 - 1 linear programming problem for which very efficient computer programs exist.

RESULTS

The result of the optimization is the closure of maximal value, which is the assembly of labelled nodes (*) in figure 1. The value of the maximal closure is 9. The sum of the values of all positive blocks is 14. This then in brief illustrate the problem in that the conventional cut off grade optimization would arrive at a value of 14, which cannot be obtained, whereas the realistic mining arrives at a value of 9.

By expanding the illustration of the problem in figure 1 and adding two lower levels (each level with block values and precedence arcs identical with those of figure 1's level), stacked upon each others as in an underground mine (figure 2), where some arcs from nodes on lower levels to nodes on higher levels have been added, we obtain a maximal closure — the assembly of the blocks with the thick walls — of a value of 22. The conventional but unrealistic, cut off grade optimization arrives at a higher value (3 x 14 = 42) namely the sum of all positive blocks.

The difference between the conventional optimization and the one presented here can be illustrated by frequency functions. Figure 3 shows the amounts of ore above the "*optimal*" cut off grade according to the conventional optimization. In figure 4 the ore, of positive as well as of negative value, which is to be

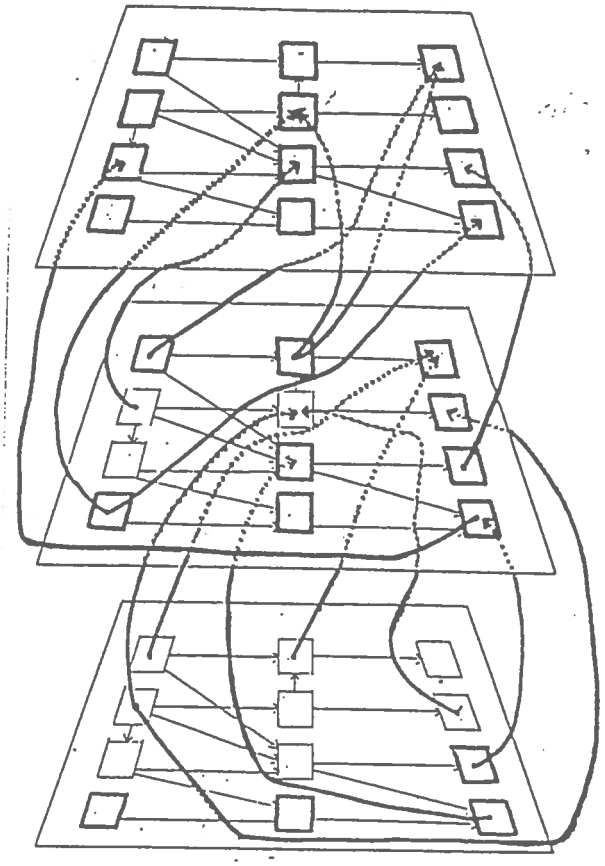

Figure 2. 3 levels with precedences.

mined according to the realistic mining sequences, is shown and the ore, positive as well as negative, which is not mined, has been shaved off.

CONCLUSION

It appears that the realistically determined amount, grade and value of a deposit are lower than the ones found by the conventional optimization.

The proposed technique uses well known mathematical and computational procedures. But in order to find the mining restrictions, the input by the practical mining engineer is crucial.

It is a good example of how operations research directly can enhance the quality of the mine valuation.

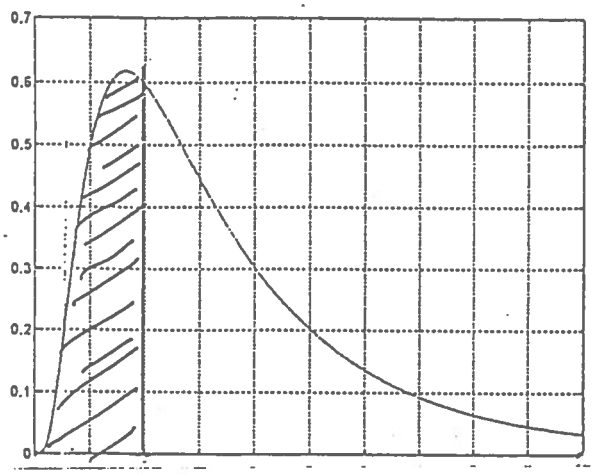

Figure 3. Cut off.

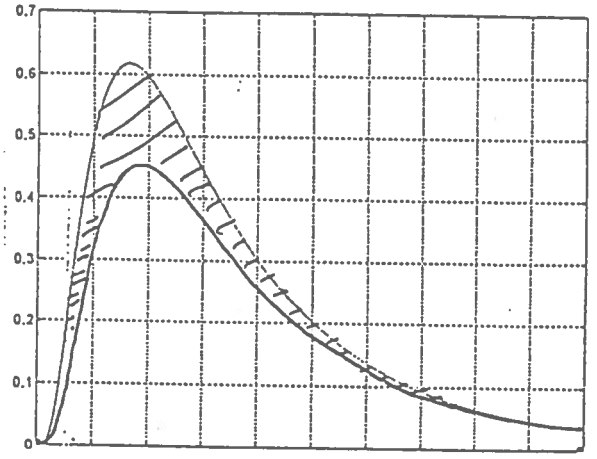

Figure 4. Shave off.

REFERENCES

Clow, Graham G., 1990
Lessons from the front lines — recent gold mine failures in Canada, CIM, AGM, Ottawa.

Picard, J.-C., 1976
Maximal closure of a graph and application to combinational problems. Management Science, Vol. 22, No. 11, pp. 1268-1272.

5.

mine planning
planification des mines

CAMI'95: 3rd Canadian Conference on Computer Applications in the Mineral Industry
Montréal, Québec, Canada, October 22-25, 1995

A Modified Network Flow Algorithm for Pit Limit Optimization

Yaohong D. Jiang
Systemes Geostat International Inc.

ABSTRACT

This paper presents an efficient, modified network flow algorithm based on the version outlined by Johnson (1968), as well as a computer implementation. Program *FLOWPIT* implements the *network flow algorithm* for pit limit optimization by linking *bounding techniques* with an efficient maximum flow algorithm to reduce memory requirement and increase speed efficiency, and by using *a conical search pattern* to allow for variable wall slopes for different pit areas. The resulting algorithm is superior to *L & G* in terms of algorithmic simplicity, and competitive to 'heuristic' floating cone algorithm in terms of speed efficiency. In addition, a necessary and sufficient condition is also identified for application of section-based bounding techniques.

RÉSUMÉ

Cet article présente un algorithme efficace de flux réticulaire basé sur celui élaboré par Johnson (1968) ainsi qu'une implantation logicielle. Le programme FLOWPIT implante l'algorithme de flux réticulaire pour l'optimisation des limites de fosses à ciel ouvert en reliant des techniques de limitation avec un algorithme efficace de flux maximum afin de réduire la demande en mémoire et augmenter la vitesse de traitement. Un patron de recherche conique est utilisé pour tenir compte des variations de pentes dans les différentes parties de la fosse. L'algorithme résultant est supérieur à L&G en terme de simplicité algorithmique et se compare à l'algorithme des cônes flottants en terme de vitesse de traitement. Une condition nécessaire et suffisante est aussi identifiée pour l'application des techniques de limitation sur section.

INTRODUCTION

One of the fundamental tasks in open-pit design is to determine the final configuration of the open pit at the end of its economic life, which will optimize ore recovery and total net profit. The mathematical formulation of the problem was solved two decades ago (Lerchs and Grossman 1965) and a number of algorithms on the topic have been published. But not all of these algorithms produce optimum results and some of them even fall pray to rather simple cases.

There are basically two rigorous optimizing techniques, namely, L & G and network flow algorithm. Lerchs and Grossman (1965) demonstrated that the optimal pit limit problem was equivalent to determining the maximal closure in a directed, weighted graph. They also mentioned that the maximal closure problem is equivalent to finding the maximum flow in a modified network. Johnson(1968) elaborated on this concept for use in multi-period scheduling for open pits and showed, for the first time, how an equivalent network could be constructed from a block model. This same concept was proved mathematically by Picard (1976).

Very efficient algorithms exist for determining the maximum flow in a network, and thereby determining the optimal pit limit. The network flow algorithm for pit optimization is thus resolved *much* faster by computer than L & G, especially when an efficient maximum flow algorithm is used. However, according to literature survey, this algorithm has found very limited industrial applications, due probably to the reason that, at the first time the technique was explicitly suggested by Johnson in 1968, the only maxflow algorithm available was Ford-Fulkerson's labeling procedure, which is known not to halt in finite steps under certain circumstances. Although more and more efficient algorithms appeared since then, the gap existing between theory and its application has prevented the mining industry from taking advantage

of them. As a result, bias has been given to L & G whenever a true optimizing technique is required for pit limit determination (Lipkewich and Borgman 1969, Chen 1976, and Whittle 1988). In addition to these, there are two other drawbacks inherent in the early version of the network flow algorithm: it requires larger RAM than L & G does; like the original L & G, it was not capable of handling multi-slope pits.

All these explain the limited industrial applications of the technique up till now. However, it will be shown that by using an efficient maxflow algorithm linked with bounding techniques and a conical search pattern, most of these limitations can be easily overcome, which in turn leads to a technique that not only guarantees optimality but also is efficient in practice.

BASIC NETWORK FLOW ALGORITHM

The network flow algorithm for pit optimization uses a maximum flow algorithm as its major ingredient. Once the maximum flow is found for the network constructed from a block model, the optimum pit can be determined. In what follows, a node (or vertex) in a network corresponds to a block in the block model. Assuming a 2D block model as shown in Figure 1a, the algorithm may be summarized as follows (Figure 1b):

1) Remove all positive vertices not covered by negative vertices in their respective closures i.e., remove ore blocks with no waste within their removal cones.
2) Construct directed arcs between an artificial source and all positive vertices. The arc capacity is equal to the node value.
3) Construct directed arcs between all negative vertices and an artificial sink. The arc capacity is equal to the absolute node value.
4) Construct a directed arc with an infinite capacity between each node i and each of those vertices which overlays node i and which does *not* overlay any other vertices that are within the removal cone of node i. These arcs represent the precedence relationships between blocks.
5) Use a maximum flow algorithm to find the maximum flow in the network. Vertices remaining in the network that can still be labeled belong to the maximum removal closure.

Obviously, the efficiency of the algorithm is dependent on Steps 4) and 5). They are further discussed in the following sections.

DESIGN AND PROGRAMMING CONSIDERATIONS

For the network flow algorithm to be of practical use, the following considerations have been taken into account.

Bounding Techniques

Bounding techniques comprise a group of techniques used to limit the search for the optimum pit by defining upper and/or lower bounds to the optimal pit. In the 17th APCOM, Barnes and Johnson (1982) presented a Fundamental Theorem of Bounding:

> "Assume a given economic model, and an initial pit design (not necessarily optimum) which is feasible under some pit slope definition of interest. Consider the economic block model created by removing the blocks contained in the initial pit design. Now, assume a second pit slope definition which is less severe than the initial pit slope definition of interest. If the optimum pit design for the modified economic block model using the second, less severe, pit definition does not contain any blocks, then the initial pit design is an outer bounding design."

As Barnes and Johnson pointed out, the implication of this theorem is powerful and useful. For example, consider an economic block model and a given pit slope definition of interest. Also assume that a less severe pit slope definition is available, accomplished by a fast efficient algorithm for calculating the optimum ultimate pit under this less severe definition. In such a situation, this fast algorithm can be used to find an outer bounding pit, which will, in most cases, contain only a fraction of the blocks contained in the whole block model. Subsequent optimization needs only to be applied to this fraction so that both memory and speed efficiencies is achieved. The 'fast' algorithms they proposed are:

1) Block Model Reduction,
2) Prepass, i.e. consider only positive blocks and those negative blocks that belong to the union of the cones constructed from these positive blocks;

-1	-1	-1	+1	-1
-1	+3	-1	+2	-1
-1	+2	-1	+2	-1

Figure 1a A hypothetical 2D block model

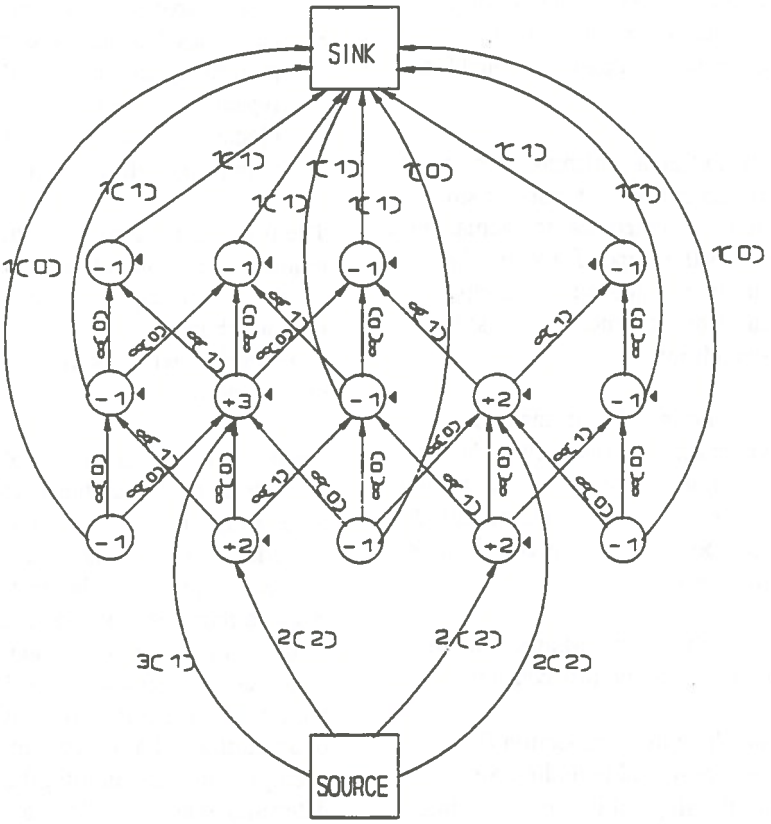

Figure 1b The basic network flow algorithm

3) Optimal Cross Sections Bound
4) 2½D Projection Bound
5) Best Valued Cross Section Bound
6) 3-D Dynamic Programming Bound

The first two bounding algorithms are simple to program. The last one is based on Johnson's 3D Dynamic Programming Algorithm and requires much more work. Algorithms 3), 4) and 5) are all based on Lerchs and Grossman 2D algorithm and are relatively straightforward to program. Since they all work on sections, we refer to them as *section-based bounding algorithms*.

Unfortunately, application of the Fundamental Theorem of Bounding using a section-based bounding algorithm is not as straightforward as the algorithm itself. Since all of these section-based bounding algorithms use Lerchs and Grossman 2D algorithm, the slope in section is constant and stipulated by the block dimension. For example, in case of cubic blocks, the slope is 45°.

In application of the bounding algorithms, Barnes and Johnson introduced the so-called "generalized slope definition" and implicitly assumed that the actual slope used in section is same as the slope of interest. This restriction is too severe in practice, since it simply means that in most cases block dimension must be adjusted to meet this condition.

For the section-based bounding algorithms to be of practical use, we have relaxed the restriction. *As long as the slope in section stipulated by block dimension is no smaller than the slope of interest*, a section-based bounding algorithm can be applied. This condition is both necessary and sufficient.

Therefore, to properly apply a section-based bounding algorithm, the following three-step procedure is recommended:

1) Make sure that pit slope in cross section θ_c embodied in an section-based bounding algorithm is no smaller than the slope of interest θ_i. If this condition is not met, stop. No proper bounding pit can be found using any of these three bounding algorithms. Otherwise goto Step 2);
2) Apply any of the section-based bounding algorithms to obtain a pit P;
3) If $\theta_c == \theta_i$, stop. P is a bounding pit. Otherwise, with the slope(s) of interest, construct cones using all of the *boundary* blocks in P as base blocks. The *union* of these cones with P is a proper bounding pit.

In the program developed, a combination of three bounding techniques was used to reduce the memory requirement for the network flow algorithm. These are: *layer cake (introducing data layer by layer), prepass,* and *modified best valued cross section bound.*

Pit Slopes

There are primarily two techniques for specifying the slope angle(s) of a pit:

1) Using analytical geometry, determine which block centers lie within a frustum (or an elliptical cone or hyperboloid) extending from a block or a set of blocks considered for removal and intersecting the current surface topography.
2) Define precedence relationships by using block addresses. This leads to establishing support patterns to approximate the shape of cones. A typical example is to use 5:1 and 9:1 overlaying blocks or 5:1 overlaying blocks plus a *knight move* to approximate a 45° slope in case of cubic blocks.

The first technique is much more direct, although requires more computational time if not programmed carefully. It is capable of establishing multi-slopes without changing the sizes of the blocks used in normal computation, whereas this must be done with the second method.

Chen (1976) used a conical search pattern to allow the variable slopes to be considered when using a L & G based program. In his approach, the search pattern or precedence constraints for a given block is a group of indices, representing the locations of the blocks which must be removed before a given block can be extracted. It forms a three dimensional cone (truncated or not), which is often referred to as the 'removal cone'. The pattern was generated by a set of predetermined pairs of azimuths and dips. The linear interpolation method is employed in calculating the dips of the blocks to determine whether a block at a specified level should be included or not. The same search pattern is used in the program developed.

If not programmed properly, the process of establishing search pattern for a block could affect the efficiency of the whole algorithm, since such a pattern has to be generated for all the blocks which are to be used as cone bases. This means almost all the blocks in the block model, if no bounding techniques are used. In

fact, establishing a search pattern for a given block is essential regardless of the method used for determination of final pit limit when a variable slope is required. The most straight-forward approach is to compute the azimuth and dip of a line between the centers of the given block (served as the cone base) and the block to be tested for inclusion. This involves at least divisions, and/or trigonometric function calls — a potentially time consuming process as the number of blocks to be tested for inclusion for a given base block increases exponentially as the level of the base block increases. A better approach is to form a 'conical template' once and use it repetitively to establish actual conical search patterns.

Computing the template *bd[][][]* is a simple process and involves calls to trigonometric function *tan2()* for determining the azimuth of a block within the bounding pyramid (Figure 2) of the cone base *(ci, cj, ck)*, but requires only one pass through the pyramid. A detailed algorithm can be found in Jiang (1991).

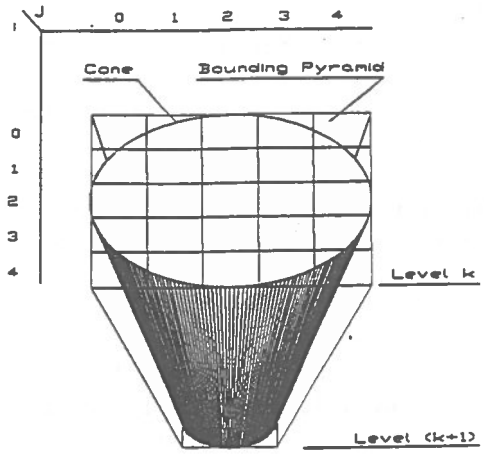

Figure 2 A cone and its bounding pyramid

This template is a 'complete' cone: it is not truncated with respect to the boundary of block model. For example, given a block model *ni×nj×nk*, then *bd[][][nk-k]* in Figure 2 will be filled with:

bd[0][0][nk-k] = bd[0][4][nk-k] = 1;
bd[1][0][nk-k] = bd[1][4][nk-k] = 3;
bd[0][1][nk-k] = bd[0][2][nk-k]=
bd[0][3][nk-k] = 0;
bd[1][1][nk-k] = bd[1][2][nk-k]=
bd[1][3][nk-k] = 4;

Once the template is established, the actual conical search pattern for a given block can be easily formed using only integer plus, minus and logical operators.

Given *A* and *S*, a set of given azimuths and the corresponding set of maximum slope angles respectively. Use *min_s* to denote the minimum of set *S*. The maximum number of rows for the conical template is computed as: *nc* = 2*(*nk*-1) / tan(*min_s*)+1. The coordinate of the base block of the template cone is computed as: (*ci, cj, ck*) = (*nc/2, nc/2, nk-1*). Assuming that a 2D array *ibd[0:2][0:nk-1]* exists, where *ibd[0][k]* and *ibd[1][k]* are the minimum and maximum i indices on level k of the bounding pyramid of block *(bi, bj, bk)* respectively, then the search pattern or the removal cone *nbd[0:1][0:ni-1][0:nk-1]* of block *(bi, bj, bk)* can be computed as shown in the algorithm *FormSearchPattern* in Figure 3. Note that the upper bound of the second dimension, i.e. *ni-1*, of the array nbd[][][] is different from that of array *bd[][][]*, i.e. *nc-1*.

```
Algorithm FormSearchPattern
  (ni, nj, nk, ci, cj, ck, bi, bj, bk, nc,
   ibd[][], bd[][][], nbd[][][])
Begin
  for k from 0 to bk-1
    for i from ibd[0][k] to ibd[1][k] do
      n0 ← i + ci - bi;
      n1 ← bj - cj;
      nbd0 ← bd[0][n0][ck-k] + n1;
      nbd1 ← bd[1][n0][ck-k] + n1;
      { any blocks in row i on level k
        are included in search pattern? }
      if (nbd0 < 0 or nbd1 > nj-1) then
        nbd[0][i][ck-k] ← 32767;
        nbd[1][i][ck-k] ← 32766;
      else { truncate the pattern if needed }
        if (nbd0 < 0) nbd0 ← 0;
        if (nbd1 > nj-1) nbd1 ← nj-1;
        nbd[0][i][ck-k] ← nbd0;
        nbd[1][i][ck-k] ← nbd1;
      end if
    end for i
  end for k
End Algorithm;
```

Figure 3 Algorithm for establishing conical search pattern from a template

The procedure first determines the search pattern according to the template. If no blocks in row i on level k fall within the pattern, a bigger value (32767) is assigned to the lower bound *nbd[0][i][ck-k]* than that (32766) assigned to the upper bound *nbd[1][i][ck-k]* to indicate this situation. The procedure then checks to see if the pattern exceeds the block model boundary; if

yes, the pattern is truncated with respect to this boundary.

CONSTRUCTION OF NETWORK

Step 4) establishes the precedence constraints between blocks. The precedence constraints for a block (referred to as *base block*) consist of a set of blocks within the three dimensional removal cone of the base block. This cone extends upward to intersect the top level of the block model.

Firstly, we need the following notations:

G: A directed graph with vertex set *V* and edge set *E*.

B: Block model. We have $B = V$ and $|B| = ni \times nj \times nk$, where ni, nj, and nk are the number of rows, columns and levels of the block model respectively.

CT: A conical template. It is a 3D complete cone with the base at block (*ni/2*, *nj/2*, *nk/2*) extending to intersect the top level of the block model. Constructing the template needs to be done only once.

C: Removal cone of block $B(i,j,k) \subset B$. *C* can be constructed using the conical template *CT* by modifying the boundary of *CT* as required (Jiang, 1991). We further assume $B(i,j,k) \propto C$. Please refer to Figure 4.

IC: Inverted cone of block $B(i1, j1, k1) \subset C$. An inverted cone is similar to the normal removal cone except that it extends toward the bottom of the block model. In this case, the bottom level of *IC* equals to *k* on which block *B(i, j, k)* lies. We further assume $B(i1,j1,k1) \propto IC$. Please refer to Figure 4.

θ: Slope angle of the pit, ranging usually between 40° and 65°.

Then, to determine if an arc should be constructed from *B(i, j, k)* to *B(i1, j1, k1)*, we need only check if $C \cap CT = \varnothing$ (Figure 4). If yes, we use the *ConstructArc* function to allocate the space for it as is done in algorithm *FormNetwork*.

Note that algorithm *FormNetwork* is completely general: if we replace slope θ with a set of slope angles for different pit areas and make corresponding changes in the algorithm, the algorithm will form a network capable of representing a variable-slope pit.

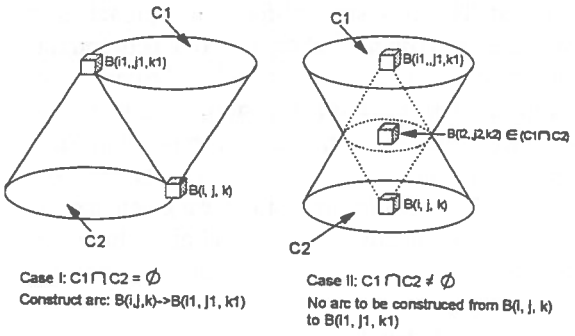

Figure 4 Condition for adding an arc between two blocks

```
Algorithm FormNetwork(B, θ, G(V, E))
{ Input:
    B — block model of dimension ni × nj × nk
    θ — pit slope angle
  Output:
    G — a graph with vertex set V & edge set E }
Begin
  |E|← 0;                    { initialize # of edges }
  CT ← FormConeTemplate(B);
  for k from 0 to nk-1       { for each level }
    for j from 0 to nj-1     { for each column }
      for i from 0 to ni-1 do  { for each row }
        { form cone C of B(i,j,k) }
        C ← FormCone(B, CT, i, j, k, θ);
        for m from 0 to |C |-1 do
          { for each block within C , form
            inverted cone IC of B(i1,j1,k1). }
          IC ← FormInvertedCone
                (B, CT, k, i1,j1,k1, θ);
          {if C ∩ CT = ∅, construct an arc }
          if (Intersection(C, IC) = NULL) then
            Arc ← ConstructArc
                  (B(i, j, k), B (i1, j1, k1));
            Add(E, Arc);
            |E| ← |E| + 1;
          end if
        end for m
      end for i
    end for j
  end for k
End Algorithm;
```

Figure 5 Algorithm for generating network from a given block model

Choosing An efficient Maxflow Algorithm

Since the network flow algorithm for pit optimization is based on determining the maxflow in a network, an efficient maxflow algorithm is required. During the last two decades a series of faster and faster algorithms have been devised for the maxflow problem by exploiting the idea of augmenting along many paths simultaneously (e.g. Dinic 1970) and by developing more efficient data structures (e.g. Sleator and Tarjan 1983). These are shown in Table 1, in which n denotes number of nodes and m number of edges, and the big Oh notation $O()$ represents the worse case time complexity of the corresponding algorithm.

The time complexities of these algorithms all depends on n, but some on m as well. Therefore, we need to analyze the density of the network, which is defined as the ratio m/n. For a dense graph, where there exists an arc between almost every pair of nodes, i.e. $m/n \approx n$, the algorithm due to Karzanov (1974) or Maholtra et al. (1978), with complexity of $O(n^3)$ is desired. For all other networks, sparse, non-sparse, or non-dense, the algorithm due to Ahuja and Orlin (1989) is fastest. For networks constructed from a block model, m is usually in the range of $(5n, 20n)$, depending on the slope angle and block dimension. Usually, bigger a slope is, smaller m will be. For instance, assuming a cubic block and constant 45° slope, the 5:1 and 9:1 overlaying support pattern is enough to approximate the slope. In this case, $m \approx 9n$, where n equals to number of blocks in the block model or in the bounding pit (if any bounding algorithms are applied). Therefore, for our purpose, the algorithm due to Ahuja and Orlin (1989) is desired.

TABLE 1 Complexities of Maxflow Algorithms

Author(s)	Time Complexity
Ford-Fulkerson (1956)	no bound
Edmonds and Karp (1972)	$O(nm^2)$
Dinic (1970)	$O(n^2m)$
Karzanov (1974)	$O(n^3)$
Maholtra et al. (1978)	$O(n^3)$
Cherkasky (1977)	$O(n^2m^{1/2})$
Galil (1978)	$O(n^{3/5}m^{2/3})$
Galil et al. (1979)	$O(nm \log^2 n)$
Sleator & Tarjan (1983)	$O(nm \log n)$
Goldberg & Tarjan (1986)	$O(nm \log(n^2/m))$
Ahuja & Orlin (1989)	$O(nm+n^2 \log U)$

Unfortunately, the algorithm of Ahuja and Orlin was not actually used because the research described in this paper had begun before the algorithm was published. However, an implementation of the network algorithm using Ahuja and Orlin's maxflow algorithm was reported by Yegulalp and Arias (1992).

In particular, both Edmonds and Karp's algorithm and Karzanov's algorithm have been adapted and programmed. Although the Karzanov's algorithm runs much faster, its current implementation requires more RAM.

COMPUTER PROGRAM

Program FLOWPIT implements the network flow algorithm, incorporating all the efficiency tricks as described in this paper. For the purpose of comparison, a simple floating cone algorithm is also implemented. The floating cone algorithm adapted works as follows: start searching from the beginning for positive blocks. Once such a block is found, a cone is constructed to intersect the topography. If the total value of the blocks within the cone is positive, these blocks belong to the final pit limit and are 'removed' from the block model; the procedure then goes back to the very beginning and start the search again. Otherwise the search continues to the next block in the block model. The word 'simple' is used to indicate the fact that adjacent blocks are not combined to form composite cones which should be checked together.

The FLOWPIT program consists of five modules: PREPASS, NWFEK, NWFKZ, FCONE and OUTPUT. The PREPASS module is used to obtain an outer bounding pit. This module is extremely fast and is designed to give a rough idea about how many blocks can be excluded from further considerations. The FCONE module implements the simple floating cone method described above. Both NWFEK and NWFKZ modules implement the network flow algorithm, but the former uses the Edmonds and Karp's algorithm and the latter employs the Karzanov's method. The OUTPUT module prints out the results of the pit design, which includes a summary of materials included in the final pit limit and a plan view of the pit.

Figure 6 shows the flow chart for either NWFEK or

NWFKZ module. The outer bounding pit Ω referred to in this flow chart is obtained by using *best valued cross section bounding* algorithm according to the three-step procedure described above.

A hypothetical block model with block dimension 20ft ×20ft×20ft and 23×80×80 blocks was used to test the program on a 486-33 with 8 MB RAM. The slope used is 45° throughout. The result is shown in Table 2. The pit limit obtained by either of the network flow modules is better than that obtained by the floating cone module: the value of the former is 4.6% higher than that of the latter and the in-pit material (including ore and waste) is 28.81% more.

Table 2 also shows the effect of bounding techniques. The simple prepass and best valued cross section bound contain 43245 blocks and 16852 blocks respectively, i.e., about 30% and 11.5% of the total blocks in the block model respectively. The combination of *layer cake*, *prepass*, and *modified best valued cross section bounding*, which are activated in the two network flow modules, has limited the maximum number of blocks to be considered by the optimization procedure at each level to no more than 8671 blocks (note that this number is not listed in the table). This greatly reduced both processing time and memory requirement.

Figure 7 plots running times against block model sizes. It clearly shows that the NWFKZ module which employs Karzanov's preflow push method is competitive with our implementation of the floating cone algorithm, whereas the NWFEK module is much slower than the both.

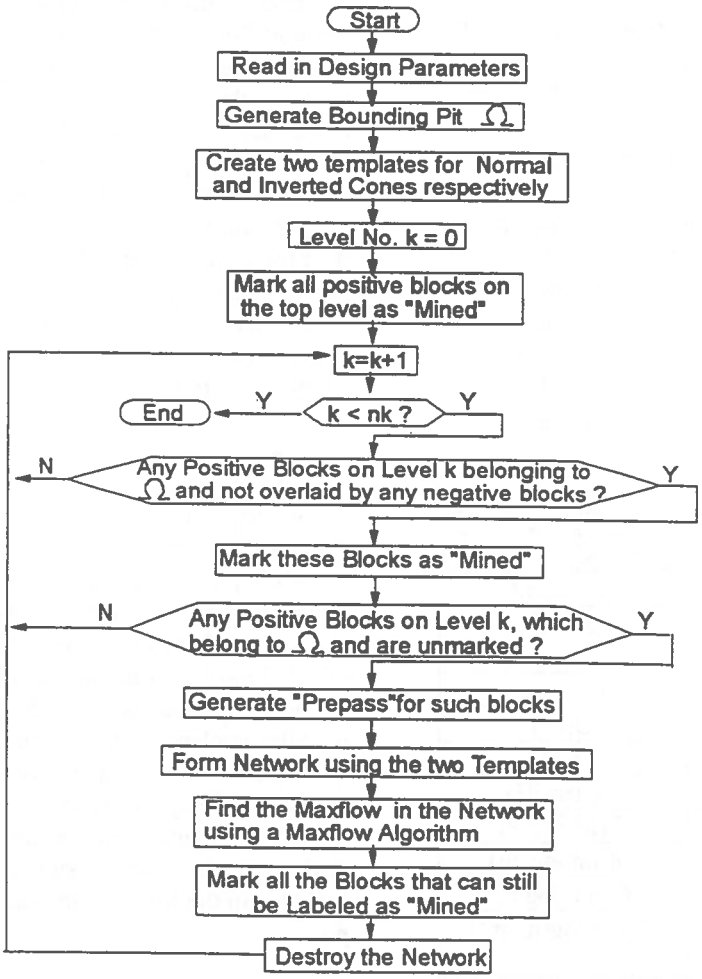

Figure 6 Flow chart for the NWFEK or NWFKZ module

TABLE 2 Comparison of the Results obtained by different Modules

Module Name	Blocks in bounding pit	Total Pit Value (mil $cdn)	Total No. of blocks in Pit		Total CPU (min.)	CPU for forming network (min.)
			Ore	Waste		
NWFKZ	16852 (in BVCSB*)	43.426	2513	3947	115	25
NWFEK	16852 (in BVCSB*)	43.426	2513	3947	170	23
FCONE	16852 (in BVCSB*)	41.518	1645	3355	120	
PREPASS	43245	-154.524	34431	8814	5	

*BVCSB — Best Valued Cross Section Bound

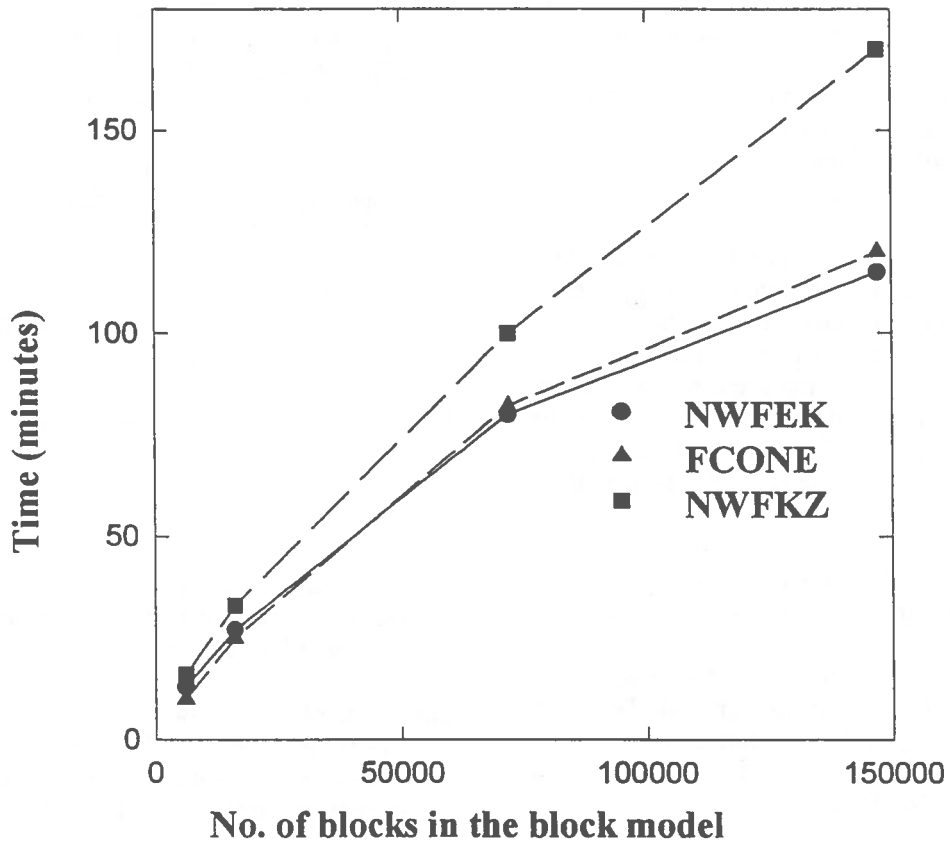

Figure 7 Comparison of running times

CONCLUSIONS

Although Lerchs and Grossman (1965) proved in their famous paper that their algorithm halts in finite steps, its time complexity in terms of the size of network, i.e., number of nodes and/or arcs in the network, remains unknown. On the contrast, the time complexity of the network flow algorithm is governed by the maxflow algorithm employed. Very efficient algorithms for the maxflow problem exist and continue to appear.

In this paper, it is shown that the network flow algorithm can be efficiently implemented by properly linking bounding techniques with an efficient maxflow algorithm. In addition, the difficulty in dealing with multi-slope pits in a rigorous optimizing algorithm can be overcome by establishing the precedence constraints between blocks using a conical search pattern.

An efficient algorithm for establishing conical search patterns using a pre-computed template is given, as well as an algorithm for generating networks capable of representing variable-slope pits.

The resulting network flow algorithm as implemented in program FLOWPIT is superior to L & G in terms of algorithmic simplicity, and competitive to heuristic floating cone algorithms in terms of speed. Furthermore, a noticeable improvement in speed can be foreseen if the maxflow algorithm of Ahuja and Orlin is used and/or if an inner bounding algorithm is also applied to an outer bounding pit before the maxflow algorithm is invoked.

A necessary and sufficient condition for application of section-based bounding techniques is also identified

Finally, the work described in this paper was completed in 1991 and remains unpublished except for a MSc. thesis (Jiang, 1991). Therefore, its is independent of a similar approach described by Yegulalp and Arias (1992).

ACKNOWLEDGMENT

Thanks are due to Robert de l'Etoile at Systemes Geostat International Inc. for translating the abstract into French.

REFERENCES

Ahuja, R.K. and Orlin, J.B., 1989. A Fast and Simple Algorithm for the Maximum Flow Problem. In Operations Research, vol. 37, No. 5, Sept.—Oct., pp. 748-759.

Barnes, R.J. and Johnson, T.B., 1982. Bounding Techniques for the Ultimate Pit Limit Problem. In *17th APCOM*, T.B. Johnson and R.J. Barnes (Ed.). S.A.I.M.E, Port City Press.

Chen, T., 1976. 3D Pit Design with Variable Wall Slope Capacities. In R.V. Ramani (Ed.), *14th APCOM*. AIME, New York.

Jiang, Y., 1991. *Pit Limit Optimization and Fault Mapping by Computer*. MSc thesis, Dept. of Mining Engineering, Queen's University.

Johnson, T.B., 1968. *Optimum Open-pit Mine Production Scheduling*. Ph.D Thesis. Operations Research centre, University of California, Berckeley., 120pp.

Lerchs, H., and Grossman, I.F., 1965. Optimum Design of Open Pit Mines. In *Canadian Institute of Mining Bulletin*. Jan.

Lipkewich, M.P., and Borgman, L. 1969. Two and Three Dimensional Pit Design Optimization Techniques. In A decade of Digital Computing in the mineral Industry. AIME, New York.

Picard J.C., 1976. Maximal Closure of A Graph and Applications to Combinatorial Problems. In *Management Science*, Vol. 22, No. 11, July, 1976.

Whittle, J., 1988. Beyond Optimization in Open-Pit Design. In *Computer Applications in the Mineral Industry (First Canadian Conference)*. A. A. Malkema Publishers, Brookfield, U.S.A.

CAMI'95: 3rd Canadian Conference on Computer Applications in the Mineral Industry
Montréal, Québec, Canada, October 22-25, 1995

Solid Modelling Techniques for Underground Hard-Rock Mine Design and Planning

Lucio D. Pareja and Charles W. Pelley
Department of Mining Engineering
Queen's University, Kingston, Ontario, Canada

ABSTRACT:

Two fundamental components of an integrated approach to underground hard-rock mine design and planning are: a database management system capable of storing, accessing, retrieving and manipulating complex mining data in an efficient, consistent and error-free manner; and a computer-based system that allows the representation of ore deposits and geological features, as well as the interactive design of underground openings and production scheduling. This paper discusses solid modelling techniques that facilitate the development of such an integrated approach. The focus is on the design and development of a modelling system that allows the efficient manipulation of all types of mining data; provides suitable design and planning tools for all stages of the process; and supports the integral evaluation of mining strategies.

RÉSUMÉ:

Deux composantes fondamentales d'une approche intégrée à la conception et la planification des mines souterraines en roches dures sont: un système de gestion de base de données capable de stocker, recouvrer, accéder, et manipuler des données minières complexes de manière efficace, consistante et sans erreur et un système à base d'ordinateur qui permet la représentation des dépôts miniers et des caractéristiques géologiques, aussi bien que la conception interactive des ouvrages souterrains et la planification de production. Cet article discute les techniques de modélisation de solide qui facilitent le développement d'une telle approche intégrée. L'emphase est mise sur la conception et le développement d'un système de modélisation qui permet la manipulation de données minières de toutes sortes, fournit des outils de conception et de planification adéquats pour toutes les étapes du procédé, et supporte l'évaluation intégrale des stratégies minières.

1 INTRODUCTION

The use of solid modelling techniques for mining applications has been extensively investigated in recent years. Specific topics of research have ranged from the modelling of orebodies and other "natural" objects (Smart, 1986; Gargantini, 1989; Bak et al., 1992), to underground mine design (Henley and Wheeler, 1988; Houlding and Stoakes, 1990), mine feasibility studies (Baxter and Hooper, 1992), and complete mining information management systems (Kavouras, 1987; Bak, 1991). However, most of the work carried out to date has focused on solving problems associated with the models themselves, neglecting the engineering and mining sides of the issue. There also seems to be some misconceptions regarding the type of modelling technique that meets the underground mining requirements, particularly in the area of mine design and planning.

1.1 Underground Hard-Rock Mine Design and Planning

Underground hard-rock mine design and planning is an inherently complex process. The diversity of the tasks involved, their high degree of interdependence, and the need to carry them out in a multi-pass manner determine its interdisciplinary and iterative nature. The attributes of underground orebodies (physical dimensions, grade and tonnage distributions, depth, and structural and geotechnical characteristics) make it a truly three-dimensional (3-D) problem. Mining sequencing, an important component of the underground mine design and planning process, is also influenced and/or restricted by factors such as the need to preserve the minable conditions of the remaining ore reserves; the need to provide safe working environments; the location and capacity of the main extraction facility; and the high amount of development work required before the start of any production activity. The large databases

involved, and the complex 3-D data interrelationships further complicate mine design and planning. Its unique characteristics make it very difficult to develop the integrated strategic approach needed to support the decision making process and facilitate efficient and adequate responses to changes in the design, planning and operational parameters.

1.2 The Role of Interactive Computer Graphics

Traditionally, graphical and non-graphical information involved in underground mine design and planning has been managed with the help of two-dimensional (2-D) geological, surveying and topographical maps. However, this is a very inefficient, and sometimes inappropriate, way of dealing with complex 3-D data. Due to the difficulty in making updates and incorporating new information, the evaluation of alternatives is unnecessarily restricted, and the possibility of defining an optimization procedure virtually eliminated.

Our highly developed pattern recognition capabilities enable us to perceive and process graphical data rapidly and efficiently (remember the ancient Chinese proverb "a picture is worth ten thousand words"?). Graphics, therefore, provides one of the most natural means of communicating with a computer. Computer graphics is concerned with the pictorial synthesis of real or imaginary objects from their computer-based models. It includes the creation, storage and manipulation of models and images of objects. Modern computer graphics is "interactive" because the user controls the contents, structure and appearance of the objects and of their displayed images by using input devices such as a keyboard or a mouse (Foley and Van Dam, 1982).

Surface and solid modelling are two computer graphics techniques particularly relevant to underground mine design and planning. They can enable us to store, manipulate and analyze the complex 3-D objects encountered in typical underground mining situations, thus facilitating an integrated mine design and planning approach and the development of an integrated mining database capable of storing both spatial and non-spatial information. User interface design is another computer graphics technique applicable to the integration process, but since it usually requires extensive customization to fit the specific needs of an operation, it will not be dealt with in this paper. It should be noted that computer graphics only complements mining engineering, and must be used in conjunction with additional tools and methods developed specifically for solving mining problems. Computer graphics provides the means to use them more efficiently (Houlding and Stoakes, 1990).

1.3 Objective and Scope of the Paper

The objective of this paper is to discuss the use of solid modelling techniques for underground hard-rock mining from a mine design and planning point of view. Due to the perspective adopted, the analysis concentrates on the requirements of the design and planning process, rather than on the details of the technique adopted. The focus on hard-rock mining narrows the analysis to underground base- and precious-metals operations in which the strength of the rock mass precludes the use of existing continuous mechanical excavating machines.

2 INTEGRATED UNDERGROUND HARD-ROCK MINE DESIGN AND PLANNING

Mine design and planning is characterized by its interdisciplinary and iterative characteristics (for example, see Wade et al., 1988 and Houlding, 1992 for discussions of the interdisciplinary features of open pit and underground mining, respectively). The additional complexity of the underground case, as discussed in the previous section, is rooted on the 3-D nature of underground mining. This complicates data processing and the development of appropriate links between the various tasks and studies involved (see Figure 1).

The current "phased" approach to the underground mine design and planning problem is not suitable for the demanding nature of modern operations. For instance, it does not allow the efficient evaluation of alternative designs and production plans, and does not lend itself to the formulation and development of mining strategies. Similarly, it is not easy to determine the impact of the introduction of new technology on grade control, support requirements, or the mine's long-term profitability. The available data are not properly used, and new information cannot be easily incorporated into the design and planning process. Its compartmentalized character makes it very difficult to share information between the groups of people involved, and virtually impossible to maintain data consistency and integrity. On the other hand, manual methods and 2-D solutions are acceptable in simple cases, such as regular vein-type deposits located at moderate depths. But if the geological and geotechnical characteristics are complex, the mine design and certain aspects of the production plan such as mining sequencing can become extremely troublesome to carry out and non-optimal solutions may be obtained.

2.1 Elements to Integrate

The following major areas of underground mine design and planning must be part of the integrated approach:

- Geological interpretation
  This includes the tasks of organizing the exploration data in an adequate database and providing interfaces for interactive, 3-D geological interpretation. The database incorporates numerical (e.g. grades, sample locations), textual (e.g. description of rocks and minerals) and graphical elements (e.g. geological structures).
- Ore reserve estimation
  This involves several interrelated tasks such as statistical and geostatistical analysis of sample data, orebody modelling and the estimation of geological (*in situ*) and minable (recoverable) reserves.
- Permanent openings design
  The design of permanent underground openings includes the specification of the location and basic design parameters of shafts, ramps, main levels, etc.
- Mine layout design
  Mine layout design involves the design of openings whose characteristics change according to the requirements of the operation. Important design issues include the dimensioning of stopes and pillars, the layout of stopes and pillars within the orebody, etc.
- Mining sequencing
  Mining sequencing is concerned with the interaction between the mining and extraction methods, the mine layout and the extraction sequence (Pelley, 1994). It involves the determination of the overall direction of mining and the sequence of extraction of stopes and pillars.
- Extraction systems design
  This task is closely related to mining sequencing. It comprises the analysis of stope configuration, preferred direction of stope retreat, and ore extraction from the stope.
- Production scheduling
  The production schedule is the backbone of any mining plan. Its objective is to plan the timing and rate of all mining activities so that the quality and quantity of the ore delivered is ensured (Wooller, 1992). It forms the basis of the development, equipment, and manpower schedules.
- Financial analysis
  Financial analysis is concerned with the development of evaluation indicators such as internal rate of return (IRR) and net present value (NPV), and the projection of operating costs, revenues, financing requirements, investment schedules, etc. Results obtained at this stage are used to make decisions or back-feed any of the previous stages.

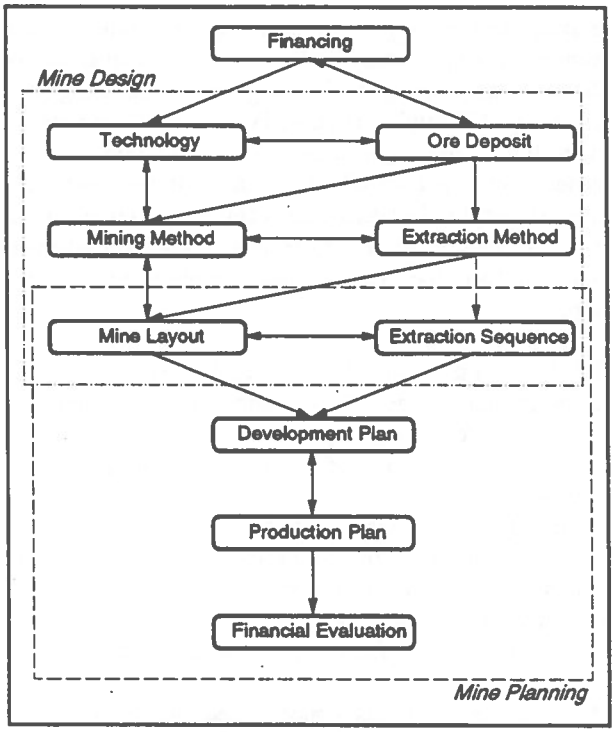

Figure 1: Underground mine design and planning.

2.2 Integration Tools

The successful integration of underground mine design and planning requires that the theoretical/philosophical approach be backed by appropriate tools. There are two types of such tools: generic tools that support several aspects of the design and planning process simultaneously; and specialized tools, used to address particular issues or engineering problems. Generic tools are needed for the management of non-spatial data (both textual and numerical) and spatial data. They are provided by a combination of database management and computer graphics techniques. An "integrated" mining database management system should:

- provide fast access to the information requested;
- make all the data in the database available for use;
- enable the user to make complex queries and fast updates; and,
- enforce data integrity and consistency.

Surface and solid modelling, in conjunction with the integrated mining database, must provide the following capabilities (Bak et al., 1989; Kavouras, 1989):

- definition and modification of 3-D objects;
- effective visualization;
- calculation of the integral properties; and,
- information retrieval through spatial and non-spatial searches.

Specialized tools are used to carry out engineering work on the above-mentioned design and planning areas. The emergence and widespread use of computer-assisted

mining engineering tools such as geostatistics and numerical stress analysis have greatly facilitated the development of integrated underground mine design and planning. Although this paper is not directly concerned with them, the high degree of interaction between generic and specialized tools makes it necessary that they are explicitly taken into account in integrating the process. Failure to recognize this interaction will certainly affect the validity and applicability of the approach.

2.3 Development of a Comprehensive Approach

Underground mine design and planning activities involve the following steps:

- manipulation of orebody and surrounding rock mass information;
- underground excavation design;
- determination of the optimum mining sequence to achieve the previous design;
- scheduling of actual mining activities; and,
- economic and/or financial evaluation of the design.

Previous research has concentrated on the first two steps, i.e., on the development of tools that facilitate the manipulation of geological and mining objects. This was the primary objective of programs carried out at the universities of New Brunswick (Smart, 1986; Reeler, 1987; Kavouras, 1987; Kavouras et al., 1988) and London (Bak and Mill, 1989; Prissang and Skala, 1990; Bak, 1991; Bak et al., 1992). They aimed at addressing specific computer graphics issues, mainly in the area of solid modelling. Systems capable of supporting interactive orebody modelling, ore reserve estimation and the manipulation of 3-D data were developed, but they fell short of linking their approach to mine design and planning. On the other hand, a review of published material on computer-assisted underground hard-rock mine design and planning indicates that a comprehensive approach has yet to be developed (Henley and Wheeler, 1988; Houlding and Stoakes, 1990; Houlding, 1992; Wooller, 1992).

A comprehensive approach recognizes the need to rely on computer graphics techniques to integrate the process. Furthermore, it is based on the observation that, in order to be of any practical use and support the above-mentioned activities and the actual operation of the mine, it must facilitate:

- full and efficient access to the integrated mining database;
- 3-D modelling of orebodies, geological/geotechnical features, and underground excavations; and,
- interactive evaluation of the validity, economic viability and practicality of designs and production plans.

3 INTRODUCTION TO SURFACE MODELLING

Bruce (1989) has identified three different types of 3-D surfaces used in mining engineering:

- surfaces that define underground excavations. Some excavations such as shafts, drifts, ramps and raises have regular or standard geometry, and can be approximated by simple shapes that are described mathematically (cylinders, conic sections, etc.);
- "geometric-based" surfaces such as faults and bedding planes, whose limits are defined by sampling. Even though these surfaces can in theory be described by simple mathematical functions, the need to obtain accurate and efficient representations demands the use of more complex ones; and,
- "attribute-based" surfaces such as ore grade cut-off limits and rock quality variations, determined according to calculated/estimated parameters. They also require complex representation methods.

Surface modelling is a branch of geometric modelling concerned with the mathematical representation and design of surfaces. There are two common 3-D representations of 3-D surfaces: polygon meshes and parametric surfaces (Foley and Van Dam, 1982). A polygon mesh is a set of connected polygonally bounded planar surfaces and is defined by a collection of vertices, edges and polygons. Polygon meshes are adequate for representing flat-faced objects but are rarely satisfactory for curve-faced ones. Parametric surfaces, on the other hand, are widely used to model curve-faced objects in a number of interactive computer graphics applications such as computer-aided design (CAD) and computer-aided manufacturing (CAM).

3.1 Parametric Surfaces

Parametric surfaces are generalizations of parametric curves. A parametric curve is one for which co-ordinates x, y, and z are each represented as a n^{th} order polynomial of some parameter t. The parametric representation of 3-D curves significantly reduces the difficulties associated with non-parametric curves, because it allows closed and multiple-valued functions to be easily defined and replaces the use of slopes with that of tangent vectors. The major advantages of parametric surfaces are the following:

- Complex surfaces with multiple values for a single value of x and y and infinite slopes can be modelled.
- Local control is provided, i.e., a change in a control point (one of the points that define the surface) only affects a local piece of the surface.
- Both interpolation and approximation of control points can be made, depending on the application requirements.

- They are computationally efficient.
- They facilitate the display and interactive manipulation of the surfaces.

The most common forms of parametric surfaces are:

- *Bézier surfaces*, based on Bézier curves. Some of the control points required to specify a patch interpolate the surface thus providing precise control. They are also attractive due to their convex-hull property and easy sub-division.
- *Non-rational B-spline surfaces*, based on uniform and non-uniform non-rational B-splines. They only approximate the control points but have local control, convex-hull property and easy sub-division. B-spline surfaces are relatively simple to implement and lend themselves to interactive design (see Figure 2).
- *Non-uniform rational B-spline (NURBS) surfaces*. They are based on non-uniform rational B-spline curves which are, roughly speaking, a quotient of two splines. In addition to the characteristics outlined for their non-rational counterparts, they have two important properties: first, they are invariant under projective transformations, such as perspective projections. Second, they can define precisely any of the conic sections. Their implementation is somewhat more complex than that of non-rational splines and they are not as computationally efficient.

3.2 Selection of a Surface Representation Method

The choice of surface representation form depends on several factors, including the type of objects to be modelled, the degree of accuracy required, the type of information used to define the surfaces, and the computing power available. Each of the types of 3-D surfaces encountered in underground mining has its own set of specific modelling requirements. Underground openings are interactively created by the user according to the location of the orebody boundaries and taking into account design, planning and operational needs and constraints. The user interface is in this case of critical importance, and must provide tools for constructing, modifying, storing and destroying designs. Geometric- and attribute-based surfaces, on the other hand, can in theory be created automatically, with little or no input from the user. This is the case of standard interpolation techniques used to create fault, bedding, and "minable" ore surfaces. A discussion of the applicability of automatic contouring or similar techniques to produce such surfaces is beyond the scope of this paper. Nonetheless, the modelling system should provide editing capabilities so that the user is able to modify the designs and test their validity interactively.

The widespread use of NURBS in CAD/CAM environments is an indicator of their excellent design capabilities. Given the increased computing power of modern workstations and the availability of efficient algorithms for curve and surface design, NURBS seem to offer important advantages over other representations for the modelling of mining- and geo-objects (Fisher and Wales, 1989). They are as follows:

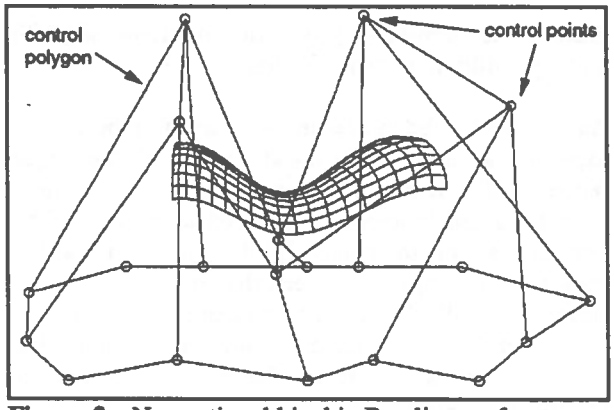

Figure 2: Non-rational bicubic B-spline surface.

- a common mathematical form is used to represent standard analytical shapes and free-form surfaces;
- a unified database can store all types of surfaces;
- it provides flexibility to the design process by allowing to manipulate the control vertices and the weights;
- it is relatively fast (in terms of computing time);
- the data storage requirements are reduced due to the parametrization of the elements; and,
- a NURBS model has scale, rotation, translation, shear, parallel projection, and perspective projection invariance.

As is the case of other free-from representation schemes, NURBS also have drawbacks (Piegl, 1991):

- additional storage is needed to define traditional curves and surfaces such as circles and ellipses;
- some interrogation techniques such as surface/surface intersection, are more efficient or work better in traditional forms; and,
- some basic algorithms are subject to numerical instability.

4 INTRODUCTION TO SOLID MODELLING

Solid modelling is a branch of geometric modelling concerned with the representation of objects that are enclosed by an assembly of surfaces. The objective of solid modelling systems is the creation of models that are complete representations of physical solid objects, i.e., representations that are adequate for providing

answers to arbitrary geometric questions algorithmically, without human intervention.

An effective solid modelling system must be able to express the three-dimensional nature of the object represented. For instance, any specified point in space must be unambiguously determined to be part of the object or outside the object. In other words, it must be possible to distinguish between the inside, outside, and surface of a 3-D object and to compute properties of the object that depend on this distinction. A solid modelling system consists of three "levels of abstraction" (Hoffmann, 1989):

- The user interface, in which the user interacts with the modelling system through a design language.
- The mathematical and algorithmic infrastructure that implements the conceptual operations available in the user interface and the auxiliary tools needed by them.
- The "substratum", which consists of arithmetic and symbolic computations used as "primitives" by the algorithmic infrastructure.

Existing solid modelling techniques can be categorized into three generic classes: constructive, boundary and decomposition models (Mäntylä, 1988; Bak, 1991).

4.1 Constructive Models

Constructive models describe solid objects as a collection of primitive point sets. The construction operators used to combine such primitives are general and include "Boolean" operations and rigid transformations.

- Sweep representations
  A solid is defined as the volume that is swept by a 2-D cross-sectional figure along a curve. There are rotational, translational and general sweep models.
- Constructive solid geometry (CSG)
  This model consists of a family of schemes for representing solids as Boolean constructions or combinations of solid components via regularized set operations (Bak, 1991). CSG representations are ordered binary trees in which non-terminal nodes represent operators and terminal nodes are either primitives leaves or transformation leaves (Günther, 1988).

4.2 Boundary Models

Also called boundary representations or "B-reps", they represent the solid object by its boundary, which is decomposed into a set of faces, edges and vertices. The result is an explicit model that is based on a combined topological and geometric description of the object.

- Planar polygon boundary model (polyhedral boundary representation). The faces used to model the surface of the object are planar polygons described by a set of straight lines or edges.
- Curved surface boundary model (non-polyhedral boundary representation). The faces are parametric (usually bicubic) surface patches which are described by known points, vectors and curves.

4.3 Decomposition Models

Solids are described as a collection of primitive point sets that are glued together. Variations of the method depend on the type of primitive point sets used.

- Primitive instancing
  This method makes the implicit assumption that all of the possible object shapes are known *a priori*, and are defined parametrically. Specific instances of the objects are created by changing the scale and dimension parameters.
- Space subdivision
  The space subdivision model consists of a set of cubes or units of space that are completely (or partially) contained in it. If the cubes are assumed to be non-overlapping and of uniform size and orientation, the resulting model is a regular subdivision and is called an exhaustive enumeration. A typical example of an exhaustive enumeration model is the block model commonly used in open pit mining applications. If the size of each unit of space is changed to fit the characteristics of the object of interest, an adaptive subdivision model is obtained. The octree representation is the most prominent adaptive subdivision scheme. It recursively subdivides the object being modelled into eight equal sized cubes or octants. The process is applied until all generated cubes are either entirely contained in the model or entirely disjoint from it (Gargantini, 1989).
- Cell decomposition
  Cell decomposition models an object by discrete, non-overlapping units of space, or cells. However, instead of being cubic or rectangular, as in space subdivision schemes, the cells in this case can be any solid model which is topologically equivalent to a sphere. Therefore, they have the advantage of providing a general domain without approximation.

4.4 Selecting the Appropriate Method

The choice of the most suitable solid modelling method depends on the type of application. Each of the classes previously discussed has its own advantages and disadvantages. A summary evaluation of their main properties is presented in Table 1. The criteria employed are (Günther, 1988; Mäntylä, 1988; Bak, 1991):

- Expressive power, determined by the extent of the domain (i.e., the number of objects that can be modelled) and the accuracy to which the domain elements can be modelled.

- Validity, determined by the extent of the range, i.e., by the number of different solids that can be represented. It ensures that only meaningful solids are created and/or manipulated.
- Unambiguity, which ensures that a representation corresponds to a single model.
- Uniqueness, needed to determine the identity of an object and distinguish it from other objects.
- Conciseness, determined by the amount of storage space needed for the representations.
- Closure of operators. Operations such as model construction and rigid transformations are said to "close" if they preserve the validity of the representation.
- Ease of model creation.
- Computational ease, indicated by the ability to calculate solid properties such as volume and surface area.
- Applicability, determined by the type of solid objects that can be modelled efficiently with the scheme.

Table 1 clearly shows that there is not a single model that is better than the others. The selection is always dependent on the specific application requirements. For instance, constructive representations, not capable of modelling irregular shapes, are not applicable to mining. B-reps, on the other hand, have been used in underground mining environments, but in conjunction with a space subdivision scheme (octree encoding) that functions as the primary representation (Bak and Mill, 1989; Bak, 1991). This is because, in spite of their drawbacks (model creation is not easy and visualization is inefficient), octrees allow the modelling and facilitate the analysis of heterogeneous solids such as orebodies.

5 PROPOSED APPROACH

Hoffmann (1989) noted that *"it is no longer thought realistic to envision a comprehensive solid-modeling system that satisfies the needs of all potential users"*. Underground hard-rock mining requires a modelling approach that specifically addresses its unique features, discussed in Section 2. Two additional characteristics are the need to take time into account, critical to mining sequencing, production scheduling and economic and financial evaluation, and the uncertainty associated with some of the information such as ore reserve estimates and location of orebody limits. They establish the "evolutionary" nature of mine design and planning.

Although it was not focused on mine design and planning, previous research demonstrated that a single representation scheme would not be able to meet the underground mining requirements, and hybrid representations were developed (Kavouras, 1987; Bak, 1991). On the other hand, maintaining multiple representations of a 3-D object is not a trivial task: it requires advanced automated integrity control to ensure validity and consistency between the different models (Kavouras, 1987). It is now proposed that, instead of simultaneously using two solid modelling representations, such as B-reps for the enclosing surface and octrees for the interior of the solid, a hybrid system based on NURBS and linear octrees should be used. NURBS would be employed to interactively design underground excavations, model surface topography, carry out geological interpretation, and visualize the mining- and geo-objects. Octrees would store attribute information such as volume, tonnage and grade of excavations, ore deposits and other geological features.

5.1 NURBS Modelling

A NURBS implementation allows the creation of several types of surfaces (Piegl, 1991). Extruded surfaces, natural quadrics and surfaces of revolution are particularly applicable to underground mining. Extruded surfaces are created by extruding a profile curve in a certain direction for a given distance. The natural quadrics are the plane, cylinder, cone and sphere. Surfaces of revolution are obtained by defining a profile curve and rotating it around an arbitrary axis.

Surface design methods include interpolation, fitting and cross-sectional design. The first two are automatic methods used when large amounts of data more or less regularly distributed are available. Their theoretical foundation is well understood (Piegl, 1991). Cross-sectional design is an interactive surface creation technique suitable for geological interpretation (which has traditionally been carried out in sections), stope design and mining sequencing. Skinning, sweeping (a special case of skinning that uses a constant section curve) and swinging (a generalization of rotational sweeping) are the most frequently used cross-sectional techniques.

Due to the focus on integrated mine design and planning, the NURBS modelling component is critical to the success of the proposed system. In fact, the ability to interactively model ore deposits, design excavations and plan mining activities sets it apart from other approaches developed in the past (Henley and Wheeler, 1988; Houlding and Stoakes, 1990; Baxter and Hooper, 1992). The development of efficient algorithms that support the interactive design of the above-mentioned surfaces in an underground mining environment is particularly important. Special emphasis must be placed on addressing common surface design problems expected to arise often in mining applications, including surface-surface intersection.

TABLE 1: Summary evaluation of solid modelling representation schemes.

	Constructive Models		Boundary Models (B-reps)		Decomposition Models		
	Sweep representations	Constructive solid geometry (CSG)	Planar polygon boundary	Curved surface boundary	Primitive instancing	Space subdivision	Cell decomposition
Expressive Power	general and exact domain	extensive and exact domain	extensive domain, but not exact (planar faces)	domain is extensive and exact	domain determined by families of instances	general domain (objects are only approximated)	general
Validity	difficult to ensure (degeneracy may occur)	depends on primitives and operators	relatively easy to ensure	relatively easy to ensure	depends on families of instances	units of space are valid solid models	Each cell must be tested (slow)
Unambiguity	unambiguous	valid CSG trees are unambiguous	unambiguous	unambiguous	unambiguous	unambiguous	unambiguous
Uniqueness	not unique	not necessarily unique	not necessarily unique	not necessarily unique	instances are not unique	unique (for a fixed resolution)	not unique
Conciseness	relatively concise	varies according to primitives and geometric complexity	not concise	more concise than polyhedral representations	parametric representation used is concise	not concise	relatively concise
Closure of Operations	closure is not guaranteed	CSG representations are closed to ensure validity	rigid operations close, but set operations may not close	depends on the surfaces used	closed if primitives do not intersect	most operations are closed (exception: arbitrary rotation)	the mathematics are unknown or computationally expensive
Ease of Model Creation	relatively easy to create	regular shapes are easy to create, complex ones can be cumbersome	complex (description languages, triangulations and CSG conversions)	complex model creation	models are easily created (simple mathematical shapes)	converted from other schemes (restrictive and time-consuming)	complex, usually converted from other representations
Computational Ease	complex mathematics & Boolean operations	only search operators are hard to compute	Boolean operations complex to implement	computationally complex and time-consuming	properties are easily calculated	simple but slow algorithms	complex operations
Applicability	limited	wide applicability (CAD/CAM)	limited	limited, used in surface modelling	very limited	reduced by slow algorithms	limited

Sources: Günther, 1988; Mäntylä, 1988; Bak, 1991.

5.2 Linear Octree Modelling

An octree is a rooted, directed tree generated by recursive subdivision of an initial $2^n \times 2^n \times 2^n$ cubic universe into nodes or octants. If all the single volume elements (voxels) that form a node have the same attributes, it becomes a leaf with those attributes, otherwise the octant is subdivided into eight sub-octants and the process is repeated until either only leaves are left (i.e., all the remaining nodes have voxels with the same attributes) or *n* subdivisions have taken place. In the simplest case, only two attributes are considered: black for nodes that are part of the object being modelled, white for nodes that are not.

A linear octree is a compressed form of the standard octree. Its main feature is that it only stores the description of the leaves that belong to the object being modelled. Linear octree encoding is carried out as follows:

- The locational or octal code of each node is generated by appending, from left to right, the octal digit that identifies it, starting with the largest octant. The octal code represents the path from the root of the corresponding octree to the node (Bak, 1991).
- The grouping factor of each node is obtained by finding the integer number in the range {0, 1, ... , n - 1} that represents the node's size.
- Each node is then labelled with its corresponding locational code and grouping factor.
- The linear octree is the sorted array of locational codes of the black nodes, each listed with its corresponding grouping factor. Octree encoding is, thus, both a representation scheme and a data structure (Kavouras, 1987).

The internal manipulation of an object's linear octree representation requires algorithms and/or mathematical tools that facilitate the evaluation of the solid's characteristics. Algorithms to carry out the following tasks have already been developed and, in some cases, tested (Gargantini, 1989):

- given the locational codes (sorted or not), determine the three-dimensional border of the solid;
- given a set of border voxels, find the enclosed volume;
- given a linear octree, find its connected components;
- given two linear octrees, find their union, intersection and difference; and,
- given a set of polygons (3-D space), digitize them.

Since the applicability of octree encoding to underground mining has been already established (Bak, 1991), the focus of ongoing research is on the development of efficient algorithms for octree creation.

5.3 Interaction Between Representations

In the proposed system linear octree representations will be created from NURBS surfaces. The NURBS → linear octree conversion, which is conceptually similar to the B-rep → linear octree conversions discussed by Bak and Mill (1989), results in some loss of surface information. Such a loss, however, depends on the "resolution" of the octree model and is not significant for the intended purposes (Kavouras, 1987). There is no need to carry out "reverse" conversions, i.e., from linear octrees to NURBS surfaces. This is because all the modelling (interactive and automatic) and editing of the surfaces of the solid models will be performed using the NURBS-based system.

In order to ensure the validity of the solid produced, the closure of the surfaces that define it must be checked before the conversion takes place. The complexity of this problem depends on the modelling tools available. Algorithms and integrity control measures are required to address this and other similar modelling problems.

6 CONCLUSION

Underground hard-rock mine design and planning is a complicated, interdisciplinary, interactive and time-consuming process critical to the economic and financial viability of an operation. The integration of all the tasks and studies involved depends on the ability to efficiently store and manipulate complex 3-D information that describes the mine structure, ore deposit and surrounding rock mass. This can be accomplished only by means of a computer-assisted mine design and planning system.

A solid modelling approach that incorporates NURBS surfaces for the modelling of geological features and interactive design of underground excavations, and linear octree encoding for their internal representation has been proposed. Its main advantages are the use of a unified mine design environment and the need to maintain only one solid model and database structure. The validity and applicability of the proposed approach will depend on the development of efficient conversion algorithms capable of supporting consistent simultaneous surface and solid representations.

REFERENCES

Bak, P.R.G., 1991.
Applied Solid Modelling in Mineral Resources Engineering. Unpublished Ph.D. Thesis, University

of London (Imperial College of Science, Technology and Medicine), London, UK, 220 p.

Bak, P.R.G., Cram, D.L. and Prissang, R., 1992.
Interactive Evaluation of Linear Octree Encoded Deposit Models. 23rd Int. Symp. on the Application of Computers and Operations Research in the Mineral Industry. Tucson, AZ, pp. 691-700.

Bak, P.R.G. and Mill A.J.B., 1989.
Three dimensional representation in a Geoscientific Resource Management System for the minerals industry. Three Dimensional Applications in Geographic Information Systems, J. Raper, ed., Taylor & Francis, London, pp. 155-182.

Baxter, A.R. and Hooper, G.B., 1992.
Use of 'Three-dimensional solids modelling' system for Baluba Centre/South Limb feasibility study at ZCCM, Ltd. Trans. Instn. Mining and Metallurgy, Vol. 101, Section A, pp. A41-A46.

Bruce, R.M., 1989.
Report of discussions by the minerals exploration interest group. Proc. NATO Advanced Research Workshop on Three-Dimensional Modeling with Geoscientific Information Systems. Santa Barbara, CA, pp. 391-396.

Fisher, T.R. and Wales, R.Q., 1989.
Three dimensional solid modeling of geo-objects using non-uniform rational b-splines (NURBS). Proc. NATO Advanced Research Workshop on Three-Dimensional Modeling with Geoscientific Information Systems. Santa Barbara, CA, pp. 85-105.

Foley, J.D. and Van Dam A., 1982.
Fundamentals of Interactive Computer Graphics. Addison Wesley, Reading, Mass., 664 p.

Gargantini, I., 1989.
Modeling natural objects via octrees. Proc. NATO Advanced Research Workshop on Three-Dimensional Modeling with Geoscientific Information Systems. Santa Barbara, CA, pp. 145-157.

Günther, O., 1988.
Efficient Structures for Geometric Data Management. Springer-Verlag, Berlin, Germany, 135 p.

Henley, S. and Wheeler, A.J., 1988.
The use of solid modelling in underground mine design. Proc. 1st Canadian Conference on Computer Applications in the Mineral Industry. Quebec, PQ, pp. 359-364.

Hoffmann, C.M., 1989.
Geometric and Solid Modeling: An Introduction. Morgan Kaufmann, San Mateo, CA, 338 p.

Houlding, S.W., 1992.
Real Time Grade Control in Mine-Planning & Production. 23rd Int. Symp. on the Application of Computers and Operations Research in the Mineral Industry. Tucson, AZ, pp. 746-755.

Houlding, S.W. and Stoakes, M.A., 1990.
Mine activity and resource scheduling with use of 'Three-dimensional component modelling'. Trans. Instn. Mining and Metallurgy, Vol. 99, Section A, pp. A53-A59.

Kavouras, M., 1987.
A Spatial Information System for the Geosciences. Unpublished Ph.D. Thesis, The University of New Brunswick, Fredericton, NB, Canada, 231 p.

Kavouras, M., 1989.
A spatial information system with advanced modeling capabilities. Proc. NATO Advanced Research Workshop on Three-Dimensional Modeling with Geoscientific Information Systems. Santa Barbara, CA, pp. 59-67.

Kavouras, M., Masry, S.E., Smart, J.R. and Reeler, E.C., 1988.
An advanced geo-information system for mining applications. Proc. 1st Canadian Conference on Computer Applications in the Mineral Industry. Quebec, PQ, pp. 511-515.

Mäntylä, M., 1988
An Introduction to Solid Modeling. Computer Science Press, Rockville, Maryland, 401 p.

Pelley, C.W.P., 1994.
A Study of Sequencing Strategy for Steep, Tabular, Hardrock Orebodies. Unpublished Ph.D. Thesis, McGill University, Montreal, PQ, Canada, 311 p.

Piegl, L., 1991.
On NURBS: A Survey. IEEE Computer Graphics & Applications, Vol. 11, No. 1, Jan. 1991, pp. 55-71.

Prissang, R. and Skala, W., 1990.
An Octree-Encoded 3D Variable Block Model for the Representation of Ore Grades in Underground Mining. Proc. 22nd Int. Symp. APCOM. Berlin, West Germany, Vol. 3, pp. 137-148.

Reeler, E.C., 1987.
The Manipulation of Linear Octrees in a Three Dimensional Digital Mapping System. Unpublished M.Sc. Thesis, The University of New Brunswick, Fredericton, NB, Canada, 124 p.

Smart, J.R., 1986.
Three-Dimensional Modelling of Irregular Natural Objects. Unpublished M.Sc. Thesis, The University of New Brunswick, Fredericton, NB, Canada, 108 p.

Wade, N.H., Naderi, F. and Nikols, D., 1988.
Role of the computer in managing and applying geotechnical data to surface mine design. Proc. 1st Canadian Conference on Computer Applications in the Mineral Industry. Quebec, PQ, pp. 339-352.

Wooller, R., 1992.
Production Scheduling System. Trans. Instn. Mining and Metallurgy, Vol. 101, Section A, pp. A47-A54.

CAMI'95:3rd Canadian Conference on Computer Applications in the Mineral Industry
Montréal, Québec, Canada, October 22-25, 1995

Geometric Modelling for the Mining Dilution Control

Diogo Cauppers, Luis Guerreiro, J. Pinto Rodrigues
SOMINCOR, Neves Corvo, Castro Verde, Portugal.

José Almeida, Amilcar Soares
Centro de Valorização de Recursos Minerais, Instituto Superior Técnico
Av. Rovisco Pais, 1096 Lisboa Codex, Portugal

ABSTRACT

The dilution of ore grades with waste as a result of mining operations is one of the fundamental factors in the reserves calculation and reconciliation procedures. Three main different dilution sources can be found in an underground selective mine method: firstly, waste from the backfill of the previously mined stope(s), secondly, dilution resulting from the barren contacts of the mineralization and thirdly, dilution between ore types. In a selective mining method like cut-fill, the dilution may easily reach a two digit percentrise of the average grades.

This paper describes a geometric modelling system to monitor the dilution of a mining method. The system is divided in two main modules:

i) A **geometric data base** (BDMINLIB) to store the inflow of topographic information of points from the roof, floor and sidewall of the mined stopes, the 3-D shapes of the stopes with estimated surfaces of roof and floor, the geometry of the union of the stopes corresponding to a monthly production, the 3-D shapes of the dilution areas and the geostatistical estimated morphology of the different oretypes of the orebody;

ii) A **geometric modelling kit** to perform the basic CAD operations of geometric modelling, the geostatistical estimation of the roof and floor of the stopes, and to calculate the intersection between stopes - dilution due to backfill - and between the stopes and the host rock - dilution due to barren formations.

The system is implemented in Neves-Corvo mine.

1. INTRODUCTION

In selective underground mining methods, the dilution of ore reserves with waste, resulting from the mining operation, can reach significant levels which must be accounted for the reserve calculation and reconciliation balances.

The main objective of a selective mining method, like cut and fill, is to mine separately and distinctly the different ore types and the waste. Among the different sources of dilution in a cut and fill mining operation, the two main waste dilution's can significantly affects the metal reserves calculation: the one resulting from the backfill contamination from the previously mined stope(s) and the dilution from the barren contacts with the mineralization.

This paper presents a methodology, based on a geometric modeling approach, to calculate the dilution pertaining to a mining operation. This methodology is supported by two main modules:

i) a **geometric data base** to organise the inflow of raw data from the mine survey consisting of spatial point coordinates of the roof, floor and sidewalls of the mined stopes before backfilling. The geometry of the designed stopes and dilution areas are also stored in this data base.
ii) a **geometric modelling kit** to perform the basic CAD operations and spatial inference. The purpose of this module is to model the geometry of the stopes, the boundaries of the intersections between stopes and the 3-D global shape of the entire mined level. These geometric entities are organised and structured in the previous data base.

The accounting and control of the different kinds of dilution are made monthly for each mine fronts.

This mining dilution control system is implemented at Neves Corvo mine.

2. THE DESCRIPTION OF THE MINING METHOD

2.1 Neves Corvo Deposit

The Neves Corvo deposits are located in Southern Portugal towards the western end of the Iberian Pyritic Belt (Fig. 1). The initial discovery was made in 1977 as a result of diamond drilling of selected gravimetric anomalies. Further drilling outlined 5 massive sulphide deposits called Neves, Corvo, Graça, Lombador and Zambujal (Murray and Real, 1990).

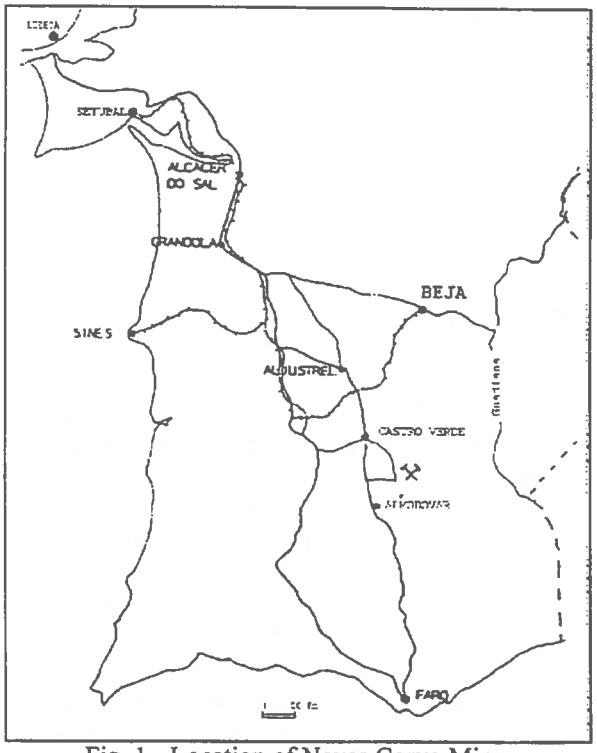

Fig. 1 - Location of Neves Corvo Mine.

Preliminary evaluations showed the copper rich deposits of Corvo and Graça to be viable, and as recently as 1994 the Neves deposit was brought into production. The additional two deposits contain copper and zinc and are the focus of an ongoing viability study.

2.2 Ore Types

The orebodies of Neves Corvo are lenses of massive sulphides with important mineralization of the upper and lower wall rocks and are similar, in some respects, to other deposits in the Iberian Pyrite Belt. However, they are unique in the high copper and tin grades and unusual in their strong metal zonation patterns.

The orebodies are located at the top of a complex volcano-sedimentary group. The rocks have been folded into a gentle anticline with several sets of sub-vertical faults intersecting and displacing the deposits.

Subsequently the ore was divide into the following categories: MC - Massive Sulphide Copper Ore and MH - Massive Sulphide Copper Ore high content in penalty elements (As, Sb, Zn, Hg). These two ore types feed the copper Concentrator at a rate of 1.400.000 tons per annum. The MH ore is treated in batches of approximately 10.000 t.

The third ore type - MS - Massive Sulphide Copper Ore with Tin grades above cut-off feeds a copper/tin circuit of the Tin Concentrator at a rate of 300.000 t per annum.

The last two ore types: MT - Massive Tin Ore and RT - Shale hosted tin ore feed the tin only circuit of the Tin Concentrator at a rate of 100.000 t per annum.

The great number of ore types, and their high unit values, as well as the complex flat lying nature of the ore (±25°) required the implementation of a selective mining method which could guarantee maximum extraction with lowest dilutions (Teixeira and Caupers, 1990, Caupers *et al*, 1993). The stoping method selected is a variant of the Cut & Fill mining method, namely Drift & Fill.

2.3 Stoping Method

The mining method is basically very simple, from a ramp located in the footwall (FW), drifts are driven parallel to the strike of the orebody and at a distance from the footwall contact determined by the maximum inclination that the mining equipment can efficiently operate (18%). These drifts are repeated every 20m in depth.

Crosscuts are then driven down until they intersect the ore. They then level off and the ore is crosscuted to the hangingwall (HW), usually determined by a grade cut-off. The number of crosscuts largely depends on the size of the ore block, fault intersections, number of ore types and production targets for the area.

Once the crosscuts have reached the "hangingwall" stoping essentially follows one of two strategies: in areas where the ore has been intersected and displaced by faults each crosscut will mine out the ore within a pair of faults. In these cases the ore will be mined out by longitudinal stopes from HW to FW, see Fig. 2. Upon completing a stope, for which the spans are a function of the geotechnical characteristics of the area, it is backfilled with hydraulic fill with a fence at the crosscut.

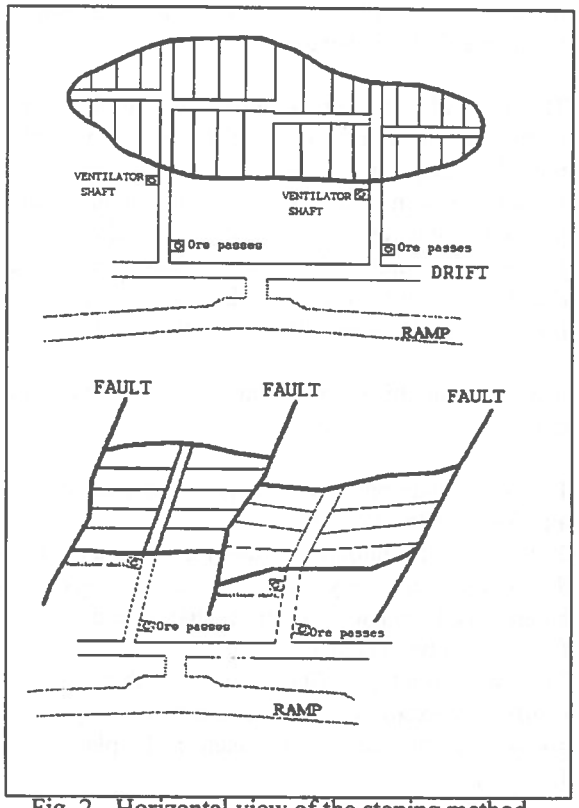

Fig. 2 - Horizontal view of the stoping method.

In areas with few faults longitudinal drifts are driven from each cross cut through the middle of the ore. Each one of these drifts is typically 50m long and defines a mining panel. From this drift transverse stopes are opened towards the HW and FW for which once again the span is a function of the geotechnical characteristics, see fig 3. Once completed the mining of a transverse stope it is hydraulically filled with a fence in the longitudinal drift.

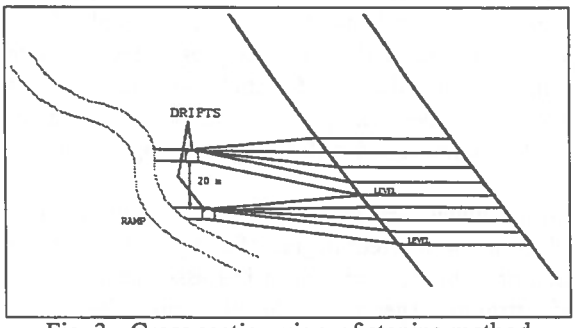

Fig. 3 - Cross section view of stoping method.

For both cases the stoping is repeated until the level is mined out at which time the back of the crosscut is raise for the next level and the sequence is repeated. Each level is 5m in height.

The backfill plays an important role in this mining method in not only providing the working platform but also local and regional stability. The backfill allows one to mine a stope along side, without which it would be necessary to leave ore pillars. It also prevents loosening of the level above, which can drastically reduce the workable span and increase instability of the sidewalls of the following level.

It is clear that this mining method is subjected to three chief sources of dilution:

1) Backfill dilution: Hydraulic fill from the sidewall(s) and from the level below;
2) Host Rock Dilution: i) Sulphides of grades below the cutoff or Graywackes from the geological hangingwall contact; ii) Blackshales and volcanic from the footwall contact;
3) Between ore types: Blast rounds which may contain insufficient/excessive of one ore type to justify it going to another ore types stream in the plants (Luis, J., 1993).

The software developed is intended to at this stage estimate and account fort the first source of dilution and subsequently the second source.

3. GEOMETRIC DATABASE

3.1 General Description

Geometrical models of stopes require a database to store, retrieve and manipulate all data involved. This particular kind of database - a geographic database - consists on a collection of spatial referenced attributes, which can be managed by the set of modelling programs developed in this particular application.

All attributes are related to one geometric object, which has a different degree of complexity: point, arc, area or volume. Each object has associated one table of attributes (geometric location and description), which can be inputted or calculated. The set of geometric objects suggests a hierarchical structure, which was implemented in the design of this database. The hierarchical structure follows the sequence of the complexity of geographic objects (Mortenson, 1985).

Based on each geographic characteristics and complexity (2D or 3D), they can be catalogued in a set of main types, corresponding to a set of associated topological rules. Following this rules, one program can easily decode the database structure and has access to the geographic and other object attributes, corresponding each one to a specific record in the associated attribute table.

3.2 The BDMINLIB Database

The BDMINLIB is composed by a set of three record tables (each one for the information related to the different hierarquical components of each stope model - points, arcs or areas and volumes) and pointers between records of this list of attributes. The connection between tables using pointers simplify and increase speed in the access to the information related to each object, located in three tables - coordinates and descriptive attributes.

The structure of attributes tables used in this particular case of geographic models are shown in fig 4. Each set of data files (one database) store information related to each level of the mine. In the same database, are stored different class of objects, which are involved in the different steps of the modelling and have particular characteristics (see TABLE 1).

BDMINLIB object code	Description	Provenience
10,15,20	Sidewall contours	Topography
30	Floor points	Topography
35	Roof points	Topography
45	Other mining objects: ramp, shafts, etc.	Topography
50	Stope in exploitation	Contour model
60	Mined or Backfill stope	Contour model

TABLE 1 - Classes of objects stored in BDMINLIB database

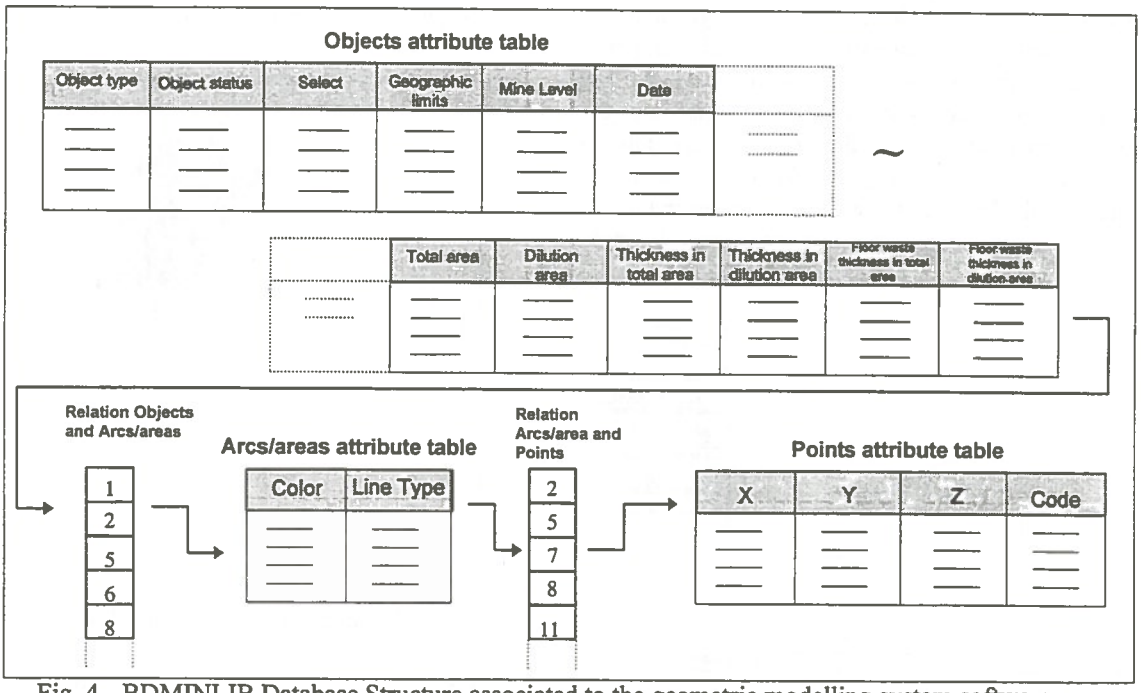

Fig. 4 - BDMINLIB Database Structure associated to the geometric modelling system software.

4. GEOMETRIC MODELLING KIT

The geometric modelling kit is composed of three main tool blocks that perform the design of the stopes, the spatial interpolation of the geometry of the roof and floor and the calculation of the different dilution's.

4.1 Design of the Stopes and Definition of Geometric Boundaries of Dilution Areas

The system input the daily topographic data pertaining to stopes which have just been mined or backfilled.

As the dilution control is made on a monthly basis, the stopes (or parts of them) are designed with CAD primitives from their position at the end of the month based on topographic data of the sidewalls (Fig. 5). After coding them as being in a *mined* or *backfill* state they are stored and organised in the geometric data base.

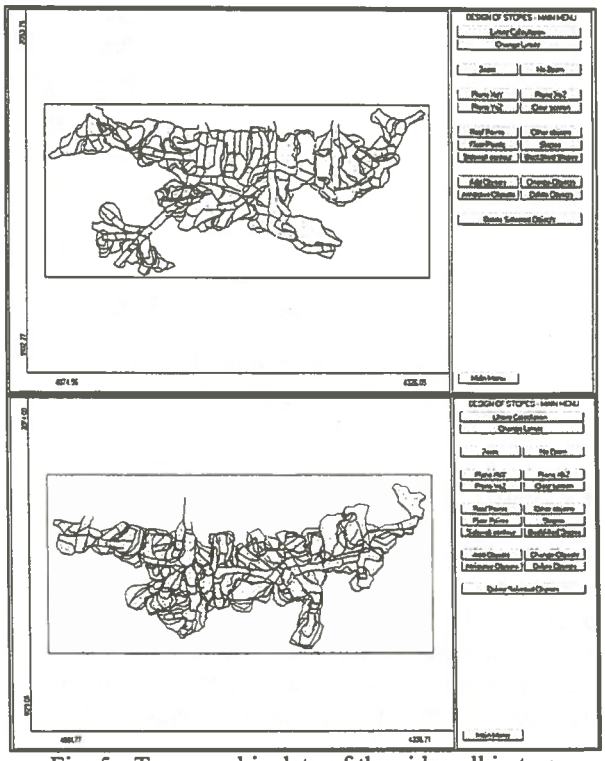

Fig. 5 - Topographic data of the sidewall in two consecutive mine levels.

For each mined and designed stope a browse of the data base is made in order to extract the geometry of the adjacent and already backfilled stope(s). Subsequently the intersection between the mined and the backfilled stope is calculated. In this step the geometric boundaries of the dilution areas are defined in the horizontal plane (Fig. 6). All these operations are made with 2D vectorial polygons representing the boundaries of the stopes and dilution areas (Almeida and Soares, 1994).

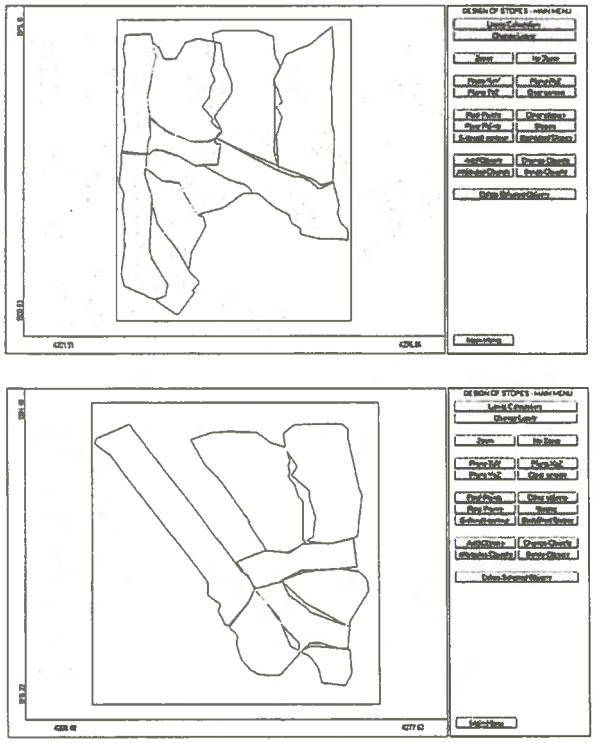

Fig. 6 - Desing of stopes in two consecutive mine levels.

4.2 Spatial Interpolation of the Roof and Floor

The objective of this step is to derive the volumes corresponding to the 2D boundaries of the stopes and dilution areas calculated in the previous step. Thus, the spatial inference of the floor and roof of the mined stope and the adjacent dilution areas is performed in accordance to the following methodological sequence:

i) Rasterization of the dilution areas, limited by vectorial polygons, in order to fill them with a regular grid of points. An adaptative grid technique is used to make the density of the grid proportional to the area of the polygon to be filled (Fig. 7);

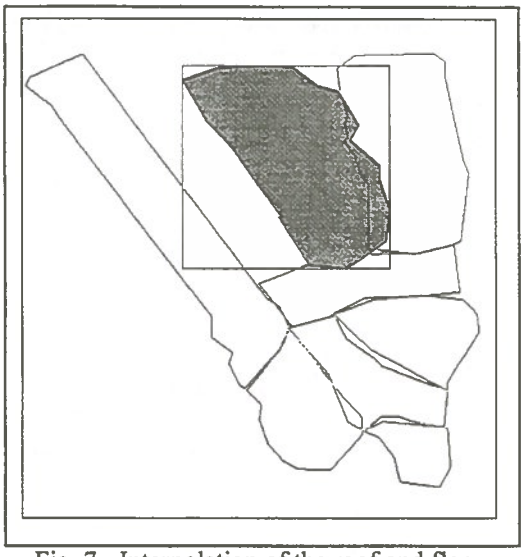

Fig. 7 - Interpolation of the roof and floor.

ii) Selection of topographic coordinates of the roof and floor of all points surrounding the mined out stope. These points are used for the spatial inference of the roof and floor of the mined stope and the roof of the previous level stopes;

iii) Finally all points of the adapted regular grid, corresponding to the stope and dilution areas, are estimated with the geostatistical technique of kriging. For estimation purposes a global variogram model, with an anisotropy effect proportional to the main average dimensions of the orebody layer, was adopted. The variogram model is systematically updated.

4.3 Dilution Calculation

The geometric modelling kit contains a set of primitives to perform the basic operations - intersections and unions - to calculate the volumes of selected areas: total volume of the mined stope, volume of sidewall dilution areas and volume of floor dilution areas. For technical control purposes it is convenient to separate the backfill dilution resulting from the previous level stopes - *floor dilution* - from that of the adjacent stopes - *sidewall dilution.*

For the sidewall dilution, the intersections between stopes of the same level are made with the vectorial

format of the 2D polygons representing the horizontal boundaries of the stopes (Fig. 8).

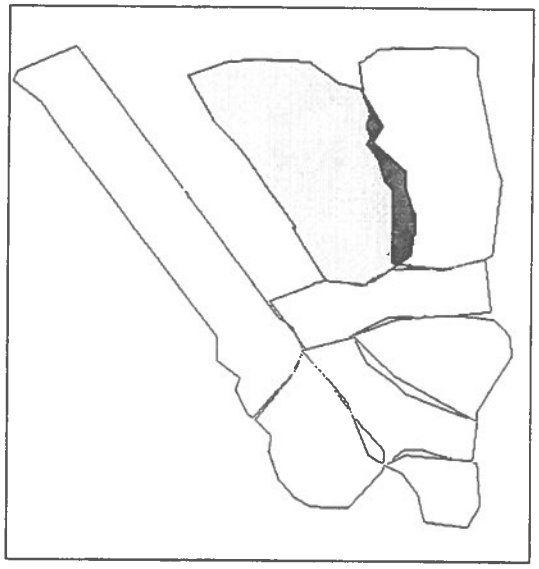

Fig. 8 - Sidewall dilution evaluation.

The floor dilution is calculated with the rasterized version of the stopes. This means that the intersections are calculated between estimated points of the floor of the mined stope and the roof of the previous level stopes - backfilled - (Fig 9).

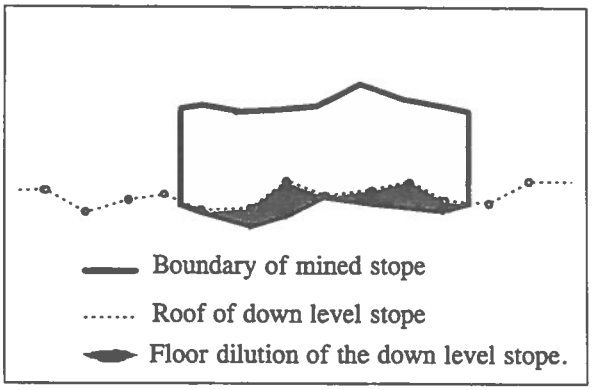

Fig. 9 - Floor dilution evaluation.

5. FINAL COMMENTS

. The calculated dilution values are reported for each panel (see table 1) and allow dilution to be controlled as a function of:

i) different mining operation performances resulting from varying conditions as well as varying equipment for different sites;

ii) different oretypes, which is essential for the reconciliation balances between the broken and treated ore.

. The system is now prepared to include the dilution calculation of the barren contacts with the mineralization. In fact, once the estimated morphology of the oretypes and barren contacts is organised in the geometric data base in a rasterized format - a regular grid of estimated values of the probability to belong to the different oretypes - the intersections with the boundaries of the stopes and consequent calculation of dilution is performed in a similar way as the floor dilution.

Acknowledgements

We would like to thank to António Salvador for the careful revision of this paper.

REFERENCES

ALMEIDA, J. and SOARES, A., 1994.
A Geometric Modelling System for Mineral Resources Based on a Graphic Object Oriented Tool Kit Developed in C Language. Proceedings, 1st Regional APCOM SYMPOSIUM, Bled, Slovenia, pp. 253-262.

CAUPERS, D.L., GUERREIRO, L., RODRIGUES, J.P. and SOARES, A., 1993
Automatic Blending System at Neves Corvo Mine. Proceedings of the XXIV APCOM CONGRESS, (Elbrond J. and Tang, Xiaoli, Editors) Montreal, Canada, Vol.2, pp. 27-34.

LUIS, J., SOARES, A., GONZAGA, J., SILVA, F: and FERREIRA, A., 1993
Geostatistical Characterization of the Shape of an Orebody by Using Mining and Geological Data. Proceedings of the XXIV APCOM CONGRESS, (Elbrond J. and Tang, Xiaoli, Editors) Montreal, Canada, Vol.2, pp. 402-409.

MORTENSON, M.E. , 1985
Geometric Modelling, John Wiley Sons, Inc, 763p.

MURRAY, DN. and REAL, F., 1990
The Technical Side of Copper Mining - The Neves Corvo Mine. Metal Bulletin's 4th International Cooper Conference, Santiago.

TEIXEIRA, L.A. and CAUPERS, D.J., 1990
Computerized Planning at Neves Corvo Copper Mine, Portugal. Transactions of the Institution of Mining and Metallurgy, Section A, Mining Industry, Vol. 99, pp. A60-A64.

6.

rock mechanics
mécaniqque des roches

CAMI'95: 3rd Canadian Conference on Computer Applications in the Mineral Industry
Montréal, Québec, Canada, October 22-25, 1995

Optimizing Seismic Characterization Of Longwall Coal Mine Overburden Using CAD And Computer-Enhanced Techniques: Case Study From Longwall Mining Operations, Western Maryland, USA

Karen Kluger Cohen, Michael A. Trevits
U.S. Bureau of Mines, Pittsburgh Research Center
Pittsburgh, Pennsylvania, USA

Douglas Rudenko
Vibra-Tech, Hazleton, Pennsylvania, USA

ABSTRACT:

Seismic studies conducted to determine coal mine overburden conditions can provide valuable information about rock mass properties and other geotechnical quantities useful for mine operators. Improvements in the manner in which these seismic data are presented, especially with respect to mining operations, would increase their utility for mine operators and aid in understanding their significance for mining. In this study, surface seismic data were integrated with mine site information using CAD and other computer-enhanced techniques toward achieving this goal. Seismic refraction surveys were conducted over a longwall coal mining operation in western Maryland, USA to investigate subsidence-related changes in mine overburden. The longwall panel mined was about 2.5 m (8 ft) thick and was located about 137-168 m (450-550 ft) below the ground surface. Surveys were conducted along lines transverse and longitudinal to the panel prior to mining, when the longwall face was located beneath the survey lines, and when the longwall face passed the survey lines. Data analyses included determination of seismic velocities, depth to and thicknesses of multiple layers, and changes in overburden velocities as mining progressed. Significant results included the delineation of the soil cover from upper bedrock, velocities for these layers, and changes in velocities of these layers as mining progressed. With few exceptions, the trend was for velocities to decrease in both the soil and upper bedrock after the longwall face advanced passed the survey lines a distance comparable to the overburden thickness. The velocity changes were attributed to changes in fracture density, compaction, water saturation, material density, and state-of-stress. The study demonstrated the value of seismic data to characterize large areas affected by undermining.

RÉSUMÉ:

Les études sismiques effectuées afin de déterminer les conditions des couvertures des mines de charbon peuvent fournir de précieuses informations concernant les propriétés des masses de roche et autres quantités géotechniques utiles aux exploitants de mines. Les améliorations dans la façon de présenter ces données sismiques, surtout en ce qui concerne les exploitations minières, augmenteraient leur utilité pour les exploitants de mines et aideraient à comprendre leur importance pour l'exploitation minière. Dans cette étude, les données de surfaces sismiques ont été intégrées aux informations concernant les sites des mines en utilisant CAD et d'autres techniques améliorées de l'informatique pour atteindre ce but. Des sondages de réfraction sismique ont été effectués sur une exploitation minière par longwall dans l'ouest du Maryland, aux Etats-Unis, afin d'examiner les changements relatifs à l'effondrement dans la couverture des mines. Le panneau longwall exploité était d'environ 2,5 m (6 pi.) d'épaisseur et se trouvait à environ 137-168 m (450-550 pi.) sous la surface de la terre. On a effectué des sondages selon des lignes transversales et longitudinales au panneau avant d'exploiter, lorsque la face longwall se trouvait sous les lignes de sondage, et lorsque la face longwall dépassait les lignes de sondage. Les analyses de données comprenaient la détermination des vélocités sismiques, la profondeur jusqu'aux couches multiples ainsi que leur épaisseur, et les changements dans les vélocités de couverture à mesure que l'exploitation

progressait. Les résultats importants comprennent la délinéation de la couverture du sol à partir de la roche de fond supérieure, les vélocités de ces couches, et les changements de vélocité dans ces couches au fur et à mesure de l'exploitation. Nonobstant quelques exceptions, les vélocités avaient tendance à diminuer dans la terre et dans la roche de fond supérieure lorsque la face longwall avançait passé les lignes de sondage d'une distance comparable à l'épaisseur de la couverture. Les changements dans la vélocité étaient attribués à des changements dans la densité de cassure, le tassement, la saturation par l'eau, la densité du matériau, et l'état de contrainte. L'étude a démontré l'importance des données sismiques pour caractériser de grandes surfaces affectées par l'affouillement.

INTRODUCTION

This investigation was conducted at a site of longwall mining operations in the northern Appalachian coalfield (Fig. 1) and focused on seismic characterization of overburden deformational response as a function of longwall face advancement. In longwall mining, typically 100 pct extraction is achieved by removal of coal panels whose width and length dimensions are on the order of 100's of meters. During removal of the panel, the mine roof is hydraulically supported at the face as the coal is removed. As the mine face advances, the roof support is advanced and the previously mined area is allowed to collapse in a controlled manner. The greatest percentage of resultant overburden deformation is short-lived in terms of time interval of mining. The specifics of overburden deformation depend on the mine dimensions, overburden thickness and character, and other geologic conditions. The deformation commonly propagates to the surface and is manifest as a vertical change in surface elevation called subsidence. The effects of this ground movement include modification to surface terrain, change in surface drainage, potential for change to the groundwater regime, and potential damage to infrastructure including buildings and utilities.

In 1977 the United States Congress enacted the Surface Mining Control and Reclamation Act (SMCRA) that required mine operators to develop approved plans for subsidence because of the potential effects described above. As a consequence of this legislation, many subsidence studies have since been conducted in the United States. These studies have focused upon developing predictive subsidence models for surface ground movement and conducting field measurements of surface and subsurface overburden response (Peng, 1992). This investigation focused on the unconventional use of a geophysical methodology, the seismic refraction method, to remotely characterize overburden response to mining.

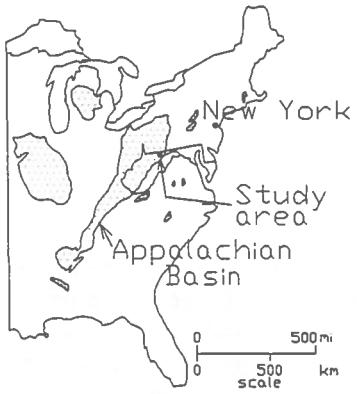

Figure 1. Eastern United States coalfields and the location of this study in the northern Appalachians.

SCOPE OF STUDY

Overburden response to longwall mining operations has been studied for decades. A simple model described by Peng (1992), that serves as an aid to visualize overburden response, defines four zones of overburden response (Fig. 2): (1) caved zone of immediate mine roof where all stratification is lost; (2) fractured zone (strata are broken but bedding remains); (3) continuous deformation or bending zone where strata can, but are not likely, to be broken, and deformation is transferred to and through; and (4) soil zone whose brittle or plastic response is dependent on the physical properties of the material comprising this zone.

Sophisticated subsidence prediction models are available and many have been summarized by Peng (1992) and other researchers. In addition to these prediction models, studies of surface movement above longwall panels have provided abundant field data. The well established dynamic subsidence profile obtained at the surface transverse to the longwall panel, shows a maximum sag at the panel centerline with vertical movement diminishing to either side (Fig. 2). The factors affecting the shape of this profile

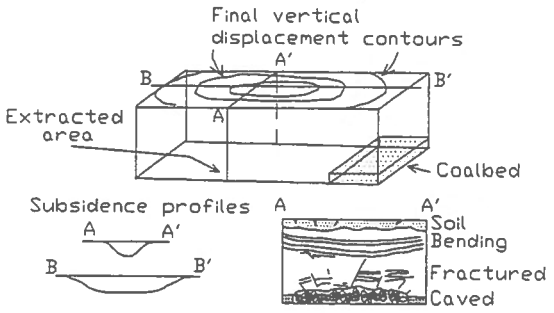

Figure 2. Block sketch for longwall panel extraction that shows final subsidence trough and cross-sections with subsidence profiles and four zones of overburden (Peng, 1992) based on deformational response. Diagrammatic and not to scale.

include but are not limited to the following: width, length, and height of the mined-out area; depth of mining; physical properties of overburden; effects of multiple panels mined; and time (Peng, 1992; Gray and Bruhn, 1984). In addition to these factors, measurement of overburden response is conventionally presented in terms of progression of mining (face advancement) or end of mining. For example, in the northern Appalachian coalfield, the relationship between subsidence, overburden thickness, and face advancement has been observed to be on the order of the following (Gray and Bruhn, 1984): if h is the thickness of the overburden, 90 pct of subsidence is completed when the face has advanced 0.75h to 1.0h beyond the point of observation, and subsidence is complete when the face is 1.25h to 1.75h beyond the point of observation.

Overburden response is an interest from both an environmental point of view and a requirement by law, and numerous methods for studying and measuring these phenomena have been developed. Field measurements of both surface and subsurface deformation have been made using techniques such as standard surveying of monuments, tiltmeters, time domain reflectometry (TDR), and borehole extensometers (Peng, 1992). Multiple point measurements are needed to understand overburden deformation response over large areas, therefore these techniques become expensive and time consuming.

In this study, an unconventional use of the seismic refraction method was tested to assess mine overburden response to mining operations. The goal of this seismic characterization was to determine overburden changes that occur shortly after mining above longwall operations. Advantages of this technique include that the methodology is nonintrusive and large amounts of subsurface data can be acquired rapidly. In designing this study, it was anticipated that overburden changes could be measured in terms of seismic properties (especially velocities) of the overburden and these, in turn, could then be related to physical properties of the rockmass. Some results from this study were previously reported by ICF Technology, Inc. (1992) and Rudenko et al. (1990).

FIELD INVESTIGATION

Description of Field Site and Seismic Data Acquisition

The site of investigation was located in western Maryland near the Maryland-West Virginia border (Fig. 1) in the Allegheny Plateau Province of the Appalachians. At the location of the surveys, longwall mining operations took place about 137-168 m (450-550 ft) below the ground surface in the Upper Freeport Coalbed. Bedrock consisted of the Pennsylvanian-aged Allegheny and Conemaugh Formations composed of interbedded shale, siltstone, sandstone, conglomerate, and coal (Fig. 3). The longwall panel extracted during this study was approximately 2.5 m (8 ft) in height, 160 m (525 ft) wide, and 1,013 m (3,325 ft) in length (Fig. 4). An adjacent panel located to the northeast of the panel studied in this investigation was previously extracted.

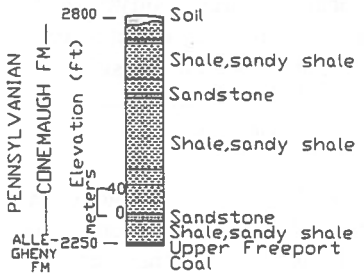

Figure 3. Stratigraphy of study area.

The objective of the seismic refraction surveys was to monitor mine overburden changes during longwall face advancement using a series of lines both transverse to and along the panel centerline (Fig. 4). Monitoring was completed at three different time intervals of face advancement that spanned approximately one month. As a result, subsurface cross-sectional data were obtained along both the

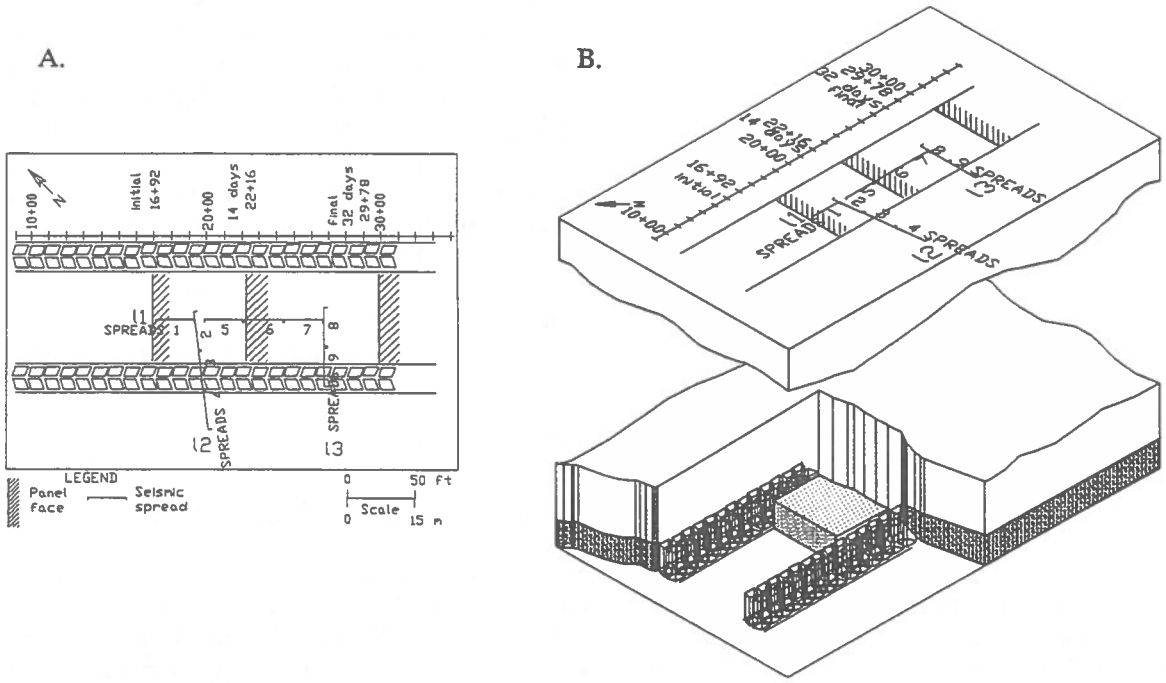

Figure 4. Plan of mine and seismic lines (A) transformed to 3-D section (B) with CAD and accessory modeler.

length and width of the panel. A total of three survey lines were completed during each interval of measurement (Fig. 4). The line along the panel centerline consisted of four spreads (l_1). Two lines were surveyed transverse to the panel; one consisted of three spreads (l_2) and the other consisted of two spreads (l_3). Each spread used 12 geophones that were positioned at 6.1 m (20 ft) intervals; this resulted in a total length of 67 m (220 ft) for each spread. Geophone locations were surveyed during each seismic monitoring period to determine elevations. Survey monuments were also positioned along each seismic line and these were also monitored to measure ground movement.

Dynamite (0.45 kg (1 lb) charges) detonated in augered shot holes was used to generate compressional seismic waves that were detected using vertical geophones. Shot points were also surveyed during the monitoring period. Shear wave studies were also conducted but will not be discussed. Numerous shots were completed for each spread contained within a given line. Shot offsets differed relative to the spread endpoints. Shots were completed at the beginning and end of each spread and midway on the spread. Forward and reverse shots with long offsets were also completed; the offset distances for these were approximately the length of the spread.

Results

In the following, only the compressional seismic wave results and interpretations will be presented. Typical seismic records acquired during the seismic monitoring are presented in Figure 5. These data represent two spreads (2 and 3) combined from line 2 positioned transverse to the panel. Results from the premining survey and the survey completed about a month later are provided. In the latter, the longwall face had progressed past the survey area and was 324 m (1,062 ft) from the line (l_2) containing these two spreads.

First arrivals on these records represent compressional seismic wave energy propagating through the overburden by way of a direct or refracted path (direct and refracted arrivals). Traveltime plots were developed from these records for further analyses of subsurface velocities (Fig. 6). These were completed by picking first arrival traveltimes from the seismic records and plotting distance of receiver along the survey line versus the time of the first arrival. Seismic refraction analyses were completed using interactive computer programs that perform forward modeling based on a ray tracing routine (Ackermann et al., 1982). The number of subsurface layers detected, corresponding velocities, and depth to these layers were determined from these analyses and are

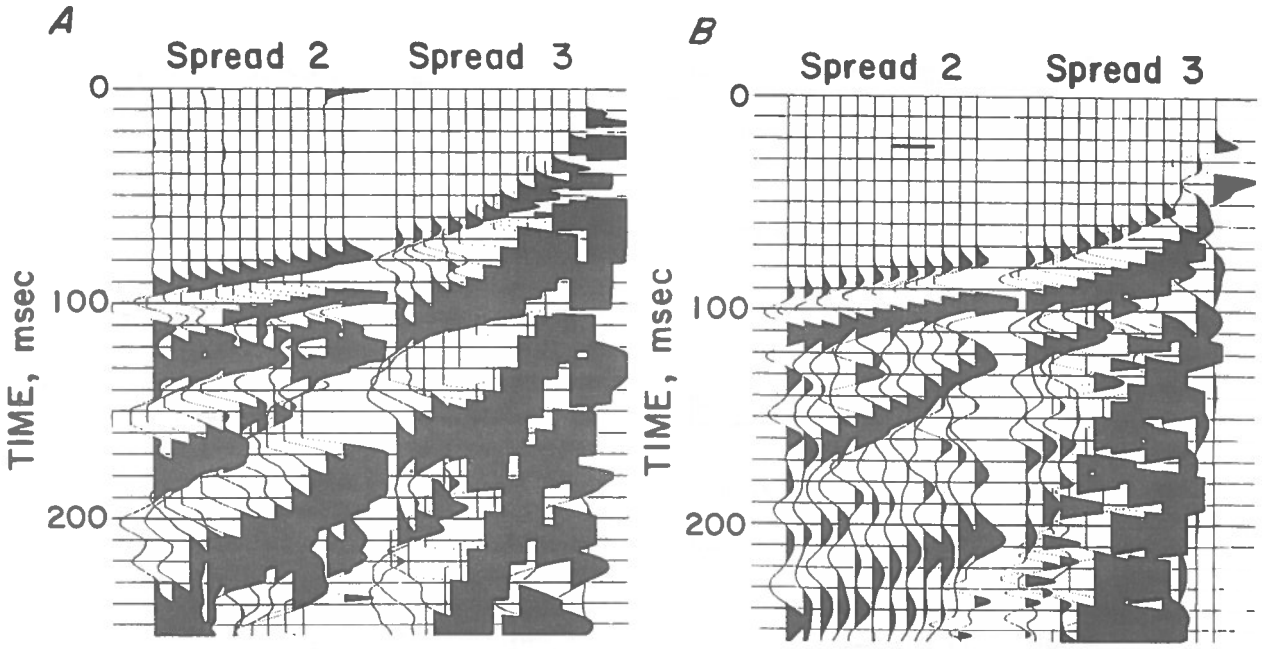

Figure 5. Seismic records from spreads 2 (far, reversed offset) and 3 (near, reversed offset) (l_2) along the panel centerline acquired during two different times of face advancement. A. Premining (initial). B. Final.

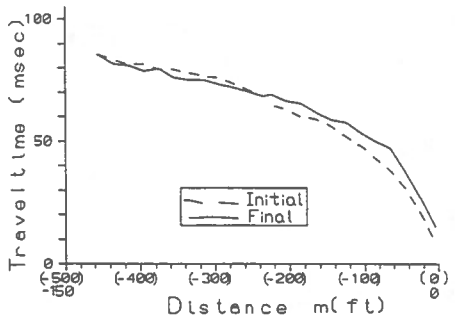

Figure 6. Traveltime plots for spreads 2 and 3 (l_2). Plots determined from records shown in Figure 5.

presented on depth sections. The subsurface velocity models that were determined for spread 2 are provided in Figures 7a and b. These models represent only the first and last monitoring completed and were derived from data shown in Figure 6.

For spread 2, a three-layer case was developed (Fig. 7). During the first time monitored (Fig. 7a) the uppermost velocity layer ranged from 610-823 meters per second (mps) (2,000-2,700 feet per second (fps))and the middle layer was 1,128 mps (3,700 fps); these velocities suggest that these layers were the unconsolidated soil mantle and weathered bedrock. The underlying highest velocity layer was detected at approximately 12-15 m (40-50 ft) deep and had an initial velocity of 3,139 mps (10,300 fps). This higher velocity layer is interpreted as bedrock. A knowledge of the stratigraphy (Fig. 3) in the area, combined with drillhole data, suggest that the uppermost bedrock is likely shale and sandy shale with minor beds of sandstone. The velocity observed is typical for these lithologies. The velocity model is also shown for the survey conducted about one month later (Fig. 7b). Comparing the two depth sections modeled for the initial and final monitoring, it is clear that velocities changed and, in some cases, configuration of layers changed.

The traveltime analyses and subsurface velocity models developed and described above were completed for all the seismic refraction surveys conducted during the three monitoring times over the course of one month (ICF Kaiser, 1992). Results for two additional spreads (1 and 7) are presented in Figures 7c-f. Velocity models for the initial and final seismic monitoring are provided. It is apparent from these data that the trend was for velocities to change after mining passed and, furthermore, they were more likely to decrease after mining. The greatest percent changes were observed in the soil layer.

Results from all of these survey lines have been synthesized into a 3-D overburden model composed of

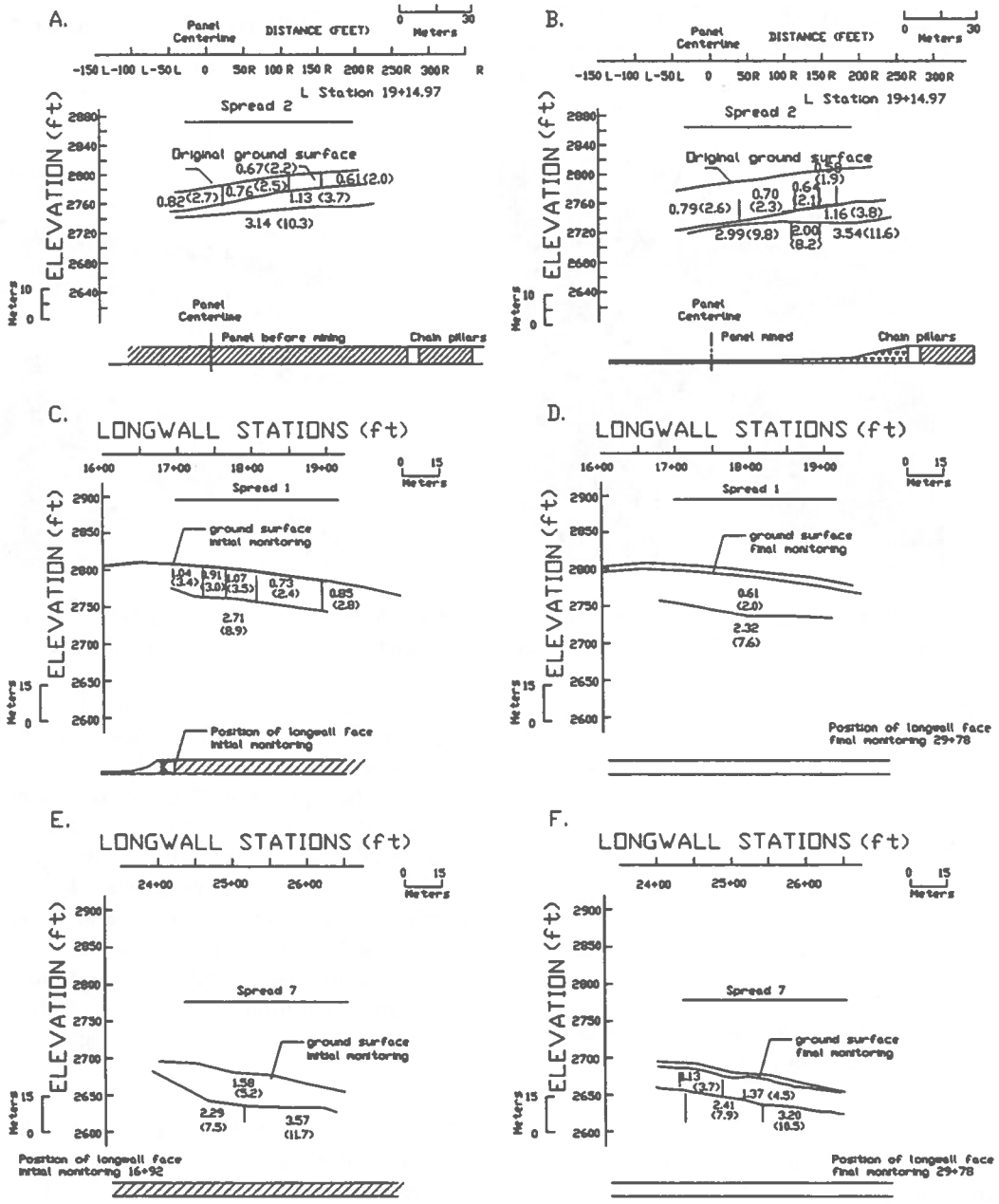

Figure 7. Modeled depth sections containing velocities for spreads 2, 1 and 7 acquired during initial and final monitoring. Velocities in kilometers per second (kilofeet per second). Spreads 1 and 7 were along the panel centerline and spread 2 was transverse to the panel. A. Spread 2, initial. B. Spread 2, final. C. Spread 1, initial. D. Spread 1, final. E. Spread 7, initial. F. Spread 7, final.

multiple layers and their associated velocities determined from the seismic refraction data (Fig. 8). To simplify this model, velocity ranges were assigned to each layer based on compartmental velocity values within each layer. Only the initial survey velocities are shown in this figure.

Lines transverse to the panel were modeled with three velocity layers (depth of about 15 m (50 ft)) and lines

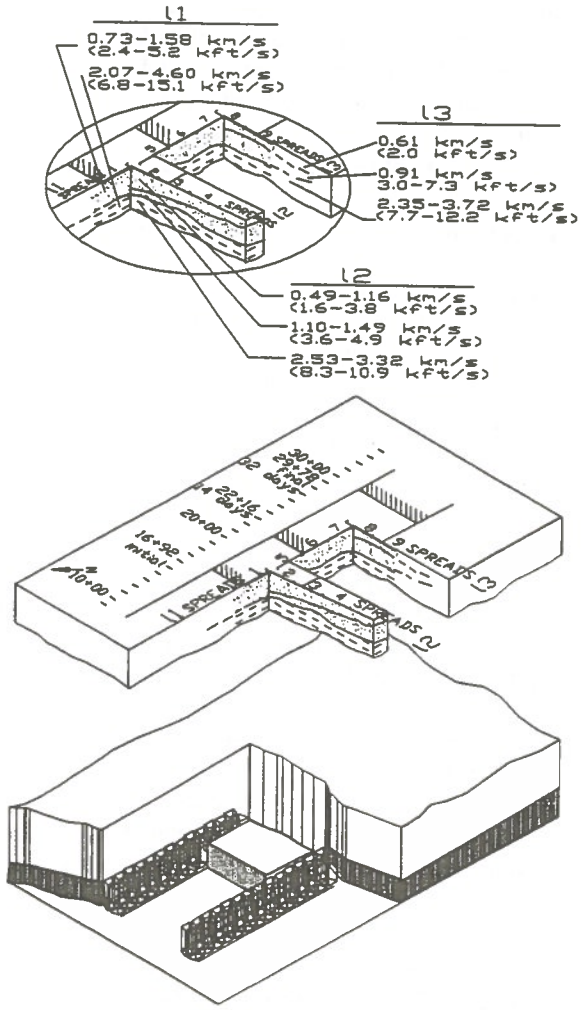

Figure 8. Three-dimensional diagram of study area with initial seismic velocities. Velocities in kilometers per second (km/s) and kilofeet per second (kft/s).

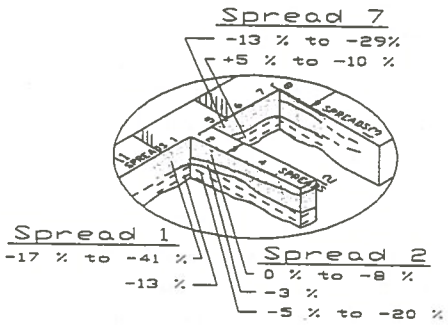

Figure 9. Percent (%) change in velocities between initial and final monitoring for spreads 1, 2, and 7.

longitudinal to the panel were modeled with two velocity layers (depth of about 18 m (60 ft)). For the lines transverse to the panel shown with three layers, it is likely that the uppermost layer represents unconsolidated soil cover. The intermediate layer likely represents soil and the weathered top of bedrock. The remaining deepest and highest velocity layer represents bedrock, most likely interbedded shale and sandstone.

The survey lines along the panel centerline were modeled with two velocity layers. The uppermost layer likely represents soil cover and weathered bedrock and the underlying layer is interpreted as bedrock. The range of velocity values in both the unconsolidated and bedrock layers infer the heterogeneous nature of these layers. In the unconsolidated mantle, important factors that affect velocity values include soil composition (i.e. clayey or sandy), compaction, and degree of water saturation. For bedrock, similar factors control velocity values, but rock lithology is probably the most important. Furthermore, degree of weathering and fracturing also controls bedrock velocities.

These data were also developed for the second and third interval of monitoring as the longwall face passed beneath the survey lines and to a point 97 m (319 ft) beyond spreads 8 and 9 of line 2 (Figs. 4 and 8). Total velocity changes measured over the entire time interval of monitoring were determined from these data; they can be compared to and explained in terms of overburden deformation and subsidence that occurred in response to undermining. These data are provided for the spreads given as examples (spreads 1, 2, and 7). In Figure 9, they are shown as a percentage change from initial velocity values. Deformation in the mine overburden as the face advanced was ultimately manifest at the surface as subsidence. The deformation also resulted in physical property changes in the overburden rockmass that affected propagation of seismic waves.

DISCUSSION OF FUNDAMENTAL PROPERTIES OF LONGWALL MINE OVERBURDEN ASSESSED WITH SEISMIC INVESTIGATION

Subsurface velocity models presented in Figures 7, 8, and 9 substantiate that deformation in the overburden was accompanied by and produced physical property changes that affected propagation of seismic waves. According to the theory of elasticity and seismic wave

propagation, compressional wave velocity is a function of only the elastic constants and density. However, there is abundant literature to support that other rockmass physical properties affect seismic wave propagation. These include but are not limited to the following: fracture density; compaction or induration; fluid saturation; porosity; and state-of-stress. For example, increased fracture or crack density tends to decrease seismic velocity and attenuate seismic energy. These physical properties can effectively alter the elastic constants and/or density of a rockmass to change the seismic velocity. What is the relationship of these physical properties changes to deformation of longwall overburden?

Recall that previous workers have developed a simple model for mine overburden response that divides overburden deformation into four zones (from the mine level, upward; Fig. 2): the caved zone; the fractured zone; the zone of bending or continuous deformation; and the soil zone. Researchers (Peng, 1992) have even developed mathematical expressions to determine the height of these zones, with important controlling factors arising from specific mining and geologic conditions. Dimensions of these zones have been estimated such that the combined caved and fractured zones typically range from 20 to 30 times the mining height.

Using this estimate for the combined caved and fractured zones, along with the mining height of 2.4 m (8 ft), it is estimated that the combined caved and fractured zones extended from 48.8-73.1 m (160-240 ft) above the mine level at this site. In terms of depth below the surface (the mine level was at a depth of 137-168 m (450-550 ft)), the upper extent of the caved and fractured zones would be found at depths of 64-88.4 m (210-290 ft) to 94.5-118.9 m (310-390 ft). It is clear that the subsurface velocity models developed in this investigation (Figs. 7, 8, and 9) and the overburden they represent were probably located in the soil zone and zone of bending or continuous deformation, well above the zones of caving and fracturing. Therefore, the seismic velocity changes measured in this investigation were a direct result of the propagation of seismic waves that traveled only through these two uppermost zones of overburden. As a result, it was these two uppermost zones that were the focus of this study.

There are some rockmass physical properties and property changes within these two zones that can be interpreted from the seismic results. In Figure 7, specific examples were provided that illustrated velocity models developed for spreads located along the longwall panel centerline (spreads 1 and 7) and transverse to the panel (spread 2). For spreads 1 and 2, the mine face had advanced more than one overburden thickness past the spreads during the last monitoring period, so it is likely that most subsidence and deformation had been completed. This was not the case for spread 7, for which the face was significantly less than one overburden thickness past the end of the spread. (Overburden thickness was about 137.1 m (450 ft) here and the mine face had progressed to 97.2 m (319 ft) past the end of the spread.) It is likely that deformation and accompanying subsidence was incomplete at this time for spread 7.

Spread 1 was located along the panel centerline. Thus, in a subsidence profile developed transverse to the centerline it was located at the position where maximum vertical displacement is predicted. The depth section in Figure 7 shows a two-layer velocity model derived for both the initial and final monitoring, and these two layers were interpreted as soil and bedrock. Initial bedrock velocity values suggest it was interbedded shale and sandstone. Because a single velocity was modeled for this layer, it was probable that the bedrock was rather homogeneous over the area. One month after mining passed, the bedrock velocity decreased to about 13 pct of its original value. The overlying unconsolidated layer appeared to be more heterogeneous during the initial monitoring, based on the wider range of velocity values. Decreases in velocity were also observed in this layer as the face passed. Velocity changes were greater than those observed for the underlying bedrock and, for the soil cover, decreased 17-41 pct. A wider range of velocity values observed in the soil cover, combined with greater velocity changes observed in this layer after mining, were two trends noted in much of the seismic data. These are most likely due to variations in soil character (sand, clay, etc.), compaction, and saturation. The latter two properties would be more readily altered than some rockmass properties as deformation is transferred to the soil cover. Increased fracture density along with changes in compaction and saturation are likely causes for velocities to decrease in the soil cover.

Velocity changes in the bedrock observed after mining were smaller. Changes could represent phenomena such as increased fracture density and/or decreased water saturation. It is apparent that the deformation

experienced by the bedrock was transferred to the overlying soil cover because the ground surface subsided. Because the final seismic velocities measured in both bedrock and soil cover were modeled as rather consistent over the length of the spread, this suggests that the deformation transferred from upper bedrock units to soil cover was rather uniform. Finally, monuments surveyed along spread 1 had total elevation decreases that ranged from 1.40-1.46 m (4.6-4.8 ft). The small range of final values suggests that surface deformations appeared to be distributed rather uniformly over the length of the spread.

Spread 7 was also located along the panel centerline and on the same survey line as spread 1 (Figs. 4 and 6). An important difference was that at the time the final seismic survey was completed, the mine face advanced a distance that was less than one overburden thickness away. Thus, deformation of the overburden beneath this spread and accompanying subsidence was not likely completed. In the initial monitoring, the soil layer appeared rather uniform according to the single velocity value modeled (this velocity value of 1,524 mps (5,000 fps) is often used for water saturated sediments). The underlying bedrock was modeled with two velocities and this suggests the presence of several lithologies within this layer, perhaps a shale and sandstone. After mining, the soil cover velocities were more variable and decreased by 13-29 pct; these observations may be attributed to increased fracture density, change in compaction, loss of water, and/or the differential response of different soil types. The underlying bedrock was modeled with two velocity values; one had an increase of 5 pct and the other decreased 10 pct. Monuments surveyed along spread 7 had total elevation decreases that ranged from 1.40-1.04 m (4.6-3.4 ft). Because of the position of the spread along the centerline, it is expected that all values would be approximately the same and similar to those observed for spread 1. The wider range of observed subsidence for spread 7 supports the interpretation that deformational response and accompanying subsidence was incomplete. Again, it is apparent that along this spread deformation was transferred from bedrock to the soil cover. Velocity changes in both upper bedrock and soil cover were observed. As was observed for spread 1, the soil cover had the greatest changes in seismic velocities. After the mine face advanced past the survey lines, velocity changes were observed in both the upper bedrock and soil cover.

Spread 2 was located transverse to the panel and offend spread 1 (Figs. 4 and 7). The seismic refraction data were modeled to produce a depth section with a three-layer velocity case. According to the velocity data obtained during the initial monitoring period, the two uppermost layers were interpreted as unconsolidated cover and weathered bedrock, and the third highest velocity layer was interpreted as bedrock. The bedrock velocity value was higher than that obtained for spread 1. This suggests a change in lithology, possibly, from shale to sandstone; it could also represent directional velocity variations due to anisotropy. As was the case for spread 1, the soil cover showed the higher variability in initial velocity values. After mining passed, changes in the velocities were observed. Most were in a negative sense, resulting in velocity decreases. The uppermost soil cover decreased a maximum of 8 pct. The underlying bedrock decreased about 5-20 pct. It is apparent that deformation transferred from bedrock to the soil cover. Monuments surveyed along this spread displayed decreases in elevation ranging from 0.58-1.37 m (1.9-4.5 ft). Compared to spreads 1 and 7, this is a greater range of elevation changes. Because this line is transverse to the panel, this greater variability in subsidence is to be expected. For a subsidence profile transverse to the panel, subsidence should be a maximum along the centerline and should decrease toward the edge of the panel, eventually reaching zero. Along the spread, deformation was not uniform and the resultant differential effect may have produced a wider range of velocities.

The examples provided in this discussion represent the general trends that were observed during monitoring the longwall overburden at this site. In addition to these physical property changes, there is evidence in the literature that the state-of-stress condition (compressional versus tensional) over mine excavations affects seismic velocities. There is a physical basis for this because state-of-stress can affect rockmass elastic moduli and rockmass density. It is probable that a relationship exists between some of the seismic velocity anomalies observed in this study, and state-of-stress conditions that resulted from mining operations.

SUMMARY AND CONCLUSIONS

The goal of this investigation was to utilize the propagation of seismic waves to characterize the overburden before, during, and after the mine face

had advanced beneath the seismic refraction survey lines. Use of geophysical technologies such as this can potentially reduce the cost of determining overburden response to mining because large subsurface areas can be surveyed and characterized quickly. Results from the lines surveyed along the panel centerline and transverse to it showed compressional seismic wave velocities were likely to change and, most likely, to decrease, as the mine face advanced past the survey lines. The depth sections modeled from the seismic data were in the uppermost 18.3 m (60 ft) of mine overburden. Therefore, the changes were measured within the uppermost two zones identified in simple models for longwall panel overburden deformation: the zone of bending (above the fractured zone) and the soil zone. Deformation transferred from the mine level through all four zones to the surface was documented by conventional land surveying.

Other trends interpreted from the seismic results were the following. In the initial monitoring conditions, the soil zone tended to be more heterogeneous than the bedrock. Furthermore, the soil cover tended to become even more heterogeneous after deformation due to mining. The soil zone also had a tendency to show greater changes in the velocities after mining passed compared to the underlying bedrock. The bedrock seismic velocities tended to also change, but these usually were not as great. This is likely due to the greater strength of rockmass compared to unconsolidated material and weathered bedrock, providing a greater resistance to deform and bring about physical changes. It is probable that physical property changes responsible for velocity changes included some or all of the following: increased fracture density; change in fluid saturation; change in material compaction; and change in material density. It is also possible that state-of-stress conditions in the bedrock and soil cover affected velocity measurements.

It is clear that this seismic field investigation provided results that documented physical property changes in overburden in response to deformation. However, it should be noted that the strongest interpretations are provided when these data are integrated with other information such as surface monument survey and borehole data. In addition, it should be cautioned that results from this one study cannot and should not be extrapolated to all longwall panel overburden conditions. This study site consisted of a particular set of mining and geologic conditions unique to the site. Based on this and previous similar studies, it is apparent that seismic data can contribute valuable information to our understanding of overburden deformation and surface subsidence, especially when integrated with all available, relevant data. Future studies selecting seismic methods as a tool to aid overburden characterization should carefully plan seismic experimental design according to site conditions and information objectives, and then integrate the seismic results with all other available overburden response data.

ACKNOWLEDGMENTS

We are grateful to the following for their technical review of this manuscript: James W. Reil, Sr., Vibra-Tech, Hazleton, PA; Dr. Larry Powell, U.S. Bureau of Mines, Twin Cities Research Center, Minneapolis, MN; Paul Jeran, U.S. Bureau of Mines, Pittsburgh Research Center, Pittsburgh, PA; and Raymond Aufmuth, U.S. Bureau of Mines, Washington, D.C.

REFERENCES

Ackermann, H.D., Pankratz, L.W. and Dansereau, D.A., 1982. A Comprehensive System for Interpreting Seismic Refraction Arrival-time Data Using Interactive Computer Methods. USGS Open File Report 8-1065, 265 p.

Gray, R.E. and Bruhn, R.W., 1984. Coal mine subsidence-eastern United States. In Reviews in Eng. Geol. Vol. VI: Man induced Land Subsidence, ed. Thomas L. Holzer, The Geol. Soc. of America, Boulder, CO, pp. 123-149.

ICF Technology Inc./SRW, 1992. Final Report: Design and Implementation of a Monitoring System to Detect Imminent Subsidence in the Anthracite Region of Northeastern Pennsylvania, USBM Contract J0178024, 204 p.

Peng, S., 1992. Surface Subsidence Engineering. Society of Mining, Metallurgy, and Exploration, Inc., Littleton, CO, 161 p.

Rudenko, D., Walker, J.S., Richardson, A.M., Ackermann, H.D. and Reil, J.W., 1990. P-wave and S-wave velocity measurements related to subsidence over a longwall mine (Abstract). SEG 59th Annual Meeting Extended Abstracts, Dallas, TX, pp. 363-367.

CAMI'95: 3rd Canadian Conference on Computer Applications in the Mineral Industry
Montréal, Québec, Canada, October 22-25, 1995

Nonlinear Approach for Determining Design Criteria for Yield Pillar Performance

William C. Smith, Dennis R. Dolinar, and Khamis Y. Haramy
Mining Engineers, Denver Research Center, U.S. Bureau of Mines, Denver, CO

ABSTRACT

The U.S. Bureau of Mines (USBM) is using laboratory and computer-based techniques to investigate the post-failure behavior of yielding pillars and pillar reinforcement techniques to control entry deformation. Laboratory studies to evaluate various reinforcement techniques for controlling yield pillar deformation were conducted. A cracking and crushing computer model is used to evaluate potential tensile and compressive failure planes within pillars of various widths to assess the degree of yielding and stress redistribution; an elasto-plastic model was applicable for studying the behavior of reinforced yield pillars. These procedures effectively account for the residual pillar strength, important in yield pillar design.

RÉSUMÉ

Le U.S. Bureau of Mines (USBM) utilise les techniques de laboratoire et d'ordinateur pour evaluer le fonctionnement des piliers, et des piliers avec les supports, après le concassage pour controller l'alteration des galeries des couloirs. Les études de laboratoire ont été utiliser pour evaluer plusiers techniques de supporter à controller l'alteration des piliers. Un modèle en ciment a utilisé pour calculer les distributions des forces, et les planes de concassage de tractions et de compression dans les piliers à plusiers dimensions. Un modèle "elasto-plastic" a appliqué pour étudier le fonctionnement des piliers avec les supports. Cette méthode calcule effectivement la résistance des piliers après le concassage, qui est plus important dans le dessein des piliers.

INTRODUCTION

Predicting stress distributions and resultant deformations around mine openings constitute an important practical problem. Field and laboratory measurements confirm the presence of progressive failure processes along gateroads. Such strain-softening behaviors require nonlinear material models to fully describe the coal, roof, and floor interactions and the accompanying stress transfers. Simple linear elastic models are useful to determine high stress states in rock masses prior to yielding, but cannot predict the critical path of the changing stress state in the rock mass and residual strength after yielding. This paper presents an approach to studying the post-failure behavior of yield pillars using results from laboratory tests and numerical modeling, namely, hypoelastic and elasto-plastic material models.

Yield pillars are engineered structures that use controlled failure to transfer high loads onto more competent structures such as abutment pillars. The mechanical behavior of pillars undergoing significant deformation while maintaining residual strength requires further investigation. Designing yield pillars based on strain-softening and residual strength characteristics may be a more valid approach than current approaches, which rely primarily on empirical and/or analytical methods for pillar sizing.

Dimensioning yield pillar systems is an inexact science. Poorly dimensioned yield pillars can either result in premature entry closure (when undersized) or adverse stress conditions (when oversized). Two possible extreme outcomes might be yield pillars that fail too violently or yield pillars that do not fail but transfer excessively high abutment stresses onto the roof or adjacent seam. Applying support and thereby changing the post-failure behavior of yield pillars, a subject of this paper, represents one means for controlling pillar failure to prevent premature entry closure by improving stress conditions in the vicinity of mining.

BACKGROUND

Several approaches have been taken by researchers to evaluate yield pillar behavior using laboratory testing and computer modeling. Laboratory studies have shown that highly fractured yield pillars can exhibit significant increases in residual strength with the application of reinforcement such as wire-rope wrapping and/or bolting. Continued research by the Bureau is suggesting a functional relationship between the energy capacity provided by the reinforcement and the subsequent pillar post-failure behavior.

In the past, computer modeling studies have been conducted using an elastic approach to model a nonlinear problem. Other researchers have used iterative techniques (Park and Ash, 1985). A modification of the linear-elastic, progressive failure procedure was developed by the USBM to help account for gob loading in the model (Kripakov and Melvin, 1983 and Dixon et al, 1985). This technique uses a pseudo-elastic approach that reduces elastic rock mass properties as different zones begin to fail. This process is continued through further iterations until all the elements are stabilized. The result is a rock mass that exhibits strain-softening behavior in those zones where failure has been reached. Most available methods use the Mohr-Coulomb or the Hoek and Brown criteria to assess failure. Elastic-plastic models assuming Von Mises criteria have been also used to simulate a yielding pillar (Bensehamdi et al, 1992).

Researchers have shown that soft rock such as coal can be effectively modeled using the elastic-plastic model (Maier and Hueckel, 1979 and Tandanand and Thill, 1987). These models generally follow Hooke's law to describe the stress/strain relationship in plane strain up to failure. For nonlinear material behavior, the onset of plastic deformations is determined by a yield function and general isotropic hardening and softening laws to describe post-yield behavior such as residual strength. Numerical and laboratory studies have shown that brittle materials such as coal, which may undergo major fracturing, can be described as elasto-plastic materials when significant deformation perpendicular to the direction of principal loading occurs (Tandanand and Thill, 1987). Referring to brittle or pseudo-ductile material as elasto-plastic assumes that fracturing is fairly consistent in the material with no dominant single fracture or sets of fractures that govern overall material behavior. In general, this assumption is less likely to be true for unsupported yield pillars where the lack of support confinement with the existence of cleats would more likely permit the development of large fracture surfaces. The addition of confinement would tend to hold more material in place and allow more consistent microfracturing to occur, resulting in more controlled failure. This suggests that yield pillar support could be effectively studied using elastic-plastic models.

A basic model for yield pillars might be one that simulates cracking and crushing-- a condition shown to exist in the laboratory. Depicting such behavior in brittle materials is generally complex. Models that simulate such behavior are limited to concrete structures studies such as nuclear reactor containment vessels and large hydroelectric projects. These models can track potential failure surfaces in yieldable materials indicating where cracking and crushing is likely to occur in the material. The authors have adapted such a model after Bathe et al, 1989 for the study of unsupported yield pillars in longwall coal mining.

YIELD PILLAR AND REINFORCED PILLAR ANALYSIS

Laboratory Models

Coalcrete model pillars, with material properties approximating those of a typical Western coal were used in this study (Dolinar, 1993). The model pillars had width-to-height ratios of 2, 3, and 4 and were either unreinforced or reinforced with a continuous strap or regular pattern of grouted bolts. To obtain the post-failure or yield characteristics of the model pillars, the specimens were deformed in compression to a strain level of 18 pct. During the tests, the applied loads and axial deformations of the specimens were monitored. Laboratory tests are assumed to represent an actual physical model of the response of a yield pillar to load including the development of fractures. The data obtained from the laboratory models provided both inputs for physical properties required by the numerical models and a means for validating and verifying the numerical model outputs.

Numerical Models

Method of analysis: The finite-element code ADINA was used in the analysis. Whereas many linear elastic models require 5 or fewer material property inputs, nonlinear models may require 30 or more. Since obtaining the stress/strain curve for the material is more important than any individual or group of material property inputs, particular attention to the stress/strain curves for the yielding materials is emphasized. In this study, stress/strain curves were computed for supported and unsupported yield pillars. Supported yield pillars were modeled based on varying the yield strength to simulate different bolting intensities (Dolinar, 1993). Subsequently, adjustments were made on the model property inputs for each pillar type to enable closer curve fitting of laboratory results. This was done by constructing a finite-element model of the laboratory uniaxial tests and attempting to match the stress/strain curve of the actual laboratory data with the model output. This approach introduces a valid check on the post-failure behavior of the yield pillar model material prior to simulations with the longwall finite-element model.

Two nonlinear model types were used in this yield pillar study. The *concrete* or *cracking* model was used to evaluate potential cracking and crushing zones in the yield pillar. The *elastic-plastic* model was used to study how gateroad stability can be enhanced by changing the levels of support, thereby changing the post-failure behavior of the yield pillar.

Concrete model: A general three-dimensional concrete model is available in ADINA that can be used for either two- or three-dimensional elements that exhibit many of the nonlinear characteristics of brittle-behaving materials. The constitutive model is hypoelastic, meaning it only allows for linear behavior at fairly low stress levels by using failure surfaces to re-establish a modified uniaxial stress-strain law at higher stress (even multiaxial) levels. Failure surfaces are established using principal stresses to determine if failure is occurring and whether that failure is compressional (crushing) or tensile (cracking). Strain softening is unidirectional, in the direction of cracking, with cracking, and multidirectional with crushing. Cracks can close and become inactive during subsequent solution steps depending on the direction of principal stresses. Observations of coal pillars suggest that similar cracking and crushing processes occur in coal pillars (Jeremic, 1980).

The model inputs allow the modeling of a wide range of brittle materials including coal. Inputs for coal and the accompanying multistress tables for coal in the model were estimated based on laboratory triaxial testing on coalcrete, a concrete material having coal-like properties (Dolinar, 1993). The stress/strain curve obtained from laboratory uniaxial testing was used to calibrate the curves from the concrete constitutive model using unconfined coalcrete properties. Once calibrated, the input properties were then used in the large scale mining problem as yield pillar properties. The aim in this model is to identify potential failure planes and resultant deformation and stress redistributions in the yield pillar present during post-failure. This would be an important check on whether the yield pillar has yielded or not.

Elastic-Plastic Model: The elastic-plastic model employs the von Mises failure criterion with bilinear isotropic hardening. For nonlinear material behavior, the plastic state is defined by:

- A yield function to specify the beginning of deformation,
- A flow rule to define the plastic straining, and
- A softening and hardening rule to define the yield surface with plastic straining.

The elasto-plastic model requires the following input to describe nonlinear behavior: Poisson's ratio, the initial Young's modulus up to the point of yielding, the yield or failure strength, and the post-yield Young's modulus based on laboratory tests.

Supported yield pillars were studied using the elasto-plastic model. The purpose for this part of the study was to show how different yield pillar support strategies can affect the load distributions throughout the pillar, thereby affecting the manner in which yielding occurs.

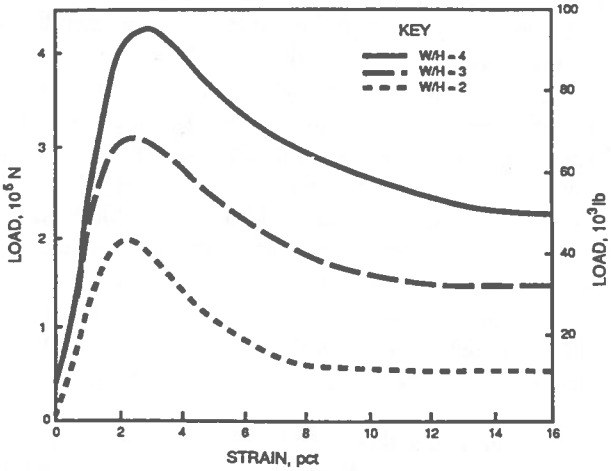

Figure 1. Typical load-deformation curves for three different geometries of unreinforced model pillars.

DATA ANALYSIS AND RESULTS

The load-deformation curves for the laboratory-tested unreinforced model pillars are shown in figure 1. Both the maximum compressive and residual strength of the pillars increase with width. Previous research has shown that the intact center portion of the pillar that remains after testing also increases with the width of the pillar

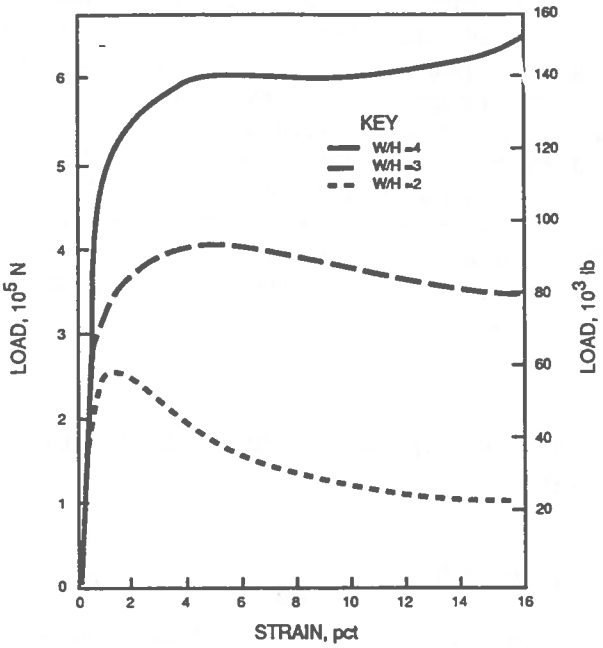

Figure 2a. Typical load-deformation curves for three different geometries of model pillars reinforced with bolts.

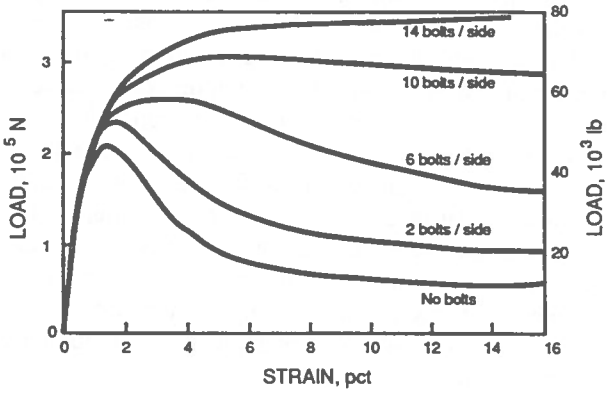

Figure 2b. Typical load-deformation curves for model pillars reinforced with different bolt densities.

(Dolinar, 1993). Figures 2a and 2b show the load-deformation curves for the model pillars reinforced with grouted bolts. The greater the bolt density and pillar width, the higher the compressive and residual strengths. Both the reinforced and unreinforced pillars exhibit nonlinear behavior where, with increasing pillar width and reinforcement, the pillar behavior approaches that of an elastic-plastic material. These load-deformation curves were used to establish the necessary pillar properties such as yield strength to account for various bolt densities.

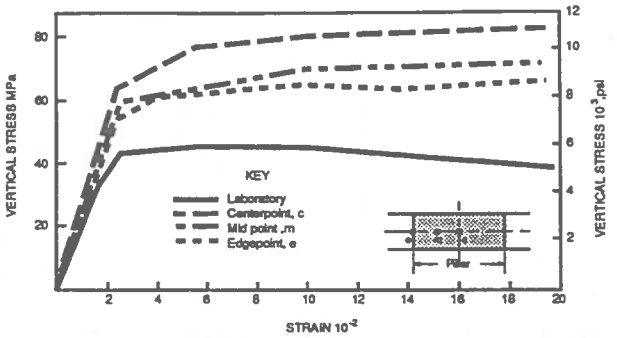

Figure 3. Load-deformation curves showing slight differences in numerical model based on point location in the pillar.

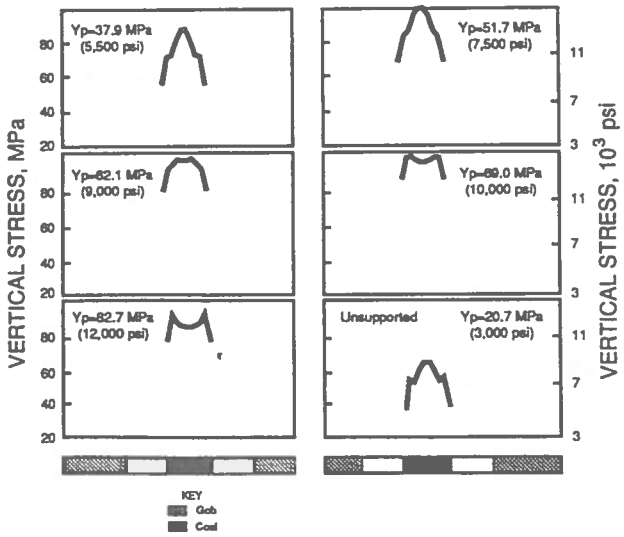

Figure 4. Pillar stress profiles for various reinforcement levels during yield point.

Figure 3 shows the load-deformation curves used to adjust the numerical results with the elastic-plastic response of the laboratory models (note slight differences in the maximum stress levels based on point-location in the pillar). The yield point of the material is used to simulate a given level of reinforcement. A yield point of 23.4 MPa (3,400 psi) is used to approximate the behavior of the unsupported pillar based solely on the laboratory determinations. Yield points above this value represent model pillars that are reinforced at increasing support levels. In addition, the general shapes of the load-deformation curves from the constitutive model were revised to more closely reflect the laboratory curves as previously discussed.

In the numerical modeling, three stages of one mining cycle were evaluated for a yield pillar in a two-entry system: both panels unmined, panel 1 mined, and panels 1 and 2 mined. Figure 4 shows the pillar stress profiles for a depth of 915 m (3,000 ft) for a range of reinforcement conditions when two panels are mined. The increase in the yield point represents an increase in reinforcement. With reinforcement, the stress profile across the pillar changes as does the peak stress and its location. Figure 5 shows the stress profiles for different levels of reinforcement with respect to various mining depths. The three depths evaluated were 457.5, 701.5, and 915 m (1,500, 2,300, and 3,000 ft). The increase in depth changes the stress profile and the magnitude of the peak stress.

Estimations of the material properties of the pillar, seam, roof, and floor are necessary inputs into the numerical model when determining stress distributions in the vicinity of mining. Knowledge of the gob material properties are similarly important, but extremely difficult to estimate because of the gob's unconsolidated, highly-broken, and fragmented structure. Lacking good information on the material properties presents a dilemma as shown in figure 6 which shows a highly variable pillar stress profile (high sensitivity) for different

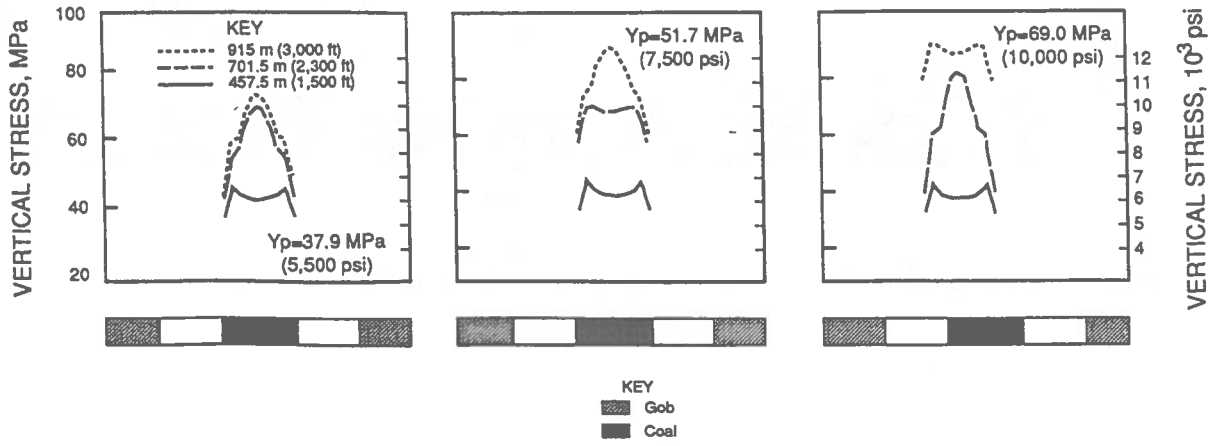

Figure 5. Pillar stress profiles for various depths.

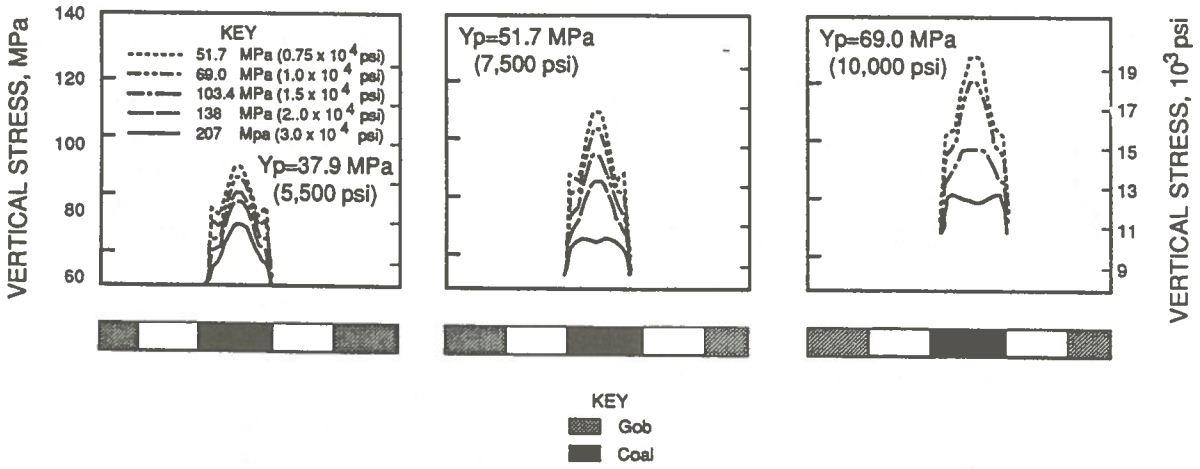

Figure 6. Pillar stress profiles for various stiffnesses (Young's Modulus).

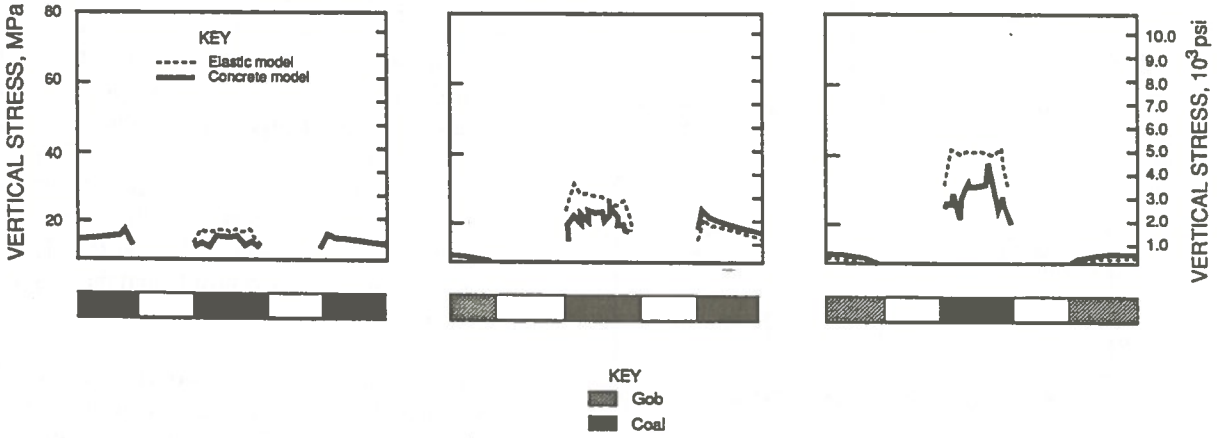

Figure 7. Pillar stress profiles comparing concrete and elastic model results.

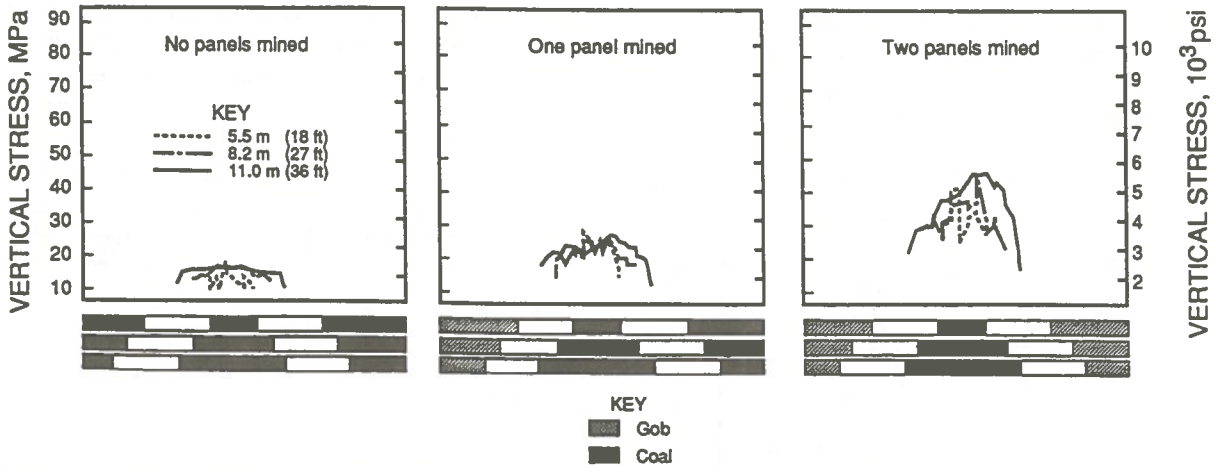

Figure 8. Pillar stress profiles for three different pillar widths using concrete model.

elastic moduli. The difficult-to-determine gob properties can have a great impact on the pillar stresses since a slight error in the estimation of a material property, such as elastic modulus may result in substantial over or under-estimation of stress levels surrounding the pillar.

In figure 7, a comparison is made between the stress profiles across a pillar for the linear-elastic and concrete models for the three mining steps using a 8.2-m (27-ft) wide pillar. The concrete model results in lower pillar stresses as well as a more irregular stress pattern. Figure 8 shows the stress profile using the concrete model for a 5.5-, 8.2-, and 11.0-m (18-, 27-, and 36-ft) wide yield pillar. These three pillar widths correspond to width/height ratios of two, three, and four. Figure 9 shows the fracture patterns that are generated in each of these pillars after the final mining step. Both tensile fractures and crushing are noted with the pillar width influencing the fracture pattern.

DISCUSSION

The pillars tested in the laboratory are assumed to represent a physical model of a yield pillar where an extensive fracture system is developed, and the load-deformation curves represent an average pillar performance. Both reinforced and unreinforced pillars show nonlinear post-failure behavior. For the unreinforced pillars, the drop in the post-failure load is due to the loss of bearing area as material spalls from the pillar. As the pillar width increases, so does the area of the remaining intact portion of the pillar at a given strain, which is responsible for most of the residual strength. Under such large strains, this pillar remnant is deforming plastically.

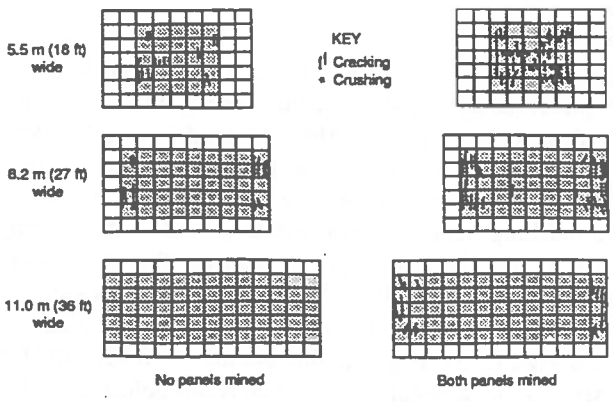

Figure 9. Concrete model showing behavior for three different pillar widths.

With bolt reinforcement, the spalled material is retained, resulting in an increase in the residual strength. The bolt reinforcement also adds confinement to the pillar, thus increasing the maximum compressive strength. The post-failure performance of the pillars is also varied by the level of reinforcement applied to the pillars. The reinforcement continues to resist the deformation of the fractured material on the outer edges of the pillars, thus assisting in maintaining the higher residual strength. This elasto-plastic behavior of the reinforced model yield pillars is influenced by changes in pillar geometry and levels of reinforcement. Similarly, this type of behavior was used to simulate the application of reinforcement to pillars in the numerical models. The numerical modeling is necessary to determine how the reinforced pillars would react under gateroad conditions because the loads and energy input into the pillars will depend on the in situ conditions. Since these tests are modeled experiments, the pillar sizes can be scaled. If the height of the model is scaled to a 2.7-m (9-ft) high coal seam, the pillar widths tested would be 5.4, 8.2, and 11 m (18, 27, and 36 ft).

With the elastic-plastic models, the level of reinforcement was simulated by changing the yield point of the material. The stress profile does vary across the pillar with an increase in the yield point or reinforcement (figure 5). As the yield point or level of reinforcement is increased, less of the pillar yields. These are also the types of conditions that were observed in the laboratory tests. Further, the stress profiles do approximate that of the laboratory tests where, after yield, the highest stresses remain in the remnant pillar. Peak stresses developed in the models do reach a limiting value. Additional support beyond a certain level would not have an effect on the maximum pillar stress but only on the stress distribution. However, this is the result of the total amount of energy that the surrounding mine structure would impart into the pillar and is controlled by depth and mining configuration. These parameters, therefore, become a factor in determining the level of reinforcement required to produce acceptable pillar or entry behavior.

Increasing the depth affects the pillar stress distribution, with the peak stress shifting from the outer edge of the pillar when the behavior is mainly elastic to the pillar core when the pillar yields. The level of pillar reinforcement is clearly tied to the mining depth as shown in figure 5. At the shallower depths, less reinforcement is required to improve pillar stability than at deeper depths.

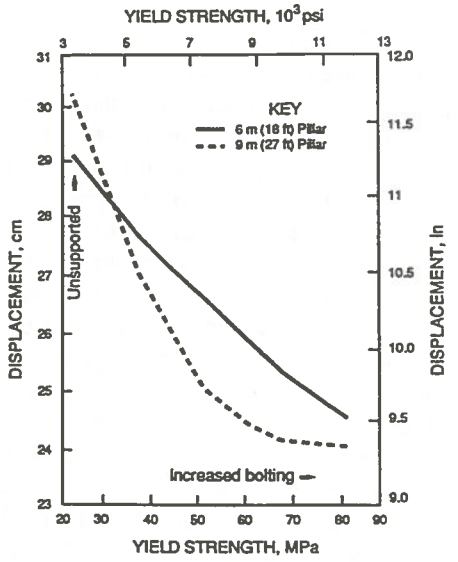

Figure 10. Yield pillar displacement versus yield strength for two pillar widths.

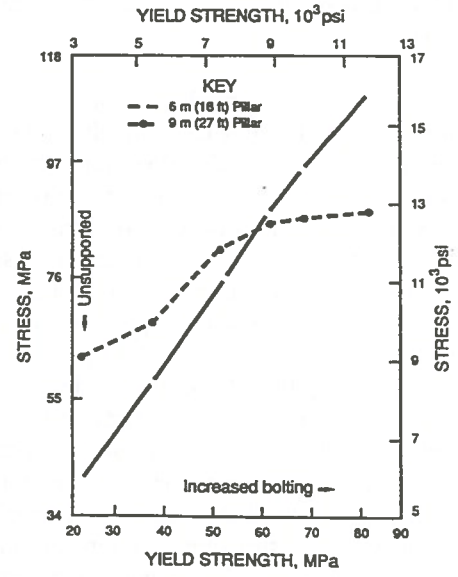

Figure 11. Yield pillar stress versus yield strength for two pillar widths.

Pillar width is another factor that affects the required level of reinforcement. Assuming the results from the numerical model, the average pillar displacements and stresses differ significantly from a 5.5- to an 8.2-m (18- to a 27-ft) wide pillar at the same level of reinforcement as shown in figures 10 and 11. At lower reinforcement levels, the 5.5 m (18 ft) pillars show more yield and therefore less stress. The narrower pillar is therefore more sensitive to changes in reinforcement. At higher levels of reinforcement, the average stress on the wider pillar remains constant, whereas the average stress on the narrower pillar steadily increases with additional support. This indicates that for a given depth or energy supplied to the pillar, the behavior of the wider pillar is essentially elastic, and the behavior of the narrow pillar is more inelastic since a significant portion of the narrow pillar yielded, though a central pillar core remains.

Mine structures surrounding the yield pillar such as the gob will also influence the amount of load the pillar will carry and, therefore, influence the degree of reinforcement required. For the purpose of this study, the gob was assumed to have linear elastic properties; a Young's modulus of 137.9 MPa (20,000 psi) was assigned to the gob based on other research experience (Kripakov et al, 1990). Significant stress changes occur in supported pillar performance when the gob modulus is allowed to vary up to ±50% (figure 6). This problem is further compounded by the realization that gob properties undergo dynamic changes and behave differently than the intact coal seam.

Another important aspect is how pillar and entry deformation is affected by pillar reinforcement. As the stress distribution along the top surface (pillar/roof interface) of the pillar begins to level out at the higher yield pillar strengths, so does the vertical deformation. Figure 12 shows the effect of an increasing yield strength of the pillar for one-panel and two-panel mining. Because pillar stress levels for one-panel mining are at or below the yield stress levels, no discernible differences in vertical pillar deformation can be seen at the higher yield strengths, i.e. > 51.7 MPa (7,500 psi). When pillar stress levels exceed the higher yield strengths, as evidenced in the two-panel mining sequence, a pattern emerges—as the yield strength increases, the rate of change of the downward displacement decreases. Figure 10 shows the parabolic relationship between increased yield strength (bolting) and pillar deformation for a 8.2-m (27-ft) wide yield pillar.

The greatest reduction of vertical deformation, for such a pillar, occurs at a moderate bolting level, with an equivalent yield strength (for this model) of 37.9 MPa (5,500 psi). Increasing the bolting intensity (yield strength equivalent) beyond the moderate level, results in diminishing returns. For instance, moderate bolting support of the yield pillar reduces the downward displacement by nearly 2.5 cm (1.0 in); this represents an increase in yield strength from an unsupported pillar of 13.8 MPa (2,000 psi). Adding another 13.8 MPa (2,000 psi) of yield strength reduces downward deformation by 1.25 cm (0.5 inch); adding a third 13.8 MPa (2,000 psi)

of yield strength reduces downward deformation by .5 cm (0.2 inch); and finally a fourth 13.8 MPa (2,000 psi) of yield strength reduces downward deformation by only an additional 0.25 cm (0.1 in).

Modeling the unreinforced yield pillar was difficult because of its nonlinear behavior, but was possible using the concrete model. The concrete model presents an insight into the load-carrying characteristics of an unsupported yield pillar. Unlike the normally smooth, symmetrical stress profiles obtained for linear elastic depictions of mine pillars, figure 7 shows a much more irregular stress distribution, suggesting both stress hardening and stress softening occurring in the pillar simultaneously as cracks develop, open, and close. This indicates yielding has occurred throughout the pillar, while still capable of resisting a reduced loading (approximately a 25% reduction in ultimate strength when compared to the linear elastic model). The most severe stress softening occurs along the pillar margins as expected and progresses inward as mining progresses.

Ideally, the yield pillar should exhibit a failure zone that ultimately intersects from one side to the other. As indicated in figure 9, the 5.5-m (18-ft) wide yield pillar meets that objective, but shows a diagonal potential failure zone through the pillar early in the mining cycle after the extraction of the first panel. During the second panel extraction, the 5.5-m (18-ft) wide pillar undergoes crushing failure in addition to a more stable tensile failure. The 8.2- m (27-ft) wide pillar shows a more gradual potential progression of tensile failure through the last mining step and shows the development of a potential tensile plane through the center of the pillar with no crushing behavior. Depending on the degree of pillar yielding desired at a particular mining step and based on the given material properties and mine conditions, a yield pillar ranging from 5.5 to 8.2 m (18 to 27 ft) wide by 2.7 m (9 ft) high suffices for purposes of this investigation. This corresponds to width-to-depth ratios of less than 2%, which, according to some empirical evidence, may lead to a pillar that suffers a state of full or partial failure (Chaturvedula and Bhattacharyya, 1992).

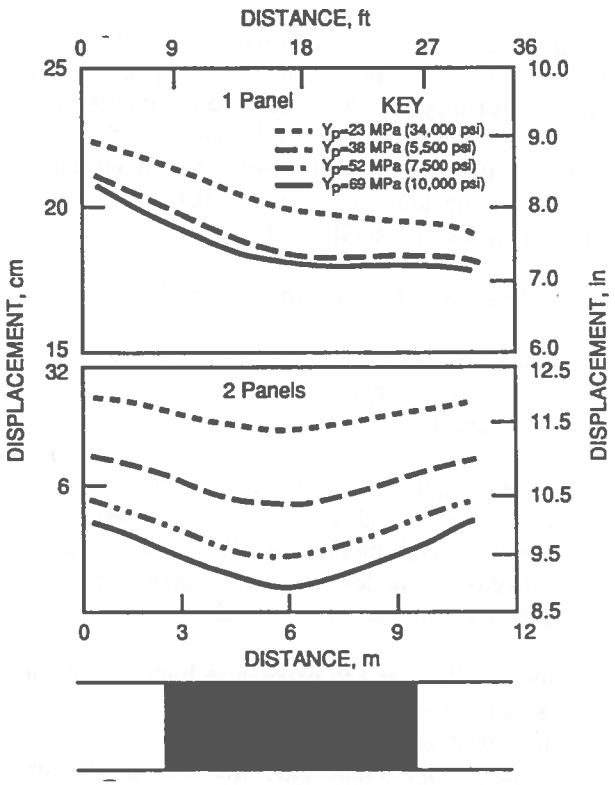

Figure 12. Displacement along top of yield pillar for different yield strengths.

SUMMARY AND CONCLUSION

A tool for simulating pillar performance consistent with the laboratory observation of a model pillar has been presented in this paper. The concrete model shows promise as a viable constitutive model for simulating yield pillars in longwall coal mines. As a cracking and crushing model, the concrete model can be used to assess the degree a yield pillar has yielded in a manner consistent with laboratory observations. For this study, it was used to determine the yieldability of a pillar with given dimension and assumed physical properties.

The second part of the study, to study the performance of a supported yield pillar, involved developing an elastic-plastic model with a stress/strain behavior similar to data obtained from laboratory models. The yield strengths of the model were varied to represent varying bolt densities. Other parameters (mining sequence, depth, and properties of the pillar and gob) that affected supported yield pillar performance were also studied.

Both the cracking and elastic-plastic models account for residual strength in the yield pillar after failure. The concrete model can provide information on possible failure planes within the intact pillar. The elastic-plastic model usefully provides information on the magnitude and direction of displacements of material within the pillar. Applying both models can be helpful in performing stability analysis of yield pillars if failure

criteria based on field investigations can be established for site-specific cases. In a similar light, engineering the proper level of support to an overstressed, underdesigned yield pillar would require considerable empirical and site-specific data on yield pillar performance and more detailed investigations on support/coal interactions, particularly in the failed pillar regime.

Other findings can be drawn from this study:

1) Significant differences in levels of support measured by increasing the support level do not occur until high stresses are present.

2) Increasing depth not only results in increasing peak pillar stresses, but also in the shape of the stress profile distributed through the pillar. This shape is also affected by the level of support applied prior to the removal of the two mine panels.

3) Narrower pillars tend to experience higher levels of stress as the yield strength of the pillar is increased (such as increased bolting), whereas stress levels in wider pillars tend to flatten at lower stress levels with no measurable benefit if additional bolts are installed.

4) Slight changes in the gob modulus (Young's) can have dramatic effects in the degree of yield pillar deformations, particularly when Young's modulus is very small. Knowing that the gob might have unusually low stiffness or high vertical height could be cause for concern and require the need for additional support if large pillar displacements are to be avoided.

REFERENCES

PARK, D.W. and ASH, N.F., 1985.
Stability analysis of entries in a deep coal mine using finite element method. Proceedings, 2nd Conference on Use of Computers in the Coal Industry, Tuscaloosa, AL. Soc. Min. Eng. AIME, pp. 11-20.

KRIPAKOV, N.P. and MELVIN, M.T., 1983.
A computer program to simulate progressive rock failure around coal mine entries. Proceedings, 1st Conference on Use of Computers in the Coal Industry, Morgantown, WV, Soc. Min. Eng. AIME, pp. 487-502.

DIXON, J.D., MAHTAB, M.A., and SMELSER, T.W., 1985.
Procedures for determining support of excavations in highly yielding ground. BuMines RI 8990, 19 pp.

BENSEHAMDI, S., PORTER, I., and SINGH, R., 1992
Elasto-plastic finite element structural stability analysis of room and pillar mine workings. Proceedings, 11th International Conference on Ground Control in Mining, N.S.W., Australia, pp. 84-91.

MAIER, G. and HUECKEL, T., 1979.
Non-associated and coupled flow rules of elasto-plasticity for rock-like materials. Int. J. of Rock Mech. and Min. Sci. and Geomech Abstr., Vol. 16, pp. 77-92.

TANDANAND, S. and THILL, R.E., 1987.
Mechanical behavior of coal measure rocks: elastic-inelastic behavior. BuMines RI 9109, 1987, 25 pp.

DOLINAR, D.R., 1993.
Techniques to increase yield pillar residual strength. Proceedings, 12th Conference on Ground Control in Mining, Morgantown, WV, pp. 284-291.

BATHE, K.J., WALCZAK, J., WELCH, A., and MISTRY, N., 1989.
Nonlinear analysis of concrete structures. Computers and Structures, Vol. 32, No. 3/4, pp. 563-590.

JEREMIC, M.L., 1980.
Influence of shear deformation structures in coal on selecting methods of mining. Rock Mechanics. Vol. 13, pp. 23-38.

KRIPAKOV, N.P, BECKETT, L.A., DONATO, D.A., and DURR, J.S., 1990.
Computer-assisted mine design procedures for longwall mining. BuMines RI 9172, 38 pp.

CHATURVEDULA, V.K. and BHATTACHARYYA, A.K., 1992.
Design of yield pillars in the southern coal field of New South Wales. Proceedings, 11th International Conference on Ground Control in Mining, N.S.W., Australia, 6 pp.

CAMI'95: 3rd Canadian Conference on Computer Applications in the Mineral Industry
Montréal, Québec, Canada, October 22-25, 1995

Application of Numerical Modeling to the Analysis of Strata Interactions

Hamid Maleki
Spokane Research Center, U.S. Bureau of Mines, Spokane, WA USA

Robert W. McKibbin
Spokane Research Center, U.S. Bureau of Mines, Spokane, WA USA

Fredrick M. Jones
Spokane Research Center, U.S. Bureau of Mines, Spokane, WA USA

Richard A. Wheeler
Spokane Research Center, U.S. Bureau of Mines, Spokane, WA USA

ABSTRACT

The U.S. Bureau of Mines implemented an integrated laboratory and field measurement program to develop techniques for assessing roof stability problems. Because of the complexity of roof, floor, and pillar interactions, many measurements were collected, both from the seam and the mine roof and floor. These measurements provided critical input to numerical models and allowed researchers to identify the failure mechanism. In addition, lithology and roof conditions were mapped, and cores were tested at the beginning and end of monitoring to assess structural damage.

Supplementary support systems to control roof deformation were installed when roof deformation approached 60 mm and seismic wave velocity was reduced by 17 pct. It was shown that failure was initiated in the mine floor and spread to the pillar and the roof. The field measurements were essential for understanding strata interaction and provided essential input for numerical models. In particular, a model incorporating the strain-softening material behavior for the floor showed best agreement between measured deformation patterns and the calculated results.

INTRODUCTION

The U.S. Bureau of Mines (USBM) implemented a geophysical instrumentation program in a southern Wyoming mine to study changes in roof stability during development mining. These measurements were complemented by detailed mapping, core testing, and collection of static measurements so that techniques could be developed for detecting roof stability problems. This case study was unique in providing integrated measurements of a mine roof, floor, and pillar and in tracking failure growth around mining excavations.

In this study, it was important to relate measured changes in dynamic properties to roof "stability." Roof stability has traditionally been related to the volume of roof falls, roof deformation rate, or amount of roof deformation. However, because there was no roof fall in the test section, an assessment of stability was based on the extent of deformation and fracturing.

The measurements described in this paper were obtained from two locations having similar geologic and support conditions. The measurements from site 1 are briefly reviewed to characterize changes in roof, floor, and pillar (also see Maleki et al., 1993). Additional measurements were recently obtained from site 2 to characterize the residual strength of the mine floor; these measurements are important for numerical analyses of inelastic strata deformation and for understanding the failure mechanisms in this mine. Based on these analyses, a modeling procedure was developed to evaluate strata interactions.

GEOTECHNICAL SETTING

A southwestern Wyoming trona mine was selected from among four mines in Colorado and Wyoming. Site selection was based on a review of geotechnical data from these mines as well as experience gained from studying another 10 U.S. coal mines.

Figure 1 presents generalized lithology, rock structure, rock quality designation (RQD), and compressive strength of a core taken from the mine roof at site 1 at the working face. Triaxial strengths were obtained from previous measurements completed by the Colorado School of Mines, Golden, CO.

The minable seam is 3.3 m high and is located 426 m below the surface. Immediate roof consists of 0.6 m of trona with minor marlstone laminations and is overlain by a sequence of marlstone, trona, and shortite inclusions. RQD's vary between 75 and 90 pct in the mine roof, and uniaxial compressive strengths vary between 3 and 27 MPa. Laboratory tests of the mechanical properties of the mine floor rock have been very limited, but the floor marlstones are the weakest stratigraphic horizon.

Trona was determined to be the stiffest component of the strata near the excavation. Young's modulus for trona was 17.24 GPa, three times higher than for the marlstones of the mine roof or floor. Specific gravity was in the range of 2 to 2.4.

USBM researchers measured the in situ stress field in the basin in which the mine was located using overcoring techniques and USBM deformation gauges in three boreholes. The measured stresses were east = 9.4 MPa, north = 15 MPa, vertical = 19 MPa, east-north shear = 2.8 MPa, north-vertical shear = -0.2 MPa, and east-vertical shear = 0.9 MPa. Both vertical and horizontal stresses were greater than expected from overburden weight. Similar measurements at the mine have confirmed the orientation of stresses, but magnitudes were 50 pct lower in the mine roof.

The geological setting of this mine favored large amounts of deformation in the mine floor, roof, and pillar. Thus an instrumentation program was developed to study the deformation and failure process near the mining excavations, with an emphasis on monitoring changes in roof conditions.

INSTRUMENTATION PLAN AND MONITORING PROGRAM

A detailed instrumentation plan was developed to measure changes in wave velocity in the mine roof and to relate these measurements to strata fracturing and roof stability. The following work was done at site 1.

- Crosshole seismic surveys at 1-month intervals,
- Biweekly deformation measurements in the mine roof, pillar, and floor,
- Biweekly stress change measurements within the seam, and
- Mapping, borehole observations, and core testing in the mine roof either during monthly monitoring or at the beginning and end of the monitoring program.

The instruments were installed in a three-entry development system using 5.2- by 13.4-m pillars and 5.2-m spans. Figure 2 shows the instrument layout and the mining geometry at site 1. At installation time, the development face was 50 m from the instruments. Development continued for 320 m before a 60-m-wide mechanized face was set up and retreated toward the instruments.

Seismic Measurements

The crosshole seismic layout is shown in Figure 2. Accelerometers were attached to the roof and installed in a receiver hole using a setting device. These accelerometers had a flat frequency response ranging from 1 to 6,000 Hz. An impact unit was used as the energy source. The impact unit consisted of a point-resin-anchored rock bolt, a 1.5-m-long steel rod, and a 7.2-kg cylindrical steel mass. The rod was attached to the point-resin-anchored bolts at the time of measurement. These bolts were anchored at 0.5, 1, 1.5, 2, 2.5, and 3 m into the roof in a semicircular pattern. The steel mass had a hole along its axis, permitting it to slide vertically along the rod as it struck a plate. The steel mass was then free dropped from a height of 1.2 m to create an energy source. A steel plate at the end of the rod stopped the sliding mass during operation. The surfaces of the plate and the mass were machined to give consistent, repeatable impacts. The solid contact between the mass and the plate allowed the data acquisition board to be triggered at the same time energy was introduced into the rock. This

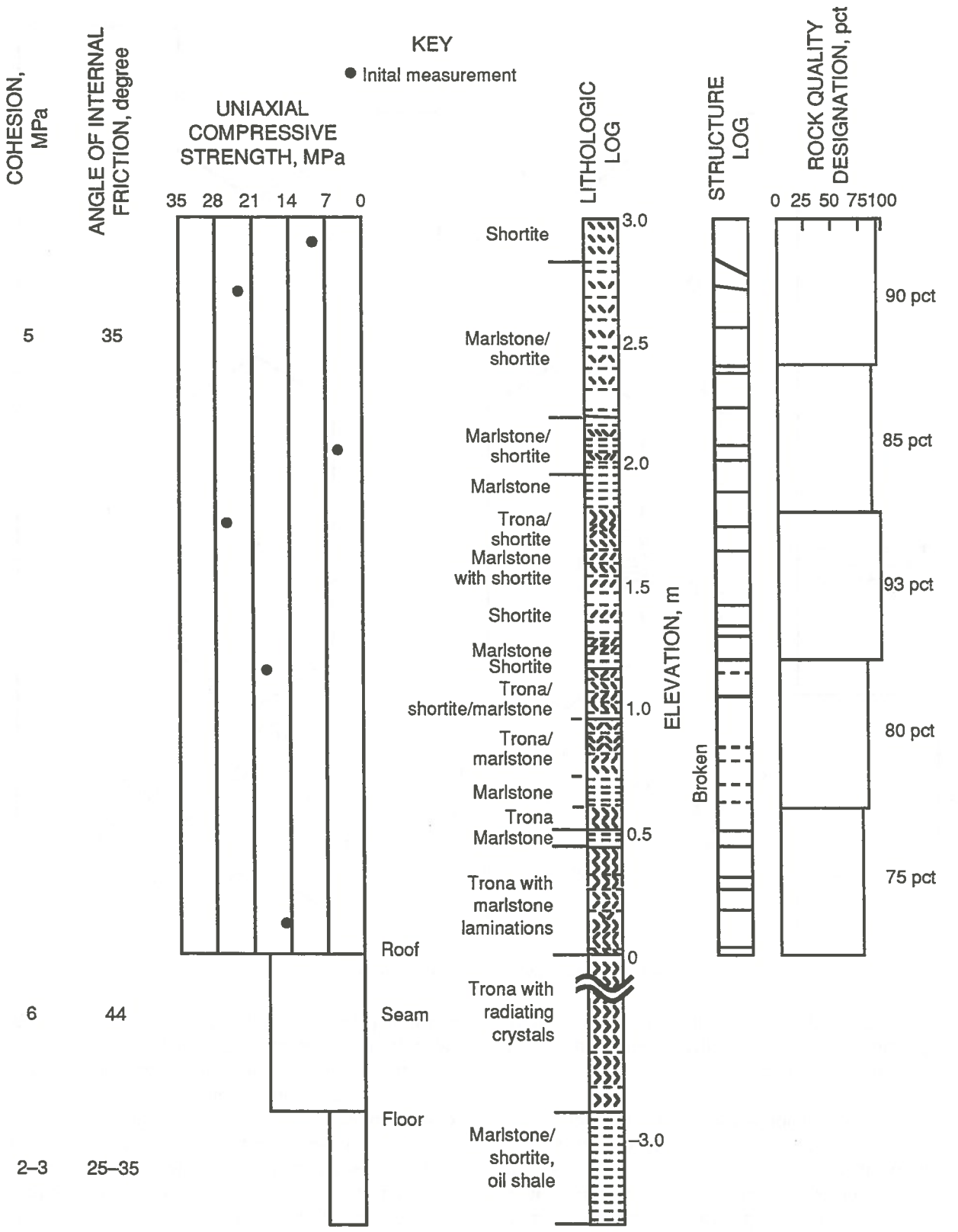

Figure 1. Lithology, structure, and rock strength at beginning of monitoring program.

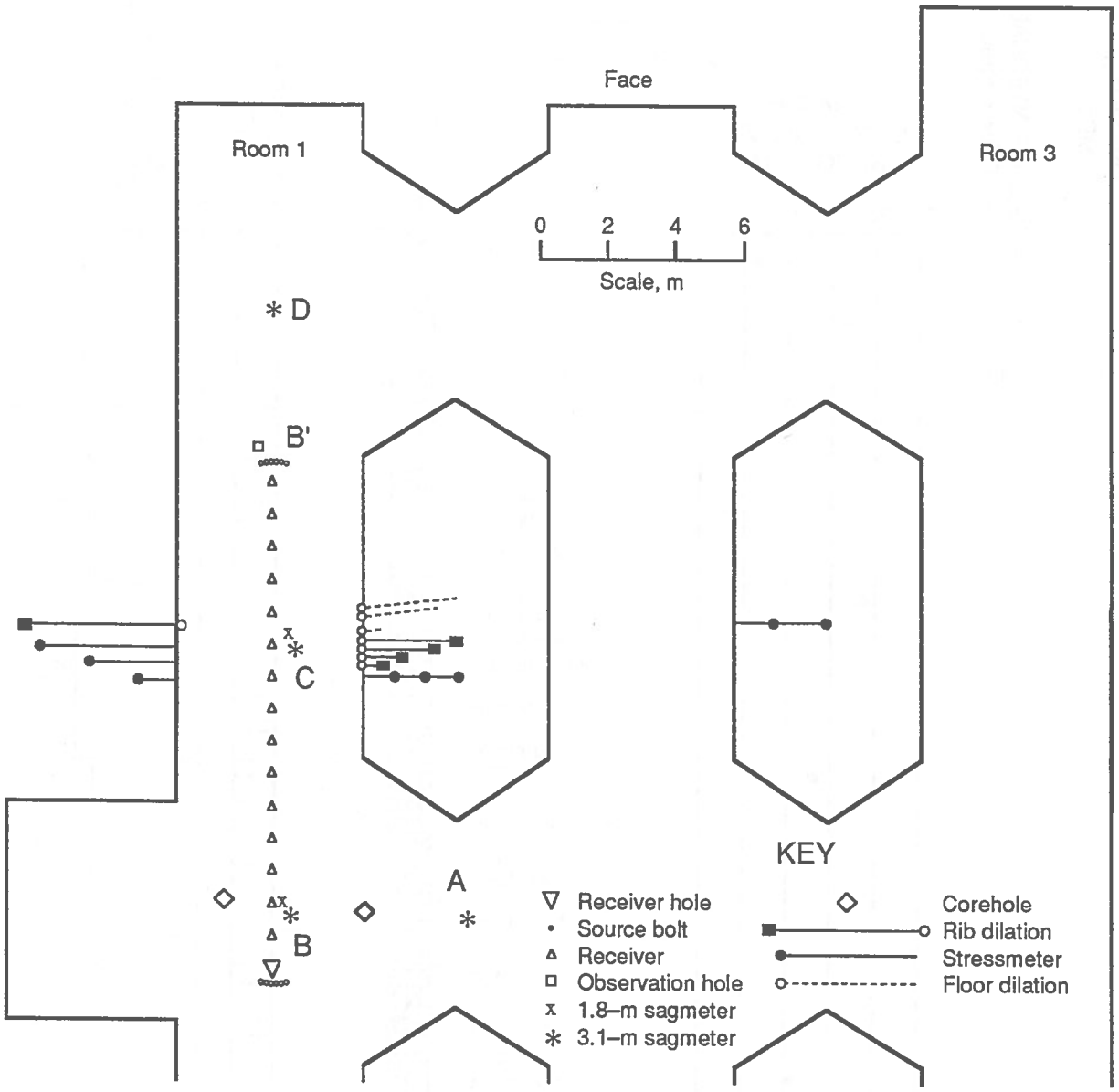

Figure 2. Plan view of instrument layout at site 1.

mechanism was designed to minimize error caused by triggering. The data acquisition system is described in a paper by Maleki et al. (1992).

Using seismic tomographic techniques (Schneider, 1990; Jessop et al., 1992), one may construct a velocity or attenuation map of the zone of interest. In this study, crosshole seismic travel-time tomography of the mine roof was implemented along cross section B-B' (Fig. 2). Tomography is a mathematical inversion technique for imaging the areal distribution of a physical property of a solid object. Measurements of physical properties on the plane of interest can be taken from measurements obtained at the boundaries. A series expansion technique using an iterative, reweighted, least-squares method was used. Pixel dimension was approximately 75 cm in both the horizontal and vertical directions, which was compatible with the resolution for this study. For ray tracing, minimum time wave-front modeling was utilized (Jessop et al., 1992). A constant average velocity of the medium was used initially in the iterative process. First P-wave arrivals were picked for the tomographic calculations. Selective shear wave arrivals were used

for calculating dynamic properties. Shear arrivals were picked using shot-gather plots and velocity ratio (P/S) considerations.

The resolution of the seismic method depends on the dominant wavelength in the signal. A frequency analysis of the recorded signal showed that the predominant frequency of the signal was 1.5 kHz. Since the seismic velocity of the trona was about 4,200 m/s, the dominant wavelength was at best 2.8 m. A practical rule of thumb to determine resolution is that the seismic method should afford the resolution of features with a 1/4-wavelength dimension. The resolution of the system used in this study was at least 70 cm. The sampling frequency study was 25 kHz, and the trace length was 40 milliseconds. The accuracy of triggering for this system was 40 microseconds. This time gave a 17-cm error in a medium of 4,200 m/s.

Static Measurements

An array of extensometers was installed at site 1 to measure relative roof movements. The extensometers were anchored 1.8 and 3.1 m above the roof. In addition, borehole observations were carried out at locations B and B' (Fig. 2) using a borescope to map fracture propagation in the roof and observe changes in roof moisture during the monitoring period. Two cores were obtained from the roof to compare physical properties at the beginning and end of the monitoring program. Roof appearance was also mapped to monitor development of fracture patterns in the roof.

Seam instruments consisted of vibrating wire stressmeters placed in the pillars and solid block and rib movement pins anchored 0.6, 1.2, 2.1, and 2.7 m into the pillar; relative lateral movements were measured using a tape extensometer attached to a 5-m-deep reference point in the solid block. These stressmeters and floor movement pins were installed to monitor pillar response and roof-pillar-floor interactions. The pins were anchored diagonally below the pillars at depths of 0.9, 2.1, and 3 m into the floor; a tape extensometer and the same 5-m-deep reference point were used for these measurements.

In addition, at site 2, three sets of floor bearing tests were completed at the beginning of the measurement program and an overcoring stress measurement profile was obtained across a mine pillar at the termination of the monitoring. Site 2 was located in an adjacent panel in the vicinity of site 1 where geologic conditions were similar.

RESULTS

Measurements of changes in strata deformation, fracturing, and dynamic properties from site 1 were combined with absolute pillar stress measurements and results of floor bearing tests from site 2.

Significant changes in seismic wave velocities, amount of roof separation, and number of roof fractures occurred during the monitoring period. Supplementary support, consisting of 2.4-m-long fully grouted resin bolts and straps to control roof deformation, was installed on day 80 (i.e., 80 days after development mining). Roof, pillar, and floor movements were all large, indicating inelastic deformation and complex interactions around the excavation.

There were three time windows that had some significance in this analysis. During the first week after development mining, stresses and rates of deformation changed rapidly as a result of face advance. Movements gradually slowed within 7 to 80 days after mining; supplementary support was installed at the end of this phase. Ground movement accelerated again up to day 120 as the face retreated. At this time, the mechanized retreat face was near the instruments.

Data analyses focused either on day 80, when supplementary support was installed, or on day 120, when monitoring was terminated. Wave velocity was estimated for day 80 on the basis of tomographic data collected before and after the monitoring dates. Numerical modeling was completed for day 80 to exclude any influence of the retreating face position on the measured stresses and deformations.

Roof Behavior and Support Requirements

Seismic tomography and relative roof movements were calculated along the B-B' cross section to show the relationship among wave propagation velocities, roof movements, and support requirements.

Significant changes in velocity were measured during the 120-day monitoring period (Fig. 3). Furthermore, there was a relationship between wave velocity

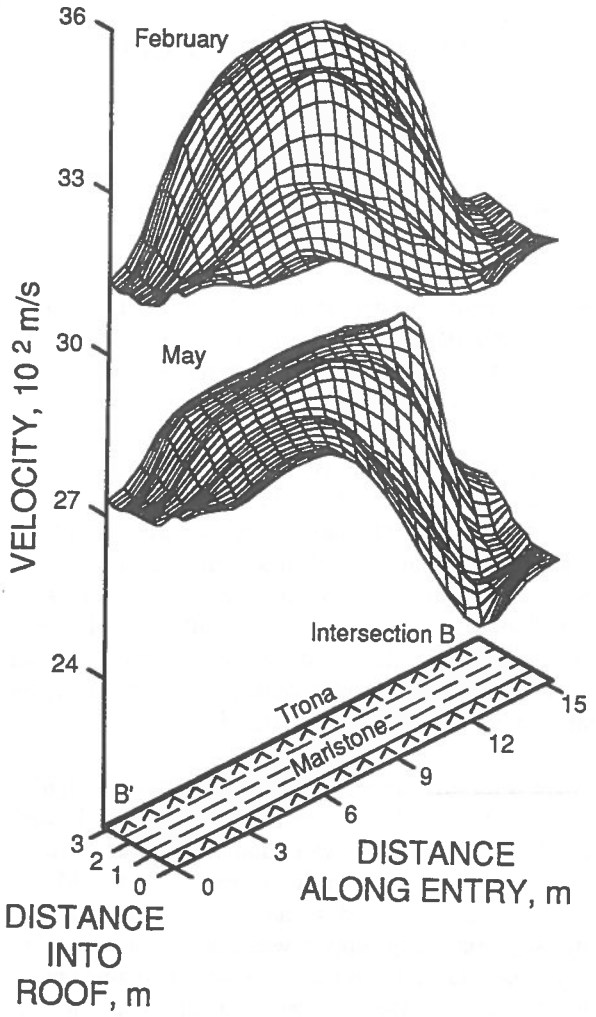

Figure 3. Wave velocity profile history at beginning and end of monitoring program.

patterns and mining geometry, i.e., velocities were lowest at the intersections where bed separation was most extensive, both in and out of the plane of measurement (B-B'). Also, velocities increased higher in the roof because there was less bed separation at these horizons, a finding that was supported by the deformation measurements. In other words, the velocity pattern was controlled by fractures.

Velocities decreased most significantly (up to 22 pct) over time at the B intersection. At midpillar, velocity decreased by 15 pct; since the amount of bed separation was almost the same during monitoring (Fig. 4), the calculated changes in velocity must have been caused either by fracturing out of the plane of seismic measurements or by differences in roof confinement stresses. Figure 4 shows the total roof deformation profile using the 3.1-m-deep extensometers.

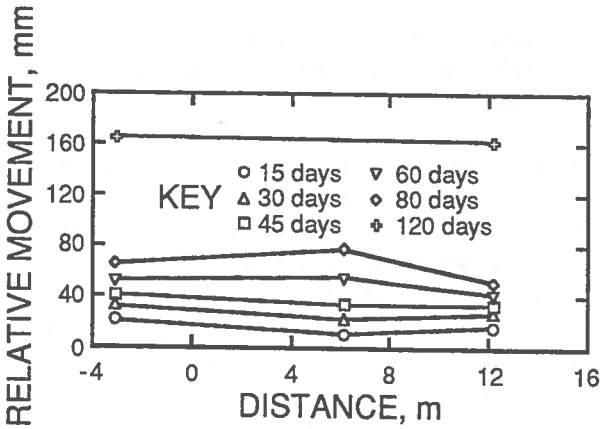

Figure 4. Relative roof movement profile along cross section B-B'.

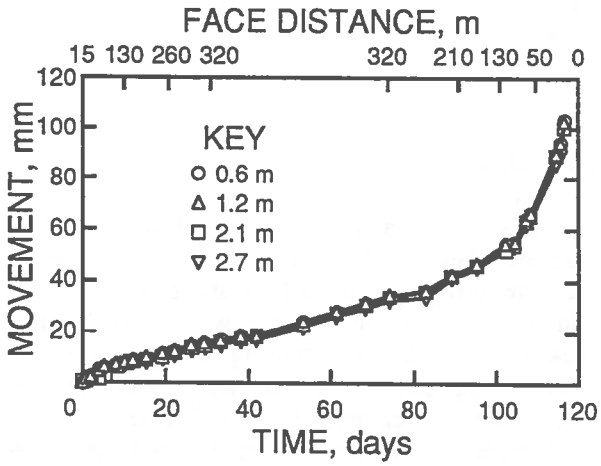

Figure 5. History of lateral pillar movement.

A relationship between velocity changes and supplementary support requirements may be tentatively established for this mine using these measurements. On day 80, wave velocities were reduced by approximately 17 pct at the intersection. The roof had deformed 60 mm since development. Therefore, changes in wave velocity greater than or equal to 15 pct may be used as a preliminary criterion for allocating supplementary support.

Seam Response

The pattern and magnitude of uniform lateral pillar movements (Fig. 5) could be the result of (1) the pillar shifting toward the solid block and/or (2) the pillar dilating 35 mm, which indicates 1 pct lateral strain at day 80. The former possibility is supported by numerical models and the occurrence of brittle

failure of the mine floor. The latter is supported by yielding within the pillar, where values for measured strain exceed values for elastic strain obtained during laboratory testing.

Overcoring stress measurements were completed across a 5.5-m-wide pillar at site 2 (Fig. 6), when the retreat face was 30 m from the measurement location. The average pillar stress (area under the curve) was 7.3 MPa; compared with calculated elastic pillar stresses, these measurements were significantly lower, confirming that the composite pillar-floor material had failed.

Floor Behavior

Approximately a meter of floor heave occurred in the test area. Within a few days of mining, the amount of floor heave reached 250 mm, necessitating mining of the floor. This reduced pillar confinement, increased the lateral movement rate of the pillar, and enhanced the uniformity of pillar movements (Fig. 5).

Since the maximum amount of strata deformation always occurred in the mine floor, it is believed that the failure process began below the pillars, probably as a result of the penetration of the much stiffer trona pillar into the floor (Fig. 7). This process was associated with crack formation, heaving, and load transfer from the pillar area to the solid block. The failure of floor marlstones was brittle in nature, extending at least 2 m into the floor.

Three in situ measurements were collected from site 2 to study the residual strength of the mine floor; these floor-bearing tests were completed during development mining. Typical results gave a peak strength of 7.5 to 18 MPa and a residual strength of 3 to 14 MPa. In comparison to calculated floor stresses, these measurements were significantly lower, indicating that failure occurred first in the floor.

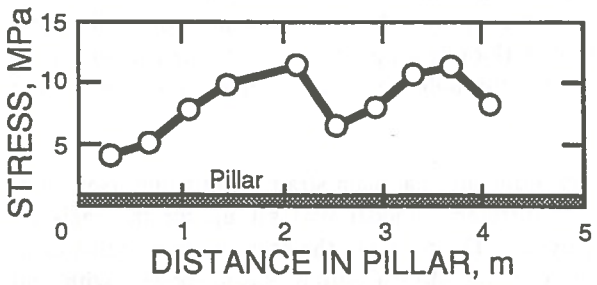

Figure 6. Profile of vertical pillar stress.

Pillar penetration into the mine floor caused differential movement between the pillar and the solid block. This contributed to the formation of a 15-cm-wide zone of crushed rock near the solid block in the mine roof (Fig. 8).

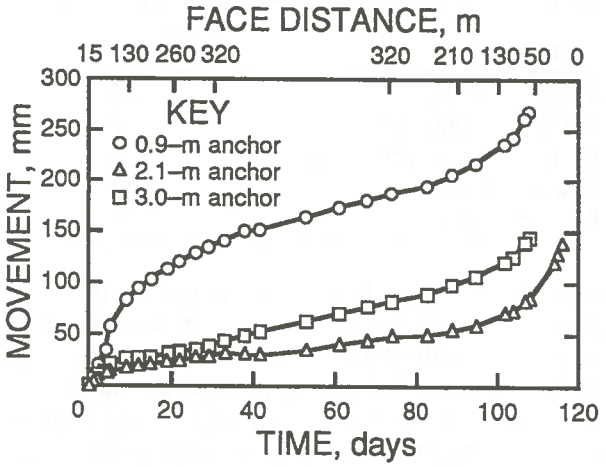

Figure 7. Profile of floor movement beneath pillar.

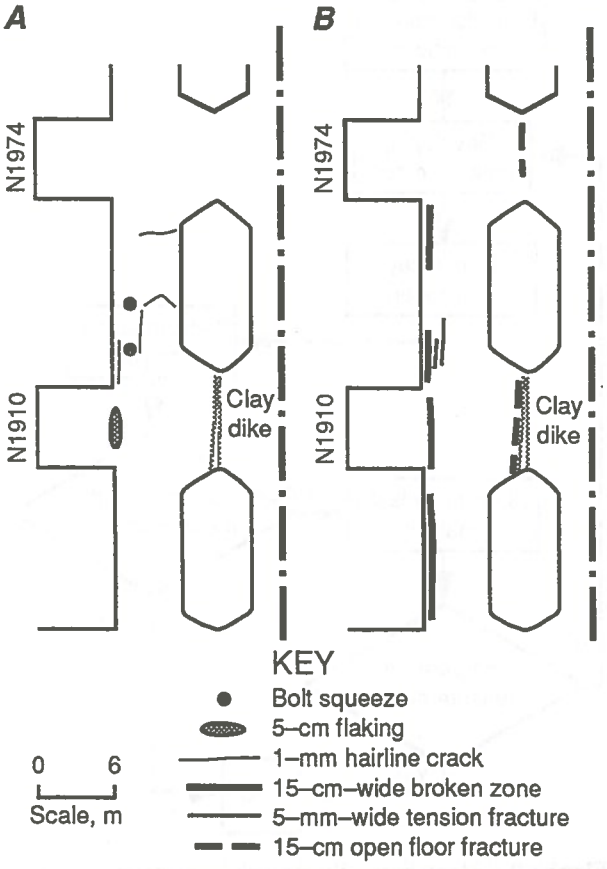

Figure 8. Map of fracturing at day 80 (*A*) and end (*B*) of monitoring program.

In summary, roof stability deteriorated in the test section by day 80, requiring supplementary support; this conclusion was based on measured changes in roof deformation, roof appearance (Fig. 8), roof bed separation and shifting, and dynamic properties (Table 1).

TABLE 1. Calculated changes in dynamic properties.

Factor	Percent change
Seismic velocity	21
Maximum amplitude	22
Dominant frequency	48
Young's modulus	51
Poisson's ratio	125

Changes in roof stability were influenced by roof, pillar, and floor interactions; in particular, the low residual strength of the mine floor seemed to be a controlling factor influencing ground movements and the location of the broken zone near the solid block (Fig. 8). The next step was to validate the proposed failure mechanism through the application of a numerical model.

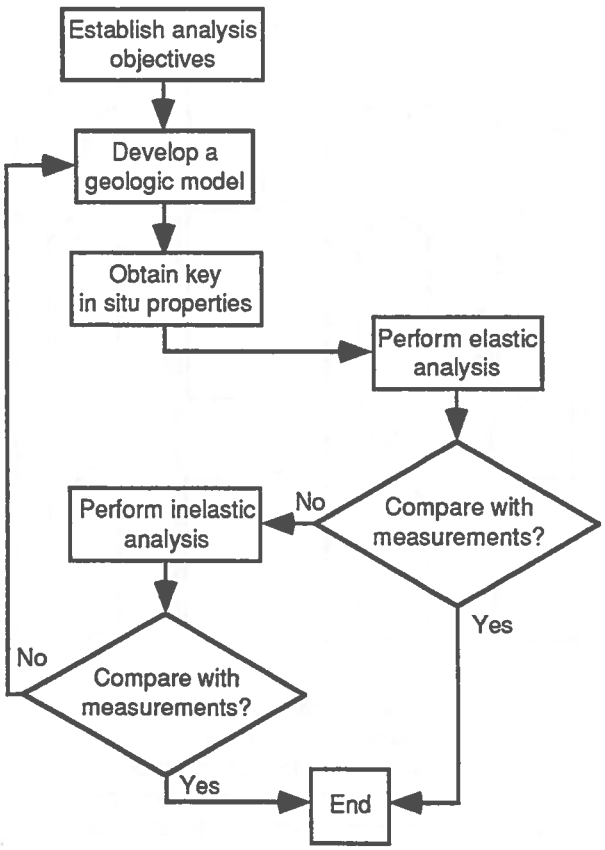

Figure 9. Flowchart illustrating modeling steps required for nonlinear analysis.

FAILURE MECHANISM

A numerical modeling procedure was developed to analyze strata interactions and study failure mechanisms. Both two-dimensional, finite-difference and three-dimensional, displacement-discontinuity methods were used in this study. The latter was important for modeling the actual three-dimensional geometry of the test section, including both rooms and crosscuts. The two-dimensional analysis simplified the geometry, but allowed elastic and inelastic deformations to be calculated both within the seam and in the roof and floor at instrument locations in the midpillar.

Figure 9 presents the modeling procedures; the objective of this exercise was to determine the source mechanism for the changes in roof stability. In particular, the formation of the broken zone near the solid block and the uniform lateral pillar deformation needed to be understood.

The simplified model used in these analyses included only the essential geologic features, such as the contrast in the stiffness of the seam versus stiffness of roof and floor, and consideration of time-dependent properties of the seam material. Values for material properties were based on laboratory tests of the core, measured bearing capacity of the floor, and published data on creep for salt and trona. Model loads were estimated on the basis of the available stress measurements for the basin in which the mine was located.

Simple elastic analyses were completed first; these analyses were not in agreement with measured deformation patterns but provided valuable input for the inelastic analyses. For example, the displacement-discontinuity models showed that pillar stresses were several times higher than the measured residual strength of the mine floor, which identified the need for inelastic modeling of the mine floor (Fig. 10). Note that all pillar stress measurements were bounded by measured floor bearing capacity, confirming that residual floor bearing capacity influenced the total load transfer through the pillar during the entire mining cycle.

A two-dimensional plain strain, continuum, isotropic, finite-difference model was set up for the inelastic analyses. The roof and the seam were modeled elastically while Mohr-Columb plastic models with and without strain-softening were used to model the mine

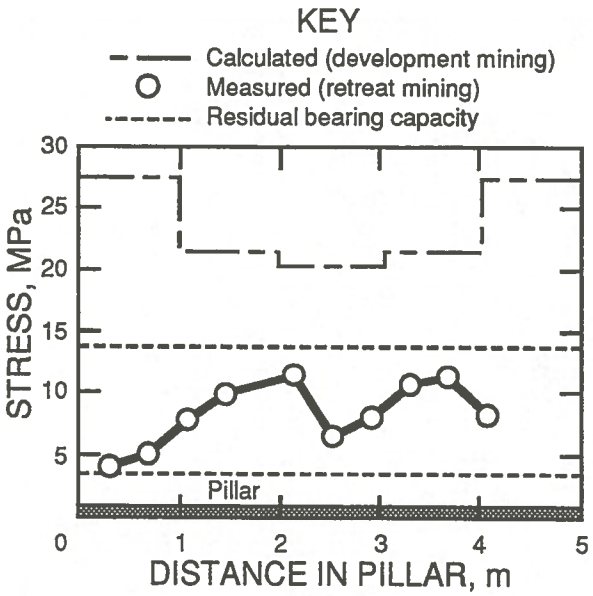

Figure 10. Comparison of measured and calculated pillar stresses, and residual floor bearing capacity.

floor. Other analyzed conditions included an elastic seam with inelastic modeling of roof and floor and an elastic roof and floor, and time-dependent analysis (creep) of the seam.

Pillar stress measurements provided important input parameters for an inelastic analysis. Strain-softening models require input on variations of cohesion, friction, and dilatancy with plastic strain and are based on Mohr-Columb elastoplasticity with nonassociated flow rule. An iterative procedure was used to determine a piecewise linear reduction in cohesion so that the calculated average pillar stress was in agreement with the measured stresses.

A model using an elastic seam and roof plus a strain-softening floor produced high compressive stresses at the corner of the solid block (Fig. 11) and was in general agreement with the measured lateral pillar movement pattern and the extent of failure in the mine floor (>2 m); this agreement confirmed that primary failure occurred in the mine floor as a result of pillar penetration into the brittle marlstone. This process was associated with lateral shifting of the pillars toward the solid block, contributing to the crushing failure of the mine roof at that location.

CONCLUSIONS

The stability of the mine roof was influenced by inelastic deformation of the mine floor as well as the pillars. The complex interactions among roof, floor, and pillar can be analyzed through careful placement of instruments, data analysis, and the application of numerical models. In situ measurements of the bearing capacity of the mine floor and pillar stress profiles were shown to be important input parameters for inelastic analysis and for the successful application of numerical models. The numerical modeling was helpful in identifying failure growth around mine excavations and verifying different hypotheses regarding floor and pillar behavior.

REFERENCES

Jessop J.A., Friedel M.J., Tweeton D.R. and Jackson M.J., 1992. Fracture detection with seismic cross-hole tomography for solution control in a stope. Proceedings, SAGEEP.

Maleki H., Ibrahim W., Jung Y. and Edminster P.A., 1992. Development of an integrated monitoring system for evaluating roof stability. Proceedings, 4th Conference on Ground Control for Midwestern U.S. Coal Mines, Mt. Vernon, IL, pp. 255-271.

Maleki H., Jung Y. and Hollberg K., 1993. Case study of monitoring changes in roof stability. International Journal of Rock Mechanics and Mining Sciences and Geomechanics Abstracts, Vol. 30, No. 7, Pergamon Press, pp. 1395-1401.

Schneider W.A., Jr., 1990. A three-dimensional physical modeling applying tomographic inversion and seismic migration to the tunnel detection problem. Ph.D. dissertation, Colorado School of Mines, Golden, CO.

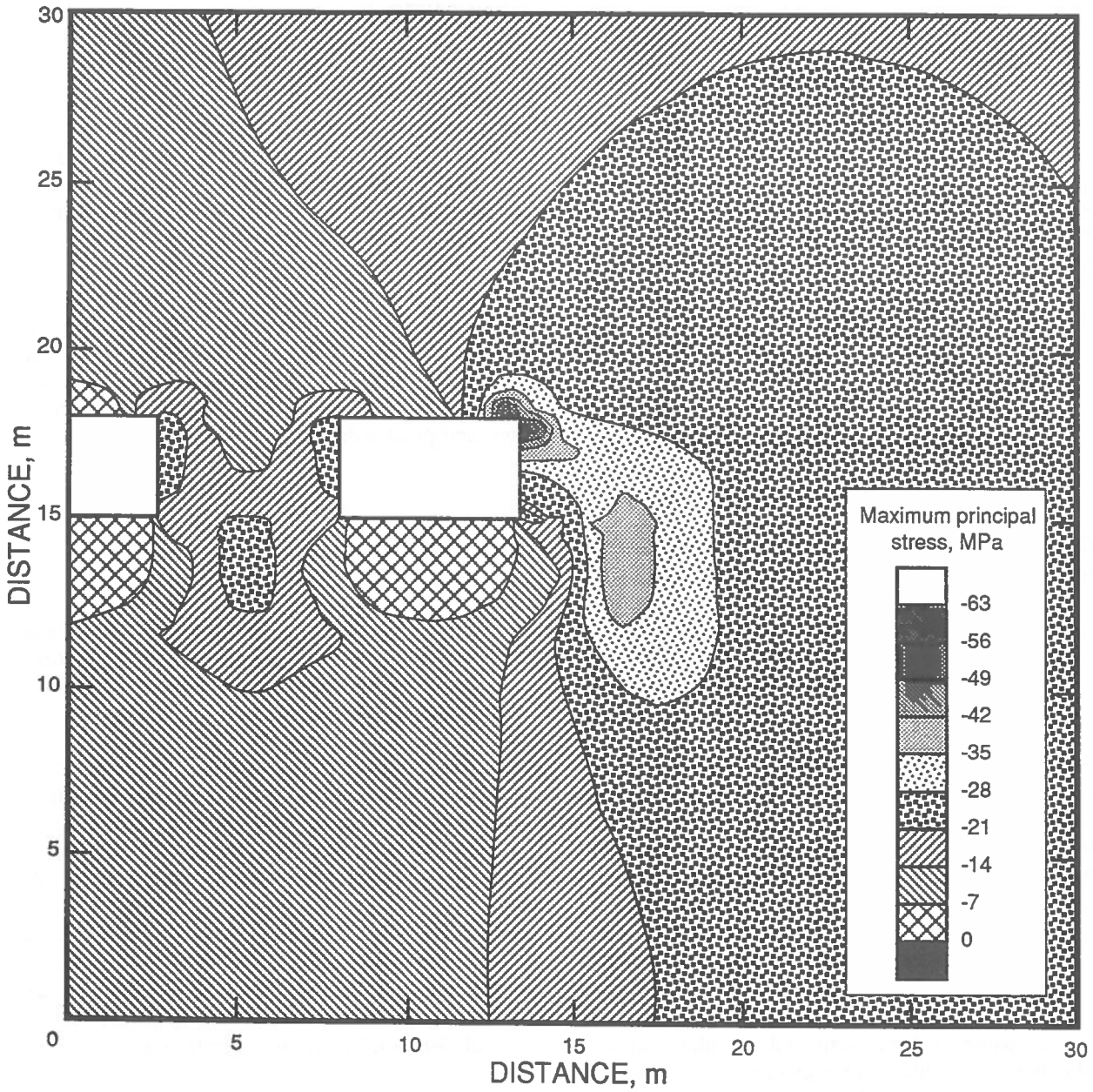

Figure 11. Maximum principal stress contours.

CAMI'95: 3rd Canadian Conference on Computer Applications in the Mineral Industry
Montréal, Québec, Canada, October 22-25, 1995

Overview of Recent Developments by USBM in Coal Mine Design Using Numerical Modeling Techniques

Nicholas P. Kripakov, Meng-Cherng Sun
U.S. Bureau of Mines, Denver, Colorado, USA

Scott. M. Oelfke
Colorado School of Mines, Golden, Colorado, USA

ABSTRACT:

The U.S. Bureau of Mines (USBM) conducts research to develop simple and practical computer-based tools to assist mine planners in assessing the structural stability of underground mine structures. This paper presents USBM developments in coal mine design using numerical modeling techniques: past, present, and future. More specifically, the capabilities of two boundary-element-based computer programs, MULSIM/PC and MULSIM/NL, released during the past few years are described, and examples presented to demonstrate their application toward solving typical ground control problems occurring in United States coal mine operations. More recent developments describe an analysis procedure that couples a series of boundary-element and finite-element models to evaluate the potential progressive failure of a yielding pillar gate road system. Results of the model(s) are discussed in the context of their significance in practical mine design. In addition, some advanced modeling techniques using discrete-element methods are also presented as a preview of future USBM research.

RÉSUMÉ:

Le Bureau des Mines des États-Unis fait des recherches à développer les méthodes des calculatrices plus simples et practiques pour aider les ouvriers des mines à évaluer la stabilité structurelle des edifices dans les mines souterraines. Dans l'article on traite les développements à les desseins des houillères usant les techniques du modelages numèriques au temps passé, à present, et dans le futur. Spécifiquement, les capabilités de deux programmes de calculatrices, qui ont basé sur les éléments-limités, MULSIM/PC et MULSIM/NL, ont discuté. Il y a aussi les exemples qui démontrent les applications des programmes pour solutionnant les problèmes de controllé le terrain typique des houillères aux États-Unis. Les développements nouveaux décrivent une méthode d'analyse qui utilise une serie des éléments-limités et des éléments-finis en combinaison pour évaluer la panne progressive d'une système des pilier fléchissant dans les galeries. Les résultats de modelages ont discuté à ce sujet de leur importance à la dessein de mine practique. En plus, les autres techniques du modelage qui utilisent
les méthodes des éléments-discrets ont présenté à une préview des recherches futur.

INTRODUCTION

Large- and small-scale rock mass failures in underground coal mines continue to cause accidents involving loss of life, extensive damage, and serious production delays. Such events can result in significant economic losses to a mining company and the Nation when untimely failures lead to abandonment and sterilization of mineral reserves. Numerical modeling techniques provide a powerful analysis approach by accounting for the myriad of factors that contribute toward such failures. These factors include local stress fields, mine geometry, geology, surface topography, mechanical properties of the rock, and mining-induced loading. Modeling provides insight into the causes of the failure process, which, in turn, may result in

elimination/reduction of these instabilities through improved mine design.

The USBM is actively developing and applying different numerical methods and computer codes toward solving typical ground control problems common to many operations in the United States. Progress has been achieved in demonstrating the potential usefulness of these tools on a mine-wide scale. However, a gap still exists between theory and practice toward applying these techniques for more detailed, site-specific problems. Often, a learning curve must be overcome in setting up appropriate meshes and determining representative input material property values. For the mining industry to take full advantage of these technologies, one USBM goal is to provide easy-to-use, well-tested software for mining engineers to assess their own situations. Output from this software must be in a form immediately useful to mine management responsible for making daily engineering and operational decisions; otherwise, it will not be used.

This paper presents an overview of USBM developments in mine design using numerical modeling techniques. Brief descriptions of the capabilities and limitations of each code are given. However, the emphasis of the paper is on practical examples.

Past Developments

Programs MULSIM/PC and MULSIM/NL are two boundary-element codes developed and released by the USBM during the past few years. These programs are formulated to calculate stresses and displacements in plan view as illustrated in figure 1. MULSIM/PC is limited to linear-elastic calculations. Utilizing a user-friendly preprocessor, models can be rapidly set up to obtain first approximations of stress concentrations in multiple-seam settings on a gross scale. The code is also set up to calculate offseam boundary input information to more detailed finite-element models. MULSIM/NL advances analysis capability by providing options for inputting nonlinear material behavior, performing energy release calculations, and running a series of mining steps. It is particularly useful for analyzing catastrophic large-scale mine collapses. A brief description of the basic capabilities of each code with practical examples follows.

MULSIM/PC: MULSIM/PC (Donato, 1992) is based on a variation of the boundary-element method, often called the displacement-discontinuity approach, developed originally by Crouch and Fairhurst (1973) and later enhanced by Sinha (1979, 1982) and Beckett and Madrid (1988). This technique is based on a mathematical model in which a tabular seam is represented as a singular plane in a homogeneous, isotropic, elastic medium. A mine plan is represented by a grid in plan view, as conceptually illustrated in figure 1. The program provides the capability to analyze many mining situations involving one or two seams and can incorporate wide-scale effects of load transfer and stress concentrations experienced by particular pillars, unmined coal blocks, and artificial structural elements (Beckett and Madrid, 1988).

MULSIM/PC is best suited for analyzing mine plans in a relatively uniform rock mass. If major geologic discontinuities, such as faults, heavy jointing, or rolls are present and are believed to affect the stress pattern significantly, then applying other numerical techniques capable of greater structural detail may be more appropriate.

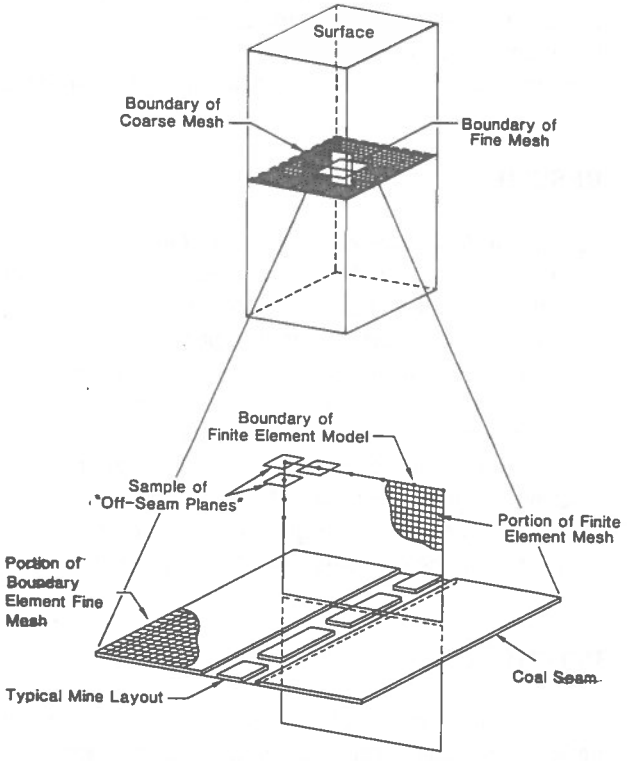

Figure 1. Typical mine layout and displacement-discontinuity grid.

Twenty-six different material property sets can be specified. In addition, the user is allowed to insert an additional material model to simulate gob, packwalls, and/or cribs. This inserted-material model uses a linear stress-strain relationship assuming a zero stress state at zero seam closure. An extraction ratio value is used to account for reduced material properties in the blocks that include some mined-out areas.

Recommended hardware requirements include an IBM compatible 486 PC with a math coprocessor, 1 Mbyte of RAM, VGA graphics, and a mouse for the preprocessor. USBM Information Circular (Donato, 1992) fully documents the MULSIM/PC program, including an example input file with output results. Also described are the companion mesh-generating preprocessing program, PREMUL, and the two- and three-dimensional postprocessing plotting programs, MUL2D and MUL3D, used in conjunction with MULSIM/PC. A complete user's guide is also provided for each of the programs. For a detailed explanation of the mathematical theories and techniques incorporated within MULSIM/PC, see references, (Crouch and Fairhurst, 1973; Sinha, 1982; Salamon, 1964; Mozumdar, 1974, 1978; Crouch and Starfield, 1983).

Example using MULSIM/PC - multiple seam interaction problem: The following example taken from reference (Donato, 1990), demonstrates how MULSIM/PC can be used to calculate stress interaction effects in a multiple seam setting. A longwall panel situated under 1,600 ft of overburden was mined underneath abandoned room-and-pillar workings located approximately 70 ft above. Figure 2 illustrates the geometry and dimensions of the upper and lower seams. Note the relative size of the MULSIM grid. The assumed in situ stress field included a vertical loading of 1.1 psi per foot of depth and a horizontal loading of 0.55 psi per foot of depth. The elastic properties used in the models are summarized in Table 1. Typical stress outputs are illustrated in figures 3 through 4.

Figure 3 presents three-dimensional vertical stress plots in a fishnet format. Note that the lower seam loading is affected by two major mechanisms: one is the redistribution of overburden weight caused by the overlying remnant structures; the second is load transfer caused by lower seam panel mining. Both mechanisms continuously superimpose their loads to give a combined concentration of stress on the lower seam. The modeled portion of the upper seam is no longer being mined, so it was assumed that its effect on the lower seam was constant. In contrast, load transfer caused by mining

TABLE 1. Effective elastic material property values used in this analysis.

Material	Modulus of elasticity, psi	Poisson's ratio	Cohesion, psi
Rock mass .	400,000	0.15	NAp
Coal	200,000	NAp	500.0
Yielded coal	100,000	NAp	250.0
Gob	5,000	NAp	0.0

NAp Not applicable

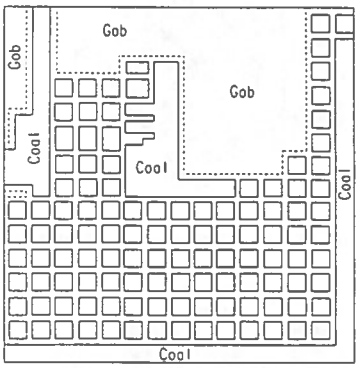

a. Upper seam.

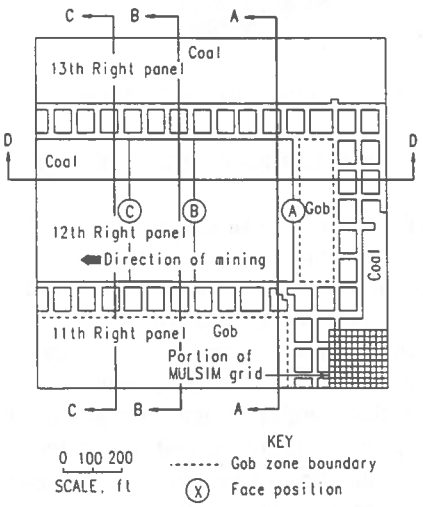

b. Lower seam.

Figure 2. Geometry and dimensions of MULSIM/PC example.

the lower seam panel varies according to face location. Of particular note is the heavy concentration of weight transferred through the 70-ft interburden layer onto the headgate entry of the lower seam from the large remnant pillar in the upper seam.

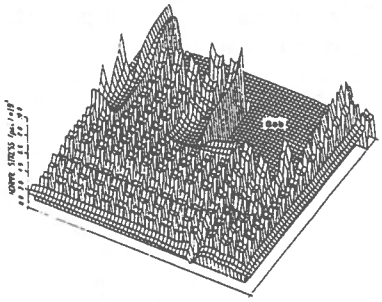

a. Upper seam.

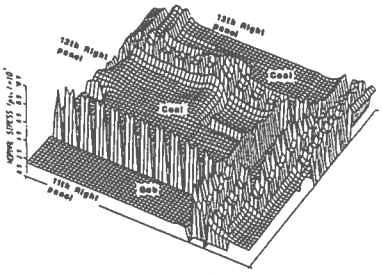

b. Lower seam for face position A (figure 2).

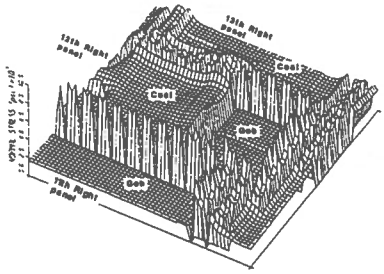

c. Lower seam for face position B (figure 2).

Figure 3. Three-dimensional vertical stress plots.

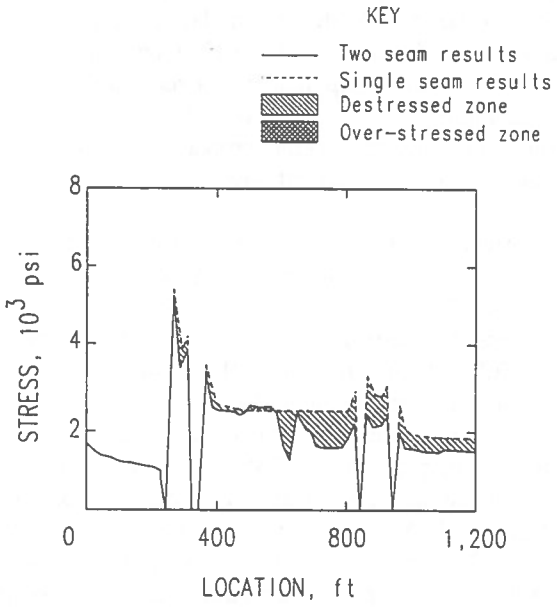

a. Cross-section A-A.

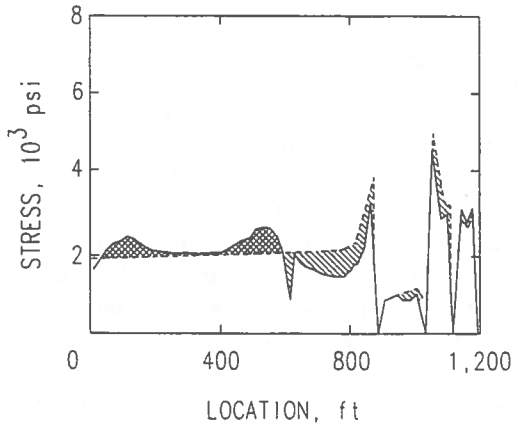

b. Cross-section D-D.

Figure 4. Two-dimensional vertical stress plots comparing two-seam versus single-seam mining results.

Figure 4 shows typical two-dimensional vertical stress plots taken through selected locations in the model. Figures 4a and 4b compare the distribution of stress at Section A-A and Section D-D (figure 2), respectively, with and without upper seam mining. Note how the presence of the unmined remnant pillar in the upper seam affects the overall pressure distributions along the chain pillars in the headgate and across the longwall face. Clearly, this type of information is of great value to a mine operator as he develops plans to retreat his longwall face.

MULSIM/NL: MULSIM/NL (Zipf, 1992) is the latest version of the USBM suite of boundary-element programs designed for calculating stresses and displacements (i.e., convergence) in coal mines or thin, tabular, metalliferous veins. MULSIM/NL analyzes one to four parallel seams that have any orientation with respect to the earth's surface. Three main features distinguish MULSIM/NL from its predecessors: (1) nonlinear material models, (2) multiple mining steps, and (3) comprehensive energy release and strain energy computations. MULSIM/NL has six material models for the in-seam material including (1) linear elastic for coal, (2) strain softening, (3) elastic plastic, (4) bilinear hardening, (5) strain hardening, and (6) linear elastic for

gob. The multiple-mining-step capability enables the user to simulate a changing mine geometry automatically. The ability to perform energy release calculations allows one to compare, on a very crude scale, the bump potential of different mine designs and extraction sequences within the limitations of static analyses. MULSIM/NL contains an energy subroutine that uses the calculated stresses and displacements at each block and element to evaluate detailed energy changes for each mining step. This subroutine computes various ERR quantities for the entire model, as well as various strain energy values for each element. Cook, et. al., (1966) developed the original ERR concept, and research found that ERR correlated well with the incidence of devastating rock bursts in deep underground South African gold mines. It is hypothesized that the ERR will also correlate with the incidence of coal mine bumps.

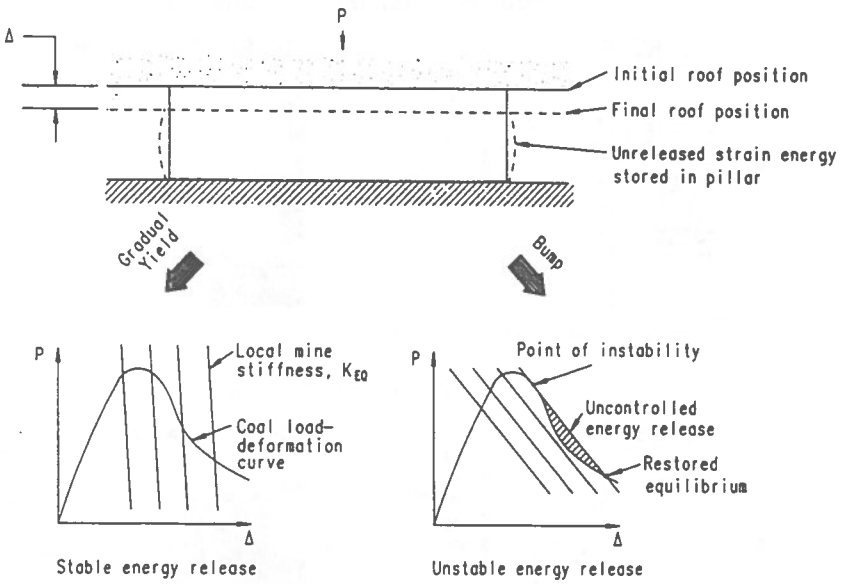

Figure 5. Stable and unstable failure in a coal mine pillar.

MULSIM/NL can also be run on a PC. But for large, computationally intensive models, a workstation environment is recommended. Minimum hardware requirements include a 486 IBM compatible PC with a math coprocessor and 8 megabytes of RAM. USBM Information Circular (Zipf, 1992) documents the MULSIM/NL application and practitioner's manual, including a number of example input files with output results. Preprocessing and postprocessing software is also provided with the program. Users interested in the mathematical and programming details are referred to reference (Zipf, IC 9321, 1992). Reference (Zipf, 1994) provides excellent suggestions and guidelines for input parameters for MULSIM/NL.

Example model analysis: Although rare, massive pillar collapses can be devastating. The most infamous collapse occurred in 1960 at Coalbrook North Colliery located in South Africa. Byran et al., (1966) report that thousands of pillars collapsed over a 750-acre area in 5 minutes, killing 437 miners. The joint Coal Board (University of South Wales) (University of New S. Wales School of Mines, 1993) reported three massive pillar collapses in Australia between 1990 and 1993. Chase, et al., (1994) report that on 11 recent occasions, massive pillar collapses have occurred in 6 southern West Virginia coal mines. The USBM is conducting research to gain a fundamental understanding of the cause(s) of such events. As part of this research, numerical techniques are being used to access the potential for particular designs to fail catastrophically.

Applying the concepts proposed by Salamon (1970), illustrated in figure 5 (Kripakov and Rockwell, 1989), it is possible to simulate and distinguish numerically, between sudden, massive pillar collapses and stable, progressive pillar failures. Figure 6 shows calculated stresses and displacements before and after the simulated pillar collapse that actually occurred in a West Virginia coal mine. Note that before the collapse, pillar splitting had been completed in eight rows of pillars plus two pillars in the 9th row. Close examination of the stresses indicates that most of the fenders approached the peak stress of 11 MPa (1,600 psi). Splitting just one more pillar in the 9th row triggered disaster. An unstable "chain reaction" developed. As one pillar failed, load transferred to adjacent pillars, causing others to fail. Displacement (convergence) in the panel increased dramatically after the failure.

The MULSIM/NL analysis showed that failure does not follow mining progressively. When a certain mine stability criterion is violated, a small increment of additional mining leads to a much larger increment of additional failure. With a realistic model, it is possible to examine different pillar geometries and different extraction sequences that might prevent a massive pillar

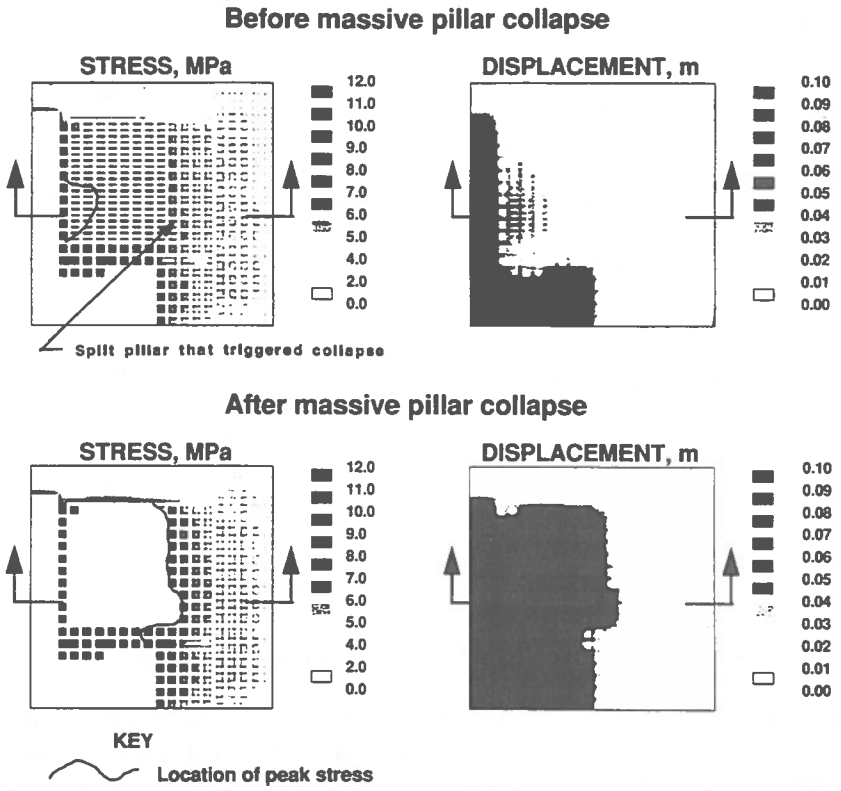

Figure 6. MULSIM/NL results comparing stresses and displacements before and after an unstable mine failure.

collapse. The biggest unknown in this kind of analysis is the shape of the complete stress-strain curve. Back analysis of other massive pillar collapses might provide additional information (Chase, Mark and Zipf, 1994).

Current Developments

A more recent development by the Bureau is an analysis procedure (Kripakov, Sun and Donato, 1994) that couples a series of boundary-element and finite-element models to evaluate the potential progressive failure of a yielding pillar gate road system for a given set of mining parameters. This approach was developed to approximate the simulation of a complex three-dimensional problem with two, two-dimensional models. Full three-dimensional finite-element models require a voluminous amount of input data, a high-speed minicomputer, and are costly to run. The proposed procedure reduces many of the complexities inherent in three-dimensional analysis, yet produces results useful for making everyday engineering decisions.

The theoretical approach is illustrated in figure 1. The idea of coupling two-dimensional, boundary-element models with two-dimensional, finite-element models was originally proposed by Kripakov, et al, 1990. This concept has now been combined with the progressive failure procedure proposed by Kripakov and Melvin, 1983, and automated. The procedure is set up to calculate the progressive failure around the periphery of a mine opening for different stages of mining. For each simulated face position, two distinct and separate phases of computer modeling are performed. Output from the first phase of modeling is used as input to the second phase of modeling.

The first phase of modeling considers a designated portion of a mine layout in plan view. This phase uses the displacement-discontinuity approach to determine the overall large-scale mining-induced stresses imposed on all remaining in-seam support structures. It also determines mining-induced in-seam displacement values and additional displacement values at designated off-seam locations for a particular face position. Load effects include overburden weight, load concentrations resulting from nearby mined-out workings in overlying or underlying seams, and lateral load transfer resulting from adjacent mined-out gob zones in longwall panels.

The second phase of modeling isolates and studies a specific area of interest in greater detail with a vertical section view. This vertical section is represented by a two-dimensional, finite-element window model. Computed displacements from the displacement-discontinuity model are used as input values to the finite-element model at common interface points between models. For the sake of simplicity and practicality, it is assumed that the out-of-plane displacements obtained from the displacement-discontinuity model have a negligible effect on the final results obtained from the finite-element plane-strain analysis, and, in this sense, displacement continuity or compatibility is maintained between the two modeling approaches (Kripakov, Beckett, Donato, and Durr, 1990).

Nonlinear behavior is approximated by utilizing a pseudo-elastic approach described in reference 18. Very briefly, stress output from the finite-element model is compared with a two-dimensional Mohr-Coulomb failure criterion. As failure is predicted to occur in each individual element, the elastic rock mass properties are iteratively updated until no additional failure occurs. At this point, the solution process is terminated and the output graphically displayed showing the degree and extent of weakening or deterioration that has occurred into the coal pillar rib, roof, and floor. In addition, an exaggerated plot of entry squeezing and deformation can be displayed. The first phase of modeling utilizes the USBM MULSIM/PC computer program (Donato, 1992). The second phase of modeling utilizes a finite-element code called ADINA (Bathe, 1975, rev. 1993). Although ADINA provides a more general preprocessor program, the USBM is using a special preprocessing program developed in-house to generate meshes specifically designed to simulate mining problems. Postprocessing software used with this procedure was also developed in-house in order to generate specialized output plots. These plots focus on the portion of the finite-element mesh of interest to the user, usually the area around the gate road, and delineate the degree and extent of yielding by a changing material property number or by one of a rainbow of colors in each element. This program will also plot the displaced mesh at any scale desired. In addition, two-dimensional stress distributions can be plotted through any desired vertical cross section of interest.

At this time, hardware requirements to run this procedure are as follows: In order to run the MULSIM/PC program and the associated preprocessing and postprocessing programs, a minimum of an IBM compatible 486 PC with a math coprocessor and 1 Mbyte of RAM, a mouse, and VGA graphics are recommended. The ADINA program currently runs on an HP workstation with a network connection to the PC for data transfer and plotting. ADINA is a commercially available code and cannot be distributed by the Bureau; however, this procedure can be incorporated into any linear-elastic finite element program.

Example Model Analysis: Yield pillar systems have become an alternative to conventional abutment pillar or combination abutment-yield pillar designs. Typically, under western U.S. mining conditions, these systems have proven more stable and economic when compared to abutment pillars at mining depths greater than 450 m

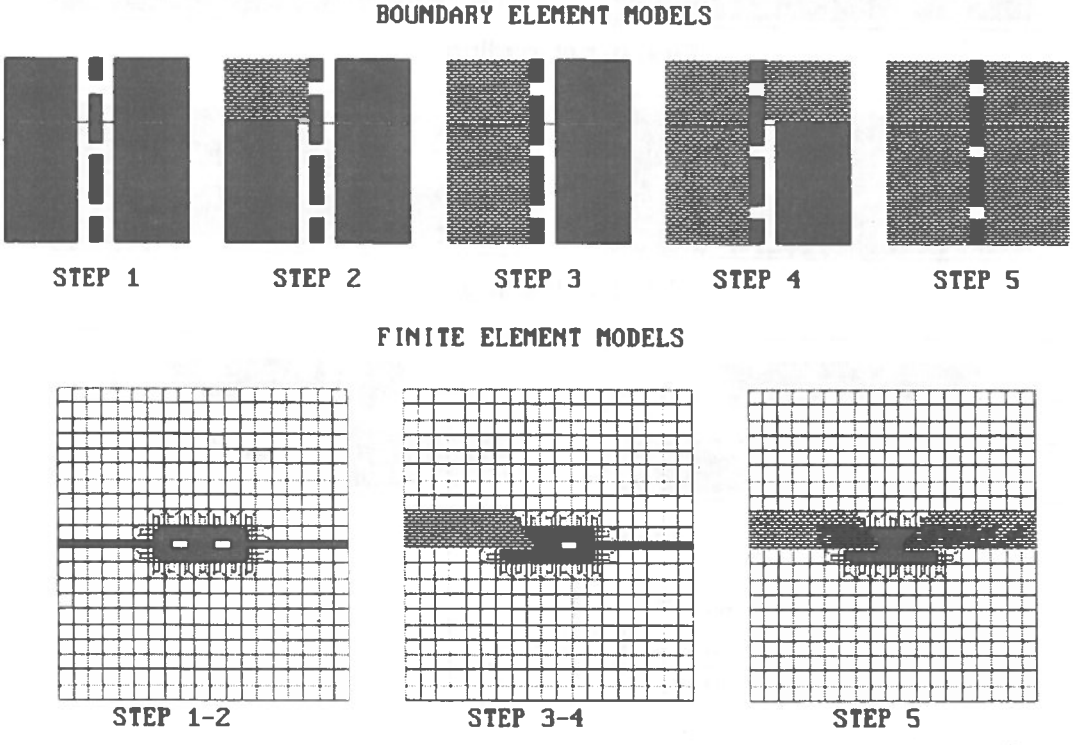

Figure 7. Geometries and meshes used in example analysis. Upper figures depict the five face positions modeled with MULSIM/PC. Lower figures show finite-element vertical section models.

(1,476 ft), where severe coal bump conditions often exist, or when roof stability and floor heave become problematic as a result of an improper design (DeMarco, 1994). This example is used to illustrate the application of the USBM progressive failure procedure.

The five small squares at the top of figure 7 show a plan view of a longwall mine layout using boundary-element models for different mining stages. For this example, the mining depth is assumed to be 458 m (1,500 ft) and the pillar width is 9.1 m (30 ft). Five

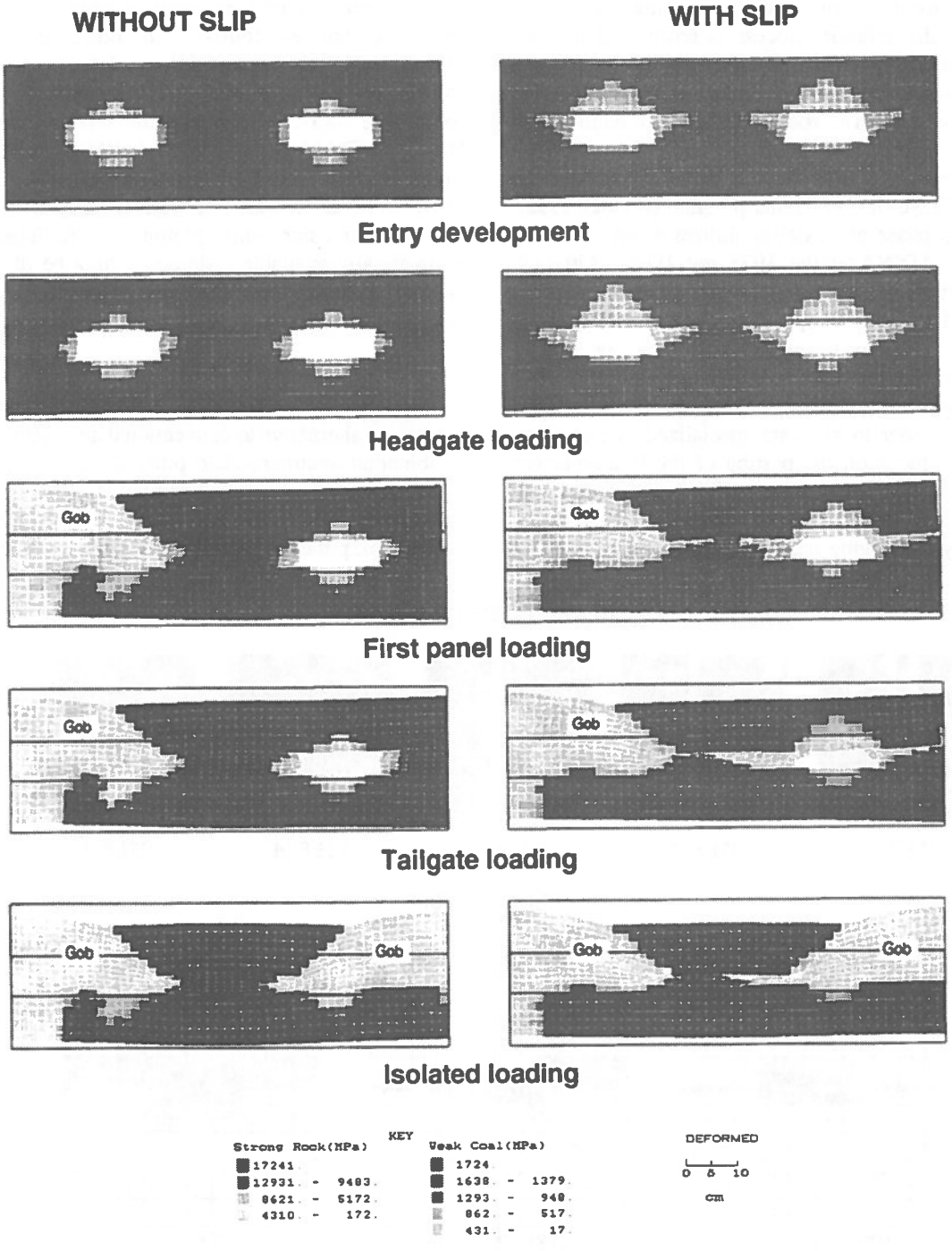

Figure 8. Progressive failure predicted to occur around mine opening as a function of face position.

mining stages are simulated. Step 1 represents initial entry development; step 2, headgate loading just as the face approaches; step 3, first panel mined; step 4, tailgate loading as the second panel approaches; step 5, both panels mined. These models are run to generate the boundary-displacement conditions for the more detailed finite-element analysis to follow. The three finite-element meshes used for these analyses are depicted by the three larger squares at the bottom of figure 7. These models represent vertical planes taken through the common section lines cut through the boundary-element models.

Figure 8 illustrates the progressive failure predicted to occur around a typical mine opening at different mining stages for the case of a weak coal seam sandwiched between a strong roof and a strong floor, with and without the effects of slip occurring at the coal/roof interface. For these numerical examples, slip means that unrestricted horizontal movement can occur along the horizontal slip line. These two conditions (unrestricted slip and no slip) represent the limits of two bounds from an analysis point of view. Reality probably falls somewhere in between. Results clearly illustrate that interface slip plays a major role in how a pillar and the entry behave. The absence of slip provides confining strength to the pillar, thus reducing the degree and extent of overall yielding. It also shows that, with excessive pillar rib yielding, the effective span of material over the opening increases, causing the weakened failed tensile zone to extend vertically, which would probably require additional supplementary support.

Future Developments

The USBM is sponsoring, through a contract with the Colorado School of Mines, the development of a general purpose, explicit, fully deformable discrete-element code for use in mine modeling. Work has proceeded in two areas: first, a graphical user interface has been written that allows a user to interactively create models and view the results of the subsequent analysis; second, an object-oriented C++ discrete-element code has been developed using a geomechanics class library written specifically for this project. Discrete-element methods allow for deformations within blocks as well as for large-scale rotational and translational movements between blocks due to external forces acting on block boundaries. Some commercial programs such as UDEC (Universal Distinct Element Code) (Cundell, 1980) use a finite-difference scheme to implement block deformability. Finite-differencing provides fast and accurate solutions to a wide variety of linear and nonlinear elastic problems. In this implementation, a finite-element approach has been adopted in order to avoid the overly stiff behavior commonly observed when finite-difference triangles are used in plastic analyses. Quadrilateral finite elements coupled with a reduced integration scheme are being used to enhance element performance when plastic strain hardening and softening is incorporated into the code to model the constitutive behavior of coal seams and pillars. In the current implementation, computational expense has been minimized by using one point quadrature to integrate over the element areas, and hourglassing has been prevented in the element "zero energy modes" by using a simple artificial stiffness technique developed by Flanagan and Belytschko, (1981). Reduced integration schemes often produce a more accurate solution in plastic analysis because they prevent elements from "locking up" after yielding.

Example Problem: Figure 9 shows the problem domain modeled. The problem represents a 30-ft wide pillar developed in a 10-ft thick coal seam using 20-ft wide entries. The mine structure has been divided into five types of deformable blocks representing the panels, the yield pillar, and the overlying and underlying country rock. Plane strain, linear elastic conditions are assumed to apply, and the relevant material properties are listed in Table 2.

Table 2. Material properties for the DEM elastic model.

Material	Modulus of elasticity, psi	Poisson's ratio	Angle of internal friction, deg.
Host rock . .	2.5×10^6	0.15	500.0
Coal seam . .	2.5×10^5	0.30	250.0

Vertical stresses equal to overburden were applied, and the model was allowed to reach the in situ stress state existing in the rock before gate road development. After excavation, the entire mesh was allowed to reach a state of static equilibrium by applying a fraction of critical damping to the equations of motion governing block movement. Figure 9a clearly shows the development of high vertical stresses in the pillar and the panels adjacent to the gate roads as well as high horizontal stresses (figure 9b) in the floor and roof rock. The higher horizontal stresses observed in the coal are due to its higher Poisson's ratio of 0.3. Currently the code is being extended to incorporate plastic strain

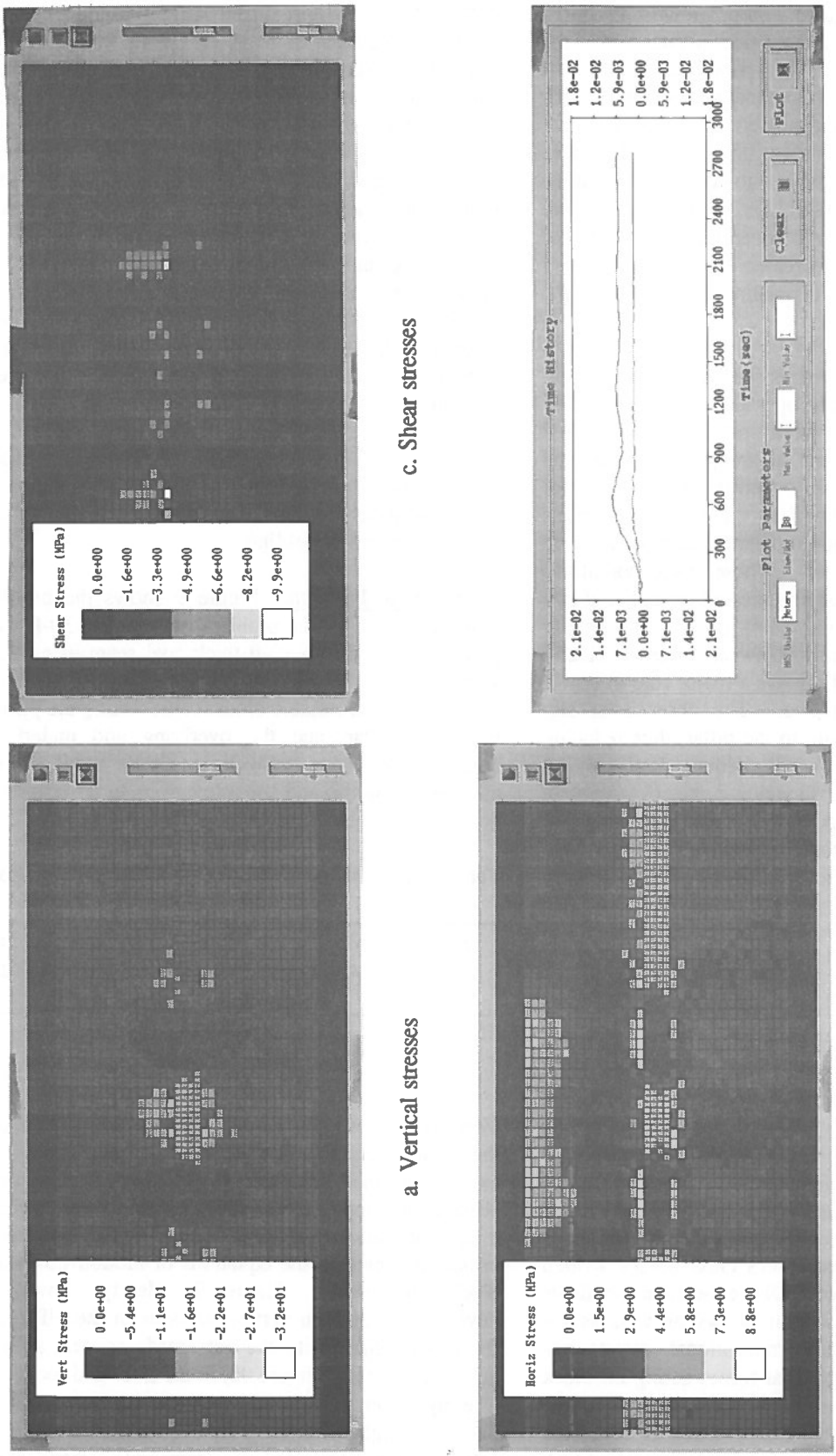

a. Vertical stresses

b. Horizontal stresses

c. Shear stresses

d. Damping history of an element located at midheightof the pillar rib.

Figure 9. Results of discrete element model analysis surrounding a pillar and entry system following development mining.

softening in the panels and yield pillars and will ultimately be used to simulate pillar yielding in a variety of mine conditions. Shear stresses are shown in figure 9c. Figure 9d is an example of the damping history of one element (midheight of left pillar rib) to show the solution has stabilized.

CONCLUSIONS

This paper has attempted to give a general overview of USBM research and development in the area of applying numerical modeling techniques toward evaluating practical mining-related ground control problems. It is often argued that model results, seemingly, do not match the real world in terms of an absolute quantitative correlation. The fact is that they seldom do, particularly in the field of earth sciences. There are simply too many variables that are unknown. An article in the February issue of Science magazine (Oreskes, 1994) pointed out, "*...verification and validation of numerical models of natural systems is impossible. This is because natural systems are never closed and because model results are always non-unique. Models can be confirmed by the demonstration of agreement between observation and prediction, but confirmation is inherently partial... models can only be evaluated in relative terms, and their predictive value is always open to question. The primary value of models is heuristic.*" In other words, the models will never give exact answers, but should be thought of as a means to provide insight as to what may be going on. It is envisioned that future USBM research will continually build upon past work and will spark interest in others to experiment independently with their own models.

REFERENCES

BATHE, K.J., 1975, 1993.
ADINA, A Finite Element Program for Automatic Dynamic Incremental Nonlinear Analysis, Military Institute of Technology, Mechanical Engineering Department, Cambridge, Massachusetts, Report. No. 82448-1, (Sept. 1975, rev. 1993), pp. 435.

BECKETT, L.A. and MADRID, R.S., 1988.
MULSIM/BM - A Structural Analysis Computer Program for Mine Design, U.S.Bureau of Mines (USBM), IC 9168, Denver, Colorado, pp. 302.

BRYAN, A., BRYAN, G. and FOUCHE, J., 1966.
Some Problems of Strata Control and Support in Pillar Workings, The Mining Engineer, V. 123, pp. 238-254.

CHASE, F.E., MARK, C. and ZIPF, R.K., 1994.
The Massive Collapse of Coal Pillars - Case Histories from the United States, Proceedings of the 13th Conference on Ground Control in Mining, W. Virginia University, Morgantown, W. Virginia, August, 1994, pp. 69-80.

CROUCH, S.L. and FAIRHURST, C., 1973.
The Mechanics of Coal Mine Bumps and the Interaction Between Coal Pillars, Mine Roof, and Floor," (contract H0101778, Univ. MN). USBM, Minneapolis, Minnesota, OFR 53-73, NTIS PB 222 898, pp. 88.

CROUCH, S.L. and STARFIELD, A.M., 1983.
Boundary Element Methods in Solid Mechanics," Allen & Unwin, pp. 322.

CUNDELL, P.A., 1980.
UDEC - A Generalized Distinct Element Program for Modelling Jointed Rock, Final Technical Report to European Research Office, U.S. Army, Contract DAJA37-79-C-0548, NTIS Order No. AD-A087 610-2.

DEMARCO, M.J., 1994.
Yielding Pillar Gate Road Design Considerations for Longwall Mining, USBM Special Publication, January, 1994, New Technology for Longwall Ground Control, pp.19-36.

DONATO, D.A., 1990.
An Application of MULSIM/PC in a Coal Mine Structural Analysis, Proceedings of Use of Computers in the Coal Industry, Grayson, Wang & Sanford (eds), Rotterdam, ISBN 90 6191 1176, pp. 85-95.

DONATO, D.A., 1992.
MULSIM/PC - A Personal-Computer-Based Structural Analysis Program for Mine Design in Deep Tabular Deposits, USBM, Denver, Colorado, IC 9325, pp. 56.

FLANAGAN, D.P. and BELYTSCHKO, T., 1981.
A Uniform Strain Hexahedron and Quadrilateral with Orthogonal Hourglass Control, Proceedings of International Journal for Numerical Methods in Engineering, Vol. 17, pp. 679-706.

KRIPAKOV, N.P., BECKETT, L.A., DONATO, D.A. and DURR, J.S., 1990. Computer-Assisted Mine Design Procedures of Longwall Mining, USBM, Denver, Colorado, RI 9172, pp 38.

KRIPAKOV, N.P. and MELVIN, M.T., 1983.
A Computer Procedure to Simulate Progressive Rock Failure Around Coal Mine Entries, Proceedings of First Conference on Use of Computers in the Coal Industry W. Virginia University, Morgantown, W. Virginia, Society for Mining, Metallurgy and Exploration, AIME, New York, pp. 487-502.

KRIPAKOV, N.P. and ROCKWELL, L.E., 1989.
Application of Numerical Modeling Techniques for Gateroad Design in Bump Prone Mines, Proceedings of American Mining Congress Coal Convention and Longwall U.S.A Exhibition and Conference, Pittsburgh, Pennsylvania, pp. 12.

KRIPAKOV, N.P., SUN, M.C. and DONATO, D.A., 1994. Automation of a Progressive Failure Procedure for Analysis of Underground Mine Pillar Designs, Proceedings of 13th Intl. Conference on Ground Control in Mining, W. Virginia University, Morgantown, W. Virginia, pp. 58-68.

MOZUMDAR, B.J., 1974.
A Mathematical Model of Ground Movement Due to Underground Mining, Ph.D. Thesis, Pennsylvania State Univ., pp. 134. 1978, Univ. Microfilms Int., Ann Arbor, Michigan, fac. 75-9815.

ORESTES, N., FRECHETTE, K.S., and K. BELITZ, 1994. Verification, Validation, and Confirmation of Numerical Models in the Earth Sciences, Science Magazine, 263, pp. 641-646.

SALAMON, M.D.G., 1964.
Elastic Analysis of Displacements and Stresses Induced by the Mining of Seam or Reef Deposits, Journal S. African Institute Mining & Metallurgy, pt. 3, v. 64, No. 10, pp. 468- 500; pt. 4, v. 65, No. 5, pp. 319-338.

SALAMON, M.D.G., 1970.
Stability, Instability and Design of Pillar Workings," Intl. Journal Rock Mechanics and Mining Sciences, Vol. 7, Pergamon Press, pp. 613-631.

SINHA, K.P., 1979.
Displacement Discontinuity Technique for Analyzing Stresses and Displacements Due to Mining in Seam Deposits," Ph.D. Thesis, Univ. Minnesota. 1982, Univ. Microfilms Int., Ann Arbor, MI, fac. 7918390, pp. 311.

UNIVERSITY OF NEW SOUTH WALES, SCHOOL OF MINES. (Joint Coal Board), April, 1993 Issue No. 1., "Strata Control for Mine Design."

ZIPF, R.K., 1992.
MULSIM/NL Application and Practitioner's Manual, USBM, Denver, Colorado, IC 9322, pp. 48.

ZIPF, R.K., 1992.
MULSIM/NL Theoretical and Programmer's Manual, USBM, Denver, Colorado, IC 9321, pp. 52

ZIPF, R.K., January, 1994.
Longwall Mine Design with MULSIM/NL, USBM Special Publication, Proceedings of U.S. Bureau of Mines Technology Transfer Seminar on New Technology for Longwall Ground Control, pp. 37-51.

CAMI'95: 3rd Canadian Conference on Computer Applications in the Mineral Industry
Montréal, Québec, Canada, October 22-25, 1995

Development of a Discrete Element Code for Mine Modeling

S.M. Oelfke
Research assistant, Colorado School of Mines, Golden, CO.

G.G.W. Mustoe
Associate professor, Colorado School of Mines, Golden, CO.

ABSTRACT:

This paper describes research being conducted under a cooperative agreement between the Colorado School of Mines and the U.S. Bureau of Mines, Denver Research Center to develop a public domain discrete element software package for modeling ground control failures in coal mines. In the software under development, an updated Lagrangian approach is used to extend the usual rigid block DEM model by incorporating elasto-plastic block deformability using quadrilateral finite elements. One point integration with hourglass control is used to reduce computational expense. This formulation is implemented in an object oriented C++ program integrated with a graphical user interface to simplify model construction and provide for rapid analysis of results. Simple analyses to simulate pillar failure have been performed to validate the computational algorithms.

RESUMÉ:

Cet article décrit le résultat de la collaboration entre Colorado School of Mines et le U.S. Bureau of Mines, Denver Research Center, pour développer un logiciel de modélisation et de simulation, par éléments finis, des instabilités dans les mines de charbon. Dans ce logiciel du domain publique, encore en développement, une nouvelle extension á la méthode de Lagrange est utilisée pour tenir compte de la déformation élasto-plastique des blocs qui jusq'á lors étaient considérés comme rigides dans les modeéles de DEM classiques. Une intégration du premier ordre avec hourglass control" est utilisée afin de réduire les temps de calcul. Cette méthode est implémentée dans un programme orienté objet, écrit en C++, avec une interface utilisateur simplifiant la construction des modéles et permettant une analyse rapide de résultats. De simples études simulants de mauvais comportements de pilliers ont étéés conduites dans le but de valider l'algorithme.

1 Introduction

Common types of failures in underground openings are difficult to model because not all relevant failure mechanisms can be described using finite or boundary element analysis. Failures occur due to sliding along joints and discontinuities, due to plastic and viscoplastic flow in the floor and wall rock, or due to a combination of these and other factors. In addition, the influence of extraction processes during mining may cause dynamic changes in the surrounding rock mass. Modern mining practices often introduce water into a mined opening which can drastically reduce rock strength and cause weak floor rock to 'swell'. Similarly, steel sets or packwalls installed for stabilization may produce bearing capacity failure and 'punch' into the floor causing it to heave. While our understanding of these conditions is not complete, and comprehensive modeling techniques to analyze them are perhaps

years away, discrete element methods that incorporate block deformability have shown potential for successfully modeling the range of discontinuous deformation possible in underground mines.

2 DEM-FEM Code

The U.S. Bureau of Mines under a contract with the Colorado School of Mines is developing a hybrid discrete element-finite element code to model floor heave and pillar failure in underground coal mines. Discrete element methods (DEM's) were first proposed by Peter Cundall (Cundall, 1971; Cundall and Strack, 1979) in the 1970's. Other researchers have built upon their work and have added mechanisms for cracking (Hocking et al., 1987) and block deformability (Barbosa and Ghaboussi, 1992). In a series of papers describing the so-called 'discrete finite element method', Barbosa and Ghaboussi use a modified Total Lagrangian formulation to model each discrete block element as a finite element. External contact forces acting on the surface of each block are added to internal forces computed from standard finite element analysis. In this paper, a velocity-based updated Lagrangian approach for treating elasto-plastic block deformability in quadrilateral elements has been implemented in an object-oriented program. The program has been developed as a C++ class library, and may be used as either a deformable discrete element program or a large strain explicit finite element program. The object-oriented framework has enhanced the development of effective data structures in the program by allowing logical parts of the problem domain to be modeled as separate objects. Access to these objects is accomplished either through classes or through methods attached to the objects themselves. The program is actually a collection of classes that implement the data structures and algorithms associated with the motions of individual DEM blocks and several types of finite elements. The primary advantage of using finite elements for block deformability instead of the more usual finite differences is that it allows the analyst to draw upon the considerable body of knowledge gained in nonlinear finite element analysis over the last three decades. The main disadvantage is increased computation time, but this limitation has been reduced considerably in the program by using one point quadrature to integrate the element stresses and then applying anti-hourglassing to control the element zero-energy modes.

2.1 Theory

In discrete element computations, central difference schemes are used to integrate the equations of motion and have the advantages of decreased storage costs and relatively simple implementation. In the present formulation, an explicit method is used to solve the equations of motion and is given as

$$[M]\{\ddot{U}\}^n + \alpha[M]\{\dot{U}\}^n = \{F_{ext}\}^n - \{F_{int}\}^n \quad (1)$$

where $[M]$ is the matrix of nodal masses, $\{\dot{U}\}$ and $\{\ddot{U}\}$ are the vectors of nodal acceleration and velocity, α is the damping proportionality factor, and $\{F_{ext}\}$ and $\{F_{int}\}$ are the external and internal force vectors acting at the element nodes. The external forces in (1) are generated at corner-edge contacts between adjacent blocks, and are computed at each timestep as

$$\{F\} = [K]\{\Delta u\}, \quad (2)$$

where $[K]$ is the block stiffness matrix and $\{\Delta u\}$ is the vector of incremental shear and normal displacements at the point of contact. We define a slip condition, f, such that

$$f = |F_s| + \mu F_n, \quad (3)$$

where μ is the friction coefficient and F_n and F_s are the normal and shear force components at the point of contact respectively. A simple Coulomb constitutive law may be defined using the sense of the incremental shear displacements, Δu_s, as

$$F_s = -\text{sign}(\Delta u_s)\ |\mu F_n|. \quad (4)$$

Plastic sliding between blocks now occurs only when the condition defined in (4) is met. This method is identical to the method used in the Northwestern University Rigid Block Model (NURBM) to evaluate corner-edge contact forces between blocks (O'Connor, 1988), except that

the nodal force vectors are not summed at the block centroids, but rather added to the internal forces acting at each node.

The internal forces in equation (1) are computed at the element nodes as

$$\{F_{int}\} = \int_V [B]^T \{\sigma\}\, dV, \qquad (5)$$

where, $[B]^T$ is the transpose of the strain displacement matrix assembled using the derivatives of the element shape functions and $\{\sigma\}$ refers to the Cauchy stresses computed at the element Gauss points when numerical integration is used to evaluate the integral. In the implementation proposed in this paper, a velocity-based formulation, as opposed to the displacement formulation proposed by Barbosa and Ghaboussi, is used to evaluate (5). This formulation has the advantage of eliminating the necessity of referring tensor quantities $(\sigma, \epsilon, \dot{\epsilon})$ to an intermediate reference configuration and provides a natural framework for solving problems involving plastic and viscoplastic deformations in rock. It has been previously implemented in explicit FEM methods by Belytschko, 1990, and Flanagan and Belytschko, 1986, and in implicit FEM methods by Baudel et al., 1986, and Chenot, 1988. The central feature of the method is the calculation of the updated stress, $\{\sigma'\}$, via the stress rate tensor, $\{\dot{\sigma}\}$, and timestep, Δt, so that

$$\{\sigma'\} = \{\sigma\} + \{\dot{\sigma}\}\,\Delta t. \qquad (6)$$

The stress rate is evaluated by decomposing the element velocity gradient, $\dot{u}_{i,j}$, into the symmetric rate of deformation tensor $\mathbf{D}$ and antisymmetric spin tensor, $\mathbf{\Omega}$.

$$\dot{u}_{i,j} = \frac{1}{2}\left(\frac{\partial \dot{u}_j}{\partial x_i} + \frac{\partial \dot{u}_i}{\partial x_j}\right) + \frac{1}{2}\left(\frac{\partial \dot{u}_j}{\partial x_i} - \frac{\partial \dot{u}_i}{\partial x_j}\right) \qquad (7)$$

where the first and second quantities on the r.h.s refer to $\mathbf{D}$ and $\mathbf{\Omega}$, respectively. For small displacements, the rate of deformation tensor is closely approximated by the strain rate tensor, $\dot{\epsilon}$, so the stress increment is evaluated as

$$\{\Delta\sigma\} = [E]\{\dot{\epsilon}\}\,\Delta t, \qquad (8)$$

where $[E]$ is the matrix of elastic properties. If a body is not undergoing large rotations with respect to an observer's frame of reference, the stress rate is simply the material derivative of the stress tensor. But in general, the stress rate is not frame indifferent even though the stress is, and equation (6) must be modified to ensure that incremental objectivity is maintained. Using the definition of the objective Jaumann stress rate tensor (Malvern, 1969),

$$\{\mathring{\sigma}\} = \{\dot{\sigma}\} + \{\sigma\}[\Omega] - [\Omega]\{\sigma\}, \qquad (9)$$

and substituting $\{\mathring{\sigma}\}$ for $\{\dot{\sigma}\}$ in (6) and integrating gives

$$\{\sigma'\} = \{\sigma\} + \{\sigma\}[\alpha] + [\alpha]^T\{\sigma\} + \{\dot{\sigma}\}\,\Delta t, \qquad (10)$$

where $[\alpha] = [\Omega]\,\Delta t$ for small rotations and $\dot{\sigma}$ is the stress rate tensor defined in (6). The requirement that the elements of $[\alpha]$ be small is due to the fact that a valid transformation $[\tilde{\sigma}] = [Q]^T[\sigma][Q]$ must exist. For small rotations, $(\theta << 1)$, the transformation matrix $[Q]$ may be decomposed so that

$$[\mathbf{Q}] = \begin{bmatrix} 0 & -\theta \\ \theta & 0 \end{bmatrix} + \begin{bmatrix} 1 & 0 \\ 0 & 1 \end{bmatrix}. \qquad (11)$$

Performing the transformation and neglecting higher order terms gives

$$[\tilde{\sigma}] = [\sigma] + [\alpha][\sigma] + [\alpha]^T[\sigma], \qquad (12)$$

which corresponds to (10) above. The finite element discretization is then formulated in the usual manner for isoparametric elements.

2.2 Reduced Integration

One drawback of a combined finite element-discrete element formulation is the computational expense incurred when using four-point quadrature to integrate the element stresses. Compared with finite difference schemes, finite elements can impose severe computational penal-

ties when implemented in explicit DEM codes. A potential solution to this problem, is to use one-point quadrature to integrate over the element stresses. While this technique can reduce the expense by more than a factor of three, it can also result in certain element deformation modes remaining stressless. If these modes are excited, the element mesh begins to deform into distinctive "hourglassing" or "keystoning" patterns that quickly become dominant and destroy the quality of the solution.

Over the past two decades, Ted Belytschko and his students have pioneered methods to control hourglassing by adding artificial forces to stiffen the hourglassing modes (Flanagan and Belytschko, 1980, Belytschko and Tsay, 1983). Their algorithms have been successfully implemented in the DEM-FEM code described in this paper. Briefly, their technique is to isolate the element hourglassing modes independently of the element rigid body and uniform strain modes. In the following discussion, the convention holds that lowercase subscripts have a range of two, representing the spatial coordinate directions, and uppercase subscripts have a range of four, corresponding to the element nodes. For the case of a four node isoparametric element integrated with one point quadrature, it can be shown that at the integrating point certain deformation modes will lead to zero element strains. If $B_{j,I}$, are the derivatives of the isoparametric shape functions defined as

$$\frac{1}{4}\begin{bmatrix} -(1-\eta) & -(1+\eta) & (1+\eta) & (1-\eta) \\ -(1-\xi) & (1-\xi) & (1+\xi) & -(1+\xi) \end{bmatrix} \tag{13}$$

and Γ_I is the nodal shape vector for one of the hourglassing deformation modes

$$\Gamma_I = \{1, 0, -1, 0, 1, 0, -1, 0\}, \tag{14}$$

expanding $B_{j,I}$ into a 3x8 matrix and taking the inner product of 13 and 14, we find that the element strains become zero at the integrating point $(\xi = 0, \eta = 0)$. This rather contrived example illustrates that the element does not strain when it deforms in the manner associated with the nodal shape vector. However, in the general case, the element may deform into any arbitrary geometry, and the task becomes to isolate the general nodal shape vector independently of deformations caused by the uniform strain and rigid body modes. Flanagan and Belytschko, 1980, calculate this vector as

$$\gamma_I = \Gamma_I - \frac{1}{A} B_{i,I} x_{i,J} \Gamma_J \tag{15}$$

and then use it to find the portion of the element velocity field, $\dot{q}_i$, that contributes to hourglassing

$$\dot{q}_i = \frac{1}{2} \dot{u}_{i,I} \gamma_I. \tag{16}$$

In equation (15), $x_{i,J}$ refers to the element nodal coordinates. The anti-hourglass forces applied to the element nodes are computed by

$$\dot{f}^{HG}_{i,I} = \frac{1}{2} \dot{Q}_i \gamma_I. \tag{17}$$

where $\dot{Q}_i$ is the hourglass stiffness rate defined as

$$\dot{Q}_i = \kappa \frac{\lambda + 2\mu}{2} \frac{B_{i,I} B_{i,I}}{A} \dot{q}_i, \tag{18}$$

λ and μ are the well known lame constants, A is the element area, and κ, is a stiffness parameter that controls the degree of anti-hourglassing applied to the mesh. Flanagan and Belytschko recommend that κ be given a value less than 0.5 for best results. This hourglass control scheme was found to be simple to implement into the DEM-FEM program and quite effective at controlling hourglassing without degrading the quality of the solution.

2.3 Time Integration

In explicit time integration schemes, the variables describing the kinematic behavior of a body must be calculated by direct integration of the equations of motion. The computational algorithm used in this formulation is quite simple and requires that the velocities, accelerations, and displacements be found at each timestep. The updated velocities and displacements are computed as

$$\{\dot{U}\}^{n+\frac{1}{2}} = \{\dot{U}\}^{n-\frac{1}{2}} + \{\ddot{U}\}^{n}\Delta t, \qquad (19)$$

$$\{U\}^{n+1} = \{U\}^{n} + \{\dot{U}\}^{n+\frac{1}{2}}\Delta t, \qquad (20)$$

subject to the initial conditions

$$\{U^{\circ}\} = \{U(0)\}; \;\; \{\dot{U}\}^{-\frac{1}{2}} = \{\dot{U}(0)\}, \;\; n = 0. \qquad (21)$$

The current element velocities and displacements must be found in order to calculate the external and internal nodal forces defined in (1). $\{F_{ext}\}$ and $\{F_{int}\}$ are then assembled into a resultant force vector and used to find the updated nodal accelerations so that

$$\{\ddot{U}\}^{n+1} = [M]^{-1}\Big[\{F_{ext}\}^{n+1} - \{F_{int}\}^{n+1} - \alpha[M]\{\dot{U}\}^{n+\frac{1}{2}}\Big]. \qquad (22)$$

In the explicit formulation described here, a stiffness matrix is never formed, and provided the nodal mass matrix is diagonal, a system of equations is never solved. This results in considerable computational simplification and often in less computational expense than that required by implicit methods. In general, explicit methods can model complex non-linear geometric and material behavior more easily than implicit methods. However, they are only conditionally stable, and in certain cases, the minimum timestep must be made very small. It might be noted that although implicit methods are unconditionally stable, the accuracy of the solution may degenerate if too large a timestep is used.

2.4 OOP Implementation

An object-oriented C++ program using the National Institutes of Health (NIH) class library was written to perform the necessary computations. The overall structure of the program was designed using class templates for handling linked lists of blocks and elements and NIH classes for handling the matrix and vector operations. The computationally intensive finite element calculations were implemented as methods in the element classes. A listing of the main program is shown below to illustrate the application of object-oriented programming concepts to DEM computations.

```
DataBase * database = new DataBase ();

void main( int argc, char* argv[] )
{
 BodySystem BlockSystem;

 try {
  arg_failure( argc );

  vect<DataFileOutput*> fp( argc );
  InputFile in_fp = InputFile( argv[1] );

OutputFile out_fp = OutputFile( argv[2] );

  for (int i=0; i<num_files; i++, arg++) {
    theDatabase->addFile( argv[arg] );
    fp[i] = theDatabase->getOutputFile();
  }
  for (i=0; i<num_parameters; i++, arg++)
   parameters[i] = argv[arg];

  for (i=0; i<num_options; i++, arg++)
   options[i] = argv[arg];

  BlockSystem.setConstants();
  BlockSystem.readOn();
  BlockSystem.moveOn()
  BlockSystem.saveObject( out_fp.ref() );

 } catch ( input_handler error )
       { error.diagnostic(); }
}
```

3 Examples

Coal pillars exhibit complex nonlinear behavior in response to induced stresses, and any useful model of pillar constitutive behavior must be able to reproduce the progressive yielding that leads to failure when pillars are subjected to excessive loads. One widely used failure criterion for coal is Mohr-Coulomb plasticity. Wilson,1972 proposed that coal pillars obey a Mohr-Coulomb yield criterion and speculated that, after continued loading, they become differentiated into an elastic core surrounded by a nonlinear yield zone. The extent of this yield zone was assumed to be dependent upon factors such as coal strength, overburden, degree of strain softening and the condition of the roof and floor rocks. Wilson's pillar model was subsequently confirmed in studies where the load-deformation response of coal pillars was measured in situ (Wagner, 1974).

3.1 Plasticity Model

To test the ability of the DEM-FEM program to model pillar failure, a 2.5x2.5 meter pillar was analyzed in plane strain using 256 quadrilateral elements (Fig.1). The mesh was horizontally constrained at both the top and bottom nodes and then incrementally loaded by applying a constant vertical velocity to the top nodes only. The strain softening portion of the pillar stress-strain curve was implemented in the program by reducing the cohesive strength of the coal as a function of the total plastic strain. The Mohr-Coulomb material properties and failure surface for the test case are shown in figure 2.

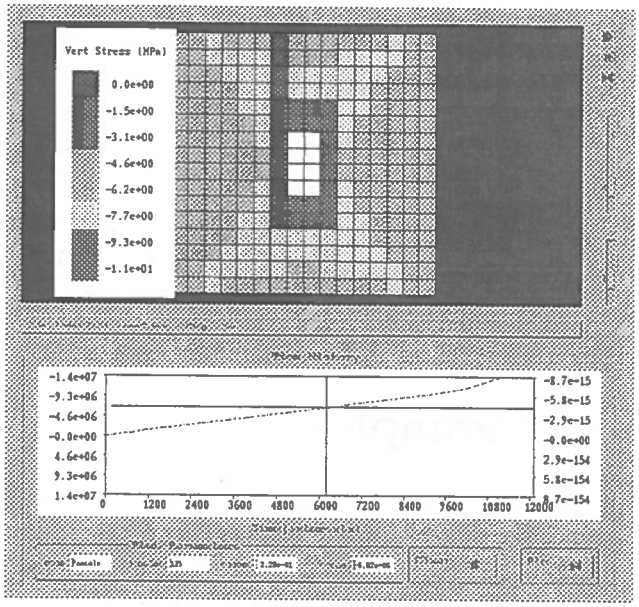

FIG. 1. Pillar stresses after ultimate strength is reached and yielding is well underway. The graphical user interface was developed specifically for the DEM-FEM code and was written in C++ using the X-Window Motif library.

During the course of the analysis, the ultimate strength of the test pillar was found to be greatly influenced by the degree of softening used in the model. When the softening tangent modulus became less than one half the Youngs modulus of the coal, the pillar failed in a controlled manner.

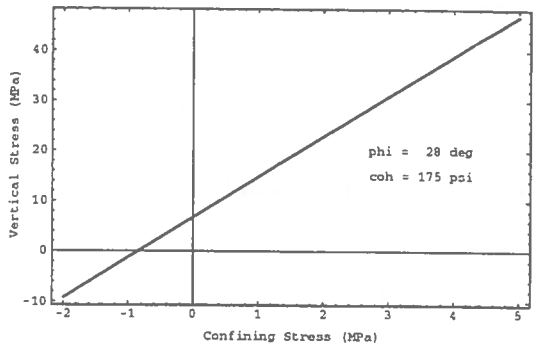

FIG. 2. Mohr-Coulomb yield criterion, shown in principal stress space, used in the test problem. Youngs modulus and Poisson's ratio of the coal are 0.29 GPa and 0.3. The cohesive strength and angle of internal friction of the coal are 1.2 MPa and $\phi = 28$ degrees respectively.

But in analyses where the strain softening tangent modulus was over-steepened, the pillar failed rapidly as the program to failed to converge to a stable solution. Rapid failure is expected when a pillar experiences a sudden loss in cohesive strength because the overlying rock converges with more energy than the pillar is able to store as elastic strain energy. In the test case, the strain softening tangent modulus was taken to be twenty percent of the Young's modulus of the coal, and the pillar failed in a controlled manner. A plot of average vertical pillar stress versus

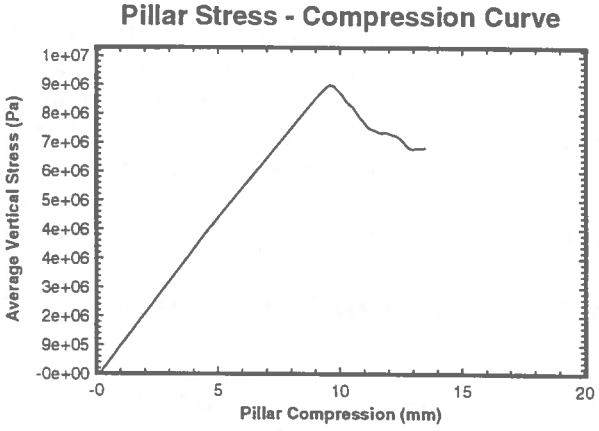

FIG. 3. Stress-Compression curve for 2.5x2.5 meter pillar. The pillar reached a maximum strength of 8.9 MPa before beginning to fail in a controlled manner.

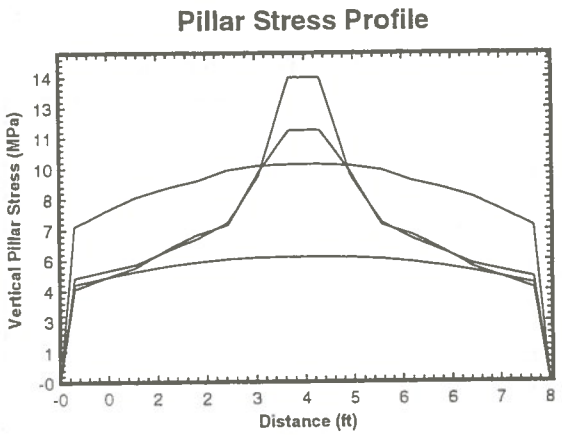

FIG. 4. Vertical mid-rib stresses in test pillar. Pillar stress profiles correspond to points shown on the loading curve in figure 3.

axial deformation in the test pillar is shown in figure 3, and illustrates the ability of the program to reproduce the classic failure mode described by Wagner(1974). During initial loading, the mid-rib stresses rose nearly uniformly as the pillar passed through the elastic and strain hardening portions of its loading curve. Shortly before the pillar reached maximum strength, elements along its edge began to soften, and the pillar became zoned into an elastic core and a strain softening outer skin. Vertical stress profiles at various points along the loading curve are shown in figure 4 and clearly show the progressive nature of the failure.

3.2 Gateroad Design

An additional test problem to determine the mid-rib pillar stresses in a two entry gateroad system was selected as a check on the accuracy of the block motion, contact processing and contact detection algorithms in the DEM-FEM code. The dimensions and relevant material and geometric properties for the model are listed in figure 5. The problem domain was divided into five deformable blocks representing the panels, yield pillar and overlying and underlying country rock. Plane strain, linear elastic conditions were assumed to apply for the country rock, and the coal was modeled as a Mohr-Coulomb material with a cohesive strength of 1.2 MPa and an internal friction angle of 28 degrees. Vertical stresses equal to 110 meters of overburden were applied

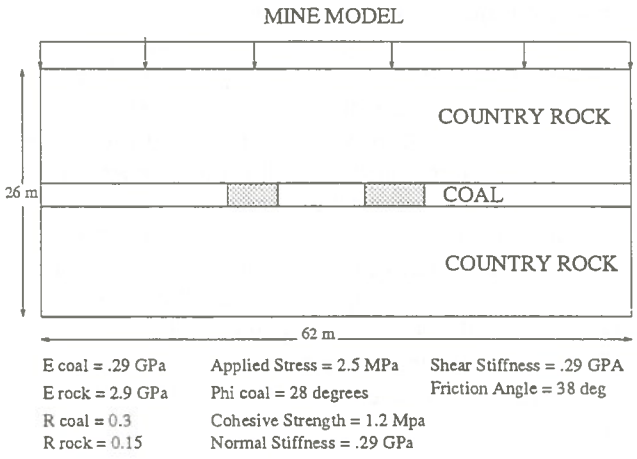

FIG. 5. Model parameters for two entry gateroad test problem.

and the model was allowed model to reach the stress state existing in the rock before gateroad development. After excavation, a fraction of critical damping was applied to the equations of motion governing block movement, and the mesh was allowed to reach a state of static equilibrium.

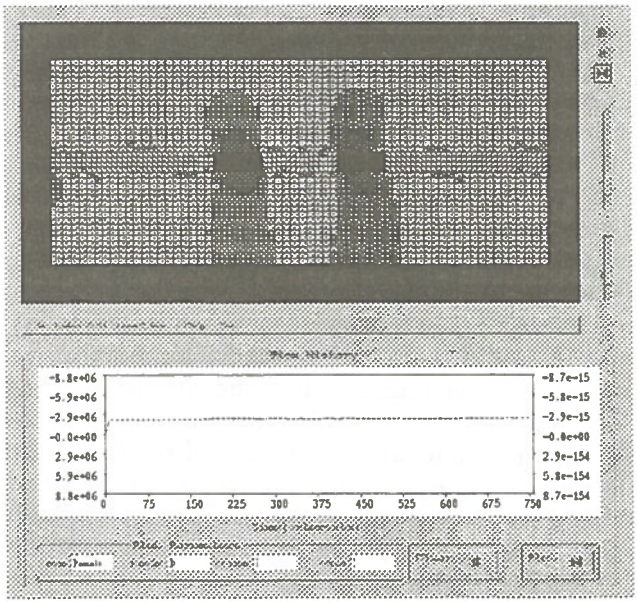

FIG. 6. Vertical stresses around two entry gateroad system after development.

Due to the low stress conditions, the central pillar exhibited mainly elastic behavior with only fourteen of sixty-four pillar elements yielding before the model reached equilibrium. This type of load response is typical of yield pillars upon development and before the passage of the longwall face causes vertical stresses to increase around the gateroads. A profile of the maximum mid-rib vertical stresses in the pillar is shown in figure 6. The plot shows spurious oscilations in the stresses due mainly to lack of adequate edge to edge contact damping between the blocks. This is an area for further research. Although this example problem is conceptually simple, it did allow the authors to verify that the program was transfering stresses correctly across block boundaries.

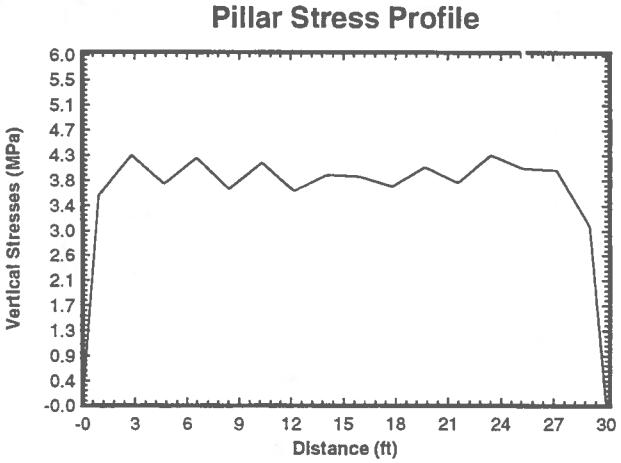

FIG. 7. Vertical mid-rib stresses in gateroad pillar after model reached static equilibrium.

3.3 Future Work

The FEM-DEM software package is still under development, and several additions are planned to make it a more robust tool for geomechanical modeling. Future work includes the addition of a Hoek-Brown plasticity model, a visco-plastic model, and a better contact damping algorithm. The most critical feature yet to be implemented is a more realistic contact model that would allow widely used joint models such as the Barton-Bandis and continuously yielding models to be added to the software. Ultimately, the software will be used to investigate rock mass behavior in heave-prone coal mines. The highly nonlinear behavior of coals and shales contributes to the floor heave problems that are common in these mines, and DEM software capable of modeling deformability is essential for accurate prediction of the extent of heaving.

In addition to the DEM-FEM software, a graphical user interface is being developed that will allow a user to build models, execute program runs, and analyze results directly at the computer screen. The interface is being written using the X-Window Motif library, chosen so that most of the graphics code will be readily portable to other platforms running UNIX.

4 Conclusions

In this paper, an updated Lagrangian approach for treating elasto-plastic block deformability using quadrilateral elements has been described as well as recent U.S. Bureau of Mines progress toward integrating object-oriented discrete element software into a comprehensive graphical user interface suitable for technology transfer to Bureau of Mines customers. This approach to implementing deformable discrete elements may have wide applicability if it simplifies the introduction of more realistic plastic and viscoplastic constitutive models into discrete element models, a necessary step for modeling complex geomechanical phenomena such as coal mine floor heave and mining-induced surface subsidence.

References

[1] Cundall, P.A., 1971,
A computer model for simulating progressive large-scale movements in blocky rock systems. Proc., Int. Symposium on Rock Fracture, Nancy, paper **II-8**, 12 p.

[2] Cundall, P.A., and Strack D.L., 1979, A discrete numerical model for granular assemblies: Geotechnique, **Vol. 29, No. 1**, 47-65.

[3] Hocking, G., Mustoe, G.G.W., and Williams, J.R., Dynamic analysis for generalized three dimensional contact and fracturing of multiple Bodies, NUMETA 87, A.A. Balkema, Rotterdam, 1987.

[4] Barbosa, R., and Ghaboussi, J., 1992, Discrete finite element method: Eng. Computations, **9**, 253-266.

[5] O'Connor, K.M., 1988, Distinct Element Modeling and Analysis of Mining Induced Subsidence, Unpublished PhD thesis, Northwestern University, pp. 175.

[6] Belytschko, T., Nonlinear FEA: explicit methods and crashworthiness: Notes for IBM Sponsored Workshop on Computational Mechanics, Breckenridge, CO, Sept 1990, pp. 96.

[7] Flanagan, D.P., and Belytschko, T., 1981, A uniform strain hexahedron and quadrilateral with orthogonal hourglass control: Int. J. Num. Meth. Eng., **Vol.17**, 679-706.

[8] Baudel, H.J., Abouaf, M., and Chenot, J.L., 1986, An implicit and incremental formulation for the solution of elastoplastic problems by the finite element method: Computers and Structures, **Vol. 22, No. 5**, 801-814.

[9] Chenot, J.L., 1988, Elastoplastic and viscoplastic deformation processes: Eng. Computations, **Vol. 5**, 2-9.

[10] Belytschko, T., and Tsay, C., 1983, A stabilization procedure for the quadrilateral plate element with one point quadrature: Int. J. Num. Meth. Eng., **Vol. 19**, 405-419.

[11] Malvern, L.E., 1969, *Introduction to the Mechanics of a Continuous Medium.* Englewood Cliffs, N.J.: Prentice-Hall, Inc.

[12] Wilson, A.H., 1972, An hypothesis concerning pillar stability: Min. Eng. (London), **Vol. 131, No. 141** , 409-417.

[13] Wagner, H, 1974, Determination of the complete load-deformation characteristics of coal pillars: *in* Proceedings of the Third Congress of the International Society for Rock Mechanics, Denver, CO, 1076-1081.

CAMI'95: 3rd Canadian Conference on Computer Applications in the Mineral Industry
Montréal, Québec, Canada, October 22-25, 1995

Geostatistical Techniques and Multiple Parameter Mapping for Ground Control in Mining

Jennifer Riefenberg
U. S. Bureau of Mines, Denver Research Center

ABSTRACT

Geostatistical techniques have been used for many years in the mining industry for estimating reserves and ore body modeling. A new technological approach, by the U.S. Bureau of Mines (USBM), utilizes geostatistical methods for modeling various geotechnical parameters in underground coal mines to predict ground control hazards. The broad applications in geostatistical analyses for mapping parameters such as mine roof and floor quality may prove to be significant for many mining and rock mechanics applications. Geostatistical tools and methods can be utilized to gain relevant information about roof and floor quality changes, among other factors, even in the absence of abundant data. A brief description of geostatistics and a preliminary case study are presented to demonstrate the incorporation of geostatistics into the Multiple Parameter Mapping (MPM) hazard index.

RÉSUMÉ

Les techniques géostatisticales ont été utiliser pour plusiers ans à l'industrie minière quand on a estimé et on a modelé les rèserves et les gisements minerai. Une technique nouveau qui a développé à le Bureau de Mines des États-Unis, a utilisé les méthodes géostatistiques à modeler plusiers paramètres géotechnicales des houillères souterraines pour prédire les dangers de controlé de terrain. Les grandes applications à l'analyse géostatisticale sont utiliser pour arrangments des paramètres de la qualité de le plafond et le fond de la mine prouve être important pour beacoup des applications de minière et des méchaniques des roches. Les méthodes géostatisticales utiliseront de gagner l'information des changements de qualité de le plafond et le fond même s'il n'y a pas assez des données. Dans l'article on traite une description des géostatistiques avec une étude de cas pour démontrer l'utilsation des géostatistiques dans l'index de danger de Multiple Parameter Mapping (MPM).

INTRODUCTION

One of the major research areas that the USBM is focussed on is understanding the mechanisms and alleviating the hazard associated with ground failure. Although great strides have been made in reducing the number of injuries and deaths associated with mining in the United States, approximately 100 workers are killed and 25,000 are injured each year. Ground control research in underground mines involves identifying causes of failure and taking measures to prevent and/or eliminate the associated hazards. Numerous parameters affect ground control problems including geology, roof and floor quality, pillar and entry design, mining-induced stresses, groundwater, and ground support. Determining what parameters and how much each parameter affects ground hazard is a more difficult task that changes with each site-specific problem. By developing technologies through which numerous parameters may be combined and mapped relative to their locally derived importance level is an effective tool for preventing or eliminating failure. As part of this mapping capability, many geotechnical parameters must be modeled throughout a mining area albeit based on limited data points. Geostatistical modeling provides the capability for systematically mapping field data. Field data that have been incorporated into a systematic map may then be included in a MPM system for further analysis.

BACKGROUND

Geostatistical methods include the application of powerful statistical techniques for analyzing spatial data. For complete discussions on theory and methodology see, for example, JOURNEL and HUIJBREGTS (1978) and ISAAKS and SRIVASTAVA (1989). Utilized heavily in mining for many years, geostatistics have become synonymous with ore reserve estimation. While ore reserve estimation is a significant field, geostatistics cannot be limited to this sole analysis of spatial data. There are numerous potential applications for geostatistics in the analysis of any spatially oriented data. In addition, although the field of geostatistics is built upon solid statistical theoretical methods, one need not be an expert in the theory in order to perform basic geostatistical analyses; similar to not needing to be an expert in statistical methods to utilize standard statistical measures (e.g., mean, median, analysis of variance, etc.). One only need be aware of the potential misuses and recognize the limitations inherent in the data.

A technology is currently under development at the USBM that effectively combines various geotechnical parameters associated with ground control into a single hazard index map. This technology is Multiple Parameter Mapping (MPM), (RIEFENBERG, 1994a, 1995). A critical part of this MPM system is the ability to integrate various geotechnical parameters into a map. The entire processing and mapping sequence is being developed for the personal computing environment.Typically, many of the geotechnical parameters that are important to determining susceptibility to ground failure hazard are only measurable on an irregular set of points in space. Geostatistical analysis is a mechanism for modeling these various, irregularly sampled parameters throughout an area. Few geostatistical analyses pertaining to underground mining in applications outside of ore reserve estimation exist (see, for example, MANAGEMENT ENGINEERS, INC., et. al., 1981). This limited research is due, in part, to the mysticism surrounding geostatistics and the lack of people exposed to the field of geostatistics.

GEO-EAS is a public domain geostatistical analysis software package developed under contract with the U.S. Environmental Protection Agency (ENGLUND and SPARKS, 1986). This package is a powerful tool for compiling general statistics, performing variogram analyses, and estimating using simple or ordinary kriging on spatial data. Geostatistical analysis, in general, is a two-part process: (1) variogram analysis and selection, and (2) kriging, or estimation of missing data on a regular grid. The term kriging is simply a moniker for the specific system of Lagrangian equations used for estimating spatial data. This system of equations is a Best Linear Unbiased Estimator (BLUE) approach and was first introduced by KRIGE (1951, 1970).

EXAMPLE STUDY USING GEOSTATISTICS

Oftentimes limited data points, such as drill core logs and underground observation, are the only available information in mining. Useful information is available from these drill core data and underground observations, although often significant data related to ground control are not collected. For example, with few underground observations and drill core data, roof quality ratings can be determined. Figure 1 shows a plan view mine map schematic drawing with roof quality ratings shown at points corresponding to six underground exposures and 26 drill hole locations. These roof quality ratings are determined using the Coal Mine Roof Rating (CMRR) (MOLINDA and MARK, 1994), which ranks the structural competence of coal measure roof strata on a 0 - 100 scale, with 0 being extremely weak and 100 correspondingly strong. With scattered and limited data points hand contouring to extrapolate roof quality ratings is a limited option at best, with no real methodology to rely upon. A contouring program may provide reasonable results although with no information on the estimation error or ability to place confidence on the estimations. For these reasons, geostatistics appears to be the logical approach to analyzing these spatial data (RIEFENBERG, 1994a, b).

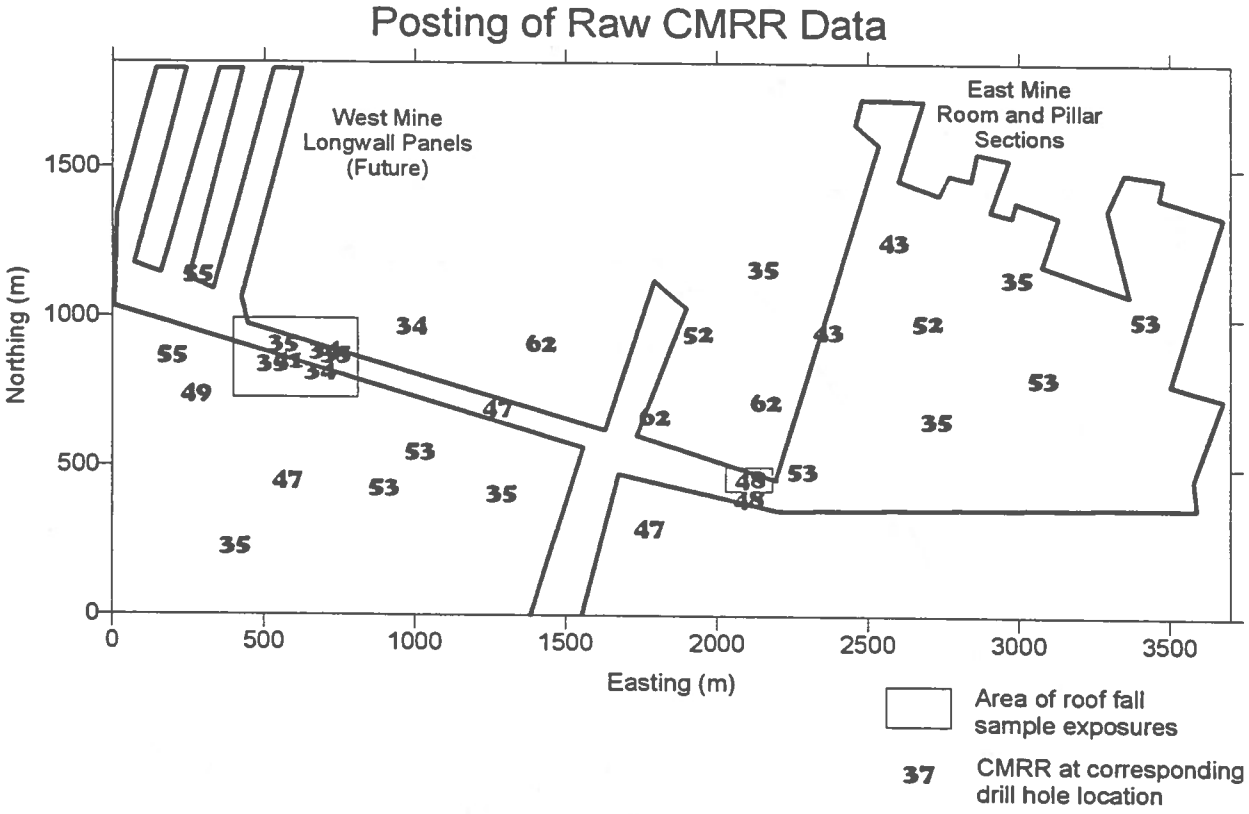

Figure 1. Plan view of generalized mine map with CMRR values from roof exposures and drill hole observations.

As stated previously, geostatistics consists of two parts: variogram analysis and kriging (estimation). Variogram analysis is the determination of a model based upon the variance in the data with respect to their inherent spatial relationship. A variogram is determined using the following equation:

$$(1) \quad \hat{\upsilon}_{ij} = \sigma^2 - \hat{C}_{ij}$$

where $\hat{\upsilon}_{ij}$ is the variogram function, $\hat{C}$ is the covariance between pairs of random variables (i, j), and σ^2 is the sample variance. As shown in figure 2, a plot is made from the data where the independent variable is mean spacing (between data points) and the dependent variable is mean sample variance for this set of points. The figure shows a variogram calculated using the data presented in figure 1. Point A in the figure shows that if an average radial distance of approximately 700 m between data points is used, the average variance value is calculated to be approximately 85 from 44 pairs of data points. A model curve is then determined that best represents the spatial relationship shown on the variogram. The most typical model curves are of the spherical and exponential families, although normal and linear relationships are also sometimes considered. Two assumptions are necessary for this model determination: (1) Data at closer spacings are typically assumed to be more important than data far away from one another; and (2) at some distance away, data typically reach some level beyond which all data points contribute the same importance in estimation (and less than nearer data) - thus the applicability of the spherical and/or exponential model curves. A couple of observations can be made

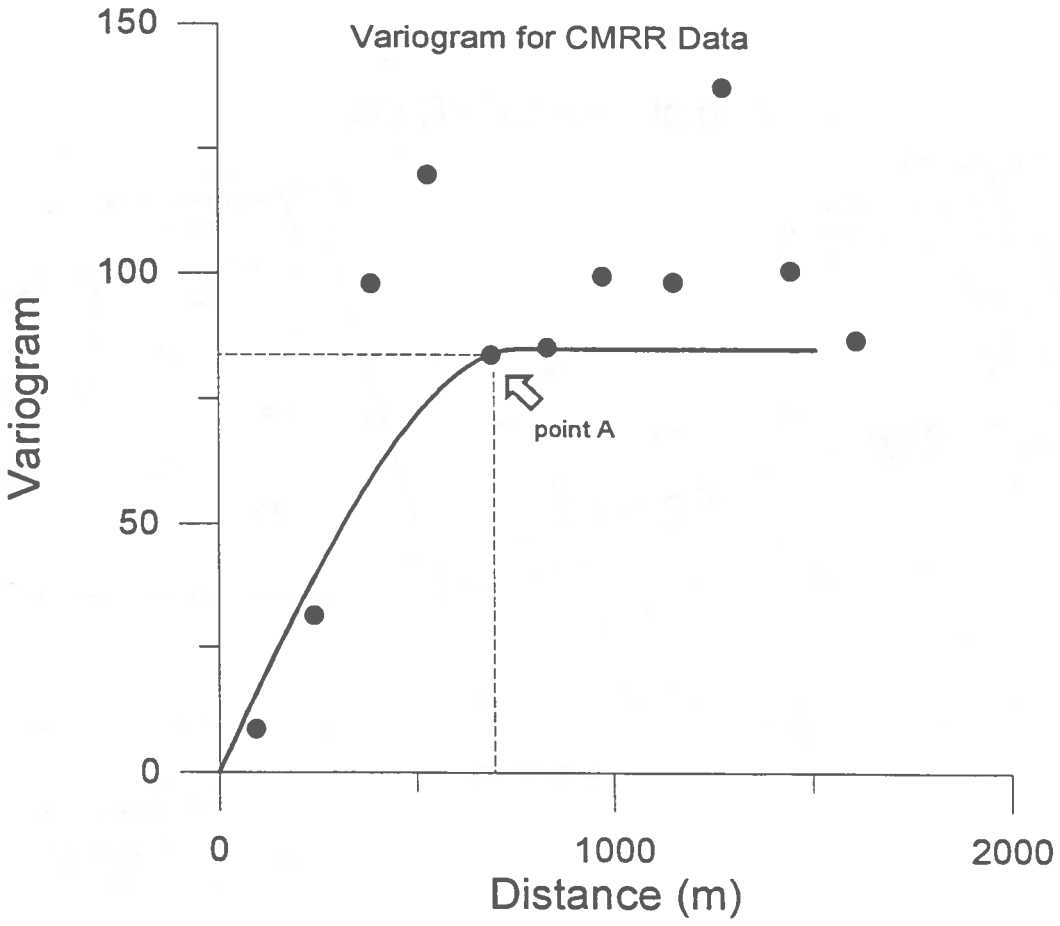

Figure 2. Variogram for CMRR data from roof exposures and drill core observations, also showing spherical model curve. Point A represents an average distance of approximately 700 m resulting in a mean variogram value (variance) of approximately 85.

in analyzing the variogram. One can determine if the data sampling is adequate or if there are "holes" that might need be filled in -- in other words, optimize drill hole sampling (LEDVINA, 1994). One can also determine the orientation and expanse of spatial relationships present in the data. The variogram is a powerful tool for understanding spatial relationships between data points. In addition, the model curve determined from the variogram analysis is used as a starting point in the kriging (or estimation) process. Even using a less-than-ideal variogram resulting from few data points can provide a reasonable map of the data. Confidence is simply a function of confidence in the original data set and any assumptions made.

Kriging, the second part of geostatistical analysis, is the computation of estimates for data on a regular grid. In other words, unsampled areas within the original sample data set are estimated using a system of equations that minimizes the estimation variance. The forms of the kriging equations are as follows:

$$(2) \qquad \sum_{j=1}^{n} w_j \hat{C}_{ij} + \mu = \hat{C}_{i0} \quad \forall\, i = 1, \ldots, n$$

and,

$$(3) \qquad \sum_{i=1}^{n} w_i = 1,$$

where w_j are the j estimation weights, μ is the Lagrange parameter, and n is the number of samples. In practice, the covariances are not actually used but, rather, the variance function, $\hat{\upsilon}_{ij}$, from the variogram (refer to equation 1). In addition, estimation errors are readily computed using the following formula (in terms of the variogram):

$$(4) \qquad \sigma_R^2 = \sum_{i=1}^{n} w_i \hat{\upsilon}_{i0} + \mu.$$

Kriging is performed either using a block or point estimate. The kriging used in this manuscript is known as normal or ordinary kriging. There are many other forms of kriging, such as cokriging, Bayesian kriging, indicator kriging, etc.; however, a description of each of these methods is beyond the scope of this manuscript. A number of references are available that describe each of these methods in more detail.

Figure 3 shows a plot of kriged estimates from the sample set of data presented in figure 2. As shown in this figure, a regular grid of points is plotted with each point an estimation of the roof quality rating, based on the original data points (figure 1). Figure 4 is then a contour plot of the kriged estimates from figure 3. Contouring aids in the visualization of the kriged estimates grid. As mentioned previously, one of the strengths of utilizing geostatistics is that estimation errors are also known. Figure 5 shows a plot of the estimation errors associated with figures 3 and 4. As expected, the error is higher farther from the original data points and lower nearer to the original data points. Confidence intervals may be determined using larger and more complete data sets, assuming determinable distribution of the errors and spatial relationships present in the original data set that can be modeled with a variogram-type curve.

RESULTS

In this simple example, the main result from the geostatistical modeling of roof quality ratings is the development of a mine-wide map from which a hazard potential map is based. Those areas exhibiting relatively weaker roof and/or those areas where dramatic changes in roof quality occur over a small radius may indicate potential roof control problem areas as mining progresses. The east side of the mine is sealed thus there are no opportunities to investigate roof falls in this area. However, according to historical accounts from the mine, areas in the (sealed) northcentral portion of the east mine experienced severe ground failure conditions. These general bad ground areas occur in relative agreement with those areas modeled to show weakest roof. Based on past experience, one might expect similar ground conditions in the current mining area to the southwestern side of the mine. Indeed, and unfortunately, poor ground conditions have been experienced in the current section. In this example, further analysis is warranted; however, preliminary reassessments of the existing ground control plan should be considered and based on past experience in similar "hazard" areas.

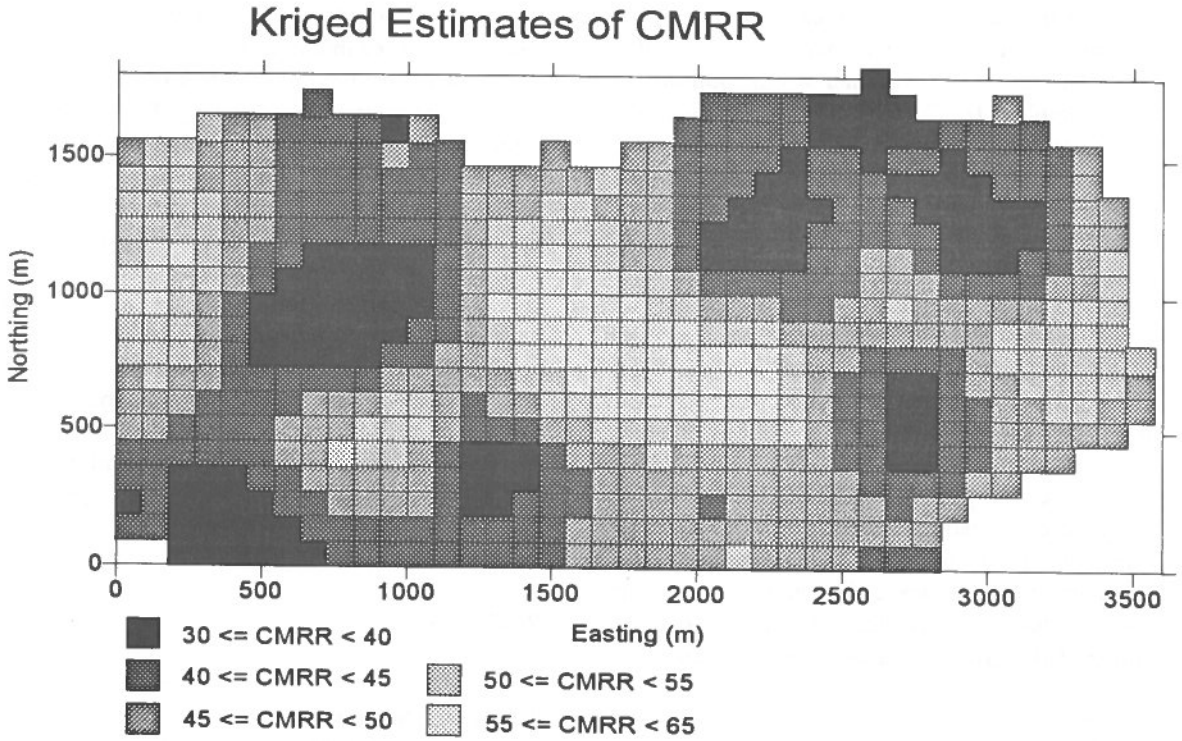

Figure 3. Modeled CMRR using kriging for estimation.

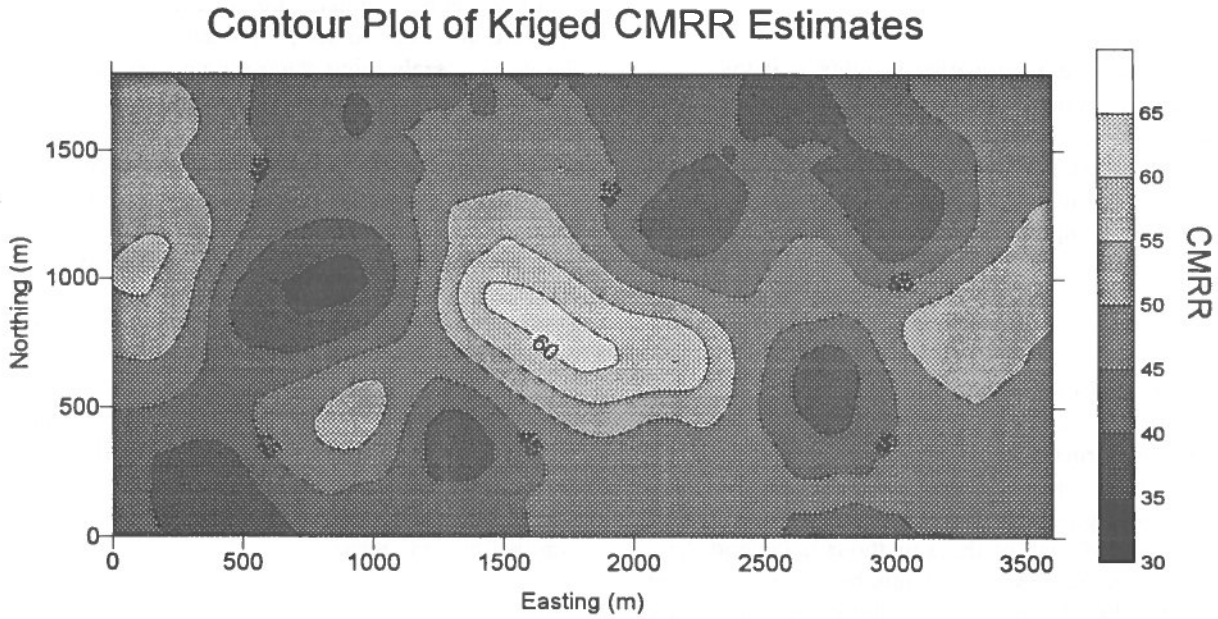

Figure 4. Contour plot of CMRR's modeled using kriging (geostatistics).

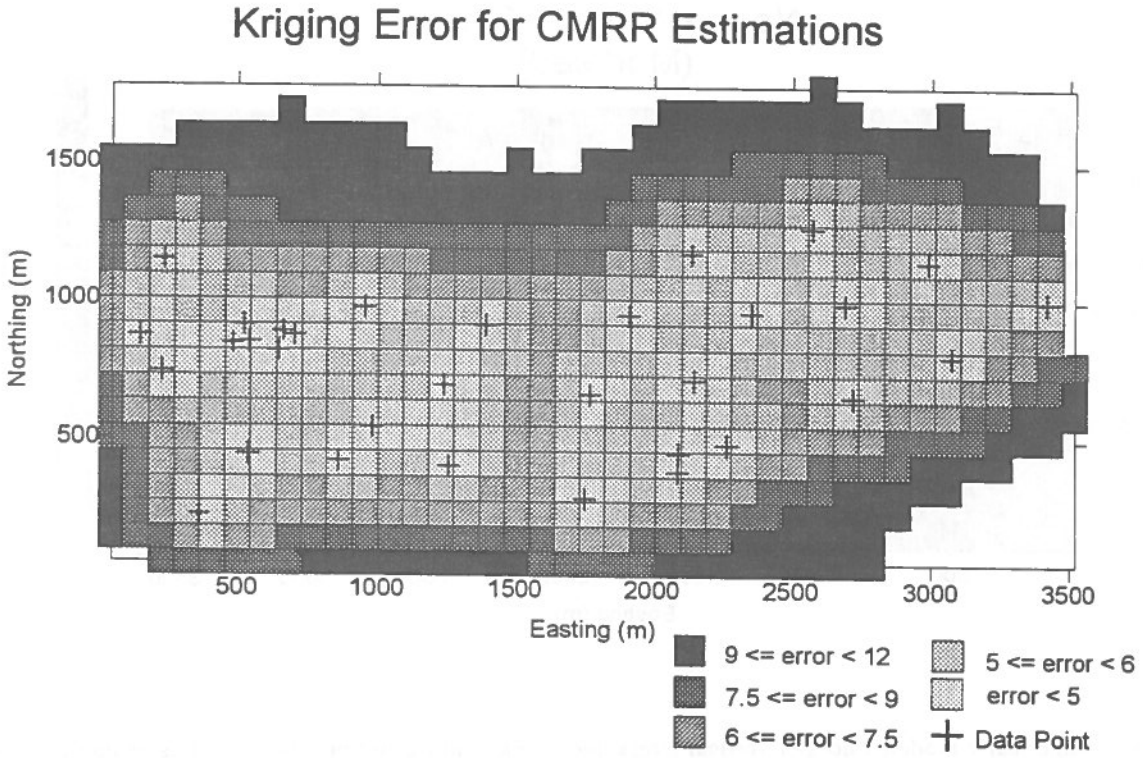

Figure 5. Plot of kriging error (kriging standard deviation) resulting from model CMRR estimations. Note that lowest error is nearest to actual data points, as would be expected.

FUTURE DIRECTIONS - MULTIPLE PARAMETER MAPPING (MPM)

Multiple Parameter Mapping (MPM) is an extension of the example presented in this report. MPM advances the process significantly through the ability to combine various geotechnical parameters into a single hazard index map. For a more complete discussion of the MPM technology see RIEFENBERG, 1995. Geographic Information Systems (GIS) technology is also a useful method for overlaying multiple parameters onto a single display; however, typically, these displays show only cut-off values for the various parameters, whereas MPM retains the continuity inherent in the data. Geostatistically modeled parameters are combined with other parameters (such as stresses determined using numerical modeling techniques) into a single hazard index and then mapped. Figure 6 shows a map of the numerically modeled vertical stress corresponding to the example in the report. In this example, only current mining (the East mine side) has been modeled. Figure 7 shows an example hazard map using the MPM method that is a weighted combination of geostatistically modeled CMRR and numerically modeled vertical stress, where the CMRR was assumed approximately twice as important as the stress. Thus, the map in figure 7 is roughly 2*CMRR + Stress. Note that both the hazard potential areas as indicated by the CMRR model (figure 4) and additional high-stress areas (figure 6) are retained. With this approach, hazard recognition and potential may be better delineated and implemented into the mine design and support processes.

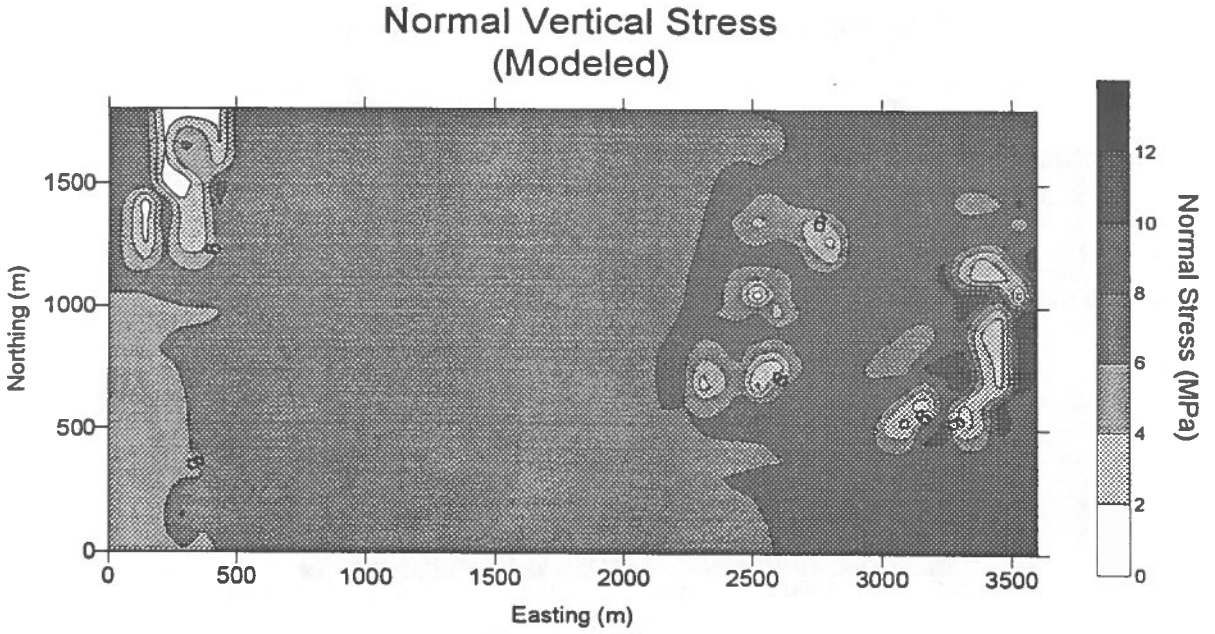

Figure 6. Numerically modeled normal vertical stress due to material extraction. Note, in this example, current and future mining (of the west mine) have been modeled.

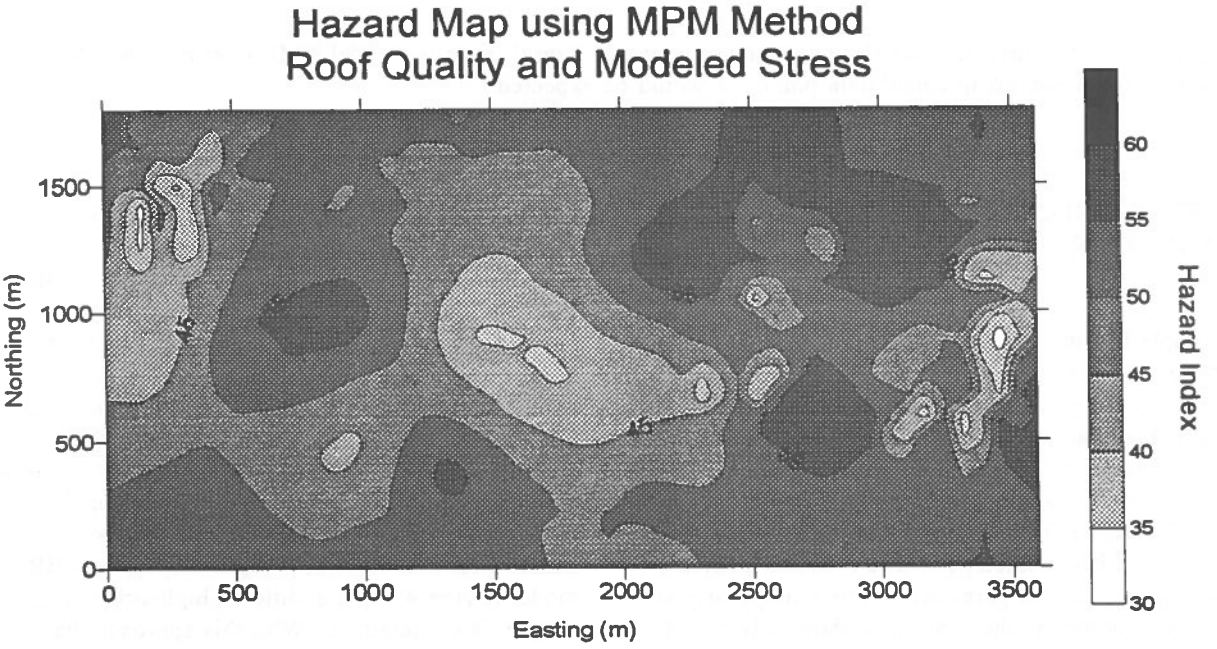

Figure 7. Example hazard index map using MPM technology. Map is a composite of CMRR and numerically modeled stress. Hazard index scale of (0 - 100) with 100 representing greatest relative hazard potential.

REFERENCES

ENGLUND, E. and SPARKS, A., 1988.
GEO-EAS (Geostatistical Environmental Assessment Software) User's Guide. Environmental Monitoring Systems Laboratory, Office of R&D, U.S. EPA, Las Vegas, NV, 196 pp.

ISAAKS, E. H., and SRIVASTAVA, R. M., 1989.
Applied Geostatistics. Oxford University Press, New York, Oxford, 561 pp.

JOURNAL, A. G., and HUIJBREGTS, Ch. J., 1978.
Mining Geostatistics. Academic Press, San Diego, CA, 600 pp.

KRIGE, D. G., 1951.
A Statistical Approach to Some Mine Valuations and Allied Problems at the Witwatersrand. Unpublished Master's Thesis, Univ. of Witwatersrand.

KRIGE, D. G., 1970.
The Role of Mathematical Statistics in Improved Ore Valuation Techniques in South African Gold Mines. Topics in Mathematical Geology, Consultants Bureau, New York and London.

LEDVINA, C.T., et. al., 1994.
Geostatistical Guidance of Exploration in Roof Control - How Many Drill Holes are Enough? Proceedings of the Fifth Conference on Ground Control for Midwest U.S. Coal Mines, Ed. by Y. P. Chugh and G. A. Beasley, Collinsville, IL, pp. 14 - 30.

MANAGEMENT ENGINEERS, INC., et. al., 1981.
Application of Geostatistics to Coal Resource Characterization and Mine Planning: Final Report. DOE/PC/30113-T7, 260 pp.

MOLINDA, G. M. and MARK, C., 1994.
The Coal Mine Roof Rating (CMRR): A Practical Rock Mass Classification for Coal Mines. USBM IC 9387, Pittsburgh, PA, 39 pp.

RIEFENBERG, J., 1994a.
Hazard Mapping Combining Geostatistical Modeling of Coal Mine Roof Quality Ratings with Numerical Modeling of Stress Data. Proceedings of the 13th International Conference on Ground Control in Mining, Morgantown, WV, pp. 261-268, 1994a.

----, 1994b.
Geostatistical Modeling of Coal Mine Roof Quality for Hazard Mapping. Proc. of the 5th Conference on Ground Control in Midwestern U.S. Coal Mines, Collinsville, IL, pp. 31 - 40.

----, 1995.
Multiple Parameter Mapping and Geostatistical Modeling of Coal Mine Roof Quality. Proceedings of the Third Int'l. Symp. on Mine Mech. and Automation, June, 1995, (to be published).

CAMI'95: 3rd Canadian Conference on Computer Applications in the Mineral Industry
Montréal, Québec, Canada, October 22-25, 1995

Application of Computer Models to Underground Coal Mine Design in the Sydney Coalfield, Nova Scotia.

Peter Cain
Section Head, Strata Control,
CANMET-MRL Cape Breton Coal Research Laboratory, Sydney, N.S.

ABSTRACT

Numerical modeling of coal mine structures is complicated by the complex material properties and the development of yield zones around openings at even the most shallow depths. Simple elastic models can give only the broadest indications of anticipated conditions. More complex models, incorporating non-linear material properties and the definition of failure zones, are now available, although even these cannot provide definitive values of stress and closure.
Numerical models have only recently been applied to the geomechanics problems of the Sydney Coalfield, and their use has been restricted to fairly simple situations lending themselves to incremental design. The paper describes three examples of applications in the Sydney Coalfield.

RESUME

La modélisation numérique des mines de charbon est rendue plus difficile à cause des propriétés complexes des matériaux et du développement des zones de rupture autour des ouvertures, même à la plus faible profondeur. Les modèles simple élastique ne peuvent donner que des indications générales des conditions anticipées. Des modèles plus complexes qui comportent des propriétés non linéaires des matériaux sont présentement disponsibles, malgré que même ceux-ci ne peuvent donner les valeurs exactes des contraintes et des déformations.
Les modèles numériques ont été récemment utilisés dans les problèmes de géomécanique au Sydney Coalfield. Leur utilisation a quand même été limitée aux solutions simples. Cette publication explique trois exemples d'application dans Sydney Coalfield.

INTRODUCTION

Numerical modeling for mine design is an accepted practice in the hard rock mining industry where elastic rock properties allow for fairly simple model formulation and therefore generally short execution times. In soft rock mines, particularly coal mines in which extensive failure of the rock occurs around openings, the model formulation must be more complicated to reflect the rock properties and behaviour.
The complexity of models suitable for application in soft rock environments used to restrict them to mainframe platforms, with the result that modeling was time-consuming and expensive. The rapid development of powerful personal computers (486 and 586 chips, large RAM capacity and high capacity hard disks) now allows many of these programs to be run at

the desktop. The salt and potash industries have benefited from this in particular, with several programs (e.g., FLAC) now available for sophisticated modeling of evaporite mining environments.

Numerical models fall into a number of categories, based on the theoretical methods used. These categories are shown in Table 1, along with some examples of those that have been used in coal mining applications. This paper does not purport to be an exhaustive treatment of the subject of numerical modeling. The examples given are those which have been evaluated at some time or another for use in the Sydney Coalfield.

TABLE 1: Categories of numerical model, with examples used in coal mines

Type of Model	Examples
Finite Element - Linear Elastic	SAP2D[1], MSAP2D[2]
Finite Element - Other	PCEPFE[1], EZ-TOOLS[2], NUFEP[3], FEOMP[4]
Finite Difference	FLAC[5]
Boundary Element - Direct Method	PCBEM[1]
Boundary Element - Displacement Discontinuity	MULSIM/NL[6], PCMINTAB[1]
Influence Function Models	SUBCALC[3], SWIFT[3]
Other Theoretical Models	ALPS[6], MONVER[6]

Sources: 1: CANMET-MRL; 2: McGill University Mining Department; 3: Nottingham University Mining Department; 4: University of Edmonton Mining Department; 5: Itasca Inc.; 6: USBM.

The case histories described below are those modeling applications that best describe the current use of models in the coalfield. At present, these applications are in the fields of strata interaction (NUFEP, MULSIM), subsidence (SWIFT), and the use of the model FEOMP to examine the potential for sandstone/gas outbursts. Those readers interested in a more complete treatment of the various modeling techniques are referred to the sources given and to Brown (1987).

STRATA INTERACTION

The longwall coal faces of Phalen Colliery in the Sydney Coalfield of Nova Scotia extract coal from the Phalen Seam lying about 140 m beneath extensive workings in the Harbour Seam.

The Harbour Seam workings are the result of extraction carried out in Lingan and No. 26 Collieries. Although the No. 26 workings have been flooded since about 1984 following the closure of the mine, the Lingan workings were dry. The collieries were separated by a barrier of solid coal of between 90 and 300 m in width.

In 1993, while the 5 East Panel at Phalen Colliery worked underneath this barrier pillar, a substantial quantity of water broke through from No. 26 Colliery workings immediately above and into the previously dry Lingan workings. This unexpected incident resulted in the closure of Lingan Colliery and the formation of an hydraulic connection between the No. 26 and Lingan Colliery workings (Cain et al, 1994).

Phalen Colliery was now working under two sets of flooded workings, and the Cape Breton Development Corporation (CBDC) was concerned about the possibility of an hydraulic connection developing between the now abandoned, flooded, Harbour Seam workings and the working Phalen Colliery below. As part of the Joint Collaborative Research Agreement between CBDC and CANMET, the Cape Breton Coal Research Laboratory undertook to investigate the effects of working adjacent coal seams using two different numerical models.

(1) The Mining Department of Nottingham University (UK) was contracted to model the interaction between the Harbour and Phalen Seams using its non-linear finite element model, NUFEP. This work explored the relationship between mine layout and the development of tensile strains in the overlying rock mass. Tensile strains high enough to result in open fractures would present significant risks of water flow from the abandoned Harbour Seam into the active Phalen Seam workings below.

(2) CBCRL staff assisted CBDC by using a numerical model to try to predict loads on pillars left in the Harbour Seam. This work formed part of a hazard

analysis study compiled by CBDC. The analysis included consideration of a number of geological and mining factors, one of which was the remnant stress at the Harbour Seam horizon after extraction. This was modeled using MULSIM/NL, a boundary element (displacement discontinuity) method developed by the USBM at Denver (Zipf, 1993).

Recent work has shown that a direct connection, with the consequent possibilities of a major inrush, is not likely, although research continues to develop an understanding of the effect of mining interaction and interburden permeability.

The NUFEP Model

NUFEP was developed by the Nottingham University Mining Department in the U.K. to model both surface subsidence and interaction effects. The finite element model allows the user to model post-failure properties of the rock based on a modified Mohr-Coulomb failure criterion under transversely isotropic plane strain conditions. During the calculation process the model determines whether an element has failed based on the failure criterion, and then calculates new Young's Modulus values. Lower post failure modulus values result in more dramatic post failure movement. The model itself is described in more detail elsewhere (CANMET, 1994).

To increase the degree of confidence in the model output, NUFEP was calibrated against predicted subsidence values for a range of extraction geometries. Subsidence prediction methods used in the UK are fairly advanced and have proved to be accurate to within ±10% in most cases. Model output was compared to subsidence predictions and model parameters - specifically material properties - were adjusted until the subsidence predicted by NUFEP closely matched that predicted by standard design methods.

By calibrating the model to accurately predicted surface movements, it is anticipated that subsurface movements, especially the tensile strains developed in the interburden between the two seams, will reasonably represent those found in-situ. The development of subsidence in the Sydney Coalfield has been shown to differ somewhat from the UK (CANMET, 1993). However, at the width-depth ratios of the panels modeled, there is little difference between the Sydney Coalfield subsidence development and the subsidence developed over panels in the UK. The results obtained are therefore probably fairly close to those that would be seen on a fully calibrated model. Stress predictions, however, are not calibrated, and are therefore regarded with some caution.

Modeling Results

NUFEP was used to predict stresses and strains induced between the Phalen and Harbour Seams as a result of extracting five longwall panels, three in the Harbour Seam, and two in the Phalen Seam below. The modeled mining sequence was the same as the mining sequence in-situ (Reddish et al, 1994).

Figure 1 illustrates the modeled strata displacement after completion of mining all panels. The development of a subsidence profile is clearly indicated. More significantly, the displacement of the Harbour Seam pillars towards the Phalen Seam is clearly shown. This effect has been observed in many coalfields, where the subsidence developed over pillars has appeared to be larger than obtained by subsidence calculations. The drawback of many subsidence calculation procedures is that they do not take into account pillar failure or floor punching, both of which can contribute to the amounts of subsidence observed at the surface.

Figure 2 shows the contoured tensile strains developed in the model. Zones of tensile strain greater than 10 mm/m are shaded. The strains indicated are maximum strain vectors, and do not necessarily correspond to horizontal strain values often quoted as subsidence guidelines..

Low strains are indicated around and above the centre panel in the Harbour Seam, with strain abutments at the edges of the extracted area. Tensile strain concentrations occur at the pillar edges in the Harbour Seam, and on the dip sides of panels in the Phalen Seam. A concentration of tensile strains appears as a band between the dip side of Phalen 4 East and the rise side of Harbour 2 East.

Strain concentrations at the pillar edge indicate a potential cause for concern with respect to the development of interburden fractures where pillars in the Phalen Seam are offset from those in the Harbour

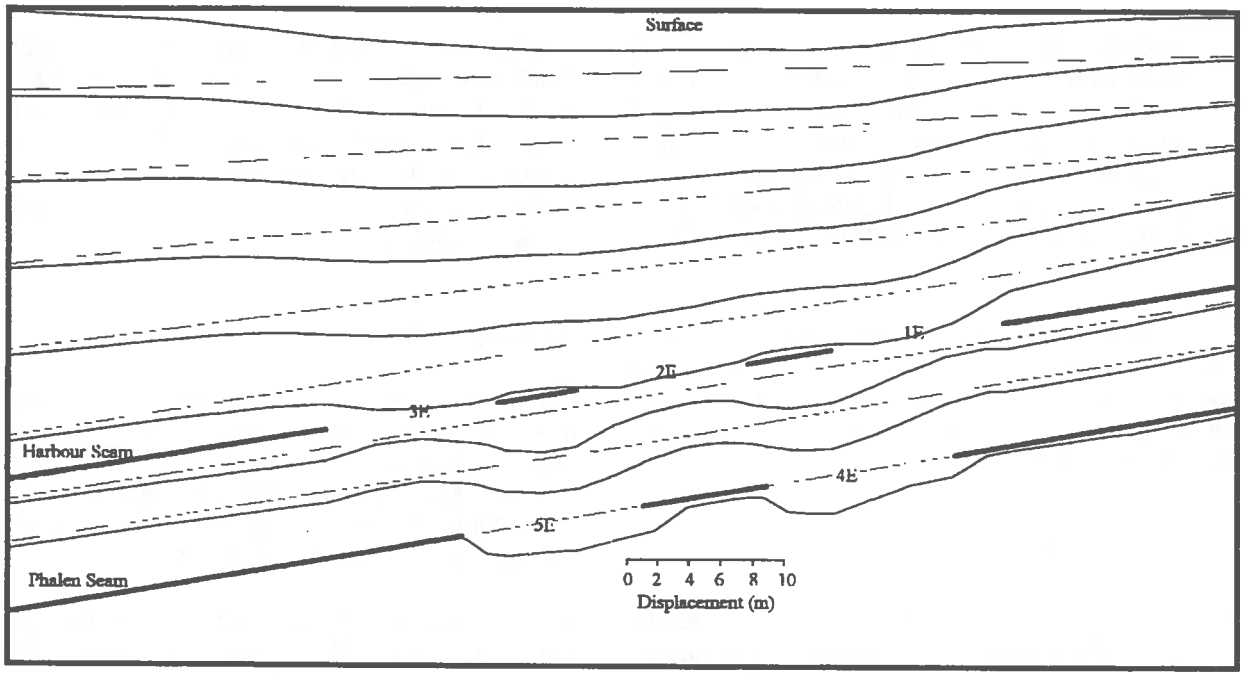

Figure 1: Strata displacement at selected horizons modeled by NUFEP

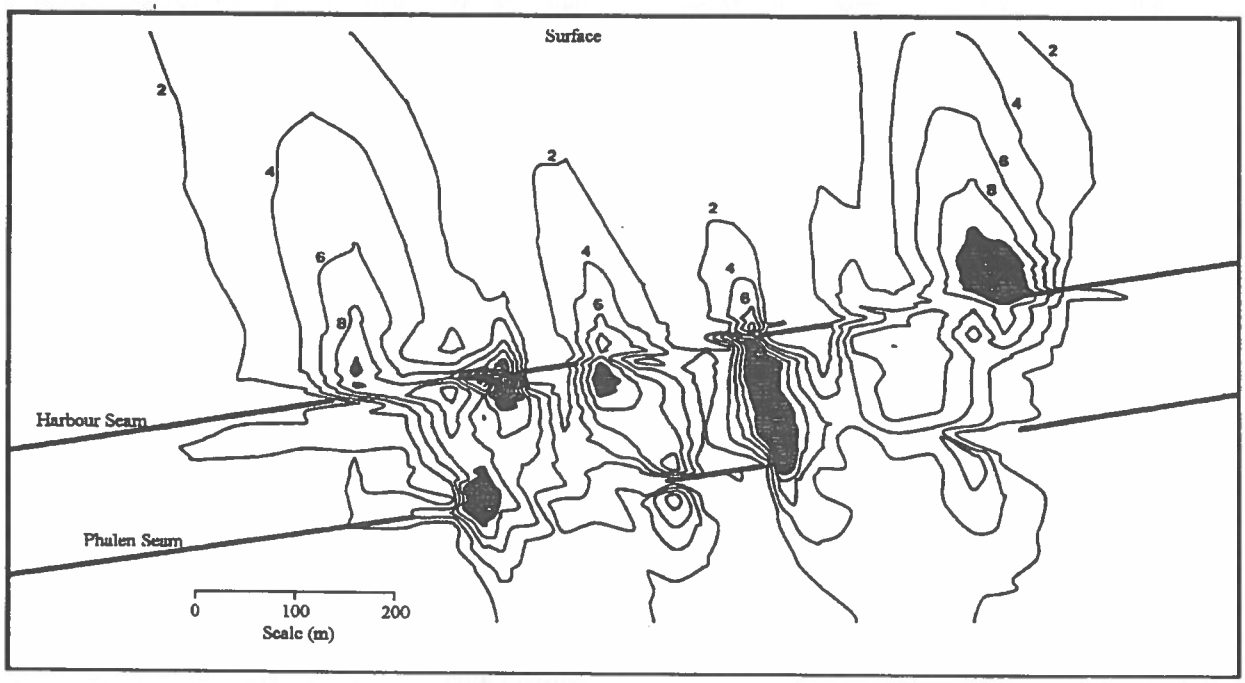

Figure 2: Strains modeled by NUFEP (shaded areas represent strains > 10 mm/m)

Seam. These fractures could theoretically provide pathways for the migration of water between the workings.

Contoured minor principal stress (surcharge) results (Figure 3) show a similar but less well defined pattern to the strain values. Surcharge loads are concentrated at outside pillar edges, and there is a zone of surcharge loading that corresponds to the strain concentration between the dip side of Phalen 4 East and the rise side of Harbour 2 East.

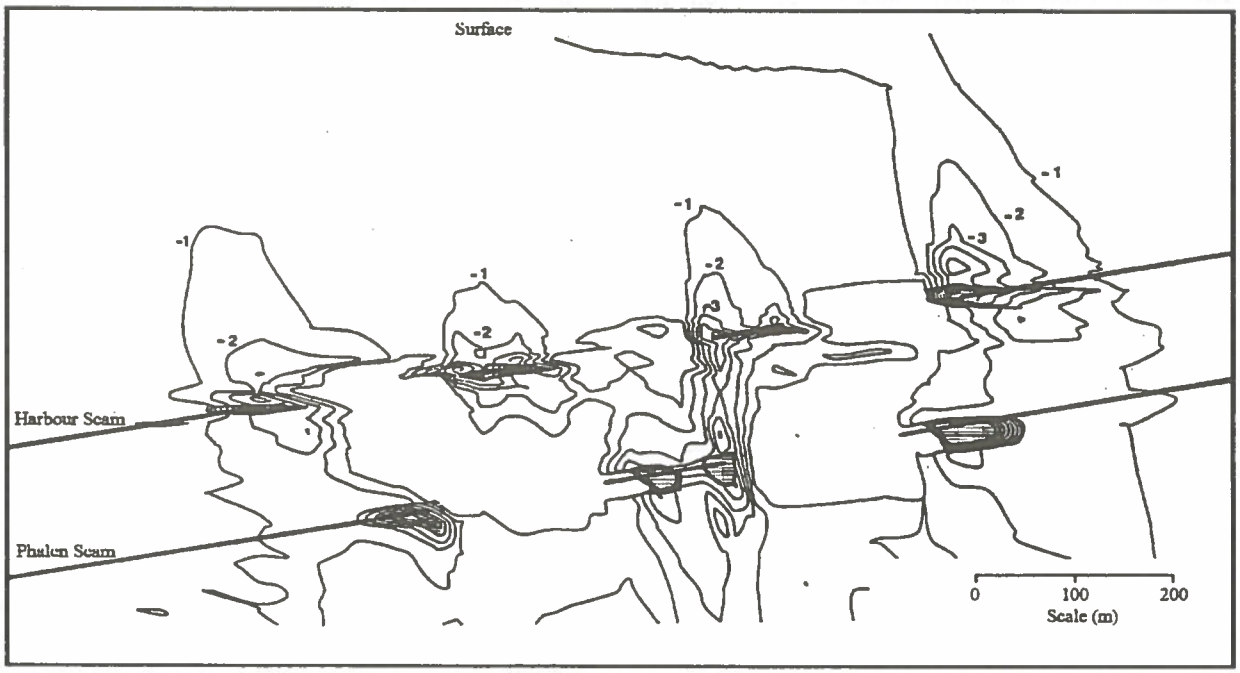

Figure 3: Surcharge Stresses modeled by NUFEP

MULSIM/NL

The USBM version of MULSIM (MULSIM/NL) is an updated and enhanced version of numerical mine modeling software originally developed by K.P. Sinha (1979). Designed to perform structural analysis of parallel multiple coal seams; it employs a variation of the boundary element method known as three-dimensional displacement discontinuity. This modeling technique sees the coal seam described as a grid in plan view and then calculates the stresses and ground movements that result from "extraction" of grid elements (Zipf, 1993).

The mine area to be modeled is divided into a coarse mesh of square blocks. The area of detailed interest is further subdivided into a finer mesh of elements that represent either mined or unmined sections of the coal seam. Stresses and displacements are calculated at the element level based on the interactive effect of element

displacements for the entire model. Model stiffness is calculated from seam elasticity coefficients derived from the elastic properties of the rock mass (Young's Modulus, Poisson's Ratio). MULSIM/NL allows a 50 x 50 coarse grid and a fine mesh array of up to 150 x 150 (120 x 120 for PC's with only 4Mb of RAM).

MULSIM/NL has the capability to model twenty-six unique material properties and to distinguish between the seam and packing materials. These materials may be based on any of six material models, as follows:

- linear elastic,
- strain softening,
- elastic plastic,
- bilinear hardening,
- strain hardening, and
- linear elastic gob materials.

The model assumes that the seam bearing rock-mass is homogeneous and it is not recommended for use in areas where significant faulting occurs. This is the major disadvantage of the model. It is MULSIM's ability to model multiple coal seams (two in the PC version, four on mainframes) that separates it from its competition and makes it an attractive modeling tool for use in the Sydney Coalfield.

Modeling Results

The area of interest in the Harbour Seam was gridded in 50 m squares. The percentage extraction in each of these squares was determined using a proprietary drafting package. The entire area of interest was too large to be modeled in one run, so it was divided into six blocks, each of which was 1000 m square. Each MULSIM run modeled a 1500 m square block, the overlap being necessary to eliminate edge effects.

The seam materials were modeled based on the percentage extraction, with the elastic and shear modulus values reduced in proportion to the percentage extraction. Linear elastic material properties were selected, and longwall wastes were modeled as totally extracted (i.e., no attempt was made to allow for support offered by the compacted gob). This approach was selected for two reasons. Firstly, the purpose of the model was to indicate zones of stress concentration, rather than actual stress values. Secondly, the model grid was considered too coarse to benefit from the use of other material properties, which would have increased the run times of the model.

The model was run as a single stage model, and the normal stress data for each block was extracted as a text file using the MULSIM/NL post-processor, and concatenated to produce a single file for the entire area. This file was further processed to add the ratio between the modeled stress and the predicted in-situ vertical stress, to normalize the data for presentation.

The results of the modeling (normalized stress levels) for a 1000 m by 3000 m block are shown in Figure 4. The layout of the Harbour Seam workings can be seen from the stress surcharge on the pillars, and the stress relaxation in the panels. It is the concentration of stresses that is thought to be responsible for the development of fractures from which the two sandstone aquifers above the Phalen Seam can drain into the workings.

Future work will include the modeling of the Phalen Seam extraction, in sequence, to indicate possible dynamic effects on the Phalen Seam, and possibly the inclusion of non-linear material properties. It may also be possible to determine stress levels at some intermediate horizon to determine the potential for fracture development.

SUBSIDENCE

Considerable effort has been directed towards the development of a subsidence prediction model for the Sydney Coalfield based on local case history data. The compilation and evaluation of local case histories are described by CANMET (1993). As a result of that work, it was possible to develop a subsidence prediction model, SWIFT. Details of the model and it's development are described in CANMET (1994).

The SWIFT Model

The SWIFT model is an upgrade of the SUBCALC model (CANMET, 1993) developed initially by the University of Nottingham, UK. The SUBCALC program code has been substantially optimized by development of common subroutines, and it has been compiled in the TurboPascal programming language. In addition to modifications to program structure, the user interface has been re-worked to be more user-friendly, and view screens incorporated for checking data.

An influence function is used to describe the amount by which an underground extraction affects the surface. Assuming an infinitesimal element at depth H to be extracted, it will create an elementary trough at the surface; the deepest point of the trough is vertically over the extraction element, and the trough decreases towards to the limit line. The amount of subsidence at an arbitrary point in the trough varies according to its position. Consequently the subsidence can be stated as a function of the position of the point by means of either radial distance from the trough central point, or the zone angle.

Conversely, it is also possible to start from a surface point above an extraction area, and find the amount of influence caused by the extraction. The extraction area can be divided into a number of extraction elements, and each of the elements has a different influence on the amount of subsidence at the surface point because of their different positions. Any extraction outside the influence area will have no effect on the surface point. The amount of influence caused by an extraction element is determined by the so called influence function. From the view of reciprocity, the influence function profile should coincide with the function of an elementary trough profile. An influence function actually reflects the effect of an extraction element on the surface. There are many kinds of influence functions; they are either derived empirically or are based on theoretical assumptions. Both models, SUBCALC and SWIFT, its derivative developed for this work, use the stochastic influence function.

Displacement can be calculated with the aid of the focal point theory. This assumes that each extraction element exerts an influence on a surface point such that it attracts the point to move towards it by an amount. This movement vector can be analyzed into two orthogonal components. The component in the

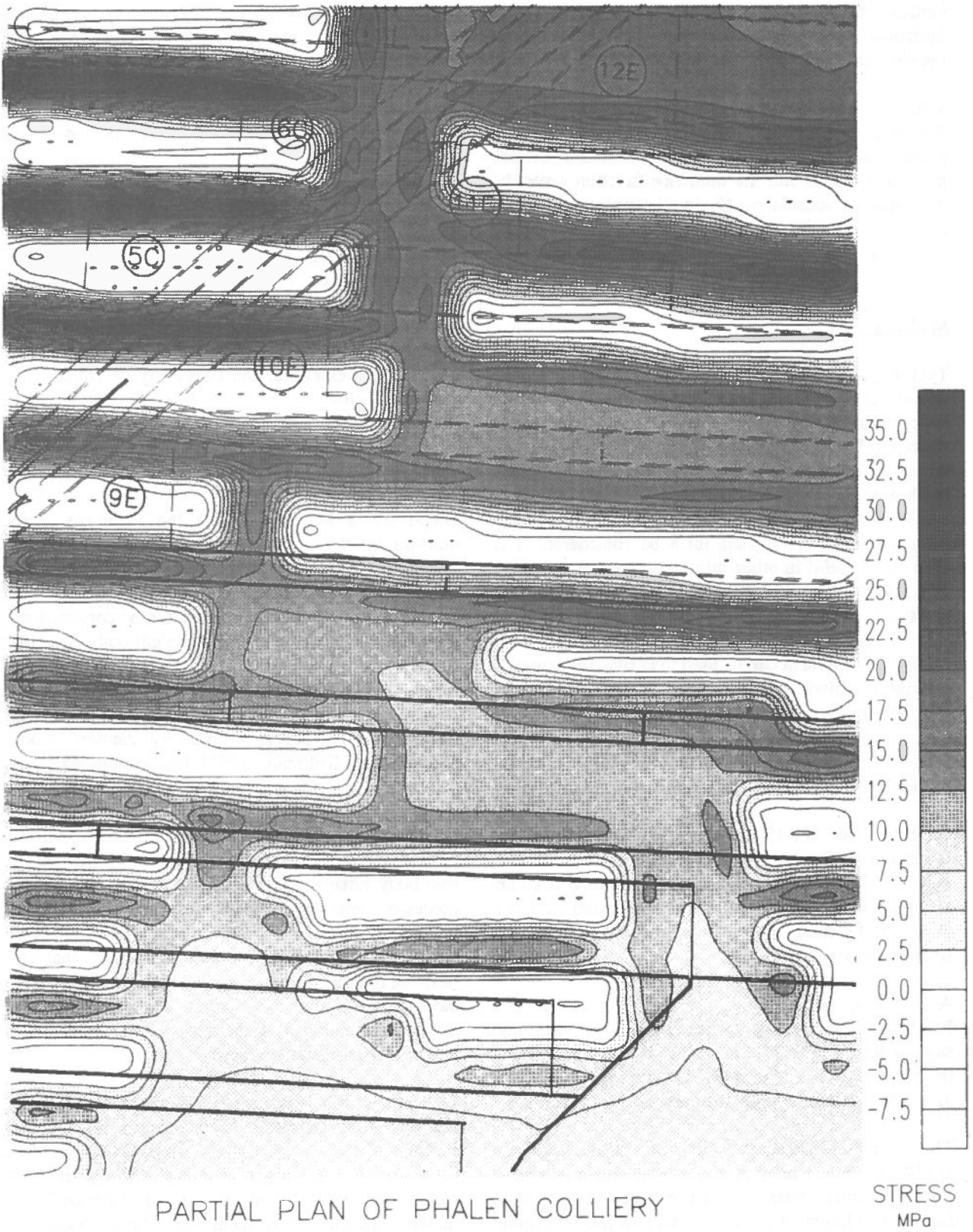

Figure 4: Residual Stresses in the Harbour Seam predicted by MULSIM/NL overlaid on a plan of the Phalen Seam

vertical direction is subsidence, and the other is horizontal radial displacement caused by extraction of the element.

With this assumption it is possible to calculate the displacement in conjunction with the subsidence. Focal point theory actually provides the directions of surface point movement, and the influence function gives the magnitude of subsidence. Having determined these two factors the amount of horizontal displacement can be calculated.

Modeling Results

Typical prediction results are shown in Figure 5. The subsidence and strain values from the model output file have been plotted using a proprietary spreadsheet package. A major advantage of SWIFT is that it can produce a subsidence profile over any line or surface (within certain limits relating to the number of points). While this is useful in coal mining applications if the influence of several panels must be considered, it is even more useful in other mining environments where extraction of irregular shapes and thicknesses is practiced. Because subsidence values are based on a calibrated influence function, field data from any mining environment can be used to derive the required calibration values, and the model adapted to a wide range of mining environments.

SANDSTONE/GAS OUTBURSTS

On September 28, 1994 Phalen Colliery suffered its first sandstone/gas outburst. The outburst occurred in a main development at a depth of 697 m, and released an estimated 1350 m^3 of gas (mostly methane) into the mine. Eight mine arches were destroyed, and one worker was seriously injured.

At the time of the event, a Voest-Alpine AM 75 Roadheader was cutting out the face prior to installing steel arches. The cutting head was in sandstone when the event occurred. The AM 75, which weighs nearly 52 t, was displaced 2 m by the outburst.

The event itself presented a dilemma. All development at Phalen Colliery is by mechanical means to maintain the development rates required to support production from retreat longwall coalfaces. Much of the remaining coal is closely overlain by a thick (5 to 25 m) bed of sandstone. The base of the sandstone is an irregular erosive contact that frequently approaches, and sometimes erodes, the coal seam. The accepted method of countering sandstone/gas outbursts - boring and firing with men in safe areas - would slow development advance and seriously jeopardize the economic viability of the mine.

A muti-facetted research program has been established jointly between CBCRL and CBDC to investigate the problem (Cain, 1995). The research involves investigation of material properties, in-situ gas pressures, microseismic monitoring and investigation of safe mining methods for outburst prone ground. An useful tool in this work is the numerical model FEOMP, developed at the University of Alberta, and described below.

FEOMP

Based on a knowledge that the principle factors controlling the initiation of an outburst were the effective stress regime at the point and time of failure and the properties of the rock , it seemed reasonable to assume that a numerical model could be constructed to simulate the initiation of sandstone/gas outbursts.

Chen (1994) described the development of a finite element model to simulate outburst initiation. This was developed after previous boundary element models (Barron and Kullman, 1994) had demonstrated the concept.

The finite element model simulates perfect elastic-plastic rock materials. Gas pressures are simulated as a true body force in the model. After each run, a post-processor determines which elements have failed in tension, which have failed in shear, and which are stable. The program then removes elements that have failed in tension (to simulate an outburst), and de-gases those elements that have failed in shear. The model then iterates until either the cavity shape stabilizes, or the cavity progresses to infinity.

The model has successfully predicted initiation of sandstone gas outbursts from outburst sites during calibration testing, although as expected the results are sensitive to the input material properties. The dimensions of cavities obtained using the model have shown reasonable agreement with those observed at outburst sites. Parametric studies conducted using the

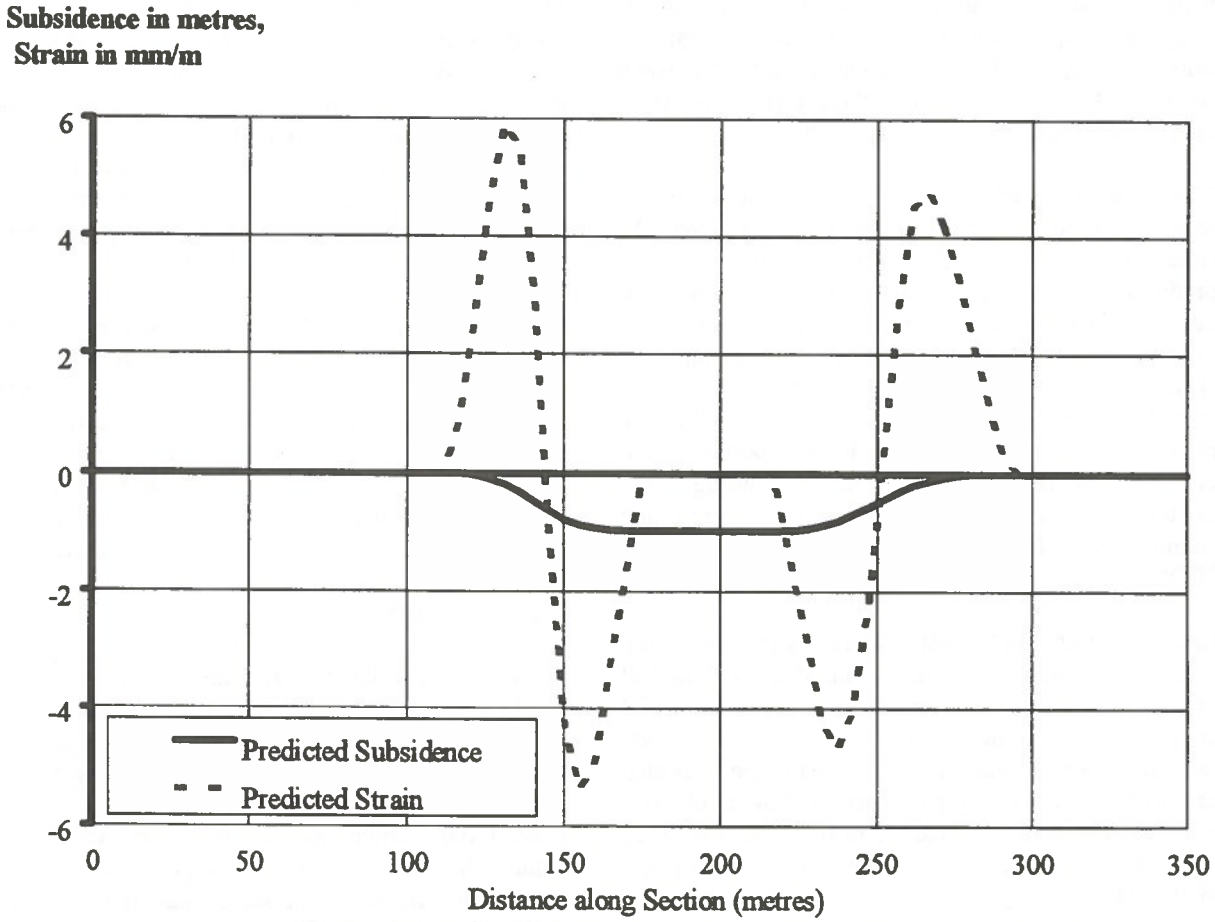

Figure 5: SWIFT Predictions of subsidence and strain over a shallow dipping extraction

model have provided valuable insights into the initiation and mechanism of the outburst events.

Model Results

FEOMP was used to examine the effect of changing the shape of openings on the potential for outbursts. Previous work has shown that for an outburst to occur, sandstone must be exposed in the roof of an arched roadway. At Phalen Colliery, all gateroad development is by rectangular, in-seam roadways. There was a question as to whether the tensile stresses induced by the bending of the roof beam into the roadway would contribute to the initiation of an outburst, and this was investigated using the model.

This model is discussed by Chen et al (1995) in these proceedings, and examples of its use and output are more appropriately found in that contribution.

DISCUSSION

The use of numerical models in the Sydney Coalfield in the future appears to be well established on the basis of the present successes, limited as they are.

Particularly important in the selection of a model is its ease of use, especially in the model building and post-processing phases. Although NUFEP is a mainframe-based model, the other models described rely on simple, easy to use, PC-based packages that produce output amenable to further processing or manipulation. As a result, the models can be run quickly and results obtained and manipulated with ease.

The basic assumptions of most continuum mechanics (i.e., that modeled materials will reasonably obey simple material behaviour rules, and that critical values for material properties can be reasonably predicted) are generally invalid in the design of coal mine structures. We should not expect to be able to

predict strains, closures or subsidence by simply plugging experimentally derived values into a numerical model. How else might a numerical model be used? At the present state of the technology, there are two potential methods of approach.

The first approach is to use an elastic model, recognizing its shortcomings, and knowing that the results are not the 'true' values. The stress changes predicted by an elastic analysis stress values so derived, however, generally have some significance and can be used to subjectively predict post-failure behaviour. An elastic analysis can also provide an objective framework for analogy building when analyzing the performance of a structure. This is an important use of numerical procedures because it acknowledges the existence of unknown factors but tries to detect and quantify them. The use of NUFEP, MULSIM/NL, and FEOMP in the Sydney Coalfield follow this approach.

Another use of simple elastic models is in incremental design. For example, when a number of longwall panels are driven at increasing depth it may be useful to calculate the change in stress fields between each face and thereby subjectively estimate the expected deterioration of opening performance. This is planned as the next stage in the analysis of interaction between the Harbour and Phalen Seams, to be carried out using MULSIM/NL

The second approach to modeling is to use sophisticated models that allow for exotic material behaviour, in particular post-failure characteristics. In the case of potash mining, there is reason to believe that such models can be made to yield useful predictive results. Flow rules for evaporites be modeled objectively with some degree of certainty, and the parameters required to derive these flow rules can be obtained with relative ease.

In general, however, moving to more sophisticated models requires the accurate determination of more material characteristics to describe the non-linear behaviour. Given the difficulty in establishing accurately even the Young's Moduli for rock masses in tension and compression, there is clearly little prospect of accurately determining other factors from laboratory testing.

What such models can do, however, is to show realistic qualitative properties that less sophisticated models cannot. If, for example, the possible benefit of a support system in terms of reducing the failed zone is being investigated, a model that will allow for failure is clearly needed. There is almost inevitably a circularity in the process by which material values are chosen. Input data for an unsupported case may be arbitrarily adjusted to give a realistic failure zone, and it may then be hoped that a second case (e.g., after the addition of support) will give a realistic measure of the change in the failure zone.

This process is planned for future modeling of gateroad supports and the development of design criteria. The confidence which one can apply to such a process depends on the suitability of the material model and the accuracy of the derived material properties. In general, one uses sophisticated material models to model situations where the structural properties require such sophistication; for qualitative similitude, rather than to regain the predictive design process of the mechanical engineer.

The most likely platform for this modeling is FLAC, largely due to its widespread use in the soft rock industry, excellent software support, and in particular its ease of use. FLAC has been widely used in the Australian coal industry, where it has been found to be a useful and reliable tool. Similar experience has been obtained in the Canadian salt and potash industry, and the software has been used occasionally during contract work in the Sydney Coalfield.

Although numerical modeling is not a regularly used tool in the Sydney Coalfield, the utility of a number of methods and models has been explored, and a number of numerical modeling applications have been attempted. All of the applications to date have examined rock mass behaviour, rather than the behaviour around single openings. They have all been pragmatic applications of the technique, looking for changes in behaviour and conditions rather than definitive results. The results obtained thus far are encouraging. Model results seem to reflect in-situ behaviour, and are providing guidance in mine design.

ACKNOWLEDGMENTS

The author acknowledges the assistance the CBDC Geology Department for the presentation of the MULSIM/NL results. The views expressed are those of the author alone, and may not represent those of CBDC or CANMET.

REFERENCES

BARRON, K., and KULLMAN, D., 1990,
Modeling of Outbursts at No 26 Colliery, Glace Bay, Nova Scotia. Part 2: Proposed Outburst mechanism and Model, Mining Science and Technology, v 11 pp 261-268.

BROWN, E.T., (Editor), 1987
Analytical and Computational Methods in Engineering Rock Mechanics. Allen and Unwin, London, ISBN 0-04-620020-7

CAIN, P. et al, 1994
Water inflows at Phalen Colliery in the Sydney Coalfield and their relation to interaction of workings. Proceedings 5th Int. Mine Water Congress, September 18-23, Nottingham, U.K.

CAIN, P., 1995
A summary of Canadian research into sandstone/gas outbursts. Proceedings 26th Int. Conf. of Safety in Mines Research Institutes, September 4-8, Katowice, Poland.

CHEN, X. et al, 1995
Finite Element Model for Outbursts in Underground Mines. Proceedings, 3rd Can. Conf. on Computer Applications in the Mineral Industry, October 22-25, 1995, Montreal.

CANMET, 1993
Evaluation of Mining Subsidence Field Data, Cape Breton, N.S. Final Report by Jacques, Whitford and Associates Ltd on DSS Contract File # 23440-1-9127, March 31, 1993.

CANMET, 1994:
Development of a Sydney Coalfield Subsidence Model. Final Report by Jacques, Whitford and Associates Ltd on DSS Contract File # 23440-2-9221, March 31, 1994.

CHEN, X. 1994,
A Numerical Model for Outbursts in Coal Mines, Ph.D. Thesis, University of Alberta, Canada.

REDDISH, D., et al. 1994
Modeling of caving over the Lingan and Phalen Mines in the Sydney Coalfield, Cape Breton. Proceedings 5th Int. Mine Water Congress, September 18-23, Nottingham, U.K.

SINHA, K.P., 1979:
Displacement Discontinuity Technique for Analyzing Stresses and Displacements Due to Mining in Seam Deposits. Ph.D. Thesis, Univ MN, Ann Arbour, MI, 311 pp.

ZIPF, K, 1993
New developments in MULSIM/NL - a boundary element method program for stress analysis of coal mines. Proceedings 1st Can. Symp. on Numerical Modeling Applications in Mining and Geomechanics, March 27-30, Montreal.

CAMI'95: 3rd Canadian Conference on Computer Applications in the Mineral Industry
Montréal, Québec, Canada, October 22-25, 1995

Tunnel Stability Assessment during Rockbursts

Pavel Vasak and Peter K. Kaiser
Geomechanics Research Centre, Laurentian University
Sudbury, Ontario P3E 2C6

ABSTRACT:

An observational modelling approach (OMA) is applied to the problem of dynamically induced tunnel failure. A two-dimensional plane-strain FLAC model with a plane shear wave input is used for the simulations. Dynamic damage is reasonably well simulated by a constant stress deviator failure criterion and three types of rockmass damage processes are numerically simulated; shear damage, tensile damage, and block ejection. Through the use of a case study the concepts of dynamic damage propagation and accumulation are discussed. The effects of rockmass strength and seismic wave amplitude are presented as a strength vs. peak particle velocity vs. damage chart.

RÉSUMÉ:

Une approche de modélisation par observation (OMA) est appliquée au problème de rupture dynamique dans un tunnel. Le programme FLAC a été utilisé pour les simulations. C'est un modèle bidimensionel de déformation plane utilisant une onde de cisaillement plane. Le dommage dynamique est assez bien représenté par un critère de rupture à contrainte déviatorique constante, et trois types de processus de dommage du massif rocheux sont simulés, soit; en cisaillement, en tension, et l'éjection de blocs. Les concepts de propagation et d'accumulation de dommage dynamique seront discutés à travers les études de cas. Les effets de la résistance du massif rocheux et de l'amplitude de l'onde séismique seront présentés dans un graphique montrant la résistance du massif vs ppv vs dommage.

INTRODUCTION

Rockbursts are seismic events causing damage to underground openings by the sudden and violent failure of rock. They are triggered by the shock waves, generated by nearby seismic activity, which travel through the rock mass. The source of these waves may be implosional (pillar bursts), explosional (blasting), or shear failure (fault slip), or a combination thereof (Hedley, 1992). Damage occurs as the seismic shock waves encounter an opening (mining drift or stope). Rockbursts fall into three basic categories based on the damage mechanism; seismically induced ground falls, block ejections, and crushing or fracturing of rock near the opening (Kaiser, 1993).

Large events encountered in a mining environment are generally caused by fault slip mechanisms. These are characterized by a wave with relatively small P-wave velocity amplitude followed by more complex shear wave signals of much larger amplitude (Figure 1). The superimposed 50 Hz synthetic wave in Figure 1 was used for modelling and is explained in a later section. Most of the rockburst damage during fault slip events is induced by the shear waves. The focus of this paper is

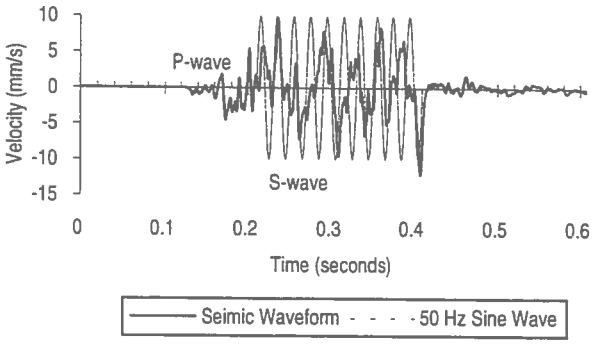

Figure 1. Typical seismic waveform for fault slip events.

on modelling the damage created by shear waves near an isolated tunnel. We are primarily interested in the rock crushing or fracturing mechanism and use a continuum model for this purpose. However, block ejection was also simulated since tensile fracture is allowed in the model. Seismically induced falls of ground are a structurally controlled discontinuum problem better handled by discrete element methods, and are beyond the scope of this paper.

NATURE OF SEISMIC WAVES

The reason that most rockburst damage is induced by shear waves lies in the fundamental difference in the nature of the two propagating wave types and the fact that typical P-wave velocity amplitudes are in the order of only 0.2 to 0.3 times the S-wave amplitude. By only considering low frequency (long wavelength) waves passing through an elastic rockmass, the nature of a wave can be investigated pseudo-statically simply by superimposing the dynamic stress components onto the in-situ stress field.

Taking a worst case approach, a compressional wave will cause the largest stress increase in the rockmass when the direction of propagation is in the direction of the major principal stress (Figure 2). A shear wave, on the other hand, will create the largest stress increase when the direction of propagation is about 45 degrees to the principal stress direction and the positive phase of the S-wave coincides with the major principal stress direction (Figure 3). The effects of the two independent processes are summarized in Figure 4 which shows

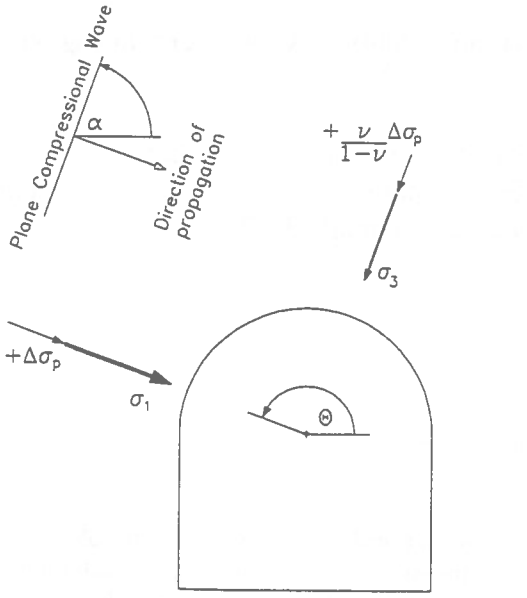

Figure 2. Pseudo-static stress due to plane compressional wave.

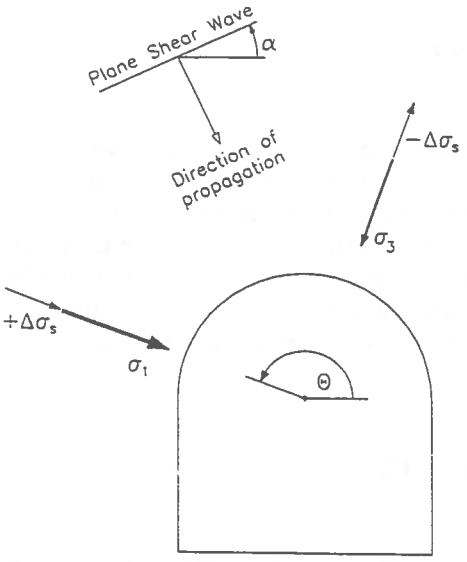

Figure 3. Pseudo-static stress due to plane shear wave.

stress shifts for the P-wave, and a stress circle expansion or contraction for the S-wave in terms of Mohr circles. Peak velocity amplitudes of 1.0 and 0.25 m/s, which result in $\Delta\sigma_s$ = 7 and $\Delta\sigma_p$ = 2.9 MPa, are assumed for the S- and P-waves, respectively.

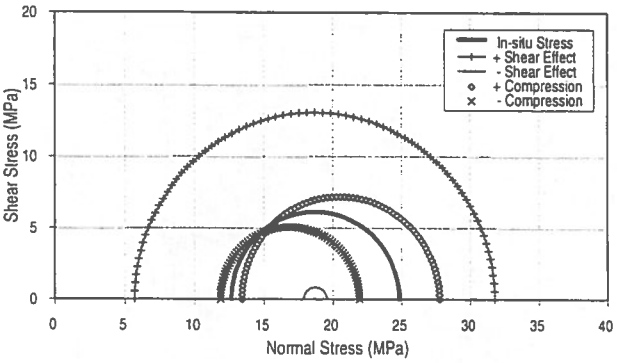

Figure 4. Mohr circles showing in-situ pseudo-static stresses.

Depending on the phase of the waveform, both favourable (negative phase) and critical (positive phase) stress conditions are created. The critical conditions, in terms of tunnel instability, arise from the increase in the stress deviator. Because of the nature of the shear wave, the dynamic stress change is more critical than that of the P-wave. Hence, it has the propensity to cause more severe damage.

FLAC DYNAMIC MODEL

For the numerical analysis, a two-dimensional plane-strain model with a plane stress wave input was adopted. FLAC was chosen as the modelling tool because its explicit solution scheme solves the equations of motion, and the code is efficient in dealing with the type of non-linear problem presented here. Another important consideration is the ability to randomize the material properties, within finite difference zones, by specifying a mean and standard deviation. Randomization of both grid and material properties reduces mesh influence on the failure propagation process.

Figure 5 shows the geometry and boundary conditions for the model used in the FLAC analysis. It consists of a 4 by 4.5 m horseshoe tunnel in a 40 by 40 m grid.

The finite difference grid for the horseshoe shaped tunnel is generated by cutting the floor segment out of a mesh originally created for a circular tunnel. The

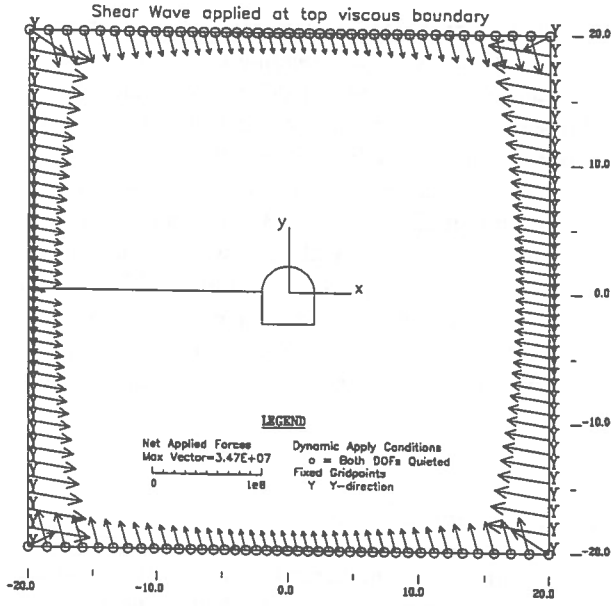

Figure 5. FLAC model geometry and boundary conditions for plane shear wave.

advantage of this approach lies in the ability to cut the floor segment at any orientation, relative to the applied seismic wave, without having to change the boundary conditions. The boundary conditions for the dynamic analysis are a critical feature in the model. To propagate a waveform through the model without boundary reflections, fixed boundaries are required perpendicular to the direction of wave propagation, and viscous boundaries are required in the direction of propagation to absorb the stress wave. A plane stress wave is applied at the top viscous boundary and propagates down toward the bottom viscous boundary. In this case, the vertical boundaries are fixed in the Y-direction because a shear wave is applied. The boundary must be fixed in the X-direction for a P-wave.

Plane Wave Approximation

A shear wave is typically a complex multiple pulse wave composed of many superimposed frequencies. Each seismic event has its own unique characteristics which cannot be accounted for in a generic sense, especially if frequency content and duration are considered. Butler and Aswegen (1993) show, from a large sampling of events in South Africa, that large

magnitude events (> 2.0 local magnitude) typically have a dominant low frequency, ranging between 10 and 50 Hz. Canadian experience (Hedley, 1992 and Kaiser, 1993) shows a similar range of 15 to 50 Hz. For the purpose of this modelling effort, the shear wave is represented by successive sine pulses having uniform velocity amplitudes at 50 Hz frequency (50 m wavelength). This synthetic waveform, shown superimposed on the seismic waveform in Figure 1, is a compromise to achieve numerical efficiency. It takes less time to run a shorter wavelength (high frequency) event, because larger timesteps can be used in the explicit solution scheme.

Remedies for Mesh Effects

When dealing with numerical simulations of failure processes, a primary concern is whether the size and shape of the mesh affect the results. It is known from previous modelling (see examples in FLAC manual, Itasca, 1993) that grid size and grid orientation play an important role in the shear failure process, particularly in a homogeneous material. Several remedies are available to reduce the grid effect (Itasca,1993):

1) Decrease zone size, i.e. increase the number of zones, in the plastic region;
2) Slight random distribution of material properties will allow shear failure to nucleate and propagate freely in the material; and
3) Use a non-uniform grid; small deviations from a smooth grid are sufficient (J. Tinucci, pers. com.).

All three remedies were applied to the model. Tensile strength and density are randomly varied in the zones and the finite difference grid is randomly perturbed to create non-uniformity of zoning (Figure 6; right half).

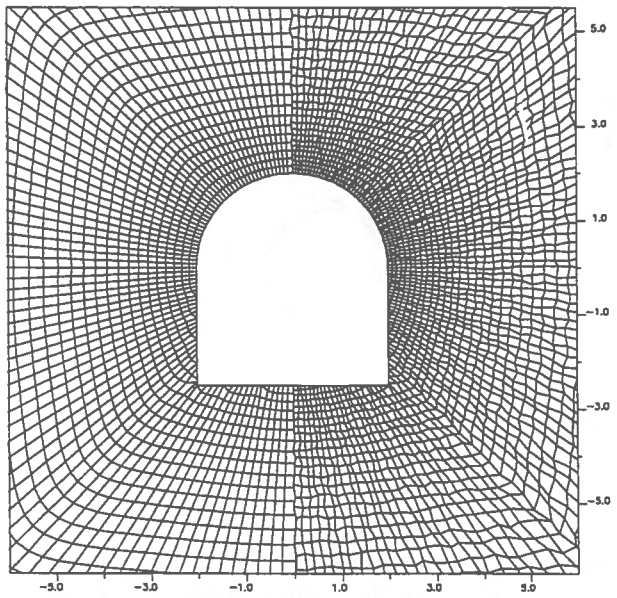

Figure 6. Randomization of 40 by 160 zone uniform grid (left half) to 60 by 240 non-uniform grid (right half).

ROCKMASS FAILURE CRITERION

A Mohr-Coulomb failure criterion derived from previous mine-scale modelling was used for the initial phase of the work. However, it became evident that the use of such traditional failure criteria is not valid for simulating the near-surface behaviour in dynamic tunnel-scale models. The primary reason for this is that strength is greatly underestimated close to the perimeter of the tunnel where the rockmass approaches an unconfined state. For this reason, the model over-predicts the extent of failure around the tunnel (Figure 7) to the extent that the whole model will fail when ppvs exceed relatively low threshold values. Several alternate Mohr-Coulomb models were investigated, again with little improvement when compared to field damage records. Consequently, an observational modelling approach (OMA) was applied to establish a meaningful criterion for the simulation of dynamically induced near-surface rockmass failure (Kaiser, 1994).

Brittle Failure Criterion

The pulse or wave-like nature of the superimposed dynamic stress acts only temporarily and the effect of the wave is primarily to initiate failure. The OMA for the tunnel instability problem is based on several important field observations from the Underground Research Laboratory (AECL) in Canada (Martin and Chandler, 1994):

1) The rockmass immediately adjacent to an underground excavation has little, or no, confinement and its strength is essentially the

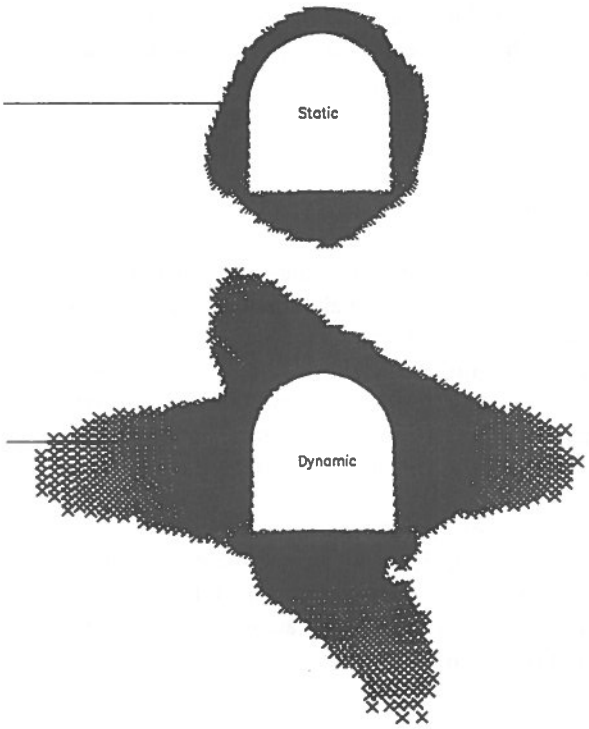

Figure 7. Mohr-Coulomb model showing regions of static and dynamic rockmass damage (cohesion = 7 MPa, friction = 35°).

unconfined compressive strength.

2) Micro-seismicity around an opening is an indicator of rock damage or failure initiation rather than peak or ultimate strength failure.
3) As failure progresses in brittle rocks, cohesive strength is rapidly lost and if unconfined, the rockmass strength rapidly drops to zero.
4) Friction, due to confinement, must be mobilized to stop the damage processes around the opening, and large confining stresses (12 to 15 MPa) were required to suppress the damage process at the URL.

Based on this evidence, the deviatoric failure initiation criterion described by Kaiser (1994) was adopted. Rockmass failure is defined by a constant deviator criterion (Martin and Chandler, 1994; Castro, 1995) where the onset of fracture initiation is characterized solely by cohesion loss. As failure progresses with plastic straining, the internal friction angle is mobilized and is assumed to increase from zero to 35°, whereas

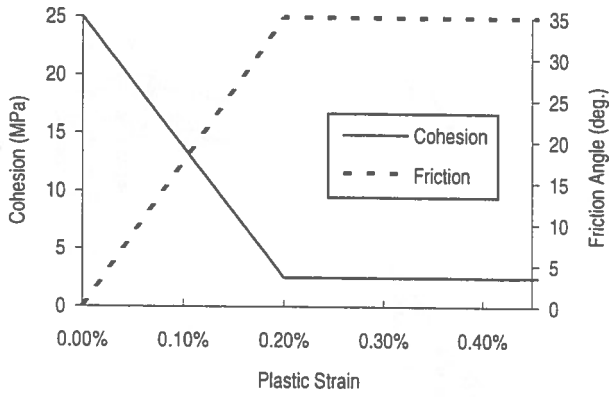

Figure 8. Brittle failure criterion used in FLAC model.

the cohesion drops from its peak value and is assumed to reach 1/10 of peak at the point when friction is fully mobilized (Figure 8).

CASE STUDY

The FLAC model was developed to study the problems encountered in an operating mine experiencing large rockbursts causing severe damage. The chosen geometry, rockmass properties and in-situ stress are site specific. Modelling results are presented in the form of a case study, but the dynamic failure process is representative of typical situations encountered at other mines.

Damage records and photographic evidence show three regions of tunnel instability (Figure 9); two regions of overbreak corresponding to the principal stress orientation, and floor heave which is common. Overbreaks often occur even under static conditions and were used to back-analyze the static rockmass strength. In areas prone to rockbursts, the rockmass is highly jointed and typical properties, used in the FLAC model to simulate ground conditions, are listed in Table 1.

The calibration of the failure criterion is based solely on numerical correlations with observations noted in overbreak records. Allowing 0.2% plastic strain for full friction mobilization and cohesion loss yields consistent locations and overbreak damage volumes. Elastic analysis gives circumferential stresses in the range of 40 to 75 MPa in the overbreak zones which suggest that

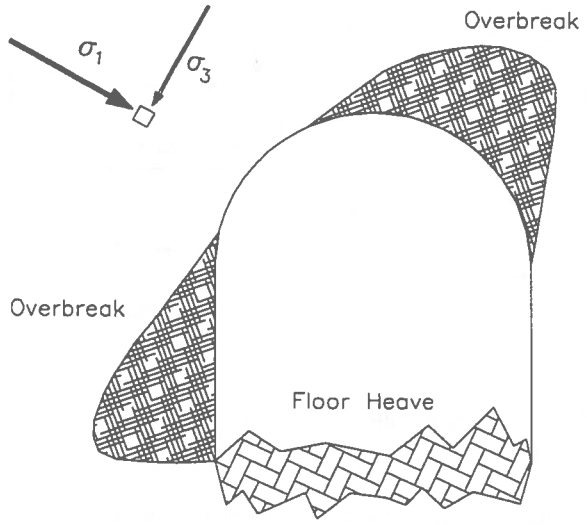

Figure 9. Typical damaged tunnel profile showing areas of overbreak.

the rockmass unconfined compressive strength must also be in this range.

TABLE 1 In-situ Stress and Rockmass Properties used in Case Study.

Axial Stress (out-of-plane)	36.8 MPa
Major Principal Stress (in-plane)	24.8 MPa
Minor Principal Stress (in-plane)	12.6 MPa
Theta Angle	160 degrees
Young's Modulus	42.0 GPa
Poisson's Ratio	0.22
Density	2800 ± 17 kg/m^3
Tensile Strength	5.0 ± 0.1 MPa
Cohesive Strength	21 to 37 MPa

TUNNEL INSTABILITY

Rockmass failure occurs when the rock strength is exceeded. It is characterized by the loss of load-carrying capacity and manifests itself as physical damage. Several common modes of failure are recognized; flexure, direct tension, shear failure, and crushing or compression failure (Goodman, 1980). Rockmass failure is a complex process involving one or more of these failure modes. The following discussion is based on the definitions provided by Goodman (1980).

Tensile Fracture

Flexure refers to failure caused by bending and is characterized by the development and propagation of tensile cracks. In its classical sense, it is usually associated with the sagging of roof beams under the force of gravity but, because seismic waves can accelerate rock in any direction, flexural forces may induce tensile cracks anywhere around an excavation.

Direct tension failure occurs when rock breaks in tension. It is difficult to separate the direct tension and flexure modes when dealing with dynamic processes, therefore, the term "tensile fracture" is used to refer to rockmass fracture processes.

Shear Damage

Shear failure refers to the formation of, and slip along, rupture surfaces created in the rock when shear stresses exceed the rock strength. The rupture surfaces result from the coalescence of small tensile cracks. Crushing or compression failure occurs under high stress loads and is a complex combination of tensile fracture and shear failure. Both shear and compression failure modes are characterized by a loss of cohesive strength followed by rockmass disintegration. The term "shear damage" is used for this loss of rock cohesion.

Numerical Simulation of Dynamic Damage

The ability to simulate realistic damage mechanisms with the FLAC model is demonstrated in Figure 10 which shows the dynamic damage caused by a relatively small (ppv = 0.5 m/s) shear wave travelling in the vertical direction. Three damage mechanisms are reflected by this figure. The first two are directly related to rockmass failure; shear damage in the minor pre-event (or static) principal stress direction, and tensile fracture initiation and propagation from stress raises at the corners of the tunnel. The third mechanism, block ejection from the floor, is a consequence of the tensile fracture mechanism. Blocks of rock bounded by tensile fractures are accelerated by seismic energy transfer and

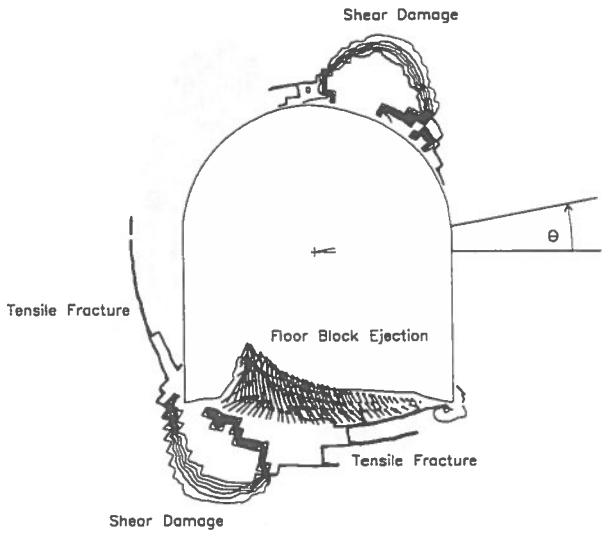

Figure 10. Dynamic damage processes around a horse-shoe shaped tunnel.

ejected into the tunnel. These blocks are ejected in the FLAC model because the tensile zones, between the rockmass and the blocks, can no longer sustain the tensile stresses caused by the outward motion of the blocks.

DAMAGE ACCUMULATION AND DAMAGE HISTORY

Damage accumulation and damage history are important aspects of the dynamic failure process. Starting with a tunnel which has not experienced previous seismicity, the accumulation of damage can be traced (Figure 11). Static stress concentrations cause initial damage in the floor corners and localized damage in the roof. The first stress wave amplifies these stress concentrations and initiates tensile fracturing from the corners, and shear damage in the minor principal direction. Subsequent shear waves propagate the tensile fractures in the floor and walls and may create blocks which can be ejected into the tunnel. Shear damage increases in response to the amount of tensile damage around the opening. With sufficiently high ppv and repeated cycles, the tensile cracks can coalesce and create an equivalent circular shaped zone of tensile fracture around the tunnel. The volume of shear damage, in this case, increases slightly in response to the larger equivalent tunnel diameter, creating an overall elliptically shaped damage zone. The shape of the ellipse is a function of the imposed static stress ratio (σ_1/σ_3).

The extent of newly created dynamic damage is a function of the previous damage history of a tunnel. For an equal magnitude event, a previously undamaged tunnel will experience more severe incremental damage than a previously damaged tunnel. This is readily apparent by comparing the increase in dynamically induced damage between the static case and wave 1, and waves 3 and 4, in Figure 11. The latter show very little additional rockmass failure, however block ejection will still occur if the blocks are not anchored.

INTERDEPENDENCE OF STRENGTH, PPV AND DAMAGE

For support design, the extent and depth of rock fracturing must be anticipated (Kaiser et al., 1995). Hence, the primary focus of the analysis was to evaluate the extent of dynamic damage as a function of rockmass strength and event magnitude. To avoid the complication of selecting an appropriate magnitude-ppv scaling relationship, the input in the model was simply given as the peak particle velocity amplitude (ppv) of the seismic wave arriving at the tunnel, irrespective of how much energy is lost between source and target.

The evaluation of dynamic damage is complicated by the previous damage history of a tunnel and the duration of a seismic event (number of cycles). Both these factors are uncertain, therefore, a simplified approach is taken and two basic assumptions are made; the tunnel has no prior seismic damage history, but static damage is accounted for; and the shear wave is approximated by a single sine wave because the greatest amount of damage is done by the first shear pulse.

Using these assumptions, a strength-ppv-damage relationship is obtained (Figure 12). Dynamic damage is presented in terms of a damage ratio, i.e., the damage volume is normalized to the initial tunnel volume. The damage volume is the sum of shear damage and the volume of rock which is ejected into the tunnel. Two notable trends are apparent:

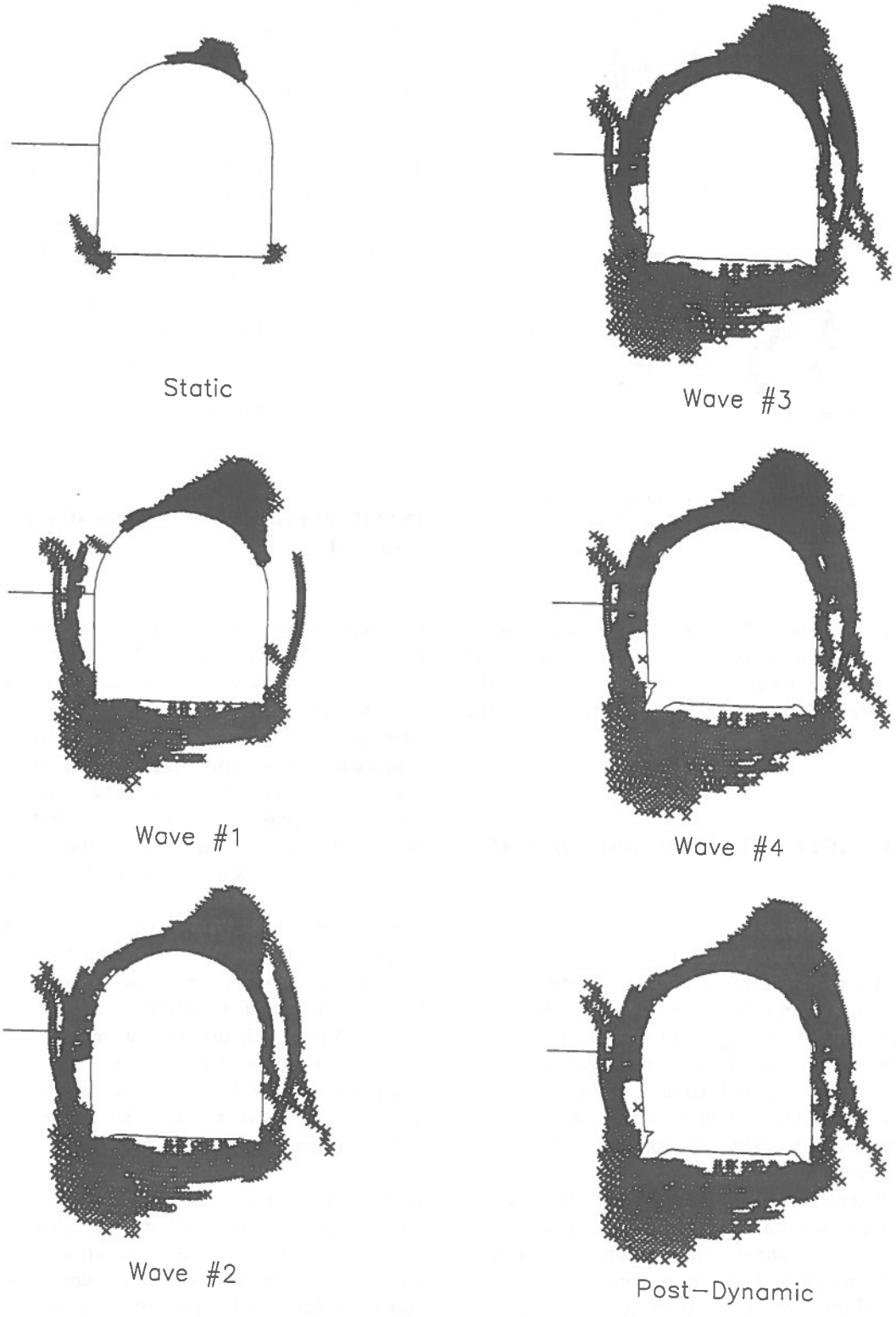

Figure 11. Accumulated damage caused by 1 m/s ppv sinusoidal wave.

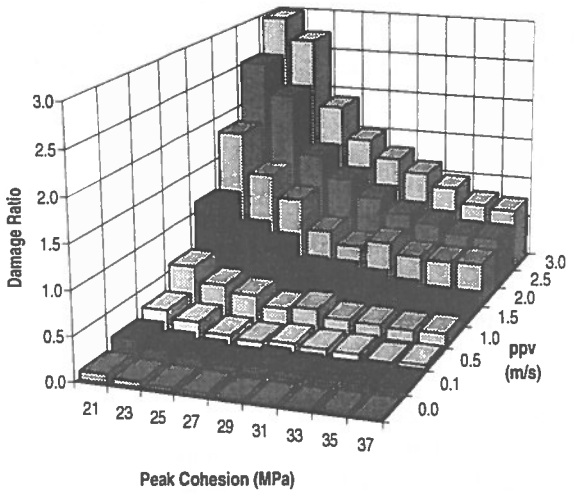

Figure 12. Dynamic damage ratio as a function of rockmass cohesion and ppv.

1) Irrespective of rockmass strength, there is a sudden increase in damage volume at about 1.0 to 1.5 m/s ppv at transition to block ejection. Tensile fractures do not develop fully below 1.0 m/s ppv so little, if any, block ejection occurs (floor heave only). At higher ppvs, the tensile fractures propagate to form blocks in the floor and walls. These blocks are ejected into the tunnel by the high wave energy.

2) Shear damage is highly sensitive to rockmass strength, particularly in weaker rocks. The volume of damage increases about threefold between 30 and 20 MPa cohesion. Shear damage lessens considerably with strength, whereas the volume of ejected rock remains fixed because tensile fracture is a geometric effect.

DISCUSSION

Several concepts which are not covered in this paper are briefly introduced here. Multiple shear waves tend to create a (nearly) circular tensile fracture pattern around the horseshoe shaped tunnel. If the fractures develop fully, then subsequent seismic damage can be modelled by a circular tunnel with a radius equivalent to the fractured zone radius. It was found, for the case study conditions, that maximum block ejection velocities are about 1.5 times the wave ppv.

The directionality of a seismic wave relative to a tunnel was investigated. Both pseudo-static analysis and dynamic modelling of incident waves at different orientations revealed that the damage mechanisms and the extent of dynamic damage are similar, regardless of the wave orientation (alpha in Figure 3). This is due to the nature of a shear wave, particularly the stress reversals which accompany reversals in the direction of motion as the wave passes. For example, the same dynamic stress increase is experienced by a tunnel regardless of whether the wave travels in the horizontal or the vertical direction.

For large shear wave ppvs, tensile zones propagate from the damaged zone around the tunnel into the rockmass at about 45 degrees (Figure 11). These tensile zones are a consequence of the brittle failure criterion used in the analysis, and may not be real. As previously stated, the failure criterion is based on the onset of fracture initiation which occurs under low confinement close to the tunnel perimeter. The development of a confinement dependent failure criterion is the next logical step in the study and application of dynamic failure simulation.

CONCLUSIONS

By using the observational modelling approach (OMA), dynamically induced tunnel failure can be reasonably simulated by a constant stress deviator criterion. In the criterion, failure is defined as the onset of fracture initiation and is characterized by rockmass cohesion loss. For the case study, the simulated failure processes agree with field observations for both static and dynamic situations.

Three types of dynamic damage processes are numerically simulated; shear damage, tensile damage, and block ejection. Shear damage occurs in the regions of high stress concentration oriented in the minor principal in-situ stress direction. Tensile fractures initiate in the corners of the floor and propagate to form a circular pattern around the horseshoe shaped tunnel. The rock bounded by these fractures becomes detached from the rockmass and may be ejected into the tunnel.

Dynamic damage is accumulated as successive shear

waves hit an excavation. The first wave starts the damage processes and subsequent shear waves propagate tensile fractures and increase the volume of shear damage around the tunnel. Because of this process, the extent of dynamically induced damage is dependent on a tunnel's previous damage history. For an equal magnitude seismic event, a previously undamaged tunnel will experience more severe damage than a previously damaged tunnel.

For support design, the extent and depth of rock fracturing must be anticipated, therefore, a parametric analysis which focused on rockmass strength and event magnitude was conducted. The strength-ppv-damage relationship yielded two notable trends; there is a sudden increase in damage volumes for ppvs greater than 1.0 m/s ppv because blocks of rock in the floor and walls are ejected at the higher ppvs; and shear damage is highly sensitive to rockmass strength, particularly in weaker rocks.

ACKNOWLEDGEMENTS

The dynamic modelling was sponsored in part by the Mining Research Directorate (MRD) as part of the Canadian Rockburst Research Project (CRRP). John Tinucci of Itasca provided valuable assistance in setting up the FLAC model. Sean Maloney and Richard Brummer, both at the Geomechanics Research Centre, provided valuable insights and comments about the subject matter.

REFERENCES

Butler, A.G., and Aswegen, G., 1993.
Ground velocity relationships based on a large sample of underground measurements in two South African mining regions. Rockbursts and Seismicity in Mines, R.P Young (ed.), Balkema, Rotterdam, pp. 41-59.

Castro, L.A.M., 1995.
Analysis of brittle rockmass failure around deep excavations. Ph.D. Thesis, Department of Civil Engineering, University of Toronto, Toronto, Canada (in preparation).

Itasca, 1993.
FLAC v.3.2 Manual, Itasca Consulting Group, Inc., Minneapolis, Minnesota, 3 vols.

Goodman, R.E., 1980.
Introduction to Rock Mechanics, John Wiley & Sons, New York, pp. 50-52.

Hedley, D.F.G., 1992.
Rockburst Handbook for Ontario Mines. CANMET Special Report SP92-1E, 305 p.

Kaiser, P.K., 1993.
Keynote address: Support of tunnels in burst-prone ground - Toward a rational methodology. Rockbursts and Seismicity in Mines, R.P Young (ed.), Balkema, Rotterdam, pp. 13-27.

Kaiser, P.K., 1994.
Observational modelling approach for design of underground excavations. SANGORM'94 - The Application of Numerical Modelling in Geotechnical Engineering, South African National Group on Rock Mechanics, Pretoria, pp. 1-7.

Kaiser, P.K., Tannant, D.D., and McCreath, D.R., 1995.
Support of tunnels in burst-prone ground. Paper submitted to ISRM Congress, 1995, Tokyo, in press.

Martin, C.D., and Chandler, N.A., 1994.
The progressive fracture of Lac du Bonnet granite. Int. J. Rock Mech. Min. Sci & Geomech. Abstr. Vol. 31, No. 6, pp. 643-659.

Tinnuci, J., 1994.
Itasca Consulting Group, Inc., Minneapolis, Minnesota, Personal communication.

CAMI'95: 3rd Canadian Conference on Computer Applications in the Mineral Industry
Montréal, Québec, Canada, October 22-25, 1995

A Simple Method for the Alleviation of Dynamic Phenomena in Mine Structures

M. Al Heib
INERIS - Ecole des Mines de Nancy - France

P. Bigarre, J.P. Josien
INERIS 60550 Verneuil en Halatte - France

Y. Guise
HBCM - U.E. Provence - France

ABSTRACT

Dynamic floor heavage in deep coal mines may be alleviated using extensive floor slotting before mining operations start. Clearly identified as efficient from *in situ* observations, this method has been tested on numerical simulations of the fractured rock mass. Stress/strain relief in the floor has been qualified and compared with measurements.

Results show that floor slotting is an attractive method for Rockbursting alleviation as well as safe and economical to work out.

RÉSUMÉ

Dans cet article, nous avons cherché à apprécier l'efficacité de cette méthode par la modélisation numérique. Nous avons utilisé le code UDEC basé sur l'approche des éléments distincts. Cette modélisation valide la méthode et met en évidence son efficacité confirmé par les observations et mesures in situ. Elle permet également de comprendre le rôle positive du procédé employé. Les résultats sont très encourageants. Nous avons mis en évidence que l'efficacité de la saignée est d'autant plus importante que les contraintes initiales horizontales sont très fortes.

1. INTRODUCTION

The management of the Provence Operations Unit of the Houillères du Bassin du Centre et du Midi (Charbonnages de France Group) has drawn up a geological engineering scheme to control dynamic phenomena. This programme introduces a coherent approach tailored to the development of workings in the mine. It is based essentially on methods of relieving stresses around roadways. In principle, the different methods involve eliminating original and induced stress concentrations and modifying the brittle character of the rock mass. If this objective is not achieved, the slot would make it possible to initiate the phenomenon at an appropriate time.

Stress relief holes have been known and used for a very long time. A new method was recently introduced which involves simply making a slot in roadway floors.

In this article, we shall begin by describing the principle of the method and the resources necessary for its application. We shall then give a comparison between a zone to which this method has been applied and one to which it has not.

A numerical simulation using the distinct element method has been carried out to determine the role of the slot and the mechanisms this type of stress relief involves.

2. PRINCIPLE OF THE METHOD

A slot is made parallel to the centre line of the roadway. This allows controlled operation with regard dynamic phenomena in the wall and dissipation of the stored energy. Figure 1 shows the roadways in which slots were made. The slot can be produced by a machine fitted with a disk cutter (Fig. 2). The slots currently used by HBCM are 90 cm deep and 15 cm wide. For satisfactory operation, the slot must be produced before the seam is worked. Subsequently the slot is monitored over time to assess its effectiveness.

Figure 3 shows how the width of the slot changes as a function of distance from the cutting face. After the first pass, the measured width is only 7 to 8 cm on the average instead of 15, indicating a closure of the order of 8 cm, virtually half the initial width. It may also be noted that slip between strata is fostered because the

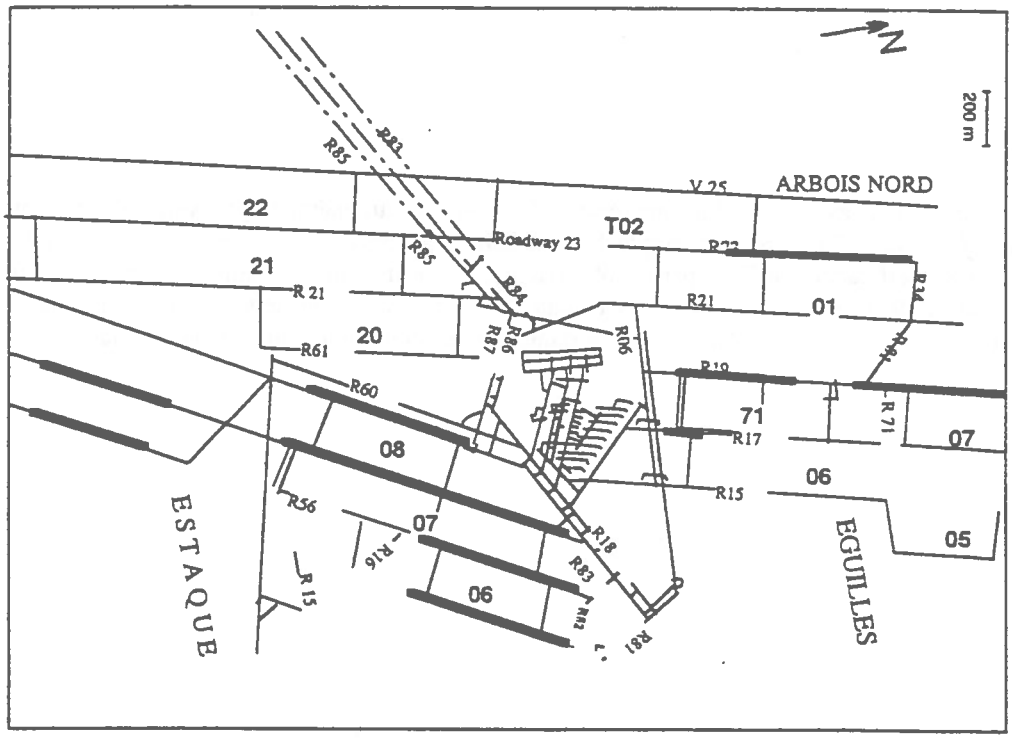

Fig. 1 : Location of slots

measurements and the follow-up observations have often shown a stepped shape. Since 1992 all roadways have been treated with this method.

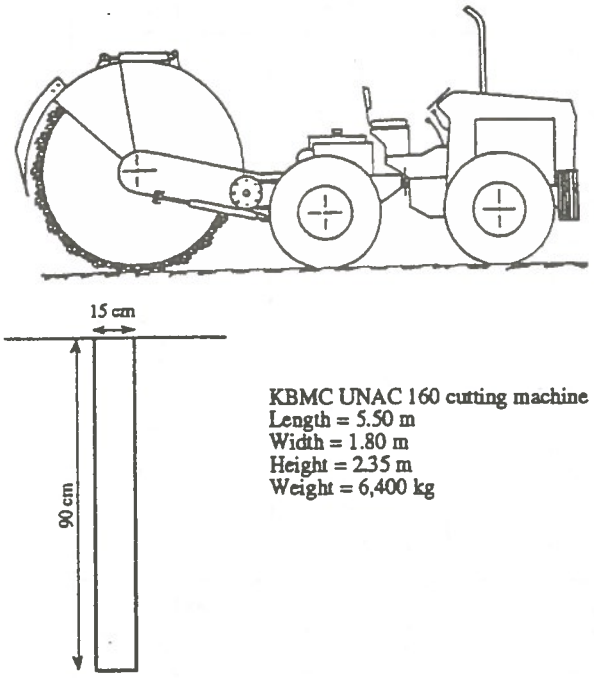

Fig. 2 : UNAC cutting machine

3. COMPARISON OF TREATED AND UNTREATED ZONES

A number of faces distributed through all districts were systematically monitored. Table 1 shows that no floor heave was recorded in the treated zones. In the main roadway, no suspicious event was recorded in the treated zones but two suspicious events were recorded in the non-treated zones. Comparison is more difficult in the auxiliary roadways.

4. NUMERICAL SIMULATION

The aim of numerical simulation is mainly to understand the stress relief mechanism introduced by the slot in the roadway wall. It is also possible to evaluate the efficiency of the slot in eliminating any danger of wall bowing. The question arises as to whether cutting the slot in the wall of the roadway does not also modify the behaviour and stresses in the roadway facing.

Many parameters influence behaviour, and numerical modelling will also make it possible to determine the influence of each.

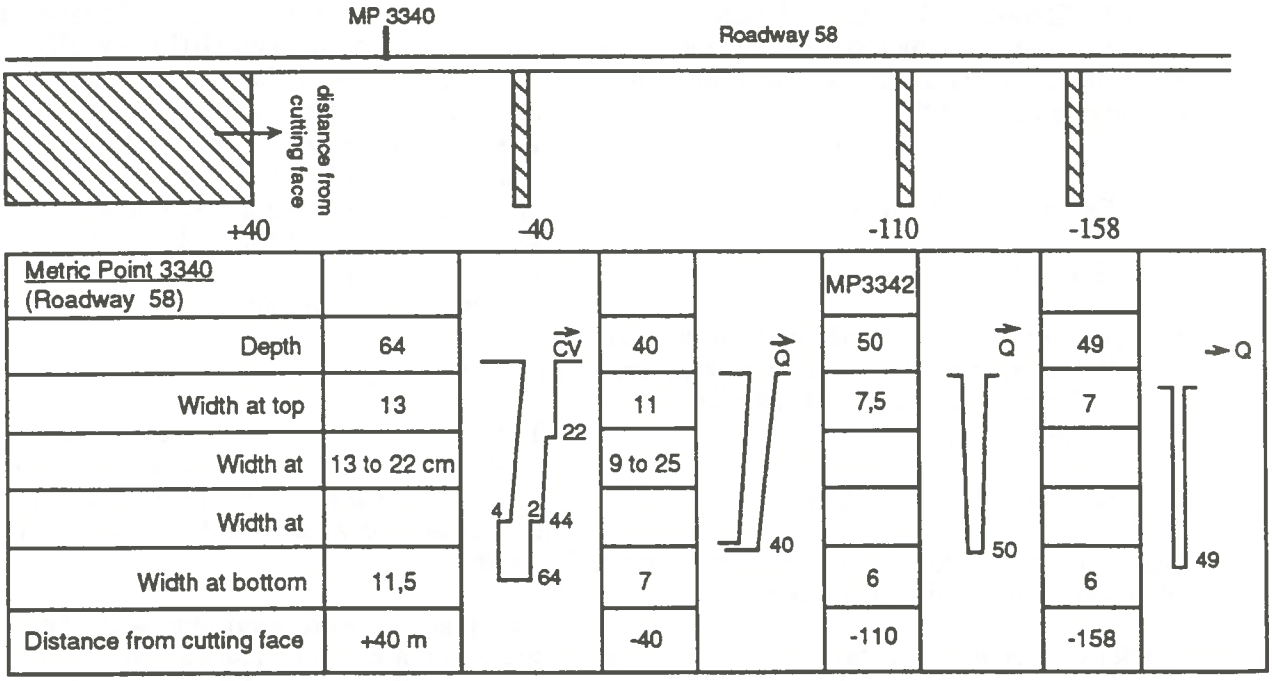

Metric Point 3340 (Roadway 58)					MP3342			
Depth	64		40		50		49	
Width at top	13		11		7,5		7	
Width at	13 to 22 cm		9 to 25					
Width at								
Width at bottom	11,5		7		6		6	
Distance from cutting face	+40 m		-40		-110		-158	

Fig. 3 : Slot changes as a function of distance from the cutting face 17 measured at metric points 3340 and 3342

	TMP		TMA	
	Slotted zone	Non-slotted zone	Slotted zone	Non-slotted zone
ESTAQUE 06			06/01/92 08/01/92	
ESTAQUE T17			28/06/92 06/08/92 04/09/92	CT 243 15/04/92
ESTAQUE T07			06/01/92	
EGUILLES T06		CT 242 18/11/91 06/12/91		11/01/91 14/01/91
EGUILLES T07				
EGUILLES T71				06/11/92 at cutting 19/01/93

Légende : CT 242 = ground heave n° 242
18/11/91 = suspicious event on 18/11/91

Table 1 : Effectiveness of the slot

The UDEC code (ITASCA, 1994) was used. The choice of numerical method (distinct elements) was determined by the substantial stratification for the operation of the slot.

4.1 Description of a model

* Geometry

The roadways excavated in Provence are virtually rectangular in section, 6 m wide and 3 m high. The workings involve alternate seams of coal and beds of limestone.

* Geological characteristics

The strata in the Provence mine mainly consist of very hard rocks (Rc > 100 MPa).

INERIS carried out laboratory tests to characterise the coal and the strata in the roof and walls (TRITSCH, 1993 and GHOREYCHI, 1982). A reducing coefficient of 0.5 was adopted so as to take fracturing and the real characteristics of the rock into account (BIENAWSKI, 1989). The rocky strata behave in an elastic-plastic manner. The Mohr-Coulomb plasticity criterion was chosen. However the stratification joints were not characterised owing to the difficulties of sampling and testing the joints. The joints were therefore modelled on the basis of theoretical and practical considerations and a number of observations.

* Loading

The initial stresses have been measured over a long period. The results showed that the Provence mine was characterised by major horizontal stresses between 1 and 3 times the vertical stress.

Two loadings were used, one with the vertical stress and a horizontal stress twice as high, the other with the same vertical stress but a horizontal stress of 0.5 times the vertical stress.

The phases of calculation were as follows:

- the roadway excavation phase;

- the slot production phase;

- the advance of the cutting face.

4.2 Results and interpretation

By analysing the parameters it is possible to quantify and analyse the behaviour of the roadway. These parameters are the deformation, the movements of joints and the new stress distribution.

The displacements induced by the production of the slot are found to be in the roadway wall. The displacement caused is equal to a third of the displacement induced by the gallery (Fig. 4).

Changes in the slot depend on the initial horizontal stresses. It can be seen (Fig. 5) that the slot begins to function as soon as it is cut with mobilisation of the joints. The slot is deformed by a greater amount for the simulation of a cutting face.[1](*)

The final closure state is of the same order of magnitude as that obtained by the in situ measurements after the cutting pass. The joints in the roadway wall undergo slippage induced by shear stresses. Joint shearing also occurs in the roof supports, which agrees with the observed process of roof damage.

Comparison of the two simulations with and without slots show the value of the slot. The extension of the slip zones due to shear is much greater when no slot is present (Figs. 6 and 7).

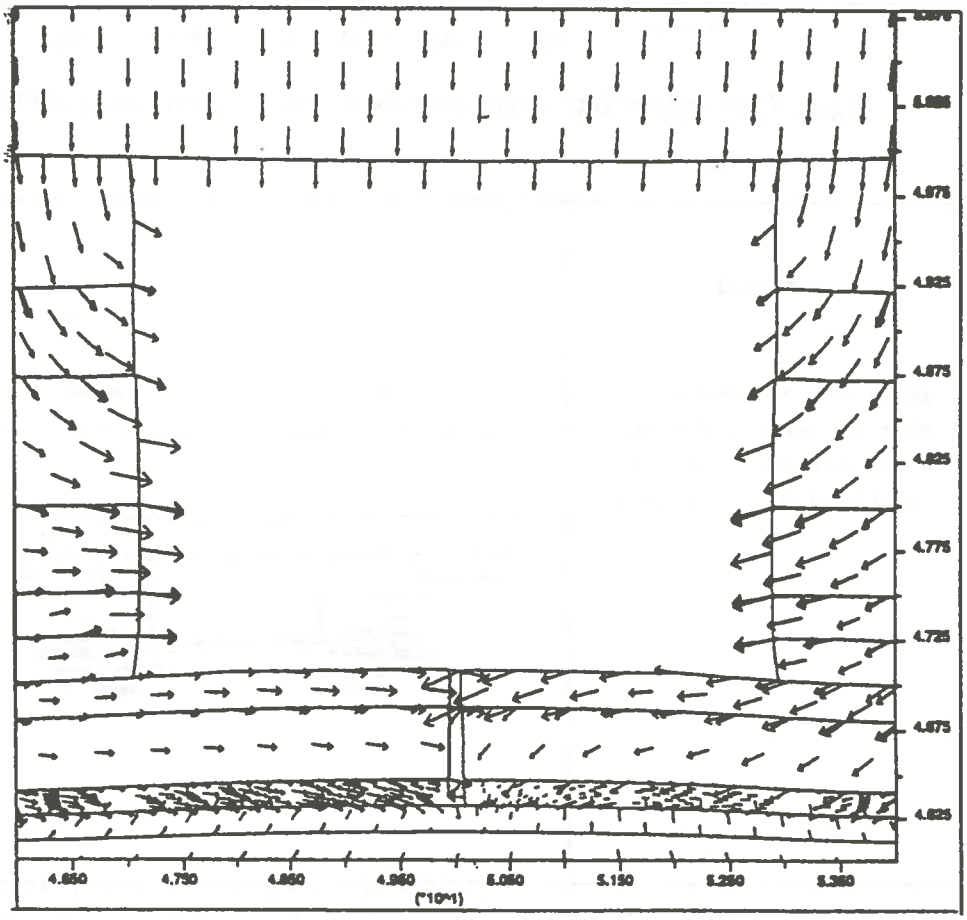

Fig. 4 : Displacements induced only by production of the slot

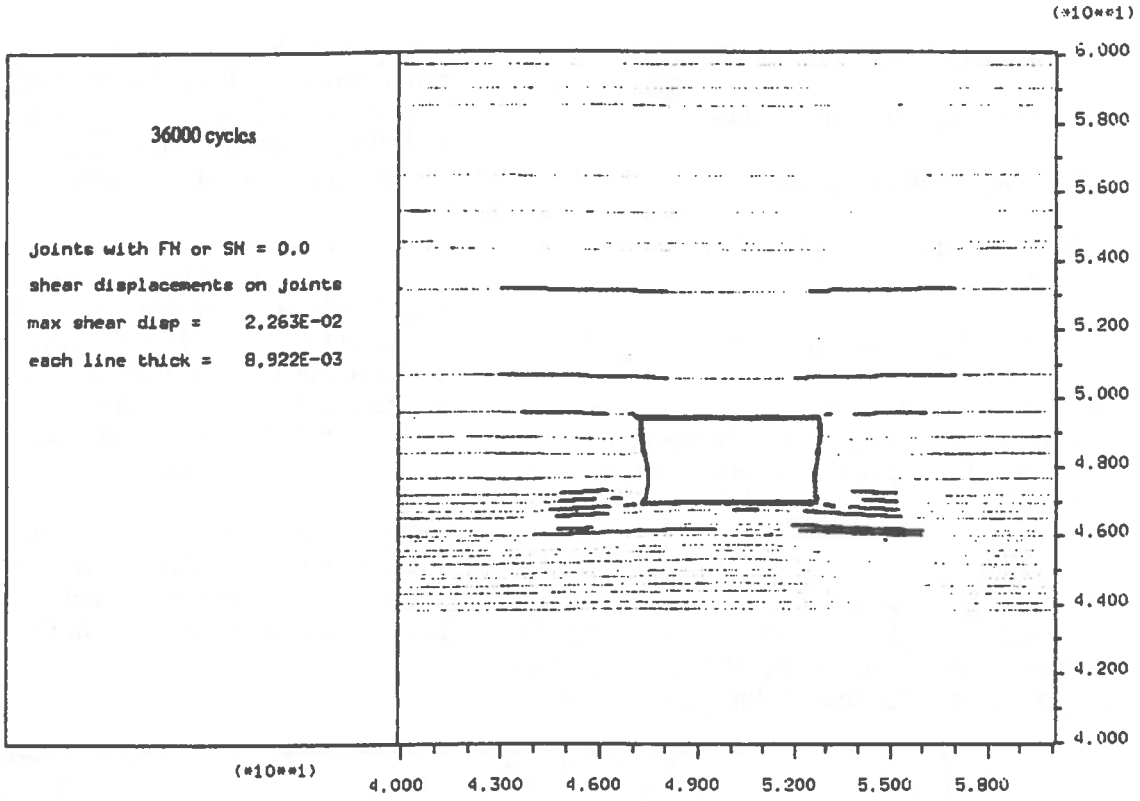

Fig. 6 : Shear displacements of joints after slotting with a vertical loading of 30 MPa

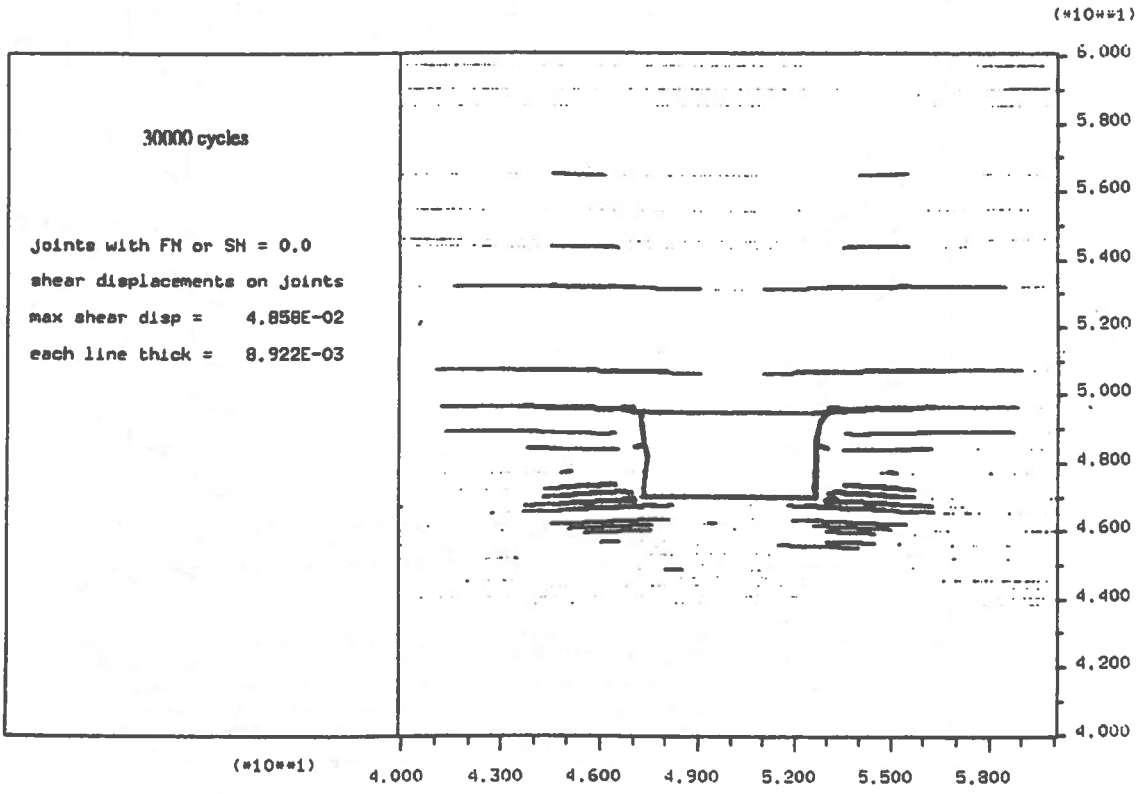

Fig. 7 : Shear displacements of joints without slotting and a vertical loading of 30 MPa

The high horizontal stresses are localised at the bottom and middle of the wall (60 MPa). Following cutting of the slot, these stresses fall significantly (40 MPa). The stress relief introduced is of the order of 30%. This relief is not limited only to the wall. The facings are also stress relieved over a considerable distance (Figs. 8 and 9).

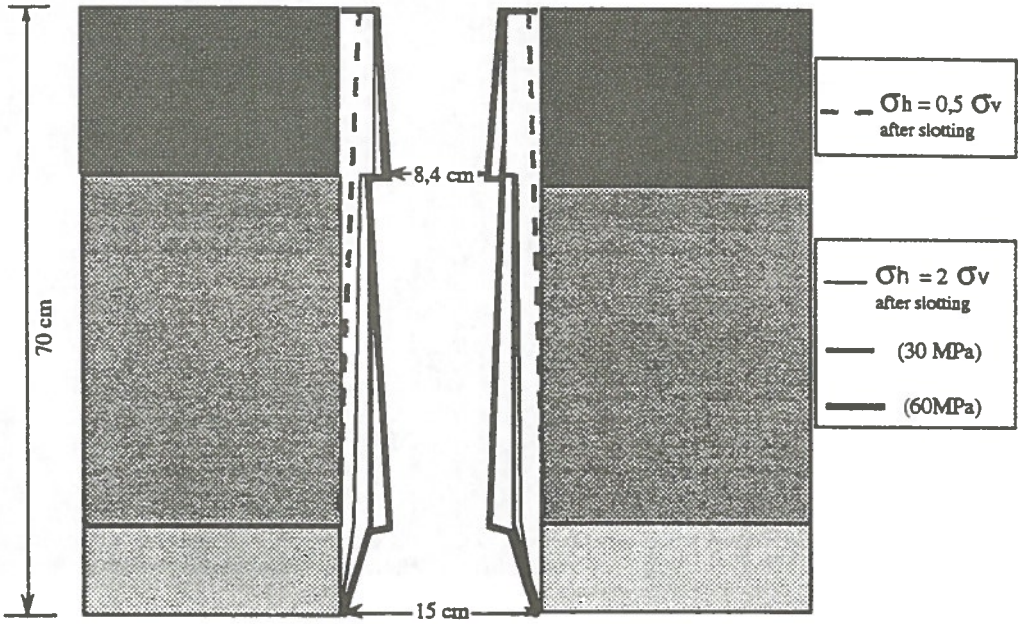

Fig. 5 : Slot section as a function of distance from cutting face

5. CONCLUSION

In this article we have analysed the behaviour of the rock mass in the vicinity of roadways treated by slots. Comparison of in situ observations in the treated zones with those made in untreated zones demonstrated the efficiency of this method and led to its being incorporated in the geological scheme for controlling dynamic phenomena.

The numerical modelling approach was used to analyse and quantify the role played by the slot. The results show that the slot makes an effective contribution to stress relieving the wall in the case of high initial horizontal stresses and to stress relieving the roadway facing.

The deformations and displacements obtained by the calculation are comparable with the in situ measurements.

6. REFERENCES

ITASCA, 1994.
UDEC ; Universal Distinct Element Code. Version 2.0
Minneapolis, Minnesota 55415 USA.

TRITSCH, J.J., 1993.
Examen géomécanique du sondage n° 834
U.E. Provence - Quartier Arbois Nord - INERIS France

GHOREYCHI, M., 1982.
Comportement du charbon de Provence sous forte charge de confinement.
CERCHAR - France

BIENIAWSKI, Z.T., 1989.
Rock Mechanics Design in Mining and Tunneling
Rotterdam, A.A. Balkema.

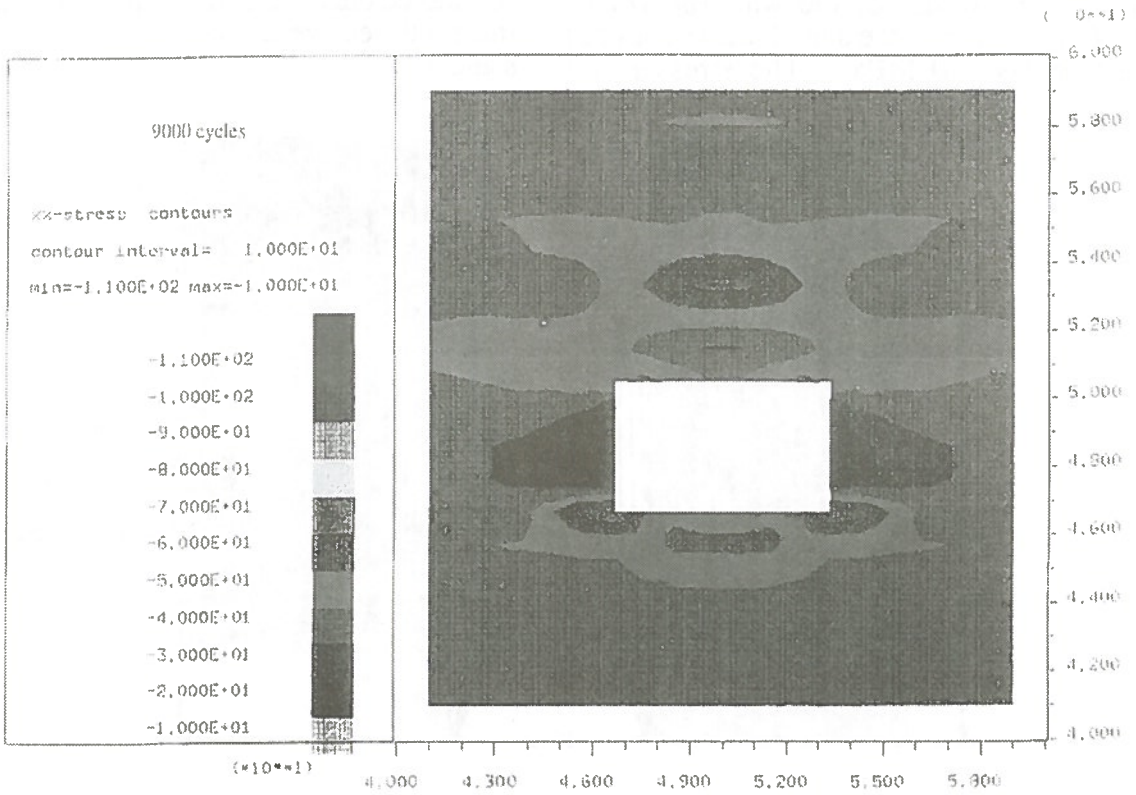

Fig. 8 : Contours of horizontal stresses σxx before slotting

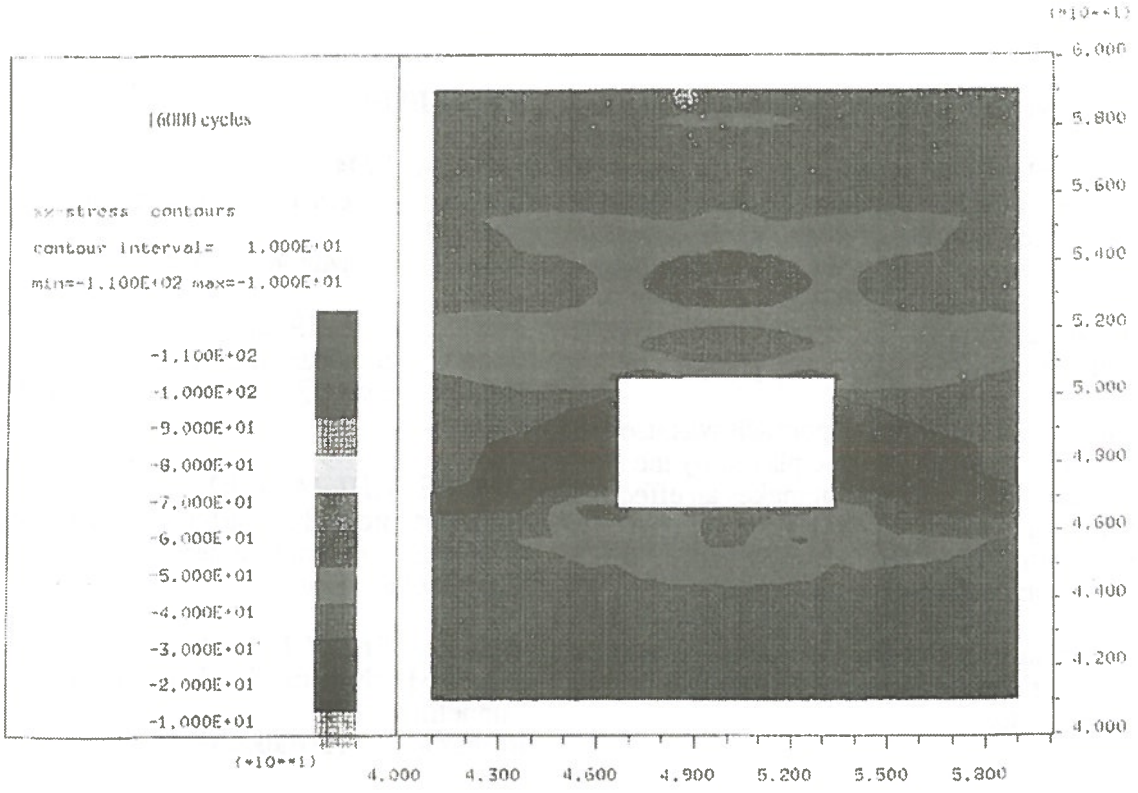

Fig 9 : Contours of horizontal stresses σxx after slotting

CAMI'95:3rd Canadian Conference on Computer Applications in the Mineral Industry
Montréal, Québec, Canada, October 22-25, 1995

Finite Element Model for the Outbursts in Underground Mines

Xiaoqin Chen, Kenneth Barron
Department of Mining Metallurgical and Petroleum Engineering
University of Alberta, Edmonton, Alberta

David Chan
Department of Civil Engineering
University of Alberta, Edmonton, Alberta

ABSTRACT

An outburst is defined as the violent ejection of gas and rock in a mine opening. Modeling has been found useful in the investigation of the mechanisms responsible for outbursts. Many models have been proposed, but few are able to simulate the whole process of an outburst from initiation to termination. In this study a new model has been developed based on the current knowledge of outburst behavior and numerical techniques. The model is able to evaluate the influence of various parameters, which are measurable in the field, on the initiation and post-initiation behavior of an outburst.

The model has been used to simulate the outbursts in #26 Colliery, Sydney, Nova Scotia. It was found that the model results agreed quite well with the measured outburst cavities. The cavity size, shape and growth showed close similarity between the model and the field observations. This indicates that the spalling mechanism of an outburst, inherent in the model, may offer a viable explanation for the outburst mechanism.

RÉSUMÉ

Une explosion est définie comme étant une violente éjection de gaz et de pierres dans une galarie minière. La modélisation s'est révélée utile lors des études des mécanismes responsables des explosions. On a proposé plusieurs modèles mais peu sont capables de simuler le processus complet d'une explosion du début à la fin. Nous avons développé un nouveau modèle basé sur les connaissances actuelles du comportement des explosions et sur des techniques numériques. Ce modèle est capable d'évaluer l'influence de paramètres divers, mesurables sur le terrain, à propos du comportement d'initiation et post-initiation d'une explosion.

On a utilisé ce modèle pour simuler des explosions dans la houillère # 26 de Sydney, Nouvelle Écosse. Nous avons trouvé que les résultats du modèle s'accordaient parfaitement avec les cavités d'explosions mesurées. La taille, la forme et la croissance de la cavité ont montré des similitudes proches entre le modèle et les observations sur le terrain. Ceci indique que le mécanisme de spallation d'une explosion, inhérent au modèle, peut offrir une explication valable du mécanisme d'une explosion.

INTRODUCTION

An instantaneous outburst was defined by Hargraves (1980), as the violent projection of coal and gas away from the freshly exposed coal in mining, either breaking into or in development of the seam. However, outbursts have been experienced in other mines, such as salt and potash (GIMM et al 1964, MAHTAB 1982) and from strata other than coal, such as sandstone overlying the coal seam (ASTON et al 1985). It is believed that all of these violent failures have been caused by the same basic mechanism. In a more generalized sense, an outburst can be defined as the violent ejection of gas and rock from a freshly exposed face in mining operations.

Past investigations have shown that many factors influence the initiation of an outburst, and many models have been proposed. Unfortunately, few of them have managed to quantitatively address the influence of the mechanical factors, such as the field stresses, gas pressure, opening geometry and geology of the area on outburst initiation, let alone their influence on outburst propagation and cessation.

FINITE ELEMENT MODEL

Mechanical Description of the Outbursts

From a mechanistic point of view, outbursts can be considered to be the result of mechanical failure of rock due to the combined effects of field stresses and pore gas pressure. If the effective stress exceeds the tensile strength of the rock, the rock fails in tension and spalls from the host rock. The detached rock may be completely shattered by the gas pressure destroying its structure, resulting in very fine particles. The expanding gas will transport this debris.

In the literature, the terms "sudden" or "instantaneous" are frequently used to describe the outburst process. In fact, the process continues over a time period from a fraction of a second to a few seconds or even longer. During this period, it is believed that the above described process is carried out in cycles, and is called the spalling. The spalling process continues until some mechanism is invoked to stop the outburst, leaving a cavity of a specific size.

The role of shear failure in the outburst mechanism is not as obvious as that of tensile failure. The "onion skin" texture left behind on the surface of the cavity wall after termination of an outburst implies some effects of shear failure. According to the experience from outbursts at #26 colliery, it was found that the sandstone with such a texture was substantially weaker than the original rock mass. This suggests that the sandstone has sheared during the bursting, but remained in the place without being expelled. It is not an unreasonable to assume that the gas has been released completely in this portion of sandstone.

The mechanical process described above can be condensed to outline the outburst mechanism as follows:

- An outburst is a tensile stress failure phenomenon.
- Effective stresses can be used to describe the stress state.
- Two basic failure modes (tensile and shear) are both observed in the outburst process; while tensile failure disintegrates intact rock, shear failure weakens rock and may cause some disintegration (to be proven in practice).
- Gas pressure acts as the transportation tool, in addition to being one component of effective stresses.
- A rapid spalling process is in effect, which leads to progressive failure.
- Stable conditions must be achieved before an outburst terminates.

Model Assumptions

Based on the outburst mechanism outlined above and the selection of finite element method as the method to evaluate the stress state in rock mass, the assumptions for the model can be summarized as follows:

1). Small deformation is assumed to prevail throughout the system, allowing the application of the finite element method code to the model.

2). The rock simulated in the model follows a perfect elasto-plastic constitutive relationship. The plastic deformations beyond the yield strength abide by the associated flow rule developed by Reyes and Deere (REYES, 1966), while Drucker-Prager's generalized failure criterion (DRUCKER, 1952) determines the yield condition.

3). The effective stress concept is adopted to describe the combined effects of the field stresses and gas pressure, and to define all failure criteria used in the model.

4). The elements representing the rock failed in the tensile mode are "removed" from system in each cycle of the spalling process, leaving a geometrically altered boundary for next cycle of the spalling.

5). The elements representing the rock failed in the shear mode "remain in the place" for the current cycle, but are de-gassed instantaneously in the next cycle.

6). The spalling process is simulated by the reiterations of the cycles and only stops when a stable boundary shape is formed or when it is apparent that the spalling will continue indefinitely.

The model is formulated by considering the FEM governing equation, degassification and removal of the failed elements.

Derivation of the Governing Equation

For a discretized 3-D irregular domain, the general finite element equation can be expressed as:

$$\sum_{n=1}^{ele.}\int_{v_e}\delta\varepsilon_{ij}\sigma_{ij}dv=\sum_{n=1}^{ele.}\int_{v_e}\delta u_i F_i dv+\sum_{n=1}^{ele.}\int_{s_e}\delta u_i T_i ds \qquad (1)$$

where, $\sum_{n=1}^{ele}$ summarizes all the elements discretized in the domain; $\int_v$, $\int_s$ indicate integration over the element body and portion of element surface subjected to traction respectively. δu_i is the "kinematically admissible displacement field" (virtual displacement imposed on the body), while $\delta\varepsilon_{ij}$ represents the associated virtual strain field distributed over the whole body. σ_{ij} represents the total stress tensor; Fi and Ti represent the external body forces and tractions on element surfaces.

According to the effective stress concept, in terms of effective stress and gas pressure the total stress can be expressed in tensor form as the following:

$$\sigma_{ij}=\sigma'_{ij}+p\Delta_{ij} \qquad (2)$$

where, σ'_{ij} - effective stress tensor;
p - pore gas pressure;
Δ_{ij} - Keronecker delta (or substitution tensor); $\Delta_{ij}=\begin{cases}1 & i=j\\ 0 & i\neq j\end{cases}$.

Substituting Eq. (2) into Eq.(1) and adjusting the terms gives:

$$\sum_{n=1}^{ele.}\int_{v_e}\delta\varepsilon_{ij}\sigma'_{ij}dv = \sum_{n=1}^{ele.}\int_{v_e}\delta u_i F_i dv+\sum_{n=1}^{ele.}\int_{s_e}\delta u_i T_i ds-\sum_{n=1}^{ele.}\int_{v_e}\delta\varepsilon_{ij}p\Delta_{ij}dv \qquad (3)$$

For a two dimensional rectangular element as shown in Fig. 1, the equation (4) can be derived from Eq. (3) as:

$$\langle\delta\underline{q}\rangle\{Q\}'_e=\int_{v_e}\delta\varepsilon_{ij}\sigma'_{ij}dv \qquad (4)$$

Since $\langle\delta\underline{q}\rangle$ is an arbitrary permissible displacement vector, Eq. (4) requires:

$$\sum_{n=1}^{ele.}\{Q\}'_e=\sum_{n=1}^{ele.}\{P_b\}_e+\sum_{n=1}^{ele.}\{P_t\}_e+\sum_{n=1}^{ele.}\{P_{gp}\}_e \qquad (5)$$

or $$\{Q\}'=\{R\} \qquad (6)$$

Equation (5) or (6) is the governing equation for the domain with pore gas pressure. The finite element equation for a plain strain conditions can be obtained as:

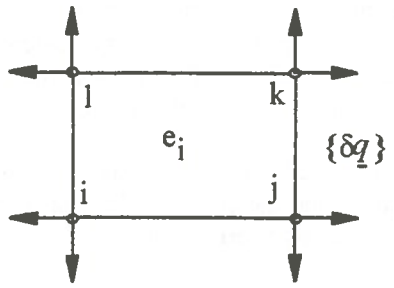

Figure 1. A 2-D Rectangular Element with Postulated Nodal Forces and Associated Nodal Displacement Vector $\{\delta q\}$

$$[K]\{q\} = \{R\} \qquad (7)$$

Where, [K] is the global stiffness of the system which is assembled from the element stiffness $[k]_e$.

In formulating this FEM equation, no material behavior has been specified. The calculations, then, are valid for any material. According to the assumption that the materials in the model are elasto-plastic, the [c] matrix for perfect elasto-plastic relation of a Mohr-Coulomb type material developed by Reyes and Deere (1986) will be used in this equation.

Because the material dealt with by the model is assumed to be non-linear, an incremental approach has to be adopted. In the incremental analysis, the loads, stresses and displacements for any incremental step can be written as $\{R_n\}$, $\{\sigma_n\}$ and $\{q_n\}$. The current $\{\sigma_n\}$ and $\{q_n\}$ are regarded as the initial stresses and displacements for the next loading increment. Thus the matrix form of the governing equation (7) is expressed as:

$$[K_{n+1}]\{q_{n+1}-q_n\} = [K_{n+1}]\{\Delta q_n\} = \{\Delta R_n\} \qquad (8)$$

Where, $\Delta R_n = \sum_{n=1}^{ele.} \left[\{\Delta P_b\} + \{\Delta P_t\} + \{\Delta P_{gp}\}\right]$

and $\{\Delta P_b\}$, $\{\Delta P_t\}$ and $\{\Delta P_{gp}\}$ are the increments of the respective external loading.

In a nonlinear analysis, the stiffness is dependent on the current stress state and has to be re-evaluated at small increments of load starting from the previously determined conditions. For the perfect elasto-plastic nonlinear material, however, the whole external loading is applied at once in the first cycle, by assuming all elements to be elastic to begin with. Since the problem is non-linear, the solution may not be correct if the stress state exceeds the strength of the material. In this case, a stepwise linear relationship between yielding of one element to another is assumed for the analysis.

Gas Pressure Consideration

The gas pressure within the specific strata is assumed to be uniformly distributed. At the periphery of the excavation, the gas pressure changes stepwise from atmospheric to the in situ gas pressure. If the stratum is sheared, it is assumed that the gas will escape instantaneously. By initially specifying a pre-existing shear zone or creating a shear zone from the previous cycle, the step distribution of the gas pressure moves towards the inside of the strata.

In the light of this assumption for gas pressure distribution, there are two aspects to be considered in the formulation of the model. First the gas pressure, in terms of the effective stress concept, can be readily treated as an extra loading component. It can be evaluated by this equation:

$$\{P_{gp}\}_e = \int_{V_e} [B]^T p\{L\} dv \qquad (9)$$

Secondly, the model assumes that instantaneous degassing occurs in the shear zone. This instantaneous degassing is simulated mathematically by applying an equal but opposite gas pressure loading to those sheared elements in the next iteration. The loading forces, therefore, can be readily calculated as follows:

$$\{P_{gp}\}_e = \int_{V_e} [B]^T (-p)\{L\} dv \qquad (10)$$

Excavation of the Material

According to assumption 4), the tensile failed elements should be removed from the system. The observations of the outbursts in situ reveal that there are basically two physical processes involved in association with the failed rock being removed. In most cases, the rock failed in tension may receive very high energy of motion transmitted from high potential energy stored in compressed gas and from the strained solid rock. The broken rock, therefore, piles up at a distance away from the spalling surface and provides virtually no back support to the boundary of the cavity. This scenario is called the "empty" cavity formulation.

In contrast, the broken rock may not obtain enough energy to be transported far from the spalling surface. It will quickly pile up in front of the spalling surface and provides back support to it. Even though the broken rock piles up right in front of the surface, the back support can be very small. When considering the "choke up" case reported by Gray (GRAY, 1981) and other discussions about the factors terminating an outburst event (GOLDER ASSOCIATES, 1987), this filled cavity assumption may describe some extreme situations in situ.

In order to simulate the above two described basic mechanisms without altering the program, the model adopts the approach of reducing the Young's modulus of the "removed" elements to a very low value or to a specific prescribed value. The procedures for the simulation follow the general method for analysis of geometrically altered structures revised by Ghaboussi and Pechnold (GHABOUSSI, 1984).

According to this general analysis method, if $\bar{P}$ expresses the nodal external load vector and $\bar{I}$ is the internal resisting force vector that can be computed from element stresses as:

$$\bar{I} = \sum_{i=1}^{ele} L_i^T \int_v B_i^T \sigma_i dv \qquad (11),$$

The residual load vector $\bar{R}$ can be calculated as:

$$\bar{R} = \bar{P} - \bar{I} \qquad (12)$$

When the elements and their associated external loads and internal stresses are removed from the element system at the beginning of increment n, the standard nonlinear formulation of FEM will apply as long as the load vector is modified appropriately to take into account the initial disturbance and inequilibrium due to altering the system. This modified residual load vector $\bar{R}_n^*$ can be computed by:

$$\bar{R}_n^* = \bar{P}_{n-1} - \bar{I}_{n-1}^* \qquad (13)$$

where, $\bar{P}_{n-1}$ indicates all the effects of external loads at increment n-1, which is regarded as unchanged when the system geometrically changed at the beginning of increment n. $\bar{I}_{n-1}^*$ represents the effects of internal stress change in those elements which are currently active. It accounts for the change due to the fact that the elements removed from system will no longer contribute to the internal resisting force vector. The load vector, revised by removing elements, therefore, can be expressed as:

$$\bar{R}_n = \Delta\bar{P} + \bar{R}_n^* = \bar{P}_n - \bar{P}_{n-1} + \bar{P}_{n-1} - \bar{I}_{n-1}^* = \bar{P}_n - \bar{I}_{n-1}^* \qquad (14)$$

Specifically in this model, $\bar{P}_n$ will be zero because the elements will be removed only after the system has been equilibrated and the tensile failed elements have been determined. Denoting $\bar{I}_{n-1}$ as the internal nodal force vector without removing the elements, and $\bar{I}'_{n-1}$ as the internal nodal force vector after removing the elements, then, $\bar{I}_{n-1}^*$ is obtained from:

$$\bar{I}_{n-1}^* = \bar{I}_{n-1} - \bar{I}'_{n-1} \qquad (15)$$

The Finite Element Model

The model is composed of three parts: the pre-processor, FEM model program and the post-processor. The pre-processor will prepare the input data file and the post-processor graphically presents the results, while the FEM model program constitutes the core of the model. Fig. 2 shows the

simplified logical flow diagram for the FEM model program. The program is built up from two distinctly functional modules that will fulfill every task depicted in the diagram. The first module realizes the finite element stress calculations and is able to handle the gas pressure under the effective stress concept for a given condition. The second module has the function of identifying the elements failed in tension and in shear and they will be removed or retained accordingly.

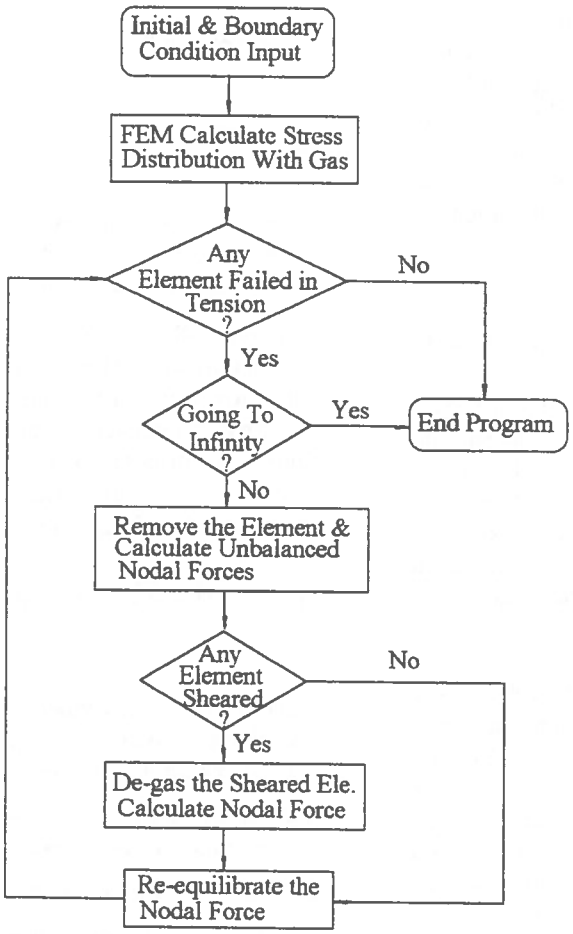

Figure 2. Model Flow Chart

The shear failure criterion is included in the FEM program (assuming that a yield element has been sheared). The failure criterion for tension uses the direct comparison of the stress and strength (i.e., $\sigma_3<\sigma_t$, σ_3 is the minor principle stress and σ_t is the tensile strength of the rock). The modeling is carried out logically according to following the steps:

1). The given boundary conditions, external loading conditions and gas pressure are prepared as input data by use of a pre-processor. The first module is called to calculate the stress distribution around the initial underground excavation.

2). Each element is then examined to test whether it has failed in tension, in shear or has not yet failed, by calling the second module. If no element has failed in tension within the gas bearing stratum, the program terminates, either not initiating an outburst or stabilizing at some specific size cavity (if it is not the first iteration). Otherwise, the program carries on to the next step.

3). Those elements failed in tension are "removed". This changes the boundary geometry of the opening. The residual stresses, by altering the geometry, can be computed according to the general method. Those elements failing in shear (yielded) will be degassed. The resulting nodal forces can be computed from Eq. (15).

4). The nodal forces induced from both "removing" and "degassing" elements will cause unbalance to the system. The first module is called again to re-equilibrate the system, which produces the redistributed stress field around the newly formed opening through spalling.

5). With such a redistributed stress field, step 2), 3) and 4) successively iterate until it terminates at a stabilized cavity or is deemed to carry on indefinitely.

COMPARISON OF MODEL RESULTS AND FIELD DATA

The last two outbursts at No. 26 Colliery occurred in the main deep development. The investigations of these outbursts have accumulated enough field data for model verification. These two outbursts will be used as cases to compare with the model results.

Outbursts at No. 26 Colliery

The outbursts at No. 26 Colliery started in the summer of 1977 when the workings reached a depth of 700 meters below the sea level. Since then, 37 events have been recorded as rock outbursts. During the event period, the frequency and intensity of outbursts increased with the depth. Prior to June 1983, gas was neither detected and tested nor recorded after the rock outbursts. In the later events, however, a large volume of gas was detected after each initiation. The details of each outburst were summarized by Kullman (KULLMAN, 1989) and also reported by Golder Associates (GOLDER ASSOCIATES, 1987).

The outbursts occurred exclusively in the development entries when driven into virgin coal where the sandstone erosion channel was located within 2.5 meters above the top of the coal seam. The bursting formation was invariably sandstone, sometimes with siltstone inter-beds. The failure face exposed within the outburst cavities had a typical "onion skin" texture. The failed material was generally pulverized.

The cavity formed in the last two outbursts at No. 26 Colliery was mapped in longitudinal direction and at fourteen cross sections. Fig. 3 shows the longitudinal and selected cross sections. Three cross sections were selected for comparison because they have different areas of sandstone exposed over the crown of the entry.

Modeling and the Results

The rock properties used in the modeling of the two outbursts are summarized in table 1. The simplified geology around the entry and the entry geometry are depicted in Fig. 4.

From this comparison, it is concluded that the model results agree well with the outburst cavities observed in the field. The cavity size, cavity shape and cavity growth showed substantial similarity between model results and reality. This indicates that the spalling mechanism of outbursts, hypothesized in this model, may offer a viable explanation for the outburst mechanism.

Elasto-Plastic Properties and Strength Parameters of the Rock Table 1

Elasto-plastic properties	Young's Modulus E (GPa)	Poisons Ratio μ	Friction Angle ϕ (°)	Cohesion c (MPa)
Siltstone	26.15	0.36	35	20
Sandstone	18.5	0.18	30	18
Strength parameters	Uniaxial Strength σ_c (MPa)	Tensile Strength σ_t (MPa)	H&B Const m	H&B Const s
Siltstone	50.5	-11.4	4.2	1.0
Sandstone	48.4	-2.9	14.9	1.0

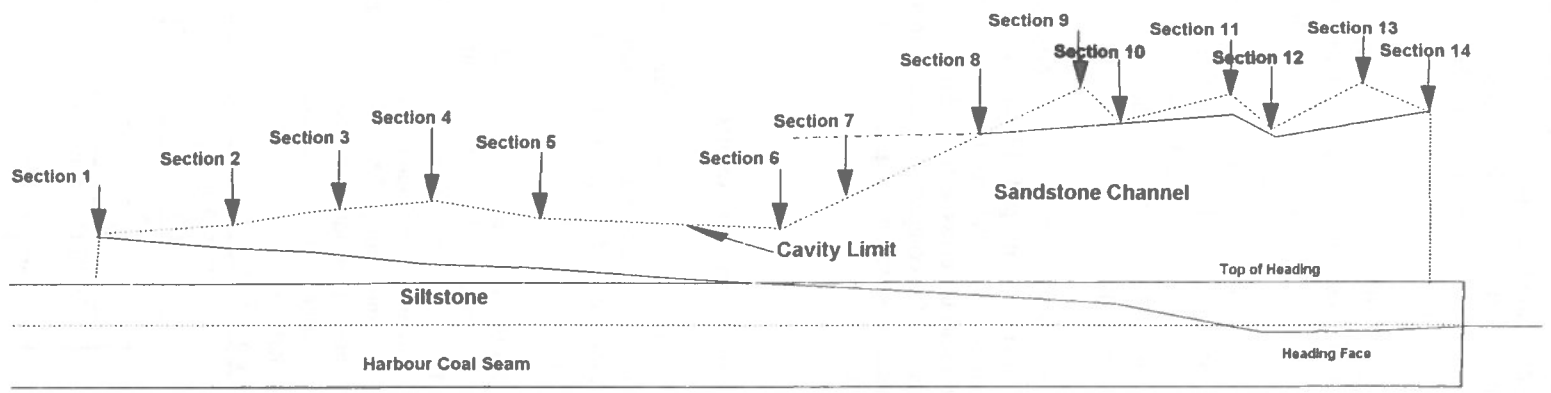

Logitudinal Section of Cavity from Outburst #36 and #37

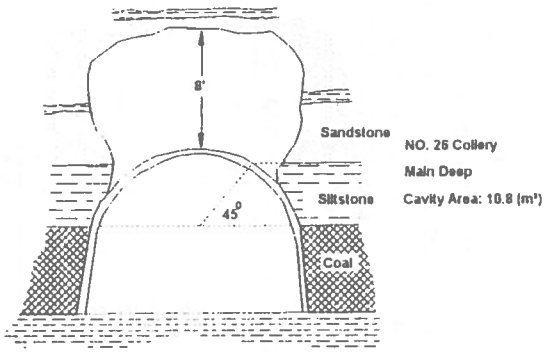

NO. 25 Colliery
Main Deep
Cavity Area: 10.8 (m²)

Section 7: 44' Down From Intersection

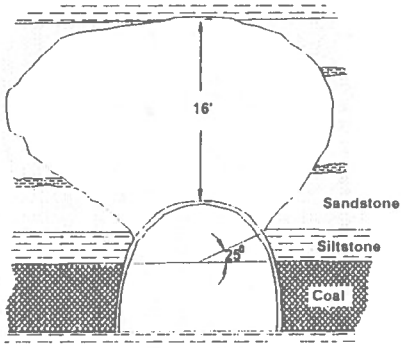

No. 26 Colliery
Main Deep
Cavity Area: 40.0 (m

Section10: 80' Below Intersection

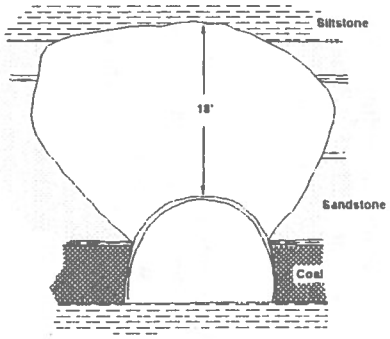

No.26 Colliery
Main Deep
Cavity Area: 50.4 (m²)

Section 12: 68.5' Below X-Cut

Figure 3. In-situ Outburst Cavity. Longitudinal and selected Cross Sections - No. 26 Colliery, Sydney, Nova Scotia

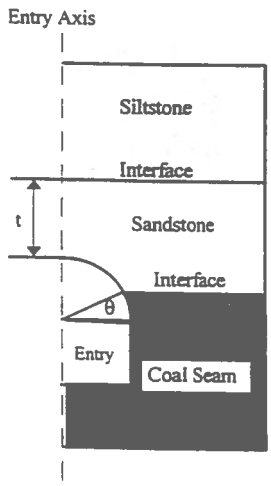

t - Sandstone height
θ - Exposure angle

Figure 4. Entry Geometry and Geology

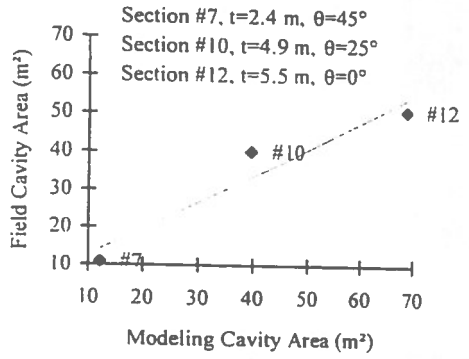

Fig. 6. Comparison of Stabilized Cavity Areas from the Field and Model Simulation.

A number of trial runs were conducted with the selected exposure angle by assuming different gas pressures. The resulting cavity from modeling was compared with that of the selected cross section. A comparison between the cavity and a selected in situ cross section is shown in Fig. 5. Fig. 6 compares the model and field cavity sizes for three cross sections.

MODEL APPLICATION

The model was also used to conduct a series of parametric studies. The results from these studies have shown very favorable support to the model through the similarities shared with field observations (CHEN, 1995). Field observations and model results all suggest that outburst tends to become more severe (more broken material expelled) as the gas pressure increases. An outburst case was reported by Gray (GRAY, 1980) in which the cavity left by the outburst measured 21 m long, and a total of 300 m³ (400 tons) broken material was expelled. There is no detailed information available about this outburst, but it was certain that the unusual size of the cavity was related to the high gas energy (pressure). The parametric study by using this model indicated that when gas pressure increases beyond a certain magnitude, the spalling process tends to continue to indefinitely. This means that a very large (deep) cavity may form and the outburst would terminate due to some other mechanisms (such as broken material "choking" it).

The results of an analysis of the influence of sandstone height and exposure angles are also similar to the observations in the field.

Through such parametric studies, it may be possible to draw some conclusions which can be utilized in preventative measures. The most obvious example is the study of pre-existing shear zones. This study indicates that by pre-defining a shear zone (degassing zone) the outburst become less likely to occur. The study of the other parameters, such as exposure angle and sandstone thickness, may also be used to develop guide lines for prevention. For example, the exposure angle can be adjusted by changing the position of entry in the formation to minimize the possibility of outburst initiation.

The model can be used to attempt a prediction, as well as to assess preventive measures for a particular situation. In the parametric studies, the model was used to find out the gas pressure that initiates an outburst. As many factors have been considered in the model, which may be directly or indirectly responsible for the outburst phenomenon, the application of the model to specific cases may be more useful than doing "general" analyses with the model. However, care must be exercised since it is

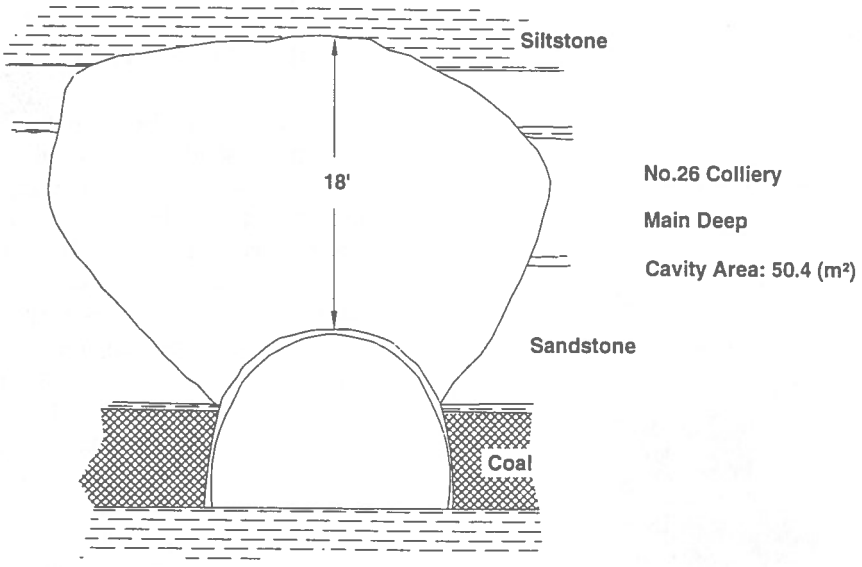

Section 12: 66.5' Below X-Cut

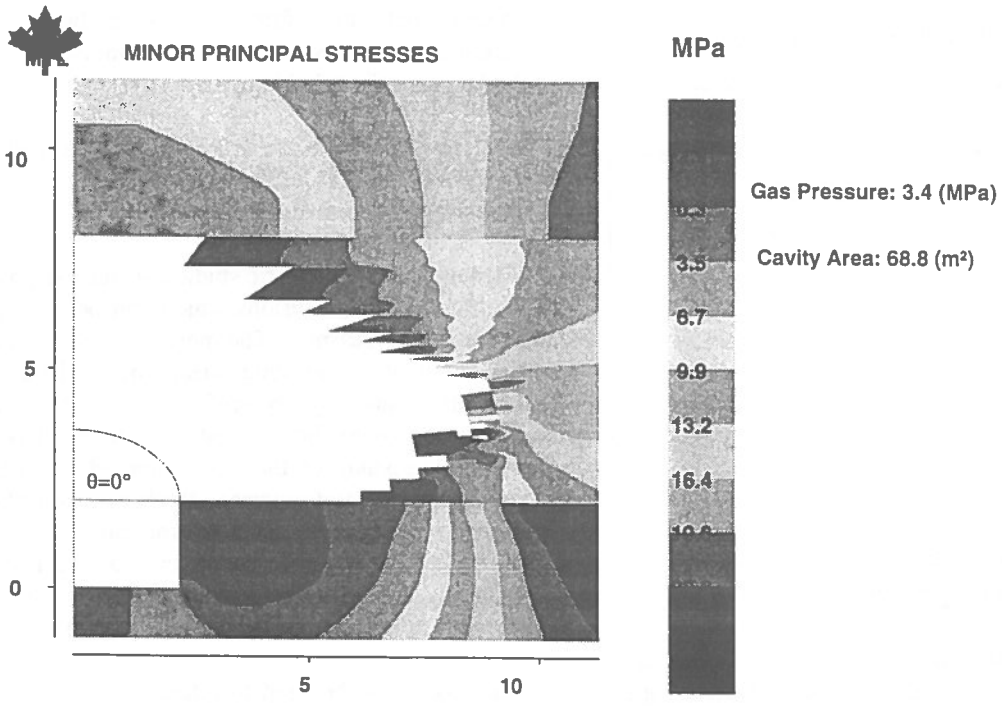

Two dimensional outburst model for a deep opening - sigh/sigv=1.1

Figure 5. Comparison of In-situ Cavity Area of Cross Section 12 and Model Result

believed that the model is more suitable to make a comparison of the relative merits of two mining schemes, rather than relying on the absolute values at this stage of the research.

CONCLUSIONS

Many models for the outbursts occurring in underground mines have been proposed in the past. Most of them are descriptive in nature, or difficult to apply to engineering practice. The model described here has shown potential for further growth as a more sophisticated tool for analyzing outbursts.

Compared with other models, the following advantages of this model have been realized:

1). This model is a practical tool which demands only conventional field data for execution.

2). The model can be easily adapted to cope with most local conditions. Because the finite element method is designed to evaluate the stress states, any material constitutive relationship could be dealt with. Major faults or other geological features of concern might also be simulated.

3). Operation of the model is straightforward. As soon as the input files are prepared, the model executes to produce the final results.

4). The model has a potential for further development. It is easy to incorporate any failure criterion and new algorithms associated with the outburst phenomenon. The energy aspect of outbursts could be easily incorporated into the model through a proper modification.

The comparison between the model and the case history from No. 26 Colliery shows satisfactory results. The parametric analysis also provides strong support to the verification. This may indicate that the mechanism inherent in the model has offered a viable explanation of the actual mechanism of outbursts.

There are some limitations to this model at this development stage. The model still requires further verification from case histories. Until such field data is forthcoming, it will not be possible to fully verify this or any other outburst model. The current model can only handle the perfect elasto-plastic material, more material constitutive relationships should be included in the program. A better finite element selection and finite element algorithm to handle the non-linearity may speed up the execution of the model.

It is strongly recommended that a 3-D model be developed to address the end effects of the entry face. As most outbursts occur in the development entry headings, a 3-D model could simulate the stress state more realistically, so that more reliable results could be expected.

REFERENCES

ASTON, T. R. C. & CAIN, P., 1985
Gas and rock outbursts at No. 26 Colliery, Sydney coalfield, Nova Scotia - a case history. Proc. 21st Int. Conf. Safety in Mines Research Inst., Sydney, Australia, 139-146.

CHEN, X., BARRON, K. & D. CHAN, 1995
Few factors influencing outbursts in underground coal mines, Intl. Symp. on Management and Control of High Gas Emission and Outbursts in Underground Coal Mines, Wollongong, Australia.

DRUCKER, D. C. & PRAGER, W., 1952
Soil mechanics and plastic analysis or limit design. Q. App. Math. v. 10, 157-165.

GHABOUSSI, J. & PECKNOLD, D. A., 1984
Implement finite element analysis of geometrically altered structures. Intl. J. Num. Meth. Eng. v. 20, 2051-2064.

GIMM, W. A. R. & PFORR, H., 1964
Breaking behavior of salt rock under rock bursts and gas outbursts. Proc. 4th Intl. Conf. on Strata Control and Rock Mech. : 434-449. Colorado, U. S. A..

GOLDER ASSOCIATES, 1987
Development of an outburst model for the Sydney coalfield Cape Breton, Nova Scotia. Contract Report (DSS Contract No. 23440-6-9025).

GRAY, I., 1980
The mechanism of, and energy release associated with outbursts. Symp. on Occurrence, Prediction and Control of Outbursts in Coal Mines, Southern Queensland Branch, Austr. Inst. Mining and Metall., Australia, 111-126.

HARGRAVES, A. J., 1983
Instantaneous outbursts of coal and gas - A review. Proc. Australas. Inst. Min. Metall., 285, 1-37.

KULLMAN, D. H., 1988
Modeling of outbursts at No.26 colliery, Glace Bay, Nova Scotia. MSc. Thesis, University of Alberta.

MAHTAB, M. A., 1982
Geomechanical aspects of gas outbursts in Louisiana salt mines. Bulletin of the Association Engineering Geologists 19(4), 389-400.

REYES, S. F. & DEERE, D. V., 1966
Elastic-plastic analysis of underground openings by finite element method. Proc. First Congr. Int. Society of Rock Mechanics, Lisbon, 477-483.

CAMI'95: 3rd Canadian Conference on Computer Applications in the Mineral Industry
Montréal, Québec, Canada, October 22-25, 1995

Energy Considerations in Geomechanical Mine Design

Murray Grabinsky, Brent Corkum, John Curran
University of Toronto, Toronto, Ontario

Vassilios N. Kazakidis
MRD-Mining Research Directorate, Sudbury, Ontario

ABSTRACT:

An understanding of the energy changes associated with progressive mining is believed to be important for good geomechanical design of underground mines. The relevant work and energy balances have been carefully considered and are available in the published literature. However, the use of these relationships has apparently not been widespread in practical mine design, likely owing to the fact that the energy calculations are generally not automatically performed in current software analysis tools. The work presented here considers the work and energy components that can be easily calculated from an elastic analysis performed using the Boundary Element Method. A procedure is then developed for deriving the *incremental* work and energy components from the results of the elastic analyses of the initial and final mining geometries. The theoretical results are incorporated in a utility used with the elastic analysis program *Examine*^{3D}. Application to a generic sequencing of mining stopes is demonstrated.

RÉSUMÉ:

La compréhension des changements d'énergie adjoints à l'exploitation progressive des mines est généralement regardée comme essentiel pour du bon dessin géomécanique des mines exploitées souterrainement. Les équilibres de travail et de l'énérgie ont été soigneusement examinés et sont disponibles dans la littérature publiée. Cependant l'emploi de ces relations est toujours relativement rare dans la domaine du dessin des mines, probablement parce que les calculs des énergies ne sont habituellement pas automatiquement effectués avec les moyens d'analyse en software courant. Le travail presenté ici prend en considération les composantes de travail et d'énergie, qui peuvent facilement être calculées avec une analyse élastique en utilisant la méthode 'Boundary Element Method'. Ceci fait, on developpe un procédé pour le tirage des composantes *d'accroissement* du travail et de l'énergie à partir des résultats de l'analyse elastique des initiaux et finals géométries des mines. Les résultats théoriques sont unis dans une application basée sur le programme d'analyse élastique *Examine*^{3D} . L'application pour enchaînement générique de gradins des mines est expliqué.

INTRODUCTION

Mining is normally an ongoing or progressive process in which the volume excavated is increased over time. Energy changes are associated with the changing excavation geometry, and an understanding of the nature of these energy changes is believed to be important in developing mining strategies that mitigate the damaging effects of energy accumulations which result in rockbursts.

Cook and co-workers (Cook 1962, 1963, Cook et al. 1966) were some of the first to call attention to the significance of energy changes associated with mining. Later work considered the energy changes in more detail (Walsh 1977 and Brady and Brown 1981), although it was not until recently that the matter was considered fully in a formal manner (Salamon 1984).

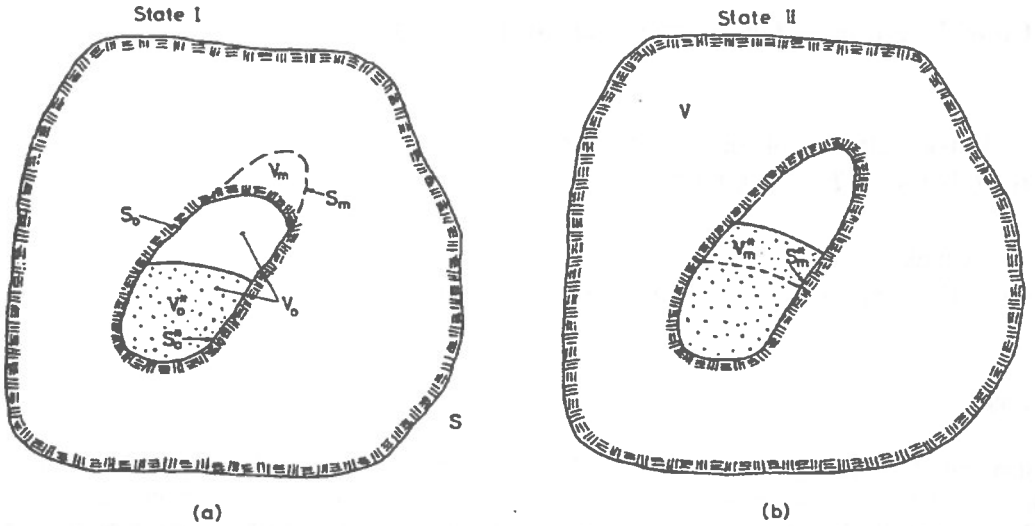

Figure 1. Definition of geometries for incremental mining (from Salamon 1984)

Despite these advances, the calculations for energy changes have not been incorporated into available numerical modelling tools for mine design to the same extent as have, for example, the calculations for strength factors based on popular rock mass failure criteria. This state of affairs is, however, changing (e.g., Tinucci and Verona 1991 and Christianson and Board 1993). One of the objectives of this work, then, is to improve the energy calculation capabilities of a practical elastic analysis and design tool, *Examine*^{3D}.

Previously, the Rock Engineering Group (Department of Civil Engineering, University of Toronto) produced an Energy Balance Utility for use with *Examine*^{3D} (Corkum et al. 1994). This utility calculates certain energy quantities by explicit area integration over the surface of the modelled excavation and then makes some assumptions in order to determine the remaining energy quantities. It also performs a strain energy density calculation at user-defined field points surrounding the excavated volume. All calculations are made assuming an unsupported excavation and that all material is excavated in a single step. Although the implementation is specific to *Examine*^{3D}, the ideas are general and could equally as well be applied to other elastic boundary element analysis tools.

The objective of this work is to determine a method for calculating the energy components due to incremental mining using energy quantities derived from existing analyses (which assume excavation in a single step). The theoretical relations are checked using results from analytic solutions to two- and three-dimensional problems. An important finding is that not all incremental energy components can be calculated conveniently, and therefore consideration is also given to the developments that would be required in order to determine these remaining energy terms. Finally, the development and implementation of various utility programs is considered, and the application to a typical mining scenario is demonstrated.

WORK AND ENERGY COMPONENTS

Here, the descriptions of work and energy components and associated notation is generally consistent with that used by Salamon (1984), and is provided below for sake of completeness. Salamon considers initial (state I) and final (state II) mining stages as shown in Figure 1. In the current work, support (including backfill) is not considered. The relevant terms are then:

- **W** the work done by the far-field tractions riding through incremental mining-induced displacements on surface **S**,
- **Um** the strain energy originally contained in the volume mined **Vm**,
- **Uc** the additional strain energy added to the remaining rock **V** due to the incremental mining,

Wr the released (unrecoverable) energy associated with the incremental mining, and

Wk the kinetic energy associated with the incremental mining.

Term **Wk** may be thought of in two ways: If in state I **Vm** was to be removed and a set of complementary tractions applied to the surface **Sm** so that the remaining rock was unaffected, then 1) **Wk** would be the work done in slowly removing these surface tractions; 2) **Wk** would be the kinetic energy added to the rock as a result of the surface tractions being removed suddenly (in fact, an amount 2·**Wk** would be added, but an amount **Wk** would be dissipated through natural rock mass damping during transitory vibration).

Salamon (1984) developed the energy balance relations suitable for analyzing the energy changes associated with incremental mining, vis.

$$(W + Um) - Uc = Wr > 0 \qquad \text{(Eq. 1)}$$

or

$$W = Uc + Wk \qquad \text{(Eq. 2)}$$

where

$$Wr = Um + Wk \qquad \text{(Eq. 3).}$$

Note that **W** and **Um** are the only two *sources* of incremental energy in the system, and that **Uc** is the only *stored* incremental energy. Therefore the energy balance equation (Eq. 1) expresses the difference between the *expended* and *stored* energy increments, which must be equal to the released energy **Wr**, a positive quantity. Further, the released energy can only come from the strain energy **Um** stored in the unmined material and the work **Wk** done at the newly-excavated surface **Sm**, hence Eq. 3. Algebraic manipulation yields Eq. 2. To summarize,

W+Um is the energy available to do work,

Uc is the transformed recoverable (stored) energy, and

Um+Wk becomes the transformed unrecoverable (released) energy called **Wr**.

COMPUTATION OF WORK AND ENERGY COMPONENTS

Through a contract with the Canadian Rockburst Research Program, an Energy Utility (Corkum et al. 1994) was developed for use with the elastic boundary element analysis program *Examine*^{3D}. This Utility calculates the quantities **Um** and **Wk**, and then computes **Wr** (which is normally the quantity of interest for design purposes) using Eq. 3. It is important to note that *Examine*^{3D} inherently assumes that the excavation is extracted in a single step. In this case, **Wk** is easily computed by performing surface integration over the boundary elements used in the model to define the excavation geometry. The term **Um** is also easily computed as the product of the excavation volume and the strain energy density due to the initial stress field. Furthermore, it has been suggested that for an infinite body problem **Uc** = **Wk** (e.g., Cook 1963) and therefore **W** = 2·**Wk** from Eq. 2.

Now, mining is a progressive process, and what is desired for design purposes is an understanding of how **Wr** varies with incremental mining. This may be done by considering two elastic analyses A and B corresponding to the initial (state I) and final (state II) geometries respectively.

For an *Examine*^{3D} analysis of the initial mining stage, denote the initial mined volume $\mathbf{Vm}^{A}$ and the computed work and energy components $\mathbf{Um}^{A}$ and $\mathbf{Wk}^{A}$. The energy relationships are then used to determine $\mathbf{Wr}^{A} = \mathbf{Um}^{A} + \mathbf{Wk}^{A}$, $\mathbf{W}^{A} = 2\cdot\mathbf{Wk}^{A}$, and $\mathbf{Uc}^{A} = \mathbf{Wk}^{A}$. A similar procedure is carried out for the final stage, with associated quantities being designated using superscript ^{B}. Note that for the incremental mining case of interest, $\mathbf{Vm} = \mathbf{Vm}^{B} - \mathbf{Vm}^{A}$.

Since the system is linear elastic we must have $\mathbf{W} = \mathbf{W}^{B} - \mathbf{W}^{A}$. The same cannot be immediately said for **Wr**, however, owing to its dependence on **Um** and **Wk**. In particular, note that $\mathbf{Um} \neq \mathbf{Um}^{B} - \mathbf{Um}^{A}$ and $\mathbf{Wk} \neq \mathbf{Wk}^{B} - \mathbf{Wk}^{A}$. However, it turns out that in fact it *is* the case that $\mathbf{Wr} = \mathbf{Wr}^{B} - \mathbf{Wr}^{A}$ as will be shown next. Equation 1 can be rearranged into the form

$$Wr = W - (Uc - Um) \qquad \text{(Eq. 4).}$$

The term (**Uc** - **Um**) can be recast considering different strain energy terms. Let **U'** denote the strain energy stored in the original unmined volume **V+Vm** (state I), computed as

$$\mathbf{U'} = \int_{V} \phi^{P} dV + \int_{Vm} \phi^{P} dV = \int_{V} \phi^{P} dV + \mathbf{Um}$$

where ϕ is the strain energy density function and ϕ^P denotes the strain energy density in the initial state (state I). Also let **U** denote the strain energy contained in the final unmined volume **V** (state II), computed as

$$\mathbf{U} = \int_{V} \phi dV .$$

Therefore **Uc = U - (U' - Um)**, or **(Uc - Um) = (U - U')** and equation 4 then becomes

$$\mathbf{Wr} = \mathbf{W} - (\mathbf{U} - \mathbf{U'}) \qquad \text{(Eq. 5).}$$

When states I and II are analyzed using *Examine*^{3D}, we have that

$$\mathbf{U'} = \int_{V+Vm} \phi^{i} dV + \mathbf{Uc}^{A}$$

and

$$\mathbf{U} = \int_{V} \phi^{i} dV + \mathbf{Uc}^{B}$$

where ϕ^i is dependent on the in situ stresses. The term **(U - U')** then becomes

$$(\mathbf{U} - \mathbf{U'}) = (\mathbf{Uc}^{B} - \mathbf{Uc}^{A}) - \int_{Vm} \phi^{i} dV .$$

Further, when a *uniform initial stress field* exists we have that

$$\int_{Vm} \phi^{i} dV = \phi^{i}\, \mathbf{Vm} = \phi^{i}\, (\mathbf{Vm}^{B} - \mathbf{Vm}^{A})$$

$$= (\mathbf{Um}^{B} - \mathbf{Um}^{A}).$$

Combining these results and substituting into equation 5 gives the result

$$\mathbf{Wr} = (\mathbf{W}^{B} - \mathbf{W}^{A}) - (\mathbf{Uc}^{B} - \mathbf{Uc}^{A}) + (\mathbf{Um}^{B} - \mathbf{Um}^{A})$$

and since $\mathbf{Wr}^{A} = \mathbf{W}^{A} - (\mathbf{Uc}^{A} - \mathbf{Um}^{A})$ and similarly for $\mathbf{Wr}^{B}$, we obtain the desired result

$$\mathbf{Wr} = (\mathbf{Wr}^{B} - \mathbf{Wr}^{A}) \qquad \text{(Eq. 6).}$$

To summarize, *Examine*^{3D} computes the energy release **Wr** for a given excavation geometry by assuming the entire volume has been removed in a single step. For the case of an incremental stage of mining, two *Examine*^{3D} analyses corresponding to the initial and final excavation geometries can be conducted, and the incremental release of energy can be calculated using the algebraic relation given by Equation 6.

It should be noted that there are three remaining incremental energy terms: **Um**, **Wk** and **Uc**. However, there are only two remaining independent energy relations. One way of solving this problem would be to develop the two meshes used for stages I and II so that the mesh for stage I was a subset of that for stage II. Field results for the stage I analysis could then be computed on the surface of the stage II mesh forming the surface **Sm**, providing a basis for computing **Um**. The energy relations **Wk = Wr - Um** and **Uc = W - Wk** could then be used to determine the remaining quantities of interest.

VERIFICATION OF UTILITY PROGRAM

The foregoing theoretical relationships for incremental work and energy terms have been implemented in a utility program called *ENCOMP* for use with *Examine*^{3D}. The theoretical relationships, as well as their implementation in program *ENCOMP*, have been verified using analytic solutions available for circular tunnels and spherical cavities. Details of the verification study are given in Grabinsky et al. (1994).

EXAMPLE APPLICATION

The following example illustrates use of the utility program *ENCOMP* in conjunction with *Examine*^{3D}, applied to the analysis of sequencing alternatives for extraction of a sill pillar in a steeply dipping orebody. Although this example is fictitious, the problem geometry and stress field are typical of conditions found at many Canadian Shield mines.

The example orebody is about 10 meters thick, measures approximately 60 meters along strike and 100 meters vertically, and dips at about 50° (Figure 2). A sill pillar roughly 10 meters in height remains at the center of the body and is to be extracted in a series of 6 adjacent stopes. The in situ stresses are assumed to be

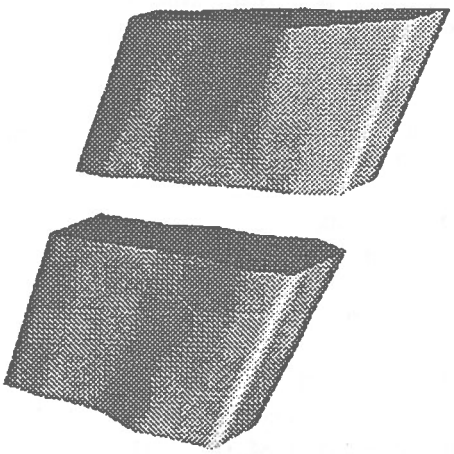

Figure 2. Perspective view of the initial geometry of the example orebody (pillar between the two solieds).

20 MPa vertically, 30 MPa along strike and 50 MPa across strike. Two different stope sequencing alternatives are to be considered: 1) extraction proceeding along strike; 2) extraction of alternate stopes in two passes (Figures 3, 5).

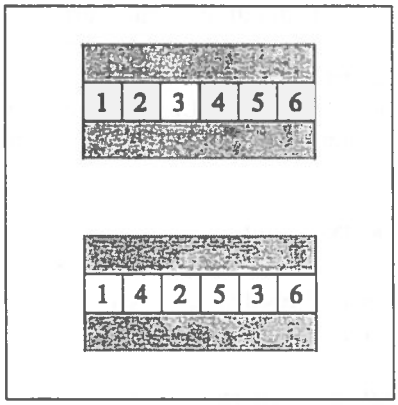

Figure 3. Alternative sequencing strategies for extraction of the example sill pillar: sequence 1 (top) and sequence 2 (bottom).

The results for these two options are presented in Table 1 and Figure 4. When considering these results it is important to keep in mind that the behaviour of the real system is assumed to be essentially linear elastic - i.e., the sill pillar has not yet undergone significant damage. Note that the released energy increment for the whole pillar is the same for both sequencing scenarios (i.e., both columns sum to the same value), as expected for a linear analysis. However, the rate of energy release is markedly different. The first stope sequencing option produces a comparatively smooth energy release rate; the second option results in lower release rates for the first three stopes but then a significant jump in release rate for the fourth and fifth stopes (note that **Wr** for stope 5 is more than double that for stopes 2 and 3).

Table 1. Incremental energy release **Wr** (MJ) during pillar extraction for two sequencing alternatives.

Stope extracted	**Wr**, sequence 1	**Wr**, sequence 2
1	0.485	0.485
2	1.002	0.935
3	1.477	0.941
4	1.643	1.603
5	1.726	2.369
6	0.863	0.863
Totals:	7.196	7.196

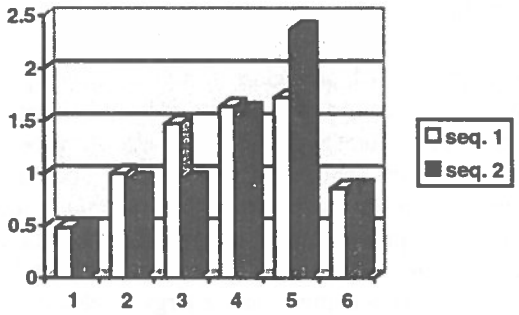

Figure 4. Incremental energy release **Wr** during pillar extraction for two sequencing alternatives (extracted stope number on the bottom axis).

In practice, operational details often predominate in deciding which sequencing option to follow. Suppose, however, that moderate difficulties (i.e., the onset of nonlinear response) were encountered after extraction of the first three stopes: if option 1 is being followed, then we might assume that energy releases associated with extraction of the remaining stopes will not be any *more* severe, and the current mining methods will be appropriate; if option 2 is being followed, then we might assume that significant increases in energy releases will be associated with mining of the remaining stopes, and the mining methodology will have to be suitably modified given the mining difficulties already encountered.

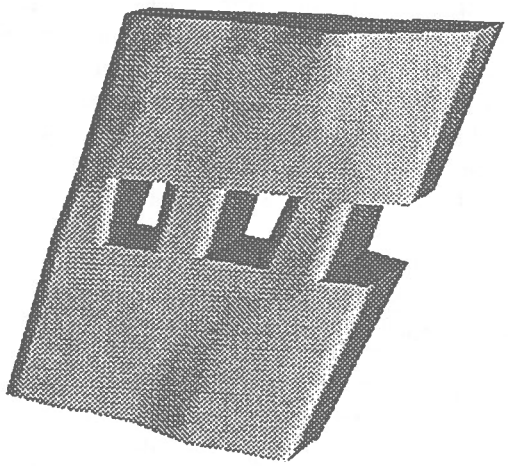

Figure 5. Extraction of first three stopes, sequence 2.

CONCLUSIONS

A straightforward procedure has been developed for analyzing the energy release rates due to incremental mining. The efficiency of the calculation procedure, coupled with the user-friendly modelling capabilities of *Examine*^{3D}, make it possible for the mine design engineer to quickly carry out a series of parametric studies in order to effectively determine the influence of mine sequencing on energy release. This information, coupled with energy density information and the more traditional results produced by analyses (e.g., stress concentrations and strength factors), enhance the designers ability to develop rational analysis and design procedures.

ACKNOWLEDGMENTS

This work was supported through a contract with the Mining Research Directorate, Canadian Rockburst Research Program.

REFERENCES

Brady, B.H.G. and Brown, E.T., 1981
Energy changes and stability in underground mining: design applications of boundary element methods. Trans. Instn Min. Metall. (Section A: Mining Ind.) Vol. 90, pp. A61-A68.

Christianson, M. and Board, M., 1993
Energy Calculations in UDEC. Minneapolis: Itasca Consulting Group, Inc. 73 pp.

Cook, N.G.W., 1962
The seismic location of rockbursts. Proc. 5th Symp. on Rock Mech. Oxford: Pergamon Press, 1963. pp. 493-516.

Cook, N.G.W., 1963
The basic mechanics of rockbursts. J. S. Afr. Inst. Min. Metall. Vol. 64, pp. 71-81.

Cook, N.G.W., Hoek, E., Pretorius, J.P.G., Ortlepp, W.D. and Salamon, M.D.G., 1966
Rock mechanics applied to the study of rockbursts. J. S. Afr. Inst. Min. Metall. Vol. 66, pp. 436-528.

Corkum, B.T., Grabinsky, M. and Curran, J.H., 1994
Examine^{3D} Energy Balance Utility. Toronto: Dept. Civil Engineering Publication No. RG-94-04-30, University of Toronto. 22 pp.

Grabinsky, M., Corkum, B.T. and Curran, J.H., 1994
The use of boundary element programs in calculating the energy release due to progressive mining. Toronto: Dept. Civil Engineering Publication No. RG-94-08-31, University of Toronto. 16 pp.

Salamon, M.D.G., 1984
Energy considerations in rock mechanics: fundamental results. J. S. Afr. Inst. Min. Metall. Vol. 84, no. 8, pp. 233-246.

Tinucci, J.P. and Verona, P., 1991
Report on Incorporation of Energy Balance Equations Into the FLAC Code. Minneapolis: Itasca Consulting Group, Inc. 52 pp.

Walsh, J.B., 1977
Energy changes due to mining. Int. J. Rock Mech. Min. Sci. Vol. 14, pp. 25-33.

CAMI'95:3rd Canadian Conference on Computer Applications in the Mineral Industry
Montréal, Québec, Canada, October 22-25, 1995

3D Finite Element Modelling of Mine-and-Fill Sequences

Hani S. Mitri, Lin Zhang and Keyvan Fotoohi
Department of Mining and Metallurgical Engineering
McGill University, Montreal, Quebec

ABSTRACT:

The paper describes a new 3-dimensional finite element modelling technique for the simulation of mine-and-fill sequences in hard rock mines. The technique is implemented in the numerical code GENA3D developed at McGill University. Targeted for hard rockburst prone mines, the code calculates the so called mining-induced strain energy density as well as the energy loss/gain due to initial stresses, associated with each mining step. These can serve as a basis for the evaluation of the potential of violent rock failure or rockburst. The benefits of modelling mining steps, as opposed to modelling the final mine scenario are demonstrated in a practical hard rock mine case study. It is shown that while stresses may be only slightly different in the two cases, the mining induced energy values appear to be radically different, and hence the assessment of rockburst potential.

RÉSUMÉ:

Cet article décrit une nouvelle technique tri-dimensionnelle de modélisation en éléments finis pour la simulation des conséquences d'exploitation et remblai dans les mines de roche dure. La technique est implantée dans le code numérique GENA3D développé à l'Université McGill. Le code calcule ce que l'on appelle la densité d'énergie de déformation induite par une exploitation. Il calcule également la perte ou l'augmentation d'énergie à cause des contraintes initiales associées à chaque étape minière. Ces composants d'énergie peuvent servir comme une base pour l'évaluation du potentiel d'une rupture violente, ou coup de terrain. Les avantages de modéliser les étapes minières plutôt que de modéliser la situation minière finale sont démontrés avec un exemple pratique d'une mine de roche dure. Il est démontré que malgré que les contraintes sont presque pareilles dans les deux situations, l'énergie induite par l'exploitation est totalement différente. Par la suite, l'évaluation du potentiel de coup de terrain sera également différente.

INTRODUCTION

With the improvement of mining methods to reach greater depths and excavate more complex geometries, it became necessary to use 3-dimensional computer programs to achieve realistic results of stress analyses of rock mass. In recent years, improvements in personal computers as well as workstations have given the opportunity for the development of a series of 3-dimensional codes to use as a tool for stress/stability analysis of mining systems. These computer models were developed using finite element method, boundary element method, finite difference method, distinct element method as well as hybrid methods. Examples of such models are the finite element model BMINES and boundary element model BEAP, both developed by CANMET (Yu et al., 1990), the boundary element model EXAMINE^{3D} developed by the University of Toronto, the finite element model FEMMA developed by University of New Brunswick, the distinct element model

3DEC and the finite difference model FLAC3D, both developed by Itasca Consulting Group Ltd., the boundary element model MULSIM-NL developed by the Denver Research Center of the U.S. Bureau of Mines (Zipf, 1992), and several others.

A 3-dimensional finite element model for stress/stability of mining excavations, GENA3D, was developed at McGill University by the authors (Zhang and Mitri, 1990). This was designed to run under the PC-DOS and OS/2 systems. In 1991, the modelling of mine backfill as in situ stress-free material was incorporated. The modelling of mining induced energy (U_{mi}) for rockburst analysis was another important feature which was added to the model more recently. In 1994, another version of the model was developed to run in a UNIX environment on Silicon Graphics Indy computer.

Recently, GENA3D was developed for mine and fill sequences. With this new feature, it creates a series of output files including the principal stresses and mining induced energy after mine-backfill sequences. All of these are available to the user only with the click of a mouse to show the sequences of mine and backfill design. This paper presents this new feature of GENA3D.

MODEL DEVELOPMENT CRITERIA

In-house development of GENA3D has been motivated by a number of factors. First, it takes advantage of recent advanced compilers. This gave the numerical model a no size limit capability, with the limits being only those of the computer hardware like the size of hard disk and extended memory available. Another important component of the model is its postprocessor, which performs failure analysis using rock mass failure criteria. This component beside the ability of the mesh editor for element deletion, gives a very special credit to the model in stress/stability analysis of mining-backfill sequences plus deleting the failure zones in each step of sequences. This special capability of the model will be presented in a paper.

GENA3D is designed to model the in situ stress free material. This would allow to model mine backfill support, which at the time of placement, is acting only by its own weight and is free of mining induced stress, but as mining proceeds, the pressure inside the backfill builds up hence the benefits of backfill as a rockwall confining support. Modelling of in situ stress-free material can be used in other applications like tunnel and shaft lining. Another important feature in this model is the simulation of mine-backfill sequences. This allows the comparison between different mining scenarios, from the point of view of ground control and stability. In the case of the rockburst problem, a proper mine-backfill sequences may be determined by the comparison of mining induced energies between different mining scenarios.

MODEL FEATURES AND LIMITATIONS

The model employs the 8-node isoparametric brick elements. Geomechanical materials can be isotropic or orthotropic, their behaviour is assumed to be linear elastic. Loading conditions accounted for are the own weight of the rock mass, in situ stress, and external boundary pressure loading. The finite element equations of GENA3D are described elsewhere [Zhang and Mitri, 1992]. While the code is only linear elastic at this stage, it has a number of practical features, which make it an attractive analysis tool. These are: (1) Easy-to-use, interactive data generator, (2) User-friendly graphical interface, (3) On-line help menus, (4) Automatic room and mesh generator, (5) Mesh editor for element deletion from an already generated mesh, (6) Out-of-core solver with no limit on the number of elements, (7) Simulation of mine backfill support, (8) Calculation of mining-induced strain energy density, and (9) Failure analysis by Mohr-Coulomb or Hoek-Brown criteria. GENA3D consists of five programs: Interactive Data Generator, File Manager, Mesh Generator, Core Processor and Postprocessor.

The code is limited to static, linear elastic analysis at this stage. No provisions are currently made for dynamic loading, time-dependent analysis, nor nonlinear elastoplastic analysis. The model is also limited to the 8-node isoparametric element.

MINING INDUCED ENERGY

The need to better understand rockburst phenomena, particularly pillar and strain bursts, have led the authors to introduce the concept of calculation of mining induced strain energy densities around mine cavities [Mitri et al., 1993]. The idea is based on the assumption that rockburst phenomena can be attributed to sudden release of energy in a volume of a highly stressed rock. Thus, mining-induced strain energy (U_{mi}) may serve as an indicator to rockburst potential rather than simply relying on mining-induced stress concentration. This concept is graphically illustrated in Figure 1. Note that the energy component due to in situ stress (U_{is}) can be negative when there is energy loss, whereas the mining induced strain energy is always positive.

In mathematical form, this can be expressed as follow:

$$U_{mi} = \int_v \frac{1}{2} \Delta\varepsilon^{i\,T} (\sigma^i - \sigma^{i-1})\, dV \qquad (1)$$

$$U_{is} = \int_v \Delta\varepsilon^{i\,T} \sigma^{i-1}\, dV \qquad (2)$$

Where σ^{i-1} and σ^i are the stress tensors at mining steps i-1 and i respectively and $\Delta\varepsilon^i$ is the strain tensor increment in mining step i.

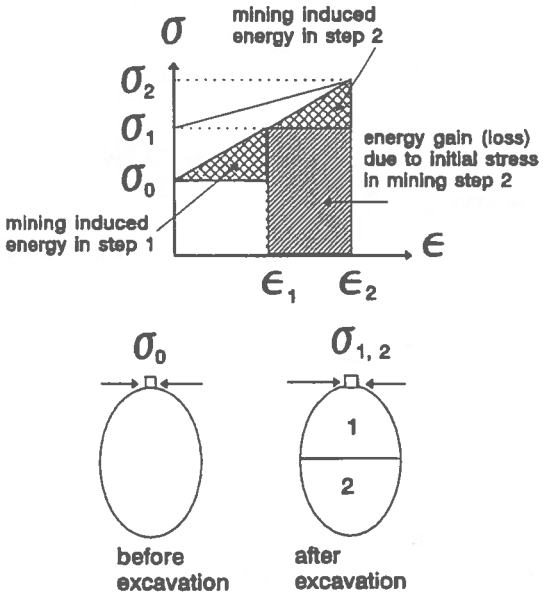

Figure 1 - The concept of mining-induced strain energy

MINE-AND-FILL SEQUENCES

A simple, yet practical procedure is implemented for the simulation of mine and fill sequences. Only the changes in load and stiffness are needed to be incorporated, in order to reach equilibrium after each mining step.
The load vector due to an excavation ΔP_e^i in a mining step i is

$$\Delta p_e^i = \int_v B^T \sigma^{i-1}\, dv \qquad (3)$$

Whereas the load vector due to the introduction/placement of backfill ΔP_b^i is

$$\Delta P_b^i = \int_v \delta_b\, [N]^T\, dv \qquad (4)$$

On the other hand the global load stiffness matrix of the system is modified. For each element excavated in mining step i, its stiffness matrix K_e^i is removed from the system. This is:

$$K_e^i = -\int_v [B]^T\, [D]\, [B]\, dv \qquad (5)$$

Whereas for each element representing a placement of backfill, the global stiffness matrix is inwarded by

$$\int_v [B]\, [D^b]\, [B]\, dv \qquad (6)$$

where $[D^b]$ is the backfill elasticity matrix.

CASE STUDY

A practical case study of a deep narrow vein underground mine was taken to demonstrate the modelling capability of GENA3D of stress/stability analysis of mining-backfill sequences. The ore body has a thickness from 5 to 15 m. with 80° dip angle as illustrated in cross section of the ore body in Figure 2. Figure 3 shows a longitudinal section of the ore body. As illustrated in Figure 3, a large section of the ore body in upper levels have been mined out and backfilled previously. The area which is to be examined through a mining-backfilling sequences is located at a depth of 1080 m. below the ground surface.

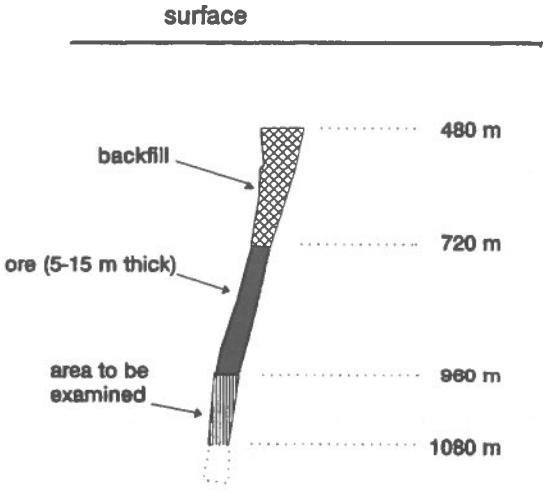

Figure 2 - Cross section of the ore body

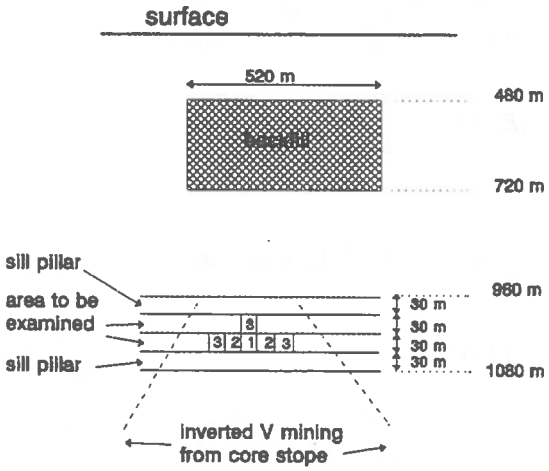

Figure 3 - Longitudinal section of the ore body

Figure 4 shows the mine-backfilled sequences of this planned area in a larger scale. This area was planned to be mined and backfilled in 3 steps. GENA3D was used for the stress/stability analysis of this area through the running of four models.

Figure 5 shows the mining-backfill scenario for models 1, 2, 3 and 4. Models 1 to 3 represent 3 mining-backfill sequences whereas model 4 has the same scenario as model 3 without conducting any mining sequences. Model 1 has only one mined stope. Model 2 is one step after model 1 with 2 new mined stopes and stope no. 1 backfilled. Model 3 is the next mining sequence with 3 new mined stopes and stope no. 2 backfilled. Model 4 is a separate model which has the same geometry of model 3 but without mining sequences. Actually, in model 4, the 3 mined stopes and 3 backfilled stopes are modelled in one step.

Table 1 presents the number of mined and backfilled stopes for different models.

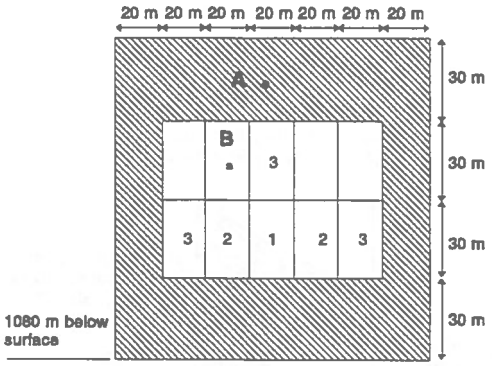

Figure 4 - mining sequences

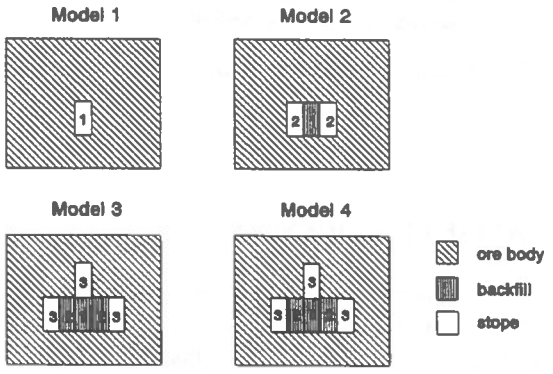

Figure 5- Mine-backfill of Models 1, 2 ,3 and 4

Table 1: Numerical models simulated

	Mined stopes	Backfilled stopes
Model 1 (step 1)	1	-
Model 2 (step 2)	1 and 2	1
Model 3 (step3)	1, 2 and 3	1 and 2
Model 4 (both mining and backfill in one step)	1, 2 and 3	1 and 2

Geomechanical Data

The rock mass is assumed to be homogeneous and isotropic with a unit weight of 0.027 MN/m^3, modulus of elasticity of 80,000 MPa and Poisson's ratio of 0.25. The hanging wall and foot wall are placed in class of fair rock (40 < RMR < 60). The Young's modulus of the rock mass (E_{rm}) was calculated from the Young's Modulus of intact rock (E_{inact}) and RMR using the following equation:

$$\frac{E_{rm}}{E_{inact}} = \frac{1}{2}\left[1 - \cos\pi\left(\frac{RMR}{100}\right)\right] \qquad (7)$$

The Young's modulus for the hanging wall and foot wall was determined as presented in Table 2.

Table 2: Geomechanical data

	E_{inact} (MPa)	RMR	E_{rm} (MPa)	ν
Hanging wall	80,000	50	40,000	0.25
Footwall	80,000	55	46,250	0.25
Ore body	80,000	65	58,160	0.25

In situ stresses vary linearly with depth, H, below ground surface and are given by:

$$\sigma_z = 0.027 * H \text{ MPa}$$
$$\sigma_x = 2.26 * \sigma_z \text{ MPa} \qquad (8)$$
$$\sigma_y = 1.51 * \sigma_z \text{ MPa}$$

A mesh of the model was created with 16,000 elements. Figure 6 shows a zoom in mesh of the examined area. Figures 7, 8, 9 and 10 show the 3 dimensional contours of mining induced strain energy of the model 1, 2, 3 and 4 respectively.

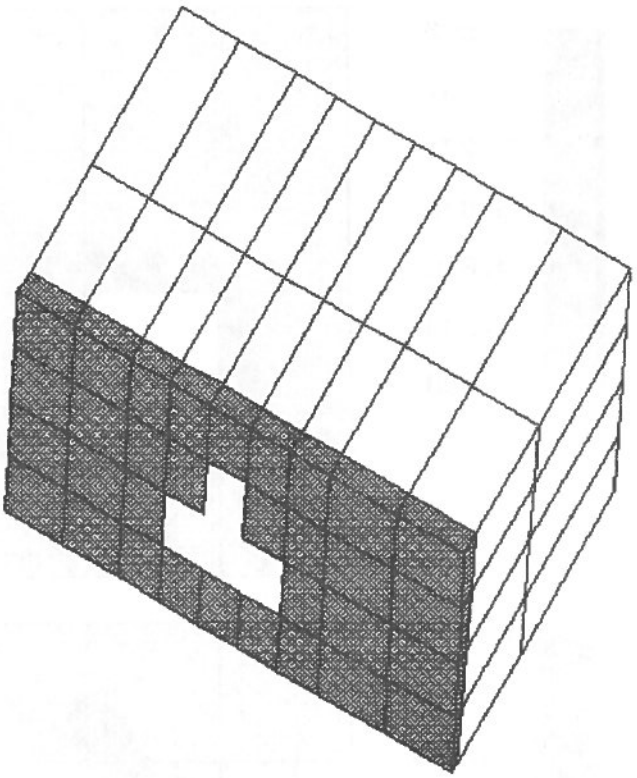

Figure 6- Finite element mesh of area examined

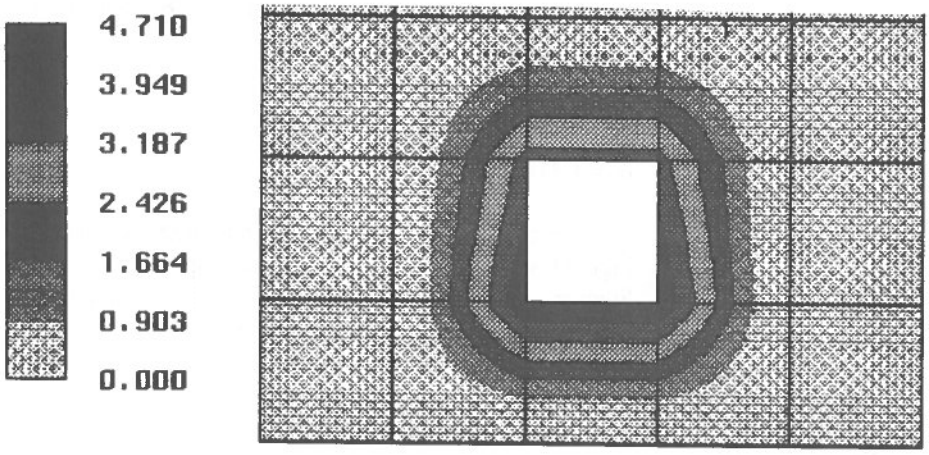

Figure 7- Mining induced strain energy of model 1 (KJ/m³)

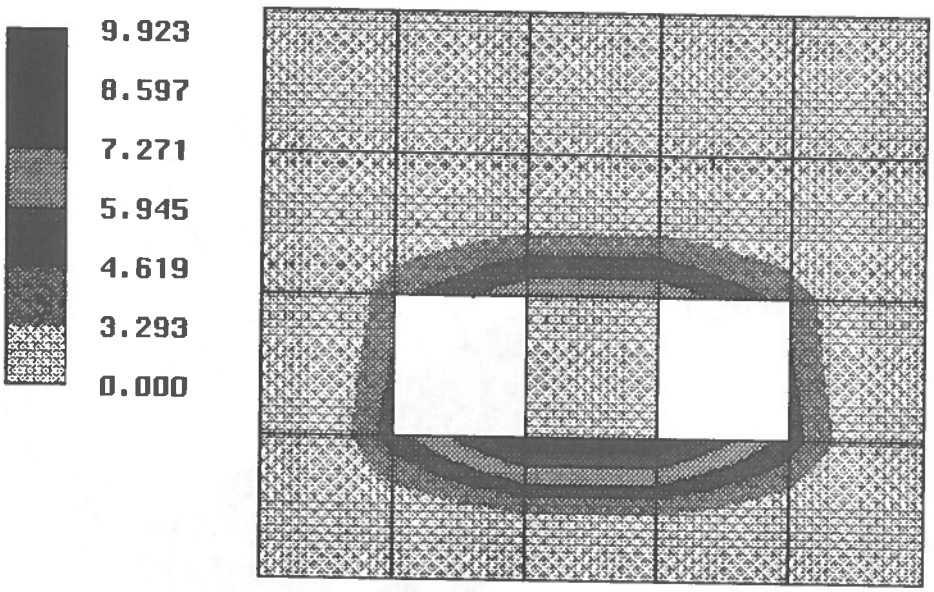

Figure 8- Mining induced strain energy of model 2 (KJ/m³)

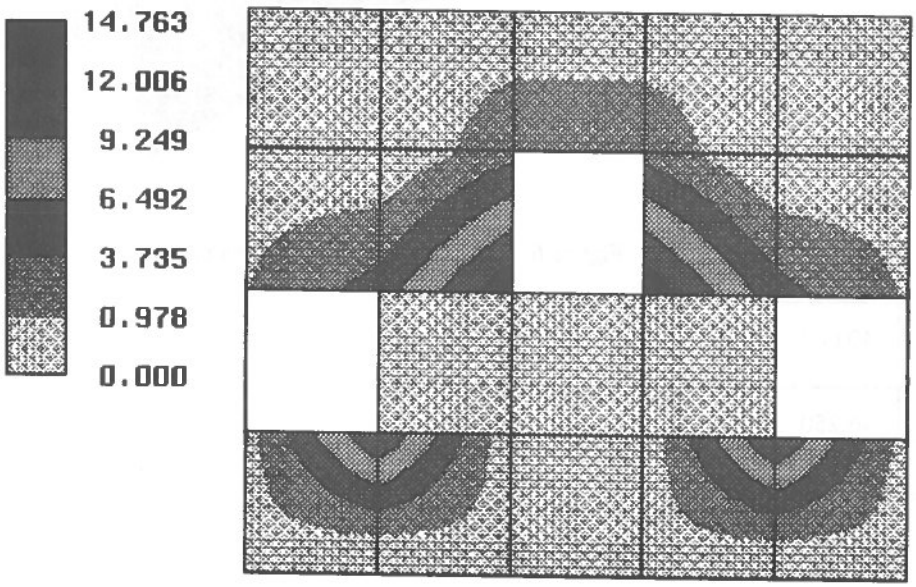

Figure 9- Mining induced strain energy of model 3 (KJ/m³)

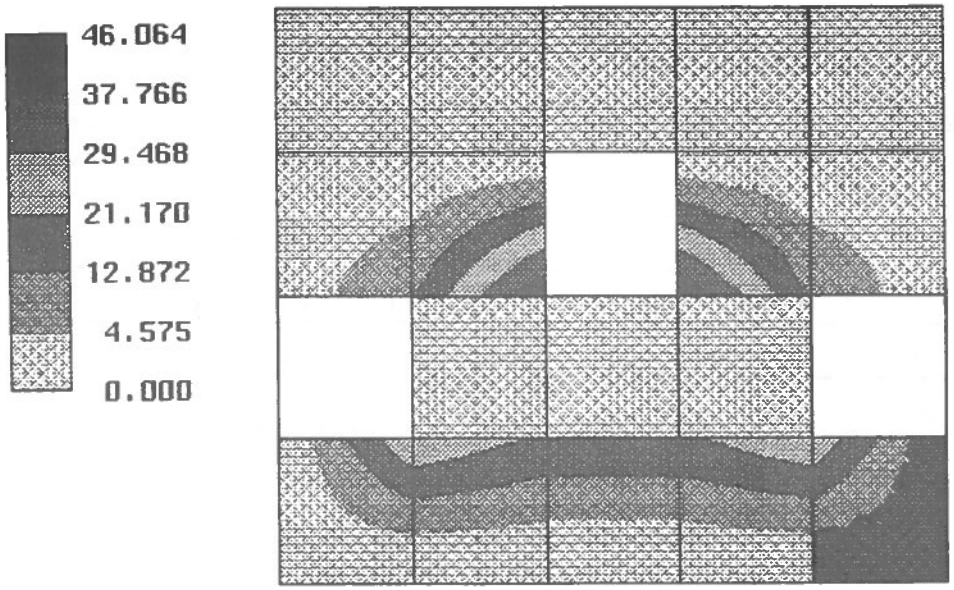

Figure 10- Mining induced strain energy of model 4 (KJ/m^3)

RESULTS

Table 3 presents the mining induced strain energy density (U_{mi}) and principal stresses (σ_1 and σ_3) at points A and B (defined in Figure 4) obtained from the 4 models simulated.

Figure 11 shows the mining induced strain energy densities at point A (defined in Figure 4) obtained from the 4 models simulated. In models 1 and 2, point A is far from the mining activity and has small energy values. In model 3, point A is in the back of the new mined stope and has a value of 1.058 KJ/m^3. On the other hand, the mining induced energy at point A from model 4 is 1.387 KJ/m^3. This is higher than the total of strain energy densities of models 1, 2 and 3 at point A.

Similarly, Figure 12 presents the mining induced strain energy densities at point B (defined in Figure 4) obtained from the 4 models simulated. In models 1 and 2, point B is not far from the mining activity and has higher energy values comparing to point A. In model 3, point B is in the pillar of the new mined stope and has a value of 3.809 KJ/m^3. On the other hand, the mining induced energy at point B from model 4 is 11.939 KJ/m^3. This is much higher than the total of strain energy densities of models 1, 2 and 3 at point B.

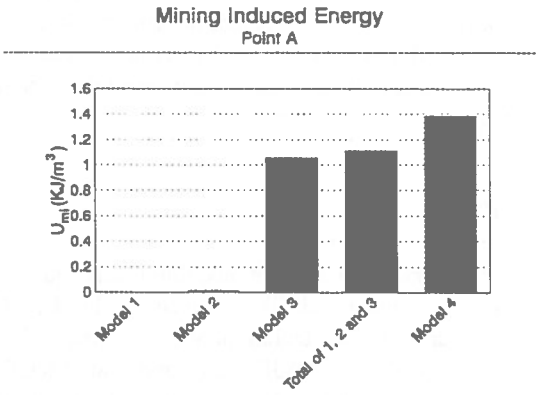

Figure 11- Mining induced energy at point A (see Figure 4)

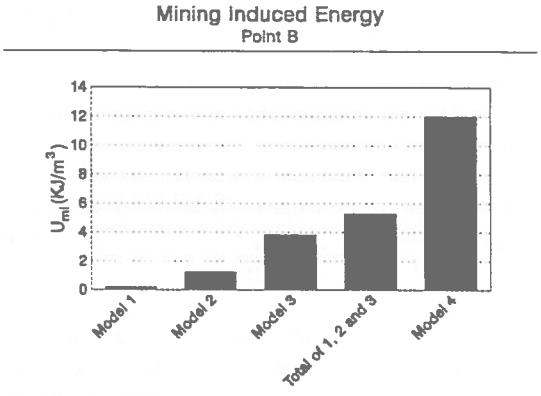

Figure 12- Mining induced energy at point B (see Figure 4)

Table 3 Mining induced energy and principal stresses

	u_{mi} KJ/m^3		σ_3 (MPa)		σ_1 (MPa)	
Point	A	B	A	B	A	B
Model 1	0.002	0.212	26.47	28.46	59.92	65.66
Model 2	0.014	1.260	26.83	32.17	61.13	77.24
Model 3	1.058	3.809	30.15	39.38	71.65	99.09
Total of 1, 2 and 3	1.111	5.281	-	-	-	-
Model 4	1.387	11.993	30.14	39.25	71.58	99.68

Figure 13 presents the principal stresses at point B obtained from 4 models simulated. The values of principal stresses at point B obtained from models 1 to 3 increased gradually. Principal stresses at point B obtained from models 3 and 4 is almost equal.

CONCLUSION

A new 3-dimensional finite element modelling technique for the simulation of mine-and-fill sequences in hard rock mines was described. This technique was implemented in the numerical code GENA3D developed at McGill University. The model computes the mining-induced strain energy density and the energy loss/gain due to initial stresses, associated with each mining step. The mathematical equations for the simulation of mine-and-fill sequences were explained. The benefits of modelling mine-and-backfill sequences, as apposed to modelling the final mine
scenario were demonstrated in a practical hard rock mine case study. The following could be concluded from the results of the case study:

- It is difficult to use simple numerical models that have no mine-and-fill simulation capability to assess the energy release associated with each mining step.

- GENA3D has the capability of the simulation of mine-backfill sequences. This allows the comparison between different mining scenarios from the point view of ground control and stability.

- Based on the hypotheses that strain burst is due to sudden release of energy, it can be concluded that mining with backfill could reduce the potential of strain burst.

- Using the new feature of GENA3D for the case of the rockburst problem, a proper mine-backfill sequences may be determined by the comparison of mining induced energy between different mining scenarios.

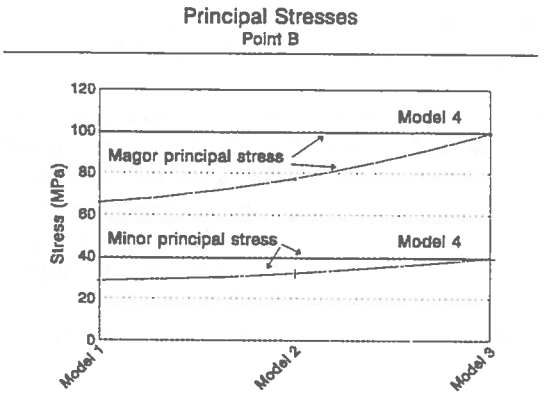

Figure 13- Principal stresses obtained from 4 models simulated

REFERENCES

Yu, Y.S., Closset, L. and Diering, J.A.C. (1990) A boundary element application package for three dimensional stress analysis of mine structures. Proc. Conf. on Stresses in Underground Struc., Ottawa, October 2-3.

Zipf, R.K. (1992) MULSIM-NL: Application and Practitioner's manual. USBM-IC, 93-22, 48p.

Zhang, L. and Mitri, H.S. (1990) Program GENA3D, version 1.0, Geometrically nonlinear analysis of 3-dimensional problems, Department of Mining and Matallurgical Engineering, McGill University, Internal Report

Zhang, L. and Mitri, H.S. (1992) 3D modelling of mine structures with backfill. CIM Bull., Vol.85, No.962, pp.89-95.

Mitri, H.S., Hassani, F.P. and Kebbe, R. (1993) A strain energy approach for the prediction of rockburst potential in underground hard rock mines. Proc. 1st Can. Symp. on Numerical Modelling Appl. in Min. &Geomech., Montreal, March 27-30, pp.228-239.

CAMI'95: 3rd Canadian Conference on Computer Applications in the Mineral Industry
Montréal, Québec, Canada, October 22-25, 1995

Coupled 3D FE Modelling of Mining in Wet Ground

William G. Pariseau
University of Utah, Salt Lake City, UT

ABSTRACT

Water complicates stress analysis for mine design because of the need to distinguish between total stress required for equilibrium and effective stress which determines strength and governs stability. A poroelastic approach based on Biot's law provides a reasonable constitutive description for initial loading in saturated ground. In this regard, diffusion of fluid pressure in jointed, porous rock introduces a time-scale that must be considered. Coupled finite element simulations of excavation in saturated rock masses indicate that effective stresses change very little after excavation, that preexcavation water pressure must be of the order of the effective stresses to influence excavation stability, and that excavation safety factors in the wet case are always less than in the dry case.

RÉSUMÉ

L'eau complique la détermination des efforts dans la conception des mines à cause du besoin de distinguer entre l'effort total exigé pour l'équilibre et l'effort efficace qui détermine la résistance et gouverne la stabilité. Une approache poroélastique fondée sur la loi de Biot pourvoit d'une description raisonnable et constitutive du chargement initial en terre saturée. A cet égard, la diffusion de la pression fluide en roche poreuse et fissurée impose une échelle de temps qui doit être considérée. Des simulations accouplée des éléments finis de l'excavations en mases de roches saturée idiquent que les efforts efficaces changent trés peu aprè l'excavation, que la pression de l'eau avant l'excavation doit être de l'ordre des efforts efficaces pour influer sur la stabilité de l'excavation et que les coefficients de sécuriteé sont toujours moins nombreux dans le cas mouillé que dans le cas sec.

INTRODUCTION

The primary rock mechanics objective in mine design is to determine whether stresses σ_{ij} will remain below the elastic limit as mining proceeds according to plan. Here, the usual subscript notation and summation convention are adopted. For example, $\sigma_{22}=\sigma_{yy}$ and $\sigma_{ii} = \sigma_{11}+\sigma_{22}+\sigma_{33}$. A comma denotes differentiation, e.g., $\partial\sigma_{yy}/\partial z = \sigma_{22,3}$. If Y is the yield function or failure criterion, then the elastic limit is locally reached when $Y(\sigma_{ij})=1$. Mohr-Coloumb, Drucker-Prager and Hoek-Brown criteria are popular in rock mechanics. Inelastic behavior in a variety of forms, such as pillar spalls, hanging wall slab formation and floor heave, become possible beyond the elastic limit. Spread of local zones of inelastic deformation may lead to larger instabilities to the detriment of safety and productivity.

In wet ground, water complicates the analysis of stress and evaluation of stability. The criterion for failure in wet ground is symbolically $Y(\sigma_{ij},\pi)$ where π is the fluid stress. By definition, the difference between total stress and the fluid stress (water pressure) contribution is effective stress σ'_{ij}, that is,

$$\sigma'_{ij} = \sigma_{ij} - c_{ij}\pi \qquad (1)$$

where the c_{ij} are material properties that allow for anisotropy. In the isotropic case $c_{ij}=\alpha\delta_{ij}$, and in soil mechanics $\alpha=1$ is a common assumption. In view of (1), the yield condition can be written in terms of

the effective stresses only, i.e., as $Y(\sigma'_{ij})$. The total stresses must still be considered in the analysis of stress for equilibrium. In this regard, the analysis of stress is clearly of central importance to meeting the prime objective.

STRESS ANALYSIS IN WET GROUND

All the usual dry mine considerations including geology and structure, past and planned mining geometry, the *in situ* stress and rock mass properties are present in wet mine stress analysis in addition to water pressure and flow. Pressure is important to stability evaluation, while flow is important to water volume estimates. The appropriate analytic model requires numerical analysis and a coupled computer code for applications.

Coupled Material Model

The mathematical model of coupled fluid flow and rock mass deformation includes consideration of equilibrium, kinematics and constitutive equations. The well-known Biot formulation for coupled fluid flow and elastic deformation may be considered the standard material model. An excellent general discussion of poroelasticity is given by Detournay and Cheng (1993). A critical review in the context of mine design is given by Pariseau and Forster (1992).

Within the range of elastic deformation the effective stresses transmitted through the solid part of the rock mass are related to the strains ϵ_{mn} in Hooke's law. Thus,

$$\sigma'_{ij} = C_{ijmn}\epsilon_{mn} \qquad (2)$$

where C_{ijmn} are the components of the elastic moduli tensor which may be anisotropic to accommodate directional features of a rock mass, perhaps associated with foliation or jointing. Substitution of (2) into (1) gives

$$\sigma_{ij} = C_{ijmn}\epsilon_{mn} + c_{ij}\pi \qquad (3)$$

Equation 3 shows that in the absence of fluid pressure change, that is, when free drainage occurs, the stress strain law is identical in form to that in the dry case. Drainage does not imply complete removal of fluid, but rather pressure decrease with free flow; the material remains saturated.

Seepage flow rate and pressure gradients are related through Darcy's law. Thus,

$$v_i = k_{ij}(\pi_{,j} + \gamma_j) \qquad (4)$$

where v_i is the fluid flow rate relative to the solid, k_{ij} are the components of the hydraulic conductivity tensor, $\pi_{,j}$ are pressure gradients, and γ_j are the components of fluid specific weight. The displacement of fluid relative to the solid is w_i, and $\partial w_i/\partial t = v_i$ where t is time. Equation 4 implies that pressure in a fluid at rest is equal to specific weight times depth of fluid to the point in question, as certainly is the case.

Water content of the rock mass is defined by $\zeta = w_{i,i}$. The relationship of fluid content to bulk solid strain and fluid pressure is

$$\zeta = -c_{ij}\epsilon_{ij} + c\pi \qquad (5)$$

As mine water moves through the rock mass pore spaces, cracks, joints and so forth, pressure changes and the rock mass deforms, thus changing the fluid content.

Equations (3), (4), (5) and the failure criterion $Y(\sigma'_{ij})$ define the material model of a saturated rock mass in which solid deformation and fluid flow are coupled, the one affecting the other.

Finite Element Model

The finite element (FE) technique is well suited for numerical solution to mining applications that involve sequential cuts and fills in initially stressed geologic media. The divergence theorem in the form of the principles of virtual work and power provides the most direct path to the numerical model in finite element form, e.g, Cui and others (1994). Thus,

$$\begin{aligned} F_u &= K_{uu}U + K_{u\pi}\pi \\ F_\pi &= K_{\pi u}\dot{U} - K'_{\pi\pi}\dot{\pi} - K_{\pi\pi}\pi \end{aligned} \qquad (6)$$

where the subscripts "u" and "π" refer to the bulk solid displacement and fluid pressure unknowns, respectively, and the overdot means time derivative. Each node has four degrees of freedom; U and π

are global vectors of node displacements and node pressure, respectively. Integration of equations (6) with respect to time is usually done using a finite difference scheme. Boundary conditions include combinations of surface traction, displacement, fluid pressure and flow rate. If the solid is considered rigid, then a conventional seepage analysis is possible. If fluid pressure changes are fixed at zero, then a conventional dry mine analysis of stress is possible. Coupled problems range between these two cases.

Many coupled codes have been reported in the literature the past decade, but few appear to be specifically intended for mining applications. Extension of an existing finite element code (UTAH3), thus became necessary. Benchmarking of the new code, UTAH4, against known analytical and numerical solutions was essential to insure reliability during subsequent testing for wet mine design (Pariseau, 1994). The "dry" case of zero fluid stress is a special case of the coupled problem. Generally there is excellent agreement with UTAH4 results. For example, Fig. 1 shows a comparison of finite element results of stress and displacement with the well-know exact solution to the problem of a circular hole excavated in a dry medium under uniform horizontal stress (hollow cylinder problem). Figure 2 compares finite element results of fluid pressure and flow with an exact solution (Detournay and Cheng, 1988) in the wet case of a circular hole excavated in initially stressed and pressurized wet ground. The horizontal preexcavation principal stresses are also equal in this test case. Dimensionless time t* is explained in the text. Such results depend to some degree on mesh refinement and computational effort.

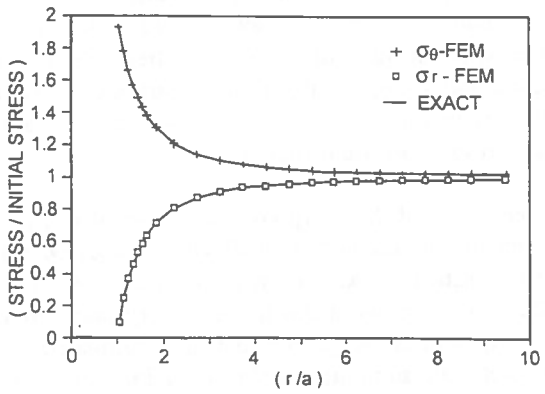

(a)

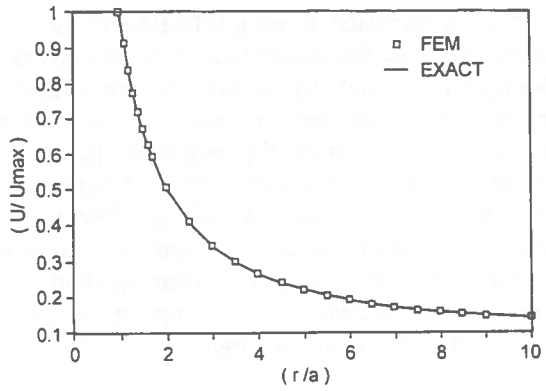

(b)

Fig. 1. Dry case comparisons of stress (a) and displacement (b) [hollow cylinder problem].

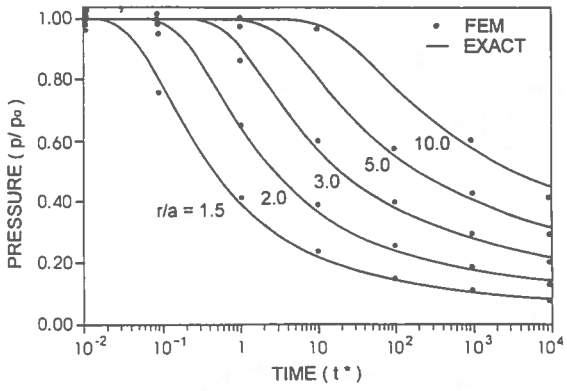

(a)

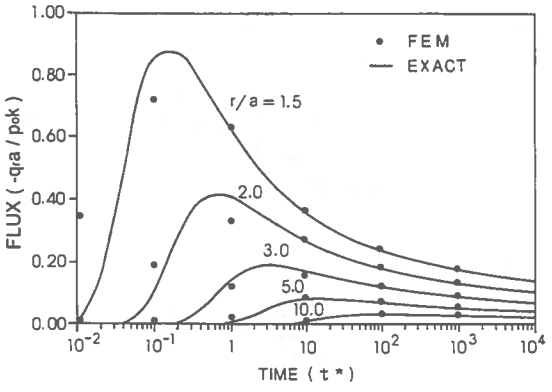

(b)

Fig. 2. Wet case comparison of fluid pressure history (a) and hole flux (b).

Previous Two-dimensional Results

Coupled calculations using UTAH4 and slab models that simulate excavation of tunnel- and shaft-like openings in initially stressed and pressurized ground indicate that the wet case safety factor at the hole wall is less than the dry case even after prolonged drainage (Pariseau, 1995). Comparisons were made using the same premining effective stresses. Premining total stress (compression) is thus greater in the wet case by the premining fluid pressure. An example is the rectangular opening of aspect ratio (W_o/H_o) of two shown in Fig 3.

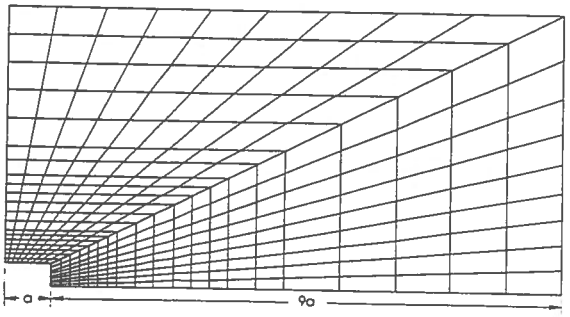

(a)

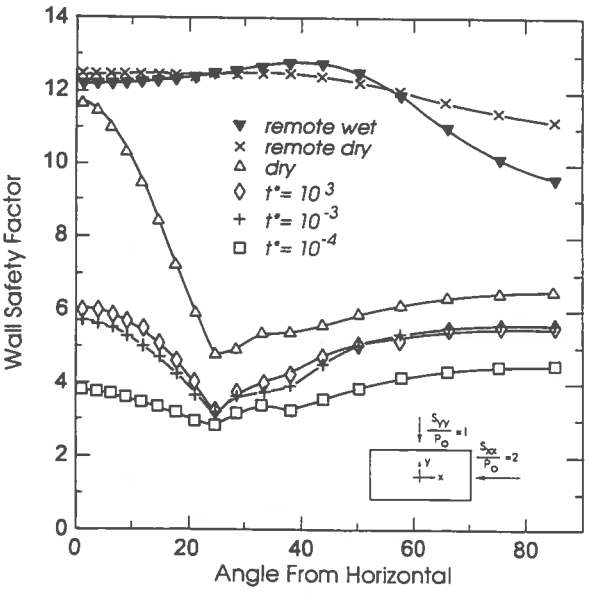

(b)

Fig. 3. Rectangular hole wall safety factor for wet and dry cases: (a) mesh (b) results.

In this calculation, the premining stress in the x-direction was twice the y-direction stress, so the opening in Fig. 3 is favorably oriented with the long dimension parallel to the major premining compression. Premining fluid stress was relatively high and equal to the y-direction premining stress. Thus, $S_{xx}/p_o = 2$, $S_{yy}/p_o = 1$, and $S_{zz}/p_o = 1$, while the premining shear stresses were zero, that is, $T_{yz}=T_{zx}=T_{xy}=0$.

The material is considered isotropic, so the coupling properties have the form $c_{ij} = \alpha\delta_{ij}$; α was set to allow for some fluid compressibility, i.e., α = 0.893. The drained elastic properties, Young's modulus E, shear modulus G were set to E/G = 2.4; the drained Poisson's ratio ν = 0.2. Also M/G = 4.18 where M is the reciprocal of the fluid compressibility coefficient, i.e., M = 1/c, $\kappa G/C_v$ = 0.538 where κ is a permeability coefficient ($k_{ij} = k\delta_{ij}$) and C_v is a consolidation coefficient (Detournay and Cheng, 1993). These property relations are the same used by Cui and others (1994). Material hydraulic conductivity was moderate, 0.0007 m/min (0.0023 ft/min), e.g. Williams and others (1986).

A dimensionless time is $t^* = C_v t/a^2$ where t=real time and a=hole dimension. In each example, time steps varied over several orders of magnitude to give a history from $t^*=10^{-4}$ to $t^*=10^{+3}$ (in increments of one-tenth each order of magnitude interval).

Rock strength corresponded to a uniaxial compressive failure strain of 1%, thus C_o/E = 0.01. Tensile strength was one-eighth compressive strength (C_o/T_o = 8), and the yield condition was quadratic. The yield condition is a paraboloid of revolution about the hydrostatic axis in principal stress space. The strength properties and yield condition allow computation of the local factor of safety which is defined as the ratio of strength to stress. Separate elastic and strength anisotropies (Pariseau, 1972) are possible in UTAH4. Associated rules of flow are used in the post-yield regime.

The effect of the sharp corner is evident in Fig. 3 where the minimum hole wall safety factor occurs. At the instant of excavation ($t=0^+$), the wet case safety factor is about 0.6 times the dry case. With prolonged drainage ($t\to\infty$), that is, depressurization, the wet wall minimum safety factor increases little, to about 0.7 times the dry case.

These and similar results for circular, elliptical and arched-rectangular openings suggest, but do not prove, that the effective stresses near the hole wall, which determine the critical stress concentration for the minimum hole wall safety factor, are established at the outset of excavation and change little with drainage time.

COUPLED EXAMPLE CALCULATIONS

Finite element analysis of even simplified coupled deformation and flow problems provides some insight into this relatively unexplored, but potentially important, region of rock mechanics and wet mine design. Examples include (1) sinking a shaft through a confined aquifer and (2) stope on stope mining in wet ground with and without hydraulic fill.

In all examples, rock mass properties are in the same dimensionless relationships as before. However, rock mass hydraulic conductivity is lower by a factor of 10^{-3}. Rock mass Young's modulus and unconfined compressive strength are 16.6 GPa and 55 MPa (2.4×10^6 psi, 8,000 psi), respectively. Fill hydraulic conductivity is "moderate", about 43 mm/hr (1.7 in./hr). Premining effective vertical stresses were either 35 or 8.7 MPa (5,060 and 1,265 psi) while the horizontal stress was either 0.25 (low) or 4.0 (high) times the vertical stress. Premining fluid pressures were low, medium or high, that is, 0.05, 0.25 or 1.00 times 8.7 Mpa (1,265 psi).

Shaft Sinking Through a Confined Aquifer

In this example, the premining effective vertical stress was 8.7 MPa (1,265 psi) while the horizontal stress was 4.0 (high) times the vertical stress (5,060 psi). Premining fluid pressure in the confined aquifer was high, that is equal to the vertical effective stress 8.7 MPa (1,265 psi). Shaft diameter was 6 m (20 ft). Lifts were 3.75 m (12.5 ft) that correspond to the vertical gradation in the finite element mesh shown in Fig. 4 which also shows the location of the aquifer and the sinking sequence implemented in the finite element model. With the exception of cut 3, multiple lifts were taken in each of the six cuts to shorten the calculations. A 10 hour "consolidation" time (10 time increments of one hour each) was allowed between cuts after penetration of the aquifer.

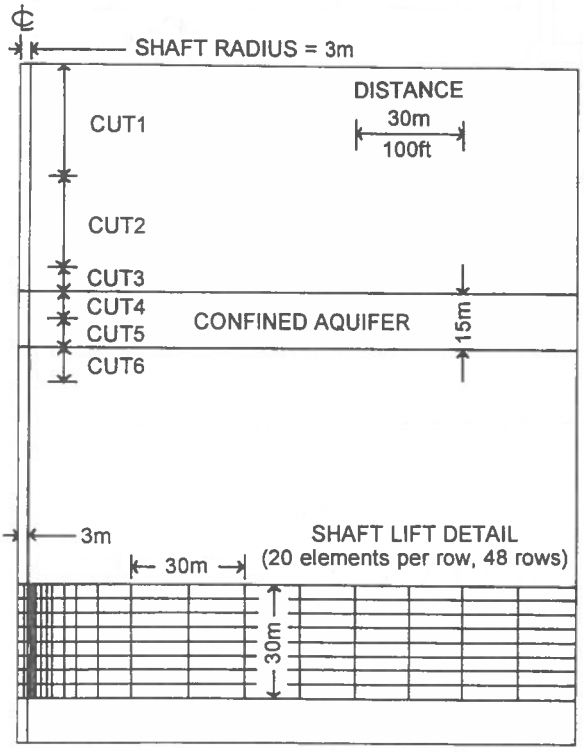

Fig. 4. Mesh geometry for shaft sinking example.

Each cut deforms the aquifer and creates pressure gradients that require time to decay to a new equilibrium state characterized by a uniform fluid pressure. Pressure decay is accompanied by fluid flow within the confined aquifer that, in turn, induces small, time-dependent displacement that adds to the instantaneous displacement caused by excavation.

Figure 5 shows the stress distribution, displacement field and fluid flow pattern in the vicinity of the shaft after the first cut. As mining approaches the aquifer, interaction between aquifer and shaft increases. Mining through the aquifer creates a large flow to the shaft that subsequently decreases with time and further deepening of the shaft, as one would expect.

Although the coupling between deformation and fluid flow is interesting and is quantified in the analysis, the consequences for shaft wall stability are small as seen in Fig. 6 which compares the "dry" shaft case (sans aquifer) with the "wet" case. The presence of the aquifer changes the safety factor distribution, but not by a significant amount. Many other practical concerns such as water handling

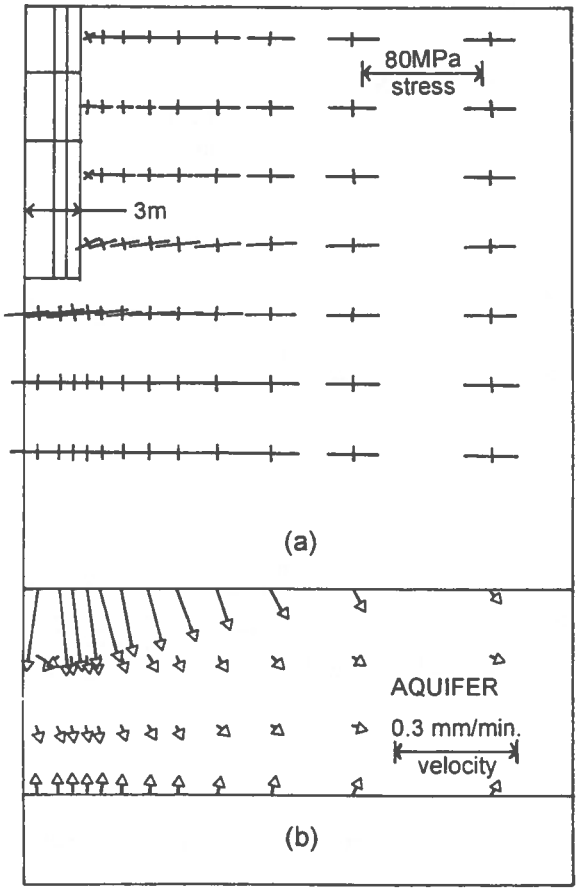

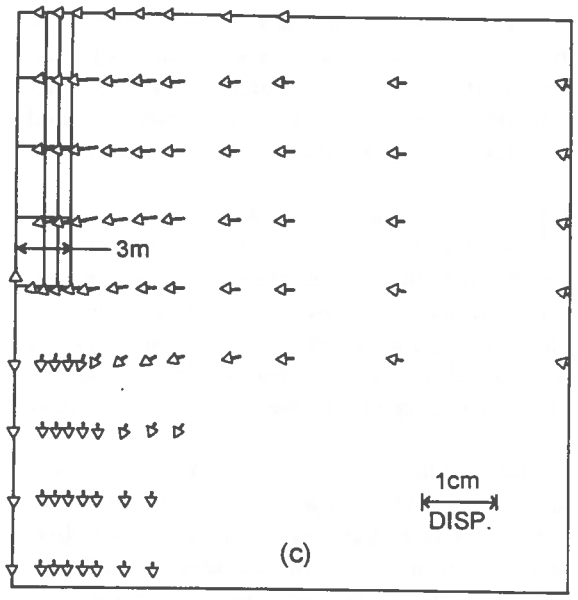

Fig. 5. Cut 1 shaft stress (a), aquifer flow pattern (b) and displacement field (c).

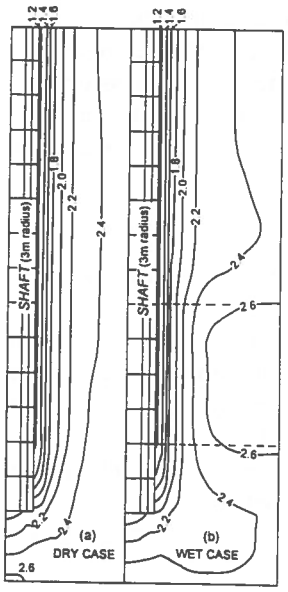

Fig. 6. Shaft safety factor distributions: (a) "dry" case, (b) "wet" case.

would, of course, need to be examined in detail in an actual engineering study of a specific site.

Stope on Stope Mining in Wet Ground

Example calculations of two 6 m (20 ft) wide by 30 m (100 ft) high vertical stopes separated by a 15 m (50 ft) pillar excavated in a deep, wet underground environment and sequential excavation of the upper stope followed by filling and excavation of the lower stope illustrate coupled behavior that is significantly different from analogous dry cases even when the premining fluid stress is small relative to the premining effective stress. Stope and mesh geometry are shown in Fig. 7. The horizontal premining stress was high (35 MPa) and the fluid pressure was medium (1.7 MPa).

Three cases were examined: (1) a dry case with both stopes mined simultaneously, (2) a wet case with the second stope (lower stope) mined about seven days after the first stope (upper stope) and (3) a wet case with hydraulic fill placed seven days after mining the upper stope and just before mining the lower stope. No time was allowed for the fill to "settle" or for additional fluid flow in the rock mass adjacent to the filled stope.

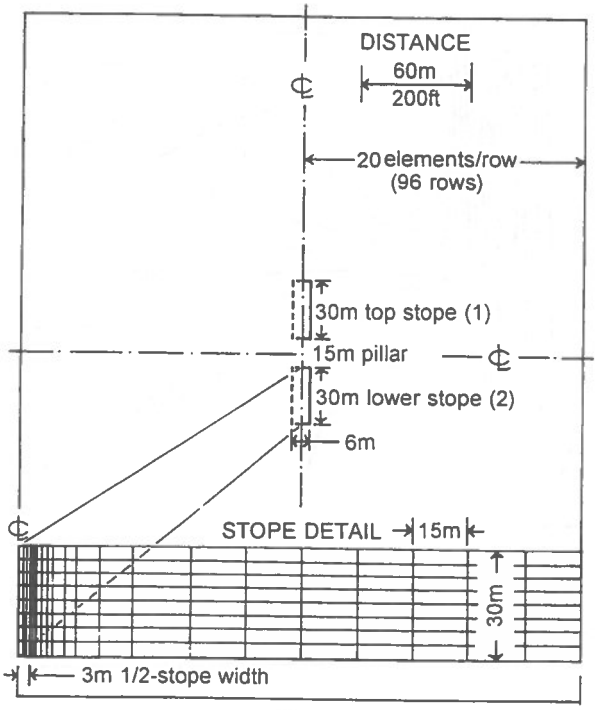

Fig. 7. Stope on stope and FE mesh geometry.

No hanging wall failure occurs in the dry case but some pillar spall is indicated by the (symmetric) safety factor distribution, shown in Fig. 8, where a small region is enclosed by a safety factor contour of one. Distribution is symmetric with respect to the (horizontal) pillar center line.

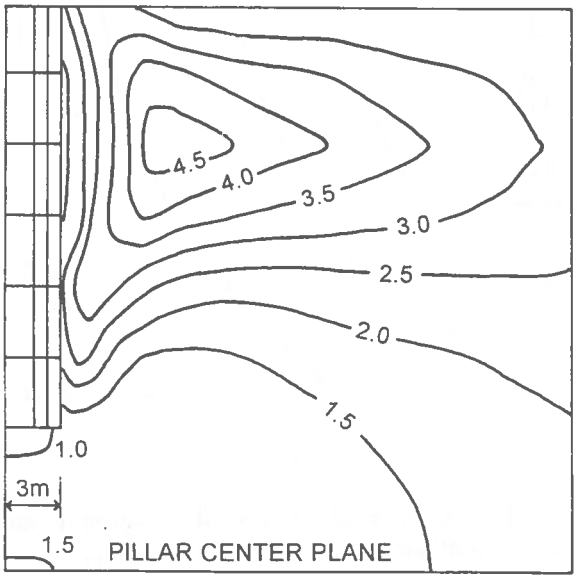

Fig. 8. Dry case safety factor distribution for stope on stope mining.

Instantaneous mining of the upper stope in the wet case results in a safety factor distribution similar to the dry case as shown in Fig. 9. Slight pillar spalling is again indicated, but the hanging wall shows a higher safety factor than in the dry case.

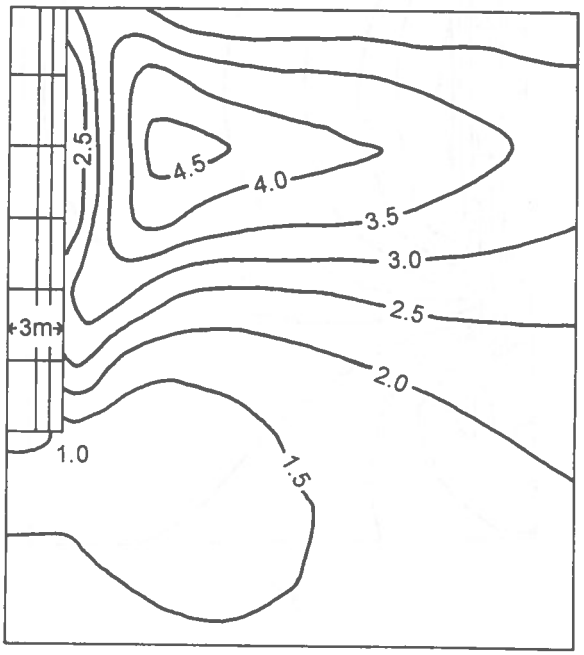

Fig. 9. Top stope wet case safety factor distribution at $t=0^+$.

The instantaneous pressure distribution induced by mining the top (first) stope is shown in Fig. 10a where positive contours indicate pressure multiples and negative contours indicate suction multiples of the premining fluid pressure. The large zone of suction in the hanging wall causes fluid to flow away from the skin of the stope into the interior, contrary to intuition, while the high pressure zone over the ribs induces flow away from the pillar. The instantaneous fluid velocity vectors are normal to the pressure contours (Fig. 10b).

The pressure distribution changes with time and induces additional displacements and changes in the stress field about the stope. Detailed calculations show that the hanging wall safety factor increases slightly the first minute after mining but then begins to decrease. After 10 minutes, failure in the hanging wall extends over the midsection for about 7.5 m (25 ft); after 10,000 minutes or about one week, the failure zone extends almost the entire height of the stope wall. Figure 11a shows the safety factor

distribution about one week after mining the first (top) stope. Meanwhile, the complex distribution of pressure and flow has changed significantly as shown in Fig. 11b.

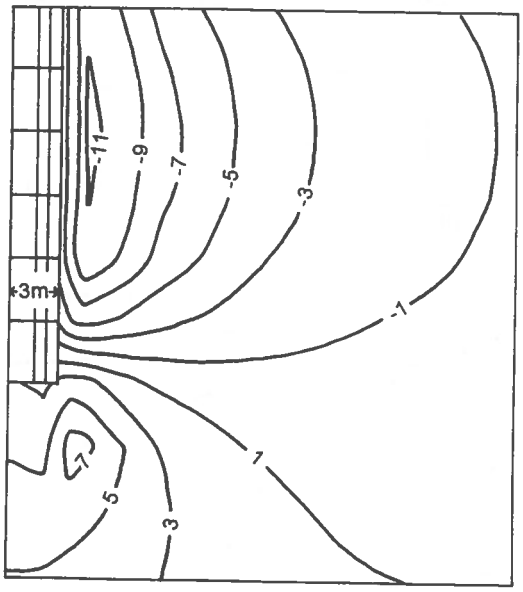

(a)

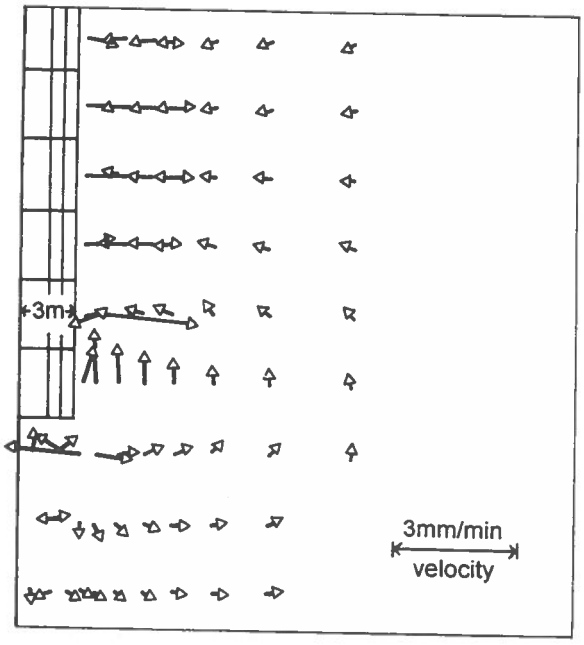

(b)

Fig. 10. (a) Top stope instantaneous fluid pressure contours. (b) Instantaneous flow pattern ($t=0^+$).

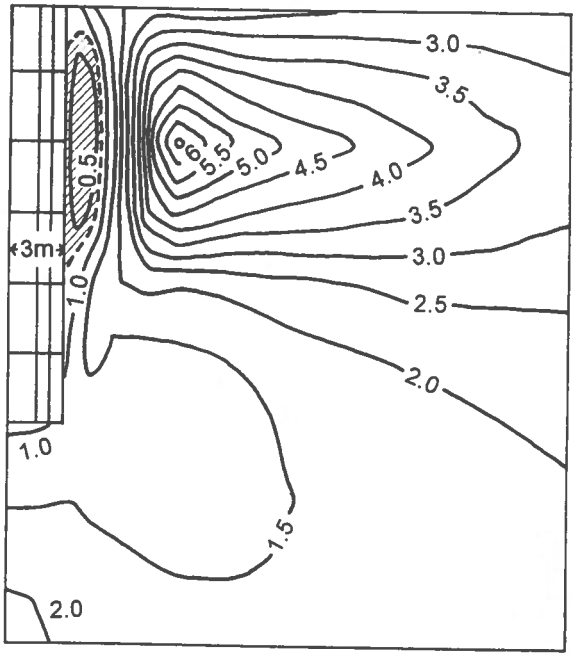

(a)

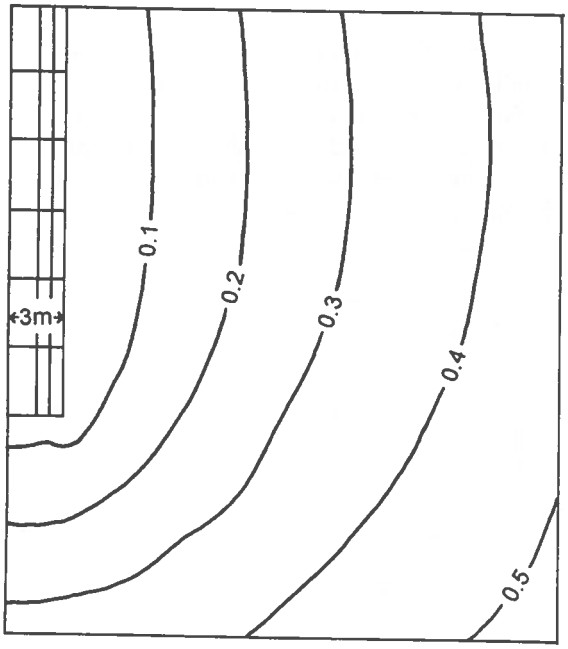

(b)

Fig. 11. Top stope safety factor distribution (a) and pressure contours (b) one week after mining.

Mining the second stope one week after the first stope induces a safety factor distribution and fluid flow pattern about the second stope that is similar to the top stope results. Interaction between stope hanging walls is slight.

However, filling the first (top) stope before mining the second (lower) stope reduces the extent of hanging wall failure in the first stope relative to the no-fill case (Fig. 11). Young's modulus of the fill is 0.001 times the rock mass Young's modulus, 0.17 GPa (24,000 psi); unconfined compressive strength is 0.55 MPa (80 psi). The hatched region in Fig. 11a shows the extent of failure in the hanging wall of the filled top stope just after mining the lower stope. The reduced failure zone extends over the middle 15 m (50 ft) rather over the full height of the top stope hanging wall. The pressure contours and fill flow pattern are shown in Fig. 12.

DISCUSSION

An important practical question in wet mine design is whether to drain in advance of mining or to allow drainage to occur after and increment of face advance. In both cases, the opening functions as a drainage gallery and the flow must be accommodated. Drainage in advance of mining may be costly while returning uncertain savings in operational costs afterwards, so a strategy of allowing drainage to occur immediately following advance of the face is economically appealing. However, the best approach cannot be decided upon without some knowledge of the amount of flow, the pressure behind the flow and how both change with time after a blast or an advance of the face. In any case, the opening must remain safe and stable.

Whether drainage is done in advance or concurrently with mining, the result at the excavation wall is still zero fluid pressure. This observation suggests that wall safety factors will be the same. However, if drainage is concurrent, fluid pressure in excess of the premining pressure may develop (Mandel-Cryer effect) inside the excavation walls and in time lead to a decrease in safety factor. For this reason, it is important to compute the fluid pressure history and evolution of the effective stresses as excavation proceeds. A simple before and after calculation could possibly overlook a dangerously low safety factor during transition to a new steady state following a face advance.

The stope on stope calculations indicate that the opposite of the Mandel-Cryer effect may occur when a zone of suction instead of elevated fluid pressure developes in the interior of the excavation wall. Stabilization of the wall may result for a short time, only to be lost with subsequent fluid flow into the suction zone and a return of saturation.

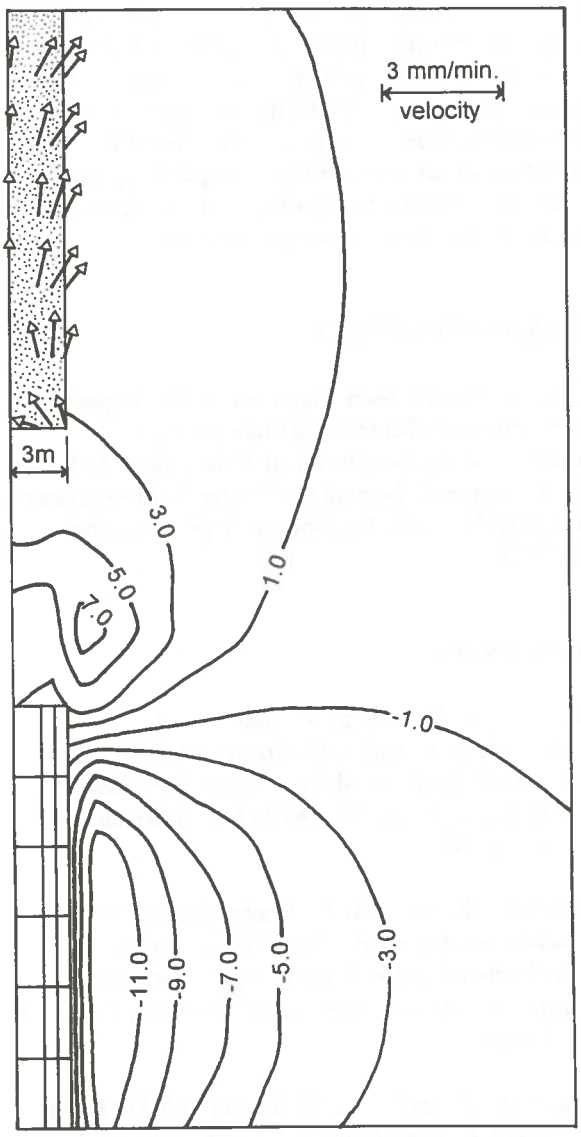

Fig. 12. Pressure distribution and fill flow pattern after mining the lower stope.

CONCLUSION

These results show: 1) the dry case is generally more favorable to stability and 2) even after considerable drainage time has elapsed, the minimum wall safety factor in the wet case is less than the dry case.

Wet mine design requires consideration of water pressure and flow which are coupled to rock mass stress and deformation. The coupled problem requires greater computational effort than dry mine stress analysis, but can be done using existing finite element technology, as briefly demonstrated here using a three-dimensional finite element program to solve several plane, axially symmetric and true three-dimensional example problems analogous to shaft and stope excavations. The procedure offers the advantage of accommodating site-specific geology, structure, excavation geometry, sequencing, and preexcavation stress, pressure and flow.

ACKNOWLEDGEMENT

This research has been supported by the Department of the Interior's Mineral Institute program administered by the Bureau of Mines through the Generic Mineral Technology Center in Mine Systems Design and Ground Control under grant number G1125251.

REFERENCES

Cui, L. A.H.-D. Cheng, V. Kaliakin, Y. Abousleiman and J.-C. Roegiers (1994) "Finite Element Analyses of Anisotropic Poroelastic Problems," *Proc.* 8th IACMAG. Balkema, pp 1567-1572.

Detournay, E. and A.H-D. Cheng (1988) "Poro-elastic Response of a Borehole in a Non-hydrostatic Stress Field," *Int.J. Rock Mech. Min. Sci. & Geomech. Abstr.* Vol. 25, No. 3, pp 171-182.

Detournay, E. and A. H.-D. Cheng (1993) "Fundamentals of Poroelasticity," *Comprehensive Rock Engineering*, Vol. 2, Pergamon, pp 113-171.

Pariseau, W.G. (1972) "Plasticity Theory for Anisotropic Rocks and Soils," *Proc.* 10th U.S. Symposium on Rock Mechanics. SME/AIME, N.Y., pp 267-295.

Pariseau, W.G. (1994) "Design Considerations for Stopes in Wet Mines," *Proc.* Twelfth Annual Workshop. GMTC - Mine Systems and Ground Control. Virginia Polytechnic Institute and State University, Blacksburg (in press).

Pariseau, W.G. (1995) "Finite Element Analysis of Water Pressure and Flow on Shaft and Tunnel Stability. SME Preprint 95-62, Annual Meeting, Denver, Colorado, March 6-9, pgs 9.

Pariseau, W.G. and C.B. Forster (1992) "Stability and Seepage in Wet Mines: A Critical Review". *Proc.* Tenth Annual Workshop. GMTC - Mine Systems and Ground Control. Virginia Polytechnic Institute and State University, Blacksburg, pp 167-178.

Williams, R.E., G.V. Winter, G.L. Bloomsburg and D.R. Ralston (1986) *Mine Hydrology*. SME, Inc., Littleton, Colorado, pp 6.

CAMI '95: 3rd Canadian Conference on Computer Applications in the Mineral Industry
Montreal, Québec, Canada, October 22-25, 1995

Modelling of Gravity Changes in Mining Areas

Anna Szostak-Chrzanowski, Adam Chrzanowski
Department of Geodesy and Geomatics Engineering,
University of New Brunswick, Fredericton, New Brunswick, Canada

Edward Popiolek
Department of Mining Surveying and Environmental Engineering
Technical University of Mining and Metallurgy, Krakow, Poland

ABSTRACT

Relocation of rock masses and resulting rock strata deformations in mining areas may produce significant local changes of the earth's gravity field. Finite Element Method (FEM), supported by FEMMA software, has been applied in a simultaneous determination of changes of gravity and deflections of the vertical caused by the relocation of mass, changes of density, and displacements of observation points. The method was used in modelling gravity changes in a large open pit mine in Poland. Gravity changes up to 18 mGal and changes of the vertical up to 4" (sec.of arc) can be expected in the mining area. The knowledge on gravity changes is important for correcting geodetic surveys of high precision and in identifying any abnormal behaviour of rock strata.

RÉSUMÉ

Le déplacement des masses rocheuses et les déformations subséquentes des assises rocheuses dans les régions minières peuvent créer des changements locaux d'importance dans le champ de gravité de la terre. La méthode d'éléments discrets (FEM), supportée par le logiciel FEMMA, a été appliquée dans la détermination simultanée des changements de gravité et des déviations verticales causé par les changements de masse, de densité et des déplacements des points d'observations. La m´thode fût utilisé pour le modelage des changements de gravité dans une mine à ciel ouvert en Pologne. On peut s'attendre à des changement de gravité allant jusqu'à 18 mGal et des déviations verticales jusqu'à a 4 secondes d'un arc dans l'étedue miniére. La connaissance des changemants de gravité est importante afin de corriger les levés géodésiques de haute précision ainsi que pour identfier quelconque anomalie dans les assises rocheuses.

INTRODUCTION

Relocation of rock masses due to mining activities may produce significant local changes to the gravity field in the vicinity of the excavated areas, stockpiled ore, and dumps of waste rocks. Besides the influence of the relocation of rock masses, the mining operation usually triggers rock strata deformations resulting in additional gravity changes due to density changes of the rock masses and displacements of observation points. The gravity changes result in local tilts of the level surface (equipotential surface of gravity) and, consequently, changes of the direction of the plumblines to which the majority of geodetic and some geotechnical measurements are referenced. Thus, if any geodetic measurements of high precision are required during the mining operation, for example, for the purpose of monitoring the stability of surface structures, they should be corrected for changes of gravity and deflection of the vertical as a function of

time. Otherwise, differences in the repeated observations (angles, distances, gyroazimuths, height differences, tilts, etc.) caused by the gravity changes could be misinterpreted as deformations of the observed object. In addition, by comparing the expected (modelled) gravity changes with the values observed with precision gravimeters, one may gain information on the behaviour of the rock masses disturbed by mining activity. The latter may give useful information on the existence of discontinuities in the rock masses and a possible presence of old mining openings. Various aspects of the mining 'microgravimetry' are discussed in Fajklewicz (1980).

The calculation of gravity changes involves solving complex integrals (summation of influences of point masses). The theory of gravity and various numerical methods used in the gravity calculations, are given in textbooks on geodesy, for example Vanicek and Krakiwsky (1986); Torge (1991); Heiskanen and Moritz (1967).

The Engineering and Mining Surveying Research Group at the University of New Brunswick has developed, within a broader research program on modelling and prediction of deformations in engineering and geosciences, a method for numerical modelling of gravity changes caused by the simultaneous effects of mass relocation and rock deformations. The method utilizes the finite element analysis supported by FEMMA (Finite Element Method for Multipurpose Applications) software developed at UNB (Szostak-Chrzanowski, 1988). The method has been used, among other uses, in modelling regional deformations and gravity changes of tectonic origin (Szostak-Chrzanowski et al., 1993) and, recently, has been applied to modelling expected gravity changes in a large open pit mine, Belchatow, in Poland. Results of the latter application are given in this paper preceeded by a brief review of the basic principle of gravity calculations and finite element modelling of gravity changes.

GRAVITATIONAL FORCES AND GRAVITY ACCELERATION

According to Newton's law of gravitation, two points with masses m and m_p attract each other with a gravitational force

$$f = (Gm/R^2)m_p \qquad (1)$$

where G is Newton's gravitational constant given as G= 6.67259 x 10^{-11} m^3kg^{-1} s^{-2} and R is the distance between the two points. Introducing a Cartesian coordinate system X,Y,Z, and denoting the coordinates of the attracting mass m by x', y', z' and the coordinates of the attracted point P by x,y,z, one can calculate the components of the gravitational force vector **F** (fig.1) of magnitude f from

$$\begin{aligned} f_X &= - f \cos\alpha = - [G\, m\, (x-x') / R^3]\, m_p \\ f_Y &= - f \cos\beta = - [G\, m\, (y-y') / R^3]\, m_p \\ f_Z &= - f \cos\gamma = - [G\, m\, (z-z') / R^3]\, m_p \end{aligned} \qquad (2)$$

where

$$R = [(x-x')^2 + (y-y')^2 + (z-z')^2]^{1/2} . \qquad (3)$$

Since force is a product of mass and acceleration (Newton's second law), the terms in brackets of eqs.(2) are components of the gravitational acceleration or, briefly, gravitation.

In the case of a solid body with volume v and density ρ, the total gravitational force acting on point P (Fig. 2) with unit mass ($m_p = 1$) will be calculated as a sum of influences of individual point masses dm of volume dv over the entire volume v. Assuming that the point masses are distributed continuously over the volume v with density

$$\rho = dm/dv \qquad (4)$$

the components of the gravitational acceleration at point P will be calculated from

$$\begin{aligned} a_x &= - G \rho_l \int_v \frac{(x - x')}{R^3}\, dv , \\ a_y &= - G \rho_l \int_v \frac{(y - y')}{R^3}\, dv , \\ \text{and} \qquad & \qquad (5) \\ a_z &= - G \rho_l \int_v \frac{(z - z')}{R^3}\, dv , \end{aligned}$$

where $dv = dx'\, dy'\, dz'$.

A point of unit mass rotating with the earth is acted upon by *gravity*, g, which is the resultant of the gravitational forces of the earth and of other celestial

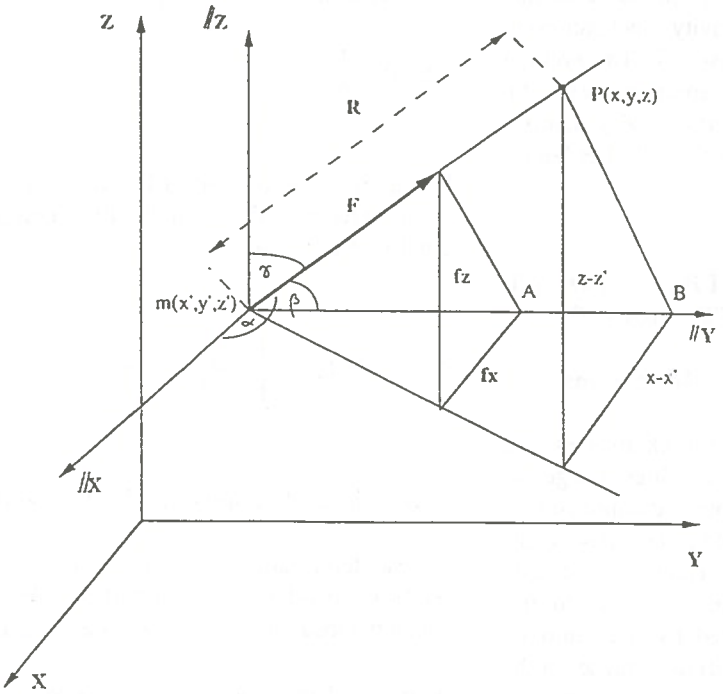

Fig. 1. The components of the gravitational force [after (Heiskanen and Moritz,1967)]

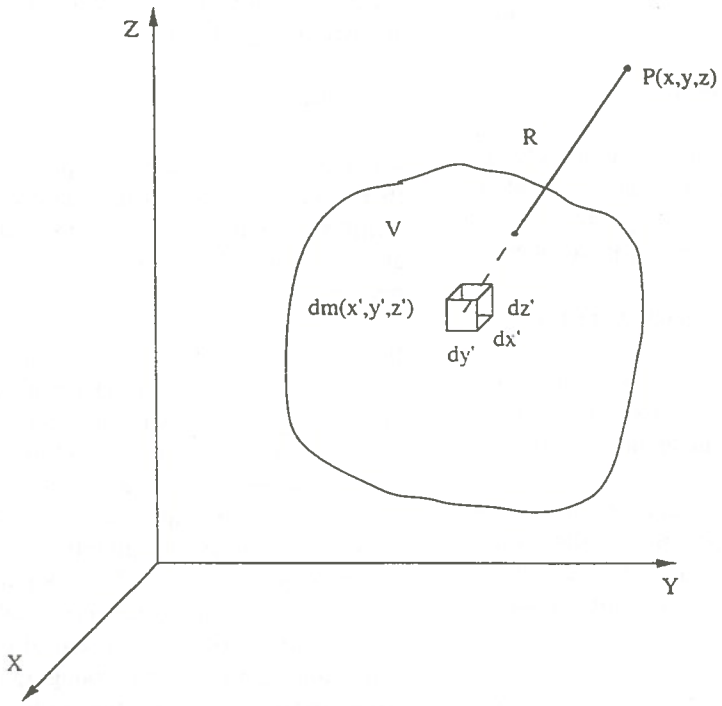

Fig. 2. Attraction of point P of unit mass by a point mass dm of a solid body [after (Heiskanen and Moritz, 1967)]

bodies, as well as the centrifugal force due to the earth's rotation. The gravity (called also gravity acceleration) is expressed in *Gals* (1 Gal = 1cmsec^{-2}). The average value of g on the earth surface is approximately 981 Gals. With the present technology, the gravity changes can be measured with an accuracy of 50 μGal or better, using portable gravimeters.

CALCULATION OF THE LOCAL CHANGES OF THE EARTH'S GRAVITY

Gravity Change due to Mass Relocations

The aforementioned relocation of rock masses and ground deformations due to mining activities change the earth's gravitational force, while other components of the earth's gravity can be considered as constant. Thus, one may determine the local gravity change, Δg, caused by the relocation of rock masses, as equal to the gravitational acceleration produced by the removed (excavated) or brought-in (stockpiled) rock masses of the given density and given geometry. Thus, for example, the x component of the gravity change, Δg_x, can be obtained from

$$\Delta g_x = a_x \qquad (6)$$

where a_x is calculated using eqs.(5).

For a convenient interpretation of the gravity changes, the axis z of the local coordinate system is oriented in the vertical direction (direction of the plumbline) at the point at which the magnitude of gravity is calculated.

Gravity Change due to Density Change

The change of density may be caused by a change in the state of stress, resulting, for example, from the deformation of the rock strata due to mining activity.

Let us assume that due to a change in the stress field in individual elements of the rock masses, the mass of the rocks remains constant but volumes of the elements change. The asssumption of constant mass is expressed by

$$\rho_1 v_1 = \rho_2 v_2 \qquad (7)$$

where ρ_1 and ρ_2 are the densities and v_1 and v_2 are volumes before and after the deformation, respectively.

The new density may be expressed as

$$\rho_2 = \rho_1 \frac{v_1}{v_2} \qquad (8)$$

Using eqs. (5), (6), and (8), one may calculate the gravity changes. For example, the z component of the gravity change, Δg_z, is

$$\Delta g_z = - G \rho_1 \frac{v_1}{v_2} \int_{v_2} \frac{(z - z')}{R^3} \, dv \, . \qquad (9)$$

Free Air and Topographic Corrections

Ground deformation caused by the mining activity may produce subsidence or uplift of the physical point at which the local gravity changes are to be determined.

A vertical displacement of the observed point changes its distance to the earth's centre of mass which changes the vertical component of gravity at the point. The increment of gravity due to the change of height is calculated approximately from (Torge, 1991; Vanicek and Krakiwsky, 1986):

$$dg_A = - b \, dH \qquad (10)$$

where b is a gravity gradient equal to -0.3086 mGal/m (here, one should not confuse m for metre with m for milliGal), and dH is the height change in metres along the plumbline. The correction (10) is called the *free air correction.*

In addition to the free air effect, the uplift or subsidence of the point produces a relative relocation of the topographic masses and, consequently, a change in the value of gravity. Therefore, eqs. (5) and (6) could be used for calculations of the gravity changes by taking a topographic area of a sufficiently large diameter around the invetigated point for the integration of the effects. The topographic correction is expected, however, to be very small in comparison with the effects of the mass relocations due to mining extraction. Therefore, the topographic correction can be approximated to the first order by the so-called Bouguer plate reduction dg_B, which corresponds to the gravitation of a horizontal plate with infinite extension and the change of height dH. The Bouguer plate

reduction dg_B is calculated from (Torge, 1991):

$$dg_B = 2 \pi G \rho_O dH \qquad (11)$$

where ρ_O is the average density of the rocks surrounding the point of calculations. The total change of gravity is calculated from the sum of gravity changes and the free air and Bouger plate corrections.

Calculations of Deflection of Vertical

Changes in the horizontal components, Δg_X and Δg_Y, of gravity, produce a change in the direction of the plumbline at the point of interest. This can be calculated (in radians) from

$$d\alpha_X = \Delta g_X / g_O$$
$$d\alpha_Y = \Delta g_Y / g_O \qquad (12)$$

where g_O is an appropriate value of absolute gravity at the point. For all practical purposes, the average value of g_O = 9.81m s^{-2} = 981 Gal can be taken for the calculations.

NUMERICAL MODELLING OF GRAVITY CHANGES

Use of the Finite Element Method

Two calculation problems are involved in the analysis of gravity changes: one is the solution of the integrals in eqs. (5) in the case of complicated geometry of the relocated mass; and the other is in the determination of the change of geometry (deformation) and resulting change in the density of the attracting object and displacements of the attracted point masses (points of observation). Although several numerical methods have been suggested by other authors for solving the integrals involved in eqs. (5) and (9), no method has been put forward addressing the simultaneous solution for the effects of the deformation. Use of the finite element method (FEM) permits the simultaneous solution by adapting the numerical solutions of integrals inherent in the FEM (involved in the calculation of the stiffness matrix of the investigated material) and by performing the load-deformation analysis on the basis of a known stress-strain relationship and geomechanical properties of the investigated material.

The total gravity change caused by a change of density is calculated as the sum of effects of density changes in each element of the finite element model using eqs. (9). The volumes v_1 and v_2 of each element are calculated from the initial and after-the-deformation (obtained from the stress-strain finite element analysis) coordinates of the nodal points.

FEMMA Software

FEMMA, Finite Element Method for Multipurpose Applications software, can be applied to either two- or three - dimensional problems in the analysis of elastic, linear-elastic, and visco-elastic deformations (Szostak-Chrzanowski A. and A. Chrzanowski, 1991), heat transfer, and rigorous propagation of random errors of the input data (Szostak-Chrzanowski et al., 1994) . The analysis of gravity changes has been added as an optional 3-D version in which the Gaussian quadrature rule is applied to solve the integrals of eqs. (5) and (9).

FEMMA uses brick elements with 8 nodal points in a 3-D analyses. The subprogramme MESHGEN generates the mesh.

Gaussian Quadrature Rule

To calculate the integral in eqs. (5), the Gaussian quadrature rule is used (Zienkiewicz and Taylor, 1989).

Let the function under the integral from eqn. (5) be represented by F(x,y,z). Then, for example, for the z component of the gravitation, we have

$$\int_v F(x,y,z)\, dv = \int_v \frac{(z - z')}{R^3}\, dv \,. \qquad (13)$$

By introducing local coordinates ξ, η, and ζ in each element, one can write:

$$\int\int\int F(x,y,z)\,dx\,dy\,dz =$$

$$= \int_{-1}^{1}\int_{-1}^{1}\int_{-1}^{1} G(\xi,\eta,\zeta)\,\det[J]\,d\xi\,d\eta\,d\zeta \qquad (14)$$

where det[J] is the determinant of Jacobian matrix. The local coordinates are chosen as

$-1 \le \xi \le 1$, $-1 \le \eta \le 1$, and $-1 \le \zeta \le 1$.

The determinant of matrix J is a magnification factor (scale factor) that yields:
volume $= dx\,dy\,dz = \mathrm{Det}J\,d\xi\,d\eta\,d\zeta$. Using the Gaussian quadrature rule, one can write:

$$\int_{-1}^{1}\int_{-1}^{1}\int_{-1}^{1} G(\xi,\eta,\zeta)\,\det[J]\,d\xi\,d\eta\,d\zeta =$$

$$= \sum_{m=1}^{n}\sum_{j=1}^{n}\sum_{i=1}^{n} W_i W_j W_m\,\det[J]\,G(\xi_i,\eta_j,\zeta_m) \qquad (15)$$

where $W_{i,j,m}$ are weights. For 2 x 2 x 2 integration points, the weights W_i, W_j, and W_m are equal to one. In order to evaluate matrix **G**, a transformation of the coordinates is necessary. The coordinate transformation is established using standard shape functions given in terms of local coordinates as explained, for example, in Zienkiewicz and Tylor (1989).

EXAMPLE OF GRAVITY CHANGES IN AN OPEN PIT MINE

Belchatow Mine

The presented method and FEMMA software have been used in calculating expected gravity and deflections of vertical changes at Belchatow, an open pit mine in Poland. The purpose of the calculations was to learn about the approximate magnitude of gravity changes which could be expected in a large mining operation and to compare the results with an earlier analysis performed by Sas (1993).

Belchatow is one of the largest open pit mines in the world producing brown coal. It started mining production in 1975. Figure 3 shows the approximate geometry and dimensions of the excavated area and of the waste rock (overburden) dump which are 2.5 x 2.6 km with the depth of 0.4 km and 2.7 x 2.7 km with a depth of 0.17 km, respectively. Table 1 shows the geomechanical parameters of the main components of the rock strata. Both the dimensions of the mine and the geomechanical data have been taken from Sas (1993) who calculated the gravity changes caused by the mining operation. In his calculations, Sas used a conventional method based on subdividing the excavated area and dump into simple geometrical blocks to facilitate analytical solutions of the integrals. His method could consider only a simplified geometry of the mine and only the influence of the mass relocation, neglecting the deformation effects.

Table 1. Geomechanical parameters of the rock mass

Rock strata	Young Modulus [GPa]	Poisson ratio	Density [gcm^{-3}]
brown coal	1.0	0.3	1.39
crushed rock & sand	0.9	0.3	1.60

In order to compare the FEMMA results with the results obtained by Sas, the same simplified geometry of the mine was used in the finite element analysis. Two analyses were performed. The first, preliminary analysis, was to estimate the approximate magnitude of influences of the mass relocation versus influences of the rock deformations (density changes and displacements of surface points). The second, the final analysis, was to perform calculations with a refined FEM mesh and using only those affecting factors which proved, in the preliminary analysis, to be dominant.

In the preliminary analysis, the whole area of the investigated rock mass was modelled as a block with dimensions 12 500 m x 12 000 m and 970 m high divided into 332 elements with 519 nodal points. The finite element analysis of the gravity changes included effects of:
1) change (relocation) of mass,
2) change of density, and
3) change of the heights of the surface points.

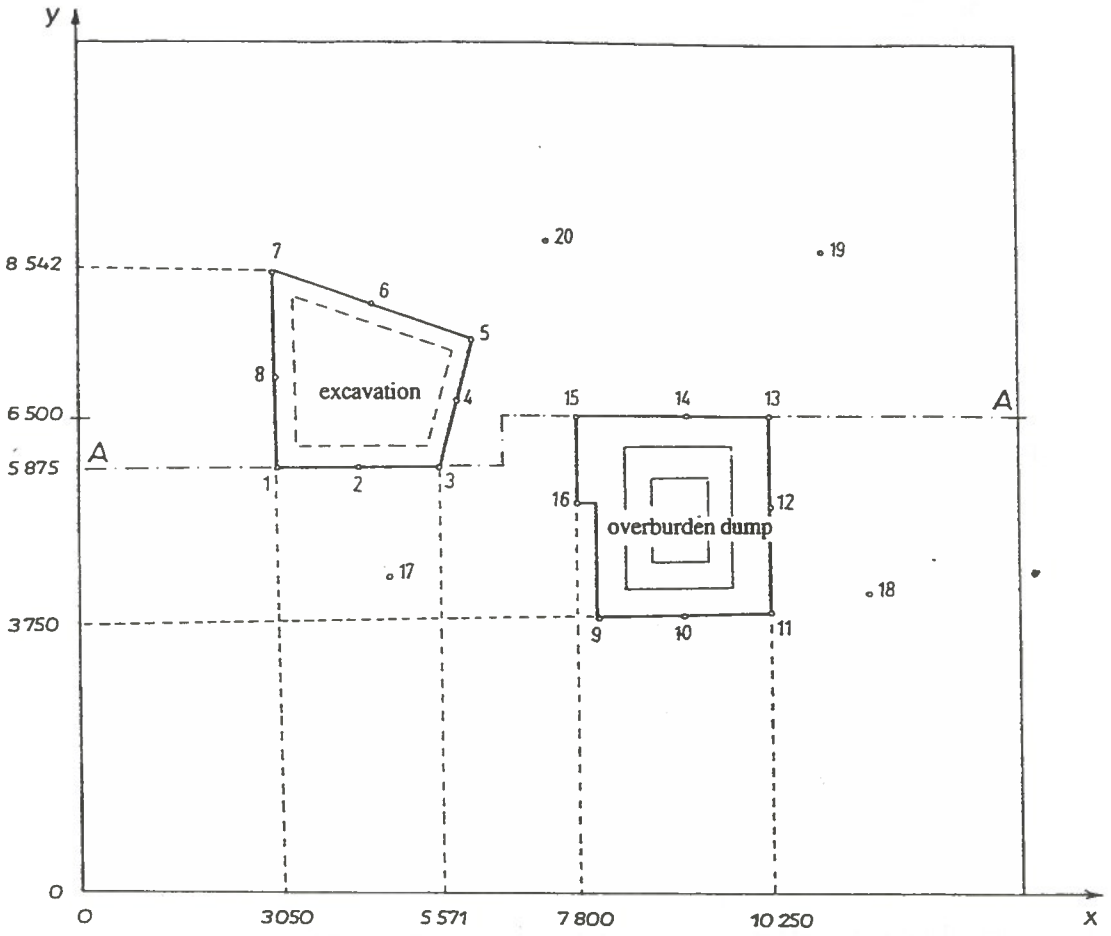

Vertical Cross-section

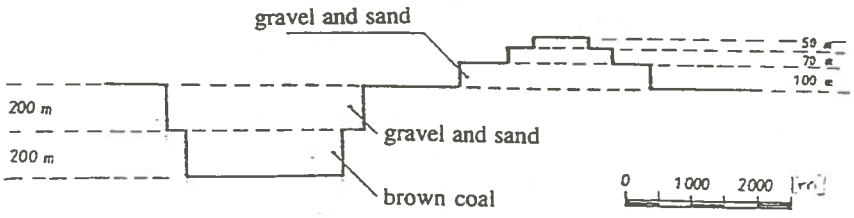

Fig. 3. Belchatow open pit mine (simplified geometry)

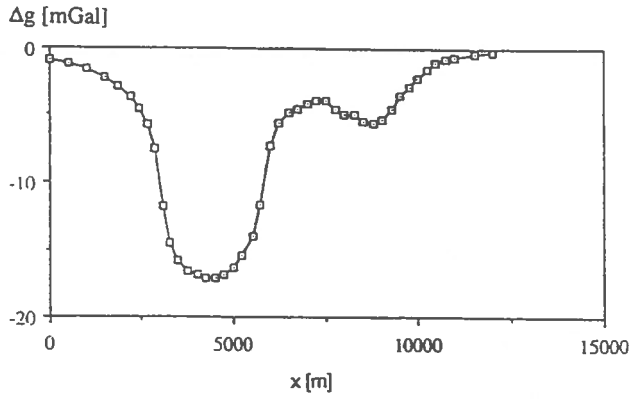

Fig. 4. Total change of gravity on the surface in A-A cross-section

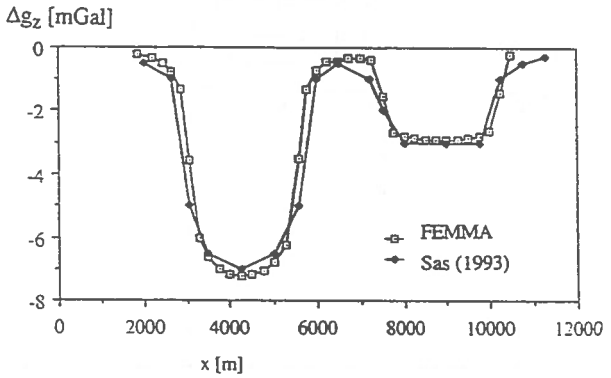

Fig.5. Vertical component of the gravity change on the surface in A-A cross-section

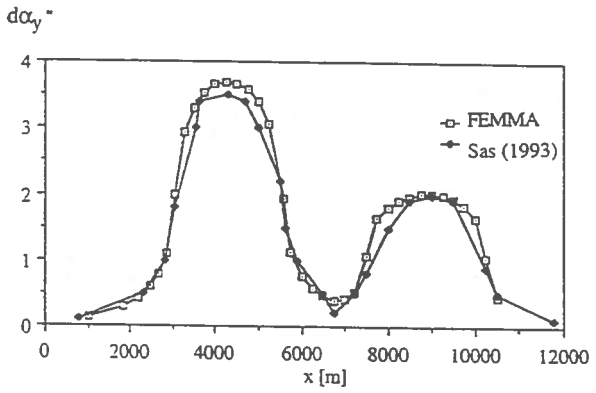

Fig. 6. Change of the deflection of vertical (y component) on the surface in A-A crossection

Table 2 shows a sample of results at surface points 2, 3, and 18 (Fig.3) for the various effects. As one can see, in this particular example, the relocation of mass is the dominating effect accounting for over 90% of the calculated gravity changes. Therefore, the final analysis was performed considering only the effect of the mass relocation. This provided also a better comparison with the results obtained by Sas.

Table 2. Results of the preliminary analysis of various effects

	Gravity change [mGal]		
Point No.	caused by mass relocation	caused by mass reloc.+ density ch.+ free air red.	caused by mass reloc.+ density ch. + free air + plate
18	- 0.64	- 0.62	- 0.60
2	- 15.05	- 14.99	- 14.86
3	- 13.71	- 13.64	- 13.52

In the final analysis, the gravity change was calculated using eqs. (5). In the FEM model, the open pit was divided into 164 elements and the dump of the overburden rocks into 153 elements. The gravity changes were calculated on the surface for an area of 12500 m x 12 000 m. The model had a total of 5385 nodal points. Figures 4 and 5 summarize results of calculations of the total and vertical (dg_z component) gravity changes, respectively, along crosssection A-A (Fig.3). Figure 5 shows also a comparison with the gravity changes calculated by Sas. A very good agreement has been obtained between the two methods of calculations. The total gravity changes, caused by the relocation of rock masses reached - 18 mGal .

The calculated components Δg_x and Δg_y of gravity changes have been used to calculate components of the deflection of vertical using equations (12). Figure 6 shows the $d\alpha_y$ components of the changes of the deflection of vertical (in seconds of arc) along the cross-section A-A as calculated with FEMMA and by Sas(1993). Again, the agreement is very good.

CONCLUSIONS

The presented method of modelling gravity changes allows for a simultaneous determination of the changes caused by relocation of masses and by deformation of the rock strata. The method is applicable to any geometry of the investigated effects (attracting masses). A good agreement with conventional calculations of gravity changes, for a simple geometry of the relocated masses, has provided a verification of the results obtained with the FEMMA software.

The presented example of effects of a large open pit mine indicates that mining activities may produce very significant gravity changes (several milliGals) and changes of the deflection of the vertical in the order of several seconds of arc.

REFERENCES

Fajklewicz, Z., 1980. Mikrograwimetria Gornicza, Wydawnictwo Slask, Poland.

Heiskanen W. and H. Moritz, 1967. Physical Geodesy, W. H. Freeman and Company, San Francisco and London, 364 p.

Sas A. M. , (1993). Redukcje Powtarzanych Pomiarow Niwelacyjnych ze wzgledu na Technogenne Przemieszczenia Mas. Ph.D. Thesis, Intytut Geodezji i Kartografii, Warsaw, Poland, 67 p.

Szostak-Chrzanowski, A., 1988. An iterative modelling of ground subsidence using non-linear elastic finite element analysis. Proceedings, 5th Int. (FIG) Symp. on Deformation Measurements, Univ.New Brunswick, 6-9 June, pp. 524-535

Szostak-Chrzanowski, A. and A. Chrzanowski, 1991. Use of Software FEMMA in 2-D and 3-D Modelling of Ground Subsidence. Proceedings, 2nd Canadian Conference on Computer Applications in the Mineral Industry, (eds.: R.Poulin, R.Pakalnis and A.L.Mular) Univ. of B. C. and The Canadian Institute of Mining, Vancouver B.C.,15-19 September, pp.689-700.

Szostak-Chrzanowski, A., A. Chrzanowski, and Y.Q. Chen, 1994. Error Propagation in the Finite Element Analysis of Deformations. Proceedings of the XXth Congress FIG, Melbourne, Australia, 5-12 March, pp.602.4/1-602.4/9

Szostak-Chrzanowski, A., A. Chrzanowski, A. Lambert, M.K. Paul,1993. Finite Element Analysis of Surface Uplift and Gravity Changes of Tectonic Origin. Proceedings of the Seventh Int. Symp. on Deformation Measurements, Can. Inst. of Geomatics, Banff, Alberta, May 3-5, pp.333 - 341.

Torge W., 1991. Geodesy, 2nd editon, Walter de Gruyter, 264 p.

Vanicek P. and E. Krakiwsky, 1986. Geodesy: the Concepts, North-Holland, 697 p.

Zienkiewicz O. C. and R. L. Tylor, 1989. The Finite Element Method, McGraw-Hill Book Company, Vol. 1 and 2.

CAMI'95: 3rd Canadian Conference on Computer Applications in the Mineral Industry
Montréal, Québec, Canada, October 22-25, 1995

Slope Stability of the Eastern Wall of Copper Mountain Open Pit Mines, Gaspé, Québec

Nadia Feknous, Richard Simard, Jacques Sarrailh
SNC-Lavalin, Montréal, Québec

Hani S. Mitri
Department of Mining and Metallurgical Engineering
McGill University, Montréal, Québec

Gaston Morin
Mines Gaspé, Noranda Mining and Exploration Inc., Gaspé, Québec

ABSTRACT:

The finite element method was used to analyze the stability of the eastern wall of Copper Mountain open pit mine, Gaspé, Quebec. The purpose of the study was to assess the overall stability of the wall at the end of a proposed mine expansion plan. Therefore, the current pit wall stability was first examined to serve as a basis for comparison. A vertical east-west section along the 21 000N, in the proposed mining expansion zone, was selected for the analysis. The pit is stratigraphically located in the Indian Cove and York River formations. These formations consist of varying proportions of metamorphosed and metasomatised interbedded calcareous siliceous siltstone and sandstone.

RÉSUMÉ:

La méthode des éléments finis a été utilisée pour analyser la stabilité du mur est de la mine à ciel ouvert Copper Mountain, Gaspé, Québec. L'objectif de l'étude est d'évaluer la stabilité du mur à la fin du plan d'expansion proposé. La stabilité du mur a d'abord été examinée pour servir de comparaison. Une section verticale est-ouest, située au 21 000N, dans la zone d'expansion proposée, a été choisie pour l'analyse. La géologie montre les formations métamorphosées et métasomatisées qui sont constituées en proportion variable de siltstone calcareux et siliceux interlités avec des gres. Les données géomécaniques et les résultats obtenus sont présentés et discutés.

HISTORY OF COPPER MOUNTAIN OPEN PIT

Mines Gaspé's mining and metallurgical facilities are located at Murdochville in north central Gaspé Peninsula (Figure 1) at an elevation of 575 m above sea level. It was in 1909 that the first indications of copper mineralization were observed in the York River and some 45 years later, the biggest underground mine in Canada was put into production. In February 1968, Copper Mountain open pit mine began production at 3,500 tonnes/day. In the meantime, improvements were carried out at the concentrator and additional equipment was installed for the treatment of 11,500 tonnes of ore per day.

In March 1973, a second concentrator, with a capacity of 22,500 tonnes/day, was put into operation to treat the ore from the expanded Copper Mountain open pit mine. An oxide ore treatment plant with a capacity to treat 5,000 tonnes/day was added. Additionally, smelter capacity was expanded to meet the increase in production and a sulfuric acid plant was put into operation.

In July 1982, mining in the underground mine ceased because of high operating costs and the low price of copper. The Copper Mountain open pit was shut down in December 1982. After the curtailment of all mining operations, Mines Gaspé took the decision in August 1984 to develop the E-32 ore body under the town of Murdochville. Since then,

exploration led to the discovery of the E-29 ore body.

The Copper Mountain deposit is located within the Indian Cove Formation and consists of a cylindrical ring of low grade mineralization, 700 m in diameter, that surrounds the porphyritic quartz monzonite intrusion. Main sulfides include pyrite, chalcopyrite and molybdenite, occuring within quartz-calcite vein stockworks or as open-space fillings within numerous joints cutting the greenish "calcareous diopsidic quartzite". Mineralization, known to occur up to a depth of 650 m below surface, shrinks in volume at depth, but the grade of the central pipe remains constant (>0.6% Cu). Using a cutoff grade of 0.2 % Cu, the geological tonnage of this deposit (ore mined out plus mineralization left in place) was estimated at approximately 200 million tonnes grading 0.4 % Cu and 0.02 % Mo. The near surface part of this deposit was oxidized and consists of limonite, malachite, chrysocolla and azurite, with a minor underlying supergene zone of chalcocite, digenite and covelite. Tonnage of the oxidized zone was estimated at 27 million tonnes grading 0.44 % Cu.

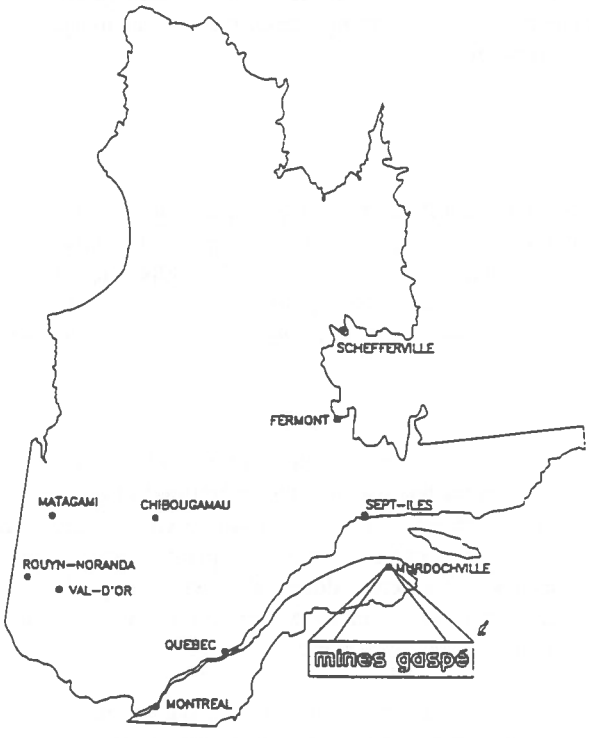

Figure 1: Location of Mines Gaspé

PROPOSED PIT EXPANSION

The proposed near future expansion of the Copper Mountain pit (Figure 2) is to take place on its eastern wall and should result in a first berm level of 1600 ft, down from the current 1710 ft level. The average slope angles above and below the 1710 level are approximately 59° and 47°, respectively. Because the berm is some 740 ft wide, the overall pit slope angle of the eastern wall is only 32°. An east-west geological section in that area showed the metamorphosed rocks located within the Indian Cove and York river formations.

LOCAL GEOLOGY

The Copper Mountain open pit mine is essentially excavated in alteration aureole where the porphyry dykes intruded up to the surface the calcareous silstone of the Indian Cove Formation. This aureole was developed in an elliptic form and can be divided in three concentric zones of different intensity of alteration, the zone of contact with porphyry is of very high alteration.

The metamorphism of the formation of York River produced quartzite, greenish to brown in color, inter-bedded with a dark brown hornfel. These rocks are visible in the north border of Copper pit, at the contact with bleached hornfel of the Indian Cove. The greenish hornfels in the border of the pit are tremolite hornfels.

Progressing toward the pit interior, are encountered porcellanite (limey-quartzite) and in the most altered part skarn or diopsidic quartzite. This is in direct contact with the porphyry intrusion and has a cylindric shape around the intrusion.

The rock is green-grey to dark green; the color becomes darker when the diopside is replaced by the hedenbergite. The porphyry contains phenocrystals of feldspar and quartz (40 to 50%) and a vitreous matrix with numerous microlites of similar composition as phenocrystals.

Oxide

The unit called "oxide", constitued of brownish rock with an earthy aspect, occupies an important section of the pit. Its limits are clear in the east sector, but are more difficult to define toward the west, since the oxide doesn't form the totality of the rock but only when it is concentrated in the fractures and the remaining rock is more or less decomposed.

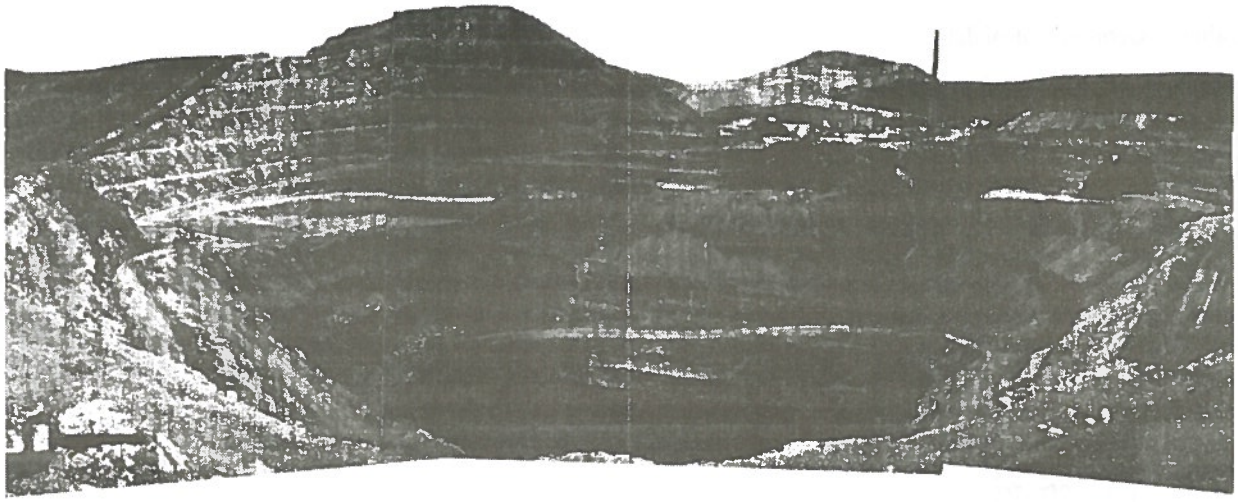

Figure 2: Copper Mountain Open Pit

The rock presents various coloration, dark red and brown with yellow and black stains, where the presence of oxides of iron and manganese (pyrolusite) is evident. The color of oxidations of copper minerals, malachite and calcosine is also very pronounced.

GEOMECHANICAL DATA

Rock Properties

Ideally, the rock mass modulus of elasticity should be determined in the field using, for example, dilatometer tests. In the absence of this data, empirical methods may be used to help estimate the rock mass modulus. In this study, the rock mass Young's moduli of elasticity, E_{rm}, were calculated as a function of the intact rock modulus, E_i and the rock mass rating, RMR. The following expression was used (Mitri et al., 1994):

$$E_{rm} = 0.5 \cdot E_i \cdot [1 - \cos\pi(RMR/100)]$$

The geomechanical data used for the purpose of numerical modelling are listed in Table 1 and were obtained from previous laboratory work done for Mines Gaspé (Charette, 1994).

In Situ Stress

Borehole slotting tests were carried out at two sites in the E-29 ore zone of Mines Gaspé in order to determine the pre mining in-situ stress (Kanduth et al., 1993). The stress determination was part of a program to characterize the rock structure in this new development for the purpose of the design of underground openings and the sequencing of mining.

A total of 132 slotting tests were carried out at two sites. In each case,the tests were performed in three HQ holes (ϕ = 76 mm). A relatively high failure rate of tests was experienced due to the very brittle nature of porcellanite rock material which caused spalling as the slot was cut.

The reported σ_2 principal in-situ stress, which is parallel to the selected section to be analyzed, ranged from 1.2 to 1.7 times the vertical stress, dipping at angles between 14° and 55°. Taking a dip angle of 20°, this gives a range of horizontal to vertical in-situ stress ratio of 1.13 to 1.6. Both extreme values obtained were used in the modelling.

NUMERICAL MODELLING

A vertical east-west section along the 21 000N was selected for the analysis. The section is located in the proposed mining expansion zone. Numerical modelling was conducted using a 2-dimensional, linear, elastic, finite element modelling software (Mitri, 1993). A finite element model consisting of 4499 quadralateral elements has been constructed (Figures 3). The model's far vertical boundary extends some 7500 ft from the pit crest whereas the bottom (horizontal) boundary extends approximately 3000 ft below the pit floor. Figure 3 illustrates the proposed expansion zone at the 1710 ft berm level.

A simple design approach has been adopted for the stability

Table 1: Geomechanical data

Rock Type	Unit Weight MN/m³	E_i GPa	RMR	E_m GPa	Poisson's Ratio	Cohesion MPa	Friction Angle
York River Formation	0.027	52.7	84	49.8	0.2	10	48°
Indian Cove	0.027	71.3	65	51.8	0.25	10	40°
Non-metamorphosed Indian Cove	0.027	65.8	85	61.7	0.2	10	48°

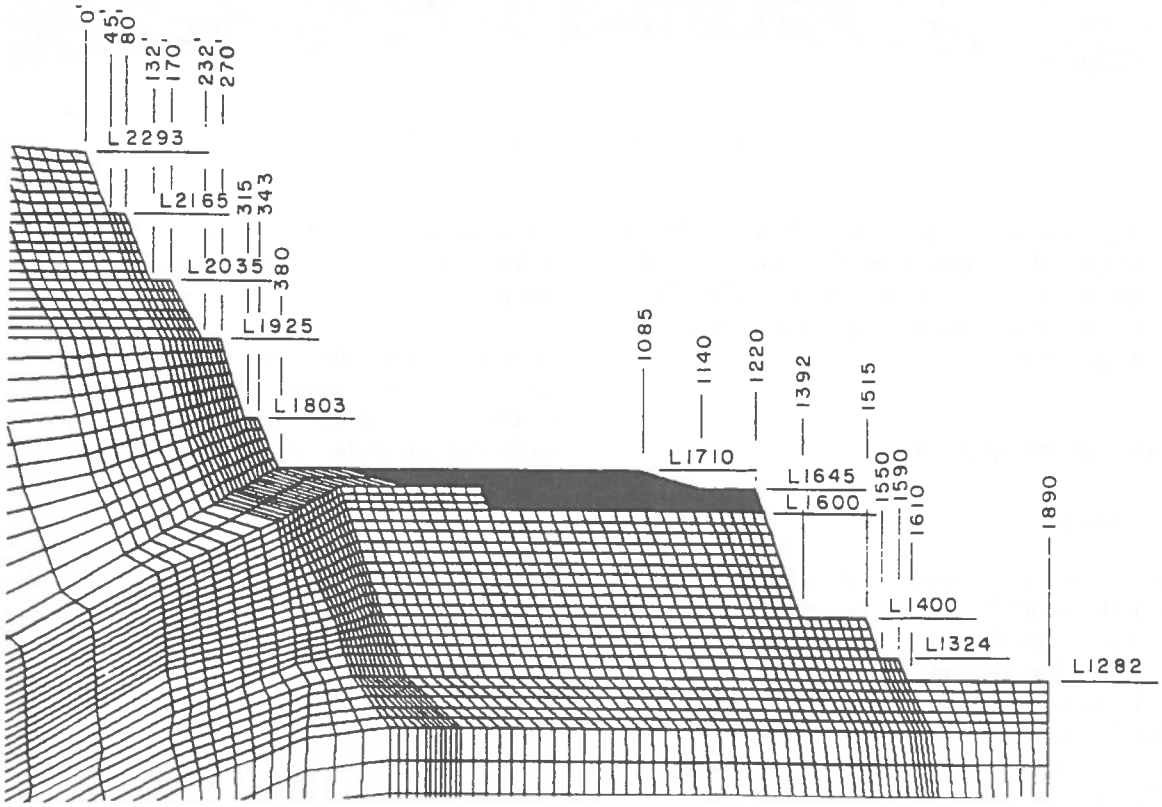

Figure 3: Finite Element Model-Zoom-in Picture Showing Berm Levels

study. First, the current (stable) pit wall was analyzed, and this condition was used as a basis to establish model validation with the set of geomechanical data described above and used in numerical modelling. The proposed mine expansion is then simulated to examine the stability of the pit wall after the excavation of the expansion zone.

Based on the observations from the site visit and the available data of water levels, it was decided that the analysis in the selected section would assume dry conditions

RESULTS

Case 1: Current Pit Slope Analysis

The results of principal stress trajectories for the two cases K=1.13 and K=1.6 indicate the development of small tensile stresses especially in the pit floor and in the 1324 and 1400 level inter-berm lifts; see Figure 4. Note that for the purpose of illustration, the tensile stress trajectories are exaggerated in scale while the compressive ones are

minimized. The tensile stresses in the pit floor are vertical hence are of little concern. The tensile stress trajectories in the 1324, 1400 and 1710 levels interberm lifts are near perpendicular to the slope face and would normally be of concern. However, their magnitude is far lower than the reported rock mass tensile strength (Charette, 1993, Miguel, 1978).

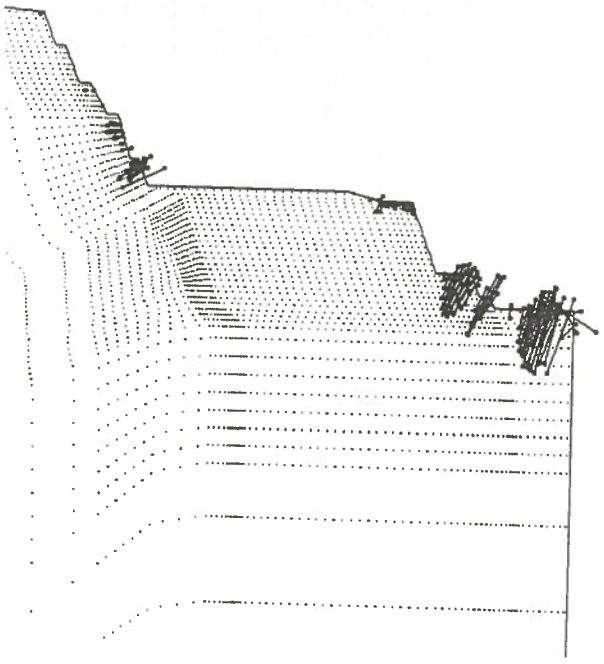

Figure 4: Tensile Stress Trajectories in the Pit Wall (k=1.6)

Additionally, the results of the horizontal and vertical stress levels in the slope for the case of K=1.6 show that the tensile stresses range from 0.19 to 0.75 MPa. The rock tensile strength as reported (Charette, 1993) is between 16 and 22 MPa. This suggests that the developed tensile stresses in the slope should not be of concern.

The resultant displacement vectors in the slope, for both cases of K=1.13 and K=1.6, indicate a general movement towards the slope face. These vectors were resolved into vertical and horizontal components (Figure 5 , for K=1.6).

In both cases, the vertical displacements indicate the following (Figure 5a):

- the lower pit levels, typically 1324 and 1400 levels have relatively larger displacements compared to levels at or above the 1710 level,
- the displacement curves shown all indicate positive upward movements to large distances from the pit face (note relative distance of 36 represents nodes approximately 220 metres from the pit face).
- the locus of zero vertical displacement of these displacement trajectories is in the far field. In fact it progressively shifts away from the slope face with depth.

Similarly, the horizontal displacements (Figure 5b) are larger for the bottom levels than the upper ones. A projection of zero horizontal displacements per levels shifts away from the face with pit depth.

When the two components are analyzed jointly, they indicate that locus of both zero vertical and horizontal displacements occur far from the slope face. The progressive shift from the face suggests that there is little probability of rock mass "daylighting" into either the slope face or pit floor.

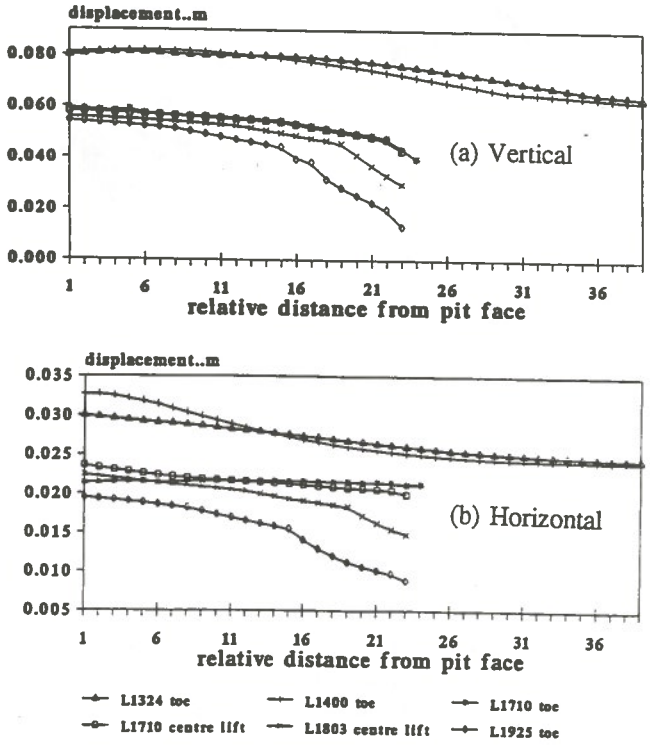

Figure 5: Variation of Vertical and Horizontal Displacements of Current Pit (K=1.6)

The slope safety factor analysis was conducted using Mohr-Coulomb criterion. It is considered that the friction angle is

45° and since the tensile strength is given (16-22 MPa) then cohesion has to assume similar values. Cohesion values of 10 MPa were used which are considerably lower than those reported by Charette (1993). The analysis was performed using the values within the ranges indicated in Table 1. The results indicate a safe slope for both K=1.13 and K=1.6.

Case 2: Final Pit Slope Analysis

Similar stress trajectories exist for the final pit slope after the mining of the proposed expansion zone as those in the current pit profile. Insignificant tensile stresses develop on the 1650 and 1710 berms (Figure 6). Elsewhere, the stresses are virtually identical.

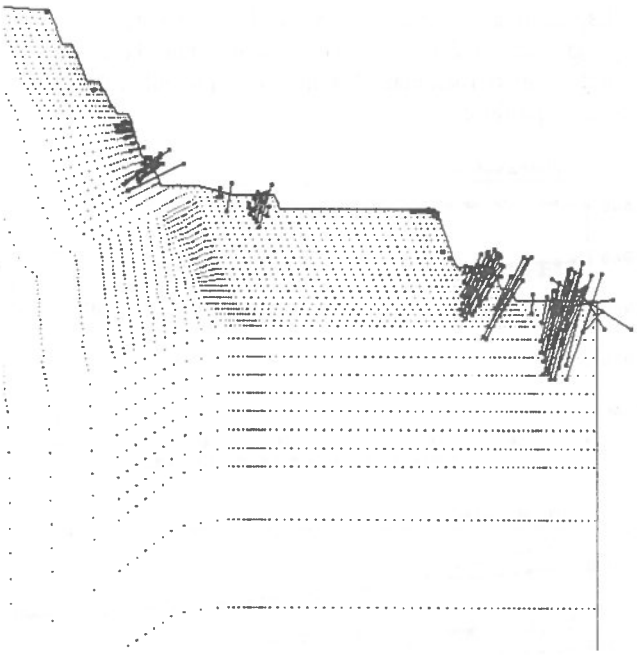

Figure 6: Tensile Stress Trajectories after Pit Expansion

Displacement vectors for K=1.6 are illustrated in Figure 7. Comparison of the current and final pit profiles is presented in Figures 8 and 9. The following comments are drawn:

- the final pit profiles for both K values are slightly larger than for the current pit profile,
- the increase in uplifting (vertical displacement)

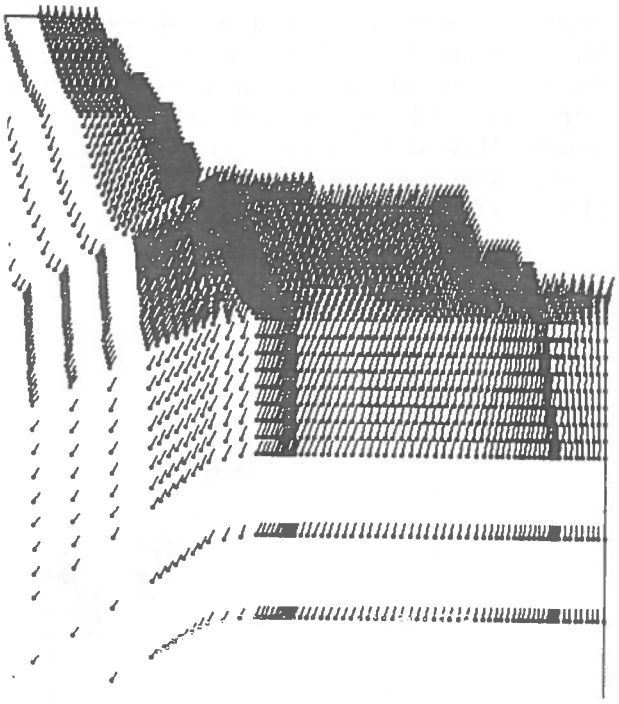

Figure 7: Displacement Vectors after Pit Expansion (k=1.6)

due to the removal of the mining cut results in an incremental displacement of very small magnitude,

- the horizontal displacements for both cases of K show strong correlation to the current pit profile displacements,
- level 1400 toe has the relative largest horizontal displacements,
- the horizontal displacements for the final pit profiles are marginally lower than in the current profile with the exception of higher levels of K=1.6,
- there is a slight shift of the zero displacement locus away from the slope face as the cut is mined out suggesting further stabilization of the slope.
- there is a slight shift of the zero displacement locus away from the slope face as the cut is mined out suggesting further stabilization of the slope.

Failure analysis was carried out using Mohr-Coulomb failure criterion. The case of K=1.13 is considerabely safer than for K=1.6. The latter, however, indicates a minimum safety level of 2 near the slope face (Figure 8).

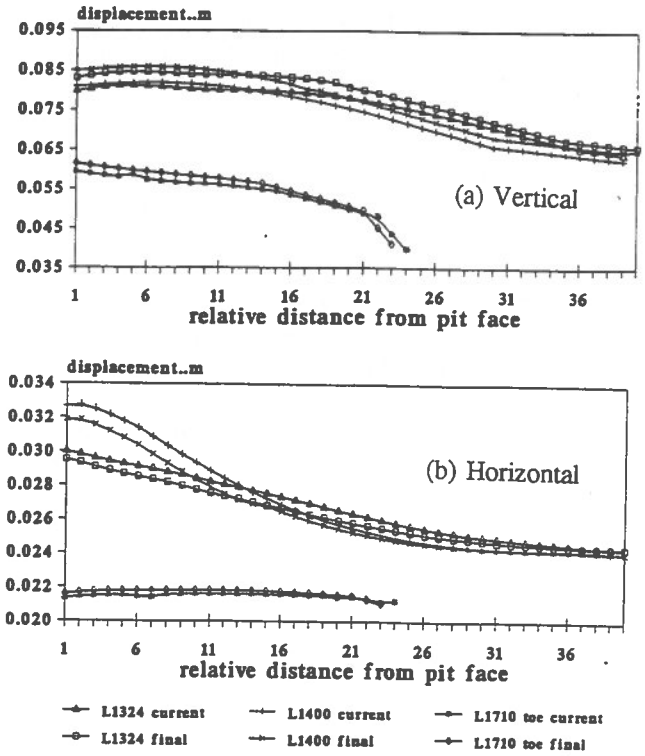

Figure 9: Comparison of Displacements BetweenCurrent and Final Pits (K=1.6)

CONCLUSIONS

The finite element method was used to analyze the eastern wall of Copper Mountain mine in the area of proposed expansion. The results indicate that there is little potential of "en-masse" failure even at extreme value of horizontal - to-vertical in situ stress of 1.6.

The proposed expansion slice geometry has virtually no effect on the overall pit slope which stays at 32°. The existence of a wide 1600 level berm similar to the current one at 1710-1680 levels enhances stability. For levels at and above the 1710 toe, no significant changes in stability are induced by the mining of the proposed slice. This is evident from the results of the displacement analysis which indicatea far field locus of zero displacement and the Mohr-Coulomb safety factor analysis indicating safety factors well above 2 near the slope face.

ACKNOWLEDGEMENT

The authors are grateful to the mining staff of Mines Gaspé Division of Noranda Mining and Exploration Inc. for their cooperation and for providing the data needed for the case study. The authors wish to thank Mr. C. Tsomondo for his work on the computer runs.

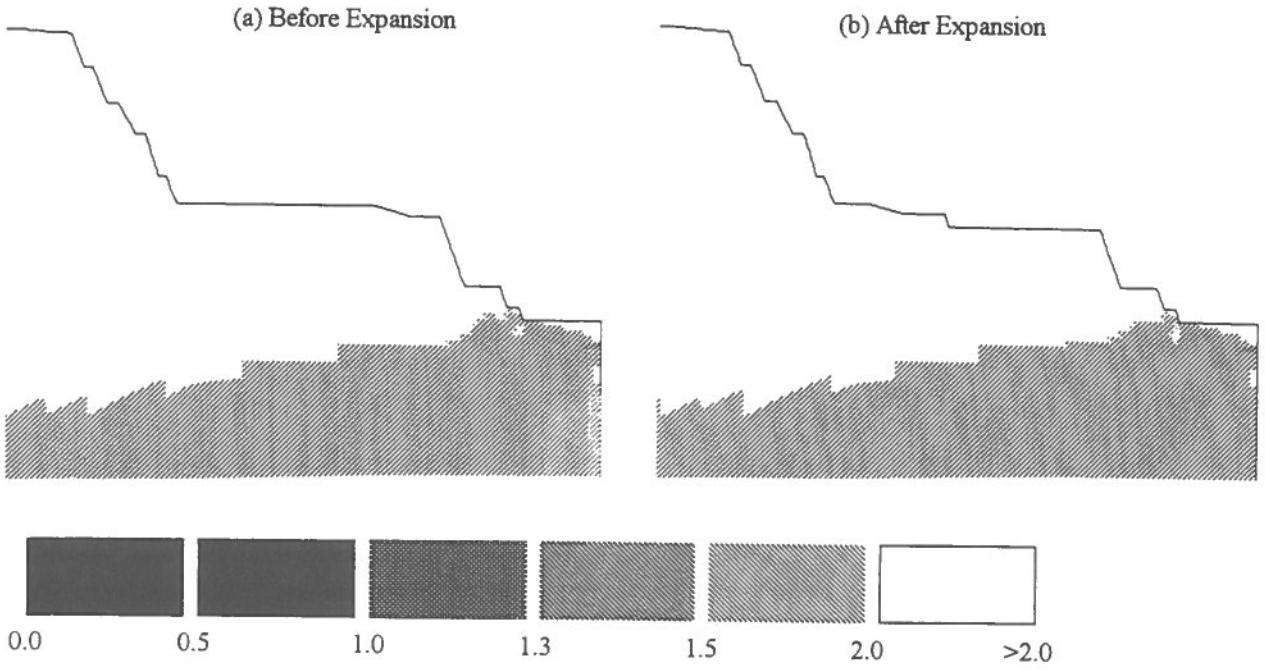

Figure 10: Safety Levels in the Pit SlopeAfter Expansion

REFERENCES

Charette, F., 1994,
Propriétés Mécaniques des Roches à Mines Gaspé. Laboratoire de Recherche Minière, CANMET.

Kanduth, H., Germain, P. and Jacob, D., 1993,
In Situ Determination at Mines Gaspé E-19 Ore Zone Using the Borehole Slotter, Noranda Technology Centre, 31 PP.

Mitri, H. S., 1993,
Finite Element Simulation of cable-bolted mine stopes. Workshop notes, McGill University, Montreal, March 28, 1993.

Mitri, H. S., Edrissi and Henning, J., 1994,
Finite Element Modelling of Cable-Bolted Stoped in Hard Rock Underground Mines. Annual Meeting of SME, February 14-17, Albuquerque, NM, Paper No. 94-116.

Mohammad, M.M., 1995
Effect of Goundwater on the Stability of Mine Excavations. M. Eng. Thesis, McGill University, (in progress).

Geocon, SNC-Shawinigan, 1994
Caractérisation Environnementale du Site de Mines Gaspé, Murdochville, Québec. Unité 7 - Méthodes d'exploitation, Rapport final, Volume 1 de 2. Minéraux Noranda Inc., Division Mines Gaspé, Aout 1994, No dossier M-5951 (006501).

CAMI'95:3rd Canadian Conference on Computer Applications in the Mineral Industry
Montréal, Québec, Canada, October 22-25, 1995

Stability Analysis of an Open Pit Wall Using a Limit Equilibrium Method

Luc Turgeon
Formerly at École Polytechnique, Montréal, Québec, Canada,
now with Inco Limited, Sudbury, Ontario, Canada

Michel Aubertin
École Polytechnique, Montréal, Québec, Canada

Yves Beauchamp
LAB Chrysotile, Inc., Thetford Mines, Québec, Canada

ABSTRACT:

The Black Lake operation of LAB Chrysotile Inc. is mining an important chrysotile-asbestos deposit by open pit. In a few years, the mine will reach a depth of about 450 meters. To investigate the potential effect of extending the mine, stability analyses have been performed. This paper presents part of this investigation. The basic geological and geomechanical information is first introduced. Stability analyses results are then presented; calculations were done with a limit equilibrium method for circular slip surfaces within the rock mass. The stability analyses were carried out for a variety of conditions, using a parametric approach. Influence factors such as strength parameters, contact plane orientation, water level, tension cracks and external loads have been considered.

RÉSUMÉ:

L'opération Black Lake de la Société minière LAB Chrysotile Inc. exploite présentement un important gisement d'amiante-chrysotile par mine à ciel ouvert. À la fin des opérations, la profondeur de la mine atteindra près de 450 mètres. Diverses analyses de stabilité de la portion nord du mur Est ont été réalisées dans le but d'évaluer les risques de rupture du massif rocheux. Le présent article décrit une partie de cette étude. Un bref résumé des données géologiques et géomécaniques utilisées dans cette étude est tout d'abord présenté. Puis on décrit ensuite les analyses de stabilité effectuées dans le but d'évaluer les possibilités de rupture profonde du massif rocheux en utilisant une méthode d'équilibre limite. Les analyses de stabilité ont été complétées en tenant compte de différentes variantes pour la résistance du massif, l'orientation des plans de contact, le niveau de la nappe phréatique, la présence de fissures de traction et les chargements externes.

INTRODUCTION

The Black Lake mining operation is located near the town of Thetford Mines, approximately 200 kilometres south-east of Montréal, Québec, Canada. The company LAB Chrysotile Inc. is mining an important chrysotile-asbestos deposit by open pit, at a rate of about 50 000 metric tons per day. The actual pit covers an area of about 1.6 by 1.2 square km, and extends to a depth of about 335 m. The eastern pit limit parallels the provincial highway and other infrastructures such as railway, water and electrical lines.

An open pit enlargement, known as the East wall extension, is currently being excavated. It will allow the mining of an extra 30 millions tons of rich asbestos ore. At the end of this extension, the mine will reach a depth of 445 m, with an average pit slope angle of 42°.

Several slope stability studies have been carried out, in the past, over the central part of this wall. Recently,

evidence of cracking and slope failure toward the north initiated an investigation of the wall stability in this area. Even if part of the wall consists of massive peridotite rock, the lower portion is believed to be composed of a weaker altered peridotite rock, commonly described as "semi-schistose" serpentinite. The economical and security aspects of the mining operations rely on the assured stability of this wall as mining progress with depth.

This paper deals with the stability analyses of the northern part of the wall. Although analyses on potential structural failures along existing discontinuities have been conducted, only rotational slip failure analyses are presented here. These analyses have been performed following an extensive site investigation and rock mass characterization. Numerical calculations, using a limit equilibrium method, have been performed to investigate various conditions by a parametric study. The main results are presented and briefly discussed.

GENERAL DESCRIPTION

The East wall of the B pit is predominantly composed of peridotite, showing varying degrees of alteration, in association with the asbestos mineralization. In its unaltered form, the peridotite is massive, but around and within the ore zones, the peridotite has been serpentinized, with the development of a "semi-schistose", or, in extreme cases, "schistose" texture, with the fractures filled by fibrous minerals. The contacts of these altered zones are frequently heavily sheared.

The geological interpretation indicates that the zones of alteration dip steeply to the east, and are bounded to the west by a talc-carbonate shear zone. This latter rock formation extends to the toe of the ultimate wall in the south, but appears to die out northwards. Similarly, the "semi-schistose" serpentinite seems to plunge northwards and dies out close to the massive granitic dyke forming the north limit of the orebody. Narrow granite veins also occur through the wall. These are typically up to 3 m thick and strike northeast-southwest, i.e., into the wall, paralleling the regional structure. This suggests that the lower section of the ultimate north end wall will be in "semi-schistose" to "schistose" serpentinite rock while the upper section will be in massive peridotite rock.

The original design of the wall was based on an overall angle of 45° for the initial cut, followed by a 180 m wide pushback, which would give a multiple angle slope, gradually flattening with depth, for an overall slope angle of 40°, over a maximum vertical height of 445 m. This design configuration involves the excavation of 12 m high operating lifts with a minimum 8 m width, using conventional truck shovel mining operations. All rock is blasted prior to excavation.

Several revisions of this design were done since, based upon additional exploration and geotechnical studies conducted over the years, together with experience gained in the mining of the upper benches of the ultimate expansion of the wall.

The proposed slope configuration essentially reflects the two basic material types that are anticipated in the wall. In the "semi-schistose" to "schistose" serpentinite, a 41° inter-ramp has been used. In the more massive, unaltered peridotite in the upper part of the wall to the north, the design inter-ramp angle is approximately 46°. The lower section of the wall is designed at an inter-ramp angle of 40° to meet previously indicated stability requirements.

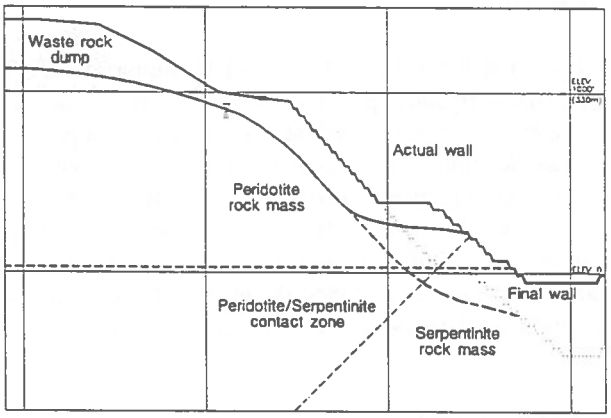

Figure 1. Schematical configuration of the East wall.

The first major instability on the East wall occurred in 1969 and involved the slumping failure of a nose at the south end of the initial cut. In order to expand the mining limits and avoid the cracks, the highway, located at the crest of the wall, was relocated to the east in 1976.

During stripping operations in the crest area, more extensive cracking was noted along virtually the entire length of the wall. Monitoring of these cracks indicated only minor movement, and consequently, mining operations proceeded back to the ultimate limits at the crest of the wall.

In the early 80's, the mining plan was revised to allow the wall to be excavated as two expansions. The mining schedule called for the intermediate cut to be mined at an accelerated rate, thereby releasing additional ore, while stripping to ultimate limits proceeded at a slower pace. In 1985, further cracking were noted on the 750 bench of the ultimate expansion with minor failure on the face.

In the early 90's, further cracking were noted on the 550 bench of the ultimate expansion. These cracks were extending northwards and a several benchscale failure occurred at the intermediate cut at the north end of the wall. Investigation showed that cracking and failure occurred at the contact between the massive peridotite and the "semi-schistose" serpentinite which extends further north than anticipated.

All failures observed since 1969 occurred during spring or fall, following heavy rainfall or snowmelt. A drainage program, involving horizontal drain holes, was implemented to relieve the excess water pressure behind the ultimate wall.

SITE INVESTIGATION AND ROCK MASS CHARACTERIZATION

Prior to performing the stability analyses of the open pit wall, a consistent site investigation campaign was done followed by a rock mass characterization. These included the following steps: review of existing geological data, structural wall mapping, geological and geotechnical core logging on diamond drill testholes and evaluation of groundwater levels.

As stated above, the north portion of the East wall is made of two different rock types: massive peridotite (weekly serpentinized) from the final crest (elevation 305 m) to bench 30 (elevation 10 m), and semi-schistose or schistose serpentinite (totally altered peridotite) from bench 30 to the ultimate pit depth (elevation -137 m). The contact between these two rock types is clear in the upper part of the final wall down to bench 390 (elevation 118 m) and has been located further north on bench 150 (elevation 45 m) by diamond drilling. However, its dip hasn't been precisely determined. For stability analysis purposes, it is considered safer to use a dip variation from horizontal to 45° E, and to retain the worst case for design (at this time).

In 1992 and 1993, a structural wall mapping campaign took place in order to identify the various structures present in the rock mass, for a structural failure analyses using the sliding block method (not presented in this article). Overall, 1 064 structural planes have been recorded on the final wall, between elevations 170 m and 130 m, on a 600 m distance, north and south of the peridotite/serpentinite contact. A pole concentration analysis was completed, and 7 major structural planes were identified (see Table 1).

Table 1. Major structural planes (strike/dip).

North portion	South portion
338°/58°	213°/80°
191°/31°	204°/63°
131°/87°	223°/71°
175°/87°	

Also, piezometer monitoring was conducted to locate approximately groundwater levels. In this study, it is assumed that the lower portion of the pit (schistose serpentinite) is moderately permeable; water has been detected on the actual faces between benches 150 and -50.

In order to characterize the rock mass, detailed geological and geotechnical core logging has been done on four non-oriented, horizontal drain holes drilled in the final wall. The core logging included determination of rock type, alteration level, joint spacing, fracture frequency, RQD, intact rock strength, condition of joints and presence of water.

The Mining Rock Mass Rating (MRMR) system, proposed by Laubsher (1977), was used for the rock mass classification. This system is versatile and gives the joint condition a large influence on the overall rating; it is a major factor for an asbestos pit wall stability. The MRMR values obtained are generally lower compared to the usual RMR system (e.g., Bieniawski, 1988). Therefore, the use of the MRMR classification instead of the RMR to characterize the rock mass can be considered as a conservative

approach.

The statistical analysis performed on the available data lead to the following results: a MRMR value of 38 (average to poor) and a standard deviation of 11 for the schistose serpentinite rock mass located south of the contact; a value of 58 (good to average) and a standard deviation of 12 for the massive peridotite rock mass located north of the contact. These values are used to calculate the rock properties constants (m) and the degree of fracturing constants (s) of the Hoek and Brown (1980) rock mass failure criterion.

MECHANICAL PROPERTIES

The mechanical properties of the rock mass can be obtained from the combination of intact rock properties and joint conditions. An estimate of the rock mass strength can also be obtained from the well-known Hoek and Brown (1980) failure criterion. This failure criterion is defined by the following equation:

$$\sigma_1' = \sigma_3' + \left[m C_o \sigma_3' + s C_o^2 \right]^{1/2} \qquad (1)$$

where σ'_1 and σ'_3 represent the major and minor principal stresses respectively; C_o is the uniaxial compressive strength of the intact rock; m and s are material constants. The uniaxial compressive strength was determined by laboratory testing. Various tests on representative core samples have given the following mean values for C_o: 143 MPa for the peridotite; 103 MPa for the serpentinite.

Because of a lack of more specific laboratory tests results, the intact rock property constant (m_i), included in the Hoek and Brown (1980) criterion, have been obtained from the values given by CANMET on somewhat similar rock types (Bétournay et al., 1991). The values provided by CANMET are lower than those proposed initially by Hoek and Brown (1980); therefore they are considered conservative and more useful for our purposes. The m_i values used are 13.5 for the peridotite and 7.3 for the serpentinite.

The value for the m and s parameters, corresponding to the rock mass properties, have been obtained from the empirical relationship proposed by Hoek (1990) (using the MRMR instead of RMR). Material constant calculations were made for the mean RMR values, and for the mean RMR values minus one standard deviation to encompass a wide proportion of the data scattering. The values obtained are presented in Table 2.

Table 2. Material parameters for the Hoek and Brown (1980) failure criterion, calculated from the Hoek (1990) relationships.

	Undisturbed rock mass		Disturbed rock mass	
	m	s	m	s
Peridotite RMR mean	3.01	0.0094	0.67	0.0009
Peridotite RMR mean - 1 std.dev.	1.96	0.0025	0.29	0.0001
Serpentinite RMR mean	0.83	0.0011	0.09	0.00004
Serpentinite RMR mean - 1 std. dev.	0.56	0.0003	0.04	0.000006

STABILITY ANALYSIS

Stability analysis constitute an integral part of the safe and functional design of rock slopes. The physical stability of a slope depends on a number of factors, including its geometry, rock mass properties and groundwater conditions.

Instabilities of a rock slope can occur as of result of various types of mechanisms, such as rock fall, toppling, buckling, and translational or rotational sliding (Hoek and Bray, 1981; Ritchard, 1987; Giani, 1992). For each type of mechanism exists one (or more) method(s) of analysis to evaluate possible failure problems.

The analyses presented in the following only deal with rotational sliding, assuming circular failure; other mechanisms have also been considered in the original study (Turgeon, 1994), but are not presented here.

Rotational sliding can occur in slopes of closely jointed,

altered or weathered rock mass. In such instances, it is appropriate to design the slope on the assumption that failure would involve a circular shape (Hoek and Bray, 1981). Such problems can be analyzed by limit equilibrium methods. Limit equilibrium analysis is useful to define the conditions at which failure occur, usually yielding a conservative evaluation. With such methods, it is considered that, at equilibrium, the forces acting to cause failure are in balance with the forces that resist failure.

Limit equilibrium analysis is the basis for many methods used for slope stability evaluations. It is commonly used for soils and other particulate media such as mine wastes and tailings (e.g., Bowles, 1984; Caldwell and Moss, 1985; Bowders and Lee, 1990; Seed and Boulanger, 1992). It is also useful to evaluate slope stability in relatively weak rock masses. The main elements of the theory has been presented and discussed by Wright (1985), Chowdury (1987) and McCarthy (1988).

Such methods consider that the failure criterion (Mohr-Coulomb, Hoek-Brown, etc.) is satisfied along an assumed failure surface. A free body is taken from the slope, and the known or assumed forces acting on the body to cause failure (overburden weight, seepage forces, imposed loads, etc.) and the shearing resistance available or required for stability are calculated. Because most practical problems are statically indeterminate, assumptions have to be made regarding the force systems and the directions of application in order to render the problem determinate.

The final result of the application of such methods is the obtention of the factor of safety (FS) usually defined as the ratio of the shearing resistance available along the failure plane to the shearing resistance necessary for equilibrium. The value of FS can be calculated directly or obtained from charts (e.g., Hoek and Bray, 1981; Charles and Soares, 1984; Hoek, 1987; Greco and Gullà, 1988). It can also be computed from numerical calculations. As the calculations have to be made for failure surfaces at several locations and with various centres of rotation, the methods are usually applied with computer codes.

In this study, the calculations were made with GSLOPE, a simple program developed for MS-DOS based microcomputers (Graham, 1988; MITRE, 1991). Among the options available, the authors have selected the Bishop's modified method (Bishop, 1955). This method is one of the most widely used and accepted procedure, as it offers a good compromise between too simplistic approaches and the more sophisticated methods. It relies on the well-known method of slices with an arc circle slip surface, and considers that the total influence of tangential forces acting on the sides of slices is small enough to be neglected.

As is the case with the majority of slope stability software packages, GSLOPE uses the Mohr-Coulomb failure criterion, as defined by the following equation:

$$\tau = c' + \sigma' \tan \phi' \qquad (2)$$

where τ is the shear strength, σ' is the effective normal stress; c' represents the cohesive strength and ϕ' the internal friction angle. Contrary to the Hoek-Brown criterion, this failure criterion is linear in the shear stress vs normal stress plane, which makes it somewhat easier to use.

The representative parameters (c', ϕ') for the Mohr-Coulomb criterion were obtained from the above mentioned Hoek-Brown criterion using the constant values calculated earlier. Conservative values of c' and ϕ' were obtained from the secant to the failure envelope defined by the Hoek-Brown criterion. The curve envelopes in the τ - σ' plane were obtained from the equations given by Hoek (1990). The two resulting criteria are shown on Figure 2.

The secant lines representing the Mohr-Coulomb criterion (no tension crack) is obtained by considering the approximate maximum value of the normal stress σ' in the event of a major (deep) failure, and the minimum value defined by a normal stress equal to 0. The c' and ϕ' parameters thus obtained give a conservative failure criterion when compared to the Hoek-Brown envelope; the parameter values are presented in Table 3.

Observations on site indicate that some cracks may appear at the crest of the wall. This can be taken into account by introducing a tension crack in the failure surface. The authors have considered that such crack may extend up to a depth H(t), and that the affected zone possesses no cohesion (c' = 0) and an internal friction angle of 30°. The tension crack depth H(t) is calculated, with Rankine's lateral pressure theory

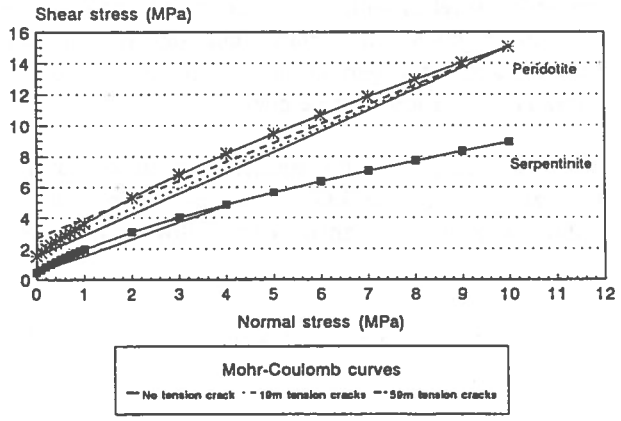

a) RMR - mean values

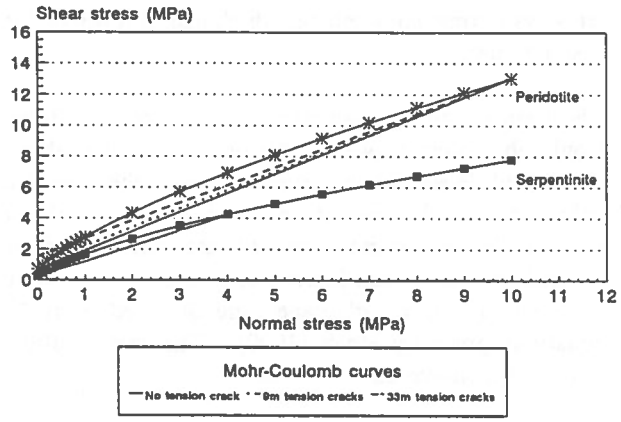

b) RMR - mean values-1 standard deviation

Figure 2. Rock mass failure envelopes using the Hoek-Brown and Mohr-Coulomb criteria.

(Bowles, 1984), using the following equation:

$$H(t) = \frac{2\,c'}{\gamma\sqrt{K_a}} \qquad (3)$$

where K_a represents the active earth pressure coefficient and γ is the unit weight of the overburden material. A minimum and maximum tension crack depth have been considered in the stability analyses. The minimum value, $H(t)_{min}$, is obtained using the estimated cohesion strength c' from Table 3. The maximum value, $H(t)_{max}$, is obtained by doing successive iterations until c' converges to the shear strength given by the Hoek-Brown criterion just below the tension crack.

When tension cracks are introduced, the c' and ϕ' parameters have to be corrected because of the changing normal stress at the upper boundary of the circular failure surface. The corrected values are presented in Table 4.

Table 3. Mohr-Coulomb parameters for the rock masses

	c' (MPa)	ϕ' (°)
Peridotite RMR mean	1.52	53.5
Peridotite RMR mean - 1 std. dev.	0.69	51.0
Serpentinite RMR mean	0.43	47.4
Serpentinite RMR mean - 1 std. dev.	0.21	45.1

Table 4. Corrected values of the Mohr-Coulomb parameters for the peridotite rock mass.

	c' (MPa)	ϕ' (°)
$H(t)_{min}$ = 19 m RMR mean	2.01	52.5
$H(t)_{max}$ = 59 m RMR mean	2.70	51.0
$H(t)_{min}$ = 9 m RMR mean - 1 stan.dev.	1.00	50.3
$H(t)_{max}$ = 33 m RMR mean - 1 stan. dev.	1.54	49.0

ANALYSES RESULTS

The slope stability analyses for the East wall have been performed in a parametric manner for the following conditions:

- rock mass properties variation (RMR mean and RMR mean - 1 standard deviation);
- dip variation of the peridotite/serpentinite contact (0° and 45°);
- effect of tension cracks of various lengths;
- effect of hydraulic pressures (obtained from in situ measurements).

Prior to performing the stability analyses for the final configuration of the wall, back analyses using the actual situation were done to validate the estimated rock mass properties and calculation approach (see case 1 on Figure 3). A total of twelve analyses were performed. The minimum factor of safety obtained for the actual wall was 1.45 using the most conservative design parameters (RMR mean - 1 standard deviation, contact dip at 0°, high hydraulic pressure and deep tension cracks). The results are listed in Table 5.

It is important to note that a lowering in the peridotite/serpentinite contact dip angle and the presence of tension cracks lower the factor of safety. In addition, hydraulic pressures can reduce the factor of safety by as much as 25% depending on the other factors.

The next step consisted in performing stability analyses of the final wall design, using the above mentioned rock mass properties. The main results are presented in Table 6. After considering the different conditions, the minimum factor of safety calculated was 1.23, using the most conservative parameters. It is less than the usually recommended value of 1.50. This low value however, takes into consideration only a minimum drainage at the top portion of the mine. If the water table could be lowered, it would reduce the hydraulic pressures in the wall and increase the factor of safety; a value of 1.56 was obtained for well drained conditions. The use of a pumping well from the final ramp (bench 30) could also increase the factor of safety.

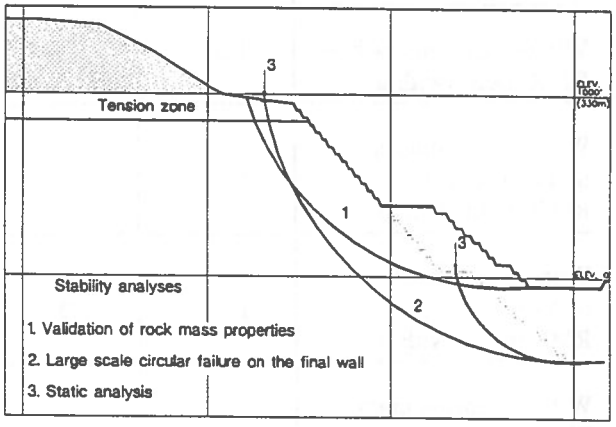

Figure 3. Schematical representation of the rotational slip surfaces.

Table 5. Factor of safety for the actual wall (considering the hydraulic pressures).

	Contact dip 0°	Contact dip 45°
Without tension crack RMR mean	1.63	1.76
With tension cracks of 19 m (min.) RMR mean	1.61	1.72
With tension cracks of 59 m (max.) RMR mean	1.54	1.62
Without tension crack RMR mean	1.50	1.61
With tension cracks of 9 m (min.) RMR mean - 1 stand.dev.	1.48	1.58
With tension cracks of 33 m (max.) RMR mean - 1 stand. dev.	1.45	1.52

Table 6. Factor of safety for the final wall.

	Contact dip 0°	Contact dip 45°
Without tension crack RMR mean, with u	1.37	1.44
With tension cracks of 19 m (min.) RMR mean, with u	1.35	1.42
With tension cracks of 59 m (max.) RMR mean, with u	1.32	1.37
Without tension crack RMR mean, without u	1.78	1.84
With tension cracks of 19 m (min.) RMR mean, without u	1.78	1.81
With tension cracks of 59 m (max.) RMR mean, without u	1.67	1.70
Without tension crack RMR mean - 1 stand. dev., with u	1.26	1.32
With tension cracks of 9 m (min.) RMR mean-1 stand. dev., with u	1.25	1.31
With tension cracks of 33m (max) RMR mean-1 stand.dev., with u	1.23	1.27
Without tension crack RMR mean - 1 stand. dev., without u	1.64	1.69
With tension cracks of 9m (min) RMR mean-1 stand.dev.without u	1.63	1.67
With tension cracks of 33m (max) RMR mean-1 stand.dev.-without u	1.56	1.57

Static analyses using external loads have also been performed in order to test the behavior of the rock mass during mining operations. A 85-ton capacity truck, fully loaded, is located on the final ramp and a transport truck, also loaded, is placed on the provincial road, near the final crest. Analyses show that for such event, two conditions become critical. A small size failure from the crest to the pit bottom can occur (FS = 1.04) and a major size failure from the ramp to the bottom can also happen (FS = 1.23). These are shown on Figure 3. These risks of failure could be greatly reduced if proper drainage measures could insure low groundwater pressures behind the wall.

The above results provide some interesting guidelines for the final design of the East wall. Some notes of caution on the significance of these results are nevertheless in order.

Although very useful for engineering purposes, limit equilibrium methods do not permit an assessment of the stress distribution in the ground nor of the deformations that occur. It also assumes that the shear strength is mobilized simultaneously at every point along the failure surface, thus neglecting the fact that failure is often a progressive phenomena.

To overcome the limitations of such assumptions, stability analyses of the wall could also be performed using other methods (e.g., Hoek and Bray, 1981; Brown, 1987; Giani, 1992; Duncan, 1992; Eberhardt and Stead, 1993; Tsomondo and Mitri, 1993).

Also, the results obtained in this paper are only valid if the material properties used in the model reflect the in-situ conditions. Additional site investigation would help to validate the adopted assumptions.

CONCLUSIONS

The main objective of this project was to perform slope stability analyses on the north portion of the East wall extension at LAB Chrysotile's Black Lake mining operation. To reach this goal, extensive work on site investigation, rock mass characterization and determination of rock properties has been completed. The ensuing parameters were then used to investigate the possible rock mass failure using the limit equilibrium method.

The analyses results show that the stability of the East wall will, to a large extent, depend on the groundwater

conditions. In fact, it has been showed that reducing the hydraulic pressure acting on the final wall would substantially increase the factor of safety.

REFERENCES

Bétournay, M.C., Gorski, B., Labrie, D., Jackson, R., Gyenge, M., 1991
New considerations in the determination of Hoek and Brown material constants. Proc. 7th Int. Cong. Rock Mechanics, Balkema, Vol. 1, pp. 195-200.

Bieniawski, Z.T., 1988
The rock mass rating (RMR) system (Geomechanics Classification) in engineering practice. Rock Classification Systems for Engineering Purposes. L. Kirkaldie (ed.), ASTM, STP 984, pp. 17-31.

Bishop, A.W., 1955
The use of the slip circle in the stability analysis of slopes. Geotechnique, Vol. 5, pp. 7-17.

Bowders, J.J., Lee, S.C., 1990
Guide for selecting an appropriate method to analyze the stability of slopes on reclaimed surface mines. Proc. Mining and Reclamation Conference and Exhibition, Charleston, West Virginia, Skousen et al. (eds.), pp. 103-110.

Bowles, J.E., 1984
Physical and Geotechnical Properties of Soils. Second edition, McGraw-Hill Inc., New York.

Brown E.T. (ed.), 1987
Analytical and Computational Methods in Engineering Rock Mechanics, Allen & Unwin.

Caldwell, J.A., Moss, A.S.E., 1985
Simplified stability analysis. Design of Non-Impounding Mine Waste Dumps. AIME, pp. 49-61.

Charles, J.A., Soares, M.M., 1984
The stability of slopes in soils with non-linear failure envelopes. Can. Geotech. J., Vol. 21, pp. 397-406.

Chowdury, R.N., 1987
Stability of soil slopes. Ground Engineer's Reference Book, F.G. Bell (ed.), Butterworths, pp. 11/1-11/16.

Duncan, J.M., 1992
State-of-the-Art: Static stability and deformation analysis. Stability and Performance of Slopes and Embankments II, Seed & Boulanger (eds.). ASCE, GSP no. 31, pp. 222-265.

Eberhardt, E., Stead, D., 1993
Numerical modelling of buckling and ploughing slope instability in surface coal mining. Proc. First Canadian Symposium on Numerical Modelling Applications in Mining and Geomechanics, Mitri, H.S. (ed.), McGill University, pp. 176-186.

Giani, G.P.,1992
Rock Slope Stability Analysis, Balkema.

Graham, J.P., 1988
A new slope stability analysis program for microcomputers. Proc. Third International Conference on Computing in Civil Engineering, Vancouver, Canada, CSCE-ASCE-CCES, Vol. 2, pp. 563-570.

Greco, V.R., Gullà, G., 1988
Slope stability charts for slip surfaces of general slope. Landslides '88, Balkema, pp. 637-642.

Hoek, E., 1987
General two-dimensional slope stability analysis. In: Analytical and Computational Methods in Engineering Rock Mechanics, E.T. Brown (ed.), Allan & Unwin, pp. 95-128.

Hoek, E., 1990
Estimating Mohr-Coulomb friction and cohesion values from the Hoek-Brown failure criterion. Int. J. Rock Mech. Min. Sci. & Geomech. Abstr., vol. 27, no. 3, pp. 227-229.

Hoek, E., Bray, J., 1981
Rock Slope Engineering. Third edition, Institution of Mining and Metallurgy, London.

Hoek, E., Brown, E.T., 1980
Empirical strength criterion for rock masses. J.Geotech. Engng. Div., ASCE, Vol. 106, pp. 1013-1035.

Laubsher, D.H., 1977
Geomechanics classification of jointed rock masses - mining applications. Trans. Inst. of Mining & Metallurgy, section A, pp. A1-A7.

McCarthy, D.F., 1988
Essentials of Soil Mechanics and Foundations. Third edition, Prentice-Hall.

MITRE Software Corporation, 1990
GSLOPE, Limit Equilibrium Slope Stability Analysis. User's Manual for Versions 3.2 and Later, 46 pages.

Ritchard, L.R., 1987
Stability of slopes in rocks. Ground Engineer's Reference Book, F.G. Bell (ed.), Butterworths,pp. 12/1-12/16.

Seed, R.P. and Boulanger, R.W. (eds.), 1992
Stability and Performance of Slopes and Embankments - II. Proc. Specialty Conf., Berkeley, California, ASCE Geotechnical Special Publication, no. 31.

Tsomondo, C.M., Mitri, H.S., 1993
Interpretation of non-structural slope failure in open-pit mining - A numerical modelling approach. Proc. First Canadian Symposium on Numerical Modelling applications in Mining and Geomechanics, Mitri, H.S. (ed.), McGill University, pp. 186-197.

Turgeon, L., 1994
Analyse de stabilité du mur final de l'extension Est - Opérations Black Lake de LAB Chrysotile Inc.. Rapport de projet de fin d'étude, Département de génie minéral, École Polytechnique de Montréal.

Wright, S.G., 1985
Limit equilibrium slope analysis. Design of Non-Impounding Mine Waste Dumps, AIME, pp. 65-77.

CAMI'95:3rd Canadian Conference on Computer Applications in the Mineral Industry
Montréal, Québec, Canada, October 22-25, 1995

Finite Element Modeling Study of a Cable Bolt Support System Installed in a Longwall Coal Mine in Western Colorado

Valois R. Shea-Albin, Dennis R. Dolinar, and Stephen C. Tadolini
U. S. Bureau of Mines, Denver Research Center

ABSTRACT:

The U.S Bureau of Mines conducted a research project to evaluate the use of cable bolts installed within a test area located in the gate road entry of a longwall coal mine in Western Colorado. To complement the design work and field evaluation, numerical modeling analyses of cable bolt behavior were performed. The mine lies within a dipping coal seam subjected to horizontal stress that exceeds overburden stress by a factor of 1.7. The cable test site was evaluated using a two-dimensional finite-element method with bolt modeling capabilities. This paper discusses a parametric study performed as part of the numerical modeling evaluation. A series of models were constructed to simulate conditions at three stages of mining: 1) after development of gate road entries, 2) after first panel mining, and 3) as the face of the second panel approaches. Bolt data was examined for each of these three mining stages to determine the effects of cribs within the test entry, the effect of dipping strata, and the effect of horizontal stress.

RÉSUMÉ

Le U.S. Bureau of Mines a lancé un projet de recherche pour évaluer l'utilisation des câbles d'ancrage installés dans un endroit d'essai qui est situé dans l'entrée d'une galérie d'une mine de charbon longtaille dans Colorado Ouest. Afin de compléter l'évaluation du chantier, une modélisation numérique des câbles d'ancrage a été effectuée. La mine est située dans une formation de charbon inclinée ou la contrainte naturelle horizontal par rapport à la contrainte naturelle verticale est de 1.7. L'endroit d'essai a été évalué en utilisant une méthode, 2-dimensionnelle, des éléments finis qui permet la modélisation câbles d'ancrage. Cette publication présente une étude de paramètres qui fait partie de l'évaluation de la modélisation numérique. Une série de modèles a été construite pour simuler les trois conditions minières suivantes: 1) après le développement des entrées d'une galerie, 2) après avoir miné le premier panneau, et 3) ont été examinées pour chaque condition ci-haut mentionèe, afin de déterminer l'effet du boisage dans l'endroit d'essai, l'influence du pendage du charbon et l'effet de la contrainte horizontale.

INTRODUCTION

Cable Bolts in U.S. Longwall Coal Mines

The U.S. Bureau of Mines is conducting a research project to investigate the use of cable bolts as an alternative to the traditional roof support strategies currently used in underground coal mines in the U.S. To evaluate the reinforcement capabilities of cable bolts, a test area was established in the tailgate entry of an underground longwall coal mine in Western Colorado. Cable bolts, although commonly used for ground support in hard-rock mines, are a relatively new type of support system for underground coal mines in the U.S.

The strategy of this project is to evaluate the effectiveness of cable bolts in supporting gate road entries of underground longwall coal mines in the western U.S. It is important to maintain stable ground within gate road entries because they serve as transportation routes to the working face for miners and equipment, access and escapeways for emergency situations, coal transportation routes, and both intake and return ventilation ways for the working face. Headgate entries, as they are called before both adjacent longwall panels are mined, can usually be supported adequately with conventional roof bolts. During the mining of the first adjacent panel, secondary support may be needed in advance of the longwall face, usually within a zone of 150 m, as abutment stresses from panel mining begin to influence ground stability within that zone. Typically, secondary support is supplied by wooden posts, hydraulic jacks, or additional roof bolts installed in strategic locations to control the effects of front and side abutment pressures induced by mining.

Tailgates entries, as they are called when the second adjacent longwall panel is mined, are used as return air and occasionally intake air passages, and travelways. Because of extraction of the second panel, tailgate entries are subjected to much higher ground pressures, increasing the difficulty in maintaining open passages in these entries. In tailgate entries, it is not as crucial to maintain completely clear entry ways, therefore, more obtrusive types of support such as cribs can be used for secondary support. Cribs, however, fill a large portion of space within the entry passage adding resistance to airflow, and crib construction contributes to the injury and accident count. Cable bolts can provide a safer, less obtrusive alternative method of secondary support in tailgate entries (McDONNELL, TADOLINI, and DiGRADO, 1994).

Description of Cable Bolts

Originally the basic cable bolt support consisted of high-strength steel cable installed and grouted with cement in a 4.1- to 6.4-cm borehole. Recent advancements in resin and cable technology permit the use of resin as an anchorage material in a 2.5- to 3.5-cm-diameter hole. The cables used for this test site are 1.5 cm in diameter with a modulus of elasticity of about 205 GPa and an ultimate strength of 245 to 265 kN.

A desirable trait of cable bolts is that, compared to conventional bolts, they tolerate a large amount of deformation, maintain a high magnitude of load, and provide a greater ultimate strength. Cables are flexible and can be coiled to about 1.2 m diameter for handling. This flexibility is another great advantage of cable supports, because a longer bolt can be handled within the restricted entry space.

For a cable support to be effective, it is necessary for the loads to be successfully transferred from the rock to the cable through the grouting material. For this study 2.1 m of resin grout is used to anchor the 4.3-m cable bolt to produce a shear bond stiffness of 138 MPa (McDONNELL, TADOLINI, and DiGRADO, 1994).

Numerical Modeling Study of Cable Bolts

To complement the design work and field evaluation of cable bolt effectiveness, finite element models were constructed to evaluate cable bolt behavior under longwall mining conditions. These models incorporated in-mine geometry and geological conditions, including stratigraphy, structure, and in-situ stresses. This paper discusses a parametric study designed to evaluate the effects of dipping strata, horizontal stresses, and placement of crib supports on cable bolt loading and elongation at three stages of mining.

The ultimate goal of this project is to provide an engineered and economically feasible roof support

system and installation design that create safe work areas under diverse and hazardous ground conditions while enhancing production.

PROJECT STUDY AREA

Geologic Setting

The mine is located in Western Colorado in coal-bearing strata of Cretaceous age. The structural setting of the mine is influenced by an anticline-synclinal configuration which gives the coal bed a strike of N45°W and dip approximately 7° to the NE. The apparent dip across the test entry is 6° N.

The magnitude and orientation of in-situ horizontal stress was measured using the overcoring technique and the borehole deformation gauge developed by the US Bureau of Mines. In the vicinity of the cable bolt test site, the maximum in-situ horizontal stress was 15 MPa at N73°E with an associated minimum in-situ horizontal stress of 10 MPa N17°W. The depth of cover at that location is 350 m. The maximum ratio of horizontal to vertical stress at that point is approximately 1.7. The plane of the model, perpendicular to the direction of mining, is oriented at N7.5°E. In this vertical plane the magnitude of the horizontal stress is approximately 11 MPa, resulting in an approximate horizontal to vertical stress ratio of 1.3 (MALEKI, McKIBBIN, and JONES, 1994).

Geometry of Cable Bolt Test Site

Figure 1 shows the plan view of the cable bolt test site. The cable bolt test site is located in the entry adjacent to the second longwall panel. The test site is 152.4 m in length, spanning four cross cuts and three pillars as shown.

The bolting and cribbing configuration is shown in figure 2, which illustrates the cable bolt test entry. The primary support in the roof consists of five conventional 2.4 m Dywidag[1] bolts, anchored with 1.2 m of resin grout. The three interior bolts are installed vertically, with two bracketing bolts oriented at an angle. The secondary support consists of four

[1] Reference to specific products does not imply endorsement by the U.S. Bureau of Mines.

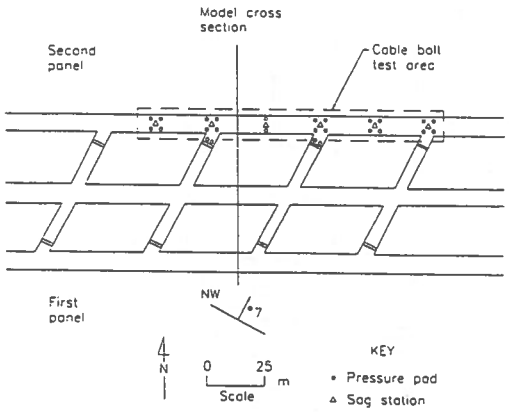

Figure 1. Plan view of cable bolt test site.

vertical cable bolts in rows spaced 1.2 m apart. In addition to cable bolts, two 1.2-by-1.2 m wooden cribs in rows spaced 2.4 m apart support the entry. The extracted coal seam ranges in thickness between 1.8 and 4 m. The mining height at the test site and within the model is 2.4 m. The gate road configuration consists of three entries 5.5 m wide, separated by coal pillars 24.4 m wide and 42.7 m long.

NUMERICAL MODELING STRATEGY

Model geometry

The numerical modeling software employed for this study was a PC-based finite element package called EZ[1]. The material property values used in the model are listed in table 1. All material properties used in the model are isotropic except for that defining failed rock along the out-of-plane axis of the model.

Modeling roof bolts

The cable bolt properties are assigned to nodes that define the location of the bolts within the finite-element mesh. These nodes are assigned bond strength values to indicate the location and strength of bolt anchors or resin-grout. A zero indicates no anchor or grout is present at that node.

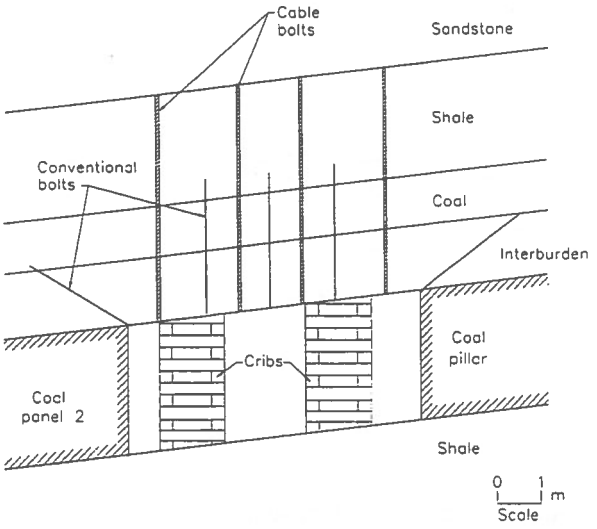

Figure 2. Cable bolt test entry.

TABLE 1. Material properties

material	Young's Modulus (GPa)	Poisson's Ratio
sandstone	49.5	0.22
coal	3.5	0.30
shale	32.6	0.24
failed rock	1.0,1.0, 0.25	0.39
interburden	3.5	0.27
cribs	0.5[2]	0.15

[2]BARCZAK and GEARHART, 1993

Model analysis

For each model case in the parametric study, a two-dimensional, plane-strain analysis was performed. Model analysis using EZ is an interactive process. The model is run one time, then the results are evaluated using a failure criteria strategy. The Mohr-Coulomb failure criteria is used for this study. Elements within the mesh with a safety factor of less than 1.0 by the failure criteria are manually reassigned the material properties of failed rock. The model is rerun with the "failed" material properties values in place. This sequence of element safety factor comparison with the failure criteria, reassignment of material properties to failed elements, and rerunning model, is repeated (usually two more times) until a stable configuration is reached and no additional elements fail. After each model run, bolt stresses can be extracted from a results documentation file, and the successive loading of bolts can be observed as progressive roof failure is modeled. After the final run, the bolts are considered to be fully loaded, and these final values are used in the parametric study.

THE PARAMETRIC STUDY

The primary purpose of the parametric study was to evaluate the effect of cribs on the stress induced within the cable bolts by running models with and without cribs in place. That study led to questions about the effects of the horizontal stress and dipping strata on cable bolt loading. Before the parametric study, it was thought that the difficulties in stabilizing the roof in the gate road entries of this mine were a direct result of the dipping strata, the horizontal stress, and the weakness of the immediate roof. The results of this study shed new light on this interpretation.

The series of models run for the parametric study includes three stages of mining: 1) after gate road entries were developed, 2) after first longwall panel was mined, and 3) during abutment stress as the second longwall face approached the test site. In the first case, voids were incorporated into the model representing the three gate road entries. In the second case, a void was added to the model to represent the extraction of the first longwall panel. In the third case, the same geometry as the second model was used with increased horizontal and vertical stress assigned to the model to simulate the front and side abutment pressures that are generated as the working face of the second panel approaches the test site. This third case represents the maximum stress conditions to which the test site is subjected.

In addition to these three mining configurations, the parametric study includes an analysis of the test site with and without dipping strata, with and without horizontal stresses, and with and without cribs. This analysis is composed of eight separate models for each mining stage to achieve all the possible

combinations of these conditions. Table 2 illustrates the parameters set up for each of the eight cases.

TABLE 2. Parameters in the eight model cases evaluated for each mining stage.

case #	dip	horiz stress	cribs
1	X	X	X
2	X	X	
3	X		X
4	X		
5		X	X
6		X	
7			X
8			

MODEL RESULTS

Results of parametric study

Bolt stresses from final model results for each of the eight cases were entered into a spreadsheet program, which facilitated the calculation of average bolt stresses and the graphing of the different permutations of bolt data. Graphs of particular use include average bolt stresses across the entries, stresses along individual bolts across entry, net elongation of bolts, and vertical displacement of roof across entry. In general, there is not a large difference in bolt stresses resulting from the dip and horizontal stress.

Stresses on Bolts

Average stress on bolts across entry: Figure 3 shows graphs of average stresses on bolts across the cable bolt test site entry for the three mining conditions, with cribs and without cribs respectively. The four cases plotted within each graph are 1) the existing conditions present at the test site, with dipping strata and horizontal stress, 2) dipping strata, no horizontal stress, 3) no dip, horizontal stress, and 4) no dip, no horizontal stress. The zero point on the x-axis of the graph corresponds to the down-dip side of the entry. Refer to figure 2 to recall the location of the cribs relative to bolts. Bolts 2 and 3 are located over cribs as are bolts 6 and 7. Odd-numbered bolts are the conventional dywidag bolts; even-numbered bolts are the cables.

The graphs show that there is very little difference between average bolt stresses for the first two mining stages, after gate road development and after first panel mining. The stress patterns are very similar with only a slight increase in average stresses on bolts after first panel mining. The only noticeable difference in the loading patterns across the entry is a slight shift in stress from the area of bolt 2 toward bolts 3 and especially bolt 4. This effect is more readily observable in the existing conditions plot of each case, with dip, horizontal stress, and cribs. Average stress on bolt 2 decreases slightly after panel mining and the average stresses of bolts 3 and especially 4 increase. This pattern is not as pronounced in the graphs with no cribs present.

The graphs all show that the existing conditions, with dip and horizontal stress, result in less average stress on the bolts across the entry, except for bolts 1 and 9, which are the angled conventional bolts that bracket the entry. Bolt stresses under the other three conditions are higher and closer in value. The second case, dip with no horizontal stress, is the second lowest stress state for the bolts on the down-dip side of the entry, but this case begins to exceed the no-dip cases at bolts 7, 8 and 9, on the up-dip side of the entry. When the strata are not dipping, the horizontal stress creates little change in the average stresses on bolts.

In the abutment stress graphs, there is less difference in average bolt stress between cases. With dipping strata, there is an increased concentration of stress in the angled bolts located downdip. This concentration is the result of rotating the entry within the existing horizontal stress field created by the effect of the dipping strata. Existing conditions show a very large difference in average stress between bolts 1 and 2.

Comparing graphs on the left side to graphs on the right side illustrates the differences in stress distribution across the entry with and without cribs in place, respectively. Without cribs to influence bolt loading, it can be more readily observed that the

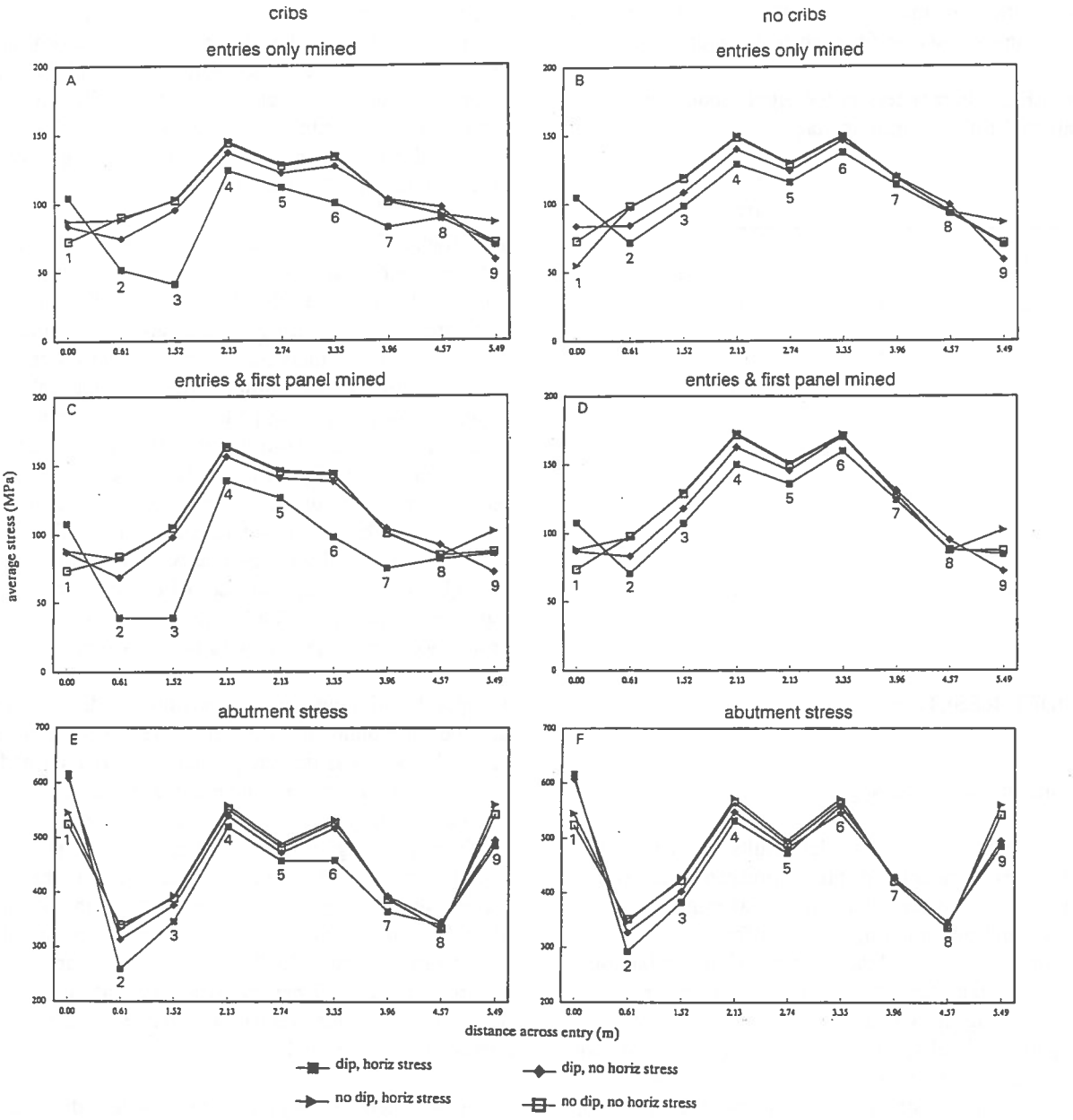

Figure 3. Average stress on bolts across entry.

stress distribution across the entry is skewed to the up-dip side for the cases with dipping strata, and, as expected, more symmetrically distributed across the entry for the no-dip cases.

Stresses on individual cable bolts across entry: To observe the distribution of stress across the entry, graphs of stress along individual cable bolts, with and without cribs, after first panel mining are the most illustrative of the mining stages modeled. These graphs are shown in figure 4. For the dipping strata cases, 4a and 4c, stresses on bolt 8 exceed those on bolt 2. When no cribs are present, this effect is still present, but less pronounced. With no cribs to support it, the stress on bolt 6 exceeds that on bolt 4, following the pattern of greater stress on the up-dip side of the entry with dipping strata.

It is interesting to observe that the effect of cribs in the entry is greatest under existing conditions, with dipping strata and horizontal stress. The greatest

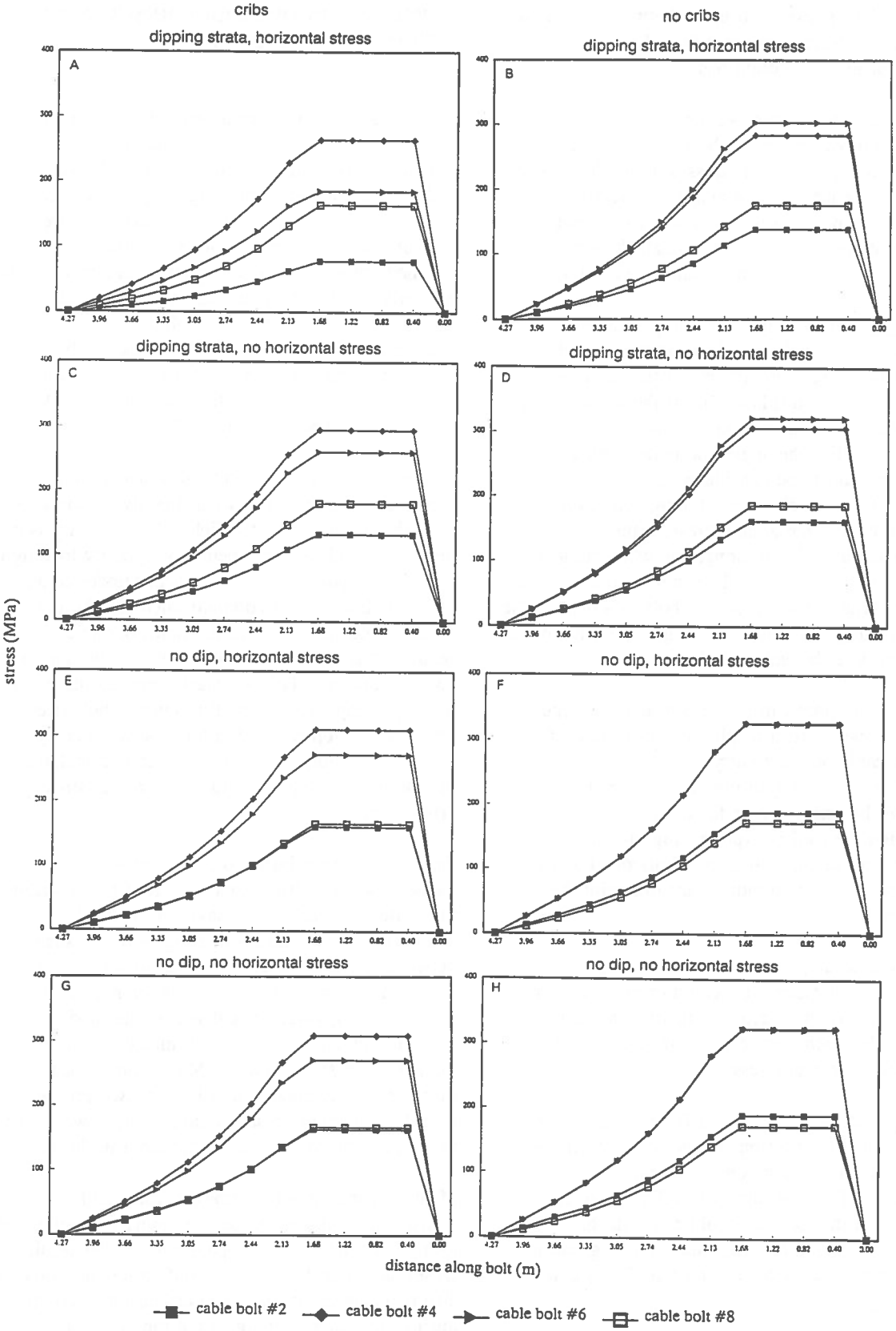

Figure 4. Stress at nodes along bolts.

increase in bolt stress is observed between the graphs of 4a and 4b, illustrating the crib and no-cribs situation for existing conditions.

For the cases with no dip, 4e through 4h, the stress on bolt 2 approaches that on bolt 8, and exceeds it for the no-crib cases. The stresses on the bolts in the middle of the entry, bolts 4 and 6, are nearly identical when no cribs are present. These four graphs illustrate once again how small the effect of horizontal stress is when the strata have no dip.

Bolt elongation: Figure 5 shows elongation of both conventional and cable bolts across the cable bolt test entry. Bolt elongation is calculated by subtracting vertical displacement of the top bolt node by displacement of the bottom bolt node for the vertical bolts. For the angled bolts horizontal displacement had to be considered as well. The graphs show that in all cases existing conditions, dipping strata and horizontal stress, result in the minimum amount of bolt elongation when compared with the other three cases. The angled bolts are the exception. The down-dip angled bolt experienced the maximum elongation under existing conditions for all mining stages, cribs and no cribs.

Comparing the graphs in figure 5 to those in figure 6, which shows vertical displacement of the roof across the cable bolt test entry after first panel mining, it is interesting to note that maximum vertical displacement occurs for existing conditions. Even though the roof is experiencing maximum deflection with dipping strata and horizontal stress, bolt elongation is a minimum compared with the other cases.

With dipping strata, but no horizontal stress, minimum roof displacement would occur, according to the model. With no dip, an intermediate amount of roof displacement would occur with very little effect from horizontal stress.

The effect of cribs, as shown in figures 5 and 6, is limited to bolts and portions of the roof directly over the cribs reducing elongation and displacement in that isolated area. The deflection of roof adjacent to cribs observed in figure 6a could result in the fracturing of roof strata in that location, suggesting that cribs may actually be detrimental in this case.

COMPARISON OF MODEL RESULTS WITH FIELD OBSERVATIONS

An attempt was made to measure bolt loads in the field using pressure pads. The pressure pads did not perform satisfactorily for this test site, because they did not have an adequate range to provide a complete loading history of the entry. A maximum stress (calculated from measured load) of 800 MPa was attained before the pressure pads ceased to function properly. Laboratory testing has determined that cable bolts fail at about 1430 MPa. Because the cable bolts in the test site did not reach failure capacity, it can be assumed that bolt stresses had not reached 1430 MPa, providing an upper limit for actual stress observed in the field.

Comparison of bolt stresses calculated through finite element model analysis is not directly comparable with that measured in the field. Model analysis of bolt stress adds a component from gravity loading of the entire model that does not occur under actual field conditions. To compare calculated bolt stress to actual values measured in the field, one must look at relative changes between bolt stress at the mining stages modeled. This approach removes the gravity loading component from all calculated bolt stresses. Stresses developed in cable bolts between entry mining and abutment stress conditions calculated by the model with dipping strata, horizontal stress, and cribs is 700 MPa.

Sag stations were installed in the test entry to measure vertical displacement of roof strata within the bolted interval. The maximum vertical displacement measured at the sag stations ranged between 2.0 and 5.6 cm. Vertical displacement of roof strata calculated by the model was determined by subtracting values calculated by the model of the first mining stage, entries only mined, from results of the abutment stress model. Maximum vertical displacement calculated in a location within the model comparable to sag station location was 5.6 cm, the upper limit of the range measured in the field.

Measurements obtained directly from field instrumentation are not the only means of collecting useful information to compare with model results. Observations of behavior of roof strata and bolts are also of value in evaluating model results. Often during first panel mining as the longwall face

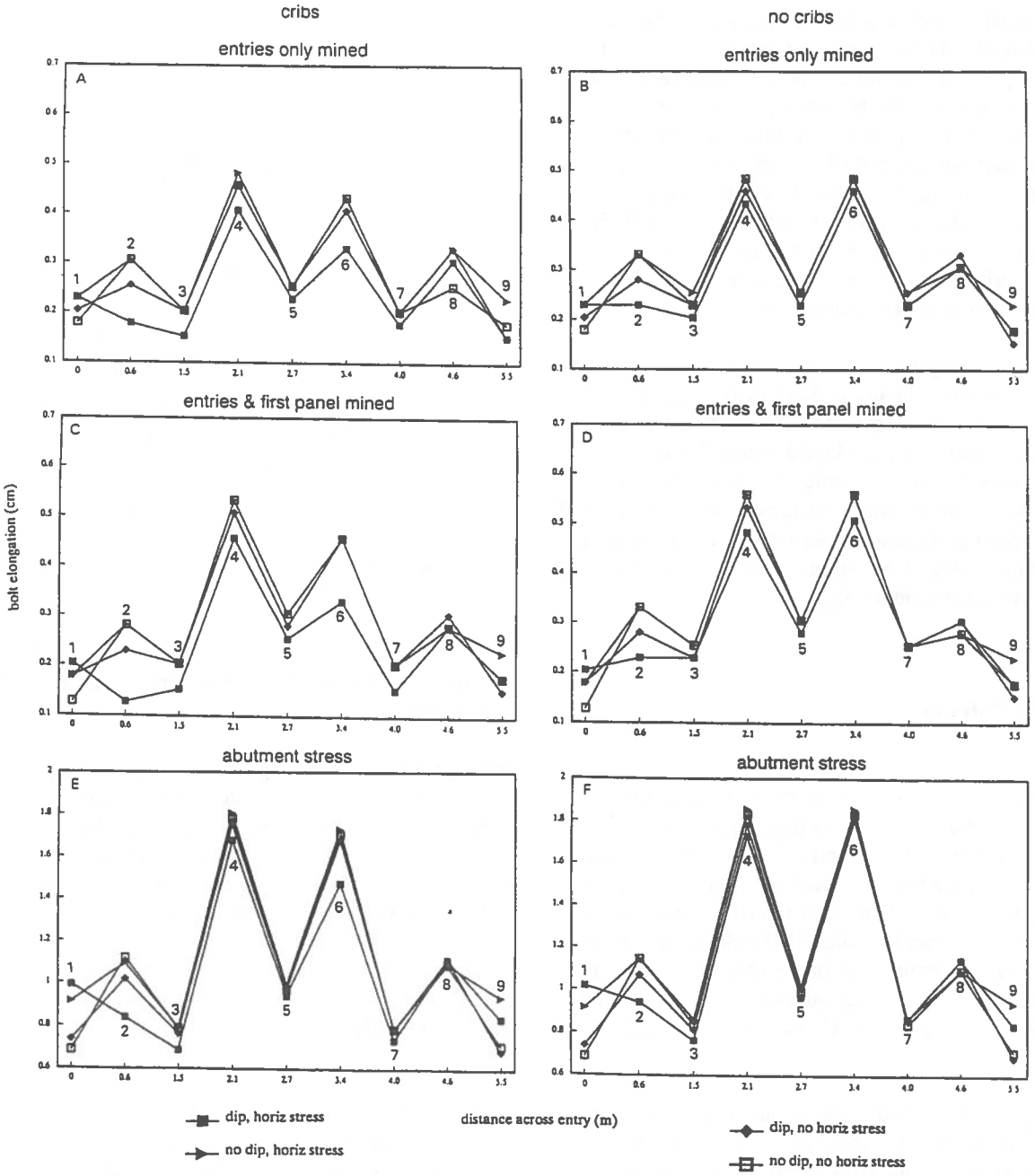

Figure 5. Elongation of bolts across entry.

approaches, roof control problems develop along the up-dip side of the entry taking the form of cutter-like roof failure. This behavior suggests that abutment stresses are developing in this portion of the entry and are observed as high stresses developing in the angled bolts of the abutment stress models. Model results indicate that high stresses develop in both angled bolts bracketing the entry, suggesting that one would expect this type of roof failure to occur along both sides of the entry. Occasionally, cutter-roof like behavior is observed along the ribline of the down-dip side of the entry, but this is not the rule. Model results, therefore, may provide useful information for gaining some understanding of the problem, but leave some questions unanswered until other factors are considered.

Model results in general suggest that the cribs in the test entry were an extraneous precaution. Although

under existing conditions, cribs reduced stress in bolts directly above them by about 40%, the model without cribs demonstrated the ultimate strength of the cables would have been adequate to carry the full load without cribs in place. Under abutment stress, models indicate that cribs have less effect on bolt stresses, resulting in a stress decrease of 18%. Although model calculations underestimate bolt stress compared to field measurements, stresses on bolts without cribs are well below the level at which cable bolts fail, even under abutment stress.

When comparing model results and field observations model limitations in simulating failed material behavior must be considered. Although a failed zone is incorporated using weakened material properties, the model still can only represent weakened material within the limits of elastic behavior. If the horizontal stress becomes a predominant factor in causing roof failure by means of non-elastic deformation, then model results no longer apply.

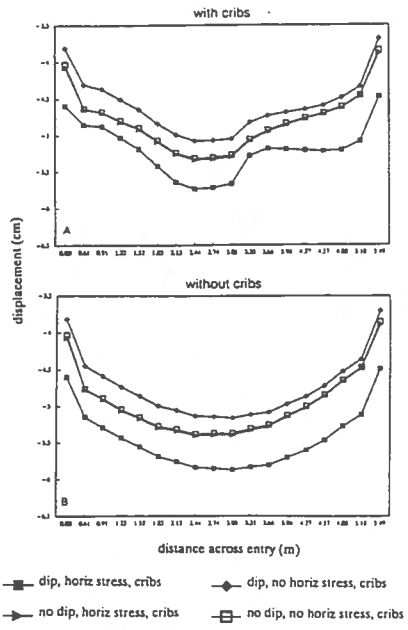

Figure 6. Vertical displacment across roof after first panel mining.

CONCLUSIONS

Numerical modeling is useful for evaluating the effects of parameters such as dipping strata, horizontal stress, and secondary support that interact together to influence bolt loading in the field test site. Through a series of numerical models, the effects of each parameter can be isolated. Model results then present an conceptual idea of the effects of stress and deformation that can contribute to the understanding of underlying causes for behavior observed in the field.

Although under existing conditions of dipping strata and horizontal stress, cribs reduced bolt load by 40%, models without cribs demonstrated that the ultimate strength of the cables would have been adequate to carry the full load without cribs in place. Even under simulated abutment stress as would occur as the working face of the second longwall panel approaches the test site, the calculated stress on the cable did not exceed their ultimate strength.

The results of this series of parametric models indicate that the combined effect of dipping strata and horizontal stress has a less detrimental effect on bolt stress than was originally thought. Comparison of average bolt stresses across the entry shows that the lowest bolt stresses were calculated for the existing conditions, although maximum roof displacement occurred. As long as behavior of roof strata observed in the field was essentially elastic, test site behavior was consistent with model results.

REFERENCES

BARCZAK, T., and GEARHART, D. Engineering Methods for the Design and Employment of Wood Cribs. USBM IC 9361, 1993, 34 pp.

MALEKI, H., McKIBBIN, R., and JONES, F. Stress Variation and Stability in a Western U.S. Coal Mine. SME Preprint 94-249, SME Annual Meeting, Albuquerque, NM, Feb 14-17, 1994, 7 pp.

McDONNELL,J., TADOLINI,S., and DiGRADO,P. Field Evaluation of Cable Bolts for Coal Mine Roof Support, USBM RI 9533, 1994, 30 pp.

CAMI'95: 3rd Canadian Conference on Computer Applications in the Mineral Industry
Montréal, Québec, Canada, October 22-25, 1995

Simulation numérique du remblayage d'un chantier de mine avec du remblai hydraulique cimenté: élaboration du modèle

Jacques Ouellet ing., Ph.D.
Département des Sciences Appliquées
Université du Québec en Abitibi-Témiscamingue, Rouyn-Noranda, Québec

Bruno Bussière ing., M.Sc.A.
Unité de Recherche et de Service en Technologie Minérale
Université du Québec en Abitibi-Témiscamingue, Rouyn-Noranda, Québec

Gilles Gagnon ing.
Mine D'Or KIENA Ltée.
Groupe Placer Dome, Val-d'Or, Québec

ABSTRACT:

A research program on cemented hydraulic backfill is underway at the University of Quebec in Abitibi-Témiscamingue. Part of these research activities are done with the support of Mine Kiena Ltd. The program includes laboratory testing, *in situ* observations and monitoring at the site of Mine Kiena. The mechanical behavior of this cemented hydraulic backfill and the *in situ* heterogeneities are described. Total pressure cells, piezometric cell and flowmeter were used to measure pressure evolution within the backfill and water drainage during the filling of a stope. Pressure readings and water flow from the stope were recorded along with backfilling operations log. The field and laboratory data will be used to build a numerical model of the backfilling of a stope. The objective of this analysis is to assess the impact of the drainage system and backfilling sequence on the stress supported by the bulkhead.

RÉSUMÉ:

Un programme de recherche sur le remblai hydraulique cimenté a été entrepris en collaboration avec Mine Kiena et l'Université du Québec en Abitibi-Témiscamingue via l'Unité de Recherche et de Service en Technique Minérale. Ces travaux comprenaient des essais ainsi qu'un ensemble d'observations in situ. Les caractéristiques mécaniques du remblai ainsi que l'hétérogénéité du remblai in situ ont été décrits. L'évolution des pressions qui se développent dans le remblai et les débits d'eau de percolation, lors de sa mise en place dans le chantier, ont été mesurés à l'aide de cellules de pression totale, d'un piezomètre et d'un débitmètre. Les données de laboratoire et in situ seront utilisées pour construire un modèle numérique de l'opération de remblayage d'un chantier de mine. L'objectif de cette analyse est d'évaluer l'effet du système de drainage et de la séquence de remblayage sur les pressions qui s'exercent sur la barricade.

INTRODUCTION

Les opérations de Mine Kiena s'intéressent aux charges que doit supporter une barricade lors des opérations de remblayage d'un chantier. Le remblai hydraulique utilisé est amené dans les chantiers sous forme d'une pulpe à 65% solide. Le taux moyen de remblayage utilisé dans le cas étudié ici était de un mètre par jour. La charge totale qu'exerce le remblai sur la barricade peut se décomposer en deux parties, la poussée du remblai qui dépend de ses caractéristiques mécaniques et une pression interstitielle qui dépend du niveau de saturation de la colonne de remblai dans le chantier. L'évaluation de la poussée du remblai sur la barricade

nécessite la connaissance des propriétés mécaniques du remblai mis en place. Dans le cas de la pression interstitielle c'est le niveau phréatique dans la colonne de remblai qui est déterminant. Pour cette composante de la charge sur la barricade, il faut connaître les caractéristiques de conductivité hydraulique du remblai in situ ainsi que la performance du système de drainage mis en place dans le chantier pour évacuer l'eau de percolation.

Notre objectif est de mesurer les pressions qui agissent sur la barricade et d'évaluer la performance du système de drainage dans cette perspective. Le programme d'investigation a donc été conçu afin de caractériser le remblai, les conditions in situ et la séquence de remblayage. Ces données permettront de définir un modèle conceptuel du remblayage du chantier. Ce modèle servira à la réalisation de simulations numériques pour évaluer les paramètres de design utilisés dans la conception de la barricade et du système de drainage des eaux de percolation.

CARACTÉRISTIQUES MÉCANIQUES

Caractéristiques physiques

Un programme d'essais au laboratoire a servi à caractériser le remblai hydraulique cimenté de Mine Kiena. Les éprouvettes d'essais ont été préparées au laboratoire à partir d'une pulpe prélevée à l'usine de remblai de la mine. Les agents de cimentation étaient ajoutés au laboratoire afin d'obtenir du remblai ayant différents rapports ciment (20:1 pour le cas du chantier étudié dans cet article) à 65% solide. Les agents liants étaient constitués d'une part ciment Portland et une part cendre pouzzolane. Le remblai était ensuite déversé dans des moules et conservés pour 28 jours dans une chambre humide à température constante. Le tableau suivant présente quelques caractéristiques physiques du remblai de mine Kiena.

TABLEAU 1: Caractéristiques physiques du remblai

Cc	0,02 à 0,21
Gs	2,79
D10	0,021 mm
D60	0,065 mm
D50	0,051 mm
Cu	3,1
<75 µm	65%

Dans ce tableau « Cc » est l'indice de compression en consolidation isotrope, « Gs » densité relative des grains solides, « D10 » le diamètre passant 10%, « D60 » le diamètre passant 60%, « D50 » le diamètre passant 50%, « Cu » le coefficient d'uniformité et « <75 µm » le passant 75 micromètres.

Comportement mécanique

Pour ce projet de recherche, l'essai de compression triaxiale à symétrie cylindrique a été sélectionné. Cet essai a été retenu pour les raisons suivantes: c'est un essai standard bien connu en mécanique des sols, relativement facile à mettre en oeuvre et qui possède une grande versatilité. L'essai non drainé a été éliminé car celui-ci nécessite la saturation de l'échantillon, une condition qui n'est pas nécessairement reproduite in situ. En conséquence, les éprouvettes ont été testées à leur teneur en eau naturelle après curage sans ajout d'eau.

Les mesures de variations de volume ont été faites par la méthode décrite dans Head (1986). Cette méthode a été utilisée avec succès par Ouellet (1992). La procédure de réalisation des essais a été maintenue, autant que possible, conforme aux normes utilisées en mécanique des sols (Bishop et Henkel, 1962). La pression interne dans l'échantillon était maintenue au niveau atmosphérique. Donc, toutes les valeurs de contraintes présentées dans ce rapport sont des contraintes effectives.

Les figures 1 et 2 illustrent quelques courbes contrainte-déformation en compression triaxiale sur un remblai hydraulique cimenté 20:1. Ces courbes contrainte-déformation sont normalisées en divisant la contrainte axiale par la contrainte radiale. L'ensemble des courbes présentées aux figures 1 et 2 donne une description complète de l'historique de déformation du remblai au cours du cisaillement.

L'examen de ces courbes contrainte-déformation permet de faire les observations suivantes:

-pour les niveaux de contraintes de confinement faibles le taux de dilatance maximum se produit seulement après le pic qui est suivi par un antiécrouïssage,

-à faible contrainte de confinement on observe la formation de plans de cisaillement bien définis sur l'éprouvette après rupture,

-pour des niveaux de contraintes de confinement plus élevés le comportement est contractant.

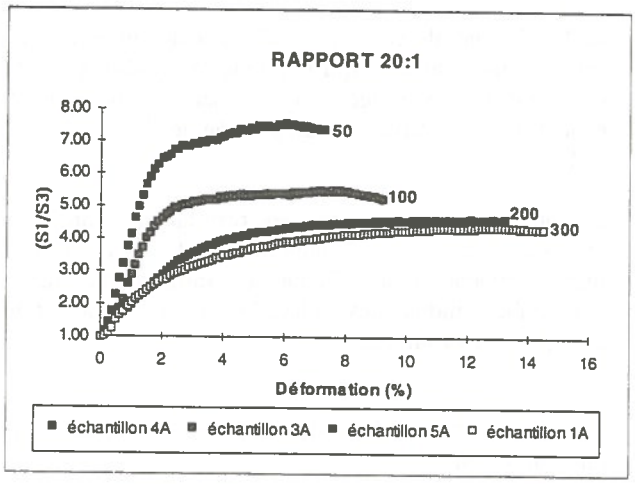

Figure 1 : Courbe contrainte-déformation remblai 20:1.

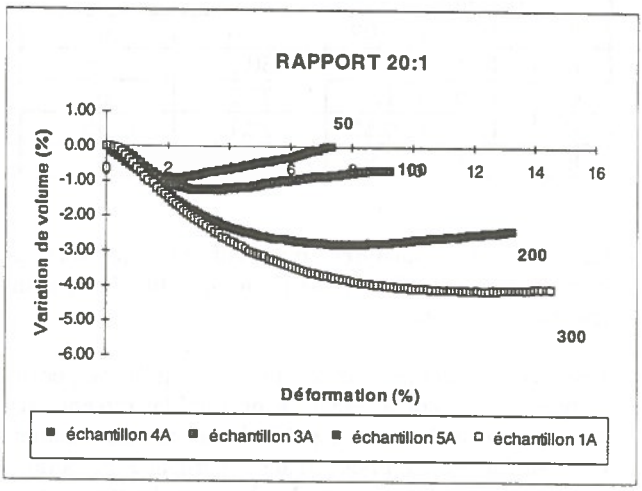

Figure 2 : Courbes de variation de volume remblai 20:1.

L'étude de ces courbes expérimentales permet de tirer certaines conclusions. La résistance au pic est principalement due au liens de cimentation; elle ne peut pas être expliquée par un processus de friction intergranulaire uniquement. Alors que la perte de résistance après le pic est due à la rupture des liens de cimentation dans le matériau.

Avec l'augmentation de la contrainte de confinement, on observe que les courbes contrainte-déformation du remblai cimenté tendent vers une courbe identique qui correspond au comportement du remblai non cimenté. Cette évolution montre que le processus de déstructuration (bris des liens de cimentation) est graduel. Cette déstructuration peut être produite soit par cisaillement ou simplement par chargement isotrope.

Ce comportement suggère une courbe enveloppe unique pour représenter la résistance ultime du remblai à contrainte moyenne élevée. À contrainte moyenne plus faible un courbe enveloppe différente existe qui dépend des caractéristiques physiques du remblai et de la quantité d'agents liants utilisée dans la préparation. Un phénomène semblable a été observé sur des sols latéritiques par Mahalinga-Iyer et Williams (1994). Mitchell et Wong (1982) ont observé un comportement similaire pour un sable cimenté. Gill et al. (1990) ont proposé un modèle de comportement pour un remblai de sel meuble qui montre des caractéristiques similaires aux matériaux meubles cimentés. Ouellet (1992) a utilisé un modèle de type Cam-Clay modifié pour reproduire le comportement d'un remblai présentant des caractéristiques similaires dans son comportement mécanique.

La figure suivante illustre les courbes enveloppes obtenues sur le remblai hydraulique de Mine Kiena dans l'espace « q-p ».

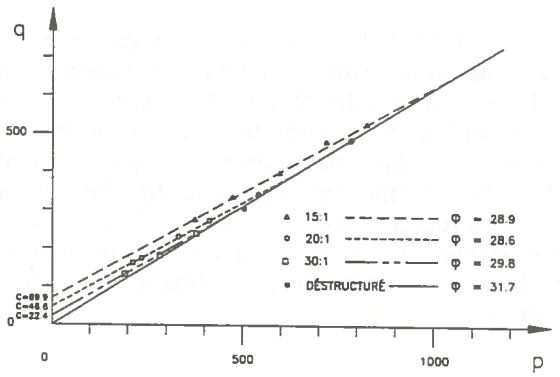

Figure 3 : Courbes enveloppes du remblai Kiena

La figure 4 montre schématiquement le modèle utilisé par Ouellet (1992) pour représenter le comportement d'un matériau meuble cimenté. Ce type de modèle permet de prendre en compte la friction ainsi que la cohésion produite par la cimentation dans la formulation mathématique du comportement contrainte-déformation.

Une description plus détaillée du modèle de comportement proposé par l'auteur principal est présentée dans Ouellet (1995).

Caractéristiques in situ:

Les caractéristiques in situ du remblai hydraulique de la mine Kiena ont été déterminées par des observations sur

le terrain et l'analyse des caractéristiques physiques d'un bloc de remblai prélevé à la base d'un chantier remblayé avec du remblai hydraulique cimenté 20:1.

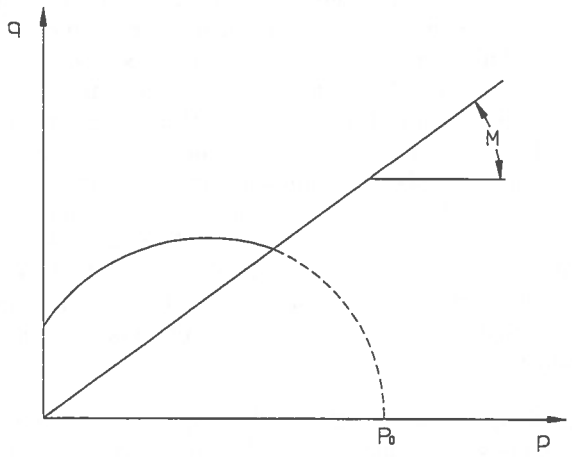

Figure 4: Illustration du critère utilisé (Ouellet, 1992).

L'examen visuel du bloc montre clairement la présence de trois strates de textures différentes. On observe une couche plus friable de 22 cm d'épaisseur entre deux couches de 4 et 6 cm respectivement qui montre une résistance mécanique plus grande que la partie centrale du bloc. Pour les fins des analyses une tranche verticale a été découpée dans le bloc. Cette tranche représentative a été ensuite subdivisée en cinq tranches dans le sens de la stratification observée sur le bloc (figure 5).

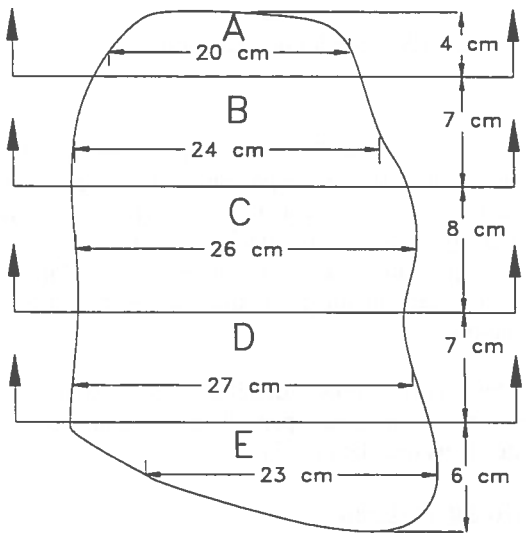

Figure 5: Schéma des coupes dans le bloc de remblai.

La bande centrale de 22 cm du bloc a été subdivisée en trois parties égales ce qui explique le nombre total de cinq tranches. Ce découpage a servi à préparer 5 échantillons identifiés chacun par une des lettres de "A" à "E".

Le tableau suivant résume les résultats des analyses réalisées sur ces échantillons. On y trouve respectivement, pour chaque échantillon, la masse volumique, l'indice des vides, la teneur en eau et le passant 75 micromètres.

TABLEAU 2: Résultats des analyses sur le bloc de remblai in situ.

	γ (gr/cm3)	e	Ww %	<75 µm %
A	1,70	1,09	27,6	65
B	1,81	1,00	30,2	75
C	1,60	1,17	25,2	65
D	1,83	0,85	22,1	55
E	1,63	0,94	14,1	45

Ces résultats d'analyses montrent que le remblai hydraulique cimenté de mine Kiena, in situ, n'est pas un matériau homogène.

Une visite effectuée sur le site de la mine a permis d'observer une coupe dénudée de remblai cimenté sur une hauteur de 4 mètres à partir de la base du chantier. Le remblai est composé d'une alternance de strates d'épaisseur moyenne de 20 à 30 cm et de strates plus dures d'environ 6 cm d'épaisseur. L'interface entre ces strates est généralement marquée par une trace blanche qui serait due, selon le personnel de la mine, à une concentration du ciment se produisant lors du lavage des conduites. Chaque séquence grossière-fine correspond à une journée de remblayage. La quantité de remblai produite en une journée étant relativement constante, l'épaisseur de cette couche de remblai est fonction de la superficie du chantier remblayé. Dans certains cas, l'épaisseur peut être de 20 à 30 cm et dans d'autres, atteindre 1 m selon les représentants de la mine. De ces observations nous pouvons conclure que l'hétérogénéité du remblai est fonction du mode de remblayage utilisé et de la géométrie du chantier.

L'anisotropie observée sur le remblai in situ a probablement une influence sur la conductivité hydraulique. Des analyses sont en cours afin de caractériser la conductivité hydraulique du remblai in situ.

DONNÉES DE TERRAIN

Un chantier a été instrumenté afin d'obtenir les données de terrain nécessaires à cette étude. Le programme d'instrumentation devait permettre de suivre l'évolution des pressions qui se développent dans le remblai lors du remblayage ainsi que la quantité d'eau qui se draine du chantier. À cette fin, deux cellules de pression totale, un piézomètre et un système Parshall avec débitmètre ont été installés dans le chantier 64-46.

Les cellules de pression totale étaient du type pneumatique (modèle EPC). Un piézomètre, modèle pneumatique FPC-2, a été utilisé pour la mesure de la pression interstitielle. Les instruments proviennent de chez RocTest Ltée. Un système Parshall avec débitmètre a été installé près de la barricade afin de suivre le débit d'eau de percolation évacué par les drains installés dans le chantier.

Une cellule de pression totale et un piézomètre ont été installés à la base et au centre du chantier. La cellule de pression a été placée dans la position horizontale afin de mesurer la pression verticale qui se développe dans le remblai à sa base. Le piézomètre a été placé à proximité de la cellule de pression, ceci pour permettre d'évaluer la contrainte effective à la base du chantier. La seconde cellule de pression totale a été placée au centre de la barricade à une élévation de 2 mètres afin de mesurer la pression qu'exerce le remblai sur la barricade. Les sorties des quatre drains installés dans le chantier étaient dérivées vers le Parshall afin de mesurer les débits d'eau de percolation. Le niveau du remblai dans le chantier était également mesuré à intervalle régulier.

La figure suivante montre la géométrie du chantier sur une vue en coupe. Ces chantiers ont, en moyenne, une dimension de 15 mètres par 20 mètres de section et une hauteur d'au moins 45 mètres. Sur cette figure l'emplacement des drains, des instruments et de la barricade peuvent être vus. Le système de drainage est constitué de 4 drains agricoles enveloppés d'un géotextile et ensuite recouvert de jute. Ces drains sont placés à intervalles réguliers sur toute la hauteur du chantier le long du mur et sortent à la base de la barricade. Le remblayage du chantier est réalisé par le biais d'une conduite localisée au sommet du chantier. Le remblayage était réalisé au rythme de 900 à 1000 tonnes de remblai par jour en moyenne. Pour ce chantier, cette quantité de remblai permet de remblayer une hauteur de 1 mètre.

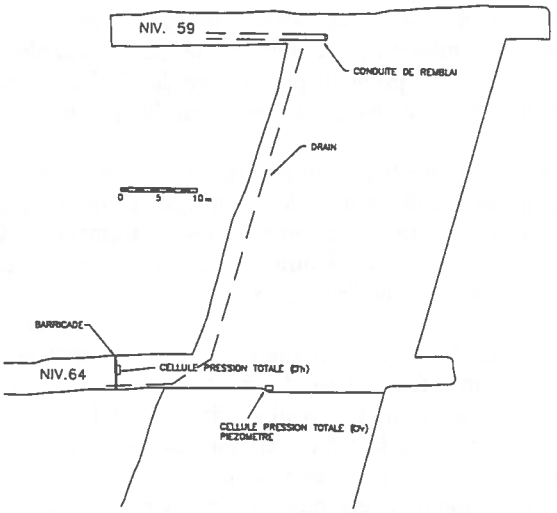

Figure 6: Vue en coupe du chantier 64-46.

La figure 7 montre le montage utilisé pour l'installation de la cellule de pression totale et du piézomètre à la base du chantier. Pour assurer l'orientation adéquate et une base stable aux instruments, une boîte en acier a été construite. Le fond de cette boîte a été remplie avec du béton et une empreinte de la cellule de pression a été faite avant la prise. La figure suivante illustre l'emplacement des instruments dans la boîte. Une fois la prise du ciment complétée, la cellule a été mise en place et fixée à l'aide de boulons.

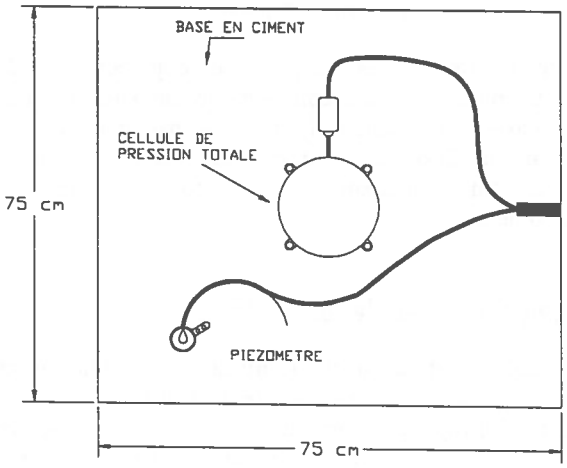

Figure 7: Schéma du boîtier.

Le piézomètre a été placé à proximité dans sa position verticale. Un guide et un contenant métallique ont été fixés dans le béton afin d'immobiliser le piézomètre

dans la bonne position. Le contenant était rempli d'eau afin de maintenir la cellule piézométrique saturée jusqu'à sa mise en place dans le chantier. Les câbles de lectures étaient protégés par un tube de PVC et amenés jusqu'au poste de lecture à l'extérieur du chantier.

L'accès du chantier étant interdit au personnel, il a été nécessaire d'utiliser un véhicule téléguidé pour préparer et mettre en place le boîtier des instruments. Un arpentage au laser a été utilisé pour vérifier que la boîte des instruments était bien au niveau.

La figure 8 montre une vue en coupe de l'installation des instruments à la base du chantier. Du stérile a servi à réaliser une base de travail au niveau. Préalablement à la mise en place, la boîte a été remplie avec du remblai non cimenté et recouverte d'un géotextile. Le boîtier des instruments a été mis en place en s'assurant que l'axe horizontal de la cellule de charge était bien parallèle au plancher du chantier. Une fois l'orientation des instruments vérifiée, la boîte a été recouverte avec du gravier afin de créer une couche de protection contre l'impact due à la chute du remblai lors des opérations de remblayage.

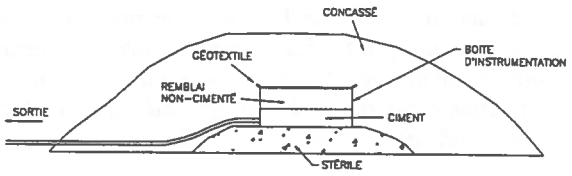

Figure 8: Schéma de mise en place.

Pour minimiser les risques de déplacements des instruments, les deux premiers mètres de hauteur ont été remblayés en amenant le remblai par une conduite passant par la barricade. Toutes les précautions ont été prises afin de s'assurer un bon fonctionnement des instruments.

Mesures in situ du chantier 64-46

Les instruments ainsi que le niveau du remblai ont été enregistrés pendant une période de 35 jours. Le journal de remblayage préparé par l'usine a été également obtenu. Ce programme de mesures a permis d'obtenir les données quotidiennes suivantes: volume d'eau déversé dans le chantier, nombre de tonnes solides, hauteur du remblai dans le chantier, volume d'eau sortie du chantier par les drains, pression interstitielle, contrainte totale verticale à la base du chantier et pression totale horizontale au centre de la barricade.

Les figures suivantes montrent quelques unes des données relevées lors de cette campagne de mesure. À la figure 9 le graphique montrant la hauteur du remblai dans le chantier en fonction du temps est illustré. La hauteur était mesurée à partir du sommet du chantier après chaque quart de remblayage. Le temps est exprimé en jour, commençant au début du remblayage (jour 1). Durant la période d'observation (35 jours) il y a eu quelques interruptions qui se traduisent par des barres manquantes sur le graphique de la figure 8.

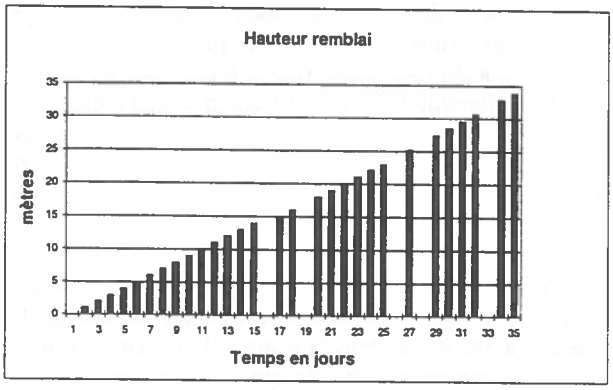

Figure 9: Élévation du remblai vs temps.

La figure 10 montre les lectures enregistrées sur les deux cellules de pression totale. La pression est exprimée en kPa et le temps en jour selon la même échelle que la figure 9. Ces courbes correspondent à des pressions totales et non pas des pressions effectives. Les interruptions sur ces courbes correspondent aux arrêts des opérations de remblayage durant la période de 35 jours.

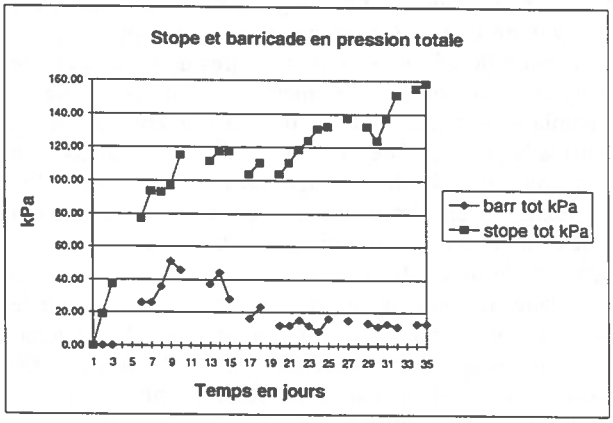

Figure 10: Lectures des cellules de pression totale.

On remarque que la cellule placée sur la barricade donne des lectures nulles sur les trois premiers jours. Ceci est dû au fait que cette cellule se situe à une

élévation de deux mètres par rapport à la base du chantier. On observe une augmentation rapide des pressions au début et une croissance graduelle pour la cellule horizontale à la base du chantier. Dans le cas de la cellule verticale sur la barricade la pression totale augmente durant les premiers jours et ensuite diminue pour finalement se stabiliser à une valeur plus ou moins constante après 15 jours.

Sur la figure 11, toutes les lectures des cellules de pression totale et du piezomètre sont illustrées. Toutefois, sur ce graphique les lectures de la cellule horizontale à la base du chantier ont été corrigées en soustrayant la pression piézométrique de la pression totale, ceci afin d'obtenir une pression effective à la base du chantier. On observe qu'en pression effective la courbe obtenue de la cellule horizontale est plus régulière et tend asymptotiquement vers une pression de 90 kPa. La tendance observée sur ces résultats se compare aux données présentées par Barret et Cowling (1980) et Grice (1989). Cette pression limite est plus faible que la pression théorique calculée avec le poids du remblai. Elle s'approche plus d'une valeur calculée avec l'équation de silos par exemple (Jahns et Brauner, 1960). Ces valeurs corrigées montre que la cellule donne une réponse stable dans le temps. Si l'on compare les courbes des figures 10 et 11 pour la cellule à la base du chantier, nous pouvons faire quelques observations. Une fois les valeurs de pression totale corrigées pour obtenir des pressions effectives, la courbe (figure 11) devient plus régulière. Les fluctuations sont attribuables surtout aux variations importantes dans la pression interstitielle (de 20 à 70 kPa).

La pression totale mesurée avec la cellule verticale placée sur la barricade montre une évolution différente pour la poussée horizontale. La pression qui s'exerce sur la barricade suit de près la valeur de la pression interstitielle. Toutefois, après les 15 premiers jours de remblayage on observe un découplage entre les lectures piezométriques et la pression sur la barricade. La courbe de pression se stabilise à une valeur d'environ 12 kPa et n'est plus influencée par les variations observées avec le piézomètre. Ce comportement indique que le remblai près de la barricade n'est pas à saturation. Le système de drains qui passent par la base de la barricade, après 15 jours de remblayage, maintient le remblai dans un état non saturé dans cette zone.

Les valeurs de pression enregistrées avec le piézomètre placé à la base du chantier ont été converties en niveau piézométrique afin d'évaluer l'évolution du niveau de saturation dans le remblai lors du remblayage. Ces données sont présentées à la figure 12. On observe une augmentation durant les périodes continue de remblayage. Suite à une interruption des opérations le niveau piézométrique baisse.

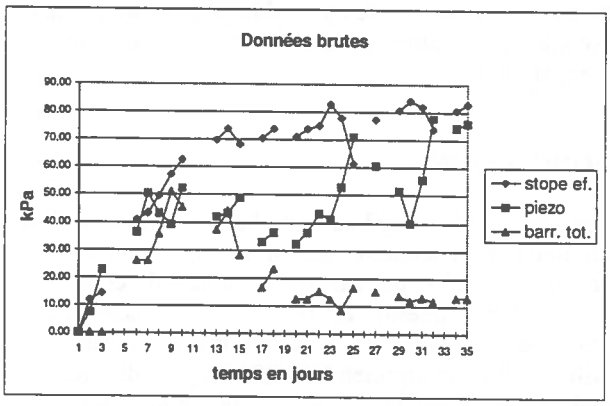

Figure 11: Pressions enregistrées dans le chantier 64-46.

Le niveau piézométrique ne dépasse pas, au cours de la période d'observation, la valeur maximum de 8 mètres. Des lectures seront prises à plus long terme pour vérifier l'évolution du niveau de saturation après que l'opération de remblayage sera terminée.

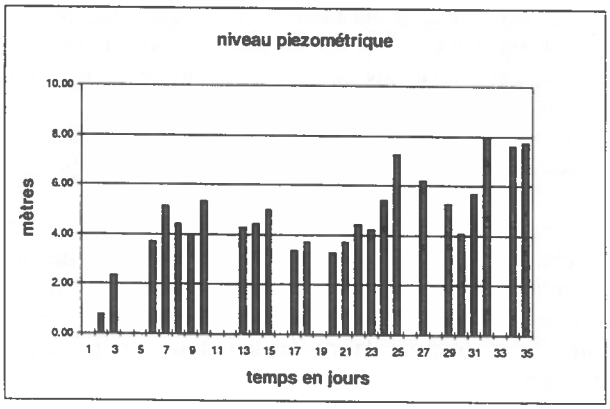

Figure 12: Niveaux piezométriques calculés.

Les données enregistrées au Parshall permettent de connaître le volume d'eau de percolation évacué par le système de drainage. Le journal de remblayage maintenu à l'usine de remblai nous indique la quantité d'eau totale qui entre dans le chantier. Ces données montrent que le système de drainage évacue de 50 à 60% de l'eau totale qui entre dans le chantier. Les teneurs en eau présentées dans le tableau 2 sont de moins de 30%. En considérant une teneur en eau mouenne de 30% et un indice des vides moyen de 1,00 le volume d'eau représenté ne permet de prendre en compte la totalité du volume d'eau qui n'a pas été intercepté par le système de drainage. Une observation faite sur le chantier du niveau inférieur montre qu'une

partie de l'eau de percolation passe par celui-ci. Aucune mesure n'ayant été prise à ce niveau il est difficile de déterminer le volume exact. Toutefois, en utilisant la teneur en eau résiduelle du remblai la majeure partie du volume d'eau utilisée dans le remblayage peut être comptabilisée.

CONCLUSIONS

Dans le remblai hydraulique l'ajout d'agents liants produit une cimentation des grains. Cette cimentation crée une cohésion qui agit sur une plage de contraintes limitée. Cette cohésion est fonction des caractéristiques physiques du remblai et de la proportion d'agents liants utilisée. Le comportement mécanique du remblai hydraulique cimenté dépend de l'historique de chargement. Le cisaillement ou un chargement isotrope peut détruire les liens de cimentation provoquant ainsi une déstructuration du matériau. Le modèle proposé par Ouellet (1992) sera utilisé comme loi de comportement pour le remblai hydraulique cimenté. Le logiciel d'éléments finis SIGMA/W de GEO-SLOPE International a été choisi pour le calcul des contraintes dans les simulations du remblayage. Ce logiciel permet les calculs en élasto-plasticité et offre deux modèles de type Cam Clay. Il permet également de faire des analyses non couplées de consolidation en prenant en compte la dissipation des pressions interstitielles. L'interaction entre les parois rocheuses sera simulée en utilisant des éléments interface (Zong et Hong, 1995).

Les analyses sur un échantillon prélevé sur le terrain et les observations faites dans un chantier montrent que le remblai hydraulique *in situ* ne peut pas être considéré comme homogène. Ces hétérogénéités devront être considérées lors de la modélisation du drainage du chantier.

Les observations *in situ* et les mesures de débits d'eau permettent de faire quelques observations. La pression sur la barricade est surtout fonction du niveau phréatique dans le remblai. La poussée que doit supporter la barricade passe par un maximum dans les premiers jours du remblayage. Par la suite, la résistance mécanique du remblai se développe et le système de drainage suffit pour maintenir un niveau de saturation inférieur à 8 mètres dans le remblai. On observe alors un découplage hydraulique entre la pression enregistrée par la cellule de pression totale sur la barricade et les lectures sur le piézomètre à la base du chantier.

Les données piézométriques montrent que le remblai n'est saturé que sur une faible hauteur par rapport à la hauteur totale. Pour les simulations numériques le logiciel SEEP/W de GEO-SLOPE International sera utilisé. Ce logiciel permet de modéliser l'écoulement en milieu non saturé. Les données expérimentales et les données de terrain permettront de caler les simulations en utilisant les débits mesurés dans le chantier.

Les données présentées dans cet article permettent de définir les paramètres nécessaires à l'élaboration des modèles numériques. Ces modèles permettront d'évaluer différentes configurations du système de drainage et leur impact sur la poussée subit par la barricade. Diverses séquences de remblayage pourront être étudiées afin de contrôler la montée de la pression sur la barricade. En effet, les données de terrain montrent que la pression maximum s'applique pour une durée limitée dans les 15 premiers mètres de remblayage.

REMERCIEMENTS

Les auteurs désirent remercier le CNRC, la Fondation de l'Université du Québec en Abitibi-Témiscamingue et Mine Kiena pour leur soutien financier.

RÉFÉRENCES

BARRET, J.R., COWLING, R., 1980. Investigations of cemented fill stability in 1100 ore body, Mount Isa Mines Ltd., Queensland, Australia. International Mining and Metallurgical Transactions, section A, Vol. 89, pp. 118-128.

BISHOP, A.W.; HENKEL, D.J. (1962) The Measurement of Soil Properties in the Triaxial Test. Edward Arnold Publisher, 227p.

GILL, D.E., OUELLET, J., CHAPUIS, R.P., 1990. Propriétés mécaniques du sel gemme meuble aux faibles pressions de confinement. Comptes rendus de la 43e Conférence Canadienne de Géotechnique, Québec, Vol. II, pp. 455-461.

GRICE, A.G., 1989. Fill research at Mount Isa Mines Ltd.. Innovations in mining with backfill technology. Proceedings of the 4th international symposium on mining with backfill, pp. 15-22.

HEAD, K.H. (1986) Manual of Soil Laboratory Testing, Vol. 1, 2 et 3. Pentech Press London. 1234p.

JAHNS, H. BRAUNER, G., 1960. Stowage pressure in steep measures. Third International conference on strata control, pp. 151-163.

MITCHELL, R.J., WONG, B.C., 1982. Behavior of cemented tailings sands. Canadian Geotechnical Journal, Vol. 19, pp. 289-295.

MAHALINGA-IYER, U., WILLIAMS, D.J., 1994. Consolidation and shear strength properties of a lateritic soil. Engineering Geology, Vol. 38, pp. 53-63.

OUELLET, J., 1992. Le sel meuble en tant que matériau de remblayage dans les mines de sel gemme. Thèse de doctorat, École Polytechnique de Montréal, 254p.

OUELLET, J., 1995. Comportement contrainte-déformation d'un remblai hydraulique cimenté pour le remblayage minier. 48e Conférence Canadienne de Géotechnique, Vancouver, Canada, septembre 1995, (à paraître).

ZONG-ZE, Y., HONG, Z., 1995. A study of deformation in the interface between soil and concrete. Computers and Geotechnics, No. 17, pp. 75-92.

CAMI'95: 3rd Canadian Conference on Computer Applications in the Mineral Industry
Montréal, Québec, Canada, October 22-25, 1995

Reducing the Amount of Cement in Backfilled Stopes

Maria Helena Leite
Department of Civil Engineering
École Polytechnique, Montréal

Robert Corthésy, Denis E. Gill, Gabriel Beaupré
Department of Mineral Engineering
École Polytechnique, Montréal

ABSTRACT:

This paper presents a new and simple solution to minimize the amount of cement required to support backfill when sequential stoping exposes a wall consisting of cemented backfill. This solution consists in building a retaining wall as the stope is being backfilled. This retaining wall, which shows a triangular profile, is built within the backfilled stope and contains a higher concentration of cement than the rest of the backfill in the stope. Such a cemented backfill "dam" retains the fill in the stope when pillars are recovered. The results of failure analyses performed with FLAC, a finite differences program which is particularly interesting for modelling this type of problem, are presented. A simple economic evaluation shows that important savings can be achieved with this new solution compared to the conventionnal constant cement content backfill.

RÉSUMÉ:

Cet article présente une solution simple et originale pour minimiser la quantité de ciment requise pour stabiliser le remblai lorsque l'exploitation séquentielle des chantiers expose un mur de remblai cimenté. La solution consiste à construire un mur de soutènement au fur et à mesure que le chantier est remblayé. Ce mur de soutènement de section verticale triangulaire est construit à l'intérieur du chantier et contient une concentration en ciment supérieure à celle du remblai contenu dans le chantier. Ce "barrage" de remblai cimenté retient le remblai dans le chantier lorsque les pilliers sont recouvrés. Les résultats des analyses de l'instabilité de l'ensemble mur-remblai à l'aide du logiciel de différences finies FLAC, particulièrement adapté à ce genre de problème, sont présentés. Une analyse économique simple montre que des économies importantes peuvent être obtenues avec cette nouvelle solution par rapport à la solution conventionnelle d'un remblai à teneur de ciment constante.

INTRODUCTION

As the mineral ressources have to be mined at ever increasing depths, the use of backfill has gained importance. Rockfill, low-density and high-density hydraulic backfill and paste backfill support systems are becoming increasingly popular in underground mines in order to minimize the cost of ground control.

In sequential stoping, one needs to add Portland cement to the backfill to insure that pillars can be recovered in between backfilled stopes without having backfill wall instabilities.

Contrary to what is generally believed, the use of cement in hydraulic backfill does not give much aditionnal support to the stope walls. Due to its emplacement technique leading to high void ratios and to a very heterogeneous body, the relative stiffness of the cemented backfill when compared to the stiffness of the country rock mass will not keep the stope walls from converging into the backfill. Depending on the mining and filling sequence, the use of cement might even have an adverse effect as it minimizes the pressure the fill material will exert on the hanging wall and foot wall in the lower portions of stopes, as the height of the backfill is increased.

Moreover, whatever the mining sequence is, the convergence of the country rock into the stope will proceed until a stabilizing pressure is reached. If this pressure is high, the backfill goes through a severe consolidation process, the void ratio and water content decreases, and the links between the particles created by the cement might be destroyed. Cement improves the support ability of backfill only when the stabilizing pressure is low compared to the collapsing pressure of the backfill, the latter being related to the cement content.

When using sequencial stoping (primary, secondary and sometimes tertiary), the adition of cement in the backfill becomes more important, as it will give support to the support (backfill) itself, since unconfined backfill walls will be exposed and will have to be able to whitstand their own weight and vibrations due to blasting. The stability of freestanding vertical faces of cemented backfill has been studied through the use of the limit equilibrium approach (Mitchell et al., 1982; Chen and Jiao, 1991) and physical models (Mitchell at al., 1982).

The object of this paper is to present how the retaining wall concept can applied to the support of backfill when second (or tertiary) stage open stope mining is done.

RETAINING WALL CONCEPT

Retaining walls have been used for as long as can be remembered. In mines, bulkheads in backfilled stopes are a direct application of the retaining wall concept. The new idea introduced in the present paper is to build a gravity retaining wall inside the stope as it is being backfilled. For open stoping methods requiring the stope to be emptied before being backfilled, the construction of the wall can be achieved by isolating a triangular portion of the stope using a geomembrane or a sisal curtain. This curtain will keep the high and low cement content fill from migrating from one section of the stope to the other. The stope is then backfilled with a high cement ratio in the retaining wall section and a lower cement ratio in the rest of the stope. This can be done by using two mixing stations and filling both sections of the stope simultaneoulsy, controlling the inflow in both sections, or by using one mixing station and filling the retaining wall and stope sections with lifts of a few feet, changing the cement content for each section. This operation requires relativeley regular stope walls so the geomembrane curtain isolates the retaining wall section from the rest of the stope. The curtain could be lowered along inclined cables attached to the stope back and floor. Figure 1 illutrates this solution. A simpler solution which would not require any curtain for open stopes, would be to drop the high cement content fill near the pillar wall so the natural slope of the flowing material will give the fill a triangular shape. The problem is that the slope will not be very steep unless paste backfill is used. This smoother slope will require more high cement content backfill. Depending on the cost of building a curtain, this solution might be economical. Another solution would be to excavate only a portion of the stope with the required triangular shape (or any desired shape) and then backfill it with the high cement content fill. However, blasting against this backfilled portion of the stope might damage the retaining wall.

For cut and fill mining, where pillars might be recovered in secondary long-hole stopes, the wall can be constructed in a much simpler way, as easy access to the stope is possible. Figure 2 shows the geometry the wall can have in a cut and fill stope as it is being built in sequential lifts.

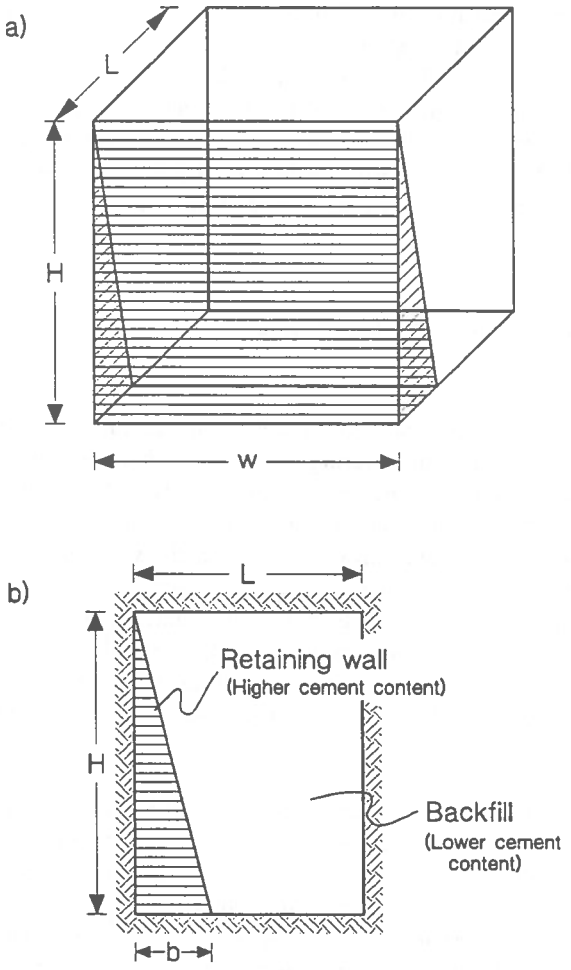

Figure 1 - Schematic view of the retaining wall concept

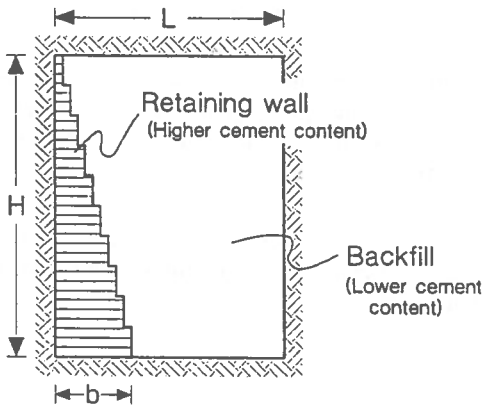

Figure 2 - Wall geometry in cut and fill stope

Prior to putting effort in developping an adequate backfill emplacement technique, it must be demonstrated that the retaining wall concept allows savings that can justify the extra work involved in the placement of the wall. In the following sections, stability analyses are done in order to determine if a retaining wall allows to minimize the total quantity of cement used for a given stope geometry.

RETAINING WALL STABILITY ANALYSIS

The stability of a gravity retaining wall depends, among others, on the pressures acting on it. It is well understood today that the distribution of earth pressures acting on a retaining wall is related to the deformation conditions and to the existing soil-wall friction conditions. The classical theories of Rankine and Coulomb are based on specific assumptions concerning these two points and the shape of the potential failure surface. When using these theories, a great amount of judgement is needed in order to evaluate the adequacy of these assumptions to the case under consideration. With this kind of analysis, the wall is considered to be perfectly rigid and the soil inside the failure surface is considered to be a rigid body.

Once the earth-pressure distribution against the wall is established, its overall stability can be evaluated. For a gravity retaining wall, the following points must be analysed: the wall shall not slide along its base (Figure 3a); it shall not rotate (Figure 3b) and the soil or rock under the wall shall not fail under the pressures imposed by the latter (Figure 3c). Besides, a general deep sliding surface must not develop under the wall.

This approach, which is typical of civil engineering applications, could be extended to analyse the stope incorporating the retaining wall. However, due to the uncertainty concerning the deformation conditions existing at the retaining wall-remaining backfill interface, the authors have decided to adopt another approach to analyse the stability of the backfilled stope.

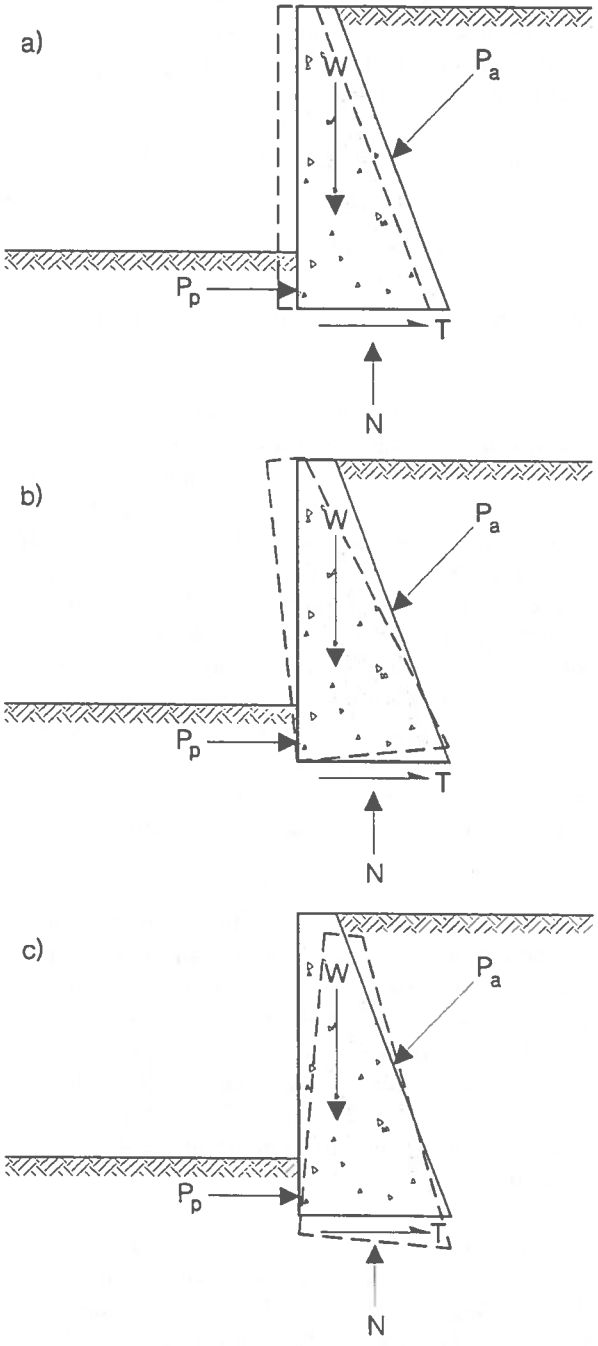

Figure 3 - Failure modes for a gravity retaining wall: a) sliding; b) rotation; c) foundation failure.

With the developpement of sophisticated numerical codes over the last 20 years, the influence of many aspects on the earth-pressure distribution can be evaluated more realistically. These include more representative soil behaviour, the construction steps and the deformability of the retaining structure, to name a few (Peck, 1990). For this reason, the cases presented in this paper have been analysed using a comercially available finite differences code named FLAC (Itasca Consulting Group., 1993). The details of such analyses are described in the following.

NUMERICAL ANALYSES

The analyses have been done considering a plane strain situation. Refering to Figure 1, this means that w is assumed to be much larger than H and L. If this condition is not verified, a 3D analysis must be done so that the shear stresses acting on the vertical stope walls perpendicular to the cross section shown in Figure 1b can be taken into account. These shear stresses contribute to increase the stability of the retaining wall. The plane strain assumption which has been retained for the sake of simplicity, is on the safe side.

Both the high cement content backfill forming the retaining wall and the low cement content backfill are assumed to be elasto-plastic Mohr-Coulomb materials, the yielding function being characterized by the cohesion (c) and the friction angle (ϕ). The elastic behaviour is characterized by the bulk modulus (K) and the shear modulus (G). The strength and deformability parameters of a cemented backfill are highly dependent on the cement content. Other factors affecting these parameters are the kind of backfill used (sand, tailings or rockfill), the curing time and the slurry density and the emplacement method.

Table 1 shows the values of Young's modulus (E) adopted for the preliminary analyses presented in this paper as a function of the cement content (Thomas et al., 1979).

The uniaxial compressive strength C_o (MPa) was estimated using the following relationship (Chen and Jiao, 1991):

$$C_o = Ae^{BC} \qquad (1)$$

where A=.2359, B=14.494, C is the percentage in cement by weight. In order to calculate the values of c, T_o (uniaxial tensile strength), K and G to be input in the analyses from the values shown in Table 1, the following relations have been used:

$$c = \frac{C_o(1 - \sin\phi)}{2\cos\phi} \quad (2)$$

$$T_o = \frac{c}{\tan\phi} \quad (3)$$

$$G = \frac{E}{2(1+\nu)} \quad (4)$$

$$K = \frac{E}{3(1-2\nu)} \quad (5)$$

Table 1

CEMENT CONTENT (% by weigth)	E (MPa)
2	25.7†
4	47.6†
6	90.3
8	185.0
10	206.0
12	301.0
14	467.0
16	643.0

† Estimated values

The friction angle ϕ has been chosen as 30° which is a reasonable lower bound for cemented backfill. The slurry unit weigth was considered to be 19.62 kN/m^3 and the Poisson's ratio (ν) was considered to be 0.1.

The cross section adopted in the analyses is that shown in Figure 1 where H=60 m, L=60 m and b=35 m. The excavation sequence was simulated in 8 steps by making the points located on the vertical boundary of the retaining wall free to move in the x direction from the bottom until the top of the stope, as indicated in Figure 4, where only three such steps are shown.

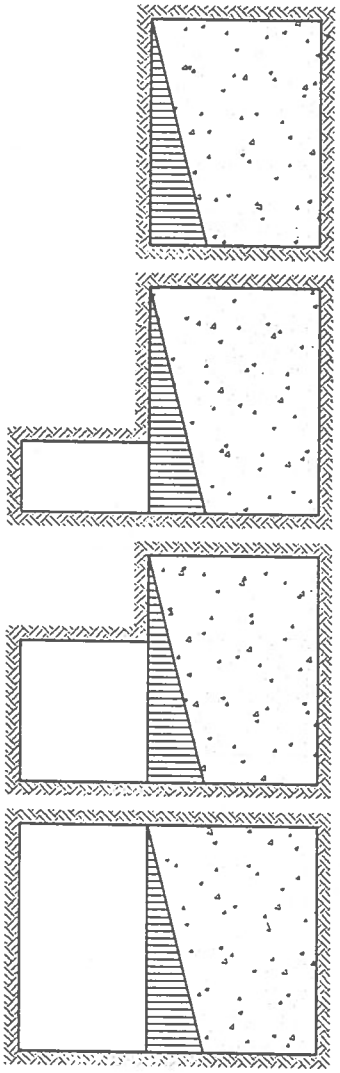

Figure 4 - Excavation sequence used in the numerical model

Two groups of analyses have been performed: the first one comprises stopes showing a uniform cement content backfill and the second one comprises stopes

For the stope backfilled using the new concept of builting a retaining wall, a minimum cement content of 2% has been chosen to the backfill behind the retaining wall. For the retaining wall itself, the cement content has been decreased until failure was observed for a cement content of 12.75%. As for the preceeding cases, the points in a yielding condition as well as the displacements at the end of the excavation are shown in Figures 7a and 7b.

a)

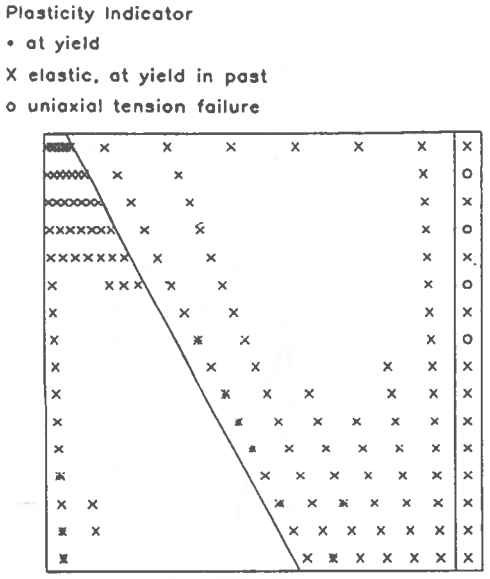

b)

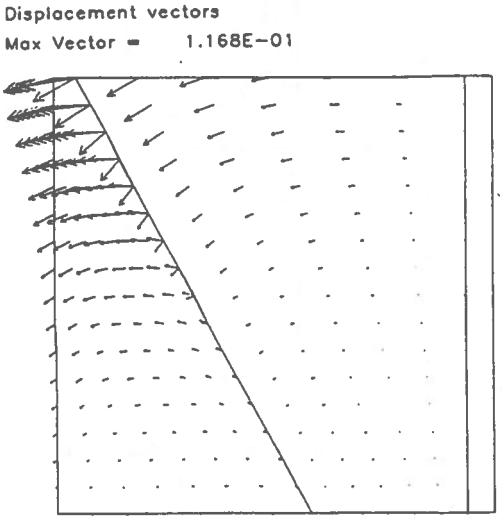

Figure 7 - Stable backfill with the retaining wall

COST ANALYSIS

In order to evaluate the costs related to the 8.7% uniform cement content and the 12.75%-2% retaining wall stope solutions, a cost comparison was done in terms of cement costs alone. Assuming the price of $150/ton for the Portland cement, the results are the following, considering an unitary width stope:

- 8.7% uniform cement content stope:

Cement weigth	= 625 ton
Cement cost	= $ 93 750

- 12.75%-2% retaining wall stope:

Cement weigth	= 389 ton
Cement cost	= $ 58 350

DISCUSSION

The analyses presented in this paper are only preliminary results of an ongoing research project. The aim of the paper is to show how the amount of cement in backfill can be reduced through the use of a retaining wall built inside the stope as it is backfilled. The results presented here should be regarded as relative rather than absolute values.

To take the maximum advantage of this new backfill concept, more work must be done in order fo find the optimum combination "cement content-retaining wall dimensions" for each case under consideration. In the present study, a single geometry of retaining wall has been analysed. If other retaining wall geometries had been analysed, another ideal cement content ratio could have been found for the retaining wall and remaining stope sections.

Some assumptions have been done for the numerical analyses as, for instance, the existence of plane strain conditions and the backfill strength and deformability parameters. However, these assumptions affect the retaining wall and backfilled sections identically.

In this paper, the damage to the retaining wall due to blasting was not investigated. If for a given blasting

backfilled using the retaining wall concept presented here. In both cases, the cement content in the whole stope (for the first group of analyses) and in the retaining wall and remaining stope (for the second group) has been decreased from an initially high value until the stope showed instability.

Such a case is shown in Figure 5. In this case the whole stope was considered to be backfilled with a uniform cement content of 5%. The results shown in figure 5 refer to the end of the excavation sequence. In Figure 5a, points at yield are identified by asterisks and in Figure 5b, the displacements in the same excavation stage are shown.

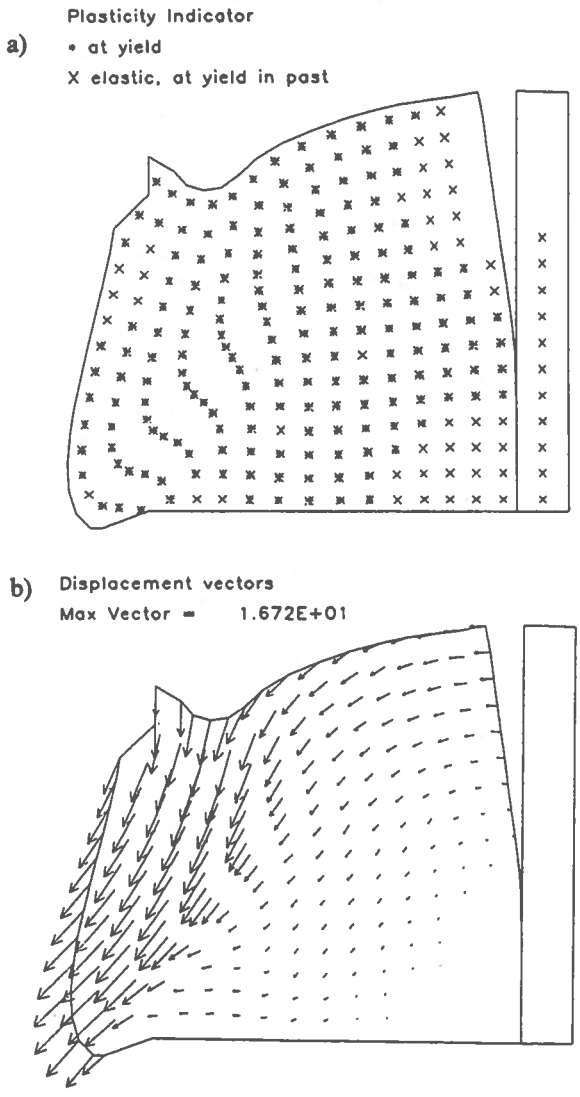

Figure 5 - 5% cement content backfill failure

As one can see, the excavation of the adjacent pillar caused the general failure of the backfill.

The lowest cement content assuring the stability of the uniformly backfilled stopes was found to be 8.7%. Figures 6a and 6b show the results of this analysis for this cement content in the backfilled stope. Only a few points are in a yielding condition and the displacements are very small (less than 4.6 mm for the 60 m height stope).

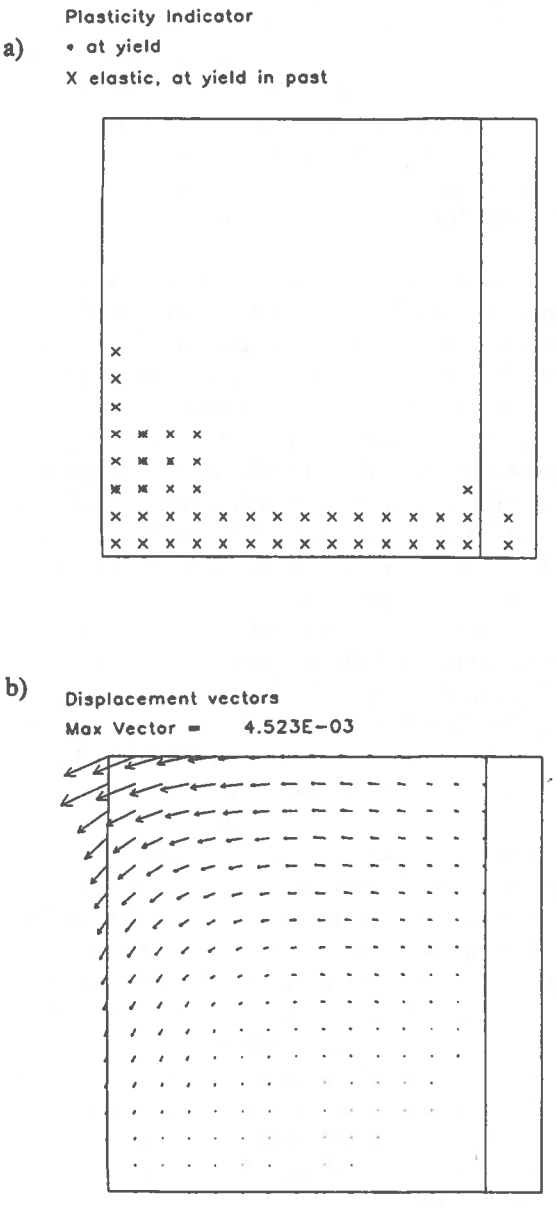

Figure 6 - Stability with 8.7% cement content

procedure a damage factor can be determined, the geometry and mechanical properties of the retaining wall can be modified to withstand the vibrations caused by blasting.

CONCLUSION

The paper presents a new and simple solution to minimize the amount of cement required to support backfill when sequential stoping exposes a wall consisting of cemented backfill. This solution consists in building a retaining wall within the backfilled stope which contains a higher concentration of cement than the rest of the fill in the stope, as it is being backfilled.

The cement content in both the retaining wall and the remaining backfill have been established through numerical analyses with the commercially available finite differences program, FLAC. These analyses have shown that, for the case under consideration (stope and retaining wall geometries, retaining wall and backfill strength and deformability parameters, excavation sequence), a cement content of 12.75% for the retaining wall and of 2% for the remaining backfill assures the stability of the backfill once the vertical wall is exposed by the excavation. To assure the stability with a uniform cement content, a 8.7% cement content backfill should be used. From a rough evaluation, the proposed solution allows savings of more than $35 000 per meter of width of stope with a 60 m by 60 m excavation. The longer the stope, the more important the savings will be.

It is important to note that the paper presented preliminary results and that the aim of the paper was to show the potential of the proposed solution. The ideal combination of retaining wall geometry and cement content to be used must be established for each case under consideration. The influence of the deformability parameters, yield criterion and strength parameters of both the retaining wall and the backfill, of the shear stresses along the vertical walls, the nature of the retaining wall-backfill interface and the damage caused by blasting are the subjects of the ongoing research.

ACKNOWLEDGEMENTS

The authors wish to thank the National Research Council of Canada for grants no WFA015669, OGP0089752 and OGP 0003412.

REFERENCES

Chen, J., Jiao, D., 1991
A design procedure for cemented fill for open stoping operations. Min. Sci. and Tech., Vol. 12, pp. 333-343.

Itasca Consulting Group, 1993
FLAC, Vol.2: Verification Problems and Example Applications.

Mitchell, R.J., Olsen, R.S., Smith, J.D., 1982
Model studies on cemented tailings used in mine backfill. Can. Geotech. J., Vol. 19, pp. 14-28.

Peck, R.B., 1990
Fifty years of lateral earth support. Proc. Conf. on Design and Performance of Earth Retaining Structures (Editors: P.C. Lambe and L.A. Hansen), pp. 1-7.

Thomas, E.G., Nantel, L.H., Notley, K.R., 1979
Fill technology in underground metalliferous mines. International Academic Services Limited, Kingston, Canada.

CAMI'95: 3rd Canadian Conference on Computer Applications in the Mineral Industry
Montréal, Québec, Canada, October 22-25, 1995

A preliminary assessment of mechanical characteristics of stiff backfills under confinement

Behrouz Arjang
Mining Research Laboratories, CANMET, NRCan, Ottawa, Canada
Graham Swan
Falconbridge Limited, Sudbury Operations, Ontario, Canada

ABSTRACT: In mining operations, an alternative to cemented tailings is the use of cemented and uncemented rockfill, "stiff backfill", which provides a backfill of higher stiffness. This paper presents the results of large-scale laboratory compression tests on combination of cemented and uncemented rockfills with selected ranges of tailings. Compressibility data, stress-strain, and stress-stiffness relationships of rockfills under confinement are evaluated. The experimental data suggest that the material composition and porosity strongly influence the mechanical properties of rockfills. For uncemented material with 5:1 rockfill-tailings ratio, low porosity fills are obtained which produced deformation modulus of up to 2.3 GPa. This demonstrates that in stiff backfill design crucial factors are void-filling and the material composition rather than the cementitious properties of a binder agent. The stress-stiffness relationship shows an initial high stiffness for cemented rockfills with a significant reduction in stiffness as the stress increases. This suggests that in mining applications, where closure strains expected to exceed 1%, the use of cement to achieve the required stiffness appears to be questionable.

RÉSUMÉ: Dans les opérations minières, l'utilisation d'enrochements cimentés et non cimentés, «remblai rigide» ayant une plus grande résistance à la flexion, au lieu de résidus cimentés, constitue une solution de rechange. Dans ce document, l'auteur présente les résultats d'essais de compression en laboratoire, réalisés sur une grande échelle, au moyen d'enrochements cimentés et non cimentés combinés à une gamme de résidus sélectionnés. Les données relatives à la compressibilité, à l'effort et à la déformation ainsi que les rapports entre l'effort et la rigidité des enrochements sous confinement ont été évalués. Les données expérimentales suggèrent que la composition et la porosité des matériaux ont un impact considérable sur les propriétés mécaniques des enrochements. Les matériaux non cimentés dont le rapport enrochements-résidus est de 5 à 1, fournissent des produits de remblayage peu poreux dont le module de déformation peut atteindre 2,3 GPa. Ceci démontre que les facteurs décisifs dans la conception d'un remblai rigide sont la composition des matériaux et le fait de combler les vides plutôt que les propriétés hydrauliques de l'agent liant. La rapport entre l'effort et la rigidité démontre que les enrochements cimentés ont une rigidité initiale plus élevée qui diminue considérablement à mesure que l'effort augmente. Ce phénomène semble indiquer que dans les applications minières, quand on prévoit que les déformations de fermeture seront de plus de 1 %, l'utilisation du ciment pour obtenir la rigidité requise est sujette à caution.

INTRODUCTION

In cut-and-fill mining operations, various type of materials have been used as backfill which include mixture of sand and gravel, mill tailings, cemented tailings and waste rock.

Presently, utilization of cemented fills is a common practice in most hard rock mines. High strength cemented fills made it possible to apply bulk mining methods, contributing to a reduction in mining costs. However, with regard to the cost of cement and other binders, many attempts have been made in optimizing the quantities used.

An alternative to the cemented tailings has been the use of cemented rockfills, "stiff backfill", which provides a fill of substantially higher stiffness. Increased interest of mine operators in utilization of stiff backfill materials has initiated in situ and large-scale laboratory assessment of mechanical properties of cemented and uncemented rockfills (Annor and Millette 1991, Arjang 1991, Grice 1989, Hedley and Quesnel 1991, Swan 1991, Yu 1987). In rockburst-prone mines, the evidence

suggests that the use of stiff backfills has significantly contributed to the alleviation of seismic activities (Hedley 1992).

Experimental data on strength and deformation characteristics of rockfills are limited. This initiated the present large-scale laboratory testing on rockfill material mixed with a combination of tailings and cement. The paper represents the results from the confined compression tests and evaluates the effectiveness of additives and the function of packing density on mechanical properties of cemented and uncemented rockfills.

TESTING MATERIAL

The rockfill and unclassified tailings material were obtained from Deep Copper Mine of Falconbridge Ltd. A total of about 4000 kg of rockfill (development waste rock) and 300 kg of tailings material were used to prepare the specimens. For cemented rockfill test specimens, Portland cement (type 10) was used as a binder. Particle size analyses were carried out on four shipments of rockfill material. Particle size distributions for these materials are plotted in Figure 1. The rockfill material comprised a maximum particle size of 150 mm with a range of coarse aggregates (>10 mm) 43-55%, and the fine aggregates (<10 mm) 45-57%, of the composition. The Coefficient of Uniformity of rockfill material was in the range of 28 to 45. The specific gravity of the rock and tailings were determined on randomly selected samples. Average density values of 2920 kg/m^3 for rock and 2200 kg/m^3 for the tailings material were used for volume calculations.

SPECIMEN PREPARATION

As described in Table 1, ten specimens were prepared with rockfill (RF) and various proportions of rockfill with tailings (RFT), cemented rockfill with tailings (CRFT) and cemented rockfill (CRF). Each test specimen was prepared from the content of individual shipment supplied in 45-gallon drums. Samples RF-01 and RF-02 were prepared from pure RF material with approximately 10% moisture content. The remaining rockfill and tailings materials were dried at room temperature. The required proportions of rockfill and tailings or cement were mixed to a uniform consistency in a 0.25 m^3 capacity cement mixer. In the case of tailings or cement addition to RF, a pulp density of about 35 % was maintained.

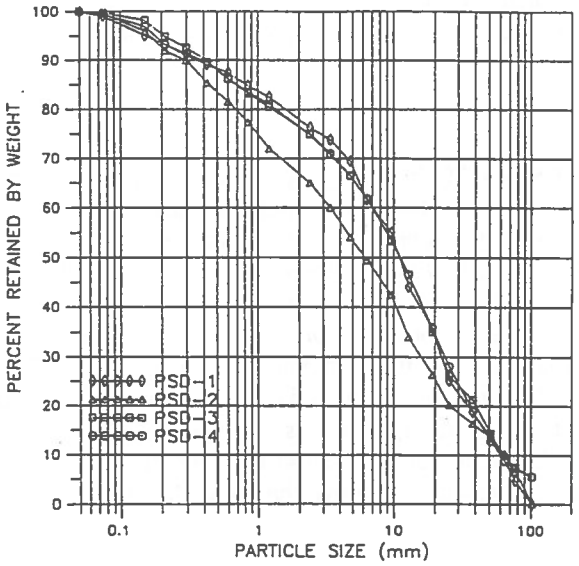

Figure 1. Particle size distribution of rockfills.

TABLE 1. Specimens description

Specimen ID	Material % by weight RF	TG	CT	Porosity %	Remarks
RF-01	100	0	0	25.7	Wet RF
RF-02	100	0	0	25.5	Wet RF
RFT-03	90	10	0	20.3	RF & TG
RFT-04	90	10	0	19.4	at 35 %
RFT-05	80	20	0	16.5	pulp
RFT-06	80	20	0	14.3	density
CRFT-07	90	8	2	20.4	As above,
CRFT-08	90	5	5	24.7	cemented
CRF-09	98	0	2	25.4	As above,
CRF-10	95	0	5	21.9	no TG

Material: rockfill (RF), unclassified tailings (TG), cement (CT), rockfill with tailings (RFT), cemented rockfill (CRF),cemented rockfill with tailings (CRFT)

A 14 mm thick steel cylinder, internal diameter 0.5 m and height of 1.0 m, was used for confinement of test specimen. The test cylinder was perforated at the periphery of the bottom portion to facilitate drainage of excess water and minimize pore water pressure buildup during the process of compression. To reduce friction, a thick layer of grease was applied to the inner wall of the test cylinder which was subsequently covered with 1 mm thick Teflon coated plastic sheets. The RF or premixed test material was placed in the cylinder in about 20 cm thick layers, and was manually compacted at each step using a 1.5 m long stud. During material placement, every effort was made to maintain a standard compaction procedure. A small portion of fine particles mixture was used to cap the prepared test specimens by creating a levelled surface. Cemented specimens were cured for a period of 14 days at room temperature with a relative humidity of 65%. Prior to compression testing, 76 mm thick steel discs with a diameter of 47.7 cm (smaller than the internal diameter of steel cylinder) were placed on the prepared test specimen.

CONFINED COMPRESSION TESTS

The set-up for the confined compression tests is shown in Figure 2. To monitor and measure the axial deformation, three displacement transducers spaced at 120 degree intervals were placed around the test cylinder. The radial deformation was monitored by three LVDTs connected to metal straps wrapped around the centre and at the top and bottom portions of test cylinder.

The confined specimen was compressed uniaxially by an 18 MN capacity, closed-loop electrohydraulic compression testing machine. A constant loading rate of 2.5 KN/sec, equivalent to an axial stress rate of 0.014 MPa/sec, was maintained. All test specimens were compressed uniformly to a maximum load of 9 MN, corresponding to an axial stress of about 50 MPa. For each test, incremental axial load, axial and radial displacements were monitored. All axial and radial displacements were continuously recorded by datalogger at a rate of 1 sample/min. In addition, the compression load and the axial displacement response were recorded by an x-y recorder to control the testing process and to provide an initial output.

Upon completion of each test, the compacted fill

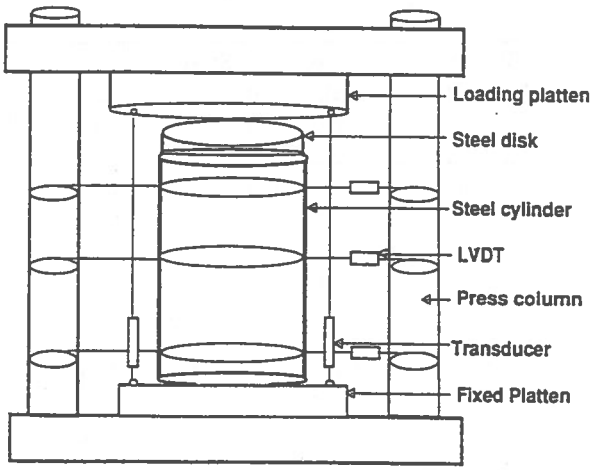

Figure 2. Set-up for confined uniaxial compression tests.

material was removed from the cylinder and dried at room temperature. From the measured dry weight the final porosity (void ratio) of test specimens was determined.
The radial confining pressure was estimated using the expression:

$$P = E\,h\,\Delta / 2\,r^2$$

where E is the elastic modulus for steel, h and r are respectively the thickness and radius of steel cylinder and Δ is the measured radial expansion. At the maximum stress of about 50 MPa, radial expansion in the order of 1.7 to 3.0 mm was determined for the test cylinders.

COMPRESSIBILITY CHARACTERISTICS OF FILLS

Table 2 summarizes the compressibility characteristics of the tested fill materials under confinement at 4% axial strain, 2.5 MPa radial confinement and at maximum axial stress of 50 MPa. Load-displacement responses from the uniaxial compression tests for cemented and uncemented fills are plotted in Figure 3 to 5. Figure 6 represents combined stress-strain curves for all ten specimens.

The relationships between the axial stress and fill deformation modulus are plotted in Figure 7. Figure 8

TABLE 2. Cemented and uncemented rockfills summarized data

Specimen ID	4% A. Strain				2.5 MPa Conf. Stress				50 MPa A. Stress			
	σ_1 MPa	σ_c MPa	n %	E GPa	σ_1 MPa	ε %	n %	E GPa	σ_c MPa	ε %	n %	E GPa
RF-01	4.2	0.0	22.0	0.10	24.0	11.3	14.5	0.55	12.4	14.6	11.6	0.97
RF-02	4.2	0.0	22.0	0.10	24.0	11.3	14.5	0.55	12.4	14.4	11.5	0.97
RFT-03	20.4	2.0	15.6	0.80	22.0	4.3	15.5	0.88	22.0	6.6	14.3	1.43
RFT-04	23.4	1.2	15.2	1.35	31.0	4.4	15.0	1.50	24.0	5.6	14.6	1.63
RFT-05	18.8	1.6	12.0	0.63	22.0	4.5	12.0	0.68	24.0	4.4	9.8	1.00
RFT-06	40.6	5.4	10.5	2.28	31.0	3.5	10.8	1.85	21.6	7.6	10.5	2.28
CRFT-07	31.4	3.4	16.5	0.96	26.0	3.2	17.4	0.85	16.0	5.8	15.3	1.06
CRFT-08	26.6	3.4	20.7	0.62	25.0	3.8	21.0	0.62	22.7	8.0	17.6	0.62
CRF-09	9.5	0.3	21.0	0.20	23.0	9.3	16.0	0.33	13.0	13.2	12.6	1.14
CRF-10	34.8	3.8	17.8	0.54	26.0	2.3	19.7	0.61	24.0	7.0	15.7	0.50

Note : σ_1 , Axial stress; σ_c , Confining stress; ε, Axial strain; n, Porosity; E, Deformation modulus.

shows the relationship between deformation modulus and the initial void ratio from present tests and the small-scale testing on fills reported by Beaudry (1991). For all ten test specimens, Figure 9 presents calculated theoretical values of porosity as a function of fill deformation modulus. The values represent the tangent deformation modulus for a given stress level.

The results of compression testing can be summarized as follows:

a) The stress-strain relationships indicate a general distinction between the cemented and uncemented fill material, disregard tailings as additive.

b) Compressibility characteristics of rockfill (RF-01, RF-02) and rockfill with low cement content (CRF-09,with 2% cement) are similar, as shown by stress strain responses.

c) Initially, at low axial stress up to 16 MPa, corresponding to an axial strain of < 4%, rockfills with sufficient cement content to coat the rock fragments (CRF-10) and cemented rockfills with tailings additions (CRFT-07, CRFT-08) have a greater stiffness than the pure rockfill, but as the bond breaks down with increasing axial stress the fill stiffness reduces (Figure 7).

d) At a low axial stress level, the cemented rockfills with 2-5% cement and 5-8% tailings (CRFT-07, CRFT-08) show similar deformation characteristics, but as the stress increases the cemented rockfill with higher fine content (CRFT-07) shows higher stiffness.

e) Generally, at high axial stress of about 20-50 Ma, rockfills with 10-20% tailings content, RFT, show superior stiffness compared to CRF and CRFT materials with no or lower tailings contents.

f) The results confirmed that a initial void ratio or porosity as low as 15% can be achieved in a laboratory scale from compaction of fill material having a rockfill-tailings ratio of 5:1 (e.g., specimen RFT-06; 80% rockfill, 20% tailings). If a pulp density of about 50% is maintained, the specified backfill (RFT 5:1) produces deformation modulus in excess of 2.0 GPa.

g) Theoretical initial porosity of cemented fills lies in the range of 20-25%, while the porosity values determined for uncemented rockfills with tailings content of 10-20% are less than 20%. As the axial stress increases, the compacted final porosity of RFT material is in the order of 12 to 15% compared to CRF and CRFT materials which, generally, exceeds 15% (Figure 9)

h) Under confined conditions and high stress levels, it appears that 2 to 5% cement in rockfills without the tailings content has no measurable effect on fill deformation characteristics.

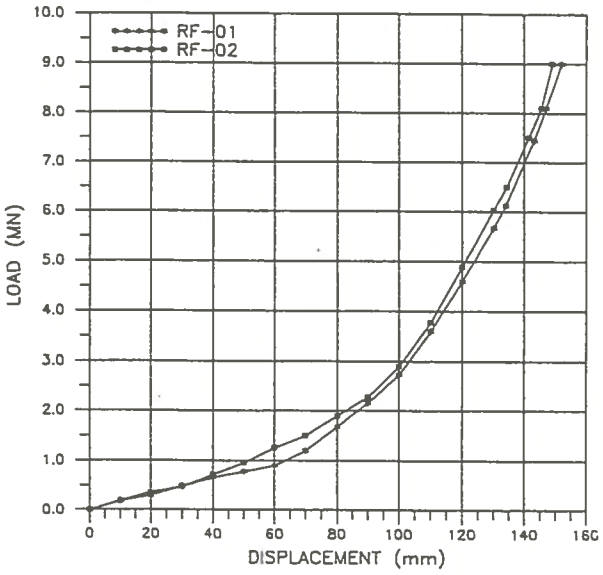

Figure 3. Load-displacement curves for rockfill (RF)

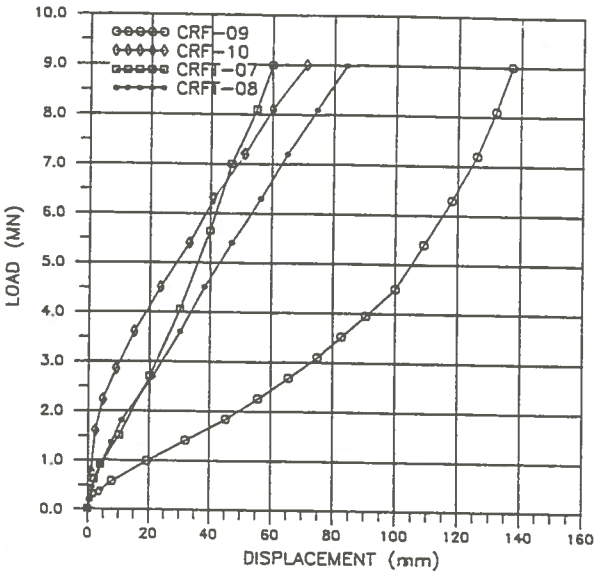

Figure 5. Load-displacement curves for cemented rockfill/tailings (CRFT) and cemented rockfill (CRF).

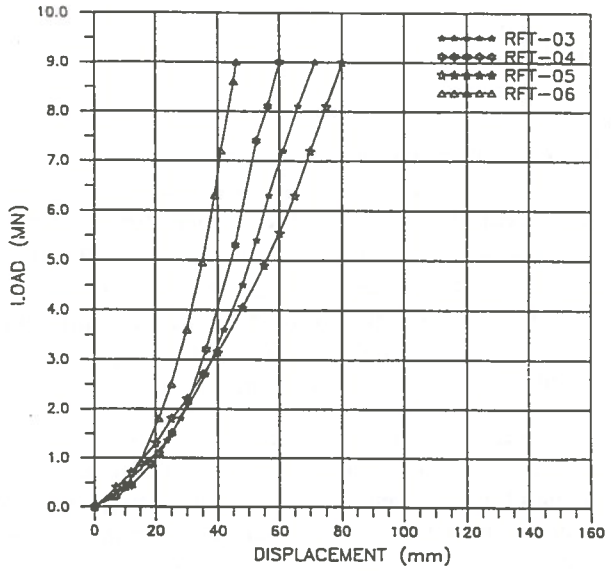

Figure 4. Load-displacement curves for rockfill / tailings (RFT).

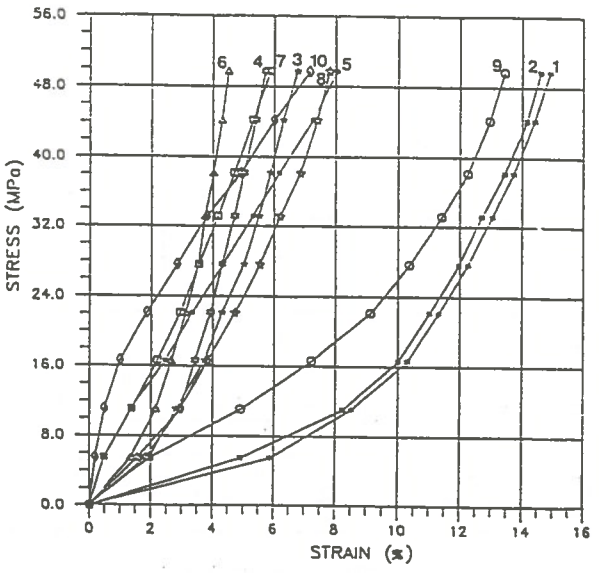

Figure 6. Combined stress-strain curves from compression tests: (1,2) RF-01 and RF-02; (3-6) RFT-03, RFT-04, RFT-05, RFT-06; (7) CRFT-07; (8) CRFT-08; (9) CRF-09; (10) CRF-10.

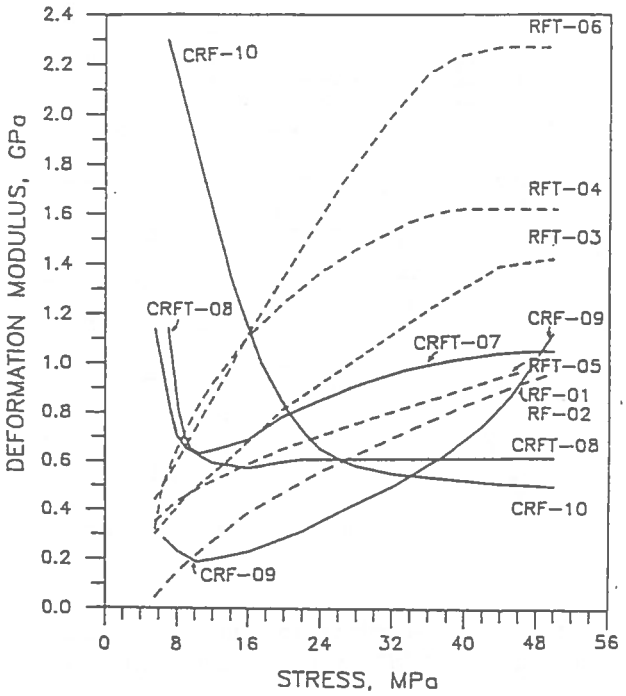

Figure 7. Stress-fill deformation modulus relationship of cemented and uncemented rockfills.

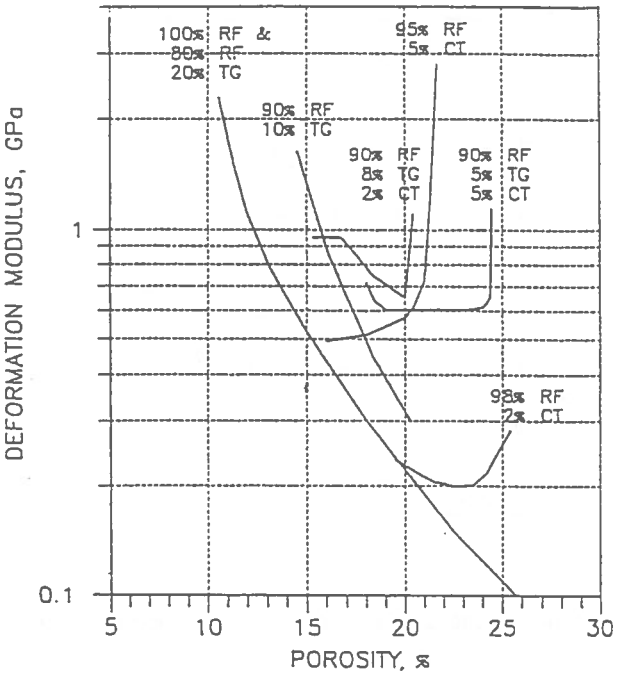

Figure 9. Cemented and uncemented fill deformation as a function of porosity.

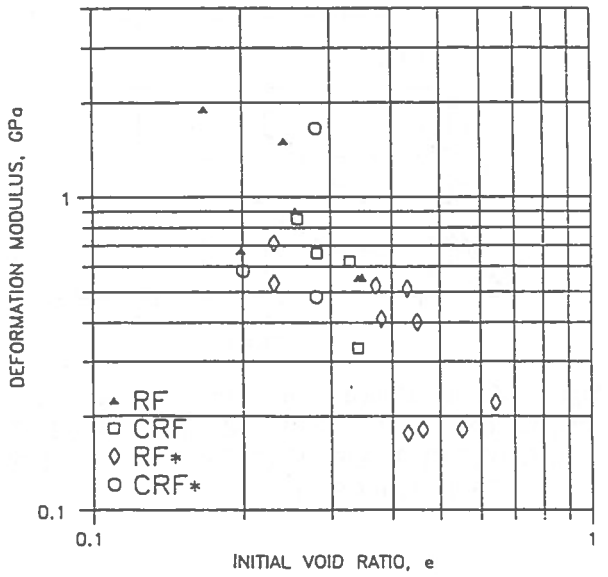

Figure 8. Fill deformation modulus-initial void ratic relationship of cemented and uncemented rockfills; (*) small-scale tests.

DISCUSSION

The present testing method is considered as a simple approach to identify the initial compressibility characteristics of stiff backfills. The steel cylinder provides an adequate lateral confinement at low stress levels and 4% axial strain. At higher axial stress levels, however, the interaction between the steel confinement cylinder / fill material and the effect of expansion of cylinder need to be further defined

Additional experimental work of similar scale on cemented and uncemented rockfills will further enhance the validity of present data. However, testing needs to be conducted under more controlled conditions and the following main factors should be considered:

a) Determination of particle size distribution for all rockfill materials,
b) Improvements in sample preparation, initial/final porosity determinations and compaction procedure,
c) Maintaining a controlled curing condition of cemented test specimens similar to an underground environment,
d) Conducting a minimum of 3 tests for each composite sample.

The results suggest that backfills with stiffness in excess of 2.0 GPa can been achieved in a laboratory scale. In a cut-and-fill mining operation, high in situ fill stiffness has been obtained by an improved fill handling and placement technique (Hopkins, 1988). Assuming tightly placed rockfill with a minimum void, e.g. a 5:1 RFT, the wall convergence in a stope is expected to compact the fill material and, to a significant degree, increase the stiffness. The load bearing capacity of fill will continue to increase with increasing closure. The experience gained on the use of stiff backfills in the cut-and-fill mining is further discussed by Swan et al. (1993).

CONCLUSIONS

The results of limited experimental work suggest that the material composition and porosity strongly influence the mechanical characteristics of cemented and uncemented rockfills. Under controlled laboratory-scale conditions, low porosity backfills with high stiffness have been obtained from uncemented material with a rockfill-tailings ratio of 5:1, compacted at a pulp density of about 35 %.

The initial compressibility data on variety of cemented and uncemented rockfills demonstrated that in stiff backfill design, crucial factors are the void-filling and material composition rather than the cementitious properties of a binder agent. However, these factors need to be further studied under experimental laboratory scale as well as in situ testing conditions.

The stress-stiffness relationships indicate an initial high stiffness for cemented rockfills with a significant reduction in fill stiffness as the stress increases. This suggests that, in cut-and-fill mining applications where closure strains expected to exceed 1%, the use of cement to achieve the required stiffness appears to be questionable.

REFERENCES

ANNOR, A. and MILLETTE, D., 1991.
Laboratory studies optimization of aggregate mix compositions for cemented rockfill, Part 1: Progress Report, Stiff Backfill Project. CANMET/MRL, Division Report, MRL 91-115 (TR).

ARJANG, B., 1992.
Large-scale testing on compressibility characteristics of stiff backfill. CANMET/MRL, Division Report, MRL 92-044 (TR).

ARJANG, B. and STEVENS, K., 1991.
Utilization of stiff backfill in alleviation of rockbursts Part 2A: Laboratory-scale dilatometer testing of cemented rockfill. CANMET/MRL, Division Report, MRL 92- 096 (TR).

BEAUDRY, M., 1991.
Small-scale testing on rockfills. Internal Report, Falconbridge Ltd.

GRICE, A.G., 1989.
Field research at Mount Isa Mines Limited. Proceedings, 4th International Symposium on Mining with Backfill, Montreal.

HEDLEY, D.G.F. and QUESNEL, W.J.E., 1991.
Stiff Backfill Project at Lac's Macassa Mine MRD Technical Progress Report.

HEDLEY, D.G.F., 1992.
Rockburst handbook for Ontario hardrock mines. Special Report SP 92-1E, CANMET/MRL, Energy, Mines and Resources Canada.

HOPKINS, P.H., 1988.
Strathcona Deep Copper zone consolidated rockfill options- background data. Internal Report, Falconbridge Ltd.

SWAN, G., 1991.
On cemented and uncemented rockfill in overhand cut-and-fill mining. Internal Report, Faconbridge Ltd.

SWAN, G., ARJANG, B. and HEDLEY, D.G.F., 1993.
On the use of rockfills in overhand cut-and-fill mining. Proceedings International Congress on Mine Design, Kingston, Ontario.

YU, T.R., 1987.
Ground support with consolidated rockfill. Underground Support Systems, CIM Special Volume 35.

CAMI'95: 3rd Canadian Conference on Computer Applications in the Mineral Industry
Montréal, Québec, Canada, October 22-25, 1995

Stability of Mine Backfilled Stopes in Faulted Rock Mass

Keyvan Fotoohi and Hani S. Mitri
Department of Mining and Metallurgical Engineering
McGill University, Montreal, Quebec

ABSTRACT:

A problem of four undeground mine-backfilled stopes located in the vicinity of a pair of inetsecting faults is analyzed using a nonlinear boundary element technique. The characteristics of the faults are determined from the field through "tilt"tests, Schmidt Hammer tests and direct measurement of thickness. Backfill was modelled by applying equivalent pressure at the stope periphery. Numerical modelling was carried out using SATURN software system developed in-house. It allows for the simulation of opening boundaries using Fictitious Stress elements and the fault using Displacement Discontinuity elements. The latter treats the nonlinear behaviour of the fault using Barton-Bandis nonlinear joint model. The comparison of results with both observations and seismic events in the field shows good agreement.

RÉSUMÉ:

Un problème de quatre chantiers d'abattage remblayés qui sont situés dans la proximité et au croisement de deux failles est analysé en utilisant la technique d'éléments frontières. Les caractéristiques des failles sur les chantiers sont déterminées par les essais de "tilt" et Schmidt Hammer et par des mesures directes d'épaisseur. Le remblai a été modélisé en appliquant des pressions équivalentes à la périphérie du chantier. La modélisation numérique a été faite par le système SATURN qui a été développé à McGill. Il permet la simulation des ouvertures en utilisant des éléments "Fictitious Stress" et de la faille par les éléments "Displacement Discontinuity". Ce dernier traite le comportement nonlinéaire de la faille en utilisant le modèle du joint nonlinéaire de Barton-Bandis. Les résultats numériques concordent avec les observations et les événements sismiques aux chantiers.

INTRODUCTION

In recent year, the application of boundary element method in mining design has been increasing due to its advantages over other numerical methods. Such advantages can be summarized as: (a) simple data preparation, (b) less computer memory requirement, (c) high computational speed. A boundary element model for stress/stability analysis of underground excavations in the vicinity of faults, namely SATURN, has been developed in house recently (Fotoohi, 1993). Application of the numerical model is an essential step of its development as an efficient design tool which focuses on its ability to solve mining problem for which it was developed. The application of the model at Kidd Creek Mine, Ontario is presented herein.

NUMERICAL MODEL

SATURN is an acronym for Stress Analysis of Tunnels

and Underground excavation with Nonlinear discontinuities. SATURN is designed to model 2-D problems in geomechanics, with up to 5 different homogeneous, isotropic solid materials as well as two choices of linear or nonlinear modelling of fault deformation and peak strength model. In fault deformation, the linear behaviour is characterized by Goodman's model (Goodman, 1976) whereas the nonlinear behaviour is based on Barton-Bandis' model (Barton et al., 1985). In peak strength analysis, the linear model uses Mohr-Coulomb and the nonlinear peak strength model employs the mobilized nonlinear shear strength envelope of Barton-Bandis.

SATURN software system consists of a main program called SATURN and its pre- and postprocessors which are called DRAW and SHOW respectively.

CASE STUDY

The case study was taken from No. 1 mine at Kidd Creek mines. Kidd Creek mines are located 27 *Km* north of the city of Timmins, Ontario. The orebody of Kidd Creek is a massive sulphide deposit with surface dimensions of 168 m width by a 670 *m* length (Yu and Quesnel, 1984). The orebody contains zinc, copper, silver, tin, lead and cadmium and strikes almost due north and dips about 75 to 85 east.

The blasthole stoping method and stope-pillar extraction sequence with delayed backfilling is used in No.1 mine at Kidd Creek mines. The stope width is 15 *m*, with a wide from 55 to 75 *m* and the length varied from 90 to 150 *m*.

The plan view of 2300 level at No. 1 mine is divided into two zones which are named south zone and north zone. The north zone of level 2300 was chosen for case study. The main structure of the north zone is NB (North-B) fault. The main purpose of this case study was the stress analysis of the north zone at 2300 level considering the NB fault. Figure 1 shows a plan view of mining sequence in north zone at 2300 level.

Mining retreat in the north zone is in general from hanging wall to foot wall, with longitudinal retreat varying to fit in with constraints resulting from past mining. The present sequence in the middle of the north zone comprises four stopes which are marked A, B, C and D from hanging wall to foot wall (Fig. 1). SATURN is used to examine the behaviour of the NB fault when mining activity takes place close to the fault (mining proceeds from stope A to stope D).

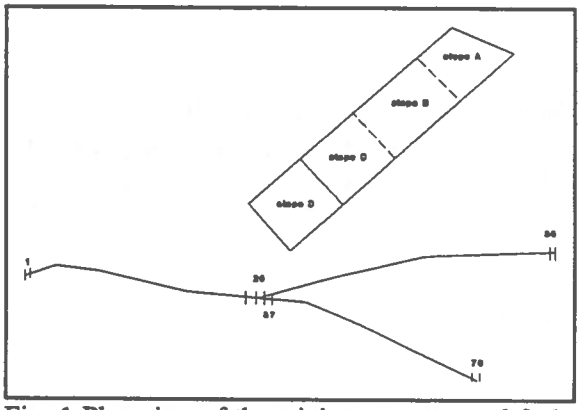

Fig. 1 Plan view of the mining sequence and faults in the north zone at 2300 level

INPUT DATA

There were three documents which report on the in situ stress at Kidd Creek mines (Fotoohi, 1993). The insitu stress after averaging the available data was taken as σ_1 = 52 MPa and σ_2 = 39 MPa. The direction of horizontal principal stresses is E-W for the major principal stress and, N-S for the minor principal stress.

The average value of available rock mass properties to be used for input data files are as follows; E = 67 GPa and υ = 0.28 (Henning, 1991)

THE CHARACTERISTICS OF STRUCTURES

The NB fault is visible in 2300, 2400 and 2500 levels (levels 2400 and 2500 are one and two levels lower than the level 2300 respectively). The data were collected from three levels and their average values were used. For any trace of fault in a tunnel, the Schmidt hammer was used to measure the "rebound on weathered and saturated joint" (r) and, "Rebound on unweathered dry rock" (R). The thickness of the fault was measured by vernier callipers. Also, the basic friction angle (φ_b) of joints was found by tilt test. The collected data for NB fault at 2300, 2400 and 2500 levels have been presented elsewhere (Fotoohi, 1993). The average values of the characteristics of NB fault is presented in Table 1.

Table 1 The average of characteristics of NB fault between 2300 and 2500 levels at No.1 mine

Level	r	R	φ_r	Thickness (mm)	JRC
2300	34	48	30	13	11
2400	29	48	35	6	10
2500	29	47	34	9.5	13
average	31	48	33	10	11

The data from Table 1 was used for calculating the final input data. The final values describing the characteristics of the fault which was used for input data file are presented in Table 2.

Table 2 Characteristics of fault NB for using in SATURN

K_{ni} MPa/m	K_{si} MPa/m	V_{jm} mm	V_{jp} mm	JRC	JCS MPa	φ_r	σ_c MPa
13,000	3,500	9	9	11	46	33	160

BACKFILL SUPPORT

Various types of consolidated backfill such as rock fill, sand fill and cement slag rock fill are used at Kidd Creek Mines (Yu & Counter, 1983). Backfill is used for secondary pillar recovery. The design of backfill is based on the strength requirements for standing over an exposed face with the dimensions of 120 m high and 70 m long. The fill requires a compressive strength of 2.8 MPa after 28 days of curing, if only the gravity load is considered. A safety factor of 2.5 is applied to allow for additional blast loading and the reduction of fill strength due to inadequate mixing, which gives a design strength of 7 MPa.

In boundary element method, backfill can be modelled by considering only the gravity load. If the density of cemented rock fill is 2,000 Kg/m^3, then the gravity load due to 100 m high backfill is : $P = \gamma * H =$ 2,000 * 100 = 200,000 Kg/m^3 = 2 MPa. The gravity load of rock fill may change from 0 to 2 MPa by changing the height of fill stope from 0 to 100 m. On the other hand, based on the theory of passive and active pressure of consolidated soil, the gravity load causes a lateral pressure on the rock walls of a stope. The ratio of lateral to vertical gravity load is between 0.33 and 10. Considering the rockfill as a consolidated backfill, the value of the gravity load might be between 0.66 to 20 MPa at the bottom of filled stope.

In this case study, the presence of backfill in a stope is simulated by applying a constant normal stress on the boundary of stopes. Based on the available information which was given before, it was decided that the constant normal stresses be 2 MPa.

NUMERICAL MODELLING TECHNIQUE

SATURN was used to predict the movement along the NB fault during mining and backfill sequence (Fig. 1). A total of four numerical models were constructed to help examine the fault behaviour. Table 3 describes the modelled scenarios. The number of elements for modelling the fault and stopes as well as run times are recorded in Table 4.

Table 3 Numerical models constructed for the case study.

Model	Explanation
1	Stope A is mined out
2	Stope A is backfilled and B is mined out
3	Stopes A and B are backfilled and C is mined out
4	Stopes A, B and C are backfilled and D is mined out

Table 4 The number of elements and run times of different models.

Model	Fault (DD)	Stope (FS)	Iterations	Run Time (min)
1	78	30	20	33
2	78	50	20	49
3	78	65	20	69
4	78	82	20	92

DISCUSSION OF RESULTS

The results of model 4 representing the last mining sequence are presented in Figures 2 to 5 which are listed below.

Figures 2 and 3 present the displacements in the rock mass in x and y directions respectively. In general, the maximum displacement in the rock mass is concentrated in the right-lower part of stopes, the area between the stope D and the NB fault.

Figures 4 and 5 show the major and minor principal stresses in the rock mass. The maximum principal stress is concentrated at the corners of the stope, especially in the corner of stope D and connection point of branches of fault NB. The contours of minimum principal stress show some tension around the stope D.

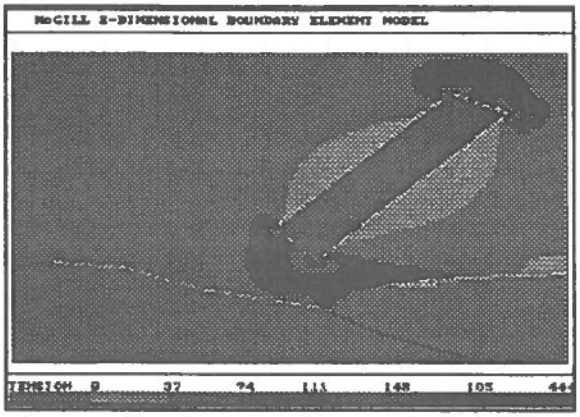

Fig. 4 Major principal stresses in the rock mass - case 4

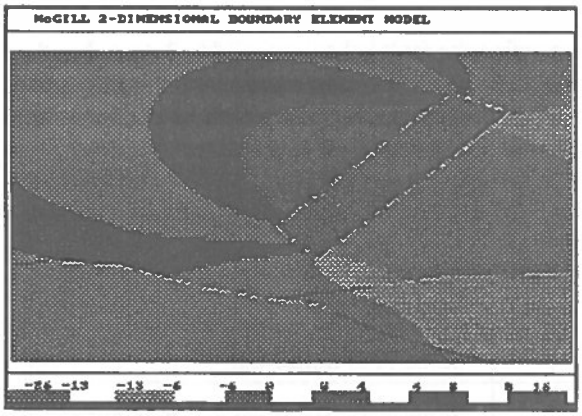

Fig. 2 *X*-Displacements in the rock mass - case 4

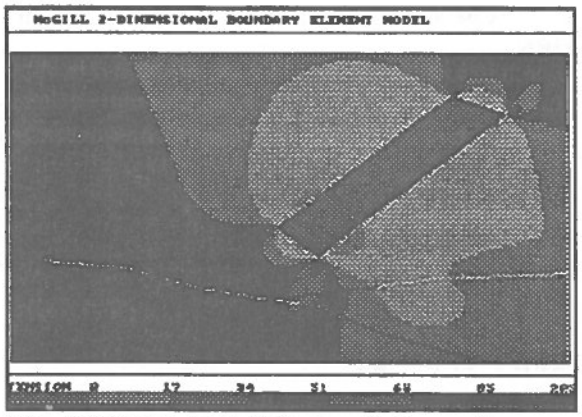

Fig. 5 Minor principal stresses in the rock mass - case 4

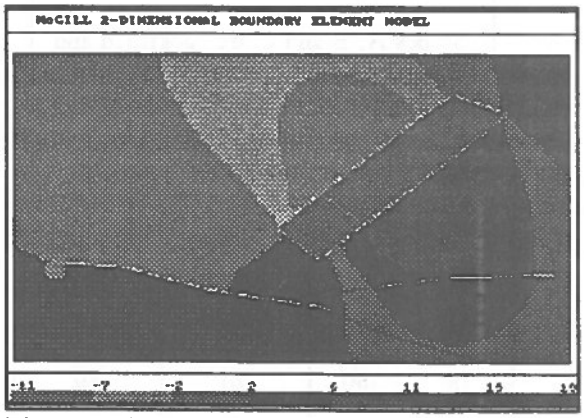

Fig. 3 *Y*-Displacements in the rock mass - case 4

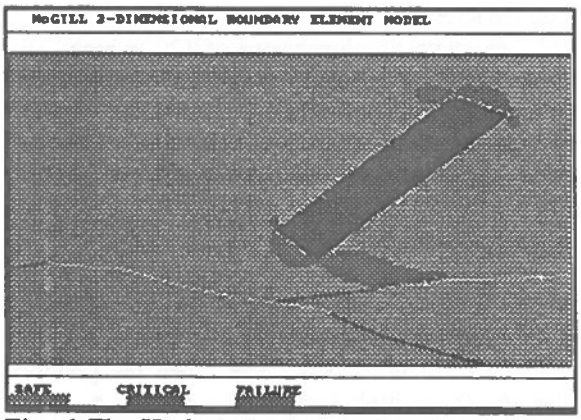

Fig. 6 The Hoek & Brown's safety factors of the rock mass - case 4

The results of the four mining sequences with backfill simulation are presented in the curves in Figures 7 to 12. A discussion of the results is given below.

For simplification in the discussion below, the NB fault is divided into three parts and named as follows 1: elements 1 to 26 in left side are named L, elements 27 to 56 in right side are named R1 and elements 57 to 80 in right side are named R2. These three parts are presented in the figures by two separate lines on element 26 and 56.

Figure 7 shows the variation of the distribution of normal stress along the NB fault during the mining-backfill sequence of stopes A to D. Whereas the normal stress in part L does not change very much, in parts R1 and R2 it changes considerably. The normal stress in the right side is increased for the elements 26 to 32 and elements 57 to 65 and decreased for the remaining parts.

Figure 8 shows the shear stress along the NB fault during the mining-backfill sequences of steps A to D. The shear stress is increased in the three sections, these are: elements 1 to 5 in part L, elements 27 to 40 in part R1 and elements 70 to 80 in part R2. The first and third sections (elements 1 to 5 and 70 to 80) may have a regular release of energy since the normal stress is constant or decreased (Fig. 7) which makes it possible that energy will be released slowly. The second part (elements 27 to 42) may have a violent energy release since the normal stress increases (Fig. 7) and hence can prevent the gradual release of shear stress.Figure 9 shows the distribution of shear stiffness along the NB fault during the mining-backfill sequence. This particular figure shows the nonlinear behaviour of fault during the stress variation. The value of shear stiffness is increased significantly in three sections (element 1 to 5 in part L, element 27 to 42 in part R1 and element 65 to 80 in part R2). A comparison between Figures 8 and 9 show that the shear stiffness and stress are increased almost at the same zone along the fault. This explains how the nonlinear deformation analysis of the fault can lead to stress concentration zone along the fault.

Figure 10 shows the distribution of shear displacement along the fault. Shear displacement is increased in three sections significantly (elements 6 to 26 part L, elements 32 to 46 part R1 and elements 57 to 65 part R2). The comparison between Figures 7 and 10 show that the reduction of normal stress is situated almost at the zone where the shear movement appeared. The zone of elements 32 to 56 of part R1 has very high movement (between 2 to 12 times the peak shear displacement) which should be considered for support design.

Figure 11 shows the distribution of the normal stiffness along the NB fault. The area of increase of normal stiffness is almost the same as that where the normal stress is increased (Fig. 7). The sudden sharp decrease of normal stress occurred in the same area where the shear displacement exceeded the value of the peak shear displacement. As it is explained later (Fig. 9), the normal stiffness is decreased by a coefficient (*FK*) for the case of unlocked fault.

Figure 12 shows the distribution of normal displacements along the NB fault. This curve shows that the normal displacement has almost the same behaviour as normal stress (Fig. 7).
Figure 6 shows the safety factors in the rock mass using Hoek and Brown failure criterion. The Hoek and Brown parameters were determined as follows:

$$m = 2 \quad s = 0.5 \qquad \sigma_c = 160 \text{ MPa}$$

The contours of safety factors show that the failure and critical zones are located between the corner of stope D and the NB fault.

CONCLUSION OF THE CASE STUDY

The results of the case study undertaken at the 2300 level, No.1 mine are presented in Fig. 13. The explanation of the results is given below:

(a) The zone of intersection of two branches of the NB fault has a potential of rockburst which should be monitored by seismometric station.

(b) The second zone which is in the middle of parts R1 and R2 shows a significant shear and normal displacement movement. The control on this zone movement may be improved by installation of cable bolt support. Also, the monitoring of extensometer would be useful for the controlling of movement.

Comparison of results showed a good agreement with what is being observed in the mine.

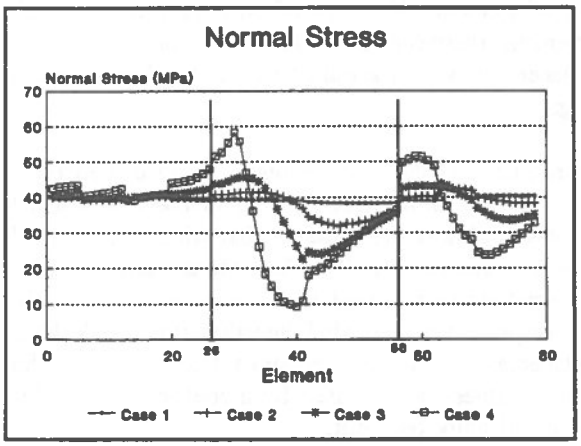

Fig. 7 Normal stress distribution along the NB fault

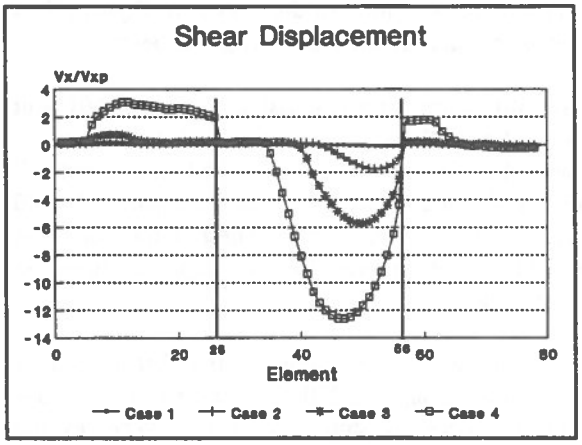

Fig. 10 Shear displacement distribution along the NB fault

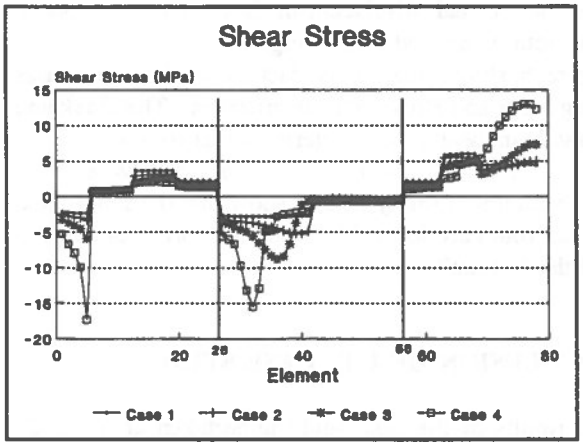

Fig. 8 Shear stress distribution along the NB fault

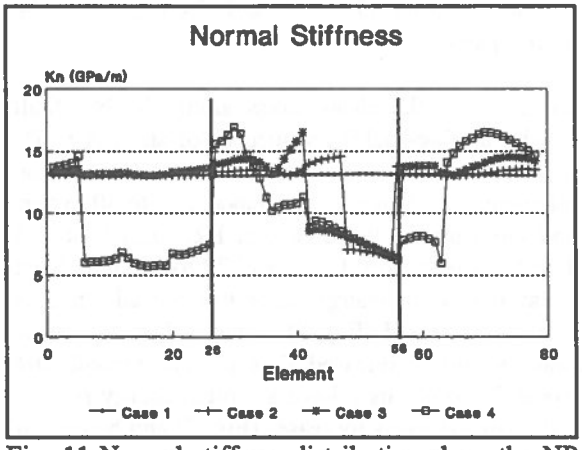

Fig. 11 Normal stiffness distribution along the NB fault

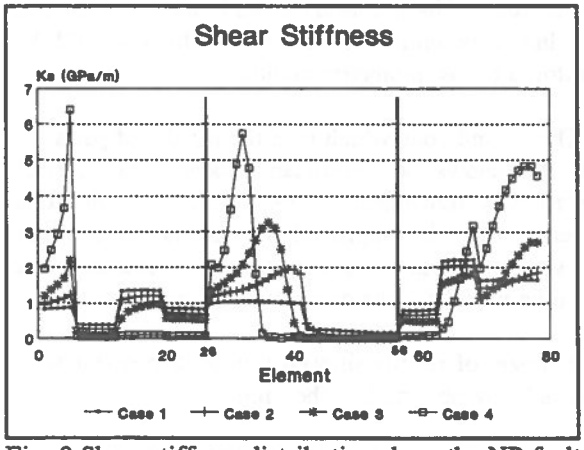

Fig. 9 Shear stiffness distribution along the NB fault

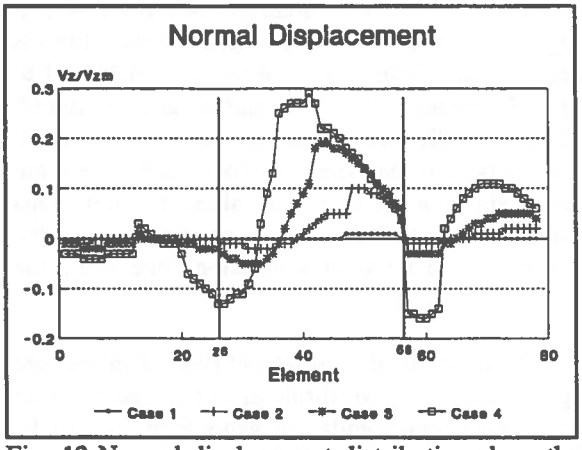

Fig. 12 Normal displacement distribution along the NB fault

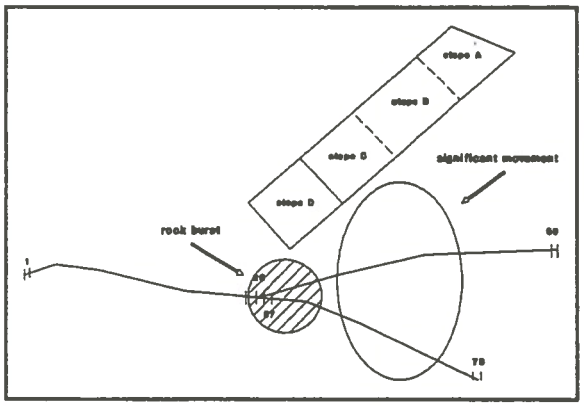

Fig. 13 Conclusion of the results of case study of 2300 level No.1 mine

SUMMARY

The behaviour of the NB fault and the rock mass at the 2300 level of the No.1 mine, Kidd Creek Mines, Timmins, Ontario was examined by numerical modelling using SATURN software system. The characteristics of the faults NB and NC at levels 2300, 2400 and 2500 were collected from the field using "tilt" test, "Schmidt hammer" test and direct measurements of thickness. The result of field tests are presented and the average values are used for the modelling work.

Backfill is modelled by applying normal stresses on boundary of pillar-stope. The numerical modelling technique is based on simulating four different cases representing mining-backfill sequence of four stopes. SATURN is used for treating all data files and results are presented graphically.

The discussion of results is presented in Fig. 13 which shows a zone of significant movement along the fault and also, an improvement of a zone with a potential of rockburst. The comparison of results of SATURN with both observations and the seismometric events in the field shows good agreement.

The following conclusions can be drawn from this case study:

- Stress and displacement distributions around underground openings are significantly effected by the presence of discontinuities in the rock mass. This class of the problems is analysed more conveniently with boundary element methods.

- The boundary element method can be developed to accommodate both nonlinear mechanical behaviour and nonlinear peak strength of joints.

- It appears that rock mechanics numerical models would be more powerful when they are completed with experimental models that are derived after years of dedicated research both in field and laboratory.

ACKNOWLEDGEMENT

This work has been funded by a research grant from the Natural Science and Engineering Research Council of Canada (NSERC). The authors are grateful for NSERC's financial support. The authors wish to thank the mine staff at Kidd Creek mine for their help and for providing the data.

REFERENCES

Fotoohi, K., 1993
Nonlinear Boundary Element Analysis of Rock Mass with Discontinuities, Ph.D. Thesis, McGill University, Montreal, Canada.

Goodman, R. E., 1976,
'*Methods of Geological Engineering*', West, St. Paul.

Barton, N. R., Bandis, S. and Bakhtar, K., 1985
'Strength, deformation and conductivity coupling of rock joints', *Int. J. of Rock Mech. and Min. Sci. & Geomech. Abstr.*, **22**, 121-140

Yu T.B., and Quesnel W.J., 1984
'*Applied rock mechanics for blasthole stoping at Kidd Creek Mines*', chapter 4

Henning J.G., 1991
'Analysis of south zone sill pillar rock bursting - part A', *Falconbridge Limited, Kidd Creek Division, Internal report*

Yu T. B., and Counter, 1983
'Backfill practice and technology at Kidd Creek Mines', *Canadian Mining and Metallurgical Bulletin*, August

Real Time Geomechanical Monitoring at the Waste Isolation Pilot Plant

Jackie L. Francke, Rey C. Carrasco, Robert E. Lewis, Dennis E. Mathieu
Westinghouse Electric Corporation
Waste Isolation Division, Carlsbad, New Mexico, USA

ABSTRACT:

This paper describes the installation and operational capabilities of a recently installed CONSPEC 400 ground control monitoring system to be used in real time monitoring of underground geomechanical instruments. The system was installed at the Waste Isolation Pilot Plant (WIPP) in Carlsbad, New Mexico to monitor deformation and stress changes occurring in the rock over time. From a central operating station, the system can poll 15,000 points at a scan rate of 10 milliseconds and plot and display real time and historical data. In addition, alarms can be set to indicate significant changes in underground conditions. The acquired information enables immediate assessments of the underground to be performed and ensures that safe ground conditions are maintained using state-of-the-art monitoring techniques.

ABREGE:

Cet article décrit l'installation et les capacités operationelles d'un moniteur control, CONSPEC 400, qui a été installé recemment et qui peut (ou doit) être utilisé comme appareil de surveillance pour instruments de mesure géomechaniques installés sous terre. Ce système a été installé au Site de Stockage et d'Isolment de Déchet Nucléaire (Waste Isolation Pilot Plant—WIPP) à Carlsbad dans l'état du Nouveau Mexique, afin d'observer continuellement la déformation et les changements de contrainte (stress) dans la roche avec le temps. D'une station d'opération centrale, ce système est capable de mesurer et d'enregistrer 15,000 points de donnée dans une période de 10 millisecondes et simultanément, ce système est capable d'obtenir une image graphique en temps réel aussi bien que d'extraire des données historiques accumulées en mémoire. Il est en plus possible de régler les systèmes d'alarme dont cet instrument est dottés afin d'indiquer des changements significatifs dans les conditions souterraines. L'information aquisé par l'usage de ce système de surveillance (de pointe), permet l'évaluation immédiate et l'assurance à tout moment de la sécurité des conditions du sous-sol.

INTRODUCTION

The Waste Isolation Pilot Plant (WIPP) is being developed near Carlsbad, New Mexico, for the disposal of transuranic nuclear waste in bedded evaporite deposits 2,150 feet (655 meters) below the surface. WIPP was authorized by Congress in 1979 Public Law 96-164 to provide "... a research and development facility to demonstrate the safe disposal of radioactive

wastes resulting from the defense activities and programs of the United States exempted from regulation by the Nuclear Regulatory Commission." To fulfill this mission, the U. S. Department of Energy (DOE) has constructed a full-scale facility to demonstrate both technical and operational principles of the permanent isolation of transuranic waste. The facility design also utilizes past in-situ studies and experiments in salt.

WIPP Geomechanical Monitoring Program

The WIPP Geomechanical monitoring program was started in 1983 during the construction phase. During this time, data was being collected for design validation of the underground workings. As part of the site and preliminary design validation process, a monitoring system was installed in the underground for collection of geomechanical data. Following the completion of the construction phase, the geomechanical data collection was maintained and additional instrumentation added to the system.

The focus of the geomechanical monitoring program was switched from design validation to routine monitoring of deformation and stress changes occurring in the underground excavations. The information collected provides assessments of the stability and performance of underground ground conditions and contributes to the initial interpretations of long-term behavior of underground openings.

Over time, the number of instruments have increased to over 1000 instruments and consist of remotely read, borehole extensometers, load cells, strain gages and piezometers and manually read convergence points. Instruments are read on a routine basis and reported in annual reports.

CONSPEC 400 Ground Control Monitoring System

In 1994, as part of an on going Interagency Agreement between the Department of Energy (DOE) and U.S. Department of Interior, Bureau of Mines (USBM), a ground control monitoring system (GCMS) was installed for real time monitoring of underground conditions at the WIPP.

The remote GCMS was initially developed by the USBM to study the effects of state-of-the-art, high-speed, automated longwall mining on ground stability under various geologic conditions. The GCMS was installed to monitor in real time the effect of rapid mining on pillar and face loading, stress redistribution in and around the longwall panel, and caving characteristics of the roof conditions (Hanna, et al., 1991). The GCMS proved to be a valuable tool for detecting the location of high-stress zones, and warning of deteriorating ground conditions. The GCMS provided continuous data acquisition and virtually instantaneous update of field data within a comparable time frame. This immediate feedback is of vital importance when rapidly changing ground conditions exist in underground excavations.

The benefits and potential use of the GCMS for monitoring ground conditions in the underground at the WIPP were recognized and in July 1994, the CONSPEC 400 (CONSPEC Ltd.) Ground Control Monitoring System was installed, expanding the current geomechanical instrumentation system to include real time monitoring with state-of-the-art data acquisition techniques.

INSTALLATION

The GCMS can be divided into the surface and underground installations (Figure 1) connected together by a single fiber optics cable that originates at the central operating station and terminates at an underground mini station.

Underground Installations

The underground installations begin at the Waste Shaft collar where the fiber optics cable enters the shaft and terminates at a converter located underground. Data is converted from light to an electrical signal and vice versa by the converter. The underground operating station consists of a CONSPEC 400 system which serves as a backup to the surface central operating station, should communications between the central operating station and underground instrumentation be severed. The mini system consists of a 486, 33 MHz, IBM compatible with a 200 megabyte hard drive connected to a 500 VA uninterruptible power supply available if needed in the event of a power outage.

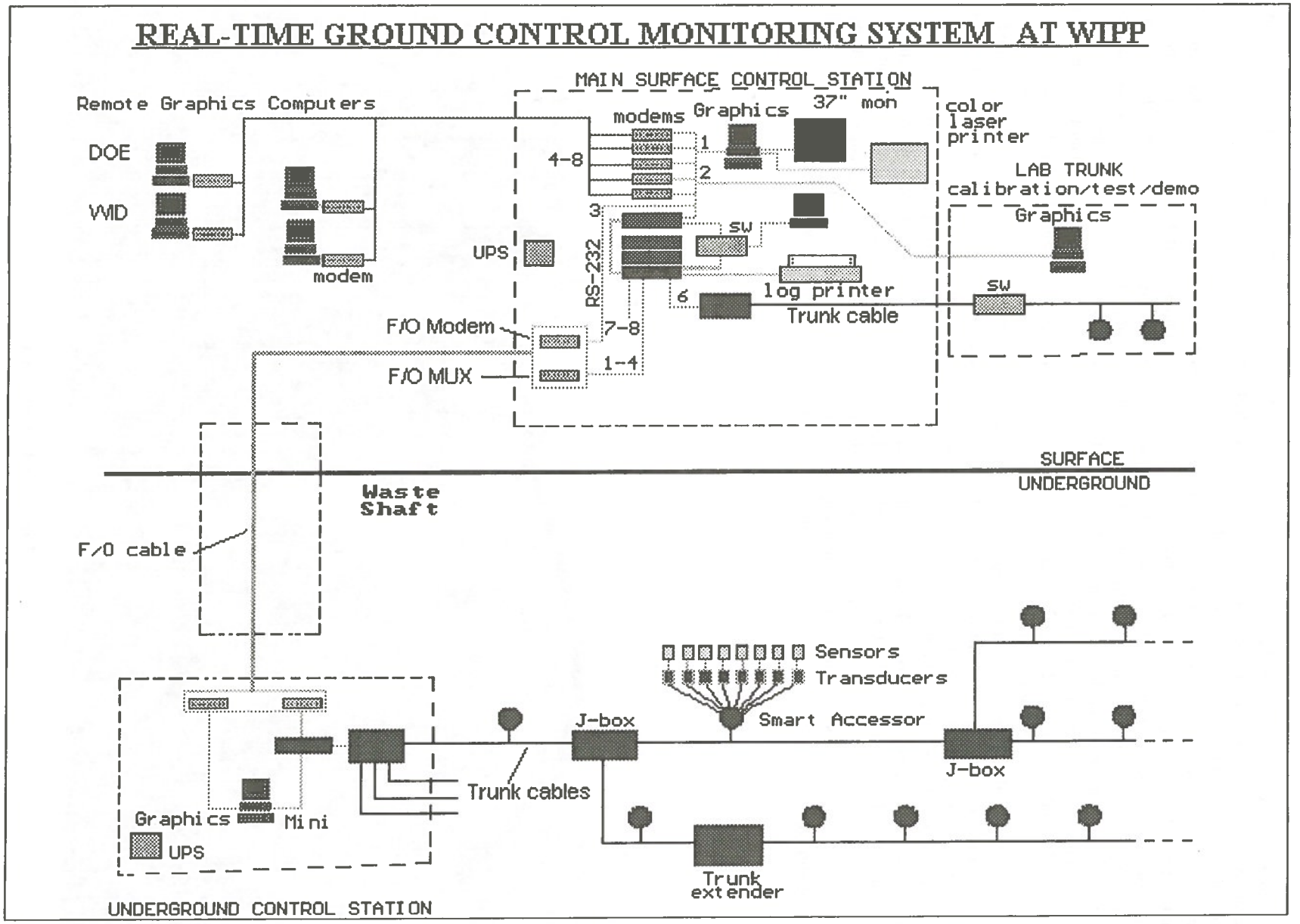

Figure 1 GCMS Flowchart

In addition to serving as a backup to the central operating system, the mini system maintains communications with underground accessors via trunk cables. Approximately 14,000 feet (4300 meters) of trunk cable have been installed throughout the underground, originating from the mini system and terminating at various locations throughout the underground. The trunk cable is a four conductor cable with two 12 AWG and two 18 AWG conductors. A 12 AWG conductor carries 24 VDC supply to the accessors, the second 12 AWG conductor acts as a common for the other three conductors. The two 18 AWG conductors serve as communication lines, one carries data in digital format from the accessors to the primary and the other carries digital data from the primary to the accessor. Logic levels for the communication lines are ten volts for a logic 1 and zero volts for a logic 0. Since the GCMS uses a seven bit address, each trunk is capable of accommodating 128 individually addressed accessors. Currently, there are three trunk cables running throughout the underground.

The accessors serve as multifunction analog to digital converters that are directly linked to the geomechanical instruments (Figure 2). During installation, each accessor is programmed with a unique address sequence that identifies itself to the system. The accessors convert instrumentation data from analog to digital status prior to transmitting to the converter located at the underground mini operating station. Currently, a total of 28 accessors are installed at various locations throughout the underground. The accessors range in capacity from one to sixteen channels. Communication from the central operating station to an accessor consists of a two byte word. The first byte is the accessor address and the second byte is the command to be executed, typically this will be a "read" command although not presently used at the WIPP, commandable devices can be connected to

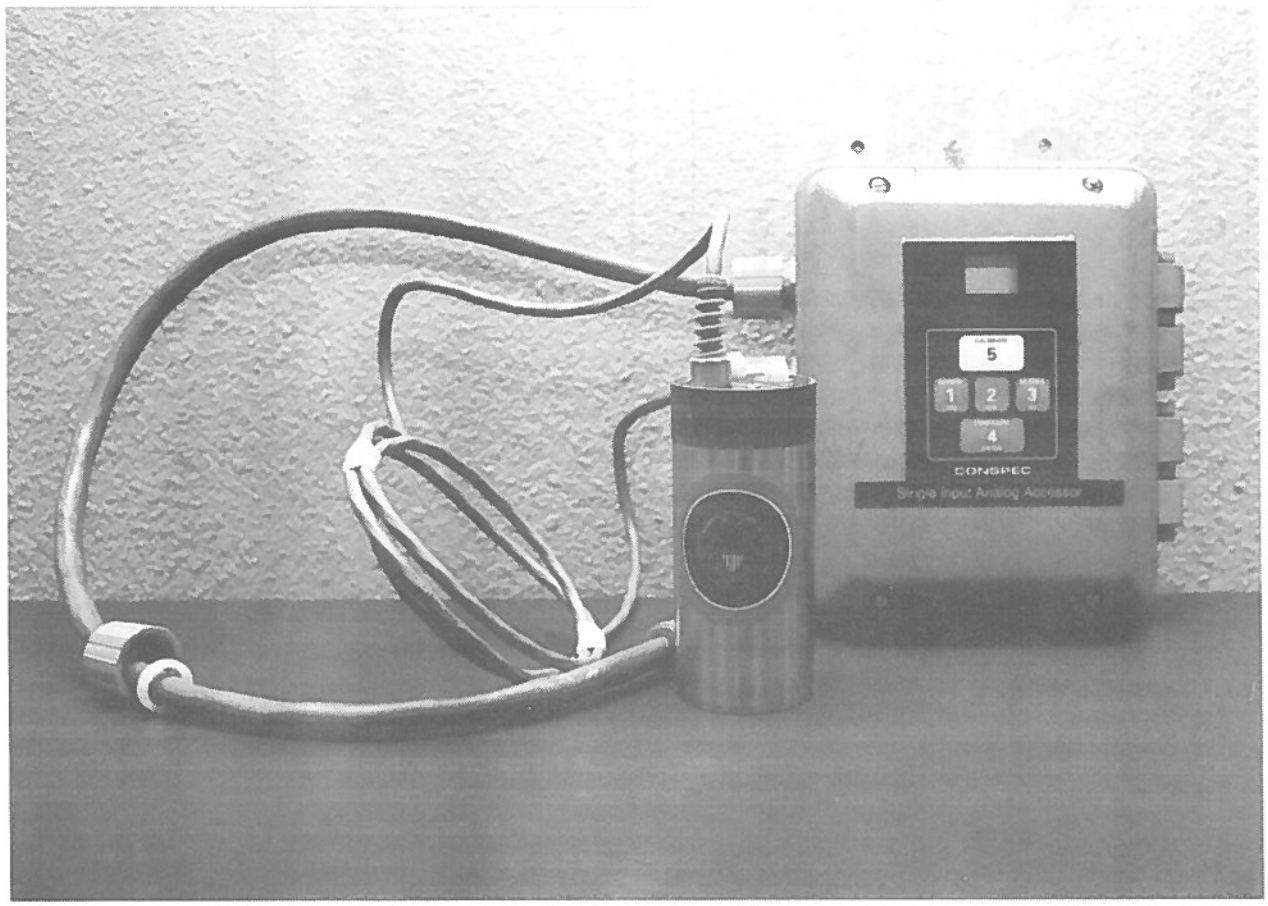

Figure 2 Typical Underground Accessor

the trunk that can be turned on and off under software controlled by the central operating station. The accessor will respond with two bytes, the first being its address or identification and the second being the data value.

Currently, both eight and twelve bit accessors are being used at the WIPP and a 16 bit accessor is under development. Each accessor contains a microprocessor and both volatile and nonvolatile memory. In addition, to microprocessor RAM, Erasable Programmable Read Only Memory (EPROM) is present and stores the accessor program which is automatically loaded upon power up or accessor reset. An Electrically Erasable Programmable Read Only Memory (EEPROM) stores individual instrument and accessor setup parameters. These parameters include instrument type (voltage or current), number of readings to average, and instrument span values. The parameters are entered by the user at the accessor location using the keyboard provided on the accessor box. In addition, the setup parameters are retained during a power outage. Upon the restoration of power, the EEPROM is read and the parameters are once again available to the microprocessor. The binary values returned from the accessors are converted to engineering units through the use of a multiplier termed the CFACTOR. The CFACTOR is internally calculated based on the range of the instrument and the accessor bit size as follows:

$$\text{CFACTOR} = \frac{A}{2^n - 1}$$

where n = bit size
and A = upper range of the instrument

The engineering value is then calculated as follows:

Engineering Value = binary value * CFACTOR

Currently, the accessors are monitoring vibrating wire extensometers, ultrasonic distance meters, pressure transducers, rockbolt load cells, and joint meters located throughout the underground.

Surface Installation

On the surface, a CONSPEC 400 operating station was installed. The central station is comprised of four computers, one 37-inch (94-cm) and two 20-inch (51-cm) color monitors, two printers and an uninterruptible power supply all housed in a four section console (Figure 3).

The primary computer is a 486, 33 MHz, IBM compatible with a 80 megabyte hard drive and serves as the primary processing unit that communicates with the underground accessors and continuously polls each accessor. As the heart of the GCMS, the primary computer polls continuously and saves only readings changed from the previous polling sequence. The changed readings, referred to as "change of state" readings are then automatically written to the second computer known as the multitasking computer.

The multitasking computer is a 486, 33 MHz, IBM compatible with a 450 megabyte hard drive that serves as a network file server. This computer enables up to sixteen remote users to view the data in plot format or in real time polling status at their remote stations. Although remote users have access to the stored change of state files, alterations to the data can not be performed.

The third computer is equivalent to the primary computer and serves as a stand-by to the primary computer should problems arise.

The fourth computer is a graphics terminal and is also considered a remote user. The graphics terminal is used to create and display a graphical representation of the data for each selected instrument and also provides data trending capabilities.

GCMS GRAPHICS

Using commercial software along with custom software developed by CONSPEC and USBM, a user friendly, menu-driven central operating station has been developed.

The system allows the operator to transfer data to other graphics software to enhance the data display capabilities. Color plots can be printed within a short time frame allowing immediate assessments of underground conditions to be performed.

All data information for the plots is stored on the multitasking computer which downloads the files to a graphics terminal upon initiation of the plotting commands.

Figure 3 CONSPEC 400 Central Operating Station

It is at the graphics terminal where alarm points can be set by the operator. An alarm editor provides the operator with the option to designate points that are not currently in view, but very important for immediate access.

The designated points, referred to as "alarm points" go into an alarm condition when the alarm criteria has been exceeded. A message is then displayed on the screen indicating an alarm. In addition, all alarm points within the system can be viewed by the operator. An instrument that is in an alarm mode will be highlighted in red. An instrument that is within the expected conditions is highlighted in green. While viewing all points, an individual point may be selected and a graph can be plotted showing the status of the point.

Currently, the alarm file on the GCMS can hold up to 100 alarm points and only one plot of an alarm point can be viewed at a time.

In addition to the alarm graphics, the GCMS allows the user to view the data as analog bar graphs, analog trend graphs, and contour plots.

Using the CONSPEC trending program, a remote user can extract the change of state files from the multitasking terminal and present data in a trend graph. The trend graphs show the historical values of the instrument.

The contour plots provide the operator with a three dimensional view of an area. Figure 4 shows a load distribution plot of a Panel test room using data from 286 rockbolt load cells. The load cells are currently monitored on the preexisting Geomechanical

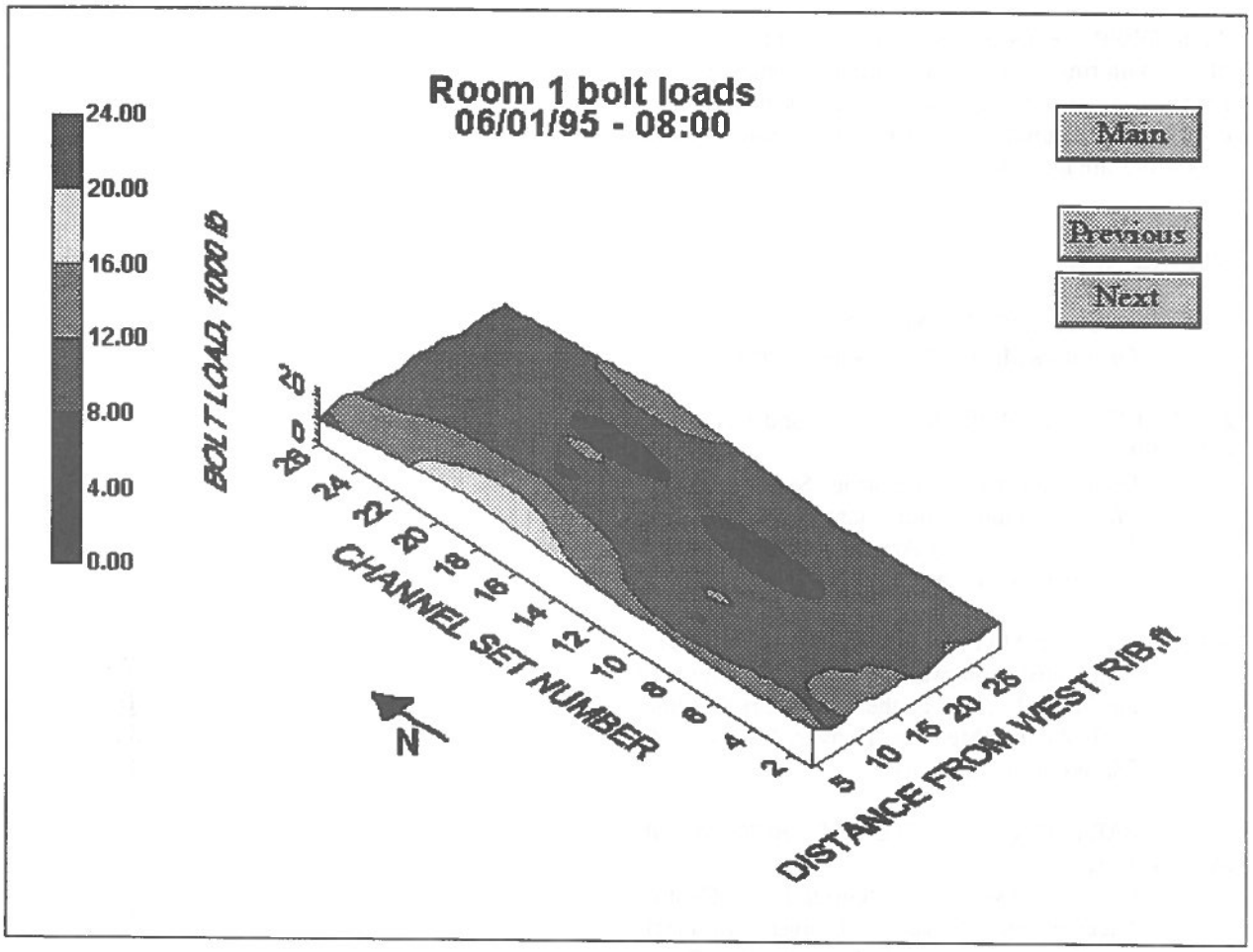

Figure 4 Load Distribution 3-D Plot of Panel Test Room

Instrumentation System and the data is converted for use on the GCMS.

CONCLUSIONS

Since the CONSPEC 400 ground control monitoring system has been installed less than a year, full capabilities have not yet been implemented. However, the GCMS has enhanced the preexisting instrumentation system with its real time monitoring techniques, alarm system, and immediate graphics capabilities.

Future enhancements to the system include:

- installation of additional geomechanical instrumentation to provide additional coverage of underground conditions,
- development of monitoring techniques to monitor microseismic instruments from the GCMS,
- enhancement of data analysis tasks to better understand rock behavior in the underground, and
- incorporation of live video to provide visual monitoring of critical areas.

Overall, the GCMS is a monitoring system that combines state-of-the-art mine monitoring with automated computer analysis techniques. In an environment where rapidly changing ground conditions may exist, such as in areas of active mining, the system serves as a valuable tool for detecting locations of high stress zones, and provides early warning of potential ground control problems.

At the WIPP, the GCMS provides an additional means of monitoring and evaluating geologic and geomechanical data necessary to assess underground conditions required to ensure that safe ground conditions are maintained.

REFERENCES

CONSPEC CONTROLS LIMITED,
Operators Manual, Downsview, Ontario

FRANCKE, J.L., CARRASCO, R.C., and CARNEY, C.B., 1992
Geomechanical Monitoring Sytstem at the Waste Isolation Pilot Plant, Carlsbad, New Mexico, CIM 94th Annual General Meeting, Montreal, April 26-30.

HANNA, K., HARAMY, K. and RITZEL, T.R., 1991
Automated Longwall Mining for Improved Health and Safety at the Foidel Creek Mine. SME Annual Meeting, Denver, February 25-28, preprint no. 91-165

U.S. DEPARTMENT OF INTERIOR, BUREAU OF MINES, 1991
Computer-Assisted Ground Control Management System, Denver Research Center, Denver, May, Technology News 381

Work sponsored by the U.S. Department of Energy under DOE contract No. DE-AC04-86AL31950.

CAMI'95: 3rd Canadian Conference on Computer Applications in the Mineral Industry
Montréal, Québec, Canada, October 22-25, 1995

Estimation of Surface Subsidence at the Waste Isolation Pilot Plant

Craig A. Givens, Miguel A. Valdivia, and Saeid Saeb
International Technology Corporation, Albuquerque, New Mexico, USA

Christopher T. Francke and Stanley J. Patchet
Waste Isolation Division, Westinghouse Electric Corporation, Carlsbad, New Mexico, USA

ABSTRACT:
Subsidence effects at the WIPP site were estimated using numerical methods as well as the influence function method and NCB method because a single universally accepted method is not available for salt. The use of parallel methods and the agreement between their results greatly enhanced the confidence in the analysis because the prediction would not depend on the assumptions inherent in a single method.

RÉSUMÉ:
Les effets d'affaissement a site WIPP etaient estimés en utilisant les méthodes numériques et aussi avec la méthode de fonction d'influence et la méthode de NCB. Ceci est à cause de non-existence d'une seule méthode acceptable universale pour le sel. L'utilisation des méthodes en paralleles et l'accord entre leurs resultats augmentent la confidence des resultats obtenue parceque la prediction ne dépend pas sur les suppositions inherentes d'une seule méthode.

1 INTRODUCTION

The Waste Isolation Pilot Plant (WIPP) is located in southeastern New Mexico about fifty kilometers east of Carlsbad. The United States Congress authorized WIPP in 1979 (Public Law 96-164) to provide "... a research and development facility to demonstrate the safe disposal of radioactive wastes resulting from the defense activities and programs of the United States..." The WIPP intends to receive, handle, and permanently dispose of transuranic (TRU) waste. To fulfill this mission, the U.S. Department of Energy is constructing a full scale facility to demonstrate both technical and operational principles of the permanent isolation of TRU waste.

The underground facility consists of (1) the main shaft area and associated access drifts; (2) a waste emplacement area to the south of the main shaft area that consists of eight panels of seven rooms each to be used for the disposal of TRU radioactive waste (only Panel 1 is presently excavated); and (3) an experimental area for non-radioactive experiments developed to the north of the main shaft area. Figure 1 presents a schematic view of the underground facilities at the WIPP site.

This paper investigates various computer and non-computer methods for predicting surface subsidence over the WIPP underground facility. It also compares the results of these methods to assess the level of confidence for applying these methods in bedded evaporite deposits.

2 GEOLOGY AND STRATIGRAPHY

The underground facility at the WIPP is located approximately 650 meters (m) below the surface in bedded salt of the Permian Salado Formation of southeast New Mexico. Figure 2 shows the generalized stratigraphy of the WIPP facility. Over 300 m of impermeable evaporite deposits separate the facility horizon from overlying sedimentary formations, and 600 m of evaporites lie below the facility horizon and provide a barrier against underlying Permian limestones and sandstones.

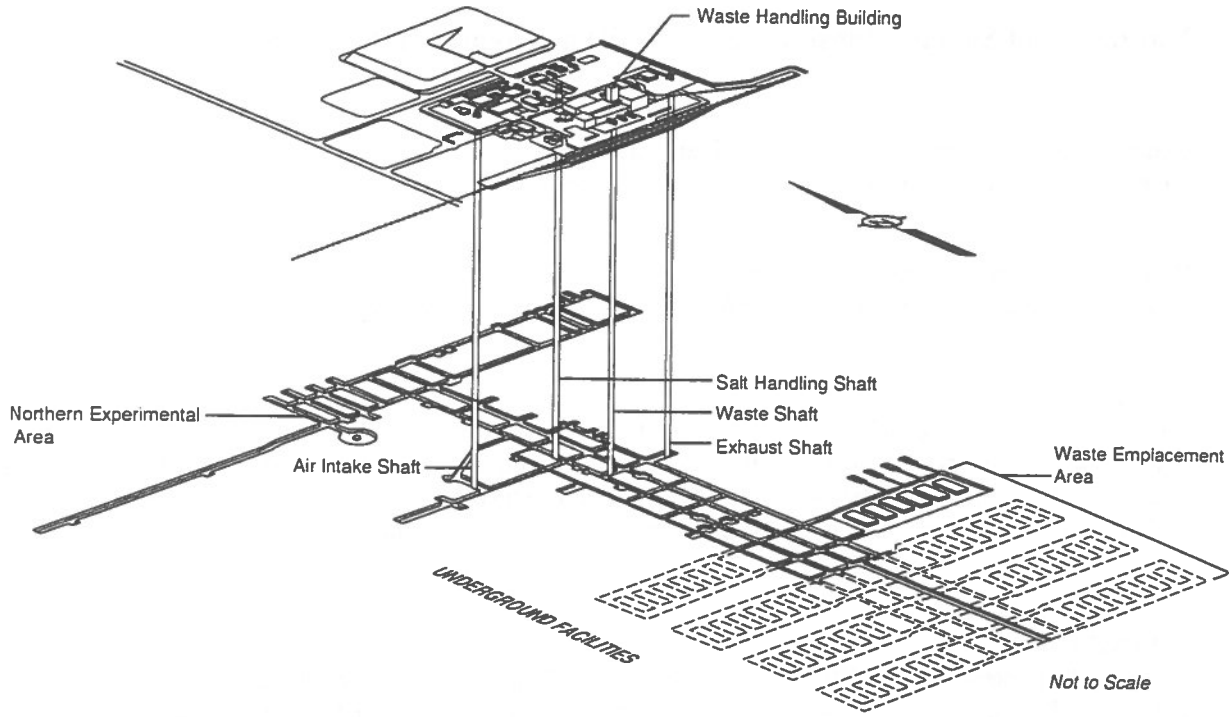

Figure 1
Surface and Underground Layout of the WIPP Facility

The facility horizon lies within an evaporite sequence consisting of halite, argillaceous halite, and polyhalite. Observations indicate that these beds are laterally continuous.

After excavation of an opening, stresses in the surrounding rock redistribute. In rock salt, the excavation responds initially by elastic deformation due to stress redistribution, and subsequently by inelastic, time-dependent deformation due to deviatoric stresses. As a result of this time-dependent behavior, known as creep, the surrounding rock mass tends to slowly move toward and into the opening.

3 BACKGROUND

Previous subsidence predictions for the WIPP site have been presented in published reports (DOE, 1980, 1990; SNL/NM, 1991). These predictions were based on various methods and present a range of maximum subsidence values from 0.09 to 1.0 m. Investigation of subsidence has been performed for potash and salt mining operations around the world (Bawden and Mottahed, 1986; Salas, 1979; Steed et al., 1985; Whittaker and Reddish, 1989).

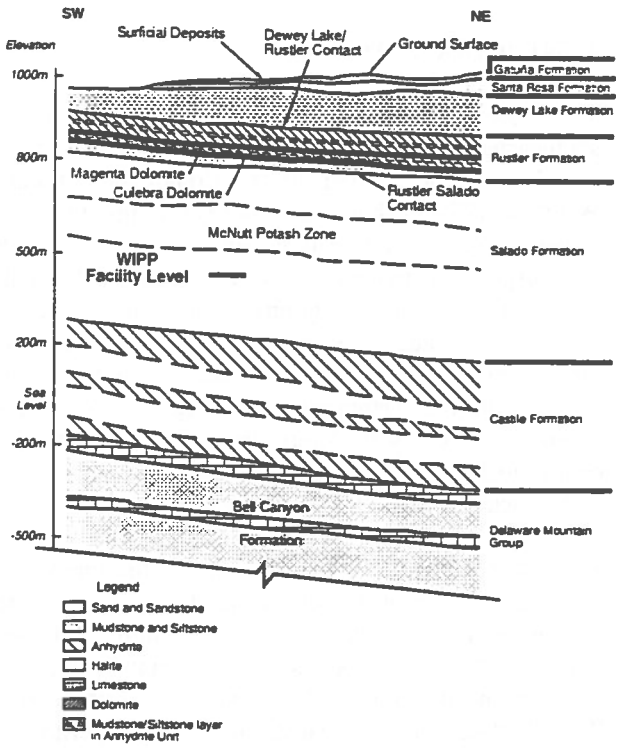

Figure 2
Generalized Stratigraphic Cross Section of the WIPP Site

The previous subsidence investigations in bedded potash and salt were reviewed to assess the subsidence prediction methods used and the applicability of each method to bedded evaporites.

4 SUBSIDENCE ANALYSIS

The amount of vertical surface subsidence expected to occur over the WIPP underground facility was calculated using three different computer and non-computer methods. A summary of the methods used and an analysis of their applicability to bedded evaporite deposits in southeast New Mexico are presented. The results of the subsidence prediction analyses for WIPP using these methods are also presented.

4.1 Subsidence Prediction Methods

This section presents calculational and computer modeling approaches performed to determine the surface subsidence over the WIPP underground facility. The influence function method estimates the amount of subsidence expected from the underground excavations. The National Coal Board (NCB) method (NCB, 1975) was also used for analysis of subsidence. A detailed description of the numerical modeling using the Fast Lagrangian Analysis of Continua (FLAC) code (Itasca, 1991) is also given.

4.1.1 Influence function method. The influence function method provides a profile of the expected shape of the subsidence trough and the lateral extent of influence on the surface subsidence. This method assumes that each point in an underground excavation has a circular region of influence on the surface subsidence around that point. Therefore, in an underground opening, neighboring extraction elements generate identical subsidence basins at the surface. By superimposing the influence of all extraction elements, it becomes possible to calculate the total subsidence of a given point at the surface. The limit angle determines the area of influence. The circle is centered on the surface and its radius is given by (Kratzsch, 1983):

$$R = H \cot(\gamma) \qquad (1)$$

where R is the radius of the influence area, H is the depth of the excavation and γ is the limit angle from the horizon. Within this influence area, the subsidence profile will gradually reach a maximum value, S_{max}. The maximum expected subsidence is a function of the dimensions of the workings and therefore is directly proportional to the seam height and the extraction ratio:

$$S_{max} = a\,M \qquad (2)$$

where S_{max} is the maximum value of subsidence, a is the extraction ratio, and M is the height of the underground opening.

4.1.2 NCB method. The NCB method is an empirical method based on case histories of coal mining in the United Kingdom. The NCB developed an extensive program of scientific study and investigation of coal mining subsidence in the United Kingdom during the period from 1950 to 1965 (NCB, 1975). Field investigations were set up, and detailed measurements were made of subsidence, lateral displacement, ground strains, and tilt in many different mining and geological conditions. In addition, comparisons were made between British and German experiences, knowledge, and observations of mining subsidence.

The NCB empirical method consists essentially of a series of tables of data, charts, and graphs from which subsidence data can be derived and which relate to specific mining situations. Graphs are presented to provide correction factors for these specific mining conditions, such as length of the panel, pillar size between panels, and time since excavation. The general geological conditions are not considered as an individual parameter, since most of the observations related to similar overburden (Whittaker and Reddish, 1989).

4.1.3 FLAC modeling. FLAC is a finite difference code used to calculate stress, strain, and displacements around modeled excavations. It is used here to calculate the amount of subsidence at the surface. FLAC software has been used to develop numerical models of the underground excavations at the WIPP since 1991. FLAC is a two-dimensional explicit finite difference code that simulates the behavior of rock and soil-like structures. The WIPP Reference Creep Law (Krieg, 1984) is built into FLAC and has been verified to Nuclear Regulatory Commission standards (Itasca, 1988). FLAC is distributed by Itasca Consulting Group, Inc., of Minneapolis, Minnesota.

4.2 Validation of the Methods Using Area Potash Mines

Potash mining companies and their consultants performed the majority of the investigations of

subsidence associated with potash mines in southeastern New Mexico. A summary of some of these reports and information received directly from the area potash mines is presented by Powers (1993). Subsidence observations from these WIPP area mines are extremely valuable for estimating the ground reaction and the amount and extent of surface subsidence to be expected over the WIPP underground.

Although the WIPP site is comparable to the potash mines in southeastern New Mexico, there are differences in stratigraphic position, depth, extraction ratio and layout. However, the overlying stratigraphic units are similar, as is the surface topography. The depth of the WIPP repository (approximately 650 m) is greater than the depth of most of the area potash mines. The extraction ratios within the potash mines are typically about 65 percent or greater with local extraction ratios approaching 97 percent in certain cases. The proposed WIPP extraction ratio is about 22 percent (SNL/NM, 1991), which is much lower than the area potash mines and should produce much less subsidence at the surface.

The potash mines of southeastern New Mexico have investigated ground-control problems in the upper Salado Formation for more than 60 years and surface subsidence for more than 40 years. The potash mines have used conventional room and pillar mining, secondary mining where old pillars are removed, and modified long-wall mining methods. Mining techniques used include drilling and blasting, as well as the use of continuous mining machines.

Large-volume underground mining commonly produces measurable surface subsidence. Within the Carlsbad Potash District, mines have demonstrably caused surface subsidence, resulting in fractures at the surface, ponding, road- and railroad-grade subsidence, and other effects. The principal mine subsidence data consist of networks of surface leveling baselines. In 1977, the National Geodetic Survey (NGS) established a baseline over large areas of southeastern New Mexico, including the WIPP site and some potash mines. A re-survey by NGS in 1981 revealed broad changes in elevation. The mine baseline and networks show much larger and rapid response due to high extraction ratios. Surface subsidence over a panel that has undergone secondary mining can begin within days to weeks and can be generally complete within about two years. Tension within surface rocks, as well as more readily observed subsidence, occurs within an angle of draw of about 35 degrees (measured from the vertical).

No local mine identically compares to the WIPP, but the subsidence data collected from area potash mines provide some insight into the expected surface subsidence conditions at the WIPP. The potash mine data were used in this study as a benchmark to validate the Influence Function and NCB subsidence prediction methods for the stratigraphy associated with the WIPP site.

In order to verify the applicability of the method to the particular stratigraphy found near the WIPP site, the Influence Function and NCB methods were applied to one of the potash mines located near the WIPP site. Two profiles, representing two different areas of the potash mine and two different mining methods, were used to check the applicability of the methods to mining in the WIPP area.

The first profile, Profile A, represents a modified long-wall mining operation. The depth of the underground workings is 305 m, the panel width is 457 m, the initial height of the opening was 2.13 m and the extraction ratio is 0.92 (Powers, 1993).

The second profile, Profile B, represents a room-and-pillar configuration. The depth of the underground workings used in the calculations was 305 m, the width was 945 m, the initial height of the openings was 3.81 m and the extraction ratio was 0.83.

Assuming a limit angle of 60 degrees, the influence function circle for the underground workings of both profiles is calculated from equation (1) as:

$$R = (305\ \text{m})\ \cot(60°) = 176.1\ \text{m}$$

Using a computer-aided drawing system, the influence function circle was superimposed along the profile on a scaled layout of the underground excavation. The center of the influence function circle is placed on nodes along the two profile lines. For each of these nodes an influence factor is calculated. The influence factors were calculated for each node across the potash mine profiles and are plotted in Figure 3.

Field measurements of subsidence from the potash mine were used to compare the accuracy of the influence function method as applied to the potash mine stratigraphy. It is assumed that maximum subsidence was almost reached when the field data were taken. Figure 3 also presents the shape of the subsidence trough observed using the field measurements and provides a comparison with the predicted subsidence. The calculated subsidence along Profile A substantially

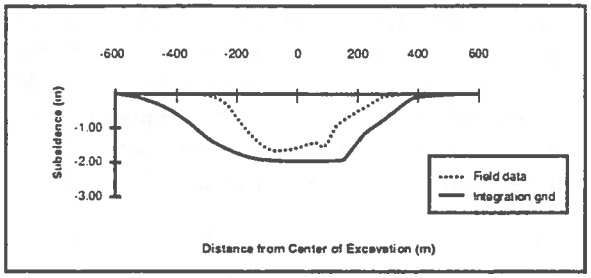

(a) Total Subsidence–Profile A

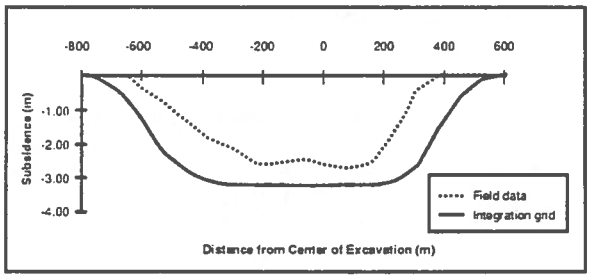

(b) Total Subsidence–Profile B

Figure 3
Comparison of Influence Function Method Results with Actual Field Measurements Across Potash Mine Profiles A and B

differs from the actual field data by overestimating the amount of subsidence observed. However, this profile is located in the corner of the mined area, which could limit the amount of observed subsidence.

Profile B is in better agreement, with the maximum predicted subsidence (3.16 m) being slightly greater than the maximum observed surface subsidence (2.80 m). The difference between observed and predicted surface subsidence may also indicate that subsidence activity is not yet complete. Because of the good agreement in subsidence profile and maximum subsidence between the influence function method and the field observations, the influence function method is expected to give reliable predictions of surface subsidence over the WIPP

The NCB method was then applied to the same two profiles. For the application of the NCB method, the area of pillars were ignored, and all of the underground workings were treated as a single panel. To do this, an "equivalent seam height" for the panel was calculated by multiplying the height of the opening by the extraction ratio yielding 1.96 m for Profile A and 3.16 m for Profile B.

For Profile A, the maximum subsidence was calculated by multiplying the equivalent seam height by the subsidence factor of 0.88 taken from a graph provided in the NCB Subsidence Engineers' Handbook (NCB, 1975). The subsidence factor was based on the depth and width of the mined panel. The maximum subsidence calculated was 1.72 m and the shape of the subsidence profile was predicted using factors provided by the NCB (NCB, 1975).

For Profile B, the subsidence factor was 0.95 because of the greater width of the excavation. The maximum surface subsidence was estimated to be 3.00 m. The predicted and actual subsidence profiles for both Profile A and B are presented in Figure 4.

Based on the results of this comparison, the NCB method appears to be a suitable tool for estimating total surface subsidence at excavations with high extraction ratios in the stratigraphy near the WIPP site.

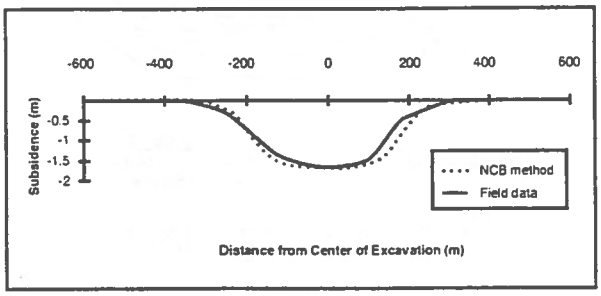

(a) Total Expected Subsidence–Profile A

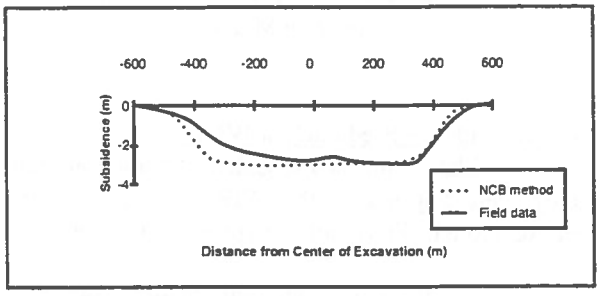

(b) Total Expected Subsidence–Profile B

Figure 4
Comparison of NCB Method Results with Actual Field Measurements Across Potash Mine Profiles A and B

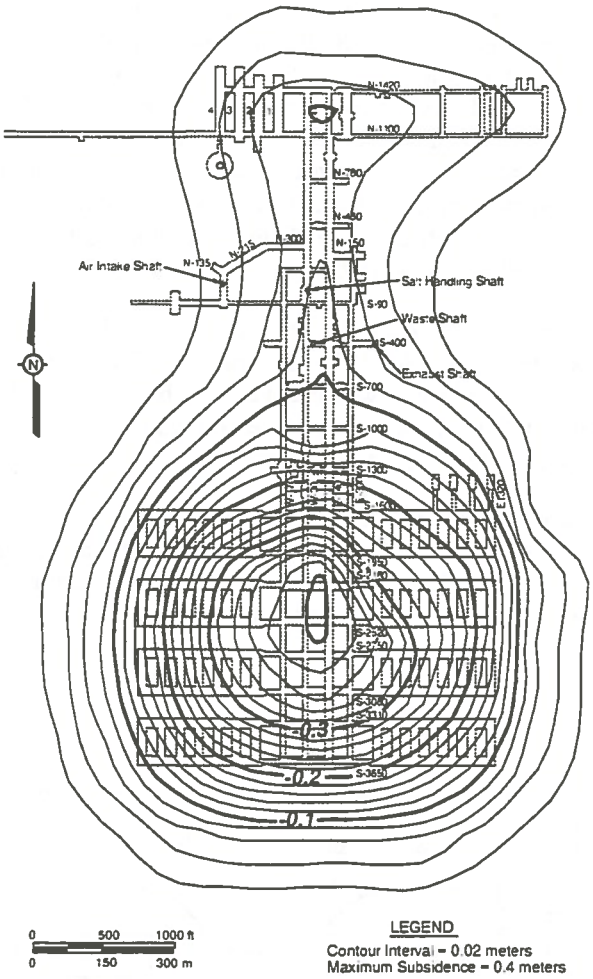

Note:
Present surface topography in this area varies by more than 3 meters.
Subsidence will not create a basin and should not be visible.

Figure 5
Contour Plot of Maximum Expected Surface Subsidence at the WIPP Site—Influence Function Method

4.3 Subsidence Prediction at WIPP

After validating the two subsidence prediction methods, they were applied to the WIPP site along with the FLAC model. The results are presented below.

4.3.1 Influence function method results. The graphical influence function method was applied to the WIPP site underground layout. Using a depth of 650 m and a limit angle of 60 degrees in equation (1), the radius of the influence circle is calculated to be 372 m. Again using computer-aided design software, the influence circle was placed over each of the difference nodes of a regular grid overlaying a scale drawing of the WIPP underground. The influence factor was calculated for each node of the grid. Multiplying the influence factors by the maximum expected subsidence, a layout of the expected subsidence is obtained. Figure 5 presents the predicted subsidence contours for the WIPP. The maximum expected subsidence in the WIPP underground would be in the waste emplacement area and is predicted to be 0.56 m if the rooms are empty and 0.40 m if the rooms are filled with TRU waste.

4.3.2 NCB method results. The NCB method was applied to the WIPP underground. The subsidence basin shape and magnitude for the entire facility were calculated by superposition.

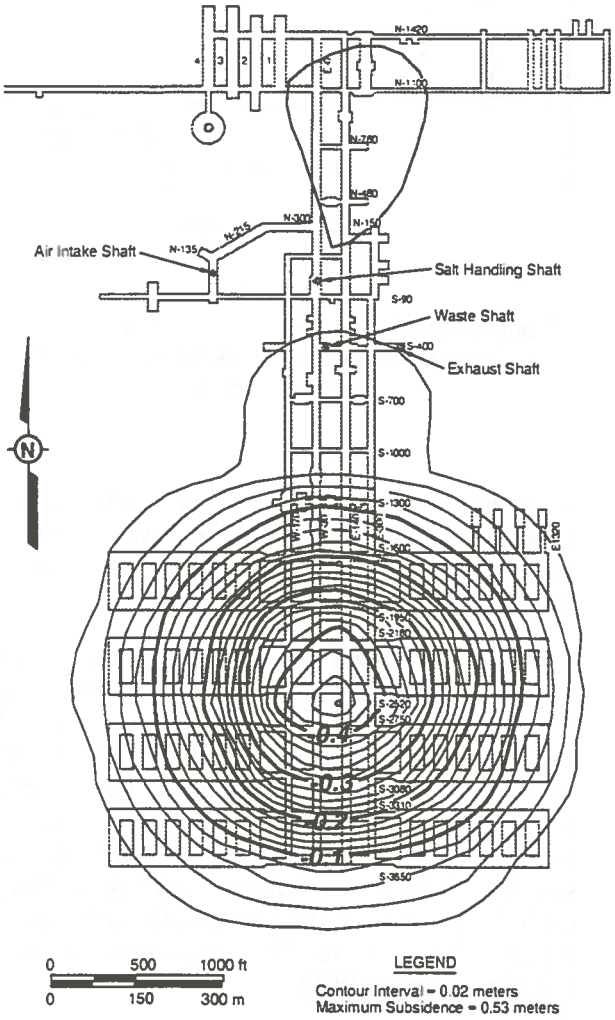

Note:
Present surface topography in this area varies by more than 3 meters.
Subsidence will not create a basin and should not be visible.

Figure 6
Contour Plot of Maximum Expected Surface Subsidence at the WIPP Site—National Coal Board Method

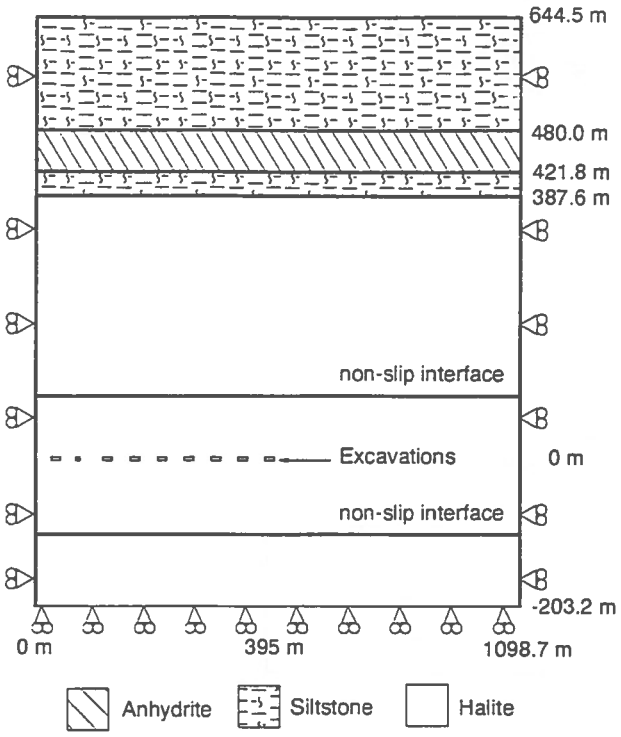

Figure 7
Subsidence Model Boundary Conditions
and Stratigraphy

Figure 6 shows the subsidence contour at the surface. The NCB analysis of the WIPP site reveals that maximum expected subsidence would occur over the waste emplacement area. The maximum expected subsidence in this area is 0.73 m assuming the area is empty and 0.53 m assuming the area is filled with TRU waste. 4.3.3 FLAC modeling results. A FLAC model containing two disposal panels and four access drifts (half by symmetry), was used to determine the curvature and depth of the subsidence trough. Figure 7 shows the boundary conditions and stratigraphy used in the model. The upper boundary of the model simulated the ground surface and was 644 m above the excavations. The lower boundary was 203 m below the excavations. The right boundary was about 740 m away from the right-most excavation. Boundary locations were selected so as to capture the shape of the subsidence trough.

The FLAC model was run to 380 model years. At that point, the maximum vertical subsidence was 0.48 m. The subsidence rate was about 0.4 millimeter per year. At 380 model years, the remaining volume of the excavations was about 12 percent of the original. An estimation of the final subsidence that would have been achieved was made by dividing the 380 model-year subsidence results by 0.88, giving a final maximum vertical subsidence value of 0.55 m. Table 1 summarizes the results of the model. Results are shown for the conditions at the ground surface, at the Culebra Dolomite level, and at a position 335 m from the edge of the panel, which is the distance of the waste shaft from the waste emplacement area. The 50-model-year and the estimated final values are given for all locations.

Figure 8 shows the shape of the surface subsidence trough at various times. Figure 9 shows the variation in shape of the subsidence trough with depth.

5 SUMMARY AND CONCLUSIONS

Each of the different methods used in the assessment were verified separately for use with the WIPP site stratigraphy. The influence function and NCB methods were validated against two case histories of potash mines in the vicinity of WIPP and found to be suitable for estimating total surface subsidence in bedded evaporite deposits in southeastern New Mexico.

Despite the fact that the different methods are based on very different principles, all of the prediction methods yielded comparable results (Table 2). The maximum subsidence was obtained for the case of empty panels at the waste storage area. The magnitude of subsidence over the WIPP facility predicted by these analyses is not expected to significantly affect repository operations.

Work sponsored by the U.S. Department of Energy under DOE contract No. DE-AC04-86AL31950.

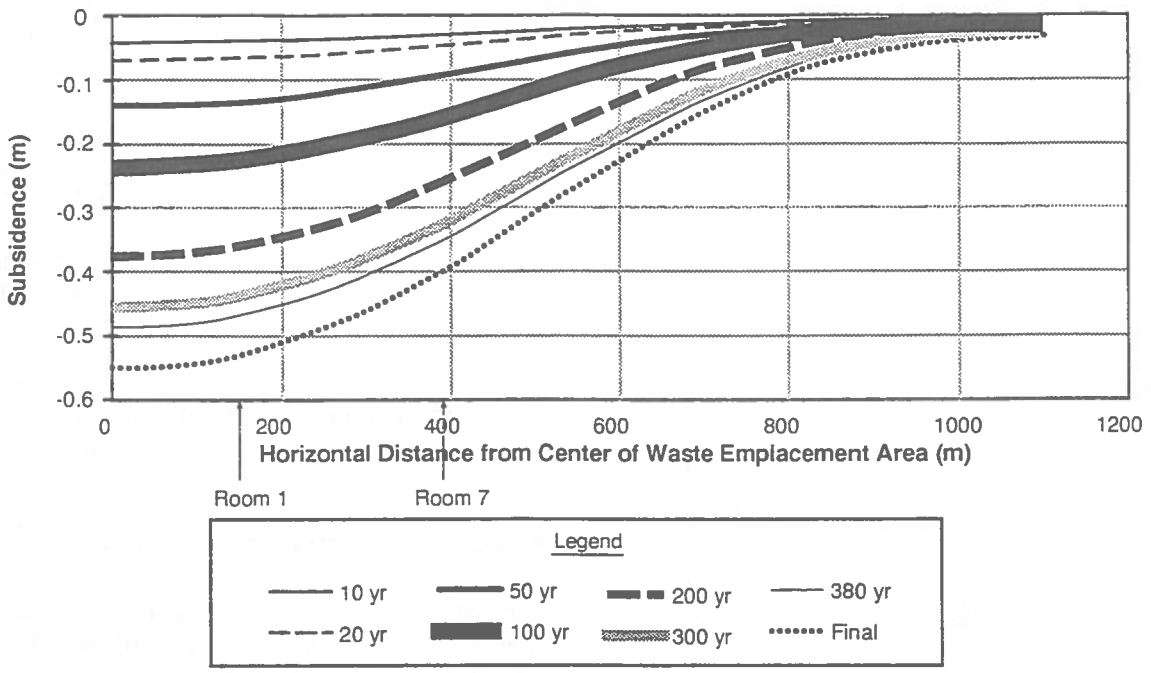

Figure 8
Subsidence Profile at Surface—FLAC Model

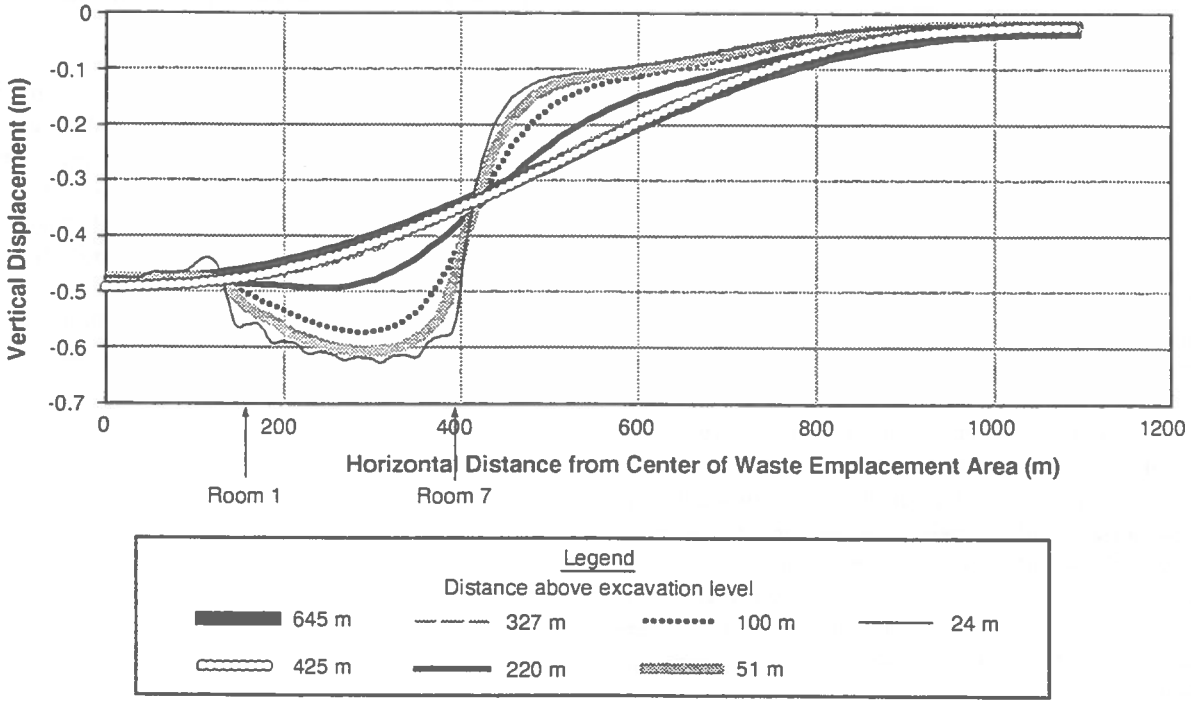

Figure 9
Subsidence Profiles at Various Depths–FLAC Model

TABLE 1 Summary of FLAC Full-Panel Model Results

Measurements at the Surface	Value	Distance from the Center of the Waste Emplacement Area
Maximum horizontal displacement (at 50 yrs)	4.4 cm	501 m
Maximum horizontal displacement (final)	14.1 cm	577 m
Maximum vertical displacement (at 50 yrs)	14.2 cm	0 m
Maximum vertical displacement (final)	54.9 cm	0 m
Maximum compressive horizontal strain (at 50 yrs)	-0.013%	63 m
Maximum compressive horizontal strain (final)	-0.035%	42 m
Maximum tensile horizontal strain (at 50 yrs)	0.011%	697 m
Maximum tensile horizontal strain (final)	0.053%	849 m
Maximum trough slope (at 50 yrs)	0.014 deg	418 m
Maximum trough slope (final)	0.048 deg	523 m

TABLE 2 Summary of Subsidence Prediction Results

Undeground Area	Contents of Excavation	Subsidence		
		Influence Function Method (m)	NCB Method (m)	FLAC Full-Panel Model (m)
Waste emplacement area[a]	Empty	0.56	0.73	0.55
	Waste only	0.40	0.53	N.A.
Shaft pillar area	Empty	0.10	0.04	0.13[b]
Northern experimental area	Empty	0.08	0.02	N.A.

[a] Waste emplacement area includes Panel 1 through 8; 2 through 8 are not yet excavated
[b] At the Waste Shaft

6 REFERENCES

BAWDEN, W.F., and MOTTAHED, P., 1986.
Comparison of three subsidence prediction techniques applied to Saskatchewan potash mining. Proceedings, 88th Annual Meeting of C.I.M., Montreal. Paper No. 89.

ITASCA CONSULTING GROUP, INC., 1988.
Thermal-mechanical benchmark testing of FLAC. *NRC-02-05-002*, prepared for the U.S. Nuclear Regulatory Commission, Division of Waste Management, Minneapolis.

ITASCA CONSULTING GROUP, INC., 1991.
FLAC user's manual. Minneapolis.

KRATZSCH, H., 1983.
Mining subsidence engineering. Springer-Verlag. New York.

KRIEG, R.D., 1984.
Reference stratigraphy and rock properties for the Waste Isolation Pilot Plant. *SAND83-1908*, Sandia National Laboratories, Albuquerque.

NATIONAL COAL BOARD (NCB), 1975.
Subsidence engineer's handbook. National Coal Board, London.

POWERS, D.W., 1993.
Background report on subsidence studies for the potash mines and WIPP site area, southeastern New Mexico. IT Corporation. Internal Distribution. Albuquerque.

SALAS, J.A.J., 1979.
Two subsidence cases in Spain. Proceedings, International Society of Rock Mechanics 4th International Congress on Rock Mechanics, Montreal, Vol. 3, pp. 369-373.

SANDIA NATIONAL LABORATORIES/NEW MEXICO (SNL/NM), 1991.
WIPP Performance Assessment Division (WPAD), preliminary comparison with 40 CFR part 191, subpart B for the Waste Isolation Pilot Plant, December 1991. *SAND91-0893*. Vol 1: Methodology & Results. Sandia National Laboratories, Albuquerque.

STEED, C., BAWDEN, W.F., COODE, A.M. and MOTTAHED, P., 1985.
Subsidence prediction for Saskatchewan potash mines. Proceedings, 26th U.S. Symposium on Rock Mechanics, Rapid City. Ed. E. Ashworth, A.A. Balkema, Boston.

U.S. DEPARTMENT OF ENERGY (DOE), 1990.
Final safety analysis report (FSAR), Waste Isolation Pilot Plant. *WP 02-9*, Rev. 0, U.S. Department of Energy, Washington, D.C.

U.S. DEPARTMENT OF ENERGY (DOE), 1980.
Final environmental impact statement (FEIS), Waste Isolation Pilot Plant. *DOE/EIS-0026*, U.S. Department of Energy, Washington, D.C.

WHITTAKER, B. N. and REDDISH, D.J., 1989.
Subsidence: occurrence, prediction and control. Elsevier Science Publishing Co., Inc., New York.

CAMI'95: 3rd Canadian Conference on Computer Applications in the Mineral Industry
Montréal, Québec, Canada, October 22-25, 1995

Application of the Inactive Mines Database

James B. Vance
Group Leader, Inactive Mines Project, CANMET, Elliot Lake Lab, Box 100, 99 Spine Road, Elliot Lake, ON, P5A 2J6

John R. Walmsley
Data Systems Specialist, Inactive Mines Project, CANMET, Elliot Lake Lab, Box 100, 99 Spine Road, Elliot Lake, ON, P5A 2J6

Marc C. Bétournay
Manager, Canadian Mining Technology Laboratory, 555 Booth St., Ottawa, ON, K1A 0G1

ABSTRACT

The Inactive Mines Database of CANMET is an advanced data management tool with implications for the full mining cycle, from exploration and production to decommissioning and long term monitoring. An in-house developed database management interface program provides access to digital documentation of inactive, abandoned and currently decommissioning mine sites in Canada. It includes knowledge based options for analysis of such features as crown pillar stability and tailings runout potential from the information in storage. Access to the database is possible for a range of communication links and microcomputer hardware by mining, civil, regulatory and scientific end users at remote locations. Details concerning the database and networking/interlinking capabilities will be discussed.

The documentation in progress covers mines in Ontario and Nova Scotia and includes: digital 3D mine models reconstructed from original mine drawings; surface features including tailings sites; selected files providing background details in text, drawings and photos about the site; historical information including production records, ground failures and environmental issues; research and/or engineering site reports related to shallow underground openings or tailings areas; and other pertinent data such as ownership, location coordinates, and GIS themes. Application of the database to case studies and its use in analysis of crown pillar stability and tailings runout potential is the focus of the paper.

RÉSUMÉ

La Banque de données CANMET des mines orphelines est un outil de fine pointe de gestion d'information touchant au cycle minier, de l'exploration à la production, à la fermeture et le suivi à long terme. Un logiciel d'interface créé à l'interne permet l'accès à la documentation digitalisée de mines canadiennes inactives, ophelines et en voie de fermeture. Celle-ci comprend l'expertise pour l'analyse, telle celles des piliers de surface, et l'étandue de la rupture de haldes stérile. L'accès à cette banque se fait à partir de liens de communication divers et de micro-ordinateurs en usage dans le domaine minier, civil, provincial ou scientifique, même en région éloingée. Les détails des fonctions du réseau sont présentés.

La documentation présentement disponsible traites des sites en Ontario et Nouvelle-Écosse et comprend: des modèles 3D digitalisés à partir de plans de mine; infrastructure, comprennant les haldes de stérile; autres détails du site en forme de textes, dessins ou photos; l'historique de la production, effrondrements, et sujets environnementaux; des rapports de recherches ou de comportements des piliers de surfaces, haldes de stérile; et autres information telles l'appartenance, coodonnées, et éléments GIS. L'application de l'information contenue dans cette banque sur des cas d'étude et l'analyse de piliers de surface et le potentiel pour l'écoulement de stérile est le point central de cet article.

INTRODUCTION

The responsibility for identifying and cataloguing hazardous mine sites often lies with various civilian agencies. Registering these sites is best performed using modern computing and database management technology which is capable of storing data pertinent to the large numbers of mines, range of mining practices and information for analysis or remediation. In Canada, this has lead to the development of a database by a federal government department, CANMET of Natural Resources Canada, in liaison with provincial authorities charged with responsibility for public safety in regard to inactive mines.

The project design facilitates application of CANMET's vast expertise in the areas of shallow stope stability issues, research into specific stability related subjects, numerical modelling, and application of dedicated instrumentation.

This effort, the Inactive Mines Project, is responsible for the development and maintenance of an advanced information archiving and retrieval system (IAMIIS, the InActive Mines Integrated Information System) comprised of a database of inactive mines and the user interface. The Inactive Mines Database (IAM Database) contains: literal description of mine features; spatial information in the form of maps and 3D models; important written records and references; and results of physical stability analyses and monitoring. The sites documented are based on priorities identified together with project partners, at this time, the provinces of Ontario and Nova Scotia.

The system allows access to the database by civil, industrial, regulatory and scientific end users at remote locations. The links may range from a remote site with only a basic computer and modem to an institutional user with advanced equipment, CAD software and experienced operators.

The IAM Database: provides secure, easily retrievable historical site information which could be required at any future time; facilitates analysis and decision making for present land use and rehabilitation requirements in view of the mining legacy; permits the use of dedicated methods as suggested by Bétournay, 1995, to assess stability; and promotes future analysis and development of improved land use and rehabilitation methods.

THE INACTIVE MINES INTEGRATED INFORMATION SYSTEM

The information system for the Inactive Mines Project meets the following requirements of the project's mandate:

- captures existing, relevant data
- provides easy, selective data retrieval
- possesses an adaptable database structure
- provides interface capabilities between the data and analytical/expert systems
- provides data that is current.

To meet these requirements, the Inactive Mines Integrated Information System (IAMIIS) was designed as a flexible system capable of evolution as the understanding of the impact of inactive mine sites on the environment evolves and as computer technology and its application to the treatment of this understanding progresses.

The system has three basic components as illustrated in Figure 1. Although they are functionally interdependent at the logical level, the development of one component can physically progress without modification of the others.

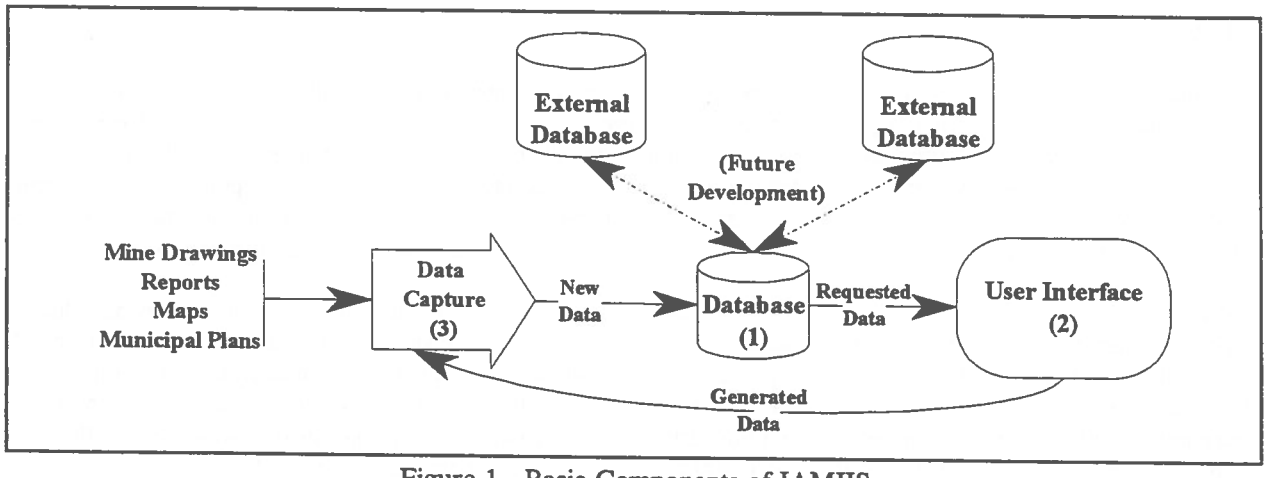

Figure 1. Basic Components of IAMIIS

INACTIVE MINES DATABASE STRUCTURE

The Inactive Mines Database is comprised of attribute data and documents data. Attribute data are singular characteristics which combine to describe inactive mine site. Documents data are literary and graphical representations of information concerning inactive mines which have been converted into digital format.

Attribute Data

Sets of attribute data which describe common themes or features are grouped into tables as shown in Figure 2. Each table contains an identifier, unique to the specific minesite, to for link all attributes which combine to describe that particular site.

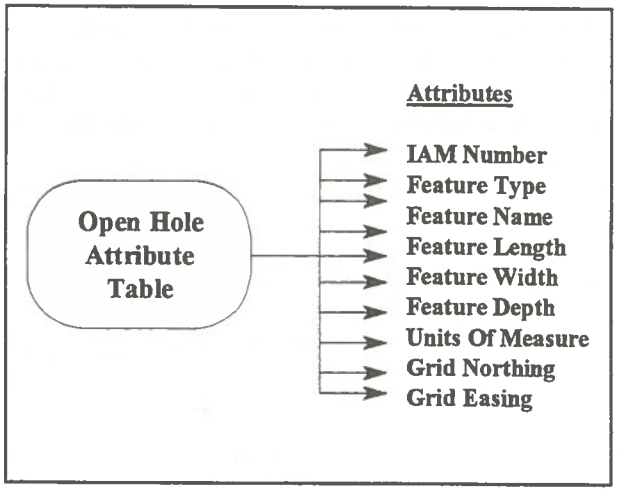

Figure 2. Example of an Attribute Table

It was beyond the scope of the project to define an exhaustive list of attributes of inactive mine sites. Instead, the database structure was designed to be open ended and was initially built around a core set of attributes. This flexibility is accomplished by the use of a *data dictionary*. The data dictionary is a file which contains a listing of the IAM attributes and their associated tables. To add an attribute to the database, a new record is appended to the data dictionary.

Because the client base will cover many disciplines and regions, a common nomenclature for the contents of the attributes can not be assumed. To provide a translation of terms used at the time of attribute data capture *dictionary tables* are provided. A dictionary table is a list of the terms used and an accompanying description for each term. The user can view the appropriate dictionary table to get a clear definition of unfamiliar words.

Documents Data

The documents data is comprised of four separate databases; text references, graphics references, GIS coverages and archived data. Figure 3 shows the structural relationship between documents data and attribute data. Text references are ASCII versions of reports, articles, memos and clippings which deal with inactive mines either specifically or generally. Graphics references are digital two dimensional and three dimensional vector drawings and imaged representations of inactive mines. GIS coverages are maps which geographically relate inactive mines and their features to their environment. Archived data mainly includes the imaged versions of text and drawings which have been converted to one of the other three types of documents data. The documents are individual files which reside on the system hardware for reference. The user has access to these documents through the user interface.

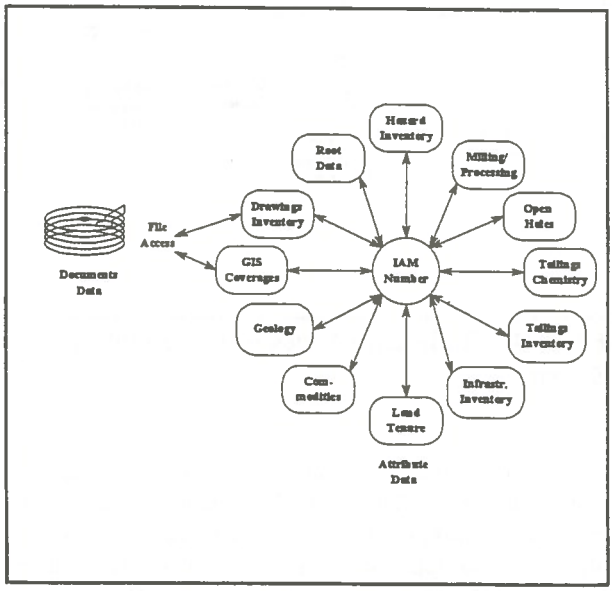

Figure 3. IAM Database Structure

User Interface

Access to the IAM Database is provided by the InActive Mines Integrated Information System (IAMIIS), a combination of in-house developed and commercially

available software depicted in Figure 4. This system provides a graphical user interface to the database. Users can perform complex queries of the attribute data to create *selection sets* consisting of only the data they wish to view. These queries produce customizable reports which display a listing of the available data for each site which satisfy the search criteria. If the user chooses to view the actual documents, the user interface will launch the appropriate software to display the selected format type. The interface also allows direct browsing of the documents database and manual selection of documents for viewing.

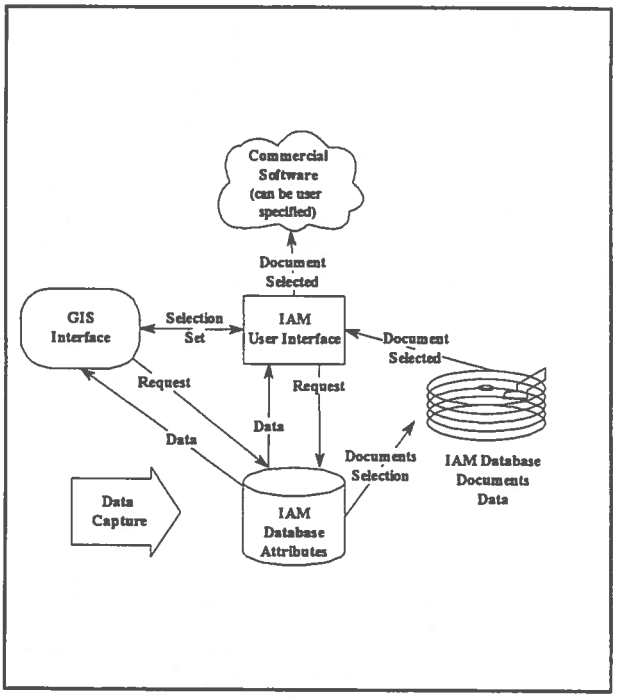

Figure 4. The Inactive Mines Integrated Information System

Creating selection sets using spatial search criteria is possible through a Geographic Information System (GIS). For spatial searches the user is presented with a map depicting geographic relationships and may create subsets of data which meet certain spatial criteria. The GIS is an information management system which also allows the user to perform certain types of queries of some of the attribute data which are not necessarily spatial in nature.

Access to the IAM Database

A wide range of options for obtaining information contained in the IAM database are available. The preferred mode is electronic linkup, which utilises the full capabilities of the system. However, it is recognised that some of the most significant situations in which the data may be of importance could be under conditions which preclude direct electronic access. Some information can be quickly sent by facsimile to a location which does not have the requisite computer capabilities for direct access. Provision of data for an emergency at a remote site not served by telecommunications or where outside communications have been interrupted, can be made by sending hard copies of the required information by air, including use.

At the present time, direct electronic access to the IAMIIS is provided via modem using "remote control" communications software. With remote control software the user takes control of a communications server located at the IAM office and linked to the IAM network. The only communication between the two computers is keyboard/mouse input from the remote computer and screen updates to the remote computer. No actual data is physically sent to the remote computer unless the user requests a permitted file transfer. Figure 7 illustrates this system.

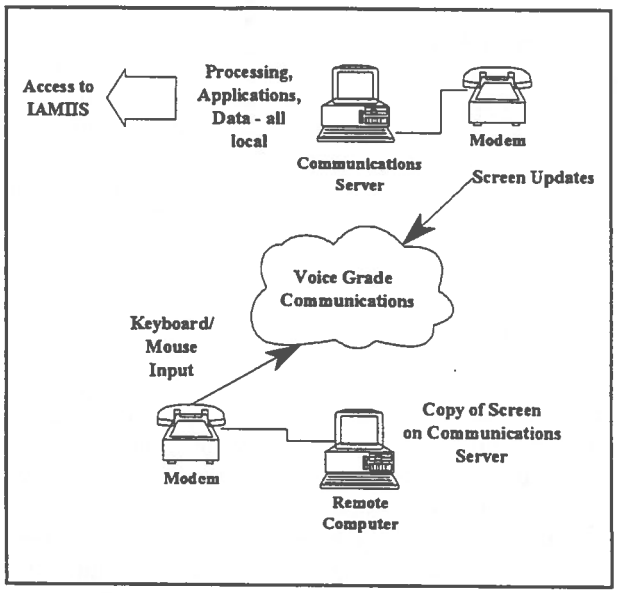

Figure 5. Remote Communications

The only requirements to use the remote control communication are: compatible software at host and remote terminal locations; SVGA graphics at the remote site; and high speed modems (9600 bps minimum).

This mode of communication makes the system available to any remote computer which has access to a phone line. In the near future the use of cellular phones and satellite phones will make the system available virtually anywhere.

APPLICATIONS OF THE DATABASE

As described by Vance et al, 1995, availability of the IAM database serves at least three important functions: the information can rapidly be made available to remote locations during an emergency; information may be provided to support planning for rehabilitation, alternative land use and municipal purposes; and technology transfer will support further research.

Support in Emergency Situations

Three types of emergency situations in which the IAMIIS could make an important contribution are: collapse of a crown pillar into shallow stopes underlying or near to surface infrastructure such as a roadway or building; breach of a tailings dam, threatening washout of a roadway and inundation of downstream infrastructure by liquefied tailings; and help in identifying the source of contamination which threatens the water supply for a community.

For these types of situations the Inactive Mines centre is able to respond to requests by provincial, municipal or other officials to provide supporting information. Under normal circumstances, within hours of the initial contact with a representative at the remote site, a computer link could be established and a graphical image detailing the area of concern could be available at the remote municipality. The full capabilities and modes of interaction will be largely dependant on the computer hardware and software at the remote site and the time availability, computer expertise and engineering knowledge of the onsite representative. With minimal capabilities, the field site can interact as a remote terminal of the Inactive Mines network with the Inactive Mines staff assisting in selecting the best graphics images for visualizing the scope of the problem and requirements for remediation.

Support for Planning

The IAM database is an important compliment to planning for such matters as site rehabilitation, alternative land use, municipal permitting and identification of existing hazardous situations. The database information on underground features provides knowledge of spatial relationships of shallow openings/crown pillars and usually will include a record of past instabilities. The location and nature of surface features such as mine and civil infrastructure and the location of spoil sites can be related both to the underground workings and to current land use plans under evaluation.

The database serves two main purposes in rehabilitation planning: it allows for assessment of rehabilitation requirements in the context of the local environment by relating all underground and surface features; and it enhances reliability of development plans, facilitating economic comparison of alternate rehabilitation schemes by providing information such as volumes of unfilled mine openings or volume and location of surface tailings.

For municipal planning purposes the IAM database will provide an important tool in exercising due diligence in evaluating land use proposals. It allows for rapid determination of potential hazards left by mining operations and examination of possible risks caused by encroachment of the planned use on the former mine site.

The IAM database will assist mining companies in evaluation of inactive sites being considered for acquisition as it facilitates assessment of outstanding environmental liabilities associated with the site. This information may be important in deciding whether or not to proceed and may enter into the consideration of the net value of the mineral rights

A major contribution of the IAM database to alternative land use planning is its ability to show both underground and surficial features, while containing important historical and reference information about the site. This can provide essential support for decisions involving routing of services and siting of structures. It will support planning for traditional civil projects such as road construction and residential developments, as well as support non-traditional uses such as geothermal heat recovery projects.

Technology Transfer for Research and Analysis Support

The IAM database provides an information base for research and development of dedicated methods to resolve the issues of inactive mines and their relationships with their environs. Future users such as mining companies, environmental consultants, civil engineers, universities and other researchers, may use the database as an aid in developing an improved understanding of the direct impacts of inactive sites and of rehabilitation methods.

Future opportunities for technology transfer in support of expert systems approaches to decision making include: development of new dedicated analytical methods for assessing physical stability; analysis of results of ongoing monitoring programmes and comparison of data to threshold values; integration of physical stability assessments with expert systems routines to aid in priorizing sites for rehabilitation; analysis of effectiveness of rehabilitation methods and review of cost effectiveness of alternatives for various classes of sites; and assessments for insurance purposes, such as economic comparisons of

probabilities of loss related to the cost of various risk mitigation alternatives.

CASE HISTORIES

Although still in the early stages of development, the IAM database has already seen use in the resolution of inactive mines issues. It has been used for planning of site investigations, identification of spatial relationships, planning for remediation purposes, and in at least one case was instrumental in identifying the potential of a hazardous situation due to an inadequate surface crown pillar.

Case History Number 1

The first case where the IAM database has contributed to remediation at an inactive minesite involves a former gold producer in Ontario. The underground workings at this site, which completed mining in the 1950's, were known to be in the vicinity of a road which is the sole land access for several northern communities and commercial developments. A review of the 3D site physical model revealed that the depth to the old mine workings was less than 10 metres. The location of the stope walls was not known as the available historical information was limited to level plans and a longitudinal section. More information was needed about its geometry and integrity in order to evaluate the safety of the roadway.

A two phase drilling program was undertaken at the site to more precisely identify the relationships between surface and the mine openings. The drilling confirmed that the original modelling of the depth of workings below surface was accurate (correct to within 0.3 metres). Figure 6 shows the relative location of surface, the road, overburden, stope outline and projection of drillholes.

The overburden was not shown on any of the drawings in the source documents and thus not incorporated into the graphics model. Drilling showed the overburden to be a thick layer of unconsolidated, incompetent coarse sand. The rock crown above the stope was relatively thin. Drilling also identified a zone of yielded ground, characterized by voids up to 0.3 metres wide, above the back of the stope. Under the western edge of the road barely more than 1 metre of rock support remains between the yielded ground and the unconsolidated overburden material.

Chips recovered during drilling showed the rock to be iron formation. The rapid drill penetration rate lead the drillers to report that the ground was "very soft". The walls of several of the holes were inspected with CANMET's downhole fibre optic video camera. This examination showed the rock to be highly fractured, jointed and locally foliated. Rust stains were seen extending from some of the fractures suggesting a high degree of oxidization of the iron minerals, probably due to water percolation through open fractures.

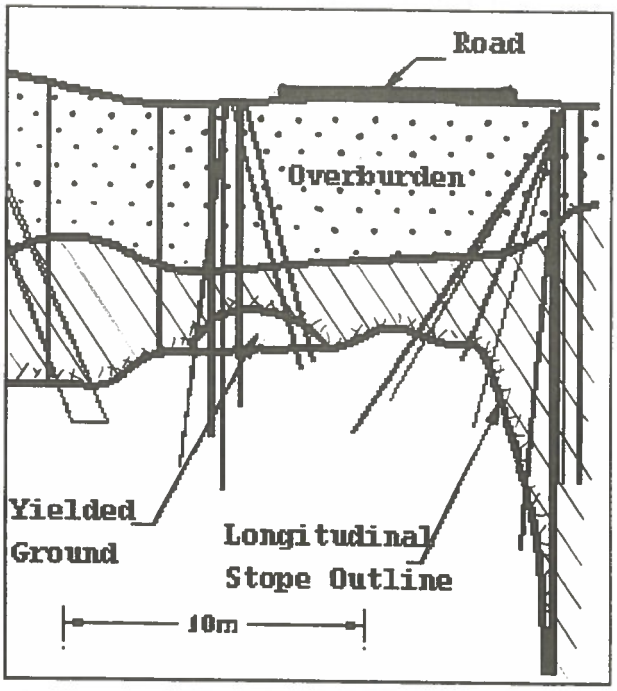

Figure 6. Longitudinal section showing location of road above mine workings.

The location data determined by drilling were incorporated into the site 3D model. An overlay was prepared to show the location of the stope outline superimposed on a photograph of the site taken from atop the headframe. This representation showed that the surface pavement of the road contained cracks running parallel to and about 2 metres outside the edges of the stope. Interpretation of the field data identified two potential failure mechanisms, plug failure and chimneying disintegration as discussed by Bétournay, 1995.

The identification and interpretation of the surface cracks as being related to the shallow crown pillar lead to an immediate meeting with the road owners. They made a decision that, since the safety of the road could not be assured, a remmediation plan would be developed. In the interim, visual inspection of the site was conducted twice daily by a competent official. Remmediation in the form of a bridging structure was completed several months later.

Case History Number 2

The IAM database has been usefully employed at another former Ontario gold producer where several public buildings and a road are located in close proximity to a shallow crown pillar. It has been necessary to identify the extent and immediacy of potential hazards. Figure 7 shows the relative locations of the features of concern.

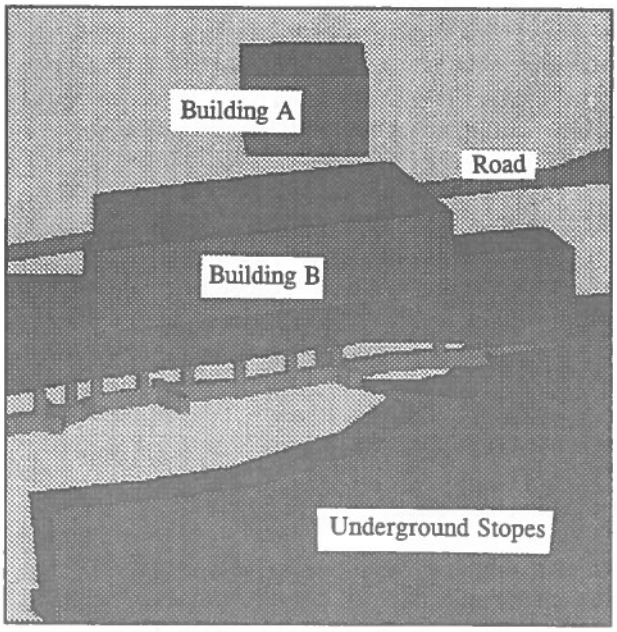

Figure 7. Perspective view showing relative location of features.

The 3D model from the IAM database helped to understand the spatial relationships between the buildings and the road with the underlying stopes. This allowed for strategic siting of drillholes to delineate the areas of concern with more precision and to evaluate the condition of the surface crown pillar. Information obtained from the drilling and resulting interpretations have been incorporated into the database.

A major element of the site work at this location has been the use of one of CANMET's dedicated methodologies, time domain reflectometry (TDR), to evaluate locations, types and rates of deformation of the surface crown pillar. The TDR method provides information about discontinuities in the rock mass and permits interpretation and analysis of the stability of the rock mass (Aston et al, 1994). The resulting information of the time dependant deformation produced by this method are of critical importance in evaluating the immediacy of requirements to ensure public safety.

The IAM database has provision for inclusion of the most recent data from instrumented studies such as TDR. With its easy access of up to date, site specific graphical and text information, the system is well suited to improve the time utilization of scientists and engineers involved in similar studies

Case History Number 3

The 3D model from the IAM database has been provided to a mining exploration company interested in the potential for finding additional ore reserves at an inactive mine site. Because the site was not decommissioned to modern standards when the former operator ceased mining, the potential buyer must evaluate the ore reserve in the context of any preexisting environmental liabilities as well as closeout costs related to future mine development.

As shown in Figure 8, the former operations at the site featured both underground and open pit mining. The prospective buyer has used the 3D model to better understand the relationships of the former mine workings with the environment.

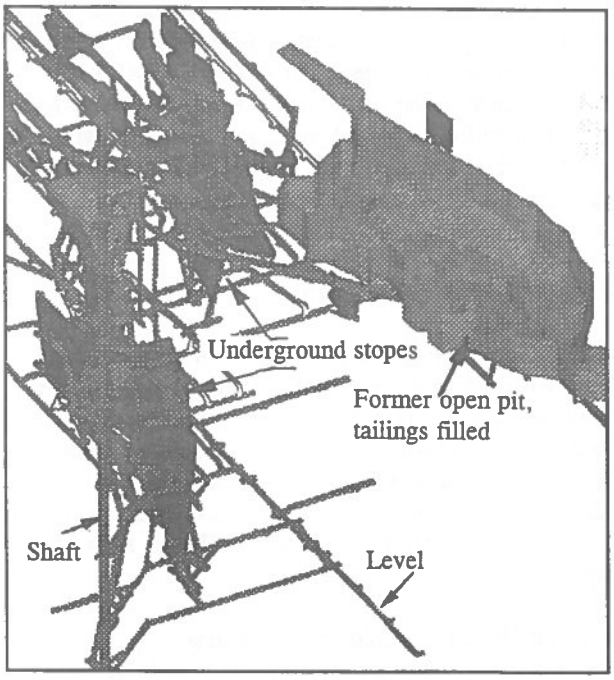

Figure 8. Perspective view of mine openings

This modern computer treatment of the site information also facilitates the visualization of trends in the geometry of the previously mined ore and could lead to identification of new drill targets.

Case History Number 4

Site information from the IAM database has been used by an engineering company for planning and evaluation of a project to recover geothermal energy via water stored in the underground workings of an inactive mine site.

The information allowed for determination of the spatial relationship between major volumes of underground openings with the target energy users on surface. It permitted layout of the most favourable locations for pumping and heat exchanger systems. It also provided for estimates of the volume of openings available for the heat storage reservoir.

This project evaluation showed a promising return on investment and implementation is now being considered by the energy consumers involved. As the project proceeds further, the IAM database information will become useful to the relevant municipal authorities who must exercise due diligence before permitting this usage.

If the heat recovery system is successfully demonstrated, there could be a potential to use the technique at a number of inactive mine sites within Canadian communities. The system could provide sufficient information for planning purposes as described here. In addition, IAMIIS is well suited to perform the search and list inactive sites which are not backfilled (ie suited to act as a reservoir) within a specified distance of a municipality for any geographic region covered by the database.

SUPPORT FOR ANALYSIS

IAMIIS has been developed with provision to support dedicated analytical methods for evaluation of the data. Analysis may be required to determine the potential hazards associated with a site. Tools already developed in the project for this purpose are the flow out distance of tailings model and an Autocad to numerical model interface to evaluate the rock mass. Future analytical tools could improve decision making.

Flow out Distance of Liquefied Tailings

The Flow out Distance of Liquefied Tailings model, described by Garga and Khan, 1995, provides a valuable tool to estimate and understand the downstream risk in the event of a breached tailings containment structure. Now that it is understood that the problems of acid mine drainage can be minimized by subaqueous deposition of acid generating mine wastes, the trend is towards more flooded tailings at active sites and at remediated inactive sites.

In their review of worldwide historical failures of tailings, Garga and Khan, 1995, found that flow out distances were independent of whether the breach of the tailings impoundment structure was seismically induced, or originated from other causes such as erosion after exceeding spillway capacity. The validation of the flow out calculation method by back analysis showed that it was equally valid for both seismically induced and non-seismic breaches.

The underlying principles of the flow out calculation method were developed by Lucia, 1981. Garga and Khan have adapted the method for application by computation of values entered in a commercial spreadsheet format. In future, the flow out algorithm may be incorporated in IAMIIS with provision to extract the required site parameters from the database (if available) and automatically perform the analysis.

Numerical Modelling

Part of the project has seen the development of an interface to import 3D mine drawings developed in AutoCAD®, to a format which can be processed directly by numerical modelling software. This translator, GEOGEN, creates files in the format of MINE DESIGNER, described by Thomson, 1993. These files in turn are directly used by the boundary element method for stress analysis, BEAP3D (YU et al, 1990).

Under applicable circumstances, numerical methods are an important tool for evaluation of stability of mines including shallow crown pillars. An important advantage of incorporation of the numerical modelling capabilities into IAMIIS is that, given availability of adequate rock properties for sites, processing may be performed to assist in judgement of the stability issues.

It is anticipated that future development will include provision of linkages to other rock mechanics analysis routines. Under consideration at the present time are interfaces to CANMET's block spring model, BSM, described by Wang, 1992.

RISK ANALYSIS AND EXPERT SYSTEMS

A logical extension of the use of the IAM database is in support of risk analysis and expert systems approaches to inactive mines issues. Input from risk analysis and expert systems will assist decision making by:

- identifying sites which may be hazardous
- priorizing hazardous sites for rehabilitation based on level of risk
- allowing for comparative assessment of site decommissioning strategies based on risk and cost factors

Identification of Hazardous Sites

Mackasey, 1989 discusses the problems and importance of identifying the "hidden hazards" related to inactive mines. The IAM database contains information which can lead to the identification of these hidden hazards where the seriousness of the problem had previously been unrecognised. This would be achieved by processing information in the database through custom algorithms which quantify the key characteristics of the site. Examples of this capability are the tailings flow out model and the numerical modelling capability, both previously described.

Using other information included in the database, the consequences of risk events may be assessed. Results of the risk of tailings flow out distance analysis would identify an area which could be inundated in the event of a breach. Where demographics information is available as a GIS coverage, the potential for direct effects on the population may be determined.

A future goal is to develop algorithms which would operate on ecosystem information in the database to evaluate potential physical and chemical consequences on the environment. The listing by drainage basin and sub- basin will permit rapid assessment of downstream areas which may be affected.

The estimation of ground stability using numerical and other analytical tools provides a measure of the potential risk to public safety through failure of shallow crown pillars. These methods allow a reasonable precision in delineating the area at risk, so that identification may be made of civil infrastructure which could be affected.

The database is an excellent tool for rapid identification of sites meeting specific criteria which may become recognized as an indicator of a hazard at some future date. The computer based information can be queried to locate and list all sites meeting the criteria.

Site Prioritization

The issue of site prioritization is important for establishing the relative urgency of rehabilitation needs amongst sites. It is sometimes necessary to establish a chronological sequence of rehabilitation works according to such criteria as immediacy of the problem, consequence of delays or availability of resources (crews, equipment, finances).

The database provides a framework by which an orderly ranking of sites can be performed using the expert systems approach. Ranking algorithms tailored to meet the needs of individual provinces can be developed. Once in place, the algorithm can be applied to all or any subset of sites.

Decommissioning Strategies

The IAM database supports the development of decommissioning strategies by facilitating a review of historical data and by the capability of filtering information according to specified criteria.

The historical information may be processed to reveal trends in decommissioning strategies. Suitably developed, it may permit quantification of cost/benefit ratios of alternative strategies for risk mitigation by various rehabilitation measures. Analysis of the records should reveal candidate strategies which have been successful under similar mining and/or mineralogical regimes, and may point out strategies which have been ineffective in the past and therefore not economically viable.

The potential correlations which may result from this orderly review of the database has important implications for present and future mining endeavours. It may provide a reasonable basis upon which to project feasible decommissioning methods for a prospective site, by comparing it to historical sites with similar mineralogical, mining or other parameters. If done effectively, this should expedite the permitting process by providing a sensible basis for development of the closure plans which most jurisdictions now require before advanced exploration can begin on the site. A sensible basis will also exist for suggesting reasonable levels of financial assurance if this is required as part of the permitting process.

CONCLUSIONS

The IAM database is an effective new tool for providing information related to the issues of inactive mines. The user is provided with an effective interface to permit easy and logical retrieval of the information.

The value of the system in contributing to added public safety has already been demonstrated at sites where remediation has been completed or is being planned. It has been of value in providing site specific background information to mining industry participants evaluating the economics of reactivating a former producing property. It has also contributed to the engineering design of a proposal to utilize old mine workings as a geothermal reservoir.

The system provides the tools and information to improve decision making regarding the decommissioning of mines through risk analysis and expert systems evaluations. These approaches should also expedite the permitting process.

REFERENCES

ASTON, T., BÉTOURNAY, M. C., HILL J., AND CHARETTE, F., 1994.
Application of TDR for monitoring the long term behaviour of Canadian abandoned metal mines. CANMET Report MRL 94-040(OPJ); CANMET; Natural Resources Canada.

BÉTOURNAY, M. C., 1995.
The stability of shallow stopes of hard rock mines. Ph. D. Thesis, McGill University, Montreal, Quebec. 611p.

GARGA, V. K. and KHAN,M. A., 1995.
Review and comparison of a deterministic/probabilistic model for estimating flow out distance of breached tailings. Report to MRL, CANMET, Natural Resources Canada.

LUCIA, P. C., 1981.
Review of experiences with flow failures of tailings dams and waste impoundments. Ph.D. dissertation, University of California, USA.

MACKASEY, W. O., 1989.
Concepts on Dealing with Abandoned Mine Hazards. International Conference Proceedings, Surface Crown Pillar Evaluation for Active and Abandoned Metal Mines, M. C. Bétournay, ed; Special Report SP89-5; CANMET; Natural Resources Canada. pp 135-141.

THOMSON, S., 1993.
Mine Designer - An automated graphical data generation program integrating numerical modelling with the mine design process. CANMET Report MRL 93-087(TR), CANMET, Natural Resources Canada.

VANCE, J. B., WALMSLEY, J. R. and BÉTOURNAY, M. C., 1995.
Inactive Mines Database, Sudbury '95 Proceedings, Sudbury.

WANG, B., 1992.
Introducing BSM. A computer program of the Block-Spring Model for analysing jointed rocks. CANMET report MRL 92-124(TR), CANMET, Natural Resources Canada.

Yu, Y. S., CLOSSET, L. and DEARING, J. A. C., 1990.
BEAP3D - A boundary element application package for three-dimensional stress analysis of mine structures. Proceedings of Specialty Conference, Stresses in Underground Structures, G. Herget, ed; CANMET, Natural Resources Canada. pp 140-150.

Stability Assessment of an Inactive Mine Using the Block-Spring Model

Baolin Wang, Yang S. Yu and Tim Aston
Mining Research Laboratories, CANMET, Natural Resources Canada, Ottawa, Ontario, Canada, K1A 0G1

ABSTRACT

This paper presents a study of an inactive mine in Canada, using a Block-Spring Model (BSM) to assess the integrity of surface crown pillars and that of the hangingwall/footwall related to the safety of surrounding structures. The effect of removal of the crown pillars on regional stability was also examined. The studies indicated that the near vertical narrow stopes were in a meta-stable state. The surface crown pillars were not crucial to the stability of the shallow stopes. Small displacements of the rocks were observed around the stopes even with the surface crown pillars removed. The stable condition of the stopes was considered to be due to the near surface proximity of the stopes, the very low regional horizontal tectonic stresses and the fact that the stope walls are nearly vertical and therefore behave as nearly free standing wall structures.

RÉSUMÉ

Ce papier décrit une étude de modélisation d'une mine abandonnée au Canada pour évaluer l'intégralité du pilier de surface, de l'éponte inférieur et de l'éponte supérieur avec l'aide du logiciel de Modèle bloc-resort (BSM) dans le but d'obtenir le degré de sécurité des structures avoisinantes. L'effet sur la stabilité régionale a aussi été examiné dans le cas ou le pilier de surface est complètement exploité. Les études indiquent que les chantiers étroits et près de la verticale sont dans un état quasi stable. Le pilier de surface n'est pas critique pour la stabilité des chantiers peu profonds. L'étude de modélisation indique que de petits déplacements du rock autour des ouvertures, même en excluant le pilier de surface. La condition stable des chantiers est due à leur proximité de la surface, aux très faibles contraintes tectoniques horizontales et, du fait que les parois des chantiers sont près de la verticale, ainsi ils se comportent pratiquement comme des structures verticales auto-portantes.

INTRODUCTION

In late 1993 and early 1994, the CANMET Mining Research Laboratories undertook an investigation of the shallow surface crown pillars located over the abandoned Howey and Hasaga mine workings in the Red Lake township (Aston and Bétournay, 1994). The purpose of the project was to confirm the location and dimensions of the two surface crown pillars, verify the integrity of the shallow stope peripheral zones and undertake a detailed geomechanical investigation to quantify the rock mass properties and assess their potential behaviour. Numerical modelling studies were carried out for three cross-sections. The results indicated that all three sections modelled appeared to be in a "meta-stable" state, whereby "no conditions exist requiring immediate concern, unless deterioration starts to occur within the crown pillar and/or stope"

(Yu and Wang, 1994). However, it was also recommended that further analysis be undertaken to assess the potential impact of deteriorating structural elements, i.e. the crown pillar, at the sites.

In early 1995, additional modelling studies were conducted to assess the impact of removing the surface crown pillars on the stability of the stope walls. Further investigation indicated that the stopes at all three sites examined were in "meta-stable" condition both with and without the pillars.

The work described here examines the numerical modelling studies of the three cross-sections of the inactive mine stopes using the BSM software, a Block-Spring Model for jointed rocks. For verification purpose, one of the cross-sections was also analysed using CANSAFE software, an elasto-plastic Finite Element model.

BACKGROUND INFORMATION

Geometry

At the Howey Workings - Hammel Road Site, the stope width was found to be in the order of 15 m (50 ft), with a crown pillar thickness varying from about 7.6 m (25 ft) over the centreline to 3.4 m (11 ft) near the crown/hangingwall intersection (Fig. 1). The stope was found to be open to a depth of about 90 m (300 ft) (Aston and Bétournay, 1994), The overburden thickness varies between 2.4 – 3 m (8 – 10 ft).

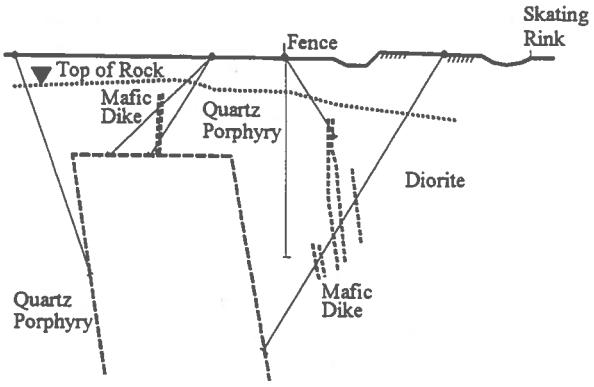

Fig. 1. A typical section showing structural features & the stope at the Howey Workings – Hammel Road Site

At the Howey Workings - Chicken Chef Site, the stope width is about 7.6 m (25 ft), with a crown pillar thickness of between 10.7 – 11.3 m (35 – 37 ft) (Fig. 2). The overburden thickness varies between 4.6 and 7.6 m (15 – 25 ft).

At the Hasaga Site, the stope width appears to vary between 12.2 – 13.7 m (40 – 45 ft), with a crown pillar thickness varying from 7.6 – 9.1 m (25 – 30 ft) (Fig. 3). The overburden thickness varies between 3.4 and 4.6 m (11 – 15 ft).

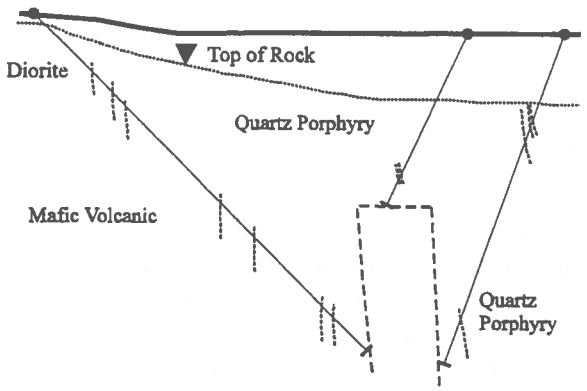

Fig. 2. A typical section showing structural features & the stope at the Howey Workings – Chicken Chef Site

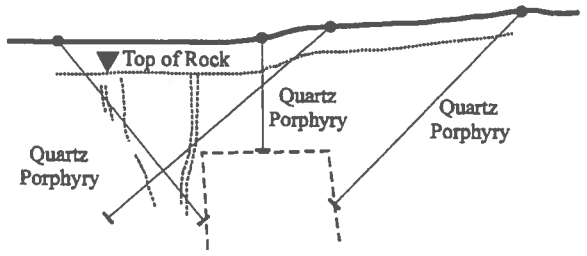

Fig. 3. A typical section showing structural features and the stope at the Hasaga Workings

Geological Conditions

Across the Howey and Hasaga sites, the overburden material generally appears to represent a mixture of clay and fill material comprising sand, gravel and crushed rock.

Throughout the Howey and Hasaga workings, the predominant rock type is a quartz porphyry, although some zones of quartz sericitic schist are found, along with localised diorite, mafic dykes and mafic volcanics. The quartz porphyry contains various degrees of sericitization and foliation across the workings. However, the hangingwall, ore and footwall zones are not well defined by specific (identifier) units, but rather merge with one another.

Structurally, the orebody has a Dip Direction of 155° (Dip 85°), with the predominant features being: Foliation Planes (Dip Direction 170°, Dip 75°); a coincident Joint Set 1 (Dip Direction 170°, Dip 78°); Joint Set 2 - Transverse Vertical (Dip Direction 75°, Dip 74°); and Joint Set 3 - Sub Horizontal (Dip Direction 325°, Dip 22°).

The size of the core pieces associated with the separations coincident with the foliation planes was found to vary considerably and range from < 2 cm to > 20 cm. The separation of the Set 1 joints, paralleling the foliation planes appeared to vary from about 0.5 m to 3.0 m. Similarly, Joint Sets 2 and 3 were found to vary irregularly, with distances ranging from 0.5 m to 2 - 3 m . The discontinuous spacing of the Set 2 and 3 joints suggests the formation of isolated blocks within the rock mass, rather than one continuous blocky mass.

The foliation planes and Set 1 joints were generally very tightly healed, while the condition of the Set 2 and Set 3 joints was found to vary considerably. However, evidence of open joints and/or separation planes was apparent via the presence of degrees of water staining on the plane surface, although no apparent correlation could be found between the degree of staining and either their spacing or spatial location.

The rock mass quality across the Howey and Hasaga workings was found to vary from Poor to Fair, as defined by the NGI Q - System, although it is probably higher, when the intact, in-situ nature of the rock mass is taken into consideration.

The in-situ stresses in the Red Lake Mine area have been observed to be under gravity loading conditions (Aston and Bétournay, 1994).

DESCRIPTION OF THE NUMERICAL MODELS

Block-Spring Model (BSM)

The Block Spring Model (BSM) is a recently developed technique for analysing the stress and deformation of jointed rock masses (Wang, 1991; Wang and Garga, 1993). Essentially, the model simulates rock masses using an assemblage of blocks, constructed from a grid of differently shaped polygons, which in turn represents naturally formed discontinuities within the rock mass. The model algorithm is formulated on the basis of equilibrium conditions for the blocks and solved using a global stiffness matrix. An iterative approach is used to simulate large block displacements. BSM is particularly well suited for: the analysis of stresses and deformations in jointed rock masses; rock blocks undergoing large displacements; and the prediction of unstable blocks around mine openings. The model is therefore considered appropriate and well suited for the shallow, near surface conditions found at the Howey and Hasaga sites.

CANSAFE Model

CANSAFE is a two dimensional elasto-plastic finite element program, which is capable of performing linear elastic and elasto-plastic stress analysis of rock structures as well as slope stability analysis (Mining Research Laboratories, 1994). Due to the non-linearity of the jointed rock masses and the difficulties for the finite element model to simulate discontinuities to a large extent, the rock masses must be considered as a continuum with the overall properties reduced. Therefore, an elasto-plastic analysis was carried out for the Howey - Hammel Road cross-section to confirm the findings of the Block-Spring Model. The Drucker-Prager failure criterion was utilised in the analysis.

NUMERICAL MODELLING STUDIES

Establishment of the Models

Three cross-sections as sketched in Figs. 1, 2 and 3 were analysed using BSM software. Two sets of joints were simulated in these BSM models: one parallel to the stope walls and the other one perpendicular to the stope walls. The BSM studies were carried out by varying the rock joint spacing and the rock joint

properties. The joint spacing in close proximity to the stope varies from 3 m to 1 m, while away from the stope boundary, the joint spacing varies from 5–10 m to 2–3 m. Fig. 4 shows a typical mesh of the BSM models.

An upper and a lower limits of the rock mass properties were established based on the best available information as shown in Table 1.

The cross-section at the Howey Workings – Hammel Road Site (Fig. 1) was also analysed using the CANSAFE software. Based on the geometry of the BSM model, a CANSAFE model for this section was created. The non-linear behaviour of the jointed rock masses was simulated by reducing the overall material properties attributed to the effect of the discontinuities of the rocks. The reduced rock mass properties were determined based on the laboratory testing data and empirical relations reported by Deere (1964), which are listed in Table 2.

Table 1. Material properties of the rock masses used in the BSM models

Area	Type	E MPa	μ	γ MN/m³	K_n upper/lower MPa/m	K_s upper/lower MPa/m	C upper/lower MPa	φ upper/lower (°)
H/W	Intact	78,840	0.25	0.027			25.37	37.6
	Joint set 1				7,884	788.4	0.25	37.6
					2,000	200.0	0.25	37.6
	Joint set 2				7,884	788.4	0.25	37.6
					2,000	200.0	0.25	37.6
F/W	Intact	79,570	0.25	0.027			27.80	36.1
	Joint set 1				7,957	795.7	0.28	36.1
					2,000	200.0	0.28	36.1
	Joint set 2				7,884	788.4	0.25	37.6
					2,000	200.0	0.25	37.6
ORE	Intact	75,310	0.25	0.027			24.42	39.2
	Joint set 1				7,531	753.1	0.24	39.2
					2,000	200.0	0.24	39.2
	Joint set 2				7,884	788.4	0.25	37.6
					2,000	200.0	0.25	37.6

Note: E = Young's Modulus; μ = Poisson's Ratio;
γ = Unit Weight;
K_n = Normal stiffness; K_s = Shear stiffness;
C = Cohesion; φ = Friction angle.

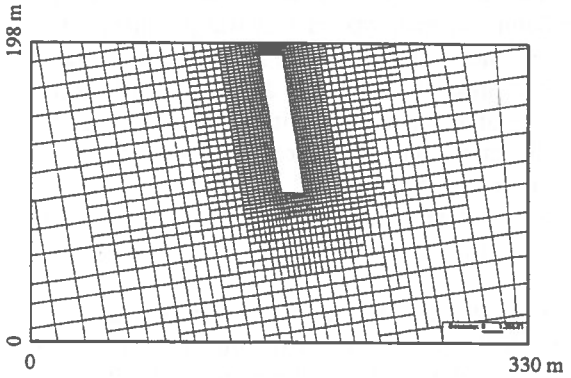

Fig. 4. A typical mesh showing the BSM model of the cross-section at Howey Workings – Hammel Road Site

Table 2. Rock mass properties used in the CANSAFE model

Area	Young's Modulus (MPa)	Poisson's Ratio	Unit Weight (MN/m³)	Cohesion (MPa)	Friction Angle (°)
H/W	7884	0.25	0.027	2.54	37
F/W	7957	0.25	0.027	2.78	36
Ore	7531	0.25	0.027	2.44	39

Results and Discussions

Hammel Road Site - BSM model: This section was analysed using BSM in four cases:

Case 1: wider joint spacing, upper bound properties;
Case 2: wider joint spacing, lower bound properties;
Case 3: closer joint spacing, upper bound properties;
Case 4: closer joint spacing, lower bound properties.

Figs. 5, 6, 7 and 8 show the principal stresses and displacements of the rocks with close joints and lower bound joint properties (Case 4). The results of other models show the similar patterns, with varying magnitudes, of stresses and displacements.

The BSM results indicated that varying the rock mass properties from upper to lower bounds had little impact on the resulting stresses. The resultant stress concentration observed in the crown pillar is relatively low, in an order of 0.6 MPa at the hanging wall corner and 1.2 MPa at the footwall corner.

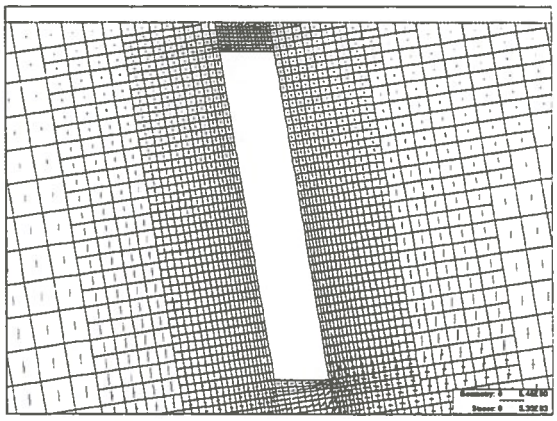

Fig. 5. Hammel Road Site - BSM model: pricipal stresses with pillar

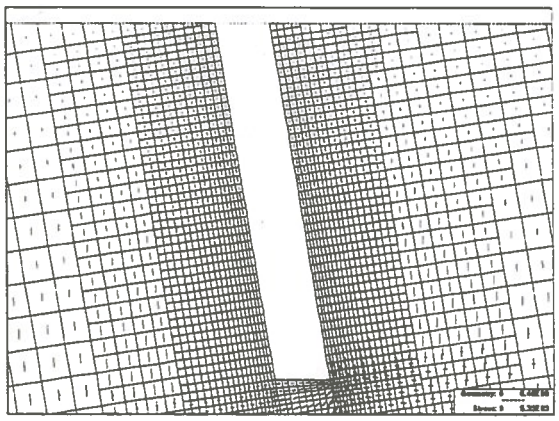

Fig. 6. Hammel Road Site - BSM model: pricipal stresses without pillar

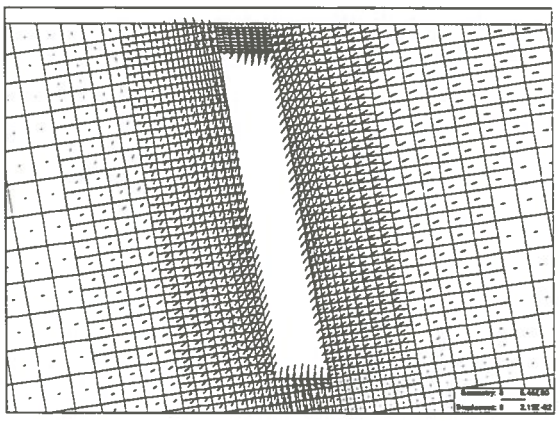

Fig. 7. Hammel Road Site - BSM model: displacements with pillar

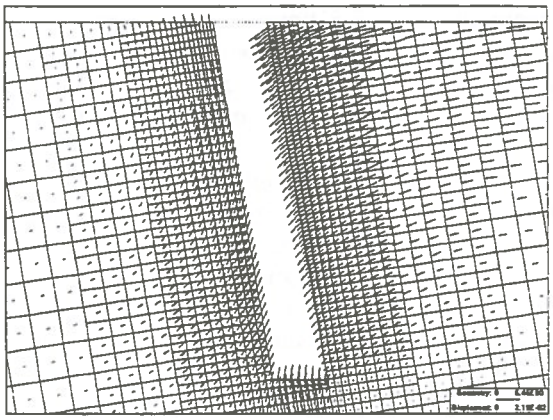

Fig. 8. Hammel Road Site - BSM model: displacements without pillar

When the crown pillar is removed, stresses around the pillar area are discharged and accompanied by a small increase in tension located principally in the hangingwall and close to ground level. The maximum observed tensile stress is about 0.2 MPa, which is considered low and should not cause instability of the stope walls.

Although removal of the pillar resulted in increased displacement of the rock masses for both the wider and closer joint spacing patterns, all four cases indicated no resulting structural failure (fatal rock mass/block movements) of the hangingwall or footwall after removal of the pillar.

The changes of the rock displacements are more noticeable due to the removal of the pillar, the reduction of material properties and the reduction of the joint spacing. The displacements of the blocks adjacent to the pillar in the hangingwall side are doubled, from 11.8 to 24.1 mm in the worst case 4, when the pillar is removed (Table 3). However, all these four cases indicated no structural failure after the pillar is removed. The displacements of the blocks in the hangingwall side pillar shoulder were increased from 4.8 mm to 15.6 mm and from 6.1 mm to 24.1 mm due to the reduction of the material properties from the upper bound to the lower bound cases. As a result of the reduction of the joint spacing under lower bound material properties, the block movements are increased from 15.6 mm to 24.1 mm at the pillar shoulder hangingwall side. In general, referring to the pillar shoulder at the hangingwall side, the displacement is increased about 2 times when the pillar

is removed; about 3.5 times when the properties are reduced and about 1.4 times when the joint spacing is reduced. However, the overall condition of the stope is "meta-stable" and the displacements are small.

The low stresses, small displacements and structural integrity are probably due to the near surface proximity of the stope to ground surface and the very low, horizontal tectonic stress components. In addition, the fact the stope walls are nearly vertical therefore behaving as near free standing walls may also be important.

Table 3. Howey - Hammel Road Site: Displacements of the shoulder of the pillar

Case	Displacement with Pillar (mm)	Displacement without Pillar (mm)
(1)	2.4	4.8
(2)	8.2	15.6
(3)	3.3	6.1
(4)	11.8	24.1

Hammel Road Site - CANSAFE model: To better understand the stress and deformation behaviour of the rock masses around the Red Lake stopes and to verify with the BSM results, a CANSAFE model was established based on the BSM model for the section at the Hammel Road Site. The analysis was undertaken using the elasto-plastic feature of the CANSAFE with Drucker-Prager failure criterion.

The principal stresses and the displacements of the rocks around the stopes are shown in Figs. 9, 10, 11 and 12. Some minor tension developed in the hangingwall side and extended further when the pillar is removed. The stresses are slightly concentrated in the pillar and the stresses in the pillar shoulders are released after the pillar is removed. These phenomena are very similar to what were observed in the BSM models (Figs. 5 and 6).

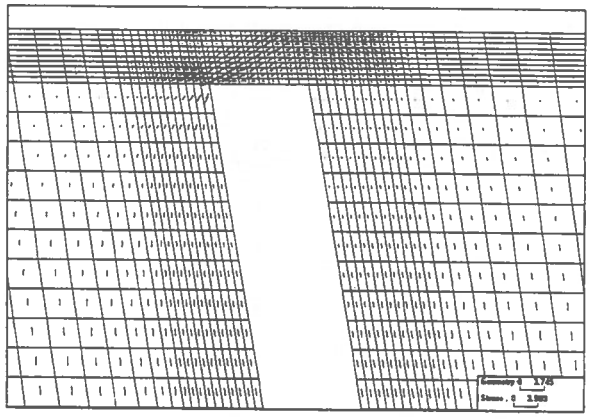

Fig. 9. Hammel Road Site - CANSAFE model: principal stresses with pillar

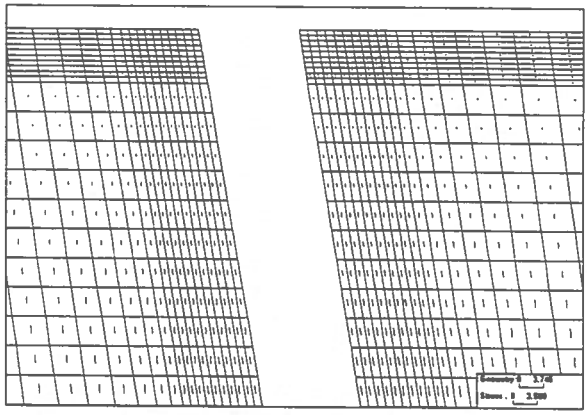

Fig. 10. Hammel Road Site - CANSAFE model: principal stresses without pillar

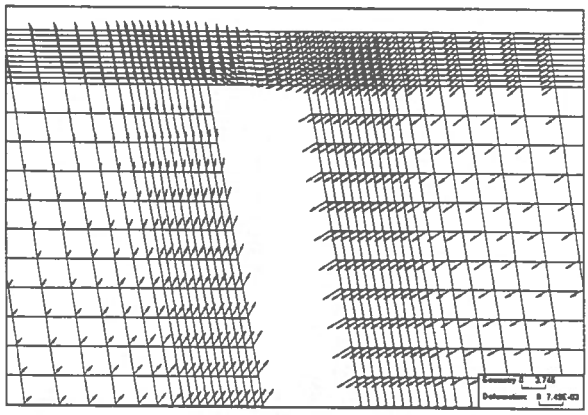

Fig. 11. Hammel Road Site - CANSAFE model: displacement distribution with pillar

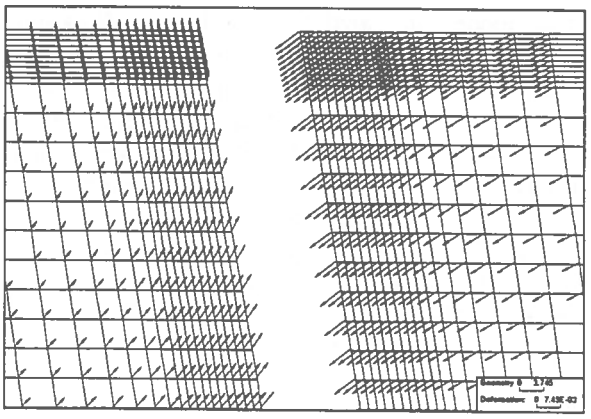

Fig. 12. Hammel Road Site - CANSAFE model: displacement distribution without pillar

The displacement distributions (Figs. 11 and 12) indicated the same pattern as that obtained from the BSM models (Figs. 7 and 8). The displacements at the hangingwall side shoulder of the pillar is about 4.2 mm with the pillar in place and about 8.8 mm when the pillar is removed, which are within the range of the BSM results under the upper and lower bound conditions with closer joint spacing (Table 4). Similar to the BSM results, the CANSAFE model did not indicate any severe situation which might cause serious safety concerns. As explained in the BSM analysis, this could be due to the low stress condition in this shallow area. The CANSAFE results further confirmed that the BSM predictions are reasonable under the same loading conditions.

Table 4. Comparison of pillar shoulder movements between BSM and CANSAFE results

Case	BSM upper bound (mm)	BSM lower bound (mm)	CANSAFE (mm)
With pillar	3.3	11.8	4.2
No pillar	6.1	24.1	8.8

Howey Working - Chicken Chef Site: The stope is relatively narrower and the surface crown pillar is thicker at this section. Three cases were studied at this section using BSM models:

Case 1: wider joint spacing, upper bound properties;
Case 2: wider joint spacing, lower bound properties;
Case 3: closer joint spacing, lower bound properties.

The analyses indicated that this section is potentially more stable than the section at the Hammel Road Site.

Figs. 13, 14, 15 and 16 show the principal stresses and displacements of the rocks around the stope with and without the pillar (Case 3).

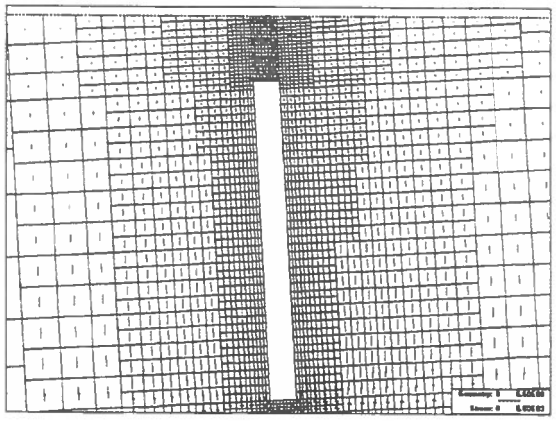

Fig. 13. Chicken Chef Site: principal stresses with pillar

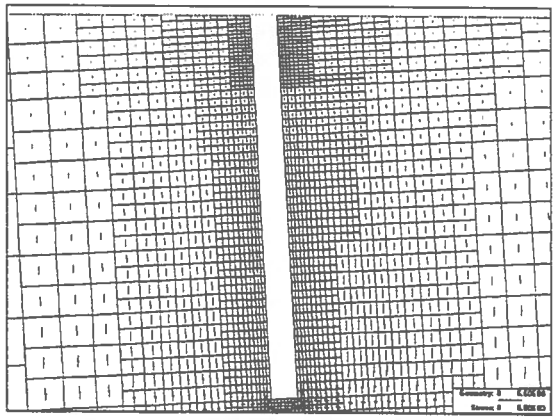

Fig. 14. Chicken Chef Site: principal stresses without pillar

Very little stress variation is observed with the change of material properties from the upper bound to the lower bound and with the reduction of the joint spacing. The factor affecting the stress distribution is the removal of the pillar. With the pillar in place, all the three models indicated a slight concentration of stresses at the pillar. The maximum stress in the pillar

is about 1.35 MPa at the footwall corner and 0.8 MPa at the hangingwall corner. After the pillar is removed, the stresses around the pillar area are discharged with some minor tension (less than 0.2 MPa) in the hangingwall.

The displacements of the pillar shoulder at this section are listed in Table 5. After the pillar is removed, the displacements around the pillar shoulder are increased. With the reduction of the joint spacing, the displacements of the stope walls are increased. Under the condition of the lower bound material properties, when the joint spacing is reduced, the pillar shoulder movements indicated an increase from 1.5 mm to 3.8 mm with the pillar in place and 3.1 mm to 4.1 mm with the pillar removed.

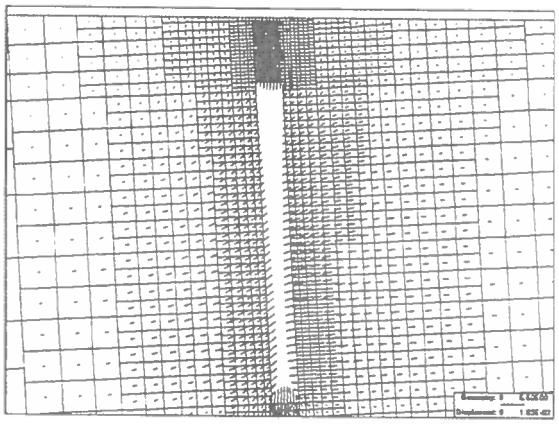

Fig. 15. Chicken Chef Site: displacements with pillar

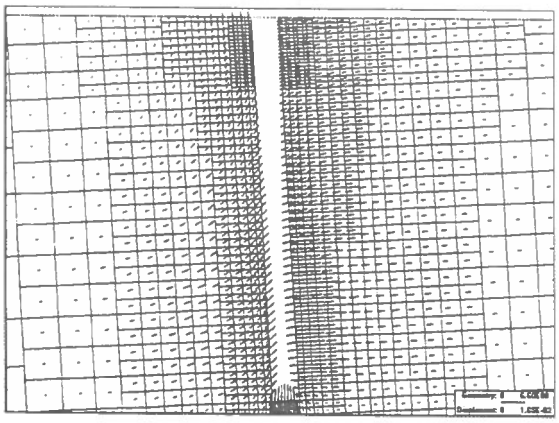

Fig. 16. Chicken Chef Site: displacements without pillar

These models indicated that the Howey Workings - Chicken Chef Site section is in "meta-stable" condition. The same reasons as mentioned in the previous section for the Hammel Road Site apply to this cross-section. The low stresses, small displacements and structural integrity are probably due to the near surface proximity of the stope to ground surface and to the very low, horizontal tectonic stress components. In addition, the fact the stope walls are nearly vertical therefore behaving as near free standing walls may also contribute to the structural integrity.

Table 5. Howey - Chicken Chef Site: Displacements of the pillar shoulder

Case	Displacement with Pillar (mm)	Displacement without Pillar (mm)
(1)	0.4	1.2
(2)	1.5	3.1
(3)	3.8	4.1

Hasaga Workings: The stress and deformation behaviour at the Hasaga Workings is very similar to the other two sites. This section was analysed using the BSM models for three cases:

Case 1: wider joint spacing, upper bound properties;
Case 2: wider joint spacing, lower bound properties;
Case 3: closer joint spacing, lower bound properties.

Figs. 17, 18, 19 and 20 show the principal stresses and the displacements of the rock around the stope at the Hasaga Workings section with closer joint spacing and lower bound joint properties (Case 3). All the three cases indicated a stress concentration in the pillar with the maximum value of about 1.0 MPa at the footwall corner and 0.6 to 0.7 MPa at the hangingwall corner. With the pillar removed, the stresses around the pillar are discharged and minor tension developed (less than 0.2 MPa) in the hangingwall side.

The displacements of the blocks at the pillar shoulder are listed in Table 6. As expected, the displacements are increased with the decrease of the material properties from the upper bound to the lower bound and with the decrease of the joint spacing. However, the BSM analysis results indicated a "meta-stable" condition at this section.

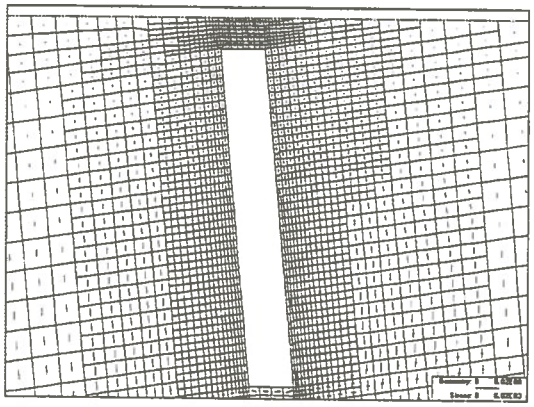

Fig. 17. Hasaga Workings: principal stresses with pillar

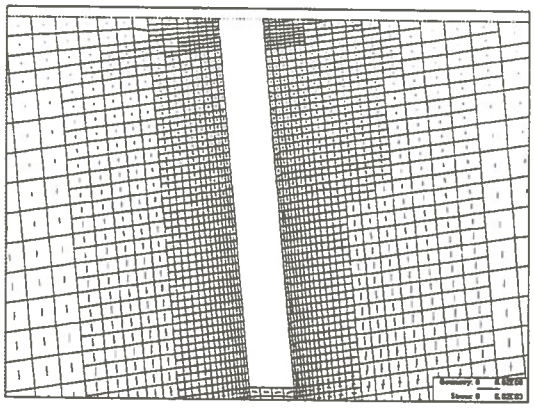

Fig. 18. Hasaga Workings: principal stresses without pillar

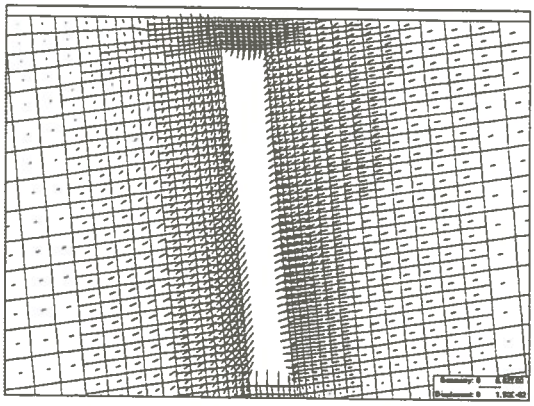

Fig. 19. Hasaga Workings: displacements with pillar

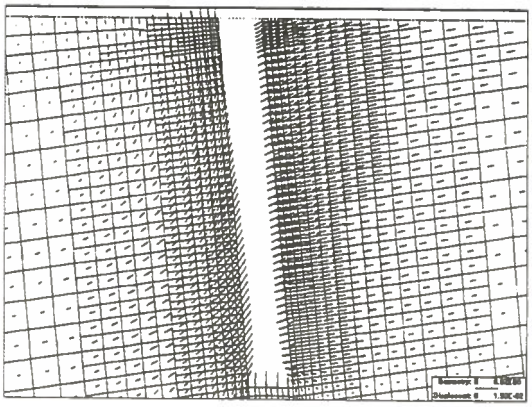

Fig. 20. Hasaga Workings: displacements without pillar

Table 6. Section 3 (Hasaga Workings): Displacements of the shoulder of the pillar

Case	Displacement with Pillar (mm)	Displacement without Pillar (mm)
(1)	0.9	2.1
(2)	3.1	6.5
(3)	6.0	8.0

CONCLUSIONS

Based on the modelling studies, it can be concluded that at each of the three sites examined, the overall condition of the stopes was in "meta-stable" condition, both with and without the pillar. The observed low displacements and stresses and overall apparent structural integrity are thought to be the result of the near surface proximity of the stopes and to the very low, regional horizontal tectonic stress components. In addition, the fact that the stope walls are nearly vertical and therefore behave as near free standing walls may also play an important role in their stability.

The analysis results indicated that BSM model is well suited for analysing stresses and deformation of jointed rock masses, especially the mines at the shallow depth.

ACKNOWLEDGEMENT

The authors wish to acknowledge the considerable assistance and help provided by the Abandoned Mines Office, Ontario Ministry of Northern Development and

Mines and the Township of Red Lake. The views expressed in this paper represent those of the authors and not necessarily those of the other parties involved.

REFERENCES

Aston, Tim and Bétournay, Marc, 1994.
Geomechanical Investigation of the Howey and Hasaga Shallow Mine Workings, Red Lake, Ontario. MRL Client Report 93-056 (CL); Prepared for the Township of Red Lake; 5 Volumes.

Deere, D.U., 1964.
Technical Description of Rock Cores for Engineering Purposes. Mech. Eng. Geol., Vol.1, pp.17-22.

Mining Research Laboratories, 1994.
CANSAFE - A Windows Application Package for Stress Analysis Using Finite Element Techniques (User's Manual). CANMET Division Report: MRL 94-046(TR). 57p.

Wang, Baolin, 1991.
A Block Spring Model for Jointed Rocks. Ph.D. Thesis, University of Ottawa, 204p.

Wang, Baolin and Garga, Vinod K., 1993.
A Numerical Method for Modelling Large Displacements of Jointed Rocks – Part I: Fundamentals. Canadian Geotechnical Journal, Vol.30, No.1; pp.96-108.

Yu, Yang and Wang, Baolin, 1994.
Geomechanical Investigation of the Howey and Hasaga Shallow Mine Workings, Red Lake, Ontario: Volume V - Numerical Modelling Study. MRL Client Report 93-056 (CL); Prepared for the Township of Red Lake, 49p.

CAMI'95: 3rd Canadian Conference on Computer Applications in the Mineral Industry
Montréal, Québec, Canada, October 22-25, 1995

Obtaining Quality Cavity Monitoring Survey Data

Sam G.L. Mah, Rimas T. Pakalnis, Richard Poulin, Lyndon M. Clark
Department of Mining and Mineral Process Engineering,
University of British Columbia, Vancouver, B.C.

ABSTRACT:

As mining technology advances towards the design of larger stopes, there exists a greater concern to better understand what controls unplanned dilution. Dilution is a quantifiable parameter that can be used as an indicator of design efficiency. Its measurement is made possible through application of cavity monitoring survey (CMS) instrumentation. Interpretation of the 3-D data can be summarized in the following five (5) steps: data calibration, CMS correction, CMS validation, cross-section generation, and dilution calculation. It follows that accurate dilution estimates will yield a valid predictive tool. In addition, a better understanding of dilution is hoped to further understand the failure mechanisms associated with instability.

RÉSUMÉ:

Avec la conception de chantiers d'abattage de plus en plus vaste, il en découle une plus grande préoccupation de mieux comprendre ce qui control la dilution non-plannifiée. La dilution est un paremètre quantifiable qui peut être utilisée comme indicateur de l'efficacité du design. Sa mesure est possible grâce à l'utilisation d'un appareil d'arpentage de cavité (AAC). L'interprétation des données 3-D peut être résumée par les cinq étapes suivantes: calibration des données, correction du AAC, validation du ACC, génération de sections et calcul de la dilution. Des estimés précis de dilution vont donnés un outil de prédiction valable. En plus, il est à espérer qu'une meilleur compréhension de la dilution va aider à mieux comprendre les méchanismes de rupture associés avec l'instabilité.

1.0 INTRODUCTION

Dilution, as used in the mining industry, implies the lowering of ore grade. It is a complex variable that can enter the various stages of mining in numerous forms (Elbrond, 1994). This important parameter can be related to quality of design. Historically, dilution has ranged from difficult to impossible in terms of quantification. At best, dilution is determined from back calculating methods (Pakalnis, 1986) using tonnage and grade values. Within the past decade, the development of sensory devices and advances in

computer technology (Schleter, 1993) have allowed mine engineers to measure dilution with a higher degree of confidence. The ability to collect and process large amounts of data, often associated with real world 3-D models, will complement the old pragmatic design methodologies of intuition and experience.

Understanding the effects of unplanned dilution is critical to optimizing designs. Possible factors affecting unplanned dilution are: cavity morphology, drilling and blasting, rock mass quality, and mining rate.

Thus the premise for this report is that dilution can be better understood if the source and quantity can be defined with a higher degree of confidence. This can be accomplished through application of new technological advances in sensor equipment and computer applications.

2.0 INSTRUMENTATION AND COMPUTER APPLICATION

The foundation of this dilution analysis is based on the ability to survey an underground opening effectively. Application of prismless laser technology has resulted in the cavity monitoring system. The instrument was developed jointly by Noranda Technology Centre (NTC) and Optech Systems (Miller et al, 1992). Since the late 1980's, the CMS has evolved and found an early acceptance to the mining industry.

2.1 CMS System

The system is comprised of three components:

- Laser Scanning Unit
- Portable Controller and CPU
- Support Package

The main component is the laser scanning unit (LSU) which utilizes a two beam laser system for distance measurements (figure 1). It is housed in a motorized fork assembly that is capable of rotating the LSU a full 360° about the boom axis and inclines up to 135° about the pivot axis.

The second component is the portable controller and CPU box. The controller handle enables the operator to remotely activate and prepare for the survey. The CPU box houses the data logger (2 Megabytes) which has the capacity for four surveys.

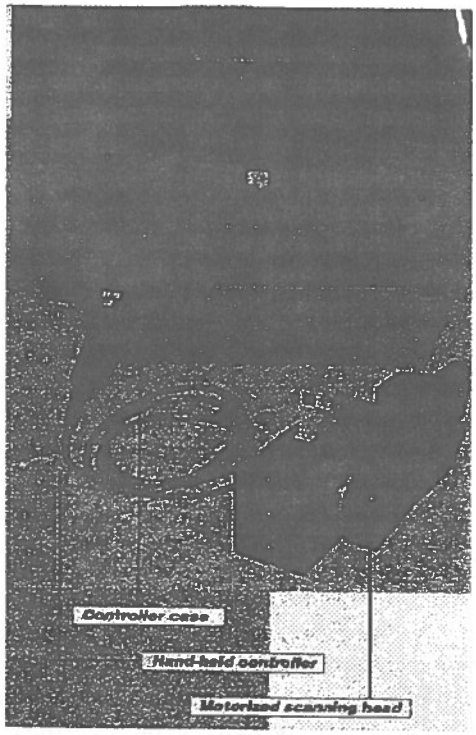

Figure 1 - "CMS System "

The third component is the support package (figure 2) which consists of a ten (10) meter segmented boom and two adjustable posts (2 - 5 m) that brace the system to the sill and back. Light weight carbon composite fibers and high density polyethylene are the materials used for the support construction.

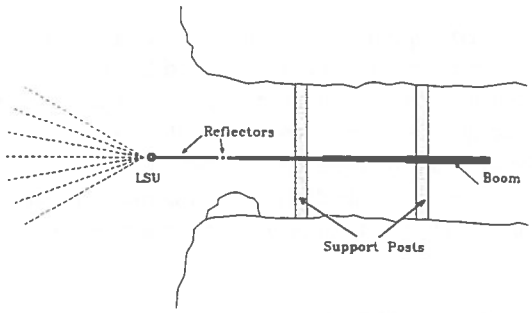

Figure 2 - "Typical CMS Set-Up"

A typical CMS set-up (figure 2) involves suspending the CMS instrument into an underground opening.

Using the remote hand-held controller, the pre-programmed scanning routine can be initiated.

2.2 Computer Software

Once the data is collected, it is then reduced and converted into the required format (XYZ coordinates, ASCII or DXF) with the supplied software. To correlate this data to current mine plans, the location of the LSU and the azimuth of the boom must be defined.

A recent survey shows that 70% of the computer automated drafting (CAD) market is dominated by AutoCAD (Orr, 1994). In particular, high end engineering applications that require 3-D capabilities and solid modeling favor AutoCAD. This is the case for the CMS application.

Of the three (3) methods for 3-D modeling (wireframe, surfaces and solids), surface modeling is the preferred method of presentation because surfaces can be shaded to eliminate visual complexity (Orr, 1993).

3.0 METHODOLOGY

Utilization of this survey information involves a five (5) step process: data calibration, CMS correction, CMS validation, cross-section generation, and dilution calculation.

3.1 Data Calibration

Super-imposing the CMS entity onto the existing 3-D mine model illustrates the discrepancies in location and overall mesh continuity (figure 3, 4 and 5).

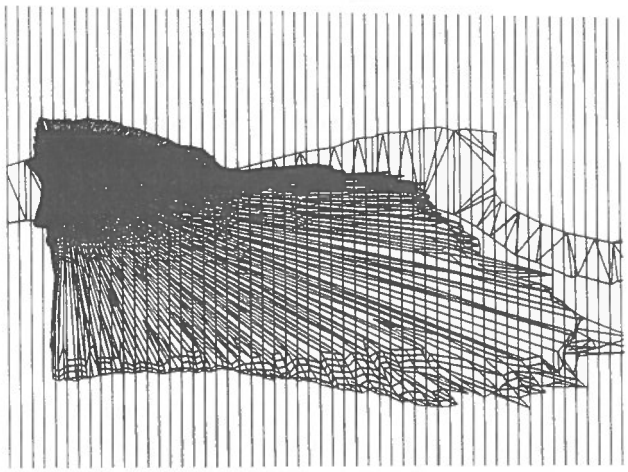

Figure 3 - "CMS Plan View"

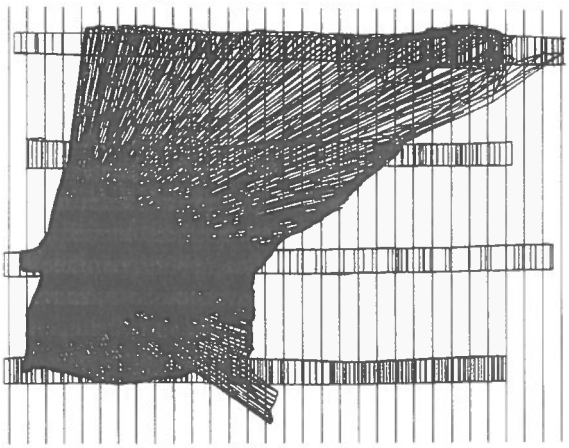

Figure 4 - "CMS Side View"

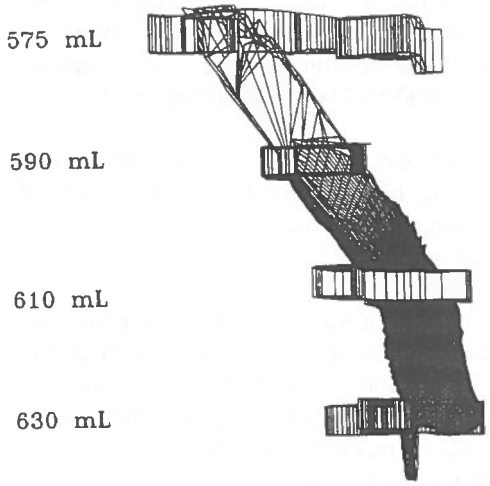

Figure 5 - "View Along Strike"

Experience has indicated that mesh location errors are translational in nature. This is largely due to its high sensitivity in defining the location of the LSU and the azimuth of the boom.

Locating the LSU is accomplished by surveying in two points (reflector locations) on the boom. The first location, closest to the LSU, is placed at a known distance from the pivoting point (0.25 m). The second point must be placed somewhere along the support boom to complete the azimuth calculation.

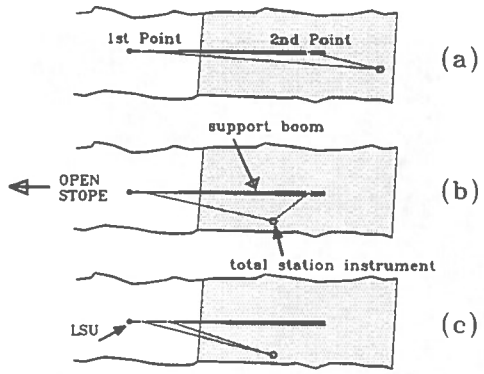

Figure 6 - "Surveying Methodology (Plan View)"

Figure 6.a shows a common survey set-up depicting the survey station located at mid drift. From this central location, it is difficult to measure the two reflector points on the boom due to the impaired line of vision. To avoid this problem, a more appropriate vantage point should be selected (figure 6.b).

In addition, because of imperfect segment connections, the boom length will sag under its own weight (figure 7). Consequently, deviations in lateral, vertical and angular directions are possible.

Experience has shown that angular deviations are not as common. The self-test performed prior to each CMS set-up involves using an internal inclinometer for leveling the LSU. Assuming that proper handling of the LSU is practiced, angular distortions are not expected to be a problem.

Therefore, translational errors are more commonly observed. It is suggested that a different approach for surveying in the boom azimuth be used to help minimize the sag effect (figure 6.c). Re-locating the second point on the boom to approximately 0.5 m from the end of the first segment is anticipated to restrict the sag effect to a single segment.

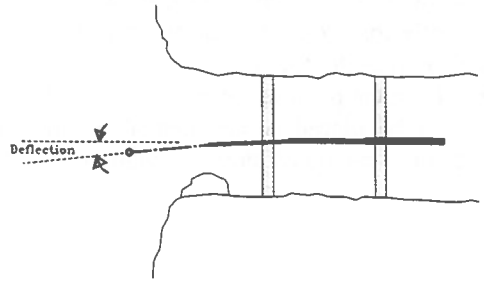

Figure 7 - "Support Boom Sag"

3.2 CMS Correction

If translation has been identified in step one, the CMS entity is re-located using known reference points.

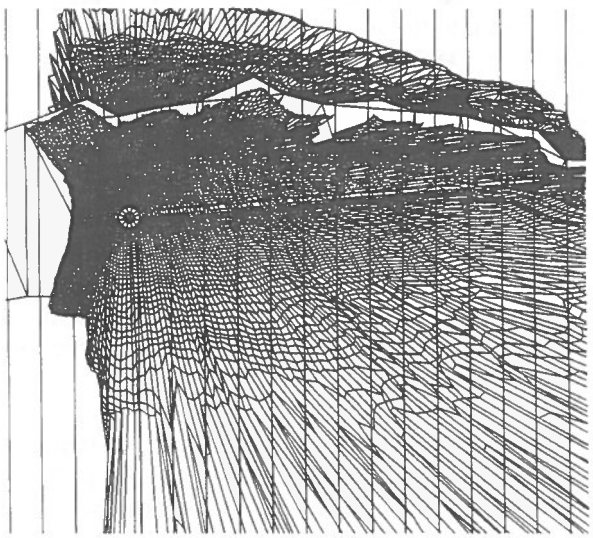

Figure 8 - "Close Up of LSU Location (Plan View)"

Using the '*<hide>*' function in AutoCAD shows the top surface contour of the CMS mesh (figure 8). In this plan view, there is a 0.25 m lateral and 0.50 m longitudinal translational error.

In essence, the portion of the CMS entity that yields the most reliable information is nearest the laser head location. The closer spaced mesh grid correlates to greater surface definition given that data density remains constant. Figure 8 distinctly shows a line separating the reliable portions of the survey from areas that may be hidden from view.

Based on this argument, the areas closest to the survey location can be used as reference points. Re-locating the CMS entity completes the model calibration process.

Similarly, this procedure can be applied in the vertical direction. Figure 4 shows an approximate 1.0 m vertical translation.

3.3 CMS Validation

Limitations of the prismless laser instrument are related to visibility problems. In optimal conditions, the LSU is capable of measuring distances up to 100 m. However, this is rarely achieved in an

underground environment. Possible visibility problems arise from suspended dust particles, gaseous by-products (blasting smoke) and moisture content (fog). In most cases, the extreme portions of the CMS entity are subject to reading errors which often result in loss of mesh continuity. These errors should be filtered from the analysis.

Another related visibility obstacle is *'line of sight'*. Laser performance is similar to human vision in that from a particular observation point, there are certain portions of the stope that are hidden from sight. Often stope cavities are irregular, largely due to geology and blasting. Therefore, selecting the laser head location is one of the controlling factors for CMS quality. Figure 9 illustrates the different approaches that can be taken for CMS setups. The stope cavity is an idealized surface showing shadow effects for indentations and protuberances. The most conservative approach (figure 9.a) shows the LSU located at mid-stope width. This location compromises CMS accuracy by averaging the shadow effects for both surface features. In order to avoid these discrepancies, at least two setups are required to sufficiently describe indentation and protuberance (figures 9.b and 9.c).

Experience has shown that the effective survey range for complex stopes is < 20 meters from the survey LSU location.

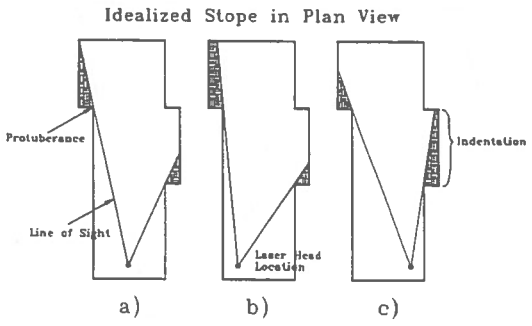

Figure 9 - "Plan View of Shadow Effects"

Note that shadow effects are equally valid in the vertical direction.

Another method employed to minimize shadow effects is accomplished by varying the data density setting. Figure 10 demonstrates the sensitivity of data density to quality CMS information.

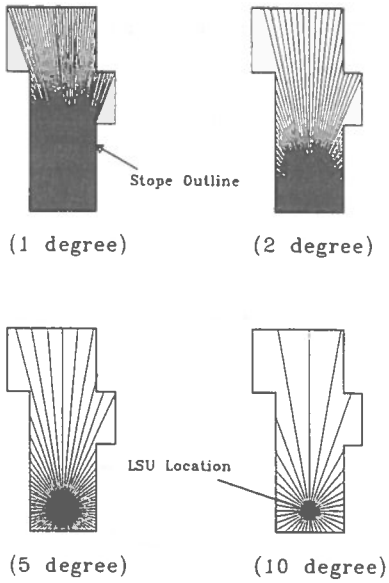

Figure 10- "Cross Sectional View of Shadow Effects"

Observe that using the 1° increment yields the best result. Current limitations of the CMS instrument restricts the operator from customizing the data density setting. Ideally, in the far-field range a high data density setting is required for obtaining a greater definition CMS grid. Conversely, a lower data density would suffice for the near-field range.

3.4 Cross-Section Generation

The next step involves generating multiple cross sectional views of the superimposed 3-D entities. This can be accomplished by manual or automated means. For AutoCAD, there are various third party software packages available on the market (written in AutoLISP or AutoCAD development support (ADS) macro language). The cross-section shown in figure 11 was generated by a program called SLICE (Oswald, 1990).

3.5 Dilution Calculation

Several assumptions are associated with determining dilution. Geological interpretation defines the stope block. Ore outlines delineated on development levels are interpolated linearly between levels. The resultant block tonnage calculated comprises the mineable reserve. Outside of this reserve are two general types of dilution: planned and unplanned (Scoble and Moss, 1994). Planned dilution is the material that is unavoidably associated with a particular mining method. Whereas, unplanned dilution is the

additional material realized from blast damage or slough.

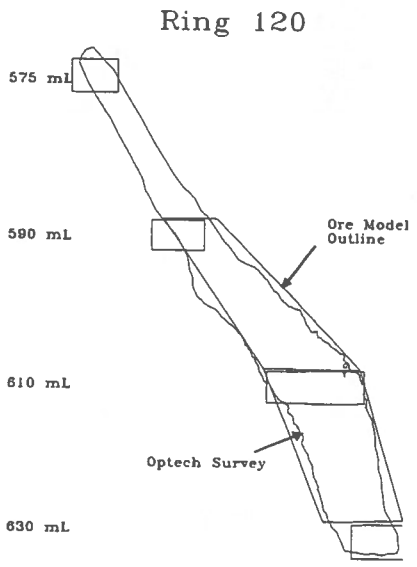

Figure 11 - "Typical Cross-Section"

For this dilution analysis, unplanned dilution will consider the excessive material gained outside the designed area (ore reserve). This can be numerically defined in the following equation.

$$\text{Dilution} = \frac{(\text{CMS Area} - \text{Ore Reserve})}{\text{Ore Reserve}} \times 100\%$$

Acceptable levels of unplanned dilution are sensitive to mining widths. Therefore, interpretation of this unitless dilution number is more meaningful if it is related to this third dimension.

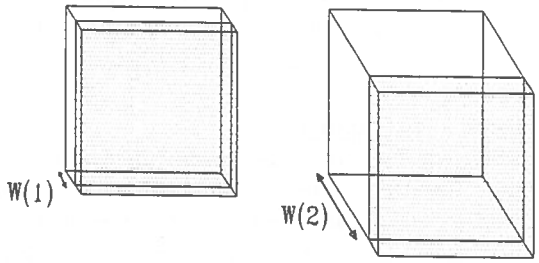

Figure 12- "Sensitivity to Mining Width"

For example, dilution realized in a narrow vein (< 5 m) stope is more critical to operational efficiency than for a wide body (> 10 m) stope (Pakalnis et al, 1995). To incorporate the effects of stope width, a dilution factor (DF) can be defined as the ratio of dilution (%) over stope width (m).

3.5.1 Proposed Methods of Data Presentation: It is proposed that dilution be related as a linear slough measurement. For a given rock material, unplanned dilution is affected by the degree of stress, structure, rock mass or any combination of the above. In this analysis, it is assumed that for large underground openings, the hanging walls are generally in relaxation (Pakalnis, 1986). For open stope methods, the rock mass is rated fair to good rock since the back should be self supporting (Resche and Romanowski, 1993). Therefore, dilution is generally realized from the walls and appears in the stope as variable sized failures along predominant geological structures. A conservative estimation assumes the worst case scenario of parallel structures relative to the open stope.

For each cross-section generated, apply the proposed CMS dilution calculation method and cumulated these values over a given wall interval. Normalizing this number over the respective wall shape factor gives the average stope dilution.

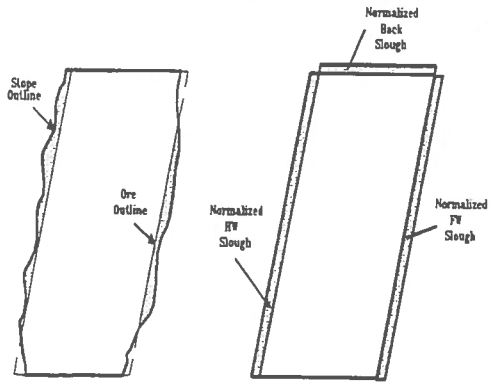

Figure 13- "Normalized Slough"

Additionally, a tonnage can be calculated for a given cross sectional thickness. Identifying the source of unplanned dilution (waste or backfill) will allow a cost to be associated with the handling of this excess material.

4.0 APPLICATION TO DESIGN

Comments on the application of this dilution analysis is given to three (3) areas of mine design: stope support, drilling and blasting, and stope design.

4.1 Stope Support

Utilization of ground support serves two purposes in mining: safety and control of slough. In open stope methods, ground support is primarily installed for dilution control since it is non-entry. The effectiveness of a ground support program can be assessed by a systematic approach. Optimizing design of pattern density or selection of ground support types are obvious benefits. The "Dilution Action Plan" as defined at the Golden Giant Mine produced an effective cable bolting program as a direct result of using the CMS dilution analysis method (Anderson and Grebenc, 1995)

4.2 Drilling and Blasting

Similarly, the effects of drilling and blasting can be evaluated quantitatively. In particular, drill deviation and blast confinement effects can be observed more clearly from CMS observations. More importantly, the effects of time can be measured. Surveys performed immediately after a blast can be assumed to show exclusively blast damage. Subsequent surveys performed in the same area will reveal the degradation of rock mass as mining progresses. Modifications in equipment selection and blasting procedures are some possible benefits.

4.3 Stope Design

The following discussion will focus primarily on two span design approaches; namely Mathew's Open Stope Design Method (Mathews et al, 1980) and the Dilution Approach (Pakalnis, 1986). Both design methods show an empirical relationship of rock mass quality to shape factor.

In short, the Mathew's method plots Stability Number (N) versus shape factor (HR). The plot indirectly defines dilution as: stable, potentially unstable and unstable areas.

Similarly the Dilution Approach shows a linear dilution relationship for a Rock Mass Rating (RMR) versus HR plot. The database for this work is comprised primarily of visual dilution assessments.

Improvements to these empirical design methods include: more accurate measurements of dilution and the identification of dilution sources.

5.0 CONCLUSIONS

Utilization of the CMS instrument as a tool for assessing quality control in the mining industry can produce beneficial results. The process of measuring dilution involves several steps for data correction. In particular, the CMS data is sensitive to infield collection methods. Selection of the LSU survey location is critical and should reflect the degree of stope geometry complexity. In some cases, two CMS surveys may be required to correlate a particular stope section. Also, the effects of sag on the support boom in terms of translation errors must be recognized. A minor adjustment in survey methodology can help minimize this effect.

The use of dilution factors, linear slough measurements and tonnage conversions are suggestions for interpreting dilution data. It is hoped that these methods would provide a universal dilution number for comparative analysis.

Further study is required to refine current empirical span design methods. With sufficient data, it is hoped that a dilution prediction tool can be created.

Acknowledging the importance that dilution has in mining, it is prudent to make every effort to obtain the most reliable data possible. With reliable dilution numbers, design engineers can make better informed decisions. The results are improved safety and optimized designs that cannot be overlooked when planning for spans that approach their critical limits.

ACKNOWLEDGMENTS

Special thanks is given to the staff at Detour Lake Mine for permission to publish their results and in particular to Mr. K. Dunne (Ground Control Engineer) for his invaluable contributions.

REFERENCES

ANDERSON, B. and GREBENC, B. 1995.
Controlling Dilution at the Golden Giant Mine, CIM Mine Operators Conference.

ELBROND, J. 1994.
Economic Effects of Ore Losses and Rock Dilution, CIM Bulletin, Vol. 87, No. 978, p. 131 - 134.

MATHEWS, K., HOEK, E., WYLLIE, D.C. and STEWART, S.B.V. 1980.
Prediction of Stable Excavation Spans for Mining at Depths Below 1,000 Meters in Hard Rock, CANMET Report 802-1571.

MILLER, F., JACOBS, D. and POTVIN, Y. 1992.
Cavity Monitoring System Update and Applications, 94th CIM Annual General Meeting, Montreal, paper #106.

ORR, J.N. 1993.
Adding A New Dimension, PC Magazine, Vol. 12, No. 4, p. 260.

ORR, J.N. 1994.
CAD's New Face, PC Magazine, Vol. 13, No. 18, p. 221- 264.

OSWALD, D., 1990
SLICE, User's Manual.

PAKALNIS, R.C., POULIN, R. and HADJIGEORGIOU, J. 1995.
Quantifying the Cost of Dilution In Underground Mines, AIME Annual Meeting, Denver.

PAKALNIS, R. 1986.
Empirical Stope Design at The Ruttan Mine, Sherritt Gordon Mine, Ph.D. Thesis (U. of British Columbia).

RESCHE, A.E. and ROMANOWSKI, J. 1993
The Success and Limitations of Mathew's Analysis for Open Stope Design at HBMS. Flin Flon Operations, 95th CIM Annual General Meeting, Calgary, paper # 136

SCHLETER, W. 1993.
AutoCAD for Windows: Stunning Speed and Jazzy Interface, but Hardware Hungry. PC Magazine, Vol. 12, No. 8, p.37 - 39.

SCOBLE, M.J. and MOSS, A. 1994.
Dilution in Underground Bulk Mining: Implications for Production Management, Geological Society Special Publication, No. 79, p. 95-108.

CAMI'95: 3rd Canadian Conference on Computer Applications in the Mineral Industry
Montréal, Québec, Canada, October 22-25, 1995

Predicting Joint Behaviour Using Artificial Neural Networks

John Hadjigeorgiou & Jean-Sébastien Lessard
Department of Mining & Metallurgical Engineering
Université Laval, Ste-Foy, Québec, Canada

Frédéric Flament
Algosys Inc., Charlesbourg, Québec, Canada

ABSTRACT:

This paper reports on use of artificial neural networks to predict shear behaviour of rock discontinuities. A series of direct shear tests were undertaken on saw-cut basalt discontinuities. The results of these tests were used for training and validation of two networks.

RÉSUMÉ:

Le présent article fait état de l'utilisation des réseaux neuronaux artificiels pour la prédiction du comportement en cisaillement des discontinuités du roc. Une série d'essais de cisaillement a été entreprise sur des discontinuités sciées dans des échantillons de basalte. Les résultats de ces essais ont été utilisés pour entraîner et tester les réseaux développés.

INTRODUCTION

This paper reports on work, currently in progress at Université Laval, on the application of artificial neural networks (ANN) to rock mechanics. This work has dealt with investigating the potential of ANN in defining the constitutive behaviour of rock discontinuities and in characterizing joint roughness.

The mechanical behaviour of natural rock discontinuities has been the subject of several theoretical and empirical studies. The inherent complexity of the problem is often made more demanding by the difficulties in selecting and quantifying the necessary input parameters for any models.

Neural networks examples of rock mechanics applications are presently limited, Hadjigeorgiou & Flament (1993). Nevertheless, they are the subject of increasing attention as both the technology evolves and its full potential begins to be realized. In particular certain tasks such as, pattern recognition and classification are better suited to neural networks. This work reports on use of pattern recognition techniques in characterizing the shear behaviour of saw-cut joints.

FEEDFORWARD ANN

Artificial neural networks consist of simple, highly interconnected, processing elements (nodes or neurons) which work in parallel. The name, neural networks, comes from the fact that their structure is inspired from

that of the brain. Each node possesses a computational feature that permits it to transform the signals it receives into a new signal that it can transmit. A neural network is often classified by the way it encodes or decodes information. The encoding of information in the network is achieved during the learning (or training) phase. Learning arises when the network modifies its internal parameters, particularly its synaptic weights, in response to external stimuli. This can be supervised, unsupervised or reinforced. The popular back-propagation learning algorithm is a supervised learning algorithm. The feedforward or feedback architecture of a network refers to the way it decodes information, that is the direction of information during recall. In a feedforward neural network the nodes are organized in input, hidden, and output layers, as seen in Figure 1. Information flow during recall is unidirectional: from input toward output nodes. Those neurons belonging to the input layer are responsible for receiving the data to be processed by the network. The output layer holds the global computation results. One or more hidden layers may be present depending on problem complexity but quite often one layer suffices. All nodes within the input layer, (I_1, I_2, ..., I_{N1}), are connected to all nodes of the first hidden layer, (H_1, H_2, ..., H_{NH}). These are subsequently connected to all nodes of the second hidden layer, if one is present, or to the nodes of the output layer (O_1, O_2, ..., O_{NO}). As shown in Figure 2, a weighting factor (W_{hn}) is associated with each connection.

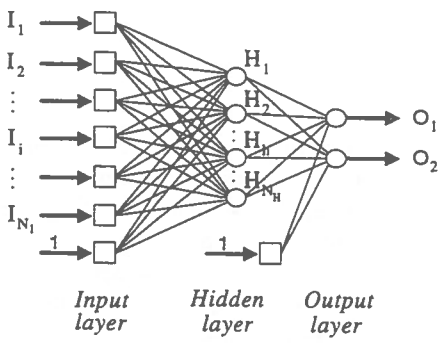

Figure 1. A feedforward neural network.

The role of the input nodes is to capture the data to be processed by the network and then transmit it to the hidden nodes. No data transformation occurs in the input nodes and the transfer is direct. Within the hidden layers several operations take place. First, the values received from the input layer nodes are multiplied by the synaptic weights of the connections. Then, each hidden node "sums" all of the weighted values it receives.

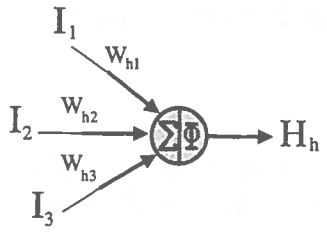

$$H_h = \Phi\left[\sum_i (W_{hi} \cdot I_i)\right]$$

Figure 2. Data processing by a neuron.

While arithmetic summation is the method most often employed, any other type of linear transformation is applicable. Finally, a nonlinear transformation, such as a hyperbolic-tangent function, is applied to the summation result. The resulting value, the activation level of the node, is then transferred to each node of the second hidden layer or of the output layer.

Although linear and nonlinear transfer functions within the output layer can be different from those of the hidden layer, the output layer has the same role as the hidden layer. The activation level of the output nodes are the network outputs or results. The general process, illustrated in Figure 2, is governed by the following equations:

$$H_h = \phi_H \left(\sum_{i=1}^{n_I} W_{ih}\, I_i\right) \quad for \quad h = 1 \rightarrow N_H$$

$$O_o = \phi_O \left(\sum_{h=1}^{n_H} W_{ho}\, H_h\right) \quad for \quad o = 1 \rightarrow N_O$$

where

- I_i is the value of the input node.
- W_{ih} is the weight associated with the connection between node i of the input layer and node h of the hidden layer.
- ϕ_H is the nonlinear transfer function of the nodes within the hidden layer.
- H_h is the activation value of hidden node h.
- W_{ho} is the weight associated with the connection between node h of the hidden layer and node o of the output layer.
- ϕ_O is the nonlinear transfer function of the nodes within the output layer.

O_o is the activation value (network output) at output node o.
N_I is the number of input nodes.
N_H is the number of hidden nodes.
N_O is the number of output nodes.

A constant node, often called bias, offset or reference, is always present except in the output layer. Its role is equivalent to the constant term in a linear regression model.

Training of a feedforward neural network using a back-propagation algorithm is achieved by presenting inputs to the network along with the desired outputs. The network processes the inputs into its own simulated outputs. The learning algorithm then evaluates an output error function that describes the difference between the desired and simulated outputs. This error function allows the determination of local error for each of the output nodes and a differential value for the synaptic weights for these nodes. The same process is repeated with all adjacent hidden layers until the input layer is reached. At that moment all synaptic weights are updated. The learning algorithm is named after the back-propagation error.

As neural networks are trained on sample data, these should be of high quality and representative of the domain. The selected examples should represent all events, that are likely to occur, in equal proportions. The training phase, and network size, can be significantly reduced by using the domain knowledge to pre-process the data. This could involve among other, scaling, compression, partitioning into sub-problems, extraction of key factors, etc.

BEHAVIOUR OF ROCK DISCONTINUITIES

The shear behaviour of rock discontinuities has been reviewed by several authors, more recently by Brady & Brown (1993). This behaviour is influenced by such considerations as surface roughness, material dilatancy, the presence of infilling or water, scale effects, and material properties.

Several models of discontinuity strength and deformation exist including empirical, Barton-Bandis (Bandis et al. 1983) and analytical, Ladan model (Ladanyi & Archambault 1970). This is an area of continuing research. In particular, problems associated with quantifying discontinuity roughness have been addressed by pseudo-static tilt tests, statistical, and fractal theory, Hsiung et al. (1993).

DETERMINATION OF JOINT ROUGHNESS

In both surface and underground mining, the presence of discontinuities can influence the stability of an excavation as well as rock mass permeability. The surface morphology of a discontinuity controls, to a large degree, its mechanical properties and its shearing resistance. In the past, deterministic, statistical and probabilistic techniques have all been used to model the discontinuity profile and predict joint behaviour.

Barton & Choubey (1977) proposed a series of ten profiles to define the degree of roughness for 10 cm long natural joints. Visual comparisons of joint profiles his chart allow the quantification of the degree of roughness by a proposed Joint Roughness Coefficient (JRC). This system however, while popular is subjective and can result in inconsistent interpretation.

The determination of joint morphology poses a considerable challenge, made even more difficult due to the influence of scale. What is defined as a planar joint at large scale can be a very undulating surface for smaller scale. In prior work with neural networks, Hadjigeorgiou & Flament (1993), Hadjigeorgiou et al. (1995), the aim was to define the profile of natural joints, approximately 1 m long. In all, 183 natural joint profiles were used. The joint morphology for each profile was then assigned a rating from one of three basic categories of smooth, average and rough.

In order to train a back-propagation neural network to classify the profiles, these were manipulated using frequency distributions. As a result of this pre-processing all profiles were described using a set of data whose cardinality was small and constant. The chosen pre-processing method also allowed the developed network to handle any length of natural discontinuity profiles. This is an important feature given in-situ variations of in joint length.

An analysis of field data profiles using the developed neural network has shown that it was possible to correctly classify the joint profiles according to their degree of roughness in 178 out of the 183 case studies, a success rate of 97%, Hadjigeorgiou et al. (1995). Furthermore, the failed predictions were very near the threshold points.

MATERIAL MODELLING USING ANN

The idea of using neural networks to predict the shear behaviour of rock discontinuities was inspired by prior

work material modelling under stress, Ghaboussi et al (1991), Pidaparti & Palakal (1993) and Millar & Clarici (1994). Their work has clearly demonstrated that neural networks provide an interesting alternative to mathematical models.

Ghaboussi & al. (1991) used back-propagation networks to model the behaviour of concrete under both monotonic biaxial and compressive uniaxial cycle loadings. For conditions of biaxial loading, a network was constructed aiming to capture the path-dependent material behaviour. They used a 6-40-40-2 architecture, i.e. 6 input nodes, two hidden layers with 40 nodes each, and two output nodes. This network was trained on nine experimental biaxial stress-strain curves. The same network architecture was employed to produce both a stress and a strain-controlled model. As input the stress-controlled model had two stresses, two strains and two stress increments. As output it used two strain increments. For the strain-controlled model, strain increments were used as input, producing stress increments as output. This allowed the network to reproduce the behaviour of concrete in a path-dependent fashion. Given a known stress-strain state and given an increment of stress or strain, it predicted an increment of the non-controlled parameter. It is interesting to note that the this network was trained in stages. The Ghaboussi et al. (1991) network was shown to produce reasonable predictions for materials outside its training data and in agreement with analytical models.

Ghaboussi et al. (1991) also employed feedforward neural networks to predict concrete behaviour when submitted to uniaxial cyclic loading. For this problem they used a 7-40-40-1 network configuration. In order to account for path-dependency they used as input three known stress-strain points and a stress increment. The output was the corresponding strain increment. Several combinations of loading cycles were used for training and testing of the network. This led to very good predictions, particularly if one considers the complexity of the problem and the limited input information. The network performance might have been further improved if input information included cycle number, and if data was differentiated into loading and unloading cycles.

Pidaparti & Palakal (1993) developed a feedforward, back-propagation neural network to predict stress-strain behaviour of graphite-epoxy laminates under monotonic and cyclic traction loadings. The network used to reproduce the behaviour of composites under monotonic traction loading used a 3-17-17-1 architecture. As input they employed the fibre angle θ, the initial stress and the stress increment, while for output they selected total strain. Training and testing were made on experimental stress-strain curves with varying fiber angles. The experimental results showed very good agreement with network predictions, for both training and validation data. Furthermore, the experimental stress-strain behaviour of graphite-epoxy laminates changes from stiffening to softening depending on the fiber angle. This complex composite behaviour was well understood by the network even though it was not explicitly introduced during learning.

The network developed to predict the behaviour of these laminates under cyclic loadings used as input nodes the fiber angle, the initial stress, the number of the current cycle and a 0/1 differentiation between loading and unloading. Total strain was still the output and the number of hidden layers and nodes was as for the first network. Although preliminary tests were good, further experimental data are needed for validation of this model.

Millar & Clarici (1994) employed a back-propagation network to predict with great accuracy the deformability behaviour of Crosland Hill sandstone. Samples were submitted to triaxial laboratory tests under five increasing confining pressures (4.5-35.0 MPa). In their work they employed as input the confining pressure, axial and radial strains and the sign of the gradient of the axial stress-axial strain curve. As output they used the axial stress. The best results were obtained with 1 hidden layer using 7 nodes. The network was successful in reproducing the axial stress-axial strain curves of the sandstone training data. It was also shown that the developed network was applicable to experimental data not part of its training field, but within the same stress range. The experimental peak stress conditions were not, however, perfectly reproduced.

Zhang & Nie (1994) also modelled the mechanical behaviour of sandstone samples using a feedforward network trained with back-propagation algorithm. The developed architecture is not fully described in the paper. It appears they used as inputs, material mineralogy, mean dry bulk density, mean saturated density, mean grain density and the effective porosity and the uniaxial compressive strength as output. In all they employed 35 samples with 34 used for training the network and one reserved for testing. This process was repeated 35 times, each time employing a different validation sample. Although this approach may be useful for smaller databases, it is not necessarily applicable for most practical situations. The predicted results reported by Zhang & Nie (1994) show excellent agreement with their constituent experimental database.

The reviewed literature suggests that neural networks can successfully predict material behaviour under different stress regimes. The appeal of the method is obvious in cases when material behaviour is governed by

several parameters, or when the governing relations are too complex to be analytically modeled. The shear behaviour of natural joints is one of these cases.

EXPERIMENTAL SET-UP

A series of direct shear tests were performed on eight dry, saw-cut basalt samples. The samples had a square shear surface of approximately 2500 mm^2, and were set in cement prior to being fitted for a portable direct shear box (model PHI-10 from Roctest). Three to six tests were performed on each sample at increasing normal stresses from 1.0 to 6.0 MPa. During testing the normal load was kept constant. A total of 40 tests was conducted at a shearing rate of approximately 2 mm/min until a displacement of 8 mm was reached. A data acquisition system was utilized to record shear displacement, and shear and normal stresses.

DEVELOPED NEURAL NETWORK

A feedforward neural network using a back-propagation learning algorithm was trained to capture the shear behaviour of the saw-cut basalt joints. This choice was made based on the success of feedforward neural networks in modelling material behaviour, as discussed earlier. In this study the commercially available ANN simulator NeuralWorks Professional II/Plus by NeuralWare Inc (1991) was used. This is a user friendly software that can simulate several neural network models.

The shear displacement and the applied normal stress recorded during laboratory testing were selected as inputs to a ANN while the shear strength was used as output. After several trials, improved network performance was achieved when the logarithmic values of shear displacement were used as input.

Several network configurations were investigated to arrive at the most performing for this particular problem. The applicability of sigmoid and hyperbolic-tangent transfer functions was examined as well as different learning coefficients. Finally the number of nodes and layers was also allowed to vary. The selected architecture has two input nodes, one hidden layer with fifteen nodes, one output node and employs a hyperbolic-tangent function for each node.

This ANN was used to predict the shear behaviour of the rock discontinuities. While it provided an acceptable overall degree of accuracy it had some difficulties in predicting shear behaviour for small deformations (less than 1.5 mm). Consequently it was felt that a higher agreement between experimental and predicted results might be achieved by using two networks. The first one (SHEAR-1) would be suited for shear displacements of up to 1.5 mm and the second (SHEAR-2) designed for the range between 1.5 to 8 mm.

Both SHEAR-1 and SHEAR-2 are feedforward neural networks using the back-propagation learning algorithm. The displacement and normal stress were used as input and the shear strength as output. SHEAR-1 has 15 nodes in its single hidden layer, while SHEAR-2 used only 7 hidden nodes. This was possible since the behaviour in the post-peak area is less complex than it is in the pre-peak area. The configuration for SHEAR-2 appears in figure 3.

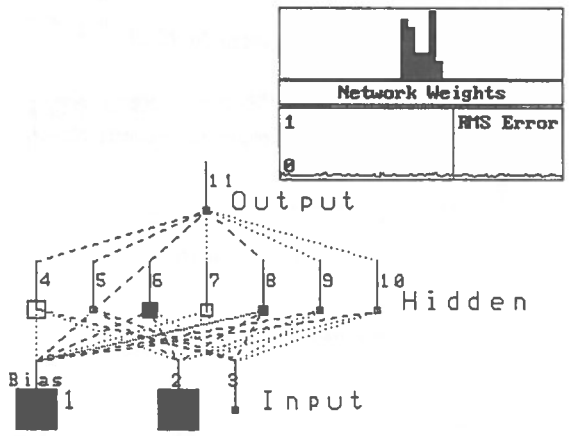

Figure 3. Neural Network architecture for SHEAR-2.

Each network was trained and tested on its applicable range of shear displacement. Both networks used 20 stress-displacement curves corresponding to four discontinuity samples for training. The learning phase for both networks was stopped when the output errors displayed were minimized and the network weights frequency histograms were stabilized, as shown in Figure 3. Learning was stopped after 50 000 iterations for SHEAR-1 and after 30 000 iterations for SHEAR-2. Finally, the networks were tested over the complete database including data not in the training files. The results are presented in the following section.

PREDICTED vs EXPERIMENTAL RESULTS

The performance of the trained networks was assessed by comparing the experimental shear strength-displacement curves to those predicted by the networks, and by determining the basic friction angle for each sample.

Figures 4 and 5 compare experimental and predicted results for basalt samples 0201 and 0302 respectively. The predictions of networks SHEAR-1 and SHEAR-2 have been combined to construct the complete shear strength-displacement curves. For presentation clarity, only one out of four points has been plotted on the graphs. The experimental results for sample 0201 were included in the training data files, while those of 0302 were only used during the validation process.

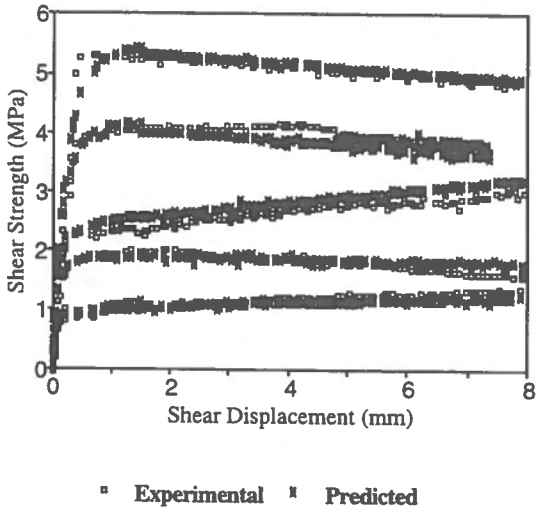

Figure 4. Experimental and predicted shear strength-displacement for sample 0201.

Several observations can be made on the basis of Figures 4 and 5. First, the networks seem to have captured the general pattern of the experimental curves. However, as with the work of Millar & Clarici (1994), it has been difficult to determine with great precision the peak zone of the curves. This is particularly true for those basalt samples not part of the training files. This is not surprising given that during the laboratory tests a manual control was employed to manipulate the hydraulic jacks of the shear box. Use of a servo-control direct-shear apparatus could arguably lead to superior sets of training data which should further improve SHEAR-1 results. SHEAR-2 was more successful in predicting the second part of the shear strength-displacement curves. As shown in both figures, there is not a perfect match at the point where the results of the two networks are integrated, but there is more than acceptable agreement for most cases.

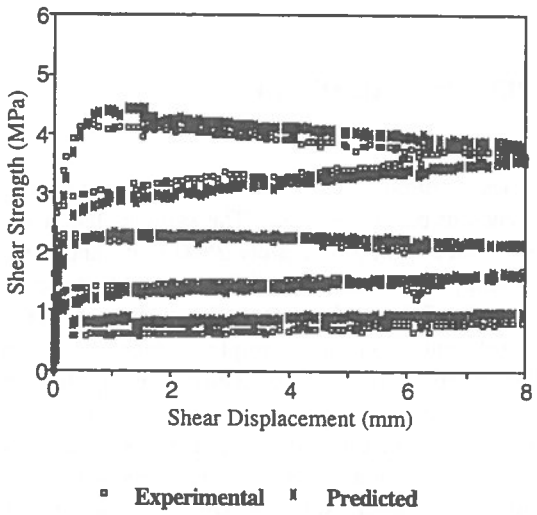

Figure 5. Experimental and predicted shear strength-displacement for sample 0302.

Finally, it can be seen that the networks tend to smooth the shear strength-displacement curves. This is because neural networks extract general patterns, not paying attention to the vagarities of the experimental shear strength-displacement curves.

Basic friction angles were determined using the shear strength-displacement curves of the saw-cut joints. The mean value of 37.7° is representative for saw-cut basalt discontinuities, as reported by Barton and Choubey (1977). The basic friction angles determined from the neural network predicted shear strength-displacement curves had a mean value of 37.4°. This represents a relative difference of only -0.8% with respect to the experimental average value. The complete results are summarized in Table 1. These results clearly demonstrate that neural networks can be used to evaluate the basic friction angle with accuracy and great input simplicity.

FUTURE WORK

Future work will aim to expand the database for discontinuities of different rock types. This will probably require more inputs to the network, such as material density and compressive strength.

TABLE 1. Comparison of experimental and predicted basic friction angles (in degrees).

Sample	Experimental	Predicted	% Diff.
0101	38.2	37.8	-1.0
0102	37.0	37.3	+0.8
0201*	36.8	36.9	+0.3
0202*	38.0	37.4	-1.6
0203*	36.1	37.2	+3.0
0204*	38.4	37.2	-3.1
0301	39.5	37.3	-5.6
0302	37.3	37.7	+1.1
Mean	37.7	37.4	-0.8

* part of training data

The influence of joint roughness on the shear behaviour of natural discontinuities will also be addressed. This is considered necessary in order to produce a realistic picture of the shear behaviour of natural joints. Prior work on the characterization of the roughness of joint profiles, Hadjigeorgiou & Flament (1995), has demonstrated that roughness can be studied and quantified in an objective manner.

The overall philosophy of future work is to attempt to keep the inputs to the networks as simple as possible. Input data that can be easily determined on field sites and produce good results will be strongly favoured over input data that cannot be easily quantified at site but may produce perfect results.

CONCLUSIONS

This paper has focused on recent developments in neural network applications in rock engineering. The fundamentals of the theory have been reviewed. While neural networks will not be suitable for every type of problem, they hold great potential in particular cases.

Present work focused on modelling the shear behaviour of natural rock joints. Preliminary works on saw-cut discontinuities showed that back-propagation neural networks can reproduce experimental shear strength-displacement curves. These are obtained with enough accuracy to find realistic values of basic friction angles. Although the developed networks were not able to perfectly reproduce every part of the shear strength-displacement curves, they were in very good agreement with the experimental results.

Based on the present work, it is felt that neural networks have the potential to predict peak and residual shear strengths of natural joints.

REFERENCES

Bandis, S.C., Lumsden, A.C. and Barton, N., 1983
Fundamentals of rock joint deformation. Int. J. Rock Mech. Min. Sci. & Geomec. Abstr. 22: pp. 112-140

Barton, N. and Choubey, V., 1977
The shear strength of joints in theory and practice. Rock Mechanics, Vol. 10, pp. 1-54

Brady, B.H.G. and Brown, E.T., 1993
Rock Mechanics for Underground Mining. Chapman & Hall, p. 571

Ghaboussi, J., Garrett, J.H.jr. and Wu, X., 1991
Knowledge-based modelling of material behaviour with neural networks. ASCE Engineering, Mechanics, vol.117, no.1, january, pp. 132-153

Hadjigeorgiou, J. and Flament, F., 1993
Neural networks applications in mining. Proc. of 24th APCOM, Elbrond J. & Tang X. (eds), pp.161-168

Hadjigeorgiou, J., Flament, F., and Germain, P. 1995
Characterization of rock joint profiles using artificial neural networks. (in preparation)

Hsiung, S.M., Ghosh, A., Ahola, M.P. and Chowdhury, A.H., 1993
Assessment of conventional methodologies for joint roughness coefficient determination. Int. J. Rock Mech. Min. Sci. & Geomech. Abstr. Vol. 30, No. 7, pp. 825-829

Ladanyi, B. and Archambault, G., 1970
Simulation of shear behaviour of a jointed rock mass. Proc. 11th Symp. on Rock Mech., pp. 105-125

Millar, D.L. and Clarici, E., 1994
Investigation of back-propagation artificial neural networks in modelling the stress-strain behaviour of sandstone rock. Proc. IEEE Int. Conf. Neural Networks, June 26-July 2, Orlando, Florida, USA, Vol.7

NeuralWare Inc., Technical Publications Group, 1991
Neural computing. Manual of NeuralWorks Professional II/Plus and NeuralWorks Explorer

Pidaparti, R.M.V. and Palakal, M.J., 1993
Material model for composites using neural networks. AIAA Journal, vol. 31, no. 8, pp. 1533-1535

Zhang, Q. and Nie, X., 1994
Prediction of rock mechanical behavior by artificial neural network. A Comparison with Traditional Method. Fourth CSMR/Integral Approach to Applied Rock Mechanics, Santiago, Chile, 10-14 may, pp. 279-287

CAMI'95: 3rd Canadian Conference on Computer Applications in the Mineral Industry
Montréal, Québec, Canada, October 22-25, 1995

Numerical Modeling of Caving Using Continuum and Micro-Mechanical Models

Loren J. Lorig
Itasca S.A., Santiago, Chile

Mark P. Board, David O. Potyondy, Matthys J. Coetzee
Itasca Consulting Group, Minneapolis, Minnesota, USA

ABSTRACT:

The prediction of cavability of rock masses is an area of primary importance in the design of block- and panel-caving mines. To date, estimates of caving potential and fragmentation have been based on empirical methods. This paper describes the use of continuum finite-difference and discontinuum micro-mechanical numerical approaches to prediction of caving behavior.

RÉSUMÉ:

La détermination du potentiel d'effondrement des massifs rocheux est un sujet de première importance pour le design des mines en blocs et panneaux. Jusqu'à présent, l'estimation du potentiel d'effondrement et de fragmentation s'est faite sur bases empiriques. Cet article décrit l'utilisation de méthodes numériques en approche continue (différences finies) et micromécanique, appliquées à la prédiction du comportement à l'effondrement.

INTRODUCTION

Block- and panel-caving methods are important mining techniques for extraction of relatively low-grade, disseminated orebodies. The method can be very cost effective when the orebody freely caves with small fragment size — a behavior typical of weaker, secondary-replacement ores. Increasingly, caving is considered as a potential method for extraction of stronger, primary ores which are characterized by high values of intact rock strength and relatively widely spaced fracturing. In the past, these ores were considered to be candidates only for methods such as blasthole open stoping. Unlike many underground mining methods, caving requires extensive development of infrastructure such as extraction drifts, draw raises and crushing facilities prior to the start of production. The major factors which impact the design of these facilities, and thus the estimate of production rate and cost, are the cavability and the resulting fragment size distribution. The initiation and sustaining of the cave as well as the beginning fragmentation will govern the early economics of the operation. As the cave progresses, the fragment size distribution will govern the design and spacing of drawpoints and the degree of secondary blasting required. Even relatively minor changes (for example, the spacing of drawpoints) can have a major impact on the economics of an operation.

Often, the decision to make the large capital expenditures necessary for development of new properties, or extensions of existing mines into new ground conditions, is based only on experience gained at other mines. This is a reasonable approach when rock mass quality and the in-situ stress state of the property in question are similar to the base of experience, but it is questionable when these conditions deviate significantly. This paper discusses recent work in the use and development of numerical techniques for prediction of rock mass cavability and fragmentation. Two approaches to these problems are discussed here: (1) a semi-empirical application of a continuum finite-difference program to estimate undercut dimensions, advance directions and sequences for initiation and self-sustaining of the cave; and (2) a discontinuum-based micro-mechanical numerical approach for representation of the processes of fracture growth and movement along joint surfaces in response to undercutting and ore extraction. In the first approach, the aim is to provide a fairly rapid, but reliable, estimate of cavability necessary for mining-method evaluation using a methodology which can account for variability in

rock quality, the in-situ stress state, and the three-dimensional geometry of the mining. The second approach, currently under evaluation, is aimed at the explicit simulation of the mechanisms of fracture growth and fragmentation in a pre-fractured rock mass when subjected to excavation. After primary fragmentation, this modeling approach allows simulation of the movement and comminution of rock blocks in the drawing ore column.

OBSERVATIONAL METHODS FOR PREDICTION OF CAVABILITY AND FRAGMENTATION

Currently, the accepted methodology for the prediction of the caving and fragmentation characteristics of rock masses is based on observational data from existing cave mines. The most commonly used approach for estimating cavability and fragmentation was developed by D. Laubscher (1990) and is based on compilation of rock mass geotechnical characteristics and caving data from numerous mines world-wide. The basis of this work is a geomechanical classification system for the rock mass intact material and joints as well as in-situ stress conditions termed the Mining Rock Mass Rating (MRMR). This classification scheme is a modification of the Rock Mass Rating (RMR) system described originally by Bieniawski (1973) in which additional adjustments are made for mining conditions including weathering, mining-induced stresses, joint orientation and blasting effects. Data on the MRMR and cavability from numerous operations were used by Laubscher (1981) to construct Fig. 1 which defines the relation between the rock mass quality and the undercut hydraulic radius for various caving characteristics of the orebody. Three caving characteristics are defined: no caving; a "transitional" zone in which caving initiates; and "free" caving, where self-sustained caving occurs. As seen in this figure, the majority of data from mines exhibiting freely caving orebodies have MRMR values of less than about 40. As will be discussed later, data gathered in stronger, well-jointed ores at several Chilean caving operations indicate that the transitional-free caving boundary may tend to flatten at higher values of the MRMR.

An additional "marginal caving" region has been proposed by Karzulovic (1995) based on experience from Chilean copper mines. Superimposed on these curves is caving data from two mines: Mine 1 in secondary ore, and Mine 2 in harder, competent ore in which caving and fragmentation were difficult. Back-analysis using the continuum modeling technique discussed in this paper is shown as a solid horizontal line starting at the predicted initiation of caving and ending at the point of self-sustained caving.

Fragmentation mechanisms in the caving rock mass have been subdivided into two classes by Laubscher, who termed them "primary" and "secondary". Primary fragmentation (also referred to as stress caving) refers to the initial block fragments produced from the cave back as

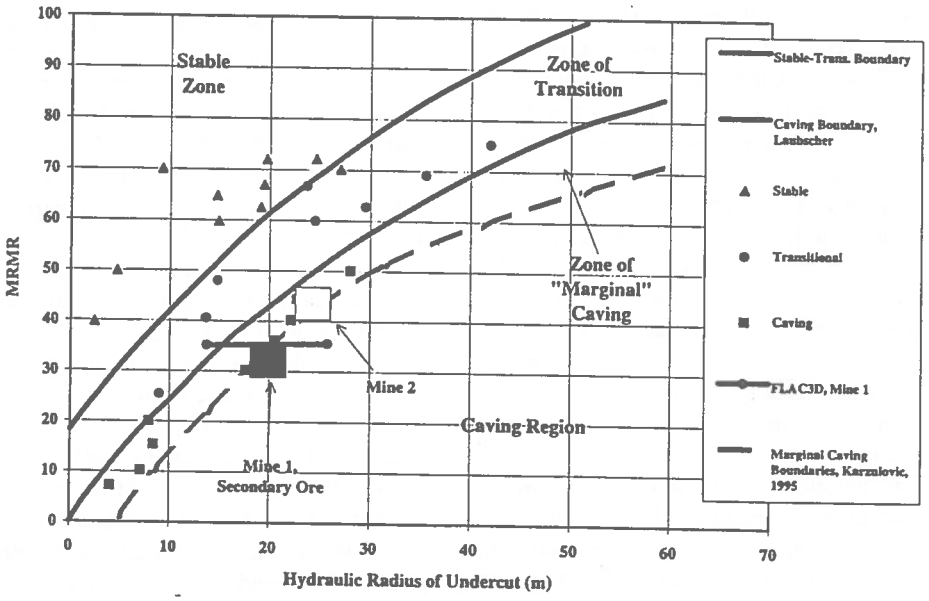

Fig. 1 Empirically derived cavability estimates as a function of undercut hydraulic radius as proposed by Laubscher (1990) and modified by Karzulovic (1995)

a result of stress redistribution caused by undercutting and cave expansion. The primary factors which control block size are the joint orientation, spacing, trace length, intact rock strength characteristics, and the ratio and magnitude of the principal stresses in the cave back. In low-stress environments with heavily jointed rocks, caving occurs primarily through shear and separation on existing joint surfaces. However, in a high-stress environment and in sparsely jointed rock masses with joint orientations characterized by high normal stresses, fragmentation may be related to intact rock fracture.

Secondary fragmentation of the detached rock fragments occurs as they are drawn down through the ore column. The degree to which further fragmentation occurs will depend on several factors, including the aspect ratio of the primary fragments, the intact rock strength, the presence of microfractures or veinlets in the rock blocks, and the height of the ore column. As pointed out by Laubscher (1981), secondary fragmentation is generally of lesser importance in governing the final fragment size distribution due to the low stresses which predominate in a drawing ore column. Esterhuizen (1994) has developed a model for predicting fragment size distribution based on the observations of Laubscher and the specification of rock mass geotechnical parameters. Bartlett (1995) reports that this model has produced good comparisons to actual fragment size distributions in ores of varying strength at the Premier Diamond Mine in South Africa.

NUMERICAL APPROACHES TO SIMULATE CAVING PROCESSES

Empirical methods, by necessity, are limited by the range and variability of the data base from which they have been developed. Unfortunately, the data base regarding cave mining is not extensive, particularly as it applies to conditions of sparsely jointed, high-strength rock masses and to a range of in-situ stress magnitudes and ratios. Numerical modeling has the potential advantage that variations in rock quality, in-situ stresses and the three-dimensional geometry typical of caving operations can be represented. However, caving is a complex, transient process involving intact rock fracture as well as slip and separation on existing fracture surfaces as undercutting and drawing of the ore proceeds. The application of numerical models to simulate caving has been performed on two levels: (1) a "gross" level in which continuum-based numerical models have been used in an attempt to identify when a state of self-sustained instability will exist in the undercut back; and (2) a "detailed" level in which the fracture and the dislodging and gravity instability of blocks in the undercut back are simulated.

At the gross level of detail, the failure and collapse prediction of the rock mass when undercut may be represented in an approximate way by using a plasticity model of some form. Rech and Lorig (1992) present a back-analysis of caving behavior of the 8100 level of the Henderson Mine using a large-strain plasticity model based on the Mohr-Coulomb failure criteria. The rock mass was treated as an equivalent isotropic material and the cohesion adjusted until an approximate match was achieved between model and field behavior. The primary goal of this sort of analysis is to examine required undercut hydraulic radii for sustained caving and to provide a platform for testing the impact of various mining strategies and rock mass qualities on caving behavior. This approach, however, gives no information on primary or secondary fragmentation or muck flow, and the ability to represent cave growth is questionable.

For these reasons, attempts have been made to model the details of caving mechanisms through the use of a discontinuum approach. Early investigations by Voegele (1978) were based on a two-dimensional, rigid block program of Cundall (1971) for examination of roof-collapse mechanisms for wide-span excavations. Using a similar approach, Lorig et al. (1989) applied a three-dimensional discontinuum approach to back-analysis of the collapse of the undercut of a blasthole stope at the East Mine in Sudbury, Ontario. These analyses explored the number and orientation of joint sets required to produce roof collapse in the absence of fracturing of intact rock. In each case, it was found that joint-related collapse alone requires a flat-lying joint set plus several additional joint sets at higher angles to produce unstable block geometries. Even then, stable arch geometries easily form when blocks with high aspect ratios are represented. These analyses have shown that the lack of a means of internal fracture of the blocks has proved to be a serious shortcoming of the rigid block models. In an attempt to overcome these problems, two-dimensional discontinuum models have been used to subdivide the rock mass into a large number of small polygonal blocks with random shape. Because the block interfaces are bonded using a Mohr-Coulomb strength criterion, the overall assemblage will behave more-or-less as an elasto-plastic material. However, because the block interfaces may shear or separate, they provide a large interconnected random network of **potential** fracture pathways. Guest and Cundall (1994) present a predictive analysis of vertical retreat-induced caving at the Bultfontein Mine in South Africa. It was found that un-

dercut spans, predicted by the modeling when sustained collapse occurred, were in reasonable agreement with field behavior.

The experience cited above has shown that both continuum and discontinuum numerical models have value for prediction of caving behavior. The continuum approach, if properly calibrated against field observations, can be used for determination of the onset of caving and, perhaps, for examination of cave growth. To examine primary and secondary fragmentation and the flow of material in the draw column, a discontinuum approach is required. In the following section, we describe a methodology for application of a three-dimensional continuum model to prediction of undercut hydraulic radii necessary for onset and for self-propagation of the cave. The methodology is applied to back-analysis of caving in weaker secondary ore and for prediction of caving in stronger, primary ores. A new approach using a micro-mechanical discontinuum model is described that allows both movement on pre-existing joint surfaces as well as fracturing in the intact solid. Both two- and three-dimensional numerical models described later have been completed and are currently being tested at caving mines in Chile and South Africa.

CAVING PREDICTION USING A CONTINUUM MODELING APPROACH

A technique similar to that suggested by Rech and Lorig (1992) has been used for the predictions of caving of secondary and primary ores for a new extraction horizon at a copper mine. The secondary ore is heavily fractured, relatively weak, and is assumed to be isotropic in its mechanical response. The primary ore is strong and brittle, with three joint sets having average spacing of approximately 1 m. Measurement of the intact-rock compressive strength and moduli have been performed as well as extensive geotechnical mapping using the MRMR system. Geotechnical mapping was used in combination with the method of Hoek and Brown (Hoek, 1990) to determine in-situ property estimates that were shown to reproduce observed field pillar collapse in the same material at upper levels. Figure 2 presents approximate Hoek-Brown failure envelopes for the secondary and primary rock. In the analyses presented here, a Mohr-Coulomb failure criterion is used in the numerical model, requiring determination of the rock mass cohesion, friction angle and tensile strength. Several options are available for determination of these values from a linear approximation to the Hoek-Brown criterion. Since failure is occurring directly in the undercut back, where confinement is low,

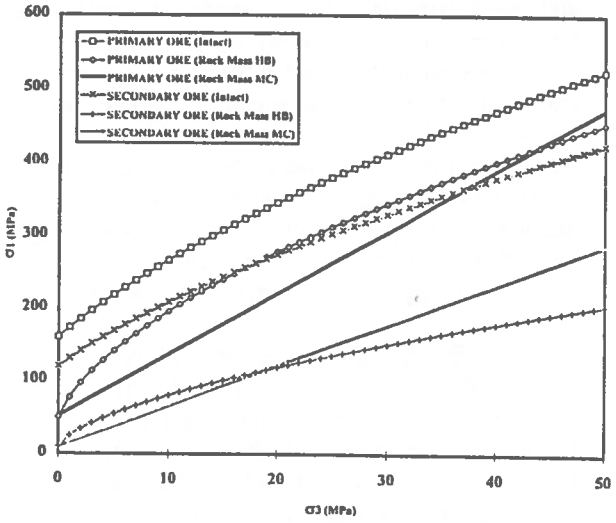

Fig. 2 Hoek-Brown failure criteria and approximate linear Mohr-Coulomb failure envelopes for primary and secondary ores

a linear approximation to the criteria is taken at a low confining stress from which the rock mass cohesion and friction angle are estimated. In-situ moduli are determined from laboratory measurements and the RMR using the approximation of Serafim and Pereira (1983). Table 1 presents the equivalent continuum rock mass properties assumed for the analyses.

The *FLAC*^{3D} explicit finite-difference program (Itasca, 1994a) was used to model the proposed undercutting direction and sequence for the new extraction horizon. The methodology employed for representation of the caving process is given in Fig. 3. The mine is located in a rugged mountainous region where the influence of topography on in-situ stresses cannot be ignored. A regional-scale model which included this topography and the existing caved regions was first developed with applied lateral stress components which best fit the stress measurements made in the mine. A mine-scale model was then constructed for the region directly surrounding the new extraction level with applied boundary stresses obtained from the regional-scale model. The in-situ rock mass is considered elastic with the stiffness properties given previously. The undercut is extracted incrementally and replaced by elements with elastoplastic material behavior and "caved rock" properties. The stresses within these "caved" elements are set to zero **initially**, and the model is run to a quasi-equilibrium condition. At this point, the stresses once carried by the mined undercut will have re-distributed to the surrounding solid mass,

TABLE 1. Properties estimate for primary and secondary ore and caved material

Unit	MRMR	UCS (MPa)	m	s	E_{field} (GPa)	Cohesion (MPa)	ϕ (°)	Tensile Strength (MPa)
Second.	30-35	120	4	0.0069	25	2	44	0.2
Primary	60-70	160	10	0.0977	55	9	51	0.9
Caved	-	-	-	-	0.5	0	35	0

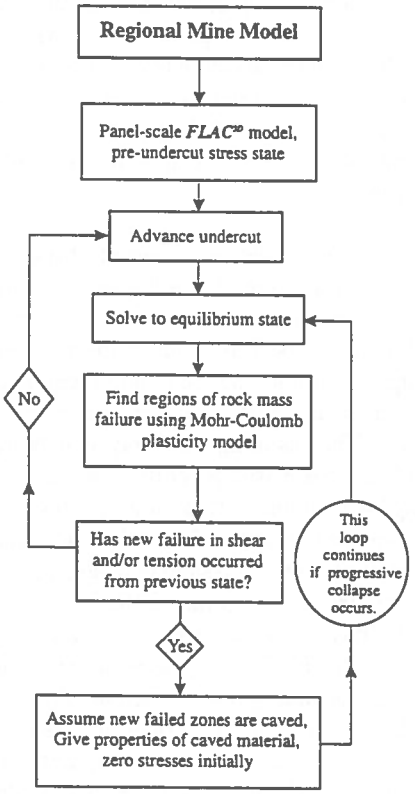

Fig. 3 Methodology for application of a continuum-based numerical model for prediction of onset of caving

and the stresses within the caved material will be gravitational and quite small in comparison. A check is made of all rock mass finite-difference zones above the undercut to determine if any have failed in tension and/or shear according to the Mohr-Coulomb criterion. If so, they are assumed to have caved. Their properties are changed to caved rock, and stresses within them are initialized to zero. The model is then run to determine the subsequent stress redistribution. The calculation cycle is repeated for the current undercut dimension until one of two conditions occurs: (1) the rock mass reaches equilibrium with a stable roof arch, or, (2) a stable roof arch cannot be maintained and the cave tends to propagate. If a stable arch is obtained, the undercut is incrementally advanced, and the process is repeated. In these analyses, intimate contact was assumed between the caved material and the rock mass, although other forms of interaction between them, such as a gap between cave back and caved material, have been used with similar overall predictions obtained.

The model of the mining panel in question is approximately 500 m wide, 900 m long, 900 m high, and is composed of 11648 quadrilateral finite-difference zones in which the elements within the cave region are 15 m cubes. In secondary ore, the cave is predicted to initiate at a hydraulic radius of approximately 13 m and becomes self-sustaining at approximately 25 m. This can be compared to Laubscher's empirical design curves presented previously in Fig. 1. As seen in this figure, the prediction agrees well with this data base and with the previous experience in the above extraction level. The primary rock is predicted to require hydraulic radii in excess of 60 m for cave initiation in this material, indicating that caving will be problematic with expected large fragmentation. Caving in rocks with such high values of MRMR is not typical, as evidenced by the lack of free-caving data in this region. Also, the model prediction indicates significantly larger required hydraulic radii than estimated in Fig. 1. Superimposed on this plot is recent data from primary rock (MRMR ~ 40 - 45) from an experimental caving area of another mine (Mine 2) in this region. The caving experience in this rock was difficult, even for hydraulic radii of 22 - 24 m. Karzulovic (1995) has modified Laubscher's original design curves based on observations in Chilean caving operations. The primary modification has been addition of a "marginal" caving area which lies between the free-caving and transitional regions. This marginal caving region also flattens more rapidly at values of MRMR greater than approximately 40. However, the precise form of these curves is not known due to a lack of caving data for these higher values of MRMR. Additionally, it is likely that a single

number such as the hydraulic radius may not be an adequate descriptor of complex undercut layouts.

Discussion

The procedure used above makes two primary simplifying assumptions: (1) the rock mass is isotropic, with the effects of geologic structures accounted for by a plastic constitutive model; (2) the stress redistribution within the rock mass is a result of the increase in dimension of the cave only, and yielding in the immediate roof of the cave will not have a great influence on this redistribution. The degree of conservatism inherent in these assumptions is not immediately obvious. However, it would appear reasonable that the assumptions make this approach more amenable to highly fractured, poor-quality materials, as evidenced by the good agreement between the secondary-ore field response and the model predictions. The utility of this method for higher-quality, poorly jointed primary rocks will be examined soon in this mine as comparisons are made during the future mining of primary ores.

A MICRO-MECHANICAL DISCONTINUUM APPROACH FOR SIMULATION OF CAVING

Introduction

During the past two years, Itasca Consulting Group, under the sponsorship of Anglo American Diamond Division and CODELCO, has developed two- and three-dimensional micro-mechanical discontinuum programs aimed at simulation of the fracture and fragmentation processes which accompany caving. These programs, *PFC*^{2D} and *PFC*^{3D} (Particle Flow Code, Itasca, 1995a and 1995b) are based on the idea that a rock mass can be represented as a large number of constituent particles (much the same as grains) whose contact stiffness and bonding behavior are simple in nature. Since the programs use a discontinuum approach for representing the interaction of the particles, the particles are free to slip or separate under applied forces as dictated by the mechanics of the system. It is possible to produce complex macroscopic behavior such as compaction, strain softening/ hardening and fracture without resorting to complex constitutive laws. The basis of the programs are described below, followed by a relatively simple caving application.

Basis of the Particle-Flow Models

A general particle-flow model simulates the mechanical behavior of a system comprised of a collection of distinct, arbitrarily shaped particles that displace independently and interact only at contacts. If the particles are assumed to be rigid, and the behavior of the contacts is characterized using a soft-contact approach, in which a finite normal stiffness is taken to represent the measurable stiffness that exists at a contact, then the mechanical behavior of such a system is described in terms of the movement of each particle and the inter-particle forces acting at each contact point. Newton's laws of motion provide the fundamental relation between particle motion and the forces causing that motion. The force system may be in static equilibrium (in which case, there is no motion), or it may be such as to cause the particles to displace.

The programs implement a particle-flow model in terms of a collection of circular and spherical particles. In addition to simulating granular flow, the particle-flow model can be used to simulate the behavior of a solid. Groups of particles can be bonded together at their contact points such that the groups behave as autonomous objects. The resulting assembly can be regarded as a "solid" that has elastic properties and is capable of "fracturing" when bonds break in a progressive manner. In addition, the broken blocks can interact with one another. This type of physical system may also be modeled by the distinct-element programs *UDEC* (Itasca, 1994b) and *3DEC* (Itasca, 1994c), which consider angular blocks. However, the PFC codes possess three advantages. First, they are potentially more efficient, since contact detection between circular/spherical objects is much simpler than contact detection between angular objects; second, there is essentially no limit to the magnitude of displacement that can be modeled; and third, it is possible for the blocks to break (since they are composed of bonded particles), unlike blocks modeled with *UDEC* or *3DEC*, which cannot break internally. A possible drawback to modeling a blocky system with the PFC codes is that the block boundaries are not planar. However, in some instances, this could prove to be useful, since surface topography of a fracture can be represented by variation of the radii of the particles which compose the surface.

A "synthetic" rock sample is modeled as a random assembly of circular/spherical particles bonded together in a dense packing. The radius magnitude and statistical distribution can be controlled to obtain a given packing density (i.e., porosity). All particles are typically assigned the same values for normal stiffness, shear stiff-

ness, and friction coefficient; the normal and shear bond strengths of the contacts satisfy a normal distribution.

Two types of bonds may be present, either individually or simultaneously, at particle contacts in a PFC model. These bonds are referred to as "contact" and "parallel" bonds. Contact bonds reproduce the effect of an adhesion acting over the vanishingly small area of the contact point — thus the name contact-point bond or, simply, contact bond. Parallel bonds reproduce the effect of additional material (e.g., cementation) deposited after the particles are in contact. The effective stiffness of this additional material acts in parallel with the contact-point stiffness — thus the name parallel bond. The contact bond can only transmit a force between the two bonded particles, while the parallel bond can transmit both a force and a moment. A detailed description of these two bonding models can be found in Itasca (1995a,b).

Contact bonds set limits on the allowable magnitudes of normal tension and shear force at contacts. If either the normal limit or the shear limit is reached, then the bond breaks, and the contact may not subsequently take tension, although compressive forces are allowed together with appropriate shear forces (limited by the friction coefficient). Parallel bonds set limits on the allowable magnitudes of normal tensile and shear stress acting on the parallel bond cross-section. If either the normal or shear limit is reached, then the bond breaks.

Distinct Element Method

The PFC codes model the movement and interaction of stressed assemblies of rigid circular/spherical particles using the distinct-element method (DEM). The DEM was introduced by Cundall (1971) for the analysis of rock mechanics problems and was then applied to soils by Cundall and Strack (1979). A thorough description of the method is given in the two-part paper of Cundall (1988) and Hart et al. (1988). The PFC codes are classified as **discrete-element** codes based on the definition in the review of Cundall and Hart (1992) because they allow finite displacements and rotations of discrete bodies (including complete detachment) and recognize new contacts automatically as the calculation progresses. The PFC codes can be viewed as simplified implementations of the DEM because of the restriction of rigid circular/spherical particles. (The general DEM can handle deformable polygonal-shaped particles.)

In the DEM, the interaction of the particles is treated as a dynamic process with states of equilibrium developing whenever the internal forces balance. The contact forces and displacements of a stressed assembly of particles are found by tracing the movements of the individual particles. Movements result from the propagation through the particle system of disturbances caused by specified wall and particle motion and/or body forces. This is a dynamic process in which the speed of propagation depends on the physical properties of the discrete system.

The dynamic behavior is represented numerically by a timestepping algorithm in which the velocities and accelerations are assumed to be constant within each timestep. The solution scheme is identical to that used by the explicit finite-difference method for continuum analysis. The DEM is based upon the idea that the timestep chosen may be so small that, during a single timestep, disturbances cannot propagate from any particle further than its immediate neighbors. Then, at all times, the forces acting on any particle are determined exclusively by its interaction with the particles with which it is in contact. Because the speed at which a disturbance can propagate is a function of the physical properties of the discrete system, the timestep can be chosen to satisfy the above constraint. The use of an explicit, as opposed to an implicit, numerical scheme makes it possible to simulate the non-linear interaction of a large number of particles without excessive memory requirements or the need for an iterative procedure.

Calibrating the PFC Models

A typical use of numerical implementations of micromechanical models, such as the PFC codes, has been to develop constitutive models for continuum calculations of boundary-value problems. In other words, the particle model has been used to understand element behavior (in terms of an assembly of several hundred or several thousand particles subjected to uniform boundary conditions), such that a continuum program could be used to solve boundary-value problems that involve complicated deformation patterns (with the element behavior derived from the particle-model tests). The spectacular increase in computing power has made it possible to model entire problems with particles such that the constitutive behavior is built into the model automatically (i.e., the constitutive behavior arises from the interaction of large numbers of particles, each of which obeys simple contact laws). The approach holds promise for certain classes of problems, such as rock fracture, where the complex constitutive behavior (arising from a large amount of both macro- and micro-cracking) is difficult to characterize accurately in terms of a continuum formulation.

The goal of the present developments is to create a synthetic material that has the same numerical properties as some specific real material and then use the synthetic material in simulating boundary-value problems. This requires that the PFC model be calibrated to reproduce laboratory behavior of the real material. The calibration consists of setting the PFC micro-properties and running numerical simulations which are compared to actual testing until both a qualitative match and a mechanistic understanding of the constitutive behavior are obtained. To some extent, this is a trial-and- error process, because there is no complete theory that can predict macroscopic behavior from microscopic properties and geometry; however, guidelines have been developed to aid in the process.

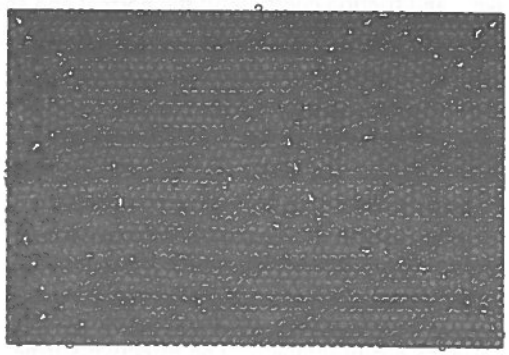

Fig. 4 Particle and block geometry for caving example

Example Problem: Caving of a Jointed Rock Mass in Two Dimensions

A highly idealized *PFC*^{2D} simulation of collapse of a jointed rock mass is given here. The objective of this exercise is to demonstrate the potential of the PFC approach for modeling caving; thus, a coarse particle and joint discretization are used. Figure 4 shows a two-dimensional representation of a "rock mass" consisting of rock blocks created by two joint sets, one horizontal and one dipping at 30°. The model is composed of 2000 circular particles whose radii are roughly 1/10 to 1/20 of the joint spacing. The set of blocks is confined by horizontal and vertical "walls" that provide lateral and vertical restraint. An initial isotropic stress state of 70 MPa is applied to the rock mass in addition to gravity prior to any excavation. (A high level of in-situ stress is applied, since it is the purpose of this example to demonstrate primary caving with significant intact block fracture.) The particles are then bonded together using contact bonds with normal and shear strengths of 10 and 100 MN, respectively, and given interparticle friction angles of 35°.

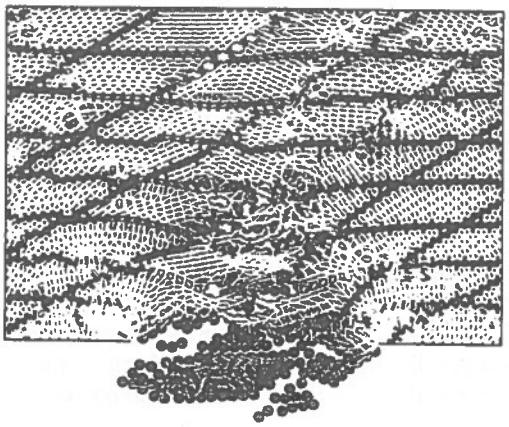

Fig. 5(a) Particle clusters early in the caving process with superimposed contact force chains

After initial stress equilibrium is attained, a central section of the bottom confining wall is removed to allow collapse. Figures 5 (a) and (b) show the collapse process at two stages. The first figure shows the particles with superimposed contact-force vectors at an early stage of of the collapse; the second figure shows a later stage in which the blocks themselves are shaded. This second figure clearly shows inter-block slip on the joints as well as fracture of the blocks in the central caving region. The initial block above the undercut falls relatively intact; however, a significant degree of comminution occurs in the caving region itself. This example indicates

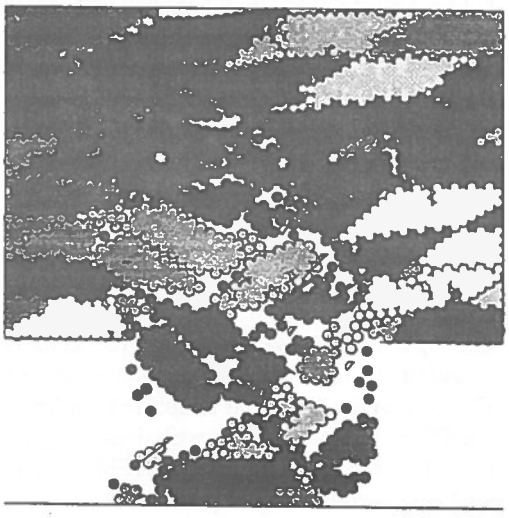

Fig. 5(b) Particle clusters after significant cave progress showing internal fracture of blocks in the zone of caving

self-sustained cave growth which propagates through the entire height of the model.

Discussion

Although demonstrated in the above example problem, caving, in general, is not well-represented by a two-dimensional approach. Currently, *PFC*^{3D} is being examined at South African and Chilean caving mines with the objective of testing the capability of this approach for prediction of cavability and reasonable estimation of fragmentation. Simulations of even portions of a caving panel may require as many as one-hundred-thousand particles. Computer memory requirements do not present a particular limitation for this technique — the greatest potential problem is the computation time required for solution of large problems. Modeling of the caving process and the draw of material in the muck column require that particle movements of tens to hundreds of meters be simulated. The solution times on existing personal computers or workstations for these extremely large problems may be of the order of weeks of time. However, given the rapid growth in speed of these computers, as well as the possible use of parallel processing, large-scale analyses such as these will soon be possible.

CONCLUSIONS

This paper presented two methods currently under investigation for the representation of caving: a continuum approach and a discontinuum micro-mechanical approach. It was shown that reasonably simple continuum models can be used for estimation of the undercut dimensions necessary for initiation and propagation of caving — at least for the case of regularly jointed, weak materials assumed to be isotropic. Comparisons to caving behavior in sparsely jointed, strong rocks are currently underway and will indicate whether the technique has wider applications. Derivation of in-situ strength properties from geotechnical mapping and the Hoek-Brown method appears to be a reasonable first approach for model input. A micro-mechanical approach for estimation of caving, fragmentation and muck flow has been developed in two and three dimensions. A simple caving problem was given here in two dimensions to illustrate the general principles of the approach to caving analysis. This approach holds the promise of providing a powerful simulation tool for caving, but it is currently limited by computational speed.

REFERENCES

BARTLETT, P.J., 1995 (in preparation).
Ph.D. Thesis. University of Pretoria, South Africa.

BIENIAWSKI, Z.T., 1973.
Engineering Classification of Jointed Rock Masses, The Civil Engineer in South Africa, 15(12), 335-343.

CUNDALL, P.A., 1971.
A computer model for simulating progressive large scale movements in blocky rock systems. Proceedings, Symposium of the International Society of Rock Mechanics, Nancy, France, Vol. 1, Paper No. II-8.

CUNDALL, P.A., 1988.
Formulation of a three-dimensional distinct element model — part I. a scheme to detect and represent contacts in a system composed of many polyhedral blocks, Int. J. Rock Mech., Min. Sci.& Geomech. Abstr., 25(3), 107-116.

CUNDALL, P.A., and HART, R., 1992.
Numerical modelling of discontinua, Int. J. Engr. Comp., 9, 101-113.

CUNDALL, P.A., and STRACK, O.D.L., 1979.
A discrete numerical model for granular assemblies, Géotechnique, 29(1), 47-65.

ESTERHUIZEN, G.S., 1994.
A model for predicting block cave fragmentation. Proceedings, Symposium on Application of Numerical Modelling in Geotech. Eng., Pretoria, RSA, pp. 147-151.

GUEST, A., and CUNDALL, P., 1994.
A three dimensional particle flow code for block cave modelling. Proceedings, Symposium on Application of Numerical Modelling in Geotech. Eng., Pretoria, RSA, pp. 15-18.

HART, R., CUNDALL, P.A. and LEMOS, J., 1988.
Formulation of a three-dimensional distinct element model — part II. mechanical calculations for motion and interaction of a system composed of many polyhedral blocks, Int. J. Rock Mech., Min. Sci. & Geomech. Abstr., 25(3), 117-125.

HOEK, E., 1990
Estimating Mohr-Coulomb friction and cohesion values from the Hoek-Brown failure criterion (technical note), Int. J. Rock Mech. Min. Sci. & Geomech. Abstr., 27(3), 227-229.

ITASCA CONSULTING GROUP, INC., 1994a.
FLAC^{3D} (**F**ast **L**agrangian **A**nalysis of **C**ontinua in **3** **D**imensions), Version 1.1, Minneapolis, Minnesota.

ITASCA CONSULTING GROUP, INC., 1994b.
UDEC (**U**niversal **D**istinct **E**lement **C**ode), Version 2.0, Minneapolis, Minnesota.

ITASCA CONSULTING GROUP, INC., 1994c.
3DEC (**3**-Dimensional **D**istinct **E**lement **C**ode), Version 1.5, Minneapolis, Minnesota.

ITASCA CONSULTING GROUP, INC., 1995a.
PFC^{2D} (**P**article **F**low **C**ode in **2** **D**imensions), Version 1.1, Minneapolis, Minnesota.

ITASCA CONSULTING GROUP, INC., 1995b.
PFC^{3D} (**P**article **F**low **C**ode in **3** **D**imensions), Version 1.0, Minneapolis, Minnesota.

KARZULOVIC, A., & ASSOC., LTDA., Santiago, Chile, 1995.
Personal communication.

LAUBSCHER, D.H., 1981.
Selection of mass underground mining methods. Design and Operation of Caving and Sublevel Stoping Mines, pp. 23-38. Society of Mining Engineering, New York.

LAUBSCHER, D.H., 1990.
Geomechanics classification system for the rating of rock mass in mine design, J. S. African Inst. Mining & Metallurgy, 90(10), 265-273.

LORIG, L. J., HART, R. D., BOARD, M. and SWAN, G., 1989.
Influence of discontinuity orientations and strength on cavability in a confined environment. Rock Mechanics As a Guide for Efficient Utilization of Natural Resources, pp. 167-174. Balkema, Rotterdam.

RECH, W.D., and LORIG, L., 1992.
Predictive numerical stress analysis of panel caving at the Henderson Mine. MASSMIN 92, pp. 55-62. SAIMM, Johannesburg.

SERAFIM, J.L., and PEREIRA, J.P., 1983.
Considerations of the Geomechanical Classification of Bieniawski. Proceedings, International Symposium on Engineering Geology and Underground Construction, Lisbon Vol. 2, pp. II-33 to II-42. LNEC, Lisbon.

VOEGELE, M., 1978.
An Interactive Graphics Based Analysis of the Support Requirements of Excavations in Jointed Rock Masses. Ph.D. Thesis, University of Minnesota.

CAMI'95:3rd Canadian Conference on Computer Applications in the Mineral Industry
Montréal, Québec, Canada, October 22-25, 1995

An Algorithm for Designing Mine Pillars with the Convergence-Confinement Method

D.E. Gill, M.H. Leite
École Polytechnique, Montréal, Québec

ABSTRACT

This paper shows how the convergence-confinement method can be extended to predict the axial stresses on pillars in uniform and non uniform multiple pillar arrays. As graphical solutions are not feasible when the number of pillars in uniform arrays is greater than four or when the number of pillars in non uniform arrays is greater than two, an algorithm which makes use of the pillar reaction curves is proposed to predict the axial stress acting on each pillar of the array. Features of the proposed algorithm are briefly discussed.

RÉSUMÉ

Cette communication montre que la méthode convergence-confinement peut être étendue à la prévision des contraintes axiales des piliers lorsqu'ils se présentent en arrangements uniformes et non-uniformes de plusieurs piliers. Puisque les solutions graphiques ne se réalisent plus avec les arrangements uniformes de plus de quatre piliers ou lorsque le nombre de piliers est supérieur à deux dans les arrangements non-uniformes, il est proposé un algorithme qui conduit à la détermination des contraintes axiales dans les piliers de l'arrangement en utilisant les courbes de réaction des piliers. Les caractéristiques de cet algorithme sont le sujet d'une briève discussion.

INTRODUCTION

Of the two fundamental approaches to the design of mine pillars, the total load approach comprises analysis methods that lead to an average state of axial stress in the pillar (total pillar load divided by the pillar effective cross sectional area) which can be compared to some uniaxial compressive rock mass strength. The tributary area method (Brady and Brown, 1985) and the deflexion method proposed by Coates (1981, 1965) are typical examples of this approach. The latter has some advantages over the other approach which involves the knowledge of the elastoplastic stress field characterizing the whole mining structure. Obtaining such a stress field requires large and sophisticated computer codes, for which input data are often not available at mines.

The convergence-confinement method (also called the characteristic lines method) for designing artificial support (support made of steel, wood, concrete, fill material, ...) has retained the attention of engineers, mainly because of its simplicity and versatility. Since its first mention by Lauffer and Seeber (1961), the method has seen many variations and developments (Ladanyi and Gill, 1988; Brown et al., 1983). Most of these were mainly within the general area of artificial support of tunnels. The convergence-confinement approach has also been used, though scarcely, to design "natural support" systems, implicitly or explicitly (Särkkä, 1984; Starfield and Wawersik, 1972; Salamon, 1970; Starfield and Fairhurst, 1968). All these applications consider only simple pillar arrays or ignore important variables.

To illustrate how the convergence-confinement method has been applied to mine pillars design, let us consider the simple two-dimensional situation described by Figure 1a. This figure shows a cross-section of two rooms of equal span, R, excavated to produce a pillar of effective width B and of height H. Since blasting produces irregular surfaces which need to be scaled, the effective width of a pillar is its expected minimum width. In order to determine a ground reaction curve for this situation, the pillar is replaced by a series of uniformly distributed stress (see Figure 1b) of various magnitudes, σ_{ya}, and the displacement distributions calculated assuming plane strain conditions (the pillar is long in the direction normal to the cross section shown). To plot a ground reaction curve as that on the interaction diagram shown in Figure 1c, the average displacement, v, accross the uniformly loaded area is retained. The pillar reaction curves are obtained by plotting the pillar axial stress, σ_{ya}, against the convergence accross the centre line of the pillar at the pillar-stope wall interface, v, assuming a specific state of stress in the pillar; for both pillar and country rock masses showing linear elastic behaviour, theses reaction curves are linear (see Figure 1c). On this interaction diagram, the intersection of the ground reaction line with the pillar reaction line gives the convergence-confinement equilibrium condition. The coordinates of this intersection point are the axial pillar stress (ordinate) and the pillar convergence at their centre line (abscissa), respectively. Data used for producing Figure 1c are those of Case I described below and the ground reaction curve has been generated using a numerical stress analysis code as suggested by Brady (1979).

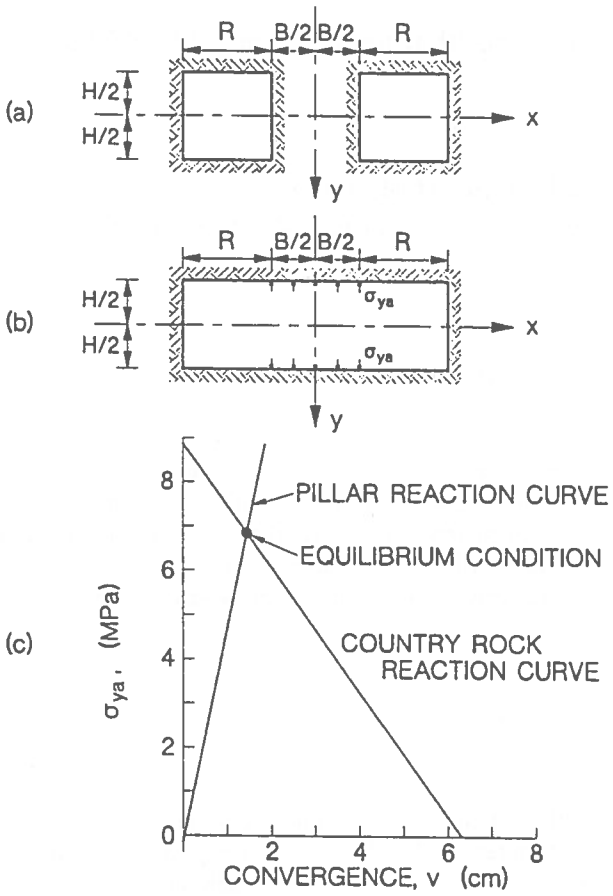

FIGURE 1 - Dimensionning pillars with the convergence-confinement method: (a) a cross section through a mining area consisting of a single vertical pillar array; (b) model for obtaining ground reaction curves; (c) interaction diagram.

Varying R (the room span) yields ground reaction curves different from that of Figure 1c. Having two rooms of different spans for the case illustrated in Figure 1a would give, all other parameters remaining the same, a ground reaction curve which would differ from that shown in Figure 1c. However, the equilibrium conditions would be obtained as described above. As the axial pillar stress would be the same on the pillars of a uniform two-pillar array, the above described graphical procedure can be applied without modification. Gill et al. (1994) have extended this graphical procedure to non-uniform two-pillar arrays and to uniform arrays of three and four pillars; the complexity arises from the fact that the axial pillar stresses are interrelated.

Moreover, if there is a lack of uniformity in either a three or in a four-pillar array, or if more than four pillars are involved, the array being uniform or not, the extended graphical solutions are no longer feasible. Gill et al. (1994) have demonstrated that the convergence-confinement method can be generalized and extended to predict the axial stresses in pillars in any uniform and non-uniform multiple pillar arrays. To do so, an algorithm should be used to predict the axial stress acting on each pillar of the array. This algorithm makes use of the pillar reaction curves only. The ground reaction curves are not required. To describe pillar reaction curves, Gill et al. (1994) have also proposed mathematical models, which take into account the fact that mine pillars are made from pre-stressed rock masses. As the computer code required to run the algorithm (including the part that is calculating the

displacement v) is very simple compared to those allowing proper determination of elastoplastic stress fields, the proposed design method keeps all the advantages of the total load group of methods.

The present paper describes the above mentioned algorithm, including the convergence controlling procedure. As the use of the algorithm requires the input of initial axial pillar stresses, of a stress increment step and of a tolerance, their effect on the number of iterations to be performed is illustrated and commented through a simple case. In order to show the potential of the algorithm, a more complex case is subsequently briefly presented.

MODELLING PILLAR REACTION CURVES

In the present paper, the proposed algorithm is used to design rib, transverse or longitudinal pillars. These are pillars having one of their cross-sectional dimensions much longer than their effective width. The coordinates system used is the one shown in Figure 1a. The longer cross sectional dimension of the pillar coincides with the z-axis. Let us assume that the principal pre-mining stress components σ_{xo}, σ_{yo} and σ_{zo} act parallel to the x, y and z axes, respectively. The rock mass into which the pillar is created is assumed to be homogeneous, isotropic and linear elastic. The axial loading of the pillar is considered to generate an uniformly distributed axial stress. Plane strain conditions are considered to exist along the z-axis.

Any rock mass portion that is left as a mine pillar is subjected to pre-mining stresses before the ore in its surrounding area is excavated. As stoping proceeds, such a block of rock is subjected to stress changes originating from two sources: (i) its lateral confinement is reduced to zero and (ii) its axial load is increased because of its support function. These two sources of changes act simultaneously. Modelling these stress changes leads to the following equation for axial pillar stress σ_{ya} (Gill et al., 1994):

$$\sigma_{ya} = \sigma_{yo} - \nu\sigma_{xo}/(1 - \nu) + 2Ev/[H(1 - \nu^2)] \qquad (1)$$

In this equation, E and ν are respectively the pillar rock mass Young's modulus and Poisson's ratio, H is the height of the pillar (see Figure 1a) and v is the average axial deflexion of the pillar at the pillar-country rock interface ($y = \pm H/2$). Gill et al. (1994) have also proposed an expression for pillars in which the larger cross-section dimension is comparable to the width of the pillar.

DESCRIPTION OF THE ALGORITHM

In the following description of the proposed algorithm, reference is made to a simple case. This case, which is identified as Case I hereafter, is the uniform three-pillar array illustrated by the cross-section in Figure 2; assuming R = 20,0 m, B = 20,0 m and H = 20,0 m, the general extraction ratio is 0,571. Such an arrangement yields a local extraction ratio of 0,500 for each pillar.

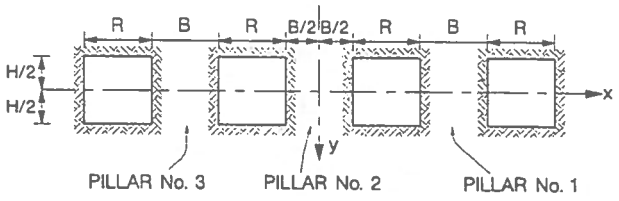

FIGURE 2 - A regular three-pillar array: cross section through the mining area.

The pre-mining state of stress is as follows: σ_{xo} = 10,0 MPa, σ_{zo} = 5,1 MPa and σ_{yo} = 5,0 MPa. The pillar elastic constants are E = 4,276 GPa and ν = 0,34. Even though it is not necessary, the country rock elastic constants are considered to be the same in the present paper. Substituting the appropriate values into equation 1, the pillar reaction curve is:

$$\sigma_{ya} = 8{,}865 - 140{,}2v \quad \text{(MPa)} \qquad (2)$$

The latter applies to the three pillars because they have the same width. It should be noted that this case could also be solved using the extended graphical solution proposed by Gill et al. (1994).

The algorithm, is presented as a flow chart in Figure 3. As a starting point, initial uniformly distributed axial pillar stresses are assumed to act on every pillar strip. A single initial guess can be assumed for all the strips although the axial stresses of pillars no. 1 and no. 3 are expected to be different from that of pillar no. 2. A

proper initial guest is the value of the pre-mining principal stress component parallel to the pillar axes (σ_{yo} for Case I, which is 5 MPa).

The resulting axial displacement (v) for every strip is computed using any numerical method code. In this paper, these calculations have been done with a boundary element code adapted from BOUDEM (Hoek and Brown, 1980) which is integrated into the algorithm. The axial displacement is averaged over each strip; one obtains one average displacement for pillars no. 1 and no. 3, and one average displacement for pillar no. 2 (see Table 1, column 4, line 1 and 2). These average displacements are then substituted into the pillar reaction curve given by equation 2.As can be seen in Table 1, one finds 26,63 MPa for both pillar no. 1 and pillar no. 3, and 32,30 MPa for pillar no. 2.

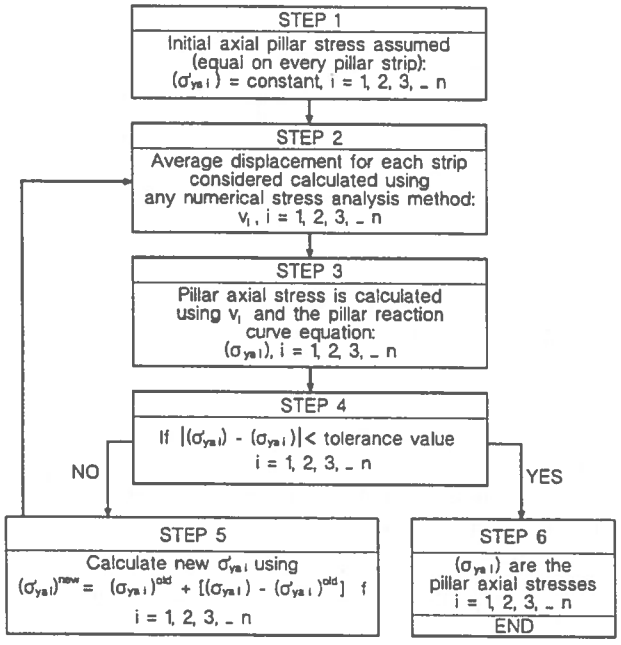

FIGURE 3 - The flow chart of the proposed algorithm.

The axial stress so calculated for each pillar is compared with the assumed axial stress acting on the corresponding strip; if, in all cases, the difference between the calculated and the assumed axial pillar stress is smaller than a tolerance value (for instance, a certain percentage of the pre-mining stress component parallel to the axis of the pillar), the axial pillar stresses calculated using the pillar reaction curve equations constitute the solution of the problem. Otherwise, new pillar axial stresses $[(\sigma'_{ya})_i^{new}]$ are calculated using the following equation:

$$(\sigma'_{ya})_i^{new} = (\sigma'_{ya})_i^{old} + [(\sigma_{ya})_i - (\sigma'_{ya})_i^{old}]\, f \qquad (3)$$

with i = 1, 2, 3, ... n.

In equation 3, n is the number of pillars on which different axial stresses are expected, $(\sigma'_{ya})_i^{old}$ are the last pillar axial stresses that were assumed to act on the strip corresponding to pillar number i, $(\sigma_{ya})_i$ are the axial stresses calculated for pillar number i using the pillar reaction curve equations and f, an appropriate fraction. For Case I, n = 2 (i = 1 for pillars no. 1 and no. 3, and i = 2 for pillar no. 2).

The proper value for parameter f has to be introduced in the algorithm after the first iteration cycle to set the stress increment step. The following equation is proposed to determine a maximum practical value for f, considering that the tributary area pillar design method is the most conservative (Coates, 1965) of all the total load design methods:

$$f < [\sigma_{yo}(1 - \rho)]/\{\rho[(\sigma_{ya})_i - \sigma_{yo}]\} \qquad (4)$$

where σ_{yo} is the pre-mining principal stress component parallel to the pillar axes, σ_{ya} is the largest of all axial pillar stresses calculated in the first iteration cycle using equation 2, and ρ is the local extraction ratio for the pillar with this largest axial stress. Applying equation 4 to Case I gives f < 0,183. A value of 0,100 was selected to produce Table 1.

For the example presented here, let us consider a severe tolerance value of 0,05 MPa (1% of the pre-mining principal stress component parallel to the pillar axis). As the difference between the calculated and the assumed axial pillar stresses are, after the first iteration cycle, much more larger than 0,05 MPa (see Table 1, column 6, line 1 and 2), equation 3 is used to calculate new axial pillar stresses for the second iteration cycle; values obtained are 7,163 MPa for both pillar no. 1 and pillar no. 3, and 7,730 MPa for pillar no. 2.

These new axial pillar stresses are now assumed to act on the pillar strips and the step involving the calculation of axial displacements with the numerical method code is redone; this leads to a new average axial displacement for each strip (see Table 1, column 4, line 3 and 4) and the iteration process is carried on.

It can be seen from Table 1 that the tolerance value of 0,05 MPa is reached at the seventh iteration. The axial stress acting on pillar no. 1 and on pillar no. 3 is 7,842 MPa while an axial stress of 8,335 MPa acts on pillar no. 2.

EFFECT OF THE NUMERICAL CODE PRECISION

The numerical model representing the cross-section shown in Figure 1a used to calculate the resulting axial displacement in the algorithm and which has lead to the results reported in Table 1 (Case I) involves 240 boundary elements. The results presented in Table 2 indicate that if this number is reduced to 160, one extra iteration cycle has to be performed to reach the selected tolerance value compared to the number of iteration cycles done with the 240 element model. Moreover, the results in this table also show that increasing the number of elements beyond 240 does not allow to reach a solution with less iteration cycles. Consequently, the proposed algorithm does not require extremely detailed modelling.

EFFECT OF THE MAGNITUDE OF THE ASSUMED INITIAL AXIAL PILLAR STRESSES

The above Case I was also solved starting with assumed initial axial pillar stresses of 6,5 MPa, 8 MPa and 9,5 MPa instead of 5,0 MPa. Table 3 summarizes the results obtained. These show that initial axial pillar stresses assumed, as suggested above, equal to the value of the pre-mining principal stress component parallel to the axis of the pillars, yield a solution with a number of iteration cycles which is close to the minimum number and thus constitutes a good initial guest.

It should be noted that an initial assumed axial pillar stress close to the solution does not necessarily lead, for a given tolerance value, to the the minimum number of iteration cycles. This is a weakness of the algorithm. Nevertheless, this number of iteration cycles remains close to the minimum.

EFFECT OF THE MAGNITUDE OF PARAMETER f

Column 7 of Table 1 gives the sum of the squares of the differences between the pillar strip stresses and the calculated axial pillar stresses for all pillars after each iteration cycle. This sum should decrease relatively fast from one iteration cycle to the other (96% from the first iteration cycle to the second for the example of Table 1) if a proper value is used for f. This means that the algorithm converges rapidly toward a solution. If the sum decreases too slowly (e.g., 10%), this means that the value assumed for f is either too close to the non converging value or too small compared to the optimum value. In both of these cases, the number of iteration cycles to be performed to reach a solution will be too large. Consequently, the assumed value for f should be first increased; if the sum of the squares of the differences, after having redone the second iteration cycle, is greater than the previous sum of the squares, the right move would rather have been to decrease the assumed value of f. If this sum increases, it means that there is no convergence. The second iteration cycle should then be redone with a smaller value for f.

In order to illustrate the impact of the value of parameter f on the number of iteration cycles, Case I was solved with assumed f values of 0,300, 0,250, 0,200, 0,150, 0,125, 0,100, 0,075 and 0,050; in all these solutions, the assumed initial axial pillar stress was 5,0 MPa. The results obtained are presented in Table 4. The minimum number of six iteration cycles required to satisfy a tolerance of 0,05 MPa is achieved when the value of f is 0,125. These results show also that the algorithm diverges when f = 0,300, converges very slowly when f = 0,250 and requires 11 iteration cycles to yield a solution when f = 0,200; this is consistent with the upper limit of 0,183 for f given by equation 4. According to Table 3, a too small value of f leads to a slow convergence.

EFFECT OF THE MAGNITUDE OF THE TOLERANCE

It can be seen from Table 1 (f = 0,100) that if one accepts a tolerance value of 0,15 MPa (3% of σ_{yo}), only 5 iteration cycles are required and the axial stress is 7,908 MPa for pillars no. 1 and no. 3, and 8,338 MPa

for pillar no. 2. To reach a tolerance value of 0,015 MPa (0,3% of σ_{yo}), 10 iteration cycles must be performed and the axial stress is 7,823 MPa for pillars no. 1 and no. 3, and 8,358 MPa for pillar no. 2. Comparing these data, one concludes that doubling the number of iteration cycles, changes the axial pillar stresses by 1,5% or less. Considering that the pre-mining stresses are generally known with much less precision, a tolerance value of the order of a few percents of the pre-mining stress component parallel to the pillar axis is surely acceptable.

A COMPLEX CASE

To show that complex cases can be solved with the proposed algorithm, let us consider the cross section presented in Figure 4. The elastic constants to be considered in this case, called Case II hereafter, are given in Table 5.

The pre-mining principal stress components are σ_{yo} = 10,0 MPa, σ_{zo} = 5,1 MPa and σ_{xo} = 5,0 MPa. Although depth-dependent pre-mining stress components can be considered in the algorithm, it is assumed in the present case they are the same for the three pillars. The pillar reaction curves required to solve Case II are, according to equation 1:

$$\sigma_{ya} = 9{,}444 + 10101{,}0v \quad \text{(MPa, pillar no. 1)} \qquad (5)$$
$$\sigma_{ya} = 8{,}750 + 5208{,}3v \quad \text{(MPa, pillar no. 2)} \qquad (6)$$
$$\sigma_{ya} = 7{,}857 + 2747{,}3v \quad \text{(MPa, pillar no. 3)} \qquad (7)$$

The axial pillar stress assumed initially to act on every pillar strip was 25,0 MPa. The value used for f in the algorithm was 0,03. The results obtained at the tenth iteration cycle and after are presented in Table 6.

As can be seen from the results reported in this table, the axial pillar stresses calculated after fourteen iteration cycles are all within 1,0 MPa of the axial pillar stress acting on the strips. These differences are all smaller than 0,5 MPa after sixteen iteration cycles. The axial stresses obtained are then 24,84 MPa, 30,71 MPa and 29,60 MPa for pillar no. 1, pillar no. 2 and pillar no. 3, respectively.

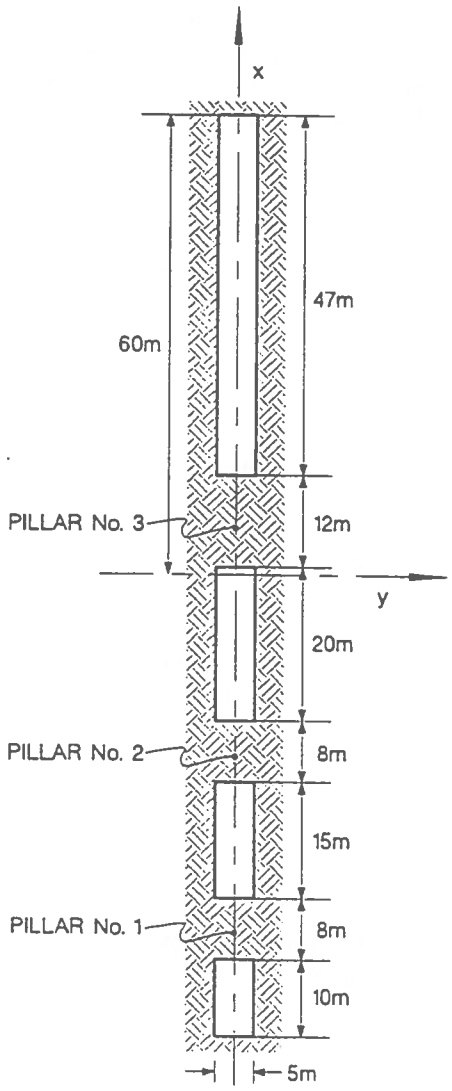

FIGURE 4 - A complex case; cross section through the mining area.

DISCUSSION

The proposed approach is general in the sense that it takes into consideration the three pre-mining principal stress components, the elastic constants of both the country and the pillar rocks, the dimensions of the pillars (width and height), their position within the mining area and their mutual interaction as far as their axial stress is concerned. Moreover, the pillar arrays do not have to be uniform and do not have to show any symmetry. Considering the elastic constants of both the country and the pillar rocks is important: it can be

shown that the pillar axial stress is a function of the ratio of these constants.

However, as with all other design methods based on the total load approach, the pillar axes must be, with the proposed approach, more or less parallel to one of the pre-mining principal stress components. The algorithm described in this paper can nevertheless be applied to inclined workings if one accepts the principle of the tributary area extension suggested by Pariseau (1982). Although not presented in this paper, the proposed algorithm can handle the design of yielding pillars.

The proposed algorithm can be extended to include fully three-dimensional problems as well as stress-strain relationships other than homogeneous isotropic linear elasticity. This implies, among other things, that numerical stress analysis codes sophisticated enough to include these features must be available.

CONCLUSION

As convergence-confinement graphical solutions are no longer feasible when the number of pillars in non uniform arrays is greater than two or when the number of pillars in uniform arrays is greater than four, an algorithm which makes use of pillar reaction curves was proposed to predict the axial stress acting on each pillar of any array.

The algorithm was described, including the convergence controlling procedure. The effect of initial axial pillar stresses, of the stress increment step and of the tolerance on the number of iteration cycles to be performed is illustrated and commented through a simple case. In order to show the potential of the algorithm a more complex case was subsequently briefly presented.

ACKNOWLEDGEMENTS

The authors gratefully acknowledge the financial support of the National Science and Engineering Research Council of Canada (Grant no. OGP0003412).

REFERENCES

Brady, B.H.G., 1979
Boundary element methods for mine design. Ph.D. Thesis, University of London.

Brady, B.H.G., Brown, E.T., 1985
Rock Mechanics for Underground Mining. George Allen & Unwin, London.

Brown, E.T., Bray, J.W., Ladanyi, B., Hoek, E., 1983
Characteristic line calculations for rock tunnels. ASCE J. Geotech. Engng., Vol. 109, No. 1, pp. 15-39.

Coates, D.F., 1965
Pillar loading Part I: Literature survey and new hypothesis. R168, Mines Branch (CANMET) Research Reports, Queen's Printer, Ottawa.

Coates, D.F., 1981
Rock Mechanics Principles. Mines Branch Monograph 874 (revised), Dep. of Energy, Mines and Resources, Canada.

Gill, D.E., Leite, M.H., Labrie, D., 1994
Designing mine pillars with the convergence-confinement method. Int. J. Rock Mech. Min. Sci., Vol. 31, No. 6, pp. 687-698.

Hoek, E., Brown, E.T., 1980
Underground excavations in Rock. Inst. Min. and Metall., London.

Ladanyi, B., Gill, D.E., 1988
Design of tunnel linings in creeping rock. Int. J. Min. and Geol. Engng., Vol.6, No. 2, pp. 113-126.

Lauffer, H., Sebber, G., 1961
Design and control of linings of pressure tunnels and shafts, based on measurements of the deformability of the rock. Proc. 7th Cong. Large Dams, Rome, Q.25, pp. 679-707.

Pariseau, W.G., 1982
Shear stability of mines in dipping seams. Proc. 23rd Symp. on Rock Mech., Issues in Rock Mech., AIME, pp. 1077-1090.

Salamon, M.D.G., 1970
Stability, instability and design of pillar workings. Int. J. Rock Mech. Min. Sci., Vol. 7, pp. 613-631.

Särkkä, P.S., 1984
The interactive dimmensioning of pillars in Finnish mines. Proc. 2nd Int. Conf. on Stability of Underground Mining (A.B. Szwilski and C.O. Brawner, Eds.), pp. 71-84.

Starfield, A.M., Fairhurst, C., 1968
How high-speed computer design of practical mine pillar systems. Eng. and Min. J., Vol. 169, pp. 78-84.

Starfield, A.M., Wawersik, W.R., 1972
Pillars as structural components in room-and-pillar mine design. Proc. 10th US Symp. Rock Mech., Austin, pp. 793-809.

TABLE 1 - Predicted pillar axial stresses after each iteration cycle for Case I

Iteration no.	Pillar no.	σ'_{yai}, MPa	v_i, m	σ_{yai}, MPa	Difference, MPa	Sum of square differences
1	1 and 3	5,000	0,055392	26,630	21,630	1213,02
	2	5,000	0,067113	32,297	27,297	
2	1 and 3	7,163	0,025041	11,956	4,793	53,84
	2	7,730	0,027793	13,286	5,556	
3	1 and 3	7,642	0,018477	8,781	1,141	2,31
	2	8,285	0,019534	9,293	1,008	
4	1 and 3	7,756	0,017019	8,077	0,321	0,112
	2	8,386	0,017859	8,483	0,097	
5	1 and 3	7,788	0,016670	7,908	0,120	0,018
	2	8,396	0,017559	8,338	-0,058	
6	1 and 3	7,800	0,016570	7,860	0,060	0,008
	2	8,390	0,017534	8,326	-0,064	
7	1 and 3	7,806	0,016532	7,842	0,036	0,004
	2	8,384	0,017554	8,335	-0,048	
8	1 and 3	7,810	0,016513	7,832	0,023	0,002
	2	8,379	0,017575	8,346	-0,033	
9	1 and 3	7,812	0,016502	7,827	0,015	0,001
	2	8,375	0,017591	8,353	-0,022	
10	1 and 3	7,814	0,016494	7,823	0,010	< 0,001
	2	8,373	0,017601	8,358	-0,015	

TABLE 2 - Effect of the number of boundary elements in the numerical model - Case I.

Number of boundary elements	Number of iteration cycles	Calculated axial pillar stresses, MPa	
		Pillars no. 1 and no. 3	Pillar no. 2
160	8	7,876	8,371
240	7	7,842	8,335
320	7	7,823	8,323

TABLE 3 - Effect of the magnitude of the assumed initial axial pillar stresses on the number of iteration cycles - Case I.

Assumed initial axial stress, MPa	Number of iteration cycles	Calculated axial pillar stresses, MPa	
		Pillars no. 1 and no. 3	Pillar no. 2
5,000	7	7,842	8,335
6,500	6	7,806	8,397
8,000	9	7,797	8,398
9,500	10	7,794	8,403

TABLE 4 - Effect of the value of the parameter f on the number of iteration cycles - Case I.

Parameter f	Number of iteration cycles	Calculated axial pillar stresses, MPa	
		Pillars no. 1 and no. 3	Pillar no. 2
0,300	No convergence	-	-
0,250	Converge very slowly; stopped after 20 cycles	-	-
0,200	11	7,858	8.412
0,150	8	7,791	8,403
0,125	6	7,834	8,342
0,100	7	7,842	8,335
0,075	10	7,843	8,346
0,050	15	7,851	8.357

TABLE 5 - Elastic constants for Case II.

Structure component	Young Modulus, GPa	Poisson's ratio
Country rock	4,276	0,34
Pillar no. 1	20,0	0,1
Pillar no. 2	10,0	0,2
Pillar no. 3	4,276	0,34

TABLE 6 - Axial pillar stresses after each iteration cycle, starting at the tenth one - Case II

Iteration no.	Pillar no.	σ'_{yai}, MPa	v_i, m	σ_{yai}, MPa	Difference, MPa
10	1	25,55	-0,00116	21,20	4,35
	2	30,07	-0,00515	35,60	-5,53
	3	29,94	-0,00807	30,04	-0,09
11	1	25,46	-0,00133	22,91	2,55
	2	30,18	-0,00481	33,81	-3,63
	3	29,94	-0,00798	29,78	0,16
12	1	25,41	-0,00140	23,62	1,79
	2	30,26	-0,00454	32,41	-2,15
	3	29,94	-0,00790	29,57	0,37
13	1	25,37	-0,00150	24,60	0,77
	2	30,30	-0,00444	31,92	-1,61
	3	29,93	-0,00793	29,65	0,28
14	1	25,36	-0,00149	24,56	0,80
	2	30,33	-0,00433	31,33	-1,01
	3	29,93	-0,00789	29,55	0,38
15	1	25,34	-0,00155	25,11	0,24
	2	30,35	-0,00429	31,14	-0,79
	3	29,92	-0,00794	29,67	0,25
16	1	25,34	-0,00152	24,84	0,49
	2	30,37	-0,00421	30,71	-0,34
	3	30,92	-0,00791	29,60	0,32

CAMI'95:3rd Canadian Conference on Computer Applications in the Mineral Industry
Montréal, Québec, Canada, October 22-25, 1995

Evaluation of Field Properties and Stress Condition by Displacement Back-Analysis Using Boundary Element Principle

Daihua (Steve) Zou
Department of Mining and Metallurgical Engineering
Technical University of Nova Scotia, Halifax, Nova Scotia

ABSTRACT

Ground stability depends on the field properties of the rock mass, the in situ stress condition and supporting systems. However, there is no practical way at present to measure rock properties in the field. The in situ stresses are usually unknown and the measured stresses vary from location to location. Ground supports if effectively applied will reinforce the ground and make the ground stronger. Therefore there are needs to evaluate the effectiveness of ground supports. This paper describes a back-analysis technique for the determination of the effective field rock properties, the equivalent in situ stresses and the effectiveness of ground supports. The technique is based on the displacement measured in the field as the primary information. It applies the principles of error minimization and boundary element method in the analysis. An inversion approach is used to arrive at a direct solution. The analysis is suitable to any shape of mine openings. A computer software which calculates the results directly is introduced. Case studies are presented and recommendations are also made for various practical applications in mining engineering.

RÉSUMÉ

La stabilité du terrain depend des propriétés du rock, telques les conditions naturelles de stress et le system de support. Parcontre il n`y a présentement aucune manière pratique de mesurer les propriétés du rock sur le terrain. Les stress naturels sont habituellement indéterminés et les mesures de ces stress varies de place en place. Les supports de terrain, si appliqués d`une facon efficace, vont renforcer le terrain et le rendre plus fort. Par conséquent, il n`est pas nécessaire d`évaluer l`efficacité des supports de terrain. Ce papier décrit une analyse technique pour déterminer les propriétés effectives du rock, le stress naturel équivalent ainsi que l`efficacité des supports de terrain. Cette technique est basée sur des mesures déplacées sur le terrain comme information primaire. Ceci s`applique au principe de minimisation d`erreur et à la methode d`elements de borne dans l`analyse. Une approche inversée est utilisée pour arriver a une solution direct. L`analyse convient pour des ouvertures minières peu importe leur forme. Un program d`ordinateur, qui calcule les resultats, est introduit. Des études de cas sont présentées et des recommendations sont faites pour des applications pratiques dans le domaine d`ingenieurie minier.

INTRODUCTION

Ground stability is one of the main concerns in the operation of underground mines. Every effort has to be made to keep the ground stable in order to maintain production and to ensure mine safety. In general, factors affecting ground stability can be grouped into two categories: the natural factors which include the effective field properties of the rock mass, the in situ stresses and the geological condition, and the controllable factors which include opening design, excavation method and supporting system. The common practice in achieving ground stability is to optimize the underground design and to reinforce the ground with supports when necessary. This practice is probably the most effective if the natural factors are well known. However they are usually uncertain. Design is therefore based on assumptions and interpretation of relevant information. The validity and the reliability of these assumptions and interpretation become a concern. For a ground control engineer, it is very important to understand the overall performance of the ground, the effective field rock properties and the stress conditions.

The field properties of a rock mass are the inherent factors of the ground. They indicate the ability of the ground to withstand external forces. Unfortunately there is no practical method to measure these properties in the field at present. They are usually interpreted from the rock properties obtained from laboratory tests of rock samples. Practice and experience in the past have indicated that interpretation is usually unreliable due to many other uncertainties in the field. The interpreted properties are often far from what would be expected from field observations. The simple fact is that the rock properties vary with the orientation (Zou, 1995a) and the location as shown in Figure 1. They also vary with the stress state in situ which is actually unknown. At present, it is technically not possible to test the properties in the size of an excavation. Therefore, there are needs to be able to determine the field properties of a rock mass, i.e., the effective properties reflecting the actual condition in the field.

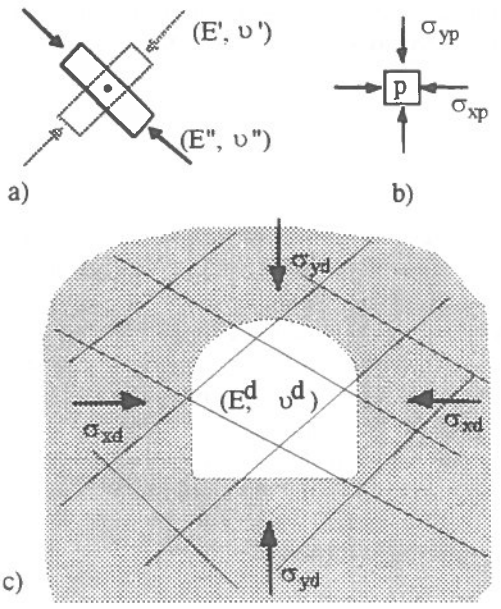

Figure 1. Variation of in situ stress state and field rock properties with location and domain size
a) orientation effects, b) stress state at point p,
c) stress state and rock properties in the domain of excavation

In situ stresses belong to the external factors which affect ground stability. They may be measured in the field by overcoring method using specially designed instrument (Leeman, 1968), such as the CSIR or CSIRO stress cell. However the common problem with field stress measurement is that the measured results often vary from location to location. Even at the same location, there could be a big variation if boreholes are drilled in different directions. As Zou and Kaiser (1990a) pointed out, the main concern with field stress measurement is the fact that the results only indicate the stress state at a point in the ground as illustrated in Figure 1 and may not be applicable to the domain of the excavation due to joints, fractures and other uncertainties in the rock mass. From the ground stability control point of view, it is important to know the stress condition in the domain containing the excavation.

The purpose of ground support is to reinforce the ground. It is therefore necessary to determine the effectiveness of supports. In the same ground, the effectively supported area will deform less than the unsupported area. The supports have equivalently increased the field properties and changed the behaviour of the rock mass. The new properties indicate the effectiveness of supports and determine the ground stability.

The most practical and effective way to evaluate the ground performance and to determine these field factors is to observe the rock mass itself in the field. The immediate visible evidence of the effects of excavation is the movement of ground around the opening. By measuring the movement and using a back-analysis technique, we can find a lot about the rock mass. In fact, back-analysis has become a powerful tool in revealing the mystery of the ground. It has been used since a decade ago in geotechnical engineering to assess the rock properties and the stress components (Sakurai and Takeuchi, 1983; Sakurai et al, 1985; Hisatake, 1991) and to evaluate the performance of tunnel linings (Yang et al, 1983; Wang et al, 1988; Hisatake and Ito, 1983) from displacement measured in the field. The analysis was usually carried out by comparison between the measured and the calculated data using the alternating variable method, a trial-and-error procedure. Quite often Finite Element Method is used to simulate the excavation. Back-analysis has also been used recently to estimate in situ stresses from stress changes monitored during excavation (Zou and Kaiser, 1990a and 1990b; Kaiser et al, 1991).

It must be noticed that application of the back-analysis technique is somewhat different in mining engineering from in geotechnical engineering. Tunnels are generally in shallow depth and lined with permanent

supports to ensure their long term stability. It is then important to evaluate the lining performance and to monitor the interaction between the rock mass and the linings. However, underground mine openings are usually at greater depth. Except for shafts, supports for mine openings are generally for a relatively short term. Unlike tunnel linings which provide relatively uniform supporting force to the rock mass, mine supports, such as rock bolts, steel beams, even steel arches generally provide concentrated supporting forces to the rock mass. Some mine openings may not be supported at all. Therefore, it is important for us to concentrate on the rock mass. Ground supports can be considered as reinforcement, i.e., as part of the rock mass.

Displacement is relatively easy to measure and usually requires simple instruments in comparison with field stress measurements. In the following, a back-analysis technique is introduced and its application in mining engineering to estimate the effective field rock properties, the effectiveness of ground supports and the in situ stresses, etc., is discussed. This technique applies boundary element method to simulate excavation and arrives at the solution directly by error minimization. From the ground support and stability control point of view, what is happening in the plane perpendicular to the opening axis is of more interest. The discussion is therefore limited to two dimensional condition. Analysis in three dimensions is possible. However the advantage of the simplicity in field displacement measurement may be lost.

BACK-ANALYSIS FORMULATION USING BOUNDARY ELEMENT PRINCIPLE

Displacements Induced By Underground Excavation

As an opening is excavated underground, the virgin stress field is disturbed and the stresses redistribute around the excavated opening by self-adjustment to reach a new state of stress equilibrium. As a result, the rock mass deforms further and moves towards the opening. The displacement induced by excavation, **u**, is the only part of deformation which can be measured. It consists of the normal and tangential components u_n and u_t, or the components u_X and u_y in x, y directions. A third component u_z along the opening axis may exist. It is however relatively small in comparison with the other two components for a long opening except near the ends or junction points. The magnitude of displacement varies with the location around the opening, the opening size, the in situ stress condition, the geology, the rock mass behaviour and properties. The displacement is the largest on the opening surface and becomes negligible at a far away place in the ground.

Simulation Of Excavation

For a circular opening, an analytical solution to the displacement can be obtained based on the stress-strain and the strain-displacement relationships. In general, the displacement in an isotropic rock can be expressed in a matrix form as a linear function of the in situ stress components

$$\mathbf{u} = \mathbf{M}\,\sigma \qquad (1)$$

where $\mathbf{u} = \{u_n , u_t\}$ is a displacement vector, $\sigma = \{\sigma_X, \sigma_y, \tau_{Xy}\}$ is a stress vector and **M** is the displacement coefficient matrix of size (2 x 3). **M** depends on the location, Young's modulus E and Poison ratio υ of the rock mass. By coordinate transformation, the two components $\{u_X , u_y\}$ can also be calculated. Thus, displacements induced by excavation are fully defined by Eqn (1).

However, except for shafts and some machine-bored openings, mine openings are rarely circular. Most of them are irregular. There may be influence from nearby excavation as well. Under these conditions, there are no analytical solutions. Numerical simulation becomes an effective method to determine the excavation-induced displacements. In the field, displacements are measured at a limited number of locations. It is only necessary to calculate the displacements at those points. In this case, boundary element method is most suitable in comparison with other numerical methods. Boundary element method has another advantage which requires no outer boundary in the model and makes it easier to prepare the input data file.

Boundary element method can be divided into three different submethods: the fictitious stress method, the displacement discontinuity method and the direct boundary integral method (Crouch and Starfield, 1983; Banerjee and Butterfield, 1981). The first method will be used in the following to demonstrate the procedure of displacement analysis.

With the fictitious stress method, the opening boundary is divided into N elements and excavation is replaced by

the fictitious stresses distributed on the boundary elements. The effects of these stresses superimpose on one another throughout the domain. Displacements $\mathbf{u}_g = \{u_x, u_y\}$ at a point in the rock induced by excavation are then expressed as functions of the fictitious stresses

$$\mathbf{u}_g = \mathbf{B}\ \mathbf{F} \qquad (2)$$

where **B** is the influential matrix of size (2 x 2N), **F** is the fictitious stress vector of size (2N x 1) and the subscript 'g' refers to the global (x, y) coordinate system.

Similarly the stress changes $\{\Delta\sigma, \Delta\tau\}$ at any point induced by excavation can also be given as functions of the fictitious stresses. This applies to the opening boundary as well. Assembling the stress changes on all boundary elements gives

$$\Delta\sigma_b = \mathbf{S}_0\,\mathbf{F} \qquad (3)$$

where $\Delta\sigma_b$ is a stress change vector of size (2N x 1) in the local (n, t) system and $\mathbf{S}_0$ is the boundary influential coefficient matrix of size (2N x 2N).

In a linearly elastic rock, the resultant stress after excavation is the sum of the original stresses and the induced-stress changes. On the boundary, the resultant stress equals the reaction pressure from supports if there are any. For unsupported free surface the resultant stress is zero and the stress changes on the boundary $\Delta\sigma_b$ are equal to the negative values of the in situ stresses

$$\Delta\sigma_b = -\mathbf{T}_s\,\sigma \qquad (4)$$

where $\mathbf{T}_s$ is the stress transformation matrix (Crouch and Starfield, 1983; Jaeger and Cook, 1976) of size (2N x 3). It converts the in situ stresses from the global (x, y) system to the values $\{\sigma, \tau\}$ on the boundary elements in the local (n, t) systems.

Solving for **F** from Eqns (3) and (4) and substituting **F** into Eqn (2) give

$$\mathbf{u}_g = \mathbf{M}_g\,\sigma \qquad (5)$$

where $\mathbf{M}_g = -\mathbf{B}\,\mathbf{S}_0^{-1}\,\mathbf{T}_s$ and the superscript "-1" refers to matrix inversion.

If the displacement is given in the local coordinate system as $\mathbf{u} = \{u_n, u_t\}$, then a transformation is needed

$$\mathbf{u} = \mathbf{T}_u\,\mathbf{u}_g \qquad (6)$$

where $\mathbf{T}_u$ is the displacement transformation matrix of size (2 x 2) which varies with the location. Replacing $\mathbf{u}_g$ by Eqn (5) in Eqn (6) gives

$$\mathbf{u} = \mathbf{M}\,\sigma \qquad (7)$$

where $\mathbf{M} = \mathbf{T}_u\ \mathbf{M}_g$.

The displacement at any point due to excavation can now be calculated from Eqn (5) or Eqn (7) if the in situ stresses are known. In a reversed order, the in situ stresses can be determined from the displacements measured in the field at a number of points. If only the normal component u_n is measured, the corresponding row of Eqn (7) can be used. As shown above, inversion of the boundary influential coefficient matrix $\mathbf{S}_0$ has to be carried out. This back-analysis process could therefore take longer computing time than boundary element modelling process where matrix inversion can be avoided if the fictitious stresses **F** are calculated directly from Eqn (3).

Field Measurement Of Displacements

The displacement induced by excavation can be measured on the opening surface or inside the rock mass. For greater sensitivity to the stress disturbance, a better location is on or near the opening surface. A tape or a rod may be used. This is possibly the cheapest way to measure the displacement. However, due to the fracture effect in the yielding zone immediately around the opening, measurements made on the opening surface tend to be larger than those expected for an elastic rock. Therefore the back-analyzed results from these data will be over-estimated unless the fracture effect is considered during the modelling of excavation or during the analysis. On the other hand, displacement can be measured in the elastic region by drilling a hole in the rock mass. In this case, an extensometer may be used. This practice is obviously more expensive but gives more realistic results. A combination of both can be used to collect more representative data.

The absolute values of both components $\{u_x, u_y\}$ or $\{u_n, u_t\}$ may not be easily measured in the field. That is because of the difficulty in locating a non-movement point as reference and the relatively low accuracy of simple instruments. In practice however, it is most

convenient to measure the relative movement and the convergence between two points.

Relative Movement Between Two Points

The relative movement can be measured between any two points along a borehole as shown in Figure 2. If a multiple anchor extensometer is installed in the rock, a number of measurements can be made at different depths along the borehole. If the relative movement, $u_{rel\text{-}i}$, between point ***a*** and point ***i*** is measured such as in Case I of Figure 2, Eqn (5) needs to be modified.

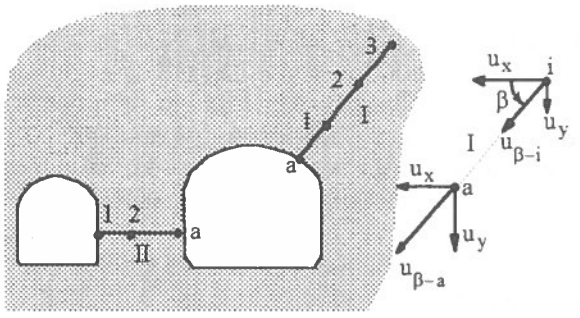

Figure 2. Relative movement measurement and calculation

Assume point ***a*** is closer to the opening surface than point ***i***, then

$$u_{rel\text{-}i} = u_{\beta\text{-}a} - u_{\beta\text{-}i} \qquad (8)$$

where $u_{\beta\text{-}a}$ is the displacement component along β direction at point ***a*** and $u_{\beta\text{-}i}$ at point ***i***. At any point, it can be shown

$$u_\beta = \mathbf{T}_\beta \, \mathbf{u}_g \qquad (9)$$

where $\mathbf{T}_\beta = [\cos\beta, \sin\beta]$.

Substituting Eqns (5) and (9) into Eqn (8) gives

$$u_{rel\text{-}i} = \mathbf{M}_{rel} \, \sigma \qquad (10)$$

where $\mathbf{M}_{rel} = \mathbf{T}_\beta (\mathbf{M}_{g\text{-}a} - \mathbf{M}_{g\text{-}i})$.

If access is available, the extensometer can be installed in advance from an adjacent opening as in Case II of Figure 2 without disturbing the excavation. Eqn (10) is still valid.

Convergence Between Two Points

Convergence is probably the easiest to measure. It is only necessary to measure the distance change between any two points in a plane as shown in Figure 3. These two points may be on the opening surface or in the rock mass. The convergence reading is the sum of the displacement components at the two points along the measurement line, i.e.,

$$u_{con} = u_{\beta\text{-}a} + u_{\beta\text{-}b} \qquad (11)$$

Similarly, $$u_{con} = \mathbf{M}_{con} \, \sigma \qquad (12)$$

where $\mathbf{M}_{con} = \mathbf{T}_\beta (\mathbf{M}_{g\text{-}a} + \mathbf{M}_{g\text{-}b})$.

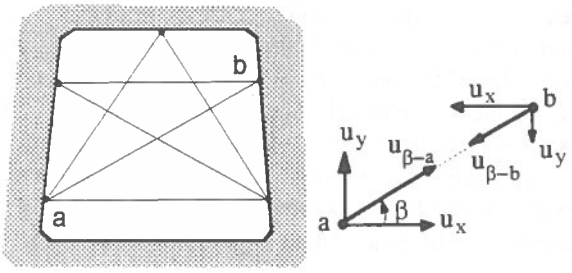

Figure 3. Convergence measurement and calculation

Eqns (5), (7), (10) and (12) can all be written in a unified format:

$$\mathbf{u}^* = \mathbf{M}^* \, \sigma \qquad (13)$$

As noticed earlier, unless the instrument is installed before excavation from a nearby access (e.g., Case II in Figure 2) or by other means, the measured value is not the total displacement induced by the excavation. If the opening to be excavated is the only access for instrumentation, initial displacement has taken place already prior to the installation of instrument. If instrument is installed as close to the excavation face as possible, the initial displacement may be relatively small in hard rocks. Its effect may be minimal, especially when the results are evaluated on a relative basis. For example, when two support systems are used in the same ground, we only need to look at the improvement of ground performance (e.g., the change of E value) if the supports and instruments are installed under the same conditions. However if more accurate

values of Young's modulus and in situ stresses are to be determined or if it is in soft rock where the initial displacement may not be small, the effect of initial movement should be taken into consideration. An option is to determine the matrix $\mathbf{M}^*$ by 3D numerical modelling and subtract the initial values from the present ones.

EVALUATION OF THE EFFECTIVE FIELD ROCK PROPERTIES AND IN SITU STRESSES

In order to provide adequate information to determine the in situ stresses, at least three measurements of displacements have to be made. A minimum of five to six is recommended for higher reliability. The instruments should be located in at least three or more directions around the opening in order to have meaningful results. Assume a total of n displacement components are measured, then Eqn (13) has the same format but different size. $\mathbf{u}^*$ becomes the assembled displacement vector of size (n x 1) and $\mathbf{M}^*$ the assembled displacement coefficient matrix of size (n x 3). In order to determine the matrix $\mathbf{M}^*$, Young's modulus E and Poisson ratio υ are needed. Both E and υ are unknown. Since 1/E is a multiplier of $\mathbf{M}^*$, let

$$\mathbf{M}^* = \mathbf{X} / E \qquad (14)$$

then Eqn (13) becomes

$$\mathbf{u}^* = \mathbf{X}\,\boldsymbol{\sigma}^* \qquad (15)$$

where $\mathbf{X}$ is the matrix $\mathbf{M}^*$ determined at E = 1.0 and $\boldsymbol{\sigma}^*$ is the normalized stress vector $\{\sigma_x/E, \sigma_y/E, \tau_{xy}/E\}$.

Eqn (15) is a set of redundant linear equations (n > 3) with three unknown parameters. Multiple linear regression analysis can be applied to find a best-fit solution to $\boldsymbol{\sigma}^*$ based on the principle of error minimization (Zou, 1995b)

$$\boldsymbol{\sigma}^{*\prime} = (\mathbf{X}^T \mathbf{X})^{-1}\ \mathbf{X}^T \mathbf{u}^* \qquad (16)$$

where the superscript "T" refers to matrix transpose.

The displacements $\mathbf{u}^{*\prime}$ corresponding to the solution $\boldsymbol{\sigma}^{*\prime}$ can be calculated by Eqn (15). The residuals, i.e., the differences between the measured and the calculated displacements can be determined. With the solution of Eqn (16), the sum of the squared residuals is the smallest among all possible solutions to $\boldsymbol{\sigma}^*$ regardless of the E value. Any outliers in the data base of measurement, namely, those with extraordinarily large residuals, can be detected and the reliability of the regression results can be tested by statistic methods (Zou, 1995b).

If the E value of the rock mass is known, the actual stress components can be determined from $\boldsymbol{\sigma}^*$. If one of the stress components is known, the *effective field Young's modulus* E_{ef} can be estimated. For example, σ_y is normally proportional to the average specific gravity γ of the rock mass and the depth H below surface. Then $E_{ef} = \gamma H/\sigma_y^*$. In Canadian shield (Herget, 1988), $\gamma = 0.023 \sim 0.034$ MPa per meter of depth. E_{ef} can be determined accordingly. In some cases, σ_y may vary from γH due to influence from geological structures and nearby excavations. Then unless under extreme conditions, an approximation of $\sigma_y = (0.5 \sim 2.0)\gamma H$ is suggested as the initial value.

Poisson ratio υ, which is normally > 0 but < 0.5, is the only property which affects the matrix $\mathbf{X}$. Its effect is small in comparison with E. It may be predetermined from laboratory tests but can also be estimated during back-analysis. If all other parameters are kept constant while υ is changed in the analysis and the sum of squared residuals is calculated, the best-fit υ value is obtained when the sum reaches the minimum. See examples later.

Computer Software DISBEM

In order to facilitate the analysis, a computer software **DISBEM** (Zou, 1994) has been developed. It combines boundary element modelling and error minimization processes together. It gives the results of $\{\sigma_x, \sigma_y, \tau_{xy}\}$ and/or E_{ef} in a single step. The required input data include the geometry of excavation, location of instruments, the measured displacements and Poisson ratio. Specific gravity of the rock mass and depth of excavation are optional but they must be provided if E_{ef} is to be evaluated. **DISBEM** is designed for practical engineers and is very easy to use. It can be run on an IBM or compatible 386 PC computer with 520 KB free RAM memory. It requires DOS version 6.0 or later and a math co-processor.

VALIDATION OF THE BACK-ANALYSIS TECHNIQUE

In order to validate the method and to demonstrate the procedure of displacement back-analysis, an example is introduced in the following. For simplicity, a circular opening of radius 2.5m is assumed in a two dimensional stress field with five extensometers installed around the opening (Figure 4). Each extensometer is anchored at the deep end and the reading is the relative movement between the collar and the anchor point. The coordinates of the measurement locations are listed in Table 1. The rock mass is assumed isotropic and linearly elastic. The Young's modulus, Poisson ratio and applied field stresses are listed in Table 2. By analytical solution, the exact extensometer readings are calculated from Eqns (1) and (10), given in Table 3. Random errors of up to 15% are added to these readings to generate the hypothetical displacement.

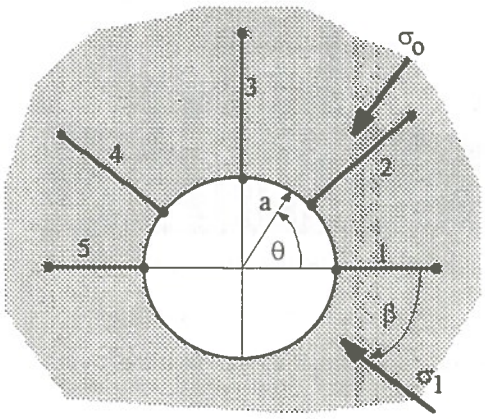

Figure 4. Relative movement measurement

Both sets of displacement data were processed using **DISBEM**. Boundary element modelling was used to simulate the excavation. σ_y is assumed to be equal to the weight of the overburden. Solutions of the in situ stresses and the Young's modulus are shown in Table 2. As can be seen, when the measurements are exact, the solutions are nearly identical to the actual ones. The very little differences are from the approximation of numerical modelling. When up to 15% errors exist in the measurements, the solutions are slightly changed. However, the differences are far less than the introduced errors of 15%. A comparison of the input and back-analyzed displacements shown in Figure 5 confirms further the validity of the method. When the input data are exact, the calculated displacements are identical to the input. When the input data contain errors, the calculated displacements tend to converge to the actual ones and have less errors than the input data.

TABLE 1 Coordinates of Extensometer Anchors

Extenso-meter	1	2	3	4	5
r/a	2.0	2.5	2.8	2.4	1.8
θ [°]	0	45	90	130	180

TABLE 2 Applied and Back-Analyzed Results

	σ_1 MPa	σ_o MPa	β [°]	E GPa	υ
Applied	42	30	43	50	0.2
Back-analyzed with exact measurements	42.12	30.04	42.9	51.2	(0.2)
Back-analyzed with hypothetic measurements	42.47	30.92	39.7	53.4	(0.2)

TABLE 3 Relative Movements [mm]

Extenso-meter	1	2	3	4	5
Exact	1.10	0.94	1.36	1.59	0.98
Errors (%)	-10	15	-15	5	-8
Hypothetic	0.99	1.09	1.16	1.67	0.90

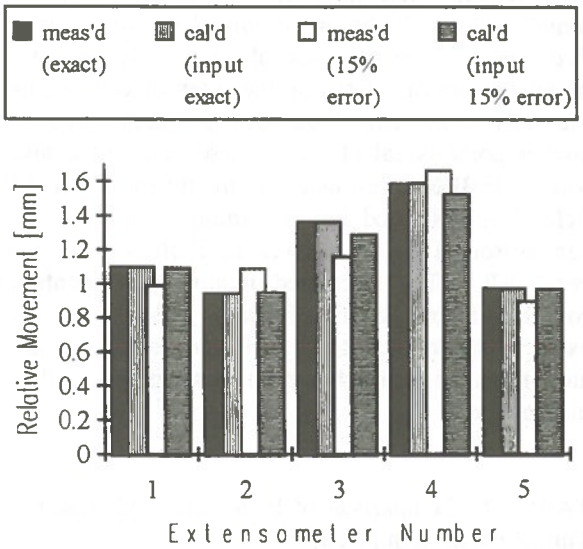

Figure 5. Comparison of input and back-calculated displacements

During above analysis, $\upsilon = 0.2$ was used. In order to check the effect of υ, the sum of squared residuals was determined for each given υ using the hypothetical data while keeping all other parameters constant. A number of analysis were carried out. The results are given in Figure 6, which indicates the best-fit value for υ is about 0.2. This example demonstrates that the in situ stresses and the field rock properties can be reasonably estimated from displacement back-analysis.

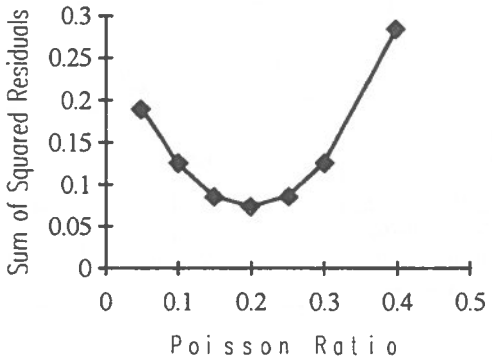

Figure 6. The best-fit Poisson ratio at minimum total errors

CASE STUDY -- TUNNEL EXCAVATION

Sakurai and Takeuchi (1983) presented a case where displacements were measured during excavation of a tunnel. Figure 7 shows the tunnel geometry and the five extensometers, for each of which only two anchor points are shown. Based on the extensometer readings, the relative movement between the collar and each anchor point is calculated. These data are analyzed using **DISBEM** to estimate the in situ stresses and the field Young's modulus assuming $\upsilon = 0.3$. A comparison of results is given in Table 4. They agree very well. The calculated relative movements are compared the measured in Figure 8. A good agreement exists at most points except at IIb and Va where Sakurai and Takeuchi showed similar discrepancy with the measurements.

TABLE 4 Comparison of Back-Analyzed Results for Tunnel Excavation [MPa]

	σ_x	σ_y	τ	E_{ef}
Sakurai, 1983	7.87	9.8	0.04	161
DISBEM	8.2	9.8	0.61	189

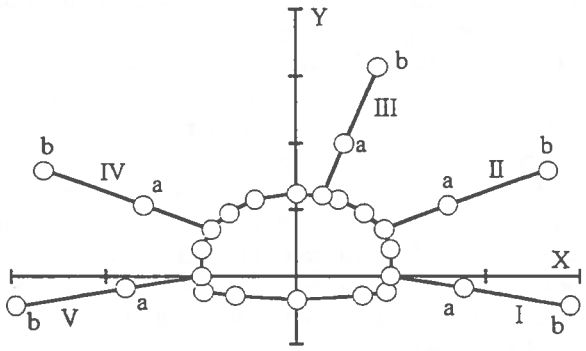

Figure 7. Displacement measurement during a tunnel excavation (After Sakurai and Takeuchi, 1983)

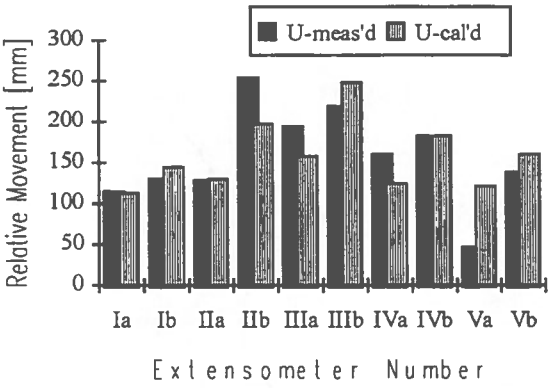

Figure 8. Relative movement comparison for tunnel excavation

The above results indicate that back-analysis technique can reasonably reproduce the ground movement as measured in the field and be used to estimate the effective field rock properties and in situ stresses.

SUGGESTED APPLICATIONS IN MINING ENGINEERING

Back-analysis technique is a powerful tool. It has a great potential in rock mechanics and mining engineering, especially in dealing with field problems. It is believed to have many applications. In the following, only a few are suggested.

Evaluation of Field Rock Properties: As has been explained before, there are needs to be able to determine the field rock properties. Direct field measurement is not feasible at present. Back-analysis offers a powerful and practical alternative. Because the input data are

from the field, the back-calculated results represents best the field condition and provides the most reliable information source for underground designs. The analysis procedure is simple as demonstrated in the case study.

Evaluation of the Effectiveness of Ground Supports: Ground supports are supposed to reinforce the ground and to change the ground behaviour. However there is a lack of proper measurement of the effectiveness of supports. Quite often, it is necessary to replace one support system by another one. Questions arise as for how effective the new system is in comparison with the old one. Back-analysis offers a practical solution. Effective supports should make the ground stronger and more stable. Equivalently they increase the properties of the rock mass when they are considered as part of the rock mass. Through the evaluation of change of field rock properties before and after installation of supports, or for two different types of supports, the effectiveness of supports can be easily and quantitatively assessed.

Calibration of numerical modelling: Very often, numerical modelling produces unrealistic results when compared with what may be observed in the field. The major problem is the assumption of the ground behaviour and rock properties used in the model. Back-analysis respects the ground itself and treats field data as the primary information. As shown in the case study, the calculated displacements can match well with the field data. The results can therefore be used to calibrate numerical modelling. In fact, if the back-analyzed in situ stresses and the field properties are used as the input data for a numerical model, realistic results comparable with field observation will be generated. Numerical modelling will then become more useful and provide more reliable information.

Evaluation of in situ stresses: Stresses in the field play another important role in ground stability. Earlier discussion has shown the importance of knowing the stresses in a domain containing the excavation. Back-analysis of measured displacement can be used to estimate the stress components acting in the domain. Stress results thus obtained are more realistic and provide more reliable information for the design and support of underground openings.

CONCLUSIONS

In this paper, a back-analysis technique has been introduced to analyze the measured displacement. It is based on the principle of error minimization and boundary element method and gives the results in one single step. It is suitable to any excavation encountered in mines regardless of the size, shape and influence from nearby excavations. It is shown through case studies to be a powerful tool in rock engineering. It can be used to estimate the effective field rock properties and in situ stresses. It can produce results which match well with the displacements measured in the field. It can also be used to evaluate quantitatively the effectiveness of ground supports. It is believed to have many prospective applications in mining engineering.

REFERENCES

Banerjee, P.K. and Butterfield, R., 1981
Boundary element methods in engineering science. McGraw-Hill Book Company, New York, 452p.

Crouch, S.L. and Starfield, A.M.,1983
Boundary element methods in solid mechanics. George Allen & Unwin, Boston, 322p.

Herget, G., 1988
Stresses in rock. A.A. Balkema, Rotterdam.

Hisatake, M., 1991
Back analysis in tunneling. Proceedings of the 1st International Workshop on Applications of Computational Mechanics in Geotechnical Engineering, Brazil, pp. 3-14.

Hisatake, M. and Ito, T., 1983
Back analysis methods to tunnel linings. Proceedings of the International Symposium on Field measurements in Geomechanics, Zurich, pp. 1047-1056.

Jaeger, J.C. and Cook, N.G.W., 1976
Fundamentals of rock mechanics. Methum & Company Ltd., London, 585p.

Kaiser, P. K., Wiles, T. D. and Zou, D. H., 1991
Two- and three-dimensional stress back analysis. Report to Atomic Energy of Canada Limited, Pinawa, 74p.

Leeman, E.R., 1968

The determination of the complete state of stress in rock in a single borehole -- laboratory and underground measurements. International Journal of Rock Mechanics and Mining Science & Geomechanics Abstracts, vol. 5, pp. 31-56.

Sakurai, S. and Takeuchi, K., 1983
Back analysis of measured displacements of tunnels. Rock Mechanics and Rock Engineering, vol. 16, pp. 173-180.

Sakurai, S., Shimizu, N. and Matsumuro, K., 1985
Evaluation of plastic zone around underground openings by means of displacement measurements. Proceedings of the 5th International Conference on Numerical Methods in Geomechanics, Japan, pp. 111-118.

Wang, S., Yang, Z. and Xue, L., 1988
The back-analysis method from displacements for viscoelastic rock mass. Proceedings of the 2nd International Symposium on Field measurements in Geomechanics, Rotterdam, pp. 1059-1068.

Yang, Z., Liu, Z. and Wang, S., 1983
A practical back-analysis method from displacements to estimate some parameters of a rock mass for design of underground openings. Proceedings of the International Symposium on Field measurements in Geomechanics, Zurich, pp. 1267-1276.

Zou, D.H., 1995a
Effects of rock behaviour and stress condition on filed stress measurement. Journal of China University of Mining and Technology, No. 1 (in press).

Zou, D.H. and Kaiser, P.K., 1990a
Determination of in situ stresses from excavation induced stress changes. Rock Mechanics and Rock Engineering, vol. 23, pp. 167-184.

Zou, D.H. and Kaiser, P.K., 1990b
Back-analysis of strain change measurements from Room 209 and shaft extension. Report to Atomic Energy of Canada Limited, Pinawa, 99p.

Zou, D.H., 1995b
Statistical regression techniques applied to borehole strain measurements. Geotechnical and Geological Engineering (in press).

Zou, D. H., 1994
Instructions for DISBEM. DZou Geomechanics International, 18p.

CAMI'95: 3rd Canadian Conference on Computer Applications in the Mineral Industry
Montréal, Québec, Canada, October 22-25, 1995

Numerical Modelling as a Tool for Stability Analysis of Shallow Stopes of Hard Rock Mines

Marc C. Bétournay
Canada Centre for Mineral and Energy Technology (CANMET), Ottawa, Ontario

Hani S. Mitri
Mining and Metallurgical Engineering, McGill University, Montreal, Quebec

ABSTRACT

Shallow stopes, usually affected by inherently weak or complex rock mass conditions, can be subject to various types of gravity driven failure mechanisms. Dedicated limit equilibrium equations and an empirical method (at $F_s = 1$) have been recently applied. Numerical modelling for shallow stopes requires that a code, commonly one of three types, reflecting the anticipated failure mechanism be used: discontinuum or block modelling to represent plug failures, ravelling failures, destratification and block caving; large strain finite element modelling to represent chimneying disintegration; and linear elastic modelling to represent competent, ineffectively jointed rock masses. Case studies are presented with modelling details and results for the three types of applications. A summary of controlling instability elements is included, along with commonly required modelling parameters to provide a focus on the nature and detail of required modelling input parameters.

RÉSUMÉ

Les chantiers peu profonds, à cause de massifs rocheux environnants faibles et complexes, sont affectés par divers types de mécanismes de rupture. Des équations d'équilibre limite particulières, et une méthode empirique (au F_s=1) ont été appliquées réçamment. La modélisation numérique pour ces chantiers requiert l'application d'un des trois types de logiciel relié au mécanisme de rupture: modélisation discontinue (en blocs) pour représenter les ruptures en bouchon, par égrainage, en strates et par foudroyage; modélisation par éléments finis à grande déformation pour représenter la désintégration en cheminée; et la modélisation linéaire élastique pour représenter les massifs compétents, peu fissurés. Des études de cas sont présentés avec exemples de modélisation et résultats pour les trois types d'application. Un sommaire des éléments qui contrôle les instabilités est inclus, de même que les paramètres communément requis pour la modélisation des chantiers peu-profonds, pour faire le point sur le type et détail de paramètres d'entrée requis.

INTRODUCTION

Canada's mining activity in metal bearing ores has primarily centered around extraction from underground stopes. Because these orebodies usually extend to the limit of bedrock, shallow stopes have been routinely created near the boundary to overburden, bodies of water, and surface infrastructure. Of these, 12% have caved to surface due to instabilities originating from stope hanging walls, crowns or footwalls.

Despite the advancements in the field of rock mechanics,

shallow stopes remain complex environments to design for. A variety of geologic terrains with variations in rock mass quality and disposition of discontinuities exist. The mining extraction method may also adversely affect the rock competence, as may the geometry and size of the opening. The geotechnical maxim "each case is a unique case" is applicable here. But unlike other engineering disciplines, the design engineer must work with materials he/she cannot change and stress levels that cannot be altered.

The mine operator in the past has had to turn, by-and-large, to conventional rock mechanics analytical and numerical design methods (theory of elasticity, continuum modelling, generic empirical methods) to address rock mass environments where failure mechanisms depend primarily on the effects of discontinuities and low rock mass strength.

STATE OF KNOWLEDGE

Because of the predominance of gravity driven failures of shallow stopes,analysis of stability and designs (Figure 1) are based on two aspects (Bétournay, 1995), recognition of in situ conditions, and failure mechanisms that can develop, shown in Figure 2: Plug failures (the sudden drop into a stope of a large but integral block which extends to the top of bedrock), ravelling failures (gradual failure from the periphery, resulting in stope enlargement towards surface), chimneying disintegration (upwardly disintegrating weak rock leaving behind "chimneys"), strata failures (from the crown, or periphery), blockcaving (free movement of a rock mass by its breakdown, towards an underground opening). In the case of competent, relatively massive rock, only partial failures occurred along shallow stope peripheries. To address these failure mechanisms, specific limit equilibrium analytical equations have been developed which reflect the mechanics of the failure process and incorporate the capability to arrive at the ultimate failure outline for comparison to the location of the bedrock surface. In this fashion a factor of safety analysis and expected location of failure can be established. Numerical modelling has been used in providing representative precise stress values for the equations. A probabilistic variant can be incorporated. Although there are some limitations in their use, they have been successful on the number of case studies reviewed (Bétournay, 1995).

A dedicated empirical approach based on failed versus stable surface crown pillar thickness or stope width (at F_s=1) using rock mass quality, stope geometry and discontinuity orientation (Golder Associates, 1990). Application of this method to case studies has been shown to be valid for discontinuity-controlled failures. Where failures are associated with weak rocks (e.g. NGI $Q < 0.5$) small variations in defining the quality of such poor rock masses yield large differences in minimum stable dimensions calculated (Bétournay et al. 1994). Failure is controlled by resistance of the rock mass to rupture.

NUMERICAL MODEL SELECTION

Approach

Application of numerical models in rock mechanics provides the possibility of obtaining approximate solutions to the behaviour of surface or underground excavations while considering a large number of influencing factors such as natural earth stresses, rock properties, ground support, and geometry of opening. Modelling of rock masses can be divided into two approaches: one approximating the mass as a continuous medium, the other a discontinuous one, regarding the mass as a group of independent blocks. The differential type of continuum models, including boundary and finite element techniques, characterize the entire region of interest. Boundary element procedures are most apt for modelling linear, homogeneous elastic systems, although certain forms of non-linearity can be treated. They provide economic means of two- and three-dimensional rock mass analysis. The finite element method is well suited to obtain continuous stress distribution in two or three dimensions and carry out estimation of mining induced fracture and weakness zones adjoining openings, by utilizing suitable failure criteria. Mining induced displacements are calculated. Irregular geometries, non-uniform material, non-uniform loadings, and location of stopes close to surface can be addressed. Non-linear material behaviour can be modelled.

Discontinuum models feature numerical procedures based on the equations of motion of blocks. The response to applied load on these relatively large block systems is calculated in time steps taking into account block interactions. The blocks can be treated as rigid or endowed with the ability to deform. This method is restricted to two dimensions unless very large computers are used. As with continuum models, it is still necessary

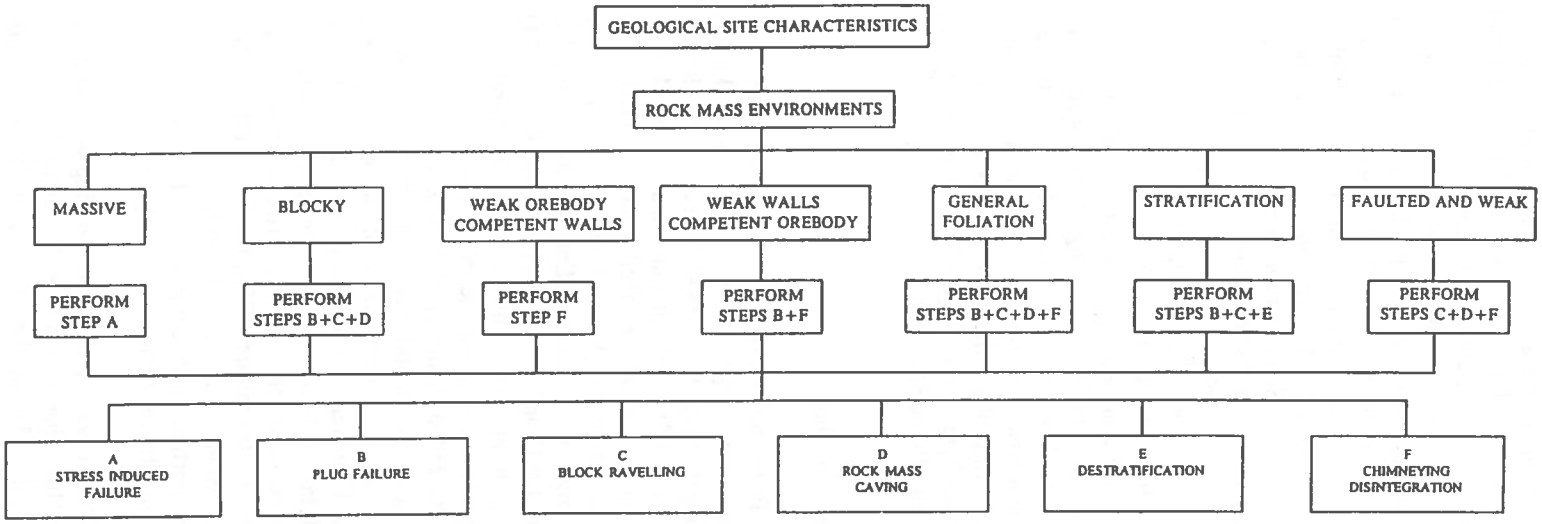

Figure 1 Stability analyses procedure for shallow stopes of hard rock mines.

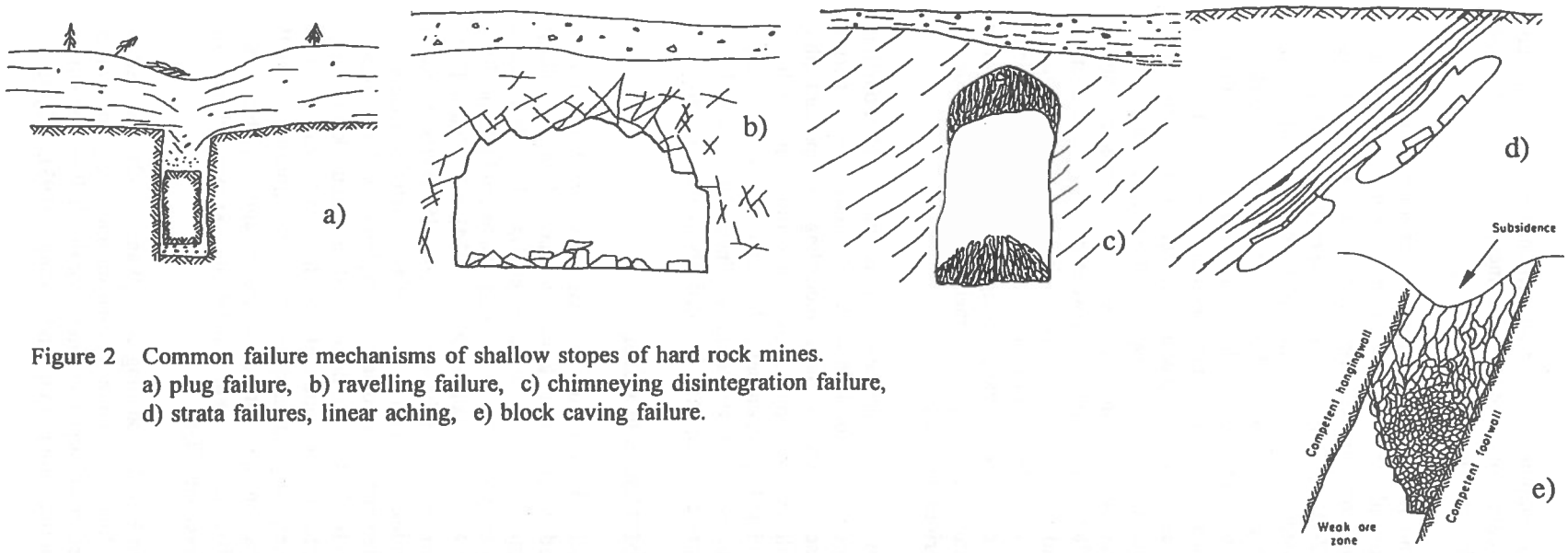

Figure 2 Common failure mechanisms of shallow stopes of hard rock mines.
a) plug failure, b) ravelling failure, c) chimneying disintegration failure,
d) strata failures, linear aching, e) block caving failure.

to compute using a pre-determined mesh, with precise location of all joints. The method however does not deliver overall factor of safety.

The selection of a particular numerical code therefore depends on a proper definition of the problem to be modelled. In examining the geometry of the opening(s) a 2-D or 3-D approach can be selected. A 2-D approach assumes that the openings, geological units and rock mass properties remain unchanged in a direction perpendicular to the 2-D section modelled. Those that are not will have such modelling predict conditions, such as redistributed stresses and displacements, which may be more accentuated than the real case. Treatment of the material load-deformation response is linear elastic when it follows a linear relation between the components of stress and strain, i.e. Hooke's law. When irrecoverable strain is produced by stressing the rock, non-linear behaviour must be considered. Finally, geological materials must also be examined in regards to their mechanical properties in various directions.

On a failure mechanism basis, numerical modelling requirements for shallow stopes fall into three categories: discontinuum or block modelling to represent plug failures, ravelling failures, destratification and block caving; large strain finite element modelling to represent chimneying disintegration; and linear elastic modelling to represent competent, ineffectively jointed rock masses.

Discontinuum modelling

Finite element modelling has been carried out on case studies that were known to have failed by block displacements in order to evaluate its effectiveness (Bétournay,1995). For the case of a 660 m high,and 70 m by 80 m plug failure (Allen, 1934), a 3D linear finite element code (Agbabian Associates, 1981) was applied in geological terrain of linear elastic material, except for filled surfaces in contact on two plug sides. Using 14,850 3D brick elements, denser mesh around the known plug surfaces, application of the Hoek and Brown failure criteria only indicated possible limit equilibrium in small areas in the immediate crown and periphery, but sufficient resistance along the known planes of movement, Figure 3.

The B.S.M. modelling code (Wang, 1992) was used to evaluate the failure mechanism and likely rock mass portions of large movements for the shallow stope of an inactive mine (Yu and Wang, 1993), Figure 4. Generalized rock mass movement was obtained but, as per current monitoring observation failure was not indicated. Use of distinct elements (UDEC code) was successful in the back analysis of a complex block failure development, Figure 5, starting with stope periphery ravelling leading to surface crown pillar de-stressing and individual block movement within it (Golder Associates, 1990). Generic analysis of surface crown pillars (Bétournay, 1995) (Golder Associates, 1990) has shown that for Canadian Shield stress fields, where the pre-mining major principal stress field is usually orthogonal to the strike of the orebody, sufficiently high redistributed compressive stresses exist to maintain the integrity of the surface crown and prevent crown ravelling or plug failures from occurring. However, when circumstances such as a high number of adjoining shallow stopes exist (e.g. in a grid, Figure 6) or when failures from the periphery increases the stope span, significant destressing occurs allowing plug failures in various cases. (Hoek, 1991) or ravelling failures (Figure 7) such as witnessed in Cobalt, Ont. (Bétournay, 1995).

Nonlinear modelling

Three different codes have been used to evaluate weak materials with large displacements and known chimneying disintegration: MSAP2D a 2D finite element code (Mitri, 1988) for elastic materials, and a 2D finite element code for elastic, perfectly plastic material and incremental plasticity (Yu and Toews, 1988) on the Belmoral mine (Commission of Enquiry: Belmoral Mine Accident, 1981) and the Brier Hill Mine (Rice, 1934) chimneying disintegration failures. In the Belmoral case, a mining step option available in the code was used to remove the failed elements and simulate the failure progress upwards. In both cases, Figures 8 and 9, areas of failure around the periphery of the opening were identified. However, results failed to indicate the ultimate extent of failure to surface as it developed. Induced compressive, and not tensile, ground stresses are responsible for the failures. This has for effect not only to break down the rock mass but also to remove part or a significant portion of its confinement thereby allowing gravity action to carry out the chimneying.

General block caving in the weak hanging wall schist of the Brier Hill Mine also occurred over its 180 m long hanging wall. Using the Hoek and Brown failure criterion, MSAP2D indicated (Figure 8) failure, which developed to surface.

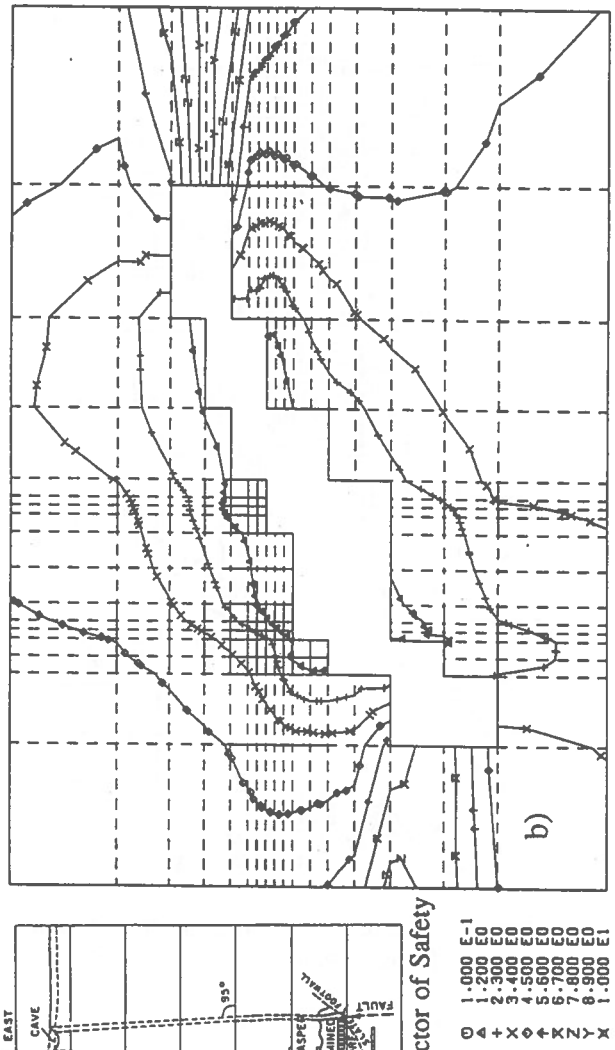

Figure 3 Plug failure of the Athens mine (Allen, 1934).
a) sections, distances in feet,
b), c) numerical modelling factors of safety.

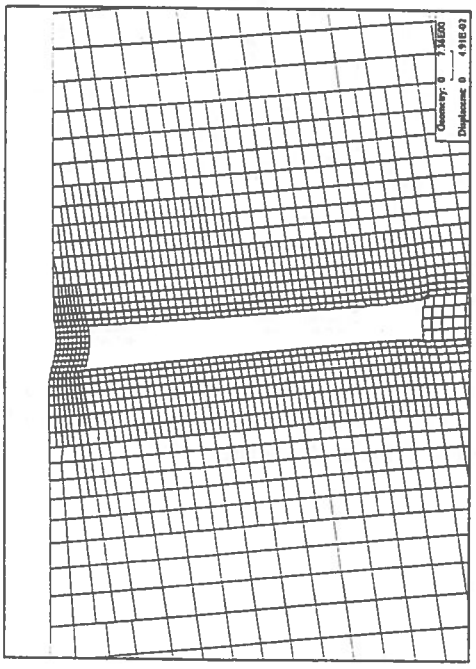

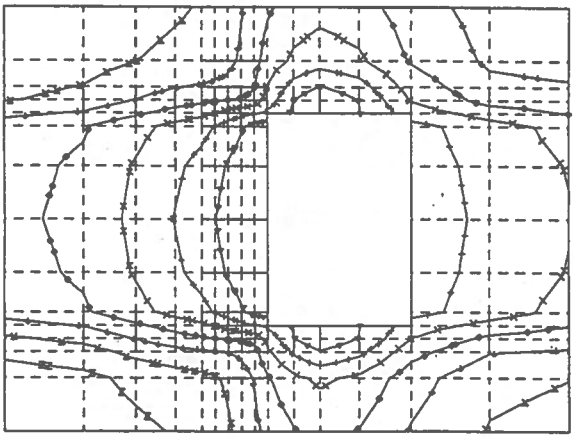

Figure 4 Exaggerated displacements of blocks around an inactive mine using discontinuum modelling (Wang, 1992).

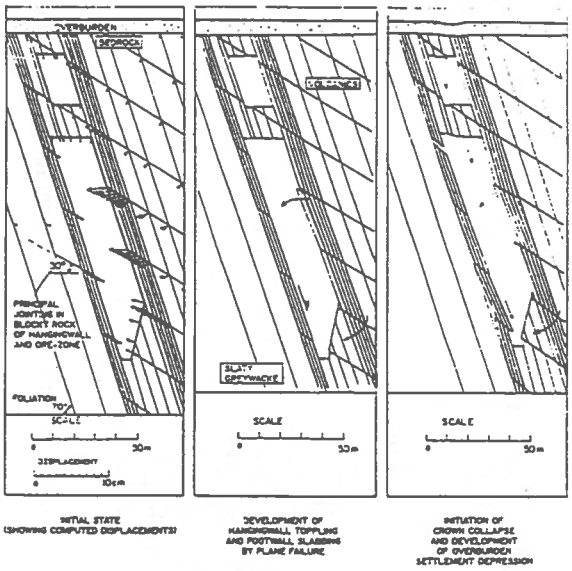

Figure 5 UDEC analysis of a complex shallow stope failure development in a discontinuous rock mass (Golder Associates, 1990).

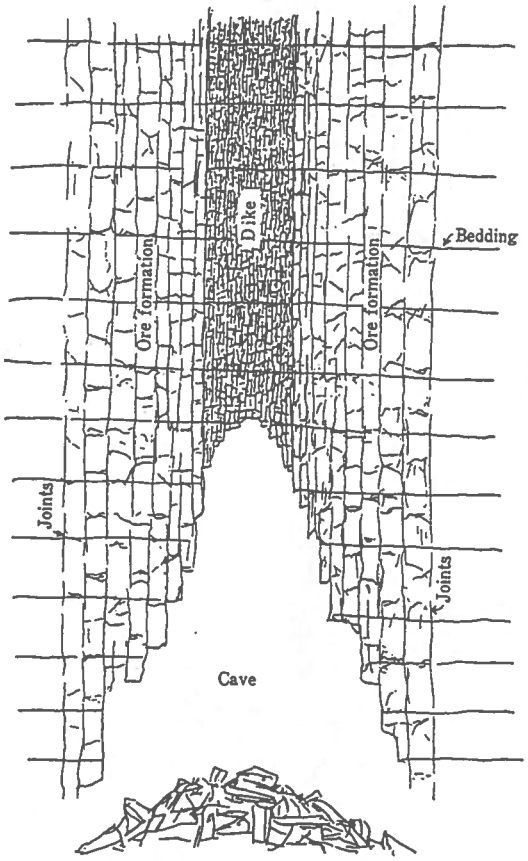

Figure 7 An example of block ravelling failure (Crane, 1929).

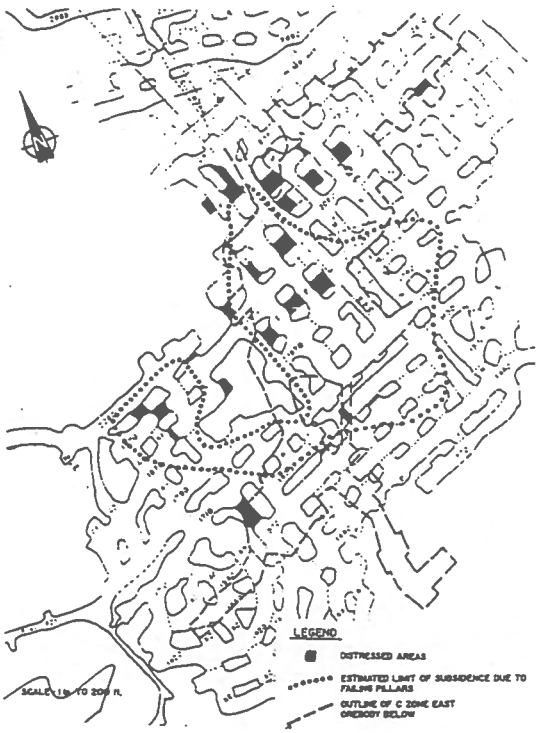

Figure 6 Plan view of proximal stopes hosting failures (Golder Associates, 1990).

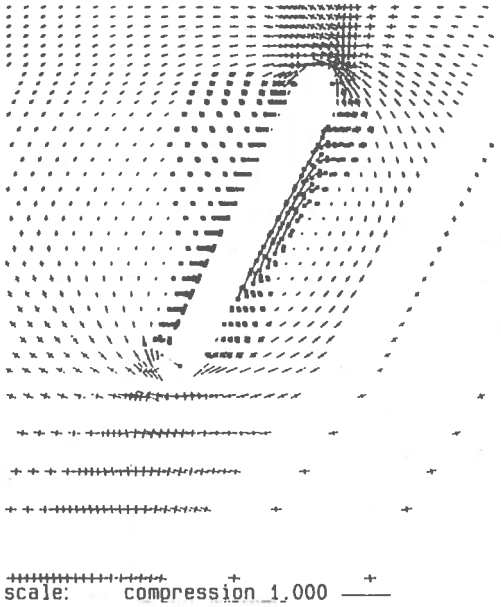

Figure 8a Enlargement of stresses around extracted area, Brier Hill Mine. Location of chimneying disintegration above opening drawn as square. Scale 1 cm = 30 m (Bétournay, 1995).

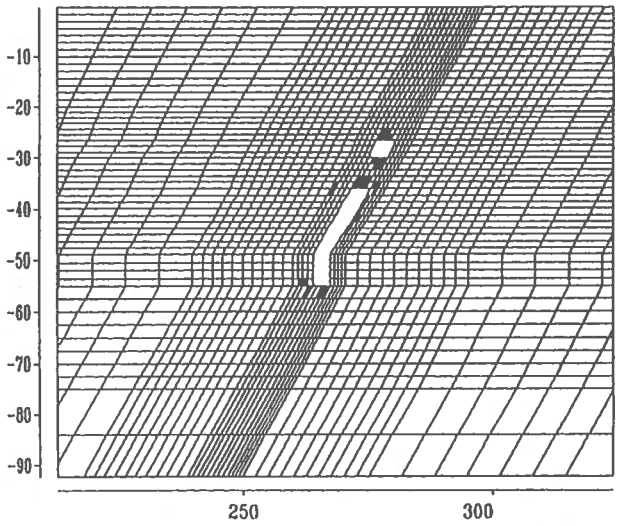

Figure 9 Failed portions of the weak rock mass after mining step two, creation of drift 1 - 7. Belmoral Mine, lengths in meters. (Bétournay, 1995).

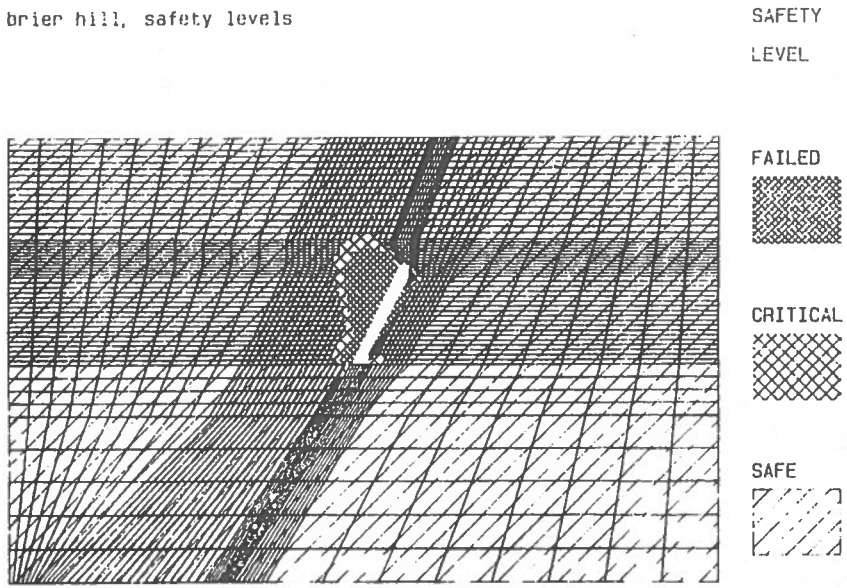

Figure 8b Hoek and Brown failure criterion safety levels for the rock mass around the extracted area, Brier Hill Mine. Scale 1 cm = 80 m (Bétournay, 1995).

In the case of severely altered rock such as the Selbaie Mine B zone (Strata Engineering, 1987) and Gays River Mine (Strata Engineering, 1991), a three-dimensional finite element code, ADINA, capable of modelling the elastic-plastic flow (large strain) of the materials was used. It allows progressive excavation variation in geometry by the application of a death and birth option for elements. Once again, compressive stresses were found to be responsible for failure within the surface crown pillar weak rock of the Selbaie Mine, and the weak hanging wall rock of the Gays River Mine. Progression of the failures was developed by the code.

Linear elastic modelling

In several cases, competent, poorly jointed rock masses were modelled using the linear elastic approach. Of particular importance was its role in identifying the surface crown pillars separating open pits and shallow stopes as being subjected to very high stresses. In this case the finite element codes used, SAP2D at Kidd Creek Mines (Hedley et al, 1979) and boundary element code BEAP3D (CANMET, 1993) for the Selbaie Mine A zone (Hamel and Charette, 1992) reflected this condition and by the application of the Drucker-Praeger, Mohr-Coulomb or Hoek and Brown failure criteria, satisfactorily represented the rock mass tensile and compressive behaviour which occurred, in the pillar, stope periphery and pit walls.

The Niobec Mine, with highly competent, massive, rock mass condition was modelled using the BMINES 3D linear elastic finite element code to represent this and the 3D layout of the open stopes. The model successfully identified zones of no confinement and tension in the surface crown pillars, due to very large surface crown pillar spans (e.g. 275 m long, 25 m wide), which reflected the failures observed (Bétournay, 1995).

Data input

Table 1 shows a summary of the important stability elements related to failure of shallow stopes. Table 2 gives the required input parameters for modelling.

In the case of weak materials it is important to understand that parametric values will be at a lower range (except for Poisson's ratio, higher) and need to be defined at low confining stresses, 0 to 5 MPa to reflect shallow stope induced stress conditions. Variations from representative values, on the more competent side, may not indicate the chimneying disintegration that occurs in weak rock masses (c_m = 0.04 - 0.14 MPa) (Bétournay, 1995). Similarly if the Hoek and Brown failure criterion

Table 1 Summary of shallow stope failure types and their causes (Bétournay, 1995)

Type of Failure	Mobilized Rock Mass	Lack of Ground Stress Clamping	Controlling Instability Elements
Rock fracturing	FW, CR, HW	No	Stress loading (p) (gravity or induced)
Plug failure	CR	Yes (s)	Near-vertical dipping continuous discontinuities (p); low friction properties (t)
Ravelling	CR, HW*	Yes (s)	Block rock mass (p); steep dipping joint (s)
Strata failure	CR, HW*	No	Stratification (p); stope span (s)
Chimneying disintegration	CR, HW	No+ (s)	Material of low cohesion (but not cohesionless (p)); small size rock mass fabric
Block caving	CR, HW	Yes (s)	Well developed jointing and blocks (p); stope span (t); tensile rock mass failure

\+ overstressed
* shallow dipping

Order of Importance: p primary, s secondary, t tertiary

Table 2 Required modelling input parameters

Dominant Failure	Required Parameters	Parameters and Tests	
Blocky and discontinuous rock masses	1,2,4,5,7,8	1. γ	material density; lab measurement
		2. υ	Poissons' ratio; unixaxial compression test
		3. m_i, σ_c	Hoek and Brown material strength parameters, unixaxial and triaxial tests, and regression calculation
		4. k_n, k_s	normal and shear stiffness of discontinuity; lab shear test
Weak rock masses	1,2,5,6,7,8	5. E_m	rock mass modules of elasticity, field dilatometer test, or rock mass rating (Bieniawski, 1973) and empirical calculation (Serafin and Pereira, 1983)
		6. c_m, ϕ_m	rock mass cohesion and angle of friction, empirical translation such as that using m_i, s_i, equations 1 & 2, (or use 7.), and calculation to field values (Hoek and Brown, 1988)
Competent, poorly jointed rock masses	1,2,5,6,7,8	7. m_j, s_j	rock mass Hoek and Brown strength parameters, using equations 1 or 2, or approximate values from Hoek and Brown (Hoek and Brown, 1988) when material is too weak to test undisturbed
		8. $\sigma_1, \sigma_2, \sigma_3$	natural ground stress measurement; in situ, in competent rock masses and preferably near surface

is applied, it has been shown that small variations in m_f and s_f values when these are in the low range result in variations in the extent of the anticipated failure zone at the low induced stress range.

The intact Mohr-Coulomb envelope and representative c and ϕ values can be scaled to field values from intact material testing by using rock mass quality and the translation equations of Hoek and Brown (Hoek and Brown, 1988) for intact (not residual strength) rock masses:

$$m_f = m_i e^{(RMR - 100)/28} \quad [1]$$

$$s_f = e^{(RMR - 100)/9} \quad [2]$$

Rock mass modulus of elasticity is ideally measured in situ, although empirical field values are possible by apply rock mass quality such as the Serafim and Pereira approach (Serafim and Pereira, 1983):

$$E_m = 10^{(RMR - 10)/40} \quad [3]$$

where RMR represents the CSIR rock mass rating (Bieniawski, 1973)

Perhaps the most difficult value to define in the field is the cohesion of weak rock masses which is the critical value for evaluating chimneying disintegration. No specific field test has been defined for this parameter. Calculation of rock mass cohesion using rock mass quality, estimates of field m and s values from the Hoek and Brown's table of representative values and calculation for c_m (Hoek and Brown, 1988) has yielded results which have been used to confirm known failures (Bétournay et al, 1994).

Significant attention is needed in performing natural ground stress measurements that are representative at the site's shallow levels. So far, published results of stress measurements in Canada usually relate to depths well below 80 m (Herget, 1984) (Arjang, 1990) leaving extrapolations to be performed for in situ stresses existing at shallow levels. Preliminary measurements at depths of 0 to 10 m have indicated non-zero horizontal stresses that can reach levels of 2 MPa (Labrie, 1991). This confirms the extrapolations (Herget, 1984). The reliability of the results require careful attention, as small micro deformations are registered, leaving very little margin for error. Measurements must be performed in sound, relatively continuous rock masses; this contrasts with the top of the bedrock which is usually altered, more intensely jointed with wider fissures.

CONCLUSIONS

Numerical modelling has been used historically to evaluate the stability, shallow stopes of hard rock mines. The application of various codes has shown that three fundamental rock mass failures originating from seven common rock mass environments require dedicated modelling codes. In the case of discontinuous rock masses defined by blocks, ravelling, plug and block caving failures require a discontinuum type code to model block movement and caving path to surface. In the case of weak rock masses where cohesion is low, routine finite element analysis, given representative values for material cohesion, will indicate stope periphery failure but not its potential for chimneying to surface. In this case, a large deformation finite element code with element death option is required. Conventionally used continuum modelling (elastic, elasto-plastic) cannot predict the nature nor the outline of the shallow stope failures to surface, failing to represent the gravity-induced movements which are for the most part piecewise and progressive (Bétournay, 1995). It can be used for competent rock masses where strength related failures are anticipated.

Modelling is fundamentally required in the case of extraction creating several proximal stopes to evaluate the significant reduction in the induced stress confinements normally provided to the surface crown pillar. This setting may host block failures, and block caving; plug failures being of special note since they occur rapidly. However, plug and ravelling failure potential within surface crown pillars is reduced substantially with discontuity inclination, the absence of low friction surfaces and shearing of intact rock interrupting the discontinuity (Bétournay, 1995).

REFERENCES

AGBABIAN ASSOCIATES, 1981.
Modernization of the BMINES computer code. Contract Report #0282022, U.S.B.M.

ALLEN, C.W., 1934.
Subsidence resulting from the Athen system of mining at Negannee, Michigan. Proceedings, Am. Ins. Min. & Met. Eng. V109, pp.195-202.

BÉTOURNAY, M.C., 1988.
Holt-McDermott mine visit: Stability Assessment of Shallow Underground Openings. Report MRL 88-72(TR); CANMET, Energy, Mines and Resources Canada

BÉTOURNAY, M.C., MITRI, H.S. and HASSANI, F., 1994.
Chimneying disintegration failure mechanisms of hard rock mines.
Proceedings, 1st North American Rock Mechanics Symposium, Austin, pp. 987-996.

BÉTOURNAY, M.C., 1995.
The stability of shallow stopes of hard rock mines. Ph.D. Thesis, McGill University

BIENIAWSKI, Z.T., 1973.
Engineering classification of rock masses. Trans. South Afr. Inst. Civil Eng., V15, pp. 335-344.

CANMET, 1993. BEAP user manual.
Report MRL 93-070(TR); CANMET, Energy Mines and Resources Canada.

Commission of Enquiry, Belmoral Mine Tragedy, 1981
Government of Quebec

GOLDER ASSOCIATES, 1990.
Crown Pillar Stability back-analyses. CANMET Contract Report 23440-8-9074/01.

HAMEL, G. and CHARETTE, F., 1992.
Projet d'évaluation de la stabilité des piliers de surface dans la fosse et des excavations souterraines, les Mines Selbaie. Report 92-093(CL). CANMET, Energy, Mines and Resources, Canada.

HEDLEY, D.G.F., HERGET, G., MILES, P. and YU, Y.S., 1979.
CANMET's rock mechanics research at Kidd Creek Mine. Report MRL 79-11(TR); CANMET, Energy, Mines and Resources Canada.

HOEK, E. and BROWN, 1988.
The Hoek and Brown failure criterion - a 1988 update. Proceedings, 15th Canadian Rock Mechanics Symposium, Toronto, pp. 31-38.

HOEK, E., 1991.
When is a design in rock engineering acceptable? Proceedings 7th International Congress on Rock Mechanics, Aachen, V3, pp. 1485-1497.

MITRI, H.S., 1988.
Finite element applications in mining engineering. McGill University, Professional Seminar Text.

RICE, G.S., 1934.
Ground movement from mining in Brier hill Mine, Norway, Michigan. Proceedings, Am. Inst. Min. & Met. Eng., V109, pp. 191-206.

Strata Engineering, 1987.
Weak rock mass model for support of surface crown pillars at Les Mines Selbaie. CANMET Contract Report 23440-5-9017.

Strata Engineering, 1991.
Gays River Mine, N.S., numerical analysis. Contract to Jacques, Whitford and Associates Ltd.

WANG, B., 1992
Introducing BSM: a computer program of the Block-Spring Model for analyzing jointed rocks.

Report MRL 92-124(TR). CANMET, Energy, Mines and Resources, Canada.

YU, Y.S. and TOEWS, N., 1988.
PCEPFE user's guide - a 2D elastic plastic finite element stress analysis package using a personal computer. Report MRL 80-95 (TR). CANMET, Energy Mines and Resources, Canada.

YU, Y.S. and Wang, B., 1993.
Geomechanical investigation of the Howey and Hasaga shallow mine workings, Red Lake, Ontario. Report MRL 93-056(CL). CANMET, Natural Resources Canada.

CAMI'95: 3rd Canadian Conference on Computer Applications in the Mineral Industry
Montréal, Québec, Canada, October 22-25, 1995

FE Simulation of Central Pillar Mining at the Homestake Mine

Jeffery C. Johnson, Melvin E. Poad
U.S. Bureau of Mines, Spokane, WA

Michael J. Stahl
Homestake Mining Company, Lead, SD

William G. Pariseau
University of Utah, Salt Lake City, UT

ABSTRACT:

In 1986, The Homestake Mining Company, the U.S. Bureau of Mines and the University of Utah initiated a cooperative study of shaft stability. The study concerned pillar mining near the Ross Shaft at the Homestake Mine. Early indications of ground control difficulties were shown to be within model expectations, and planned "wing" pillars within the main pillar were shown to be recoverable. Recent three-dimensional finite element simulations of the mining sequence for extraction of an 18 m central pillar remaining in the 60 m main pillar show some potential for skin yielding near the shaft, incremental shaft wall motion of about 1 cm and peak shaft strains of $5x10^{-4}$. The conclusion is that central pillar mining can be safely accomplished.

RÉSUMÉ

En 1986, la société Homestake Mining Company, le Service des mines des Etats-Unis et l'université d'Utah ont initié une étude coopérative de la stabilité des puits. L'étude portait sur l'exploitation par piliers abandonnés près du puit Ross à Homestake Mine. Les indications préliminaires ont montré que les difficultés de contrôler la terre sont conformes aux prévisions du modèle. Egalement, on a démontré que des piliers "ailes" planifiés à l'intérieur du pilier principal peuvent être recourvrés. Des simulations récentes en trois dimensions des éléments finis de la séquence d'exploitiation pour l'extraction d'un pilier central de 18 m que reste dans le pilier principal de 60 m démontrent du potentiel pour du fléchissement de la peau près du puit, du mouvement murale cumulatif du puit d'à peu près 1 cm et des déformations maximales du puit de $5x10^{-4}$. La conclusion c'est que l'exploitation par piliers centrales abandonnés peut être accomplie sans danger.

INTRODUCTION

The Central Pillar Project at the Homestake Mine in Lead, South Dakota, involves extraction of high grade gold ore from an 18 m (60 ft) wide pillar that remains in an originally 60 m (200 ft) wide pillar near the Ross Shaft. Location of the Homestake Mine, the Spokane Research Center and the University of Utah are shown in Fig. 1. General development of the mine and site of the shaft pillar project is shown in Fig. 2.

Shaft damage that occurred in the late 1950s led to definition of the original pillar as a block extending 30 m (100 ft) north and south along the strike of the ore body from the shaft centerline and indefinitely in the vertical direction. Figure 3 shows the horizontal extent of the original shaft pillar on the 3650 Level (depth below surface in feet). Most of the pillar ore reserve extended from the 3250 to the 3800 Level.

Figures 4a and 4b show the shaft pillar geology and a portion of the finite element model in an East-West vertical section passing through the shaft centerline.

Improved mining methods and ground control techniques led to a plan to recover as much of the original pillar ore reserves as was feasible. A series

Fig. 1. Location of the Homestake Mine.

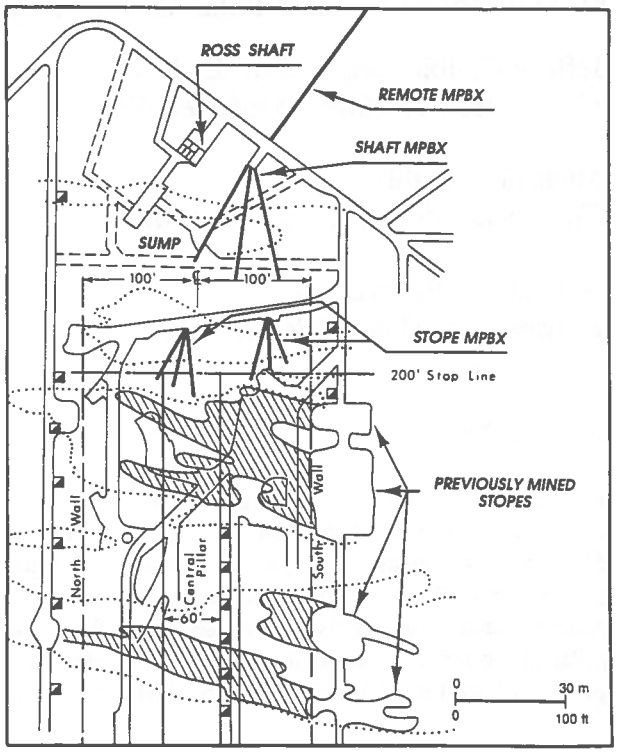

Fig. 3. Horizontal extent of the original shaft pillar on the 3650 Level.

of two-dimensional finite element analyses indicated that the Ross Shaft would remain in elastic ground and thus the potential for large-scale yielding was nil. Development began in 1987; in early 1988, the first lifts using a mechanized cut and fill method were taken below the 3650 Level. Ground control concerns arose almost immediately as a result of cracking of concrete slabs in a pump room near the shaft on the 3650 Level and renewed fracturing near the shaft station on the 3250 Level well away from the first lifts below 3650. The two-dimensional model results were brought into question, while an intensive three-dimensional finite element model was

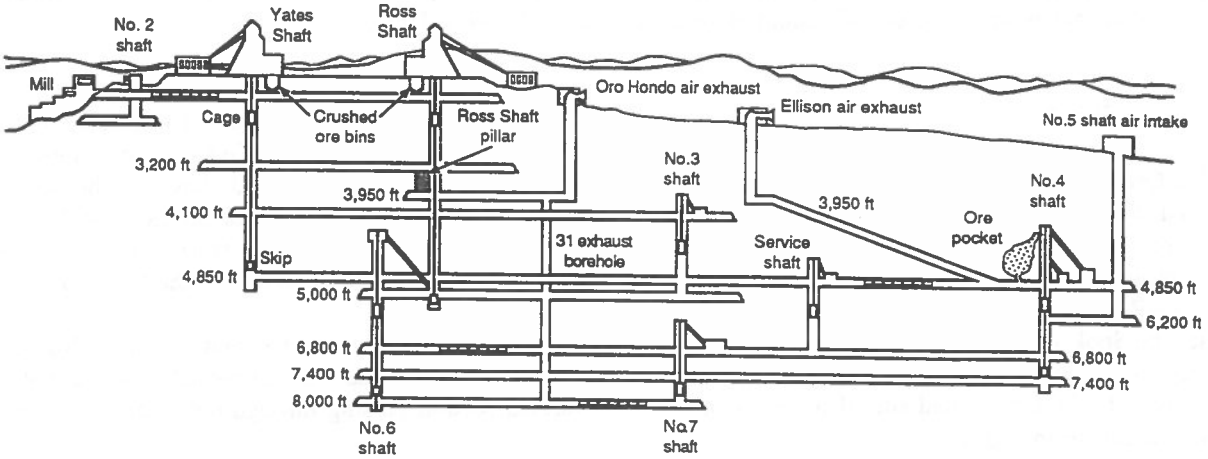

Fig. 2. General development of the Homestake Mine and location of the Ross Shaft pillar.

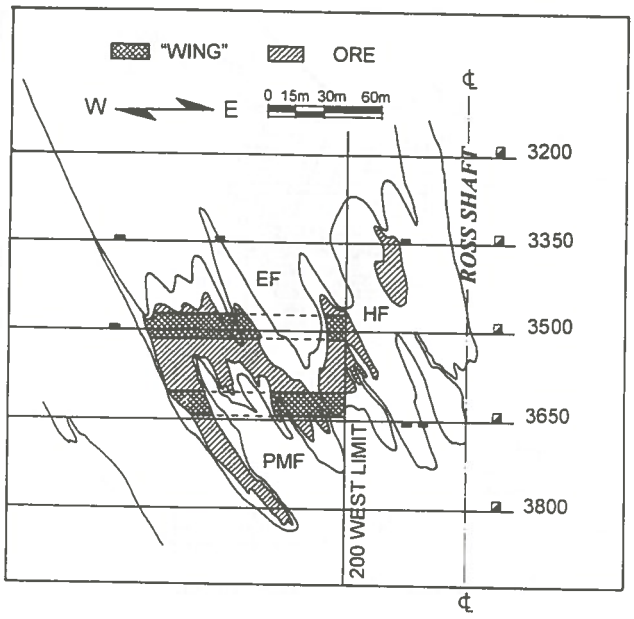

(a)

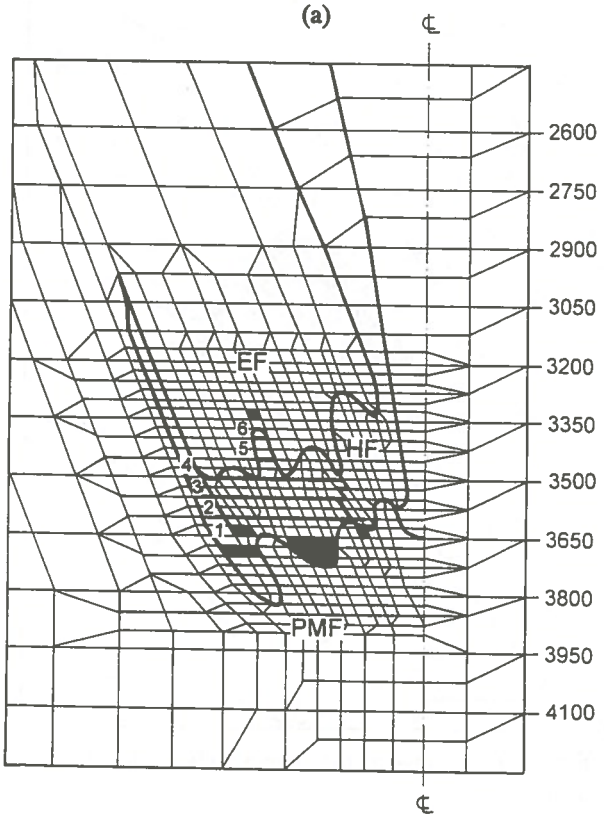

(b)

Fig. 4. (a) Shaft pillar geology in vertical section and (b) Portion of the central pillar finite element mesh in vertical section.

being implemented on a supercomputer at the University of Utah.

Examination of historical data showed that some of the difficulty was associated with long-term creep that had been accommodated by shaft guide adjustment which had reached adjustment limits. Chipping of rock and cement from behind shaft buntons allowed for recovery of adjustment space. Rebound was visually detectable at some sets.

More realistic three-dimensional model results confirmed the premining two-dimensional results in that the Ross Shaft remained in elastic ground.

Model details also revealed stress transfer occurred naturally in three dimensions and did much to explain rock mass motion near the 3650 Level pump room and near the 3250 Level shaft station. Importantly, model results showed that the worst would occur first, that measurements of displacements with borehole extensometers were within expectations, and that the logical course was to proceed with pillar mining.

Additional simulations of different pillar mining sequences suggested that recovery could be safely improved by eliminating "wing" pillars planned within the main shaft pillar (Fig. 4a). Mining of the remaining central pillar (Fig. 3) began in February, 1995. As mining proceeds, comparisons of borehole extensometer measurements with calculated readings will be used to further test model validity and the accuracy of the central pillar forecast.
mesh in vertical section.

BACKGROUND

A recent update and summary of the Ross Shaft Pillar Project is given by Poad and others (1995). Earlier progress in three-dimensional modeling is reported by Pariseau and others (1990). Complete details may be found in a series of Reports of Investigations by Pariseau and others (1995). The finite element code UTAH3 was used in all three-dimensional analyses. The program handles specified sequences of cuts and fills in initially stressed, elastic-plastic anisotropic geologic media using Hooke's law, quadratic yield and associated flow rules.

An overall view of the three-dimensional mesh is shown in Fig. 5. There are about 35,000 nodes in the mesh. A smaller but more refined mesh containing the shaft is shown in plan view in Fig. 6. Interleaving the two meshes was accomplished by using coarse mesh displacement output as fine mesh input while simulating a particular pillar mining sequence. This technique increases run times and the number of data files to be processed, but has the advantages of keeping the meshes relatively small and avoiding extreme gradation which can cause numerical difficulty. The fine mesh provides numerical detail and insures reliability in the vicinity of the shaft wall, while the coarse mesh shows a larger, stope-scale view of mining effects.

The ore at the Homestake Mine occurs in the Precambrian Homestake formation. The Poorman and Ellison formations form the foot and hanging walls, respectively, although folding can change the sequence. Foliation is well developed in the Poorman and Ellison formations and to a lesser extent in the Homestake formation. Each formation is modelled as an orthotropic elastic-plastic material.

An extensive series of laboratory tests formed a data base for estimating rock mass properties. Application of elastic and strength scale factors of 0.25 and 0.50, respectively, to the nine laboratory elastic moduli and nine strengths (three compressive, three tensile, three shear) gave the corresponding rock mass, field-scale moduli and strengths. Subsequent comparisons of model results (displacements and yield zone extents) confirmed the reasonableness of these values.

Regression analyses of calculated on measured borehole extensometer readings were used to establish the elastic properties scale factor (0.25). More subjective observations of the extent of yielding and downhole extensometer anchor loss were used to confirm the strength scale factor (0.5). An additional check on model reliability was obtained from comparisons of calculated with measured premining stresses in the center of the shaft pillar on the 3650 Level (Johnson and others, 1993). Because of the importance of the Ross Shaft, a conservative approach was taken during model validation and calibration studies. The goal was to be realistic, neither overly optimistic or pessimistic.

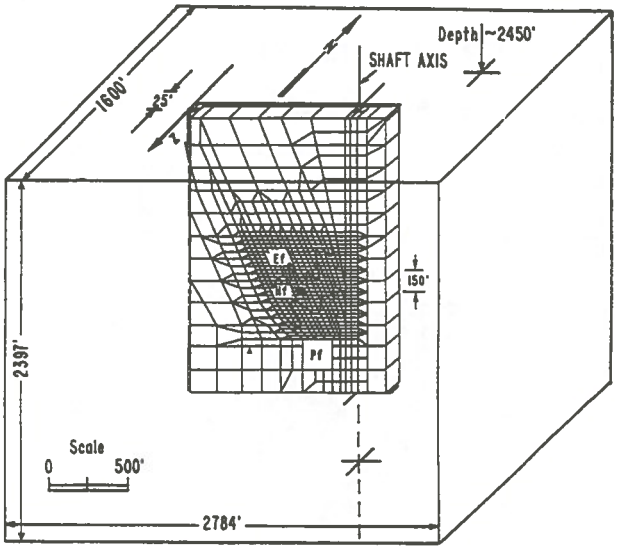

Fig. 5. Overview of the coarse mesh.

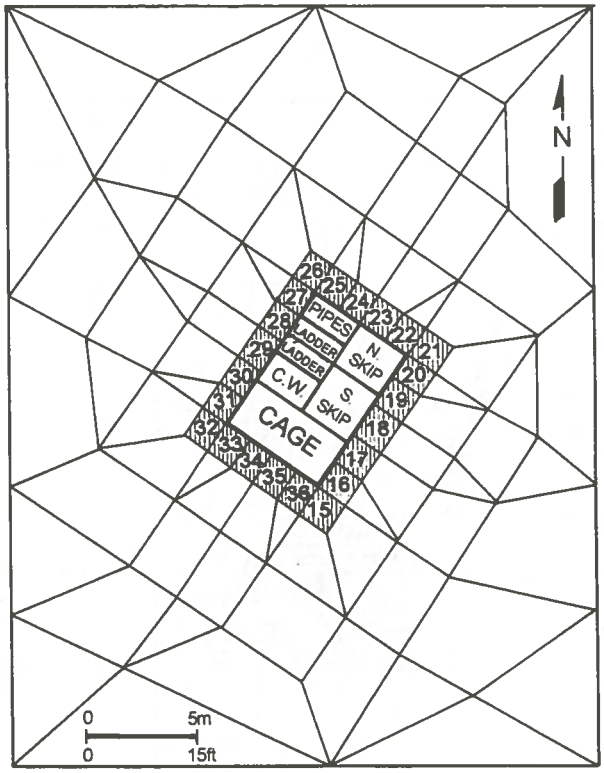

Fig. 6. Plan view of insert mesh about the Ross Shaft.

An additional array of borehole extensometers was recently installed in the central pillar to provide additional calibration data for the three-dimensional

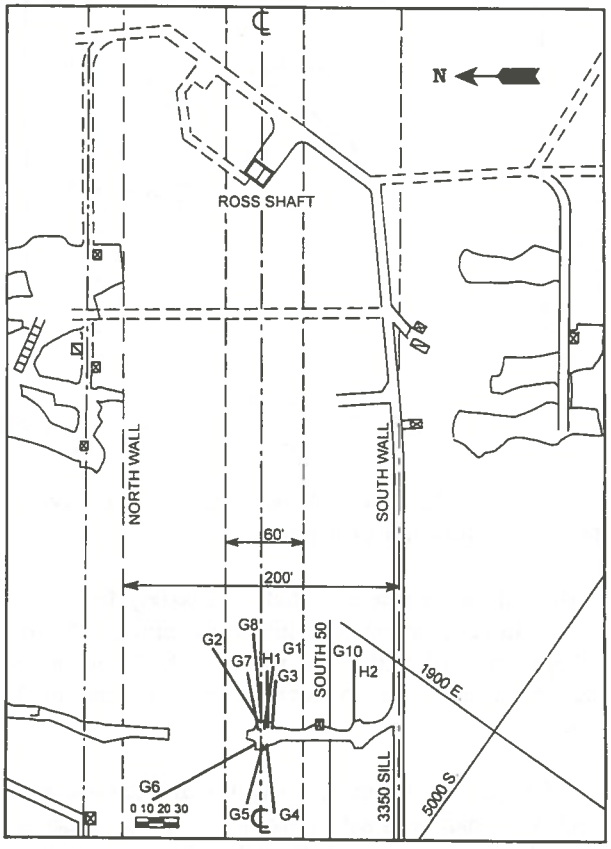

Fig. 7. Plan view of the recently installed 3350 Level borehole extensometer array.

model. Figure 7 shows a plan view of the new extensometer array from the 3350 Level where all holes were collared in an old tail drift.

CENTRAL PILLAR SIMULATION

The decision to leave an 18 m wide (60 ft) pillar within the main shaft pillar was based in part on a premining, two-dimensional finite element analysis that showed a potential for significant reduction of shaft wall displacement. Additional support was also introduced by "wing" pillars. However, subsequent analyses (later confirmed by actual mining) indicated the wing pillars were not essential. The present analysis suggests that the central pillar can also be mined without a serious threat to Ross Shaft stability.

Shaft stability here refers to the rock mass and the potential for large-scale ground movement that could close the shaft or render it inoperative. If rock mass stresses and strains enclosing the shaft are within the elastic limit, deformations are small and rock mass failure is unlikely. Small-scale yielding within the skin of the shaft is also not considered threatening because of containment of the yield zone by the adjacent mass of elastic rock and the opportunity for ground control by bolting and screening, for example. If a large-scale zone of yielding ground were to progress to the extent of entirely surrounding the shaft, a definite threat to stability would be indicated.

Structural stability of shaft buntons and framing, shaft guide alignment and so forth, while of concern, are separate issues because of different safety and stability criteria and much smaller displacement tolerances. Main shaft buntons are socketed into concrete in the Ross Shaft which is approximately 4.5 m by 6.4 m (15 ft by 21 ft) in section. If shaft steel begins to yield at a strain of 0.1%, end-on displacement of about 0.5 cm (0.2 in.) will strain the steel to the elastic limit. Displacements in bending would be similarly limited. Such small displacements are likely to be within the elastic range of shaft wall displacements and cannot be accurately estimated from finite element computations intended for large-scale rock mass stability analysis.

Inferences of stability are thus based on consideration of shaft wall safety factors, which indicate extent of yielding as well as margin of safety, and displacements, which largely determine structural stability, even though shaft wall displacements are only a rough indication of the structural response of shaft framing. All calculated data were obtained from three-dimensional finite element simulation of proposed central pillar extraction sequences. Measured displacements will be obtained from multi-point borehole extensometers (MPBXs) installed in the central pillar.

Finite Element Simulation

A total of twenty-six computer runs were used to simulate mining in the Ross Shaft pillar. The first run simulated excavation of the Ross Shaft. Mining before pillar extraction began was simulated by five additional runs. Thus, at the end of the sixth run, historical mining was complete. Runs seven through twenty followed pillar mining to the present (1994).

Simulation of central pillar mining involved six runs (twenty-one through twenty-six). Mining proceeds overhand by mechanized cut and fill; lifts are 3 m to 4 m (12 ft to 15 ft) in height. The simulated sequence combines several lifts in a single run as shown in Fig. 4b. A run requires about two hours of workstation time and about 64 Mbytes of fast memory.

All input data including geology, rock properties and *in situ* stresses were obtained from earlier project work. Output data include, displacements, strains, stresses and safety factors. In this regard, a safety factor is computed locally, that is, for each element in the mesh, according to the calculated stress state, failure criterion and rock strength assigned to each element. As customary, a safety factor greater than one signifies an elastic stress state. A safety factor of one means the element is at the elastic limit. Numerical drift can result in a safety factor less than one, although physically stress cannot actually exceed strength. Any tendency to do so, results in additional deformation.

The yield condition that marks the limit to purely elastic deformation is $Y = J^{(n/2)} + I$ where n = 2 in the present analysis, J is an anisotropic expression that reduces to the second invariant of deviatoric stress in the isotropic case, I is an anisotropic expression that reduces to the first invariant of stress in the isotropic case (Pariseau, 1972). When n=1 and isotropy prevails, one obtains the well-known Drucker-Prager yield condition. When the elastic limit is reached, $Y = 1$. The greatest value of $(J)^{1/2}$ possible is thus $(J)^{1/2}_{max} = (1\text{-}I)^{-n}$ and depends on the element stresses. The actual value is $(J)^{1/2}_{act}$ which also depends on the element stress state. The element safety factor is the ratio $fs = (J)^{1/2}_{max} / (J)^{1/2}_{act}$. Uniaxial compressive, tensile and shear failures are special cases that may arise in response to the evolving element stresses.

Shaft Wall Safety Factors

The lowest shaft wall safety factor at a given depth occurred near the shaft corner (element 27 in Fig. 6). Figure 8 shows the low element safety factor near the shaft wall at the end of the original Ross Shaft cut (CT1), at the end of historical mining (CT6), at present (August, 1994, R20) and at the end of the central pillar mining simulation (R26).

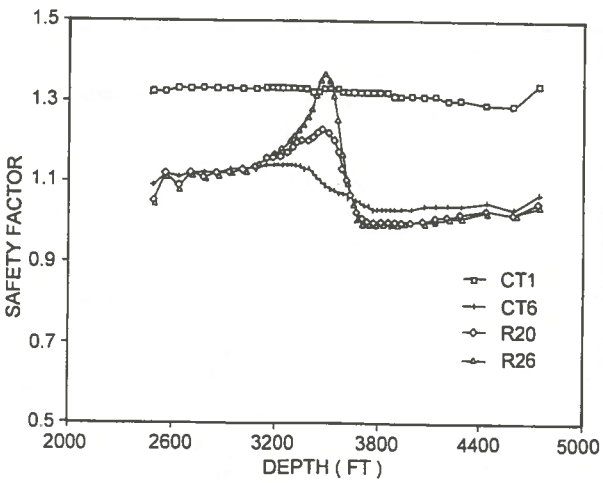

Fig. 8. Calculated low element shaft wall safety factor as a function of depth.

Most of the decrease in shaft wall safety factor occurs in conjunction with historical mining. Stress relief associated with pillar mining actually increases shaft wall safety factors between the 3200 and 3650 Levels.

Below the 3650 Level, a small additional decrease occurs in shaft wall safety factors. This decrease is enough to cause some shaft wall elements to respond inelastically as the safety factor is reduced to one. Figure 9 shows that the calculated yield zone is confined to elements at the shaft wall and is limited to a few elements near the shaft corners.

Shaft Wall Displacements

Although absolute shaft wall displacement is not a reliable index to stability, displacement calculations assist in visualizing shaft wall motions and provide a basis for estimating extensometer readings. The major component of shaft wall displacement is towards the pillar mining, that is, in an east-west direction. Figure 10 shows the calculated east-west displacement of the southeast corner of the shaft wall as a function of depth at the end of the shaft cut, the end of historical mining, at present (August, 1994) and at the end of central pillar mining (CT1, CT6, R20, R26, respectively). A negative displacement in Fig. 10 is towards the pillar. Each mining phase results in additional displacement. About a 1 cm (0.5 in.) occurs with historical mining. Pillar mining

roughly doubles shaft wall displacement. Simulation of central pillar mining indicates a further 1 cm (0.5 in.) of shaft wall displacement.

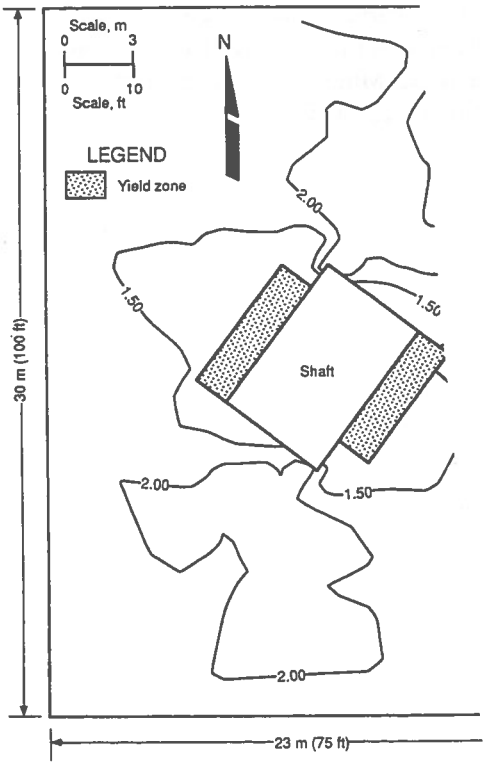

Fig. 9. Calculated contours of shaft wall safety factors with yielding extent (3650 L).

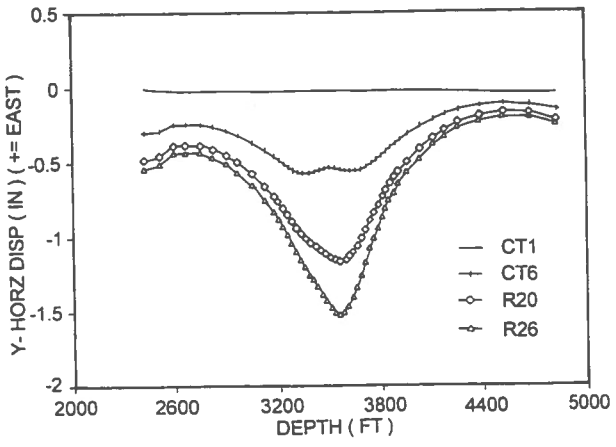

Fig. 10. Calculated east-west shaft wall displacement as a function of depth.

Relative displacements between shaft walls provide a measure of shaft deformation which may be transmitted to shaft buntons and other shaft frame components. In this regard, shaft strains are defined as relative displacements per unit of shaft dimension (width, breadth in a horizontal plane). Figure 11 shows shaft strains as a function of depth after the shaft cut, at the end of historical mining, at present (August, 1944) and at the end of the central pillar mining simulation (CT1, CT6, R20, R26, respectively). Figure 11 shows that the greatest compressive strain $3(10^{-4})$ is associated with historical mining. Pillar mining tends to deform the shaft in the opposite sense, and shows an extension strain of $5(10^{-4})$ at the end of central pillar mining. These deformations are well below a steel elastic limit of, say, 10^{-3}.

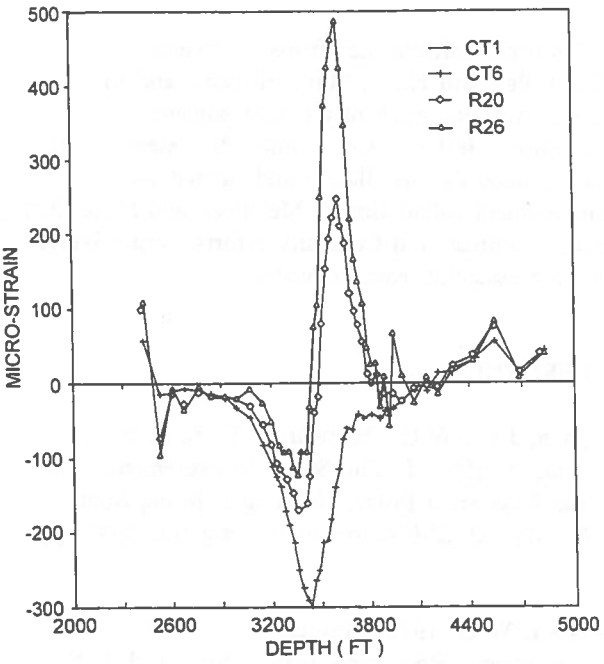

Fig. 11. Calculated shaft "strains" as a function of depth.

CONCLUSION

Three-dimensional finite element simulation of central pillar mining in the original Ross Shaft pillar at the Homestake Mine shows little decrease in shaft wall safety factors from the present (August, 1994) state which is stable. Simulation of central pillar mining also shows shaft wall displacements continue

to increase with extraction, but shaft deformations remain small. The finite element program UTAH3 was used earlier for stability analysis after the start of mining in the original pillar and provided useful guidance in the decision to continue pillar mining after initial disturbances gave pause to the mining plan. Reliability of simulation results was demonstrated and further application made to wing pillar recovery within the original pillar. Comparisons of measured with calculated borehole extensometer readings provided model calibration data. Additional data is expected from an array of extensometers installed in the central pillar portion of the original shaft pillar. The forecast is for stable shaft walls as central pillar mining proceeds.

ACKNOWLEDGEMENT

This paper reflects the efforts of several individuals. Bill Hand, Mark Filigenzi and Mike King carried out much of the extensometer installation. Jeff Johnson planned the extensometer array, guided the installation and carried out the finite element calculations. Mel Poad and Mike Stahl managed Bureau and Company efforts, respectively. All were essential team members.

REFERENCES

Johnson, J.C., W.G. Pariseau, D.F. Scott and F.M. Jenkins. 1993. In Situ Stress Measurements Near the Ross Shaft Pillar, Homestake Mine, South Dakota. USBM Report of Investigation 9446. pp 17.

Pariseau, W.G. 1972. Plasticity Theory for Anisotropic Rocks and Soils. *Proc.* 10th U.S. Symposium on Rock Mechanics. SME/AIME, N.Y., pp 267-295.

Pariseau, W.G., J.C. Johnson and S. Orr. 1990. Three-dimensional Analysis of a Shaft Pillar at the Homestake Mine. *Proc.* 31st. U.S. Symposium on Rock Mechanics. Balkema, Rotterdam, pp 529-536.

Pariseau, W.G., J.C. Johnson, M.M. McDonald and M.E. Poad. 1995. Rock Mechanics Study of Shaft Stability and Pillar Mining, Homestake Mine, Lead, South Dakota (In Three Parts). USBM Report of Investigation 9531 (Part 1), pp 20. Washington, D.C. (Parts 2 and 3 forthcoming).

Poad, M.E., W.G. Pariseau and M. Laurenti. 1995. Rock Mechanics of the Ross Shaft Pillar Project at the Homestake Mine. *Mining Engineering.* Vol. 47, No. 1, pp 80-84.

CAMI'95: 3rd Canadian Conference on Computer Applications in the Mineral Industry
Montréal, Québec, Canada, October 22-25, 1995

Numerical Modelling of Ground Deformation Associated with the Mining of Steep Tabular Orebodies

Erik Eberhardt, Doug Stead and Malcolm J. Reeves
Department of Geological Sciences, University of Saskatchewan, Saskatoon, SK, S7N 0W0

ABSTRACT

This paper presents a rock mechanics design methodology applicable to steeply dipping tabular orebodies typical of many Canadian underground hardrock mines. The first stage in this design process is the characterization of the rock mass using both *in situ* and laboratory data. The authors discuss the effects of anisotropy on rock mass behavior with reference to laboratory and field observations. The second stage in the design process involves the use of selected numerical modelling techniques to investigate ground performance in the near field rock. An approach was taken whereby several different numerical methods were used in conjunction, allowing the advantages of each method to be maximized. The design methodology employed emphasizes the importance of gaining an understanding of ground deformation mechanisms as opposed to predicting absolute behavior.

RÉSUMÉ

Ce travail présente une méthodologie de projet de la mécanique des roches s'appliquant aux corps minéralisés tabulaires à inclinaison abrupt typique de plusieurs mines souterraines à roches dures au Canada. La première étape daus le procédé de plan est la caractérisation de la masse rocheuse en utilisant des données *in situ* et de laboratoire. Les auteurs discutent des effets anisotropiques sur le comportement de la masse rocheuse en se basant sur les observations de laboratoire et du champ d'exploitation. La deuxième étape implique l'utilisation des techniques de modélisation numérique, choisies afin d'étudier le comportemeut du sol dans la roche environnante. Une étude a été faite à ce sujet òu plusieurs différeutes méthodes numériques ont été utilisé. Cela a eu pour effect de maximiser les avantages de chacune de ces méthodes. L'utilisation de cette méthodologie de projet intensifie donc l'importance de comprendre les méchanismes de la déformation du sol au lieu d'y prédire son compartement absolu.

INTRODUCTION

Open stope mining involves the formation of a large excavation to allow for the extraction of ore. The opening of these excavations is accompanied by an increase in strain energy stored in the form of stress concentrations in the near-field rock. Support for free-standing stope walls is provided through the intact strength of the orebody and host rock, and by pillars that separate the stope from previously developed openings. Cable bolting and backfill can be used to provide extra support and better ground control. Lack of control results in local failure of the wall-rock and dilution of the ore, possibly to the point where the diluted ore becomes uneconomic to mine.

Design methods can be utilized to study the effect that a large opening has on the local stress field and the stability of the stope walls. On a larger scale, they can be used to assess the global mine behaviour, allowing for the design of future stopes, pillars and development excavations. A study was undertaken to evaluate a variety of design techniques in order to develop an overall rationale which would integrate the advantages of each method. A case study involving a sill pillar failure at the Hudson Bay Mining and Smelting Co., Ltd.'s (HBMS) Trout Lake mine was used as part of this evaluation.

CASE HISTORY BACKGROUND

The Trout Lake Cu-Zn sulphide deposit was discovered in 1976, 5km northeast of Flin Flon, Manitoba. The deposit lies within the volcanic strata of the Flin Flon Greenstone Belt and is comprised of a series of en-echelon sulphide lenses, each underlain by an altered zone of chlorite schist. The case study presented in this

paper involves the modelling of the Trout Lake #4 lens sill pillar failure. The geology of the #4 lens consists of four main rock types: quartz porphyry (hangingwall), solid ore (ore zone), disseminated ore (ore zone), and chlorite schist (footwall).

Mine production called for the #4 lens to be mined in two halves, separated by a roll in the orebody where the dip steepened from 60° to 70°. During mining of the upper half of the lens, few ground control problems were experienced. In contrast, excavation of the lower half induced hangingwall sloughs with some footwall slabbing reported on almost every level. This was attributed to a combination of poor drilling and blasting, higher stresses and the foliated nature of the rock. More difficult groundfall problems began to occur after the completion of mining below the 420m level (Figure 1). Effectively, a pillar existed between the 420m level and the 390m level, with the exception of a development drift driven at the 405m level. The division of this remaining ore by the development drift into two separate pillars, would have resulted in increased stress concentrations in the pillar and possibly a reduction of the overall strength. Ground control problems were observed on the 405m level, most notably along the back of the undercut. The proposed failure mechanism is depicted in Figure 2. Unravelling of the disseminated ore and slabbing of the chlorite schist footwall led to the stronger intact solid ore being left unconfined This promoted gravity falls of large, joint-bounded, solid ore wedges, extreme mucking conditions and production delays. Cable bolting from the drift was performed, however the majority of the cables snapped. As the disseminated ore continued to unravel, large wedges continued to fall resulting in a decision to abandon the stope.

The majority of the ore in the lens was recovered and the loss was not considered that significant. Of greater concern was the possibility that with deeper mining and higher stresses, this type of failure may reoccur, increasing mining costs and operational problems.

LABORATORY AND *IN SITU* CHARACTERIZATION

Laboratory Testing

A series of laboratory tests were conducted in order to characterize the rock masses encountered at the Trout Lake mine and to determine the material parameters required for numerical modelling studies (Eberhardt et al, 1994). Testing involved rock types representing the hangingwall, the ore body and the footwall.

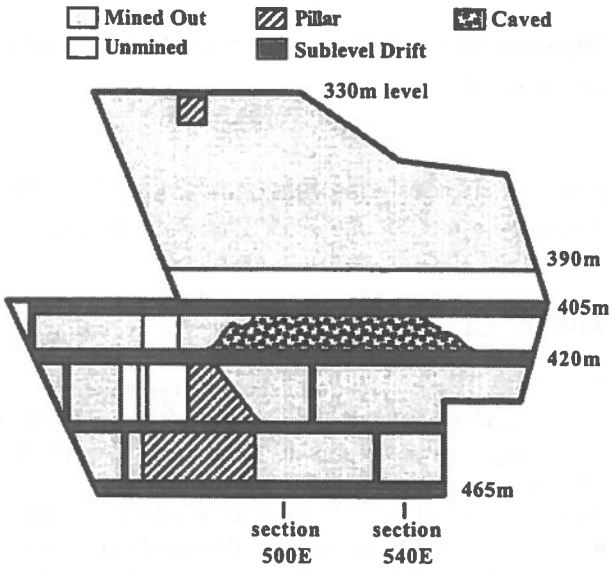

Figure 1. Sequencing of extraction for the #4 lens.

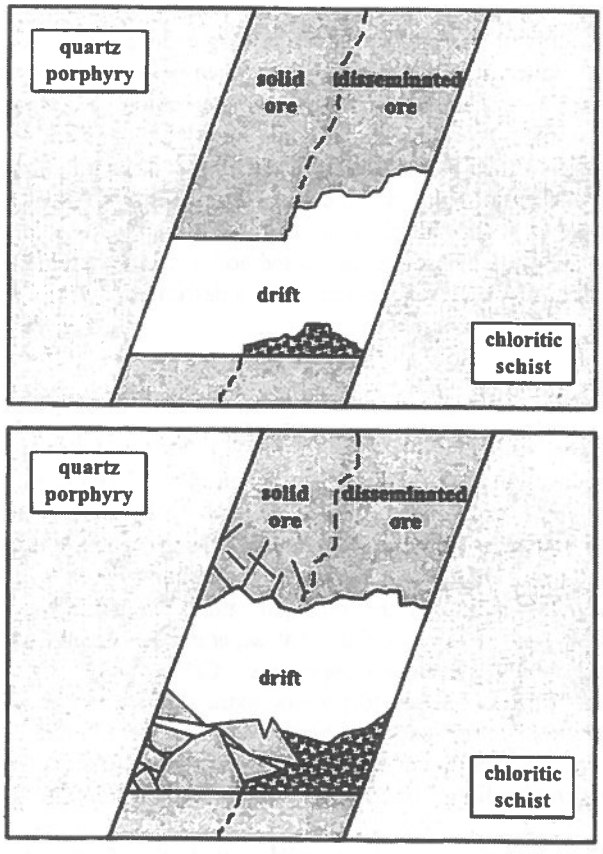

Figure 2. Proposed failure mechanism, #4 lens sill pillar.

In total, 32 triaxial, 14 uniaxial, and 67 Brazilian tests were conducted. Laboratory testing showed that the disseminated ore was approximately 50% weaker than the other rock types. The solid ore proved to be the strongest of the four rock types tested. Of the three rock types tested which exhibited varying degrees of foliation (i.e. chlorite schist, disseminated ore and quartz porphyry), the chlorite schist displayed the strongest transverse elastic isotropy, with a Young's modulus 60% higher when loaded parallel to the plane of isotropy than when loaded perpendicular to it (this anisotropy was also reflected in point load testing).

Although laboratory testing provides strength values and deformation properties for the intact rock, the ultimate strength and deformation characteristics of a rock mass is governed by the characteristics of the naturally occurring fracture systems. In some cases the intact values may be considered as a fair approximation to *in situ* behaviour, however, in most cases the quality of the rock mass as a whole must be taken into consideration.

In Situ Characterization and Empirical Design

The Mathews' method (Mathews et al, 1980), serves as one of the primary empirical design tools used at the Trout Lake mine, providing safety checks on the analysis of back support requirements and allowable span dimensions. Results obtained by Reschke and Romanowski (1993) for a number of HBMS mines in the Flin Flon area (including the Trout Lake mine), show good correlation between the collected data and the Mathews' stability design guidelines. In contrast, results obtained in the analysis of HBMS hangingwalls show that field performance does not correlate well with the type of behaviour predicted by the stability graphs.

The poor correlation in the hangingwall analysis may help in distinguishing which factors are influencing the degradation of the rock mass quality, and in addition are not properly being accounted for in the Mathews' analysis. In the case of the hangingwall, a larger exposed, or unconfined, area is involved, as opposed to the smaller area analyzed in the case of the stope back. With a larger area, the hangingwall becomes more susceptible to such factors as drilling and blasting. Drilling can have a critical destabilizing effect when it results in undercutting of the hangingwall structure (this is later demonstrated using the boundary-element numerical modelling method). Undercutting is not only the result of drillhole deviation but can also occur due to irregular geometries in the orebody. Reschke and Romanowski (1993), note that the Flin Flon area deposits are highly sheared and sinuous, thereby requiring closely spaced diamond drilling to accurately delineate the hangingwall. Unexpected hangingwall contacts and deviating drillholes result in damage to the hangingwall and increased sloughing. In addition, the sloughing extends to the next level above, making it difficult to regain control. Blasting also has an adverse effect on the quality of the rock mass, causing damage through strain-induced fracturing and/or gas penetration. Strain-induced fracturing results in the creation of new fractures and the extension of old ones, possibly forming wedges with pre-existing structural discontinuities. In order to reduce the problem of blast induced damage at the Trout Lake mine, considerable effort has been directed at optimizing blast patterns and explosive type.

Variability of laboratory and *in situ* data demonstrates that a number of factors may influence results. For example, both laboratory and *in situ* testing involve material found at depth. Effects such as microcracking and fracturing due to blasting and induced stresses must be considered as they alter the physical properties of the virgin rock. Martin (1993), has shown that intact samples obtained from a pre-stressed medium suffer irreversible damage when the far-field stresses exceed 15% of the rocks compressive strength. Considering the number of factors which may influence the results of both laboratory and *in situ* testing, it is necessary to accept laboratory and empirical values as a component in the overall design plan, modifying them to take into account scale effects and sample damage.

NUMERICAL MODELLING

Many design problems in rock mechanics involve complexities such as irregular geometry, anisotropic media and non-linear constitutive behaviour. Conventional methods of analysis, based on analytical solutions, are often impractical due to the large number of simplifications that are required to make the problem determinate. Numerical modelling design methods do not require such gross simplifications and therefore provide a means to solve more complex problems. Numerical methods can be subdivided into two main categories: integral methods (boundary-element and displacement-discontinuity methods) and differential methods (finite-difference and finite-element methods). Other numerical methods include hybrid methods, which link parts of the differential and integral methods, and discrete or distinct-element methods, developed to model jointed rock.

Both the integral and differential methods have been widely used to analyze stope designs and failures, with

the general approach being the selection of a single method which is best suited for the task at hand. In some cases, two different methods are used to analyse a problem, but in comparison, with the end result being a recommendation of one method over the other. With increasing experience and development of the different numerical methods over the past twenty years, the approach of selecting just one method best suited for the problem should no longer be required. Instead, an approach where several different methods are used in conjunction, allowing for the advantages of each method to be utilized, would seem to provide the ideal design plan. To show how such an approach allows for a comprehensive analysis of the different perspectives of stope design and analysis, modelling of the Trout Lake #4 lens sill pillar failure was completed.

Boundary-Element Method

The use of the boundary-element method in the design plan should capitalize on its speed and efficiency. These factors are best utilized in providing estimates of stress concentrations induced in the rock mass by an excavation due to its geometry. Cross-sections through the #4 lens were modelled to show how the relative stress concentrations would be effected by the different excavation geometries. Results of a 2-D boundary-element analysis using the program EXAMINE^{2D} (Curran and Corkum, 1988) showed that the highest stress concentrations occur along a 40m stretch of the sill pillar on the footwall side. This agrees with the location of the observed failure indicating that the geometry of the stope may have been an important factor in the resulting failure.

Further analysis shows that adjusting the shape of the stope by reducing the span of the roof results in a significant decrease in the stress concentrations (Figure 3). Such revisions to the final stope geometry are possible throughout the mining of the stope because of the quickness and ease with which models can be created and solved by the boundary-element method. These results also show how important accurate drilling can be since even minor deviations can result in problem geometries that are prone to large stress concentrations.

A 3-D analysis of the study area was performed using the program EXAMINE^{3D} (Curran and Corkum, 1993). The objective of the first part of the study was to analyze the effects that the surrounding excavations may have on the #4 lens. Assuming elastic isotropy, the "zone of influence" of a circular opening is five times its radius, beyond which the pre-mining stress field is not significantly different from the virgin stress field. In the case of a stoping operation, in which numerous large openings are present, the determination of the zone of influence is more complicated. The efficiency of the boundary-element program allows for such checks through the construction of large models which can incorporate the entire mine. Such a model was constructed to include all of the mined out stopes of the Trout Lake "north zone". The results of the model showed that although the excavation of the individual stopes influences the stress fields surrounding them, there is not a significant effect on the study area in question. These results justify the assumption in later models that the surrounding excavations do not have a significant effect on the #4 lens. This allows for other models to be simplified since the addition of surrounding excavations

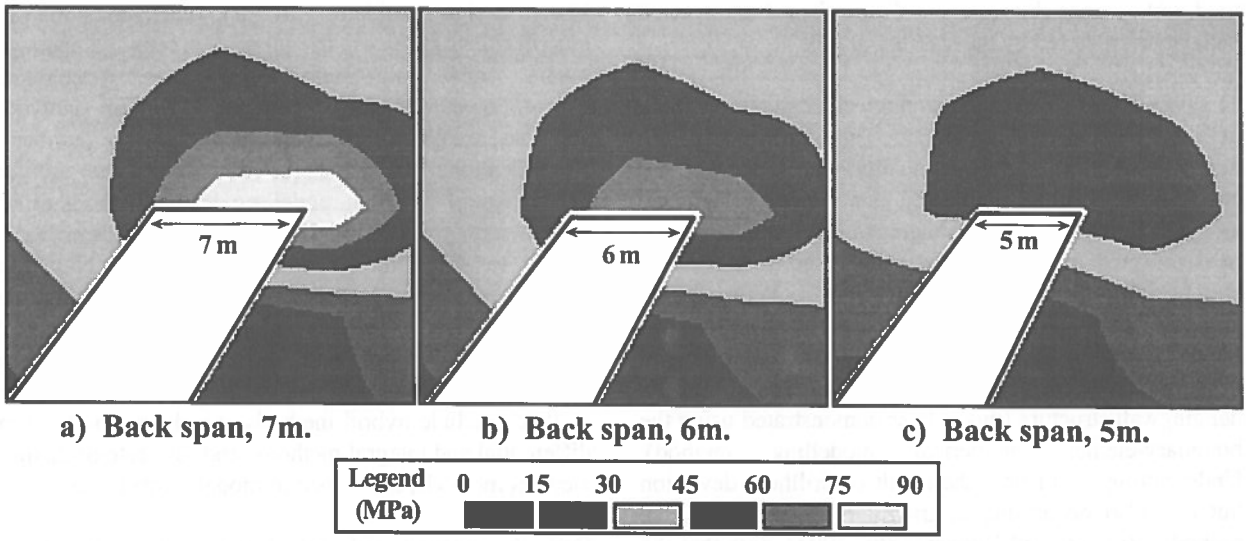

Figure 3. Effect of reducing the span of the back on the major principal stress (σ_1) concentrations.

is not essential. A further advantage to this type of analysis is that a check can be performed well ahead of excavation, based on exploration data, to determine if any highly stressed zones are to be expected from the interaction of neighbouring excavations.

The second phase of the 3-D boundary-element analysis involved the modelling of the #4 lens so as to check the effectiveness of a 2-D analysis. Using identical input parameters, the examination of the 3-D geometry allows for a check on the validity of the 2-D assumption of plane strain. The assumption of plane strain requires that strains be restricted to a single plane. Therefore, it is most accurate when the conditions of a problem are such that they involve the geometry of a body loaded uniformly over a comparatively long distance in one direction. Although this assumption can be regarded as being adequate in the modelling of a tabular orebody, the irregular geometry that is present in the third dimension requires some consideration. Initial analysis reveals that similar results are found between the 3-D and 2-D modelling, with regards to the prediction of a higher stress concentration in the vicinity of the actual failure. A direct comparison of the 2-D sections is provided in Figure 4 using sections through the 3-D model which mirror the cross-sections modelled in 2-D. This comparison shows that although both models predict a similar pattern in the stress field, the magnitude of the stresses calculated in the 2-D model are approximately 40% higher than those found by the 3-D model. Conceivably, higher stresses should be expected in 2-D models since 3-D models allow for the redistribution of stresses in the third dimension. In other words, the 3-D models allow for the stress concentrations to be partially dissipated in the third direction, whereas the 2-D models restrict the stresses to act only in the plane of analysis. This shows that 2-D modelling can overestimate the resulting stress field around an opening, thereby making the 2-D analysis more conservative.

Displacement-Discontinuity Method

The displacement-discontinuity method provides a pseudo 3-D analysis ideal for the modelling of excavations where the surfaces are close together, as in the case of a coal seam or a tabular orebody. Analysis of the #4 lens using the packages MULSIM/NL (Zipf, 1992) and EXAMINE^{TAB} (Curran et al, 1990) provide comparable results, showing increased stress levels in the pillar above the area of failure. However, as elastic models, these results do little more than confirm the results found in the 3-D boundary-element analysis. Since EXAMINE^{3D} is a true 3-D program, the 3-D boundary-element results can be regarded as a more realistic portrayal of the elastic problem.

Despite this overlap, in the case of a linear elastic analysis, the displacement-discontinuity method does allow for other useful types of analysis. Through the methods' portrayal of the problem domain as a slit in an infinite linear elastic rock mass, the use of stiffnesses between the two surfaces of the slit, representing the in-seam material, permits various non-linear material models to be used. Using the program MULSIM/NL, models were created to represent the orebody material as both a linear elastic and a non-linear elasto-plastic material (Figure 5). Detailed modelling of the sill pillar provided typical results for an elastic material, with stresses being at their highest next to the opening and decreasing away from it. The elasto-plastic model provided more interesting results showing that the stress concentrations and their relative magnitude can be significantly altered by any yield in the rock. Next to the opening, where near uniaxial stress conditions exist, a destressed zone appears representing rock which has yielded due to stresses exceeding the deviatoric yield stress of approximately 60MPa. This correlates well with plastic failure around an opening as opposed to elastic deformation in which the stresses would continue to increase. Next to the destressed zone is a zone of increasing stresses reaching magnitudes of 80MPa. Although these stresses are significantly higher than the yield stress, the *in situ* stresses in the σ_2 and σ_3 directions allow for stresses to exceed the assumed deviatoric yield point which is based on uniaxial stress conditions. The perimeter of the higher stress contours effectively outlines the new pillar boundary (i.e. rock that has not reached its full load-bearing potential). The resulting "hour glass" shape of the pillar typifies observations made regarding pillar failures in coal and potash mines. Wagner (1980), showed that the failure process in coal pillars commenced at the pillar boundary and migrated towards the centre where the core of the pillar had not reached its full load-bearing potential. Stresses throughout the pillar replicated this pattern with a destressed zone in the yielded areas, a high stress zone at the boundary of the stable material, and a gradual reduction in stresses towards the centre of the pillar. In the case of the #4 lens, the splitting of the sill pillar in half by the development drift, significantly increased the volume of yielded material thereby reducing the volume of supporting material.

Another useful feature of the displacement-discontinuity method is the ease at which it allows the analysis of progressive mine sequencing and the subsequent evaluation of intermediate results. This feature enables the user to examine stress and displacement changes as

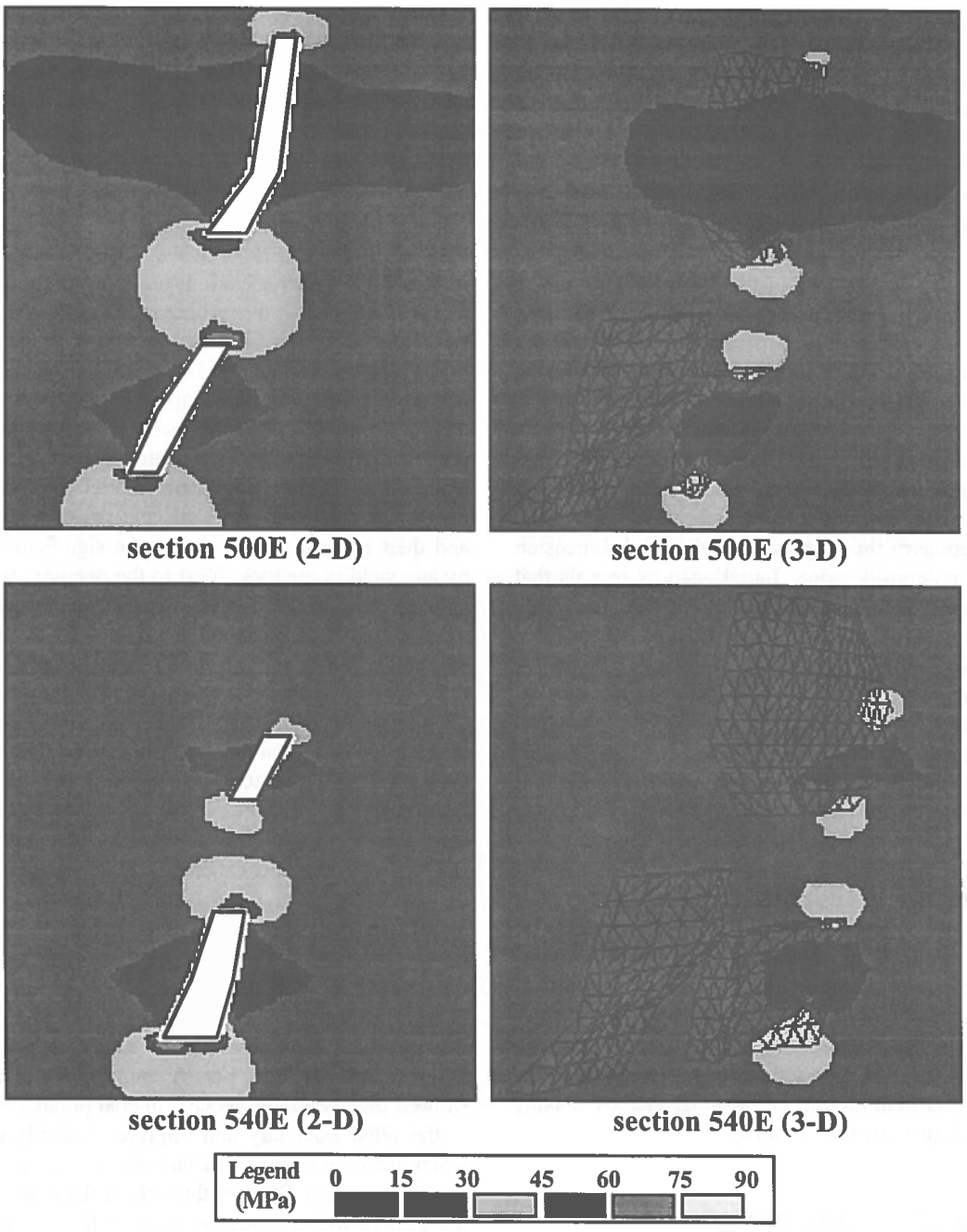

Figure 4. Comparison of 2-D and 3-D boundary-element models showing major principal stress (σ_1) concentrations.

mine development progresses. Each of the MULSIM/NL and EXAMINE^{TAB} models were created duplicating the actual excavation sequencing used in the mining of the #4 lens. Limited to a linear elastic analysis, EXAMINE^{TAB} makes this process extremely easy, allowing for a number of excavation strategies to be modelled in a relatively short period of time. However, in the case of linear elastic modelling, stress distributions around uniform geometries will be the same regardless of the intermediate steps leading up to the final geometry. Since, in most cases, the final geometry of the excavated stope will be the same, the use of the models is best applied to examining the stresses after each intermediate step. Results from the intermediate mining steps show that the actual sequencing used by the Trout Lake mine was, most likely, the optimum pattern for keeping stresses in the sill pillar to a

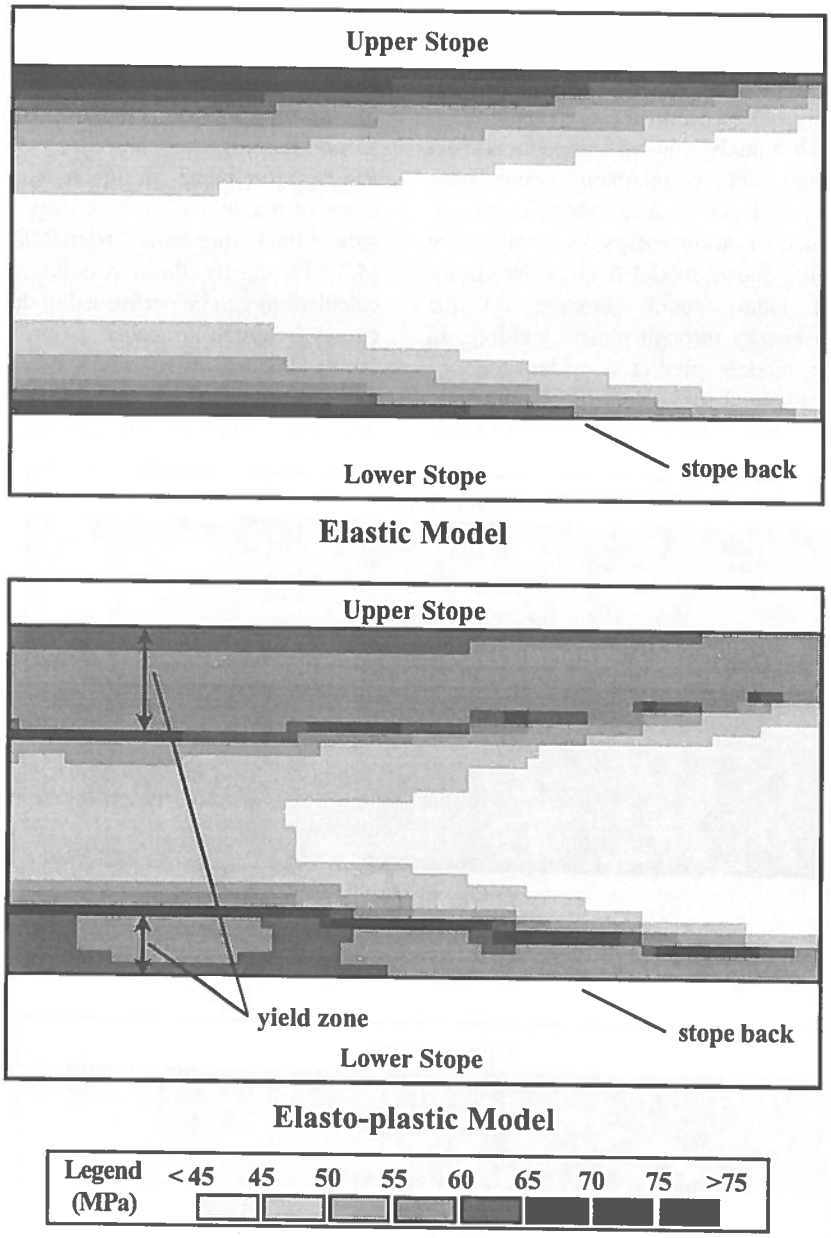

Figure 5. MULSIM/NL results showing normal stress contours along a longitudinal projection of the pillar area.

minimum. Assuming an elasto-plastic constitutive model (an option available with MULSIM/NL but not EXAMINE^{TAB}), the final stress distributions will be dependent on the sequencing since the varying zones of excavation will result in different zones of irreversible yield before the final geometry is reached. Modelling results show that without the use of intermediate mining steps, the zone of influence is greater and the stresses are higher. This would be expected since, without multiple mining steps, the amount of stress dissipation due to plastic yield would be limited. A more realistic portrayal of the resulting stress field would therefore be expected when duplicating the actual mine sequencing, since intermediate mining steps allow for large stress concentrations to gradually build up and at the same time, slowly dissipate through plastic yielding.

Another feature of the MULSIM/NL code is that it contains an energy subroutine that uses the calculated stresses and displacements at each element to determine the change in strain energy for each mining step. Changes in strain energy accompany mining induced stresses and

result in the deterioration of the rock in the periphery of the mine opening. A study into the distribution and build-up of strain energy can provide insight not only into areas of potential instability but also into the dynamics of the potential failure. Such a study was performed in respect to the #4 lens failure, with comparisons being made between linear elastic and elasto-plastic models. As was expected, the influence of strain energy was seen to be more significant in the elastic model than in the elasto-plastic model, the latter model allowing for the dissipation of strain energy through plastic yielding. In effect, elasto-plastic models predict a wider zone of failure, but a lower potential for violent failure, whereas linear elastic models, which do not limit the rate of strain energy build-up, are more prone to indicate rock burst conditions. Further analysis of the sill pillar indicates that strain energy values in the centre of the pillar are higher for the elasto-plastic model (Figure 6). Plastic yielding around the edges of the pillar results in higher stresses, and therefore higher strains, in the centre of the pillar. In terms of magnitude, strain energy values in the modelled area of the failure ranged from 0.08 to 0.14 MN*m/m^3 (or MJ). To clarify these results, simple elasticity based calculations can be performed to determine the total strain energy required to cause failure in the rock (Herget, 1988). The estimated stored strain energy at failure for the disseminated ore and the solid ore, using values determined through the laboratory testing, would be

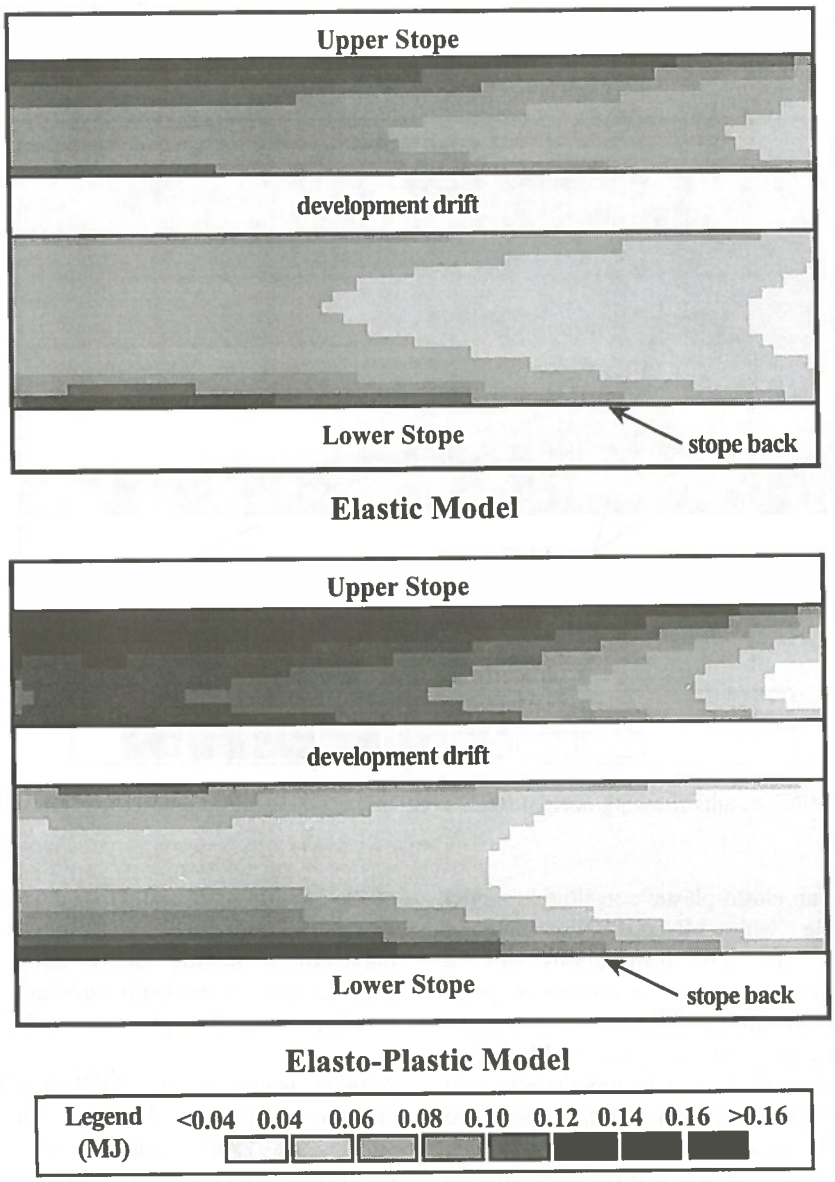

Figure 6. Linear elastic and elasto-plastic MULSIM/NL models showing total strain energy in the sill pillar.

approximately 0.06 and 0.16 MJ respectively. Although this may be regarded as a crude estimate, modelling shows that the total strain energy in the failed sill pillar fell within this range. In regards to rock burst potential, Herget (1988), notes that 1.08 MJ of stored strain energy is relatively large and has the potential for bursting if suddenly released. Although failures in the #4 lens more closely conform to a gradual plastic failure, studies into strain energy build-up and release rates may play a more critical role in the design of deeper stopes where the stresses are much higher.

Finite-Difference Method

Finite-difference and finite-element methods solve problems through the use of elements representing the problem domain and hence, allow the incorporation of a number of different material models representing both anisotropy and non-linearity. These characteristics were incorporated into the analysis of the Trout Lake mine case study. Using the 2-D finite-difference program FLAC (Itasca, 1992), three models were created to compare the results of modelling the problem domain as being elastic isotropic, transversely isotropic, and Mohr-Coulomb elasto-plastic. The models were also run to simulate the excavation of the stope in three steps. FLAC results for the three different material models showed similar results, with stress concentrations in the sill pillar varying by only a few MPa's. The similarities observed between the linear elastic and transversely isotropic models, and the results obtained through the simpler and less time consuming integral method, demonstrates the relative inefficiency of the finite-difference method in elastic modelling of homogeneous media. It is the ability of the differential method to model materials as being non-linear, along with the handling of anisotropy and inhomogeneity, that separates it from the integral method.

Using the Mohr-Coulomb elasto-plastic material model, comparisons were made between the yielded rock and the stress trajectories, providing considerable insight into the failure mechanism responsible for the #4 lens failure. Results from the modelling indicate that with the weaker strength properties of the disseminated ore, yield would begin in the disseminated ore zone (Figure 7). Assuming that this yield would result in compressive failure of the disseminated ore and therefore its subsequent unravelling, the yielded blocks were removed from the model. It should be noted that the unravelling of the disseminated

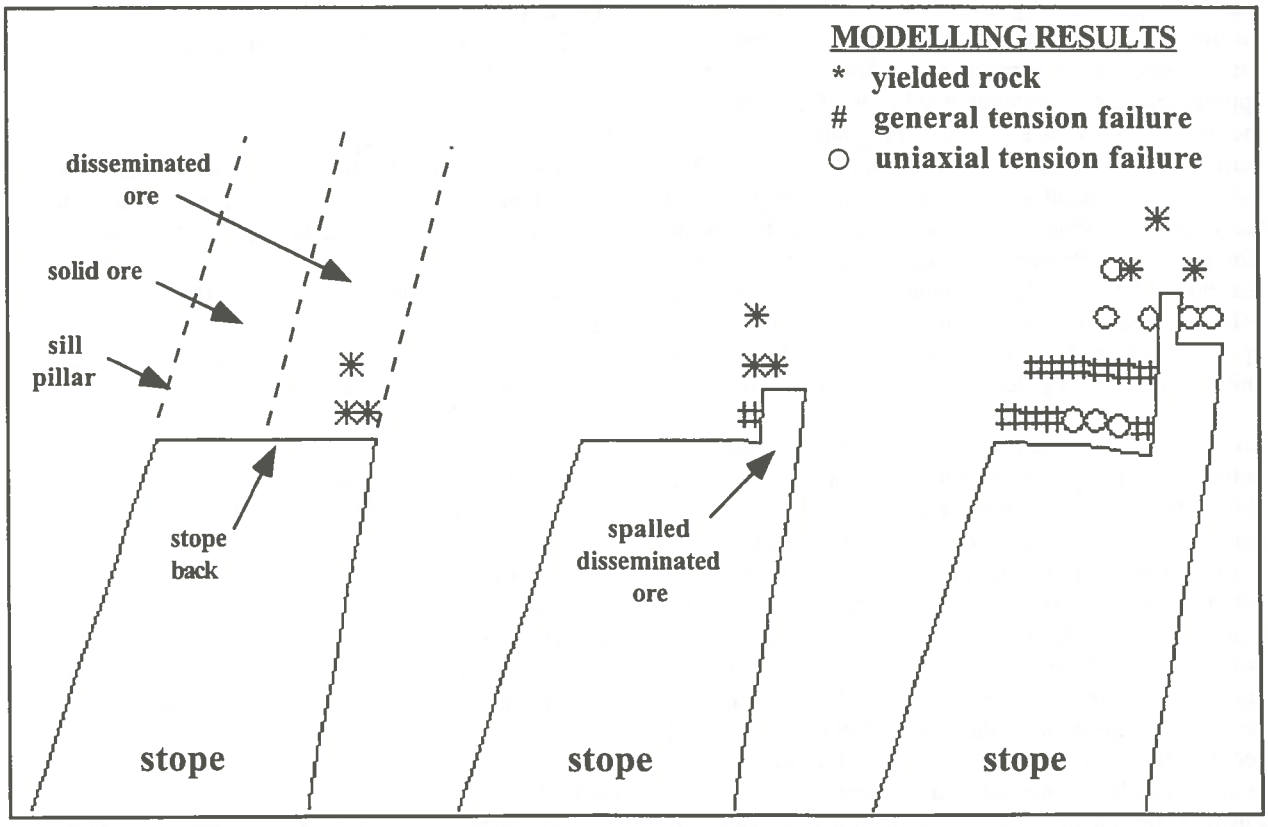

Figure 7. FLAC model showing state of yield in the rock within the sill pillar.

ore fits closely with observations made in the mine, before the large scale failure of the stope's sill pillar began. Subsequent models show that the unravelling of the disseminated ore results in a rotation of the stress field around the stope. This results in higher compressive stresses in the disseminated ore, and unconfined to tensile stresses in the adjacent solid ore. Further modelling shows that the removal of only a few cubic meters of disseminated ore through small scale compressive failures results in the continued yielding of the disseminated ore, eventually resulting in a "chimneying" effect where the propagation of failure in the disseminated ore leads to the unconfinement of the solid ore. This allows for large scale gravity wedge failures and further tensile failures.

CONCLUSION

A design methodology applicable to steeply dipping orebodies typical of many underground hardrock mines has been presented. This methodology was developed through a study on the #4 lens stope failure at the HBMS Trout Lake mine, Flin Flon, Manitoba, using elements of laboratory testing, rock mass characterization and computer modelling. Through this study, an approach was developed whereby several numerical methods could be used in conjunction, allowing for the advantages of each method to be maximized. This deviates from approaches more commonly cited in the literature where the use of only one or two programs, capable of performing a limited set of tasks, is used. The methodology includes the use of: boundary-element techniques to investigate 2-D and 3-D geometry related stress concentrations; displacement-discontinuity techniques to study pseudo 3-D elasto-plastic deformations, mine sequencing and strain energy build-ups; and finite-difference techniques to model non-linear anisotropic material yield and ground failure mechanisms.

To date, a 3-D differential analysis has not been included in this methodology. By utilizing the differential methods' ability to include different material models, a more realistic portrayal of the problem might be obtained using a 3-D non-linear finite-element or finite-difference code. Although this type of analysis provides a more realistic representation of the problem, it is also more complex and time consuming. In addition, more input data is required, more assumptions may need to be made, and the use of instrumentation data to constrain the model becomes more critical. With the eventual development of more powerful computers and more user friendly software, the inclusion of 3-D differential analysis will become more accessible and routine as a design tool.

REFERENCES

CURRAN, J.H. and CORKUM, B.T., 1988.
EXAMINE^{2D} version 3.1 users manual. Data Visualization Laboratory, University of Toronto.

CURRAN, J.H. and CORKUM, B.T., 1993.
EXAMINE^{3D} version 2.0 users manual. Data Visualization Laboratory, University of Toronto.

CURRAN, J.H. AND CORKUM, B.T. and WYLLIE, J.A., 1990.
EXAMINE^{TAB} version 1.1 users manual. Data Visualization Laboratory, University of Toronto.

EBERHARDT, E., STEAD, D. and SZCZEPANIK, Z., 1994.
Characterization of Rock Masses Within the Flin Flon Mining Area. Hudson Bay Mining and Smelting Co., Limited, Grant-in-Aid Report, 263pp.

HERGET, G., 1988.
Stresses in Rock. A.A. Balkema Publishers, Rotterdam, 179pp.

ITASCA CONSULTING GROUP, INC., 1992.
FLAC version 3.22 users manual. Itasca Consulting Group Inc., Minneapolis, 1125pp.

MARTIN, C.D., 1993.
The Strength of Massive Lac du Bonnet Granite Around Underground Openings. PhD Thesis, University of Manitoba, Winnipeg, MB, 278pp.

MATHEWS, K.E., HOEK, E., WYLLIE, D.C. and STEWART, S.B.V., 1980.
Prediction of Stable Excavations for Mining at Depths Below 1000 Metres in Hard Rock. CANMET Report 802-1571.

RESCHKE, A.E. and ROMANOWSKI, J., 1993.
The success and limitations of Mathews analysis for open stope design at HBMS, Flin Flon operations. 95th CIM Annual General Meeting, Calgary.

WAGNER, H., 1980.
Pillar design in coal mines. Journal of the South African Institute of Mining and Metallurgy: 80 (1), 37-45.

ZIPF, R.K., 1992.
MULSIM/NL Application and Practitioner's Manual. U.S. Bureau of Mines, Information Circular 9322.

CAMI'95: 3rd Canadian Conference on Computer Applications in the Mineral Industry
Montréal, Québec, Canada, October 22-25, 1995

Finite Element Analyses for the Interpretation Model of the 3D Borehole Slotter

G. He*, R. Corthésy*, D.E Gill*, M. H. Leite**,
*Department of Mineral Engineering**
*Department of Civil Engineering***
École Polytechnique, Montréal, Canada

H.H. Kanduth
Geomechanics Group
Noranda Technology Centre, Pointe-Claire, Canada

ABSTRACT:

The 3D borehole slotter is a new stress measuring technique which only requires a single borehole to obtain the complete 3D stress tensor by local stress relief without overcoring. The stress calculation model of the 3D borehole slotter is based on the following assumptions: linear elastic isotropic homogeneous rock behaviour, complete stress relief normal to the slot and plane strain condition parallel to the slot while the local stresses are being relieved. The validation of the last two hypotheses by finite element modelling is the subject of the present paper.

RÉSUMÉ:

Le "borehole slotter 3D" est une nouvelle technique de mesure de contrainte qui ne requiert qu'un seul forage pour l'obtention du tenseur de contrainte 3D, sans la nécéssité d'un surcarottage. Le modèle de calcul des contraintes du "borehole slotter 3D" est basé sur les hypothèses suivantes: comportement élastique linéaire isotrope et homogène de la roche, relâchement complet de la contrainte normale à la saignée et conditions de déformations planes parallèlement à la saignée lors de la réalisation de celle-ci. La validation de ces deux dernières hypothèses fait l'objet du présent article.

INTRODUCTION

When using instruments based on the recovery principle, the measurement of the elastic strain recovery during relaxation of the rock is generally done using strain gauges. However, gluing strain gauges or strain gauge carriers to borehole walls means that the probe is either lost or must be re-equipped after each measurement. All of the overcoring methods rely on special diamond drilling procedures. This is a costly and time-consuming procedure. But the borehole slotter avoids these problems (Sinkwitz 1993; Stacey 1993; Lawrence 1993). The 2D borehole slotter is completely self-contained in its stress release operations and strain measuring capabilities. It has been developed at James Cook University of North Queensland, Australia. Bock (1986) mentioned that the borehole slotting technique gave the in situ stress state with comparable accuracy faster, cheaper, and more reliably than overcoring and hydraulic fracturing tests. The original version is designed for use in HQ drill holes of 96 mm diameter, and uses a pneumatically driven saw to cut a slot in the borehole wall (Bock, H. 1984, 1986; Azzam, R. and Otto, B. 1987; Azzam, R. and Bock, H. 1987; Foruria 1986). A slot is cut axially into the borehole wall with a blade. Strain recovery is monitored by a strain sensor. At any given location, at least three slotting tests, with cuts in different radial directions, are made

(Corthésy 1990; Kanduth 1991).

The objective of this paper is to present the results of finite element analyses performed to validate a series of hypotheses used in the stress calculation model of the 3D borehole slotter.

3D BOREHOLE SLOTTER TECHNIQUE

The 2D borehole slotter has many advantages. But in order to get a complete 3D stress tensor, the 2D borehole slotter technique requires three non-parallel boreholes, which induces higher costs than when one hole is used.

The 3D borehole slotter should have the same advantages as the 2D borehole slotter, but it would only require a single borehole to obtain the complete 3D stress tensor by monitoring six independent changes in strains at the borehole surface by local stress relief. Figure 1 shows a 3D view of the slot parallel to the hole axis and the slot making a 45° angle with the hole axis. A half-moon-shaped slot is cut into the borehole wall, using a thin diamond-impregnated blade. The blades cuts slots 0.7 mm wide with a maximum 25 mm depth and 65 mm length. One slot is parallel to borehole and another is at a 45° angle with the borehole axis.

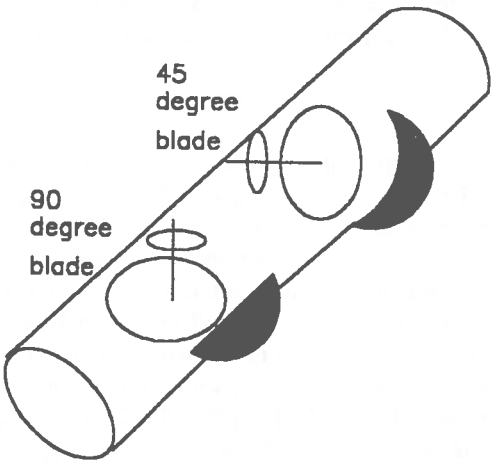

Figure 1. Schematic view of the 3D borehole slotter

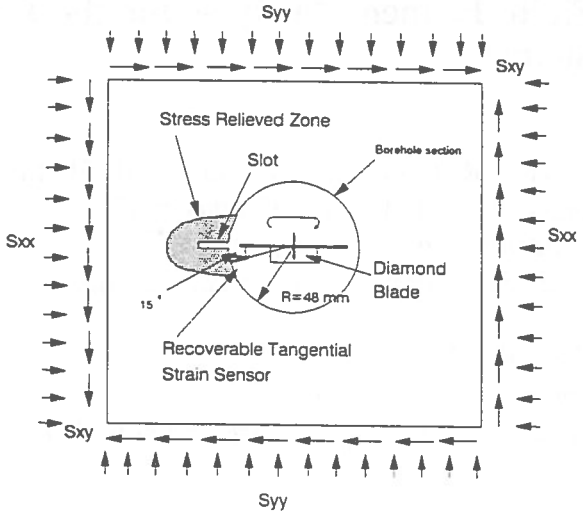

Figure 2. The principle of the 3D borehole slotter

The 3D borehole slotter is designed for borehole diameters of 96 to 105 mm. The maximum depth of use with the standard equipment is 30 m. No special preparation of the borehole wall is required.

The 3D borehole slotting instrument consists of three easily identifiable systems similar to the 2D borehole slotting instrument. These are:
1) The slotting system,
2) the recoverable strain sensor system,
3) the clamping system.

THE 3D BOREHOLE SLOTTER INTERPRETATION MODEL

The determination of the components of the field stress tensor is derived from the solution of the stress distribution around a circular hole in a body subject to a general triaxial state of stress.

Equations (1) is the expression of the recovered strain normal to a slot making an angle α with the hole axis (see figure 3). θ gives the orientation of the sensor around the borehole surface (figure 3). Sxx, Syy, Szz, Sxy, Syz, Sxz are the components the of the far field stress tensor. E and ν are Young modulus and Poisson's ratio at the measurement location.

$$\Delta\varepsilon_A=\frac{1-\nu^2}{E}\left(\frac{1}{2}\left[\left(1+2A+2\nu A\right)-\left(1+2A-2\nu A\right)B\right]S_{xx}\right.$$

$$+\frac{1}{2}\left[\left(1-2A-2\nu A\right)-\left(1-2A+2\nu A\right)B\right]S_{yy}$$

$$+\frac{1}{2}(1+B)S_{zz}-2\left[\left(1+\nu\right)C-\left(1-\nu\right)CB\right]S_{xy}$$

$$\left.+2(D\cos\theta)S_{xz}-2(D\sin\theta)S_{yz}\right) \qquad (1)$$

Where

$$A = \cos 2\theta, \qquad B = \cos 2\alpha$$

$$C = \sin 2\theta, \qquad D = \sin 2\alpha$$

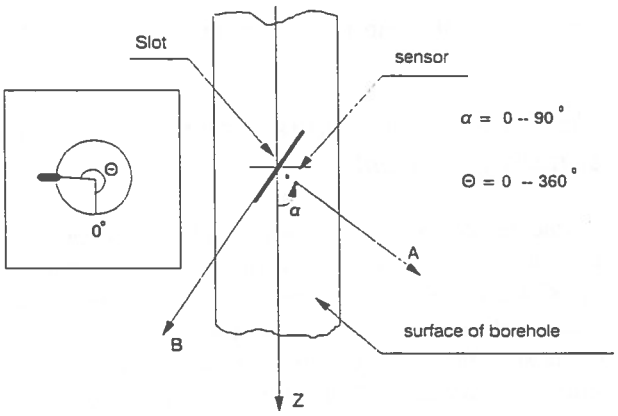

Figure 3. The slot making a α angle with the Z-axis

The development of equation (1) requires the following hypotheses:
1) Complete release of the stress component normal to the slot in its vicinity.
2) Plane strain conditions parallel to the slot while it is being cut.

It can be demonstrated that combining two different α angles in equation (1), allows the determination of the complete 3D stress tensor when measurements are repeated around the borehole surface. These α angles can be 90^0 and 45^0 as is the case with the 3D borehole slotter being developed at the Noranda Technology Centre.

FINITE ELEMENT ANALYSES

The purpose of the finite element analysis program is to verify the hypotheses used in the development of equation 1. The aspects studied include:
1. The stresses and strain distribution around the borehole before slotting.
2. The stresses and strain distribution around the borehole after slotting.
3. The degree of stress relief by slotting in the vicinity of the slot.
4. Plane strain conditions along the slot during the stress relief process.
5. The zone of influence of the slot around the borehole.

Because of the lack of symmetry when analyzing the stress and strain distribution with both the 90° and 45° slots, a 3D model had to be used. For the 90° slot model, there is one plane of symmetry. We use a half model for 90° slot and a full model for the 45° slot (Figures 4 and 5). The block geometry of the 90° slot is 100x100x50 units (X x Y x Z) and the 45° slot is 100x100x100 units (X x Y x Z). The borehole radius is 4.8 units allowing to consider the block infinite in relation with the borehole diameter.

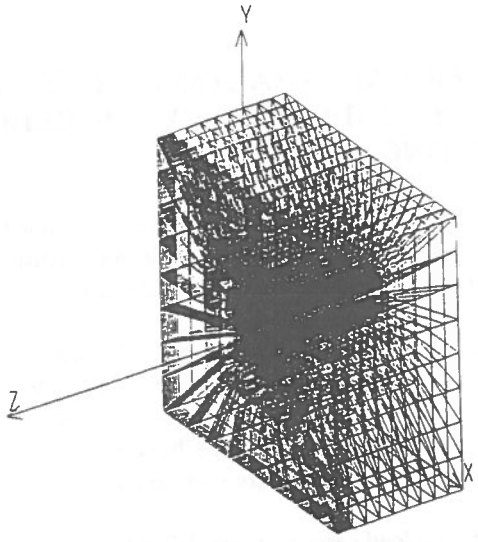

Figure 4. The 3D finite element mesh (half model) for the 90^0 slot analyses

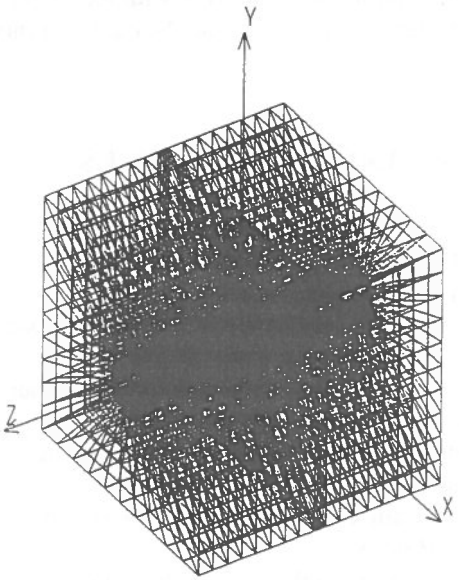

Figure 5. The 3D finite element mesh (full model) for the 45^0 slot analyses

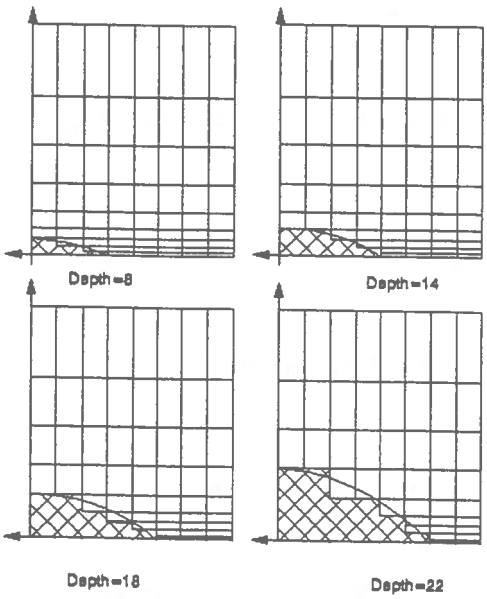

Figure 6. Finite element slotting simulation

Figures 4 and 5 illustrate the 3D finite element mesh layouts used to model the distribution of stress around the borehole periphery subject to slotting. The slot geometry is 0.07 units wide, 2.5 units deep and 6.5 units in length.

NUMERICAL ANALYSIS OF STRESS RELIEF INDUCED BY BOREHOLE SLOTTING

Figure 6 shows how the slotting process is simulated by deleting elements step by step. This approximation of the slot geometry was found to be adequate.

The model used gave less than 1.2% error on the stresses and strains compared with the theoretical solution of the unslotted borehole. Figure 7 shows numerical results compared with the theoretical solution for a given load case (before cutting the slot).

Six different load cases were modelled to investigate the influence of the external stress field on the recovered tangential stress and the stress normal to the 45^0 slot due to borehole slotting.

Verification of plane strain conditions parallel to the slot

As mentioned earlier, the finite element analyses were done to check if plane strain conditions prevail while the slotting operation is performed as assumed in the interpretation model. $\Delta\epsilon_B$ is the strain variation parallel to the slot and $\Delta\epsilon_A$ is the strain variation normal to the slot after slotting. The ratio of $\Delta\epsilon_B/\Delta\epsilon_A$ gives an indication of the degree to which plane strain conditions prevail parallel to the slot.

Table 1, shows that the ratio $\Delta\epsilon_B/\Delta\epsilon_A$ is very small for both the 90° and 45° slot geometry in the six load cases analysed, being less than 3.2% in the worst case within 7.5° arc from the slot. This result confirms the adequacy of using the hypothesis of plane strain conditions. Figure 8, as an example, illustrates the strain ratio $\Delta\epsilon_B/\Delta\epsilon_A$ for the slot parallel to the borehole axis.

The degree of stress relief

The finite element model was also used to verify the degree and extent of stress relief at the vicinity of the slot normal to it.

Equation 1 is based on the assumption that complete stress relief is achieved for the stress component normal to the border of the slot at its centre. The degree of stress relief is defined by:

$$\frac{Original\ \ stress\ \ - New\ stress}{Original\ \ stress} x\,100\ \%$$

Table 2 gives the position the strain sensor should have in order to measure 100% stress relief normal to the slot for both of the 90^0 and 45^0 slots. As table 2 shows, a 100% stress relief is attained normal to the slot within a 7.5° arc from its centre. Figure 9, as an example, illustrates the stress relief profile for slot depths varying from 2 mm to 27 mm. For a given blade geometry, the depth of the slot is the primary factor controlling the stress and strain relief process.

The strain sensor mounting system of the borehole slotter is located on the borehole surface within a 7.5° arc from the slot centre. Complete stress relief normal to the slot would be expected at this location for slots depths greater than 18 mm.

Table 1 Verification of plane strain conditions parallel to the slot

Load cases	Slot	Slot depth	The worst ratio $\Delta\epsilon_B/\Delta\epsilon_A$
Case 1 uniaxial loading Sxx=1E6	90^0 slot 45^0 slot	12.0 mm 10.6 mm	3.1% 2.8%
Case 2 uniaxial loading Syy=2e6	90^0 slot 45^0 slot	11.8 mm 9.8 mm	1.9% 2.4%
Case 3 biaxial loading Sxx:Syy=1:1	90^0 slot 45^0 slot	11.8 mm 10.6 mm	2.5% 2.8%
Case 4 biaxial loading Sxx:Syy=1:3	90^0 slot 45^0 slot	9.3 mm 9.8 mm	1.7% 2.9%
Case 5 biaxial loading Sxx:Syy=3:1	90^0 slot 45^0 slot	10.8 mm 10.6 mm	3.2% 3.2%
Case 6 triaxial loading Sxx:Syy:Szz=1:2:3	90^0 slot 45^0 slot	9.3 mm 9.8 mm	3.2% 3.1%

Table 2: Slot geometry leading to 100% stress relief normal to it within a 7.5° arc.

Load cases	From slot	Min. depth 90^0 slot	Min. depth 45^0 slot
Case 1 uniaxial loading Sxx=1E6	7.5^0	12.9 mm	18 mm
Case 2 uniaxial loading Syy=2e6	7.5^0	11.8 mm	14.1 mm
Case 3 biaxial loading Sxx:Syy=1:1	7.5^0	11.8 mm	18 mm
Case 4 biaxial loading Sxx:Syy=1:3	7.5^0	9.3 mm	14.1 mm
Case 5 biaxial loading Sxx:Syy=3:1	7.5^0	10.8 mm	18 mm
Case 6 triaxial loading Sxx:Syy:Szz=1:2:3	7.5^0	9.3 mm	14.1 mm

Table 3 gives the required slot depth to achieve 100% stress relief normal to the slot. This result is very useful for designing the 3D borehole slotter. According to table 3, the strain sensor of the 3D borehole slotter should be located at the borehole surface within 10° arc from the centre of the slot since slot depth greater than 25 mm can not be obtained.

Table 3: Strain sensor location and slot depth in order measure 100% stress relief.

Orientation from the slot	5^0	7.5^0	10^0	14^0	17^0
90^0 slot: Min. slot depth(mm)	9	12.9	19	32	38
45^0 slot: Min. slot depth(mm)	12	18	24	35	-

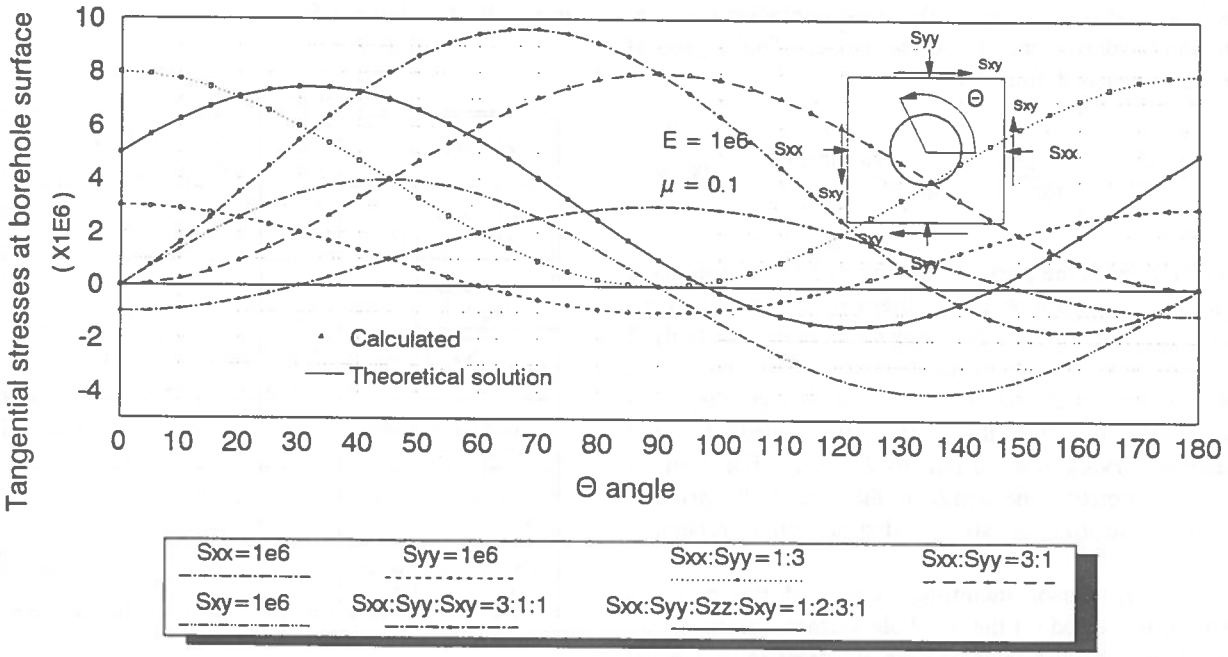

Figure 7. Comparison of finite element results with theoretical solution

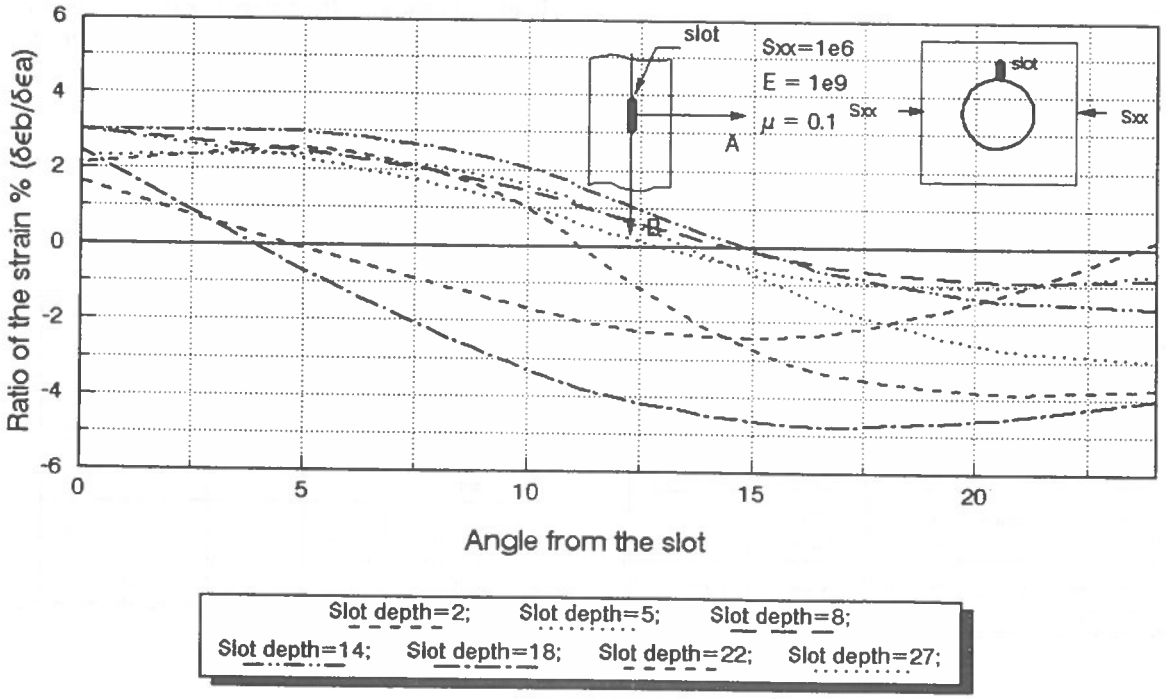

Figure 8. Strain ratio $\Delta\epsilon_B/\Delta\epsilon_A$ for the uniaxial load case

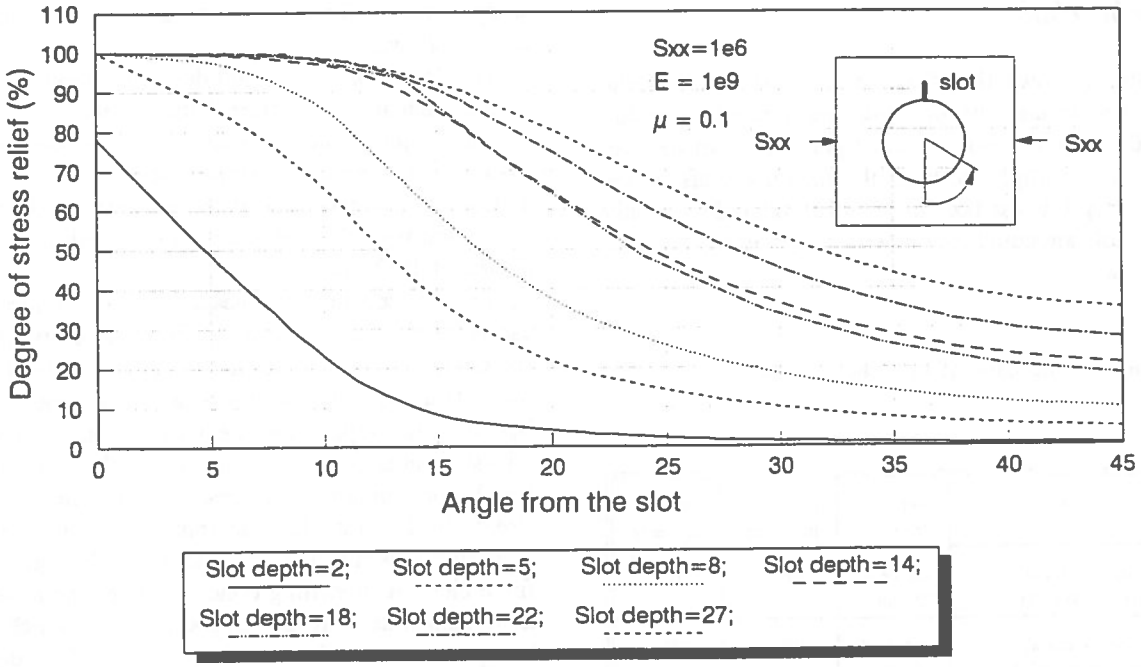

Figure 9. Degree of stress relief for the uniaxial load case

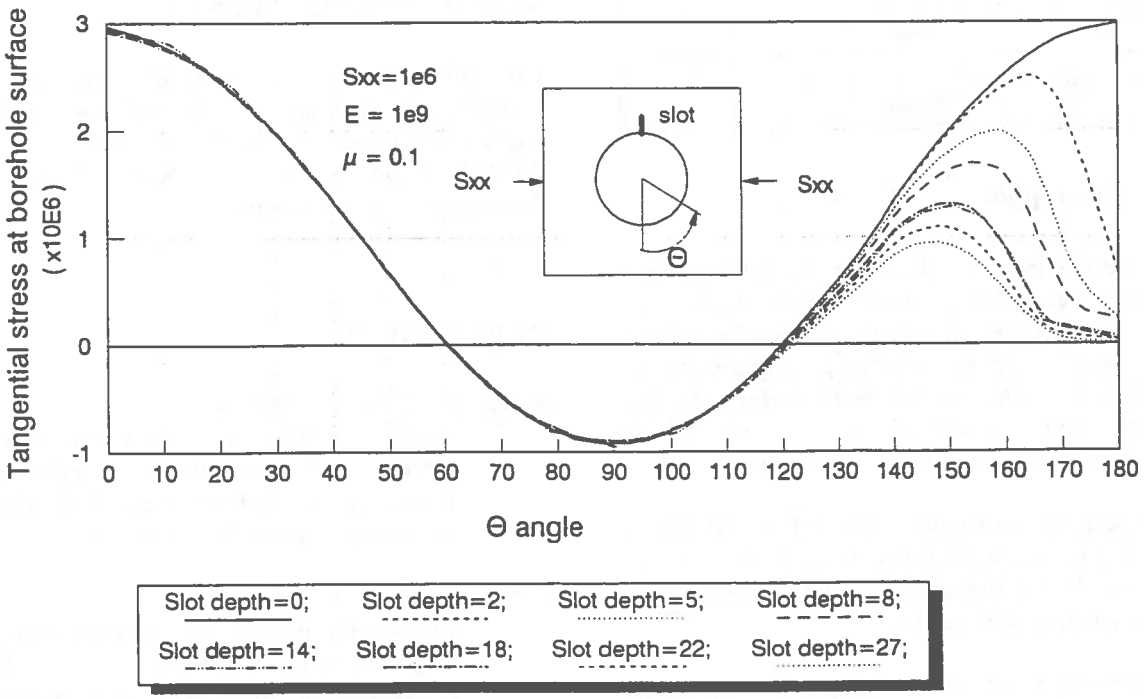

Figure 10. The influence zone of the slot for the uniaxial load case

The zone of influence of the slot around the borehole

Table 4 shows that the effects of slotting on the stresses around the borehole are limited to within ±70° from the slot. From figure 9, it can be seen that for multiple slotting, the measurements at the same depth in the borehole can be undertaken if only two slots are cut at the same depth (25 mm) at a 140° interval.

Table 4: The zone of influence of the slot

Load cases	Slot depth	90° slot Influence	45° slot Influence
Case 1 uniaxial loading Sxx=1E6	slot depth 25 mm	70°	70°
Case 2 uniaxial loading Syy=2e6	slot depth 25 mm	50°	55°
Case 3 biaxial loading Sxx:Syy=1:1	slot depth 25 mm	70°	70°
Case 4 biaxial loading Sxx:Syy=1:3	slot depth 25 mm	40°	50°
Case 5 biaxial loading Sxx:Syy=3:1	slot depth 25 mm	70°	70°
Case 6 triaxial loading Sxx:Syy:Szz=1:2:3	slot depth 25 mm	70°	70°

CONCLUSION

Borehole slotting is a relatively new, self-contained technique which should allow relatively cheap stress measurements to be carried out in boreholes without the necessity of having the drilling equipment on the site while the measurement is being performed. The borehole slotter should provide a rapid, reliable method of measuring in-situ stresses in rock.

At present, the technique is limited to a depth of about 30 m. This is a function of the length of hoses and rods. It is envisaged that the technique could be used at much greater depths.

The advantages of this technique outnumber its disadvantages. The initial evaluation of the former indicates that it is a very powerful method of determining in-situ stresses in hard rock.

The main conclusions to come out of this preliminary study of the 3D borehole slotter interpretation model are as follows:

1).The degree of stress relief due to borehole slotting is independent of the external stress field.

2).The major element to influence the degree of stress relief is the depth of the slot.

3).Complete stress relief of the borehole wall within a 7.5° arc from the slot can be accomplished for slot depths of 12.9 mm.

4).Six independent strain measurements in a borehole can be used to solve a system of equations giving the six unknowns of the 3D far field stress tensor. If more than six measurements are performed in a borehole, the supplemental equations can be used in a least squares analysis. It remains to be determined which combination is the best for obtaining the 3D stress field with the maximum accuracy when including experimental error in the solution. The finite element modelling done up to this point tends to demonstrate that the hypotheses on which the interpretation model is based are correct. In order to further validate these conclusions, an evaluation of the 3D borehole slotting technique will be made on a physical model under laboratory conditions.

ACKNOWLEDGEMENTS

The authors would like to thank The Noranda Technology Center and the Natural Sciences and Engineering Research Council of Canada (grants CRSNG OGP0089752 and OGP0003412) for financing part of this research.

REFERENCES

Azzam, R., Otto, B., 1987
Variation in the Young's modulus of rock as determined by new laboratory and in-situ testing method. 2nd Int. Symp. Field Meas. in Geomech. Kobe, Vol.1, pp112-122.

Azzam, R., Bock, H., 1987
Recoverable sensor for measurement of tangential strain at borehole walls - A key component in some innovative borehole instrumentation. 2nd. Int. Symp. Field Meas. in Geomech. Kobe, Vol. 1, pp.98-111.

Bock, H., 1986
In-situ validation of the borehole slotting stressmeter. Proc. Int. Symp. on Rock Stress Meas. Stockholm, pp.261-269.

Bock, H., Foruria, V., 1984
A recoverable borehole slotting instrument for in-situ stress measurements in rock not requiring overcoring. Int. Symp. Field Meas. in Geomech., Zurich, Rotterdam, Balkema, 1984. Vol. 1, pp.15-29.

Corthésy, R., Gill, D. E., 1990
Evaluation du modèle d'interprétation des mesures de contraintes avec le Borehole Slotter". Report for Centre de Technologie Noranda, 17p.

Foruria, V., 1986
A borehole slotting instrument for stress measurement in rock. M. Eng. Sc. thesis (James Cook University, Australia).

Kanduth, H. H., Corthésy, R.,Gill, D.E., 1991
Validation of borehole slotting as a method for in situ stress measurement. Proc. 7th. International Congress on Rock Mechanics. Aachen, pp. 527 -532.

Kanduth, H. H., Germain, P., 1990
Measurement in three of Noranda's Mines using a new borehole slotting method. Proc. of CANMET Specialty Conference on stresses in underground structures, pp.50-59.

Leeman, E.R., 1969
The "doorstopper" and triaxial rock stress measuring instruments developed by the C.S.I.R.. Journal of the South African Institute of Mining and Metallurgy. Feb. pp.305-339.

Sinkwitz, H., 1993
Analysis of the stress state in the foundation pillars of the Schwerin Castle by means of borehole slotting and dilatometer testing. Interfels News. Germany, Vol. 7. pp.3-6.

Stacey, D., 1993
Slotter stress measurements at Parabola Mine. Interfels News. Germany, Vol. 7. pp.15-16.

Lawrence, B., 1993
Borehole slotter stress measurement at the Opera House, Sydney. Interfels News. Germany, Vol. 7. pp.7-9.

7.

mining geophysics
géophysique

CAMI'95: 3rd Canadian Conference on Computer Applications in the Mineral Industry
Montréal, Québec, Canada, October 22-25, 1995

The Introduction of Continuous Seismic Monitoring at Mt Charlotte Gold Mine

Peter A. Mikula
Kalgoorlie Consolidated Gold Mines, Kalgoorlie, Australia

ABSTRACT

Continuous seismic monitoring commenced at Mt Charlotte in 1994 with the commissioning of a 32 channel PSS seismic system Mt Charlotte experiences seismicity related to an abundance of faults and geological structure. The largest event in recent years was Richter magnitude ML = 4.3. The monitoring network is about 1 km in size, with 10 triaxial geophone sites spread around the workings. Direct transmission of analogue waveform signals to the surface is achieved with very good signal fidelity. Event location accuracy is within 7m on average. The lower limit of the network is ML = -1.87, with 600 events annually exceeding this size. Distinct changes in the rate of mine seismicity have been observed over time periods of weeks and months. Events generally locate on structures which could be up to 100m, or more, from stopes. Seismic data has provided useful information to mine management on safety and production issues, and to engineers for design and support issues. Case examples of the preconditioning/yielding of a hard rock pillar, and of breakout around an orepass, illustrate the role of seismic data.

RÉSUMÉ

On a commencé à contrôler l'activité séismique de façon continue à Mt. Charlotte au moyen d'un tunnel de type PSS 32 mis en service en 1994. L'activité séismique qu'on y a enregistré est liée à la présence d'une grande quantité de failles et à la structure géologique particulière, La plus forte secousse ces dernières années s'est élevée à ML = 4,3 sur l'échelle de Richter.

Le réseau de détection s'étend sur environ 1km et comprend dix géophones disposés sur trois axes autour des mines. La transmission en surface des ondes sous formes de signaux analogues atteint un niveau de fidélité remarquable. On arrive à localiser l'origine des secousses avec un exactitude de 7 mètres en moyenne. Le réseau détecte les secousses supérieurs à ML = 1.87. Chaque année, six cents secousses dépassent cette limite. Au cours d'observation sur des périodes de semaines, puis de mois, on a pu mesurer des changements distincts dans le taux d'activité minière. En règle générale, les secousses proviennent de structures situées à une distance de cent mètres ou plus des chambres. Les données séismiques ont ainsi pu fournir des renseignements précieux aux contrôleurs des mines pour améliorer la sécurité et la production, ainsi qu'aux ingénieurs en ce qui concerne la conception et les structures de soutènement. Les cas où on a pu consolider des piliers rocheux qui risquaient de céder et éviter des échappées dans les cheminées à minerai illustrent l'utilité des contrôles séismiques.

1. INTRODUCTION

A new era of rock mechanics information commenced at Mt Charlotte Gold Mine on 24 March 1994 with the commissioning of a 32 channel PSS seismic monitoring system. At the time the system was the first of its kind in Australian mines. It provides continuous automatic monitoring and data capture of acoustic waveforms from seismic events and blasts.

Mt Charlotte has a history of experiencing seismic activity, and the idea of seismic monitoring was first suggested in 1965 in the form of a network of 4 to 8 seismometers in the area connected to a central tape recorder. Over the past 10 years the mine has experienced 6 events of Richter magnitude (ML) between 2.5 and 4.3. Yet apart from this historical record, and evidence of damage at certain sites underground, Mt Charlotte does not give the appearance of being prone to seismicity. There is a paucity of observable stress damage underground. At most, minor stress spalling or borehole breakout are seen only in limited areas close to stopes, and mirror zones are extremely rare. The only significant clue to the seismicity is rock noise occasionally heard in the vicinity of active stope faces (particularly areas with numbers of geological faults and related structures).

With the commencement of production in the new CDOB stope block at 950m depth, 27% deeper than previous extraction, the decision was made to install a seismic monitoring system. This paper describes the design and performance of the system and details the findings of the first few months of operation.

2. MT CHARLOTTE MINE

Mt Charlotte, located on the eastern boundary of Kalgoorlie, is Australia's largest underground gold mine. In 1993-94 production was 1,600,000 tonnes at an average grade of 3.0g/tonne.

Gold mineralisation occurs in a complex folded and faulted basalt/sediment sequence intruded by a dolerite sill. The major orebodies are comparatively planar, with thickness of 25 to 60m being small compared to their dip and strike dimensions. They dip subvertically and strike approximately north-south (Figure 1). Gold is associated with siliceous and carbonate stockwork veins, particularly adjacent to major subvertical faults (Charlotte, Reward, Maritana and Golden Pike). These faults are planar with displacements of 60 to 200m. A second series of faults (Neptune, Flanagan, Shea) dipping 45° to the west displace the orebodies by 10 to 150m. Most geological structure is parallel either to the quartz veins or the fault systems. The structures within the mine are of major relevance to mine induced seismicity. An example of the relatively abundant structure mapped in an area near ROB5 stope is shown in Figure 2.

Based on numerous tests, back analyses and correlation with underground observations, the properties of the dolerite rockmass and major faults are as shown in Table 1.

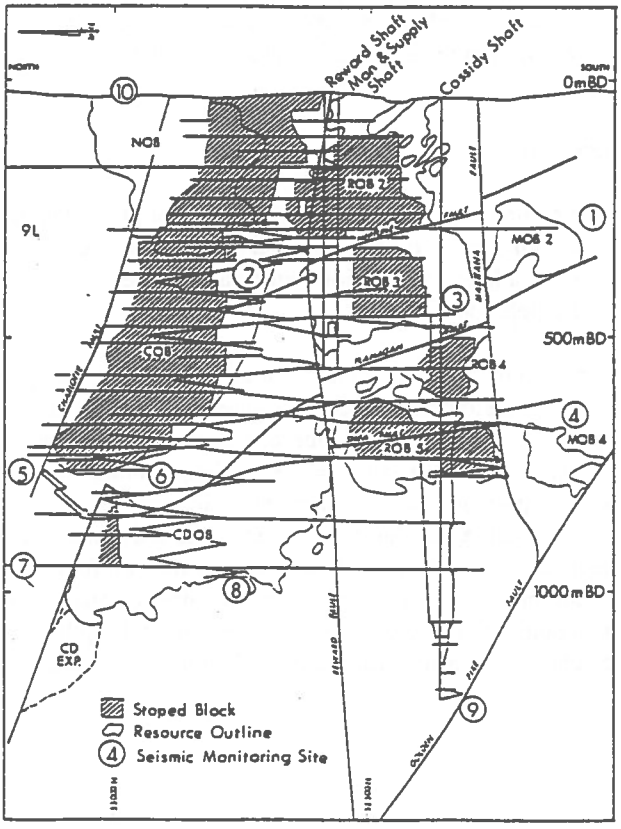

Figure 1. Mt Charlotte mine showing monitoring sites.

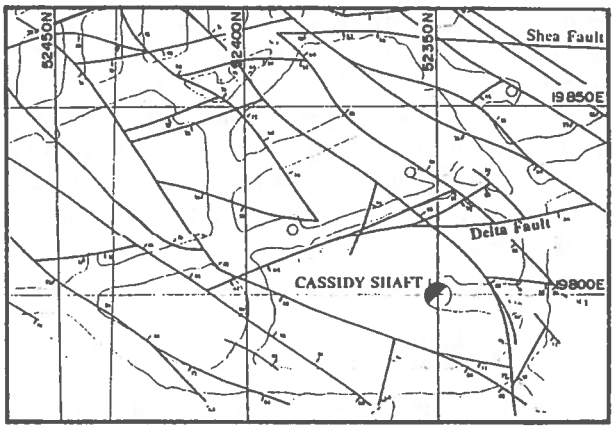

Figure 2. Faults and structures on 24 level near ROB5 stope.

TABLE 1: Static In Situ Rockmass Data

Major Faults	Shear Strength (cohesion/angle of friction) Peak 2 MPa 21.5°, Residual 1 MPa 16.5°
Dolerite	UCS 90 MPa Modulus 65 GPa Poisson's Ratio 0.26 Triaxial $\sigma 1 = 90 + 4.2\ \sigma 3$ MPa

The stress field is highly deviatoric with σ_1 oriented approximately north-south, σ_2 east-west, and σ_3 subvertical. Representative magnitudes are:
650m depth: $\sigma_1 = 60$, $\sigma_2 = 30$, $\sigma_3 = 20$ MPa
1200m depth: $\sigma_1 = 80$, $\sigma_2 = 40$, $\sigma_3 = 30$ MPa

A longhole open stoping mining method is used, whereby open stopes are mined in the block along strike, and then rib/crown pillars are mass blasted, with waste rock fill from above cascading onto the broken ore. Extraction is from drawpoint millholes below, until waste rock dilution become excessive. Blocky waste rock fill is continually added at the surface glory hole.

Ground support installed in the mine comprises resin-anchored 2.4m rebar, 8m to 15m cement grouted cable, and lately 3m cone bolts in millhole pillars susceptible to rockburst. Mt Charlotte trialed the first cone bolts in Australia in December 1993, and routine use of cone bolts commenced in 1994.

3. SEISMIC MONITORING

Continuous seismic monitoring was an untried technique in Australian mines when the decision to install a system was made. The main objectives sought from seismic monitoring were:

- observe and locate seismic events in space and time, and define their source parameters;
- characterise relationships between events;
- identify the factors influencing event occurrence, with a view to eventual control.

Whether monitoring would be worthwhile was unknown at the time. On the one hand, a great deal of study in the past had established important geomechanical principles of stope design for Mt Charlotte, leading to the possibility that new data could be superfluous. On the other hand, despite this level of knowledge, seismicity still occurred. Perhaps here it could be more easily studied, using to advantage the well defined rock types, properties and structures, together with the geomechanical understanding of the mine.

The PSS monitoring system (developed by COMRO, now CSIR, in South Africa) was chosen, mainly because it was a pragmatic design, with relatively simple hardware, yet able to meet the monitoring objectives within the constraints imposed by the mine.

4. THE PSS SEISMIC NETWORK

4.1 Network Design

The controlling requirement of the network was to monitor a volume of about 1200 x 1100 x 400m for events of ML -2 and above, with location accuracy of 10m on average. As location accuracy is about 2% of source-sensor distance, any point in the volume was ideally to be within 500m of at least three sensors. Adjacent sensors at Mt Charlotte are typically 400m apart, and do provide this location accuracy. Hangingwall and footwall drives were available to allow a good three-dimensional spread of sensor sites around the workings.

4.2 Sensors

Sensor locations are shown in Figure 1. The sensors are 4.5 Hz geophones, with a triaxial geophone cluster at each of 10 sites providing 30 channels of data in total. The geophones are grouted in 20m deep boreholes, to clear fractured rock around drives and the guided seismic wave associated with tunnels. The sites are also located remote (200m away on average) from major stoping voids and associated fracturing/loosening of rock.

Geophones were selected over accelerometers as they would respond to the desired acoustic frequencies (5 to 750 Hz range was adopted) and provide a velocity record (one integration to obtain displacement). Accelerometers were inappropriate as they respond to high frequencies (small events), and would need to be less than 300m apart in order to detect all such events.

4.3 Transmission

Signals from each sensor site are continually amplified and frequency modulated, then sent by twisted pair telephone cables to a surface computer station. Direct transmission is possible due to the compact mine size, with maximum cable lengths of 2.5km. The use of FM maintains high signal fidelity during transmission. Combined with proper earthing at the sensor site, this procedure effectively eliminates induced electrical noise in the data.

4.4 Event Data Acquisition

On surface, signals are demodulated, digitised, and as event triggers are detected from time to time, the event waveforms (for all 32 channels) are captured onto hard disk of a 486 PC. The sampling rate is 3000 Hz, with anti-aliasing filtering set at 750 Hz. A 680 msec long data window is captured for each event. Details of the PSS hardware and firmwave design and operation are given by Pattrick et al (1990). As a bonus, two channels are connected to a loudspeaker in the office, enabling events and blasts to be heard as they occur.

Spurious events are only a minor inconvenience. Electrical spikes are responsible for perhaps 5 spurious events daily, and these are easily identified and deleted. Cultural noise (nearby drilling, trucking, ore in passes, crushing) does not trigger the system. One channel at site 9 responds to crusher operation on 36 level, 90m distant. It was initially considered that to avoid spurious events, four triggers at a minimum of two sites would have to be detected before an event could be flagged. However the system has operated very satisfactorily on two triggers (even at the same site) for several months.

4.5 System Software

An initial location is computed automatically, and refined interactively later. Full waveforms are written to disk at the rate of one per minute, so locations can be computed very quickly if desired. If swamped by many event arrivals (as during blasting), the system adopts the "graceful decline" principle to delete smaller event records in favour of larger ones.

Interactive analysis is then used to compute source parameters for each event. These parameters describe the strength (magnitude, seismic moment, seismic energy), size (source radius, apparent volume) and stress conditions (stress drop, apparent stress) of an event. Waveforms are also processed for peak velocity, acceleration, displacement and first motion at each sensor site. A rigorous treatment of attenuation is included in the PSS software.

4.6 Operation and Maintenance

The time taken to operate the network, obtain accurate locations and source parameters, and do housekeeping, averages 8 hours per week, with additional hours for detailed study and application of data. System maintenance comprises calibration (10 hours underground) at three month intervals.

The system has proved very reliable in its first 12 months of operation, with no faults at any underground stations, and two circuit board changes in one of the surface data acquisition computers soon after commissioning. The PC was the biggest problem, needing a hard disk replacement. System downtime results from loss of power supply, either mine-wide (for scheduled work, or other external reasons, 20 hrs/year) or at an individual outstation (circuit breaker tripping, 6 incidents/year).

4.7 Event Location

Typical location computational error for near-field events (ie events within 500m of at least three sensors) is 7m, with best locations to 3m and most better than 15m. Probably the most significant factor in obtaining these small errors is the three-dimensional spread of network sites.

The reliability of computed locations, by comparison with development blasts at known locations, is 2 to 25m, averaging 12m. This is usually sufficient to relate events to particular geological structures. Good locations are essential for further study and interpretation of the data.

In practice, while all sensors may observe an event, P and S arrivals at some sensors are misleading, due to stope voids or fractured rock in the source-sensor path (resulting in delayed or split arrivals) or to the velocity model for the mine (see below). The interactive screen display, which shows actual arrivals in comparison to those computed (by reverse ray tracing from the computed source position), indicates which arrivals should be eliminated from the location algorithm. True P and S arrivals are generally distinct, and unaffected by reflection of signals from stope voids.

4.8 Velocity Model

A constant velocity model with Vp = 6380 m/sec and Vs = 3630 m/sec is used to represent the rockmass, with Vp and Vs calibrated from analysis of arrival times for 44 blasts at different known locations over a period of two months. While giving acceptable results, this simplified model is probably responsible for some of the anomalous arrival times observed.

5. CHARACTERISTICS OF MT CHARLOTTE SEISMICITY

Event characteristics discussed in this section are based on observations of overall event trends during commissioning and familiarisation of the monitoring system. Results from ongoing source parameter analysis will be reported at a later date.

5.1 Event Mechanisms

In general, mine-induced seismic events can be classified into two types:

- crush events, arising from failure of a highly stressed zone of rock in a stope face, pillar or similar, and releasing relatively large P-wave energies;
- shear events, arising from slip on a fault or geological structure, due to changes in shear stress and/or normal stress on the structure. These events typically release more S-wave energy, and can be very large if the structure involved is extensive.

Preliminary expectations are that the majority of Mt Charlotte events may be of this second type. This agrees with other geomechanical facts about the mine, namely

- abundant structure
- paucity of stress effects
- stresses on the major faults are known to be in balance with fault strengths.

The Gutenberg-Richter magnitude-frequency relationship for 500 near-field events over the first ten months of monitoring is shown in Figure 3. This graph shows the effective lower limit of the network is ML = -1.87, not quite as low as had been intended. However, a planned hardware change to outstation amplifiers should significantly improve detection limits. M_{max} is estimated at 3.3, somewhat less than the 4.3 maximum from recent historical data. A high M_{max} is an indication that fairly large fault structures and/or extensive regional faulting are involved.

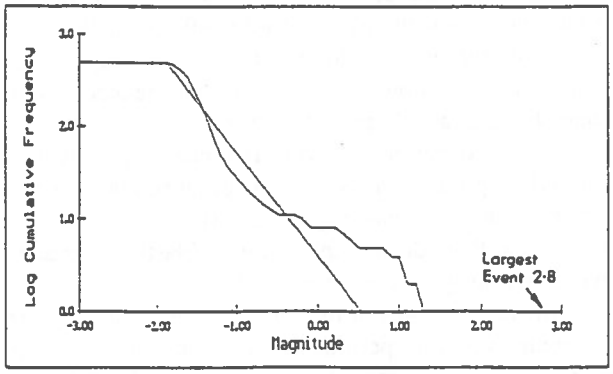

Figure 3. Magnitude-frequency diagram, 10 month period.

The average b-value is 1.1, indicative of some seismicity involving large structures influenced by tectonic stresses.

It is interesting to compare Mt Charlotte data with earthquake statistics for events in the Kalgoorlie region (Gaull et al, 1990). Differences in the two sets of data, shown in Table 2, may be due to different magnitude scales or detection limits. The regional data may include mainly larger slip events, whereas the Mt Charlotte network detects smaller events of both crush and shear types. Clearly, further analysis of the data is required.

TABLE 2: Seismicity Parameters

	Mt Charlotte PSS System	Kalgoorlie Region (Gaull et al, 1990)
ML_{min}	-1.87	3.0
ML_{max}	3.3	4.5
b-value	1.1	0.63
Avg focal depth	0.8km	2.0km
No events M>3	1.0	0.46

5.2 Event Characteristics

(a) Risk of occurrence: Figure 3 data was used to compute the general risk of occurrence of an event of size greater than a chosen magnitude. Thus the calculated occurence of an event of ML>2.5 is 1.2 annually. However, this is twice the historical record of 6 such events in 10 years at Mt Charlotte.

(b) Event trends over time: The average rate of occurrence of events ML > -1.87 is 600 annually. The actual rate ranges from no events for many days, to 20 within a few hours. Typical time-related event characteristics are (Poplawski, 1995):

- events occur mainly on production days, with a marked drop on Sundays. This is because many events are associated with blasting (Figure 4);
- other than during the 3.15pm blasting window, events are fairly random (Figure 5);
- distinct changes in the rate of mine seismicity are apparent over time periods of weeks and months. As shown in Figure 6, the rate of events in early 1995 was nearly four times greater than that in mid-1994. This last factor is of particular interest, because of an apparent coincidence of noticeably active seismic periods at Mt Charlotte and at several other mines in the Kalgoorlie region. To investigate whether some gross changes in regional stresses may underlie this phenomenon, a stress monitoring station was recently installed at 39 level. Results of this monitoring are awaited with interest.

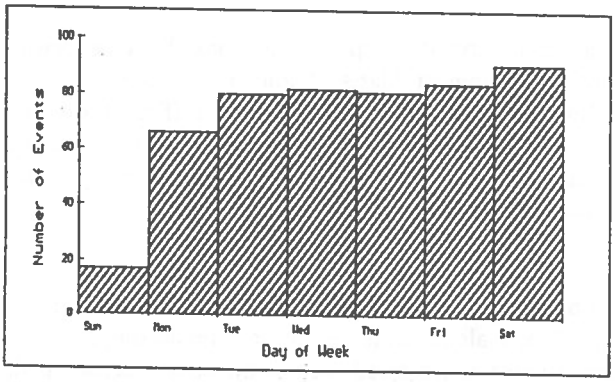

Figure 4. Event occurrence by day of week.

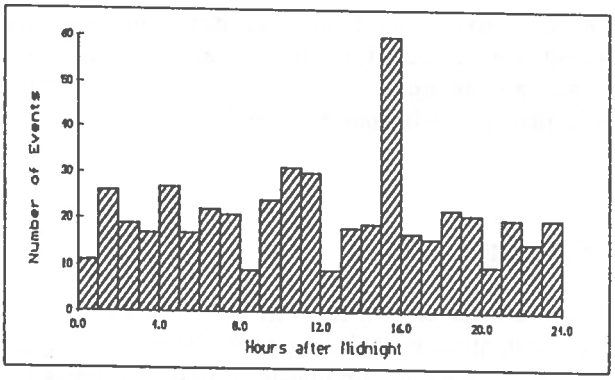

Figure 5. Event occurrence by time of day.

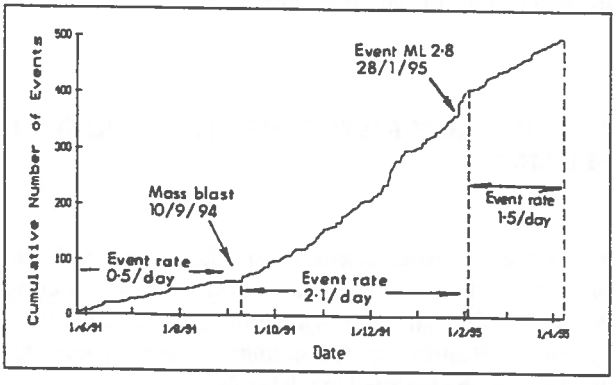

Figure 6. Cummulative event occurrence.

(c) Relationship to geometry and geology: Events have tended to cluster in three specific areas of the mine, namely:

- around active stopes (ROB5 and CDOB);
- on major faults remote from stopes;
- around a deep orepass.

In the first two cases, shearing on known and/or inferred structures is important. Events are not dominant in regions of highly stressed rock close to stopes; rather, they often locate on structures which could be up to 100m or more from stopes. An instance is the "ROB5 pipe" shown in Figure 7. Over a four month period, events located along a fuzzy sub-horizontal line, or pipe, extending eastwards from the middle of the stope for 80 metres. This line was thought to represent the intersection of two structures, but lack of any access to the area prevented further assessment. Activity on the line ceased in December 1994, to be followed a month later by a large rockburst on the west side of the stope, involving structures intersecting on a similar horizontal line.

In the case of the orepass activity, the seismicity probably indicates breakout of the pass, driven by the high horizontal stress. No access is possible to establish the presence of structures. This pass is discussed further in Section 6.3.

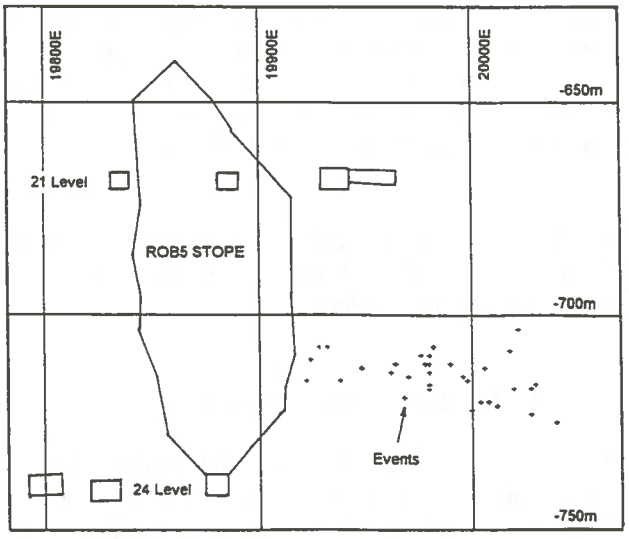

Figure 7. Section showing event cluster east of ROB5 stope.

(d) Relationship to blasts: Approximately 33% of the total number of recorded events occur within 30 minutes of blasting. There is a clear tendency for larger events to occur closer to or coincident with blasts. The diedown period, as such, does not have significance for smaller blasts, as so few events occur anyway. However for larger stope blasts, a diedown period of less than 24 hours is indicated.

A 900,000 tonne mass stope blast on 10 September 1994, affected seismicity in an unexpected way. The blast was followed by a normal diedown period, but not to previous background level. A distinct gradual rise in event rate occurred over the next two months, and persisted until a major rockburst in January 1995 (Figure 6).

(e) Relationship to damage: Since commissioning of the system, two damaging events have occurred in accessible areas. Damage from the first (ML=1.0) extended about 20m from the event source, while that from the second (ML=2.8) extended up to 100m away. Damage comprised falls, stress spalling, and shearing/opening on structures.

6.0 APPLICATION OF SEISMIC DATA

6.1 Perceived Benefits

Benefits from seismic monitoring are already apparent in several areas.

(a) Information base: Accumulation of a substantial seismic database has many potential uses, ranging from simple confirmation of whether a particular vibration felt in Kalgoorlie originated in the mine, up to complex analysis to find precursor anomalies for seismic prediction.

(b) Safety and seismic hazard: In the short term, the immediate location of larger events allows informed decisions where search and rescue may be involved. In the first ten months of monitoring, six such events occurred, of which four were coincident with blasting when the mine was clear, and the remaining two were located and found not to require action.

(c) Production downtime: Production losses have been reduced by avoiding unnecessary evacuations of

some or all of the mine, as had previously been the practice in response to larger seismic events. Production would cease until the extent of damage, if any, was established. In the first ten months of monitoring, three such instances occurred.

Monitoring of the diedown of activity following blasts or large events allows informed decisions on re-entry to affected working places, combining worker safety and mine productivity.

(d) Mine planning: Preliminary analysis of seismic data has been useful for mine planning:

- seismically active mine areas have been identified, and are now being progressively supported with cone bolts prior to mining;
- the correlation between event magnitude and damage underground is being defined;
- seismically active structures have been identified;
- seismic feedback has improved understanding of how the rockmass has responded to particular mining strategies.

6.2 Case Example: Pillar Preconditioning

Numerical modelling studies had indicated that the proposed I1 rib pillar, located between I1 and I2 open stopes in the CDOB resource (Figure 8), was at risk of violent failure. To address this risk, preconditioning of the pillar was undertaken.

Preconditioning involves physically modifying the pillar to provide it with a yielding or destressing mechanism. The modification is done before the pillar is formed, so that the mechanism allows gradual yield in pillar structures as soon as the pillar faces are exposed. By limiting stress buildup in the pillar in this way, the risk of sudden failure should be reduced.

As preconditioning was new to Mt Charlotte, several options were assessed, and a blast softening technique was adopted and implemented. Blasting was used to fracture a zone of rock across the pillar, with 17 blastholes each 53m long. Further details on the preconditioning are given by Mikula, Lee and McNabb (1995).

To date, I1 stope has been mined and the north face of the pillar formed. The south pillar face was yet to be developed at the time of writing. Conventional stress and extensometer monitoring during I1 stoping has shown effectively zero increase in pillar stress, combined with nearly 30mm closure across the preconditioned zone near the exposed stope face. Seismicity within the pillar has been minimal, in contrast to high activity in the floor of the stope. This is of critical importance, as it may mean either the preconditioning was ineffective (no yield possible), or that it worked extremely well (pillar is relaxed).

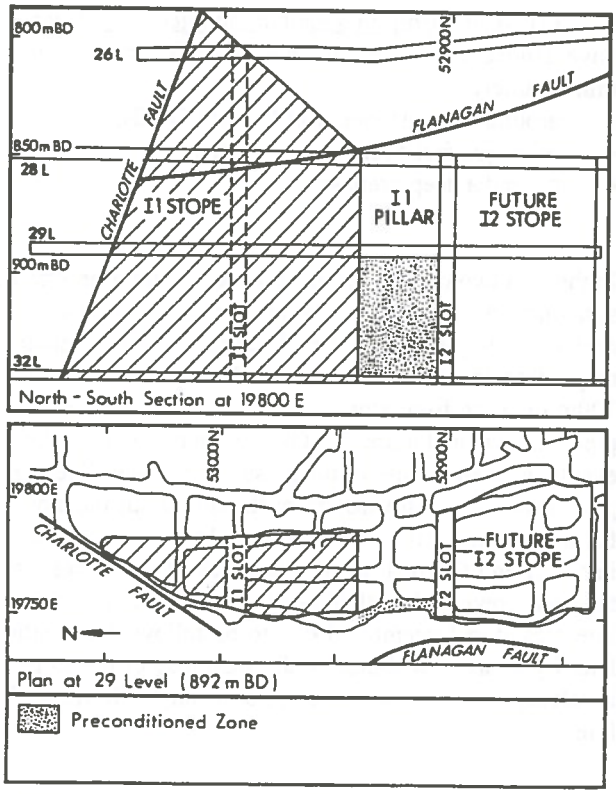

Figure 8. Preconditioned zone in I1 rib pillar.

As I2 stope is opened and the pillar is fully formed, monitoring should provide feedback on the effectiveness of this strategy.

6.3 Case Example: Orepass Breakout

An orepass subject to high horizontal stresses (exceeding 70 MPa) within the mine had experienced breakout at various times since construction. By experience it was found that keeping the pass full was the best way of controlling breakout.

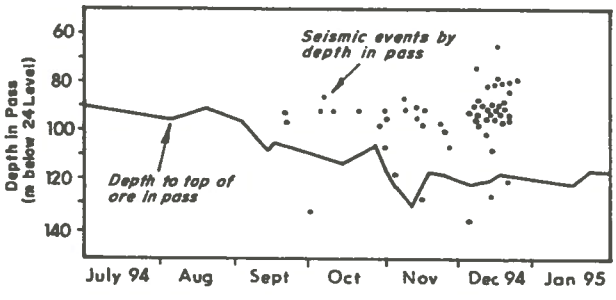

Figure 9. Event cluster at orepass, by depth and time.

Soon after installation of the seismic monitoring system, the pass was drawn down below the 90m mark, which turned out to be a critical depth. The sudden onset of seismicity is shown in Figure 9, in relation to ore level and time. Events were located all around the pass. It is concluded that these events record the breakout.

7.0 CONCLUSION

Although only preliminary analysis of the data is completed, the usefulness of seismic data at Mt Charlotte is becoming clear. The slip mechanism inferred for most Mt Charlotte events fits in well with other geomechanical aspects of the mine, and emphasises the need for good structural information prior to stoping design. It also explains why the lack of significant stress spalling in the mine does not mean lack of seismicity. Overall, seismic monitoring "sees" into the otherwise opaque rock, and records data on rock mass activity as it responds to excavation. The availability of this information results in smarter mining, with benefits to safety, productivity and planning.

REFERENCES

GAULL B.A, MICHAEL-LEIBA M.O. and RYNN, J.M.W., 1990.
Probabilistic earthquake risk maps of Australia. Australian Journal of Earth Sciences, 37, pp 169-187.

MIKULA, P.A., LEE, M. and McNABB, K., 1995.
The preconditioning and yielding of a hard rock pillar at Mt Charlotte mine. 8th Int. Congress on Rock Mechanics, Tokyo.

PATTRICK, K.W., KELLY, A.M. and SPOTTISWOODE, S.M., 1990.
A portable seismic system for rockburst applications. Technical Challenges in Deep Level Mining, Johannesburg, SAIMM, pp 1133-1146.

POPLAWSKI, R.P., 1995.
Seismic research at Mt Charlotte mine. Kalgoorlie Consolidated Gold Mines, Internal Report.

CAMI'95: 3rd Canadian Conference on Computer Applications in the Mineral Industry
Montréal, Québec, Canada, October 22-25, 1995

Three-dimensional Imaging of Underground Mine Structures Using Geophysical Tomography, with Tests for Resolution and Robustness

M. J. Jackson, M. J. Friedel, D. R. Tweeton
U.S. Bureau of Mines, 5629 Minnehaha Ave. S., Minneapolis MN 55417

D. F. Scott and T. Williams
U.S. Bureau of Mines, E. 315 Montgomery Ave., Spokane WA 99207

ABSTRACT

Three-dimensional (3-D) tomographic imaging of underground mine sites has several important advantages over two-dimensional imaging. However, because of practical limitations on source and receiver positioning, ray-path coverage is often suboptimal, and tomographic computations as a result are ill-conditioned or underdetermined; this problem may be more severe in 3-D than in 2-D. Therefore it is important to evaluate the resolving power of a 3-D data set and the robustness of the resulting tomographic images. New software from the US Bureau of Mines was designed to facilitate such evaluations, as illustrated here with a data set from an underground silver mine.

RÉSUMÉ

L'image tomographique en trois dimensions (3-D) des mines souterraines comporte quelques avantages importantes sur tomographie en deux dimensions (2-D). Cependant, à cause des limitations pratiques de la géométrie expérimentale, les calculs tomographiques sont souvent sous-estimés; ce problème peut être plus sévère en 3-D qu'en 2-D. Il est donc important d'évaluer la résolution des données en 3-D et la qualité des images obtenues. Un nouveau logiciel a été developpé par le U.S. Bureau of Mines afin de faciliter lesdites évaluations. Ce dernier est illustré ici en utilisant des données d'un mine d'argent souterraine.

INTRODUCTION

Tomographic imaging of underground mine sites provides a means of identifying safety hazards and environmental problems. In this paper we describe new software produced by the US Bureau of Mines for three-dimensional tomographic inversion of seismic or electromagnetic travel-time or amplitude data, and we illustrate its application with data from an underground mine site. The 3DTOM software provides a variety of tools for evaluating the reliability of the velocity reconstructions, in terms of the resolving power of the data and the robustness of the results.

COMPUTATIONAL METHODS

The tomographic calculations are carried out on a regular rectangular grid in three dimensions. Velocities or attenuation coefficients are specified at the nodes of the grid, and calculated between nodes by multiple linear interpolation.

Iterative Reconstruction

The inversion algorithm we use is based on the simultaneous iterative reconstruction technique, or SIRT (e.g., Gilbert, 1972; Peterson et al., 1985.). This method involves specifying an arbitrary initial model, and repeated cycles of forward travel-time computation and model updating. The forward travel-time computations are based on three-dimensional ray-tracing (described below). Model updating involves backprojection of travel-time residuals (differences between calculated and measured travel times).

Ray Tracing

We use two methods for three-dimensional ray tracing: a "bending" method (Um and Thurber, 1987) and a "network theory" approach (Moser, 1991). The bending method involves iterative perturbation of an arbitrary (often straight-line) initial path joining a source and a receiver. The network approach involves computation of minimum-time paths from a source to all receivers, along straight-line segments between nodes. Under certain circumstances the bending method may converge to a local rather than a global minimum travel time (corresponding to a later

arrival). In these cases, a ray path obtained by the network technique may be used as an initial path for the bending method.

Resolution and Robustness

Resolution is limited by both physical and mathematical considerations. The physical limitations are imposed by the wavelength of seismic energy transmitted through the rock mass (Williamson, 1991), and by refraction/diffraction of first-arriving energy around low-velocity regions (Wielandt, 1987). The latter effect precludes detailed imaging inside of low-velocity areas. These physical limitations are important in interpreting the velocity tomograms, and they will be discussed further in that context below.

The principal focus of this paper, however, concerns mathematical limitations on resolution. These are imposed by ray-path coverage, which in turn is limited by the logistics of source and receiver placement. Incomplete ray-path coverage, often a problem in two-dimensional tomographic studies (e.g., Menke, 1984; Bregman, et al., 1989), is perhaps even more common in three-dimensional studies. In an underground mine survey, sources and receivers can easily be placed in the mine openings, but the resulting set of ray paths may leave some areas entirely unsampled, and most or all of the volume may be sampled by rays with a limited range of viewing angles. Similarly, ray-path coverage is less than ideal for cross-borehole surveys using multiple boreholes. It is well known that cross-borehole data have a limited angular aperture, resulting in non-unique 2-D reconstructions (e.g., Menke, 1984). When data from several intersecting crosshole surveys are combined into a 3-D data set, the same limited subhorizontal aperture remains (i.e., no vertical ray paths). Further, the path coverage on any horizontal plane is sharply limited by the number and locations of the boreholes.

Incomplete data inevitably result in tomographic reconstructions that are non-unique (i.e., there are many possible velocity models that fit the data equally well). Moreover, with incomplete data the inversion is ill-conditioned (i.e., small changes in the data can produce large changes in the reconstruction). One method of reducing the nonuniqueness is to impose additional constraints on the reconstructions; this is described in the following section. Even after constraints are applied, however, the calculated model may not be unique.

In order to evaluate the robustness of the reconstructions, we use a set of different initial models and carry out the inversion for each of them, thus producing a corresponding set of "intermediate" models. The final model is computed by node-by-node averaging of the intermediate models (which tends to filter out features that are sensitive to the initial model), and the robustness of the final model (which varies with position) is evaluated in terms of the nodal standard deviations.

We also evaluate the mathematical resolving power of a data set by means of a "checkerboard" resolution test. We construct a three-dimensional velocity model with alternating cubes of high and low velocity. Then, using the same source and receiver positions as those in the real data, we compute synthetic travel-time data for the checkerboard model. Finally, we invert the synthetic travel times, and compare the resultant velocity model with the checkerboard model. We repeat this process for several checkerboard models with varying coarseness (i.e., length scale of velocity variation). The accuracy of the checkerboard reconstructions can be quantified by computing the correlation between the node velocities in the reconstruction and those in the original checkerboard model.

Constraints

An advantage of SIRT is that it enables the formulation and application of constraints in an explicit and straightforward way (Tweeton, 1988). Velocities in the reconstruction can easily be forced to match known boundary conditions (e.g., borehole sonic logs), and they can be restricted to plausible bounds by specifying maximum and minimum permissible values. Fuzzy constraints (Jackson and Tweeton, 1994) can be applied when there is uncertainty in any of these values; this is equivalent to taking a weighted average of constrained and unconstrained models at each iteration.

3DTOM Software

The Bureau of Mines 3DTOM software is designed for easy application of constraints based on site information, and to help evaluate resolution and robustness for three-dimensional tomography. In addition to performing the tomographic computations, 3DTOM automatically generates starting models as specified by the user. These can be used to calculate synthetic data for resolution tests, or for multiple-inversion tests of robustness.

3DTOM runs under DOS; a Unix version is under development. Source code and executables are available from the authors on request.

FIELD TEST

Here we describe the application of three-dimensional tomography to seismic data collected at an underground mine site. The site is the Lucky Friday silver mine in the Coeur d'Alene district of northern Idaho, where the

objective was to identify regions of anomalous stress that pose rockburst hazards. Results of the Lucky Friday study have been presented previously (Friedel et al., 1995), with an emphasis on geomechanical interpretation of the reconstructed seismic velocities; here we focus on questions of resolution and robustness, and show how these can be evaluated using 3DTOM.

Site Description:

The Lucky Friday mine is located in the Coeur d'Alene district of northern Idaho. Because of the hazards of rockburst activity at this and other deep silver mines in the district (e.g., Blake and Cuvelier, 1990), new methods for mapping anomalous stress concentrations are of vital interest. Seismic tomography is a potentially valuable tool because of the relation between seismic velocity and stress (e.g., Radcliffe et al., 1986).

The study area in the mine lies at a depth of approximately 1.5 km below the surface. The principal rock types are quartzite and argillite. Ore is removed from two steeply-dipping veins, and the stopes are then backfilled with sand.

Data Collection:

Approximately 2400 travel times were determined, using a sledgehammer source and 100-Hz geophones mounted on roofbolts. An analog highpass filter (500 Hz) was applied to the signals prior to recording with a 24-channel digital seismograph, and first arrival times were picked manually. Sources and receivers were located in mine drifts at two depth levels separated by approximately 60 m (referred to as the 4900 and 5100 levels, indicating their approximate depth in feet; Figure 1). There is thus a high density of horizontal ray-path sampling for those two levels, and the intervening rock mass is sampled with a moderate density by dominantly steep rays (Figures 1 and 2). The average calculated velocity for the first arrivals was approximately 4 km/s, which combined with the frequencies exceeding 500 Hz yields wavelengths of 8 m or less.

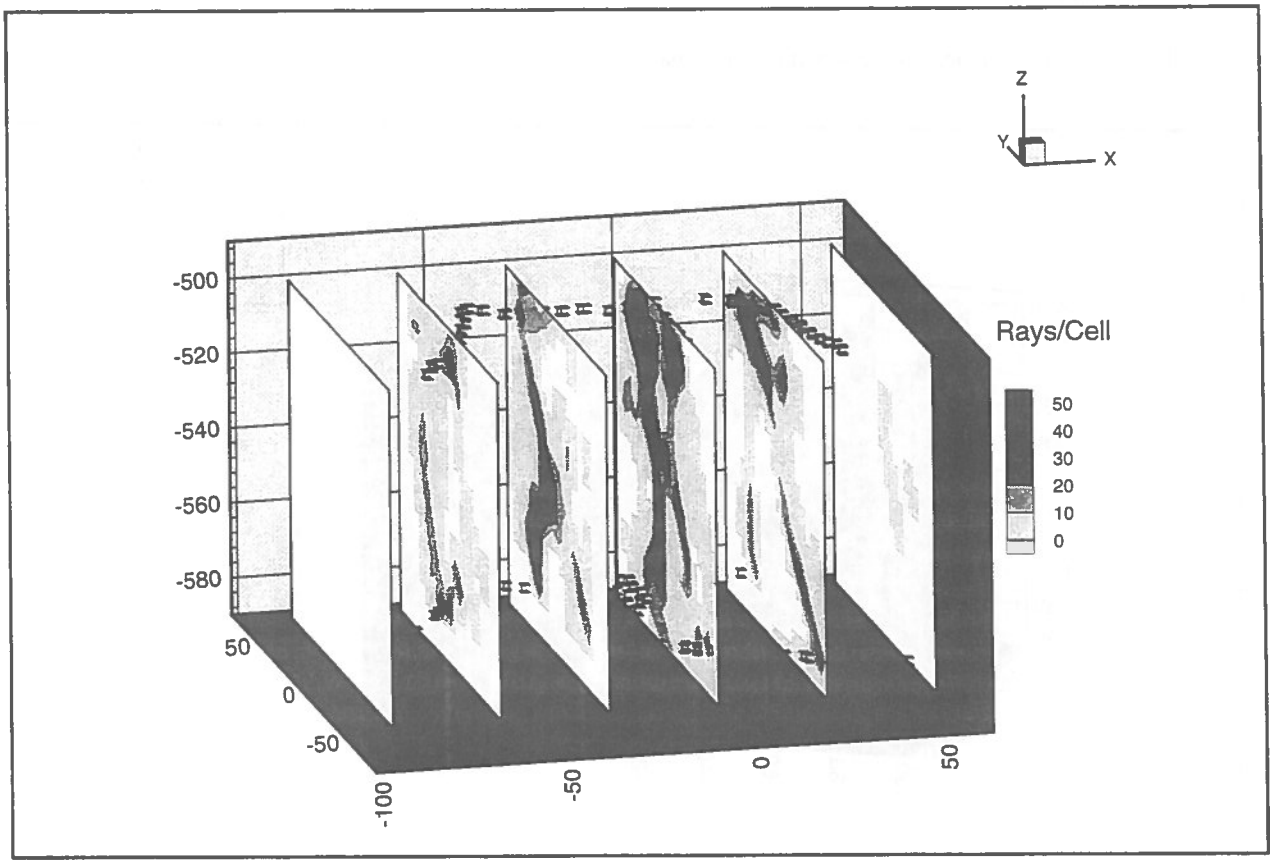

Figure 1. Raypath sampling density contoured on vertical slices through the 3-D survey volume. Symbols indicate source and receiver locations.

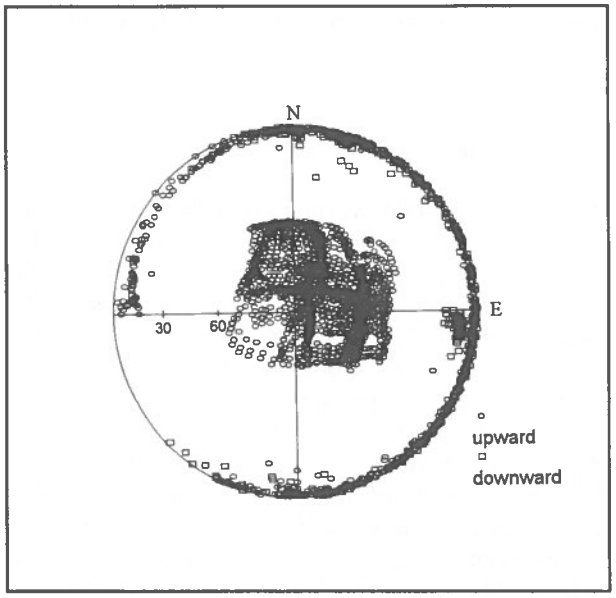

Figure 2. Stereographic projection of (straight) ray-path orientations, showing dense azimuthally-distributed subhorizontal coverage, and dense steep coverage.

Velocity Reconstruction:

The calculation grid occupies a volume with approximate dimensions of 140 by 110 by 90 m, with 10,648 nodes (22 by 22 by 22) spaced at intervals of 6.7, 5.2, and 4.2 m in the respective coordinate directions. The cell dimensions used in the calculations are thus comparable to the dominant wavelength of the seismic energy.

Twelve intermediate velocity models were generated by inverting the travel-time data twelve times, with a different initial velocity for each inversion. The initial velocities ranged from 4.7 to 6.0 km/s. In each case, the first five iterations used the straight-ray approximation, and ten subsequent iterations used the bending method for 3-D ray tracing. Figure 3 shows the final velocity model, produced by nodewise averaging of the 12 intermediate models.

The reconstructed velocities are strongly heterogeneous, varying from 1.5 to 6.0 km/s. The lowest velocities are invariably associated with the mine drifts, and are attributable to fracturing and stress relief due to excavation. The highest velocities tend to occur above the mine openings and backfilled stopes, and they can be attributed to concentration of load (due to the weight of the overburden). This interpretation has been substantiated by finite element stress modeling (Friedel et al., 1995).

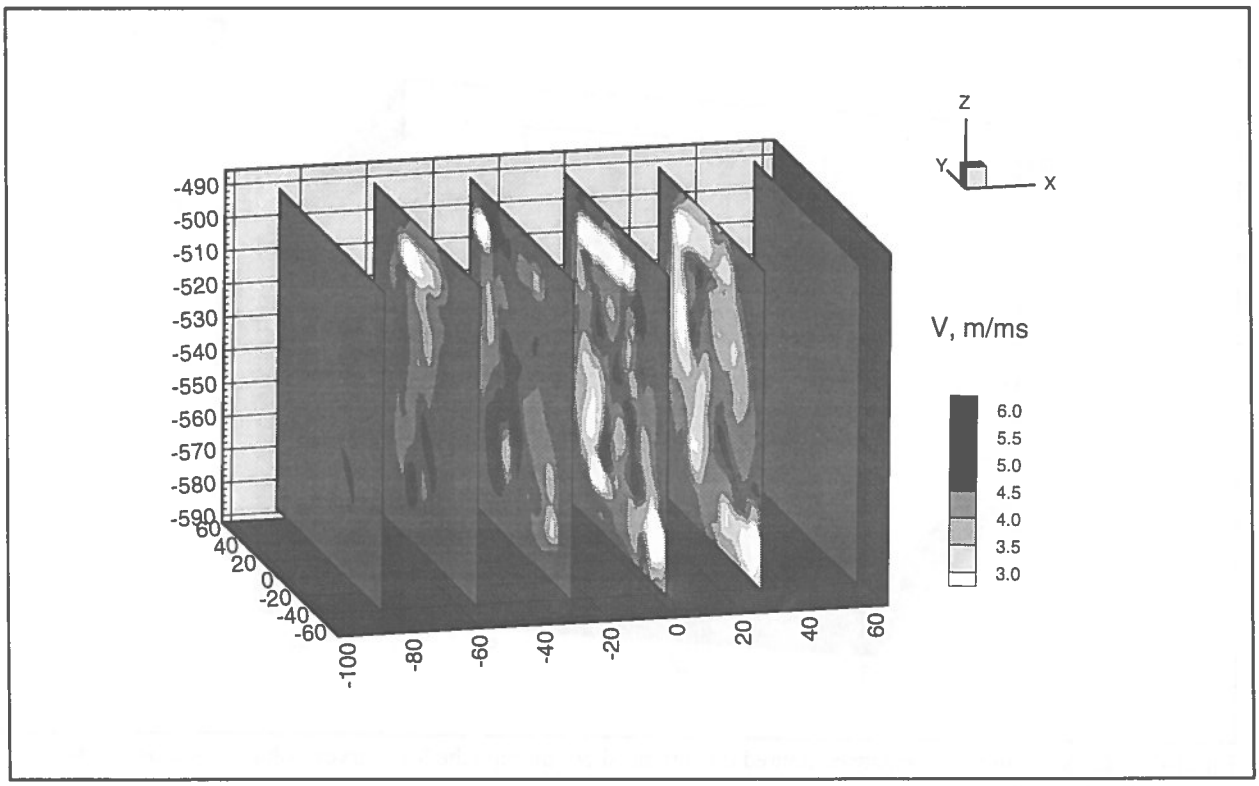

Figure 3. Velocity contoured on vertical slices through the 3-D model.

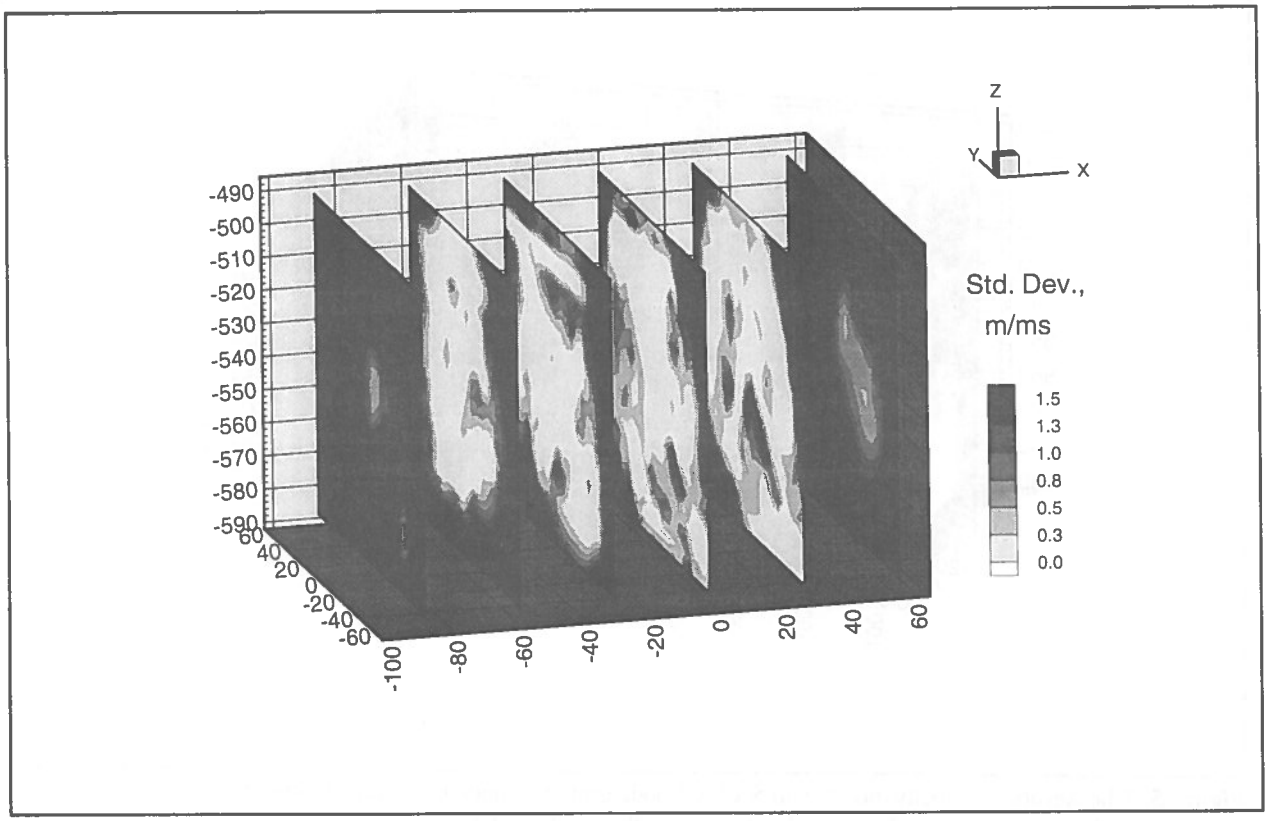

Figure 4. Contoured standard deviation of reconstructed velocities; lower values indicate greater robustness.

The contoured standard deviations (Figure 4) show that most of the principal features in the final reconstruction are robust with respect to initial model velocity. Within the portion of the grid volume that is sampled by rays, the standard deviation is almost everywhere less than that in the unsampled areas. However, a few small sampled areas show relatively high standard deviations; these areas are generally less than about 15 m in extent, and they lie between the two mine levels. At each level, the reconstructed velocities are very consistent, regardless of the value in the starting model. This robustness is due to the high density and excellent azimuthal distribution of ray paths.

Resolution Tests:

Checkerboard resolution tests were carried out for six different grids, as summarized in Table 1. The total grid volume was identical in each case.

Figures 5 and 6 illustrate the checkerboard test for the coarsest grid (5 x 5 x 5), with an average cell dimension of slightly over 30 m. Eighty-two precent of the cells (53/64) are sampled by at least one ray path. The reconstruction is reasonably accurate in depicting the large-scale velocity structure, with alternating blocks of high and low velocity; the correlation coefficient is 0.32. Accuracy tends to be reduced around the edges of the survey volume, where sampling density is low (cf. Figure 1). For the nodes in the interior of the grid, the correlation coefficient is 0.70.

Doubling the number of nodes in each direction (10 x 10 x 10) produces the checkerboard model of Figure 7, with a mean cell dimension of 13.5 m. With the finer grid, a much smaller fraction of the cells are sampled by rays; in fact a majority of the cells (418/729, or 57%) are unsampled. Nevertheless, the pattern of alternating high and low-velocity cubes is still discernible, particularly on the 4900 level (Z=503), where sampling density is highest and the raypath orientations cover a wide range of angles within the horizontal plane. Resolution is also reasonably good between the 4900 and 5100 levels, especially for the region with X coordinates between -40 and 20 (Figure 8). The correlation coefficient is 0.244 for the whole grid and 0.307 for the interior nodes. Restricting the comparison to the plane corresponding to the 4900 level yields a correlation of 0.412, and for the region bounded by X=±30 the correlation is 0.376.

Another doubling of the number of nodes in each direction (20 x 20 x 20) seriously degrades the accuracy of the

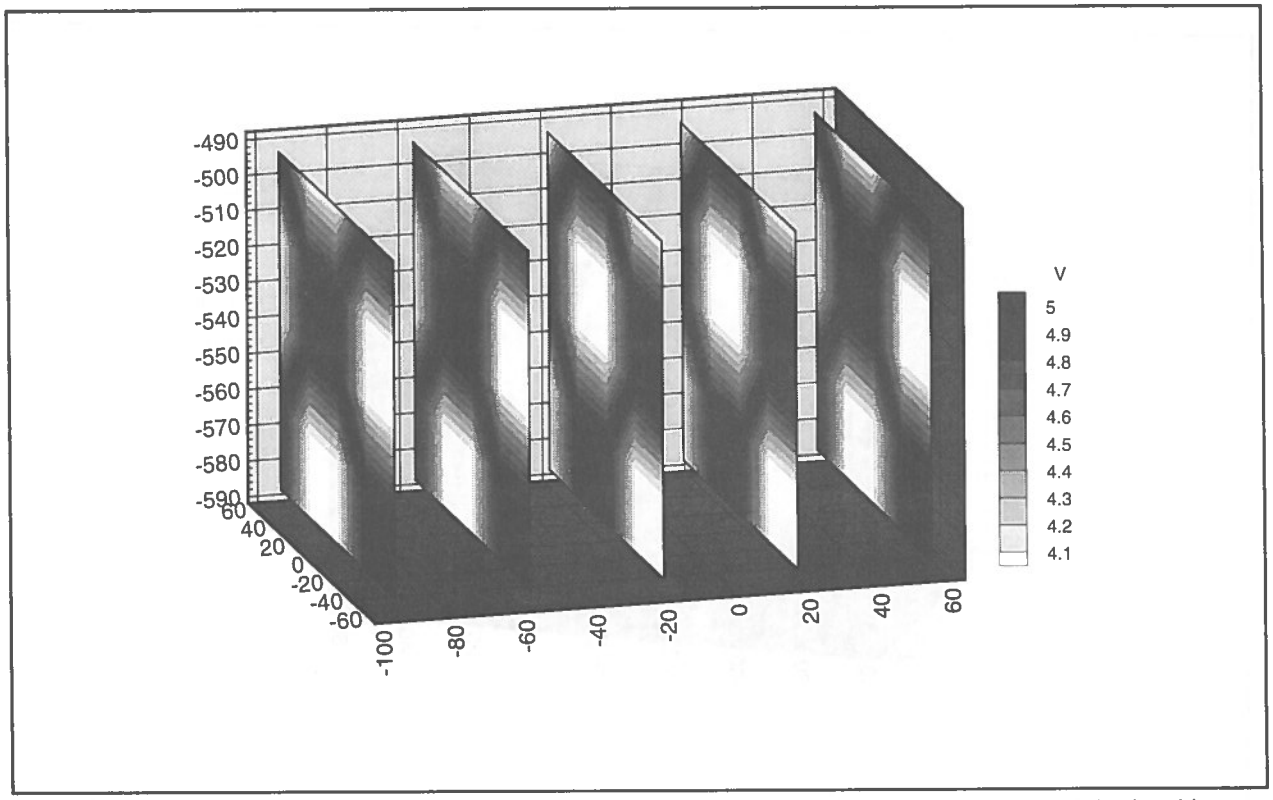

Figure 5. Checkerboard velocity model with 5 x 5 x 5 node grid. Synthetic travel times were calculated using this velocity model and the source and receiver locations from the real field data.

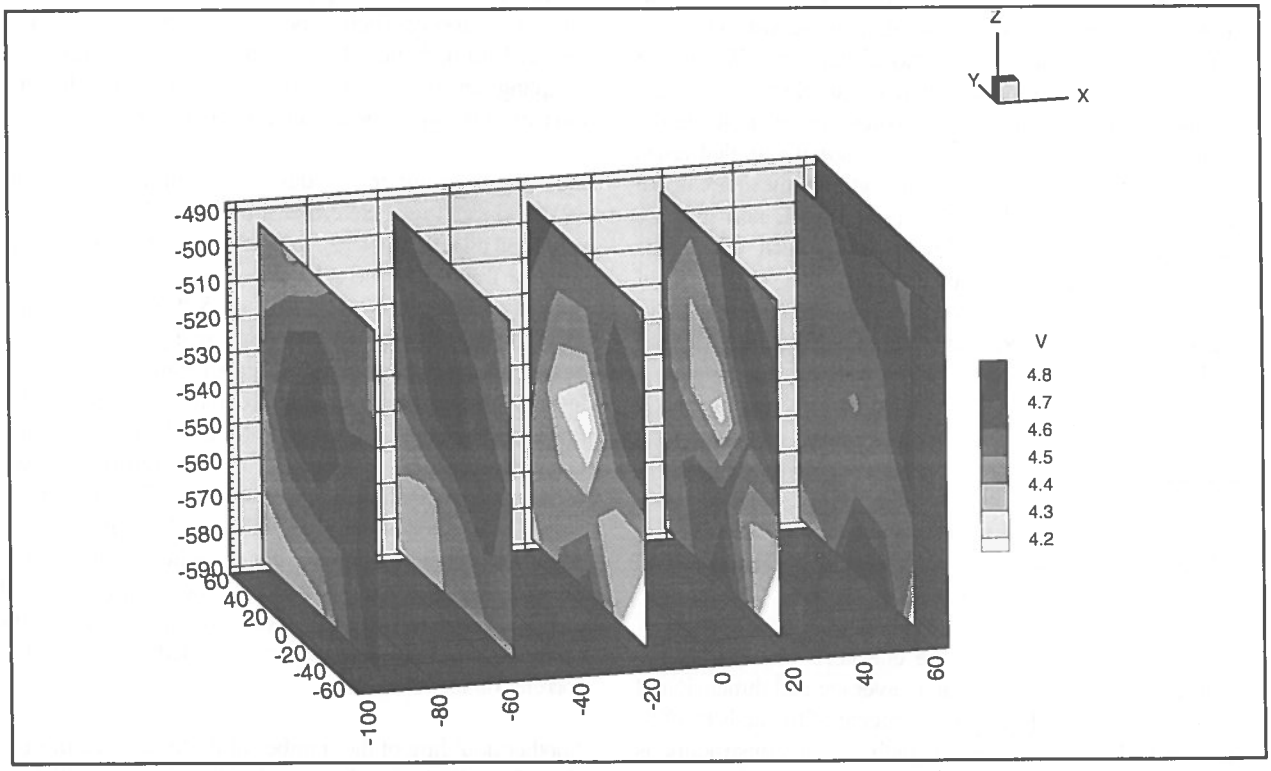

Figure 6. Reconstruction of the 5 x 5 x 5 checkerboard model from the synthetic travel times.

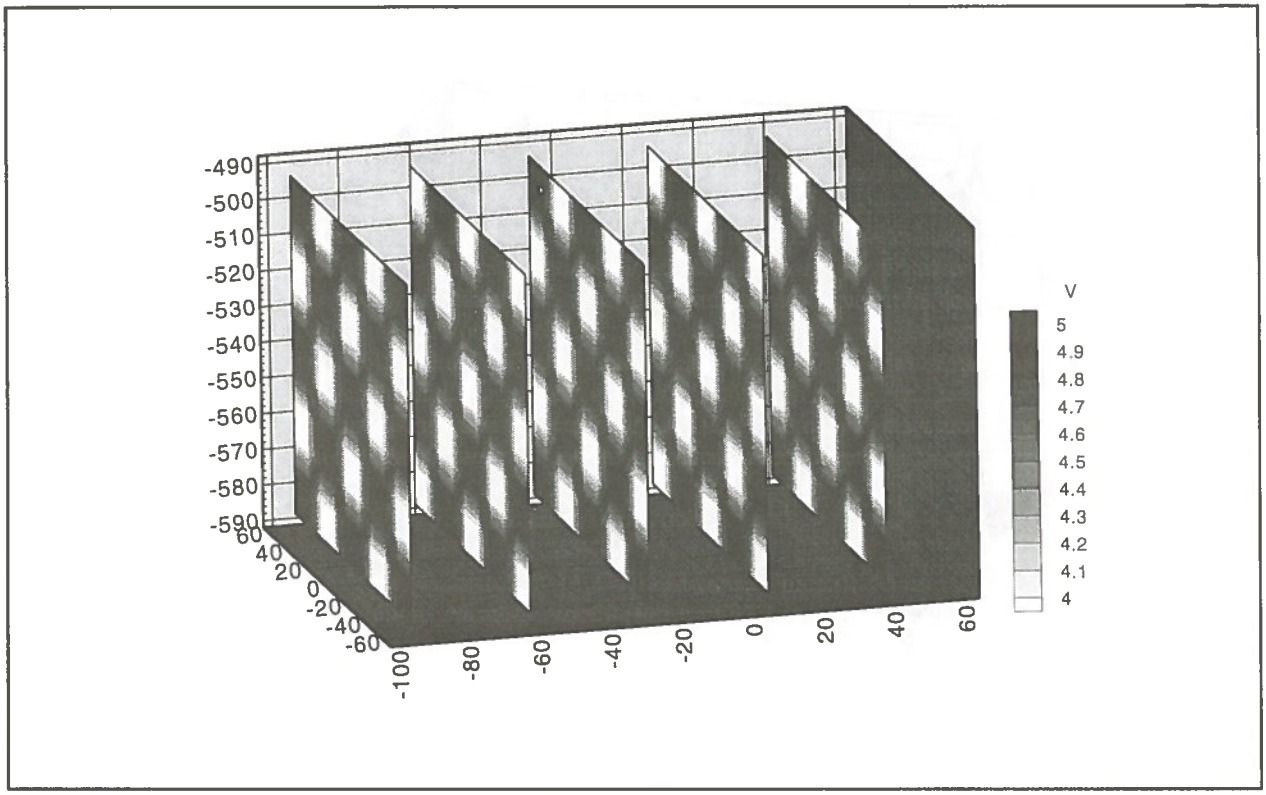

Figure 7. Checkerboard velocity model with 10 x 10 x 10 node grid. Synthetic travel times were calculated using this velocity model and the source and receiver locations from the real field data.

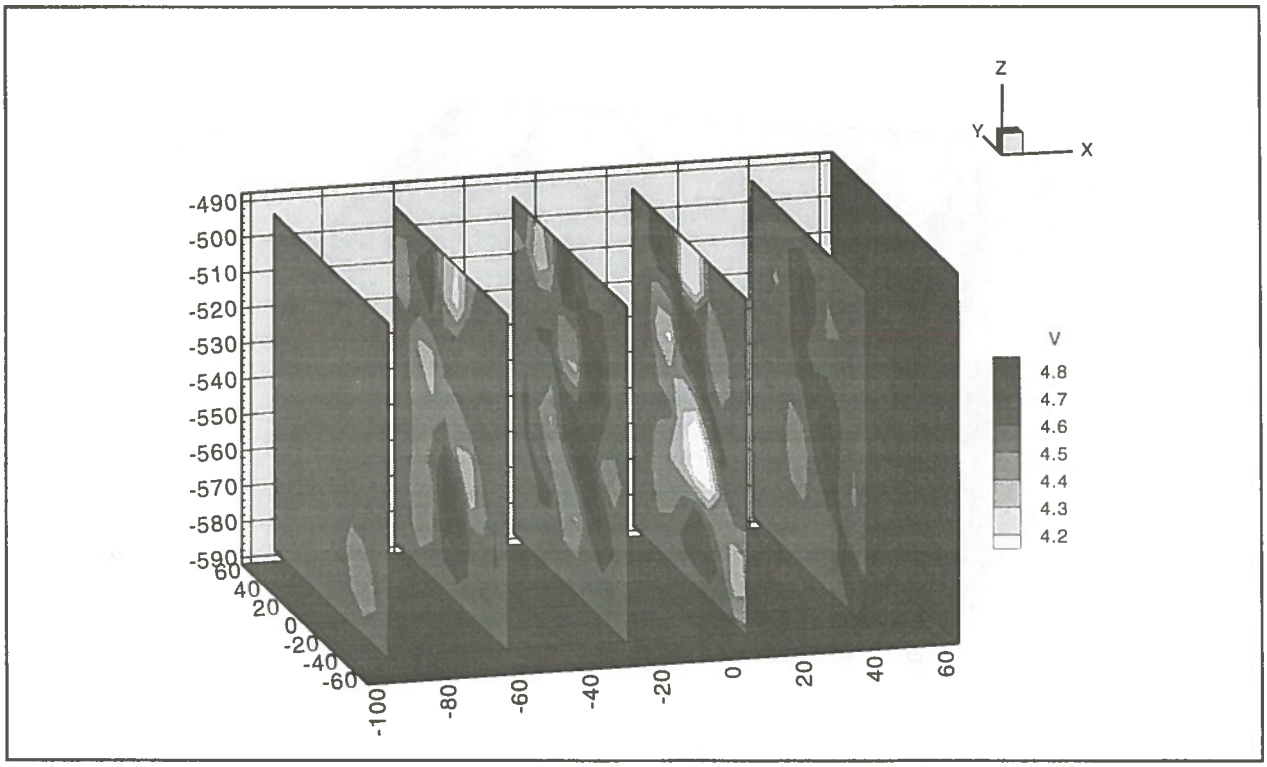

Figure 8. Reconstruction of the 10 x 10 x 10 checkerboard model from synthetic travel times.

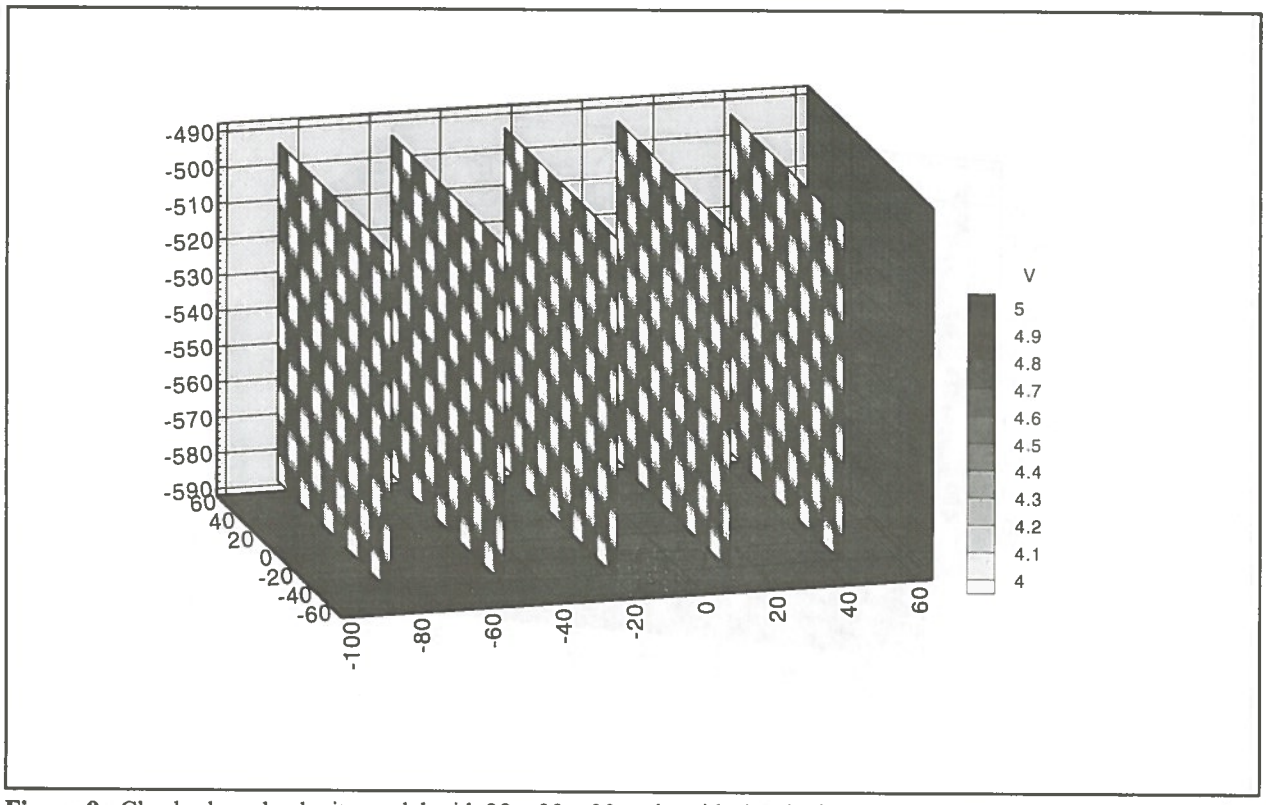

Figure 9. Checkerboard velocity model with 20 x 20 x 20 node grid. Synthetic travel times were calculated using this velocity model and the source and receiver locations from the real field data.

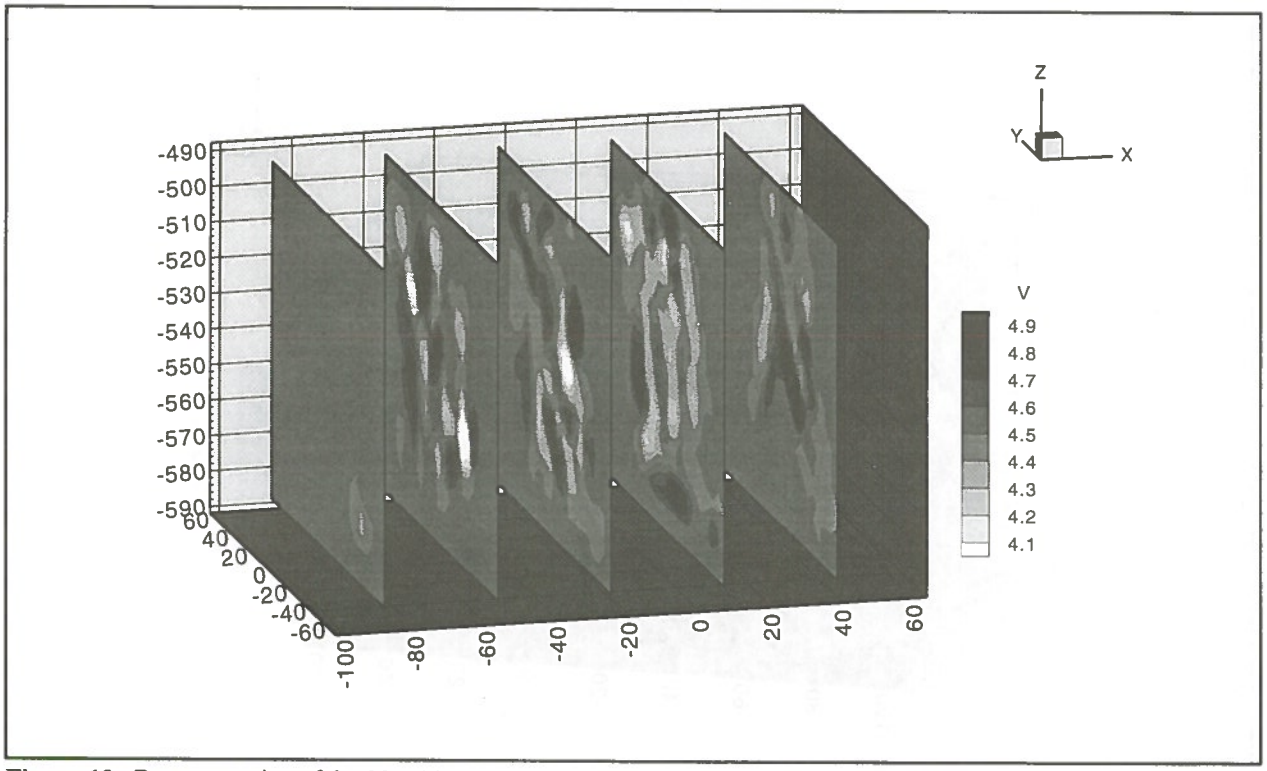

Figure 10. Reconstruction of the 20 x 20 x 20 checkerboard model from synthetic travel times.

Table 1. Grids Used for Checkerboard Resolution Tests

Grid	# of Nodes	DX (m)	DY (m)	DZ (m)	Mean Cell Dimension (m)
5 x 5 x 5	125	37.8	29.9	23.7	30.4
7 x 7 x 7	343	25.2	19.9	15.8	20.3
10 x 10 x 10	1000	16.8	13.3	10.5	13.5
15 x 15 x 15	3375	10.8	8.5	6.8	8.7
20 x 20 x 20	8000	8.0	6.3	5.0	6.4
22 x 22 x 22	10648	7.2	5.7	4.5	5.8

DX, DY, DZ: Cell dimensions in X-, Y-, and Z-directions.

reconstruction (Figures 9, 10). The checkerboard pattern is still recognizable in the regions of most dense raypath coverage, and for the 4900 level plane the correlation is 0.314. However, for the whole grid only 28% of the cells are actually sampled, and the correlation is only 0.050 (0.059 for the interior nodes). Although many of the fast and slow anomalies are represented in the reconstruction, they are often smeared out or elongated parallel to the local dominant ray-path orientation. The elongation of the reconstructed anomalies is here comparable to the cell size, a factor that accounts to a large degree for the low correlation.

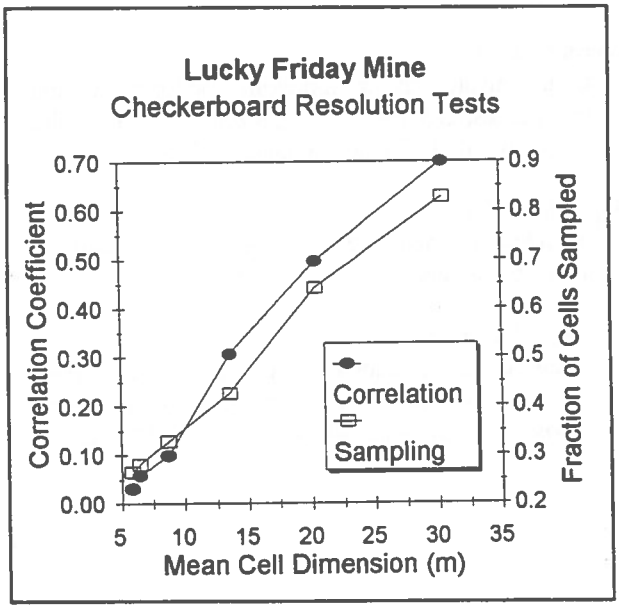

Figure 11. The fraction of cells sampled decreases with diminishing cell size, causing the accuracy of the checkerboard reconstructions (expressed as correlation coefficient) to decrease.

Figure 11 summarizes the results of checkerboard tests with varying cell sizes. As the cell dimensions are reduced, the fraction of cells sampled diminishes accordingly, in a quasi-linear fashion over the range of sizes investigated. (For the limiting case with cell size approaching zero, the fraction of cells sampled also approaches zero; for the opposite case where cells become sufficiently large, all of them will be sampled by at least one ray). The accuracy of the reconstructions also diminishes as the cell size is reduced, in part due to the decreased sampling efficiency. The dependence of correlation coefficient on cell size is nonlinear, with a sharp decrease for cell sizes less than about 13 m. The sharp drop in accuracy is probably due to a reduction in the range of viewing angles for each cell, as the number of rays per cell decreases. The result is greater smearing (relative to the size of the cells) so that fast or slow anomalies in the reconstruction overlap with both fast and slow anomalies in the original model.

DISCUSSION AND CONCLUSIONS

Velocity reconstructions for the Lucky Friday Mine site contain important information concerning the occurrence and location of anomalous stress concentrations. Principal velocity anomalies in the tomograms are broadly compatible with the results of stress modeling (Friedel et al., 1995) and laboratory studies of the stress-dependence of seismic velocity.

The velocity reconstructions are generally quite robust with respect to differences in initial velocity, due primarily to the good azimuthal ray-path coverage on the two horizontal levels. In the intervening volume, small regions of high standard deviation, typically of less than 15 m extent, show that some of the fine-scale features of the reconstructions are sensitive to initial velocity, and therefore are not reliable.

The checkerboard resolution tests also indicate that the characteristic resolution scale for this data set is around 10-12 m; the mathematical resolution is thus comparable to the physical resolution (8 m wavelength). The overall accuracy of reconstructions for finer-scale velocity variations is poor, although features as small as 5 m are well resolved in the regions of highest raypath sampling density, especially near the 4900 level and the region bounded by X=±30.

In practice, three-dimensional inversions are commonly underdetermined to a greater extent than 2-D inversions. Thus, in order to capitalize on the advantages of 3-D processing, it is essential to carefully analyze the resolution and robustness associated with reconstruction. The Bureau's 3DTOM software is designed to assist in this analysis.

REFERENCES

Blake, W. and Cuvelier, D., 1990.
Developing reinforcement requirements for rockburst conditions at Hecla's Lucky Friday mine. *Proc. 2nd International Symposium on Rockbursts and Seismicity in Mines '88*, Fairhurst (editor), A.A. Balkema, Rotterdam: 407-409.

Bregman, N. D., R. C. Bailey, and C. H. Chapman, 1989.
Crosshole seismic tomography, *Geophysics*, v. 54, pp. 200-215.

Friedel, M.J., M.J.Jackson, D.F.Scott, T.J.Williams, and M.S.Olson, 1995.
3D tomographic imaging of anomalous conditions in a deep silver mine. *Journal of Applied Geophysics*. (in press).

Gilbert, P, 1972.
Iterative methods for the three-dimensional reconstruction of an object from projections, *Journal of Theoretical Biology*, v. 36, p. 105-117.

Jackson, M.J. and Tweeton, D.R., 1994.
MIGRATOM - Geophysical tomography using wavefront migration and fuzzy constraints. *BuMines RI 9497*, 43 pp.

Menke, W., 1984.
The resolving power of cross-borehole tomography, *Geophysical Research Letters*, v. 11, p. 105-108.

Moser, T.J., 1991.
Shortest path calculation of seismic rays. *Geophysics*, 56 (1): 59-67.

Peterson, J. E., B. N. P. Paulson, and T. V. McEvilly, 1985.
Applications of algebraic reconstruction techniques to crosshole seismic data, *Geophysics*, v. 50, p. 1566-1580.

Radcliffe, K.S., R.E. Thill and J.A. Jessop, 1986.
Use of acoustic velocity for predicting stress under uniaxial compression. *115th Ann. AIME Mtg. Reprint 86-147*, 11pp..

Tweeton, D.R., 1988.
BOMTOM- a tomographic computer program with constraints to improve reconstructions for monitoring in situ mining leachate. *BuMines RI 9159*, 70 pp.

Um, J. & C.Thurber, 1987.
A fast algorithm for two-point seismic ray tracing. *Bulletin of the Seismological Society of America*, v. 77, p. 972-986.

Wielandt, E., 1987.
On the validity of the ray approximation for interpreting delay times, in *Seismic Tomography*, edited by Nolet, G., pp. 85-98, D, Reidel, Hingham, Mass.

Williamson, P.R., 1991.
A guide to the limits of resolution imposed by scattering in ray tomography. *Geophysics*, 56 (2), 202-207.

Young., R.P and S.C.Maxwell, 1992.
Seismic characterization of a highly stressed rock mass using tomographic imaging and induced seismicity. *Journal of Geophysical Research*, v. 97, p. 12361-12373.

CAMI'95: 3rd Canadian Conference on Computer Applications in the Mineral Industry
Montréal, Québec, Canada, October 22-25, 1995

Seismic Modelling of the McConnell Orebody, Sudbury Basin

Ronald A. Borsato
Seismic Definition, London, Ontario

ABSTRACT

Two-dimensional seismic models were constructed using velocity and density downhole logging measurements for the McConnell Orebody, Sudbury Basin. The purpose of the modelling was to define the seismic response of the orebody versus the host rock. Variations in orebody thickness, velocity and density were also implemented into the modelling to define the seismic response for different characteristics. The results obtained confirm that seismic data can image the McConnell Orebody within defined thickness and frequency limits.

RÉSUMÉ

Deux modèles sismiques bidimensionnels ont ètè dèveloppès à partir de mesures diagraphiques en puits pour le gisement de McConnell, bassin de Sudbury. Ces modèles avaient pour but de définir les spectres de réponse sismeque du gisement par rapport à la roche d'accueil. Des variations de l'épaisseur, de la vitesse et de la densité du gisement ont également été incorporées dans les modèles afin de déterminer les résponses sesmiques en présence de caractéristiques différentes. Les résultats obtenus permettent de confirmer que, dans le cadre d'épaisseurs et de limites de fréquence déterminées, les données sismiques peuvent illustrer le gisement de McConnell.

INTRODUCTION

The McConnell Orebody is owned by Inco Limited and is located northeast of the city of Sudbury outside the town of Garson in the Sudbury Basin (Figure 1). The Geologic Survey of Canada has recently acquired downhole logging measurements over this particular orebody. Velocity and density measurements were used to construct seismic models to define the seismic response and limits of resolution. The software used for the seismic models were supplied by Geophysical MicroComputer Applications (International) Limited of Calgary.

GEOLOGY

The McConnell Orebody is a massive sulphide feature that subcrops at surface and extends in depth to approximately 350 metres. There is a weathering layer above the bedrock which ranges from 0-12 metres. The shape, thickness, orientation and borehole delineation of this body is detailed in Figure 1.

The Geologic Survey of Canada, in cooperation with Inco Limited, acquired downhole logging measurements. Borehole #78930 was used to log the orebody. Measurements acquired are found in Figure 1. Note the significant velocity decrease and the significant density increase that the orebody exhibits.

SEISMIC MODELLING

The seismic modelling was conducted using the LOGM and STRUCT two-dimensional seismic software programs developed by Geophysical MicroComputer Applications (International) Limited of Calgary. The velocity and density

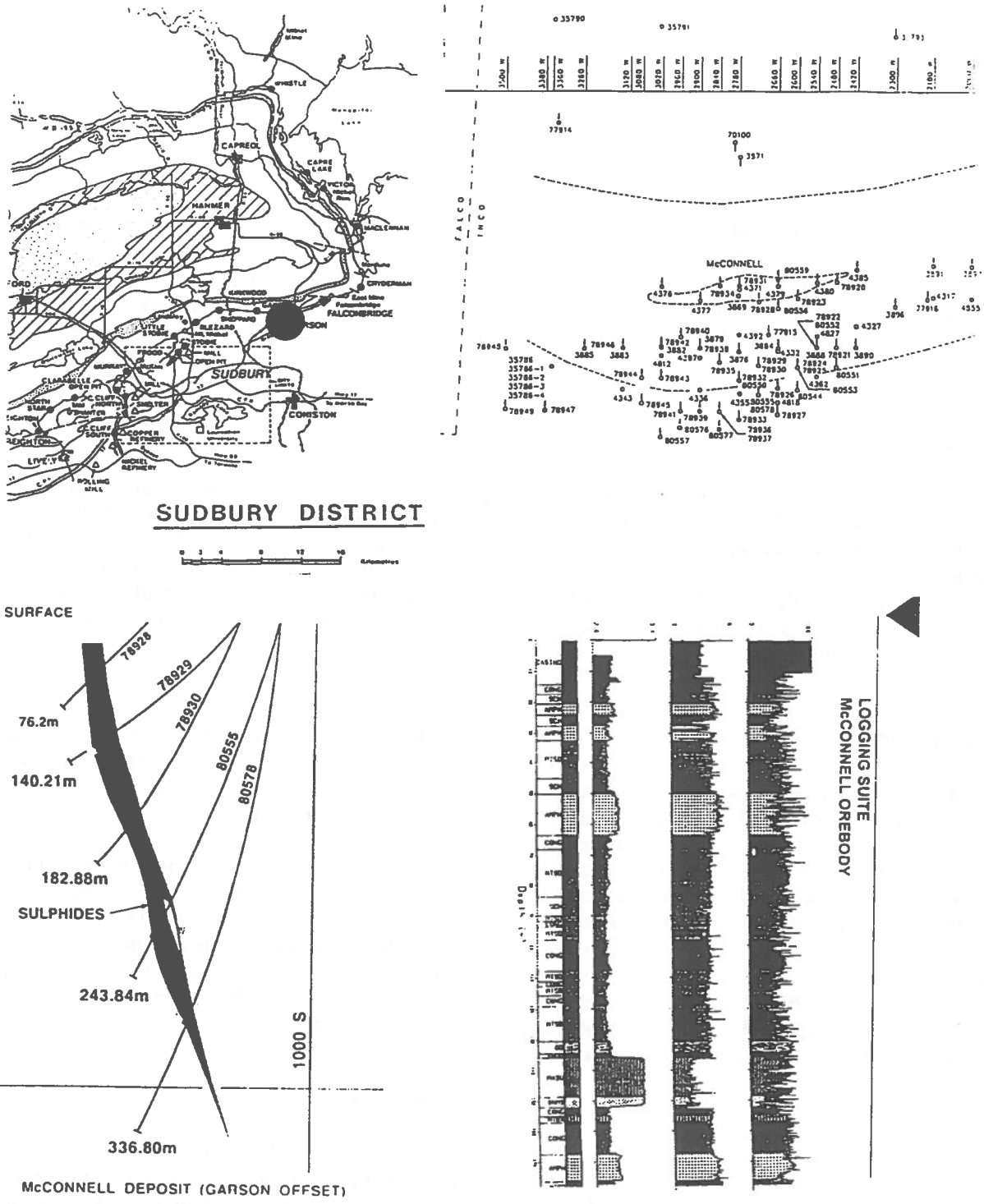

Figure 1 Location, Surface and Subsurface Geology and Borehole Logging Suite for the McConnell Orebody, Sudbury Basin.

logging curves were digitized and inserted into these software programs to define the seismic response and limits of resolution of the McConnell Orebody. In all models, except the synthetic, a cross-section of the model is generated and seismic responses at frequency ranges 10/15-80/90 hertz, 10/15-140/150 hertz and 10/15-190/200 hertz were created. This frequency range was chosen based on seismic data previously acquired over the McConnell Orebody.

Synthetic Model (Figure 2)

The first model generated was a synthetic, where the seismic waveform and frequency chosen are related to the actual borehole logs of velocity and density. The acoustic impedance created by the velocity and density differences of the orebody and host rock, creates a seismic waveform that defines the top and bottom of the orebody. The synthetic is generated with the resulting normal and reverse polarities at the different frequencies. In normal polarity, for instance, the top of the orebody is defined by a strong amplitude trough and the bottom of the orebody is defined by a strong amplitude peak.

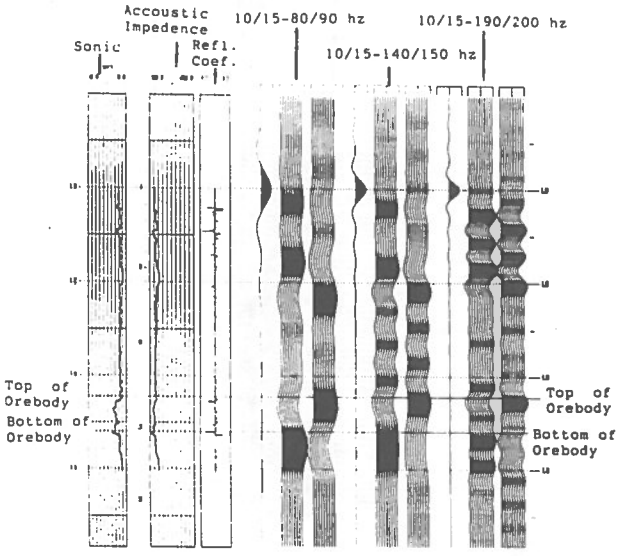

Figure 2 Synthetic Model, McConnell Orebody, Sudbury Basin.

Velocity Model (Figure 3)

The velocity model cross-section portrays a senerio, going left to right, of a host rock velocity log, an orebody velocity log and back to a host rock velocity log. Velocity only plays a role in this model without any density information. The normal polarity seismic responses all exhibit strong amplitude delineation of the orebody. The top of the orebody is defined by the trough and the bottom of the orebody is defined as the peak.

Acoustic Impedance Model (Figure 4)

The acoustic impedance model cross-section portrays a senerio, going left to right, of a host rock velocity/density log, an orebody velocity/density log and back to a host rock velocity/density log. Velocity and density information create this acoustic impedance. The normal polarity seismic responses all exhibit strong amplitude delineation of the orebody. The top of the orebody is defined by the trough and the bottom of the orebody is defined by the peak.

Thickness Variations Model (Figure 5)

The thickness variations model cross-section portrays a senerio, from left to right, of a host rock velocity/density log, a 5 metre thick orebody velocity/density log, a 10 metre thick orebody velocity/density log, the original 16 metre thick orebody velocity/density log and back to a host rock velocity/density log. The normal polarity seismic responses show some differences here. The 10/15-80/90 hertz and the 10/15-140/150 hertz seismic responses cannot resolve a 5 metre thick orebody. They are able to resolve a 10 metre thick or greater orebody. Only the 10/15-190/200 hertz seismic response was able to resolve as little as 5 metres of orebody.

Variations in Velocity Model (Figure 6)

The variations in velocity model portrays a senerio, going left to right, of a host rock velocity/density log, an orebody with velocity 3,500 metres/second velocity/density log, the original orebody with velocity 4,500 metres/second velocity/density log, an orebody with velocity 5,500 metres/second

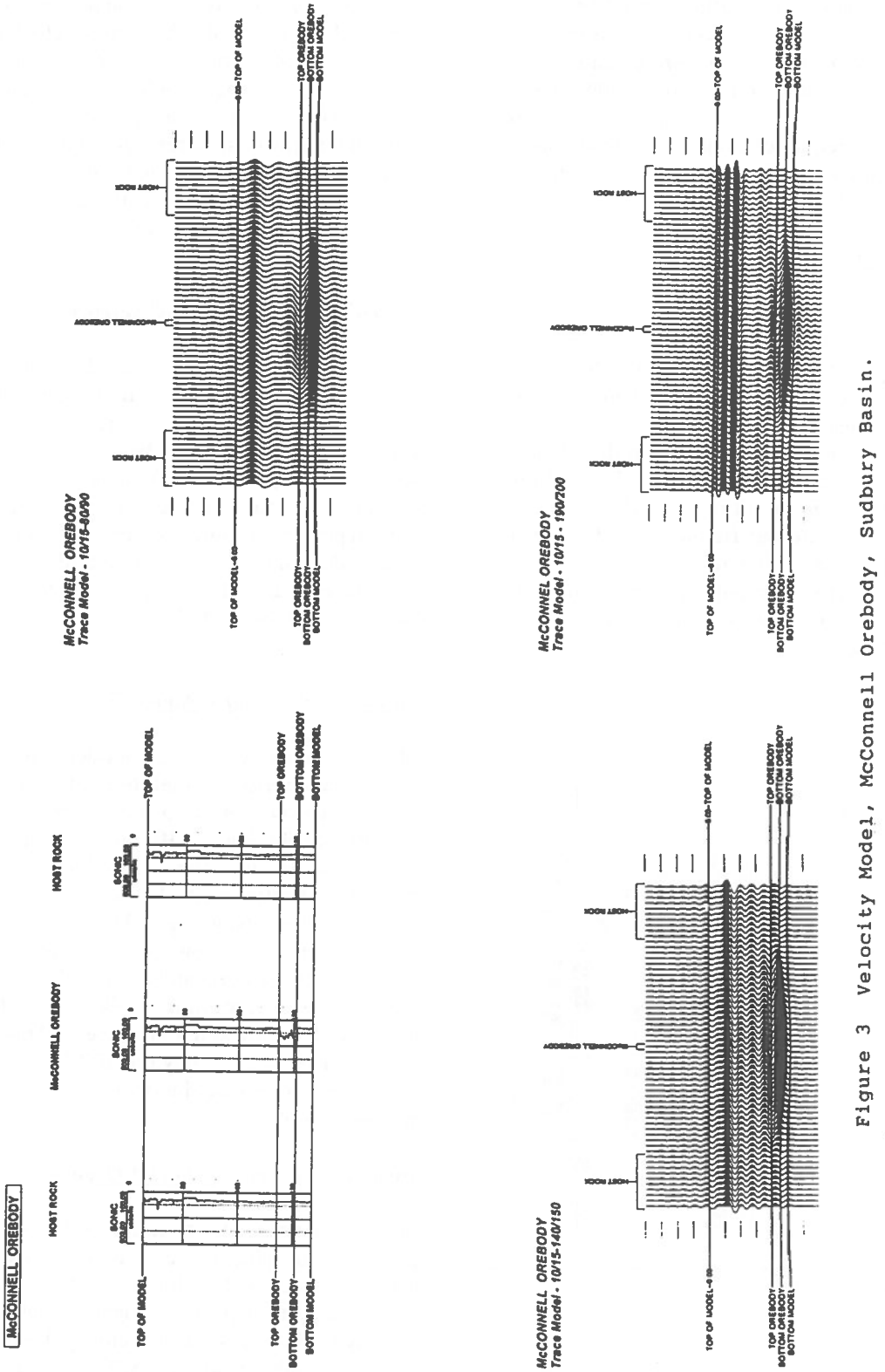

Figure 3 Velocity Model, McConnell Orebody, Sudbury Basin.

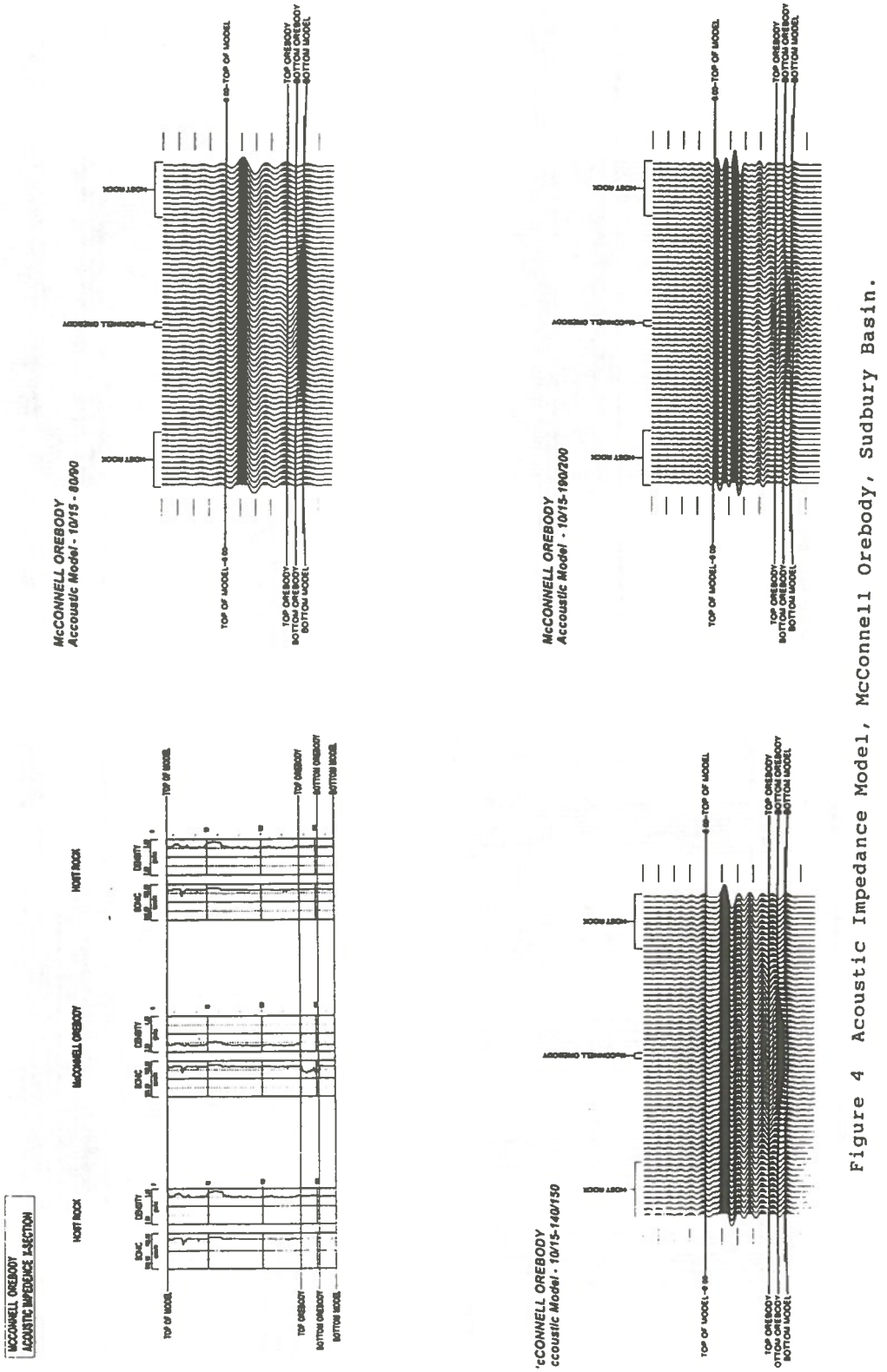

Figure 4 Acoustic Impedance Model, McConnell Orebody, Sudbury Basin.

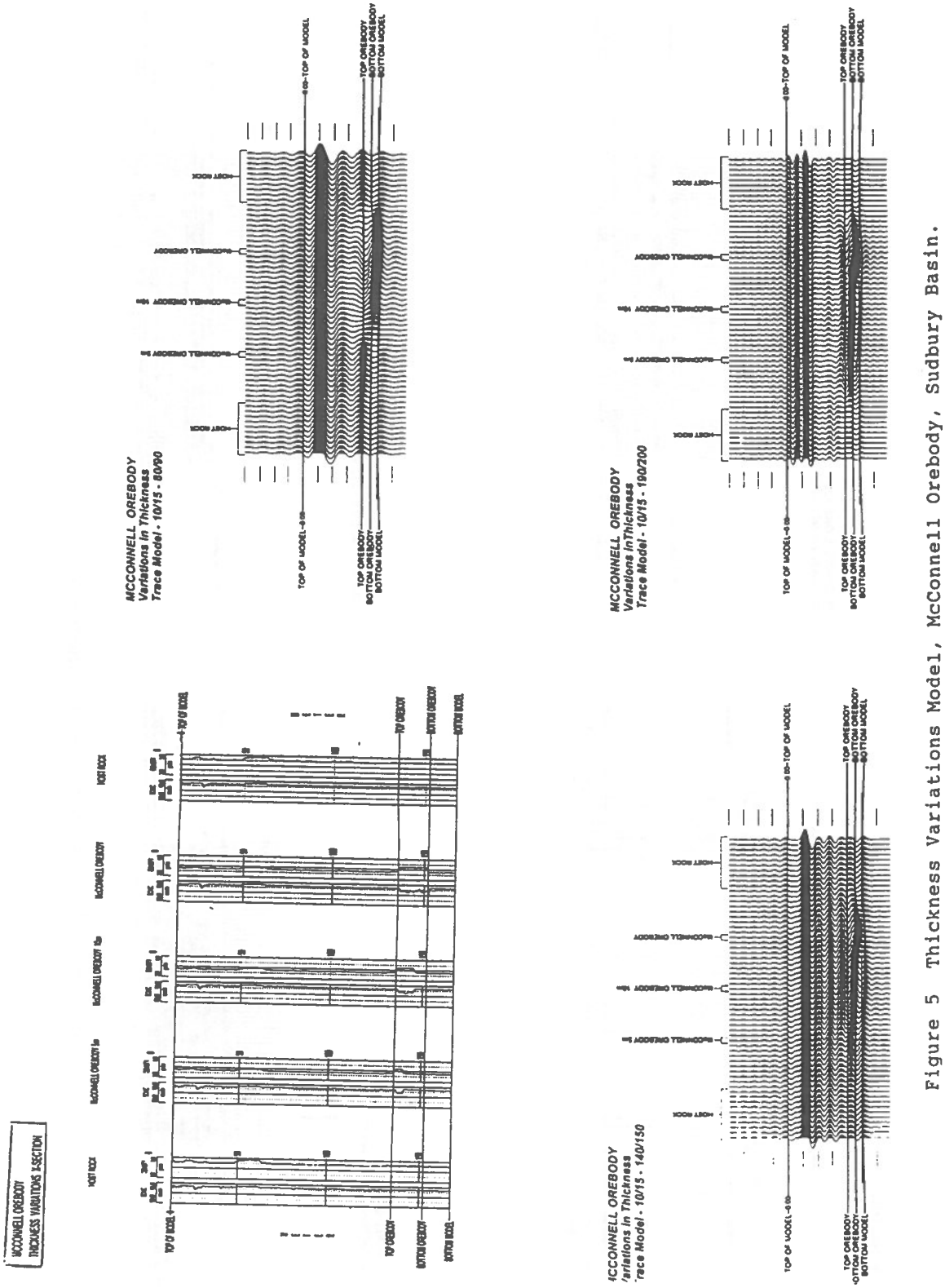

Figure 5 Thickness Variations Model, McConnell Orebody, Sudbury Basin.

velocity/density log and back to a host rock velocity/density log. Variations in velocity reflect variations in orebody grades. The normal polarity seismic responses show some differences here. At a velocity of 5,500 metres/second an orebody cannot be resolved in the frequency ranges shown here. Only at velocities of 4,500 metres/second and slower, and at a constant density, can these frequency ranges resolve the orebody from the host rock.

Variations in Density Model (Figure 7)

The variations in density model portrays a senerio, going left to right, of a host rock velocity/density log, an orebody with density 3.0 gm/cc velocity/density log, the original orebody with density 3.3 gm/cc velocity/density log, an orebody with density 3.5 gm/cc velocity /density log and back to a host rock velocity/density log. Variations in density reflect variations in orebody grades. The normal polarity seismic responses show no differences here. At these frequency ranges density values of 3.0 gm/cc to 3.5 gm/cc can be resolved seismically at the given a constant velocity.

Total Orebody Model (Figure 8)

The total orebody model was created to portray what the McConnell Orebody would look like on a two dimensional seismic profile. Boundaries were created for the weathering layer, orebody and host rock. Each cell was assigned a certain velocity and density which are constant throughout the cell. The normal polarity seismic responses each show reflectors at the base of the weathering and at the top and bottom of the orebody. The top of the orebody is defined by a trough and the bottom of the orebody is defined by a peak. Increase in frequency content results in sharpness of wavelet reflectors.

CONCLUSION

The results of the two-dimensional seismic models on the McConnell Orebody clearly demonstrates that this orebody can be imaged seismically. The only real limits to its delineation are thickness, velocity and wavelet frequency. Measurements of amplitude of wavelets should lead to fairly accurate estimates of orebody grades in conjunction with borehole information. Seismic imaging of the total orebody are possible given similar parameters to the McConnell Orebody. These total orebody seismic profiles will aid in total orebody economics and future mine design, especially in a three-dimensional case.

There certainly are sufficient velocity and density differences between the McConnell Orebody and the host rock. This should be the case for many other massive sulphide orebodies. It is critically important to acquire downhole logging information on velocity and density for as many orebodies as possible. This database will allow for further uses of seismic to delineate these economic features. Seismic is the only hope right now to truly image the orebody -host rock boundary. Once this is done mine economics, mine planning and mine extraction can be achieved more efficiently, at less cost and greater return.

ACKNOWLEDGEMENTS

Seismic Definition would like to thank Geophysical Micro Computer Applications (International) Limited of Calgary for the use of the seismic modelling software. Thanks also go to Inco Limited for providing the geology, logging information and the opportunity to present this data.

REFERENCES

Hilterman, F.J. and Liang L.C., 1983
Seismic Exploration Modelling, Geophysical Development Corporation, Dome Petroleum Ltd. In-House Course, Calgary, October 31-November 4.

Lye, A., 1984
Basic Well Logging, Southern Alberta Institute of Technology, Fall Course.

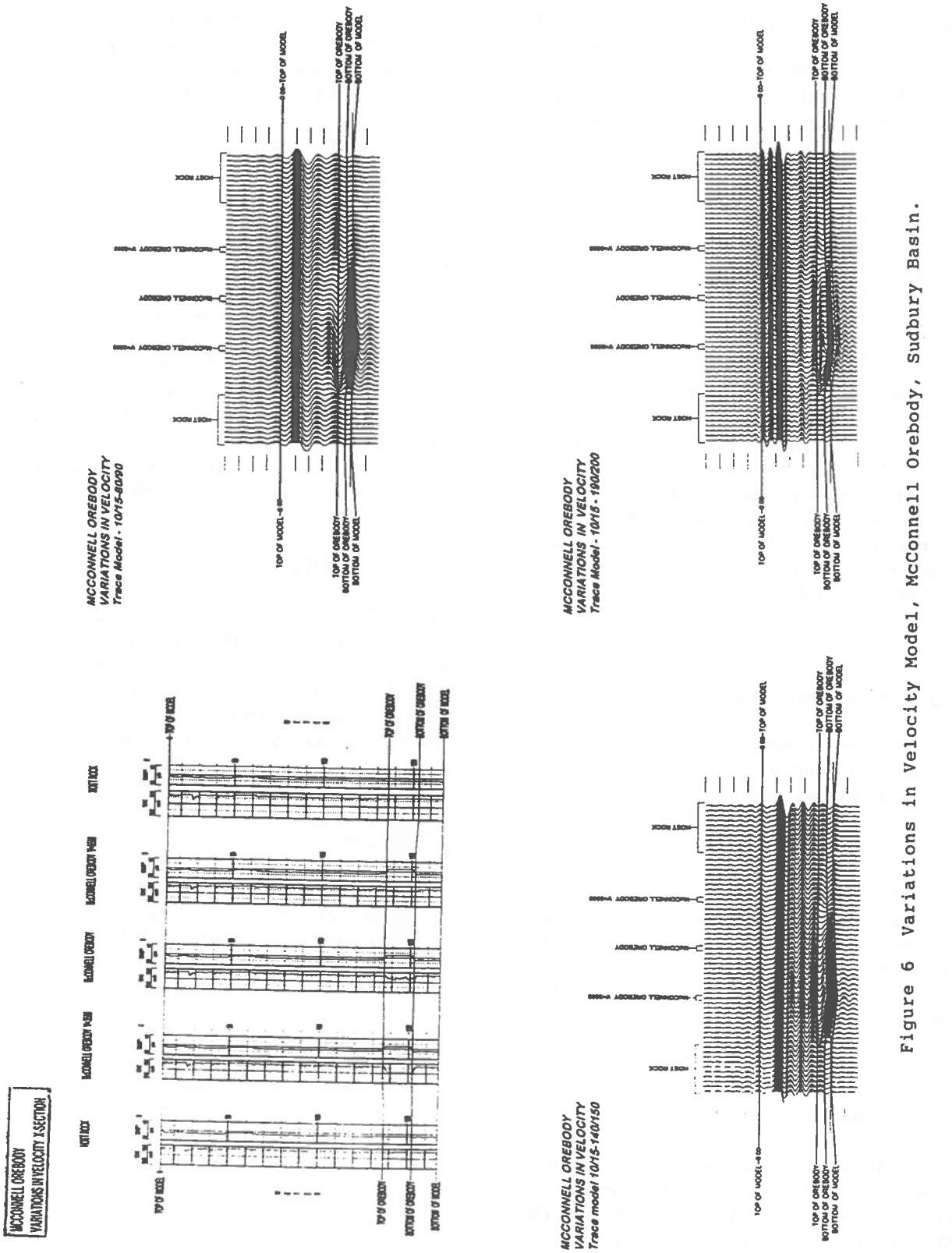

Figure 6 Variations in Velocity Model, McConnell Orebody, Sudbury Basin.

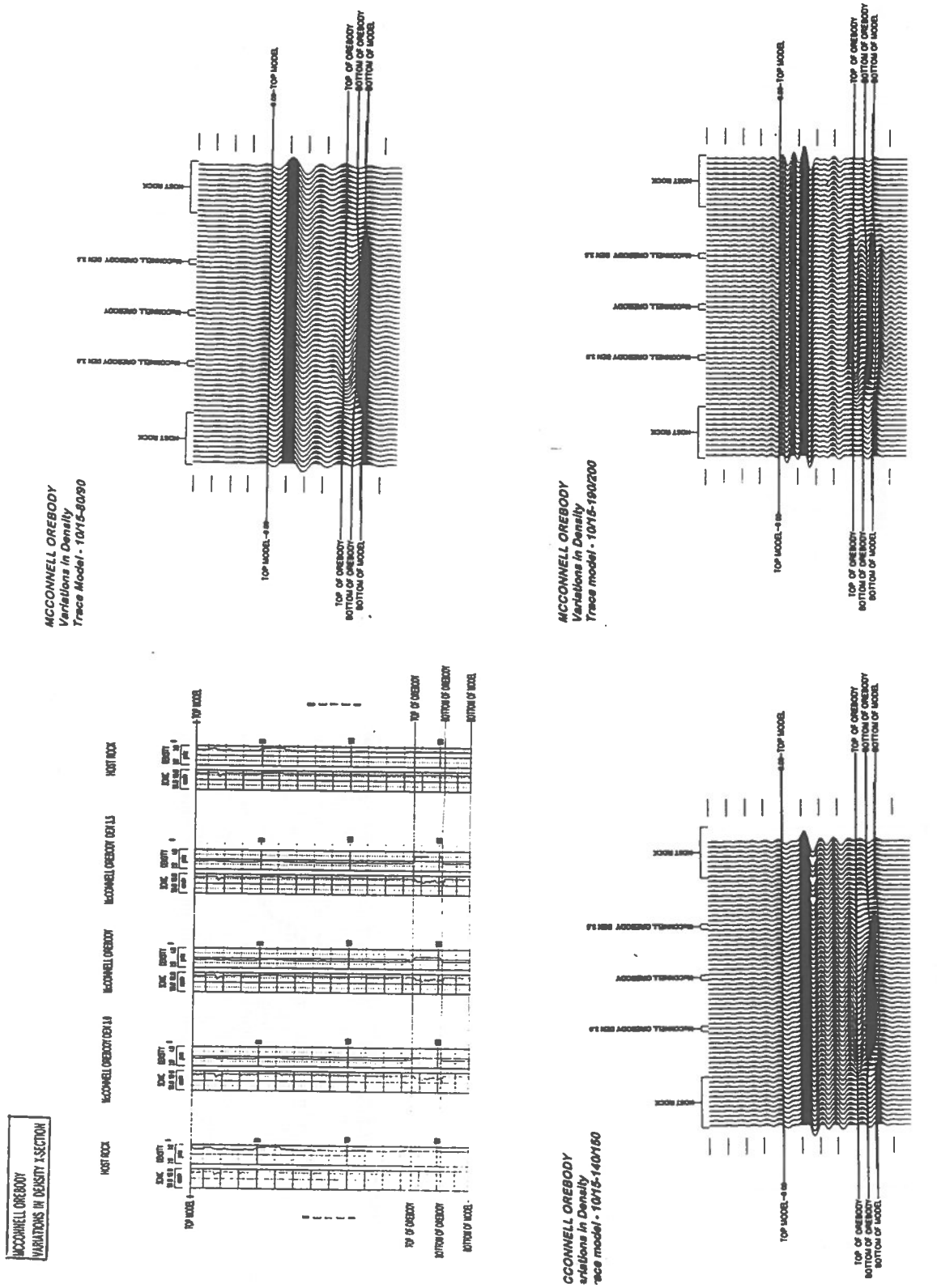

Figure 7 Variations in Density Model, McConnell Orebody, Sudbury Basin.

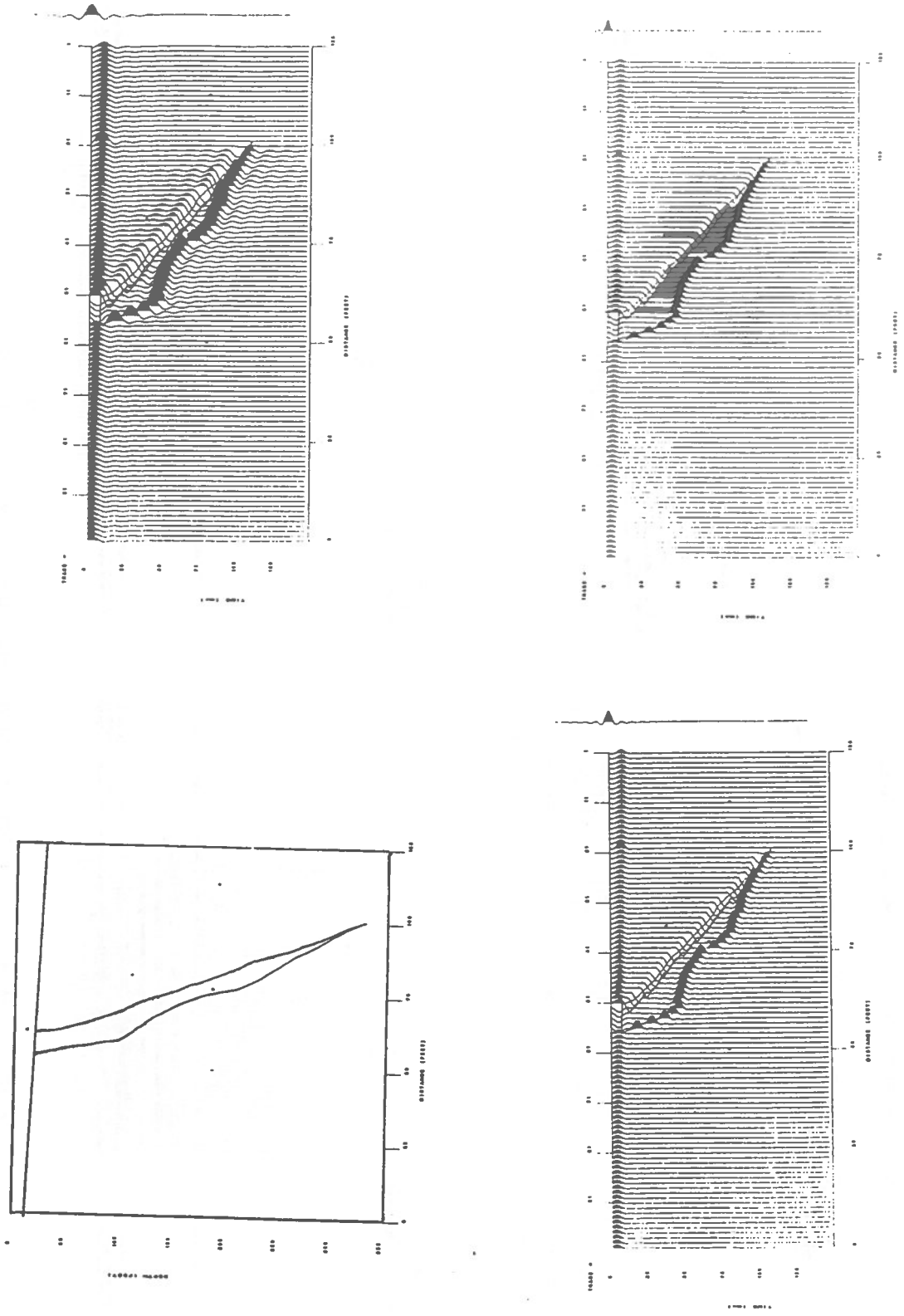

Figure 8 Total Orebody Model, McConnell Orebody, Sudbury Basin.

CAMI'95: 3rd Canadian Conference on Computer Applications in the Mineral Industry
Montréal, Québec, Canada, October 22-25, 1995

Use of Seismic Density Analyses in Burst-Prone Mines

Vassilios N. Kazakidis
MRD - Mining Research Directorate, Sudbury, Ontario

Allan R. Punkkinen
Creighton Mine, Inco Ltd, Sudbury, Ontario

Terry J. Villeneuve
Mines Research, Inco Ltd, Sudbury, Ontario

Brent T. Corkum
University of Toronto, Toronto, Ontario

ABSTRACT:

A software utility that enables the examination of spacial distribution of seismic events using three dimensional event density contouring is presented. In addition to event density analysis, the utility has the capacity to determine relative density of parameters such as total and average energy density or source parameters that are provided by full waveform microseismic systems. Output of the utility can be visualized using *EXAMINE*^{3D}, a data visualization package, where data pertaining to mine geometry, geology or results from numerical modelling can be superimposed. The use of the density utility is demonstrated through a number of examples from an Ontario hard rock mine with rockburst problems.

RÉSUMÉ:

Cet article présente un programme permettant l'examen de la distribution spatiale d'événements séismiques en trois dimenions. En plus d'analyser et de préparer des contours tri-dimensionnels du nombre d'événements, ce programme peut servir à déterminer la densité relative de paramètres tels que l'énergie totale ou moyenne, ou des paramétres de source. Les résultats peuvent êste visualisés avec le logiciel *EXAMINE*^{3D}, permettant ainsi la superposition avec les données géométriques et géologiques et la modélisation numérique. La démonstration de ce programme est faite à l'aide d'examples en provenance de mines ontariennes confrontées á des coups de terrain.

INTRODUCTION

Mining in deep underground hard-rock mines is often associated with high levels of seismic activity and rockbursting. Analysis of seismic data has become increasingly important for understanding the response of the rock mass to mining in burst-prone mines. Today for the operation of such mines, it is necessary to maintain constant monitoring of the seismic activity using microseismic systems. Such monitoring can provide to the operator information with respect to the locus, the size and the time of seismic events, as well as a number of additional information related to the seismic source.

The results of a seismic analysis can significantly affect decisions pertaining to:

- evaluation of the current state of a particular section of a mine at a given time;
- improvement of current mine planning practices;
- identification of seismically active geological features;
- identification of sources of instability near mining openings;
- evaluation of the effects of destress blasting practices;
- *calibration* of numerical models for mine design purposes.

A number of seismic systems, MP250 or full waveform, are currently operating in Canadian Mines. However, regardless of the microseismic system, in order for a seismic analysis to have the desired impact on a mine operation, it needs to be linked with the overall mine geometry, current mining sequence, and available knowledge of the mine geology. Dealing with seismic data accumulated over a period of years can be a particularly tedious task, requiring the existance of a seismic database. Visualization of the results is currently being conducted with plots of seismic events on level plans or sections using symbols to represent seismic event locations. Although this process may be adequate when dealing with a small number of data, it is not adequate to visualize the spacial distribution of a large number of seismic events or the parameters that are associated with them. A utility that enables such analysis is presented here.

DESCRIPTION OF THE DENSITY UTILITY

EDEN2 is a software utility than facilitates the determination of two and three dimenional relative density of parameters such as the event or the energy density. Density of other parameters provided by full waveform microseismic systems can also be calculated. The sequence of steps followed using the *EDEN2* program is shown in Figure 1.

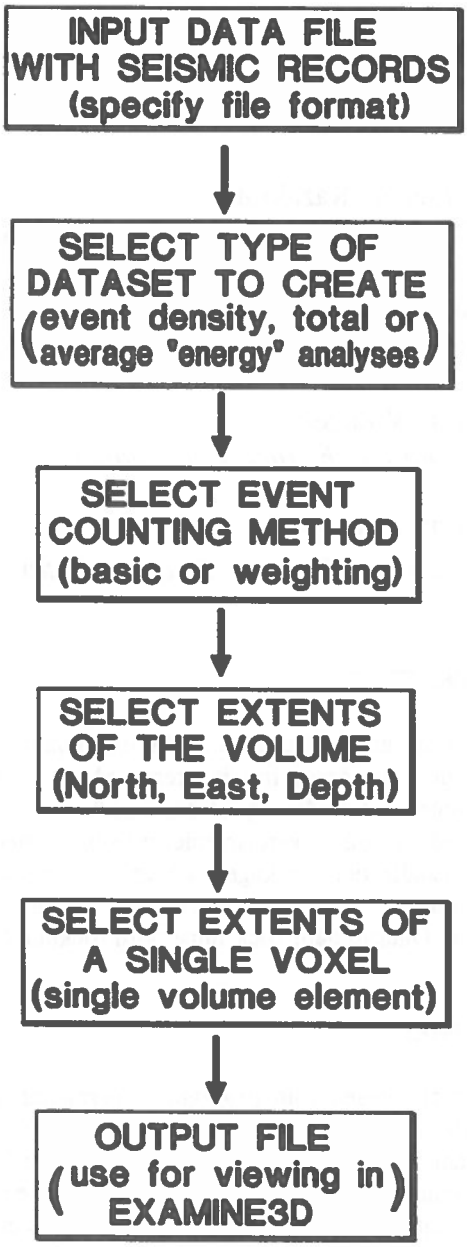

Figure 1: Sequence of steps followed using the *EDEN2* software utility

The user can choose the data set to be created based on three analyses that are supported by the utility: the event density, the total *"energy"* density, and the average *"energy"* density. With the event density the user can obtain a picture of the concentration of the seismic activity, independently of the size of the events. The total *"energy"* density describes the amount of *"energy"* seismically released per unit volume. Since the user usually is interested in a relative comparison of the contoured parameter, this parameter can be the energy contained in the waveforms, the size of the events or the number of transducers triggered. The average *"energy"* density represents the average size of events per unit volume. The energy contained in the waveforms, the size of the events or the number of transducers triggered, can be used for the calculation of this relative density. Areas with high average *"energy"* density are indicative of occurence of large magnitude events.

The user can then specify the type of the event counting technique. The basic method calculates the number of events at a grid point by simply counting the events within a single volume element (voxel) centered around the grid point. An alternative method, determines which voxel an event is in, and then weights it to the eight corner grid points using an inverse distance weighting function. The weighting factor is then multiplied by the contoured parameter to get the value added to the grid point. This weighting method tends to smooth out the event density distribution, since there is no binary classification of an event being inside or outside a voxel.

The three dimensional extents of the conducted density analysis and the size of the single voxel are determined by the program, based on the extents of the seismic record coordinates, or alternatively, can be specified by the user. The *EDEN2* program then proceeds in creating an output file which can be read directly into *EXAMINE*^{3D} (Curran and Corkum, 1994) for viewing, using SVGA resolution. Mine geometry, geological structural features and results from other analyses (e.g. numerical modelling) can be superimposed in the same views. Plotting of the views can be conducted using a postscript file format or alternatively a screen capture software.

EXAMPLES

EXAMPLE 1: Comparison between Seismic Density and Visual Observations:

Seismic activity associated with an orepass failure at INCO's Creighton Mine was analysed as shown in Kazakidis and Morrison, 1994. The data from the MP-250 system were processed through ADASLS, a source location algorithm (Ge and Mottahed, 1993), in order to improve the accuracy of the location of the events. A total of 12,700 microseismic events were found to be located in the vicinity of the orepass during a three year period. Hang-ups within the orepass that caused production delays, became common during the same time. When a laser scanline survey was conducted, it revealed that the ore pass had expanded from 2 to 17 metres (6 to 50 feet) at mid-height, while it maintained its integrity near the top and bottom (Figure 2).

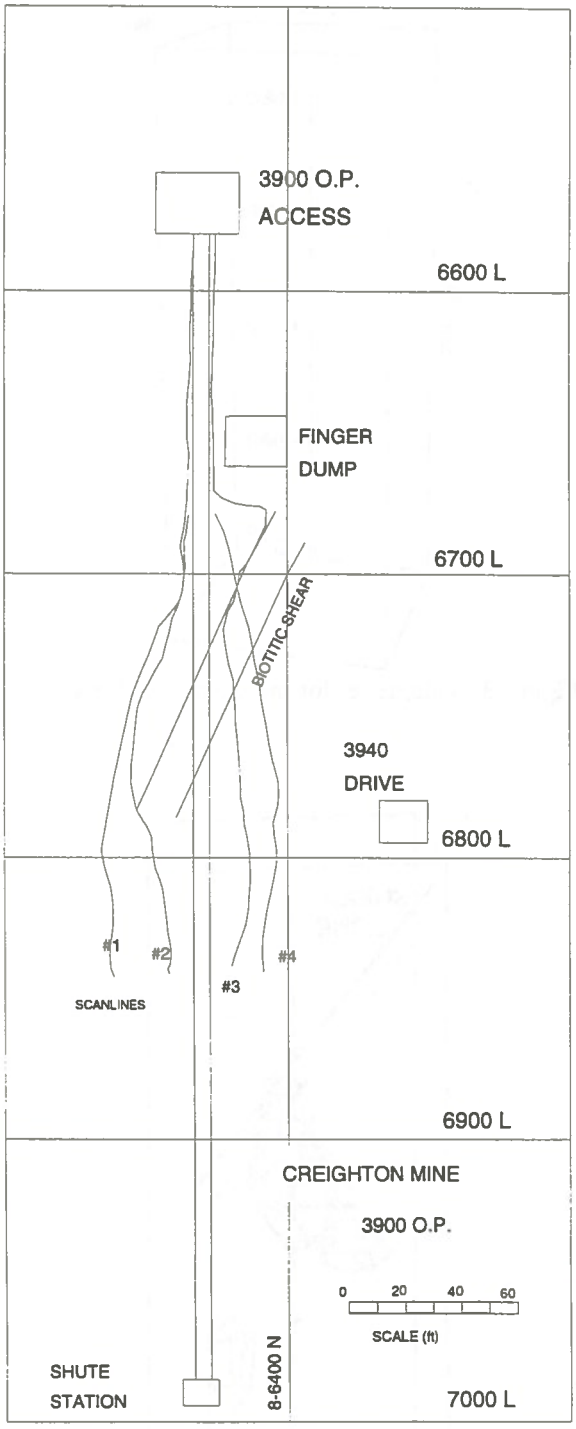

Figure 2: Laser scanline survey down the 3900 ore pass

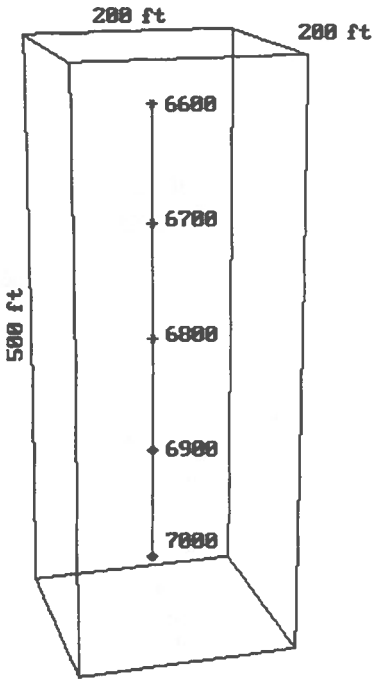

Figure 3: Volume set for the seismic analysis

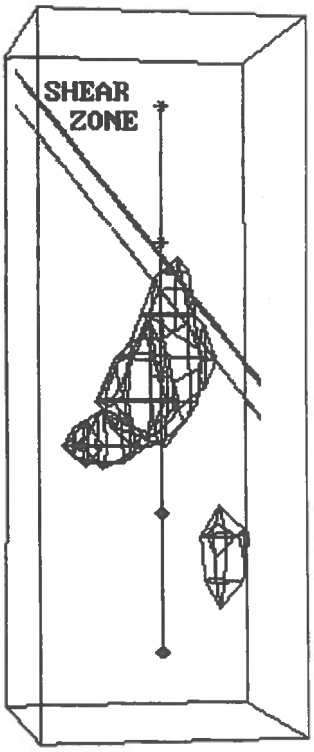

Figure 4: Event density contouring at the ore pass looking NW

Event density contouring was conducted using the available seismic records and *EDEN2* for a 61 x 61 x 152 metre area (200 x 200 x 500 feet) around the orepass and an 8 metre voxel (25 feet) (Figure 3). The results of the analysis are indicated in Figure 4. It can be seen, that, most of the microseismic activity (higher event density) was concentrated in the same area where ore pass failure was observed. Seismic density analysis was able to indicate the area of failure around the pass walls. Therefore, such analyses can be used to identify the state of an orepass before this starts creating operating problems by rapid expansion.

EXAMPLE 2: Comparison Between Seismic and Energy Densities:

The seismic density at a level of Creighton Mine was examined here for the period between April and August 1993 (Punkkinen, 1993 and Kazakidis, 1994). MP250 seismic data from Creighton's mine-wide array were used in the analysis for an area 17 metres (50 feet) above and below the level. A total of 18,600 events were found to be located within the area. In addition to the location of the events within the considered volume, the number of triggers per seismic record were used as a relative indicator for the size of the events.

The event density, total phone density and average phone density were calculated using *EDEN2* and the results were plotted in *EXAMINE*^{3D}, as shown in Figures 5, 6 and 7 respectivelly. It can be seen that both the event and the total phone density distributions (Figures 5 and 6) are similar, indicating that most of the seismic activity is located in the footwall of the level (i.e. South). It also revealed that some microseismic activity is located in the NW quadrant of

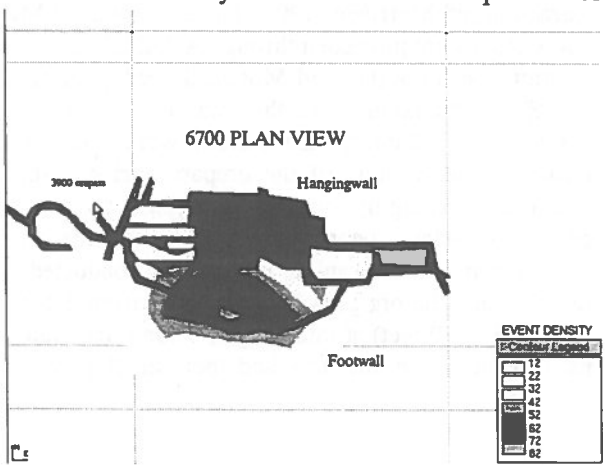

Figure 5: Event density

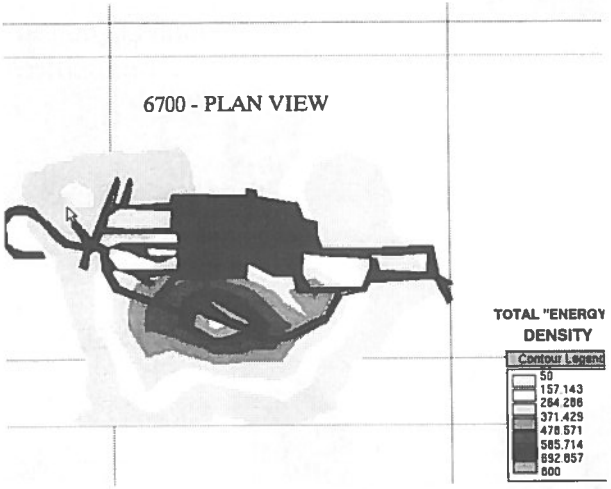

Figure 6: Total transducers triggered density

this level, where the 3900 ore pass exists (refer to the history of failure examined in the previous section, Example 1).

A completely different picture can be seen in the average phone density plot of Figure 7. Different areas are indicative of high average phone density and therefore large seismic events. The high density deep in the hangingwall (i.e. North) is, most likely, associated with the hangingwall shears with historical large magnitude event seismicity (up to m_N of 4).

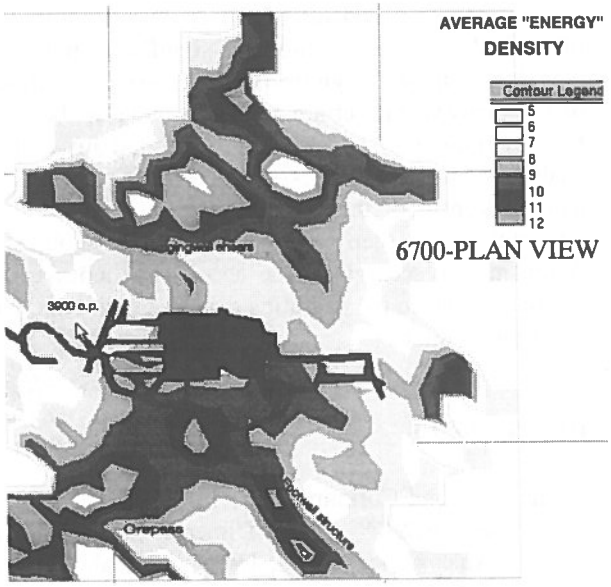

Figure 7: Average transducers triggered density

There are three high density areas in the footwall:

- the one associated with the 402 orepass (a m_N 2.3 event occurred in the area);
- the footwall ramp (a m_N 2.0 event occurred in the area) which has already indicated high concentration of small events using the event density analysis; and
- the one near a footwall structure.

Please note that there is no high density contouring in the vicinity of the 3900 orepass, since only low magnitude events were associated with this seismic activity.

The density analyses conducted here were able to indicate both the location of high microseismic activity, as well as the areas where large magnitude events occurred in association with the mine geometry (mining zone, development, orepasses) and geological structure. Such information can provide important input to mine design analyses pertaining to stope sequence, as well as location and support of mine openings.

EXAMPLE 3: Mine-Wide seismicity:

The seismic event density at Creighton Deep for the period between August 1993 to February 1994, was examined using *EDEN2*. The results were viewed with respect to the mine geometry as shown in Figure 8. It can be seen, that there are two main seismic clusters in the mine: one in the footwall between the 6800 and 6900 evels, and the other one in the Southeastern corner below the 7000 level. Location and density of large events with magnitude greater than m_N 0.5 are also superimposed in the same Figure. It can be seen that there is no clear correlation between large events and microseismic activity, except perhaps the events at the Southeastern corner below the 7000 level. One interpretation to this observation is perhaps that small events are closely related to the mine geometry while large ones to the existence of structural features.

The above analysis provides a means to explore the behaviour of the rock mass to mining for a certain time interval. The results can be used to evaluate current mine design practices, identify historical sources of instability and *calibrate* numerical models.

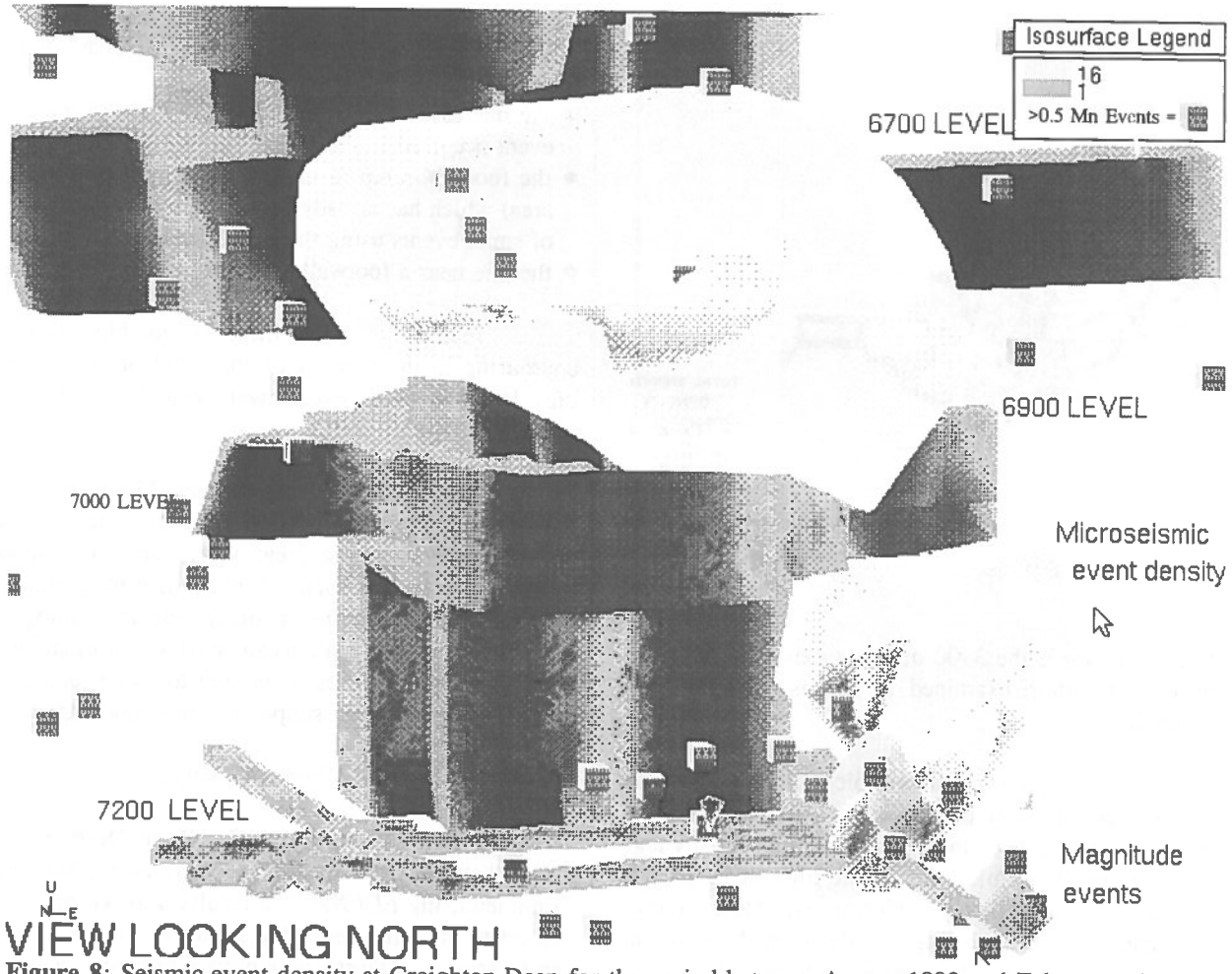

Figure 8: Seismic event density at Creighton Deep for the period between August 1993 and February 1994.

CONCLUSIONS

An *"easy to use"* software utility for seismic event density was demostrated through a number of case studies. Different types of information can be obtained by the three density analyses proposed here. In the examples included in this report, MP250 seismic data were used to demonstrate the operation and the applicability of the utility. However, should different seismic parameters be available (e.g. through full waveform system analyses), their spacial distribution can also be determined using the same utility.

It is recommended that the seismic density analysis be carried out when large amounts of seismic data are available. Application of *intelligent* source location software and errospace analyses can significantly improve the quality of the seismic event locations.

Monthly updates of the seismic density in a mine wide scale can provide significant input to planning or mine design decisions. Historical analyses of seismicity within certain areas of a mine can be used for descriptions of occurrences of ground instability, analysis of the key factors that control that instability and assessment of the current mine design practices. Alternatives can then be explored and be applied to future mining scenarios. The above can improve the safety and reduce the operating cost of an underground burst-prone mine.

REFERENCES

Curran, J.H and Corkum, B.T., 1994
EXAMINE^{3D} - Three Dimensional Excavation Analysis for Mines, Users' Manual, Version 2.2, 181 p.

Ge, M and Mottahed, P., 1993
An Automatic Data Analysis & Source Location System (ADASLS), In Rockbursts & Seismicity in Mines, Young (Ed.), Balkema, pp. 343-347.

Kazakidis, V., 1994
Seismic Density Analyses Using the EDEN2 Utility, MRD/CRRP report, 9 p.

Kazakidis, V.N. and Morrison, D.M., 1994
Analysis of Key Factors Affecting Ore Pass Stability in Highly Stressed Rock Masses: A Case Study, Proc. The 1994 ISRM Int. Symp., IV South American Congr. on Rock Mech., Workshop on Applied Rockburst Research, May 10-14, Santiago, Chile, pp. 185-197.

Punkkinen, A. 1993,
Seismicity Contours, Creighton Mine, Internal Report, 6 p.

8.

rock fragmentation
fragmentation du roc

CAMI'95: 3rd Canadian Conference on Computer Applications in the Mineral Industry
Montréal, Québec, Canada, October 22-25, 1995

Numerical Modelling of Stress-Field around Nested Blastholes

R. Yang and B. Mohanty
McMasterville Technical Centre, ICI Explosives Canada, McMasterville, Québec

Abstract

A variety of wall-control blasting practices is in use today. The more precise fracture-plane control blasting techniques, although not in common practice yet, promise to provide superior wall-control results. This paper examines the mechanics of fracture-plane control for one such technique, the *'equivalent notched hole'* design. The technique is based on drilling nested holes which consists of a central large-diameter charge hole flanked by two small-diameter satellite holes without explosives. The resulting fracture plane coincides with the diametral plane of these three holes. Numerical modelling has been carried out to map the stress field in a homogeneous medium in order to determine the locations of stress concentrations and provide blast design guidelines. The various configurations examined are, ratios of charge hole to satellite hole diameter and spacing between charge hole and satellite, for specified explosion pressure in borehole and rock type. The analysis shows that the induced stress concentration at the boundary of the satellite hole could be many times higher than the tensile strength of rock, thus promoting development of co-linear fractures. It also highlights the critical role of charge and satellite diameter ratio and spacing in the fracture plane control design.

Résumé

Il existe déjà plusieurs techniques associées au contrôle de la paroi rocheuse. Des nouvelles techniques de cisaillements engendrées par l'explosif ont été développées récemment et promettent déjà des résultats supérieurs aux méthodes courantes. Cet exposé examine le mécanisme qui contrôle le plan de rupture de la masse rocheuse par une technique surnommée *'Equivalent notched hole'* design. La technique consiste à forer un trou de grand diamètre chargé d'explosifs encadré de deux trous de petit diamètre non chargé dans un même plan. Le cisaillement ainsi créé coïncide avec un plan diamétralement orienté vers ces trois trous. La modélisation numérique a servi à localiser les champs de stress à l'intérieur d'une masse homogène et à reconnaître les endroits les plus affectés par cette concentration. Les configurations examinées sont le ratio des diamètres de forage utilisés et les espacements requis entre les trous chargés et les trous satellites, et ce pour des pressions explosives spécifiées dans une masse rocheuse connue. Les analyses démontrent que la concentration de stress aux frontières des trous satellites dépasse de beaucoup la force en tension du roc et provoque ainsi un développement accru de fissures co-linéaires. L'exposé indique comment le design primaire versus le choix des diamètres et des espacements peut avoir un rôle critique dans l'établissement du plan de cisaillement.

Introduction

Control of overbreak by means of specialized drilling and blasting techniques is important and an increasingly integral aspect of all blasting operations. However, the traditional approaches to designing wall-control blasts do not incorporate the precision required for controlling blast-generated fracture planes to satisfy the present needs in large scale mining operations. These techniques are variously grouped under the following blasting practices; line drilling, pre-splitting, cushion blasting, and buffer blasting. In line drilling a plane of weakness along the limit of excavation is created by drilling closely spaced, small diameter holes which may or may not contain any explosive. Pre-splitting is a more cost effective variation, whereby, 50 mm to 100 mm diameter holes are drilled at 0.6m to 1.2m spacing and each loaded with special explosive charges. However, the bulk of the wall-control blasts today, especially in medium to large hole applications, are carried out by means of cushion or buffer blasting. In the former, the boreholes drilled along the excavation limit are loaded lightly with explosives, with the intent of trimming off excess material after the main blast. In buffer blasting the wall-control row of holes is blasted at the same time as the main production blast. The modifications to the buffer row usually involves a reduction in burden and spacing and the explosive load in these holes.

The primary objective in all these techniques is to reduce the explosive energy density or shock in the borehole by means of lower explosive load or decoupling the explosive column from the borehole wall, and thereby minimize overbreak. Through optimum blast design and choice of explosives, it is possible to achieve a very high degree of fracture plane control in small diameter applications, as in tunnelling and construction projects (Gustafsson, 1981; Persson et al, 1993). However, in large diameter applications in stoping and open pit, the degree of wall-control achieved often falls far short of design. This is largely due to the compromises made in design and loading of the buffer row, which typically is loaded only in the toe region, and occasionally supplemented by the use of air decking above the charge. To obviate these compromises, two novel approaches based on fracture-plane control techniques, have been proposed and tested in the field with considerable success. The fracture-plane control technique involves modifying the boreholes so as to guide the propagating fracture along a specified direction. The simplest means of achieving this control is through diametral notching of the borehole (Holloway et al, 1987). An alternate method is to replace the notched hole by a nest of three holes described as the 'equivalent notched hole' (Mohanty, 1990a). This paper deals with numerical analysis of the stress field around each nest of holes for quasi-static explosion pressure in the central charge hole.

Equivalent notched hole blast*

In this approach, the equivalent notched hole (Equinox) can be shown to be a mathematical analog of the three notched hole. It consists of a nest of three holes, with the central hole containing the explosive charge being much larger in diameter than the two flanking satellite holes containing no explosives (Fig. 1). The perimeter row of holes employing this technique would consist of a series of these nested holes to provide fracture-plane control.

* U.S. Patent No. 4,690,058

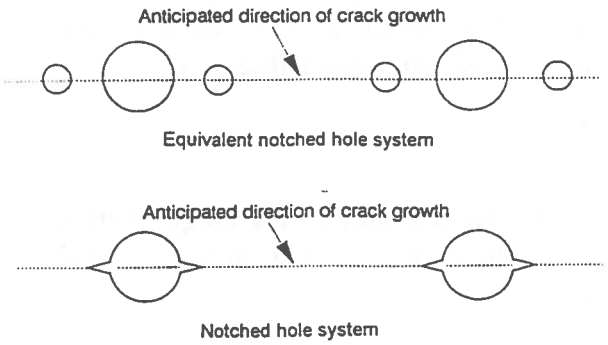

Fig. 1 Equivalent notched-hole system vs. true notched-hole system

The main advantage of this approach over others is that it requires no specialized drilling except for the small diameter satellite holes, and normal production holes can be employed as the charge holes. In the Equinox design, the explosive column is usually decoupled from the borehole wall. The degree of decoupling, type of explosive, borehole diameter ratio and spacing critically govern the outcome of the blast. Field trials supported by extensive laboratory studies in plate models have shown it to be a very promising technique (Mohanty, 1990b).

Numerical modelling of stress field

In the finite element method, the complete problem area or volume has to be discretized. Consequently, it fails to achieve fully continuous variation of stress and displacement in the problem region. In contrast, in the boundary element method, for a homogeneous and isotropic material it is necessary to discretize only the excavation boundary. Thus, fully continuous variation of stress and displacement can be calculated in the problem region. Any discretization errors are therefore induced at the boundaries only (Beer and Watson, 1992). Furthermore, boundary element method has certain advantages over finite element method in modelling blasting problems. It is much simpler to discretize the boundary of holes and free faces than to generate a finite element mesh over the complete problem area, especially in modelling multiple holes.

In this analysis, a 2-dimensional plane strain Indirect Boundary Element program (EXAMINE^{2D}) is used to compute the stress field. It is designed to be a quick and simple-to-use parametric analysis tool for investigating the influence of geometry and in situ stress variability on the stress changes in rock due to excavations (Curran and Cockburn, 1992). For modelling purpose, the rock is assumed to be an average type with the following elastic properties; Young's modulus: 40 GPa, and Poisson's ratio: 0.30. To simulate the blasting process, it is assumed that the explosive upon detonation in borehole exerts a quasi-static pressure of 2 GPa uniformly along the borehole wall. The actual pressure developed in the borehole will depend on the explosive (its detonation velocity and density) and the degree of decoupling. For a fully coupled explosive such as ANFO (Ammonium Nitrate/Fuel oil: 94/6) in 200 mm diameter borehole, the detonation pressure could exceed 4 GPa. Although the latter is very short-lived, the borehole is pressurized for a considerably longer period due to expansion and containment of the high pressure explosion gases resulting from detonation in the borehole. Therefore, assumption of a quasi-static explosion pressure in the borehole is considered a realistic approach in illustrating the stress field around the borehole. The same applies to the treatment of target rock as being an elastic body as the high borehole pressure decays extremely rapidly as one moves away from the borehole. In dealing with multiple nests, it is assumed that all the charge holes detonate exactly at the same time.

Case I. Nested holes of equal diameter

The stress field has been calculated as a function of spacing (centre of charge hole to the inside boundary of satellite hole) for two borehole diameters (100 mm and 200 mm). Fig. 2 shows the ratio of tangential stress at the boundary of the central hole along co-linear direction of holes to that on a line perpendicular to it as a function of spacing. The presence of the two satellite holes results in the tangential stress along the co-linear direction being much greater than in a direction normal to it resulting in a propagating fracture along the common diametral plane of the three holes. In the case treated, all three holes are charged with explosives and assumed to detonate simultaneously. With increasing spacing, this ratio tend to unity, as expected. However, for close spaced holes in a nest, this stress 'amplification' could exceed 200% of the value obtained without satellite holes.

Case II. Nested holes with large central charge hole flanked by two small diameter holes.

The effect of varying charge hole diameter to the satellite hole diameter ratio on the stress field is shown in Fig. 3, for a constant web thickness (i.e. width of rock between the boundaries of the charge and the satellite hole). It shows that the tangential stress (tensile) along the preferred direction rises rapidly as the ratio of diameters is increased. The rate of increase of the tensile tangential stress slows down after a ratio of ~4, although the former keeps rising in absolute terms.

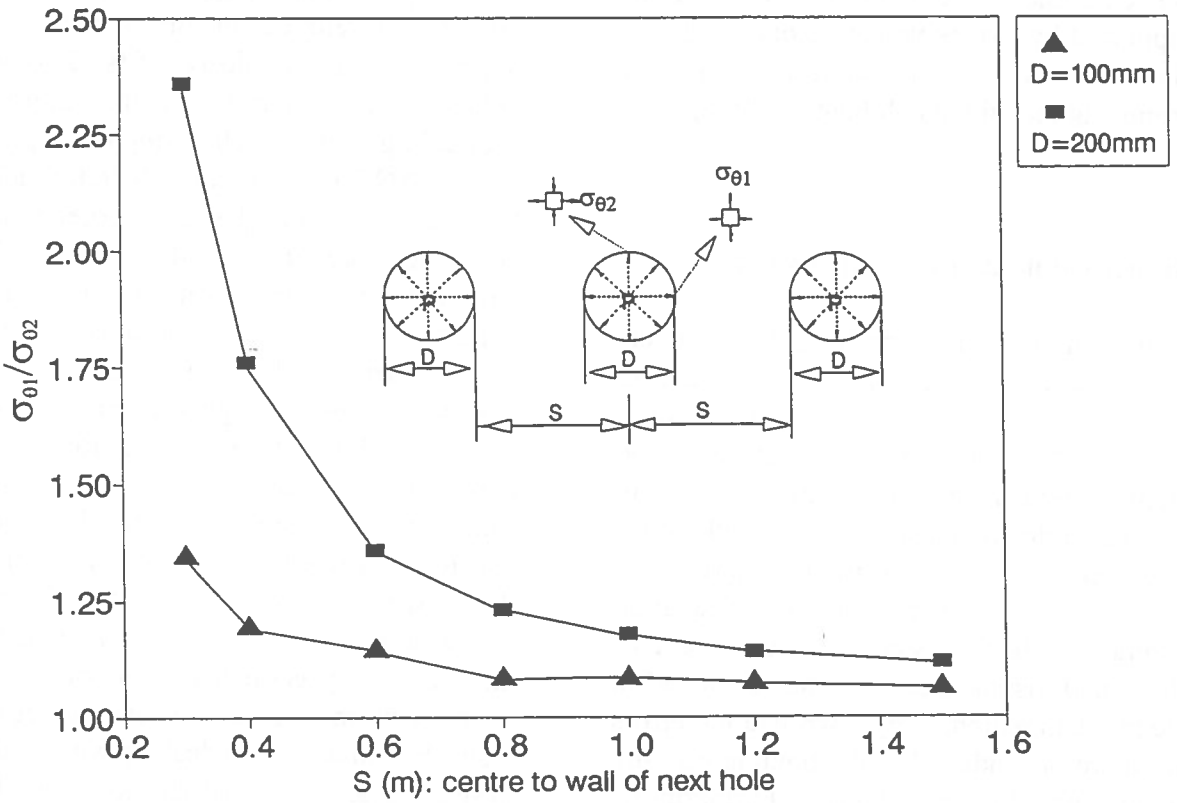

Fig. 2 Ratio of tangential stress at the boundary of the central hole on the co-linear direction of holes to that on a line perpendicular to it as a function of spacing.

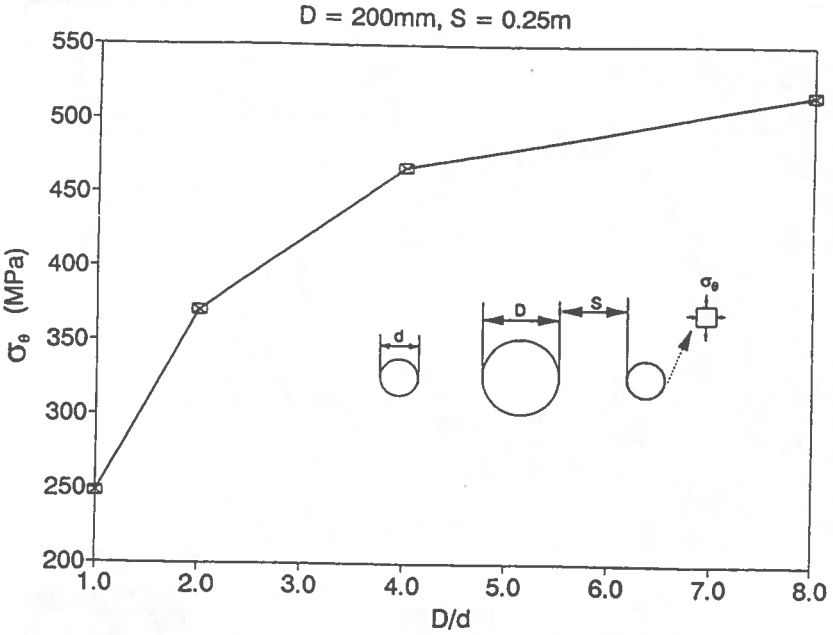

Fig. 3 Effect of varying charge hole diameter to the satellite hole diameter ratio on the tangential stress of the outer boundary of the satellite hole.

A variation of the above condition is plotted in Fig. 4, which shows the tangential stress (tensile) on the outer boundary of the satellite hole as a function of web thickness for three satellite hole diameters. It is seen that for only small web thickness there is significant advantage to having much smaller diameter satellite holes; for web thickness approaching

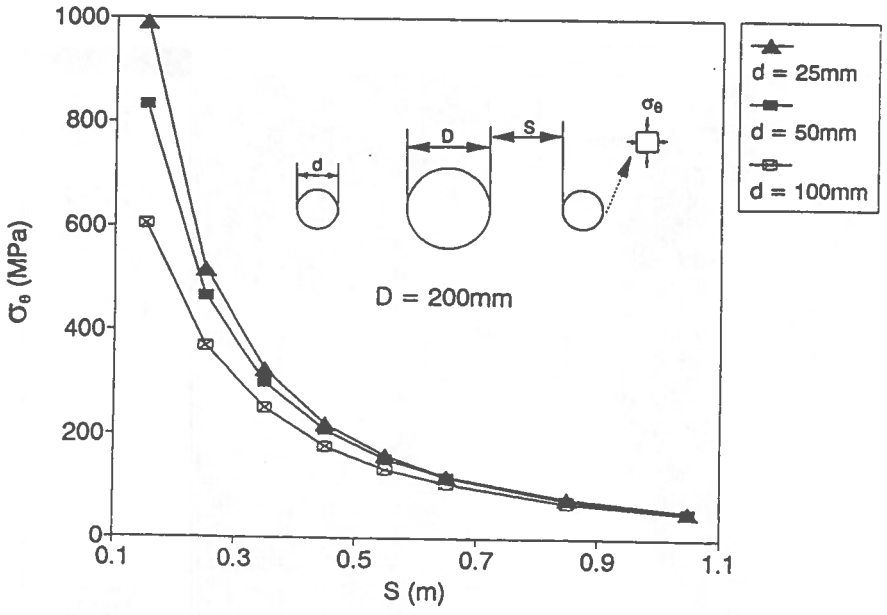

Fig. 4 Tangential stress on the outer boundary of the satellite hole as a function of web thickness for three satellite hole diameters.

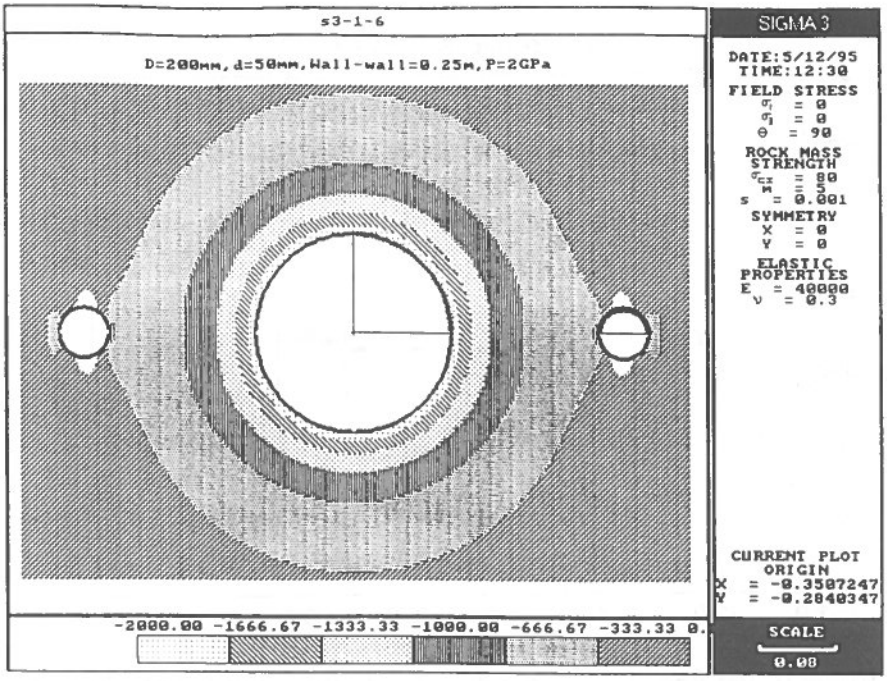

Fig. 5 Tangential stress field around an equivalent notched-hole system.

4 x charge diameter the amplitude of radial stress becomes more or less independent of the satellite hole diameter. However, for web thickness measuring 2 x charge diameters or less the stress concentrations are significantly higher for small diameter satellite holes than large ones. The 2 x charge hole diameter distance also represents a very practical range in terms of drilling, as this translates into a distance of 0.6m from the boundary of a 300 mm diameter hole.

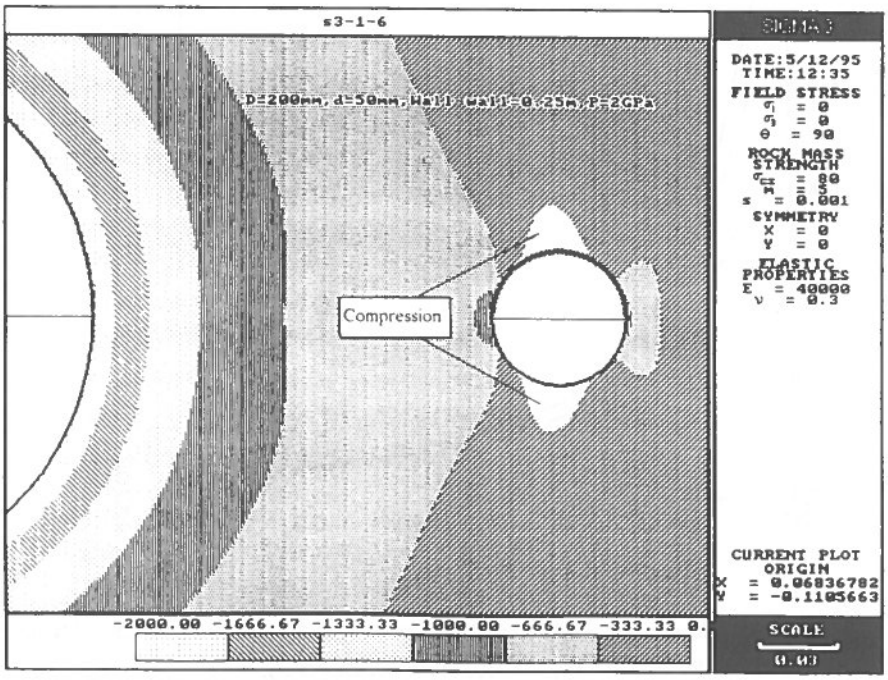

Fig. 6 Expanded view of tangential stress field around a satellite hole.

Case III. Stress field surrounding the nested holes with large pressurized central hole.

The complete tangential stress field around the nested holes is shown in Figs. 5 and 6. The tangential stress is everywhere tensile, except in the perpendicular direction at the satellite hole where it is compressive. For the configuration shown (charge hole diameter: 200 mm, satellite hole diameter: 50 mm, hole separation (web thickness): 0.25m, and borehole pressure: 2 GPa), the tensile zone extends well beyond the satellite hole. In the immediate vicinity of the outer boundary of the satellite hole, it measures in excess of 600 MPa, and beyond in excess of 300 MPa. These values are of course proportional to the initial borehole pressure chosen. By suitable decoupling of the explosive column from the borehole wall in the charge hole, the effective borehole pressure can be reduced by an order of magnitude or more. In this case, the tensile stress at the outer boundary of the satellite hole and co-linear with the charge hole would still be in excess of the average tensile strength of target rock.

The radial stress field for the same configuration is shown in Fig. 7. As expected, the stress field around the charge hole is all compressive. However, there is still a tensile component along the co-linear plane at the satellite hole boundary. This further augments the tensile zone around the satellite holes and, promotes the development of the desired fracture plane.

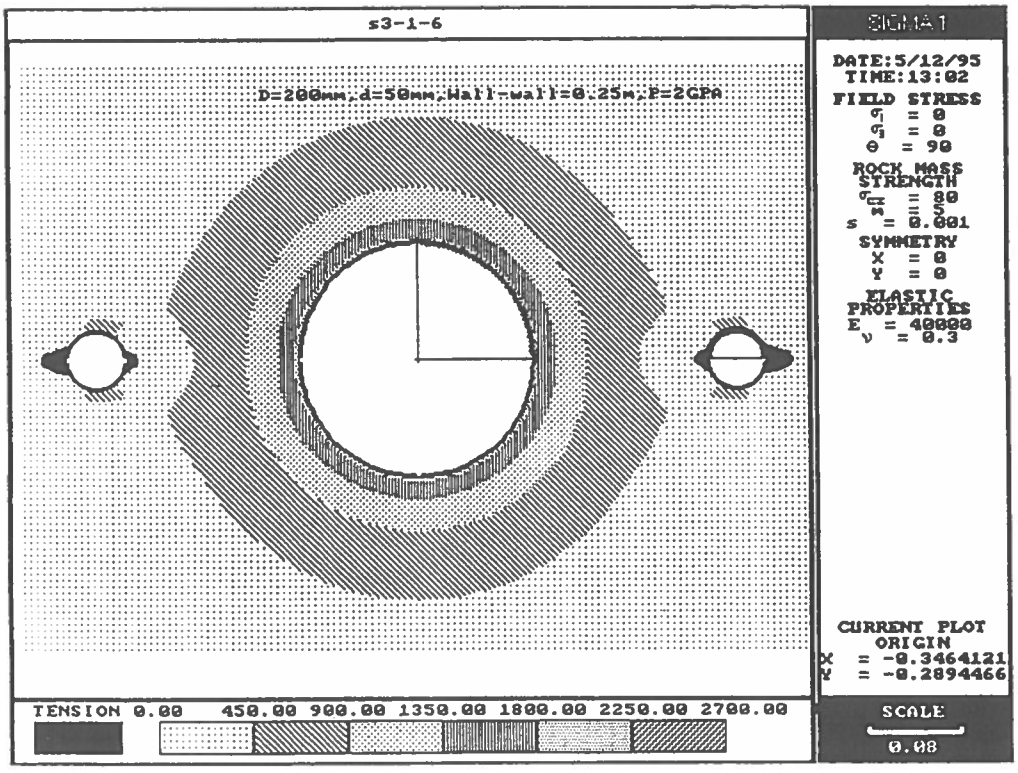

Fig. 7 Calculated radial stress field around an equivalent notched-hole system.

Conclusions

Numerical modelling of the equivalent notched hole design has confirmed the results of experimental investigations. It is now possible to obtain detailed design guidelines for various borehole diameter and spacing combinations. The analysis also showed that for small borehole spacing, significant enhancement of stress concentrations along the preferred direction occurs only when the ratio of the central charge hole diameter to that of the satellite hole is sufficiently large. The optimum range is shown to be about 3 to 5. For large diameter central charge holes this still translates into a practical range of borehole spacings which would allow easy and accurate drilling of the small diameter satellite holes. For a 200 mm charge hole and a 50 mm diameter satellite hole, this spacing could be in excess of 0.5m.

The present analysis on controlled fracture along a preferred direction applies to a homogeneous and isotropic rock. It would be necessary to extend the work to rock with joint planes and in situ stresses to obtain corresponding blast design guidelines for more typical rock mass.

References

Beer, G. and Watson, J.O.; *Introduction to Finite and Boundary Element Methods for Engineers;* J. Wiley & Sons, New York, 1992.

Curran, J.H. and Cockburn, B.T.; EXAMINE^{2D}: Excavation Analysis for MINES - Version 4.0; University of Toronto, 1992.

Gustafsson, R.; *Blasting Technique,* Dynamit Nobel Wien; Vienna, 1981.

Holloway, D.C., Bjarnhold, G., and Wilson, W.H.; A Field Study of Fracture Control Technique for Smooth Wall Blasting: Part 2; *Proc. 2nd International Symp. on Rock Fragmentation by Blasting*; Keystone, Colorado, p. 646-657 (1987).

Mohanty, B.; Explosion Generated Fractures in Rock and Rock-like Materials; *Engineering Fracture Mech.*, vol. 35, p. 889-898, 1990(a).

Mohanty, B.; Fracture-plane control blasts with satellite holes; *Proc. 3rd Int. Symp. on Rock Fragmentation by Blasting*, Australasian. Inst. Min. & Met.; Brisbane; p. 407-412, 1990(b).

Persson, P-A, Holmberg, R., and Lee J.; *Rock Blasting and Explosives Engienering;* CRC Press, Boca Raton, 1993.

Digital Imaging of Blasting Process in Field

Stephen H Chung
Technical Services, ICI Explosives Canada Inc.

ABSTRACT

Direct visualization of rock movement during blasting is an important key to understanding the blasting process, as well as optimizing blast designs and explosives performance. To achieve this, a digital camera system (HSIS-500) has been built. It is a custom made high speed solid-state camera employing an advanced charge coupled device(CCD) and dynamic random access memory (DRAM) technologies. It handles like a regular video camera but requires no film or tape as the image is recorded in digital form on memory chips and transferred to the system hard disk for storage. The system consists of two components: the camera body and hardware, and the image processing unit. The imaging rate is fixed at 425 frames/s; it can also be used in the single frame mode. The recording duration can be set at 5, 10, 15 and 20 seconds. The camera can be triggered manually or by wireless remote control, and is capable of recording transient images in extremely low lights. The captured images can be displayed immediately on a video screen or a computer monitor. The system image analysis software can be run in the field for a quick preview. The full features of the software allows the detailed motion digitization in Windows™ for obtaining target displacement as well as velocity.

The system has been in use for over a year in several mines and quarries under extreme weather conditions (-20° C to +43° C). The paper describes the basic principles and features of the digital imaging system, and its actual use in blast diagnostics and optimization, and in modelling of the blasting process.

RÉSUMÉ

La visualisation directe des mouvements du roc lors d'un sautage est un élément important qui permet de comprendre le processus du sautage, en même temps que d'optimiser le plan de tir et le rendement des explosifs. Pour effectuer cette visualisation, nous avons fait construire une caméra numérique du nom de HSIS-500. Il s'agit en fait d'une caméra vidéo transistorisée grande vitesse fabriquée sur mesure et utilisant un dispositif à couplage de charge hautement perfectionné (CCD, pour « *Charge Coupled Device* ») et une technique de mémoire à accès sélectif dynamique (DRAM, pour « *Dynamic Random Access Memory* »). L'appareil fonctionne comme une caméra-vidéo ordinaire, mais ne requiert ni pellicule ni bande puisque les images sont enregistrées numériquement sur des puces mémoire et transférées sur le disque rigide intégré à l'appareil pour y être emmagasinées. L'appareil réunit deux composantes, soit une caméra et une unité de traitement d'images. La numérisation se fait à une vitesse de 425 images à la seconde ; on peut aussi se servir de l'appareil en mode mono-image. La durée de l'enregistrement est réglable à 5, 10, 15 ou 20 secondes. La mise en marche peut se faire manuellement ou à l'aide d'une télécommande sans fil. De plus, l'appareil peut numériser des images transitoires à une très faible intensité de lumière. Les images ainsi captées peuvent être affichées instantanément sur un écran vidéo ou un moniteur d'ordinateur. Il est possible de faire tourner le logiciel d'analyse d'images de l'appareil pour visualiser brièvement les prises directement sur le chantier. À sa pleine puissance, le logiciel permet de suivre en détail le mouvement des images numérisées dans Windows[MD] et d'observer ainsi le déplacement de la cible et la vitesse de la détonation.

Cet appareil est en usage depuis plus d'un an dans diverses mines et carrières en présence de températures extrêmes (-20 °C à +43 °C). Le présent exposé définit le principe et les caractéristiques de base de la numérisation d'images. Il décrit également l'utilisation qu'on fait de cette technique pour diagnostiquer, optimiser et modéliser les opérations de sautage.

INTRODUCTION

Digital imaging technology has been developed and applied in the science and engineering research for many years. In the field of still photography, a resolution of at least 512 x 512 is required to match the quality of a photograph. However, in taking a motion picture of a blast at 300 frames per second for five seconds in order to be able to analyze the rock displacement, a total dynamic random access memory (DRAM) of 400 MB would be required. Since DRAM is an expensive item, HSIS-500 was developed using a 128 x 128 CCD sensor to capture blasting events. A fractal transformation is then used to increase the resolution of all captured images for the motion analysis. Although the resolution so obtained may not match the quality of a 16mm high speed film, digital imaging offers the ability to analyze results immediately after the blast.

PRINCIPLE OF CCD IMAGING

In terms of electronics, a CCD can best be described as a series of parallel plate capacitors which store charge. The charge is optically generated by the absorption of photons which are converted into electrical charges in the same manner as a typical photodiode sensor as shown in Figure 1. However, a major difference is that this diode is operated in the integrating mode, not the conductive mode. That is, instead of reverse biasing the diode and constantly sensing the current increase caused by the photons, a CCD photoelement senses the change in voltage induced by the collection of charge in a short period of integration. The period of integration must be shorter than around 100ms due to the fact that the CCD has a temporary space charge depletion layer created by a pulse of negative bias on the diode.

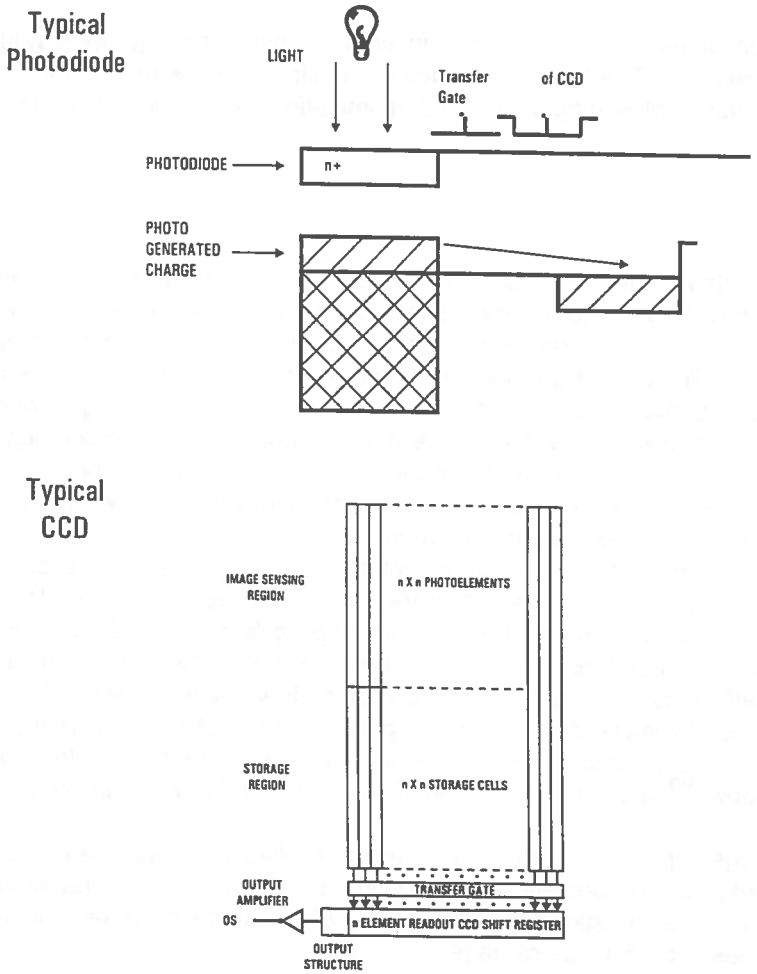

Figure 1: Comparison of typical photodiode and typical CCD

A less technical explanation of a CCD is to describe it as a sensor which is made up of a series of charge buckets which store photons in the form of electrical charge (Figure 2.). Using the bucket analogy, the charge corresponds to a drop of water. The photon to electron conversion is identical to a photodiode sensor which most optical engineers are familiar with. The major difference is that these bucket sensors or CCD photoelements, are arranged in a serial fashion which permits a large number of charge buckets to be poured into the next bucket in a serial fashion. This multiplexing is not possible with a row of photodiodes.

The camera operates the CCD sensor by providing the necessary biasing and clocking information to run the bucket or charge storage capacitors in the correct sequence. The signal charge is converted to a voltage by the sensor which is then amplified and conditioned by the camera. The exact form of the conditioning depends on the options selected.

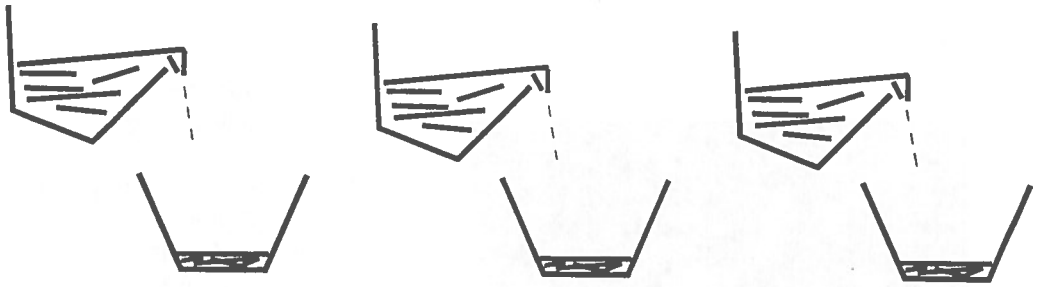

Figure 2: Hydraulic Analogy of CCD Image Sensors

THE IMAGING SYSTEM AND OPERATION

Figure 3 displays the components of the CCD imaging system HSIS-500. The system consists of (1) a high speed CCD sensor; (2) an image processor; (3) a wireless remote control triggering system; and (4) a 12-V rechargeable battery pack.

The system works like a PC. Once it is powered up, the operator may use the pre-programmed keypad to command one of the following tasks with a single key stroke:

1. View a video file and save a user defined portion in order to save storage space.
2. List and delete existing files in directory.
3. Scan disk and recover files that were not completely transferred from DRAM to hard disk due to accidental power breakdown.
4. Download files to other PCs.
5. Go to switch on the CCD sensor for viewing, focusing and standby for triggering.
6. Quit CCD sensing mode and return to normal PC operations: steps 1 to 4 above.

Steps 1 to 4 are DOS based programs designed for effective operation in field. Although the system

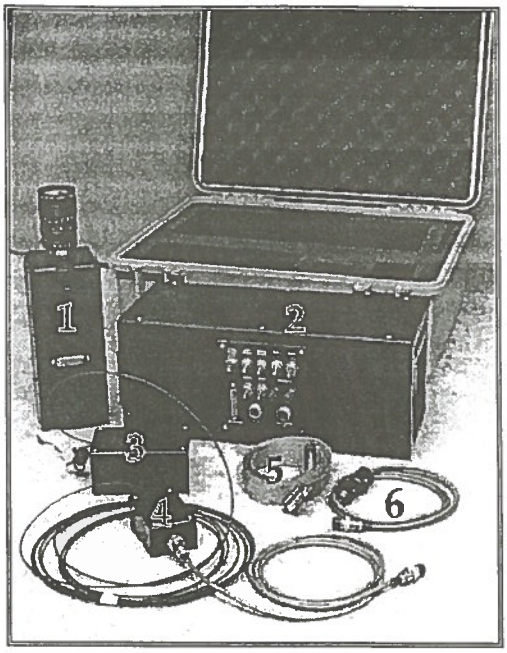

List of Components:
Transport Case

(1) High Speed CCD Sensor
(2) Image Processor (IP)
(3) & (4) Fibre Optic Trigger Receiver System
(5) Ribbon Cable
(6) Power Cord

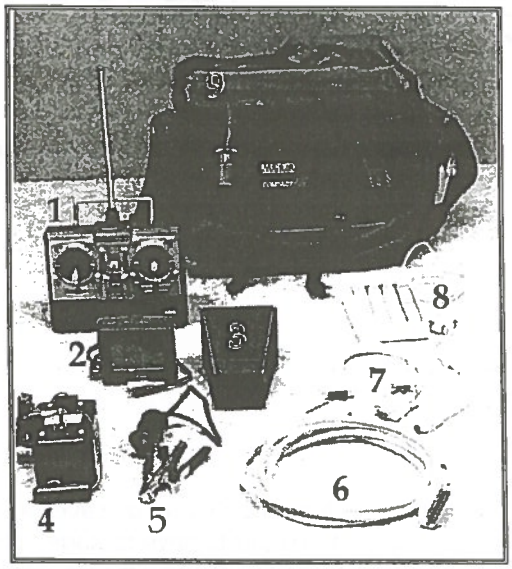

List of Components:
Shoulder Bag.

(1) Remote control trigger box
(2) 3" LCD view finder
(3) View finder visor
(4) Battery charger
(5) Back up power supply cables
(6) Data transfer cable
(7) System set up cables
(8) Keypad
(9) 12V power supply and cable (in shoulder bag)

Figure 3: System components of HSIS500 stored in it's transport case.

itself can be used to perform the analysis, it is recommended to have all the records downloaded to a desktop PC and use the Windows™ based program to do the analysis.

In the standby mode, the CCD sensor starts sampling and transmitting an image every 2.353 ms to both the VGA and video port. For viewing and focusing in the field, one may use the 3" viewing screen or a video camera equipped with a video input.

There are three triggering modes used by the system: manual, wired remote and wireless remote controls. In general, the triggering circuit is normally closed. A break in the circuit will send a signal to the system to start capturing and writing images to DRAM. If the recording timer is set for five seconds, the system will record all frames captured. If the recording timer is set at ten, fifteen or twenty seconds, the CCD sensor keeps the same sampling rate but the Image Processor writes only every second, third or fourth frames respectively. Once the preset recording time has been reached, all the images temporarily stored on the DRAM will be transferred to the hard disk and labeled automatically. All single snap shots taken before and after the blast will be filed under a different name.

REPLAY OF CAPTURED IMAGES

As described in step 1 in the previous section, the captured image can be replayed immediately on the system monitor or on the view finder of a video camera. For the conventional 16mm high speed motion picture, it would take at least a week to send and receive the processed film back before an evaluation of blasting results could be made possible.

It needs to press one single key stroke on the keypad to activate the PREVIEW function. If there are two videos stored on disk, either Video1 or Video2 can be selected for viewing. PREVIEW is a DOS program. It provides the following list of basic functions for editing files in the field:

1. To display histogram of pixel values of a selected frame.
2. To change histogram distribution of pixel values.
3. To select one of two captured videos for viewing.
4. To play a specified portion of the selected video.
5. To play a video forward or backward in a Continuous or Single Frame mode.
6. To save a portion of the video using a user defined file name.

A highly underexposed motion picture, e.g. 3 to 4 stops under normal exposure, would not yield any well defined image for analysis. However, HSIS-500 can capture useful images under the same or even worse conditions since the contrast can be adjusted and enhanced digitally as described in function 2 above. Figure 4 demonstrates an underexposed image and its variations after changing the histogram distribution of pixel values.

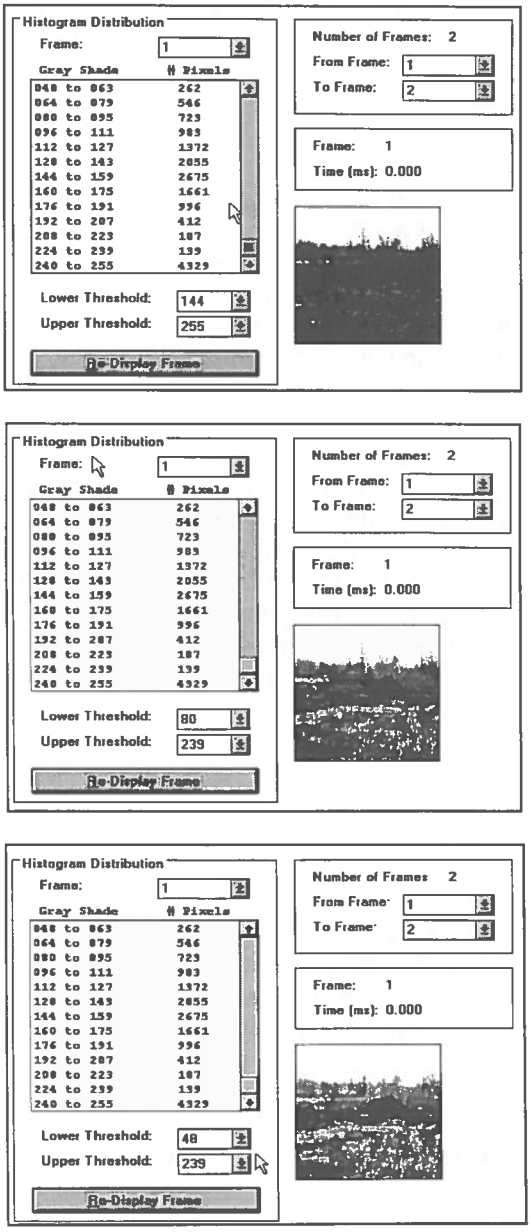

Figure 4: Correction of underexposed image by changing histogram distribution.

ANALYSIS OF IMAGES IN WINDOWS™

The full motion analysis software package runs in Windows™. The minimum hardware configuration for implementing this package includes a 486DX-33 with 8MB RAM (486 DX/2-66 or greater with 16 MB RAM recommended), a graphic card supporting 256 colors and a SVGA monitor. An absolute minimum of 100 MB hard disk is required. However, a hard disk greater than 500 MB is recommended if more than one full video file is to be analyzed.

Once the contrast of a selected raw image has been corrected, all images in the file are converted to PC Paint Brush's PCX format for further enhancement and analysis. Figure 5 shows a PCX image converted from the raw data of 128 x 128 resolution and its enhancements using fractal transformation.

The analysis of rock displacement is demonstrated in Figure 6. Frame 1 shows the scale drawn on the foreground in front of the face. This scale is used in subsequent frames for measuring displacement and velocity. The digitization procedure is straightforward. All digitized results are written to a file in ASCII format as shown in Figure 7.

RESULTS

Figures 8 shows some selected images captured with HSIS-500 from various mines and quarries. The operating condition varies from -20°C to +43°C including rain and snow blizzard.

CONCLUSIONS AND DISCUSSIONS

The HSIS-500 has performed well in the field under severe weather conditions. Digital images can be copied any number of times without changing original quality and can be replayed, enhanced and analyzed immediately. The software run in

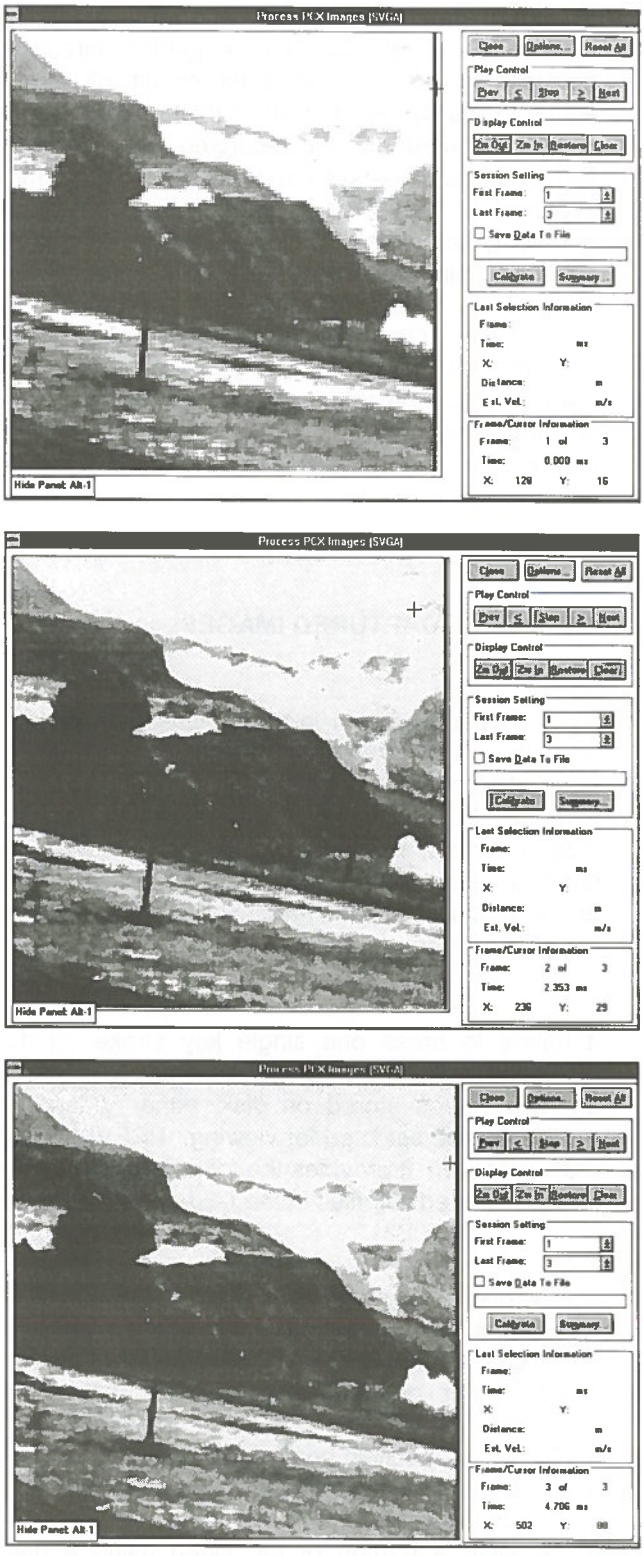

Figure 5: Expanding resolution from 128 x 128 to 256 x 256 and 512 x 512

Windows™ is user friendly, and has most of the features required for the motion analysis work.

Because the size of the CCD sensor is small (about 2 mm x 2 mm), the view of field is somewhat restricted. A change to a wide angle lens should be pursued in order to cover a wider area. The current version of the CAD sensor does not have the anti-blooming feature built-in, therefore it is not suitable for recording bright events such as a flash from the detonating cord over a dark background.

REFERENCES

1. Chung, S. H. et al, " Application of High-Speed Photography to Rock Blasting at Canadian Industries Limited - A Review". 10th Canadian Rock Mechanics Symposium, September, 1975.

2. Dalsa Inc. CCD Image Sensors - 1994 Databook.

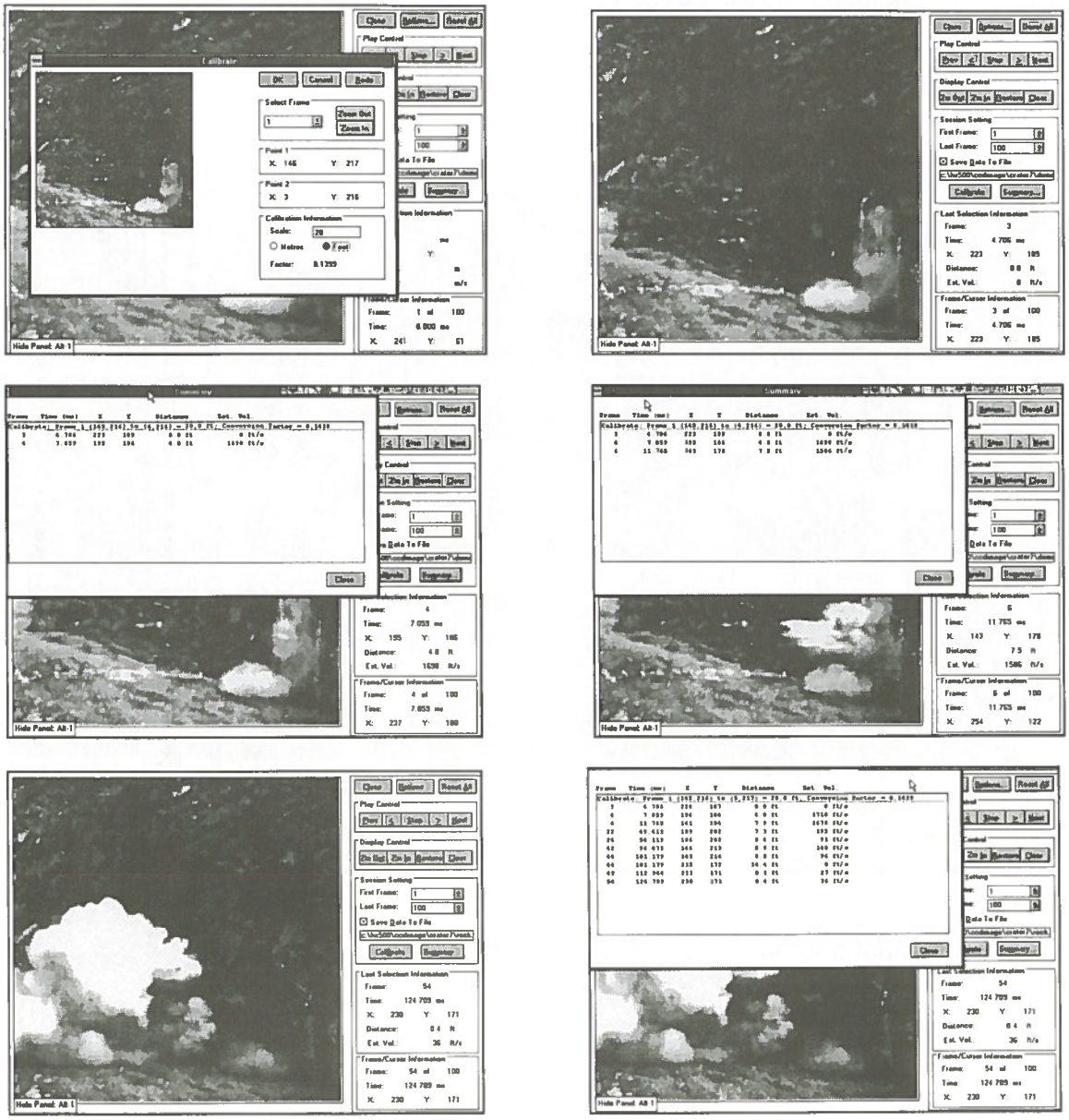

Figure 6: Motion analysis.

```
C:\HS500\CCDIMAGE\CRATER7>type demo.dat
"Calibrate: Frame 1 (145,216) to (4,216) = 20.0 ft; Conversion Factor = 0.1418"
"    3        4.706     223     189         0.0 ft            0 ft/s"
"    4        7.059     195     186         4.0 ft         1698 ft/s"
"    6       11.765     143     178         7.5 ft         1586 ft/s"
"   76      176.475     148     140         5.4 ft           33 ft/s"
"   81      188.240     143     139         0.7 ft           61 ft/s"
"   86      200.005     134     136         1.3 ft          114 ft/s"
"   90      209.417     127     137         1.0 ft          107 ft/s"
"   90      209.417     120     167         4.4 ft            0 ft/s"
"   92      214.123     118     167         0.3 ft           60 ft/s"
"Calibrate: Frame 1 (145,217) to (3,217) = 20.0 ft; Conversion Factor = 0.1408"
"    3        4.706     223     187         0.0 ft            0 ft/s"
"    4        7.059     195     186         3.9 ft         1677 ft/s"
"    6       11.765     140     185         7.7 ft         1646 ft/s"
```

Figure 7: Digitized results saved in ASCII format.

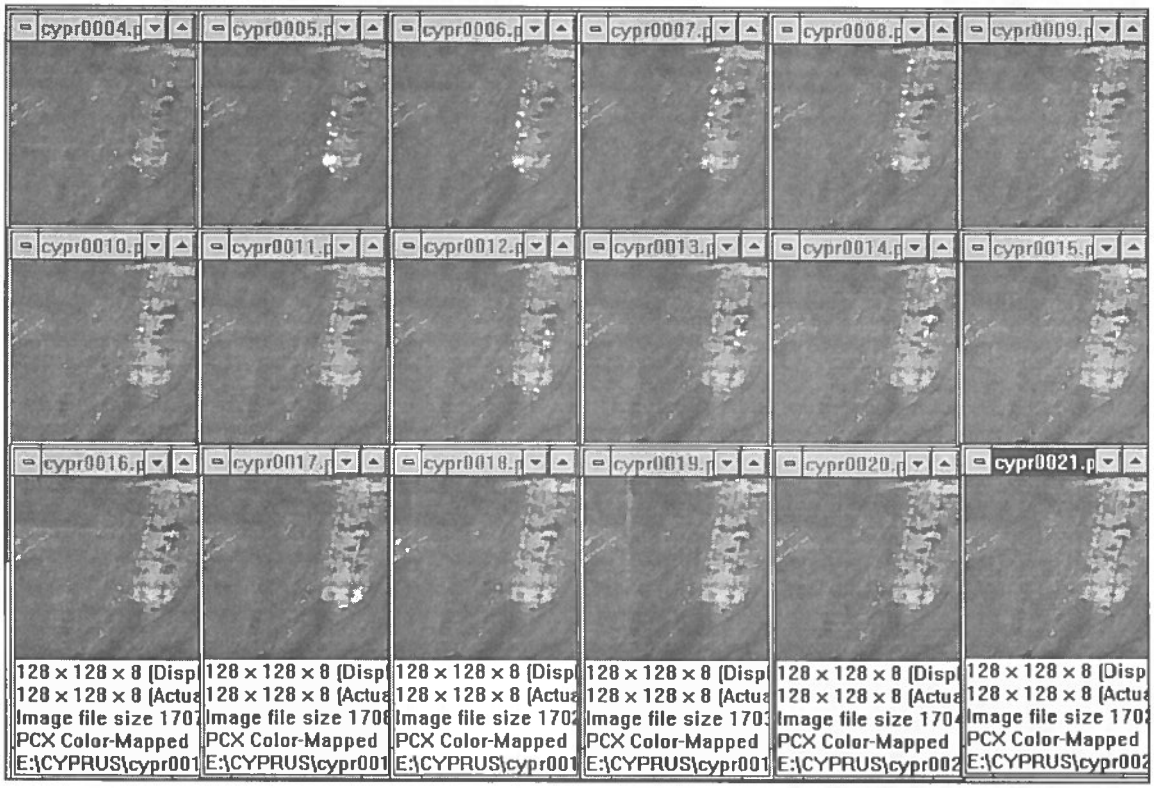

Figure 8a: Blast shot in Phoenix (Sunny, +43^{0}C)

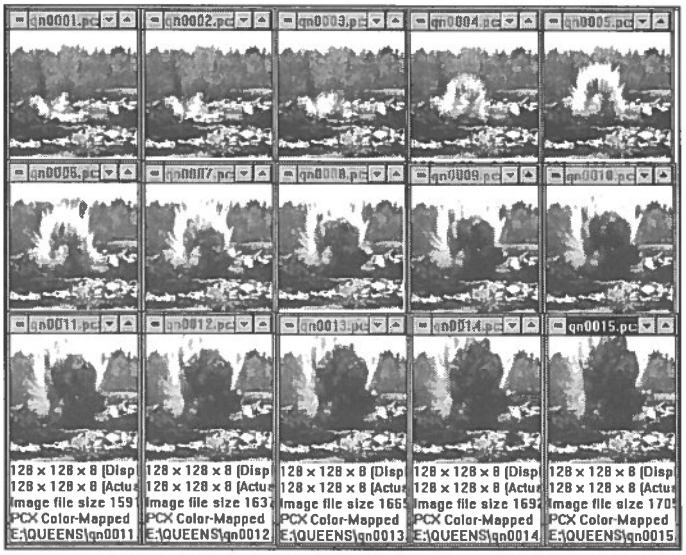

Figure 8b: Quarry shot in Kingston, Ontario (rainy).

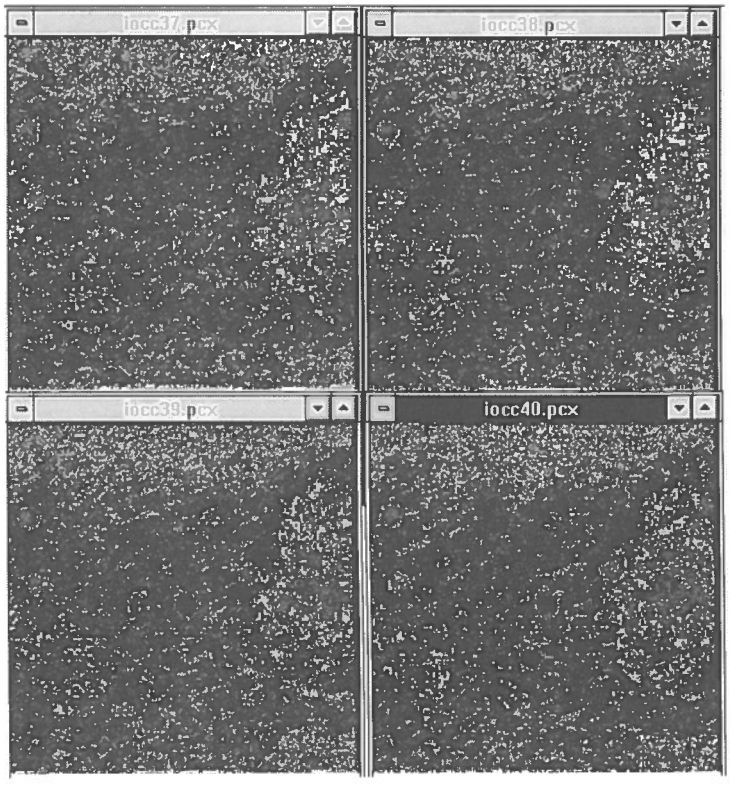

Figure 8c: Shot through snow storm in Labrador City at -20^{0}C. Detonation of trunk line is visible.

CAMI'95: 3rd Canadian Conference on Computer Applications in the Mineral Industry
Montréal, Québec, Canada, October 22-25, 1995

SHOTPlus* Blast Designer

J. Paul Tidman, Brad H. A. Brown
Group Technical Center, ICI Explosives, McMasterville, Quebec

ABSTRACT

To design a blast, one must give consideration to safety, economics, geometry, geology, production needs, and a variety of other requirements. To compare designs requires the time to develop alternatives, analyze, and then improve on them. A number of tools are available to assist with the first set of requirements, however they are poorly integrated. SHOTPlus is a program to improve the efficiency of blasting operations, by combining measurement and blast design tools, and offers the user the time and means to modify designs and explore alternatives.

Working from imported surveys or a defined drill plan, SHOTPlus facilitates the design and evaluation of sophisticated delay sequencing and blasthole charging. The program accesses databases of drilling equipment, initiation products, and explosives, including their performance characteristics. From a completed design, the program reports drill plans, loading charts and hook-up tables for the blasting engineer and the blast crew. Examples of actual applications and output are discussed.

RÉSUMÉ

Pour la préparation d'un tir de mine, on doit considérer, entre autres, la sécurité, l'économie, la géométrie, la géologie et la demande de production. La comparaison des différents scénarios de tir exige des heures pour les faire, les analyser et y ajouter des améliorations. Même s'il existe plusiers outils pour compléter le dessin, ils sont toutefois mal intégrés. ShotPlus est un progiciel qui hausse l'efficacité de gestion des tirs de mine. Il intègre des outils de mesure dans un environnement de DAO, qui permet la modification des dessins et l'exploration d'alternatif dans un environnement convivial.

Utilisant des fichiers électroniques d'arpentage importés ou un plan de forage prédéfini, SHOTPlus rend facile le dessin et l'évaluation des séquences de tirs et le mode de chargement des trous de mines. Le logiciel utilise les basses de données des équipements de forage ainsi que les explosifs et des accessoires de tirs. Une fois le dessin du tir de mine complété, on peut utiliser SHOTPlus pour imprimer une panoplie de rapports tels que le plan de forage, le plan de chargement et le plan de tir ainsi pour assister l'ingénieur en sautage et l'équipe de sautage dans l'élaboration de leur travail. Des examples d'entrée et de sortie sont présentées.

INTRODUCTION

The demand for quality improvement in mining, as in other manufacturing and service industries, is a prime focus for all concerned. Blasting is a critical phase in mining production and as such is often the target for improving efficiencies. The SHOTPlus blast designer software package has been created as a tool to assist blasting engineers who must improve the quality of their blasting operations. SHOTPlus is a full-feature Windows* program which allows the blast engineer to draft a blast design, assign initiating devices for each charge, evaluate the effect of the initiation hook-up on blast performance and report the design for implementation. This paper highlights features and then demonstrates the utility of the program by a few examples.

BLAST DESIGN

As each blast design is created for a specific location in a mine or quarry, the first step is to define the coordinate system. This is done by importing a portion of the mine plan through AutoCAD* DXF*-format files, by importing raw survey data of the site or by establishing arbitrary local coordinates. These are all accomplished through dialog boxes, which speed access even for those unfamiliar with computer operating systems. Once the coordinate system has been established, all hole locations are displayed on a scale plan view of the area. It is possible to pan across or zoom in/out of the plan view at any time in the design phase to find the most useful display.

The next stage in blast design is defining the blasthole location. There are several tools in the Toolbar which can be activated to establish one or more holes. Blastholes are defined by the coordinates of the collar of the hole, the azimuth and dip of the drill hole and the drill diameter. A second feature of a blasthole is the initiating product which will be used to set off the main blasthole charge, the in-hole initiator. This product is chosen from a database containing products available and their technical performance data.

Drilling on blast sites is usually done in regular patterns. In SHOTPlus, a single row or multiple rows can be created through an appropriate dialog box. A very useful feature is the ability to fill an irregularly-shaped polygon with a defined, regular array of blastholes. The location, size and initiation product of any single blasthole or group of blastholes can be edited simply by completing a dialog box.

The blast design is not complete until all the holes in the blast have been connected or hooked up using more initiating products on the surface. This is accomplished by selecting products compatible with the existing in-hole initiators and then pointing to the holes to be connected in sequence. The various tools used to accomplish these tasks are shown in Figure 1, including basic Windows features such as menu, action, and status bars, an edit window, and a floating Toolbar.

DATABASE

The SHOTPlus program has been designed to access a secure database of products and their technical performance data. The drill database contains information on drill production rates and diameter ranges. The initiating product database includes both electric and shock-tube initiating systems, nominal delay times and factory test results on the delay scatter statistics. Explosive product entries permit completion of the blast design for the physical blast predictions which are calculated in another program, SABReX*.

REPORTING

A given blast design may be reported at several different levels, depending on the information needed. Scale plots of most displays are available, with Blast Hole Data and Ties Legend options. Selected elements or the entire design can also be exported as, for example, a DXF-format file to include the drill pattern in the mine planning database.

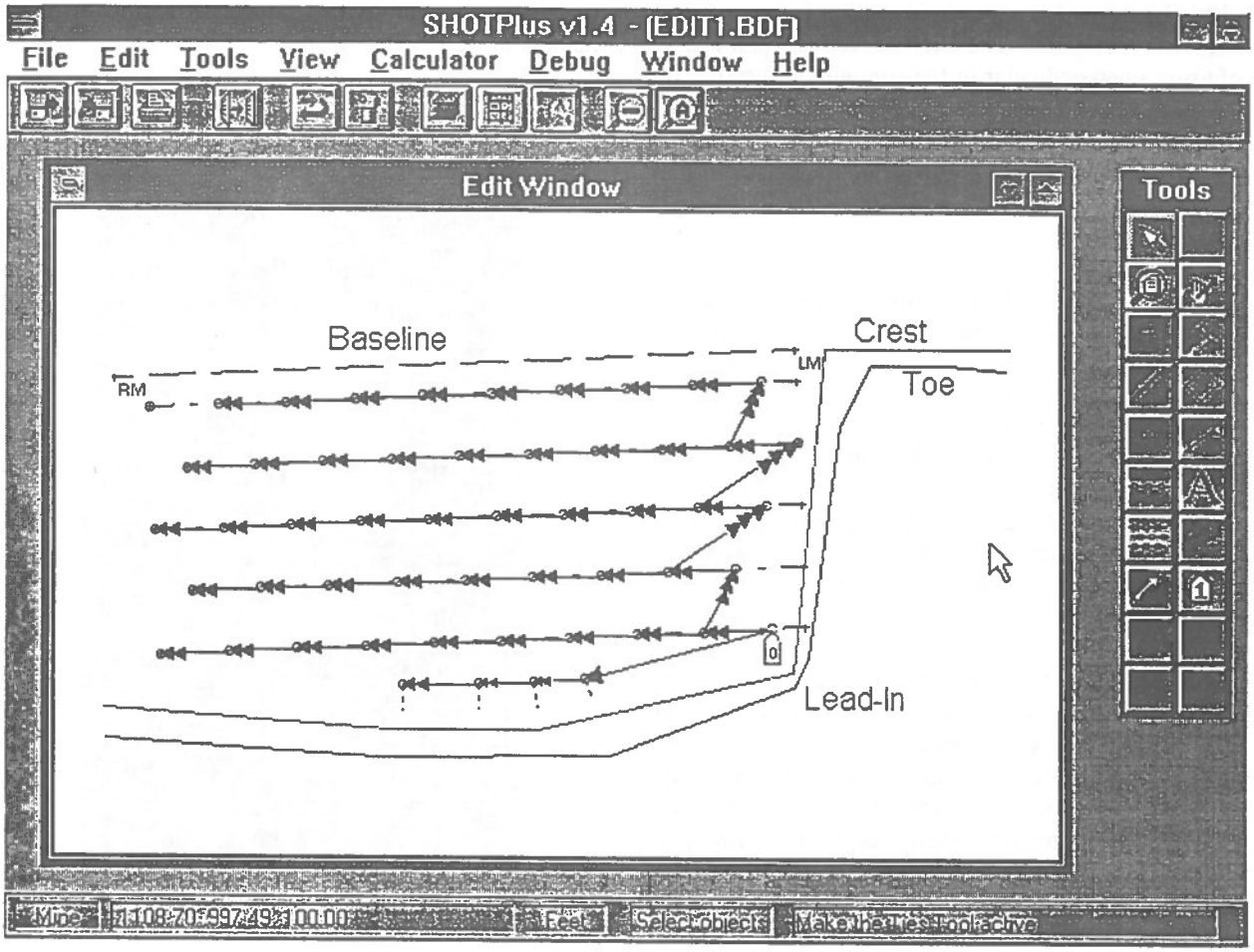

Figure 1: SHOTPlus Screen Features

The amount of information displayed overall and at each blasthole can be controlled throughout the program. Control over visibility of the various design elements allows filtering to suit the audience, such as drillers versus blast crews. A drilling plan for the drill operator will require the hole coordinates, planned depth and hole orientation plus any label used to identify the hole. The drill operator usually will not be concerned with the details of the initiation hookup. Similarly the blast loading crew will need to know the in-hole initiation product for each labeled hole and the planned depth but does not need the hole coordinates and orientation. Plots of the blast design, containing only the desired information, are previewed by the program user and then printed through the Windows print manager.

DESIGN EVALUATION

The SHOTPlus user has several options for evaluating the performance of the initiation hook-up. The first is the 'Visualize' mode which displays as a video the sequence as each initiation product fires. This is a simulation of the blast. From 'Visualize' the designer can verify both sequencing, and the time and distance between surface initiators and the main charges. Since a fully-charged blasthole may disrupt the correct functioning of nearby surface units, blast designers frequently check the progress of the surface versus in-hole detonations.

Another calculation is the 'Time Contours', which are a set of lines connecting points firing at the same time. These are useful to determine if the hole delays are uniform, indicated by equally spaced contours, or not, as shown by crowding of contours in regions of the

blast. The 'First Movement' calculation is derived from the 'Time Contours'. The 'First Movement' plot is a set of arrows perpendicular to the contours, indicating the direction of initial rock displacement during the blast. This feature is especially useful in blasts which include both ore and waste so that the boundaries between may be mapped.

The 'Burden Relief' plot presents a measure of the time between the firing of nearest neighbor holes and the explosion of the target blasthole. This time interval, scaled by the physical distance between the blastholes, is a useful indicator of whether the timing will have a strong effect on the blast result. This plot uses a range of colors to identify the various relief times achieved in the blast design. Blasting engineers have found that the height and distance rock is thrown in a blast can be controlled by this 'Burden Relief' interval.

The blast initiation design can be examined in one other manner, termed the 'Time Envelope'. This displays the number of blastholes which are to fire within a preset time interval. Blasters are frequently concerned with the intensity of ground vibrations outside the immediate blast zone. The vibration intensity can be controlled by keeping the number of holes firing during a time interval to a minimum. A default value used is 8 milliseconds, as specified by USBM test work. The 'Time Envelope' calculator can rapidly evaluate even the most complex hook-up, and can also be used to explore the design and identify the holes firing within any selected time window.

EXAMPLE 1 - Basic Initiation Design Analysis

For analysis of a basic initiation design, the user will need to input the pattern, define the initiation sequence, and then run the Initiation Calculator. For the first step, the pattern is usually defined relative to a baseline, representing a previous shot or design limit. Drawing the baseline and then selecting the Pattern tool will bring up a dialog box as shown as Figure 2.

The user simply chooses the settings and the software draws the pattern, Editing is possible and single or multiple changes may be made through appropriate dialog boxes, such as that shown in Figure 3, or by manipulating objects directly.

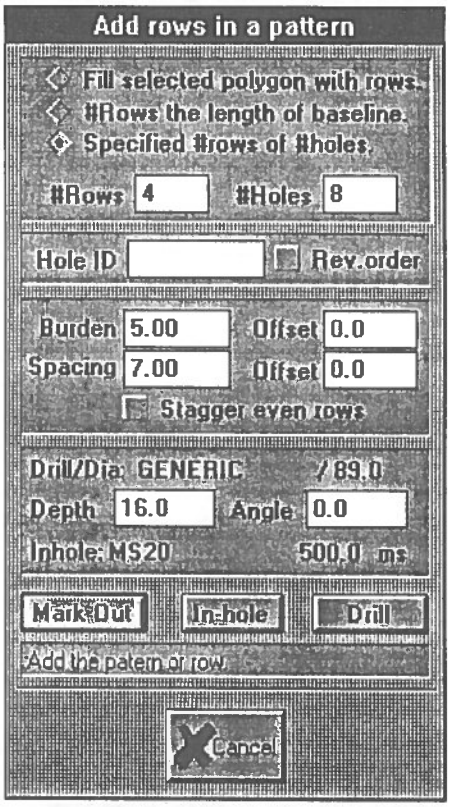

Figure 2: Pattern Definition Dialog Box

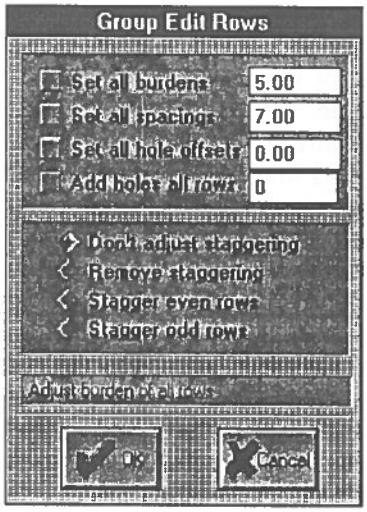

Figure 3: Example of Edit Dialog Box

The next step is to define the initiation sequence, and a critical part is locating the starting point for a blast. Using a 'Lead-In' tool, the user defines the location and time for the blast to be initiated. Next comes the 'Surface Ties' tool and customizing the palette of initiation products for the job. A default palette is shown in Figure 4. The user works with one type of unit at a time and makes connections by pointing in sequence at the holes to connect. Again, editing by deleting and replacing, or selecting and changing is possible.

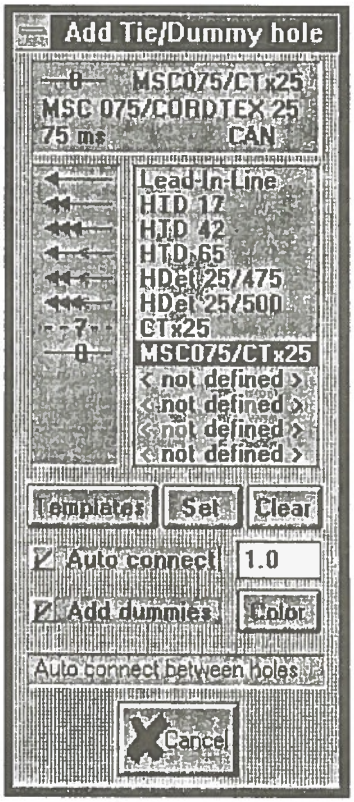

Figure 4: Surface Ties Palette

When a blast has been completely defined, the Initiating Explosives (IE) Calculator is called upon to analyze the design. In this second window, the view may be adjusted and the action buttons used to switch between 'Visualize', 'Time Contours', 'Time Envelope', 'Explore Time Envelope', 'Relief', and 'Explore Relief' modes. Examples from the IE Calculator are presented as Figures 5 and 6.

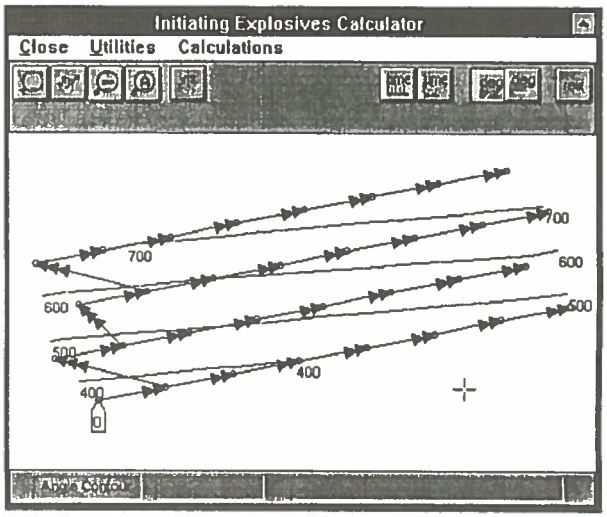

Figure 5: Contour plot from IE Calculator

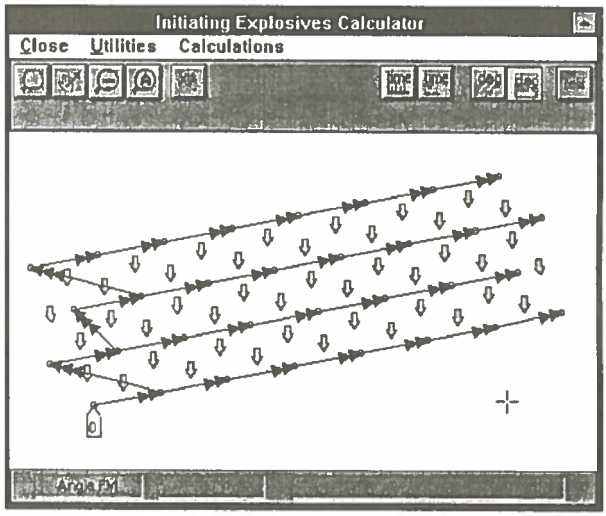

Figure 6: Plot of First Movement from IE Calculator

EXAMPLE 2 - Polygon Fill Example

A typical problem in large mining operations is to divide a bench into blasts and quickly generate plans for drilling and blasting to meet scheduling or blending requirements. In this example, a shot is required in a given irregular area of a bench, and the user must fit a prescribed blast pattern into that area. The steps can be reduced to describing the blast limits, defining the pattern, and editing to suit the overall mine design.

The first task is to define the block we wish to blast. Assuming we have the existing and proposed benches defined either from survey pick-up or computerized design, the crests and toes are plotted for both before and after the blast. From this information, a polygon can be constructed defining the limits of the blast, as is shown in Figure 7 . Alternatively, the polygon itself may be defined in a mine design package and imported along with the desired bench references.

The next step starts with deciding where to place a baseline for orienting the pattern. Typically the best orientation will be known, based on preferred directions for blasting results, mining schedule, or vibration considerations, for example.

To define the pattern, the baseline and limiting polygon are selected, and the pattern tool now allows entry of, or changes to the various parameters as seen in the first example. When done, the program draws the pattern, and the user proceeds to the third stage, to edit the design to suit wall control, minimum /maximum burden, or other considerations. The results are shown as Figures 8 and 9.

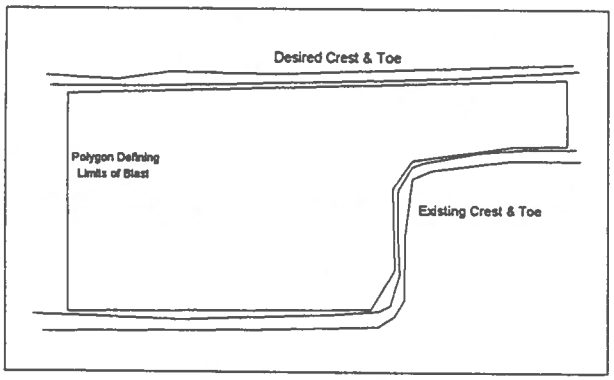

Figure 7: Limiting Benches and Polygon

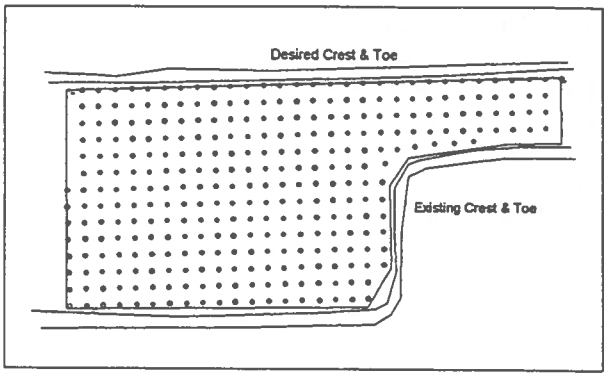

Figure 8: Pattern Filling Limiting Polygon

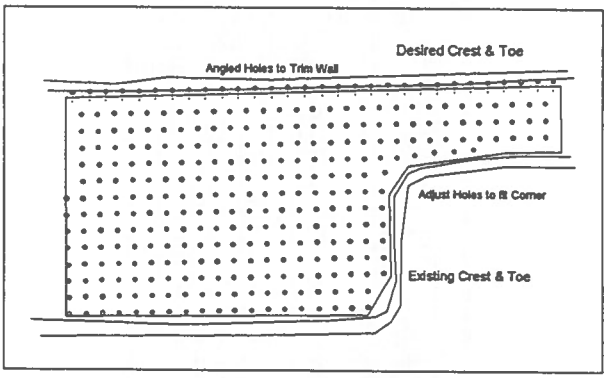

Figure 9: Edited Pattern ready for IE Design

EXAMPLE 3 - DXF File Import and Design

One of the many concerns blast design engineers face is recalling what has been done before, and effectively using that information in new designs. For this case, the task will be to import the hole locations from an upper bench and combine them with the design limits for the current bench. The goal is to design a drill pattern which does not call for drilling in bootlegs. To accomplish this, the steps will be to import the previous hole locations, to overlay and define the current bench design, and to define the pattern for drilling.

Starting from a clean slate, the import option allows access to the previous blasthole locations as a DXF-format file, complete with identification labels. To this,

the current design information is added by importing the appropriate file. The result is shown in Figure 10.

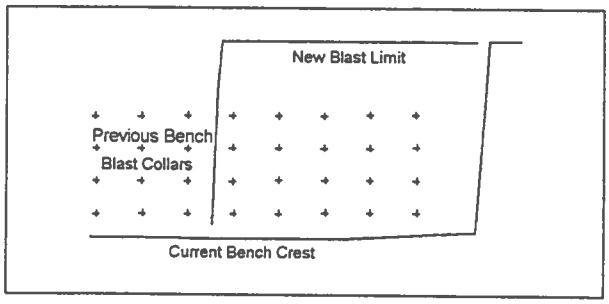

Figure 10: Imported Hole and Bench Locations

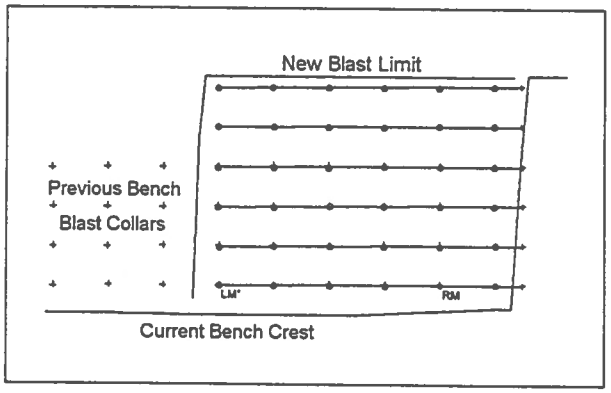

Figure 11: Baseline and Basic Pattern Defined

Next, the baseline for the new pattern will be established using the old hole locations as a guide. Once drawn, the pattern tool will allow a pattern definition including offsets to generate a design meeting the stated criteria. Figure 11 illustrates the intermediate result. A final design is shown as Figure 12 after editing to meet safe blasting and production requirements.

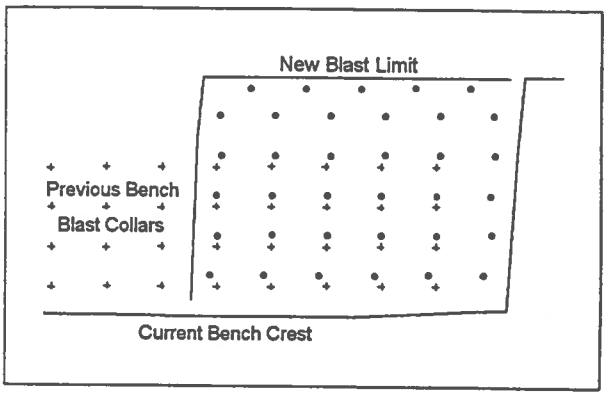

Figure 12: Final Pattern Design after Editing

CONCLUSIONS

Some of the typical applications of the SHOTPlus* Blast Designer have been presented. The package offers the drawing and analysis tools necessary for complete blast design, evaluation, and field support. Compatibility with existing mine engineering tools such as AutoCAD make it immediately useful on most sites, and the ability to tailor output to specific audiences improves its acceptance. Our experience shows that the operating environment and the program structure have made the tool easy to learn and work with, and users have been highly satisfied with the SHOTPlus Blast Designer program.

CAMI'95:3rd Canadian Conference on Computer Applications in the Mineral Industry
Montréal, Québec, Canada, October 22-25, 1995

NBLAST - Noranda's Blasthole Drilling Information System

James Leung
Noranda Technology Center

Gaétan Léonard
Flairbase Inc.

ABSTRACT:

Production blast hole drilling is a crucial and expensive operation within the hard rock mining cycle. Until recently, it was quite difficult to identify and correct problems related to this operation, mainly because of a lack of effective ways to collect the data and present the information in a useful manner. Noranda's Blasthole Database, called "Nblast", was originally developed as a research project by the Noranda Technology Center. The initial objective of the project was to assess whether or not relational database technology could be used efficiently by technicians, engineers and production supervisors to better control this very specialized mining operation. This paper describes the resulting database application, which is simple enough to be used by a wide variety of personnel (some of whom are not computer literate), and, at the same time, sophisticated enough to efficiently process highly specialized data and turn it into meaningful information leading to better decision making. The development of the Nblast system took approximately eighteen man-months of research, design, and programming. By the end of 1994, four different Noranda mine sites throughout Canada were using it on a daily basis.

RÉSUMÉ:

Dans le cycle de minage de la roche dure, le forage des trous de sautage est une opération cruciale et chère. Jusqu'à tout récemment, il était difficile d'identifier et de corriger les problèmes reliés à cette opération, parce qu'il n'existait pas de méthode efficace pour collecter les données et pour présenter l'information de façon utile. La base de données 'blasthole' de Noranda, appelée "Nblast", a été développée dans le cadre d'un projet de recherche par le Centre de Technologie Noranda. L'objectif du projet était de déterminer si la technologie des bases de données relationnelles pouvait être utilisée de façon efficace par les techniciens, ingénieurs et superviseurs de production pour contrôler cette opération minière hautement spécialisée. Ce document décrit le résultat de ce projet. L'application Nblast est suffisamment simple pour être utilisée par une large variété de personnel (qui ne connaissent pas tous les ordinateurs), et sufisamment sophistiquée pour transformer des données complexes en information utile, permettant de meilleures prises de décision. Le développement du système Nblast a pris approximativement dix-huit personnes-mois de recherche, design, et programmation. À la fin de 1994, quatre mines de Noranda à travers le Canada utilisaient l'application sur une base quotidienne.

INTRODUCTION

Nblast is a customized Windows database application dedicated to the highly specialized operations of planning and drilling blast holes in a mine. From the data entry of the driller's time sheets, the software provides useful information on: personnel, equipment, lost and unreported time, work place, and actual versus plan comparisons. The application demonstrates how powerful a well designed database can be in saving a mine site time, money and effort by streamlining and facilitating access to meaningful information.

HISTORY OF NBLAST

In late 1992, blasting engineers at the Hemlo Gold Mines in Marathon, Ontario, were looking for a better way to manage their blasting related data in order to enhance their blasting design and decision making abilities. Here is a sample of the types of questions that were asked daily at the Mine Planning group in the Mine Engineering Department:

- How many meters have been drilled so far this month?
- What is the availability of Drill #183?
- How many meters did we achieve on Bit #315?
- How did the productivity of the COP44 Hammer compare to the Bulroc Hammer in D1 Stope during the month of January?

The answers to those and other questions were buried in mounds of paper which made the retrieval of information difficult and time consuming. Furthermore, it was hard to verify the accuracy of the extracted information.

Hemlo Gold Mines could not find a commercial software package to fit their highly specialized needs. They then turned to the software designers at the Noranda Technology Center (NTC). After meeting with members of the Mine Planning group and studying their needs, NTC's designers realized that all the required information could be obtained from data that could be collected on the Driller's Time Sheets. They also concluded that a Database application would be the best way to collect this data and to produce the reports the Mine Planning engineers needed.

NTC designed Nblast in early 1993. The programming work was performed by Flairbase Inc., a Montreal based software firm specializing in the development and support of Windows Database applications. Programming started in April 1993, and the first prototype was delivered to Hemlo in July 1993 for on site testing. Feedback from the mine resulted in improvements to the product as it exists today. Customized versions of Nblast are currently installed in four Noranda mine sites and are being used daily with excellent results. The success of this software has also prompted the development of other database packages within the Noranda group. All of those packages provide data management of highly specialized mining operations, like for example: Core Logging, Cable Bolting, or Mucking.

DATABASE ADVANTAGES

Before the Nblast Database, drilling information was filed in paper files, and sometimes entered on commercial spreadsheets. Nblast clearly demonstrated the superiority of Database applications over spreadsheets for data collection and retrieval.

The major advantages of a database application are the following:

Reduced Data Redundancy and Inconsistency

Full data validation and reference checking insures that the data entered is valid. Therefore, users have more confidence in the reported information from the database.

Sharing Of Data

Because data in centralized, it follows a common format and can be exported to other software packages like spreadsheets for further analysis. When data is entered on spreadsheets, it often comes

in different formats and it can be difficult to link and analyze the data collected. It is therefore preferable to enter and query the data using a database application, then pass down the results to spreadsheets for temporary data manipulation and analysis.

Enforcing of Standards

Data entered in a database application must follow some agreed upon input formats.

Security

Database applications have the capability to restrict the rights to view and/or manipulate data according to a user's security clearance.

Data Integrity

By carefully designing the data model and applying referential integrity rules, collected data can be protected against accidental deletion or modification.

SOFTWARE DEVELOPMENT TOOL

The software development tool used to build Nblast is Paradox for Windows. Paradox was the most advanced Windows Relational Database available at the time the application was developed in PC. Although other good database packages have been introduced since (Microsoft Access for example), Paradox still has the technological edge for the following reasons:

User Interface

The design tools available within Paradox give the application designer a virtually unlimited amount of objects, colors, patterns, icons, etc. with which to design menu screens, data entry screens and forms that are both visually attractive and easy to use. In addition, a Paradox application can be programmed to incorporate all the standard Windows features users are already familiar with, like for instance MDI (Multiple Document Interface). The application can be programmed to respond to both Mouse and Keyboard commands, with helpful status messages and dialog boxes to help the user along the way. This makes Nblast user friendly and very easy to learn and operate.

Speed Of Development

Paradox uses the object oriented concept of programming, which considerably reduces the amounts of time and money required to develop and maintain applications. The reason for this is the following. With linear programming languages, any change or addition to a program often involves major changes to other sections of the program. With object oriented programming, code is attached to objects on a screen or form. Objects can be added, deleted or altered without affecting the other objects on the same screen or on other screens. In addition, objects can easily be transferred or copied to other forms, further reducing the programming time.

Performance

Most Windows database packages are relatively slow when running on a network in a multi-user environment. Paradox applications are network ready from the very start. Table and record locks are maintained automatically without affecting performance.

Upgrading

A Paradox application is easily upgradable to an SQL database which can run on a minicomputer or on a mainframe. This could be a major consideration, should the volume of data and the complexity of the required data processing grow over time.

THE KEY TO THE APPLICATION'S SUCCESS

The success of Nblast derives from two major reasons: functionality and design.

Functionality is obtained by supplying the Mine Planning group with all their information needs from

the simple data entry of the information contained in the driller's time sheets. Great care was taken in the conception and in the programming of the data entry screens in order to make the process as simple and as error free as possible. The drillers time sheets were designed so that all the required data could be collected on site. The fields on the data entry forms are validated in order to insure that the values are correct. Lookup tables are used whenever possible in order to speed up and validate the data entry process.

The other aspect of functionality is how the data is queried and reported to the end user. The user chooses the category of data to report, the start and end dates, and the items to report on (for example, Stopes RG55BH0 and RG55BH1 from March 15 to April 15, 1995). From this criteria, a general report of the drilling activity is produced. From this point, the user can drill down to a detail report of a single stope, view a down time report, a graph, etc. The user has full control of how much or how little information he or she wants to see at any given moment. With this technique, specific information that used to take hours to collect and calculate can be obtained in just a few seconds.

Design is the other reason for the success of the application. The major elements of a good design are: navigation, user friendliness, and flexibility.

Navigation within Nblast is facilitated by: the menu structure; the grouping of the major functions in logical categories (Manager, Data Entry and Query); the drill down feature of the query screens (from general to detailed information); and by the MDI (Multiple Document Interface) feature which allows many forms to be viewed at the same time.

User friendliness is essential if an application is to be accepted and utilized in the work place. This feature is realized in Nblast with: useful status messages and dialog boxes to help the user whenever necessary; full data validations on every screen; compatibility with Windows; and with logical and attractive design of each screen using boxes, buttons, frames and colors to logically group functions and data sets.

Flexibility is essential if an application is to survive the test of time. The flexible nature of the Nblast is the reason why it is now in use in four different mine sites. The application achieves this flexibility by using parameters instead of hard coded values whenever possible. This feature has, for example, allowed its use in mine sites with different shift lengths. Another aspect of flexibility is the careful design of the data model. For example: when after several months of use the size of the data started to slow down the data entry process, Flairbase was able to program an archiving function which removed time sheets from inactive Stopes, while retaining the possibility to include this archived data in queries at the user's discretion.

DESCRIPTION OF NBLAST

Nblast is divided in three main sections which are shown on the Main Menu screen. The sections are: Data Entry, Query, and Manager.

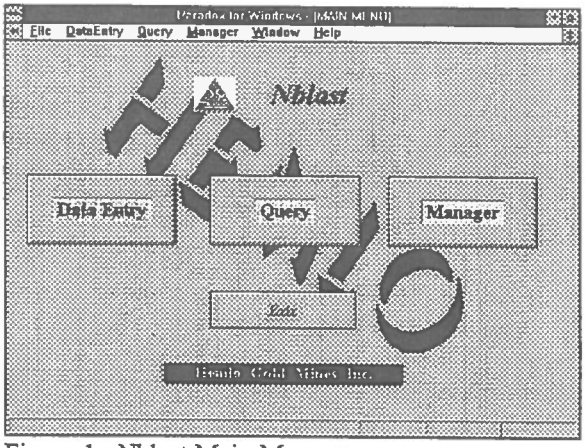

Figure 1: Nblast Main Menu

The Manager section is used to maintain the data on: Workplaces, Drills, Drill Bits, Hole Types, Employees, Hammers, Delays, and Shifts. This data is required before the other two sections of the database can be utilized. The Archiving function is also located in the Manager section.

The Data Entry section is used to enter the employee time sheets, on which all the queries are based. It is also used to enter the design (planned) layout of the blasting areas.

The Query section converts the data of the previous two sections into useful information which is presented in the form of screens, reports and graphs. The queries are grouped under seven major

categories: Total Drilling, Work Place, Employee, Drills, Drill Bits, Discarded Bits, and Hammers.

The following figure shows all the screens of the Blast Hole Database application, and how they are connected:

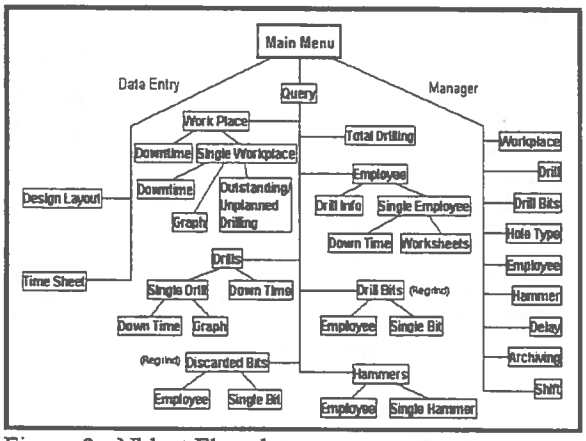

Figure 2: Nblast Flowsheet

The Manager Section

The Manager section contains nine screens. Eight of those screens are simple data entry screens used to maintain the data that defines the work areas, the equipment used, etc. This data is required before the time sheets can be entered (for example, employee # 312 must be entered in the Employee table before entering time sheets for this employee). The screen categories are:

Workplace
Drill
Drill Bit
Hole Type
Employee
Hammer
Delay
Shift

The ninth screen is Archiving, used to archive and restore data. When a workplace is archived, all the time sheets, work place data, drill data and delay data for that workplace are removed from the live tables and placed into archive tables. The archive tables are identical in structure to the live tables, and can be fully restored at any time. In addition, the data contained in the archive tables can be included in the Queries, at the user's discretion. Archiving speeds up the queries and the data entry by reducing the size of the live tables.

The Data Entry Section

The Data Entry section contains two screens: Design Layout, and Time Sheet.

Design Layout is used to enter the drilling plan. Planned drilling is entered by Location ID, which represents a specific work area within a Stope. The data entered is: planned drilling date, drill number, hole size, ring number, hole number, hole type, and hole length. The data entered in this screen will be compared in the Query screens to the actual drilling data entered in the time sheets.

Time Sheet is used to enter the actual drilling data.

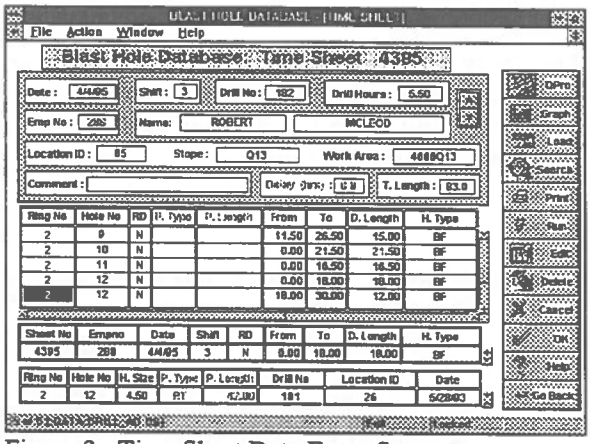

Figure 3: Time Sheet Data Entry Screen

This screen contains a lot of information. It is divided into four sections. The top two sections are for data entry, and the bottom two sections provide useful information on the data being entered.

The first data entry section (at the top of the screen, in dark gray) is the time sheet master record. It contains the data common to all the drills done by an employee on a particular shift: date, shift, drill number, drill hours, employee number, location ID, delays, and comments.

The second data entry section (the white table frame in the middle of the screen) is used to enter the details of the drilling done during the shift. Details are entered for each hole drilled, a hole being defined by a ring number and a hole number. The

data entered is: redrill (yes or no), plan hole type and length (if available), from and to values, drilled length (calculated), hole type, bit number, hammer number, completed hole (yes or no), and comments.

When the user enters the drilling details, the two information sections at the bottom of the screen get updated. The first information section (white table frame) displays the details of the last time that particular hole was worked on. If it is a first drill for that hole, that table remains blank. It is possible to view all the work done on that hole by scrolling through that table. The second information section (gray table frame) displays the design layout for that hole. If the hole has no planning, the display remains unchanged. It is possible to scroll through the entire design layout.

The Query Section

The Query section contains 27 screens. There are seven query categories: Total Drilling, Work Place, Employee, Drills, Drill Bits, Discarded Bits, and Hammers. The main navigation screen is the Query screen, where the query category and range are selected:

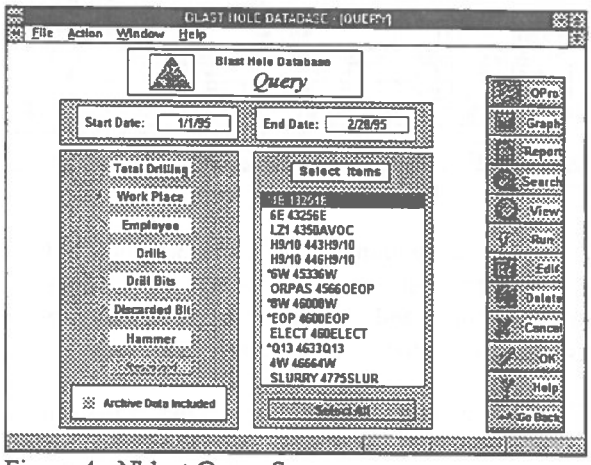

Figure 4: Nblast Query Screen

The user selects the query category, start and end dates, and the items to be queried. The Run button executes the query, displaying a screen containing general information on the selected items. The user can then use the drill down feature of the application to display subscreens containing more detailed information. Each query screen except the main query screen provides printed reports.

To illustrate the power of the database, here are three examples of query screens.

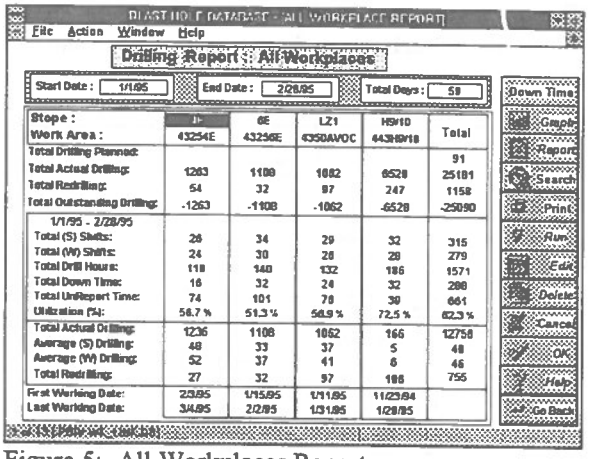

Figure 5: All Workplaces Report

Figure 5 contains general information on the drilling activity per workplace within the time interval. Each column shows a single workplace. The "Total" column adds up the data for all the selected workplaces. The data in the white sections of the screen is independent of the start/end dates; it includes all the work done in that workplace until today's date. The data in the gray section of the screen is within the start/end dates. This form makes it easy to compare plan versus actual drilling for a single workplace, or between workplaces. It also reports productivity by comparing drill hours, down time, unreported time, and utilization. Statistics are also provided on work (W) shifts versus total (S) shifts, a work shift being defined as a shift on which actual drilling has been performed.

The user can select the Down Time button to view the down time report for all workplaces, or drill down to a single workplace by double-clicking a stope or a work area. A detail screen of the drilling activity for the workplace is then displayed. From that detail screen, the user can further drill down to see the single workplace down time report, or the single workplace outstanding and unplanned drilling report, or a graph showing the drilling activity for the single workplace in the previous twelve months.

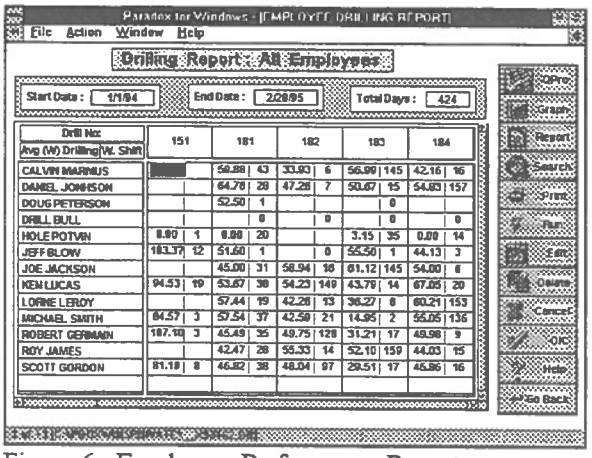

Figure 6: Employees Performance Report

Figure 6 contains general information on the drilling activity per employee within the time interval. Each line in the table frame represents one employee. Information reported is: total drilled length, total (S) shifts, work (W) shifts, average drilling per work shift, number of lost shifts, number of drills used, total drill hours, average drill hours per work shift, total down time, and total unreported time.

The user can select the More button to view the drill utilization report for all employees, or drill down to a single employee by double-clicking an employee number or last name. A detail screen of the drilling activity for the employee is then displayed. From that detail screen, the user can further drill down to see the single employee down time report, or the single employee drilling report per dates.

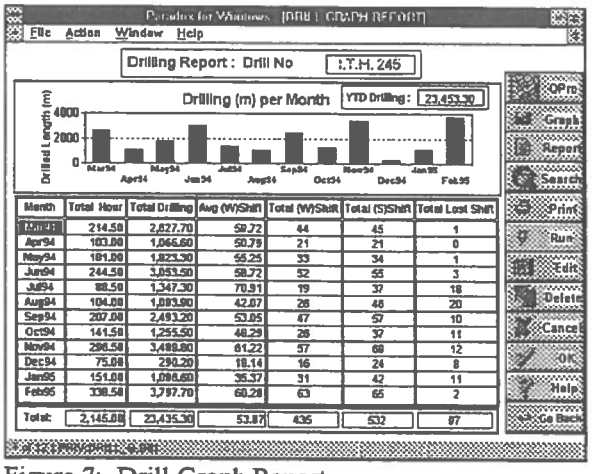

Figure 7: Drill Graph Report

Figure 7 is an example of a graph report. It shows all the drilling activity for a single drill over a twelve month period, both in graphical and in table form. The graph can be maximized to fill the entire screen by double-clicking on it. A similar graph report is available for a single workplace.

BENEFITS OF NBLAST

The main benefit of the database is the time and money saved by making information quickly and easily available. For example, preparing month end drilling reports for management is a task that used to take as long as 1.5 days to complete; Nblast does this work quickly and accurately.

The database is a powerful tool to use in the decision making process. One example from the Hemlo Gold Mine: in the fall of 1993, the database was used to help justify the purchase of three portable semi-automatic bit grinding machines. ITH bits were being sharpened by hand grinders at the drill sites. This method proved inefficient and drillers were forced to stop drilling in order to maintain an adequate supply of sharp bits. The drillers were forced to trade-off good bit sharpening for meters drilled per shift. Also, hand grinding tends to vary from driller to driller, producing inconsistent sharpening results. The net result was reduced bit life. Following the purchase of the first semi-automatic grinding machine, bit life improved 22% and grinding material consumption decreased by 30%. The new machines permit the driller to sharpen bits and drill at the same time and produce consistent grinding results. The actual drilling data stored in the database was used to demonstrate these results, leading to a decision to purchase two additional machines.

Other spin-off benefits include the ability to track bit performance by manufacturer or bit type; to do comparisons studies of hammer types; to track the number of times a bit is sharpened and the length interval between those sharpenings; to use the time sheet data for job bonus calculations; etc. All of these jobs would have been very time consuming in the past, if they would be done at all.

CONCLUSION

Nblast has demonstrated that a Relational Database Management System is the best way to collect, organize and report mining information. A well designed Database application can be used to save a mine site large amounts of time and money, to improve the Stope planning and design process, and even to give mine managers, engineers and geologists access to information they never even knew existed.

To be successful, such a highly specialized application must be carefully designed and programmed. The designer must involve the users in order to ensure that their information needs are fully satisfied, and that the data can be easily collected and entered into the system. The programmer must ensure that the application is user friendly, that it is easy to learn and operate, that the data entered is fully validated for accuracy, and that the queries are optimized to execute quickly and efficiently. If all those conditions are realized, the chances that the application will be accepted and utilized are greatly improved.

Noranda and Flairbase have jointly produced several specialized database applications for mining. Those other products cover areas like: Grinding, Cable Bolting, Grade Control, Bonus, Mucking, etc. Although not all of those applications are as complex as the Blast Hole Database, they all contribute to improving the efficiency of the Noranda mines.

REFERENCES

Noranda Technology Centre, 1995
Blast Hole Database User Guide

Borland International, 1994
Paradox for Windows Guide to ObjectPal, pp. 385-490

CAMI'95: 3rd Canadian Conference on Computer Applications in the Mineral Industry
Montréal, Québec, Canada, October 22-25, 1995

IBLAST - Noranda's interactive blasting layout and analysis system.

Per J. Lunder
Noranda Technology Centre, Pointe Claire, Quebec

ABSTRACT

IBLAST is an underground blast layout and analysis system for use with the computer aided drafting program AutoCAD®. It enables mine engineering personnel to design and produce underground open stope blasting layouts based upon existing mine geometry that is stored in AutoCAD. IBLAST is divided into seven main modules: hole layout, hole editing, hole naming and marking, data output, explosives layout, ring analysis, and time saving drafting features. IBLAST has been developed using AutoLISP® and ADS® , the development tools for AutoCAD. This paper will describe these features and the benefits that Noranda has realized from developing an in-house software package for use in mine engineering offices.

RESUME

Le logiciel IBLAST est un système de design et d'analyse du forage-sautage en souterrain, conçu pour être utilisé avec le programme de DAO AutoCAD®. IBLAST permet au personnel d'ingénierie des mines de préparer et de produire les plans de forage-sautage des chantiers ouverts souterrains directement à partir de la géométrie de la mine, déjà existante et disponible sur AutoCAD. Le logiciel IBLAST est divisé en sept modules principaux qui sont: design des trous de forage, édition des trous de forage, désignation et marquage des trous de forage, entrée de données, design des charges explosives, analyse des rangées de tir, et accessoires de dessin. IBLAST a été développé à l'aide des languages AutoLISP® et ADS® qui sont les principaux outils de développement d'AutoCAD. Cette présentation décrit les caractéristiques du logiciel ainsi que les bénéfices que Noranda a retirés du développement à l'interne de ce système destiné à ses opérations minières.

INTRODUCTION

Noranda has been committed to developing mine engineering software solutions at its operations. Beginning in 1990, blasting layout was identified as an area where significant productivity gains could be realized using computer based methods. In 1993, the existing blasting software was remolded into a software product that not only performed the basic blasthole layout elements, but also provided some analytical tools that could be used with existing blasting layouts, as opposed to reentering the data for a particular analytical application.

The initial requirements of the blasting program were to duplicate the drilling and blasting letters that are routinely produced for drillers and blasters. These letters have to be clear and consistent so as to avoid any confusion when drilling the blast holes for a stope blast. Any mis-drilling could result in costly redrilling or the firing of a ring that was not drilled to the correct design specifications.

Another important issue with the plans being distributed to drillers and blasters is that they are consistent and contain all of the information that is required to drill and load the blast successfully.

IBLAST is the current blasting program being used at a number of Noranda Group companies. The software is made up of a total of over seventy commands that are grouped logically into modules of like functionality.

PROGRAM PHILOSOPHY

Noranda's goal in developing blasting software meets two main requirements. The first is to improve engineering productivity in performing blasting layouts and to generate neat, consistent drilling and blasting letters that are given to underground personnel. The second requirement is to incorporate analytical capabilities into production blasting software so that routine spatial blasting analysis such as powder density

can be performed quickly on existing blast designs without any intermediate data manipulation steps.

In 1990, Noranda's first AutoCAD based blasting software project, BlastCAD was started. In 1993, the needs of operations were much clearer and it was decided that rather than try to incorporate all of the needed changes into BlastCAD, it would be easier to redevelop the blasting software.

BlastCAD relied extensively on complex external AutoCAD drawing entities, known as blocks, to store information relating to the blast layouts. The use of blocks meant that program instability could result if user changes were made to these external blocks. A new approach was undertaken in IBLAST. Based upon previous experience Noranda has with extended entity data (EED) as part of the AutoVENT program, it was decided to use extended entity data and simple entities wherever possible in IBLAST. The use of EED results in optimized memory requirements, flexibility when extending program features, and because the entities involved are simple entities, many of the existing editing command that AutoCAD users are already comfortable with can be used on IBLAST entities.

AUTOCAD & AMINE

AutoCAD is a computer aided drafting (CAD) package that is used extensively in Noranda Group mining operations for mine engineering purposes.

Beginning in 1990, Noranda operations began moving to AutoCAD as a means of constructing and maintaining engineering drawings and plans. These drawing are constructed in three dimensions using in-house software, collectively referred to as AMINE, developed at the Noranda Technology Centre.

AMINE can be broadly divided into two separate areas: the Drawing Manager and the Program Manager with associated application programs.

The drawing manager maintains the drawing database of CAD files. The philosophy is that one drawing layer in AutoCAD is a single drawing in the AMINE drawing database. When a user needs to work on an assembled drawing, the drawing manager performs the task of collecting the required layers and assembling them into a working drawing, At the end of the editing session, the Manager saves all of the drawing layers as individual drawing files. This approach is used to maintain a single copy of each drawing only, which is used by different engineering groups.

One requisite of using the AMINE drawing manager is that drawing and layer naming conventions are rigid for a particular minesite. This approach to drawing management ensures that duplicate file names never exist.

The program manager handles the task of loading and unloading each of the AMINE compatible applications that a particular operation may have installed. After an application is loaded, it is accessed from either the command line or from a customized menu for the particular application.

IBLAST

IBLAST is a modular program that has been developed with the user in mind. A particular software program may be extremely useful, but the user interface has a dramatic impact on how useful that software may be deemed. IBLAST makes use of the screen based user interface features of AutoCAD, namely dialogue boxes, screen menus, and pull-down menus.

IBLAST is divided into a number of modules that cover a logical grouping of the commands available to IBLAST. The individual modules are described and listed below.

- LAYOUT contains all of the functions related to the placement of blastholes and drill setups.
- DRAW contains all of the functions related to the drawing of ancillary information on the blast ring.
- NAME contains all of the functions related to the naming and marking of holes and setups.
- MODIFY contains functions used for modifying blastholes, setups and powder.
- POWDER is used to place and modify a charge or a deck on one or many blastholes.
- OUTPUT contains the functions for generating title blocks and letters. It also provides a means of exporting and importing information between IBLAST and an external database.

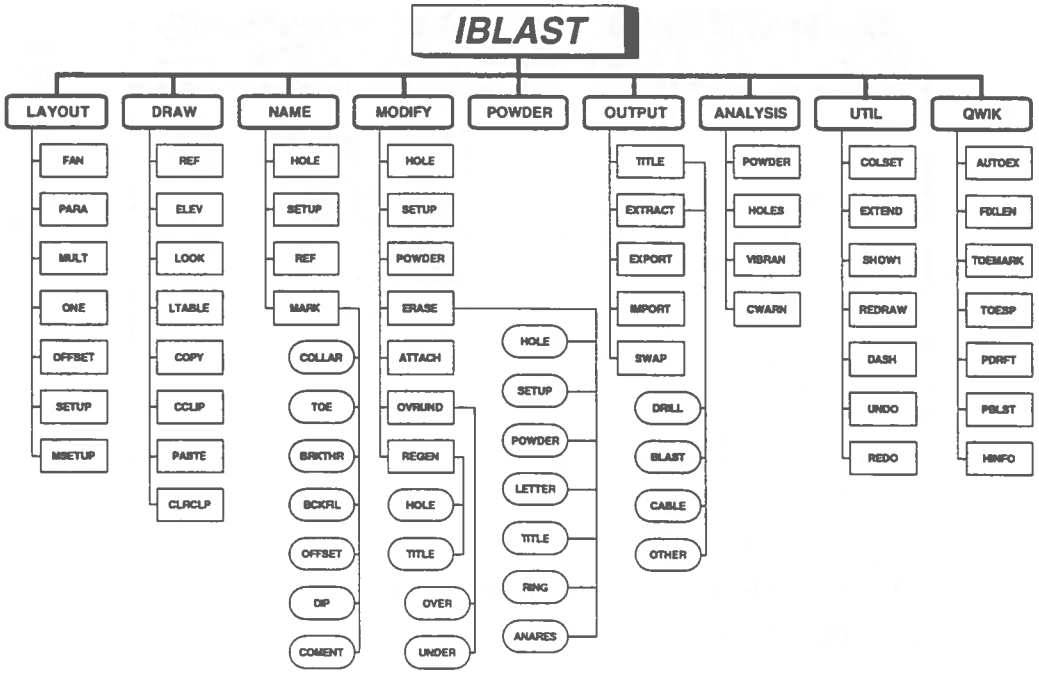

Figure 1 - IBLAST function hierarchy, main modules are listed on the top line.

- ANALYSIS contains the functions that provide analytical capability in IBLAST. These currently are hole density, powder density and an analysis for collar interference on closely spaced holes.
- UTILITIES contains functions to make the users life a little easier while using IBLAST.

Each of the major modules is described in greater detail in the sections following. Figure 1 is the IBLAST function hierarchy tree showing the major modules and the included functions.

Drawing Environment

Prior to discussing the individual modules of IBLAST, the AutoCAD drawing environment must be explained. A complete stope blast layout generally consists of a number of parallel to sub-parallel drill rings that contain blast holes, powder and other information. IBLAST is used in conjunction with AMINE and as such a single blast ring is created on a single layer. While there are some cross ring functions, IBLAST can be thought of as a two dimensional ring layout program that acts upon arbitrary plane in three-dimensional space. This means that, while the rings are two-dimensional, their spatial relationship to the other rings in the blast reflects the actual conditions in the mine. This three-dimensional information is used for the analytical portion of IBLAST.

In this context, all blasthole information for a particular ring resides on a single layer. There are situations where information on a given ring may have applicability on other rings. Examples of this are reference lines, elevation lines, mine opening labels. Functionality is provided to transfer this information between different rings.

IBLAST takes advantage of many aspects of the AutoCAD drawing environment. Commands can be accessed through either the pull down menus, the side menus, or the command line. Extensive effort has been made so that IBLAST has the look and feel of standard AutoCAD commands. In the screen layout there are a number of areas that should be noted. The top of the screen menu is used to change information related to the blast on the fly, such a powder type, paper size, output scale, drill type etc. The status line is used when necessary to keep the user aware of various information such as hole length and angle, powder and collar length etc. The command line reflects where the IBLAST command actual is. In the case of user errors, a message will be directed to the

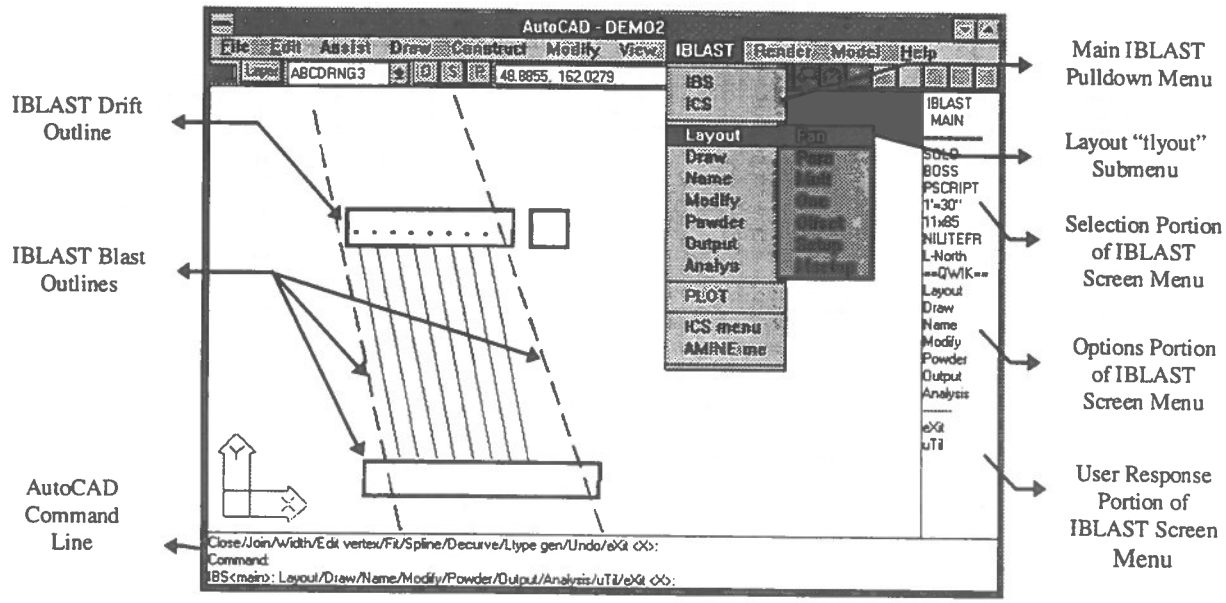

Figure 2 - Example of the IBLAST / AutoCAD Drawing Environment

command line, or in the case of more serious errors, the error will be displayed in a dialogue box which the user must acknowledge to close. Figure 2 illustrates the various aspects of the IBLAST / AutoCAD drawing screen environment.

Layout Module

The layout module is responsible for the placement of drill holes and setups on the drill ring. A number of different methods are provided for the placement of blastholes. Prior to placing the blastholes, the user must assure that the correct drill has been selected. This is done because IBLAST calculates the location of the drill setup line within the drift outline based upon the height and standoff distance of the selected drill. In addition the drill contains a design toespacing that is used for spacing the blastholes.

A major feature of the layout module is the flexibility in the mode in which the blast layout may be performed. The user has the option of selecting any of the following at the hole placement prompt: the drill line, an existing setup or an existing hole. If the drill line is selected and a setup does not exist at the selected location, a new setup will be placed. If a setup is selected or exists at that location on the drill line, then one or all of the subsequently laid out holes will be attached to the existing setup. If an existing hole is selected, the subsequently laid out holes will be located between the selected hole locations.

When laying out holes using one of the multiple hole modes, a number of options are available to the user before the completion of this particular sub-layout task. A new toespacing can be entered and the hole layout will be regenerated based upon this new toespacing. The toespacing can be increased to fit the existing holes into the range specified. The toespacing can be decreased and an additional hole added to fit the holes into the range specified. The user must then decide whether to keep the sub-layout and generate the setups or to dump the sub-layout and try a different approach.

Two options require the calculation of the toespacing based upon potentially differing lengths of holes. IBLAST uses an iterative approach in the layout so that all of the holes in a particular sub-layout will have identical toespacings. The toespacing can be defined to be calculated from either the shorter or the longer hole.

The following layout options are available, listed from the simplest method to the most complex method:

- ONE places a single hole and setup. While locating the hole a user selectable marker appears at the cursor location that indicates the current design toespacing. The command continues until the user requests an exit.

- FAN places a number of holes that will be drilled from a single setup location.

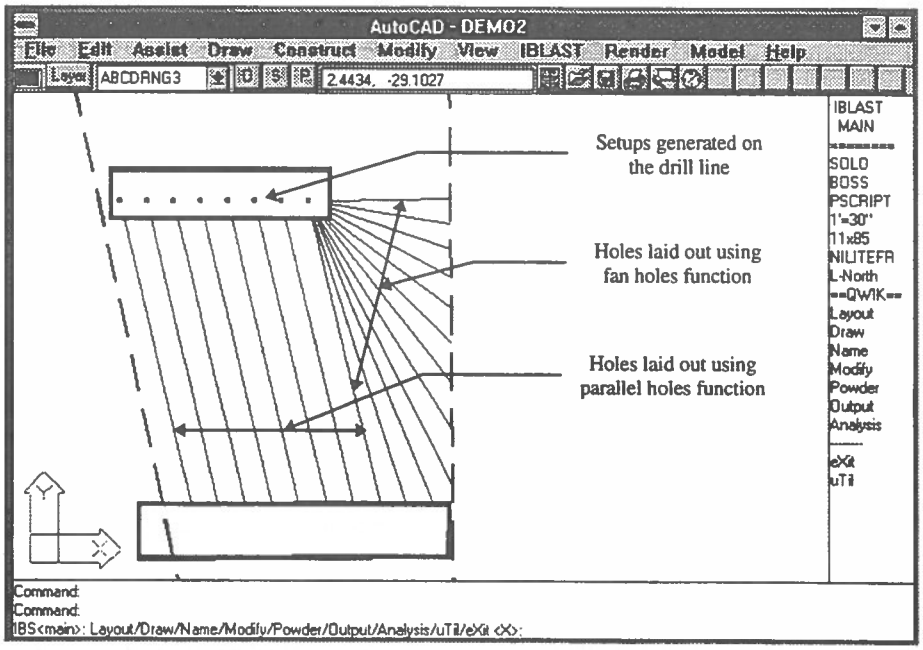

Figure 3 - Example of a layout performed with the Fan Holes and Parallel Holes functions.

- PARA places a number of parallel holes. The user specifies the location of the first hole and the end of the drill line and the program will fill the space with holes.
- MULT places a number of non parallel holes. These holes can have either a convex or concave configuration.
- OFFSET is used to place one or a number of holes parallel and offset from some drawing feature, such as a hanging wall contact. This command continues until the user requests an exit.
- SETUP(s) is use to place one or many setups only.

This overall approach to blasthole layout allows users a large flexibility in the methodology adopted to perform the layout operation. Figure 3 shows an example of a drill ring laid out using the parallel and fan holes commands of the layout module.

Draw Module

The draw module is used to place information that is not directly related to the blastholes or setups. This information includes reference lines, elevation lines, and looking arrows. In addition a number of drawing manipulation features are included such as a light-table function and a clipboard feature.

The reference line function places and labels a reference line on the current ring. If desired and the reference line exists, all subsequently laid out setups will be automatically attached to the reference line. This enables the computation of the distance to the reference line for the drill or blast letter.

The elevation line function automatically places an elevation line in the drawing and labels it with the correct elevation.

The looking arrow function places a block that is used for indicating direction, i.e. North or East, and automatically labels it with the correct direction.

The light table function enables the temporary drawing of information from other rings in the drawing on the current ring. This is useful to locate blastholes in relation to adjacent rings.

The clipboard function enables the user to copy items to the clipboard from other rings in the current blast. While intended primarily for extra information such as reference and elevation lines, it can also be used to copy blastholes from one ring to another. After being pasted, the new holes are regenerated based upon the

currently selected drift and blast outlines and, if required, new setups are generated.

Name Module

The name module is used to name and mark entities in the blast layout. The primary use of IBLAST is to generate a drill or blast letter for mine production personnel. The information presented in the letter must correspond to the holes in the "blast picture". The name holes and name setups command quickly names holes or setups and allows the user to specify any character as the initial hole number. Each subsequent entity names is an incremented from this initial value. The user also has the option of specifying which direction the naming will take place in.

The mark function enables the user to mark one or many holes with some "extra" information to be conveyed to production personnel. These marks correspond to some extra information that will be present in the output letter. The marks available are as follows:

- COLLARS places marks at each hole collar on a user specified layer.
- TOES places marks at each hole toe on a user specified layer. This and the collar marks are used to generate collar and breakthrough plans.
- BREAKTHRU places a mark to indicate the hole is expected to, or did, breakthrough to an existing mine opening.
- BACKFILL places a mark to indicate that the hole is expected to, or did, break through to an adjacent stope that is backfilled.
- OFFSET places a mark to indicate the hole is offset a certain amount in front of or behind the current ring, likely a small amount where the collars are very crowded.
- DIPRING places a mark to indicate that the hole is dipping at a certain angle from the current ring. The amount of the off dip is stored on the hole.
- COMMENT places a mark to indicate that some additional information is stored on the hole.

Marks are externally defined blocks that are unique for each mark type.

Modify Module

While laying out blastholes is an important portion of performing a blast layout, it is also important to be able to make changes to existing blast layouts with ease. In order to accomplish this in IBLAST, an extensive suite of editing capabilities have been developed.

The modify hole command enables the user to move either the startpoint or endpoint of a blasthole and will create a setup if required at the new hole position. All related entities to the blasthole are automatically moved to their correct locations in relation to the blasthole.

The modify setup command enables the user to move a setup to a new position on the drill line. If there are holes drilled from the setup, they are automatically moved to a new position that is in line with the new setup location. While the user is moving the setup, all of the attached holes are drawn interactively at the current setup position.

The modify powder/deck command allows the user to modify the collar and toe position of a column charge of powder (or deck). A marker indicating the current design toespacing is used to locate a new startpoint or endpoint of the powder/deck while showing the changing powder and collar length in the status area of the AutoCAD drawing screen.

An erase function is available that allows the following portions of the blast layout to be selectively erased:

- HOLE erases a hole and all the attached entities.
- SETUP erases a setup and all the attached holes and other entities.
- POWDER/DECK erases the powder from the selected hole.
- LETTER erases all of the letter information on the current ring.
- TITLE erases all of the title blocks on the current ring.
- RING erases the current blast ring leaving other information intact.

Additional modify commands are as follows:

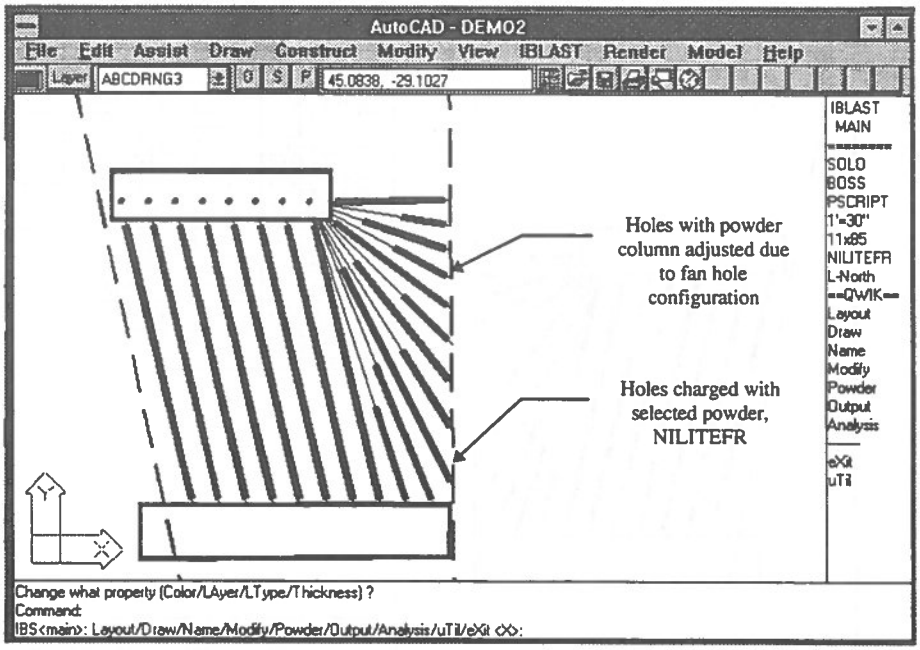

Figure 4 - Example of a drill ring that has been loaded using the Powder Function.

The attach command allows the user to specify which setups are attached to which reference lines. The over-under command allows the user to specify a constant amount for all selected holes to be either over drilled or under drilled. The regen functions allows the user to regenerate all selected holes based upon new blast and drift outlines. The regen functions can also be used to regen a title block and update all of the included attributes in the title block.

Powder Module

The powder module is used to place either a column charge or a deck on all selected blastholes. The currently selected powder is attached to the selected blastholes for the charge function. The user specifies the collar and toe distances and the powder/deck is placed on the selected holes. Included in the powder module are editing functions that allow the user to interactively adjust the location of the charge and deck endpoints. Figure 4 is and example of a ring that has been loaded using the powder charge function.

Output Module

The output function is used to generate title blocks and letters for the current ring. For each of the external blocks, there are a number of attributes that represent particular information. These blocks do not have to contain all of the allowable information. As the blocks are inserted, the existing attributes are updated with the pertinent information.

For each the title and the letter, there are four choices of type of output the user has, namely: "drill", "blast", "cable" and a generic "other" configuration. A feature of IBLAST is that intelligent title blocks are created. Prior to the insertion of a title block, the user ensures that the correct printer, paper size and scale are specified. IBLAST then creates a title block that can send itself to the correct printer. When requesting hard copy the user has merely to select the title block to plot and the IBLAST program sends the plot to the correct printer and selects the correct scale and paper size, making plotting a painless task. Figure 5 is an example of a completed blasting letter that is ready to be sent to the appropriate output device.

In addition to the tile and letter functions, there is a feature that enables IBLAST to interface with an external database. NBLAST is a database application that has been developed at the Noranda Technology Centre to track drilling and blasting operations. IBLAST can read and write ASCII files that facilitate the transfer of information to and from NBLAST. After updated drilling information has been entered in NBLAST, the user can import this information into IBLAST and the program will automatically update the

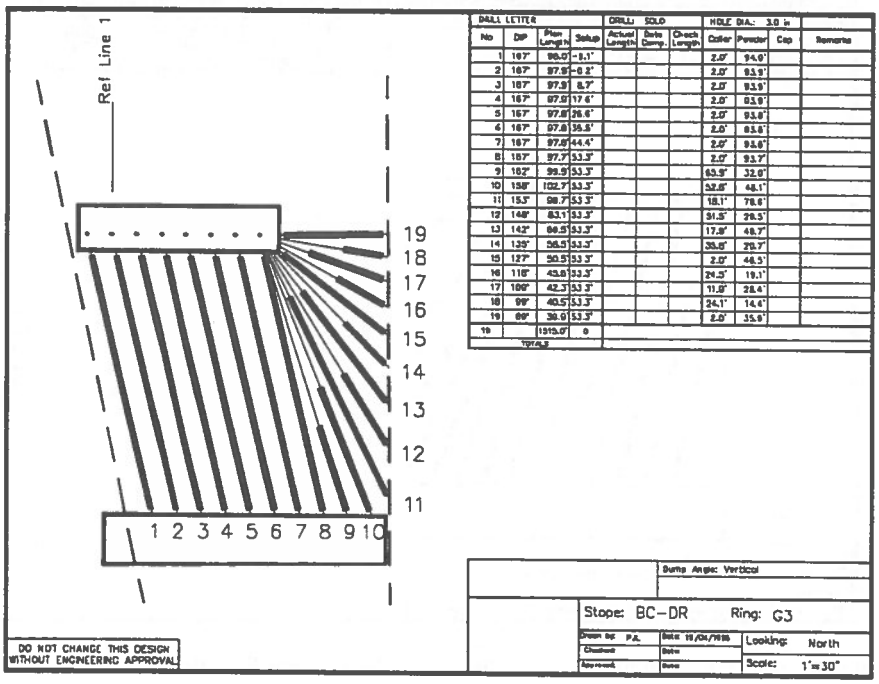

Figure 5 - Example of a completed Drilling Letter ready to be sent to the printer/plotter.

blast layout with the actual hole lengths. Holes that have been updated have their color changed to indicate the update. This information can then be used to generate an up to date blasting letter.

Analysis Module

The analysis module makes use of the three-dimensional relationship between the blastholes in the current blast. Color coded diagrams can be produced that represent the powder density or hole density. This generic approach to spatial analysis allows for the addition of other analytical relationships that may be derived in the future in relation to blasthole layout. The analysis function is driven by a dialogue box that allows the user to specify the colors and ranges of the diagram, the search radius of the density plot and other function information. Figure 6 shows the Analysis dialogue box. Also available in the analysis module is a function that will detect the potential for collar interference based upon a user selectable interference criteria.

Utility Modules

Two utility modules exist in IBLAST that are available from most locations within the program. One group of utility functions is to provide visualization helpers such as temporary hole extensions. An undo and redo feature is available for use with the layout module. Figure 7 is the hole information dialogue box that can be used to review individual blast holes in a layout.

A second utility module provides access to various control variables in the program such as toggling auto-extend holes, temporarily overriding the design toespacing, providing quick access to specifying the drift and blast entities etc.

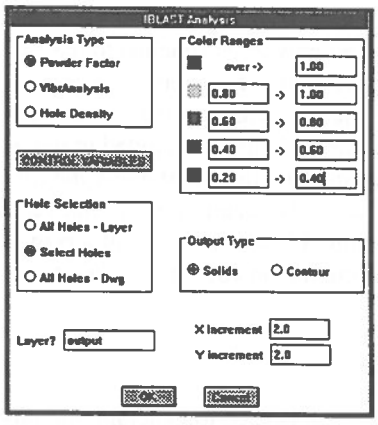

Figure 6 - The ANALYSIS function dialogue box.

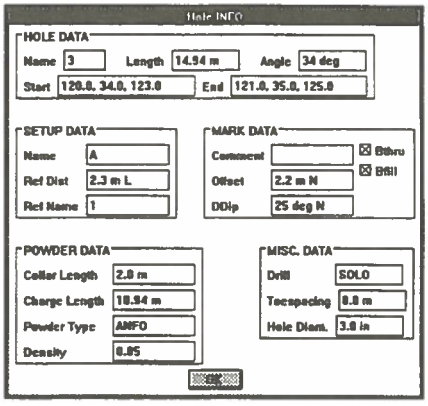

Figure 7 - The HOLE information dialogue box.

CONFIGURATION & CUSTOMIZATION

IBLAST Is designed to be used at a number of different operations which may have different software requirements, and as such extensive measures have been taken to provide flexibility for configuration and customization. Customization takes place either through the design of AutoCAD "blocks" and the selection of specific block attributes in the letter and title blocks. In addition there is an extensive configuration file that lets users specify control variables that apply to various aspects of the program.

Configuration Variables

Variables are defined for almost every feature of IBLAST. This means that there are no hard coded values in the program code. Variables define the following: powder definition, block definitions, default user responses, colors used for various entities, text height's, text offset amounts, drilling equipment specifications, user names, printers, output scales, paper size and more. This allows each installed site flexibility in shaping IBLAST to look and behave the way that they desire.

User Defined Blocks

AutoCAD blocks provide customization in how the IBLAST printed output will look. This includes the selection and location of numerous block attributes that are used in the title and letter blocks. The flexibility in block customization currently supports over thirty title block attributes and over fifty letter block attributes. When a block is inserted, IBLAST scans each of the block attributes and automatically detects if it is an "IBLAST recognized attribute". If it is, then the value will be updated with the correct IBLAST generated value. This approach allows users to change the way that their output looks by modifying the blocks that are defined for their operation. No changes to program code are required.

CONCLUSIONS

A commitment has been made by the Noranda Group of companies to develop a blasthole layout package that meets the needs of its operations. The system developed allows users to take advantage of all of the geometric mine openings and geological information that may exist at a particular mine site. It also provides a flexible and easy to use method of laying out blastholes. IBLAST could not have been developed in its present form without significant input from operations during the development and testing phase. IBLAST is currently installed at eight operating Noranda Group mines.

REFERENCES

Favreau, P. and Andrieux, P., 1993
BLASTCAD - Noranda's three-dimensional computer-aided undeground blast system. CIM Bulletin, Vol. 86, No. 967, pp. 62-68, February 1993.

Lunder, P., 1995
IBLAST, Version 1.1F, Final Documentation, Internal Noranda document.

9.

AI and knowledge based systems
intelligence artificielle

CAMI'95 : 3rd Canadian Conference on Computer Applications in the Mineral Industry
Montréal, Québec, Canada, October 22-25, 1995

LES SYSTEMES EXPERTS DANS L'INDUSTRIE MINIERE : BILAN DE L'EXPERIENCE SOUT ET ORIENTATIONS FUTURES

Y. GUENIFFEY (1), S. KOUNIALI (1, 2),
H. BAROUDI (2), et J. P. PIGUET (1, 2)

(1) *Laboratoire de Mécanique des Terrains - Ecole des Mines de Nancy*
(2) *Institut National de l'Environnement Industriel et des Risques (INERIS)*

RESUME

L'expérience accumulée depuis 1985 lors du développement de SOUT, système expert d'aide au choix du soutènement dans les galeries minières, nous a fourni un certain nombre d'enseignements susceptibles d'orienter l'utilisation future de la technologie des systèmes experts dans l'industrie minière. Plus qu'une technologie nouvelle destinée à capter «magiquement» le savoir des experts, les systèmes experts, dès lors qu'il s'agit de les appliquer en vraie grandeur, s'avèrent être d'excellents révélateurs de la nécessité d'une étape de modélisation dans le travail du géotechnicien; le «transfert de connaissances» ne réussit que s'il est une modélisation et une interprétation des données d'observation et des savoirs des experts du domaine. Ces outils doivent s'intégrer aux autres moyens informatiques, que ce soit les bases de données nécessaires à l'archivage des informations géotechniques toujours plus nombreuses, ou les codes de calculs nécessaires au dimensionnement des ouvrages. Ils doivent bénéficier des avancées faites en matière d'interface homme-machine et garantir ainsi une convivialité maximale. Cette expérience nous a permis ainsi de proposer à nos collègues des charbonnages allemands (Deutsche Montan Technologie, Essen, DMT) une nouvelle version de Sout qui intègre leur expertise, et nous a poussé à envisager, en collaboration avec nos collègues allemands et espagnols, un système intelligent de planification et de simulation d'une exploitation minière.

ABSTRACT

Since 1985, we built and experienced SOUT, a computer aided design for support in mining galleries, several points we have learned could pilot the future uses of expert-system technology in geotechnics.
Besides, more than a new technology able to capture the experts' knowledge «magically», experts systems, when they are used in a real context, teach us the absolute need for a modeling step in the geotechnician's work. The so-called «knowledge transfer» succeeds only when it is both a modeling and an interpretation of observationnal data and knowledge of experts in this field.
These tools must be combined easily with other computer tools from relationnal databases, useful to keep the more and more numerous geotechnical data, to calculation programmes necessary to design civil engineering structures. They must also benefit from the advance in man-machine studies to be as user-friendly as possible.So we have been able to propose our colleagues from the german collieries (Deutsche Montan Technologie, Essen, DMT) a new Sout version augmented with their expertise, and to consider with our german and spanish colleagues the development of an intelligent planning tool for the mining operations.

1. Introduction

1.1 Définition

SOUT est un Système «Intelligent» d'Aide à la Décision (SIAD) en matière de choix du soutènement dans les galeries minières (cf. figure 1).
Le choix d'un type de soutènement doit prendre en considération toute une série de données et satisfaire un grand nombre de contraintes ; de plus, et c'est un point très important, ce choix engage la sécurité des hommes au travail. D'autre part, les gisements exploités en Europe sont de plus en plus profonds et les coûts s'accroissent en conséquence. Disposer d'un outil intelligent d'aide à la décision dans ce domaine est évidemment un atout crucial.
La technique des Systèmes à Base de Connaissances (SBC), une des techniques de l'intelligence artificielle (IA), a été choisie, parce que, contrairement aux algorithmes informatiques classiques, elle permet :

- de formaliser la connaissance et l'expérience,
- d'intégrer le savoir des experts et de garantir la cohérence de sa mise en oeuvre,
- de faciliter la mise à jour de ce savoir, ce qui est indispensable dans un contexte qui évolue avec le gisement et avec la technologie.

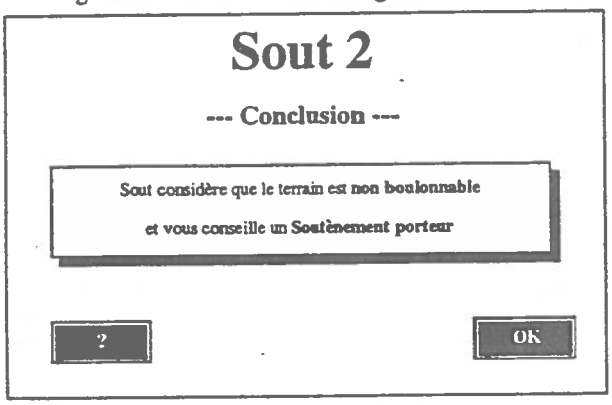

Figure 1 : Conclusion du SIAD SOUT 2 concernant le type de soutènement à mettre en place.

1.2 Les systèmes à base de connaissances

1.2.1 Généralités

Jusqu'en 1983, faire un système expert consistait en général à interroger un expert quant à son expertise et à la coder directement ; chaque règle correspondait à la réponse de l'expert à un problème dans un contexte donné. La connaissance et le savoir faire étaient mêlés étroitement. Celà conduisait à des systèmes qui certes fonctionnaient, mais dont le développement était plus ou moins anarchique, et surtout " fragiles " et difficiles à maintenir.

Depuis 1983, on parle de systèmes experts de seconde génération pour désigner les systèmes où l'on code de façon déclarative la connaissance indépendamment de la façon dont on l'utilise; on met ainsi en évidence des modèles de domaines spécifiques (classification, conception, diagnostic...) qui permettent de définir également des méthodes spécifiques d'acquisition des connaissances relatives à ces domaines.
Les explications fournies par ces systèmes ainsi conçus sont beaucoup plus qu'une simple réexposition des règles; ils sont moins fragiles, fondés qu'ils sont essentiellement sur des principes caractéristiques d'un domaine plus que sur des heuristiques ponctuelles.
La réflexion fondamentale sur la nature de l'expertise a depuis conduit à décrire plus finement des niveaux de connaissance [Newell ,1991] ; on distingue ainsi maintenant les tâches (ce qu'il y a à faire et dans quel contexte), des modèles (quel type d'information est disponible), et des méthodes (comment utiliser au mieux l'information pour tel type de tâches).
On peut préciser d'ailleurs qu'en ce qui concerne l'acquisition des connaissances relatives aux domaines d'application, on s'adresse plus aux spécialistes qu'aux experts (pour reprendre la distinction classique entre le spécialiste, dont le savoir est public, attesté par les livres et les publications, et l'expert, dont le savoir est essentiellement privé et fondé sur une expérience personnelle difficilement transmissible). La difficulté de l'acquisition des connaissances consistant plus en un problème d'interprétation et de modélisation qu'en un simple transfert au système informatique, la collaboration avec les spécialistes du domaine permet de simplifier cette phase.

Ces avancées, combinées avec l'utilisation systématique du formalisme objet, permettent maintenant de concevoir des systèmes qui réutilisent des modules développés pour d'autres applications, pour peu qu'ils correspondent à des domaines semblables ; on envisage même le partage de bases de connaissances.
De nouvelles architectures permettent d'aborder le problème de l'expertise hétérogène, celle qui résulte de la diversité des approches proposées pour résoudre un cas précis, mais aussi celle qui résulte tout simplement de la diversité des experts consultés. On parle alors de système multi-experts.

Les outils graphiques disponibles en standard sur la plupart des environnements informatiques ont grandement simplifié la réalisation d'interfaces utilisateurs conviviales (cf. § 3.1, figure 2).

Enfin, les systèmes ne sont plus isolés ; ils peuvent communiquer avec des applications standard mieux appropriées pour gérer les calculs numériques (tableurs ou codes de

calcul) et les informations de l'entreprise (bases de données). Cette intégration dans l'informatique " classique " des utilisateurs simplifie la mise en place de ces systèmes; de moins ésotériques ils en deviennent plus " utilisables ".

1.2.2 L'art de la mine

La conception et la conduite d'une exploitation minière relève plus d'un véritable " art " que d'une technique ou d'un ensemble de techniques. Les savoirs qui sont impliqués sont multiples. Cet " art de la mine " est un terrain propice à l'utilisation des méthodes de l'intelligence artificielle et plus particulièrement de celles qui permettent le développement de systèmes à base de connaissances.
Là où les méthodes classiques d'optimisation n'apportent que des réponses partielles, les systèmes experts contribuent à intégrer la complexité des domaines concernés et des tâches à résoudre. Envisagés comme des systèmes d'aide intelligente à la décision, ils remplissent une mission d'assistance auprès des exploitants plus qu'ils ne " remplacent " les experts.
En fait, l'évolution de la recherche en systèmes experts telle que nous l'avons relatée ci-dessus n'a été prise véritablement en compte que tardivement dans notre projet SOUT ; la raison évidente en est que le développement a été le fait d'ingénieurs et de chercheurs concernés principalement par la géotechnique des exploitations minières et informaticiens par nécessité, plus que celui de professionnels de l'intelligence artificielle.

2. Historique du projet SOUT

Le projet SOUT a démarré en 1985 et on peut dire qu'il a traversé, à l'image de l'intelligence artificielle et de ses applications, les trois époques suivantes :

2.1. Les débuts : le mythe de l'expert artificiel (de 1985 à 1988)

En 1985, lors de la grande époque de l'intelligence artificielle et des systèmes experts en particulier, Charbonnages de France (CdF) à décidé de confier au CERCHAR [2] la réalisation d'un système expert d'aide au choix du soutènement, avec l'idée assez répandue à l'époque, de «remplacer» les experts en soutènement. C'est ainsi qu'est né le projet SOUT.
La réalisation de la base de connaissances de cette première version s'est déroulée en plusieurs étapes, conformément aux recommandations classiques de l'époque [Waterman 86].

[2] Centre d'études et de recherches des Charbonnages de France, actuellement INERIS.

1985 : Réalisation d'une maquette de démonstration :
Au cours de cette phase, une première base de connaissances a été réalisée à partir d'une trentaine de règles. Elle a permis de tester la faisabilité du projet et de cerner les premiers problèmes liés à son développement [Baroudi 85].
1986 à 1987 : Réalisation d'un prototype de recherche :
Après une période transitoire de quelques mois, destinée à familiariser avec le domaine minier, les personnes impliquées (par l'intermédiaire d'études bibliographiques, de visites de mines et de contacts avec les exploitants), on a abordé le développement règle par règle de la base de connaissance, en prenant soin de tester chaque règle sur un certain nombre de cas judicieusement choisis.
En plus des tests effectués au CERCHAR, plusieurs démonstrations étaient présentées dans les mines, futures utilisatrices du produit.
A la fin de cette phase, la base de connaissances contenait près de 250 règles.
1988 : Réalisation d'un premier «produit final» : Fin 1988, une version 0.1 de SOUT est achevée [Baroudi & Revalor 88]. Cette version aurait du servir dans les unités d'exploitation pour choisir de manière indépendante, i.e. sans intervention d'un spécialiste humain le type de soutènement dans une galerie donnée.

2.2 La déception : Analyse de l'échec de la première phase (de 1989 à 1992)

A la fin des années 80, on s'est aperçu que les systèmes experts avaient du mal à tenir leur principale promesse («remplacer les experts»), et un sentiment général de déception s'installa. Le projet SOUT n'y échappa pas. Outre un manque cruel de convivialité et un manque d'intégration (aucun interfacage direct avec des bases de données existantes, peu d'accès immédiat à des programmes de calcul analytique ou numérique), on s'est vite aperçu qu'il y avait peu de chances pour que SOUT " remplace " l'expert en soutènement. Le système SOUT 0.1 resta alors en l'état jusqu'en 1992.

2.3 Le réalisme : Les Systèmes Intelligents d'Aide à la Décision (depuis 1992)

Depuis le début des années 90, on assiste à un nouvel essor de l'intelligence artificielle et à une redéfinition du rôle des systèmes experts : ce sont plus des systèmes d'assistance et d'aide que des systèmes destinés à remplacer les experts. Une collaboration s'est alors établie entre l'INERIS, et nos collègues des charbonnages allemands : la Deutsche Montan Technologie. Cette collaboration ainsi que les travaux de recherche et d'ingénierie réalisés depuis 1992 sont décrits en détail au paragraphe suivant.

3. Evolution du projet SOUT depuis 1992

La version 0.1 de Sout, achevée en 1988, est malheureusement restée très peu utilisée et peu d'efforts ont été consacrés à sa maintenance. L'intérêt de DMT, depuis Juillet 1992 pour les systèmes à bases de connaissances dans le domaine minier en général, et pour Sout en particulier, nous a permis, d'une part, de maintenir jusqu'à aujourd'hui une veille technologique dans le domaine des systèmes à base de connaissances, et d'autre part d'améliorer considérablement l'implémentation informatique de Sout.
Ce soutien de DMT nous a permis de " professionnaliser " le prototype expérimental Sout 0.1 réalisé à l'occasion d'une thèse de doctorat d'université [Baroudi 88] pour parvenir à la version Sout 2.0, véritable logiciel robuste, ergonomique et «prêt à l'emploi».

3.1 Re-programmation informatique de l'expertise.

La version 0.1 de Sout était principalement destinée à démontrer l'intérêt et la faisabilité d'un système expert dans le domaine minier.
Cette version Sout 0.1, bien que comportant une excellente expertise dans les domaines de la géotechnique et de l'exploitation minière, ne tirait pas pleinement parti des nouvelles méthodologies des systèmes à base de connaissances. La réalisation informatique n'était pas non plus conforme aux exigences actuelles en terme de facilité d'utilisation et de robustesse. Les interfaces étaient peu conviviales, et chaque mauvaise utilisation du prototype, ou l'introduction de données non prévues provoquait un " plantage " du programme.
Dans la version Sout 2.0, [Thoraval & al 94], [Sbierczik & al 95], nous avons mis l'accent sur une programmation selon les règles de l'art en intelligence artificielle, en tenant compte des résultats récents des recherches dans ce domaine, tout en intégrant l'expertise de Sout 0.1.
Nous avons également prévu, par l'intermédiaire de fichiers externes, la possibilité pour l'utilisateur de créer une «banque de données», lui permettant de conserver des jeux de données «types». Ce stockage sur fichiers externes permet aussi de réaliser de véritables «backtracks» (retours en arrière du raisonnement), possibilité non offerte directement par NexpertOject®[3].
Finalement, nous avons créé, avec Toolbook®[4] de véritables interfaces graphiques conviviales, tirant parti au maximum des possibilités offertes par la souris, les menus déroulants, les écrans graphiques, les boutons etc. (cf. figure 2).

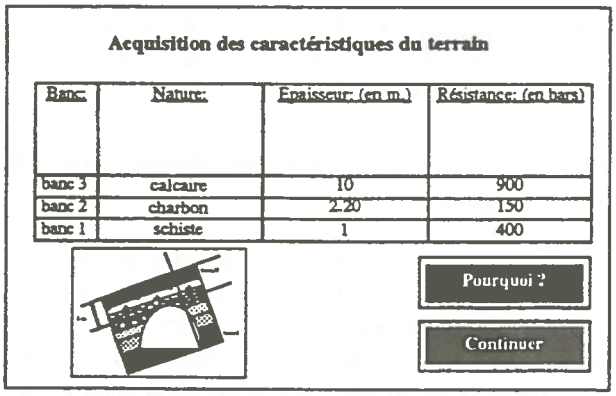

Figure 2 : Ecran graphique de saisie de la stratification au toit de la galerie.

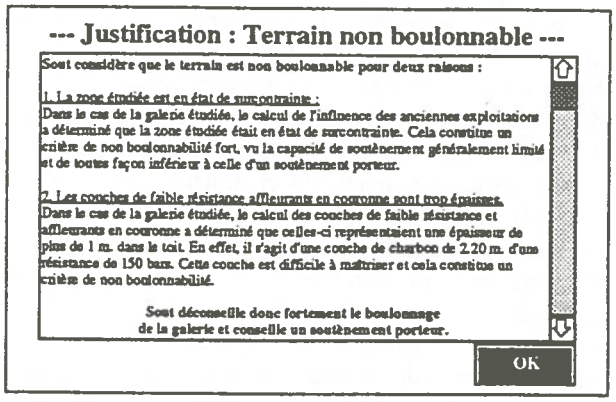

Figure 3 : Conclusion du SIAD Sout 2 concernant le type de soutènement à mettre en place.

Un effort particulier a été fait, lors du développement de la version 2.0 de Sout, pour illustrer de façon interactive le raisonnement et pour expliquer et justifier les résultats du système (Cf. figure 3).

Les utilisateurs n'ont en effet confiance que dans les résultats dont ils peuvent obtenir une justification. C'est un point très important pour que l'outil soit accepté et surtout, utilisé. C'est de plus un des atouts pour que le produit serve à des fins de formation.
Ainsi, en actionnant par exemple le bouton «?» de la figure 1, on obtient une justification sur la conclusion de Sout (Cf. figure 3).

3.2 Test du système Sout 2 par les experts allemands

La version 2 de Sout est suffisament robuste et conviviale pour être utilisée par des novices en systèmes à base de connaissances (aucune connaissance particulière dans ce domaine n'est nécessaire); c'est ainsi que Sout 2 a pu être testé et évalué par les experts de DMT.

[3] NexpertObject® est un générateur de systèmes experts développé par la société Neuron Data®
[4] Toolbook® est un générateur d'interfaces développé par la société Asymetrix®

L'expertise de SOUT a été confirmée dans son ensemble par les experts allemands. Certains points étaient traités différemment en Allemagne mais les ingénieurs reconnaissent l'intérêt de disposer également de l'expertise française, même si elle n'est pas toujours adaptée aux conditions allemandes, du moment que cette expertise est clairement identifiée comme provenant d'experts français.

3.3 Le système PLANANK 0.1

En 1994, DMT décide de réaliser, en étroite collaboration avec l'INERIS, le système à base de connaissances «Planung des Ankerausbaus» : PLANANK. Le but du projet est d'intégrer, à terme, au sein d'un même système, l'ensemble de la connaissance disponible dans les charbonnages allemands en matière de boulonnage des galeries minières afin de réaliser un logiciel complet, traitant de tous les aspects du boulonnage, et pouvant être directement utilisé par tous les ingénieurs de DMT.
Dans un premier temps, DMT a financé en 1994 la conception et la réalisation, sous le pilotage de l'INERIS, d'un système expert de planification du boulonnage dans une voie de taille : «Ankerausbau für Abbaustrecken» (Cf. figure 4).

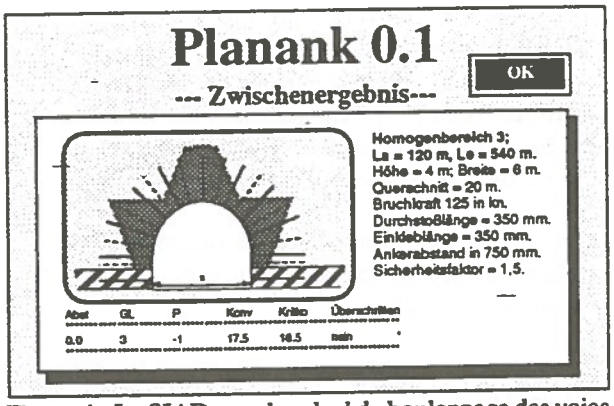

Figure 4 : Le SIAD pour le calcul du boulonnage des voies de tailles allemandes : PLANANK 0.1.

Ce système contient, conformément aux objectifs susmentionnés, la connaissance des spécialistes allemands en matière de boulonnage des voies de taille au creusement. Cette connaissance s'est avérée complémentaire et non contradictoire avec celle contenue dans SOUT.

Par ailleurs, le système PLANANK 0.1 a été particulièrement adapté aux conditions allemandes :
• il tient compte des particularités géologiques des gisements allemands (veines minces, terrains très stratifiés...),
• il intègre directement des programmes de calcul spécifiques réalisés par DMT pour le calcul de la longueur et la densité des boulons,
• il est conforme aux exigences de la législation allemande pour les schémas de boulonnage.

3.4 Objectifs pour 1995 : Le système multi-expert franco - allemand SOUT 3

Partant du système expert SOUT 2.0 ainsi que du système expert Planank 0.1, système expert de planification du boulonnage dans une voie de taille [Kouniali 95], nous nous proposons de réaliser un système multi-experts franco-allemand de calcul du schéma de boulonnage dans les galeries minières (Cf. figure 5).

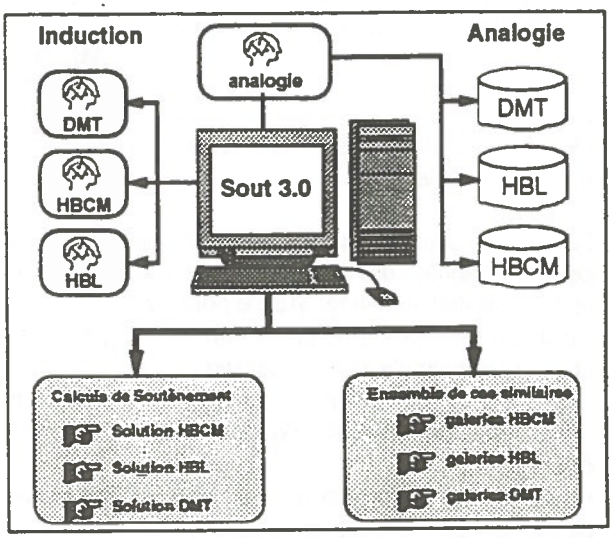

Figure 5 : Organisation du Système Multi Expert SOUT 3.

Ce travail s'effectuera dans le cadre du projet ciblé boulonnage et sera financé conjointement par la Communauté Européenne du Charbon et de l'Acier (CECA), par Charbonnages de France (CdF) du côté français, et par DMT du côté allemand.
En effet, un des principaux objectifs du projet ciblé boulonnage est la comparaison des différentes méthodes utilisées dans chaque pays pour déterminer le schéma de boulonnage des voies, afin de dégager les règles de la connaissance régissant ces méthodes. Cette connaissance est actuellement contenue, selon les pays, dans les notes de service, les textes législatifs, et surtout dans la tête des experts.

Comme il a été dit ci-dessus (Cf. & 1.2), l'approche multi-expert permet de modéliser le savoir et le savoir-faire de plusieurs experts au sein d'une base de connaissances regroupant les règles de raisonnement utilisées par les ingénieurs spécialistes dans le domaine pour définir et calculer le schéma de boulonnage en question.

Un tel système permettra d'intégrer les connaissances et l'expérience complémentaire de plusieurs spécialistes confirmés ainsi que de disposer d'un outil tout à fait unique pour la formation d'ingénieurs de spécialités différentes (Cf. figure 6).

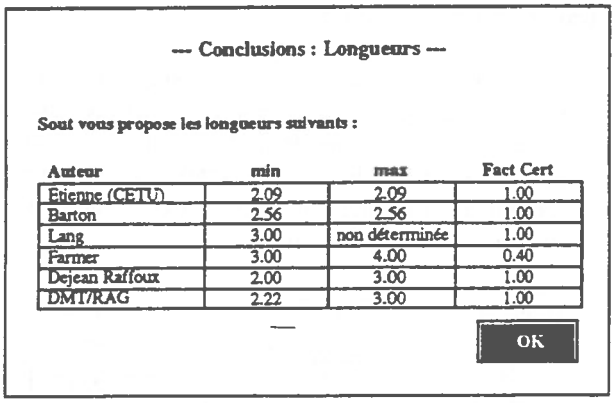

— Conclusions : Longueurs —

Sout vous propose les longueurs suivants :

Auteur	min	max	Fact Cert
Etienne (CETU)	2.09	2.09	1.00
Barton	2.56	2.56	1.00
Lang	3.00	non déterminée	1.00
Farmer	3.00	4.00	0.40
Dejean Raffoux	2.00	3.00	1.00
DMT/RAG	2.22	3.00	1.00

OK

Figure 6 : Résultats de SOUT concernant des longueurs de boulons possibles.

Le système multi-experts devra intégrer les connaissances et l'expérience des experts français et allemands dans le domaine du boulonnage afin de pouvoir :
• conserver le savoir et le savoir faire de ces spécialistes, entre autres pour d'autres spécialistes,
• servir à la formation continue des ingénieurs et des agents de maîtrise au sein de la Ruhrkohle AG (RAG), de CdF ou de DMT,
• disposer d'un outil d'aide à la décision en cas d'absence ou d'indisponibilité temporaire des experts humains.

4. SOUT et les évolutions envisagées

Les résultats récents et concluants du projet SOUT en tant que SIAD, nous ont poussés à envisager, en collaboration avec nos collègues allemands et français, un système intelligent de planification et de simulation d'une exploitation minière.

La planification d'une exploitation minière comporte, en premier lieu, une série de décisions que nous qualifierons de "décisions de premier ordre" et qui sont très étroitement conditionnées par des considérations sur la géologie et l'histoire du gisement exploité : Il s'agit de la géométrie du gisement, de sa régularité, de la position et de l'importance des failles, de l'existence et de la localisation d'anciens travaux, de l'existence, de la localisation et de l'état d'infrastructures préexistantes...

Ces décisions "du premier ordre" vont porter par exemple, sur le découpage des panneaux, l'ordre d'exploitation, la vitesse d'exploitation... Elles pourront être modifiées par la suite.

Ces premiers choix vont impliquer quasi-automatiquement un certain nombre de conséquences (par exemple en termes de créations d'infrastructures nouvelles ou de distribution des "pressions de terrains" dans le massif...). Ces conséquences sont évolutives, en ce sens qu'elles apparaîtront au fur et à mesure de la mise en oeuvre des décisions du "premier ordre". L'ensemble correspond en quelque sorte à une "initialisation " du système.

A partir de là, le projet concret d'exploitation va nécessiter un certain nombre de décisions de «2ème ordre». Leur objet est de permettre que soient remplies les conditions de réalisations des décisions «du premier ordre». Ces choix concernent :
• les méthodes de creusement des infrastructures,
• le soutènement des voies et galeries,
• les méthodes d'abattage dans les chantiers,
• le soutènement des chantiers,
• l'aérage,
• l'exhaure,
• ...
Une deuxième série de conséquences résultent de ces décisions. Elles s'expriment en terme de main d'oeuvre, de matières consommables, en investissements nécessaires, et déterminent des niveaux de production et des coûts.

Les exploitants souhaitent disposer d'un outil intelligent d'aide à la décision, permettant des modélisations tridimensionnelles poussées, pour effectuer des simulations qui donnent une idée des conséquences des décisions de planification qu'ils envisagent.

C'est un tel système intelligent de planification et de simulation d'une exploitation minière que nous envisageons maintenant de réaliser.

5. Conclusion

La conception d'un système à base de connaissances est un processus complexe qui ne s'improvise pas. Les règles de l'art impliquées dans la réalisation d'un tel système sont finalement les mêmes que celles qui gouvernent la conduite d'un projet, qu'il soit informatique ou d'ingénierie en général. Les compétences spécifiques relatives au caractère cognitif du projet sont également difficilement contournables ; c'est parce que nous nous sommes décidés à les prendre réellement en compte que les experts et les exploitants se sont mis à considérer SOUT comme un outil susceptible de faciliter leur métier et qu'ils ont accueilli favorablement les projets d'extension que nous avons mentionnés.

6 Bibliographie

[Baroudi 88] H. Baroudi. Choisir un soutènement des galeries : réalisation d'un système expert. Thèse de Doctorat Ecole des Mines-INPL, Nancy France.

[Baroudi & Revalor 88] H. Baroudi et R. Revalor. Vers un système expert pour le choix d'un soutènement en galeries. - Proceedings of the first canadian conference on computer applications in the mineral industry - Québec - 1988.

[Kouniali 95] S. Kouniali. Entwicklung eines Expertensystems zur Berechnung des Ankerausbaus für Abbaustrecken. Rapport interne INERIS / DMT, janvier 1995.

[Newell, 1991] : A. Newell. Unified Theories of Cognition. Harvard University Press, 1991.

[Sbierczik & al 95] : G. Sbierczik, W. Kammer & S. Kouniali. Entwicklung eines Expertensystems zur Optimierung des Streckenausbaus durch Einbeziehen der Abbauplannung : Rapport CECA N° 7220-AB/136, 1995.

[Thoraval & al 94] A. Thoraval, M. Al Heib & S. Kouniali. Amélioration de l'avancement des voies au charbon à grande profondeur : Rapport CECA N° 7220-AB/311, 1995.

[Waterman, 1986] D. A, Waterman. A guide to expert systems. Addison Wesley, 1986.

CAMI'95: 3rd Canadian Conference on Computer Applications in the Mineral Industry
Montréal, Québec, Canada, October 22-25, 1995

Development of A Knowledge-Based Automatic Stope Scheduling Model

Yeong Su
YLS Associates, Sudbury, Ontario

Somchet Vongpaisal
Mining Research Laboratories
CANMET, Ottawa, Ontario

Herbert Smith
Falconbridge Limited, Sudbury, Ontario

ABSTRACT:

Stope scheduling is an important mining engineering function. The process is something of an art and is a prime candidate for the application of expert systems. Due to the complex nature of stoping activities there is also a need to test tentative schedules, utilizing a simulation model, prior to implementation. Within the model the normal stoping operations are simulated by "hard wired" codes. Unusual activities and the new configurations are furnished through a set of rules. Data are entered from data bases and spreadsheets. Application of knowledge-based systems comes at the front end of the model. It instructs users how simulation data are to be prepared and how unusual activities are to flow in the model. The model in turn provides production schedules and finite capacity analysis. Although it may be beneficial for the knowledge-based systems to be applied at the end of the simulation to recommend further improvement through the analysis of output statistics, this is not done in the current version of the model.

RÉSUMÉ:

L'ordonnancement de l'abattage est une activité technique importante dans l'exploitation minière. Le procédé est presqu'un art et se prête bien à l'utilisation des systèmes experts. En raison de la nature complexe des travaux d'abattage il est nécessaire, avant de procéder, de mettre à l'essai des programmes provisoires, au moyen d'un modèle de simulation. Dan le modèle, les opérations d'abbatage ordinaires sont simulées par des codes conventionnels. Les activités inhabituelles et les nouvelles configurations sont fournies par un ensemble de règles. Les données sont introduites à partir de bases de données et de feuilles de calcul électronique. L'application de systèmes à base de connaissances se produit dans la partie frontale du modèle. L'utilisateur est informé de la façon de préparer les données de simulation et du cheminement des activités inhabituelles. Par ailleurs, le modèle fourni le calendrier de production et l'analyse finie de la capacité. Bien qu'il soit peut-être avantageux que les systèmes à base de connaissances soient utilisés à la fin de la simulation afin de recommander des améliorations par l'analyse des statistiques, ces fonctions ne sont pas exécutées par le prototype actuel.

INTRODUCTION

The ultimate goal of stope scheduling for cut-and-fill mining operations is to achieve the optimum utilization of available resources in order to obtain the best short term and long term output goals from a given stoping area. The goals may be about ore production, productivity, grade control, ground control, or simply a better prediction of what is being scheduled. The scheduling process is something of an art and is a prime candidate for the application of expert systems, the use of which has become widespread in the solutions of various problems (Su, et.al. 1993).

During the scheduling process a great number of variables have to be taken into consideration. In a typical stoping area there may be from two to thirty headings (work faces) sharing the same stoping equipment and manpower. Each heading will have the standard stoping activities including drilling, blasting, scaling, mucking, and bolting. It will also have non-standard activities such as cable bolting, cleaning up, fill preparation, and backfill cycle. There will be shift changes and limited blasting times to be considered. Manpower will vary from week to week and from weekdays to weekends and equipment will have to undergo scheduled maintenance. Headings will have different priority for various reasons and each heading will have its own parameters such as width, height, advance, and grades. Using conventional scheduling techniques, it is almost impossible to evaluate the interaction of these variables simultaneously and repeatedly. The bar chart method, the cpm-pert method, and the resources levelling method need to make many simplifying assumptions. Many essential elements which govern the output of a schedule are distorted by these same assumptions.

The very nature of a simulation model allows the actual details of stoping operations to be weaved into a virtual-reality laboratory. Many simulation models (Manula, 1973) have been developed to study alternative schedules of underground coal and open pit mining operations where mechanization has been advanced more rapidly than in underground hardrock mines. However, the obvious disadvantages associated with such fine detailing is that the programmer may find it virtually impossible to foresee the endless changes of stope configurations and re-configurations. Many models are developed to study a single subject and "thrown away" afterwards, while other models suffer high maintenance and a short life cycle. A partial solution to this would be to use the artificial intelligence simulation method (Haddock, 1989). Within the model, the normal stoping operations are simulated by "hard wired" codes. Unusual activities and new configurations are furnished through a set of rules in data form.

Through the use of an Intelligent Front End (IFE), where data is entered from a database and spreadsheets, the simulation model can have an extended useful life beyond that of the original design. The IFE instructs users how simulation data is to be prepared and how unusual activities are to flow in the model. The model, in turn, provides production schedules and finite capacity analysis via forward chaining processes. There is also some thought that "expertise" can be provided through artificial intelligence utilizing backward chaining methodology to help seek the goals that the simulation model is being designed to achieve. Such an "Intelligent Rear End" may be feasible for some simple models. It has not been seriously contemplated here for the simple reason that the model is considered as a laboratory and users know their realistic scheduling alternatives.

THE ESSENCE OF STOPE SCHEDULING

The process of stope scheduling involves the selection of a group of working headings that are to be advanced during a given time horizon; determining the nature of the work to be performed for each heading; deciding upon operating sequences and priority of headings; scheduling manpower and equipment for the work; and "forecasting" the outcome of the final schedule.

Stope scheduling is an important mining engineering function. A good schedule will provide guidelines to field crews to ensure that the short term requirements of ore production and development advance are maintained while preserving the integrity of long term needs. A lesser role, yet equally essential of stope scheduling, is to forecast stope production and supply reliable information to

the mill or other downstream operations.

It is a known fact that if the headings are allowed to sequence randomly or by miners' preference, there is a strong possibility that, sometime in the near future, one or more of the following conditions will occur:
- Productivity will suffer as the number of available working face decreases.
- Several headings will require backfilling at the same time and the fill plant will not be able to provide adequate quantities at short notice.
- Leading headings will fall behind other surrounding headings and ground control problems may ensue.
- The rate of ore production will fluctuate.
- An accurate "forecast" of production will not be possible, impeding the ability of the mill and other departments to plan their operations.
- Daily grade fluctuations will be greater.

In terms of time frame and the needs of mine management, stope scheduling can be classified into these categories:
1.) one week output schedule: Use of up-to-date information from mine captains and shiftbosses to produce weekly production forecasts. This will provide reliable information to the mill and also permit frontline supervisors to allow for events such as breakdowns.
2.) two weeks to 6 months schedule: The main purpose is to ensure that stopes are filled in a timely fashion, cable bolting is properly scheduled, and priority headings are selected such that sufficient number of working faces are available during the period.
3.) long term, 6 months to life term schedule: This is mainly for the purpose of economic analysis, the mine's long term investment commitments, and cashflow forecast.
It should be noted that stope scheduling is not usually an exercise appropriate for a front-line supervisor. The front-line supervisor's role emphasizes manpower assignment, i.e. to keep every man usefully busy during a working day. In a large mine, the stope schedule is also different from the mine's full production and development schedule which is usually of longer term and pieced together from the schedules of all stoping areas.

Fundamental differences between the above first two scheduling categories and the third long term one lie in the areas of initial conditions, degree of abstraction, and applications of the scheduling outcome. The initial conditions are those that occur during the time the scheduling process is carried out. In a "real time simulation", some of the initial conditions may be input from sensors of the mine's monitoring systems. The importance of initial conditions is reduced with a longer term schedule. Short term schedules need to take all detailed activities into consideration. The unit operations of drilling, blasting, mucking, and bolting have to be treated individually since the schedule is adversely affected by the interference between activities. The same details can be applied to the long term schedule at the expense of computation time. However, in a long term schedule the same degree of accuracy can be achieved by considering the total cycle time of breasting as a unit operation. It is obvious that the long term schedule is more appropriate for major capital investment decision making, while the short term ones are suitable for operators' mining plans. The two short term schedules are the main focus in this paper.

CONSIDERATION OF VARIABLES IN SHORT TERM SCHEDULING

In a throw away model, most variables are built into the model, leaving only a few to be enacted as inputs for experimental purposes. This eliminates the tedious task of understanding and correctly entering the input data. In the other extreme, a model can be a general purpose one, with all variables being defined by users. Functions governing the behavior of each variable and the logic that controls the interaction of these variables are also left up to the users. Such a degree of flexibility calls for a specialist to construct useable models. Nevertheless, after the project is completed, the model meets the same fate of being thrown away. The simulation language software packages such as "Cinema" (Systems Modeling Corp.,1988) and "Autosched" (AutoSimulations, 1993) give models which belong to this category. The stope schedule model presented in this paper cannot avoid the eventuality of being thrown away. In order to prolong its usability, more variables are organized in the IFE as input while the complicated relationships among these variables and others are hidden in the program.

Within a typical stoping area there may be from two to thirty headings (work faces) sharing the same stoping equipment and manpower. When scheduling the area, many variables have to be considered. Some of the essential ones in the model are listed below.

Heading Data:

These include the names, the types, and the priority of the headings. The headings are limited to three types: cut-and-fill stope, ramp and access development, and overcut and undercut (for blasthole operations). The heading data set also contains the total number of breasts in each heading, the filling group number, and how a heading is to be started (such as after a certain fill group is completed or after a certain heading is advanced to a certain breast) or how a heading is to be stopped (say, when it reaches a certain breast) and, perhaps, restarted (when a different heading reaches a certain breast). The elements of the cyclical operation (drilling, blasting, mucking, bolting, etc.), the types and nature of cycle interruptions, the current activity of a heading, and the physical parameters of each breast: width, height, advance, tonnes, % of waste inclusion, are also required.

Equipment Data:

Other than the names and the types of activity performed, the important equipment parameters are the performance rates, in terms of standard hours required to produce a cubic meter (mpu) of material, equipment status: whether the equipment is idle or active, equipment setup time, maximum number of operators that can be assigned, and the maintenance schedule: daily, weekly, and x-hundred hours inspection. Various performance rates are specified for these six heading types: stopes less than 9 m wide, stopes greater than 9 m wide, subdrift less than 6.6 m wide, subdrift greater than 6.6 m wide, overcut and undercut, and ramp development.

24-Hour Shift Schedule:

This consists of the starting time of a working shift, the starting time of actual work, and the starting time of breaks (coffee break, lunch break, quitting, etc.) during a 24-hour period for weekdays, Saturdays, and Sundays.

Manpower and Operating Days Per Week Schedule:

This includes the size of the regular crew, in terms of men per shift for weekdays, Saturdays, and Sundays for each week. The support crews for backfilling and cable bolting, and maintenance mechanics are not included. In the days per week schedule, a zero day per week is allowed. In the cases of six or seven days per week, the sixth and seventh days are interpreted as Saturdays and Sundays, respectively.

Backfill Groups:

Several headings can be grouped together in order to be filled at the same time. A total of five groups with one to ten headings per group is allowed. The standard hours required for each group, including all operations from building fill fence and pouring, to settling, are required. If the fill crew is part of the stoping crew, then the element "backfill equipment" will have to be assigned one or more operators.

Blasting Schedule:

Ten time slots are reserved during a 24-hour day where blasting is permitted. These blasting times will have to coincide with the break times of the 24-hour schedule.

General Data:

This includes identification of each experimental run, crew number, date of the study, the studied period, and the expected performance index of the crew. The performance index is the ratio of the standard hours and the actual hours that it takes to produce 1 mpu. It is similar to the bonus rate of the incentive system. The standard width for stope, subdrift, and ramp, the standard depth of advance, and the standard height for each breast, along with ore and waste densities, are specified in the general data section as common values to all breasts. This will simplify the input process if dimensions of the breast are relatively uniform among all headings.

"HARD-WIRED" VARIABLES AND LOGICS OF STOPE SCHEDULE MODEL

There are certain fundamental routines governing

the execution of a simulation model: routines that advance the simulation clock, update the succession of events, and generate variants of stochastic variables. These routines are mandatory of any simulation model and are generally the core of commercial simulation packages. In the case of the stope schedule model, there are also some indigenous variables that are considered as impractical for users to handle. These variables are hard-wired in the model. Some of them are described below.

Events and Event Handlers:

At each active heading, major events occur at these situations: the completion of an activity of a cyclical operation nature, the completion of an activity of a cycle interruption nature, the completion of a breasting cycle, the completion of all breasts, and the completion of backfilling.

Major events also occur at shift changes, lunch breaks, coffee breaks, the end of a 24-hour day and 7-day week, the end of a scheduling period, and the completion of equipment maintenance.

At the occurrence of an event, the handlers act on assigning new activity (cyclical or cycle interruption), assigning equipment to a heading or to a scheduled maintenance, assigning manpower, calculating the duration of an activity, adjusting the completion time of an activity, accumulating various statistics, and at the end, outputing the results.

Duration of an Activity

The time required to carry out an operation or an activity is input, and is measured in two different units of time: hours, and standard hours per mpu. The standard hours per mpu are input from equipment performance rates while the "hours" are input from the cycle interruptions of a heading and the required times of backfill groups.

The unit "mpu" (metric production unit) represents a cubic meter of in-situ rock (or ore) mass. The work study department establishes the standard performance rate in terms of hours per mpu for various types of stoping jobs and uses them to gauge against the actual output in order to administer the incentive system. The ratio between the standard hours earned, which is the product of the actual mpu output and the standard hours per mpu rate, and the hours worked on the measured work (the elasped time) is called the "performance index". The actual incentive earnings, or bonus rate, may be slightly different from the performance index because of the addition of other unmeasured factors such as, for example, a superintendent's adjustment.

The relationship between the performance index (D), the standard hours earned, which is the product of the output units (M) and the standard rate (U), and the hours worked (T) is:

$$T = \frac{M * U}{D} + \frac{C}{D} + \frac{B}{D}$$

where C consists of cycle interruption work hours and B consists of hours for items such as shift auxiliary allowance, extra allowance for unmeasured work or wait, etc.

Using the same principle, the model calculates the duration of each "small" activity as follows:

$$t_i = \frac{m_i * u_i}{D}, \frac{c_i}{D}, b_i, w_i$$

where w_i is the delay between activities. The total time (T) is the summation of these t_i elements. The model calculates t_i for each activity from exogenous data whenever an equipment piece is assigned to a heading. The t_i value is adjusted whenever a break time is encountered.

Manpower Assignment

Total manpower is referred to as "men per shift" in the program. A regular crew consists of those who work as a team in the same working places in all shifts during the scheduled period. The supporting crews, such as designated fill crew or cable bolting crew, who are not full time in the work area are not designated as regular members. The regular crew is the subject of manpower assignment here.

Each piece of equipment is permitted to have the maximum number of operators assigned. For example, bolting can use up to 4 persons while mucking can use up to 1.5. The actual number of persons operating a machine depends upon the availability of men at that particular moment. A

fraction of manpower such as 1.5 for mucking, as mentioned above, is allowed. If equipment is operated by a special operator and not the regular crew, then it requires zero (0) manpower.

Manpower assignment in the program is based on the minimum value between availability and requirement of manpower at the moment an event occurs. The required manpower can be either the maximum allowable men for that machine or the difference between the maximum and the number of men currently being assigned to the machine. Since the available manpower can be either 0 or greater than 0 (two cases) and the required manpower can be either 0 or greater than 0 (two cases), there are four cases to be considered when manpower is assigned to a machine. Furthermore, if manpower is assigned at a figure less than that of the maximum allowed, reassignment is carried out when new manpower becomes available.

Equipment Assignment

Each piece of equipment being used by the regular crew or by a special crew is assigned a unique coded number. A total of 15 pieces of equipment belonging to 9 different types of operations is allowed in the system. The equipment is coded from 1 to 9 with code 9 being reserved for backfilling, code 2 for loading and blasting, and code 4 and 6 for muck producing equipment such as scooptrams.

When a heading is ready for a new activity, it is assigned the necessary machine according to the following rules: if the machine performs the type of activity that is needed by the heading and if the machine is available, i.e. not down for maintenance or repair, not occupied by another heading, or not requested by another heading which has a higher priority. Even after the machine is assigned to a heading it cannot commence to work until manpower is also assigned (see manpower assignment above). Therefore, idle equipment can be caused by either no heading available or no manpower available.

The duration of the activities is calculated after equipment and manpower are assigned. There are six different working environments that affect the duration of the activity of an equipment piece. They are: stope < 9m wide, stope > 9m wide, subdrift < 6.6m wide, subdrift > 6.6m wide, stope, and development. Each piece of equipment also needs a setup time. The setup time for the regular equipment is small and is usually blended into the standard operating time. However, where a long setup time is required, such as could be the case for, say, a continuous cutting machine, then the setup time is calculated separately.

Backfilling

Backfilling can be performed in many ways. It can act as a cycle interruption or as a regular backfill operation after the end of a heading is reached. It can be carried out by the same stoping crew or by a special filling crew. It can be filled as a single heading or as a group of several headings. If a heading is assigned a filling group number and is also defined in one of the cycle interruptions or a backfill operation, the heading will undergo two filling processes, one as cycle interruption and another at the end of the heading.

Assignment of manpower, equipment, and duration of backfill activity is the same as that of other stoping activity. Equipment needed for backfill, either real or imaginary, is listed in the equipment section under code 9. In cases where special fill crews are used, the maximum number of operators required for such backfill equipment is assigned as 0. If several headings are to be filled as a group, the filling operation commences only after all headings reach their respective ends. The required filling time (including fence building and pipe installation if these are not separate items) for each group is entered as standard hours.

The filling operation is not performed for a heading (such as development headings or stopes to be left unfilled after being mined out) under the following conditions: The heading does not belong to one of the five allowed filling groups; the heading is not specified in one of the cycle interruptions .

Heading Starts and Stops

A heading is a working place where workers and machines perform activities of cyclical operations and cycle interruptions. A stope may contain one or more than one heading. Several physical working headings can also be simplified into one heading for programming purposes. All headings listed in the

input file are regarded as active headings.

A heading becomes busy when equipment and men are assigned to it. If a piece of equipment is assigned to a heading, it has to complete the task before being released to another heading. A heading has to complete the last element of the cyclical operations before considering other operations such as cycle interruptions, backfilling, or advancing to the next breast. A heading may also have to wait until a certain other heading is advanced to (and has completed) a certain breast, or it may have to wait until a certain filling group has completed filling. A heading may also have to wait to be restarted, after being halted, until a certain heading is advanced to a given breast.

The heading is considered mined out if it has completed the last activity of the cyclical operations, its current breast number is not mentioned in one of the cycle interruptions, the current breast number equals the maximum breast number, and the heading does not belong to any filling group.

Outputs

The output items include: daily tonnages for the first week, weekly production tonnages and development meters for each heading during the simulation period (a maximum of 26 weeks are output), and statistics of idle time of equipment and headings. Dates of major activity changes in each heading, i.e. starting and completing dates of stoping, starting and completing dates of backfilling, starting and completing dates of cycle interruptions are not output but are readily available in the program.

THE STOPE SCHEDULE MODULE

The module is made up from three windows: a spreadsheet handling the inputs and the outputs, a data screen handling IFE and the detailed heading data, and a main display handling all aspects of simulation.

The input portion of the spreadsheet contains the items described in the preceding section on "Consideration of Short Term Scheduling". They are listed in spreadsheet cells from "A1" to "Z95" under six different sections. Shown in Figure 1 below are cells "A1" to "C20"; this give a glimpse of the general data section and the heading section of this input file. The same spreadsheet receives output from the simulator at cells "AC1" to "BD42"; Figure 2 below shows a small section of this.

	B	C
1		
2	General Data	simulation
3	title	data
4	1996 AP01, Crew #1	02-01-95
5		
6		
7	Heading Section	
8	# heading title	types (key words)
9		stope,o/c,u/c,devel,subdrift
10		production, advance, 2 faces
11	1 36-631 ST. CUT #4	stope production standby
12	2 36-632 ST. CUT #3	stope production,2 faces
13	3 37-630 ST.CUT #7	stope production
14	4 36-1-633 ST.SILL CUT/BENCH CUT	stope production
15	5 33-1-275 B.H.PILLAR O/C	o/c,u/c production
16	6 31-0-669 DUMP X-CUT	development advance
17	7 34-1-648 ST.U/C ACCESS	development advance
18	8 36-2-607 RAMP	development advance
19	9 36-2-614 D.D.STATION	development advance
20	10 36-1-470 X-CUT	development advance

Figure 1.A Section of The Input File

	BC	BD	BE	BF	BG
1					
2	Output Section				
3	- tonnes/week for each production heading				
4	- metres/week for each development heading				
5	-please make sure that total per week on rows 41 and 42 have the cor				
6					
7			week	week	week
8		header	1	2	3
9	heading title	#	(t)	(t)	(t)
10	to be copied from column "B"		(m)	(m)	(m)
11	36-631 ST. CUT #4	1	0	0	0
12	36-632 ST. CUT #3	2	1290	2680	2680
13	37-630 ST.CUT #7	3	697	1193	1193
14	36-1-633 ST.SILL CUT/BENCH CUT	4	645	0	1290
15	33-1-275 B.H.PILLAR O/C	5	504	504	0
16	31-0-669 DUMP X-CUT	6	0	0	0
17	34-1-648 ST.U/C ACCESS	7	4	0	0
18	36-2-607 RAMP	8	0	4	7
19	36-2-614 D.D.STATION	9	4	4	0
20	36-1-470 X-CUT	10	0	4	0

Figure 2. A Section of the Output Cells

The data section and the main display of the module are prepared in the windows of the Level5 Object Expert System Tool (Information Builders Inc., 1990). A portion of the data screen, where the detailed heading information such as width, height, etc. for each breast can be added, deleted, or modified is shown in Figure 3. It also shows some of

the data that is regrouped from the spreadsheet input for data diagnosis. Other IFE routines are being added to this screen. The main display, as shown in Figure 4, contains a message box to instruct and inform users about simulation processes, a picture box, along with various textboxes, representing headings to show the stoping activities, several pushbuttons to perform the labelled actions, and a table listing showing ore production and equipment utilization statistics.

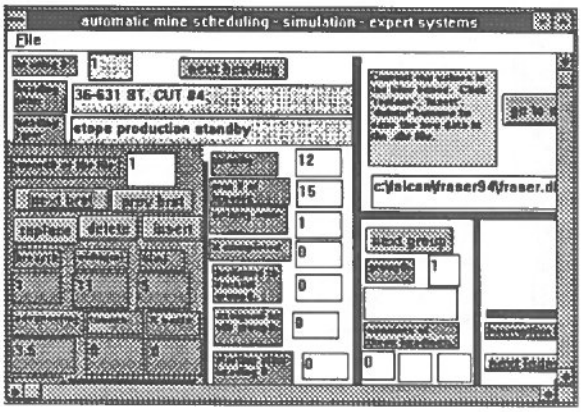

Figure 3. A Section of the Data Screen

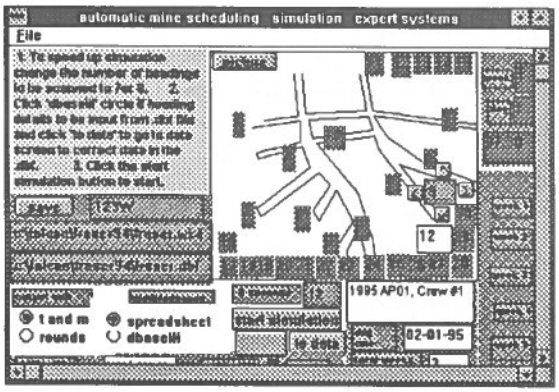

Figure 4. A Portion of the Main Display

VERIFICATION OF THE MODEL

In theory, if the actual performance index is known (which reflects the working rate during a given period) and the given standard rates are used both by the simulation and by the incentive department who issued the incentive statement, it is expected that the simulator would be able to faithfully generate an output consistent with that measured by the surveying department. Similarly, if the same parameters are used by both manual scheduling and simulation, it is also expected that the respective outcomes should be closely matched. The following simulation runs, utilizing an existing mine's historical data, were carried out to test the validity of the program.

The actual performace of crew #1 in the account period (AP) 01 to 06 of 1994 was simulated by the model. A total of six simulation runs were conducted for these six periods. Since the actual performance index and the actual manpower for each period were used for the tests, it is not a surprise that the simulation results compare closely with those of the actual, as shown in Table 1. Although this data indicates that the simulation can "duplicate" the actual situations within acceptable ranges, they are not matched perfectly. The major reason for this is as follows: The idle time of equipment and manpower are accumulated "automatically" by the simulation model, (for example, idle time of drill is 45% of the total "working" time in one of the test runs). This is not the case for a manual scheduling or for the actual calculation of miners' incentive rate. The "miners incentive statement" contains the standard shift auxiliary allowance which is approximately 26% of the "total hours worked on measured work". It also contains an "extra allowance for unmeasured work or wait" of between 13 to 24% of the "total hours worked on measured work". These "artificial" figures affect the values of performance index and it is obvious that the "allowed" allowances do not necessarily correlate precisely with the delays studied in the simulation.

Table 1. Comparisons between Simulation Output and Actual Production

		Actual tonnes	Simulated tonnes	
AP01	ore	13207	13658	103%
	stope waste	544	423	
	dev. waste	5122	4314	97%
	break (mpu)	6126	5851	96%
AP02	ore	11755	12265	104%
	stope waste	2919	2503	

	dev. waste	4329	4500	99%
	break (mpu)	6049	6116	101%
AP03	ore	27104	24879	92%
	stope waste	3379	1764	
	dev. waste	2900	2804	88%
	break (mpu)	10006	9137	91%
AP04	ore	16820	15464	92%
	stope waste	3026	2589	
	dev. waste	2480	1941	90%
	break (mpu)	6565	6313	96%
AP05	ore	18658	17226	92%
	stope waste	2327	1423	
	dev. waste	3129	2804	89%
	break (mpu)	6808	6725	99%
AP06	ore	15750	18462	117%
	stope waste	3617	3286	
	dev. waste	3678	3451	109%
	break (mpu)	7907	8034	102%
Total	ore	103294	101954	99%
	stope waste	15812	11538	73%
	dev. waste	21638	19814	92%
Total	break (mpu)*	43461	42176	97%

* simulated mpu is calculated by: ore tonnes/3.35 + waste tonnes/2.67

In order to test the performance of the model for a "longer term" case, the above six runs were combined into one run. The weighted average bonus rate of 175% was used. The results, as shown in Table 2, indicate that ore production from the stope was higher than actual, development was lower, while overall mpu was reasonably close. Such deviation was caused by some development headings being assigned a lower priority in the simulation. During the six month period, the simulation assigned priority only once, while in the actual operation, it was many times.

Table 2. Six Months Simulation Comparison

	actual	simulation	
ore tonnes	103294	119393	116%
stope waste tonnes	15812	*	
dev. meters	352	270	76%
total mpu	43461	41850	96%

* It was assumed in this test that there was no waste in the stopes.

The next test runs were carried out in order to compare the manual schedule and the automatic schedule by simulation. The schedule of three crews for account period 02 of 1995 was obtained as shown in Table 3. It should be noted that "unmeasured work or wait" with a value of 10% of the labour debit is added to the total earned credit in the manual schedule; a further 20% is added for training; also contained is 28.75% of earned S.A.A. (shift auxilliary allowance). Overall, these "adjustments" create variations between scheduled output and that of the simulation.

Table 3. Comparison Between Manual and Simulation Schedule for Crew #1, #2, and #3 in AP02, 1995

Crew		schedule	simulation	
#1	ore tonnes	14700	13897	
	dev. meters	35	49	
	total mpu	5193	5275	102%
#2	ore tonnes	24940	24409	
	dev. meters	42	25	
	total mpu	8411	7861	94%
#3	ore tonnes	13200	15138	
	dev. meters	46	46	
	total mpu	4998	5577	112%

assumption: performance rate is 170%, 20 days per period. crew #1: 12 men/day; crew #2: 21.6 men/day; crew #3: 14.4 men/day.

SUMMARY AND CONCLUSIONS

This paper presents the use of an intelligent front end (IFE) within a simulation model that performs automatic scheduling of the stope production. The simulation model assembles a variety of input variables from a spreadsheet, dBase files, and via forward chaining methods to generate weekly production and equipment utilization statistics. The purpose of the IFE in the model is to permit users to correctly and effectively handle a great number of variables as input and, therefore, increase the useful life of the simulation model.

The model has been verified with several actual data sets. These tests indicate that the model is capable of sorting out interferences within the stoping system and producing realistic, trustworthy production schedules. The need for utilizing assumptions and artificial adjustments such as those being used by other scheduling methods is completely eliminated when the simulation model is employed. Additional advantage of the simulation model include speed, accuracy, the provision of quality information re equipment utilization, and the capability to run multiple "what-if" scenarios at any time and to rapidly run new scheduling possibilities if unforseen events have a major impact on the current schedule.

The goal seeking, backward chaining simulation model may also have potential in terms of assistance to users. It is the opinion of the writers that the application of this type of artificial intelligence may be beneficial particularly to frontline supervision for daily scheduling purposes.

BIBLIOGRAPHY

AutoSimulations™:AutoSched, Finite Capacity Planning and Scheduling, Bountiful, Utah, 1993.

Cinema™, System for Simulation and Animation, Systems Modeling Corp., Sewickley, Pennsylvania, 1988

Haddock, J. and O'keffs R.M. : "Using Artificial Intelligence to Facilitate Manufacturing Systems Simulation", Computers & Industrial Engineering, 1990, pp 275 - 283.

Level5 Object™, Object-Oriented Expert System for Microsoft Windows, Reference Guide, by Information Builders Inc., New York, NY, 1990.

Manula, C.B., Ramani, R.V., and Su, Y.L. : "OPMHS - A Total System Simulation for Open Pit Mining", 11th APCOM, April 1973.

Su, Y.L., Vongpaisal, S., and Smith, H.A.: "Application of Expert System for Peak Power Management", CIM Bulletin, February 1993, pp73 - 78.

Su, Y.L., Vongpaisal, S., and Smith, H.A. : " Object-Oriented Expert System Module for Hydraulic Backfill Design", XXIV APCOM, October 1993.

10.

mining and process automation
automatisation des mines

CAMI'95: 3rd Canadian Conference on Computer Applications in the Mineral Industry
Montréal, Québec, Canada, October 22-25, 1995

A Positioning System to Aid Underground Navigation

Eric H. Hinton, P. Eng.
INCO Limited
Copper Cliff, Ontario, Canada P0M 1N0

Greg R. Baiden
INCO Limited
Copper Cliff, Ontario, Canada P0M 1N0

Nick Vagenas
Laurentian University, School of Engineering
Sudbury, Ontario, Canada P3E 2C6

Abstract

The automation revolution is being looked at by INCO Limited as a way to increase productivity and safety by keeping the work force in a safer environment. The communications system allows for the tele-operation of mobile equipment. The next hurdle that must be overcome is the positioning of equipment to carry out specific tasks. This paper looks at alternatives for finding reliable positioning systems for underground mining applications.

Résumé

INCO Limitée explore actuellement l'automation minière afin d'augmenter la productivité et la sécurité du travail pour les employés créant un environnement de travail plus sécuritaire. Le système de communication permet la téléoperation d'équipement mobile. Le prochain défi à relever est l'installation d'équipement nécessaire pour exécuter des tâches spécifiques. Ce document propose différentes options afin de trouver des systèmes fiables de positionnement pour l'équipement minier souterrain.

1. INTRODUCTION

The deepening of the current mines in Canada and the pressures put on Canadian operators from lower cost offshore producers is a driving force behind the idea of automation in mining. The definition of automation here is the use of autonomous and semi- autonomous vehicles in an underground mine and does not necessarily mean the absence of workers in the mine. The ability to compete with foreign countries becomes less possible as the technology that previously gave a huge advantage is now equalled [Scoble, 1994]. The Canadian Mining Industry's challenge is to be surpetitious (a group should be more than competitive and strive to create "monopolies of value") rather than merely competitive. [deBono, 1994]

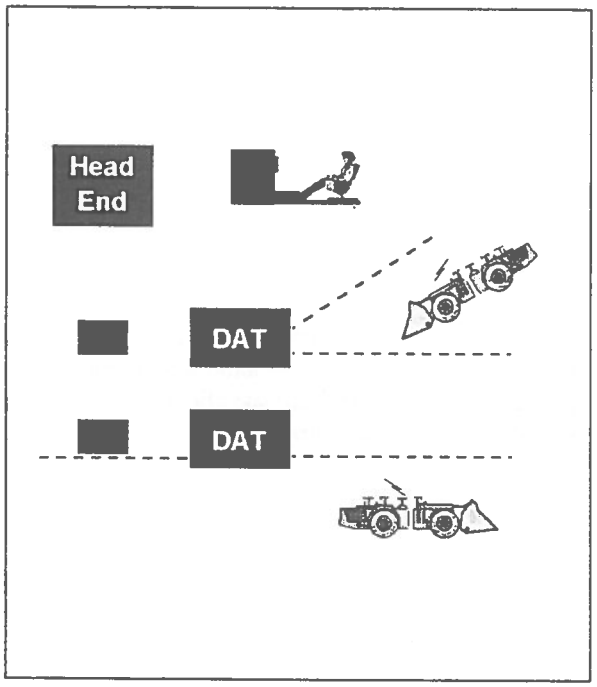

Figure 1: Generalised section of Copper Cliff North Mine showing tele-operation of untethered scooptrams.

The main issue faced by the underground operators at first was how to communicate with an untethered piece of equipment. This was addressed at INCO Limited with a broadband communication system and the development of a Distributed Antenna Translator (DAT) which allows for voice ,video and data to operate simultaneously. (See Figure 1). The DAT ensures that the video signal is the best that can be generated. [Baiden, 1993]

An issue that is now being faced by underground operators is positioning systems for automation. This puzzle is vague because navigation and positioning are often defined as the same thing. Navigation is the ability to move from one point to another and reach a designated target. Positioning is knowing where an object is with respect to a known co-ordinate system.

This paper looks at alternate positioning systems that are being studied by INCO Limited. This is a research project at the Mines Research department and the evaluation part of the project is investigated through a Master's Thesis at the Laurentian University Mining Automation Laboratory (LUMAL).

The scope of the research project is to develop a system that can address navigational subsystems for autonomous and semi-autonomous mining scenarios within the next three years. The main part of this project is the accomplishment of accurate positioning to within 10 cm of true position.

2. NAVIGATION AND POSITIONING SYSTEMS

Navigation can be broken into two main divisions: **Reference and dead reckoning**.

Reference navigation finds the position of an object with respect to external landmarks on a set co-ordinate frame. This bounds the error to an upper limit rather than one that grows with time.

Dead reckoning refers to navigation based on a combination of inertial guidance and odometry (distance measurement). The problem with dead reckoning is that error grows with time unless it is periodically updated with an outside reference system. [Anon., 1994]

Based on internal studies at INCO Limited, the combination of dead reckoning and reference guidance is considered as the most robust of approaches in any situation. The accuracy of the dual system approach will be greater than using either one alone. [Anon., 1994]

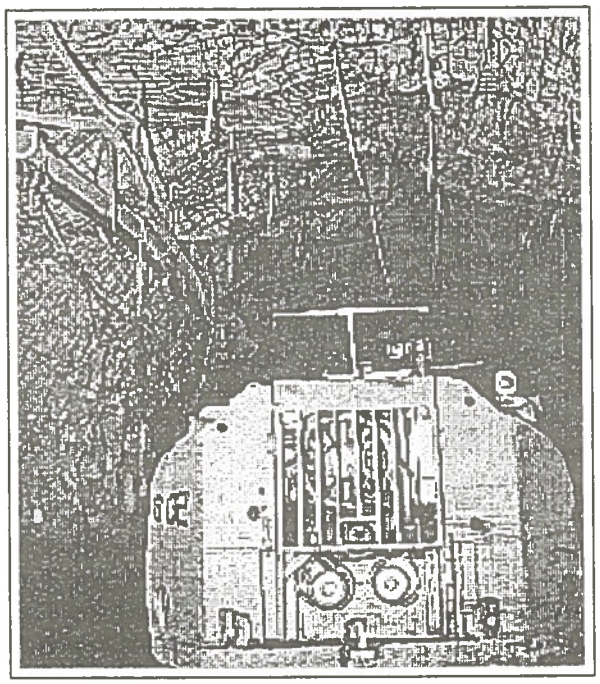

Figure 2: Scooptram operating at INCO's North Mine at Copper Cliff, Ontario using a light rope for guidance.

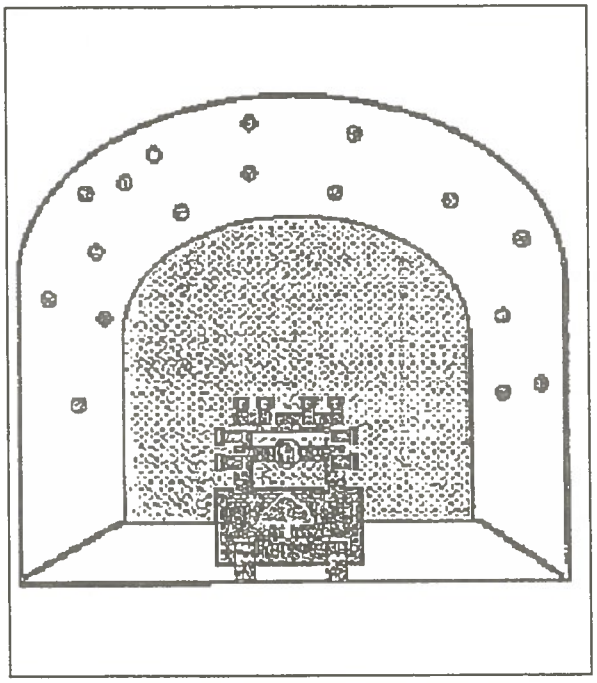

Figure 3: A vision system may be used to set up a reference grid for machines to use as navigation aids.

At present, there are four main types of navigation / guidance systems employed in underground mining. These are:

- **Buried Cable** [Kalio, 1988]
- **Overhead Trolley** [Kitchener andVollenwyder, 1988]
- **Laser based Inertial Navigation System (INS) with odometry** [Sammarco, 1994]
- **"Painted" Line Guidance** [Baiden and Henderson, 1994],[Vagenas et al 1991], [Hurteau et al 1988], (See Figure 2)

The navigation systems, which permit the machines to move from position to position, have subsystems such as path planning, collision avoidance and obstacle detection. There are other systems
that enable precision docking. A challenge for miners is to keep or exceed current operational speeds for manually driven equipment. The final objective is to have a position correction system to ensure system reliability will not be compromised.

In the case of an automated mine, mobile robots may proceed to their tasks using a navigation system. The navigation system allows for the guidance of vehicles to their tasks. A positioning
system is required to calibrate the navigation system to ensure the requested task is carried out efficiently. That is, the reliability of the navigation data is continually updated therefore zeroing any error accumulated with time. [Lawrence, 1993]. The proposed positioning system is referred to in this paper as the **Underground Positioning System (UGPS)** and the discussion focuses on sulphide orebodies common at INCO Limited's mines.

INCO Limited is considering machine positioning in depth. Four distinct variations for the UGPS strategy are:

- **Microseismic Systems**
- **Line of Sight Position Beaconing Systems** (See Figure 4)
- **Inertial Navigation Systems**
- **Very Low Frequency (VLF) Systems**
- **Passive Positioning Systems** (from an Oceanographic application)

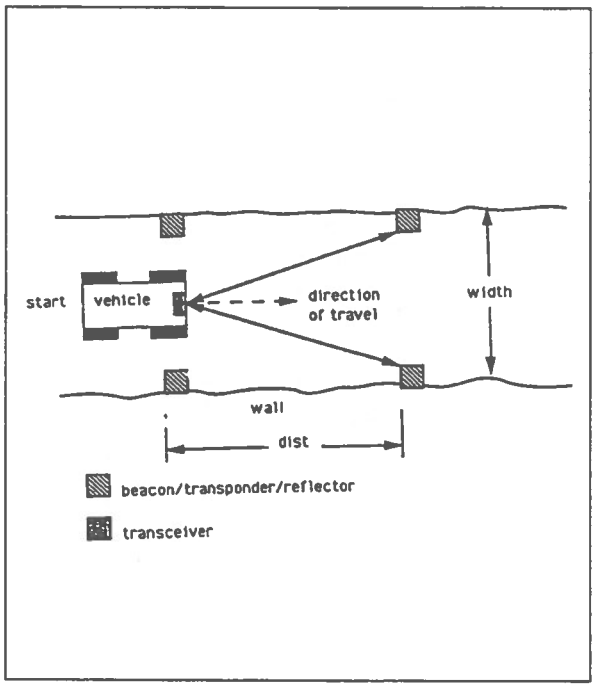

Figure 4: LOS (Line Of Sight) beacons giving the machine direction in a structured environment. This is the type of system that has been employed in automated and semi-automated factories. The name given to these robots are Automated Guided Vehicles (AGVs).

2.1 Microseismic Systems

Many mines have microseismic systems installed which are used to help locate seismic events such as rock bursts or blasts. If a machine generated enough energy to trigger the geophones it could then be located, [Blanco, 1994]. Research has been done to investigate the accuracy of this type of system., at INCO's Creighton Mine. The preliminary test demonstrated that in-the-hole (ITH) drill induced vibration can be measured and further work has been requested to improve the location algorithm.

2.2 Line of Sight Positioning Systems (LOS)

LOS uses conventional surveying techniques to identify the position of targets (passive or active). A vehicle uses this system to correct itself by trilateration (the spatial co-ordinates of a point found by measuring distances as opposed to triangulation that is the measurement of angles to find the position of a point). [Anon. 1994]. The system is simple and the technology is available; however it involves the installation of an infrastructure underground which is not advisable for an automated mine.

2.3 Inertial Navigation Systems (INS)

The United States Bureau of Mines looked into the use of an INS that would need little or no intervention [Sammarco, 1994]. They found a system from Honeywell Incorporated that uses a ring laser gyroscope in what is known as a strapped down Inertial Measurement Unit (IMU). (See Figure 5).

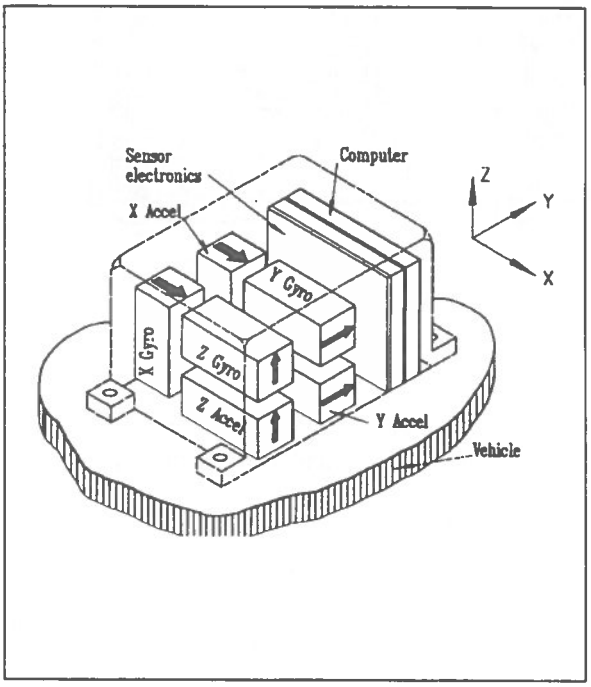

Figure 5: Typical "strapped down" Inertial Measurement Unit (IMU) which is the heart of an inertial navigation system.

The test was done on a continuous mining machine, the JOY 14CM. The IMU performed well but in order to maintain such a high degree of accuracy in the positioning system, the machine had to stop and do a zero velocity update called a ZUPT. This accounts for the rotation of the earth and removes the occurred error. To keep the accuracy of 10 cm of true position, it is required to do a ZUPT every 3 minutes for ten seconds. This means that it would be easier to use this system on pieces of equipment that would not require much movement during operation. Production drills, development jumbos, roof bolters and infrastructure

deployment vehicles may be considered as candidates for this type of system.

2.4 Very Low Frequency Systems (VLF)

Geophysics has been using the very low frequency (band width is between 10 and 300 kHz) radio waves for years in the exploration of orebodies. The next logical step was to use geophysics to determine mineralisation in production blastholes to help predict the grade of the stope and to increase ore value by leaving previously unknown rock in place.

The theory behind this system is simple but the practical application can be a breakthrough for underground autonomous and semi-autonomous equipment. The electromagnetic velocity of propagation through a medium is a function of the substance. This velocity is caused by the dielectric property of the material. If the effects of various dielectrics are known, it may be possible to work out the time for the signal to reach a point. If three such points are defined, the machine may be positioned in space by trilateration, (see Figure 6).

Literature review and discussions with researchers in geophysics have indicated that no work has been done concerning the use of VLF waves to position underground vehicles. There is an opportunity to develop such a system which can also facilitate traffic management in underground mines.

2.5 Passive Self-Calibrating Positioning System

An oceanographic system method is being investigated and it is in the Medium Frequency (MF) range rather than the Very Low Frequencies. (MF bandwidth is between 300 and 3000 kHz). This system is a passive self-calibrating radio positioning system for use in tracking ships with requirements of 20 m circular error over a distance of 100 km from the transmitters. [Dennis , 1981] Most of the work on surface navigation has been focused in the use of satellite networks for global positioning therefore the system has not been explored in any depth since the early 80's.

The attributes of this system are:

- **"provide continuous, absolute calibration and quality control 'on project' without requiring earth-fixed calibration points.**
- **minimal external Radio Frequency (RF) interference susceptibility.**
- **all signal processing must be digitised to aid in the simplification of the design of the system.**
- **The {size of the} mobile antenna will be much easier to handle since it is a medium frequency antenna and there will be no need to tune an array of transmitters.**
- **off the shelf components would be easy to purchase.**
- **since the bandwidths are narrow, there would be an increased signal to noise ratio at the MF receiver."**

The path chosen for further study is to look at the VLF and Passive Self-Calibrating Systems and conduct tests around this technology incombination with an inertial navigation system.

3. PRINCIPLES OF THE UNDERGROUND POSITIONING SYSTEM, "UGPS"

The difficulties for underground mine positioning in sulphide orebodies are the constant variations of the rock plus varying mineral dielectric properties throughout the mining claim and its effects on the wave propagation through this type of medium. One effect comes from the varying height of the water table thus the system would have to account for this type of fluctuation.

3.1 Accuracy Requirements

The required accuracy for mine orientation is in the order of 50 to 75 cm. [Chrzanowski, A. 1969]. There is a possibility to achieve higher accuracy based on new digital photogrammetric techniques. The requirements for positioning of a vehicle is 10 to 15 cm. This would allow for the timely updates and the possibility of using lower cost inertial systems for dead reckoning.

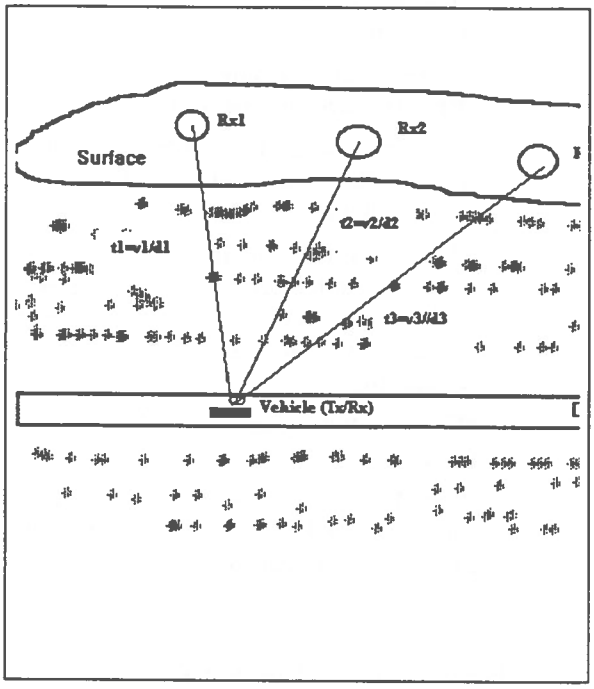

Figure 6: Basic principle of the underground positioning system. (Tx/Rx = Transceiver, Rx= Receiver, Tx= Transmitter)

3.2 Further Specifications

The UGPS must be able to help update the IMU as it drifts from its true heading with time. This is commonly called the time of flight or TOF.

Another function for the positioning system is to act as a traffic controller. The VLF/Passive based system, which is being proposed, should be able to follow equipment as it moves through the mine, enabling an operator on surface to act much like an air traffic controller except there are there machines and workers in the controlled zone.

At least three receivers are required on surface which are spread out in such a manner that they are on one side of the ore body. The reason for this is the signal will be severely distorted when going through the ore and it may be completely attenuated.

A highly stable signal source is required to generate a narrow band width signal to propagate through the rock. In the case of the offshore system used by Analytical Technology Laboratories, Cesium clocks were used in conjunction with linear power amplifiers to preserve phase stability with desired accuracy, [Dennis, 1981].

Other components of the UGPS are a transmitte.· exciter, a power amplifier, antennae, and connections to the mine wide computer system.

It is expected that the UGPS will not work inside the orebody because of the high conductivity of the sulphides. Therefore machines operating for extended periods of time within the shell of the stope would require a fairly accurate IMU for dead reckoning. When machines wander in and out of the ore body, they should be automatically positioned by the UGPS since it will be continually polling for equipment.

A scenario of the proposed system is as follows:

- *Assume a vehicle is starting at time zero and heads down a ramp. The UGPS is tracking while the self contained navigation system moves the machine into the workings. The machine reaches its destination and then requests an update to its "absolute" position and it receives co-ordinates from the UGPS. The navigation system is reset and the machine continues its duty while a traffic system monitors people and equipment throughout the mine.*

3.3 Verification of the System Function:

Periodically, the system would have to be calibrated mainly because of the change in the dielectric constant. A survey vehicle with a precise IMU having digital photogrammetry capabilities would enter the workings and request updates from the UGPS. This request would compare the vehicle's reference position with respect to a precise survey of the area to know exactly where the vehicle is positioned.

If the surveying vehicle covered the entire workings or the area of interest for that day, the UGPS information delivered to the other
machines would be accurate and the system should run smoothly.

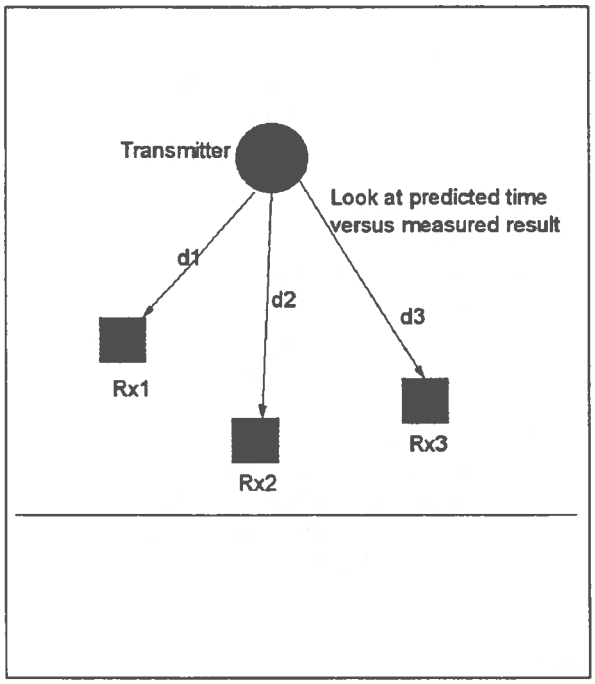

Figure 7: Schematic layout of the surface test.

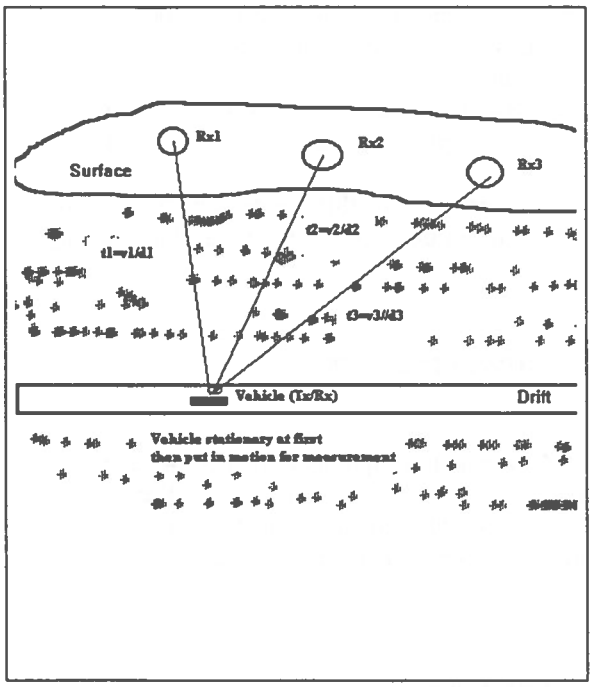

Figure 8: Measurements underground will tell if the system is viable.

4. A PROPOSAL FOR PROOF OF CONCEPT TESTS

Tests will be conducted to show how well UGPS works on surface. Can there be distinguishing features over a short time span and ensure position accuracy even with the high radio frequency noise levels expected?

Once established that the surface system works (see Figure 7) and there is evidence that the system should work underground , a more involved experiment would be set up to test different frequencies and study the results. The final test would be to identify the depth that could be reached before the ground cover shields the transmitters from the receivers. (see Figure 8)

4.1 First Test

The experiment will involve a transmitter and a receiver with a measuring device to detect time. A comparison between the theoretical answer and the field results will be made. The next step will be to vary the frequency to see the accuracy given at different values.

4.2 Second Test

The next test would involve moving underground to see if the signal can be picked up and measured with some consistency. The device that is to be located would be at rest for these two experiments.

The final test would be with a vehicle in motion. This would indicate the UGPS's effectiveness as a traffic control unit as well.

5. CONCLUSIONS

To provide consistent and reliable position information for navigating equipment in underground mines, there is a requirement to develop both a reference system and various dead reckoning systems for the autonomous and semi-autonomous machines.

The main driving force behind the use of a VLF type of system is that it requires no infrastructure in the mine to monitor the machines. This system on surface would be easy to maintain and simpler to install.

At the time of publication, the tests have not yet been performed but some of the results should be known by the conference date.
The experiment and the refinements for the prototype should be completed within a period of two years.

The discussion held in this paper should be viewed under the current trends and limitations of technology.

6. ACKNOWLEDGEMENT

Many of the practical aspects of this system have been jointly studied by Peter Cunningham, Electrical Designer, at INCO Limited and his help in bringing this idea to reality is greatly appreciated.

7. REFERENCES

Anon. 1994.
Automated Mining Vehicle Guidance and Navigation System Study. INCO Internal Report. Confidential

Arora , R.K. 1994
Global Positioning Technology and Applications , IEEE

Baiden, G.R. 1993
Combining Teleoperation with Vehicle Guidance for Improving LHD Productivity at Inco Limited pp 527-532 August 23-26 Kingston Ontario. International Congress on Mine Design

Baiden, G.R.; Henderson, E. 1994
LHD Teleoperation and Guidance: Proven Productivity Improvement Tools May 1-4 Toronto Ontario, 96th Annual General Meeting of the Canadian Institute of Mining Metallurgy and Petroleum

Blanco, Max 1994
Feasibility of an Underground Mine Equipment Positioning System March 11 Undergraduate Thesis Queen's University, Kingston Ontario

Briggs , S. M 1981
High Precision Near Shore Seafloor Positioning pp127-128 OTC 4020 May 4-7 Houston Texas Offshore Technology Conference

Brink, A. W. 1981
Automatic Position Control of a 30,000 Tons Ship During Ocean Mining Operations 205-212 OTC 4091 May 4-7 Houston Texas Offshore Technology Conference

Brophy, D.G., Euler, D.W. 1993
The Opti-Trak system, a system for automating today's LHD's and trucks. 2nd Int. Symp. Mine Mechanization and Automation. Lulea, Sweden

Chrzanowski, A. 1969
Tunnel Profiling Using a Polaroid Camera CIM Bulletin vol 72 March

Chrzanowski, A. 1967
Underground Survey Measurements-Research for Progress CIM Bulletin June

Chrzanowski, A. 1987
Some New Developments in Monitoring, Analysis and Prediction of Ground Subsidence CIM Bulletin vol 80 #901 May

deBono, Dr. E. 1994
Creative and Lateral Thinking. Mica Management Resources. Toronto

Dennis, A.R. 1981
A New Passive Technique for Offshore Navigation and Positioning 417-421 OTC 4158 May 4-7 Houston TX Offshore Technology Conference

Draper, C. S. 1981
Origins of Inertial Sept.-Oct. 5 4 Journal of Guidance and Control Boston

Hurteau, R., Piche, A., and St. Amant, M. 1988
Experimental Results of the Teleoperation and automatic guidance of LHD's. 1st IFAC Workshop on Advances in Automation of Underground Hard Rock Mining. Quebec

Kalio, P. 1988
Utilisation, automation and data transfer in the operation of LHD machines. 3rd Can. Symp. on Mining Automation, Montreal

Kitchener, L.; Vollenwyder, K. 1988
Development of a 70-ton capacity automated underground trolley truck. CIM Bulletin January. vol 81 # 909

Lovell, MC; Avery, AJ; Vernon, MW 1976
Physical Properties of Materials QC176.L66 Van Nostrand Reinhold London

Lawrence, Anthony 1993
Modern Inertial Technology: Navigation Guidance and Control TL588.5.L38 1992 New York Springer-Verlag

O'Brien, M.D. 1981
Navigation Systems for Deep Ocean Mining 441-445 OTC 3098 May 4-7 Houston TX Offshore Technology Conference

Sammarco, John J 1994
A Navigational System for Continuous Mining Machines Sensors January

Scoble, Malcolm ,1994
Competitive at Depth: Re-Engineering the Hardrock Mining Process. Proc 1st NA Rock Mechanics Symposium, Univ of Texas at Austin. June 1-3. pp 35-46 AA Balkema

Stansell, Jr. T. A. 1981
The Continuing Evolution of Satellite-Based Geodetic Positioning & Survey Navigation Capabilities 405-412 OTC 4157 May 4-7 Houston TX Offshore Technology Conf

White, Wm. 1994
Automated Surface Mines June Mining Engineering

Vagenas, N., Sjoberg, H., Wikstrom, S. 1991
Application of Remote-Controlled/Automatic Load-Haul-Dump system in Zingkgruvan. 1st Int Symp on Mine Mechanisation and Automation, Vol 1 Golden Co.

CAMI'95:3rd Canadian Conference on Computer Applications in the Mineral Industry
Montréal, Québec, Canada, October 22-25, 1995

The Total Mining System TMS™ - The Future of Open Pit Mining

Jonathan P. Peck
Aquila Mining Systems Ltd. and
Dept. of Mining & Metallurgical Engineering, McGill University.

Carl Hendricks
Aquila Mining Systems Ltd. and
Dept. of Mining & Metallurgical Engineering, McGill University.

ABSTRACT

With declining ore grades and reserves and rising production costs, open-pit mines have been looking to obtain timely and quantitative feedback on how each component in the mine is operating. Proper and timely use of this information would permit more dynamic planning as market conditions fluctuate, equipment fleets age and variations in the grade, quality, geometry and hardness of the mined material all contribute to either changing production targets or levels of achievable performance. If real-time or on-demand data would be available through the integration of equipment monitoring, locating and communication, a proactive optimizing approach to mine planning is possible.

Toward achieving a proactive planning capability in a surface mine, better two-way data and information flow between each component in the operation is required. AQUILA Mining Systems Ltd. is developing the basis for a complete and comprehensive real-time monitoring and information system called the Total Mining System or TMS™. This system is being designed to address both current and future needs of open-pit mines to enable improved productivity while minimizing cost. At a higher level, and within 5 years, TMS™ will allow for the autonomous operation and/or real-time supervisory control of mobile and stationary equipment in open-pit mines.

This paper will outline AQUILA`s TMS™ design, primarily in relation to its various subsystems and how these can be integrated to enable an Intelligent Management, Production Control and Planning Facility for surface mines.

1 INTRODUCTION

The competitiveness of today's mining environment has made cost efficient mining operations a necessity. Efficiency has been mandatory for survival in the 80's, but even with increased commodity prices in the 90's, optimized productivities and effective cost control are still needed to maximize return on the owners investment, attain a market advantage, and to maintain the operation's viability to survive the next low price cycle. In effect, good management of the mine's ore body, infrastructure and human resources are continually needed for on-going success.

In a typical mine, there are many groups that need to work together in order to attain a successful operation. For example, operations and engineering are responsible for their own jobs, setting and attaining their own particular objectives. However, close cooperation between these groups is also needed to meet the common objective of minimizing the unit cost of the mine's product. Furthermore, mine plans and cost estimates for new projects are based on exploration and development data, technical know-how and past experience. After a mine goes into production, the operating data is used to measure the operating performance and for subsequent revision of the mine plans. Operating experience is the accumulation and use of this data and as the quality and quantity of data increases, so can the quality of planning. In addition, the use of production data can provide the necessary link between mine planning and production. Both engineering and operations can increase the accuracy of their plans and decrease their reaction time as they go from long term to short term planning. For engineering, long term and short term planning can be defined as the life of mine projections down to daily plans, while for operations these can imply yearly plans down to operating control systems respectively for particular pieces of equipment.

The integration of mine engineering and mine operations efforts becomes important when defining targets to meet their common objectives. Through the installation of monitoring and locating systems on the mobile equipment, these groups have the means to readily assess their specific contribution to production. In addition, through an examination of the performance and production information from these systems, the same groups can fine-tune their approaches towards meeting common goals on a more timely basis. In this regard, this paper will discuss the possibilities, developments and current application of the following concepts:

. Increasing planning accuracy and decreasing reaction time to define and meet Mine Engineering and Mine Operations common goals.

. Using the data and information from monitoring production equipment performance, productivity and location towards meeting these goals.

2 THE POSSIBILITIES FOR OPERATING DATA AND INFORMATION

In the life of a mining project, the accuracy of planning increases with the quantity and quality of the data available. The study progresses from a "horse back" estimate through pre-feasibility and feasibility stages until finally a production decision is made. At this stage, a detailed design and the initial operating cost budget is derived. After operations begin, components of the plan are revised to correct deficiencies due to short-falls in the original assumptions and to take advantage of any new opportunities that arise.

Eventually, the various areas of the mine will reach steady state and performance data can be collected from the operating equipment through either manual or instrumented means. In the past, this data has been limited in detail, basically being mined quantities as determined by surveys, load counts or weightometer readings, cost of supplies and manpower time sheets. In addition, sampling and testing for exploration and fill-in drilling, laboratory analysis, time and load weight studies, etc. have been used to improve the information needed for planning and optimization.

Through the use of advanced, on-board monitoring and locating devices and sophisticated mine planning and information management systems, detailed operating data from the mine equipment can be obtained and assimilated to improve estimates of:

- ore versus waste rock definition per blasthole
- equipment and manpower productivities
- muckpile diggability
- dilution and mining loss
- equipment costs and availabilities

To effectively manage a mine, it is necessary to measure certain criteria which enable the various activities of the operation to be assessed in an unbiased and consistent

manner. By measuring time, cost and effort of the individual unit activities in the mine operation, prediction of performance can be refined for planning. As a result, better control of equipment application activities can be realized, and if planning is taken to the very short term, optimization will result. After all, this type of optimization happens only when the planning time interval approaches an instantaneous or real-time response.

Improved and innovative data collection and management enables better planning and forecasting. However, in a mine operation, planning must also be dynamic as market conditions fluctuate, equipment fleets age and variations in the grade, geometry and hardness of the mined material all contribute to either changing production targets or levels of achievable performance. Much like process control in a mine concentrator, monitoring the condition and output of the mining equipment, for example drills and shovels, can indicate changes in rock conditions, but can also identify wear or assist in predicting the ensuing breakdown of equipment components. Through the use of intelligent monitoring systems, change-outs can be forecast and planned, operating targets can be modified and the blast design changed. By monitoring equipment performance, analyzing the data in real-time and transmitting information on status to a central location, reaction response to any change can be immediate leading to optimization. Having an infrastructure in place to permit such a level of planning, response to change can be converted from a reactive, problem fix-up approach, to a pro-active optimizing approach -a concept associated with unit optimization and process control methodology (Gray et.al., 1991).

3 THE COMMON OBJECTIVE - OPTIMIZING UNIT RESULTS

The objective of measuring, interpreting, controlling and optimizing operating performance is to reduce or minimize operating costs. In the past, badly designed monitoring hardware and inconsistent approaches for the collection, analysis and assimilation of the data have limited their contribution towards improving optimization, control and reporting strategies in mines.

In an open pit, the drill, blast, load, haul and pit overhead functions all contribute to the effectiveness of the total operation. Decreasing the cost of one function can increase the cost of another, where it is the net bottom line effect of the combined operating functions that is important. The efficiency of the operation will normally depend on its most critical piece of equipment which in most open pit mines is the loading shovel. The performance of the shovel in turn depends on the condition of the muckpile, assuming the pit maintains consistent truck/shovel matching and fleet sizing. This leads to the strategy of conditioning the muckpile to reduce the unit mine operating costs. Shovel performance in the muckpile can, therefore, be used as an indication of the muckpile conditions or blast efficiency and how the blast affects the other operating functions. The inter-relationships between the various mine functions are demonstrated on the curves in figure 1. In the past, it has been attempted to use fragmentation and applied blasting energy to generate these curves. Both of these components contribute to easy digging, however, test work has shown that a tight or "frozen" muckpile with good fragmentation and high applied blast energy can still produce poor digging performance. For this reason, the more basic term of shovel diggability, or digging index (Hendricks et.al.,1991) is used to provide a relative indication of the muckpile characteristics. This requires a basis of definition for diggability to be derived with variations measured relative to that basis. As seen in the curves, in a given muckpile an increase in diggability is achieved by an increase in the drilling and blasting efforts, or both. This in turn reduces the unit costs of the other functions. The net result is that the optimized unit cost at any particular time and location for the total Mine Operations is at the bottom of the "U" shaped curve corresponding to a specific diggability. As with any process control situation, this is a dynamic curve which varies predominantly as the rock changes.

By using the production equipment as the measuring tool, not only is it possible to stay near the bottom of the curve, but it is also possible to see any changes which will move the curve and create a new optimum point (indicated by the dashed lines in figure 1). This shows for example, that as the rock conditions change an increase in blasting effort would be necessary to keep the shovel diggability the same. The total cost curve then indicates that the trade-off optimization point for the new conditions are a slightly more difficult digging condition.

4 ACHIEVING OPTIMIZATION THROUGH THE USE OF ADVANCED MONITORING AND LOCATING SYSTEMS

Today, a typical open pit mining operation will have in

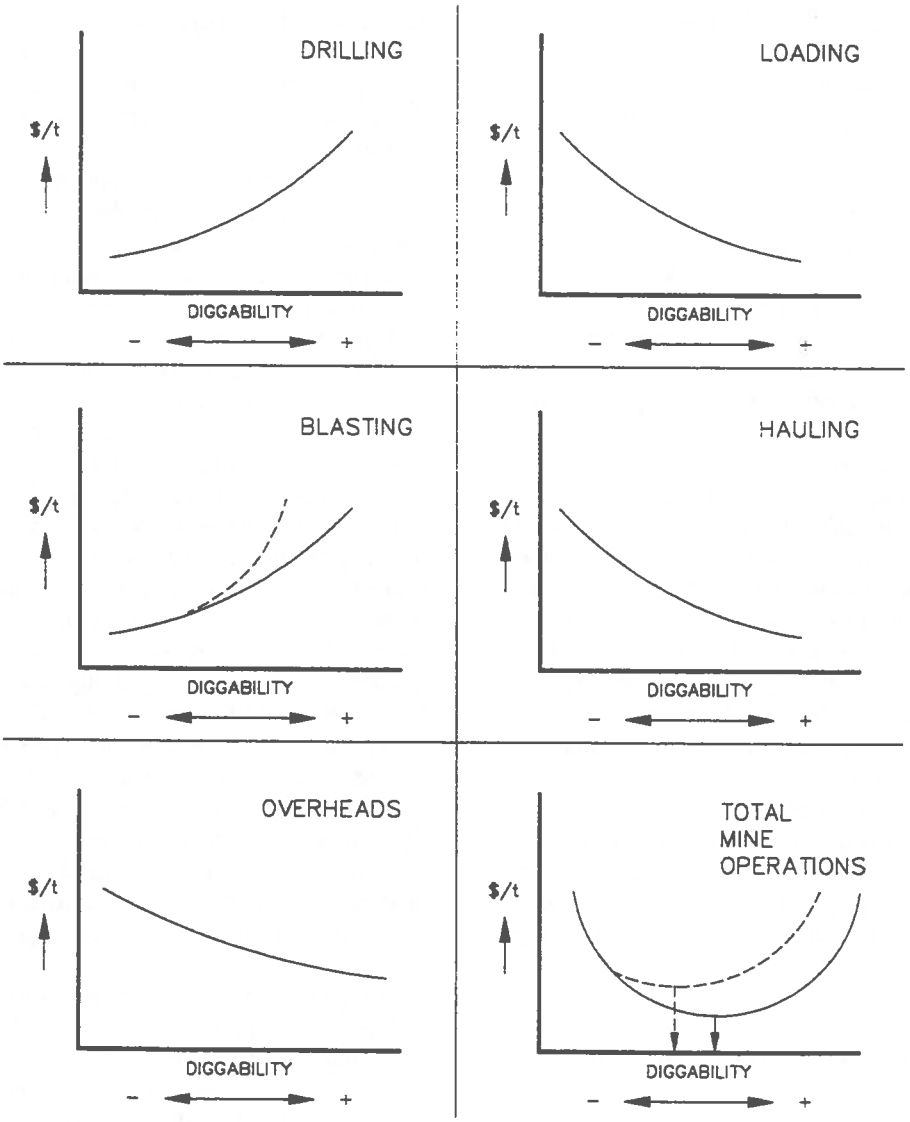

Figure 1 - Costs curves (Gold et.al.,1987).

place, stand alone software and engineering systems for mine planning and production optimization. The mine planning system - first used to model and layout the initial mining sequence for the deposit - hosts the short and long range plans for continued development of the orebody. The information used to update the mine plan and allow for informed production decisions (scheduling and sequencing) is often sporadic, slow in coming and generally hard won. This is due largely to the enormity of the physical operation, the harshness and heterogeneity of the environment and the absence of intelligent monitoring systems on the production equipment capable of collecting meaningful data on their operation and environment.

Truck dispatching systems represent the current state-of-the-art for production optimization in surface mining. These systems, through monitoring the locations and cycle time of each haultruck in the operation, make decisions (based on production targets) as to which shovel a particular truck should report to, or where a truck should dump, in order to optimize the production cycle time. These dispatch systems can be run in an auto mode, but are generally overseen by a human dispatcher.

In order that mine planning and operations can achieve the common objectives outlined earlier and towards optimizing unit costs, it will be necessary to integrate all the different mining functions. To achieve such an integration, the performance, production and locations of mobile equipment, such as drills, shovels and haultrucks, need to be monitored continuously. Towards realizing such an objective, monitoring and control systems are becoming standard features on mobile equipment in surface mines. However, the productive use of the data generated by these systems has been inhibited by the lack of suitable communication systems for their mine-wide transmission. As well, many mines become overwhelmed with the amounts of data these systems can generate in a short time period. In addition, provided the data can be transmitted, their analysis requires considerable time and effort before meaningful results can be obtained for use in decision-making.

These problems will be further amplified as the demands for real-time data/information from integrated and advanced monitoring, control and locating systems continue to increase over the next five years. As the technology matures to enable autonomous mining vehicles, it is apparent that the demands on a communication facility will increase dramatically (White and Zoschke, 1994).

5 TMS™ - THE TOTAL MINING SYSTEM

To circumvent this inevitable communications barrier, and to achieve seamless, two-way communication between each monitored and controlled component in a mine, AQUILA Mining Systems Ltd. and their strategic partners are developing the basis for a complete and comprehensive real-time monitoring, control, locating and information management system called the *Total Mining System* or TMS™ . The following elements and sub-systems will be required to bring the TMS™ concept to fruition:

- On-machine monitoring, control and positioning (GPS-based) systems;
- A production control system capable of proactive (very-short term) planning;
- An integrated database system, permitting ready access by operations, production, maintenance or management groups using flexible, application specific software;
- An open-architecture, object-oriented, mine modelling and GIS (Geographical Information System) system;
- A comprehensive mine planning system that utilizes the information and control capabilities available under TMS™;
- A bidirectional mobile communications network with adequate responsiveness and bandwidth for current needs as well as an upgrade path to meet future TMS™ enhancements and imminent developments in the field of mobile communications;

The TMS™ communication system will have an open and flexible architecture such that certain existing systems can be interfaced. The "wireless" network is the first stage of TMS™ development and will be designed to readily accommodate applications modules and hardware components as they become available. In addition, its design will facilitate the remote/autonomous control of various mobile mining machines, for example, drills, front-end loaders, shovels and trucks, in the future (Peck et.al., 1994; Peck and Gray, 1995).

Using the TMS™ framework, it will be possible to continuously track changing mining conditions based acquired on data and/or information. Once areas of concern have been identified, decisions can be made to resolve or circumvent their impact on overall productivity. Thus, the response of the mine is modified from a reactive to a proactive approach in managing the changing operating situation.

The following sections will describe the various components needing to be developed, modified and/or implemented in order to achieve full TMS™ capability.

5.1 Mine Engineering Application Systems

Computer-based (PC or mainframe) Mine Engineering Application Systems, for example Medsystem from Mintec, used in open pit mines on a daily basis, will directly benefit from the data/information made available from TMS™. As is commonly the case with software, the quality of the data in directly relates to the quality of the results or output.

These database and graphical systems generally include drilling and blasting, production statistics, and short range planning components. Without any monitoring systems, the drilling and blasting component utilizes manually acquired data such as operating hours, drilled meters, bit usage, surveyed hole locations and operator reported waste rock/ore intersections and particular problem zones (rehandle, broken ground). This latter information is critical in issuing hole-by-hole loading instructions to account for the variation in the bench geology, and is generally provided from manual driller logs. The drilling and blasting function could, however, be greatly enhanced by the information on ore versus waste rocks as obtained on a hole by hole basis in real-time from a suitable monitoring system. Such information is more consistent and reliable than driller's logs in that it is not affected by operator bias or subjectivity. Particular benefits could include improved blast pattern design, where savings relate to optimized explosive loads by precisely knowing the rock conditions in every borehole. Of particular importance in open pit coal mines, would be the ability to reduce dilution through the identification of waste versus coal in every blasthole, not only selected holes as is commonly the case with geophysical logging.

The data available from real-time GPS positioning systems will also benefit the drilling and blasting system. Benefits could be related to improvements to scheduling, utilization and fragmentation and thus overall mine productivity. Additional cost benefits would also result from eliminating the need for initial surveying in of the blastholes and pick-ups after the holes have been drilled and reducing over-/underdrilling due to the variable pit floor versus an assumed collar elevation. A major benefit of shovel locating using GPS is the accurate determination of the elevation of the tracks or dipper at all times. In this way, the operator or pit superintendent can instantly recognize whether the shovel is excavating along the designed grade and thus correct for any deviation. By tracking the location of the shovel, scheduling of the equipment, volume calculations and grade control becomes simplified, since the position of the machine within the muckpile is precisely known in real-time. Combining this position information with measured dipper loads (if suitable monitoring equipment is installed), diggability data and the geological information from drilling, accurate volumes of the excavated material (waste and ore) could be determined further improving short range plans.

The production statistics component relies on typical manual data inputs to measure productivity of both drills and shovels. Drill monitors will permit production data to be readily available in a centralized database for further compilation and reporting on such aspects as utilization, downtime and bit footage for any time period. Integration of this information within the database would also permit feedback to drilling and blasting for further optimization of both drills and bits in terms of utilization and more importantly costs. In a similar manner, shovel monitors will provide data on operating versus downtime, in addition to reliable measured weights per dipper load, hour, shift or day.

The short range planning module of mine engineering systems is usually a complex system of sub-components catering mainly to the needs of planning engineers, but retaining a strong inter-relationship with the other elements noted earlier. The effectiveness of this module is to a large part determined by the frequency of the updates and quality of the input data. In open pit coal, an important input is a geological gridded seam model. The model is built using manually interpreted and input production drillholes in addition to the data from exploration holes. Drill monitoring and positioning systems could be utilized to automatically provide real-time updates to coal seam structure within the model. In copper or iron ore, interpreted drill data could be related to zones of differing ore grade, hardness and composition permitting updates to be made in terms of sections, bench maps, and volumes for planning, scheduling, and reconciliation (Peck et.al., 1994).

5.2 Data Processing and Analysis

The volumes of data which will be obtained from the monitoring of mobile equipment performance and location on a regular basis in open pit mines, makes the need for further processing/refinement even more important. The issue of reducing the data set relates not only to hardware limitations, but also to provide to management, only the information necessary to make timely decisions. Advanced processing methods need to be integrated with suitable hardware, to reduce the data down to a manageable size. Over the past 3 years, intelligent monitoring and control systems have been developed by AQUILA and their partners using high resolution GPS positioning and on-line interpretation and control of drill and shovel variables. These systems will serve as the means to monitor the production, performance, health and position of key production equipment in surface mining (drills, shovels and trucks). These intelligent "front-ends", thus offer the potential to radically change the mine planning and production

decision-making process through advancing both the breadth and timeliness of available data and/or information.

5.3 Integration of Monitored Data and Information via TMS™

Integrated monitoring of the performance of key equipment can provide the types of data necessary to successfully maximize the benefits to be derived from all these engineering components. By having such data readily available in a centralized database, on-line or real-time decision making becomes a possibility, thus permitting improved control over the nature and quality of the recovered ore.

The concept of integrating machine performance monitored data in mine engineering and planning is not new. The Bucyrus-Erie Company proposed such a concept in 1985, for a fully integrated, computer assisted, Distributed Mine Management System (DMMS), which considered input from the monitoring of all equipment in a surface mine (LaPrairie, 1985). The proposed system was to link special purpose computer-based monitors on drills, trucks and shovels or draglines with a mine management information system. While some progress towards this end has been achieved via truck-shovel dispatch systems, for example the DISPATCH system offered by Modular Mining and the PMCS by Wenco, a higher level infrastructure will be required to achieve the objectives of TMS™, see figure 2. The unique constraints and conditions of the surface mining environment, as well as the projected evolution of communication systems towards ever increasing levels of supervised autonomy of mobile machines, will require a complex network to handle data and control functions. The requirements for broadband voice, video and data transmission for such applications far exceed the capability of any existing communication system in open-pit mines. This hybrid system would do more than manage the data flow between equipment monitors and the mine office, but would also permit remote control from the same office PC or workstation. The specific issues to be considered when designing or selecting a suitable communication network architecture for an open-pit mine are: protocol, interoperability, command status and topology.

Based on the proposed functionality for the wireless communication system, the following general requirements have been identified as a basis to commence its design:

- Maximum compatibility with existing voice and data communication systems.
- Integrated, bidirectional communication of data, voice, and video signals.
- Easy integration with different third party monitoring, control and positioning systems.
- Minimal licensing requirements.
- Data security and network integrity.
- Minimal infrastructure, installation and maintenance costs.
- Robust, proven and reliable technology.
- Capability to simultaneously handle in excess of 200 pieces of equipment.

The transmission of information, rather than data, is the key element which will determine the viability, functionality and success of the TMS™ system. As is currently the case, commercially available monitoring systems provide "data" and require considerable additional effort and time to process, analyze and interpret. At the heart of each monitoring platform in TMS™, will be the capability to automatically process the monitored data using high-level software processing techniques. Thus, the "raw" monitored data is processed on-board the machine, where only results (ie. information), are transmitted to a remote location for immediate use in the decision making. This approach will also reduce the problems associated with mass data transmission, processing, analysis, interpretation and on-board storage.

Towards this end, AQUILA's Drill and Shovel Monitoring systems currently employ such techniques to reduce the volumes of raw data stored on-board or transmitted via radio (Peck et.al., 1994). Using propriety techniques, real-time conversion of drill performance variables into rock material properties can reduce the data set by a factor of sixty. In the same manner, monitored component signals can be converted immediately as they are acquired into status alarms related to the health of the equipment. Caterpillar is currently developing a concept called the Advanced Product Services or APS, which will convert acquired data from their on-board monitoring system, the Vital Information Management System (VIMS), into useful information to identify when a problem develops. The APS will combine sensing, monitoring, on- and off-board analysis, communication, and interpretation components, towards recommending an immediate course of action to the operator. When combined with location and control subsystems, the APS will form the basis for eventually achieving a fully autonomous haultruck (Ferguson, 1994).

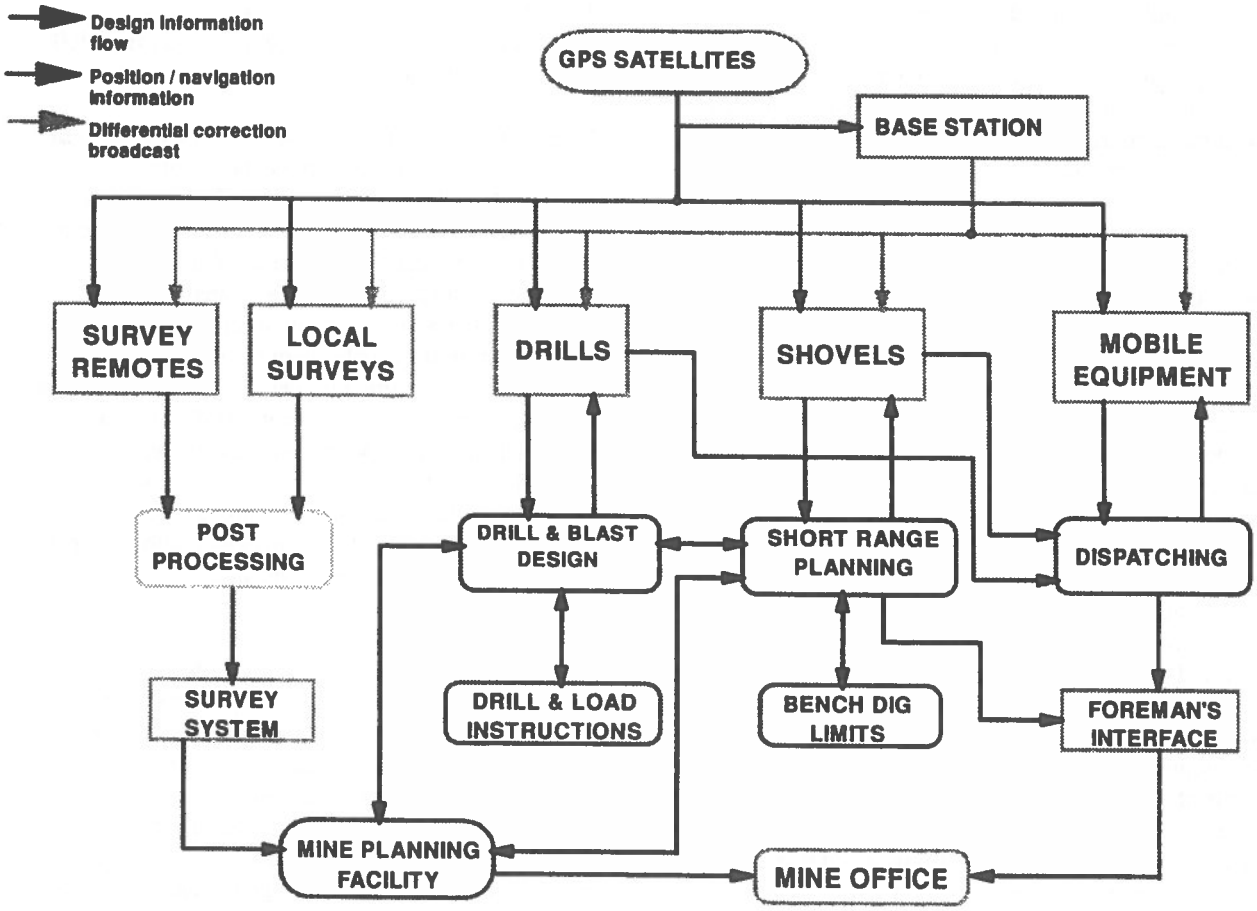

Figure 2 - The Total Mining System (Peck and Gray, 1995).

6 CONCLUSION

The issues related to the development and implementation of a TMS™ facility for a surface mine have been addressed. Many open-pit mines already have subsystems required for TMS™, installed or under development for mobile equipment. These include GPS-based ground surveying, drill navigation and shovel grade control and intelligent drill monitoring and control systems. In addition, several mines have developed customized application software for short range planning, designed to incorporate the data/information from these and other on-board systems.

When properly processed and analyzed, the information available through TMS™ can be used for optimization and process control. When this information is relayed in real-time and interfaced to a suitable database facility via a high-level communication system, it can be used by management to make timely and tangible production decisions. Thus, when TMS™ is properly and fully implemented at a mine, the available information can be used for short term unit optimization through control strategy and up to management reporting. In other words, TMS™ allows the production equipment itself to become the measuring tool.

Towards bringing TMS™ to fruition, efforts will involve the integration of machine level monitoring, control and positioning systems on all production equipment to corporate/site databases and any existing operational decision support systems in place. A unified facility, would allow corporate "strategic plans" to be passed down to the mine/mill level to formulate operational strategies, which could in turn be transferred to the supervisory levels for formulation of "dynamic tactical plans and production schedules" for short range planning. Finally, the dynamic tactical plans could be implemented through the machine level systems (intelligent front-ends).

The development of the various technologies composing TMS™, not to mention TMS™ itself, will lead to a significant build-up of an indigenous Canadian industry as is the case with AQUILA Mining Systems Ltd.. This new industry will first supply custom-designed equipment and high technology to allow Canadian mines to be more competitive on an international level. Secondly, all the sub-elements of the TMS™ system, as well as TMS™ itself, will become technology available for export to other countries, for example, the U.S., Chile, Australia and South Africa.

7 REFERENCES

FERGUSON, C. 1994.
Future of maintenance. 8th Maintenance/Engineering, Operators Conference, Paper PS-1, Sept Iles, September.

GOLD, R.D., KENNEDY, D.A. and GRAY, J.H. 1987.
A review of drilling and blasting practices at the Fording River Operations. 11th CIM District 6 Meeting, Vancouver, Canada.

GRAY, J.H., AMON, F.B. and J.P. PECK. 1991.
Integrated mine planning and production. CIM District Five Meeting, Ft. McMurray, September.

HENDRICKS, C., PECK, J. and M. SCOBLE. 1991.
Machine monitoring in surface mines. 1991 Am. Soc. Mining Eng. Ann. Meeting, Denver, Feb.

LaPRAIRIE, G.E., 1985.
Suspended load monitoring module for shovels and draglines. Proc. Mining Equipment Selection Symposium, University of Calgary and CANMET, Calgary.

PECK, J., WHITE, J.W. and VYNNE, J. 1994.
Increased productivity and reduced operating cost through drill monitoring. Baker Hughes Seminar, Johannesburg, October.

PECK, J. And GRAY, J.H. 1995.
The Total Mining System (TMS): the basis for open-pit automation. CIM Annual General Meeting, Paper 19.1, Halifax, May.

WHITE, J.W. and ZOSCHKE, L.T. 1994.
Automation of open pit mine operations is long overdue. World Mining Equipment, July/August.

CAMI'95: 3rd Canadian Conference on Computer Applications in the Mineral Industry
Montréal, Québec, Canada, October 22-25, 1995

Systems Analysis for Robotic Mining

Laura Mottola, Malcolm J. Scoble, Jonathan P. Peck
Department of Mining and Metallurgical Engineering
McGill University, Montreal, Quebec

Greg R. Baiden
INCO Ltd., Mines Research, Automation and Robotics, Copper Cliff, Ontario

ABSTRACT

Mining automation has incrementally progressed from line-of-sight remote operation to teleoperation and automatic control of mobile machines, mainly due to significant advances in underground communication systems. The present trend points towards a robotic mining environment where mobile machinery and stationary equipment will be integrated with a mine-wide information system overseeing all aspects of mining via a communication network. The successful design and implementation of the software and hardware components necessary to realize this vision depends on the level of seamless integration achieved. The complexity involved in terms of systems functionality and coherence necessitates systems analysis and computer-aided software engineering tools and techniques to actively support this integration effort. These offer both a detailed and global perspective of robotic mining systems.

This paper examines the underground hard rock robotic mining environment in terms of mobile machinery, stationary equipment, mine monitoring, and infrastructure. It attempts to relate some fundamental concepts of systems analysis to this environment and illustrates how this discipline and its tools can have a significant impact throughout the life cycle of both hardware and software components. The structure and flow of information which underlies robotic mining is then reviewed and related to the application of software engineering, information engineering , structured analysis and design, and object-oriented analysis and design. The paper concludes by considering how a specific CASE tool, System Architect©, is being used to analyze the information requirements of robotic mining systems.

RÉSUMÉ

L'automatisation minière en souterrain a connu une progression depuis l'opération à distance jusqu'au contrôle automatique d'équipements lourds grâce surtout à d'importants développements en matière de communication sous terre. Présentement, on se dirige vers un environnement minier robotique dans lequel l'équipement mobile et fixe à travers la mine serait relié à un système d'information par l'intermédiaire d'un réseau de communication. La conception et réalisation des éléments matériels et logiciels nécessaires au développement de cet environnement dépendent largement du niveau d'intégration atteint lors de la planification de ces systèmes. C'est pourquoi une analyse approfondie avec l'aide d'outils informatisés est primordiale afin d'étudier la complexité des systèmes requis. Cet article présente les composantes principales de l'environnement minier robotique, explique les concepts fondamentaux de l'analyse de systèmes et illustre comment cette discipline peut assister le développement des éléments matériels et logiciels.

INTRODUCTION

This paper is a first attempt at relating systems analysis concepts and tools to the business of mining at a time when the industry is faced with the challenge of streamlining its core processes to remain competitive. While moving from conventional mining techniques to more futuristic and leaner approaches, the fundamental problem lies in fully understanding the current mining processes in order to confidently assess the present situation, isolate bottlenecks, and identify the most critical areas needing improvement and re-engineering. This initial step is essential to the consistent and integrated development of robotic mining systems, both in terms of software and hardware. Systems analysis and computer-aided software engineering tools offer the capability to analyze present and future systems in their most abstract form, i.e. the processes they perform, down to the specifics of their implementation. In some form or another, these tools have been used to assist in the development of numerous and varied applications. The mining industry is now in a position to integrate seamlessly these proven techniques within its efforts to develop robotic mining.

UNDERGROUND ROBOTIC MINING ENVIRONMENT

Typically, underground hard rock mining is performed by accessing the orebody via a vertical shaft and a series of drifts and tunnels. Connection between levels is secured through a ramping system or the shaft itself. Mobile machinery is manually operated and consists of load-haul-dump vehicles, haulage trucks, top-hammer drills, jumbo drills, and bolting machines. Stationary equipment includes fans, pumps, a crusher, hoists, and maintenance facilities.

The ultimate goal of robotic mining is to access and exploit underground resources without the need for people to enter the mine. The ore would be retrieved by a new generation of intelligent and autonomous mobile machinery linked to surface facilities via a communication network. This fleet of robotic machinery would acquire information regarding the orebody and surrounding rock mass while mining to complement the initial exploration. The information system responsible for managing and interpreting the data from different sources would be located on the surface, although parts of its functionality may be distributed between underground equipment and a number of subsystems and databases.

A technological gap exists between the conventional and robotic mining scenarios, particularly with respect to the sensing technology necessary to gather sufficient information about the rock mass with minimal supporting infrastructure. Incremental advances in mining automation have already proven the viability of teleoperation and automatic control of mobile machinery, and progression is headed towards refining these technologies to include more sophisticated and flexible capabilities (Baiden and Henderson, 1994). The next logical step to bridge the gap between conventional and robotic mining consists of an intermediate stage, where the stationary equipment and mobile machinery utilized today is linked to an information system via a communication network. Figure 1 illustrates this concept, where a mine information system interfaces with four main underground functional areas: i) mobile machinery; ii) stationary equipment; iii) mine monitoring; and iv) infrastructure.

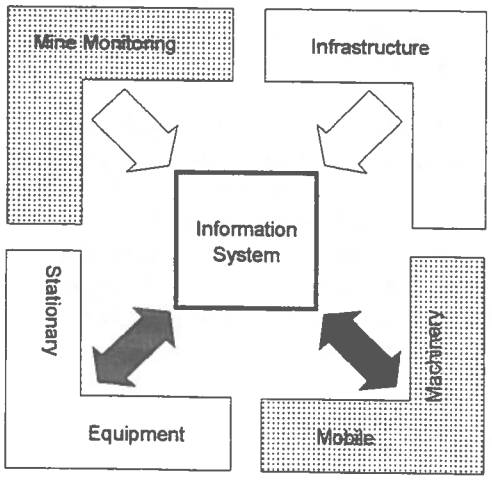

Figure 1: Overview of the mine information system

Figure 2 (at the end of the paper) offers a more detailed perspective of this diagram and the following sections describe its components.

Mobile Machinery

The basic mobile machinery found in a mechanized hard rock mine essentially comprises combinations of the following:

i) *development drill*, such as a jumbo drill, to advance underground tunnels;
ii) *bolting machine*, to mechanically support the tunnels with bolts and screens;
iii) *production drill*, such as an in-the-hole (ITH) or top-hammer drill, to drill production holes;
iv) *explosives loading machine*, to load blast holes with explosives;
v) *load-haul-dump vehicle* (LHD) and
vi) *haulage truck*, to transport material from a loading point to a dumping point.

Assuming that all of this machinery possesses teleoperation capabilities and a minimum of automatic control, then a two-way link to the mine-wide communication system is necessary to support these functions, regardless of the task to be accomplished. In addition, effective monitoring of production parameters and vital signs can be easily achieved by outfitting the machines with appropriate sensors and transmitting relevant data through the network. Hence, operating mode, production monitoring, and condition monitoring are common communication needs for all mobile machinery operating in such a preliminary robotic stage.

The specifics of production monitoring vary according to the particular function of a machine. For instance, drills would collect performance parameters such as meters drilled, feed force, torque, piston blow rate, machine vibration, etc., as well as hole deviation and perhaps metal content of the rock encountered. LHDs and haulage trucks would measure tonnage, fragmentation, and perhaps sense ore grade. Cycle times, including operating, servicing (maintenance), and idle times, are an important aspect of production monitoring which determine the utilization and availability of machinery.

Stationary Equipment

Underground stationary equipment typically consists of drainage pumps, ventilation fans, a crusher and ore bin, a hoisting system, as well as storage and maintenance facilities. Aside from the latter items, production and condition monitoring data can be gathered from all stationary equipment as it is obtained from mobile machinery. Production variables of interest would be power consumption and throughput, such as tonnes per hour for the hoist and crusher and litres per minute or cubic metres per minute for the pumps and fans respectively. Automatic control of this equipment, with occasional manual override, allows for efficient operation and energy savings.

Storage and maintenance facilities exchange a different kind of information. Inventory tracking of supplies and parts kept underground can result in just-in-time delivery of needed materials thus reducing production delays and the need to stock up. Pre-processed condition monitoring data routed to the maintenance facility can assist in preventive and predictive maintenance of both mobile machinery and stationary equipment.

Mine Monitoring

The intermediate robotic stage requires that information be gathered about the surrounding mining environment, such as groundwater flows, air quality, and ground conditions. This is achieved using sensors strategically located throughout the mine to monitor parameters such as the following:

i) *drainage*: water levels, in-flow rates, chemestry, and suspended solids;
ii) *ventilation*: air flows and air quality;
iii) *ground conditions*: stress and deformation, seismicity;
iv) *backfill*: permeability and water pressure;
v) *blasting*: fragmentation, vibration, and rock mass damage;
vi) *ore tracking*: in transit tonnage, grade, and levels (e.g. in ore passes and storage bins).

This information is valuable in monitoring the status of the production and environmental performance. Some is directly utilized as input to control stationary equipment, for example where drainage and ventilation data indicate the need to activate or shut off pumps and fans. Information related to ground conditions, backfill, blasting, and ore tracking indirectly influences mining processes such as ground support, production planning, and blast design, by characterizing the dynamic nature of the mining environment. The sensing instrumentation required to provide this kind of information adequately and reliably poses one of the greatest challenges towards achieving robotic mining.

Infrastructure

The principal underground infrastructure consists of a power distribution grid, compressed air, water, and backfill transport systems. A communications network must also be added in order to provide a mine-wide electronic link to surface. As for mobile machinery and stationary equipment, the health of infrastructure components must be monitored to ensure effective network distribution throughout the mine. Of equal importance is the status and maintenance of the sensing instrumentation described in the previous section. Also included in this category are personnel tags transmitting the location and identification of the underground workforce, possibly via a radio frequency identification (RFID) system (Knights et al., 1994).

INFORMATION STRUCTURE AND FLOW

Figure 2 (at the end of the paper) gives an overall view of the structure and flow of information in the likely transition from conventional to robotic mining. The information associated with each component block is both complex and extensive and cannot be effectively analyzed without suitable methods and tools. A systematic approach must therefore be taken to capture in detail the nature and behaviour of each individual element as well as its interaction with other components of the system. Before illustrating how systems analysis and computer-aided software engineering tools can assist in accomplishing this task in a dynamic and constructive manner, it is necessary to introduce the terminology and fundamental concepts of software engineering, its methods and tools.

Software Engineering

In a robotic mining environment software is an important driving force behind complex systems. For instance, the smooth navigation, coordination, and control of autonomous mobile machinery depends on well planned software components that integrate the individual functionality of each machine within the overall logistics of the mining operation. The planning, design, and construction of software systems is regulated by the discipline of software engineering.

Software engineering (SE) encompasses methods, tools, and procedures enabling engineers to structure and control the software development life cycle. Briefly, *SE methods*, or *techniques*, provide the technical specifications of how to develop software and *SE tools* the automated support for these methods; *SE procedures* enable the timely development of software through quality control and project management.

The *software development life cycle* comprises the following core phases:

i) *Analysis*, which involves defining system requirements and functionality, as well as the interactions between major sub-systems and the "outside world".
ii) The *design* process, which translates the logical model, built during analysis, into a physical model of the system which can be assessed before coding begins. The design phase can be broken down into preliminary (high-level) and detailed (low-level) design, depending on the level of procedural detail, data structure, architecture, and interface characterization specified.
iii) *Construction*, which consists of coding the design specifications into a machine-readable language.
iv) *Testing*, which ensures that the software performs satisfactorily.
v) *Maintenance*, or *evolution*, manages the changes made to the software once the product is delivered.
vi) *Documentation* produces a record of the software development process, system requirements, design specifications, etc. (Pressman, 1992).

These life cycle steps are essential to the development and implementation of coherent software systems, regardless of the application to which they are destined. In fact, taken out of the software context, these conceptual steps form the building blocks necessary to design and construct a variety of tools, from mechanical devices to electrical components, or on a higher level of abstraction, even processes such as mine planning or ground support.

The heart of the robotic mining environment resides in an information system which manages and compiles data from a number of sources. Understanding the nature and characteristics of the information to be manipulated is therefore of capital importance to the development of such a system. Software engineering can assist in the analysis of information requirements by means of methodologies such as Information Engineering (IE), Structured Analysis and Design (SA/D), and Object-Oriented Analysis and Design (OOA/D). The latter is rapidly gaining in popularity and may very well surpass more traditional methods in

the near future. The following sections briefly describe these methodologies.

Information Engineering

The term *information engineering* (IE) was coined in the early 1970s by James Martin. In his own words, "information engineering is defined as an interlocking set of automated techniques in which models are built up in a comprehensive knowledge base and are used to create and maintain [information] systems" (Martin, 1989). It is important to note that, while software engineering focuses on one project, information engineering examines the enterprise as a whole.

In fact, IE begins with a top management view of the enterprise by conducting an information strategy plan and progresses downward into greater detail through the analysis of a particular business area, and the design, construction, and, later maintenance of a system which implements selected processes of the business area. The information generated throughout the investigation is collected in an *encyclopedia*, a computerized repository which helps control the accuracy and validity of the knowledge base.

In the context of mining, IE can assist in gaining a more comprehensive understanding of our business by zooming in on problem areas from a wider perspective. In this respect, IE is analogous to utilizing satellite images or aerial photography to identify potential mineralization. On the other hand, structured and object-oriented techniques are concerned with the detailed analysis and design of specific systems, analogously to exploration drilling, which provides insight on the nature of the mineral deposit, and mine planning, which addresses the subsequent layout and design of the operation.

A detailed discussion of structured and object-oriented analysis and design is beyond the scope of this paper. However, the following sections briefly review the intent behind these techniques. Their application to the problem at hand is illustrated in a later section by means of a concrete mining system example.

Structured Analysis and Design

The term *structured analysis* was popularized by Tom DeMarco in 1979 by introducing the notation and techniques necessary to create information models (DeMarco, 1979). *Structured analysis* employs modeling tools and process decomposition to build a functional requirements document. *Structured design* utilizes functional partitioning and hierarchical decomposition in a top-down fashion to build a system exhibiting *high cohesion* and *low coupling*, that is with a strong functional association within a single module and weak dependence between separate modules (Topper et al., 1994).

Object-Oriented Analysis and Design

Object-oriented concepts originated in the late 1960s with the development of the Simula programming language and progressively evolved with the work of several researchers while developing object-oriented programming languages (OOPL) such as Smalltalk, Eiffel, Ada, and C++. While, at first, object-orientation may appear to be nebulous, its concepts are actually simple and compact in nature. In fact, we live in an object-oriented world, where physical objects display certain characteristics and behaviours, and where similarity is commonly recognized and categorized. This process of classification, in conjunction with object attributes and behaviour, forms the basis for object-oriented technology. The goal of *object-oriented analysis* (OOA) is to build an *object model* identifying a correct set of objects complete with attributes, methods (functions), and relationships. *Object-oriented design* (OOD) groups objects into classes, defines massaging protocols, data structures, and procedures (Rumbaugh et al., 1991.; Topper et al., 1994).

Computer-Aided Software Engineering (CASE) Tools

The need for computerized tools to assist in carrying out a methodical analysis of robotic mining systems has been emphasized throughout the paper. Because of the complexity and size of the systems involved, information engineering and structured or object-oriented techniques are best implemented in conjunction with software tools. The software industry has been experimenting with CASE technology since the early 1980s. At first, CASE products were simple diagramming tools without a repository or verification checking of models. Since then, they have evolved into sophisticated tools including requirements collection and tracking, prototyping, code generation, documentation management, and even reverse engineering from existing code. Hence today, CASE tools offer an automatic support to the entire software development life cycle. To draw a parallel with the

manufacturing industry, CASE is analogous to computer-aided engineering and computer-aided design (CAE/CAD), in terms of analysis and design of software systems, and to computer integrated manufacturing (CIM) in terms of construction, testing, and maintenance.

As part of this investigation, a number of CASE tools were evaluated to identify a suitable product for undertaking a systems analysis of robotic mining (Mottola, 1994). A set of criteria and weighting factors were used to rate the products reviewed keeping in mind the following objectives:

i) to experiment with different software engineering methodologies;
ii) to implement the resulting information models on a local area network under the OS/2 or Windows environment and interface with an Oracle relational database;
iii) at a cost not exceeding $ 5,000 US.

The importance of experimenting with different systems analysis techniques originates from the fact that the software development process is enriched by the variety of methods it incorporates. The choice of operating platform and cost were dictated by constraints on existing systems and budget. System Architect©, a product developed by Popkin Software and Systems Inc. was selected and purchased. The following section illustrates how this particular CASE tool is being used to analyze the information requirements of robotic mining systems.

SYSTEMS ANALYSIS OF THE DRILLING PROCESS

The first step in undertaking a systems analysis consists in identifying the core processes of underground hard rock mining. These are:

i) *drilling*: including production drilling with an ITH or top-hammer drill and development drilling with a jumbo drill;
ii) *explosives loading*: by means of explosives loading machines;
iii) *blasting*;
iv) *supporting*: by means of bolting machines;
v) *material handling*: including transport with LHDs and haulage trucks, as well as crushing and hoisting;
vi) and *servicing*: including maintenance of mobile machinery, stationary equipment, mine monitoring instrumentation, and infrastructure, as well as supplies management.

Each one of these core processes consists of a number of sub-processes and associated information flows. To illustrate the application of software engineering methods and tools, the process of *drilling* in particular will now be examined in detail using structured analysis techniques and System Architect©.

Figure 3 (at the end of the paper) displays the sub-processes involved in drilling with an in-the-hole (ITH) drill. The structured analysis notation chosen for this *data flow diagram* is that of Gane and Sarson (Gane and Sarson, 1979), in which external systems are represented by rectangles, processes by rectangles with rounded edges, information flows by arrows, and data stores by open rectangles. It must be understood that this is not a mere graphical representation: in fact, each object (rectangle or arrow) corresponds to a database record or entry in the System Architect© encyclopedia. Hence, these objects are meaningful entities linked to one another as shown on the figure and possessing properties and descriptions integrated within a machine-readable database. In other words, the data flow diagram constructed using System Architect© possesses another perspective or depth which cannot be represented on this figure. The following paragraphs explain the details behind each object.

Connecting and Disconnecting: Auxiliary connections are needed to provide compressed air, water, and electricity to the drill. Water flushing is used as a form of dust control and cooling while removing the drill cuttings from the bottom of the hole. The connecting time is cumulative for all three connections and is added to the time it takes to disconnect the machine from the service lines. Air, water, and electric consumptions are also recorded through monitoring of these infrastructure components. The connection data gathered is relayed to the information system database via the communications network. This link is here represented by the information flows to the data store "Connection Data". This convention is used throughout the diagram.

Machine Positioning: The machine is positioned within the working area according to its planned location given by the pattern to be drilled. The correct machine location corresponds to the position of the

drill required to collar the hole at the (x,y,z) coordinates specified in the drill pattern. Hence, machine location can be specified in terms of hole location. The positioning error can be obtained by comparing the planned versus actual location. The machine positioning time includes the time it takes to install and level the machine.

Drill Positioning: Once the machine is in place, then the drill is precisely positioned according to the drill pattern describing the hole orientation. For an ITH drill, the mast is positioned with respect to azimuth and dip angles. The drill positioning time includes all time periods required to achieve the proper orientation.

In-The-Hole Drilling: The hole is drilled to a pre-determined length specified in the drill pattern and the following performance parameters are measured while drilling: footage, feed force, torque, rotary speed, bit air pressure, bit air flow rate, piston blow rate, machine vibration, and rod vibration. Hole deviation is calculated by comparing bit location versus the planned trajectory given by the drill pattern.

Rod Handling: In the case of an ITH drill, where production holes can reach lengths of up to 130 metres, an automatic rod addition/removal mechanism is incorporated into the machine to extend the drill string. The rod handling time is cumulative during the drilling process and continuous when removing the rods once the hole is completed.

Moving: There are three means to move a drill, namely by tramming, towing, or caging. Tramming is the usual manner in which drills are temporarily displaced when blasting or moved between working areas that are on the same level. ITH drills are crawler mounted and are usually towed or carried by an LHD between levels or over long distances. When moving equipment between levels which are not connected by a ramp system, caging becomes necessary. The moving time is cumulative for these activities and includes all pre- and post-move preparation periods.

Servicing: Servicing encompasses three types of maintenance: routine, preventive, and breakdown. Routine maintenance, and associated downtime, consists of replacing consumables, such as bits, rods, and lubricants. Preventive maintenance involves continuously monitoring vital parameters of the machine subsystems, sounding alarms when thresholds are reached, and perhaps offering a preliminary diagnosis as part of an expert system. The time spent in performing preventive maintenance is accumulated separately. Breakdown maintenance results from a machine failure and tracks the time at which it occurred as well as the time it takes to diagnose it and repair it. This information allows the calculation of quantities such as mean time before failure (MTBF) and mean time to repair (MTTR) for a specific part and failure.

Idling: Idling takes into account all periods of inactivity, such as waiting for instructions.

The data flow diagram of Figure 3 is not intended to include control flows between processes, but only flows of information. The behaviour of the system is captured in another view called a state-transition diagram, which is beyond the scope of this paper. However, for the sake of clarity, non-labelled arrows have been drawn on Figure 3 to represent the sequence of activities in the drilling cycle. Note that the processes of servicing and idling have not been connected to any other process because they can take effect at any point in time.

There are a number of lessons to be learned from this exercise. For instance, the process of drilling with an ITH machine is very similar to that of drilling with a jumbo drill. Therefore, it would be preferable to design the process of drilling at a level of abstraction which enables the application of its sub-processes to different conditions. For example, when positioning the drill to match the hole orientation specified in the drill pattern, the ITH requires azimuth and dip angle adjustments whereas the jumbo requires boom rotation and lift angles and feed tilt and swing angles. This distinction could be made deeper within the definition of the drill positioning sub-process, rather than creating a whole new drilling process specifically for the jumbo drill. Similarly, the process of servicing, including routine, preventive, and breakdown maintenance, could be tailored to cater to different types of machinery and equipment. These observations call for object-orientation: essentially, object-oriented analysis techniques differ from structured techniques in that data structures and the methods (functions) that manipulate data are encapsulated locally within an object rather than in a central location. Information is accessed and updated via messages passed between objects. This configuration promotes object re-use and can potentially enhance the overall design of the information system.

CONCLUSIONS AND FURTHER WORK

The paper has described a robotic underground mining environment where an information system interfaces with four main functional areas: mobile machinery, stationary equipment, mine monitoring, and infrastructure. Software engineering concepts, methods, and tools have been introduced and related to the problem of planning and designing integrated robotic mining systems. Although this approach is new to the business of mining, systems analysis has evolved successfully in other industries and can be applied effectively to examine the present and future need for more adequate mining solutions. Currently, System Architect© is being used to analyze the interactions and information flows between mining processes in a robotic underground environment.

Future work is intended to pursue the following:

i) explore the suitability of object-oriented techniques in the analysis and design of robotic mining real-time systems;
ii) translate process specifications into a database architecture for Oracle and carry through the software development life cycle for a specific process, e.g. drilling;
iii) instrument a drill accordingly and interface it to the database via a communications network;
iv) use this platform as a test case to assess ...

ACKNOWLEDGMENTS

The authors would like to thank INCO Ltd. for permission to publish this work.

REFERENCES

BAIDEN, G.R. and HENDERSON, E., 1994.
LHD Teleoperation and Guidance: Proven Productivity Improvement Tools. 96th Annual General Meeting of the Canadian Institute of Mining, Metallurgy, and Petroleum. Toronto, Ontario. May 1-4.

DEMARCO, T., 1979.
Structured Analysis and System Specification. Prentice-Hall. Englewood Cliffs, New Jersey.

GANE, C. and SARSON, T., 1979.
Structured Systems Analysis: Tools and Techniques. Prentice-Hall. Englewood Cliffs, New Jersey.

KNIGHTS, P.F., KAIROUZ, J., DANESHMEND, L.K. and PATHAK, J., 1994.
Applications of Radio Frequency Identification Systems in Underground Mining. 6th Canadian Symposium on Mining Automation. Montreal, Quebec. October 16-19. pp. 28-33.

MARTIN, J., 1989.
Information Engineering: Introduction (Book I). Prentice-Hall. Englewood Cliffs, New Jersey.

MOTTOLA, L., 1994.
CASE Tools: Product Evaluation. INCO Ltd., Mines Research, Automation & Robotics. Sudbury, Ontario. Internal Report. December.

PRESSMAN, R.S., 1992.
Software Engineering: A Practitioner's Approach. McGraw-Hill Inc. New York, New York. 3rd ed.

RUMBAUGH, J., BLAHA, M., PREMERLANI, W., EDDY, F. and LORENSEN, W., 1991.
Object-Oriented Modeling and Design. Prentice-Hall. Englewood Cliffs, New Jersey.

TOPPER, A., OUELLETTE, D. and JORGENSEN, P., 1994.
Structured Methods: Merging Models, Techniques, and CASE. McGraw-Hill Inc. New York, New York.

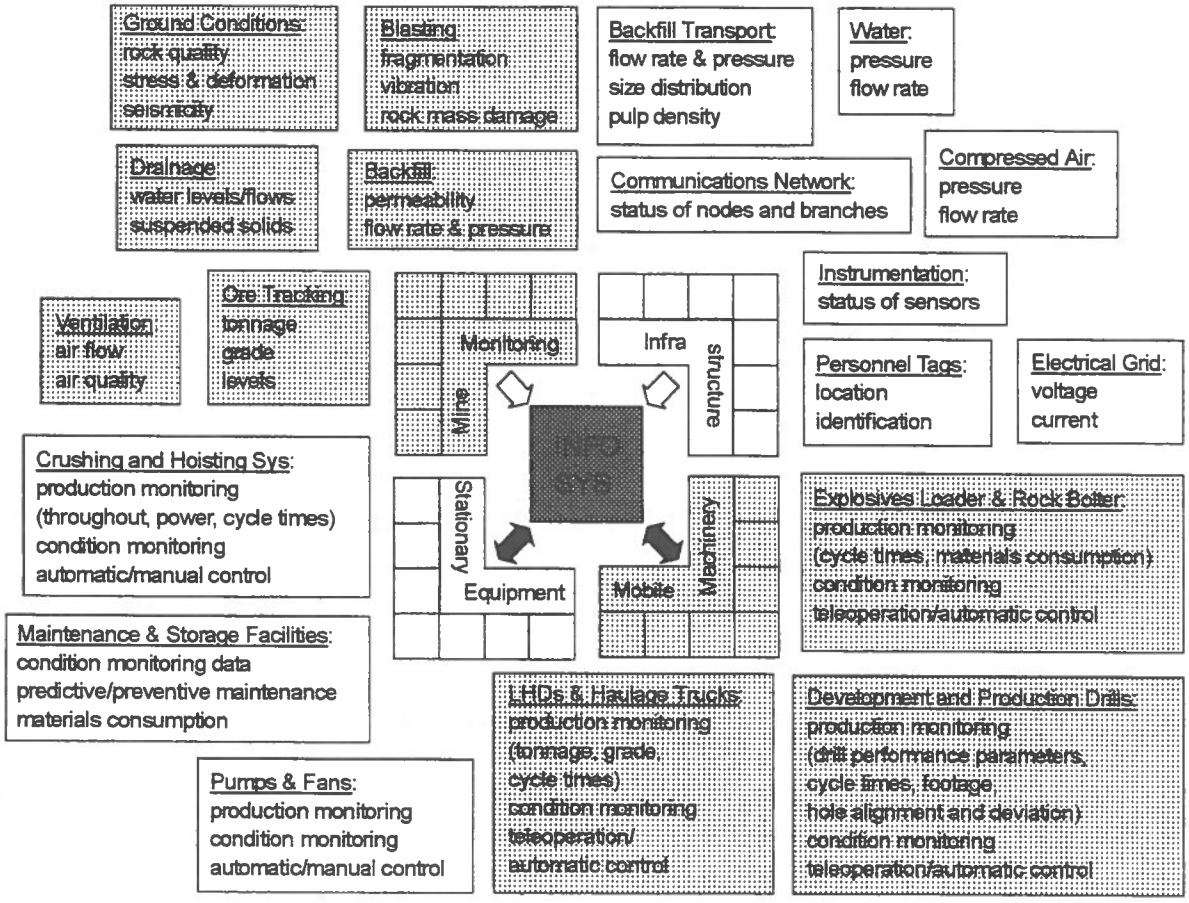

Figure 2: The mine information system

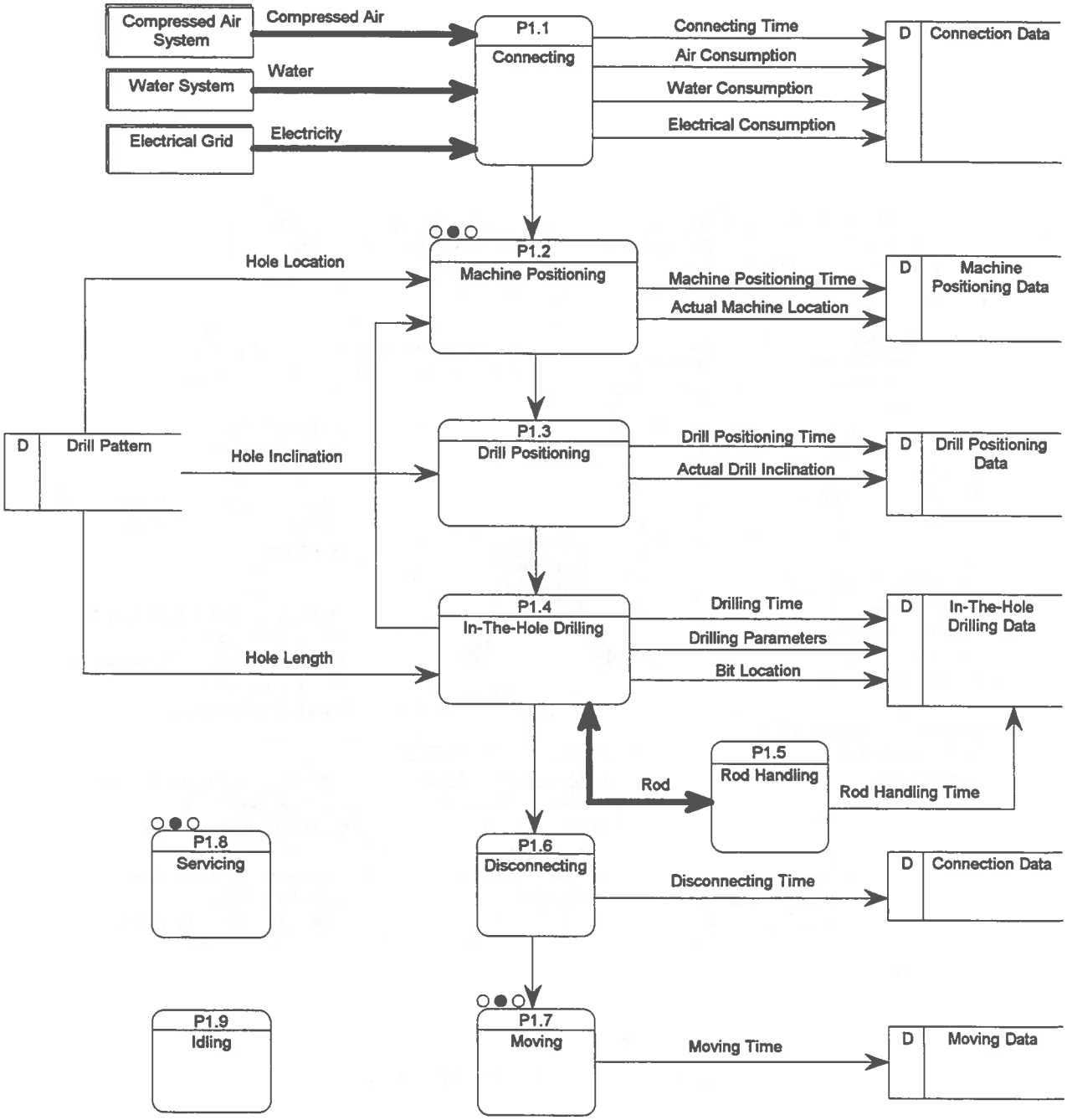

Figure 3: The drilling process (with an ITH drill)

CAMI'95: 3rd Canadian Conference on Computer Applications in the Mineral Industry
Montréal, Québec, Canada, October 22-25, 1995

Simulation Studies of Automated Truck Haulage Systems at INCO Mines

Nathalie M. Lemay, *Mining Engineer*
Inco Limited,
Copper Cliff, Ontario, Canada, P0M 1N0

Nick Vagenas, *Associate Professor*
Laurentian University, School of Engineering
Sudbury, Ontario, Canada, P3E 2C6

Allan D. Akerman, *Mechanical Engineer*
Inco Limited, Mines Research
Copper Cliff, Ontario, Canada, P0M 1N0

ABSTRACT

Computer simulation models have the potential to become valuable tools in the decision making processes mine engineers are faced with on a daily basis. METAFORA is a simulation model developed for the evaluation of transport operations in the mining industry. The model is used for the analysis of ramp haulage case studies at two of INCO Ltd's Sudbury mines. The results of the simulations are presented and discussed in this paper.

RESUME

La simulation à l'ordinateur de modèles miniers pourrait devenir d'essentiels outils pour les ingénieur(e)s miniers lors de décisions journalières. Ainsi, METAFORA est un logiciel qui fut conçue pour analyser les opérations de transportation dans l'industrie minière. Un cas typique de transport dans une rampe dans deux mines d'INCO à Sudbury furent modelés avec ce logiciel. Ce papier présente les modèles utilisés et discute des résultats obtenus.

INTRODUCTION

As a consequence of the availability of affordable and reliable computer technology, industries are increasingly relying on simulations as a tool in decision-making. Discrete event simulation models are used to represent systems in which the variables required to describe the systems, change only at discrete set of points in time (Banks and Carson, 1984).

METAFORA is a microcomputer discrete event simulation model (Vagenas and Forsman, 1992), (Forsman et al., 1992). The model combines simulation and graphical animation with Computer Aided Design (CAD). A transport layout can be created using up to 99 nodes. The haulage system can include up to ten loaders, thirty trucks, two crushers, four dumping points and a repair station. One way and/or two way traffic can be simulated. Input data can be defined deterministically or probabilistically. Six probability distributions are available, i.e. Exponential, Normal, Lognormal, Poisson, Weibull and Uniform distribution. Two sizes of loaders and trucks can be used simultaneously. Planned equipment service, equipment break downs, shift changes, and coffee and lunch breaks are easily incorporated in the simulation.

Three dispatch rules are currently available with this model: **Fixed dispatch, Maximize trucks utilization** and **Maximize shovels utilization**. Using the **Fixed dispatch** rule, the trucks travel to the initially assigned shovel and dumping points unless breakdowns occur. **Maximize trucks utilization** means that a truck is always assigned to the shovel where it is expected to be loaded earliest. **Maximize shovels utilization** means that a truck is sent to the shovel which has been waiting longest or is expected to be idle next. Other rules can easily be incorporated in the software thanks to the modular design of METAFORA. For optimum route selection during dispatching Dijkstra's shortest path algorithm is used. Detailed discussion about dispatch rules and techniques can be found in the literature e.g. (Lizotte and Bonates, 1987).

Simulation is done either as a graphical animation, where the motion of the trucks is continuously displayed on the screen, or as a text output simulation for faster execution. Among other information the text output menus display availability, utilization, number of breakdowns, operating time, service time and idling time for the loaders and the trucks. Waiting times, loading times and loaded tons are also displayed for the loaders.

METAFORA runs on IBM AT compatible computers with EGA graphics. Minimum memory requirement is 530K and the operating system must be DOS 3.1 or higher. A 10 hour shift can be simulated in less than a minute on a 33 MHz IBM compatible computer.

INCO LTD'S STOBIE AND CREIGHTON MINES

Truck haulage systems are widely used in surface and underground mining operations. The simulation model METAFORA is used at the Laurentian University Mining Automation Laboratory (**LUMAL**) for a feasibility study of proposed haulage systems at two Sudbury area underground mines of INCO Limited. Simulation studies are performed for two of INCO's Sudbury mines: Stobie Mine and Creighton Mine (Lemay, 1993).

Stobie Mine

Presently at Stobie Mine, two mining methods are used for the extraction of ore; Sublevel Caving and Vertical Retreat Mining (**VRM**). Present production is 15400 tons per day, 4000 tons of which are recovered from the VRM stopes. The mine has approximately 100 million tons of reserves, which correspond to an expected mine life of 20 years. At the present time, the mine does not use any trucks underground, but uses locomotives. However, to obtain access to reserves, Stobie Mine will be deepened. Consequently, the mine's present mucking and hoisting system needs to be modified to accommodate the new mine layout. The use of trucks for ore transportation is considered as a possible alternative.

Creighton Mine

At Creighton Mine, the VRM mining method is being used to mine a 914m thick and 305m long ore body. The present production is about 5200 tons per day (**tpd**). Creighton has enough reserves to be able to maintain this production rate for another 20 years. Similarly to Stobie mine, Creighton will be deepening its shaft from the 7200 level to the 8200 level to access additional reserves. Creighton does not presently use any underground hauling trucks. However, with the deepening of the mine, the use of underground trucks is being considered to transport the 3500 tpd that will be generated from the new levels.

STOBIE MINE CASE STUDY#1 - 39 TON TRUCK VS. 70 TON TRUCK

Case 1 - Haulage Output Comparison

Purpose: With the deepening of the Stobie mine, the purchase of underground hauling trucks is being considered. Therefore, some important questions need to be answered. For example, what size and number of trucks are required to haul the amount of ore and waste that will be produced ?

At present, INCO is using 39 ton manually driven trucks at some Sudbury mines, while Little Stobie Mine uses a 70 ton Automatic Haulage Truck (**AHT**)

to haul 3000 tpd of muck. At present, the AHT is used to haul o5n a horizontal level. It has also been tested on 20% grades, where it has achieved a speed of 1 m/sec.

Although INCO may consider the development of another 70 ton AHT to be used at Stobie Mine, it still remains uncertain as to whether this would be profitable, considering that at Stobie Mine the truck would be hauling on a grade. The purpose of Case 1 is therefore to compare the haulage outputs of the 39 ton manually driven truck and the large 70 ton AHT.

Parameters such as loading and dumping times, truck speed and operating time vary from one type of truck to another. For example, the loading time for the 70 ton truck is longer than it is for the smaller truck. However, the 70 ton truck is automatic, and thus can run for 7.5 hours per shift as compared to 5.5 hours for the manually driven 39 ton truck. The simulation model is used to compare these two types of trucks, taking into consideration the above mentioned parameters.

Input data: METAFORA is used to simulate the operation of both the 70 ton Automatic Haulage Truck and the 39 ton manually driven truck in the Stobie Mine ramp, which for our purposes is divided into 7 segments of various lengths, based on the truck speeds. These conditions are shown in Tables 1 and 2, as well as in Fig. 1.

In this case the input data from Table 3 is also included.

TABLE 1: Speed of 70 ton truck in Stobie ramp

SEGMENT	DISTANCE (m)	SPEED (km/h) (LOADED)	SPEED (km/h) (EMPTY)
1-2	30.8	8.1	8.1
2-3	215.4	16.2	16.2
3-4	15.4	8.1	16.2
4-5	7794.8	6.2	16.2
5-6	15.4	8.1	16.2
6-7	2051.4	16.2	16.2
7-8	30.8	8.1	8.1

TABLE 2: Speed of 39 ton truck in Stobie ramp

SEGMENT	DISTANCE (m)	SPEED (km/h) (LOADED)	SPEED (km/h) (EMPTY)
1-2	30.8	8.1	8.1
2-3	215.4	16.2	16.2
3-4	15.4	11.3	16.2
4-5	7794.8	8.6	16.2
5-6	15.4	11.3	16.2
6-7	2051.4	16.2	16.2
7-8	30.8	8.1	8.1

TABLE 3: Additional input data (CASE 1)

TRUCK TYPE	TRUCK CAPACITY	LOADING TIME	DUMPING TIME	SHIFT DURATION
70 Ton Truck	70 tons	68 sec.	22 sec.	7.5 hrs
39 Ton Truck	39 tons	40 sec.	90 sec.	5.5 hrs

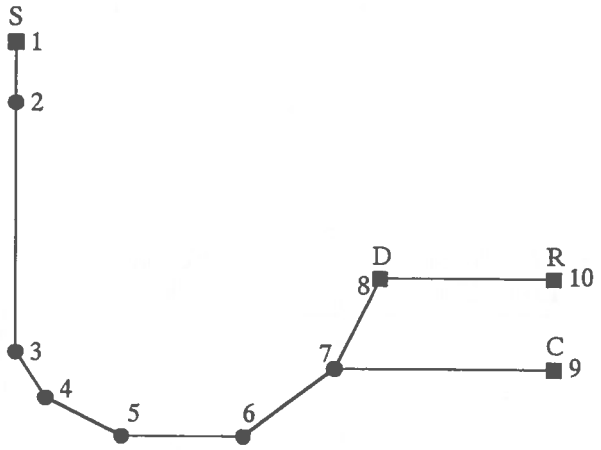

Fig. 1 Stobie mine haulage layout (as it was created in the CAD menu of METAFORA): S is a loading point, D is a dumping point, C is a crusher, R is a repair station. (Note: The figure is not drawn in proportion to the actual distances)

Simulation Results: The output obtained indicates that the 70 ton Automatic Haulage Truck is loaded 4 times during the 7.5 hour shift but completes only 3 trips to the crusher. Meanwhile, the 39 ton truck makes 3 complete trips from the loading to the dumping zone during the shift. The larger truck is somewhat slower, thus although it is operated for 2 extra hours, it completes the same number of round trips as the 39 ton truck. Results indicate that the 70 ton truck hauls and dumps 210 tons of muck in a 7.5 hour shift while the 39 ton truck handles 117 tons in a 5.5 hour shift.

Case 2 - Variation of the Truck Load Capacity

Purpose: Although it is assumed that the 70 ton truck has a capacity of 70 tons, the exact amount of material loaded in it varies. Part A of Case 2, examines the effect of variation in truck load capacity. The same exercise is performed for the 39 ton truck in Part B of Case 2.

Part A (70 ton truck), input data: The simulation model is run using the assumptions described in Table 1. However, in this case, the truck capacity is defined probabilistically using the uniform probability distribution with a low limit of 60 tons and a high limit of 80 tons. A loading time of 68 seconds, a dumping time of 22 seconds and a shift duration of 7.5 hours are used. 15 simulation runs are performed for the statistical analysis of the simulation output.

Simulation results: The average load (in tons) transported by the 70 ton truck operating 7.5 effective hours per shift is 208.5 tons with a standard deviation of 8.8 tons.

Part B (39 ton truck) input data: In Part B of the simulation study, the truck speed data from Table 2 is used. However, in this case, based on suggestions from specialists at INCO Ltd., the truck load is uniformly distributed with a low limit of 34 and a high limit of 39 tons. The 39 ton truck loading time is 40 seconds, the dumping time is 22 seconds and the shift duration is 5.5 hours. 15 simulation runs are performed.

Simulation Results: The average amount of tons hauled by the 39 ton truck is 108.4 tons per shift with a standard deviation of 2.5 tons..

Case 3 - Effect of Varying the Loading Time (39 ton truck)

Purpose: Studies performed at INCO mines have shown that the loading times of the 39 ton truck are approximately 40 seconds. However, loading times

can vary, and therefore the simulation program is used to determine if a substantial change in tons dumped per shift will occur, if the loading times vary following a theoretical probability distribution.

Input Data: The truck capacity in Case 3 is assumed to be 39 tons. The dumping time is 90 seconds and the effective shift duration is 5.5 hours. In this case however, the loading times are considered to be uniformly distributed from 30 to 40 seconds per load.

Simulation Results: 10 simulation runs indicate that a variation in loading time between 30 to 40 seconds has no effect on the total tons hauled per shift in the Stobie ramp. The 39 ton truck transports 117 tons per 5.5 hour shift.

STOBIE MINE CASE STUDY #2 - ANALYSIS OF 140 TON AUTOMATIC HAULAGE TRUCKS

Purpose: Although Study #1 compares the alternatives of using a 39 ton or a 70 ton truck, the output obtained with these two trucks is not considered as high because of the long tramming distance. Due to the expected high daily production of Stobie Mine it is proposed to evaluate the possibility of employing larger trucks. The purpose of Study #2 is to determine the number of 140 ton automatic trucks required to haul 12000 tons per day. Furthermore, since the use of more than one truck in the same ramp layout can cause traffic congestion problems, it is also necessary to determine in which sections of the ramp the trucks meet, so that bypasses can be developed to permit safe truck motion in both directions. Thanks to the built-in graphical animation feature, METAFORA is used to identify these sections.

Input Data: The ramp haulage system in Stobie mine operates for 22.5 hours per day (3 shifts/day, 7.5 hours/shift). Since it is required to determine the areas in which truck circulation is hindered, the haulage network as created in METAFORA is slightly modified. These modifications are illustrated in Fig. 2.

The top portion of the figure (segments 1 through 15) portrays the sections of the ramp used by the loaded trucks (uphill). The bottom section of Fig. 2 which is a mirror image of the top portion shows the route followed by the empty trucks (downhill). The transport layout in the CAD menu of METAFORA is drawn in more detail in order to enable a better visualization of the truck motion and to permit an easier identification of the sections in which the trucks meet. The truck speeds are shown in Table 4. For the purpose of this simulation the loading and dumping times for the 140 ton trucks are assumed to be 68 and 22 seconds, respectively. The truck capacity is 140 tons.

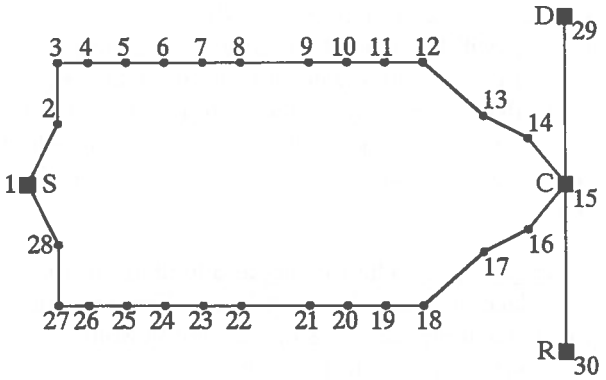

Fig. 2 Modified Stobie mine haulage layout (as it was created in the CAD menu of METAFORA): S is a loading point, D is a dumping point, C is a crusher, R is a repair station. (Note: the figure is not drawn in proportion to the actual distances)

Simulation Results: Simulation output indicates that nine 140 ton automatic trucks are required to haul 12000 tons per day of material. In fact, with these nine trucks a total of 12600 tons of material can be transported over a distance of 10139 m on a 3 shift/day schedule. However, the use of these nine trucks creates traffic problems in the ramp. It is seen through the graphical animation part of the simulation, that the trucks meet near the loading and dumping zones. More precisely they meet in segment 5-6 (24-25) in the loading zone and in segment 13-14 (16-17) in the dumping area, see Fig. 2. This can be attributed to the waiting times occurring while trucks are either being loaded or dumped. Based on the above observations, it is suggested that the maximum length of road segment that must be enlarged to permit two-way traffic, is 720 m (from node 1 to node 6) in the loading zone area and 1230 m (from node 13 to node 15) in the dumping zone. However, the latter road segment is on surface, thus no ramp

enlargement is required for this road segment.

CREIGHTON MINE CASE STUDY#1 - DETERMINING THE REQUIRED NUMBER AND SIZE OF TRUCKS

Purpose: Creighton mine is in the process of developing 5 new production levels from the 7400 level to the 8200 level. The material from the 5 levels will have to be transported to the 6950 level, from which it will be hoisted to surface. The purpose of this study, is to determine the number and size of trucks that will be required to handle the 3000 tpd of ore, in addition to the 750 tpd of waste that will be produced in the deeper levels of INCO's Creighton mine.

Input Data: The loading and hauling of ore will take place on three different levels. There are three possible hauling scenarios for Creighton Mine. These scenarios are presented in Table 5.

Creighton mine's transport layout as created in METAFORA is displayed in Fig. 3. Based on suggestions by INCO specialists, certain assumptions are made in running this particular simulation. These are:

- The trucks will operate 15 effective hrs/day (5 hrs/shift @ 3 shifts/per day)
- Loading time is 70 seconds (regardless of truck size)
- Dumping time is 22 seconds (regardless of truck size)
- Maximum haulage distance to the ramp per level is 250 m. (The road segements : 1-12, 2-3, 4-5, 6-7 and 8-9 in Fig. 3 are all 250 m)
- Maximum haulage distance from the main ramp to the dumping station, (the road segment 10-11 in Fig.3), is 100 m
- The road segments : 12-3, 3-5, 5-7, 7-9 in Fig. 3 are all 411 m
- The road segment 9-10 in Fig. 3 is 1083 m
- Truck speed for hauling in the ramp with an inclination of 15% is 6.5 km/h for both empty and loaded trucks
- Truck speed from the main level haulageways to the ramp is 15.1 km/h for both empty and loaded trucks

Simulation results: Simulation runs were performed for trucks ranging in sizes from 70 to 110 tons for each scenario, in order to determine the minimum number of trucks required for the transportation of the 3750 tons of material. By examining the simulation output it is possible to find the minimum number and size of trucks required to transport the material from each level. Table 6 summarizes the conclusions that were reached. However, these conclusions do not take into account other important parameters such as capital, operating and maintenance costs as well as the reliability of the trucks.

Thus, keeping the number and size of trucks to a minimum for each level, it is deduced that 3 trucks are required to meet the demands of scenario 1; two 70 Ton trucks, one on the 7400 level and the other on the 7600 level, and one 80 Ton truck on the 7800 level. Meanwhile, 3 trucks are necessary for scenario 2; one 70 Ton truck on the 7600 level, a second 70 Ton truck on the 7800 level and one 100 Ton truck on the 8000 level. And finally to satisfy the conditions of scenario 3, three trucks are needed; one 70 Ton truck on the 7800 level, another on the 8000 level and one 110 Ton truck on the 8200 level. However, since only three of the 5 levels are going to be mined at the same time, only 5 trucks would have to be purchased initially; two 70 ton trucks, one 80 ton, one 100 ton and one 110 ton truck.

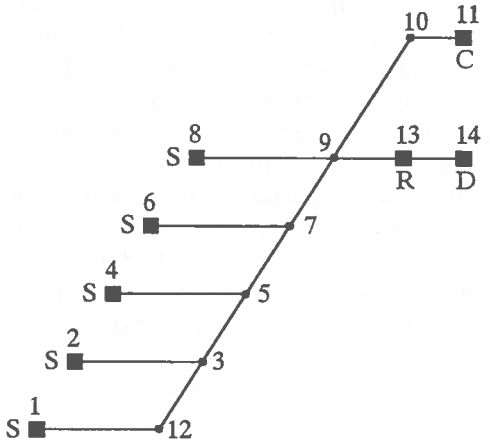

Fig. 3 Creighton mine haulage layout (as is was created in the CAD menu of METAFORA): S is a loading point, D is a dumping point, C is a crusher, R is a repair station. (note: the figure is not drawn in proportion to the actual distances)

TABLE 4: Travelling speeds for a 140 ton automatic truck in Stobie ramp

SEGMENT	DISTANCE (m)	SPEED (km/h) (LOADED)	SPEED (km/h) (EMPTY)
1-2 / 28-1	30	8.1	8.1
2-3 / 27-28	220	16.2	16.2
3-4 / 26-27	20	8.1	16.2
4-5 / 25-26	250	6.2	16.2
5-6 / 24-25	200	6.2	16.2
6-7 / 23-24	300	6.2	16.2
7-8 / 22-23	7040	6.2	16.2
8-9 / 21-22	20	8.1	16.2
9-10 / 20-21	250	16.2	16.2
10-11 / 19-20	250	16.2	16.2
11-12 / 18-19	250	16.2	16.2
12-13 / 17-18	100	16.2	16.2
13-14 / 16-17	1200	16.2	16.2
14-15 / 15-16	30	8.1	8.1

TABLE 5: Three possible hauling scenarios at Creighton mine (Table 5 continues to next page)

SCENARIO 1	
LEVEL	TONS PER DAY TO BE TRANSPORTED
7400 L	1000
7600 L	1000
7800 L	1750

SCENARIO 2	
LEVEL	TONS PER DAY TO BE TRANSPORTED
7600 L	1000
7800 L	1000
8000 L	1750

TABLE 5: (continues)

SCENARIO 3	
LEVEL	TONS PER DAY TO BE TRANSPORTED
7800 L	1000
8000 L	1000
8200 L	1750

TABLE 6: Number and size of trucks required at Creighton mine

SCENARIO 1				
LEVEL	**MINIMUM TRUCK SIZE (TONS) PER LEVEL**	**NUMBER OF TRUCKS REQUIRED**	**TONS TRANSPORTED PER TRUCK**	**TONS GENERATED PER LEVEL**
7600 L	70	1	1960	1000
7400 L	70	1	2520	1000
7800 L	80	1	1760	1750

SCENARIO 2				
LEVEL	**MINIMUM TRUCK SIZE (TONS) REQUIRED**	**NUMBER OF TRUCKS REQUIRED**	**TONS TRANSPORTED PER TRUCK**	**TONS GENERATED PER LEVEL**
7600 L	70	1	1960	1000
7800 L	70	1	1540	1000
8000 L	100	1	1900	1750

SCENARIO 3				
LEVEL	**MINIMUM TRUCK SIZE (TONS) REQUIRED**	**NUMBER OF TRUCKS REQUIRED**	**TONS TRANSPORTED PER TRUCK**	**TONS GENERATED PER LEVEL**
7800 L	70	1	1540	1000
8000 L	70	1	1330	1000
8200 L	110	1	1760	1750

FINAL COMMENTS

The use of the simulation model METAFORA was proven to be advantageous in the study of haulage systems at INCO mines. Other mathematical methods than simulation can also be used. However, the user friendliness, flexibility and adaptability of the simulation model METAFORA offered a satisfactory engineering tool for the case studies discussed previously.

In underground and open pit mining operations, truck haulage costs represent a significant portion of the total operating cost of the mine. Combined with cost and reliability data, the results obtained with METAFORA can provide useful information that can be used by mine management to make appropriate decisions regarding the development of new haulage systems, or the improvement of systems already in operation. It must be mentioned that the interpretation of the simulation results is made within the limits and assumptions of the input data employed.

REFERENCES

BANKS, J. and CARSON, J.S., 1984.
Discrete-Event System Simulation, New Jersey: Prentice Hall, Inc.

FORSMAN, B., VAGENAS, N. and LINDSTRÖM, C., 1992.
"Using METAFORA to Evaluate the Transport System in a Swedish Open-pit Mine", in the 23rd APCOM Symposium, Tucson, Arizona, USA.

LEMAY, N., 1993.
The Use of Computer Simulations for the Economic Evaluation of Haulage Systems, Undergraduate Degree Thesis, School of Engineering, Laurentian University, Sudbury, Ontario, Canada.

LIZOTTE, Y. and BONATES, E., 1987.
"Truck and Shovel Dispatching Rules Assessment Using Simulation", in Mining Science and Technology, Number 5.

METAFORA, 1990.
Metafora Computer Software Manual, 1990, : Forsman Consulting Engineers, Rafsarstig 148, S-95434 Gammelstad, Sweden.

VAGENAS, N. and FORSMAN, B., 1992.
"METAFORA: A simulator for dispatch control of truck/shovel systems in surface mines", in Simulation Conference and Annual Meeting of Scandinavian Simulation Society, Lappeenranta, Finland.

CAMI'95: 3rd Canadian Conference on Computer Applications in the Mineral Industry
Montréal, Québec, Canada, October 22-25, 1995

Self-Learning Cutting Pattern Control for a Voest-Alpine Miner

Minda Zhao (Graduate Student), Jame N. Wilson (Professor)
Control Engineering, Department of Mechanical Engineering
University of Saskatchewan, Saskatoon, SK.

ABSTRACT

This paper describes the research and development of a first and necessary step in the realization of autonomous operation, referred to as "Self-learning[1] Cutting Pattern Control", of a Voest-Alpine miner AM100. In many mining situations, manual operation of Voest-Alpine miners requires that several repetitive operations be executed by the operator. This study investigates and identifies system and control requirements necessary for repetitive operations to be executed automatically once a desired cutting pattern has been established by the operator. Computer simulation is employed to verify the control system design. The simulation results show that accurate cutting pattern control can be achieved.

RÉSUMÉ

Cette publication décrit la recherche et le développment d'une première étape nécessaire à la réalisation d'une opération autonome appelée "Auto-apprentIssage[1] du Contrôle d'un Modèle de Coupe" d'un mineur Voest-Alpine AM100. Dans plusieurs situations minières, l'opèration manuelle des miniers Voest-Alpine nécessite que plusieurs opérations répétitives soient exécutées par l'opérateur. Cette étude questionne et identifier les exigences du système et du contrôle nécessaires afin que les opérations répétitives soient effectuées automatiquement, une fois que le modèle de coupe désiré a été établi par l'opérateur. Une simulation sur ordinateur est employée pour vérifier le modèle du système de contrôle. Les résultats de la simulation démontrent que le contrôle précis du modèle de coupe peut être accompli.

INTRODUCTION

Potash is of particular importance to the agricultural industry which demands a soluble source of potassium in large quantities as a fertilizer component. At nearly all of the underground potash mines, ore excavation is mainly performed by large continuous miners [1][2]. The Voest-Alpine miner AM100, shown in Fig. 1 [2], is another major mining machine extensively employed for both production and mine rehabilitation in the potash mining industry in Saskatchewan. This is a boom-type, electro-hydraulically powered roadheader. Although its production rate is only about one sixth of that of the large continuous miners [3], the versatility of drive makes it very useful in "room and pillar" mining systems. The operational cycle of the Alpine miner, when removing a complete formation, consists of three main steps: sumping, cutting, and advancing. Once the sump has been made, the boom is then moved back and forth in horizontal passes across the width of the work face, thereby removing the ore out of the face.

The environment surrounding the mining machine is usually of high temperature, high vibration and noise levels, as well as high levels of dust. These factors

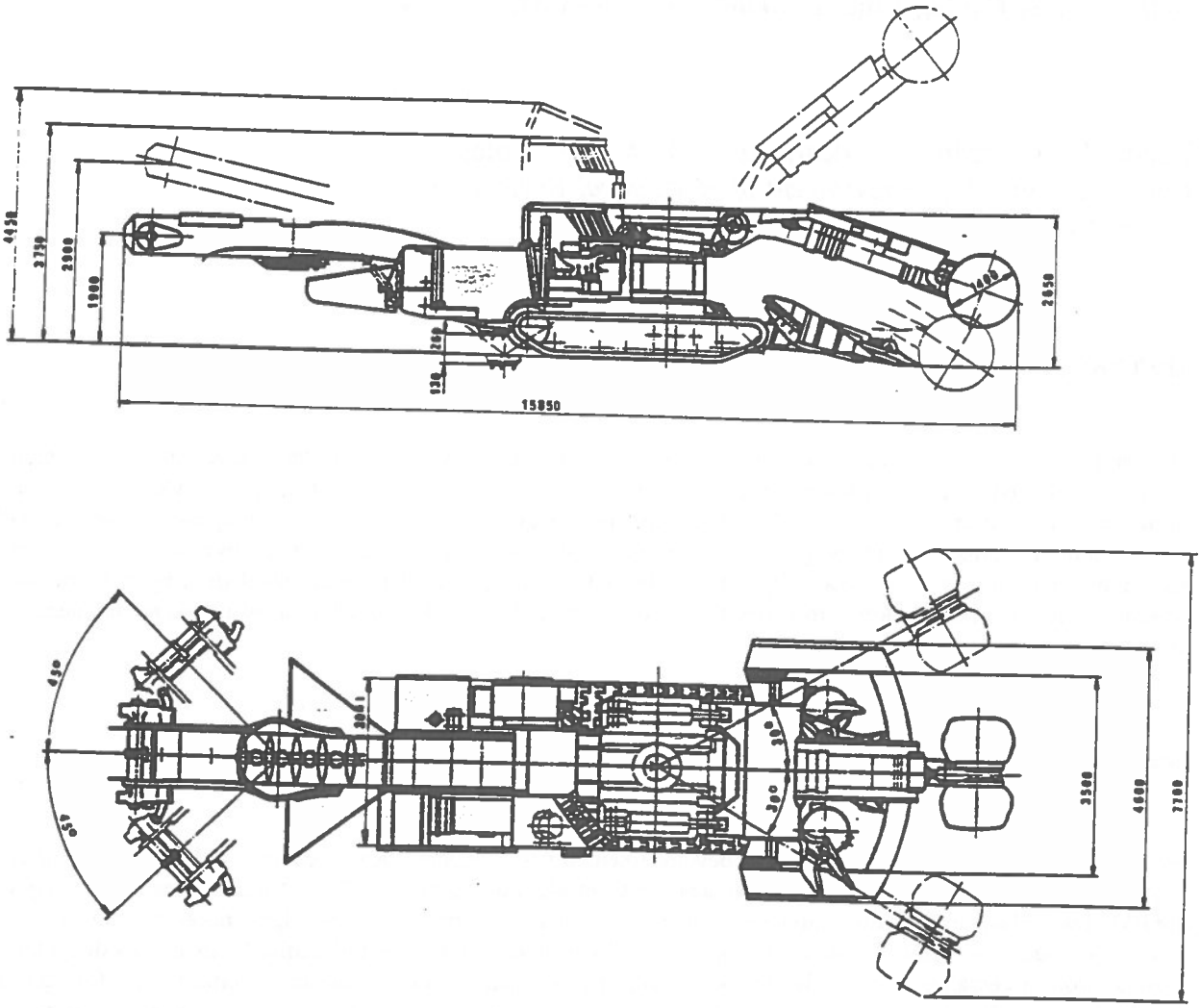

Fig. 1 Voest-Alpine Miner AM100

quickly lead to operator discomfort and fatigue. In addition, the operator's view of the cutterheads and the work face is frequently obstructed by dust and parts of the machine itself. Consequently, it is difficult for the operator to maintain accuracy and consistency in controlling the cutting functions of the miner. Therefore a reduction in productivity results.

In many mining situations, once a cutting pattern is established, the role of the operation becomes one of repeating a number of passes across the work face, followed by advance of the machine to make a new sump, and then a repeat. Therefore, repetitive operations could be executed automatically.

Predetermined cutting patterns may sometimes not be desirable in particular situations. A self-learning cutting pattern control may provide an alternate solution. The overall system schematic is shown in Fig. 2 [4]. In this approach, the operator will initially determine the cutting pattern, during which time the system will "learn and remember" the routine and subsequently carry out the same operation a number of times as dictated by the operator. However, this automatic control action must be capable of manual override by the operator. This provides the mining machine flexibility for any type of desired cutting pattern.

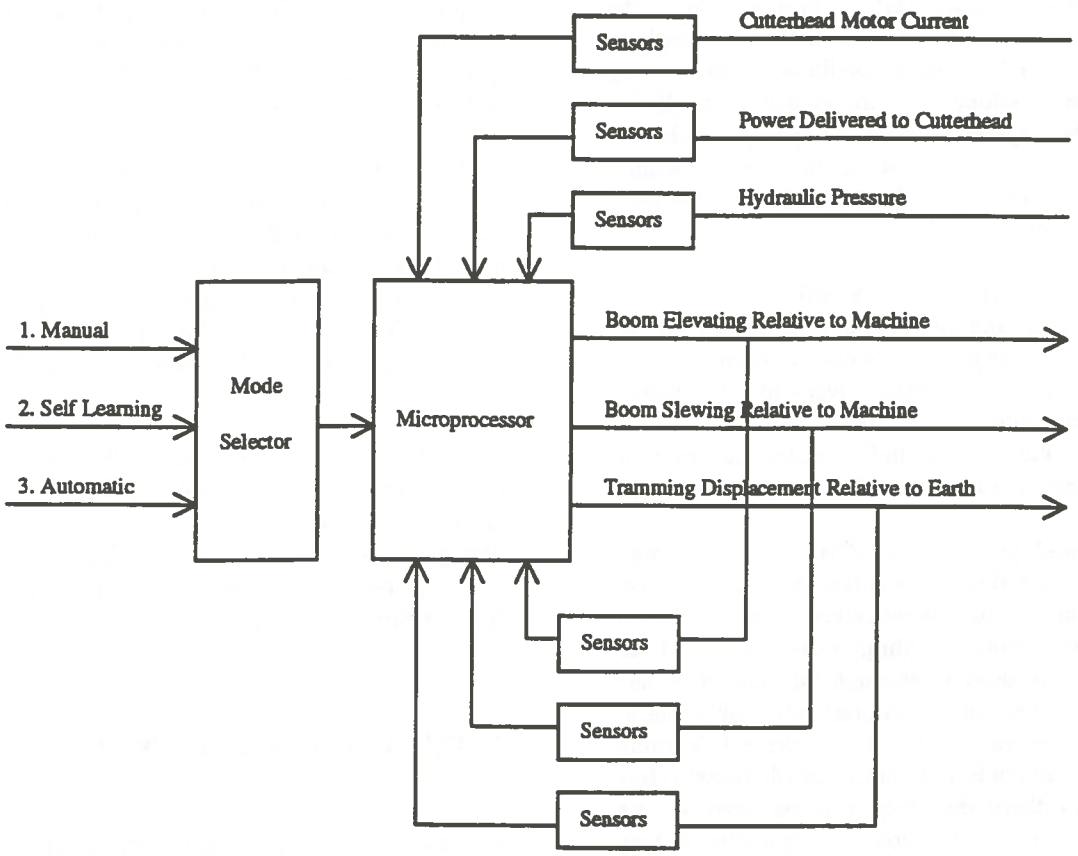

Fig. 2 Overall System Schematic

The anticipated benefits of the self-learning cutting pattern control system, if implemented, are:

1. Repetitive operations can be executed without manual control. This could result in increased productivity (e.g. the machines can operate during work breaks) and improved quality of work performed (e.g. human errors in operation can be minimized by the application of the microcomputer).

2. Although representing an incremental change in automation technology applied to this mining machine, the system would be an essential part of a fully automated system. Thus, it could be used as a vehicle by which to gain field experience and operator acceptance leading eventually to a fully automated system.

CONTROL SYSTEM REQUIREMENTS

Various parameters which must be controlled and/or measured for safety features in an automatic control system for a Voest-Alpine miner can be identified from the manual operating techniques used with the machine. The self-learning cutting pattern control is basically a position control system. The desired accuracy of the cutting pattern is 0.15 m [3]. In the automatic control system, the measurements of the cutterhead position relative to the machine, the boom movement speed, the machine advance speed and direction as well as the distance of advance, and the loading table and the rear stabilizer position relative to the machine are imperative. These measurements are believed to be more readily implemented and less vulnerable to damage than absolute measurements. It is realized that situations may be encountered in which absolute measurements may be required.

It is believed that boom movement can be determined by measuring the extension and speed of the piston rod. These measurements could indicate the cutterhead position and speed with respect to the machine by machine geometry.

In normal operation, the angular position (or speed)

of the advance motor shaft is proportional to the machine advance distance (or speed) by the machine geometry. Under certain conditions, such as very high advance settings, the tracks may slip. If this occurs, the angular position (or speed) of advance motor shaft can no longer indicate the machine advance distance (or speed). Absolute measurements may be required.

Machine overload can be identified by the cutter motor current and the hydraulic pressure in the actuators. If these parameters exceed a certain value, resulting from the machine overload, the control system could automatically adjust the control settings for boom movements and machine advance to decrease these parameters within the specified range.

The Voest-Alpine miner AM100 has various automatic internal safety monitoring systems, such as the hydraulic oil temperature, level, motor temperature, motor cooling flow, etc. If an anomalous situation is encountered, electrical and hydraulic power cut-off automatically takes place. These parameters can be fed to the self-learning cutting pattern control system as an additional safety guard. Furthermore, they can be used as the automatic control indication, for example, if they reach 75 per cent of the limit for safety, the automatic control system takes action to decrease these parameters. Records of these data also provide useful information for analyzing machine working conditions for future mining machine design.

A single board microcomputer with 4k random access memory (RAM) and 64k read only memory (ROM) can be used as a central control unit. The flexibility provided by the microcomputer-based system allows for setting up and tuning the controllers after installation on the mining machine. Furthermore, the system provides for future expansion in other control functions.

Assembly language can be used in data acquisition and control programs to obtain high speed in computation. A loop in the program must be used to monitor time lapsed and to interrupt it to execute the control routine for each sampling time in order to ensure that the sampling period remains constant for the whole control process. With this method, the sampling frequency can be kept constant irrespective of the length of the complete program. In the self-learning cutting pattern control system, the bandwidth is approximately 19 rad/sec (3 Hz) [4]. The sampling time of 0.04 seconds, is appropriate. Therefore, the single board microcomputer with an operating frequency of 4 or 5 MHz can meet the control system requirements.

Analog to digital converters (ADC) and digital to analog converters (DAC) on board are required to provide interface with the analog sensors and the proportional solenoid valve. Based on the required accuracy, an 8-bit multichannel ADC is appropriate. Based on the number of the input parameters and the controlled parameters, 16 channels of ADC and 4 channels of DAC are required.

An RS-232 serial port on board is also required for communication with a portable personal computer. This provides more flexibility for program transfers, debugging and modification, and allows for easier setting up and tuning the controllers after installation on the mining machines.

SYSTEM ANALYSIS AND MODELLING

Analysis and modelling of the boom movements and the machine advance is imperative. This analysis provides a description of the dynamic performance of the system for open-loop operation. Computer simulation is employed to examine its characteristics in the time and frequency domain, providing the foundation for the control system design. Because of the similarity in the hydraulic systems of the mining machine, analysis, modelling, and simulation of boom elevation only are presented.

The hydraulic system for boom movements is shown in Fig. 3 [4]. The vertical movements of the boom are effected via two hydraulic actuators and the horizontal movements of the boom are effected by two integrated hydraulic actuators via rack and pinion drives. These movements are controlled by a pilot control lever which is connected to a proportional directional control solenoid valve. This valve controls the direction and the magnitude of the hydraulic fluid flowrate, thus controlling both the direction and the speed of the boom movements.

Eqn. 1 gives the actuator response to the valve input signal (voltage) [4], which is of interest in linearized system design and analysis. A drop in the speed gain constant, K_q/A_p, does not adversely affect stability in

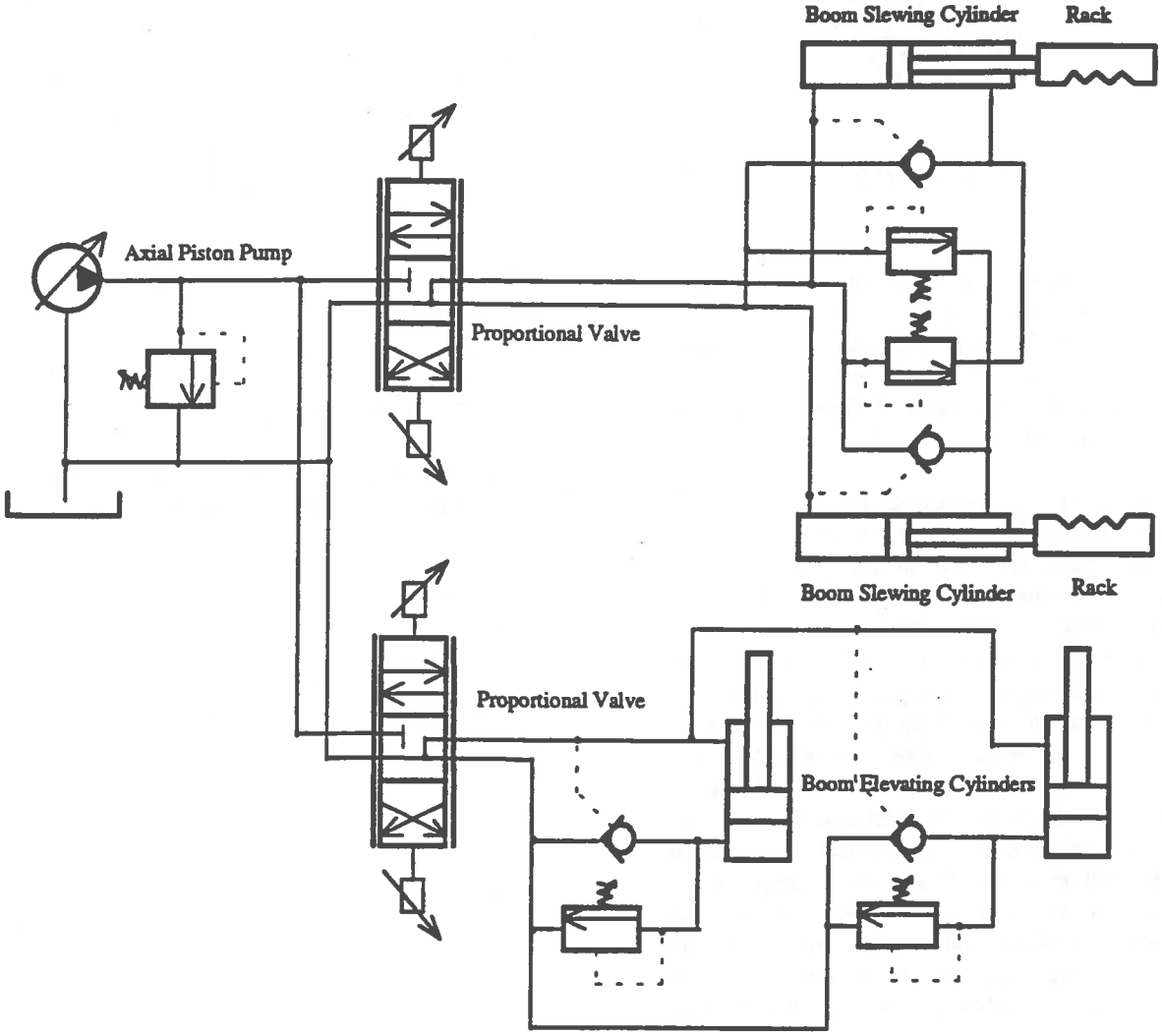

Fig. 3 Hydraulic System for Boom Movements

closed-loop control systems. In addition, the gains in the controller can always be adjusted according to the true value of the speed gain constant obtained on-site. Therefore, the product of the speed gain constant, K_q/A_p, and valve gain constant, k, of unity is used in simulation.

$$\frac{x_p}{V_i}(s) = \frac{k\frac{K_q}{A_p}}{s\left(\frac{s^2}{\omega_h^2} + \frac{2\zeta_h}{\omega_h}s + 1\right)} \qquad (1)$$

where x_p is the displacement of the piston;

V_i is the input signal (voltage) to the valve power amplifier;

k is the valve gain constant;

K_q/A_p is the speed gain constant;

ω_h is the hydraulic natural frequency (rad/sec); and

ζ_h is the hydraulic damping ratio.

$$\omega_h = \sqrt{\frac{4\beta_e A_p^2}{V_t M_t}} \qquad (2)$$

$$\zeta_h \approx 0.1 \sim 0.2 \qquad (3)$$

where β_e is the effective bulk modulus of system;
A_p is the area of the piston;
V_t is the total volume of fluid under compression in both chambers; and
M_t is the total mass of the piston and load reflected to the piston.

The parameter ω_h, expressed by Eqn. 2, is the hydraulic natural frequency due to interaction of the total load mass reflected to the piston with the hydraulic springs (due to hydraulic fluid compressibility). It establishes the overall speed of response of the valve-actuator combination for open-loop operation. ω_h sets an upper bound on the speed of response of the open-loop system. In Eqn. 2, values of all parameters except the effective bulk modulus, β_e do not vary significantly. β_e can be substantially decreased by entrained air and/or mechanical compliance. In practical situations, an effective bulk modulus of 690 MPa is suggested [5], but direct measurement is preferred. Based on the estimated or measured values of the parameters, the open-loop hydraulic natural frequency ω_h is approximately 50 rad/sec [4], as calculated by Eqn. 2.

The hydraulic damping ratio ζ_h varies widely with the valve spool positions and the load. It is minimum at the null position. Measured damping ratios for null operation are at least 0.1 or 0.2 and are often much higher [5]. ζ_h is assumed to be 0.2 for the worst stability considerations in closed-loop control system designs.

The step and frequency response from the valve input signal (voltage) to the actuator for boom elevation for open-loop operation are shown in Fig. 4. and Fig. 5 [4], respectively. The results, in fact, are normalized by dividing by $k K_q/A_p$.

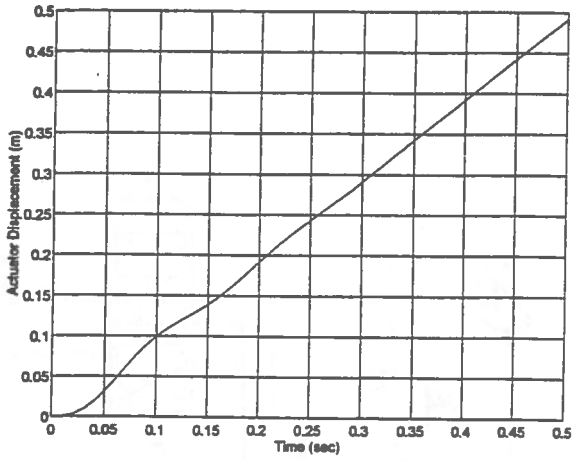

Fig. 4 Step Response from Valve Input Signal to Actuator for Open-Loop Operation

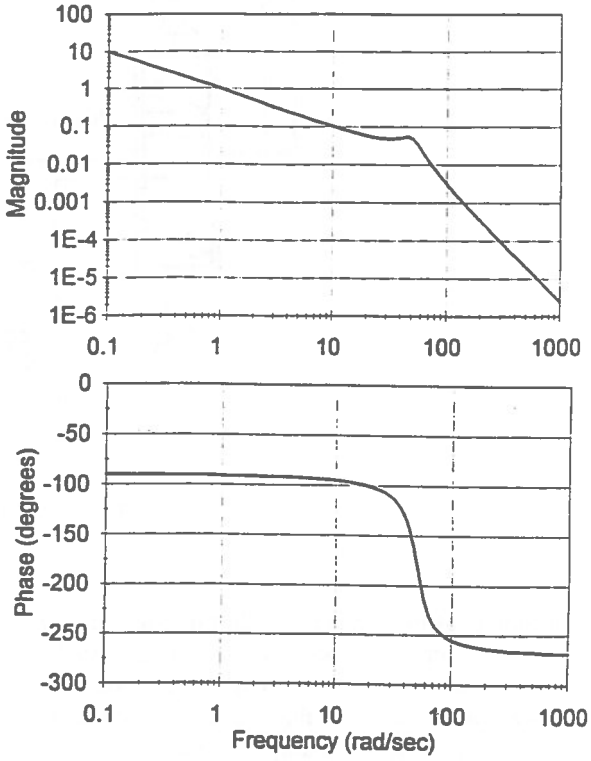

Fig. 5 Frequency Response from Valve Input Signal to Actuator for Open-Loop Operation

CONTROL SYSTEM DESIGN

The closed-loop control system is basically a position

feedback system to achieve accurate cutting pattern control. The general requirements are high accuracy, stiffness, disturbance rejection, and no overshoot. It is realized that factors such as accuracy, response, and compliance are considerations that outweigh efficiency in importance. It is also realized that various constants in the control system may have to be adjusted according to the accurate measurements on the components of the mining machine.

The cutting pattern is determined by the operator during initial cutting in the learning mode. It is described by the cutting width, the cutting span, and the cutting depth. The maximum values of these parameters measured in the learning mode are the reference inputs for the closed-loop control system. These parameters measured in the automatic mode are the outputs. The controller is designed to eliminate the difference between the reference inputs and the outputs, so that the same cutting pattern can be achieved during the automatic mode.

A proportional controller is often employed in electro-hydraulic position control systems. The larger the proportional gain constant, K_p, the higher the control accuracy and the closed-loop stiffness. It is, however, restricted by the system stability and overshoot requirements. K_p of 9.6 is suitable [4], if a proportional controller only is employed. The bandwidth of the closed-loop control system is then approximately 11 rad/sec [4].

Phase lag compensation may be used to boost low frequency gain to decrease the system steady-state error and increase the closed-loop system stiffness while retaining system stability. As was investigated, a typical overshoot of 10 per cent exists in phase lag compensation, which is undesirable in the position control system for the Voest-Alpine miner AM100. Therefore, phase lag compensation or phase lag-lead compensation is rejected.

The open-loop damping ratio, i.e. the hydraulic damping ratio ζ_h, is in the range of 0.1 to 0.2 in the worst situation which is so small that it is difficult to improve the closed-loop control system performance. If the open-loop damping ratio could be increased to be in the range of 0.4 to 1, the system stability and dynamic characteristics would be greatly improved. In addition, the higher open-loop natural frequency is also desired to improve the closed-loop system bandwidth. Therefore, the combination of the acceleration and velocity feedback in the minor loop, shown in Fig. 6, is employed [4].

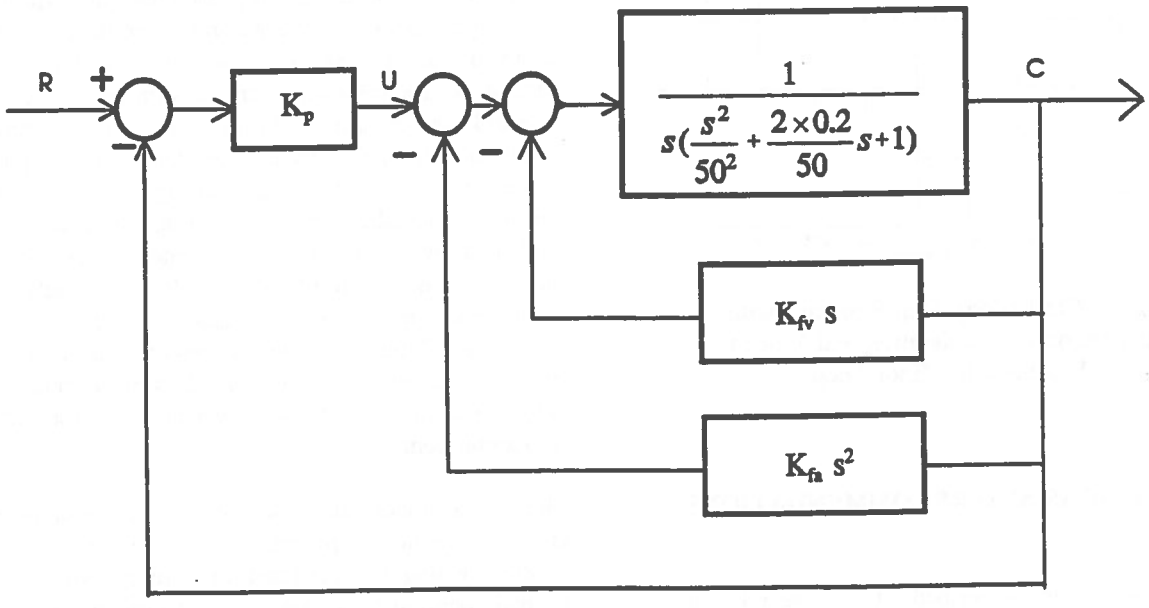

Fig. 6 Block Diagram of Acceleration and Velocity Feedback in Minor Loop

The acceleration feedback compensation increases the system open-loop damping ratio. The velocity feedback compensation increases the system open-loop natural frequency but decreases the system open-loop gain and damping ratio. However, the system overall gain can always be increased by the proportional controller, K_p. The closed-loop control performance can be greatly improved by properly selecting these gain constants.

The system closed-loop step and frequency responses with the combination of the acceleration and velocity feedback compensation in the minor loop are shown in Fig. 7 and Fig. 8, respectively. K_p of 80, K_{fa} of 0.048, and K_{fv} of 3 are used. As indicated by simulation, the system open-loop gain constant is increased from 9.6 in the proportional control system to 20 in that with acceleration and velocity feedback compensation in the minor loop. Meanwhile the bandwidth is increased from approximately 11 rad/sec to 19 rad/sec [4]. Therefore, the control system performance is greatly improved.

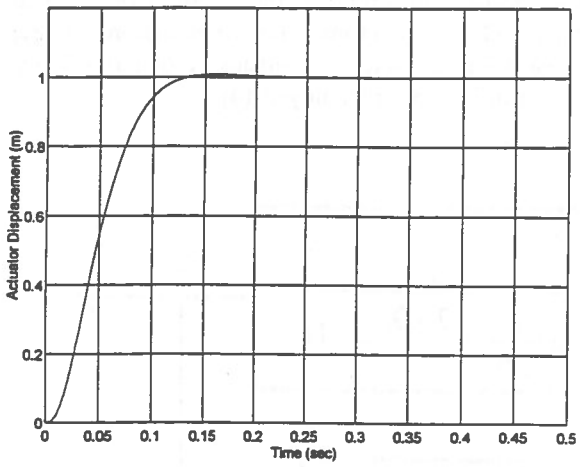

Fig. 7 Closed-loop Step Response with Combination of Acceleration and Velocity Feedback in Minor Loop

CONCLUSIONS AND RECOMMENDATIONS

This paper has described the research and development of the self-learning cutting pattern control system for the Voest-Alpine miner AM100. As indicated by computer simulation, it is capable of automatically cutting several work faces dictated by

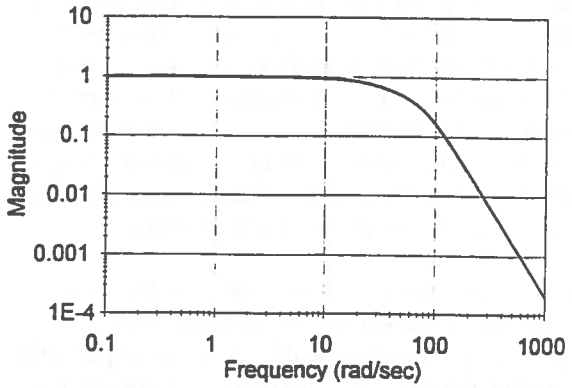

Fig. 8 Closed-loop Frequency Response with Combination of Acceleration and Velocity Feedback in Minor Loop

the operator after the initial manual operation. This would result in increased productivity and reduced operator fatigue. This also has the potential for autonomous operation of the Voest-Alpine miner AM100.

Control system designs are verified by computer simulation. The results show that accurate cutting pattern control can be achieved.

Once installed on the mining machine and adjusted for proper operation, the automatic control system could increase utilization, productivity, accuracy of cutting, and reduce manpower and maintenance costs. It could also eventually be used as part of a fully automatic control system for the Voest-Alpine miners. After the self-learning cutting pattern control system is installed on the mining machine and evaluated over some period of time, further work may be done towards developing partially autonomous operation of the machine. In order to realize this long term ideal objective, some other functions currently under manual control must be automated first, such as advance direction and horizontal control.

The central control unit used with a microcomputer is very reliable in general. However, there is a possibility that the program may jump out of its normal operating sequence as programmed and becomes unpredictable. This could possibly not only damage the mining machine but also injure people in vicinity of the machine. It is imperative to develop a watchdog timer to ensure that the program does not

fail without being detected by itself.

The controller design presented in this paper is based on the linear model and theory. However the hydraulic system is nonlinear. Therefore, a system identification technique may be used to predict the system model. The controller could be designed based on the pole-placement technique. A neural network control system could also be used in the self-learning cutting pattern control system. In this way, the neural synaptic weights could be automatically adjusted based on the system nonlinearity, variations of operating conditions, parameters, and load. Consequently, a very robust and adaptive control system could be realized.

NOTES

1. Term "Self-learning" as used in this paper pertains to the ability of the system to remember a cutting pattern and does not imply system intelligence to improve performance.

2. Numbers in brackets refer to the references listed at the end of this paper.

REFERENCES

1. VANCE, J. B. and WILSON, J. N. 1987. "Developments in Potash Miner Automation", Seminar on Future Mining Technology, Mining Division, Coal Mining Research Company, Devon, Alberta.

2. Alpine Miner AM100 Machine and System, Wajax Industries Limited., Edmonton, Alberta.

3. This research project was suggested by Noranda Minerals Inc., Central Canada Potash Division (CCP), Colonsay, Saskatchewan. The background and operational information pertaining to this project was gleaned from several meetings, field trips, written communications and discussions with CCP personnel. The information, acquired in various forms, is referred to as Ref. 3.

4. ZHAO, M., 1995. Self-learning Cutting Pattern Control for a Voest-Alpine Miner AM100, M.Sc. Thesis, University of Saskatchewan, Saskatchewan.

5. MERRITT, H. E., 1967. Hydraulic Control Systems, New York, John Wiley and Sons Inc..

ACKNOWLEDGEMENTS

This research project was supported in part by the Natural Sciences and Engineering Research Council of Canada Grant A-2754. The help of personnel, especially Mr. Marc Hout, of Noranda Minerals Inc., Central Canada Potash Division, Colonsay, SK., where the background and operational information pertaining to this research work was gleaned from, is appreciated. The assistance of Mr. Arnold J. Brockman of Ore-Site Systems, Humboldt, SK., is gratefully acknowledged.

CAMI'95: 3rd Canadian Conference on Computer Applications in the Mineral Industry
Montréal, Québec, Canada, October 22-25, 1995

Automatic Navigation Controller For An APM Five-Section Bridge Conveyor

Aaron K. Reynolds
Department of Mechanical Engineering
University of Saskatchewan, Saskatoon, Saskatchewan

James (Jim) N. Wilson
Control Engineering, Department of Mechanical Engineering
University of Saskatchewan, Saskatoon, Saskatchewan

ABSTRACT

This study describes a microprocessor-based navigational control system (NCS) for use on the APM Mineveyor which is a five-section bridge conveyor. The modular design of the NCS makes it easily adaptable to other bridge conveyors. An algorithm for processing feedback data and determining appropriate actuator controls is also developed.

Simulation results of the NCS indicate that distance offsets of the bridge conveyor up to 0.91 m (3.0 ft.) may be reduced to less than 5 percent in under 3.05 m (10.0 ft.) of bridge motion for a straight line trajectory path. Simulation results show successful bridge conveyor navigation for actual mine pattern cutting sequences.

RÉSUMÉ

Cette étude décrit un système de navigation sur microprocesseur (NCS) destiné à être utilisé sur un APM Mineveyor qui est une pont-courroie de cinq sections. Le dessin modulaire du NCS lui permet de s'adapter facilement à d'autres pont-courroies. Un algorithme analysant l'information obtenue et permettant de réajuster les contrôles fut aussi developpé.

Les résultats de la simulation du NCS indiquent que même si la trajectoire dévie de 0.91 mètre (3.0 pieds) l'erreur peut être réduite à moins de 5% et ce sur une distance de parcours de moins de 3.05 mètres (10.0 pieds) de la trajectoire linéaire de la courroie. Les résultats de la simulation démontrent que le système de navigation de la courroie peut être utilisé avec succès en conjonction avec les patrons des sequences de coupe minières.

INTRODUCTION

Underground potash mining processes evolved from the industrial revolution and led to large-scale mechanised operations. These mining techniques combined significant capital investment of large machinery with the use of human labour to produce large quantities of potash. By the end of the 1980's, a declining economy curbed the world potash demand and forced change among the producing companies. Two areas of concern were outlined. First, change was needed to reduce the input costs of production in order to salvage profit margin and company survival. Second, mine safety needed to be improved without a decrease in overall production. Mining needed to become more efficient and automation was deemed to be the best solution.

Automation can also address environmental concern while increasing production, improving efficiency, and improving the human factors or ergonomics. In an industry such as potash mining, safety is a large component of labour costs [Sanders et al, 1988]. The actions of underground mining change the working environment surrounding the operator. These changes can affect the worker by reducing visibility, causing workers to ingest dust, creating physical obstacles and hazards, and may temporarily reduce the workers ability to perform their

duty. Temporary loss of sight, hearing, touch and smell are the potential causes of accidents. In addition to the above listed environmental changes, other adverse environmental factors are encountered by underground mine workers. High temperatures, poor lighting, high noise levels, and a dry dusty atmosphere all affect the workers performance, health, comfort and safety. Automation is fulfilling the long term objective of moving the operator away from the cutting face to a more safe and stable environment, and improving production rates and overall efficiency [Klassen, 1986].

This research project was conducted to provide a concept evaluation of a navigational control system (NCS) for a five-section APM Mineveyor. After an extensive search, no suitable off the shelf navigation controller was identified for use with this type of bridge conveyor [Gauthier et al, 1992]. The ability to retro-fit a navigation controller onto existing mining equipment can save a significant amount in capital expenditure over re-developing new equipment.

This paper presents and evaluates an automatic navigation control algorithm for a five-section mobile bridge conveyor. Automatic navigation includes the tramming or driving and steering of each bridge section. This control method has been designed to operate with the APM Mineveyor Five-Section Mobile Bridge. The control method, however, can be adapted to any number of bridge conveyor sections. Bridge conveyor parameters and operation procedures are identified for the automatic control action. The parameters are then incorporated into a mobile bridge conveyor motion logic tree for use by the navigational control algorithm. A simulation program provides a mathematical analysis of the NCS performance.

BRIDGE CONVEYOR

The bridge conveyor used in this study was a five-section APM Mineveyor. This bridge conveyor system consists of five rigid conveyor sections connected to one another on a roller linkage allowing each section to extend or retract over top of the adjacent section. A side view of the mobile bridge conveyor is given in Figure 1 showing the general assembly of the five bridge sections and the mining machine [Gauthier et al, 1992]. The conveyor sections are mounted on individual drive train frames giving them independent navigational abilities. Each conveyor section frame is supported at the front on two wheels with hydraulic power to drive the wheels and adjust the swivel steering. The discharge end stacks on the adjacent conveyor section front end and is supported on a carriage on rollers that can travel back and forth on a track. This allows each conveyor section to extend or retract about 3.66 m (12.0 ft.) relative to its neighbour. The carriage system also swivels giving the bridge conveyor sections freedom to pivot more that 45 degrees relative to the adjacent bridge centre line. When extended, the bridge conveyor is approximately 76 m (250 ft.) long and can be retracted to a length of about 61 m (200 ft.). Each section has a 1.22 m (4.0 ft.) wide conveyor running the approximate 15.2 m (50 ft.) length of the bridge. The front conveyor section at the front end attaches directly to the mining machine on a fifth wheel type hitch. The back end of the discharge bridge is supported on two wheels.

NAVIGATIONAL CONTROL SYSTEM (NCS)

The automatic navigation system has two main functions of the bridge conveyor to control in order to achieve the desired output. The first function is tramming or providing drive power to produce locomotion. The second function is steering control to guide the bridge conveyor through the mine rooms without collision. These two functions are integrated to provide control signals for the positioning of the bridge conveyor.

The simplified block diagram in Figure 2 illustrates the basic navigation system inputs and outputs. The NCS for the bridge conveyor is a free ranging follower type system. The main input parameter is the location of the mining machine in relation to the bridge conveyor sections. This relative position between the mining machine and bridge conveyor determines the amount of extension in the bridge conveyor. When carriage travel extension limits are reached, the bridge conveyor must advance. Also, for accurate steering, the drive wheel steering angle is a necessary input. The feedback steering angle combined with the bridge conveyor position path, which is based on the mine cutting pattern, determine the necessary motion. The combination of these inputs to the NCS produce output signals for the tramming and steering actuators.

The navigational control system (NCS) design is based on microprocessor control. The processor is an important part of the computer assisted control system. It must operate at a number of levels. This hierarchical structure performs data acquisition and generates actuator control signals at a low level. At a higher level, it performs numerous calculations to determine the correct trajectory path based on interpretations of multiple source feedback information,

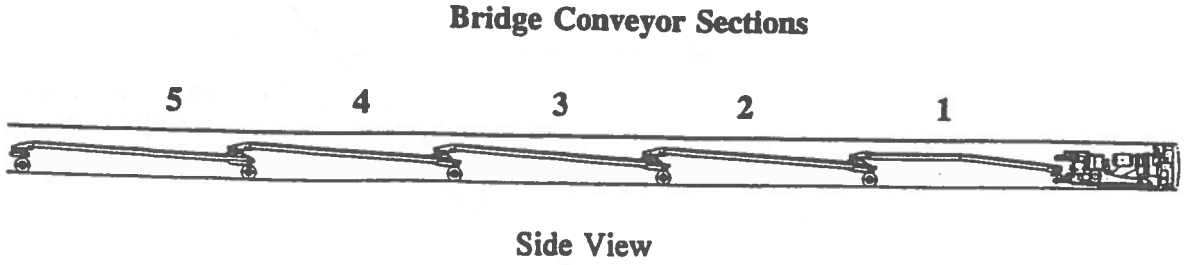

Figure 1: Schematic of Bridge Conveyor Assembly [Gauthier et al, 1992].

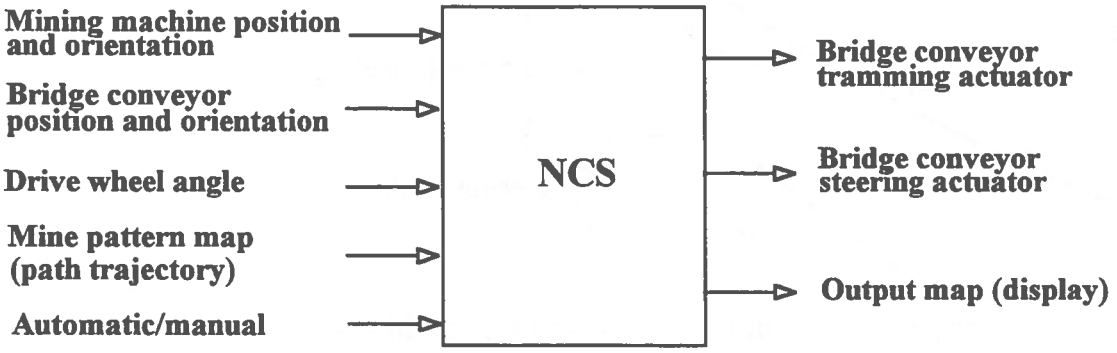

Figure 2: Simplified Block Diagram of Navigational Control System.

stored parameters and other data. Appropriate sensors for feedback measurements have previously been identified [Reynolds, 1995].

STEERING CONTROL

The steering control system operates on the basis of bridge conveyor guidance along a prescribed path. The prescribed path is represented as a polynomial curve equation by the controller. This equation is curve fitted to a set of data that represents the desired path of the bridge conveyor in the mine pattern. The polynomial curve or trajectory path provides a steering control input which the bridge conveyor should follow during normal path following operation. In order to know the position of the bridge conveyor on the trajectory curve, the bridge conveyor must know its x-y co-ordinate position in the mine. Position and heading measurements provide closed-loop bridge conveyor navigation control.

The steering control task used for bridge conveyor navigation includes an adaptation of the algorithm used by Pears and Bumby [Pears et al, 1991] to automatically steer an experimental vehicle. In their study, the steering control was based on a turning curvature determined from the trajectory path. Because of the slotted-link-type connection of the multi-section bridge conveyor, the motion of a single bridge section with a fixed steering angle does not generate a constant turning curvature. Therefore, the notion of path angle or slope angle of the polynomial trajectory curve is used. The slope angle of the trajectory path indicates how the path changes as the bridge conveyor moves along it.

The x-y co-ordinate point that is required to follow the trajectory path is the bridge conveyor wheel axis midpoint. Therefore, this point is considered a reference point for bridge conveyor location. To maintain effective steering control, it is necessary to control the steering angle of the wheels so they follow the slope angle of the trajectory curve. Also, the position offset or distance between the reference point on the bridge conveyor and the trajectory path must be controlled as the bridge conveyor advances. Figure 3 shows some of the steering control parameters.

The steering angle combined with bridge conveyor motion are the only parameters that can be controlled to navigate

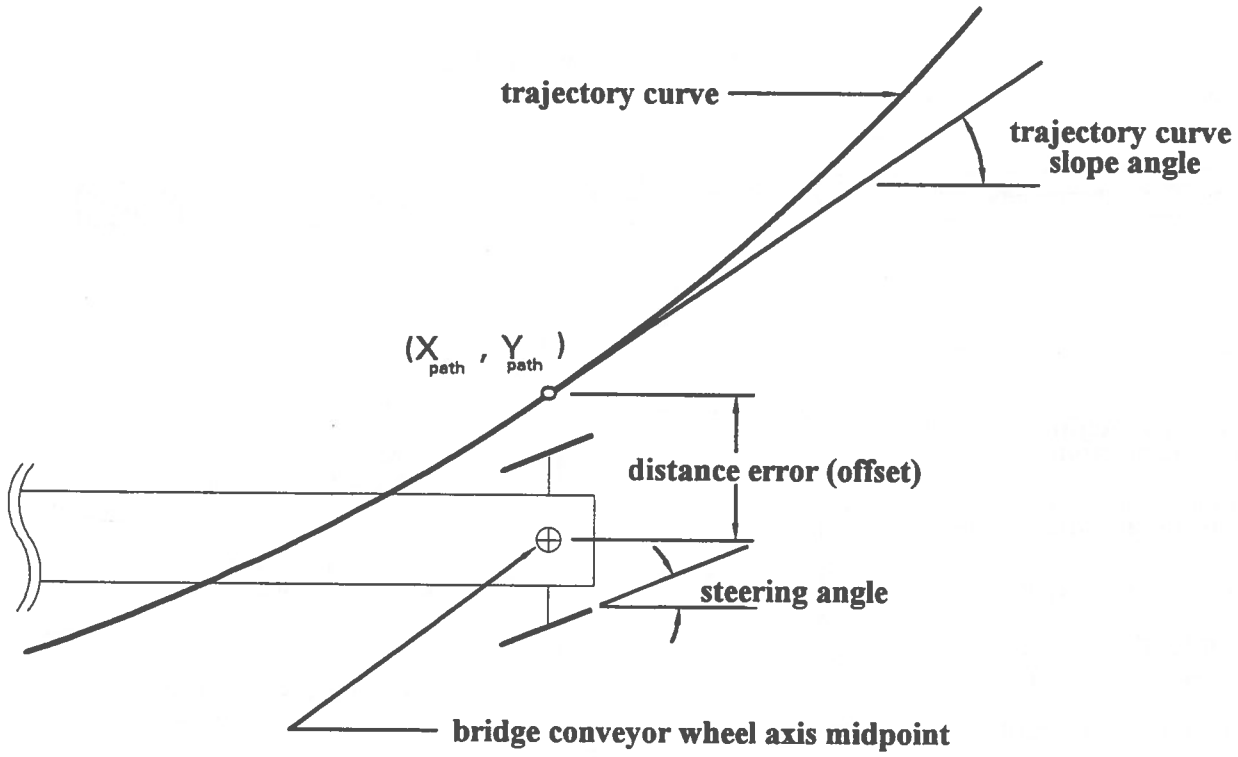

Figure 3: Steering Control Parameters

the bridge conveyor along the trajectory path. The relative amount of steer angle in relation to the desired path angle affects the way that the offset or distance error changes. For large distance errors, the steering control signal requires a large steer angle to quickly reduce this offset. As the distance error decreases, the steering control action must counter steer and approach the angle of the trajectory path. The steering control algorithm must therefore generate heading or steering angle control relative to the trajectory path heading. This control heading always points towards the trajectory path on a gradient that is relative to the distance error.

A block diagram, shown in Figure 4, illustrates the input, feedback and other control parameters of the steering control system.

TRAMMING CONTROL

The tramming control system operates on the basis of sensor recognition to activate the drive power to the wheels. The bridge conveyor tramming controller main input is the carriage travel extension limit between the first and second bridge sections. When moving forward, the tramming control task engages drive power to the wheels when the carriage travel is fully extended. The bridge conveyor motion occurs with a single section at a time in a systematic fashion. The second bridge section, the forward most section with drive wheels, is the first section to move. Drive power is engaged and the bridge section moves at a constant velocity. When the carriage travel is exhausted, the drive power is disengaged and the next section begins tramming. This procedure continues until the discharge bridge section has moved.

RESULTS AND DISCUSSION

The first tests conducted were to observe the response of the steering controller to correct a distance offset from a straight line trajectory path. The initial testing of the NCS was performed by the simulation program. Presented here are the results of investigating the motion of the second bridge conveyor section. All remaining self propelled sections will respond in a similar manner.

The second bridge section was initially positioned with a

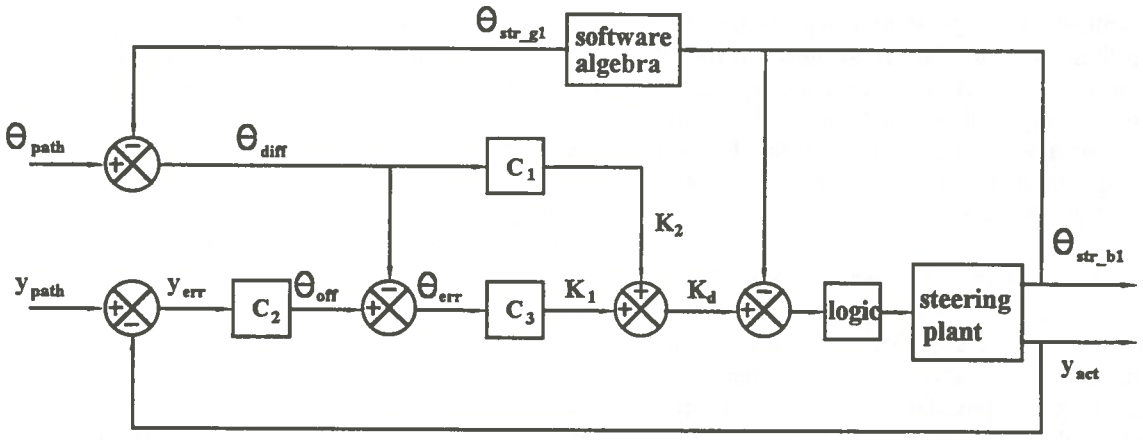

θ_{diff}	difference angle; between θ_{path} and θ_{str_gl}	C_3	controller gain value
θ_{err}	offset steering angle error	K_1	steering control angle signal
θ_{off}	controller offset steering angle	K_2	controller difference angle signal
θ_{path}	trajectory path angle	K_d	controller demand angle signal
θ_{str_bl}	bridge conveyor new local steering angle	y_{act}	bridge section y co-ordinate
θ_{str_gl}	bridge conveyor new global steering angle	y_{err}	distance error; y direction
C_1	controller gain value	y_{path}	trajectory path co-ordinate; y direction
C_2	controller gain value		

Figure 4: Steering Controller Block Diagram.

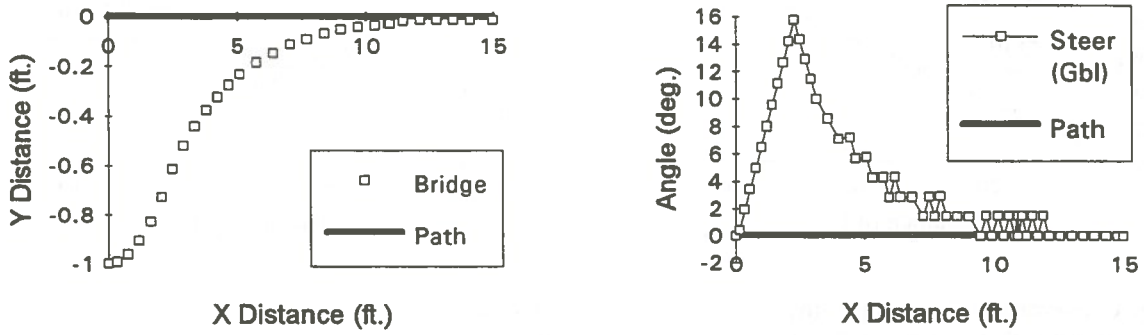

i) Bridge Conveyor and Trajectory Paths ii) Steering and Trajectory Path Angles

Figure 5: Results for 0.30m (1.0 ft.) Distance Offset; Second Bridge.

positive distance error from the desired trajectory path. The trailing bridge sections along with the mining machine were all aligned with the straight line trajectory path. All bridge sections were positioned with maximum carriage roller travel of 3.66 m (12.0 ft.). The forward velocity of each driven bridge section was 1.34 m/s (4.4 ft./s).

The first graph in Figure 5 shows the path of the bridge for a 0.30 m (1.0 ft.) distance offset. The distance error is reduced to less than 5 percent of the original offset in less than 3.05 m (10.0 ft.) which is less than one full carriage roller travel extension. From the second graph in Figure 5, the maximum steering angle was 16 degrees which was reached after approximately 0.61 m (2.0 ft.) of bridge motion. The steering angle data shows that the bridge conveyor turned left toward the prescribed path and then slowly counter steered as the bridge section approached the trajectory path. Similar results were observed for distance offsets of 0.61m (2.0 ft.) and 0.91 m (3.0 ft.).

A second set of preliminary tests were conducted on the

NCS to investigate the response to a step change in the trajectory path angle input. Bridge sections two through five were aligned on an initial path angle of 0 degrees with full forward carriage roller extension. The mining machine was initially positioned with a heading following the step input path angle. The bridge conveyor velocity was again 1.34 m/s (4.4 ft./s).

Figures 6, and 7 show the NCS response to a trajectory path angle step disturbances of 10 degrees. Figure 6 shows that near the origin of the step change, the distance error increases rapidly to a relatively small maximum value before decaying and approaching zero. The maximum distance error only reaches 0.04 m (0.13 ft.) for the 10 degree step change. Figure 7 illustrates the local steering angles quickly approach the trajectory path angle before decaying to zero as the bridge angle approaches the trajectory path angle.

The above initial analysis of the NCS was conducted in order to set up the system for the mining application. Because of the complexity of the controller, with two inputs and two outputs, a trial and error method was used to set the controller gains. A combination of the above tests were used to select appropriate controller gains to provide the results presented. Acceptable controller gains were found to be $C_1 = 4.0$, $C_2 = 1.5$, and $C_3 = 1.0$ [Reynolds, 1995].

A mine pattern test was performed on a 45 degree cut from a generic chevron pattern. A global Cartesian co-ordinate system was placed in the mine plan view with the x axis running along the centre line of the main entry room and the y axis origin at the leading wall of the chevron room. This cutting sequence was assumed to be produced in two passes. The room produced by the sequence was, therefore, 9.14 m (30.0 ft.) wide. The chevron rooms extended outward 56.39 m (185.0 ft.) from the main entry at an angle of 45 degrees from the x axis. The panel conveyor was located at 2.44 m (8.0 ft.) on the y axis and running parallel with the x axis. The bridge conveyor sections were initially located over the panel conveyor with the front end reference point of the second bridge section at the x axis zero point. Each bridge section started with full forward carriage roller travel and the mining machine was positioned against the wall of the first pass cut with a

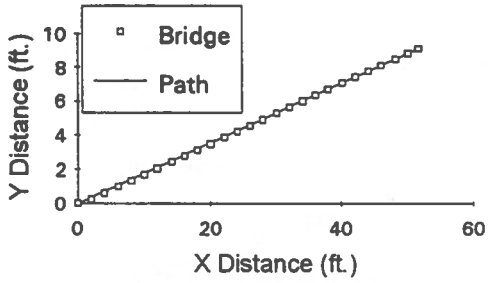

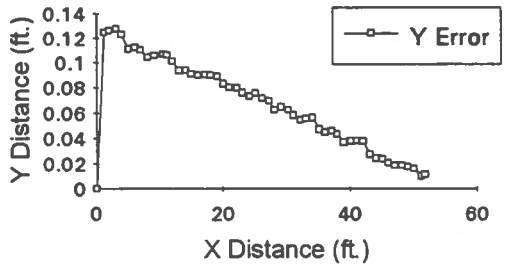

i) Bridge Conveyor and Trajectory Paths ii) Y Position Error

Figure 6: Position Output Results for 10 degree Angle Offset; Second Bridge.

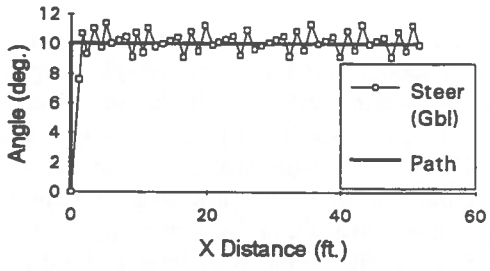

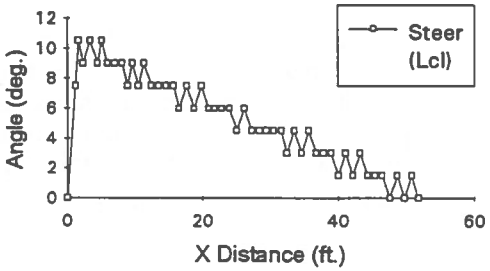

i) Steering and Trajectory Path Angles ii) Local Steering Angle

Figure 7: Angle Output Results for 10 Degree Angle Offset; Second Bridge.

heading of 45 degrees.

The first graph in Figure 8 shows a plot of the trajectory path and the path taken by the second bridge conveyor section during the mine pattern simulation. The y distance error plot shown in the second graph reveals that the bridge conveyor is not in error by more than 0.15 m (0.5 ft.) at any time during the cut. The mining machine cuts a 5.49 m (18.0 ft.) room. The bridge conveyor is 3.35 m (11.0 ft.) wide providing 1.07 m (3.5 ft.) clearance on either side. This trajectory path provides adequate navigation control for this cut. A slight discontinuity is observed as the trajectory path input equation changes from the straight line to a polynomial curve and back to the sloped straight line path. This discontinuity does not present a problem for the NCS.

Figure 9 shows angle output results from the mine pattern simulation. The first graph shows the global steering angle and the input trajectory path angle. The steering angle follows the trajectory path angle very well. The second graph shows the local angle between bridge sections two and three. This angle reaches a maximum of 46 degrees on this pass as bridge two approaches the chevron room heading and bridge three turns right past the panel conveyor tail pulley. The trajectory path sets up a

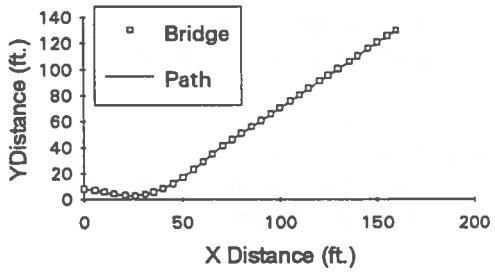

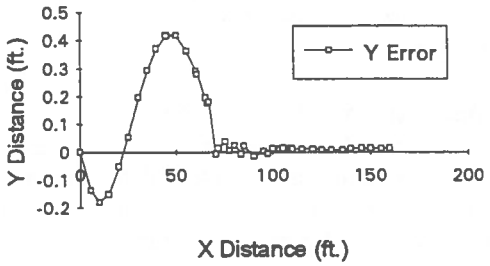

i) Bridge Conveyor and Trajectory Paths ii) Y Position Error

Figure 8: Position Output Results for Mine Pattern Cut; Second Bridge.

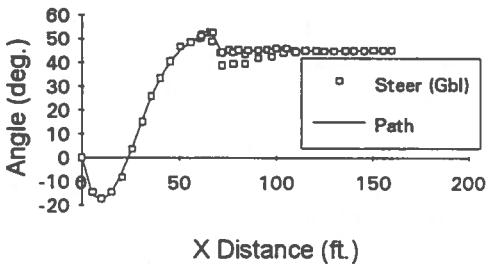

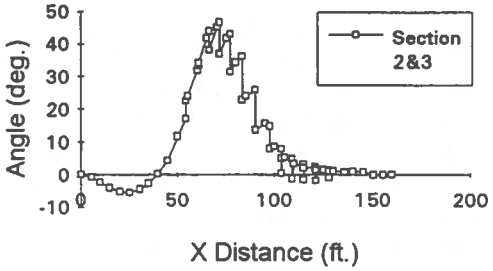

i) Steering and Trajectory Path Angles ii) Angle Between Sections 2 and 3

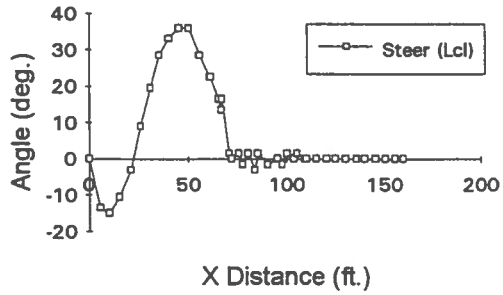

iii) Local Steering Angle

Figure 9: Angle Output Results for Mine Pattern Cut; Second Bridge.

wide sweeping turn which reduces the maximum local steering angle as shown in the third graph. The local steering angle reaches a maximum left hand turn of 34 degrees and a right hand turn angle of 16 degrees.

CONCLUSIONS

The development of a navigational control system for a multi-section bridge conveyor was analysed in this paper. This system was designed for use with a five-section APM Mineveyor but has the potential to be retro-fit to other existing bridge conveyor equipment. This could greatly reduce the capital investment for automation of a continuous haulage system.

The navigational control system (NCS) was developed with two main modules or tasks for steering and tramming control. This system has the potential to automatically control the navigation functions of the bridge conveyor. By automatically controlling the bridge conveyor, the operator could move to a more safe and comfortable environment. Further savings could be realised by reducing input and maintenance costs by allowing more continuous mining operations as well as controlling the bridge conveyor at a consistent level below maximum limits.

The NCS revealed a good response to a bridge conveyor position offset for a straight line trajectory path. An offset distance up to 0.91 m (3.0 ft.) was corrected to within 5 percent in less than 3.05 m (10.0 ft.) of forward motion. Also, the steering controller was observed to turn quickly toward the desired path followed by a counter steer to align the bridge conveyor with the proper heading. The NCS also showed good response to a step change in the input trajectory path. A step change of up to 10 degrees did not produce a distance error greater than 0.04 m (0.13 ft.). The NCS maintained proper bridge conveyor positioning in the mined rooms throughout the chevron pattern cutting sequence.

ACKNOWLEDGEMENTS

The authors would like to thank Raoul Gauthier and Mo Molavi of the Potash Corporation of Saskatchewan's Allan Division Mine, Allan, SK, for their co-operation and support of this project. Also, acknowledgement is given to NSERC for some financial assistance.

REFERENCES

GAUTHIER, R., MOLAVI, M., and TOTH, L. of the PCS Allan Division Mine, WILSON, J.N. of the Division of Control Engineering, University of Saskatchewan, and REYNOLDS, A.K. of the Department of Mechanical Engineering, University of Saskatchewan, 1992

The information, obtained in various forms, during a meeting at the PCS Allan Division Mine on September 16, 1992 with the above people is referred to in this paper as Gauthier et al.

KLASSEN, N.D., 1986.

M.Sc. Thesis, "Automatic Advance Rate Control System for a Potash Mining Machine", University of Saskatchewan, Saskatoon, SK.

PEARS, N.E. and BUMBY, J.R., 1991.

"The Steering Control of an Experimental Autonomous Vehicle", Transactions of the Institute of Measurement and Control, Vol. 13 No. 4, p.190-200.

REYNOLDS, A.K., 1995.

M.Sc. Thesis, "Automatic Navigation Controller for a Five-Section Potash Bridge Conveyor", University of Saskatchewan, Saskatoon, SK.

SANDERS, M.S. and PEAY, J.M., 1988.

Human Factors in Mining, No. 9182, Information Circular (IC), US Bureau of Mines.

CAMI'95: 3rd Canadian Conference on Computer Applications in the Mineral Industry
Montréal, Québec, Canada, October 22-25, 1995

Development of a Database and Graphic Aided Software System for Planning and Analysis of Mining Equipment

Dipl.-Ing. Thomas Schumacher and Dr.-Ing. Rainer Hünefeld
IBH, Aachen University of Technology, Germany

ABSTRACT:

In the field of mining engineering, design and planning are complex tasks, which require the knowledge of various engineering disciplines.
GRUBE (Graphisch-RechnerUnterstützter BergwerksEntwurf) is a modular databased program system, which offers computer aid for all mining departments using a 3D CAD software as user interface. Despite the data quantity and complexity, specific and uniform working conditions have to be applied to the planning of technical equipment of a pit. With the application of 3D graphics, complex data stores and their interrelations become 'palpable' for the user by suitable visualization
GRUBE-M forms the mechanical operations module of GRUBE, in which underground locations displayed as three dimensional graphic models are "equipped" interactively. Planning alternatives can be created and compared quickly in terms of technical calculations and economical analysis.

INTRODUCTION

Over the last 30 years German hardcoal production has decreased from 150 Mio. t in 1957 to 70 Mio. t in 1990, caused by a surplus on worlds energy market. Because of the high costs of the technical equipment necessary for excavating hardcoal seams of 1-2.5 m thickness at a depth of 800-1000m, coal from the world market can be imported for comparatively low prices.
Despite many economic disadvantages, local hardcoal is an important factor in the security of energy supply in Germany. Therefore, national hardcoal companies have increased their productivity, measureable by a higher performance per manshift. In 1957 the average production was 1.6 t coal per man and shift, which increased to 5.2 t in 1992, caused by higher mechanisation and automation of underground equipment.
RUHRKOHLE AG is the biggest German hardcoal company, running 15 underground hardcoal mines in the Rhein-Ruhr area, the industrial centre of Germany. The main mining method is longwall mining using shearer loader or ploughs. Each mine has its own planning offices for all mining disciplines, but all of them are controlled and supported by one head administration and a management board. Therefore, mining equipment is partly owned by the mine itself, but most of it is rented from the central equipment management, part of RUHRKOHLE AG head administration.

THE OVERALL COMPUTER CONCEPT OF RUHRKOHLE AG

Todays productivity in underground working areas cannot be increased essentially by more technical

solutions but by a more effective and qualified planning and control at the surface, leading to improved operating cycles. Various investigations and studies concluded that the integration of graphical data processing is a very promising software tool for achieving this aim.
RUHRKOHLE's concept of computer integration is structured in five layers (Fig. 1).

The first three layers concentrate on information of the actual underground operations in a mine e.g. monitoring and analysis of underground activities and conditions such as the running time of excavation machines, ventilation data received by sensors, or level control of underground coal bunkers.

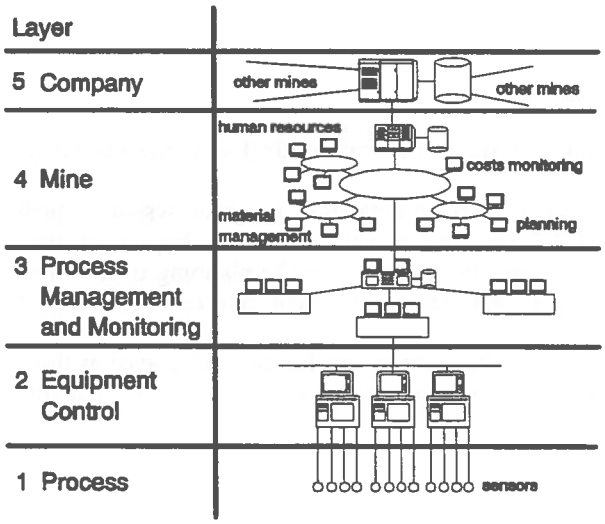

Figure 1: Five Layer Model of RUHRKOHLE AG

Monitoring, control and planning of a whole mine in terms of technical and economical aspects such as equipment planning, human resources, or material management are integrated in layer 4. Layer 5 consists of central computers for company tasks, analysis and overall management.

THE PLANNING AND CONTROLLING OFFICE OF THE FUTURE

This paper concentrates on one part of layer 4, which can be characterised as "Mine Planning".
For this part, RUHRKOHLE AG over recent years has been establishing the integration concept "The Planning and Controlling Office of the Future" (Fig. 2), which uses networked computer workstations and modular planning software.

The five main departments involved with mine planning are surveying, ventilation, operation planning, equipment planning, and electrical engineering. These are connected by a local network (Token Ring) and are equipped with one of the following computer workstations (IBM RISC System 6000):

MAP:	The mine surveying workstation
WTAP:	The mine ventilation workstation
BPAP:	The mine operation planning workstation
MTAP:	The mine equipment planning workstation
ETAP:	The mine electrical engineering workstation

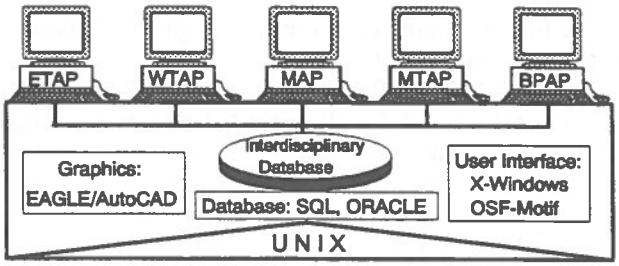

Figure 2: Planning and Controlling Office of the Future

The basic software implemented on these workstations are the IBM UNIX based operation system AIX and AIX window manager, the graphical editor EAGLE from XEAGLE Ltd. and AutoCAD from AutoDesk and the SQL database management system ORACLE from Oracle. Graphical user interfaces are implemented using the OSF/Motif toolkit.
The five workstations are connected to an interdisciplinary database implemented on a server, enabling all departments to read in data required for planning or to write data important for other departments. This database forms the foundation for most planning activities, because it contains all geometrical data concerning mine roadway systems and deposits.

The objectives of the "Planning and Contolling Office of the Future" are:

- overall improvement of planning efficiency and quality

- preparation of data required for planning activities
- rapid creation and analysis of planning alternatives
- a more detailed and precise planning
- improved visualisation of planning results through graphics
- decision making based on qualified and quantified data

THE PLANNING AND INFORMATION SYSTEM GRUBE

A part of the software used on the computer workstations is a database and graphic aided planning and information system called GRUBE, developed by Aachen University of Technology and RUHRKOHLE AG. This software is divided into submodules according to the structure of the computer workstations.

The main components of GRUBE are:

GRUBE-Perspe:	Software for surveying
GRUBE-W:	Software for ventilation
GRUBE-B:	Software for mine operation planning (time and quantity)
GRUBE-M:	Software for equipment (machine) planning
GRUBE-E:	Software for electrical engineering
GRUBE-Draft:	Software for documentation (maps, etc.) for all departments

GRUBE uses the same software mentioned before with the exception of AutoCAD, which is used on the surverying workstation only. The EAGLE graphic software enables the creation, visualisation and adaptation of three dimensional objects such as models of the underground roadway system (Fig. 3) based on the geometrical data obtained from the interdisciplinary database. Furthermore, those and other objects, like machine models, can be connected with logical attributes such as identification codes and any other data. The information generated during planning or calculation are partly transferred either to one of the department specific databases or to the interdisciplinary database.

Over recent years, certain submodules of GRUBE, in particular the ventilation module, have been successfully implemented in mines workstations.

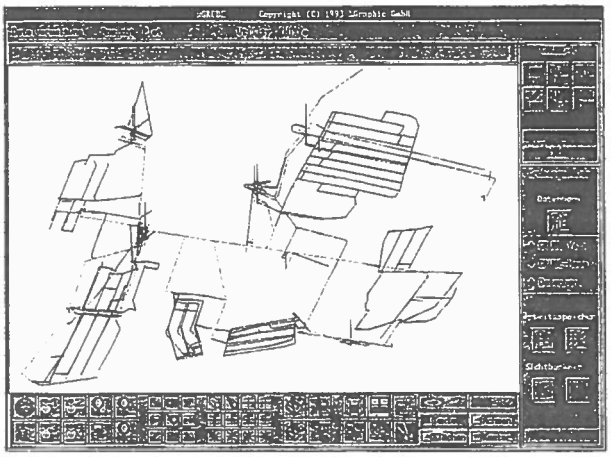

Figure 3: 3D GRUBE model of a roadway system

GRUBE-M: A SYSTEM FOR UNDERGROUND MINING EQUIPMENT

GRUBE-M forms the mining equipment planning and information module.

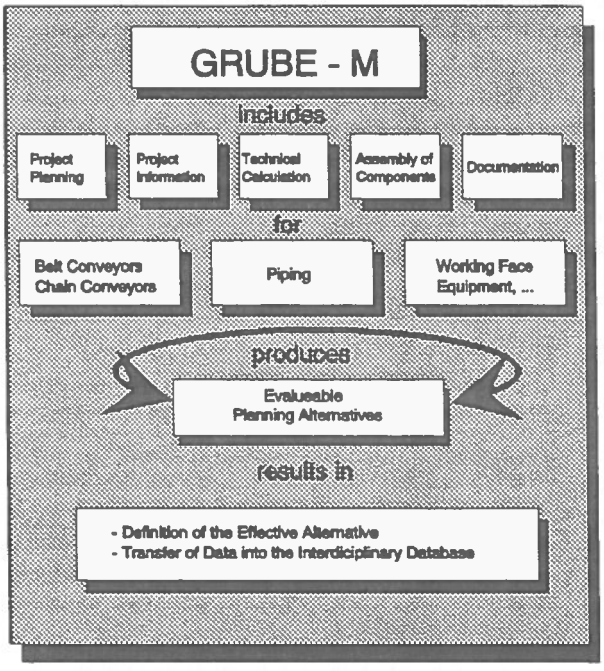

Figure 4: Overview of GRUBE-M

Starting with a defined project, which requires the employment of machines and equipment, GRUBE-M enables the user to establish and analyse planning alternatives.
The data obtained from the planning activity can be transferred to the material management department for order and delivery

Regarding functionality GRUBE-M is structured in five main submodules (Fig. 4):

- Project Planning
- Project Information
- Technical Calculation
- Assembly of Components
- Documentation

A module for generation and visualisation of mines layout is also included and forms the basis for most planning activities.
At the present, GRUBE-M concentrates on the following subjects:

- Belt Conveyors
- Chain Conveyors
- Distribution Pipes
- Working Face Equipment

As mentioned before, the strategy of GRUBE is planning based upon interdisciplinary data.

PROJECT PLANNING:
A project is roughly defined by a location, a time and the kind of activity planned by the mine. Almost every activity of an underground mine project requires the application of equipment. In this aspect, equipment means machines of higher value, e.g. belt conveyors, chain conveyors, shearer loaders, ploughs, road headers, drilling carriages, etc. Low cost equipment such as bearings, individual props or drill bits is not taken into account, because its influence on planning is considered negligible.
Before starting project planning the three dimensional model of the mines actual roadway system is loaded using the survey data. New roads and working areas can be planned also by the equipment engineer and saved "locally" in the GRUBE-M database but not back in the "global" interdisciplinary database. This means, only the surveying office is authorized to add or change binding geometrical data. Each other discipline may change or add underground roads for the creation of department specific and internal planning alternatives.

However, within the submodule "project planning", drifts and working areas related to the project are equipped using geometrical data from the model for design and technical calculation, for example while planning a belt conveyor.
The first step of planning a belt conveyor in GRUBE-M is the definition of drives and return ends position by mouseclick on the graphic model. An algorithm follows the drift line creating a conveyor belt model and returns geometrical information such as length, dipping, height of lift, downfold and upfold areas (Fig. 5), etc.. Based on this information, the position of belt feeders and supporting TT-drives may be defined as well as man riding distances. The conveyor is identified by a location id obtained from the roadway model and a number given by the planning engineer. Together, these two numbers form an unique identifyer for the conveyor, which is used in other functions.

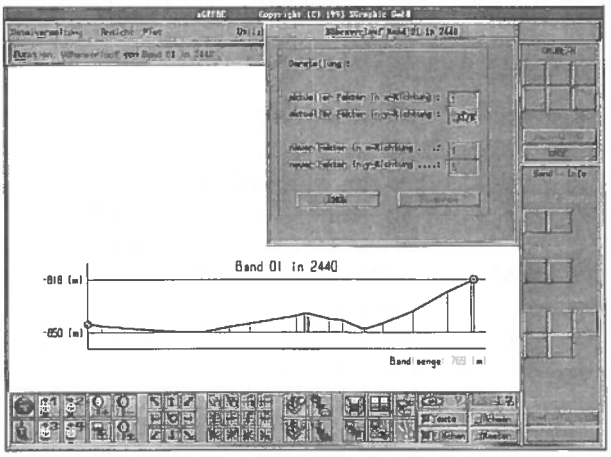

Figure 5: Contour line of a belt conveyor

The result of this planning activity is a table, describing belt conveyor segments, which forms the foundation for later technical calculation of performance and driven traction.

PROJECT INFORMATION:
Effective equipment planning and operation activities require fast and easy access to a variety of data sources such as databases, files, drawings, maps, documents, etc.. Therefore, within this submodule information can be added to or interrogated from various data sources depending on the planning subject. A high quantity of information can be linked to a conveyor model using, for example data panels as graphical user interface for

GRUBE-M database communication. Data can then be visualised in the graphic on request (Fig. 6).
Furthermore, detailed technical 2D-CAD drawings as well as standard specification sheets and various documents related to the project can be visualised on the screen and used as an additional information source.

Overviews and analysis of underground equipment forms additional support for the engineer. GRUBE-M offers answers to several kinds of questions related to machine engineering, which can be displayed either graphically or in tabular form.

TECHNICAL CALCULATION:
Technical Calculation forms one of the bases of equipment engineering. During the planning period several calculations based on operational requirements and space related situations are necessary for design and dimension of the equipment to be installed. A useful planning result requires detailed consideration of technical alternatives.

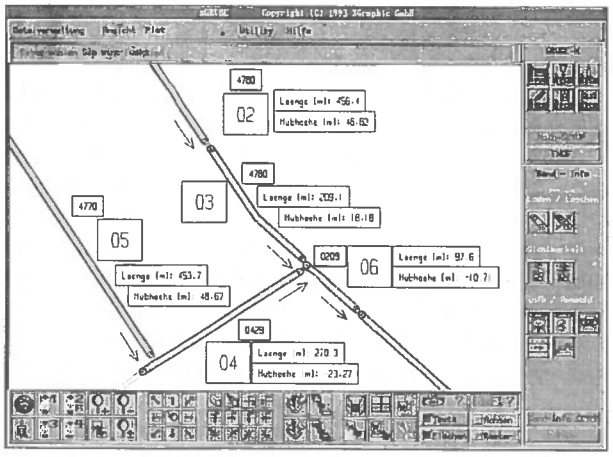

Figure 6: Graphical model of a belt conveyor system in GRUBE-M

The calculation of various technical alternatives within GRUBE-M is fast and uncomplicated, as all geometrical data are transferred automatically from the 3D model into the calculation submodule. For example, just after positioning an additional TT-drive with a certain performance on the graphic conveyor model, the calculation programm provides the engineer with actual results.
Similar calculations based on a 3D roadway model that provide real geometrical data are very useful in the area of machine anchorage and piping.

ASSEMBLY OF MACHINE COMPONENTS:
After equipment planning by means of technical considerations, the organisation and disposition of single components is a subsequent duty of the engineer. Each part required for building an installation has to be described by its technical attributes and identified for order at the central equipment management. Because of the wide variety of available equipment, describing a single component for clear and unambiguous identification can be difficult. Especially in cases of a machine breakdown during operation, the ordering of spare parts has to be carried out rapidly. This occasionally leads to the wrong part being ordered leading to extended and more expensive machine downtimes. In order to avoid losses in production, detailed information management and an easy access to data deserting equipment components forms the basis for more efficient planning and operation.
RUHRKOHLE AG maintains the database systems BIS-K and DABIB, which contain the data necessary for equipment management.
The BIS-K database contains on the one hand classification of equipment component groups and on the other hand tables containing specific technical characteristics of each group, providing a clear technical description of each component, and a unique component identification number for order.
DABIB contains economical data such as costs for renting and maintanance for each component identification number available at RUHRKOHLE AG.
By combining the data of both these (BIS-K and DABIB) systems into the planning and information system GRUBE-M, the mining engineer is able to analyse installations in terms of economy.
During planning, the technical description of all the single components of for example a belt conveyor results in a list of component identification numbers from BIS-K representing the key for cost data in DABIB. Together with the quantity of each component this information is associated with a single installation. All useful technical alternatives can be compared in economical terms to support further decisions.
During operation, a list of all single components of a conveyor belt can be generated within seconds, thus enabling fast ordering of the required spare part in case of machine breakdowns.

DOCUMENTATION:
The documentation submodule contains functionality for the creation, visualisation and output of machine application lists, graphical equipment maps, circuit diagrams, technical drawings, etc.
For example, information from the 3D project planning can be transferred to a 2D map of the roadway system

and presented with symbols. Lines, text, etc. can be added by a graphic editor, which contains further symbols for conveyors, excavation equipment, piping, etc. (Fig. 7).

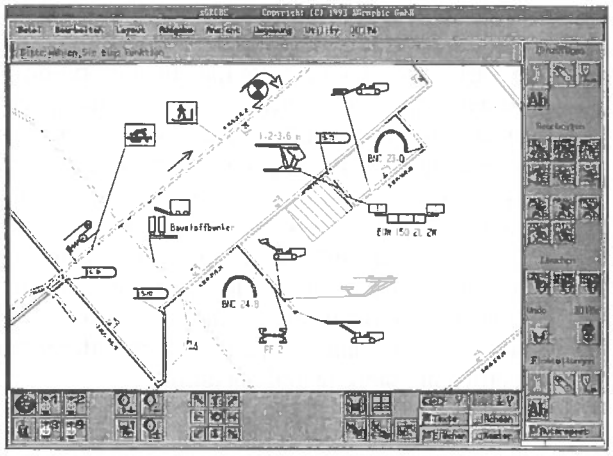

Figure 7: Equipment application map in GRUBE-Draft

GRUBE-M IN INTERDISCIPLINARY PLANNING

As mentioned before, GRUBE-M is a part of an interdisciplinary planning system. This means GRUBE-M reads in data from other disciplines important for equipment planning and transfers planning results useful for other departments into the interdisciplinary database.

Elementary information for equipment planning are:

- geological data: seam thickness, strength of coal and features of surrounding rock, etc.
- geometrical data: dipping of roads and deposit, length of drifts and roadway cross section, etc.
- mine planning data: project describtion, time limits, aimed production, mining method, etc.
- ventilation data: temperature, gas content, air cooling, etc.

Information transferred into the interdisciplinary database are:

- technical data: power requirements, generation of heat, etc.
- economical data: costs, manpower requirements, etc.

SUMMARY

Todays productivity in underground working areas cannot be increased essentially by more technical solutions but by a more effective and qualified planning and control at the surface, leading to improved operating cycles.
Various investigations and studies concluded that the integration of graphical data processing is a very promising software tool for achieving this aim.
RUHRKOHLE AG over recent years has been establishing the integration concept "The Planning and Controlling Office of the Future" for mine planning, which uses networked computer workstations and modular planning software.
The five main departments involved with mine planning are surveying, ventilation, operation planning, equipment planning, and electrical engineering. These are connected by a local network (Token Ring) and are equipped with computer workstations.
A part of the software used on the computer workstations is a database and graphic aided planning and information system called GRUBE, developed by Aachen University of Technology and RUHRKOHLE AG. This software is divided into submodules according to the structure of the computer workstations.
GRUBE-M forms the mining equipment planning and information module. Starting with a defined project, which requires the employment of machines and equipment, GRUBE-M enables the user to establish and analyse planning alternatives. The data obtained from the planning activity can be transferred to the material management department for order and delivery.
GRUBE-M is a part of an interdisciplinary planning system, i.e. GRUBE-M reads in data from other disciplines important for equipment planning and transfers planning results useful for other departments into the interdisciplinary database.

REFERENCES

1. SEELIGER, A.; KOPYCZYNSKI, F. and RUSCHITZKA, C.; 1994
Rechnerunterstütztes Planungs- und Informationssystem GRUBE-W. Glückauf 130, No.7, pg. 444-450.
2. SEELIGER, A. and KOPYCZYNSKI, F.; 1993
Computer-based ventilation planning in German coalmines. APCOM XXIV Proceedings, Vol.3, pg. 335-342, Montreal.

3. HEIERMANN, H.; 1994
Von der Mechanisierung zur Automatisierung - Bergtechnik bei der RUHRKOHLE AG, Vol. 17, Essen.

4. BRODERIUS, T.; FRIEDEHEIM, K. and HÜNEFELD R.; 1993
GRUBE-MS - Das markscheiderische Modul des Bergbauplanungssystems GRUBE. Das Markscheidewesen 100, No.2, pg. 394-400.

An Integrated Software Simulator for the Analysis of Mining Shovels

H.Wu, L. Daneshmend†, C. Hendricks and M. Scoble

Canadian Centre for Automation & Robotics in Mining,
Department of Mining and Metallurgical Engineering,
McGill University, Montréal, Québec

† now Chair in Mine-Mechanical Engineering,
Department of Mining Engineering,
Queen's University, Kingston, Ontario

ABSTRACT:

This paper addresses the software design and implementation issues relating to a comprehensive simulator which has been developed for electric mining shovels. The software involved in simulating shovel dynamics and kinematics, actuator responses, and muckpile interaction, is discussed. Issues relating to the simulation of such complex, and nonlinear, elements, are reviewed. Results from the simulator are presented and compared with actual shovel data.

1. INTRODUCTION

Electric mining shovel plays a key role in many surface mining operations. They are used as production machines in conjunction with drill and blast operations, or to move waste rock. The rate and efficiency with which these pieces of equipment operate in loading haul trucks largely determines the efficiency of the overall mining operation. Hence, most surface mining operations tend to evaluate their productivity based on the performance of their primary loading equipment. There exists considerable scope for productivity enhancement in surface mine extraction through the optimized use and operation of current excavation equipment.

A software simulator for electric mining shovels is of interest for three main uses:

1. Mine production planning and simulation.
2. Machine design.
3. Operator training.

It is apparent that the required fidelity and complexity of simulation increases as we proceed down this list. Conversely, a simulator developed for a more demanding purpose, e.g. for machine design, could provide significantly better simulation results in terms of accurately reflecting constraints on productivity.

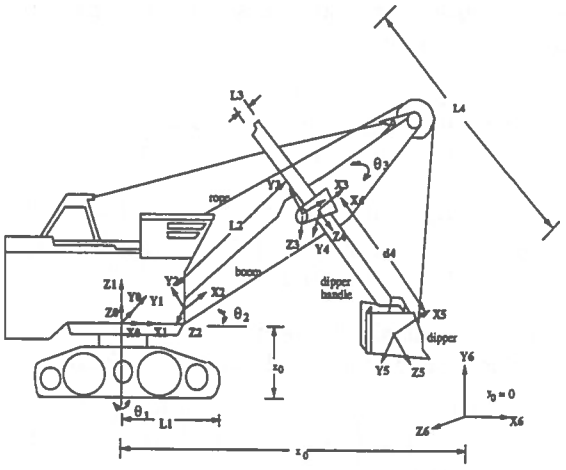

Figure 1: Electric Shovel

An electric shovel is illustrated in Figure 1. The machine consists of two major sub-systems: mechanical and electrical, corresponding to the structure and motors.

$$x_{22} = \frac{\sqrt{2}}{2}s_1((d_4(c_3 - s_3) + L_3(c_3 + s_3)) \quad (10)$$

$$x_{23} = \frac{\sqrt{2}}{2}c_1(c_3 + s_3) \quad (11)$$

$$x_{31} = 0 \quad (12)$$

$$x_{32} = \frac{\sqrt{2}}{2}((c_3 + s_3)d_4 + (s_3 - c_3)L_3) \quad (13)$$

$$x_{33} = -\frac{\sqrt{2}}{2}(c_3 - s_3) \quad (14)$$

The variables are the components of the Jacobian. The relationship between the shovel's linear velocity and angular velocity is:

$${}^0V_5 = \begin{pmatrix} x_{11} & x_{12} & x_{13} \\ x_{21} & x_{22} & x_{23} \\ x_{31} & x_{32} & x_{33} \end{pmatrix} \begin{pmatrix} \dot{\theta}_1 \\ \dot{\theta}_3 \\ \dot{d}_4 \end{pmatrix} \quad (15)$$

3.3 Rigid Body Dynamics of Shovel

The motion of the shovel arises from torques generated by the actuators and from external forces. The Newton-Euler formulation can be applied in this case. Considering that each link has symmetry (although there are some non-symmetric elements, they are negligible), one can choose the principal axes of inertia; therefore,

$${}^{c_1}I_1 = \begin{pmatrix} I_{xx1} & 0 & 0 \\ 0 & I_{yy1} & 0 \\ 0 & 0 & I_{zz1} \end{pmatrix}, {}^{c_2}I_2 = \begin{pmatrix} I_{xx2} & 0 & 0 \\ 0 & I_{yy2} & 0 \\ 0 & 0 & I_{zz2} \end{pmatrix} \quad (16)$$

$${}^{c_3}I_3 = \begin{pmatrix} I_{xx3} & 0 & 0 \\ 0 & I_{yy3} & 0 \\ 0 & 0 & I_{zz3} \end{pmatrix}, {}^{c_4}I_4 = \begin{pmatrix} I_{xx4} & 0 & 0 \\ 0 & I_{yy4} & 0 \\ 0 & 0 & I_{zz4} \end{pmatrix} \quad (17)$$

By the analysis of the bucket, one can consider the effects of the force and moment as follows:

$$f_5 = \begin{pmatrix} f_{51} \\ f_{52} \\ f_{53} \end{pmatrix} = \begin{pmatrix} f_{51} \\ 0 \\ f_{53} \end{pmatrix}, \; n_5 = \begin{pmatrix} n_{51} \\ n_{52} \\ n_{53} \end{pmatrix} = \begin{pmatrix} 0 \\ 0 \\ 0 \end{pmatrix} \quad (18)$$

After complex calculation, considering that the motion of the link 4 is prismatic and the link 2 is fixed, one obtains:

$$\begin{aligned} T_{d4} &= f_{43} + b_4\dot{d}_4 \\ T_{d3} &= n_{33} + b_3\dot{\theta}_3 \\ T_{d2} &= 0 \\ T_{d1} &= n_{13} + b_1\dot{\theta}_1 \end{aligned} \quad (19)$$

Where f_{43}, n_{33}, and n_{31} all have complex representations. Due to space limitation, these are neglected from here.

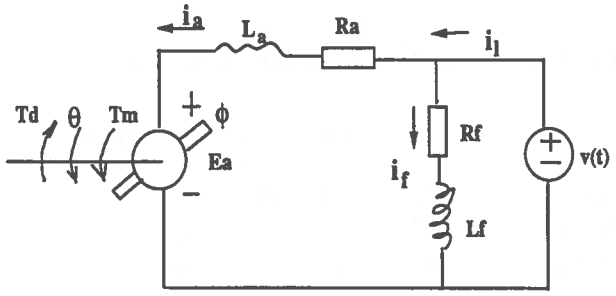

Figure 2: Circuit Diagram for DC Shunt Motor

3.4 Actuator Dynamics

The swing, hoist, and crowd motors are all DC shunt motors. The circuit diagram for a DC shunt motor is shown in Figure 2.

The equation for the armature current is:

$$v - E_a = L_a\frac{di_a}{dt} + R_a i_a \quad (20)$$

The torque balancing equation is

$$T_m = I_m\dot{\omega} + b\omega + T_d \quad (21)$$

Since the flux ϕ is constant, the torque developed by the motor is:

$$T_m = k_m\phi i_a = k_1 i_a \quad (22)$$

where k_1 is the torque constant. The back emf relation is:

$$E_a = k_b\phi\omega = k_2\omega = k_2\frac{d\theta}{dt} \quad (23)$$

where k_2 is the back emf constant.

When use a gearbox, with gearbox ratio r, set the sum of the actuator and gearbox inertias as follows:

$$I_m = I_a + I_g \quad (24)$$

Taking $\tau_1 = \frac{L_a}{R_a}$, $\tau_2 = \frac{I_m}{b}$, $x_1 = \theta$, $x_2 = \omega$, $x_3 = i_a$, and arranging the formulae, from (20) to (24), one has the DC motor's state space representation:

$$\dot{x_1} = x_2 \quad (25)$$

$$\dot{x_2} = -\frac{1}{\tau_2}x_2 + \frac{k_1}{b\tau_2}x_3 - \frac{r}{b\ tau_2}T_d \quad (26)$$

$$\dot{x_3} = -\frac{k_2}{R_a\tau_1}x_2 - \frac{1}{\tau_1}x_3 + \frac{1}{R_a\tau_1}v \quad (27)$$

The DC shunt motor system diagram is shown in Figure 3.

2. METHODOLOGY

Previous papers by the authors have concentrated upon the modelling process, which utilized both analytical and empirical techniques to formulate the shovel models (Wu et al. 1994). The simulator development was based upon these models, and the modelling and simulation processes were heavily inter-dependent: the attributes of the models defining the simulation requirements, and the results of intermediate simulation runs prompting refinement of the models.

Since the shovel may be viewed as a powered kinematic mechanism which interacts with the surrounding environment (the rock), various standard simulation techniques from the field of robotic manipulation were applicable. Hence the next section first deals with kinematics, structural dynamics, and actuator dynamics.

However, various aspects of the shovel's interaction with the muck-pile are quite unique, e.g. impacts and intermittent frictional contacts, and the simulation requirements for these were very demanding. The these are dealt with in section 4. In the simulation phase, both analytical and empirical model simulators are being set up and used to simulate and validate the electric shovel operation.

3. SIMULATION OF FREE SHOVEL MOTION

Analytical modelling describes fully the electric mining shovel itself and the external environment with which it interacts. This modelling consists of Forward Kinematics, Jacobian, Rigid Body Dynamics, Actuator/Transmission dynamics, Friction, and Impact.

3.1 Forward Kinematics of Shovel

The forward kinematics of shovel need to be derived in order to solve the trajectory generation problem of the machine. Given the joint angle vector $[\theta_1, \theta_2, \theta_3, d_4]$, find the position and orientation of the end effector of the shovel in the work location coordinate system, which is with respect to a reference coordinate system. In Figure ??, if one considers the base of the machine fixed when the shovel is digging, the frame $\{0\}$ is the world coordinate frame; frames $\{1\}$, $\{2\}$, $\{3\}$, $\{4\}$, and $\{5\}$ are fixed on the shovel machine and the frame $\{6\}$ is fixed on the location where the shovel is working. In terms of the Denavit-Hartenberg notation, and using the formula [1],

$$ {}^{i-1}_{i}T = \begin{pmatrix} c\theta_i & -s\theta_i & 0 & a_{i-1} \\ s\theta_i c\alpha_{i-1} & c\theta_i c\alpha_{i-1} & -s\alpha_{i-1} & -s\alpha_{i-1}d_i \\ s\theta_i s\alpha_{i-1} & c\theta_i s\alpha_{i-1} & c\alpha_{i-1} & c\alpha_{i-1}d_i \\ 0 & 0 & 0 & 1 \end{pmatrix} \quad (1) $$

One can obtain the bucket position with respect to the coordinate $\{6\}$ as follows:

$$ \begin{aligned} x_6 &= \frac{\sqrt{2}}{2}c_1(d_4(s_3+c_3)+L_3(c_3-s_3)) \\ &+ c_1(\frac{\sqrt{2}}{2}L_2+L_1)-x_0 \quad (2) \\ y_6 &= -\frac{\sqrt{2}}{2}(d_4(s_3-c_3)+L_3(c_3+s_3)) \\ &- \frac{\sqrt{2}}{2}L_2+z_0 \quad (3) \\ z_6 &= \frac{\sqrt{2}}{2}s_1(d_4(s_3+c_3)+L_3(c_3-s_3)) \\ &+ s_1(\frac{\sqrt{2}}{2}L_2+L_1)-y_0 \quad (4) \end{aligned} $$

3.2 Shovel Jacobian

In order to analyze the motion of a manipulator, the "Jacobian" concept is commonly utilized. The Jacobian describes the relation between the linear and angular velocity of rigid body. It is also the basis for the formulation of the shovel's dynamics which will be described in the next section. Furthermore, when one calculates the impact, one will use the shovel Jacobian.

The Jacobian is a multidimensional form of the derivative. In shovel case, it is a three dimensional matrix:

$$ {}^{0}\mathbf{J}(\theta) = \begin{pmatrix} x_{11} & x_{12} & x_{13} \\ x_{21} & x_{22} & x_{23} \\ x_{31} & x_{32} & x_{33} \end{pmatrix} \quad (5) $$

Where,

$$ \begin{aligned} x_{11} &= s_1((L_1+\frac{\sqrt{2}}{2}L_2)-\frac{\sqrt{2}}{2}L_3(s_3-c_3)) \quad (6) \\ x_{12} &= \frac{\sqrt{2}}{2}c_1((c_3-s_3)d_4+(c_3+s_3)L_3) \quad (7) \\ x_{13} &= \frac{\sqrt{2}}{2}s_1(c_3+s_3) \quad (8) \\ x_{21} &= s_1((L_1+\frac{\sqrt{2}}{2}L_2)-\frac{\sqrt{2}}{2}L_3(s_3-c_3)) \quad (9) \end{aligned} $$

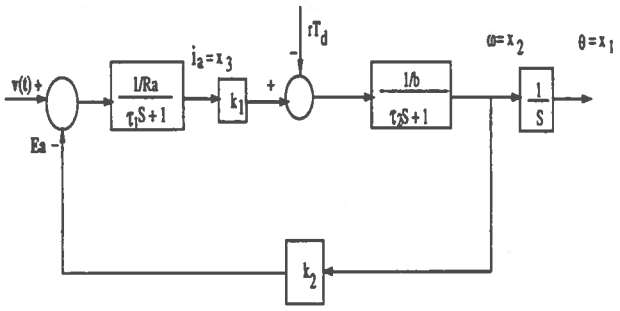

Figure 3: DC Shunt Motor System

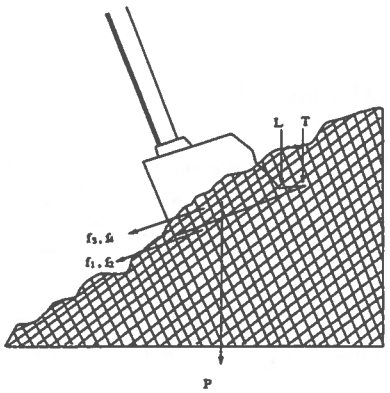

Figure 4: Forces Acting on Shovel

4. SIMULATION OF INTERACTION WITH THE MUCKPILE

The interaction between the bucket and the muckpile gives rise to forces. These forces arise either due to friction or impact.

4.1 Friction between Bucket and Muckpile

When the shovel is digging in the muckpile, a digging interaction between the bucket and the rock exists and affects the overall machine motion and performance. This interaction is an important issue which must be addressed by any model of the shovel's operation. The interaction actually includes two aspects, friction and impact. This interaction has not been studied extensively by any previous researchers. Rowlands (1991) however has studied the friction of dragline buckets, and we can obtain some insight from his work. But his work did not include impact. In addition, his friction model only represented some specific cases. We have developed these models into a general representation.

When the bucket digs in the muckpile, the torque acting on the shovel is zero; the forces acting on the shovel are shown in Figure 4. The physical significance of these notations are as follows:

P — payload weight

T — tooth friction force

L — lip friction force

f — friction forces; this includes surface friction of outer bucket bottom(f_1); surface friction of inner bucket bottom(f_2); surface friction of two outer bucket sides(f_3); surface friction of two inner bucket sides(f_4).

The surface friction of the outer and inner bottom of the bucket(f_1) and (f_2)can be expressed by:

$$f_1 = (M_b + \frac{M_p}{D}\sqrt{\Delta x_6^2 + \Delta y_6^2 + \Delta z_6^2})g\mu\cos\varphi \quad (28)$$

$$f_2 = \frac{M_p}{D_1}\sqrt{\Delta x_6^2 + \Delta y_6^2 + \Delta z_6^2}g\mu\cos\varphi \quad (29)$$

Where M_b is bucket mass; M_p is final payload; D is maximum digging distance; $\sqrt{\Delta x_6^2 + \Delta y_6^2 + \Delta z_6^2}$ is actual digging distance in work location coordinate $\{6\}$. ($\Delta x_6 = x_{61} - x_{60}$, $\Delta y_6 = y_{61} - y_{60}$, $\Delta z_6 = z_{61} - z_{60}$), $(x_{61}y_{61}z_{61})$ is destination of bucket digging; $(x_{60}y_{60}z_{60})$ is start of bucket digging; φ is digging angle; μ is coefficient of friction. D_1 is the bucket length.

The surface friction of the outer and inner bucket sides, (f_3) and (f_4), can be described by using Taylor's theory. Taylor (1948) indicated that according to Coulomb's theory of failure, the passive thrust per unit length along a stiff retaining wall can be calculated as follows:

$$P_p = \frac{\gamma H^2 K_p}{2} \quad (30)$$

where, P_p is lateral thrust per length of wall(N/m), γ is unit weight of the fill material(N/m), H is depth of material(m), K_p is passive pressure coefficient. Therefore, the surface friction of the outer and inner bucket sides, f_3 and f_4 are:

$$f_3 = \frac{\gamma n k_p}{2}(\frac{H_{fa}}{D})^2(\Delta x_6^2 + \Delta y_6^2 + \Delta z_6^2)\mu \quad (31)$$

$$f_4 = \frac{\gamma n k_p}{2}(\frac{H_{fa}}{D_1})^2(\Delta x_6^2 + \Delta y_6^2 + \Delta z_6^2)\mu \quad (32)$$

where, H_{fa} is average material height in bucket.

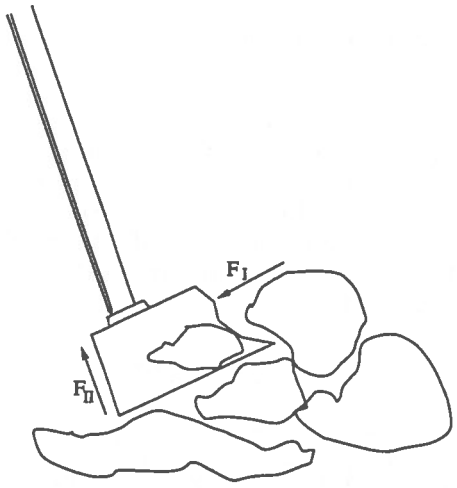

Figure 5: Impacts Acting on Shovel Machine

The friction across the teeth and lips of the bucket is a very complex problem. A model based on soil/blade cohesion and adhesion by Hettiaratchi and Reech was proposed as follows:

$$R = \gamma \chi^2 w K_r \tag{33}$$

where, R is resistive force on blade(N), γ is material unit weight (N/m^3), χ is blade tip depth, w is blade width, K_r is a factor due to gravity (derived from nomograms). Thus, can obtain the teeth force:

$$T = n_1 \gamma w_T k_r (\frac{H_{fa}}{D})^2 (\Delta x_6^2 + \Delta y_6^2 + \Delta z_6^2)\mu \tag{34}$$

$$L = n_1 \gamma w_L k_r (\frac{H_{fa}}{D})^2 (\Delta x_6^2 + \Delta y_6^2 + \Delta z_6^2)\mu \tag{35}$$

4.2 Impact between Bucket and Muckpile

During the digging process, the shovel often meets with large fragments which enter and interact with the bucket in a manner different from smaller fragments: they produce impact on the bucket and the whole machine. The impacts acting on the shovel are shown in Figure 5.

In terms of Hertz's colliding compression and deformation rule, the maximum impact is:

$$F_{max} = K_2 (\frac{5V_1^2}{4K_1K_2})^{3/5} \approx \eta V_1 \tag{36}$$

where $\eta = K_2(\frac{5}{4K_1K_2})^{3/5}$.

From the shovel Jacobian, we can get the impact along the x_5 and z_5 directions, i.e.,

$$F_I = (x_{11}\dot{\theta_1} + x_{12}\dot{\theta_3} + x_{13}\dot{d_4})\eta \tag{37}$$

$$F_{II} = (x_{31}\dot{\theta_1} + x_{32}\dot{\theta_3} + x_{33}\dot{d_4})\eta \tag{38}$$

Thus, the total force acting on the bucket is:

$$\mathbf{F} = \mathbf{F}_{x5} + \mathbf{F}_{z5} \tag{39}$$

$$\mathbf{F}_{x5} = \mathbf{f}_1 + \mathbf{f}_2 + \mathbf{f}_3 + \mathbf{f}_4 + \mathbf{T} + \mathbf{L} + \mathbf{f}_{px5} + \mathbf{F}_I \tag{40}$$

$$\mathbf{F}_{z5} = \mathbf{f}_{pz5} + \mathbf{F}_{II} \tag{41}$$

5. SIMULATOR STRUCTURE AND IMPLEMENTATION

Dynamic Modelling

The system dynamics includes the actuator dynamics and rigid body dynamics. In terms of the division of the three major actuators, one can obtain the crowd, hoist, and swing motor dynamics, respectively.

Bringing in equation (25), (26), and (27), as well as considering the three different parts of shovel, one can obtain the matrix representation as follows:

$$\frac{d}{dt}\begin{pmatrix} x_1 \\ x_2 \\ x_3 \\ x_4 \\ x_5 \\ x_6 \\ x_7 \\ x_8 \\ x_9 \end{pmatrix} = \begin{pmatrix} A_1 & 0 & 0 \\ 0 & A_2 & 0 \\ 0 & 0 & A_3 \end{pmatrix} \begin{pmatrix} x_1 \\ x_2 \\ x_3 \\ x_4 \\ x_5 \\ x_6 \\ x_7 \\ x_8 \\ x_9 \end{pmatrix}$$

$$+ \begin{pmatrix} 0 & 0 & 0 \\ 0 & 0 & 0 \\ \frac{1}{R_{a1}\tau_1} & 0 & 0 \\ 0 & 0 & 0 \\ 0 & 0 & 0 \\ 0 & \frac{1}{R_{a2}\tau_3} & 0 \\ 0 & 0 & 0 \\ 0 & 0 & 0 \\ 0 & 0 & \frac{1}{R_{a3}\tau_5} \end{pmatrix} \begin{pmatrix} v_1 \\ v_2 \\ v_3 \end{pmatrix}$$

$$- \begin{pmatrix} 0 & 0 & 0 \\ \frac{r_1}{b_1\tau_2} & 0 & 0 \\ 0 & 0 & 0 \\ 0 & 0 & 0 \\ 0 & \frac{r_2}{b_2\tau_4} & 0 \\ 0 & 0 & 0 \\ 0 & 0 & 0 \\ 0 & 0 & \frac{r_3}{b_3\tau_6} \\ 0 & 0 & 0 \end{pmatrix} \begin{pmatrix} T_{d1} \\ T_{d2} \\ T_{d3} \end{pmatrix} \tag{42}$$

Where,

$$A_1 = \begin{pmatrix} 0 & 1 & 0 \\ 0 & -\frac{1}{\tau_2} & \frac{k_1}{b_1\tau_2} \\ 0 & -\frac{k_2}{R_{a1}\tau_1} & -\frac{1}{\tau_1} \end{pmatrix}$$

$$A_2 = \begin{pmatrix} 0 & 1 & 0 \\ 0 & -\frac{1}{\tau_4} & \frac{k_3}{b_2\tau_4} \\ 0 & -\frac{k_4}{R_{a2}\tau_3} & -\frac{1}{\tau_3} \end{pmatrix}$$

$$A_3 = \begin{pmatrix} 0 & 1 & 0 \\ 0 & -\frac{1}{\tau_6} & \frac{k_5}{b_3\tau_6} \\ 0 & -\frac{k_6}{R_{a3}\tau_5} & -\frac{1}{\tau_5} \end{pmatrix}$$

The gearbox rates, r_1, r_2, and r_3 are brought into the system simulation. This is reflected in the position and velocity outputs, as well as the disturbance inputs.

Continuous-Time Controller and Saturation

The continuous-time controllers are analog control circuits which control the crowd, hoist, and swing motor's rotational velocities. For simulation purposes, one can construct the controllers in terms of the electrical and mechanical parameters of the three motors. In addition, to enhance disturbance rejection, feedforward controllers are also used.

Due to the motor's internal characteristics and constraints, the input current and generated torque cannot superpass certain values. Therefore, a saturation function must be implemented for both the motor current and torque.

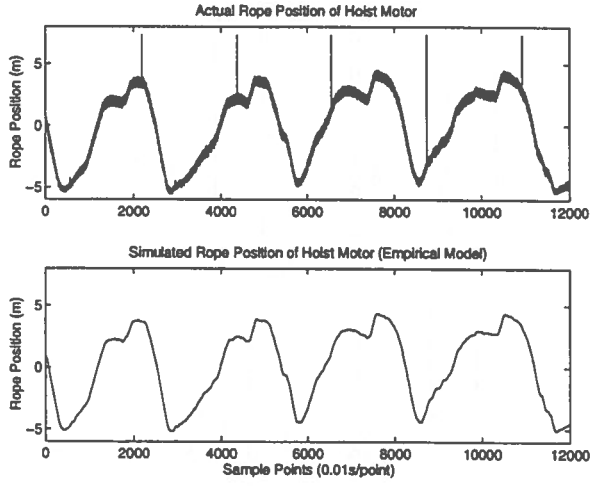

Figure 6: Actual and Simulated Rope Positions of Hoist Motor (Easy Digging)

Disturbance Simulation

The disturbances to the actuators come mainly from two parts: the shovel machine's rigid body cross-coupling and the interaction between the bucket and the muckpile during the course of digging and loading. To represent the first part, we can use formula (19). The second part is already included in T_{d1}, T_{d2}, and T_{d3}, identified as f_{51} and f_{53}, in formula (18).

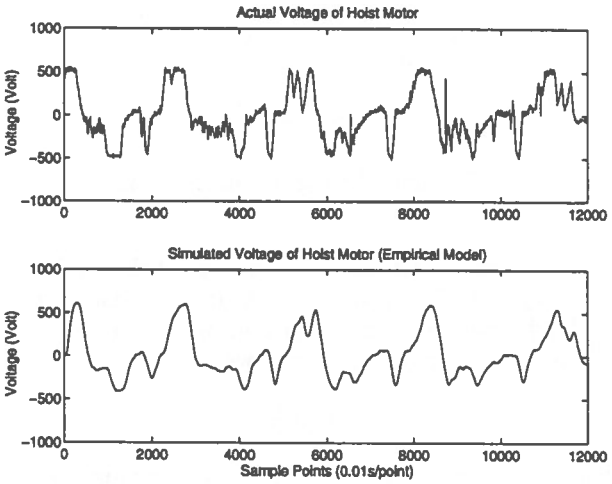

Figure 7: Actual and Simulated Voltages of Hoist Motor (Easy Digging)

6. EVALUATION OF RESULTS

The previously described shovel models were implemented and integrated using an off-the-shelf simulation software package, is *Simulink*, from the Mathworks Inc. *Simulink* is a nonlinear simulation module which runs within *Matlab*, which is also a Mathworks Inc. product. Fourth-order Runge-Kutta numerical integration algorithms were selected as providing sufficient numerical stability and accuracy while still yielding reasonable short simulaton run-times. The overall simulator software structure, in block diagram form, is shown in Figure 9.

Figure 6, Figure 7, and Figure 8 show the rope positions, voltages, and currents of hoist motor. From these figures, we can see the actual and simulated curves of trajectories and voltages have very similar shapes.The basic shapes of the currents are also roughly similar - but there is some discrepancy.

The deterioration in match between the simulator and actual shovel data is explainable in terms of the increasing frequency content as we proceed from

trajectories to voltages to currents. The experimental motor current data has much higher frequency content, and is hence much more difficult to match through discrete time simulation of the type used. However, since trajectory data is of primary interest for mine planning purposes, this is not of concern in the current work.

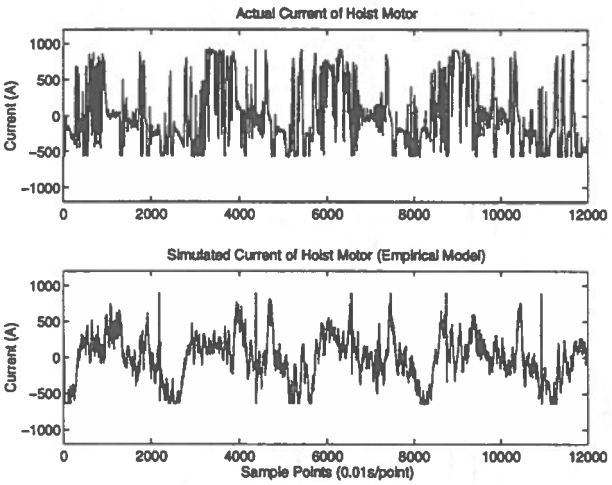

Figure 8: Actual and Simulated Currents of Hoist Motor (Easy Digging)

7. CONCLUSION

This work has demonstrated the viability of applying advanced software simulation techniques to complex mining equipment. With the continuing trend towards cheaper and more powerful computing resources, such simulation software could be be of direct benefit in various aspects of mine planning as well as operator assessment and training.

8. ACKNOWLEDGEMENTS

This work has been partially supported by the Natural Sciences and Engineering Research Council of Canada (NSERC), under s Strategic Grant.

References

[1] Craig, John J., *Introduction To Robotics Mechanics and Control*, Second Edition, Addison-Wesley Publishing Company, 1989.

[2] Guru, Bhag S., Hiziroglu, Huseyin R., *Electric Machinery and Transformers*, Horcourt Brace Javanovich, Inc., 1988.

[3] Hendricks, Carl F.B., *Performance Monitoring of Electric Mining Shovel*, unpublished Ph.D. thesis, McGill University, 1990.

[4] Hettiaratchi, D.R.P., and Reech, A.R., *The Calculation of Passive Soil Resistance*, Géotechnique 24, No.3, pp.289-310, 1974.

[5] Hollerbach, John M., *A Recursive Largrangian Formulation of Manipulator Dynamics and s Comparative Study of Dynamics Formulation Complexity*, IEEE Transaction on System, Man, and Cybernetics, Vol.SMC-10, No.11, Nov.1980.

[6] Izaguirre, A.,Hashimoto,M.,Paul,R.,Hayward,V., *A New Computational Structure for Real-Time Dynamics*, The International Journal of Robotics Research, pp.346-361,Aug.1992.

[7] Kane, Thomas R., Levinson, David A., *Dynamics: Theory and Applications*, McGraw-Hill Book Company, 1985.

[8] Ljung L. *System Identification: Theory for the User*, Prentice-Hall,Inc.,1987.

[9] P & H Inc., *Electrotorque Drive and Harnischfeger Mining Shovel Motors – Products of Harnischfeger, Research and Development.*

[10] Reece, A.R., *A Rational Approach to the Design of Earth-Moving Machines*, Journal of Terramechanics, Vol.21, No.1, pp.69-79, 1984.

[11] Rowlands, Jeffery C., *Dragline Bucket Filling*, unpublished Ph.D. thesis, University of Queensland, 1991.

[12] Spong, Mark W., Vidyasagar, M., *Robot Dynamics and Control*, John Wiley and Sons, 1988.

[13] The Math Works Inc., *Simulink Manual*, The Math Works, Inc., 1992.

[14] Wu, H., Daneshmend, L., Hendricks, C., and Scoble, M., *Systems Analysis and Modelling of an Electric Mining Shovel*, Proceedings of the 6th Canadian Symposium on Mining Automation, October 16-19 1994, Montréal, pp.163-170.

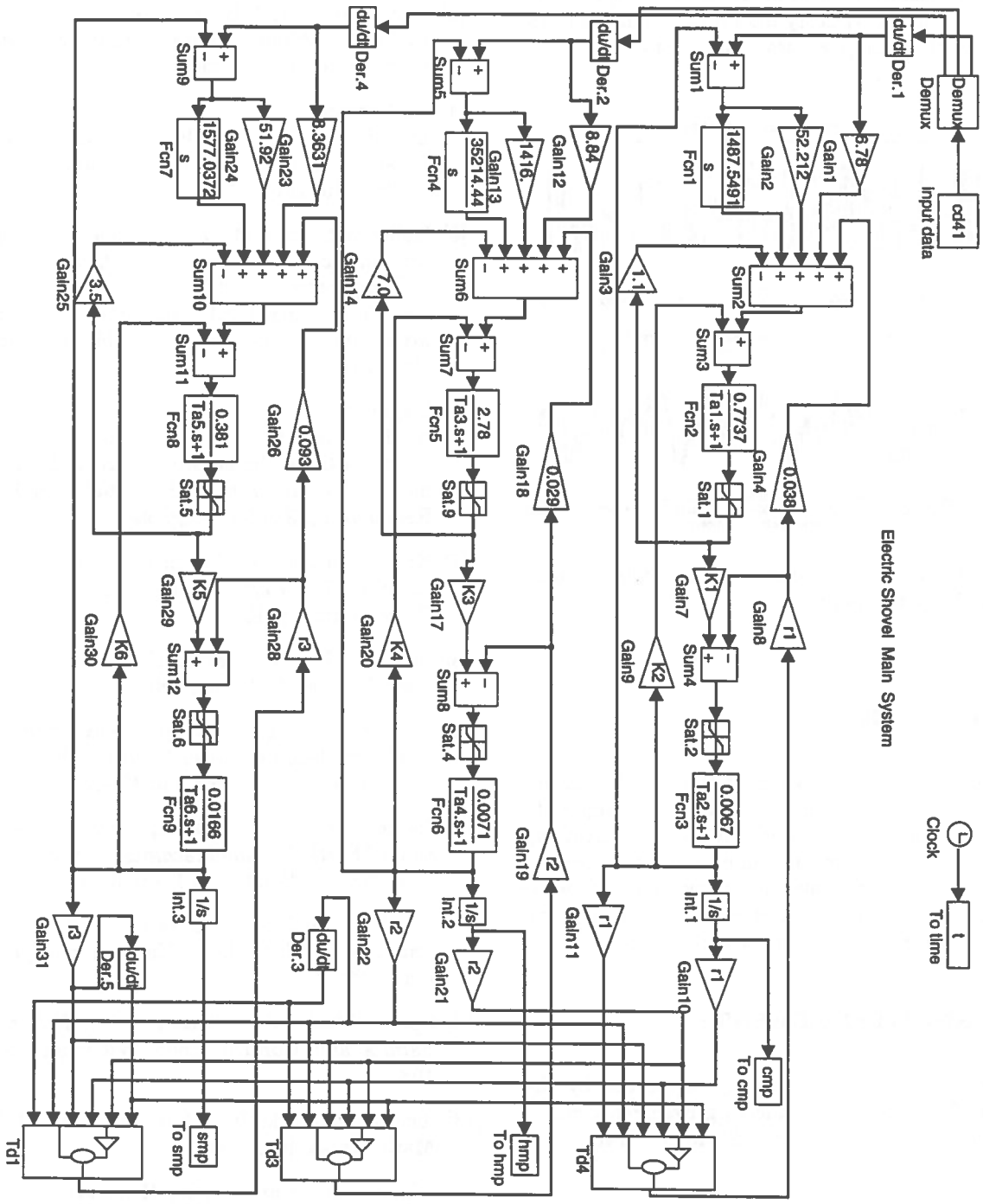

Figure 9: Electric Shovel Main System

CAMI'95: 3rd Canadian Conference on Computer Applications in the Mineral Industry
Montréal, Québec, Canada, October 22-25, 1995

A PC-Based Monitoring System for Mine Hoisting

Michael J. Beus
Spokane Research Center, U.S. Bureau of Mines, Spokane, Washington USA

Frank T. Duda, Jr.
Pittsburgh Research Center, U.S. Bureau of Mines, Pittsburgh, Pennsylvania USA

Timothy J. Orr
Spokane Research Center, U.S. Bureau of Mines, Spokane, Washington USA

ABSTRACT

The technology to enhance safety and control features for mine shaft hoists is being investigated by researchers at the U.S. Bureau of Mines (USBM). The objective of the research is to prevent injuries and fatalities related to hoist and elevator operations. Monitoring and controlling mine hoisting operations will allow hoist operators, inspectors, and maintenance personnel to increase their awareness of potentially dangerous situations and provide controls for safer operations. Process simulation and visualization software, real-time data sensing, and advanced programming techniques are being applied to this problem. Development of reliable and cost-effective sensors and data acquisition interfaces to monitor hoist loads and detect slack rope conditions is underway. Three-dimensional design software was used to visualize mine hoisting to enhance understanding of hoist operations. Quick Basic and Visual Basic (an object-oriented Windows interface) are being used for acquiring and processing hoisting data. Testing and evaluation of components are underway at USBM testing facilities. The resulting system will allow hoist personnel to assess critical operating parameters, such as hoist position, speed, acceleration, conveyance load, and rope tension.

RÉSUMÉ

La technologie, pour réhausser la sûreté et traits controllés des hissages de puits dans les mines, est sous recherche par les ingénieurs du Bureau des Mines aux États-Unis. L'objectif des recherches est de prévenir les altérations de santé et dégâts mortels au rapport des hissages et élévateurs en mines. Les observations et le controllement des activitées de hissage en mine permettra les ouvriers, inspecteurs et le personnel de maintien, d'augmenter leur perception en situations potentielles et dangereuses, et fournir des mesures de control pour des travaux de meilleure sûreté. Un procédé simulateur et programme de visualisation, sensorisation de données en temps-actuel et techniques avancées de programmatique sur ordinateur sont appliqués ă ce problem. Le développement des censeurs exacts et coût-éffectifs est entrepris, ainsi que l'interface d'acquisition de données, pour observer l'éffet du chargement des hissages et de détecter l'état du câble en détente, pendant l'abaissement. Un programme de dessin proportionné trois-dimensionel a été utilisé pour etablir une réalisation visuelle de hissage en mines et pour réaliser la compréhension des hissages eux-même. Quick Basic et Visual Basic (an object oriented Windows Interface sur ordinateur) sont utilisés pour acquir les données sur hissages. La tenue des épreuves et les évaluations des éléments constitutifs sont commencées dans les établissements d'évaluation des U.S. Bureau des Mines. Le résultat permettra le personnel du hissage d'imposer les paramètres des procédures délicates; tel sont l'état du huissage, la vitesse, l'accélération, le transport et la tension du câble.

INTRODUCTION

Mine shafts are the "lifeline" of underground mining operations. A shaft (figure 1) provides access to the network of openings used to recover the underground resource and serves as an escapeway in case of emergency. As such, a shaft must be well designed and maintained for a long and reliable service life. Hoist and elevator systems for underground metal/nonmetal mines and coal mines must meet the requirements specified in the Code of Federal Regulations (CFR), Parts 57 and 75. The Mine Safety and Health Administration (MSHA) has been reluctant to require new safeguards for elevators and hoists without fully developed technology. However, in many cases, the mining industry and hoist equipment manufacturing companies cannot justify research and development expenditures.

Researchers at the U.S. Bureau of Mines (USBM) are conducting research to develop a PC-based monitoring, inspection, and control system that will increase awareness of proper functioning of mine hoists, warn of potentially dangerous situations, and provide controls for safer operations. According to MSHA data, many of the shaft-related accidents in the United States are associated with the hoisting cycle and maintenance operations (figure 2). For example, about 10% of all injuries in U.S. metal/nonmetal mines in the period between 1985 and 1992 were related to hoisting. Of these, almost all (>90%) were related to errors by operating (i.e., hoistman or cagetender) and maintenance personnel, as opposed to injuries caused by faulty or poorly maintained equipment.

From MSHA accident reports, personnel located in areas related to muck and material loading and unloading were particularly susceptible to injury or death. A relatively common occurrence was water inundation or muck hangup in the loading pocket or ore pass. Several fatalities have occurred recently in the United States and Canada from the sudden inrush of water and muck, washing loading-pocket operators into the shaft (MSHA, 1989). Another problem occurs when spillage or equipment falls to the shaft bottom, often severely damaging shaft hardware and requiring expensive downtime and hazardous repair work. Downtime for inspection, maintenance, and repair also significantly decreases the time available for muck hoisting.

In the past 10 years, several documented mine hoist and elevator accidents (Dames and Moore, 1977) have

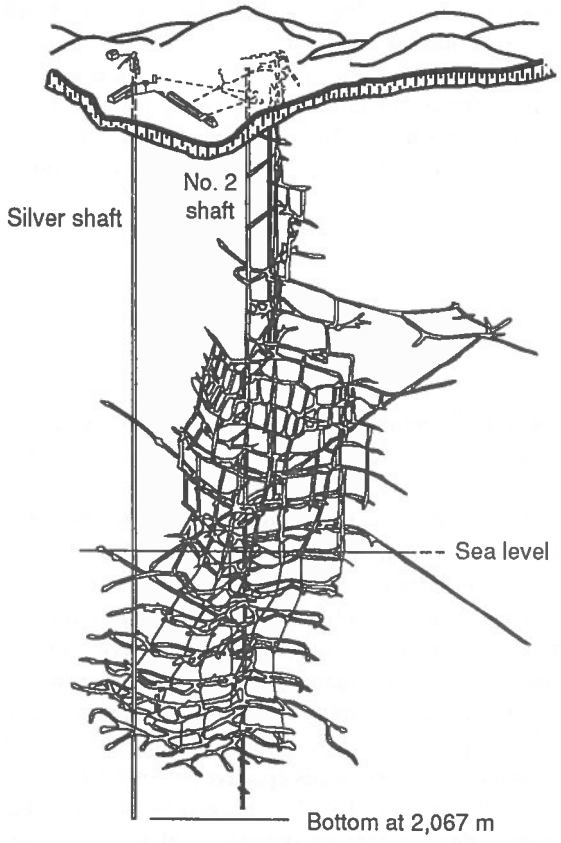

Figure 1. Typical shaft layout in deep metal mine.

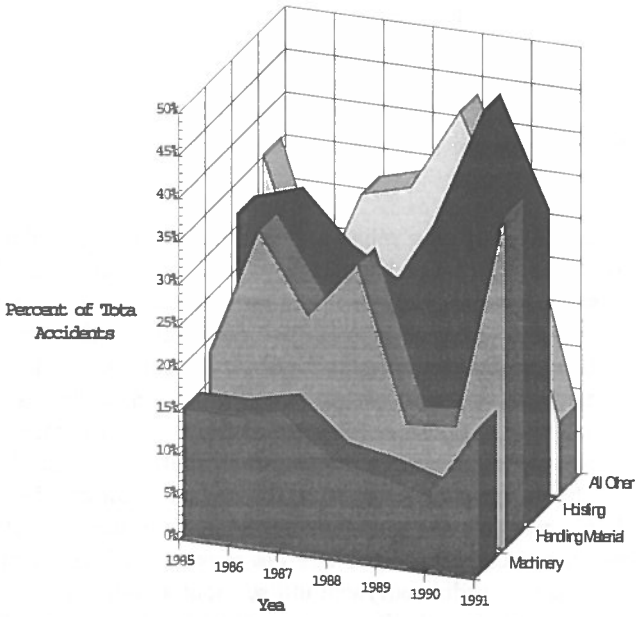

Figure 2. Shaft-related accidents in metal and nonmetal mines in the United States—1988-92.

also resulted from electrical, mechanical, and structural failures, despite MSHA requirements for periodic testing of hoist systems. All these accidents had the potential for injuring or killing miners, as did the accident at the Markham Colliery in the United Kingdom on July 30, 1973. With advances in computer technology, including process visualization, real-time data acquisition, sensors, and microcomputers, safer, more cost-effective inspection, monitoring, and control systems are possible. This paper will present some applications of computer methods and sensor development approaches to the mine hoist monitoring and inspection problem.

APPROACH

This research is being conducted at the Pittsburgh and Spokane Research Centers, in cooperation with the MSHA Technical Support Group in Pittsburgh. Components of various mine hoisting and elevator systems were assessed, including hoisting machinery, such as hoistroom controls, motors and gearboxes, and winders, and shaft infrastructure, such as support frameworks, guides, wire ropes, and skips and cages. Current technology was assessed to determine what conditions and equipment should be monitored, availability of adequate sensors, and how to process and act on the information.

Specific research tasks were defined as follows:

- Evaluate the complete shaft hoisting and materials handling process and facilities, including stations, loading pockets, and safety and control features.
- Develop a working computer model to simulate the hoisting process and delineate potential safety problems and targets for condition sensing.
- Assess currently available sensors and monitoring and process-control technology for hoisting personnel and materials in mines.
- Identify parameters to be monitored and modify or develop new sensors and data acquisition capabilities.
- Develop laboratory test facilities to conduct proof-of-concept testing.
- Develop software with hoisting process and subprocess graphics screens and collect, save, and evaluate sensor data.
- Conduct field evaluations and transfer technology to industry and MSHA.

TECHNOLOGY ASSESSMENT

Shaft hoisting technology, safety features, and standards have been assessed. Such work includes an evaluation of all safety features for hoists and elevators, existing safety standards for both hoists and elevators as well as current hoist and elevator monitoring systems and sensors (Farley et al., 1983; Barkland and Helfrich, 1988; Loynes, 1976; Cseff et al., 1981). Most monitoring and control systems have been developed and introduced in Canadian, British, and South African mines. However, indications are that cost-effective hoist monitoring systems are not widely used in the United States, particularly for smaller operations and for use with older hoisting equipment. Existing commercially available systems range in price from $50,000 to $250,000 and are largely customized to be site specific. Major cost items are sensors, data acquisition, and associated monitoring and control software.

It was concluded that research to improve sensor technology and increase information flow on operational status of the hoisting function is important. More cost-effective methods and software for automated inspection operations and sensors for determining conveyance loads, slack and tight rope, and conveyance position must be developed.

Software kits for developing personal-computer- (PC-) based data acquisition systems for enhancement and customization of current software were evaluated. State-of-the-art, factory-floor process control technology for monitoring and controlling schemes for mine hoisting operations were evaluated.

Figure 3 shows an example of a control screen layout of a deep-mine hoisting process using currently available technology. This screen incorporates cage or skip position, speed, and acceleration using various layouts of in-shaft processes. Figure 4 shows how the loading pocket may be set up and simulated, again using off-the-shelf software. However, it was deter-

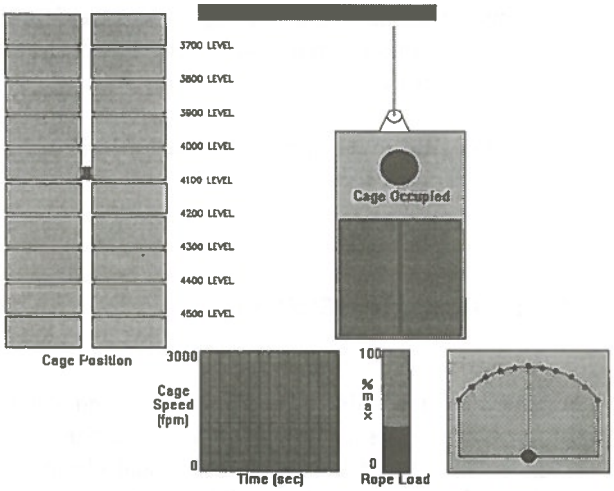

Figure 3. Control screen layout of deep mine hoisting process.

mined that existing software packages were still either too comprehensive or too expensive to be compatible with the requirements of the project. It was decided to develop in-house a public-domain data acquisition and process control software package customized for hoisting. Windows-based software appeared to offer the greatest potential for reducing cost and enhancing the user-friendly aspects of the interface between an operator and a PC screen. Powerful and comprehensive Windows-based data acquisition and process control software and hardware tools are available.

Sensor development has focused on determining conveyance position and load. Various sensors for monitoring skip or cage position and hoist velocity and acceleration have been evaluated. For example, onboard ultrasonic and a radar-based speed and distance detectors developed for the agricultural industry has been evaluated for determining the position of a skip in a shaft. A position sensor located on the conveyance eliminates the need to correct the position of the conveyance because of rope stretch. However, preliminary results indicate that these devices are not sensitive enough for accurate positioning, and the response time is insufficient for proper control.

Shaft conveyance load is identified as the other key element for enhancing hoist safety. Conveyance load monitoring in real time will detect slack or tight rope conditions resulting from shaft obstructions, rock movement, and misalignment. In addition, it will serve as a production monitor and warn of ore hangup in the skip or loading pocket. Current approaches favor inline load cells in the load path of the convey-

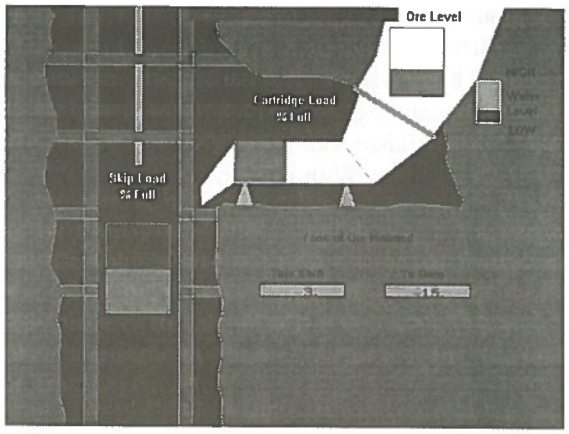

Figure 4. Simulation of loading packet with off-the-shelf software.

ance or load cells in the sheave wheel pillow blocks at the headframe. Both of these approaches have major disadvantages. Inline load cells may compromise the integrity of a wire rope, and they are costly and difficult to install, requiring a significant modification to the conveyance termination point. Pillow-block load cells weigh the total downshaft load, including the wire rope and acceleration loads. This makes determination of the net weight of the conveyance, and therefore overload conditions, difficult to determine, particularly in deep shafts where the weight of the wire rope becomes a significant part of the total load. This situation requires a very high-capacity load cell, the use of which would reduce sensitivity so that small but significant changes in the conveyance load could not be determined.

HOIST TEST FACILITIES

It was determined early on in the project that testing of new technology would be difficult to undertake in operating hoist installations. For this reason, a deep mine hoisting test facility was constructed at Spokane and a three-level elevator test facility was modified for research at the Pittsburgh Research Center. These test facilities are being used to evaluate position and load-indicator sensors, data acquisition systems, and software. The test facility in Spokane utilizes a 60-ft hoist tower to simulate the headframe and shaft, an 18-ft-deep "shaft" lined with concrete sections, a winding drum, sheave wheel assembly, and shaft skip conveyance (figure 5). A loading-unloading circuit to investigate skip loading and unloading operations has

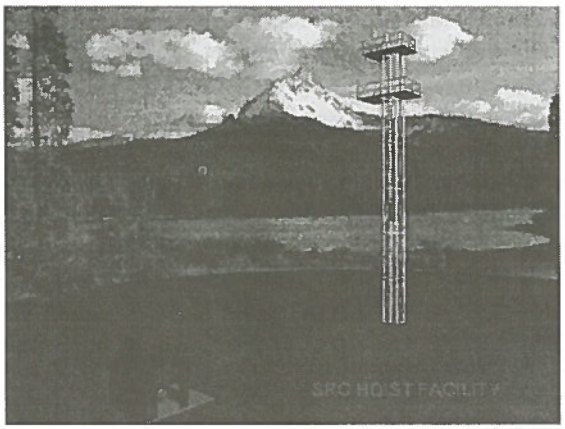

Figure 5. Hoist test facility at Spokane Research Center.

also been fabricated. A loading cartridge is equipped with balancing load cells to monitor the net weight of material in the cartridge prior to its discharge into the skip. Output from these cells and loading gate position sensors will control skip loading functions. A similar approach is used for skip discharge at the top of the headframe.

The hoist room components include a winding drum and gearbox, a motor-gearbox interface, a braking system, and a 50-hp dc motor. A digital motor controller allows sophisticated control of the dc motor through an interface to a PC. A ideal motor-velocity profile can be input using numerous parameters; the profile can be modified via feedback from sensors on the motor, such as an optical encoder, a digital tachometer, or armature current. The system is being further modified with a Simplex model Lilly hoist controller to back up the digital control system and duplicate hoisting installations currently in use.

The testing approach is aided by development of conceptual layouts in which all the features of a proposed monitoring and testing system and preliminary concepts for key sensor technology are delineated. A computer simulation of the Spokane shaft test facility was developed to allow researchers to visualize the hoisting process. This permitted delineation of target areas that might be of special concern and that would require additional sensors. An animated simulation of the test tower allowed various scenarios to be considered. The analysis also allowed computer evaluations of key structural components of the test frame and skip. Different skip and guide materials may be analyzed and the computed results correlated with the results of actual testing. For example, a more flexible guide rail alignment wheel may allow the skip to pass through tight spots with less resistance, a major cause of tight rope conditions. The computer visualization and simulation model of the test frame continues to be updated and is being used to simulate operation of the actual test hoist as features are added.

CURRENT PROGRESS

Sensors

A new approach to conveyance load sensing incorporates a design that is independent of the conveyance load path, and therefore does not compromise the integrity and safety of the wire rope. This concept is called a "flexcable" load cell. The device imbeds a slight curvature in the rope at the sensing point and is totally independent of the load-carrying function of the wire rope. A typical full bridge circuit measures bending strains on the conforming cell body as the rope is tensioned, providing the required output as pounds of tension at the conveyance termination.

Pillow-block load cells at the sheave wheel are used to verify loads from the flexcable load cell at the conveyance. Figure 6 shows a layout of the labor-

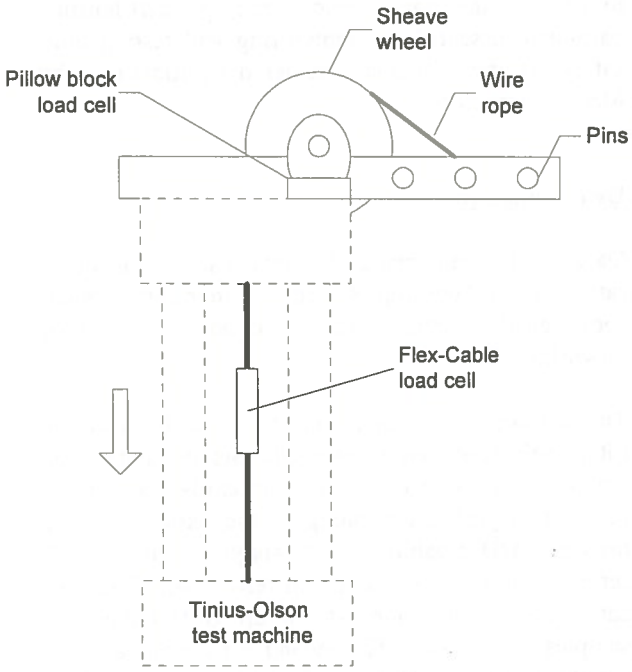

Figure 6. Layout of laboratory test setup to evaluate load cells.

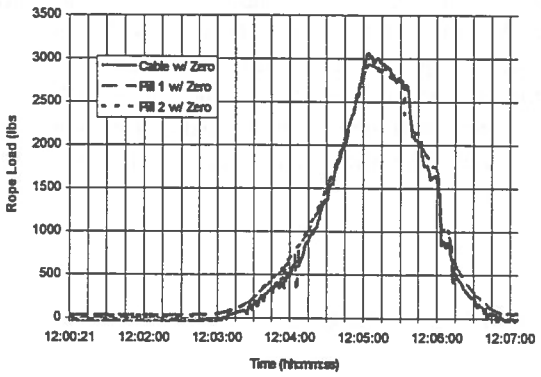

Figure 7. Comparison of results of pillow-block and flexcable load cell.

atory test setup. Results of this work show an excellent correlation between the pillow-block load cells and the flexcable cell. Figure 7 shows the results of the comparison using a laboratory test setup.

The design for conveyance position favors the use of an optical encoder mounted on a conveyance guide wheel. In addition, an encoder mounted on the winding drum and hoist motor monitors shaft revolutions and provides backup data for determining the same operating parameters. These devices provide sufficient data to establish conveyance position, and thereby velocity, and acceleration. These data are needed to develop the hoist speed curve, a shaft-hoisting parameter essential for monitoring and testing hoist safety features. This is considered a critical need by MSHA inspectors.

Data Acquisition

Data acquisition consists of a hybrid scheme incorporating both a "desktop' system for monitoring hoistroom functions coupled with an "onboard" system for downshaft monitoring.

The desktop data acquisition system utilized at the Pittsburgh Research Center consists of a 486 PC equipped with two ISA expansion cards and the appropriate signal conditioning. One expansion card provides A/D capability for 16 single-ended or 8 differential analog inputs at 12-bit resolution. The card can sustain a sampling rate of up to 100 thousand samples per second. The second expansion card is a counter-timer card that has five 16-bit counters that can be configured for frequency measurements and event count accumulations. Both cards have multiple digital I/O port capabilities. A eight-channel commercially available signal conditioner is used to make the sensor signal readable by the A/D board as well as to provide electrical protection.

At this time, the data acquisition system is being used to monitor dc hoist motor voltages and currents as well as signals from speed- and position-measuring sensors on the elevator. The sensors are hard wired into the signal conditioners. This system will be validated against the current monitoring system now used by MSHA inspectors.

Obtaining accurate and reliable data from a moving hoist conveyance in a deep shaft remains a key element of future efforts. A commercially available transmitter-receiver set was procured and installed at the Spokane Research Center for wireless transmission of load cell and encoder data from the test hoist. This unit provided a standard for evaluating prototype transmitter-receiver sets. The receiver, located at the headframe or in the hoist room, has been tested both as stand-alone equipment and with a "leaky feeder" antenna that extends the receiver's effective range. The leaky feeder antenna allows signals to be received around corners underground, such as around a rope raise and into an underground hoistroom.

A battery-operated, microcomputer-controlled signal processing board has been designed jointly by the USBM and McCoy Engineering Co., both of Spokane, WA. Functionally, this board processes data from various hoist sensor inputs and provides serial data output for a radio uplink from the conveyance to the hoist control room computer. Inputs are—

1. An analog load-cell input channel for monitoring loading of the hoist wire rope by the conveyance.

2. An analog input channel configurable for use with another load cell or with other sensors, such as accelerometers, linear potentiometers, or ultrasonic transducers.

3. A digital optical encoder input channel for monitoring the location of the conveyance in the shaft.

Analog sensor input data are sampled by the monitoring system at 100 ms intervals. This sampling rate allows data to be acquired about 10 times per second, which is adequate for evaluating satisfactory hoist operation and affecting timely control at a speed of 600 m/min or 10 m/s (1,800 ft/min or 30 ft/s). At

the completion of each sampling period, this information is combined with an updated optical encoder pulse count and transmitted as asynchronous serial data over the radio modem. A secondary RS-232 serial port output of the processing board can provide the same information to a portable computer or terminal on the conveyance itself. The conceptual data acquisition and sensor package is shown integrated into a hoist and shaft conveyance monitoring system (figure 8).

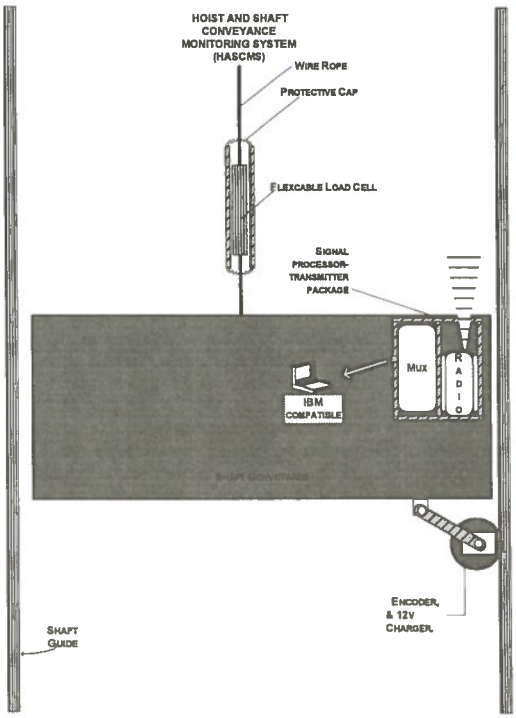

Figure 8. Hoist and shaft conveyance monitoring system.

Software

A user-friendly software interface to collect, save, analyze, and provide hoist control from sensor data input has also been developed. Visual Basic, an event-driven programming language, was selected. Instead of lengthy instructions taking weeks to write, this program is drawn. Subroutines are embedded in tool boxes of requisite functions by simple "point, click, and drag" programming. Subroutines are carried out in reaction to an event caused by either user input or internal actions. For example, events could be entered with a mouse click on a start button on the screen or input to a text box from a communications port on a PC.

Initial programming efforts resulted in a series of screens displaying hoisting data. The main menu includes eight buttons for displaying different data: "hoisting," "loading/unloading," "data-save," "calibration," "shaft inspection," "set operating limits," "set password," and "exit." The user can move anywhere in the system from either the main menu or the pull-down menus that exist in each window. For example, in figure 9, the "hoisting" window is shown with a mine shaft and conveyance represented, along with various operating parameters. The conveyance moves in accordance with position data input into the text box. Speed, acceleration, and conveyance weight are displayed as input into the text boxes. Another icon on this screen represents conveyance contents tied to warning conditions set in the operating limits window.

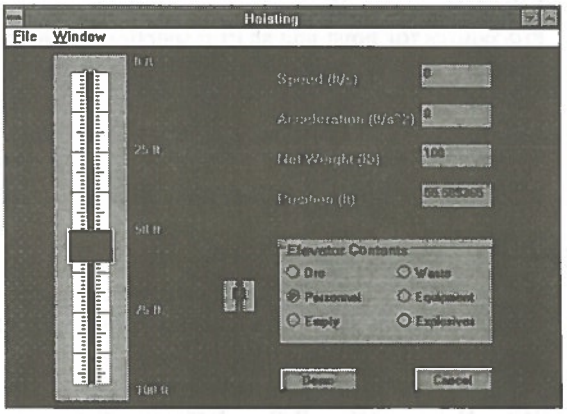

Figure 9. Computer screen showing shaft and conveyance simulation.

Updates and new capabilities are being incorporated as needed. For example, a menu bar is currently being incorporated into each process screen with a representative icon for different screens. Algorithms for time trends of rope load and conveyance speed with the effects of tight compartments from ground squeeze are also being considered. Coupled rock mass and set distortion data with slack and tight rope sensing can define potentially hazardous sections in the shaft.

SUMMARY

The major benefit arising from this research will be a reduction of injuries and fatalities related to hoist

and elevator operations. Real-time visualization of hoisting processes will provide a hoist operator with a desktop tool for control of hoisting operations in a safe and efficient manner. By integrating this function into a broader framework of hoisting process control, the research will improve the health and safety of the work place.

REFERENCES

Barkand, T.D. and Helfrich, W.J., 1988.
Application of dynamic braking to mine hoisting systems. IEEE Trans. on Industry Applications.

Cseff, J., Forbes, W.J., Mills, A.W. III, Albert, L. and Penning, F.A., 1981.
Procedures for hoist and shaft inspection and maintenance. Vol. I. Systems description and Vol. II. Inspection and maintenance procedures (Contract J0100035, V.B. Cook, Inc.). USBM OFR 196(1)-82, 310 pp.; NTIS: PB 83-148049 and USBM OFR 196(2)-82, 140 pp.; NTIS: PB 83-148056.

Dames and Moore, 1977.
Safety analysis of United States shaft-sinking operations (Contract JO155174). USBM OFR 45-78, 289 pp.; NTIS: PB 282 289.

Farley, H.L., Fish, R.B., Jeffcoat, R.L., and Hoadley, D.L., 1983.
Slack and overload rope protection system (Contract JO199008, Foster-Miller Assoc., Inc.). USBM OFR 213-83, 327 pp.; NTIS: PB 84-143460.

Loynes, E., 1976.
Safe manriding in mines. Mining Technology, December, pp. 12-21.

Mine Health and Safety Administration, Health and Safety Analysis Center, 1989.
Shaft accidents in metal/nonmetal 1989, ADA (Accident data analysis).

CAMI'95: 3rd Canadian Conference on Computer Applications in the Mineral Industry
Montréal, Québec, Canada, October 22-25, 1995

Observer-Based Path-Tracking Controller for Forward/Backward Motion of an Articulated Vehicle

Vladimir Polotski
Perception and Robotics Laboratory
Ecole Polytechnique de Montréal,
Montréal, Québec

ABSTRACT:

Using a concept of geometrical path-tracking, some specific properties of articulated vehicles have been analyzed. We consider the case of incomplete information, corresponding to the situation when only lateral deviation from the desired path can be measured. An observer-based controller is implemented for this purpose. An observer strategy with piecewise-constant gains, guarantiing almost monotonous and fast convergence is proposed. It is shown that the lack of information about the heading offset can not deteriorate the tracking process. The importance of forward/backward manoeuvres for practically useful control of LHD-vehicle has necessitated additional investigations and reliable definitions of the desired path and reference point. Presented analysis is most important for the backward motion with reference point placed in front of the vehicle, because of the computational instability arising in the calculation of the articulation angle. The theoretical conclusions and simulation results have been successfully compared with experimental tests using a reduced-size LHD vehicle available in the laboratory.

RÉSUMÉ:

Utilisant le concept du suivi géometrique du chemin, les propriétés specifiques des véhicules articulés ont été analysées. On considère le cas de l'information incomplète correspondant à la situation où seules les déviations latérales par rapport au chemin désiré peuvent être mesurées. L'utilisation de l'observateur d'etat dans la boucle du contrôle est implentée pour ce but. La stratégie d'observation avec les gains constant-par-morceaux, qui garantie la convergence rapide et presque monotone a été proposée. On a démontré que le manque d'information sur les déviations directionnelles ne peut pas détériorer le processus de suivi du chemin. L'importance du manoevre de la marche avant/arrière pour le contôle du véhicule chargeuse-navette (LHD) nécessite une analyse additionnelle y compris les définitions reliables du chemin désiré et du point de référence. Cette étude est la plus significative pour la marche arrière quand le point de référence est placé en avant du véhicule à cause d'instabilité qui apparaît dans le calcul de l'angle d'articulation dans ce cas. Les conclusions théoriques et les résultats de simulations ont été comparés aux testes expérimentaux faits avec un véhicule chargeuse-navette réduit de laboratoire.

INTRODUCTION

The path-tracking problem is the important part of mobile robot control. The classical control framework consists in partitioning of general problem to the trajectory computation (*e.g.* optimal) and to the synthesis of stabilizing controller. This approach results in the planning-tracking separation for robotics control. The desired trajectory being computed by the planning procedure is transferred to the tracking algorithm. However some problems arise in the interface between planning and tracking parts, especially if the non-rigid (*e.g* articulated) wheeled vehicles is under consideration. On the other hand the tracking procedure is based on the information about offsets from the desired path. To apply the feedback control technique the reliable estimations of those offsets have to be obtained. State observers have been used here for these purposes as an interface between available measurements and tracking algorithm.

Mechanics of wheeled mobile robots owing to nonholonomic constraints was under increasing studies last years. Differential geometry approach has been used for trajectory planning in (Fernandes, Gurvits and Li 1991). The new ideas exploiting time-transformations (Pomet, Thuilot, Bastin and Campion 1992) and nonlinear phase transformation (Canudas de Wit, Fixot and Astrom 1992), (Pomet et al. 1992), (Samson 1995) has been recently used for planning as well as for trajectory stabilization. All those works result in rather complex control strategies for planning part as well as for tracking problem.

The framework of geometrical path-tracking was proposed in (DeSantis 1993) and then generalized for the case of tractor-trailer in (DeSantis 1994). This methodology can greater simplify the resulting path-tracking controller.

Articulated vehicles being a specific type of wheeled vehicles are very important for mining applications because of their capability to follow narrow corridors and because of two units which the vehicle consists of can be separately delivered to the underground space and assembled there.

The analysis of different control problems for articulated vehicle has been performed in (DeSantis 1994) in contest of tractor-trailer and with explicit mining objectives in (Hurteau, St-Amant, Laperrière and Chevrette 1992), (Juneau, Hurteau, Freedman and Chevrette 1993). Relatively low speed of the vehicle allows to reduce the mechanical model which is used for the analysis and to limit the description of the system by the kinematic level. (Hemami 1995),(Hemami and Polotski 1995).

The conception of feedback is essential for tracking procedures because of stabilizing nature of this problem. It is important to emphasize that the real feedback should be based on the output, but the state feedback is usually considered for the sake of simplicity. The state estimation as an important step making it possible to pass from the output to the state and to fill the state feedback procedure, is less studied.

We present here the appropriate analysis and the state estimation procedure. We also present the feedback controller based on the directly measured information which is used at first in the the estimation loop and then the obtained estimation of state are used in controller loop. The separation principle (Brogan 1991) is the basis of such approach. After the synthesis of controller's and observer's gains, the analysis of the compound system has been performed. The known peaking phenomenon (Polotski 1980), (Kokotovic and Sussmann 1991) is taken into consideration and the piecewise-constant observer gain has been used. This approach allows to reduce significantly the tracking errors and makes the convergence almost monotonous. The importance of going farther than simply choose controller's and observer's gains using the separation principle for a synthesis, has been recently demonstrated in (Canudas de Wit et al. 1992)

Another question discussed in the paper is the knowledge of parameters of the desired path when they are required for controller to be used in the synthesis of tracking procedure. The complete information about the desired path and about offsets is the commonly used assumption. But the knowledge of trajectory in the workspace does not mean that it is known in the configuration space. The redundancy (or not uniqueness of inverse transformation) necessitates a special discussion of this problem. For nonholonomic systems such a question becomes more complicated: the coordinates are independent but the velocities are not. To be used in path-tracking controller the desired path has to be determined in the configuration space. An articulation angle have to be added to computed parameters for completing the description. Its computation along the desired path results in the solution of nonlinear differential equation. This problem is (computationally) stable for the forward motion but becomes unstable for the backward motion. For straight line and circular trajectories the articulation angle is constant and the computational problem becomes trivial.

In the previous works (Hurteau et al. 1992), the desired articulation angle has been computed approximatively under assumption of constant curvature. We present the procedure enable us to compute the articulation angle along the known trajectory followed in the backward manoeuver.

In the planning-tracking framework a determination of the parameters of the desired path should be placed somewhere between two parts: being relevant to the desired path these parameters are required by the tracking algorithm. Let us note that some aspects of path planning for articulated vehicle are discussed in (Lapointe and Hurteau 1991).

KINEMATIC MODEL OF ARTICULATED VEHICLE

Articulated vehicles (AV) used in mining applications belong to the class of vehicles with relatively low speed (Hurteau et al. 1992),(Hemami and Polotski 1995). Almost all "dynamical" phenomena, important for the motion of highway vehicles become negligible in this case. As a result the mechanics of the path-tracking may be totally based on the kinematics. This approach simplifies significantly the formulation of tracking problem and the synthesis of control low.

The unit under study is a two-part four-wheel vehicle articulated in the point P (see Figure 1). This vehicle can be regarded as *two connected tricycles* with steering. The steering action is performed by changing articulation angle (controlled joint scheme) or by controlling independently left and right wheels (independent control scheme). As pointed out *e.g.* in (Guldner and Utkin 1994) the tricycle model is kinematically equivalent to two wheel axle or "knife edge" (Fernandes et al. 1991) centered wheel. Therefore the steering control of an articulated vehicle can be understood as produced by a common wheel placed at the joint point P even if this wheel does not really exist.

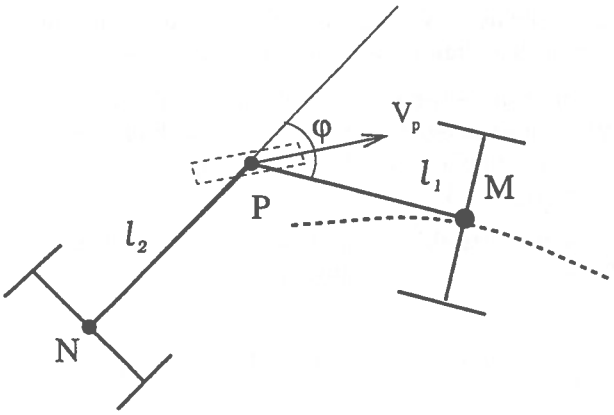

Fig. 1 Scheme of articulated vehicle.

Let M and N be the middle points of front and rear wheel axles. Let $\overline{V}_M$, $\overline{V}_N$ be the velocities of points M and N respectively. They are collinear to PM and PN due to the nonholonomic constraints imposed to the system. Suppose that one of points M and N is arbitrarily chosen as front one. Without loss of generality it is point M. The sign of velocity V_M is positive if $\overline{V}_M \uparrow\uparrow \overline{PM}$ and negative otherwise. Let denote by φ the articulation angle of the direction $\overline{PM}$ to $\overline{NP}$ (positive for anti-clockwise case). Let denote by δ the angle of velocity vector $\overline{V_P}$ with the front part $\overline{PM}$ of the vehicle $\overline{PM}$. We will consider this angle as the *generalized control input.*

The equations of motion can be obtained by easy and logical way using a concept of two tricycles and of imaginary wheel.

Let X, Y, θ be Cartesian coordinates of point M and heading angle of $\overline{PM}$ with respect to fixed Cartesian basis in the workspace.

Points P and M of the tricycle $\overline{PM}$ move with velocities V_P, V_M and we can write down

$$V_P = V_M / \cos\delta$$

$$\frac{d\theta_M}{dt} = -V_M \tan\delta / l_1 = -V_P \sin\delta / l_1 \qquad (1)$$

For another tricycle we get a similar result using the angle $(-\varphi + \delta)$ instead of δ.

$$V_P = V_N / cos(\delta - \varphi)$$

$$\frac{d\theta_N}{dt} = V_N \tan(\delta - \varphi)/l_1 = V_P \sin(\delta - \varphi)/l_2$$

Let note that the sign "+" instead of "−" appears because of the front position of the steered wheel in tricycle $\overline{NP}$ instead of the rear position in $\overline{MP}$

Therefore we obtain for $\varphi = \theta_N - \theta_M$ the following equation

$$\frac{d\varphi}{dt} = V_P \sin(\delta - \varphi)/l_2 + V_M \tan\delta / l_1 =$$

$$V_M(\tan\delta/l_1 + \sin(\delta - \varphi)/\cos\delta/l_2)$$

after some algebra we obtain

$$\frac{d\varphi}{dt} = V_M\left(\frac{tan\delta}{l_1} + \frac{\tan\delta\cos(\varphi) - \sin\varphi}{l_2}\right) \qquad (2)$$

To deduce the kinematic equations of motion we simply write the relations between velocities and derivatives of Cartesian coordinates (X, Y) together with (1) and (2), then we come to the following system

$$\frac{dX}{dt} = V_M \cos\theta \qquad (3)$$

$$\frac{dY}{dt} = V_M \sin\theta \quad (4)$$

$$\frac{d\theta}{dt} = -V_M \tan\delta/l_1 \quad (5)$$

$$\frac{d\varphi}{dt} = V_M \left(-\frac{\sin\varphi}{l_2} + \tan\delta\left(\frac{1}{l_2} + \frac{\cos\varphi}{l_1}\right)\right) \quad (6)$$

The first three equations describe the plane motion of the rigid body which has initially two degree of freedom but is described on the kinematic level and under nonholonomic constraint of rolling without skidding. The last equation is relevant to "internal" motion of an AV and is specific for this type of vehicles.

Presented deduction of motion equations is methodically interesting but they could be found elsewhere. To show the advantages of *generalized input* and two tricycles concepts we analyze the following question.

For given th motion parameters of one point among M, N, P, how can we compute the parameters of motion of two others? The answer is as follows.

Given parameters (δ, V_P) of point P we obtain for point M:

$$\omega_M = -V_P \sin\delta/l_1, \quad V_M = V_P \cos\delta \quad (7)$$

An expression for the point N can be derived by substituting $(\delta - \varphi)$ instead of δ and changing the sign because of the opposite orientation of the tricycles:

$$\omega_N = V_P \sin(\delta - \varphi)/l_2, \quad V_N = V_P \cos(\delta - \varphi) \quad (8)$$

Given parameters (ω_M, V_M) of point M we obtain for point P:

$$V_P = \sqrt{\omega_M^2 l1^2 + V_M^2}, \quad \delta = -\arctan(l_1 \omega_M / V_M) \quad (9)$$

To obtain the N-point parameters the expressions (8) and (9) are used

$$V_N = V_M \cos\varphi + \omega_M l_1 \sin\varphi \quad (10)$$

$$\omega_N = \frac{\omega_M l_1 (\omega_M l_1 \sin\varphi - V_M \cos\varphi)}{l_2 V_M} \quad (11)$$

The case when we start from point N is similar and omitted.

Presented formulas have been used for on-line calculation of motion parameters in the algorithm of teleoperation of mini-LHD (Labonté, Giraud and Polotski 1995) . They have been used for the odometry analysis of AV in (Boisgontier, Lopez and Polotski 1995) as well.

In next sections we analyse the behavior of articulation angle from divers points of view. We discuss the advantages to use it in tracking procedure. On the other hand we show that the computation of the desired value of an articulation angle becomes nontrivial in the case of backward manoeuver. Finally we show how it can be computed for general case of motion.

STABLE COMPUTING OF THE DESIRED ARTICULATION ANGLE

The importance of the feed-forward computation of the articulation angle for the quality of tracking error regulation was discussed in (Hurteau et al. 1992). We will confirm it again in the section devoted to the simulation examples (see Fig. 9 an comments). It is important to notice that the common practice for computing such terms consists in the utilization of terms proportional to φ without using its derivatives, usually referred as small values (Hurteau et al. 1992). But the value of derivative is significant for the manoeuver like a motion consisting in "folding up" of two parts of the vehicle. There can be little doubt that the derivative is neglected due to the difficulties arising from the unstable computation rather than because of its small value.

Let us denote the *generalized input* $\tan(\delta)$ by p and introduce the length $s(t)$ along the path of point M and the angular variable $\alpha = s(t)/l_2$, then we have $d\alpha = ds/l_2 = V_M\, dt/l_2$.

Changing variable in (4) from t to α and denoting $(l_2 - l_1)/(2l_1)$ by ε we obtain:

$$\frac{d\phi}{d\alpha} = sign(V_M)(p(\alpha)(\cos\varphi + 1 + 2\varepsilon) - \sin\varphi) \quad (12)$$

This equation has the type studied in (Kamke 1967) and is equivalent to Riccati equation. Changing variable from φ to $u = tan(\varphi/2)$ and writing γ for $sign(V_M)$, we get

$$\frac{du}{d\alpha} = \gamma\left(-u + p(\alpha)(1+\epsilon) - p(\alpha)\varepsilon U^2\right) \quad (13)$$

The objective of such a transformation is the following: sign(V_M) is positive for forward motion and

negative otherwise. As far as $sign(V_M)$ is a multiplier in the right-hand side of (12), the stability of motion is determined by the direction. Solution is stable for forward motion and unstable otherwise.

We give here the description of the result completely presented in (Polotski 1996).

The case $\varepsilon = 0$ corresponds to the symmetrical machine $l_1 = l_2$. Riccati equation (13) is reduced in this case to the linear one

$$\frac{du}{d\alpha} = \text{sign}(V_M)(-u + p(\alpha)) \qquad (14)$$

This equation has unique exponentially stable "attractive" solution for forward motion and an unstable one otherwise. The growing solutions for backward motion can be regarded as converging to infinity, it corresponds to the singular solution $\varphi = \pi$ of (12) (see Fig.5 in the section devoted to simulation results an corresponding comments).

The case $p = \text{const}$ corresponds to a desired path of circular shape or straight lines and was recently analyzed in (Bushnell, Mrtich, Sahai and Secor 1994). The Riccati equation has constant coefficients and can be analytically solved using reduction to the linear system. For industrial application both assumptions of small ε and slowly varying p usually hold.

For $\varepsilon = 0$ and $p = \text{const}$ two stationary solutions are

$$\varphi_1^0 = 2 \arctan(p), \quad \varphi_2^0 = \pi$$

Using small parameter approximation, two solutions engendered by φ_1^0 and φ_2^0 can be found as follows:

$$\varphi_1^0 = 2 \arctan(p(1 + \varepsilon\frac{1+2p^2}{2})),$$

$$\varphi_2^0 = 2 \arctan(\frac{2}{p\varepsilon} - \varepsilon\frac{p(1+p^2)}{2})$$

In the general case Riccati equation could be reduced to the second order system of linear differential equations. Essential property consists in the existence of two solutions, one of which is always stable, another one unstable. One can find the details in (Polotski 1996).

Unstable solutions can be made stable by simply reversing the time and the direction of motion ($\text{sign}(V_M)$). Thus equations (3)–(6) can be used to obtain the desired articulation angle along backward maneuver. Using (3) and (4) to compute θ, the *generalized input* can be subsequently determined from (5) and then (6) is used for stable computing of φ.

Using this method an iterative procedure has been proposed for general case, when the path can be partitioned into the elements required to be followed in the forward mode (so called positive elements) or in the backward mode (respectively negative).

For the sake of simplicity let suppose that the first element is positive. To determine the articulation angle along the first element we start from initial point and integrate the equation (6); this computation is stable. Instead of make the unstable computation along the next (negative) elements we choose articulation angle for final point, by executing iteratively time inverse computation we try to get the value of articulation angle obtained for final point of first element (paste condition). When the paste condition is approximatively satisfied the value of articulation angle for final point of second element becomes the initial value for the similar computation along the third element.

For many applications the situation is even simpler since the last part of iterations is unnecessary as far as the values of articulation angle in intermediate points are supposed to be given by external conditions; this is *e.g.* the case for mining applications.

OBSERVER BASED PATH-TRACKING CONTROLLER

Let T^* be the desired trajectory, $M^* \subseteq T^*$, $MM^* \perp T^*$, articulated and heading angles of desired configuration are ϕ^* and θ^*, errors (tradeoffs) are $\varepsilon_\theta = \theta - \theta^*$, $\varepsilon_\phi = \varphi - \varphi^*$, $n = M\bar{M}^*$.

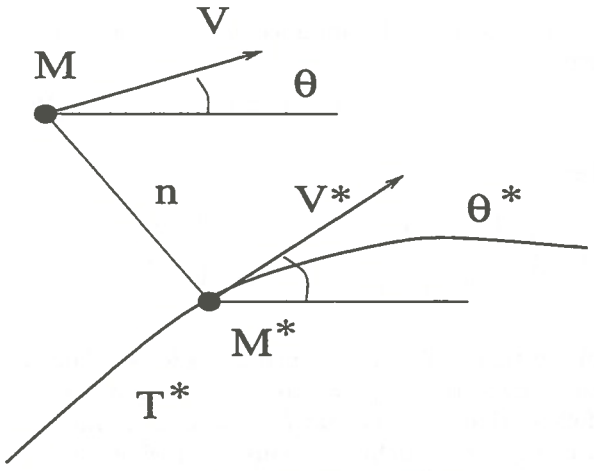

Fig. 2 Projection motion

We follow here the geometrical path-tracking framework proposed in (DeSantis 1993). We have to note

that obtained equation are not equivalent to the linearization along the curve T^* because of the fact that the motion of point M^* (the projection of the point M) is taken into account.

Let U – be the heading control input $(\tan(\delta)/l_1$ in term of (3–6) We will write down the motion equation in linearized form along the desired path and using S as independent variable $(dS = V(t)\,dt)$. We should point out that more general wherefores of this technique related to time transformation (Pomet et al. 1992) is recently given in (Samson 1995).

$$\frac{dn}{dS} = \varepsilon_\theta$$

$$\frac{d\varepsilon_\theta}{dS} = U \qquad (15)$$

$$\frac{d\varepsilon_\phi}{dS} = \varepsilon_\phi\, a(S) + U\, b(S)$$

where $a(S) = -1/l_2 + U^* \sin\varphi/l_1$, $b(S) = 1/l_1 + \cos\varphi/l_1$

The obtained equations describe the motion with respect to the given path *i.e.* displacement along the path and the velocity of such motion are not taken into account. Then the order of the system has been reduced to 3 and number of inputs to 1. The position is completely described by three parameters: normal and directional (heading) offsets and articulated angle (new parameter with respect to the case of conventional vehicle). But only one velocity is required to complete the kinematic description due to nonholonomic structure of motion constraints (DeSantis 1994), (Hurteau et al. 1992)

Let us write down the obtained equations in matrix form:

$$\frac{dZ}{dS} = A\,Z + B\,U, \qquad (16)$$

where

$$A = \begin{pmatrix} 0 & 1 & 0 \\ 0 & 0 & 0 \\ 0 & 0 & a(S) \end{pmatrix}, \qquad B = \begin{pmatrix} 0 \\ 1 \\ b(S) \end{pmatrix}$$

This system is obviously controllable for stationary desired trajectories ($\varphi^* = const$, $U^* = const$, hence it follows that $a(S) = const$, $b(S) = const$). One can verify that controllability occurs for a wide class of non-stationary desired trajectories as well. Using a well criterion for controllability of time-varying systems (Brogan 1991) $rank(K_1\,K_2\,K_3) = 3$ where for our case

$K_1 = B$, $K_2 = AB - dB/dS$,

$K_3 = A^2B - 2A - dB/dS - B\,dA/dS + d^2B/dS^2$.

The identity $\det(K_1K_2K_3) \equiv 0$ is the very tight (and almost exotic) restriction imposed on $a(S)$ and $b(S)$ and does not occur for general case of nonstationary paths.

If φ, φ^*, $(\theta - \theta^*)$, n - are directly available for feedback construction the classical methods could be used for tracking control (Hurteau et al. 1992),(DeSantis 1993). Such an assumption is fulfilled *e.g.* when the desired path is materialized by the guideline.

A more realistic approach consists in the observability analysis of the system taking into account the structure of outputs. Such "information filling" of control algorithms is discussed below.

We analyse at first the possibility to eliminate the heading offset from the output available for feedback. It should be noted that this parameter is rather difficult to measure for unstructured mining environment in particular. The range finders of different types also deliver the information about the distance from the object rather then directional information ((Juneau et al. 1993), which is sometimes extracted using approximative derivation or similar procedure. Suppose that φ, n are measured and $\check{\varphi}$, $\check{n}$ become available. The output matrix in this case is

$$C = \begin{pmatrix} c_1 \\ c_2 \end{pmatrix} = \begin{pmatrix} 1 & 0 & 0 \\ 0 & 0 & 1 \end{pmatrix} \qquad (17)$$

To prove the observability it sufficient to compute matrix CA and check that c_1, $c_1\,A$, c_2 - are linearly independent. Although matrix A is nonstationary the criterion is identical to stationary case because of special structure of matrix C. Therefore including *e.g.* full order Kalman-type observer in the feedback loop the tracking controller could be designed in the following form:

$$\frac{d\tilde{Z}}{dS} = A\,\tilde{Z} + K_{ob}(\check{Z} - \tilde{Z}) + B\,U, \quad \tilde{Z}(0) = 0,$$

$$U = k_4\tilde{Z}_1 + k_5\tilde{Z}_2 + k_6\tilde{Z}_3$$

The observer gain matrix is as follows:

$$K_{ob} = \begin{pmatrix} k_1 & 0 & 0 \\ k_2 & 0 & 0 \\ 0 & 0 & k_3 + a \end{pmatrix} \qquad (18)$$

The gain coefficients in observer and controller can be chosen to guarantee the appropriate decay of tracking error *e.g.* by placing the poles in the point $\lambda_i = -\mu$, $(1 = 1, \ldots, 6)$

$$k_1 = 2\mu,\ k_2 = -\mu^2,\ k_3 = \mu,$$

Then the solutions will be bounded by arbitrary fast exponentially decaying function.

If the linear combination $q_1 n + q_2 \varepsilon_\theta$ is measured instead of n we have almost the same result:

$$C_q = \begin{pmatrix} c_{1q} \\ c_2 \end{pmatrix} = \begin{pmatrix} q_1 & q_2 & 0 \\ 0 & 0 & 1 \end{pmatrix} \qquad (19)$$

One can easy check the observability verifying that if $q_1 \neq 0$ then $det(A^* c_{1q}^*, C_q^*) \neq 0$.

It is known that requiring fast decay of the response, we may obtain the large peaks in transition processes (Kokotovic and Sussmann 1991), (Hemami and Polotski 1995). Being high for purely linear system the peaks may practically destroy the controller in nonlinear case.

To improve the transient behavior (decreasing the peaks arising from observer fast dynamics) the piecewise-constant gain in observer has been proposed in (Polotski 1980).

For our case it simply required to choose the gain vector k_1, k_2 for the process within $(0, T)$ as follows:

$$k_1 = k_1(t) = \begin{cases} \mu & if \quad t \leq T/2 \\ 2\mu & if \quad t > T/2 \end{cases}$$

$$k_2 = k_2(t) = \begin{cases} 0 & if \quad t \leq T/2 \\ -\mu^2 & if \quad t > T/2 \end{cases}$$

It is important to emphasize that an observer based design could be extended to the case of erroneous measurements.

Let us suppose that φ is measured with an unknown constant error

$$\breve{\varphi} = \varphi + g \qquad (20)$$

this model arises from the natural assumption about an existence of the constant error of zero setting.

Considering g as an additional variable and denoting it by Z_4 we obtain the system

$$\frac{dZ'}{dS} = A'\,Z' + B'\,U, \qquad Y' = C'Z \qquad (21)$$

Where

$$A' = \begin{pmatrix} 0 & 1 & 0 & 0 \\ 0 & 0 & 0 & 0 \\ 0 & 0 & a(S) & 0 \\ 0 & 0 & 0 & 0 \end{pmatrix}, \qquad B' = \begin{pmatrix} 0 \\ 1 \\ b(S) \\ 0 \end{pmatrix},$$

$$C' = \begin{pmatrix} c_1' \\ c_2' \end{pmatrix} = \begin{pmatrix} 1 & 0 & 0 & 0 \\ 0 & 0 & 1 & 1 \end{pmatrix} \qquad (22)$$

The system is uncontrollable but the controllable part is observable with measurements (20). Using presented approach we may design the full order observer for extended system, partially stabilize the system in the subspace spanned on $(n, \varepsilon_\theta, \varepsilon_\phi)$ (and not including g) and use the piecewise-constant observer gain to improve the transient quality.

SIMULATION RESULTS

As a first example we present the simulation using MATLAB package of the backward motion of AV along the convex trajectory consisting of four straight line parts and four transient elements between them. Workspace trajectory is presented in Fig. 3 and time-history in Fig. 4.

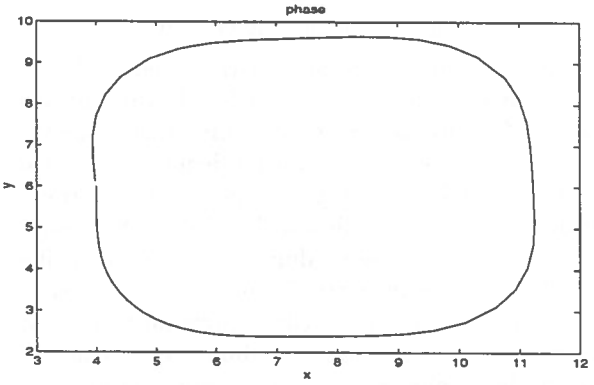

Fig. 3 Backward manoeuver(workspace)

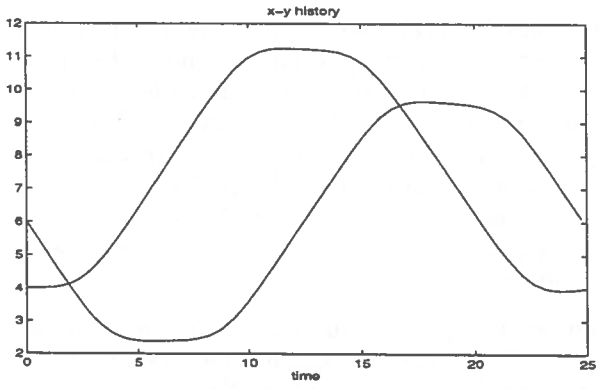

Fig. 4 Backward manoeuver(time)

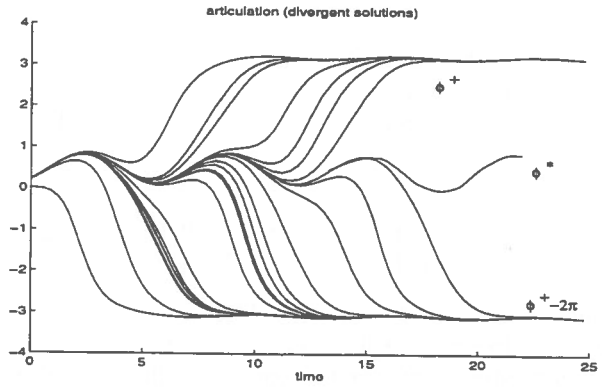

Fig. 5 Direct computation (unstable).

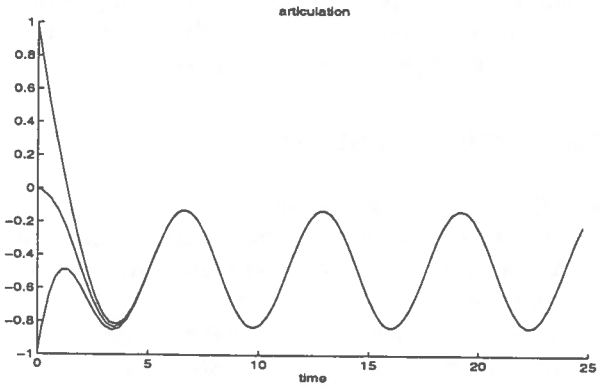

Fig. 6 Inverse-time computation.

Trying to compute the articulation angle behavior in the direct time we get immediately the unstable family of solutions. Starting from small neighborhood near unstable solution (let denote it $\varphi^*(t)$) all solutions quickly converge to the stable solution (let denote it $\varphi^+(t)$) which is closed to π. Such solutions have no much sense during long period of time but their appearance simply means that the angle ϕ will come very fast to the saturation value. On the figure 5 an example of instability is presented by the family of solutions with very closed initial values $(.2156 \pm 10^{-4})$.

To escape from this complication the time inversion has been used. Starting from final moment of time (25 s. for the simulation example under consideration) and choosing arbitrary initial condition (*e.g.* equal to zero), the integration of differential equation (5) has been performed (see Fig.6) Inversing the time again we get the articulation angle along the required path and it can be used for tracking procedure.

Another group of simulation results refer to the same S-shaped trajectory (with a 4m radius of two semi-circles). The machine is slightly asymmetric $(l_1 = 1.1m,\ l_2 = .9m)$, the value of articulation angle is bounded by 40°. The vehicle is initially biased along Y–direction, is oriented transversely to the correct direction and moves with constant speed 1m/s for 25s.

In Fig.7,8 the tracking with the state space controller is presented. In Fig. 7 the dash-dotted line corresponds to the desired path and the solid line to the path generated by using tracking algorithm.

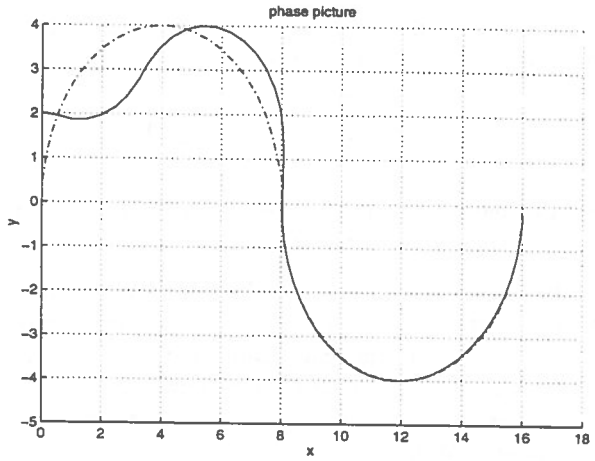

Fig. 7 State-feedback tracking (workspace)

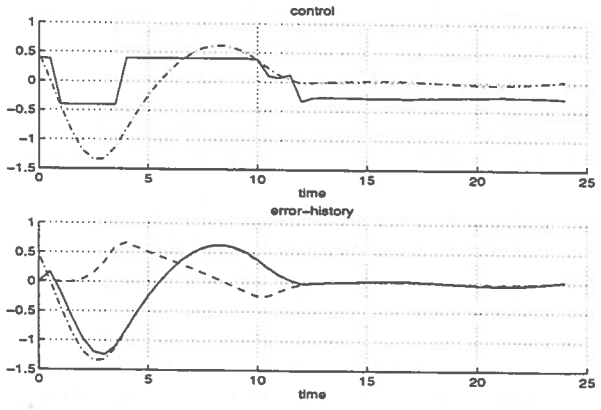

Fig. 8 State-feedback tracking (time)

The time evolution of errors is presented in Fig. 8. In the top part of the figure control (*generalized input*) is shown by solid line and distance-error by dashed line. In the bottom part of the figure one can see the error of estimated distance (dash-dotted line), exact distance error (solid line), orientation error (dashed line).

Fig. 9 shows how the knowledge of the desired articulation angle improves the quality of tracking (solid line corresponds to unknown desired value of articulation angle, dashed line to known articulation angle

being used in the control algorithm together with output feedback and $\mu = 1.5$).

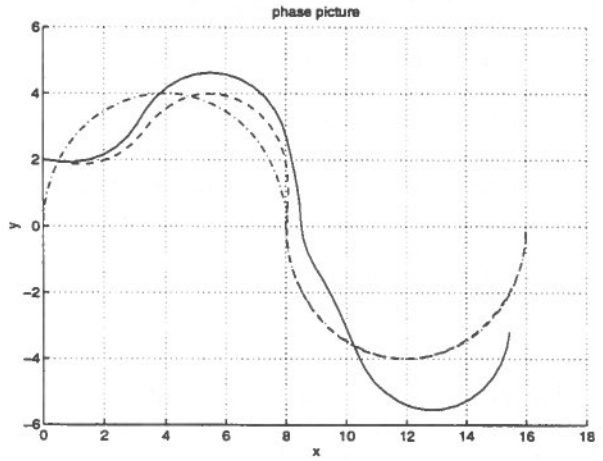

Fig.9 Effect of precalculation.

Fig.10 illustrates the sensitivity to the choice of constant gain in controller loop as well as in observer loop. We are trying to make the convergence faster, by increasing the gains (dashed line corresponds to controller gain 1.5 and observer gain 5; solid line corresponds to both controller and observer gains 5).

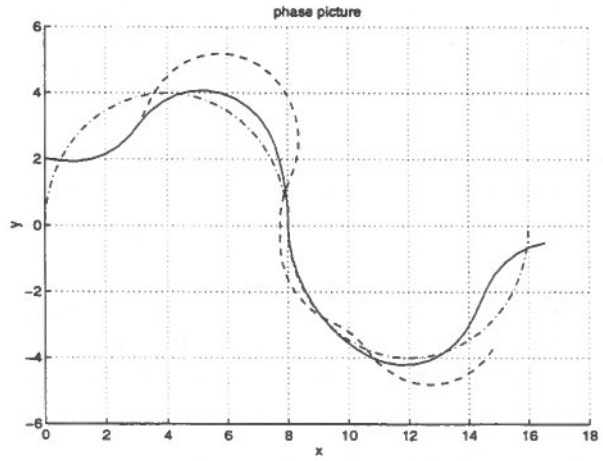

Fig.10 Gain comparison.

Fig. 11,12 illustrate the possibility to increase the gain in both observer and controller loop up to 3 (solid lines) using the piecewise-constant strategy. They are comparable to Fig. 7 and Fig. 8 respectively. For constant gains the deviations from the desired path increase, but piecewise-constant gain in observer when switching at the moments $t \simeq 5s$ and $t \simeq 17s$ improves the convergence and makes it fast and almost monotonous.

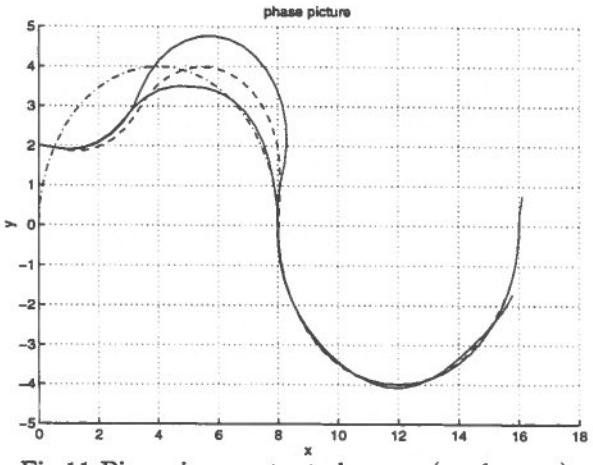

Fig.11 Piecewise-constant observer (workspace).

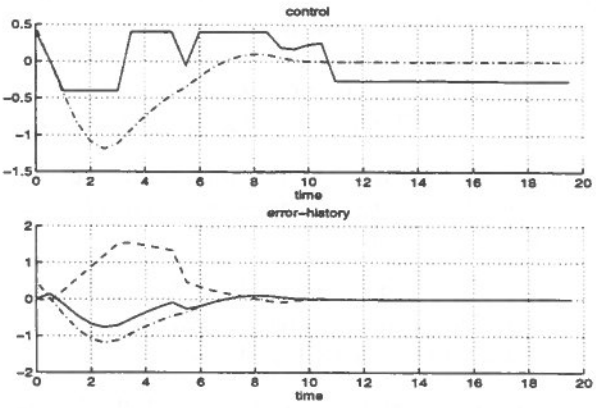

Fig.12 Piecewise-constant observer (time).

CONCLUSIONS

The paper deals with the motion control problem for articulated vehicle. The path-tracking algorithm based on limited amount of information consisting of lateral offsets from the desired path, desired and measured values of articulation angle has been proposed. An observer with piecewise-constant gain is included in the controller in order to estimate the lacking part of state parameters. Special method for the calculation of the desired articulation angle along the backward manoeuver has been derived in order to avoid the computational instability.

ACKNOWLEDGMENT

This work is supported by the NSERC program of Industry-University Partnerships (NSERC-Noranda Chair in Mining Automation).

REFERENCES

Boisgontier, X., Lopez, P. and Polotski, V.: 1995, Position estimation for an articulated mobile robot, *Proceedings of the Canadian Conference on Electrical and Computer Engineering.*

Brogan, W.: 1991, *Modern Control Theory*, Englwood Cliffs, NJ:Prentice Hall.

Bushnell, L., Mrtich, B., Sahai, A. and Secor, A.: 1994, Off tracking bounds for a car pulling trailers with kingpin hitching, *Proceedings of the 33rd Conference on Decision and Control*, Lake Buena Vista, FL, pp. 2944–2947.

Canudas de Wit, C., Fixot, N. and Astrom, K.: 1992, Trajectory tracking in robot manipulators via nonlinear estimating state feedback, *IEEE Transactions on Robotics and Automation, 12, 1980, pp.1640-1648.* **8**(12), 138–144.

DeSantis, R.: 1993, Path-tracking for a car-like robot, *Proceedings of American Control Conference*, pp. 64–68.

DeSantis, R.: 1994, Path-tracking for a tractor-trailer-like robot, *International Journal of Robotics Research* **13**(6), 533–544.

Fernandes, C., Gurvits, L. and Li, Z.: 1991, Foundations of autom. & remote control, 12, 1980, pp.1640-1648. nonholonomic motion planning, *Proceedings of the IEEE International Conference on Robotics and Automation*, pp. 1–112.

Guldner, J. and Utkin, V.: 1994, Stabilization of non-holonomic mobile robots using lyapunov functions for navigation and sliding mode control, *Proceedings of the Conference on Decision and Control*, pp. 2967–2972.

Hemami, A.: 1995, Steering control problem formulation of a tricycle-model vehicle, *To appear in International Journal of Control.*

Hemami, A. and Polotski, V.: 1995, Path tracking control problem formulation of an lhd-loader, *Submited to International Journal of Robotics Research.*

Hurteau, R., St-Amant, M., Laperrière, Y. and Chevrette, G.: 1992, Optical guidance system for underground mine vehicles, *Proceedings of the IEEE International Conference on Robotics and Automation*, Nice, France, pp. 639–644.

Juneau, L., Hurteau, R., Freedman, P. and Chevrette, G.: 1993, Using laser range data to model tunnel curvature for the automatic guidance of a mining vehicle, *Proceedings of the Second IEEE Conference on Control Applications*, Vancouver, BC, pp. 643–648.

Kamke, E.: 1967, *DifferentialGleichungen*, Verbesserte Auflage, Leipzig.

Kokotovic, P. and Sussmann, H.: 1991, The peaking phenomenon and the global stabilization of nonlinear systems, *IEEE Transactions on Automatic Control* **36**(4), 424–440.

Labonté, F., Giraud, J.-L. and Polotski, V.: 1995, Telerobotic issues in the operation of an lhd vehicle, *Proceedings of Third Canadian Conference on Computer Application in the Mineral Industry.*

Lapointe, S. and Hurteau, R.: 1991, Kinematics modelling and local path planning for articulated mobile robots, *Congrés Canadien en Génie Élecrique et Informatique*, pp. 73.3.3.1–73.3.3.4.

Polotski, V.: 1980, Estimation of the state of single-output linear systems by means of observers, *Automation and Remote Control* **22**(12), 1640–1648.

Polotski, V.: 1996, Motion of articulated vehicle and behavior of the solution of riccati equation, *to be published in Dynamic Systems and Applications.*

Pomet, J., Thuilot, B., Bastin, G. and Campion, G.: 1992, A hybrid srategy for the feedback stabilization of nonholonomic mobil robots, *Proceedings of the IEEE International Conference on Robotics and Automation*, pp. 129–134.

Samson, C.: 1995, Control of chained systems with application to path following and time-varying point-stabilization of mobile robots, *IEEE Transactions on Automatic Control* **40**(1), 64–77.

CAMI'95: 3rd Canadian Conference on Computer Applications in the Mineral Industry
Montréal, Québec, Canada, October 22-25, 1995

Robust Computer Vision Techniques for Rock Fragmentation and Loading Analysis

A. Bedair, L. Daneshmend†, C. Hendricks and M. Scoble

Canadian Centre for Automation & Robotics in Mining,
Department of Mining and Metallurgical Engineering,
McGill University, Montréal, Québec

† now Chair in Mine-Mechanical Engineering
Department of Mining Engineering
Queen's University, Kingston, Ontario

ABSTRACT:

Analysis of rock fragmentation is of relevance to various operations and processes in the minerals industry. This paper focuses on image analysis techniques for evaluation of fragmentation in an open-pit muck-pile, and presents a novel methodology for automatic image analysis of rock fragmentation. The methodology uses image smoothing and edge detection techniques to automatically extract fragment contours from muck-pile images. These contour images are then analyzed using a novel segmentation technique which is based upon the characteristics of the muck-pile, resulting in identification of distinct rock fragments. Partially occluded fragments are identified, and contour closure algorithms are used to predict their overall shape. A geometry-based weighting function is used to predict the probability of a specific fragment passing through a sieve mesh of a particular size. The overall size distribution is then computed based on the weighting functions, as well as the estimated volume of each fragment.

RÉSUME:

L'analyse de la fragmentation des rochers est d'une importance pour plusieurs operations et processus dans l'industrie minérale. Cet article se concentre sur les techniques dans les analyses des images pour l'évaluation des fragmentations dans un open-pit muck-pile, et présente une nouvelleté dans la methodologie de l'automization des analyses des images des rochers fragmentés. La methode proposée utilise le concept du polissage (smoothing) des images et la détéction des bordures (edges) pour extraire les contours des images du muck-pile. Ces contours sont analysés a leurs tour avec une nouvelle methode de segmentation basée sur les characteristiques du muck-pile, ce qui en resulte l'identification distincte des fragments des roches. Les contours partiellement identifiés et les algorithmes des fermetures des contours sont utilisés pour estimer leurs formes globale. Une fonction basée sur des poids a partir de formes geometrique est utilisée pour prédire la probabilité des fragments specifique poids des fonctions utilisées, autant au volume estimé de chaque fragment.

INTRODUCTION

Many operations and processes in the minerals industry can benefit from quantitative analysis of the size of rock fragments: the potential applications range from cuttings analysis in mechanical mining machines; to evaluation of loading conditions for scoops and shovels; onto oversize detection on crush-

ers and in conveyors; and through to mineral processing operations. This paper focuses on a specific type of mining operation: open-pit mining using drills and shovels. The fragment size analysis in such an operation is unique in terms of the context in which the fragments must be viewed - the muck pile generated by blasting. In addition, due to its location outdoors, the muckpile is prone to the vagaries of nature in terms of lighting and precipitation.

The surface mining process in question can be viewed as consisting of a number of sequential operations including drilling, blasting, loading, hauling and crushing. Drilling and blasting, being the primary production operations, have a major impact on the performance and cost of subsequent operations. The main objective of the drilling and blasting operations is to obtain optimum fragmentation within safety and economic limits.

The results of the blasting process are affected by many parameters such as rock composition, layer thickness, type of explosives, etc. As a result, an evaluation process is required after each blast to assess its effectiveness. One of the parameters that can be used in the evaluation process is fragment size distribution. Similarly, the size of rock fragments has a direct bearing on the loading of the rock by shovels into haul trucks - poor fragmentation leads to hard digging, resulting in low productivity and high maintenance costs.

Fragment size distribution in such operations has traditionally been determined by sieving analysis, which is a time consuming and labour intensive process. Hence actual size distributions have tended to be obtained infrequently, and have been prone to human bias in the sampling process. It is clearly desirable to have a more consistent and effective way of obtaining fragment size distribution on a widespread basis, since this would facilitate the enhancement of production quality control, as well as furthering the automation of surface mining operations.

DIGITAL IMAGE ANALYSIS OF A MUCK-PILE

There has been a considerable level of research activity, for over a decade, focused on the use of digital image analysis techniques to measure the size distribution of rock fragments on the surface of muckpiles. The problem of fragment size distribution can be decomposed into two sub-problems, namely:

1. The rock fragment's identification and measurement.
2. Estimation of the overall size distribution.

The first sub-problem addresses the issue of identifying fragments from the digital image by determining its boundary. Work on this aspect has been relatively neglected. The favoured approach has been to rely upon manual tracing of contours, resulting in subjective measurements which are very tedious and labour-intensive to obtain. Alternatively, some researchers have resorted to classical edge-detection techniques which were developed for other applications and hence do not cater to the specifications of the muck-pile image processing problem. Along with the identification comes the measurement of fragment size. Several researchers have utilized concepts and techniques from machine vision to obtain measurements of fragments [Hunter et al., 1990].

The second sub-problem is the estimation of the overall size distribution of the pile. The solution to this problem is highly dependent on the accuracy of the measurements obtained from the solution of the first sub-problem.

Some of the properties that characterize muck-pile images and make this such a unique and challenging problem, are:

- **Surface Texture:** each fragment possesses a textured surface; in addition, the pile itself is not of uniform texture. This poses a problem since conventional image processing boundary detection algorithms tend to be highly sensitive to texture variations.
- **Multifaceted Fragments:** rock fragments may have more than one face visible in an image. This may result in an edge detection algorithm determining that a fragment boundary exists at what is actually a face boundary.
- **View Location:** the images acquired vary with the viewing angle, elevation and distance.
- **Illumination:** natural lighting can vary in intensity and angle of incidence. This can have a very significant effect due to shadows, and loss of contrast.
- **Environment:** rain and surface moisture can dramatically affect the image properties. Snow can obscure fragments.

All of these properties contribute to the quality of the digital image to be analyzed as will be shown in the rest of this paper.

MUCK-PILE MODEL FOR SEGMENTATION

The surface of the muck-pile modelled as being divided into three layers. This division is adopted

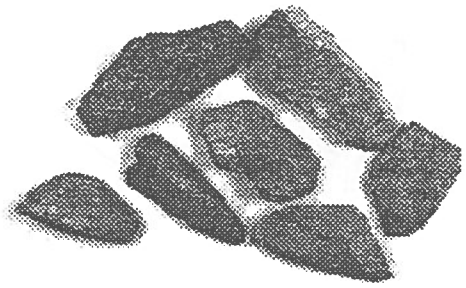

Figure 1: Shadow connected contours

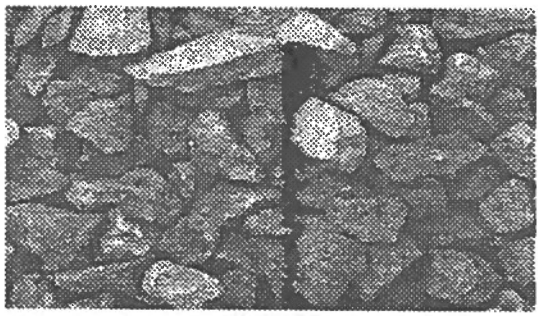

Figure 2: Overlapping rocks

to simplify the fragment segmentation and measurement sub-problems. The three layers in question are the top layer, middle layer, and background layer, L_1, L_2, and L_3 respectively. In measuring the fragments, only the fragments in the top and middle layers will be considered. The criterion used to classify fragments into one of these layers is based on their convexity. The modelling methodology can be summarized as follows:

- A rock is in the top layer, $R \in L_1$, if its contour is closed and convex.
- For non-convex contours: one of the following cases applies
  - Two rocks both in the top layer, i.e. R_1, $R_2 \in L_1$(e.g. see Figure 1).
  - One rock in the top layer and one rock in the second layer, i.e. $R_1 \in L_1$ and $R_2 \in L_2$ (e.g. see Figure 2).
  - One rock in the background layer, i.e. $R \in L_3$.
- If one convex rock R_1 contains an other convex rock R_2 (i.e. $R_2 \in R_1$): the contained rock R_2 will be considered as texture on the surface of R_1.

BOUNDARY DETECTION

Actual rock fragments do not possess smooth surfaces; this usually results in "noisy" images. To be able to apply contour extraction algorithms (a process which is based on detecting intensity discontinuities), a pre-processing (smoothing) of the image is needed to reduce the image artifacts (i.e. to eliminate high frequency components).

Many algorithms have been developed in the field of computer vision to smooth noisy images [Mastin, 1985]. The problems associated with most of these filters is that they either do not preserve image features such as edges or they are computationally expensive ([Chin and Yeh, 1983], [Saint-Marc et al., 1991]). For example, in applying a low pass filter in the frequency domain, due to the nature of the image, occlusion boundaries can be lost to the background in some cases.

The noise in the digital image can significantly be reduced using a Crimmins filter [Crimmins, 1985]. Being a nonlinear filter, it has the property of smoothing the speckles - represented as a narrow winding walls and valleys- and preserving contour features. This filter was first used in assisting radar image interpretation.

Cascading the smoothing process of images by an edge detection algorithm, such as a Canny filter [Canny, 1986], we can obtain reasonable contour extraction. Figure 3 presents the result of applying a Canny filter to the image shown in Figure 2, firstly without pre-processing with the Crimmins filter, and then with Crimmins pre-processing.

EDGE LINKING

Fragment contours are fairly difficult to discriminate from other sources of edge features. This is evident from Figure 3 (b) , where the image preprocessing yields an image with numerous unconnected edge segments. Hence a robust method of extracting these contours from the pre-processed image is needed.

The first step is to apply a thinning algorithm to enhance the contour segments; this may result in breaking one segment into several smaller segments. Small gaps between these segments are then completed by adapting a simple heuristic methodology, in which the end points are extended along their tangents for each segment.

A database for contour segments is then built in which each segment is represented by two end points and their tangents. Using the outer contour we ap-

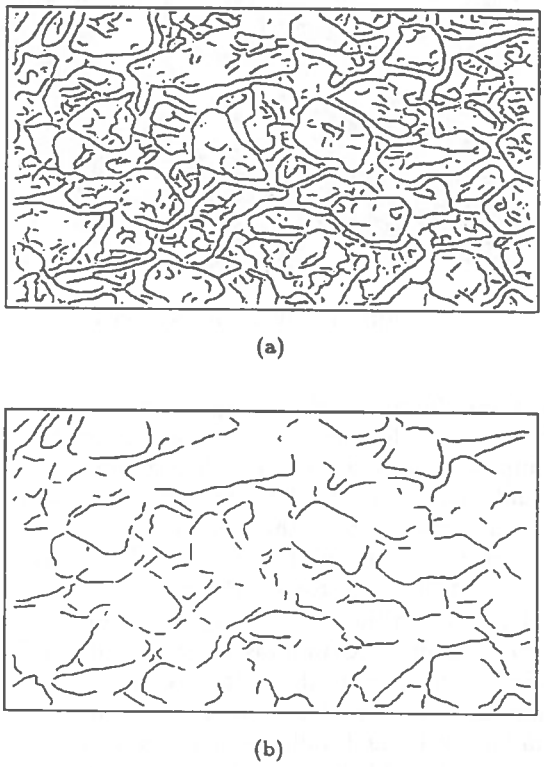

Figure 3: Result of Canny filter: (a) Before smoothing, (b) After smoothing.

ply a search strategy for finding the nearest segment (with variation of the tangent angle within +/- 20 at the nearest end point without intersecting with other segments) for one end and bind them together. Only one junction is allowed at each point.

This results in dividing the contour of the pile into regions. In each region, we check for contour segments and closed contours and classify them according to their length. We retain only long segments and discard short ones; similarly, we retain only long contours - i.e. small bounded areas are removed. The resulting contour image is shown in Figure 5 (a). Points where three curve segments meet (T-junctions) are identified using a crossing index algorithm. These points (T-junctions) will play a major part in solving the overlapping problem.

To compute the hidden part of a fragment in the second layer, a third order spline ($S(t)$) is constructed linking the two end points. Given the two end points $(x(0), y(0))$ and $(x(1), y(1))$ and tangents $(x'(0), y'(0))$ and $(x'(1), y'(1))$, $\mathbf{S}(t) = (x(t), y(t))$

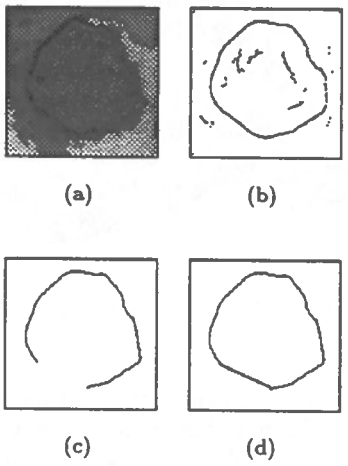

Figure 4: Result of contour completion algorithm: (a) Rock sample, (b) Complete contour of the fragment, (c) Result of overlapping, (d) Contour completion.

can be computed iteratively as follows:

$$\begin{bmatrix} x(t) & y(t) \end{bmatrix} = \begin{bmatrix} t^3 & t^2 & t & 1 \end{bmatrix} \cdot \begin{bmatrix} 2 & -2 & \xi & \xi \\ -3 & 3 & -2\xi & -\xi \\ 0 & 0 & \xi & 0 \\ 1 & 0 & 0 & 0 \end{bmatrix} \cdot \begin{bmatrix} x(0) & y(0) \\ x(1) & y(1) \\ x'(0) & y'(0) \\ x'(1) & y'(1) \end{bmatrix} \quad (1)$$

The spline $\mathbf{S}(t)$ minimizes the sum of length and curvature squared, where ξ is the speed of the spline at both $t = 0$ and $t = 1$, which varies to minimize the integral

$$\int_{t=0}^{1} (\nu + \alpha\kappa^2)\sqrt{x'^2(t) + y'^2(t)}dt$$

where κ is the curvature and ν and α are constants. Figure 4 demonstrates the result of applying this algorithm for one rock. Applying this algorithm to the image of the pile shown in Figure 3 (b), taking in to consideration that grouping of the contour segments are used to form convex rocks, and marking the junction points, the image can be decomposed into the first and second layers as shown in Figure 5.

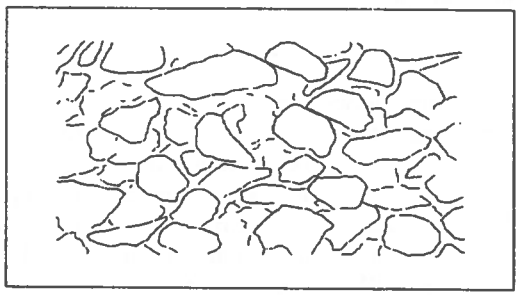

(a)

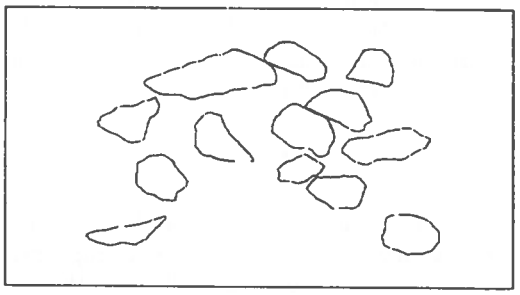

(b)

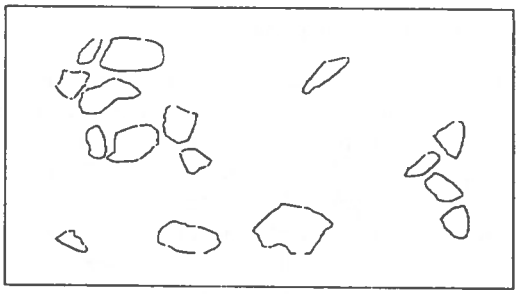

(c)

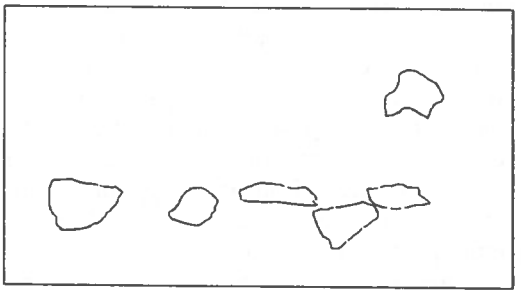

(d)

Figure 5: Contours of the rock pile: (a) Composite layers, (b) First layer, (b) First Part of the second layer, (c) Second part of the second layer

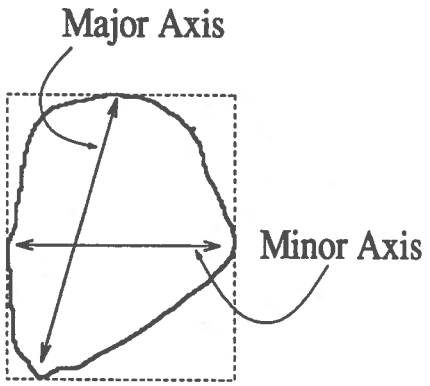

Figure 6: Major and Minor axes of a fragment

FRAGMENT SIZE MEASUREMENT

Fragment geometry and orientation are the two major factors that control the sieving process. Though both of them are non-deterministic, many researchers have tried to use a unique model for the geometry, and have ignored the orientation [Maerz et al., 1987], [Nie and Rustan, 1987], [Grainger and Paine, 1990], [Paley et al., 1990], [Farmer et al., 1991], [Doucet and Lizotte, 1992], [Schleifer et al., 1993], [Ouchterlony et al., 1990] and [Kemeny et al., 1993].

In general, fragments resulting from a blast do not possess regular shapes. This is due to the various factors that control the blasting process and the nature of the rocks (e.g. chemical composition, layer thickness, etc.). In addition, depending on its orientation, the fragment can pass through the grid in some cases whereas its passage is blocked in others. A reasonable approximation to each individual fragment is required. To derive this approximation, it is important to understand the mechanism of the sieving process. The sieving process can be viewed as size classification. For a fragment to pass through a certain grid size, the fragment size needs to satisfy certain criteria imposed by the grid.

Assuming that a fragment contour (projection on a plane) forms a regular, convex, closed curve, the fragment size can be characterized by the length of both its major and minor axes. Both the major and minor axes (A_M and A_m respectively) will be used to compute the weight function $W(t)$ which is considered the symbolic model of a fragment. These axes form a limit for the grid size S_i in which the weight function has a value different from 0 and 1, i.e. $S_i \in]A_m, A_M[\Leftrightarrow W(t) \in]0,1[$. The weight function, as will be shown in the next section, has a major role in computing the size distribution of fragments on a muck-pile surface.

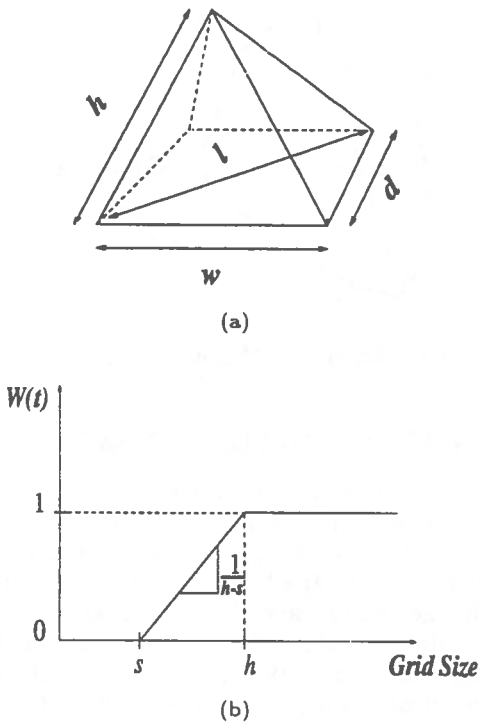

Figure 7: Size measurement: (a) Pyramid, (b) $W(t)$ verses Grid size

FRAGMENT SIZE CLASSIFICATION

Based upon the above definition, sieving can be viewed as a size measurement technique which imposes two dimensional classification criteria (the grid) on three dimensional objects. Thus sieving may be modelled using object shape descriptor(s) which are evaluated by a classification function: we can use $W(t)$, the weight function presented above, for this purpose.

The weight function $W_i(t)$ for a specific object i, depends on the orientation t, of the object with respect to the grid and its value varies between 0 and 1. In other words

$$0 \leq W(t) \leq 1$$

where t is the orientation of the object when it contacts the grid.

To demonstrate this, we consider the case of the pyramid shown in Figure 7. The parameters that control its passage through the grid at any time are l and h. (Note that l is a function of w and d.) The smallest grid size, s, which will allow passage of this object is given by

$$s = max(w, d)$$

and this grid size will only allow passage if the base of the pyramid is oriented parallel to the grid surface.

In contrast, the smallest grid size which will allow passage of this object at *any* orientation is given by the fragment's largest dimension, which is h, if $h \geq s$. Assuming then, that the grid size is less than s, $W(t)$ will have a value of zero, regardless of the orientation of the pyramid, since it cannot pass through the grid. As the grid size increases, the value $W(t)$ will start to increase from zero until it is equal to one, $W(t) = 1$ i.e. the grid will pass the object always, when the grid size reaches h. Assuming that $W(t)$ is a linear function:

$$W(d_i, t) = \frac{d_i - s}{h - s} \qquad (2)$$

The weighting remains constant at 1 for further increases in grid size. Figure 7 shows a graphical representation of $W(t)$ versus grid size for the case of the pyramid. We have chosen to approximate $W(t)$ as a straight line function.

SIZE DISTRIBUTION

The first step in determining the size distribution is the measurement of individual fragments, in terms of determining their major and minor axes, "P" and "M" respectively. The next step is to perform a "virtual sieving" analysis. Here, rather than using a simple pass/stop sieving criterion based on one length parameter as employed by previous researchers, use is made of the weighting function $W(t)$.

As in conventional sieving, we test the fragments to see which mesh (grid) size will retain them. This done by comparing the size of a particular mesh, d_j, with the interval of the weight function for a particular fragment, i, i.e. the interval between m_i and l_i. If the mesh size lies in that interval, it is *possible* that the fragment would pass through to the next size, with a probability proportional to $W_i(d_j, t)$. We can then look at the next mesh size, d_{j+1}, and check if it lies within the interval between m_i and l_i, and then propagate probabilities accordingly.

This "virtual" sieving procedure is repeated for each fragment. The size distribution can then be obtained by accumulating the probabilities of the fragments which might pass through a particular mesh size according to the following equation:

$$W_T(d_j, t) = \frac{1}{T} \sum_{i=1}^{T} W_i(d_j, t)$$

where $W_i(d_j, t)$ is computed using equation 2. However this would result in a distribution in terms of the *number* of fragments versus mesh size. In contrast, standard mining practice is to plot the distribution in terms of the *weight* of fragments versus mesh size.

We propose to correct for the weight of the fragments by multiplying the probability of a fragment passing through a size with an estimated fragment volume. One possible technique of estimating fragment volume is to calculate the volume of an ellipsoid with the same minor and major axis dimensions as the fragment.

CONCLUSION

This paper has presented an integrated methodology for completely automated image analysis of rock fragmentation. The major contributions of this research to date have been:

1. Utilization of pre-processing techniques (Crimmins filtering followed by Canny filtering) which result in a less noisy image from which to extract fragment contours.

2. Development of model-based techniques which rely upon the inherent nature of the muck-pile to simplify segmentation.

3. Formulation of contour closure techniques for estimating the contour of partially occluded fragments.

4. Automatic measurement of major and minor axes of identified rock fragments yielding shape information rather than area information typically used by other researchers.

5. Development of a weighting function based on the fragment shape information, to quantify in a probabilistic manner, the likelihood of a specific fragment passing through various mesh sizes.

Continuing work is focused on testing the robustness of this methodology under various muck-pile conditions, and comparing its performance against manual and semi-automated size distribution measurements.

ACKNOWLEDGEMENTS

This work has been partially funded by the Natural Sciences and Engineering Research Council of Canada (NSERC) under a Strategic Grant, and by the Institute for Robotics and Intelligent Systems (IRIS) under project ISDE-1.

References

[Canny, 1986] Canny, J. (1986). A computational approach to edge detection. *IEEE Transactions on Pattern Analysis and Machine Intelligence*, Vol. PAMI-8(No. 6):679 – 698.

[Chin and Yeh, 1983] Chin, R. and Yeh, C. (1983). Quantitative evaluation of some edge-preserving noise-smoothing techniques. *Computer Vision, Graphics, and Image Processing*, Vol. 23(No. 1):67 – 91.

[Crimmins, 1985] Crimmins, T. (1985). Geometric filter for speckle reduction. *Applied Optics*, Vol. 24(No. 10):1438 – 1443.

[Doucet and Lizotte, 1992] Doucet, C. and Lizotte, Y. (1992). Rock fragmentation assessment by digital photography analysis. Technical Report MRL 92-116 (TR), Mining Research Laboratories, CANMET, Val d'Or Quebec.

[Farmer et al., 1991] Farmer, I., Kemeny, J., and McDoniel, C. (1991). Analysis of rock fragmentation in bench blasting using digital image processing after blasting by photographic method. In *Proceedings of the International Congress on Rock Mechanics*, pages 1037 – 1042, Aachen, Germany.

[Grainger and Paine, 1990] Grainger, K. and Paine, G. (1990). The development and application of photographic fragmentation sizing assessment technique for blast analysis. In *Proceedings to the Third International Symposium on Rock Fragmentation by Blasting*, pages 255 – 258, Brisbane, Austria.

[Hunter et al., 1990] Hunter, G., McDermott, C., Miles, N., Singh, A., and Scoble, M. (1990). A review of image analysis techniques for measuring blast fragmentation. *Mining Science and Technology*, Vol. 11:19 – 36.

[Kemeny et al., 1993] Kemeny, J., Devgan, A., Hagaman, R., and Wu, X. (1993). Analysis of rock fragmentation using digital image processing. *Journal of Geotechnical Engineering*, Vol. 119(No. 7):1144 – 1160.

[Maerz et al., 1987] Maerz, N., Franklin, J., and Coursen, D. (1987). Fragmentation measurement for experimental blasting in virginia. In *Society of Explosives Engineers Proceedings of the Third Mini-Symposium on Explosives and Blasting Research*, pages 56 – 70, Miami, FL.

[Mastin, 1985] Mastin, G. (1985). Adaptive filters for digital image noise smoothing: An evaluation. *Computer Vision, Graphics, and Image Processing*, Vol. 31(No. 1):103 – 121.

[Nie and Rustan, 1987] Nie, S.-L. and Rustan, A. (1987). Techniques and procedures in analyzing fragmentation after blasting by photographic method. In *Proceeding of the Second International Symposium on Rock Fragmentation by Blasting*, pages 102 – 113, Colorado.

[Ouchterlony et al., 1990] Ouchterlony, F., Niklasson, B., and Abrahamsson, S. (1990). Fragmentation monitoring of production blasts of mrica. In *Proceedings to the Third International Symposium on Rock Fragmentation by Blasting*, pages 283 – 289, Brisbane, Austria.

[Paley et al., 1990] Paley, N., Lyman, G., and Kavetsky, A. (1990). Optical blast fragmentation assessment. In *Proceedings to the Third International Symposium on Rock Fragmentation by Blasting*, pages 291 – 301, Brisbane Austria.

[Saint-Marc et al., 1991] Saint-Marc, P., Chen, J., and Medioni, G. (1991). Adaptive smoothing: A general tool for early vision. *IEEE Transactions on Pattern Analysis and Machine Intelligence*, Vol. 13(No. 6):514 – 529.

[Schleifer et al., 1993] Schleifer, J., Chavez, R., Leblin, D., and Grollier, S. (1993). Grain size distribution analysis for blasting by means of image processing. In Elbrond, J. and Tang, X., editors, *Proceedings of the International Symposium on the Application of Computers and Operations Research in the Mineral Industries*, pages 361 – 367, Montreal, Quebec.

CAMI'95: 3rd Canadian Conference on Computer Applications in the Mineral Industry
Montréal, Québec, Canada, October 22-25, 1995

Telerobotics Issues in the Operation of a LHD Vehicle

Françoys Labonté, Jean-Luc Giraud, Vladimir Polotski
Perception and Robotics Laboratory
Ecole Polytechnique de Montréal,
Montréal, Québec

ABSTRACT:

Complete automation of LHD vehicles cannot be expected, at least in a short term range, and other solutions such as teleoperation and partial automation must be studied. A situation where operation modes of a LHD vehicle can alternate between supervised control (teleoperation) and autonomous control is considered. In this context the problems of path planning, path tracking, efficient data transmission, and development of teleoperation interfaces are addressed. Some perceptual characteristics of the human visual system are exploited for the improvement of data transmission protocols and for the development of efficient teleoperation interfaces. A path planning procedure based on a simplified mechanical model of the vehicle is proposed: nonholonomic constraints and articulated structure are replaced by appropriate geometrical constraints. Path-tracking controllers using a kinematic model of the articulated vehicle are also presented. A setup for the teleoperation of a reduced-size LHD vehicle is used for experimental validation of the proposed methods.

RÉSUMÉ:

Une automatison complète de véhicules chargeuse-navette (LHD) n'est pas envisageable, du moins à court terme, et d'autres solutions telles la téléopération et l'automatisation partielle doivent être étudiées. Une situation où les modes d'opération d'une chargeuse-navette peuvent alterner entre le contrôle supervisé (téléopération) et le contrôle autonome est considérée. Dans ce contexte, les problèmes de suivi de chemin, de planification de trajectoire, de transmission efficace de données et de développement d'interfaces de téléopération sont traités. Certaines caractéristiques perceptuelles du système visuel humain sont exploitées pour l'amélioration de protocoles de transmission de données et pour le développement d'interfaces de téléopération. Une procédure de planification de chemin basée sur un modèle mécanique simplifié du véhicule est proposée: les contraintes non-holonomiques sont remplacées par des contraintes géométriques appropriées. Des contrôleurs pour le suivi de trajectoire qui utilisent un modèle cinématique du véhicule articulé sont aussi présentés. Un banc d'essai pour la téléopération d'un véhicule chargeuse-navette réduit est utilisé pour la validation expérimentale des méthodes proposées.

INTRODUCTION

The automation of mining operations requires the development of autonomous and intelligent vehicles to bring back the ore from the digging sites where human presence is undesirable and hazardous. This automation may lead to significant increases in productivity, safety, and working conditions. Nevertheless complete automation cannot be expected, at least in a short term range, and other solutions such as teleoperation and partial automation must be considered.

Mining environments are often weakly structured and operator supervision is often required to accomplish complex tasks which are difficult to automate. However there also exists simpler tasks that can be accomplished without operator supervision, given the availability of appropriate automatic control tools. Flexible strategies of partial automation and teleoperation include path planning, path tracking, efficient data transmission, and development of teleoperation interfaces. These problems are addressed here in the context of the partial automation of a LHD vehicle.

Typical tasks for LHD vehicles consist in loading the ore at a digging site, hauling it to a dumping site, and going back to the digging site. This series of

tasks is performed repeatdly under the control of a human operator located on the vehicle. A complexity analysis of the tasks involved in this series of operations shows that vehicle navigation to go back and forth from one site to the other can possibly be accomplished without operator supervision. One possible method for autonomous navigation consists in following an optical guide on the ceiling (Hurteau, St-Amant, Laperrière and Chevrette 1992). Other approaches which do not require physical modifications to the environment must also be considered in order to obtain increased autonomy. For instance, it might be possible to exploit some kind of knowledge about the global topology of the mine corridors to automatically generate an appropriate trajectory. It might also be possible to rely on some landmarks already present in the mine for other purposes to generate local trajectories.

Once a trajectory is generated, the problem of path following must also be addressed. Due to various sources of errors, such as wheel slippage and positional encoder imprecision, the vehicle might not be located exactly at the position where it is estimated to be, and thus, methods to evaluate its exact position and relocate it on its trajectory must be devised.

The problems of path planning and path following are discussed in details in section 2. The proposed path planning procedure is based on a simplified mechanical model of the vehicle: nonholonomic constraints and articulated structure are replaced by appropriate geometrical constraints. Photometric cameras are used for obstacle detection. The presence of an obstacle immediately causes, if necessary, the generation of a new trajectory, which is then translated to a a new reference-path in the path-tracking algorithm. Path-tracking controllers have been developed using a detailed kinematic model of the articulated vehicle.

On the other hand, the digging and loading tasks cannot be so easily automated for LHD vehicles, and teleoperation must be considered. Teleoperator performance critically depends on his ability to obtain an accurate perception of the remote environment where the LHD is located, and on his capacity to control the vehicle operation in a natural way. In order to provide the operator with the required perceptual information, special considerations must be taken into account in the design of the teleoperation interface at the control station. For instance, depth perception can be enhanced by using a control station equipped with stereoscopic viewing capability.

Efficient data transmission protocols must also be devised in order to maximize the amount of information provided to the operator while at the same time minimizing transmission delays. In order to obtain stereoscopic viewing at the control station, the number of images to be transmitted must be doubled, and consequently image compression schemes must be considered because of the limited bandwidth of the available communication channels.

The design of efficient data transmission protocols and the conception of teleoperation interfaces are considered in section 1. The proposed approach consists in exploiting some perceptual characteristics of the human visual system for the design of image compression algorithms and for the development of user-friendly interfaces. Strategies for the dynamic allocation of spatial resolution exploit the fact that stereoscopic acuity is highest in the central region of the visual field — which generally corresponds to the current region of interest — and much lower in the periphery. A teleoperation interface consisting of a central window for the presentation of detailed stereoscopic information and of surrounding windows with additional information about the vehicle status has been developed, as well as a method for the compression of stereoscopic images.

A setup for the teleoperation of a reduced-size LHD vehicle has been constructed and used for experimental validation of the proposed methods. A low cost teleoperation station with stereoscopic display capabilities permits to control the robot from a remote location. This setup is described in details in section 3. Experimental results consist in the successful demonstration of the teleoperation of a sequence of actions such as reaching the loading destination, loading a pile of rocks, and dumping the loaded rocks at the target destination. Future works on this project are also discussed.

1 SUPERVISED LHD OPERATION

A situation where operation modes of a LHD vehicle can alternate between supervised control (teleoperation) and autonomous control is considered. Digging and loading are performed under supervised control. The mode of operation is switched to autonomous control to haul the ore at the dumping site. A teleoperation station with stereoscopic viewing capabilities is used to increase depth perception of the operator. Two important problems related to the design of this kind of control station are addressed in this section. The first one concerns the transmission of the stereoscopic information from the remote site to

the control station, and the second one the conception of the teleoperation interface. The autonomous mode of operation of the LHD vehicle is discussed in the next section.

1.1 Stereoscopic Coding

The use of a teleoperation station with stereoscopic viewing capabilities leads to an increase by a factor of two in the number of images to be transmitted. One possible solution to deal with this problem consists simply in increasing the bandwidth of the communication channels. However, the high costs associated with the expansion of these channels make this solution unattractive. Nevertheless, without any bandwidth increase, it is still possible to transmit a significant amount of information by using efficient image compression algorithms. These algorithms should exploit the intra-image spatial redundancy, the temporal redundancy, and the stereoscopic redundancy. Intra-image spatial redundancy depends on object continuity: given a pixel belonging to an object in an image, chances are that neighboring pixels belong to the same object and possess similar intensity values. Temporal redundancy is due to motion continuity: small changes are expected between successive images of a moving scene. Stereoscopic redundancy comes from the fact that the same scene is viewed from two slightly different viewpoints.

The exploitation of intra-image and temporal redundancies have been topics of investigation for a long time in the field of image coding (Jain 1989). Studies related to the exploitation of stereoscopic redundancy are more recent and less numerous. Most of the proposed stereoscopic coding algorithms use disparity compensation — the prediction of one image of the pair from disparity vectors calculated with respect to the other image —, e.g. Tamtaoui and Labit (1991), Kopernik and Pelé (1992). A major drawback associated with these methods is that accurate disparity vectors can generally only be obtained at the expense of prohibitive computation times. Since the human visual system can effortlessly perform stereoscopic matching, it might not be desirable for applications requiring fast computation times to allow some computing resources to this task. Other approaches which do not require an explicit matching between the two images of the stereoscopic pair might turn out to be more adequate.

The perceptual characteristics of the human observer must also be taken into account in the design of the coding algorithms. There already exists some algorithms which exploit the contrast sensitivity, masking effects or spectral response of the human visual system (e.g. see (N. Jayant, J. Johnston, and R. Safranek 1993)). Some properties related to stereoscopic vision such as the magnitude and spatial frequencies of disparity vectors giving rise to perceivable changes in depth have also been considered (Steurer 1992). However, there remains some properties related to stereoscopic vision that have not been fully exploited yet. It is well known that spatial and depth stereoscopic acuity is highest in the center of the visual field and decreases rapidly with retinal eccentricity. Consequently, stereoscopic acuity is highest around the fixation point of the eyes whose position highly depends on attentional processes. Based on these observations, the coding problem can be formulated in two distinct parts: the coding of a central region of interest with a detailed three-dimensional vision, and the coding of a peripheral region with less details.

We propose a coding method based on the notion of region of interest in order to limit the spatial extent of the transmitted stereoscopic information as well as its depth resolution. The method does not attempt to recover exact disparity values by means of an explicit matching process. The coding system consist of two modules and its architecture is illustrated in Figure 1. The first module is dedicated to the prediction of the location of the region of interest, which is then used by the second module to compress the stereoscopic sequence. The principal requirement for the coding algorithm is that it should lead to small reconstruction errors in the region of interest; more important errors can be tolerated for the background.

It is assumed here that the fixation points of the eyes are a good indicator of the position of the region of interest and that there exists only one region of interest at any given time. Even if these conditions are not always verified, they generally hold in typical viewing situations (Viviani 1990). One possible method to predict the position of the region of interest is to directly measure eye movements of the observer. However, delays might be introduced in the prediction loop. It can be that by the time the region of interest is presented to the operator, his focus of attention has shifted to another region in the image. This might cause some serious performance degradation for interactive tasks such as teleoperation. Another possibility is to predict the position of the region of interest directly from the content of the stereoscopic sequence. It might be possible to determine fixation points of the eyes as a function of the

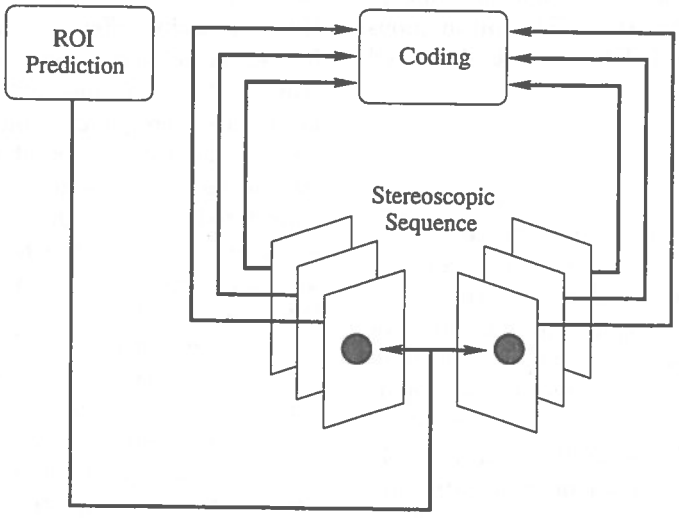

Figure 1: Architecture of the proposed coding system.

type of motion present in a stereoscopic sequence. Psychophysical experiments are currently underway to evaluate this possibility.

Once the position of the region of interest is known in both images, this information is used to encode the stereoscopic sequence. As a first step in the development of the coding module, only static stereo pairs are considered. A compatible image is created by averaging pixels at corresponding location in both images after one of the two images has been shifted in order to obtain superposition of the region of interest. A compatible image corresponds to an image that would be seen from a viewpoint between the two cameras used to capture the stereo pair (De Vleeschauwer 1991). Difference values to reconstruct both images from the compatible image are kept. These difference values are expected to be small since they correspond to the same scene viewed from two slightly different viewpoints. A wavelet transform is applied to the compatible image. Instead of truncating all the small amplitude coefficients, as is usually done in wavelet-based coding scheme, an algorithm to select the coefficients that are required to reconstruct the region of interest with small errors is proposed. Wavelet coefficients and difference values are quantized and entropy coded. A coarser quantization is applied to difference values corresponding to the background. For reconstruction, an inverse wavelet transform is performed to reconstruct the compatible image. Difference values are used to reconstruct both images of the stereo pair from the compatible image. As desired, small reconstruction errors are obtained for the region of interest and more important errors are present in the background.

1.2 Teleoperation Interface

A number of problems must be addressed for the design of teleoperation interfaces. A general presentation ergonomics must be defined. This aspect concerns the selection of the information to be presented, the spatial distribution of this information, the fusion of different sources of information, and the level of interaction of the operator with this information. The perceptual characteristics of the operator must be studied to determine the impact of transmission delays, transfer of attention, and the importance and the content of peripheral vision. The selection of presentation devices (e.g. telepresence helmet, stereoscopic display, ...) and the coupling between these devices and the sensors (e.g. a head tracker controlling camera motion) must also be considered. Design strategies and devices to provide the sensory information must be selected in order to provide the operator with sufficient information to accomplish efficiently and safely his tasks.

In order to efficiently control a LHD vehicle, the operator should perceive depth. Depth perception can be obtained by stereoscopy, which is based on the fact that the two slightly different viewpoints provided by the two eyes are used by the human visual system to infer depth. Motion parallax, which corresponds to a change in viewpoint when the head of the observer moves, should also be available to

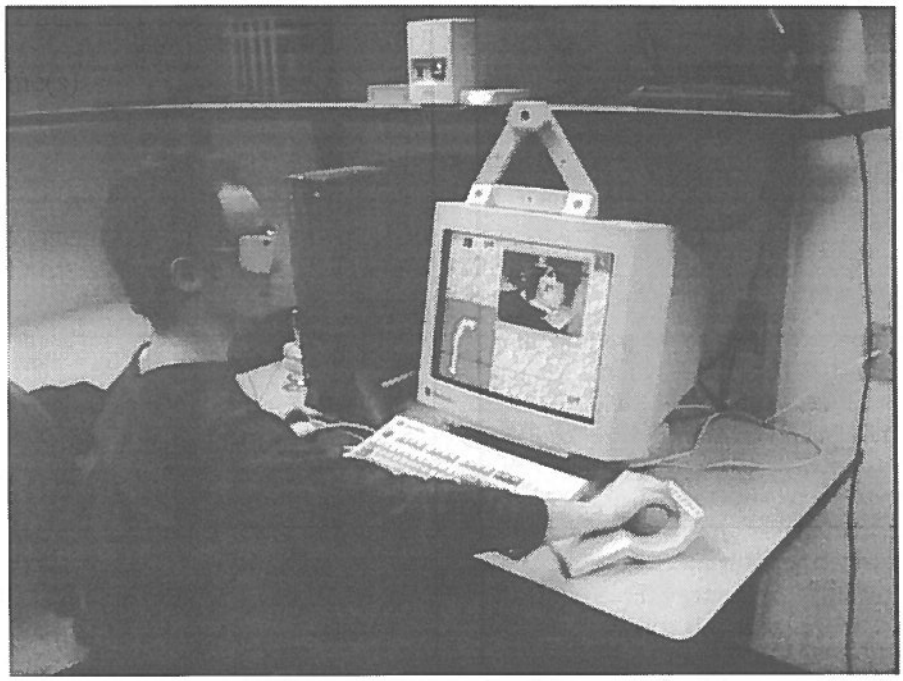

Figure 2: The teleoperation station.

the operator because it can provide important information about the structure of the scene under observation. A knowledge of the strategies used by the operator to control the vehicle can certainly be helpful for the conception of the interface. These strategies are closely related to the way attentional resources are dynamically allocated during the execution of a task. Psychophysical experiments are currently under way to study how attention is allocated as a function of the type of motion present in a stereoscopic sequence. Results of these studies will eventually lead to the development of a teleoperation interface incorporating the coding strategies based on the notion of region of interest discussed in the previous subsection.

A teleoperation interface with stereoscopic display capabilities has been developed to study the effectiveness of this mode of presentation of information for the teleoperation of a reduced-size LHD vehicle. This vehicle is described in details in section 3. Stereoscopic effects are achieved by a Silicon Graphics computer with stereo display capabilities and a pair of polarized glasses. The teleoperation station is illustrated in Figure 2. The computer is directly connected to a pair of stereo cameras located on the vehicle, and displays in real-time the scene in front of the robot. Changes in operator head position are detected by a head tracker, and control the orientation of the cameras on the robot. The operator controls the actual displacements of the robot and of the bucket with a Spaceball input device. On the screen of the control station, the central window displays in stereo the region in front of the robot. Surrounding this window, three two-dimensional windows show 3D models of the vehicle, the cameras, and the bucket. These views are provided to help the operator estimate the position in space of these elements. In addition, he can interactively examine the model representation without actually moving the vehicle in order to disambiguate confusing perceptual situations. Various control buttons and display panels are also located around this central window. The operator interacts with these buttons to control the robot and acquire information about its current state. Precise information about the vehicle status is also available in alpha-numerical format.

2 AUTONOMOUS NAVIGATION

The standard approach to vehicle control problems consists in separating them into two parts: determining where to go (path planning) and how to actually get there (path tracking). This is the general framework for robot control, or even more gener-

ally for any control system — the determination of a nominal trajectory, and the design of a controller for tracking this trajectory —. These problems are addressed here in the context of the autonomous navigation of a LHD vehicle. The most important features of this vehicle are that it has no steered wheels and possesses a single articulation between the front and the end units.

2.1 Path Planning

Typical exploitation zones in underground mines consist of corridors that are generally long and narrow, and of more or less broad halls. The problem of control (including both planning and tracking) for corridors is rather specific and has been studied by a number of researchers. In (Hurteau et al. 1992) the problem of path tracking is analyzed using an optical guide physically constituting the desired path to be followed. In (Juneau, Hurteau, Freedman and Chevrette 1993) the desired path is considered as the "skeleton" line of the tunnel. The desired position is calculated from the known width of the tunnel and from measured distances from the wall. In this case the path is obtained from local measurements, and thus need not be physically represented, by means of an optical guide for instance. This kind of planning procedure is very local; in this paper more global path planning procedure are considered, i.e. how to get from a starting location to a target location. The problem of obstacle avoidance has not been addressed in the above-mentioned approaches. This problem is particularly important when a LHD is moving in a hall. Obstacles such as pieces of rock or machines working at the same place might suddenly appear in the view field of the LHD. Obstacles locations that were unknown at planning time now become prohibited and must be avoided. Strategies for avoidance of static and moving obstacles by means of path replanning are presented in this section. The simplified kinematic model of the LHD that is used for path planning and replanning is presented first.

An articulated vehicle (AV), such as a LHD vehicle, is more complex to control than a regular car, which is kinematically equivalent to a unicycle. For the purpose of rough path planning it is sufficient to approximate an AV by the moving point of the articulation, under restrictions imposed on its velocity, acceleration and radius of curvature. The last restriction is related to the limited articulation angle of the vehicle. Namely, if the upper bound for the articulation angle is α^+ (see Figure 3) and the distance from articulation point P to the central point of front (respectively rear) wheel axe M (N) is l_1 (l_2), then the radius of curvature for admissible M-point (N-point) trajectory has lower bound $R_M^+ = (l_2 + l_1\, cos(\alpha^+))/sin(\alpha^+)$ ($R_N^+ = (l_1 + l_2\, cos(\alpha^+))/sin(\alpha^+)$). We present here both formulas because l_1 and l_2 are not necessarily equal for all AVs. The choice of a reference point (typically different for forward and backward motion), for which the path should be planned, determines the choice of the appropriate relation. The simplified kinematic model of a moving point is used for path planning. The bounded curvature guarantees that calculated trajectory can be executed by the AV.

The planning procedure consists in the determination of the sequence of primitives, which when all concatenated one after the other, constitute the desired trajectory. Each primitive can be a straight line, the arc of a circle with allowed (lower bounded) radius, a transition element, or a "folding" element which permits to change the angle between the two units of the LHD vehicle. These primitives can be followed with constant speed or constant acceleration. The lower bounded radius guarantees that the trajectory can be followed by the LHD because its articulated structure and bounded articulated angle are taken into account. The constraint on the radius is tighter than the real limitations on the shape of the LHD trajectory: they are equivalent only for stationary trajectories. The "folding" element gives the possibility to change the future direction of motion; it starts and ends with zero speed. This specific maneuver consists in changing the articulation angle of the vehicle without inducing a translational motion, i.e. in "folding" the vehicle from a straight configuration to a configuration where the front and rear units make an angle α^+. It can be executed with a fixed reference point, and therefore corresponds to a radius of zero. Such kind of maneuvers are considered in the proposed planning procedure to obtain a more realistic class of planned trajectories. In order to link together elements with different radius, transition elements are computed following a procedure proposed in (Nelson 1989). The planning procedure is applied initially to compute a path through a hall with known obstacles (forbidden areas), going from a starting point to a target point. The same trajectory can also be used to come back from the target point to the starting point.

Given a trajectory to be followed, the LHD vehicle, equipped with videosensors, repeatedly checks in the heading direction for the presence of obstacles. When the detection subsystem signals the presence of an obstacle, the obstacle relative velocity, its dis-

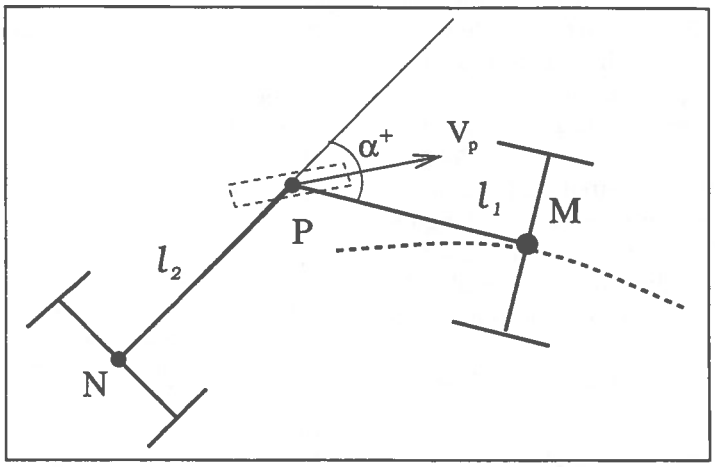

Figure 3: Kinematic model of the articulated vehicle.

tance from the vehicle, and the time and point of estimated collision are computed. For the case of moving obstacles the system generates new control laws consisting in reducing the speed (or braking if necessary) along the old path. If it is not sufficient to stop, or to reach the estimated collision point after the obstacle has left it, a new path must be computed. This path must avoid the estimated collision point and bypass this point on the side opposite to the obstacle velocity direction. In order to take into account the dimension of the LHD vehicle, obstacles are expanded, using either a circle for rough calculation, or a polygonal approximation for refined calculation. For the case of fixed obstacles, for which the estimated speed equals zero, an attempt is made to generate a new trajectory in real-time without reducing the speed of the vehicle. If this is accomplished successfully, the new path is followed. In cases for which it is not possible to generate a new path fast enough, the vehicle reduces its speed or stops until a new path is available.

For the moment there is no proof that this procedure of obstacle avoidance cannot fail (in contrast with classical cases where such proofs have been given, see e.g. (Latombe 1991)). Therefore, teleoperator intervention should be considered in cases for which the replanning procedure might fail. In these cases, the replanning procedure should be switched to a semi-autonomous mode where teleoperator assistance is used to supervise the replanning procedure. However, it is expected that operator intervention will only rarely be required and that autonomous navigation will be possible most of the time.

2.2 Path Tracking

Following a planning (or replanning) procedure, the desired trajectory becomes available and must now be followed. The path tracking procedure provides the steering actions that permit to follow the desired trajectory. The geometric path tracking approach developed in (DeSantis 1994) is used here. This procedure consists in designing a controller which stabilize the desired path in the work space. Such a controller depends on the actuator and sensor structure available for the particular vehicle under consideration. Actual LHD vehicles possess a common wheel drive and actuator controlling the articulation angle. The experimental LHD vehicle used in our laboratory and described in details in section 3 possesses an articulation actuator and four wheels which are independently controlled. This results in a redundant control structure. In order to exploit this redundancy and make possible the transfer of experimental results from the test vehicle to real ones, the analysis is divided into two phases. At first the generalized control, defined as the behavior of an imagined steered wheel placed at the articulation point (the point V_p in Figure 3), is considered. This approach makes it possible to avoid the analysis of the exact AV structure and to consider the AV as a pair of two connected tricycles. This allows to use some results obtained for tricycle-model vehicle (Hemami 1995). As a second step the generalized input is used to compute the control signal for the real actuators. Naturally, this analysis is different for industrial LHD vehicles and for the experimental LHD vehicle in our laboratory.

In order to make the vehicle follow the desired tra-

jectory, the path-tracking controller can use some information about the desired path and about the vehicle deviations from this path. It is also possible to develop a tracking algorithm based only on vehicle deviations which does not use any information about the desired trajectory (Hemami and Polotski 1995). Knowledge about the desired path curvature can also be used to significantly reduce tracking errors. The usefulness of the estimation of curvature has been demonstrated in (Juneau et al. 1993). The required amount of information to implement a particular approach depends on the required knowledge of path parameters and on the availability of sensor information.

Usually internal parameters of motion, such as wheels angular velocity and articulation angle (with its derivative), are usually available with industrial LHD as well as with our experimental vehicle. For navigation in mine corridors, external sensor information about distances from the walls (Juneau et al. 1993) can be transformed into deviations from "skeleton-lines". For navigation in the halls only internal information is available. Improvements in the estimation of the position delivered by internal sensors (odometry) can be achieved by fusing data coming from redundant sources of information (4 velocities and 2 articulation parameters among which only 4 values are independent).

Due to the relatively low speed required to operate a LHD vehicle , the kinematic model has been used for the controller design. For motion in the halls, position estimation is based on odometric data. In the case of motion in the corridors, a state observer (Brogan 1991) is used for the estimation of the vehicle offsets from the desired path under the supposition that only the lateral offset can be directly measured. Because of the observability of linearized systems, the heading offset can be reconstructed using a state observer with arbitrary fast dynamics. The pole placement technique is used for the analysis of the compound system (controller plus observer).

3 EXPERIMENTAL SETUP

An experimental setup for the teleoperation of a reduced-size LHD vehicle from a remote control station has been developed in our laboratory. The custom-made LHD vehicle, illustrated in Figure 4, possesses kinematic constraints similar to the one of an actual LHD vehicle. Its size is approximately 1 meter high, 1.5 meter long, and 60 cm wide. Ten actuators are used to operate the vehicle. It is propulsed by 4 DC electrical motors, one for each wheel. One electrical cylinder is used to control the articulation of the vehicle. Three powerful electrical cylinders control the motion of the bucket along two independent directions. The bucket can lift up to 100 pounds. The camera platform can be oriented along the pan, tilt and lift directions by three electrical motors. The vehicle possesses two batteries which give up to 10 hours of autonomy.

An on-board industrial 486DX33 PC computer with a 230 Mbytes hard disk equipped with a special suspension to minimize vibrations is used to control the actuators. Each actuator possesses one optical encoder and one Pulse Width Modulation amplifier. Three Quadrature Decoder Board, which can each be connected to 4 actuators, are used to read the optical encoders. Two Digital/Analogical boards, each with 24 digital inputs and 6 analogical outputs are used to transmit the commands from the computer to the amplifier of the actuators. An Ethernet card is used to connect the teleoperation station to the on-board computer. Commands from the control station and state information from the vehicle are transmitted via this communication card. The QNX exploitation system with the TCP/IP communication protocol is used to obtain real-time operation of the vehicle. For the moment, images from the two cameras are directly transmitted to the teleoperation station, but as mentioned in section 1.1, image coders for stereoscopic sequences are currently under development. Three independent control processes, one for each group of actuators (propulsion, bucket, camera), have been developed using PI controllers with sampling times going from 10 to 20 msec. These processes communicate through shared memory with a communication server. Special care has been taken to develop a modular and flexible architecture that can easily be modified according to the current needs. Data coming in and out of the controllers can easily be analyzed since they can be saved in a format compatible with the MATLAB software. An extensive analysis of the performance of different controllers can thus easily be achieved.

The teleoperation station has already been described in section 1.2. The teleoperation of a sequence of actions consisting in reaching a source destination, loading a pile of rocks, and dumping the loaded rocks at a target destination, has been accomplished successfully. Future works include comparative studies of the performance of different controllers and of different path planning algorithms, the incorporation of a compression module for the transmission of stereoscopic sequences, and studies related to the

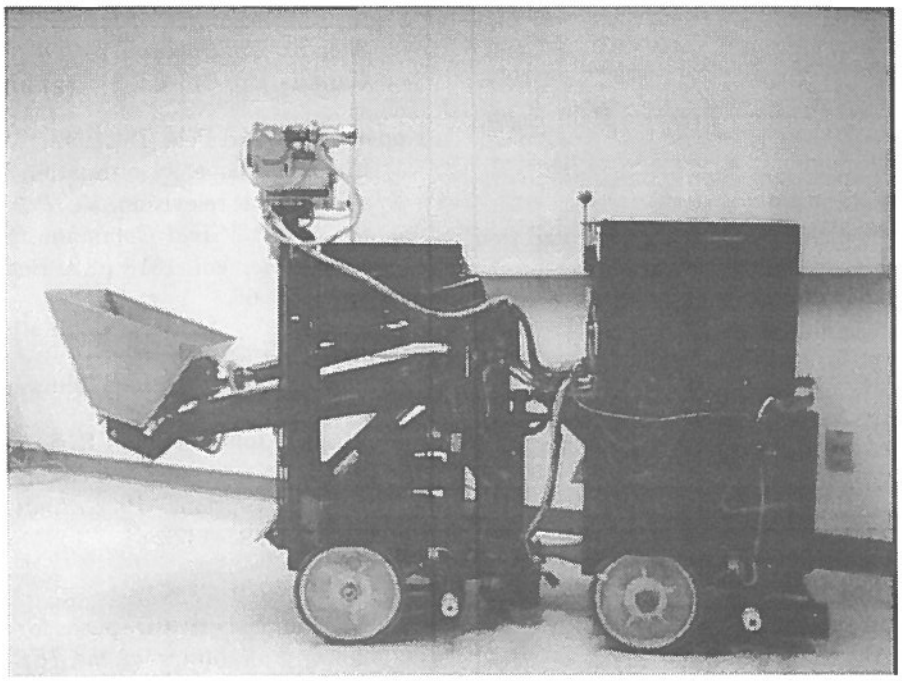

Figure 4: The reduced-size LHD vehicle.

ergonomics of the teleoperation station and to operator performance.

ACKNOWLEDGMENT

This work is supported by the NSERC-Noranda Industrial Chair in Mining Automation. F. Labonté is supported by a FCAR scholarship.

REFERENCES

Brogan, W., 1991
Modern Control Theory, Prentice Hall, Englewood Cliffs, NJ.

De Vleeschauwer, D., 1991
Coding of the disparity field and the correction signal in predictive 3DTV coding, *Proceedings of the 1st International Festival of 3D Images*, Paris, France, pp. 213–221.

DeSantis, R., 1994
Path-tracking for a tractor-trailer-like robot, *International Journal of Robotics Research* **13**(6), 533–544.

Hemami, A., 1995
Steering control problem formulation of a tricycle-model vehicle, *To appear in International Journal of Control.*

Hemami, A. and Polotski, V., 1995
Path tracking control problem formulation of an LHD-loader, *Submited to International Journal of Robotics Research.*

Hurteau, R., St-Amant, M., Laperrière, Y. and Chevrette, G., 1992
Optical guidance system for underground mine vehicles, *Proceedings of the IEEE International Conference on Robotics and Automation*, Nice, France, pp. 639–644.

Jain, A., 1989
Fundamentals of digital image processing, Prentice Hall, Englewood Cliffs, NJ.

Juneau, L., Hurteau, R., Freedman, P. and Chevrette, G., 1993
Using laser range data to model tunnel curvature for the automatic guidance of a mining vehicle, *Proceedings of the Second IEEE Conference on Control Applications*, Vancouver, BC, Canada, pp. 643–648.

Kopernik, A. and Pelé, D., 1992
Improved disparity estimation for the coding of stereoscopic television, *VCIP'92. Proceedings of the SPIE: Visual Communications and Image Processing*, Vol. 1818 pt.3, Boston, MA, USA, pp. 1155–66.

Latombe, J., 1991
Robot Motion Planning, Kluwer, Boston.

N. Jayant, J. Johnston, and R. Safranek, 1993
Signal compression based on models of human perception, *Proceedings of the IEEE* **81**(10), 1385–1422.

Nelson, W., 1989
Continuous-curvature paths for autonomous vehicles, *Proceedings of the IEEE International Conference on Robotics and Automation*, Nice, France, pp. 1260–1264.

Steurer, J., 1992
Coding stereoscopic images for the human observer, *Proceedings of the European Workshop on 3DTV Signal Processing*, Rennes, France.

Tamtaoui, A. and Labit, C., 1991
Constrained disparity and motion estimators for 3DTV image sequence coding, *Signal Processing: Image Communication* 4(1), 45–54.

Viviani, P., 1990
Eye movements in visual search: Cognitive, perceptual and motor control aspects, *in* E. Kowler (ed.), *Eye movements and their role in visual and cognitive processes*, Vol. 4 of *Reviews of oculomotor research*, Elsevier, chapter 8.

11.

mining infrastructure
infrastructures des mines

CAMI'95: 3rd Canadian Conference on Computer Applications in the Mineral Industry
Montréal, Québec, Canada, October 22-25, 1995

System Safety Principles for the Design of Underground Mobile Machine Systems

Glenn Atkinson
Ontario Natural Resources Safety Association
North Bay, Ontario

Malcolm Scoble
Department of Mining and Metallurgical Engineering
McGill University, Montreal, Quebec

ABSTRACT:

In the search for both efficiency and personnel safety several mining companies are investigating mining machine automation strategies. This paper proposes that the principles of system safety be incorporated into the concept and design of these automated machine systems in order to fully realize the potential safety benefits. Background information in system safety and selected hazards related to automated mining systems are presented. A discussion of factors related to hazard analysis and risk assessment follows. Software failure modes, software failure risk classification methods used in other industries, as well as human factors issues are considered. The paper concludes with what are considered to be key issues to be addressed in future research and development of mining automation machine systems.

Introduction:

Mobile machines in underground mines have become larger and more powerful in the search for economies of scale. An example of this is the current size of LHD and haulage trucks that are used in hard rock bulk mining methods. This current phase of mechanization is likely to be followed by the teleoperation and eventual robotization of such machines. Teleoperation has the potential to increase the safety of the operator by relocation to a less hazardous environment. In order to do so a system safety evaluation should be carried out to identify, analyze, and control unacceptable health and safety risks, prior to implementing such systems. This is of particular importance in the transition to automation with our limited system operating experience. If a hazard related to teleoperation were to result in a serious injury in this early mining automation phase, then the effect may be to seriously retard any further advancement of automation and the resulting potential benefits to safety.

Many existing base and precious metal mines struggle to extend their underground reserves, invariably by deepening. This leads to operating bulk mining equipment in more stressed and often rock burst prone ground. [Scoble 1994] One approach to dealing with risk to the underground machine operator is to relocate the operator from this environment through the teleoperation of mining machines. The system safety related to mining at depth as well as other possible demanding future operating environments should be identified and accounted for in the automated system. This transitional phase of automation will still require the intervention of personnel underground for breakdown maintenance and work in non-automated adjacent developments. Currently work is being done by a number of companies to introduce mine machine automation in varying degrees.[AUTOMIN 6, 1994] This paper does not investigate the rationale underlying this, but rather considers the safety implications of automating these systems.

A preliminary safety analysis for a teleoperated mining machine system has been initiated jointly by the Ontario Natural Resources Safety Association (ONRSA), INCO Ltd. and McGill University. Since this analysis is in

progress all the needs and issues have not necessarily been identified and addressed. It is clear however that the success of implementing underground automation will be very sensitive to any incidence of accidents or unanticipated safety hazards.

This paper intends to present background information in system safety, note selected hazards identified to date, and propose factors to consider in assessing the risks associated with these. The hazards are considered to result from either hardware, software, or human error. A discussion of methods to assess the risks associated with software failure follows. The paper concludes with a list of outstanding issues that will be investigated in the future.

System Safety

Traditional safety is more a reaction to an event, (accident) rather than a planned, coordinated procedure to control losses. Traditional safety practitioners often use accidents to identify where hazard controls are required. This approach led to the viewpoint that "regulations are written in blood". [Stevenson 1991] Throughout industrialization, technology, management concepts, and society as a whole advanced, however, safety practices had remained relatively unchanged. After the onset of the atomic age, a more exacting, planned and systematic approach to accident prevention was needed. The U.S. Air Force and the aerospace industries recognized the need for system safety and developed MIL-STD-882 in 1969. [MIL-STD-882] From this beginning , system safety principles and techniques are now being broadly adopted by standard and regulatory writing bodies. [Manuelle 1994] System safety is based in the concepts that:

- accidents result from numerous interacting causes
- each accident cause and interaction can be logically identified and evaluated
- solutions can be developed to control each cause. [U.S. Dept. Of Labour 1986]

Stevenson gives this definition of system safety:

> "...the effort to make things as safe as is practical by systematically using engineering and management tools to identify, analyze, and control hazards." , [Stevenson 1991]

There are over 90 documented hazard identification techniques listed in the System Safety Society handbook. [System Safety Analysis Handbook 1993] These can be classified as either inductive or deductive hazard identification techniques. Inductive methods pick a starting point, e.g. a component failure, and identify the related consequences. Examples from this suite of techniques are: What If analysis and Failure Modes and Effects Analysis (FMEA). Deductive methods start with an undesireable event (e.g. accident) and determine the causes or combinations of causes that led to this event. Examples of deductive techniques are Fault Tree Analysis (FTA) and Event Tree Analysis.

An inductive technique is often used to identify hazards at the concept and early design phase. The techniques typically reduce a system to be analyzed into groups of increasingly smaller subsystems. Each of these subsystems are studied, often by a team of specialists, to identify adverse system effects that could be initiated by a behavior or failure mode of the subsystem. Each technique provides a process to follow to ensure systematic coverage of hazard identification.

Use of hazard identification techniques assumes there is a design sufficiently complete to be analyzed. A conceptual design can be evaluated using less sophisticated techniques to identify gross system hazards. As the detailed design progresses, more specialized hazard identification techniques can be used depending on the nature of the hazard, and the type of system being analyzed. The process of hazard identification, risk assessment and control is integrated throughout the design process. The result is a design that has been influenced from the concept phase through detailed design to minimize risk.

This is the process currently underway among ONRSA, INCO Ltd. and with McGill University collaboration in developing a traffic control system for teleoperated mining machines. A technique used to date is a form of HAZOP analysis. This technique identifies the design intention of each of the traffic control subsystems and applies the HAZOP guide words of no, more, less, as well as, other than, part of, and reverse, to these in order to help create images of possible adverse effects. One hazard identified in the preliminary hazard analysis (PHA) is that of collision between an automated machine and a non-automated machine or pedestrian. At a point when the design is further defined, a deductive technique like Fault Tree Analysis (FTA) could be used to identify all the causes or combination of causes that could lead to this undesired top event (collision).

Mining Hazards

Mining hazards include those that could result in losses to people, equipment, material, or the environment. These can be broadly classified as hazards that result in possible injury, and other losses. The focus of this paper is on hazards resulting in injury to personnel. Underground mobile machine systems pose several hazard considerations. The environment comprises a series of underground development excavations serving as the means of ingress/egress for normal and emergency requirements and also as ventilation ducts. Fires underground present a major risk to personnel. LHD and haulage truck fires are not uncommon in conventional mining practice, [MOL 1993], and are usually extinguished by the operator prior to becoming a substantial loss. When electronic hardware and software is used to automate these machines, then fire potential, and its effect on other personnel in the mine, both from smoke inhalation and possibly blocking a critical means of egress, must be considered.

Automated mobile machines represent substantial mass and energy relative to pedestrians or personnel vehicles which may require access into automated zones. One major hazard is collision between an automated and non-automated machine or pedestrian. Some form of human tolerant traffic control will be required. Human tolerant refers to a design that does not include a single point failure opportunity directly related to human judgement or reflexes. This system must also incorporate the ability to respond to an emergency situation that may develop either inside or outside the automated zone. Performing breakdown maintenance is another mode of system operation that requires analysis. In this mode the machines may behave unexpectedly and pose hazards to those in the immediate vicinity or those that must approach the vehicle for diagnosis and repair.

Evaluating Risk and Performance

The risk estimation for an identified hazard involves weighing a number of factors that affect the severity of hazard consequences, and the probability that these consequences will occur. [CSA Q634 1992] It is considered that risk estimation should consider but not necessarily be limited to the following.

The probability of occurrence is considered to be a function of the *frequency and duration of exposure*, the *probability of occurrence of a hazardous event given exposure*, and the *possibility to avoid or limit harm.*

Frequency and duration of exposure:
Consider the personnel that could be affected by the machinery. Factors such as the time spent in the danger zone, the number of persons requiring access and the frequency of access should be considered.

Probability of occurrence of a hazardous event given exposure:
Consider all modes of machine operation such as but not limited to; commissioning, start-up, operation, maintenance, shut-down, and disposal. Is it necessary to suspend safety functions during maintenance, and is any operating and accident history available for similar systems? Is reliability information available? Finally, what is the ability for personnel to defeat the safety measures? Is there an incentive to defeat or circumvent the safety measures? Does the safety device slow down production, interfere with other activities or preferences of the operator? Is it difficult to use, are other persons than the operator involved, and is the safety device recognized or accepted for its function? Is the safety device easy to maintain? If the safety devices can not be maintained then this can encourage defeat of the safety measure to allow continued use of the machinery. Programmable electronic systems introduce an additional possibility to defeat them if access to the safety related software is not properly designed and monitored. Risk estimation should identify where safety related functions are not separated from other machine functions.

Possibility to avoid or limit harm:
Does the hazardous event appear suddenly or slowly? How are personnel made aware of the risk: by general information, direct observation, or through indicating devices? Would it be characterized as possible, possible under some circumstances, or impossible for the personnel to avoid the hazard consequence using reflexes, agility, or a possible escape route? Finally, does the operator have experience and knowledge of the machinery, similar machinery or have no experience?

Hazard Control:

The reliability and effectiveness of any recommended control should be appropriate to the risk presented from

the hazard. For example, if a particular hazard consequence is assessed as causing a critical injury, and likely to occur several times over the life of the system, a control strategy using only procedures, training, and personal protective equipment (P.P.E.) would be insufficient. A higher order of control would be necessary which may be supplemented with training. A widely accepted order of precedence for hazard control is: design to eliminate or reduce the hazard, safety devices, warning devices, and P.P.E. and training. [Roland 1990]

Although training, experience and ability can affect the risk, none of these factors should be used as a substitute for hazard elimination, risk reduction by safe design or safeguarding where these measures can be implemented.

Nature and Applications of Software Tools

Software is being used increasingly for system logic and to facilitate automation of mining machines. Computers and software have the potential to provide increased versatility and power, improved performance, greater efficiency, and decreased cost. The extent that computers may increase safety is a matter of current debate. Even when a computer can improve safety, the end result may not be an increase in the safety of the system. For example, although technological improvements reduce the possibility of aircraft accidents substantially, they also allow those making the decisions to run greater risks in search of increased performance.[Leveson 1986]

Many of the system safety techniques that have been developed to analyze electromechanical systems do not seem to apply when computers are introduced. The major reasons stem from the differences between hardware and software. System safety techniques are primarily designed to cope with random system component failures. Human design errors are not considered since these have been eliminated through extensive prior use and experience. This is not the case for software which is often application specific.

The risk assessment used for system hazards, excluding software, relies on assessing the probability and severity of the hazard consequence. For hazards associated with software it is difficult at best to determine the probability of a hazard. One approach suggested by the MIL-STD-882C is to consider the potential severity and the degree of control that software exercises over the hardware. The degree of control is defined using software control categories. These are defined in the MIL-STD-882-C as;

I) Software exercises autonomous control over potentially hazardous hardware systems, subsystems or components without the possibility of intervention to preclude the occurrence of a hazard. Failure of the software or a failure to prevent an event leads directly to a hazard's occurrence.

IIa) Software exercises control over potentially hazardous hardware systems, subsystem, or components allowing time for intervention by independent safety systems to mitigate the hazard. However, these systems by themselves are not considered adequate.

IIb) Software item displays information requiring immediate operator action to mitigate a hazard. Software failures will allow or fail to prevent the hazard's occurrence.

IIIa) Software often issues commands over potentially hazardous hardware systems, subsystems or components requiring human action to complete the control function. There are several, redundant, independent safety measures for each hazardous event.

IIIb) Software generates information of a safety critical nature used to make safety critical decisions. There are several, redundant, independent safety measures for each hazardous event.

IV) Software does not control safety critical hardware systems, subsystems, or components and does not provide safety critical information.

In reference to chemical process plants [Dombrowski 1991] suggests five classes of interlock on the basis of the hazard consequence potential for damage. The highest class interlock , class A, is designed to prevent personnel injury or a significant environmental release of hazardous material. Interlocks in this class have no other approved independent backup system if the primary safety interlock fails. The lowest class of interlock includes low risk categories that are designed to prevent minor equipment damage and insignificant production losses. A corresponding set of design requirements is presented for each class of interlock. For example, one option for class A interlocks is a two-out-of-two voting scheme with non-identical microprocessors, sensors, and programming by two independent programmers. Further details of this approach can be found in the references. Essentially the risk estimation for software safety classifies only the

potential severity of consequences since it is deemed to be impractical and perhaps unrealistic to assess the probability for software failure.

The application of fault tolerant techniques through redundant software may not increase safety enough to justify the cost of producing multiple versions of the software. [Leveson 1986] Perhaps the most important consideration is that most fault tolerant methods do not solve the problem of erroneous requirements. Determining the requirements for software is a major source of software problems and may be the most important with respect to safety. Functional requirements often focus on what the system shall do, safety requirements must also include what the system shall not do.

Software control faults may involve

- failure to perform a required function
- performing a function not required.
- timing or sequencing problems
- failure to recognize a hazardous condition requiring corrective action
- producing the wrong response to a hazardous condition

There are a number of techniques that can be formally applied in the validation of software for safety. (Fault Tree Analysis, Petri Net Analysis, Sneak software analysis)[Leveson 1986] There are advantages and limitations to each of these. In general there is also the danger in over-emphasizing the models and forgetting the many assumptions that are implied. Another problem cited with formal safety assessment is the "Titanic effect." The Titanic was thought to be so safe that some normal safety procedures were neglected, resulting in the loss of many more lives than may have been necessary. The Titanic had five water tight cells rupture and there had never before been an accident where more than four water tight cells had ruptured. The mistake was in placing too much faith in the assumptions and the models and not in taking measures in case they were incorrect.

The goal stated by Nancy Leveson is to reduce the amount of software that affects safety. (And thus reduce the verification effort involved)

Human Factors Issues

From a system safety perspective human factors must be considered in a much different way than hardware elements. Hardware elements respond largely as a two step model, a simple stimulus-response type reaction. Generally speaking, if a stimulus is applied to a human, there are a wide variety of responses other than simply "doing", or "not doing". There is a mediation step after the stimulus where the person thinks over the decision on the basis of prior knowledge, goals, experience, emotions, and other factors. This mediation process has two effects, it introduces delays and provides potential for a wide range of responses. Hardware is designed to withstand the anticipated stresses of its operating environment. e.g. temperature, pressure, vibration etc. Additional stressors which affect the operator such as emotion, physical and mental stresses play a role in their response. Essentially, when dealing with humans in system safety, there are much higher failure rates and much wider variability in those failure rates both from person to person and within the same individual at different times. In a simulation evaluating almost 1000 operator actions, 66% fall into the simple "did do" and "did not do" choices typically included in an operator action event tree. The remaining 34% of the actions were almost evenly distributed among actions that led to a more favorable outcome, had no direct effect on outcome, and actions which led to an unfavorable outcome.[Nertney, R.J.1985] This last option requires special attention by the safety analyst since it represents the opportunity for a catastrophic loss.

One qualitative method to assess the potential effect of humans on the system is to look at the places where the human is expected to take action. This involves the resolution of required human design intervention into sequences of tasks, then individual tasks, and steps to complete the task. The probability of the operator making a mistake is judged as being high or low, and if they do make a mistake whether the consequences are likely to be high or low. This process is intended to locate those steps in which the operator taking action might or might not cause an adverse system condition or loss.

An assessment of the likelihood and severity of consequence is estimated for the eventuality that the entire sequence of tasks is not performed or performed in a manner other that intended. This same process is then applied to each of the tasks, and the steps for each of the tasks. There are two advantages to this technique. First a comparison can be made to note if any individual steps, or tasks, had a higher estimated risk than the entire sequence of tasks that they comprise. This would prompt the analyst or team to review those discrepancies.

Secondly, the specific steps within a task that pose the greatest risk are identified and can be the focus of hazard control effort.

The human factors safety analysis is valid only for the system design used in the analysis. Any changes made to the system in terms of people, procedures, management controls, or changes in hardware can invalidate any of the analytical results. The tighter or more controls applied to a system, then the more sensitive it becomes to changes.[Woods D.D. 1994] It is worth noting that when designing fully automated systems, human errors reflect back into the system through system maintenance, installation errors, and software programming.

Some specific human factor issues related to teleoperated mining machine systems are considered to be the following. For teleoperation of multiple machines the ability to switch from one type of machine to another without confusing the various functions of the controls available on the console is a key challenge. Another issue is the lack of, or incomplete sensory feed back when the teleoperator is removed not only spatially but also temporally, functionally, and cognitively from the process. Teleoperators are also often aware of an unnatural sensation or dizziness caused by the small but perceptible time lags between the time a command is issued to the time the machine actually responds.[Golde1994]

Questions have been raised in Europe as to whether the human controller who has to intervene in an exceptional case will be properly placed and able to do so. A study of an automated steel plant in the Netherlands [Leveson 1986] found serious productivity problems resulting from the changed role of the human operators. The operators did not know when to take over from the computer, and they became unsure of themselves.

The current evidence appears to be that, although humans do make mistakes, computers also make mistakes, and removing humans totally from the loop in favor of so called expert systems or total computer control is probably not desirable.

Key issues & future R&D

To design an effective, efficient and safe mining automation system we should incorporate system safety principles throughout each phase of the project. The capacity and limitations of people, hardware and software, must be recognized and analyzed within the context of the design mission and the operating environment. System safety offers an abundance of techniques that have been adopted in various forms for the chemical, nuclear, U.S. Air Force, and military. The challenge is to select a process and suite of tools to assist the systems engineer to identify and assess hazards for each unique system and control these to an acceptable level of risk.

The ONRSA, INCO Ltd., and McGill University have initiated a process to use the principles of system safety in the development of teleoperation of underground mining machines. This analysis is not complete at present and therefore we have not identified all the needs and issues to date. Some of the outstanding key issues relating to underground mobile machine systems to be addressed are: machine fires, machine recovery and maintenance, emergency response, extent and form of human supervisory control, and the traffic control system associated with the interaction both between machines and between machines and humans. It is clear however, that the success of implementing underground automation will be very sensitive to any incidence of accident or unanticipated safety hazard.

References:

AUTOMIN 6, 1994
Proceedings of the 6th Canadian Symposium on Mining Automation, Canadian Center for Automation and Robotics in Mining (CCARM), Montreal, 16-19, September, 1994

CSA-Q634-M92, 1991
Risk Analysis Requirements and Guidelines, Quality Management A National Standard of Canada, Rexdale, Ontario

Dombrowski, L.R., 1991
Separation of Interlocking and Regulatory Control in Programmable Electronic Systems, Instrumentation Society of America, Volume 30, Number 4

Golde, P. And Scoble, M., 1994
Teleoperation and Human Factors in Underground Hardrock Mining, 6th Canadian Symposium on Mining Automation, CCARM,

October 16-19, 1994, Montreal

Gowen, L.D., Collofello, J.S., 1995
Design-Phase Considerations For Safety-Critical Software Systems, Professional Safety, Journal of the American Society of Safety Engineers, April 1995

Leveson, N., 1986
Software Safety: Why, What, and How, Department of Information and Computer Science, University of California, Irvine

Manuele, F., 1994
Future Directions for the Practice of Safety, ONRSA, Mining Health and Safety Conference, May 5, 1994, Toronto

MIL-STD-882C, 1993
Military Standard System Safety Program Requirements, U.S. Department of Defence, Global Engineering Documents, Emglewood Califronia

Ministry of Labour, 1994
A Summary of Accidents Involving Underground Mobile Vehicles in Ontario mines for the Year 1993, Mining Health & Safety Program, Sudbury, Ontario

Nertney, R.J. and Horman, R.L., 1985
The Impact of the Human on System Safety Analysis, DOE 76-45/32, SSDC-32, United States Department of Energy, pp 12-16

Roland, H.E., and Moriarty, B., 1990
System Safety Engineering and Management, 2nd ed. "A Wiley-Interscience publication" pp 12-17

Scoble, M., 1994
"Competitive at Depth:Re-engineering the Hardrock Mining Process", Proceedings of the 1st North American Rock Mechanics Symposium, University of Texas at Austin, 1-3 June, 1994, P.P.Nelson ed., Balkema, Rotterdam, pp 35-46.

Stevenson, J., 1991
System Safety 2000, A Practical Guide for Planning, Managing, and Conducting System Safety Programs. Pub. Van Nostrand Reinhold, pp 13

System Safety Society, 1993
System Safety Analysis Handbook, 1st ed. System Safety Society, Albuquerque, New Mexico

U.S. Department of Labour, 1986
System Safety Engineering, Safety Manual No. 15, Mine Safety and Health Administration, National Mine Health and Safety Academy.

Woods D.D., Johannesen L.J., Cook, R.I., and Sarter N.B., 1994
Behind Human Error: Cognitive Systems, Computers , and Hindsight, Crew System Ergonomics Information Analysis Center, Wright-Patterson Air Force Base, Ohio, pp. 28, 48-50

CAMI'95: 3rd Canadian Conference on Computer Applications in the Mineral Industry
Montréal, Québec, Canada, October 22-25, 1995

EOLAVAL - An Integrated Mine Ventilation Design Software

Kostas Fytas
Department of Mining & Metallurgy
Laval, University, Québec

Pierre Thibault,
Quebec Mining Association Inc.

ABSTRACT

This paper presents EOLAVAL, an integrated mine ventilation design software. It is a user friendly fully interactive computer package which can be used to carry out the following aspects of underground mine ventilation design : mine ventilation network analysis and simulation, economic design of an airway, auxiliary ventilation design, calculation of a mine air heating plant, and evaluation of pressure losses in a mine shaft. This paper concludes with the presentation of a case study illustrating the use of the computer package in mine ventilation design.

RESUMÉ

Cet article présente EOLAVAL, un logiciel intégré de conception de ventilation minière. Il s'agit d'un logiciel convivial et complètement interactif qui peut être utilisé pour effectuer les aspects suivants de conception de ventilation minière : l'analyse et la simulation des réseaux de ventilation minière, le dimensionnement économique d'une conduite, la conception de ventilation auxiliaire, la conception de systèmes de chauffage et l'évaluation de pertes de pression dans un puits. Cet article conclut avec la présentation d'un exemple pratique qui montre l'utilisation du logiciel dans la conception de ventilation minière.

INTRODUCTION

Mine ventilation planning is an important part of the overall mine planning process. Computer simulation of ventilation networks has been one of the earliest applications of computer technology into mine planning. Since then computer assisted ventilation planning is a routine practice in all underground mines. Computer simulation of ventilation networks is very important in evaluating various alternatives in mine ventilation (Hartman, 1982) such as :

- evaluation of alternative ventilation paths;
- evaluation of alternative shapes and sizes of ventilation raises and shafts;
- choosing the appropriate type and location of mine fans;
- choosing the appropriate type of fans and duct sizes for auxiliary ventilation.

EOLAVAL is a user friendly, fully interactive computer package for mine ventilation planning. It can be used to carry out the following aspects of underground mine ventilation design (Figure 1) :

- mine ventilation network analysis and simulation;
- evaluation of mine shaft pressure losses
- economic design (shape and size) of an airway (shaft, ventilation raise, ramp or drift);
- auxiliary ventilation design;
- calculation of mine air heating plants;
- evaluation of fan operating point as a function of temperatures (dry and humid) and barometric pressure.

MINE VENTILATION NETWORK ANALYSIS AND SIMULATION

Ventilation network analysis and simulation involve the following steps :

- creation of the network data file;
- preparation of a data file for the simulation;
- simulation of ventilation network;
- evaluation of alternative ventilation paths using simulation;
- choosing the best (in terms of head losses) ventilation configuration.

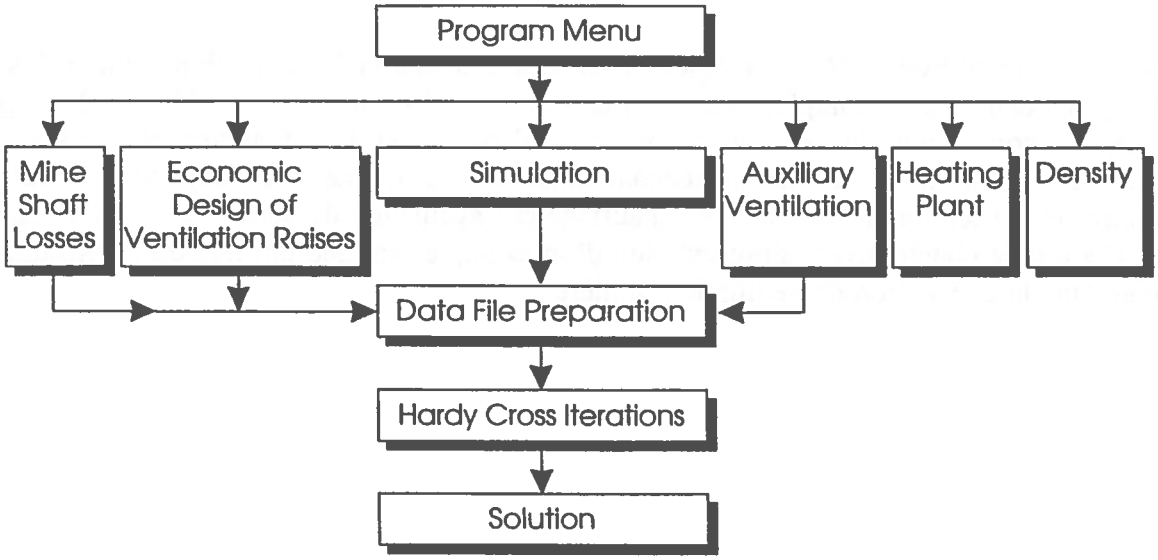

Figure 1 - Flow chart of EOLAVAL program

Creating and editing the network data file.

The user has two options : either to create a new data file or to edit an existing one. Creating a new data file is completely interactive; the user enters the following data for the ventilation network :

- number of branches and nodes;
- for each branch the user is prompted to enter the following :
  - branch number
  - initial node
  - end node
  - branch name
  - branch surface
  - branch perimeter
  - friction factor (K)
  - shape factor
  - branch length
  - air quantity (initial estimation)
  - fixed quantity branch (yes or no)

In editing an existing data file the user has the following options :

- add a new branch;
- add a new node;
- eliminate a branch;
- eliminate a node;
- modify the attributes of a specific branch.

Editing of an existing file is completely interactive and a new data file is created at the end of each editing session.

Preparation of a data file for the simulation.

It is a preliminary step where EOLAVAL creates a simulation data file using the initial network data file. The preparation of the simulation data file involves the calculation of the branch resistances from their geometrical characteristics (surface, perimeter, friction factor, shape factor and length) and the verification of air quantity balance for each node.

Simulation of ventilation network.

This is the final step where EOLAVAL simulates and balances the ventilation network using the Hardy-Cross method. The output from this simulation involves the following information :

- summary of data file;
- summary of resistance data file;
- head losses for each branch;
- regulator and fan requirements in the network;
- final air quantity in each branch.

Evaluation of alternative ventilation paths using simulation.

There are several ways in ventilating an underground mine. The ventilation engineer however should choose the ventilation configuration which corresponds to the lowest pressure losses. Therefore, the evaluation of several alternative configurations is of paramount importance to the design of an efficient ventilation network. This is particularly important when designing future expansions of the ventilation network as the mine evolves through time. This is going to be further illustrated in the practical example of this paper.

EVALUATION OF MINE SHAFT PRESSURE LOSSES

It is well known that in a typical mine ventilation network the resistance of mine shafts may account for 40% to 90% of the

mine total resistance (McPherson, 1993). It is therefore very important to calculate shaft losses as precisely as possible especially when designing a new mine. EOLAVAL offers the possibility of analytically calculating these losses using the analytical formulas developed by McPherson.

The user enters interactively the geometrical characteristics of the mine shaft (such as surface, perimeter, length, air quantity, air density, surface and configuration of buntons, cables, pipes and guides, speed of conveyances and their configuration). The computer output involves the total friction and chock losses along with the equivalent friction factor (K) of the mine shaft.

ECONOMIC DESIGN OF AIRWAYS

One of the most efficient ways in lowering the cost of ventilation of a mine lies in the right selection of the size and shape of the airways since these two variables are closely related to the head losses due to friction. It is therefore very important for the ventilation engineer to consider many alternatives of airway shape and size in order to minimize energy costs. This is particularly true when designing new expansions of the ventilation network.

EOLAVAL allows the user to optimize the dimensions of a ventilation raise by examining several alternatives in terms of shape and size. The user enters the length of the raise, mine life, interest rates, friction factor (K), airflow and electricity costs. The program has built-in several shape and size options (ex. circular, rectangular, driven conventionally, by long holes, by the Alimak method, etc.) with their corresponding excavation cost (per m^3 or pi^3). These costs can be modified by the user. Subsequently, EOLAVAL calculates the yearly ventilation cost (excavation and operations cost) according to the procedure outlined by Mutmansky (in Hartman, 1982), for a single and a double ventilation raise. It is then up to the ventilation engineer to choose the best alternative of shape and size also taking into account other specific considerations. This is also illustrated in the practical case study of the paper.

AUXILIARY VENTILATION DESIGN

EOLAVAL also allows the user to design auxiliary ventilation systems by choosing the fan and tubing dimensions. The user enters the following data related to the auxiliary ventilation requirements :

- air quantity requirements;
- total tubing length;
- tubing configuration (standard length and fittings);
- tube diameter;
- tubing type (ex. rigid, flexible, flexible reinforced).

EOLAVAL has built-in the friction and chock losses as a function of the tube diameter for each type of tubing. It produces an output which specifies the auxiliary fan characteristics (head, air quantity) for the particular application. If the required air quantity is not compatible with the specifications of a certain tubing diameter the user is prompted to modify the type and diameter of tubing.

CALCULATION OF MINE AIR HEATING PLANTS

The design of a heating system for mine ventilation is an essential part of the mine ventilation design process in Québec and all over Canada. EOLAVAL allows the ventilation engineer to design a mine air heating plant taking into account the climatic conditions of the mine site. The user is prompted to enter the following data :

- duration of heating system operation (months);
- average temperature for each month;
- desired air temperature entering the mine;
- air quantity.

Based on the above data, EOLAVAL computes the power and energy requirements of the heating plant per month and for the total heating period.

EVALUATION OF AIR DENSITY FLUCTUATIONS

The operating point of the mine main fan may change as air density fluctuates. EOLAVAL provides for the evaluation of density fluctuation effects on the fan operating point. The user is prompted to enter the dry and humid air temperatures along with the barometric pressure. He also enters the fan operating point (quantity of air, fan head) at standard conditions. EOLAVAL computes the air density using the psychrometric formulas and then it calculates the new fan operating point.

CASE STUDY

The following part of the paper presents a practical case study where the potential of EOLAVAL in designing mine ventilation systems is illustrated. Figure 2 presents the mine ventilation network of an underground mine in Québec. The objective of this case study is to calculate the air quantity distribution in the network in one hand and to compute the operating point of the main fan and booster fans. In order to facilitate modeling of the mine ventilation network, it is recommended that the user takes into account only the main ventilation airways. The user enters an initial estimate of the air quantity and airflow direction in each branch.

Once a network sketch is completed the next step is to build the network file interactively using the appropritate option of EOLAVAL. The network file associated to figure 2 is shown in figure 3. Following the creation of the network data file, EOLAVAL creates the simulation input data file by calculating the resistance of each airway and by verifying if the quantity of air is balanced at each node. The next step is the simulation itself. The simulation through the Hardy Cross interations will produce the real air quantity and its direction in each branch. The program will also calculate the static head of the main fan, the static head developed by the booster fans and the head losses of the regulators within the network.

Table 1 shows the results of the simulation. It gives the head losses of each branch and the quantity of air flowing in each branch along with the static head losses of the fixed quantity branches. In the example illustrated here the solution shows us that the main fan

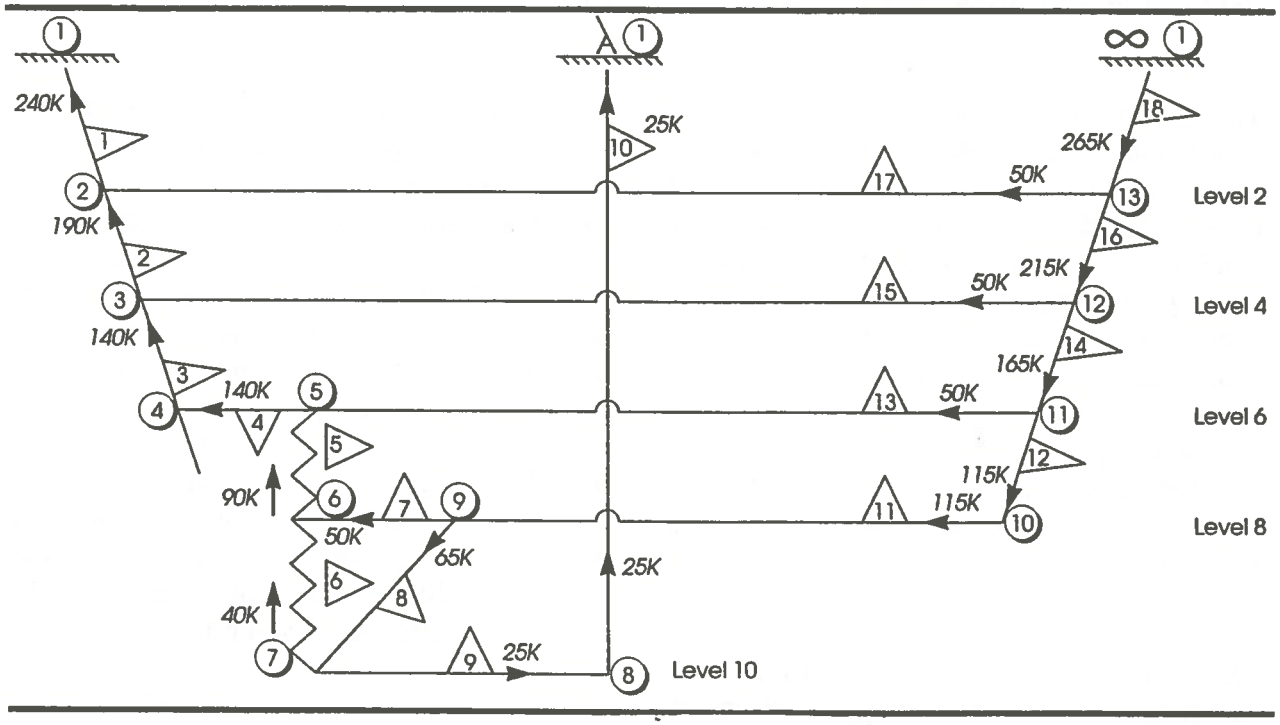

Figure 2 - Ventilation network of case study

```
18, 13
 2,  3,  2,EXHAURE NIV4-NIV2   , 100.0,  40.0, 120,   1.0, 357.0, 190.0,NON
 3,  4,  3,EXHAURE NIV6-NIV4   , 100.0,  40.0, 120,   1.0, 357.0, 140.0,NON
 4,  5,  4,NIV.6 ZONE OUEST    , 120.0,  44.0, 100,   1.0, 400.0, 140.0,NON
 5,  6,  5,RAMPE 6 AU 8        , 180.0,  54.0,  90,   1.0,1500.0,  90.0,NON
 6,  7,  6,RAMPE 10 AU 8       , 180.0,  54.0,  90,   1.0,1500.0,  40.0,NON
 7,  9,  6,NIV 8 ZONE OUEST    , 120.0,  44.0, 100,   1.0, 200.0,  50.0,OUI
 8,  9,  7,VENT RAISE 8 AU 10  , 120.0,  44.0, 100,   1.0, 357.0,  65.0,NON
 9,  7,  8,NIVEAU 10           , 120.0,  44.0, 100,   1.0, 100.0,  25.0,OUI
10,  8,  1,PUITS 10-SURF       , 192.0,  64.0,  90,   1.0,1640.0,  25.0,NON
11, 10,  9,NIV-8 ZONE EST      , 120.0,  44.0, 100,   1.0, 500.0, 115.0,NON
12, 11, 10,VENT RAISE 6 AU 8   , 110.0,  45.0, 110,   1.0, 357.0, 115.0,NON
13, 11,  5,NIV 6 ZONE EST      , 120.0,  44.0, 100,   1.0, 800.0,  50.0,OUI
14, 12, 11,VENT RAISE 4 AU 6   , 110.0,  45.0, 110,   1.0, 357.0, 165.0,NON
15, 12,  3,NIVEAU 4            , 120.0,  44.0, 100,   1.0,1500.0,  50.0,OUI
16, 13, 12,VENT RAISE 2 AU 4   , 110.0,  45.0, 110,   1.0, 357.0, 215.0,NON
17, 13,  2,NIVEAU 2            , 120.0,  44.0, 100,   1.0,1500.0,  50.0,OUI
18,  1, 13,VENT RAISE SURF AU 2, 110.0,  45.0, 100,   1.0, 357.0, 265.0,OUI
 1,  2,  1,EXHAURE NIV2-SURFACE, 100.0,  40.0, 120,   1.0, 357.0, 240.0,NON
```

Figure 3 - Data file for figure 2

TABLE 1 - Simulation results (for figure 1)

Airway	Initial node	End node	Air quantity (cfm)	Head loss (in)	Fan/regulator (in)
1	2	1	240 000	1.89	
2	3	2	190 000	1.18	
3	4	3	140 000	0.64	
4	5	4	140 000	0.38	
5	6	5	90 000	0.19	
6	7	6	40 000	0.04	
7	9	6	50 000	0.02	0.08 REG
8	9	7	65 000	0.07	
9	7	8	25 000	0.03	4.33 REG
10	8	1	25 000	0.01	
11	10	9	115 000	0.32	
12	11	10	115 000	0.33	
13	11	5	50 000	0.09	0.87 REG
14	12	11	165 000	0.69	
15	12	3	50 000	0.18	2.51 REG
16	13	12	215 000	1.18	
17	13	2	50 000	0.18	4.88 REG
18	1	13	265 000	1.63	8.59 FAN

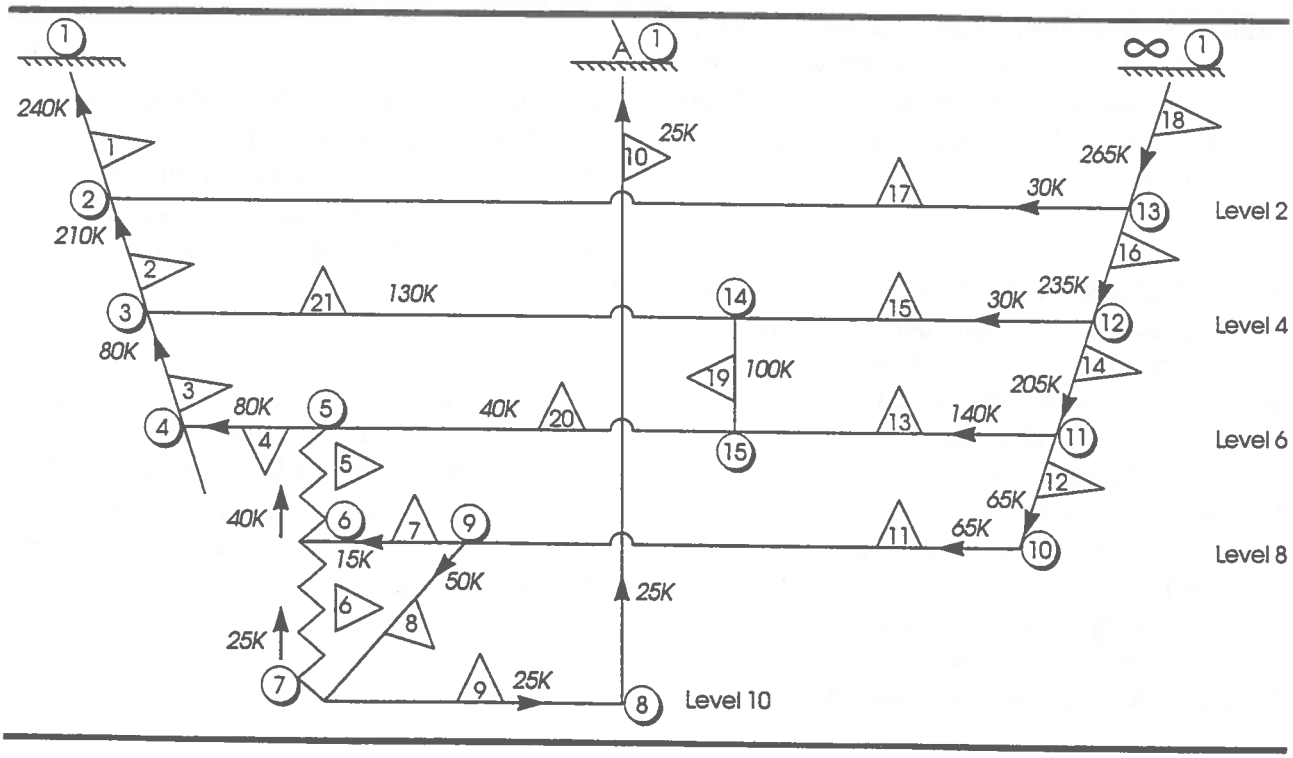

Figure 4 - Modified ventilation network (with raise).

(branch 18) would have to operate at a static pressure of 8.6 in. of water in order to obtain the air distribution specified in the data file. The negative values (branches 7, 9, 13, 15, 17) represent the head losses of the regulators which have to be placed on the specific branches.

These results allow the user to select a fan which meets the air quantity and static head requirements and also to correctly calculate the regulators dimensions. The program can also be used to verify the effect of adding new branches in the network as the mine develops through time. The example illustrated in figure 4 shows the addition of a ventilation raise between levels 6 and 4 and the new air distribution which is requested.

Three questions need to be answered in this example : what is the most economic size of the raise (circular raise) ?; what will be the new operating point of the surface fan ? and do we need to change the regulators dimensions ?

In order to answer the first question, we can use EOLAVAL to calculate the economic dimensions of the raise. EOLAVAL requires the following input data (listed on table 2) :

- length of the raise (ft);
- life of the mine (years);
- interest rate (%);
- quantity of air flowing through the raise (cfm);
- hours of operation per year;
- electricity cost ($ /kwh);
- excavation cost for the raise ($ /pi^3).

The program has built-in several options of rais shape and size raise with their corresponding excavation costs. The program is built in such a way that we can change any of these values (dimensions or excavation costs). The results obtained from EOLAVAL are shown in table 2. For a circular raise (type of raise chosen) we can see that the minimum cost corresponds to a 10 feet diameter raise. The program produces the total cost per year for one raise or two parallel raises.

The next step is to go back to EOLAVAL and modify the network file to fit the network shown in figure 4. This consists of adding three branches and two nodes in the network and changing the quantity of air in the branches where necessary. EOLAVAL is run again to find the new air quantity distribution and the static heads of the booster fans and the regulators head losses in the network.

The results obtained (table 3) show that the static head (main fan) drops to 8.1 in. of water (branch 18) and that in order to obtain 100 000 cfm in the new raise (branch 19) we will have to use a booster fan of 0.21 in. of static head in this branch.

The user should be aware that the precision obtained depends on the accuracy of the data used. It is also very useful to compare the results expected with the real values obtained in order to verify the precision of the simulation.

TABLE 2 - Economic design of ventilation raise, results

Type of ventilation raise	Dimensions (feet)	Excavation cost ($/ft^3)	Total annual cost ($)	
			One raise	Two parallel raises
Conventional	5 x 6	5.42	22 747	45 265
	5 x 8	4.75	26 494	52 872
	6 x 6	6.77	33 982	67 820
	6 x 8	4.38	29 284	58 496
	8 x 8	2.53	22 541	45 048
	8 x 10	2.08	23 156	46 293
Alimak	8 x 8	5.27	46 933	93 832
	10 x 10	2.45	34 084	68 157
Long hole	5 x 5	3.92	13 836	27 313
	6 x 6	4.05	20 362	40 580
	8 x 8	4.42	39 366	78 698
	10 x 10	0.59	8 213	16 414
Down the hole	6 x 6	3.78	19 010	37 876
	7 x 7	3.78	25 801	51 535
	10 x 10	2.54	35 336	70 661
	17 x 17	0.56	22 511	45 022
Circular (Roger)	3	32.47	35 715	64 796
	5	33.40	91 513	182 510
	6	10.68	42 120	84 033
	7	18.39	98 495	196 894
	10	3.83	41 849	83 683

Data of the problem

Ventilation raise length	:	350 ft
Mine life	:	5 years
Interest rate	:	12 %
Friction factor (K)	:	40
Air quantity	:	100 000 ft^3
Operating hours/year	:	7 200
Electricity cost (¢/kwh)	:	5

TABLE 3 - Simulation results with raise (figure 4)

Airway	Initial node	End node	Air quantity (cfm)	Head loss (in of water)	Fan/regulator (in of water)
1	2	1	240	1.89	
2	3	2	210	1.45	
3	4	3	80	0.21	
4	5	4	80	0.12	
5	6	5	40	0.03	
6	7	6	25	0.01	
7	9	6	15	0.02	0.05 REG
8	9	7	50	0.04	
9	7	8	25	0.03	3.72 REG
10	8	1	25	0.01	
11	10	9	65	0.10	
12	11	10	65	0.10	
13	11	15	140	0.29	0.02 FAN
14	12	11	205	1.07	
15	12	14	30	0.04	1.26 REG
16	13	12	235	1.41	
17	13	2	30	0.06	4.51 REG
18	1	13	265	1.63	8.10 FAN
19	15	14	100	0.17	0.21 FAN
20	15	5	40	0.04	
21	14	3	130	0.41	

PROGRAM APPLICATIONS

EOLAVAL has been developed in the Department of Mining & Metallurgy at Laval University in collaboration with the Québec Mining Association in order to provide a practical and easy to use mine ventilation planning tool to the Québec Mining Industry. Since its application has been distributed by the Québec Mining Association to all mines in the province of Québec where it is being used extensively on a routine basics. At the same time it has been used as a teaching tool at Laval University.

Possible areas of applications of EOLAVAL are :

1. Designing the ventilation system of a new mine :
   - evaluation of alternative ventilation configurations;
   - optimisation of airway shape and size;
   - design of auxiliary ventilation systems;
   - design of mine air heating plants;
   - evaluation of mine shaft pressure losses;
   - evaluation of the effects of air density fluctuations on the fan operating point.
2. Design of ventilation network expansions as the mine evolves through time.

REFERENCES

Hartman, Howard, Mutmansky Jan and Wang Y., *Mine Ventilation and Air Conditioning*, Wiley Interscience, 1982.

McPherson, Malcolm, *Subsurface Ventilation and Environmental Engineering*, Chapman & Hall, 1993.

CAMI'95: 3rd Canadian Conference on Computer Applications in the Mineral Industry
Montreal, Quebec, Canada, October 22-25, 1995

Mine Ventilation: Waste Heat Recovery

L. Henry Smith, David C. Arthur
Williams Operating Corp.,Marathon, Ontario, V.B. Cook Co. Limited, Thunder Bay, Ontario

Hani Mitri
Department of Mining and Metallurgical Engineering
McGill University, Montreal, Quebec

ABSTRACT

The Williams Mine is Canada's largest gold producer, with annual production of 450,000 ounces from 2,300,000 tonnes of ore. Highly mechanized and automated underground mining practices are employed in order to achieve and maintain high levels of productivity and minimize costs.

The Mine Ventilation System is modified to include a new Vent Raise and Variable Pitch Vane-Axial Fan. This addition allows several fan installations underground to be decommissioned. A substantial net savings in installed horse power is achieved.

Heating costs associated with underground ventilation air are a significant portion of mine operating costs. Air heating costs are substantially reduced by recovering heat from upcast exhaust air, mine water and compressor cooling circuits. This waste heat is used to supplement propane fired air heating systems for underground ventilation air. An additional benefit is the availability of a heat sink for summer cooling of the compressors.

System design, energy savings data and payback calculations are presented.

Keywords Energy Savings, Heat Exchanger, Heat Recovery, Mine Ventilation, Propane Burner, Vane-Axial Fan, Variable Frequency Drive

MINE SITE

The Williams Mine is situated in the Hemlo area of Northwestern Ontario. It is operated by Williams Operating Corporation which is owned equally by Teck Corporation and Homestake Canada Inc. The mine is one of three adjacent properties which form the Hemlo Gold Camp.

The mine commenced operation in 1985 at a nominal capacity of 3,000 tonnes per day. Through an ongoing capital development program, the production rate of the property achieved its design capacity of 6,000 tonnes per day in 1989. Figure 1 shows the Property Plan with the locations of the new Fan and Heat Recovery System.

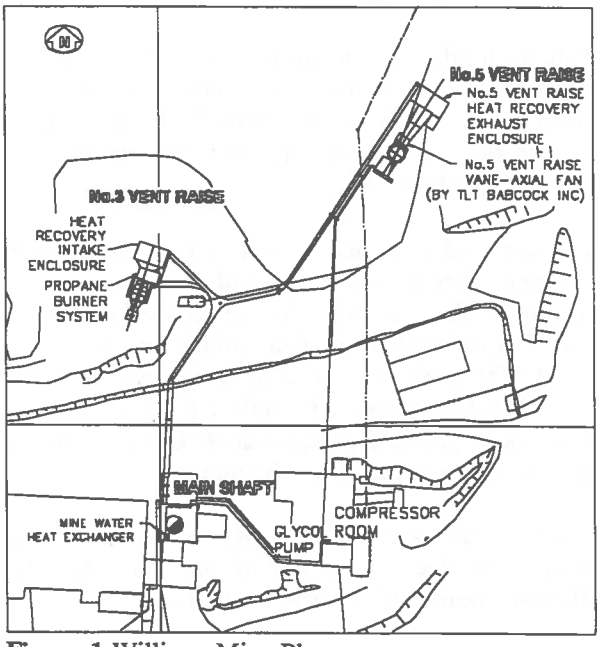

Figure 1 Williams Mine Plan

MINE VENTILATION

When the mine was placed in full operation in 1989, the capacity of the ventilation system underground was established at 475,000 l/s (1,000,000 cfm). This air entered the mine via the Main Shaft. Exhaust air was up-cast through one of three Vent Raises: one near the Main Shaft, and two in the general mine workings.

As mining progressed, an increasing number of headings were vying for ventilation. It became more difficult to maintain adequate ventilation in each working area. The operating tendency was to add increasing numbers of underground fans to alleviate the problem.

VENTILATION MODIFICATIONS

Ontario Hydro performed an Energy Audit in June of 1993. One item identified which had the potential to yield large energy savings was the Mine Ventilation System. Specifically, the recommendation involved reducing the total connected horse-power required to drive the Ventilation System.

Planning for the construction of a new Ventilation Raise to facilitate ongoing mining was started in 1993. The intent was to extend a raise from the lowest working level to the surface, and ultimately to connect every level and sub-level.

Increased headings and distances were required as mining progressed which impacted on air volumes and pressures. To compensate for the additional distances, provision to increase the total volume to 710,000 l/s (1,500,000 cfm) was included in the plan. It was scheduled that by 1995, 615,000 l/s (1,300,000 cfm) would be required; the additional 95,000 l/s (200,000 cfm) would be available for the future.

Energy conservation was a large concern as well. Head-losses due to friction in the Raise and fan efficiency were two key items to address.

The new Vent Raise was driven at 6mϕ for the top 915m then at 4.25 to 5.5mϕ for the lower 305m to reduce friction losses to an economic minimum.

Several fan styles, configurations and manufacturers were considered before final selection was made. Centrifugal and Vane-axial Fans were evaluated for efficiency, sound power level, workmanship and cost. A TLT-Babcock Model No. 37.5/18.0-1 Variable-Pitch-in-Motion Vane Axial Fan was selected. This fan is 85 to 90% efficient in the expected operating range.

The new fan was installed on surface. Initially, the fan was operated at 310,000 l/s (650,000 cfm) to reach the 1995 ventilation target of 615,000 l/s (1,300,000 cfm) total. If required in future, the fan is capable of 400,000 l/s (850,000 cfm).

Part of the plan was to reverse the direction of the Shaft Ventilation Raise (No.3 Vent Raise), in order to down-cast more air into the mine. No.3 Vent Raise would become an Intake Raise with the capacity of 140,000 l/s (300,000 cfm).

At the same time as the Ventilation system was being studied, the potential for recovering waste heat from the exhausted Up-cast Air, Mine Water and Air Compressors and using it to pre-heat Down-cast Air was being investigated.

HEAT RECOVERY: FEASIBILITY STUDY

V.B. Cook Co. Limited was retained to complete a feasibility study of Heat Recovery opportunities on the Williams mine property.

Several factors make Heat Recovery potentially viable on the site:

- the Exhaust and Intake Raises are relatively close together making for economic piping runs for heat transfer fluid.
- the site does not have access to natural gas for Down-cast air heating and must rely on more expensive propane for fuel.

A flowsheet was developed for a closed loop glycol system. At the same time discussions were carried out with a glycol-to-air heat exchanger supplier to develop the design parameters:

- glycol flow for efficient heat transfer; heat exchanger sizes
- entering temperatures for the glycol and air
- exiting temperatures for the glycol and air.

These new heat exchangers were required at the No.3 and No.5 Vent Raises, and the Main Shaft.

The existing heat exchangers at the shaft required supplemental units to exchange the additional heat available. The compressor cooling system modifications required the conversion of the compressors from the existing water-to-glycol-to-air system to a new glycol-to-air system. Interaction with the compressor manufacturer and the heat exchanger supplier established the system design temperatures for this portion of the new heat recovery system.

The last portion of the system included heat recovery from the mine water. The mine water is brought to surface through the mine shaft, passes through a water-to-glycol heat exchanger, and then out the Mine Portal. The existing mine water pumps are designed to run at Off-Peak times. In order to utilize the water for heat recovery, one pump is required to run continuously at a lower flow rate. A pump analysis was required to review the best means to accomplish this and to determine the modification costs.

Environment Canada provided day-to-day weather temperature data averaged over 32 years in the area of the Williams Operating Corporation's mine. A spreadsheet was constructed from this data. The spreadsheet was used to determine:

- the number of heating hours to estimate the energy required to heat the downcast air
- the potential heat recovery
- the temperature difference available.

Upon completion of the flowsheet, the operating parameters were established and the energy balance completed. Two approaches were considered: one single glycol loop and a two loop glycol system. The energy balance was used in conjunction with the Heating Load Spreadsheet to determine:

- the net financial benefit
- the propane savings in heating the downcast air
- the increased costs in pumping of water and glycol
- the increased fan horse-power costs resulting from the installation of heat exchangers
- the summer savings resulting from more efficient compressor cooling.

Heat added to the system from fans and pumps was not included in overall savings calculations. It was considered that this heat will offset thermal losses from pipelines.

Heat Exchanger Performance Approximation

Heat exchanger performances were approximated using the NTU (Number of Heat Transfer Units) method.

The NTU method is based on a heat exchanger's Effectiveness (E), Capacity Ratio (C) and Number of Heat Transfer Units (NTU):

$$E = \frac{\text{Actual Heat Transfer Rate}}{\text{Maximum possible heat transfer rate with given flow rates and inlet conditions}}$$

$$C = \frac{\text{Min. Value of Mass Flow x Heat Cap.}}{\text{Maximum Value of Mass Flow x Heat Capacity}}$$

$$NTU = \frac{\text{Heat Transfer Coefficient of Heat Exchanger x Area of Heat Exchanger}}{\text{Minimum Value of Mass Flow x Heat Capacity}}$$

The heat transfer coefficients used in the performance estimate were derived from information supplied by the heat exchanger manufacturers.

Results using the NTU method correlated well with manufacturer supplied data.

Several alternate piping and equipment configurations were studied before recommending the system as described below. Figure 2 shows the Flow Diagram for the Heat Recovery System.

The feasibility study concluded that $500,000.00 per year gross energy savings could be achieved at an estimated capital cost of $1,700,000.00. The project was approved based on a 3.8 year payback.

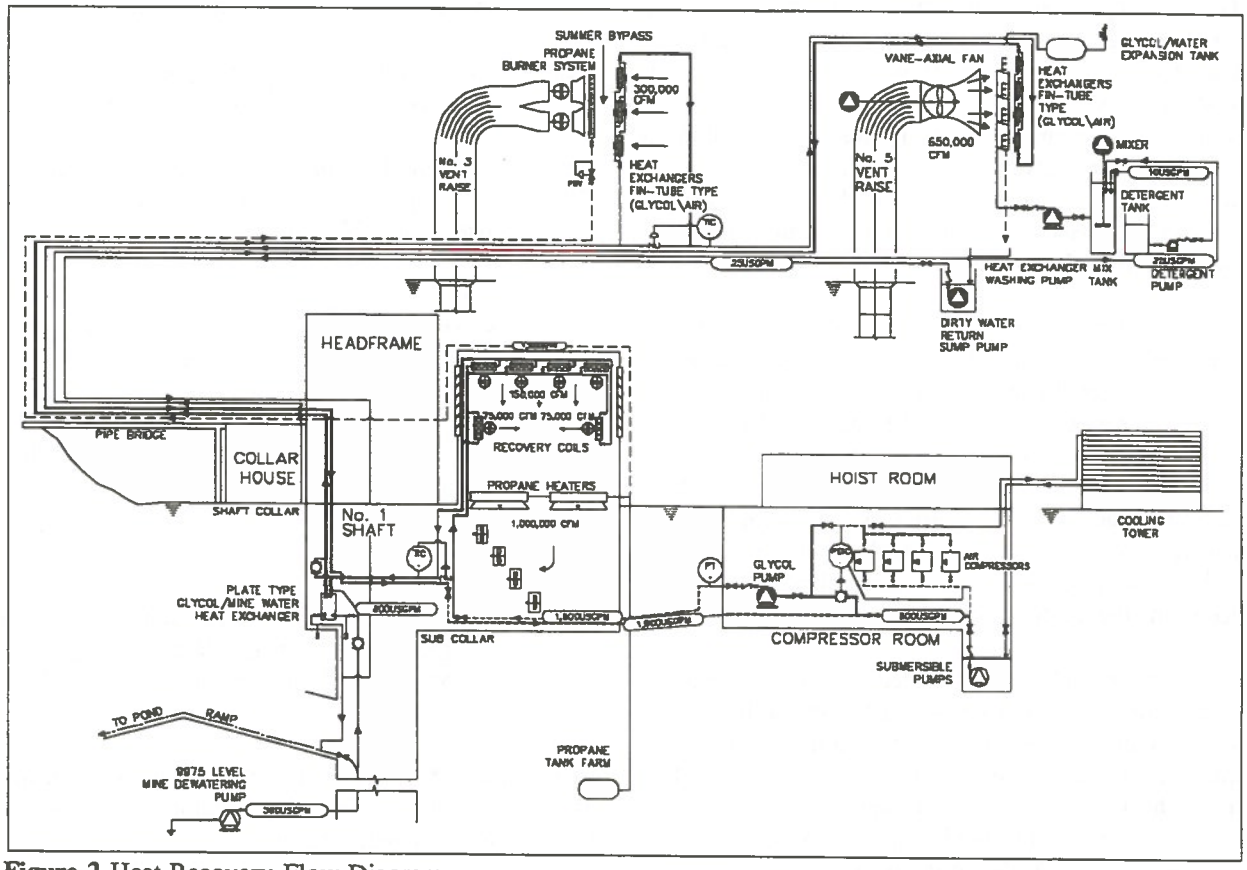

Figure 2 Heat Recovery Flow Diagram

DETAILED ENGINEERING AND CONSTRUCTION

E.S. Fox Ltd. and V.B. Cook Co. Limited entered into a partnership to complete the detailed engineering and construction for the project.

The work under the contract included:

- the installation of a new exhaust fan at No. 5 Raise
- conversion of the existing exhaust fans at No. 3 Raise to supply service
- provision of propane fired air heating at No. 3 Raise with gas supply from the main tank farm
- provisions for Waste Heat Recovery.

System Configuration: Winter

During winter, the system recovers heat from the ventilation exhaust, mine water discharge, and compressor inter-coolers and after-coolers, discharging it to the mine ventilation intakes at the shaft and No. 3 Raise. The circuit is arranged so that the low-grade heat sources, the mine water and vent exhaust, are immediately downstream of the heat rejection points. This maximizes the temperature differential available for Heat Recovery from these low temperature sources.

The circuit provides for low temperature control of the glycol to avoid freezing the heat exchangers, and for bypassing to maintain glycol flow volume when compressors or coils are running at part load, or are out of service.

System Configuration: Summer

During summer, the flow direction remains the same, but the mine water and exhaust air become the lowest temperatures available in the system, and heat from the compressors is rejected at these points.

Compressor Room

One glycol circulating pump is located in the compressor room. Piping is laid out to accommodate a second pump in future if desired. A 185 kW (250 Hp) Variable Frequency Drive (VFD) is installed to maintain a constant flow rate in the glycol circuit.

The VFD is necessary in the system because of the difference in winter and summer operation. In the summer the coils at the Main Shaft and the No.3 Vent Raise are bypassed, substantially reducing the total system head. Power requirements are reduced from 135 to 50 kW (180 to 70 Hp). The electrical savings by installing the VFD paid for the additional expense of the drive in one season. A VFD is perfectly suited to this application.

A pressure reducing valve between the compressor glycol supply and return headers maintains a predetermined pressure differential across the compressors, while allowing excess flow to bypass should the compressor cooling demand be less than the total system flow.

Shaft Ventilation Intake

The existing heat recovery coils in the intake structure are retained, and are augmented by additional coils mounted vertically around the walls. These coils have their own fans, as in the original installation. This minimizes the pressure drop through the intake structure during the summer when heating is not needed.

A temperature sensor in the glycol return header operates a bypass valve between the supply and return headers, maintaining a minimum downstream temperature of 1°C. During the summer this valve is positioned open to reduce pressure drop in the system.

Mine Water Heat Exchanger

The mine water discharge line is extended up the shaft from the adit level to supply the existing plate heat exchanger, and returned down to the adit for discharge to the sedimentation pond. This return line also serves as the sewer for coil wash water from the No. 5 Raise exchanger coils.

It is necessary to adjust the discharge rate of the mine pumps to provide a continuous water supply: the 9975 Level pumps are now operating about 20 hours per day. This is done by means of a manually adjusted throttling valve. Water supply to the 9975 sump will remain under the existing automated level control system.

A summer glycol bypass valve is provided to reduce pressure drop and allow the exchanger to be disassembled for annual servicing.

No. 3 Vent Raise

The existing exhaust fans are reinstalled in the opposite direction to work as supply fans. They are fitted with intake bells, and propane fired heaters are installed in a new intake structure. Heat recovery coils are installed vertically in the walls of an additional structure ahead of the propane burners. These coils are mounted on racks so as to be serviceable by boom truck and lift platform from the exterior. Individual coil banks have isolation valves so that servicing need not remove the entire system from service. Figure 3 shows the Plan at No.3 Vent Raise.

Propane is supplied through a pipeline from the main tank farm. The exposed sections of pipeline are insulated to prevent the occurrence of condensation problems.

Bypass and temperature control valves are installed between glycol supply and return headers, similar to the Main Shaft arrangement.

Louvres are installed in parallel with the heat recovery coils to reduce intake pressure drop in summer.

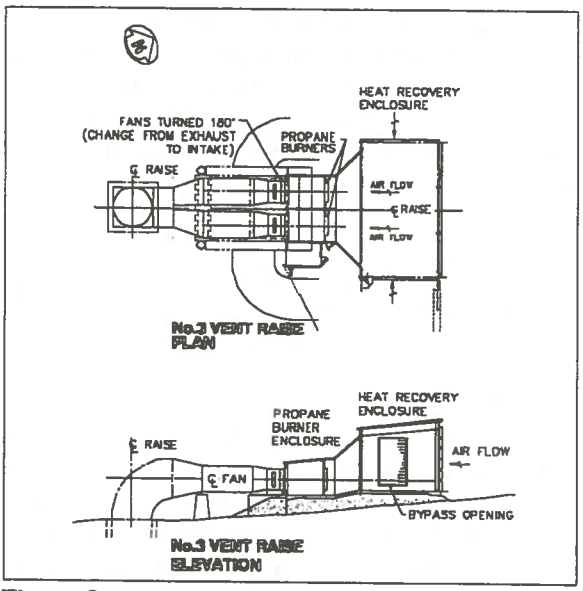

Figure 3 No.3 Ventilation Raise

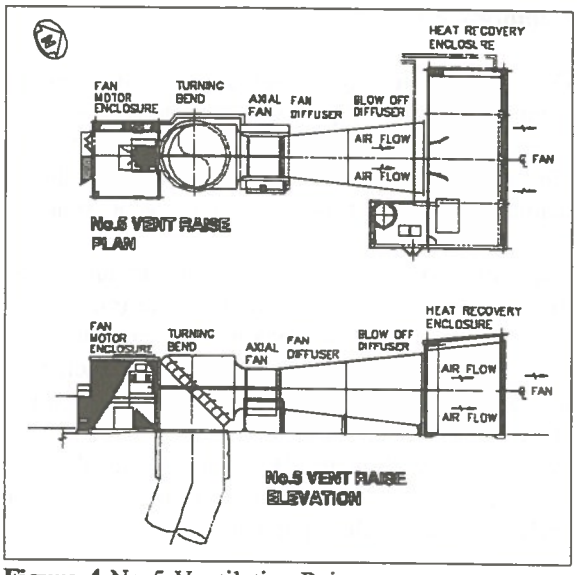

Figure 4 No.5 Ventilation Raise

No. 5 Vent Raise

The TLT Babcock Exhaust Fan is direct-driven through a jack shaft extending across the top of the raise to an elevated motor room on the south side. Figure 5 shows the Plan at No.5 Vent Raise.

The heat recovery equipment is housed in a steel framed structure attached to the discharge of the fan diffusers. The equipment includes heat exchange coils similar to those used in the No. 3 Raise, but in larger numbers to suit the larger air volume.

The coils in this area are subject to heavy fouling from the mine exhaust air; a spray cleaning system is provided remove build-up. This system includes a detergent storage tank with transfer pump, a detergent/water mixing tank, and a spray pump and nozzle system to cover the entire coil bank. The sprays are sectionalized to reduce peak water demand, and are sequenced by a PLC.

Condensate and wash water are collected in a sump and pumped away to the sedimentation pond by a float-controlled sump pump.

The layout provides for single-pass washing of the coils, but the arrangement is adaptable to recirculation of the detergent solution if this should be found practical.

The water supply and drain lines are used only intermittently, and are thus insulated and heat traced.

OPERATING EXPERIENCE

START-UP

The No.5 Exhaust Fan was commissioned at reduced volume of 210,000 l/s (450,000 cfm) on November 20, 1994. The fan was started at reduced volume because most of the underground break-throughs to the new Vent Raise were not yet complete.

During the course of the next several days, Heat Recovery System parameters were varied to optimize performance. The Air Compressor circuit was not tied in initially, to give operations time to become familiar with the other parts of the system before making it critical to mining.

It was apparent early in the trials that the system would meet and exceed the calculated Heat Recovery.

The volume of the fan was progressively increased to 310,000 l/s (650,000 cfm) as levels were connected to the system. All available levels were connected by the end of January 1995. During this same time frame, the Air Compressors were tied into the system.

OPERATION

Outside temperatures in December and most of January were unseasonably warm. When the temperatures did return to the norm at the end of January, it became evident that the system had the ability to remove more heat from the glycol than could be added. System parameters were revised from the original to allow more heat to be rejected at the No.3 Vent Raise and less at the Main Shaft. This was achieved by manually adjusting the Summer By-pass Valves at the Main Shaft to allow increased flow to short-circuit around these coils.

The increased net volume of air flowing through the mine workings had an unexpected effect: the average temperature of the Exhaust Air dropped from 15°C to 12°C. The overall level of Heat Recovery still met design expectations.

ECONOMIC ANALYSIS

Heat Recovery

Now that the system has been in operation for several months, the estimated savings have been confirmed. Propane savings for the period from start-up to February 28, 1995 are estimated to be $287,000.00. Projecting this over the entire heating season yields $500,000.00.

Fan Installation

The installation of the No.5 Vent Raise Fan facilitated the off-loading of 20 small horse-power fans located underground, after all levels were tied into the new Raise. Power consumption underground was reduced by 1,000,000 KWhr/month during January and February 1995 from the same period in 1994. The expectation to achieve 30% increase in system overall volume with no increase in horse-power was realized. In fact, horse-power was reduced. This equates to an additional savings of $500,000.00 per year.

FUTURE PLANS

Using the experience gained with this project, Williams Operating Corporation will study the remainder of the Ventilation System. The objective will be to improve the efficiency of the underground fan system and increase the ability to recover heat from exhaust air.

CONCLUSIONS

The Heat Recovery part of this project is an example of true energy conservation because it directly reduces the consumption of fuel.

The technologies employed are directly adaptable to any mine which preheats Down-cast air with propane.

ACKNOWLEDGEMENTS

The authors wish to recognize Jack Jeffries, Jack Morris, Don Nelson, Eric Schraml, and the Project Teams at Williams Operating Corporation, E.S. Fox Limited and V.B. Cook Co. Limited who contributed to the success of this project.

CAMI'95:3rd Canadian Conference on Computer Applications in the Mineral Industry
Montréal, Québec, Canada, October 22-25, 1995

AutoVENT - AutoCAD based ventilation modelling software.

Per J. Lunder
Noranda Technology Centre, Pointe Claire, Quebec

ABSTRACT

AutoVENT is an underground ventilation simulation and survey system for use within the computer aided drafting package AutoCAD®. It enables mine ventilation personnel to design and test underground ventilation networks quickly, utilizing existing mine geometry that is stored in AutoCAD. AutoVENT is divided into 2 main modules: survey and simulation. The survey module is used to generate ventilation plans quickly and the simulation module is used to perform ventilation simulations using a Hardy Cross algorithm to solve the flow problems. A third module to aid in simulation visualization is currently under development. AutoVENT was originally developed using AutoLISP and external executable programs. The current version was developed entirely using ADS, the advanced development system for AutoCAD. AutoVENT is currently in use at approximately ten Noranda Group operations.

RESUME

AutoVENT est un système de simulation et d'investigation de ventilation souterraine. On l'utilise à l'intérieur d'AutoCAD®: un ensemble de dessins assisté par ordinateur. AutoVENT permet de concevoir et de tester rapidement les réseaux souterrains de ventilation en utilisant la géométrie de la mine déjà implantée dans AutoCAD. AutoVENT est divisé en deux modules principaux: investigation et simulation. Le module d'investigation sert à créer rapidement des plans de ventilation tandis que le module de simulation est utilisé pour des simulations de ventilation avec l'algorithme Hardy Cross pour résoudre les problèmes d'écoulement. Un troisième module aidant à visualiser les simulations est actuellement en développement. AutoVENT a été développé à l'origine avec AutoLISP ainsi que des programmes externes exécutables. La version actuelle a été développée entièrement avec ADS, le système avancé de développement d'AutoCAD. AutoVENT est maintenant utilisé dans environ dix opérations du Groupe Noranda.

INTRODUCTION

Mine ventilation is critical to all underground mining operations. Regulatory agencies require that certain quantities and quality level for mine air be maintained at locations where mine personnel are traveling or working. In order to effectively design and monitor ventilation networks at Noranda Group operations, a software program known as AutoVENT has been developed.

AutoVENT makes use of three-dimensional mine plans that exist in AutoCAD, a mainstream CAD package, at Noranda group operations.

AutoVENT has been developed for "unsophisticated" computer users, that is users who may not have an in-depth knowledge of CAD or computers. As such the user interface developed is simple and easy to understand. AutoVENT runs entirely within AutoCAD as a sub-program.

AUTOCAD & AMINE

AutoCAD is a computer aided drafting (CAD) package that is used extensively in Noranda Group mining operations for mine engineering purposes.

Beginning in 1990, Noranda operations began moving to AutoCAD as a means of constructing and maintaining engineering drawings and plans. These drawing are constructed in three dimensions using in-house software, collectively referred to as AMINE, developed at the Noranda Technology Centre.

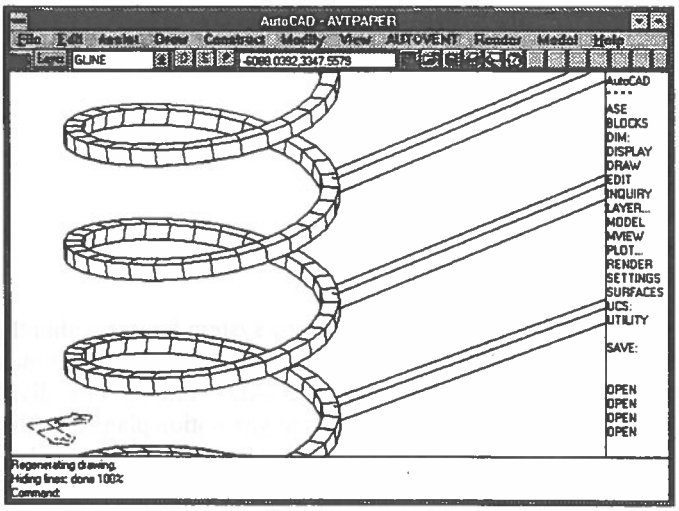

Figure 1 Conceptualized isometric three-dimensional view showing a ramp and sub-levels.

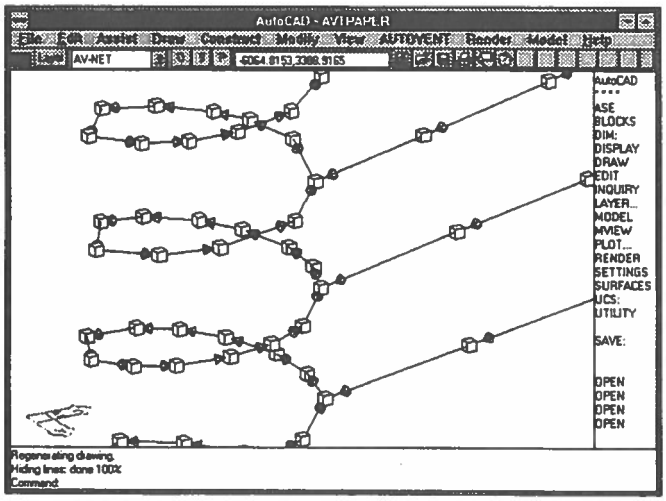

Figure 2 Sample ventilation network constructed on the mine openings shown in Figure 1.

AMINE can be broadly divided into two separate areas: the Drawing Manager and the Program Manager with associated application programs.

The drawing manager maintains the drawing database of CAD files. The philosophy is that one drawing layer in AutoCAD is a single drawing in the AMINE drawing database. When a user needs to work on an assembled drawing, the drawing manager performs the task of collecting the required layers and assembling them into a working drawing, At the end of the editing session, the drawing manager saves all of the drawing layers as individual drawing files. This approach is used to maintain a single copy of each drawing only, which is used by different engineering groups.

One requisite of using the AMINE drawing manager is that drawing and layer naming conventions are rigid for a particular minesite. This approach to drawing management ensures that duplicate file names never exist.

The program manager handles the task of loading and unloading each of the AMINE compatible applications that a particular operation may have installed. After an application is loaded it is accessed from either the command line or from a customized menu for the particular application.

Figure 1 and Figure 2 show the relationship between a three-dimensional mine plan that would have been created using AMINE layout tools and an AutoVENT

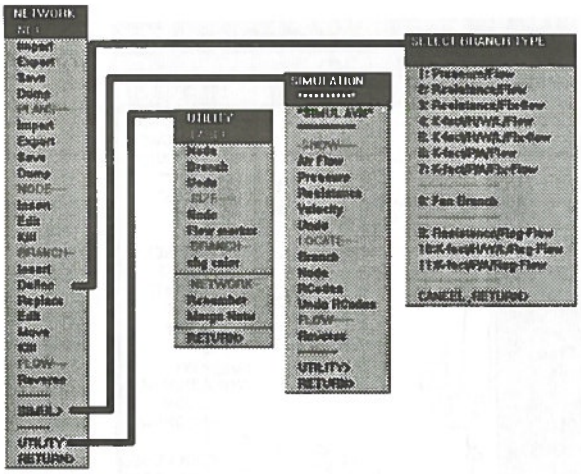

Figure 3 Menu tree for the AutoVENT simulation module.

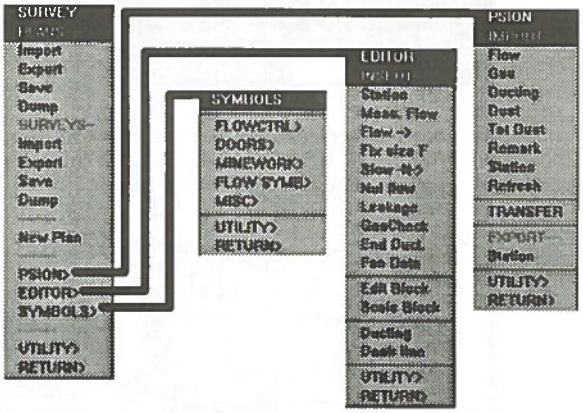

Figure 4 Menu tree for the AutoVENT survey module.

ventilation network constructed using the same mine plans.

AUTOVENT - OVERVIEW & PHILOSOPHY

AutoVENT is currently divided into two discrete modules: Survey and Simulation. The survey module is used to aid mine ventilation technicians in the task of maintaining mine ventilation plans. The simulation module is used to investigate current ventilation scenarios or to plan new ventilation networks. Each of these modules functions independently of the other. However, in order to validate simulation results, the current survey plans may be required. A third module is currently under development which will enable ventilation personnel to visualize the results of simulation modelling.

The personnel involved in mine ventilation have a good knowledge of ventilation procedures, however, they may not have a good knowledge of mine CAD systems or other computer knowledge. In order to make AutoVENT as usable as possible, a user interface has been developed that minimizes the CAD knowledge required to run AutoVENT. Figure 3 shows the AutoCAD menu structure used to access the AutoVENT simulation module. Figure 4 shows the AutoCAD menu structure used to access the AutoVENT survey module.

AutoVENT makes use of the AutoCAD menu capabilities to structure the commands for the user. For example, when file actions are required, a list of all of the available files for a particular operation are presented in a list on the screen menu at the right side of the AutoCAD editing window. The user then selects the files which they want to use to process.

AutoVENT is written in "C" in order to take advantage of AutoCAD's advanced development system (ADS). Prior to the current version of AutoVENT, development had taken place in AutoLISP and the simulation had been performed by an external DOS program. This involved the construction of external ASCII data files that were required to move information between AutoVENT and the simulation modules. In the current version, the simulation module is written into the AutoVENT program code, thus eliminating the need to use external programs. This modification has resulted in a greater than tenfold increase in simulation performance. This means that the user can spend less time running simulations and more time analyzing them.

SURVEY

The purpose of the survey module is to aid in the construction and maintenance of ventilation survey plans. There are three main sections in survey:

- Symbols
- Editor
- Psion

The survey module is designed to be used by ventilation personnel to maintain mine ventilation plans. Figure 5 is an example of a ventilation survey

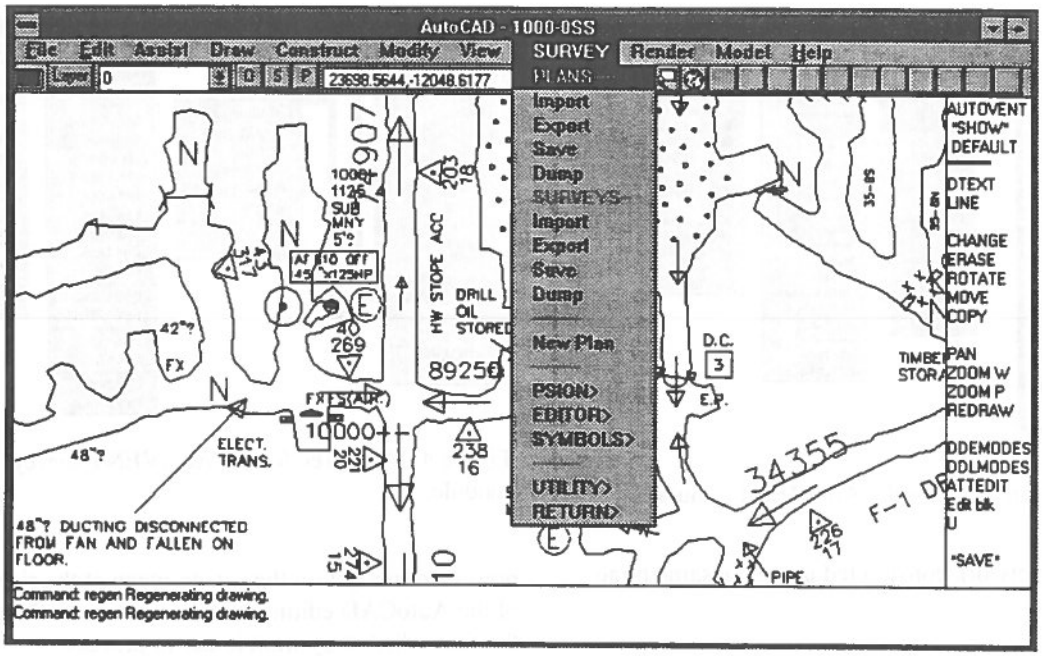

Figure 5 Example of a ventilation survey plan constructed on top of an existing mine survey plan.

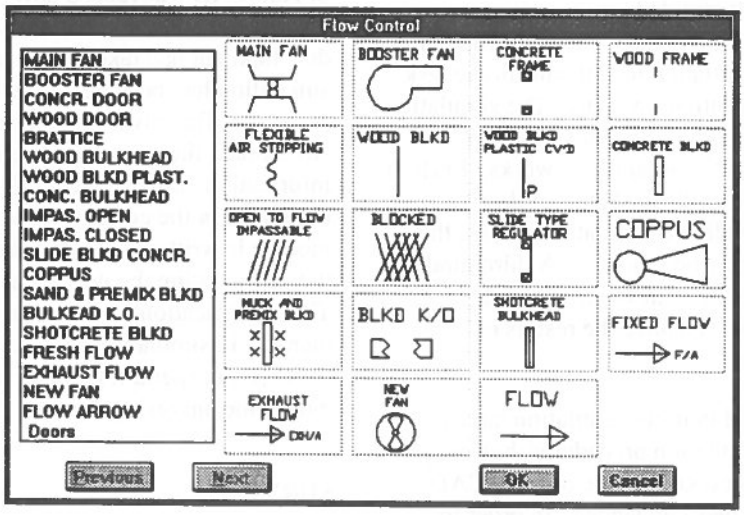

Figure 6 Autovent survey icon dialogue box used to select various ventilation symbols for insertion.

plan that includes surveyed mine workings and various ventilation symbols.

Symbols

The symbols section allows the user to select from a library of ventilation symbols for insertion into the current drawing. Upon insertionof the symbol, the user interactively scales and rotates the symbol at the desired location. There are five symbol libraries that the user can select symbols from as follows:

- Flow control symbols
- Mine doors symbols
- Mine working symbols
- Flow symbols
- Miscellaneous symbols

Figure 6 shows the icon dialogue box to aid in the selection and insertion of flow control symbols on a ventilation survey plan.

Editor

The editor is used to insert AutoCAD blocks that have defined attributes. These symbols are used to indicate numeric or other values on ventilation plans. Example of symbols inserted using the editor option are:

- ventilation stations
- measured flow markers
- bulkhead leakage
- gas checks

Psion

A link to a PSION handheld computer has been developed for AutoVENT. Ventilation technicians can use the PSION to enter gas or flow readings at defined locations in the mine while performing ventilation surveys. Upon returning to surface, the ventilation technicians then connect the PSION to an AutoVENT PC via an RS232 serial link and then transfer the results of the daily survey to a database file on the AutoVENT PC. Then, while in AutoVENT, the ventilation stations that exist in a particular survey plan can then be updated with the latest information recorded underground.

SIMULATION

The purpose of the simulation module is to construct ventilation networks that can be modelled in order to analyze mine air flows. The construction of an AutoVENT network is performed in true three-dimensional space so that it represents the actual spatial mine conditions. A Hardy-Cross algorithm is used to solve the ventilation network. Thermodynamic properties are not considered at the current time.

Numerical modelling methods have in the past used data files that generally include the following two sections: nodes and elements (or in this case branches). The nodal section defines the spatial location of the junction point of two or more branches. The branch information includes to which noes the branch is connected and the physical properties of the branch and the starting or last values of the parameters for which the model is being solved for. The construction of these data files is a cumbersome and lengthy task with the potential for clerical errors,

AutoVENT does not require that these data files be built. The drawing file in which the model (or network) is constructed contains all of the information necessary for performing the network simulation. When a simulation is executed, the node and branch relationship is extracted directly from the entities in the network.

Network construction in AutoVENT is a three stage process:

The first step is to place nodes at the branch junction points in the model. Because of Noranda's use of AMINE to maintain three dimensional mine models, this process involves the placement of nodes directly on the three dimensional mine opening.

The second step is to insert branches between the nodes that have been previously placed. Each branch represents a mine opening or a section of a mine opening such as a drift, raise, shaft etc.

The third step is to assign the branch with physical properties and default values for the model parameters. This is known as branch definition.

Figure 7 shows an expanded view of a portion of an AutoVENT network illustrating the various elements of the network.

There are a number of branch definition options that can be used as follows:

- variable flow
- fixed flow
- regulated flow
- fan branches

Fan branches are assigned from an external fan file that contains the fan properties defined for all fans at a particular operation. In order for the model to run, either fixed flow branches or fan branches must be present in order to provide a driving force for air flow.

In addition the physical properties of the branch may be defined in a number of ways as follows:

- pressure
- resistance
- k factor / branch height / branch width / branch length
- k factor / branch area / branch length.

On branches where length is an definable attribute, the default value is the three-dimensional distance calculated between the two nodes to which the branch is connected. The user can override this value to simulate a shorter or longer branch and place any value

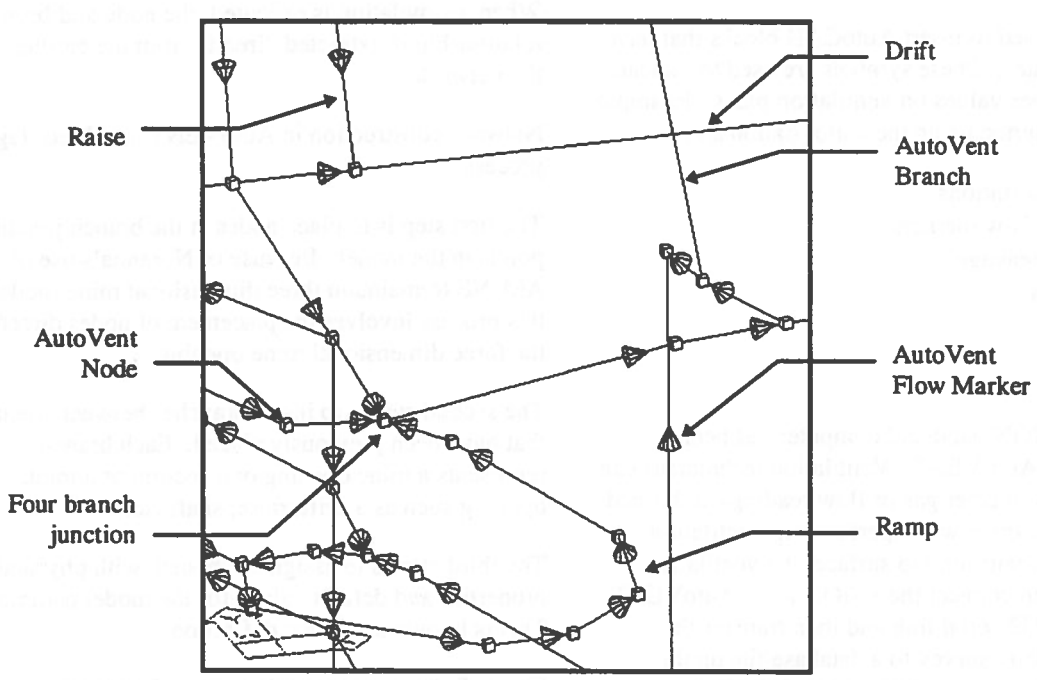

Figure 7 Detailed view of ventilation network showing various AutoVENT entities.

to this branch and that value will be subsequently used in the simulation.

Following the completion of model construction or modification, the user selects the "simulation" option from the network menu and the simulation will execute. If there are no errors in model construction, all the branches in the model will be updated with the results of the network simulation:

- new branch pressure
- new flow value
- branch state

In order to see any immediate changes in the network, the user can run the RCODES (result codes) command to identify any changes in the model. Branch changes are identified based upon the following criteria:

- flow reversal
- fans outside their defined operating range
- fixed flows that cannot be met
- regulated flows that do not have adequate flow to be regulated

The RCODES are shown as a colored circle placed upon the branches in question.

VISUALIZATION

As ventilation of larger mining operation grow, they become extremely complex and it can be difficult to assess the implications of model changes on other portions of the model.

Visualization of branch data can take place in a number of methods. A feature of AutoCAD is that drawing entities can be assigned any color available under the current color palette. When performing visualization tasks, the entity colors are temporarily changed and the user defined colors are stored on the entity as extended entity data (EED) so that the original colors can be restored at a later time. The branches are color coded by a value range and corresponding color. The following factors can be visualized:

- pressure
- resistance
- k factor
- flow values

This provides a rapid means of assessing a model visually for some factor. Figure 8 is the visualization control dialogue box.

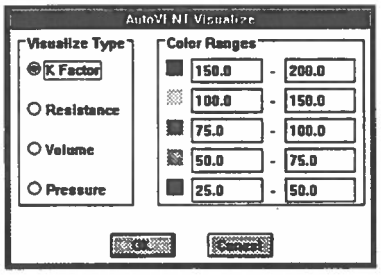

Figure 8 AutoVENT visualization control dialogue box.

A second visualization tool provided is the means to track airflow through a balanced ventilation simulation. This is performed by a user selecting a node as a starting point and the criteria on which to proceed with the flow tracking. The flow tracing will continue until one of two criteria are met: the track has proceeded a user defined number of branches from the starting node or the original airflow has been diluted by other airflow's below a user specified level. This feature can be used to track the following for example: exhaust gases after a blast, exhaust form diesel equipment or smoke from an underground fire. It should be noted that in the case of a mine fire the effects of the thermal nature of a fire are not considered.

CONCLUSIONS

AutoVENT is used successfully at a number of Noranda group operations for the purpose of maintaining mine ventilation plans and performing mine ventilation simulations. The benefits of performing ventilation simulations directly upon mine plans are that:

- simulations can be performed quickly.
- networks can be modified easily based upon new mining information.
- results can be presented in a manner that is easy to visualize.

REFERENCES

Dasys, A.A., Morasse, L.S., 1991.
AutoVENT - Graphically based computer aided ventilation design. Proceeding 2nd Canadian Conference on Computer Application in the Mining Industry, Vancouver, Vol. 1, pp.255-262.

Anon, 1993.
AutoVENT Version 3.0, Users Manual, Internal Noranda document.

Tien, J.C., 1994.
Practical mine ventilation design and control, Short course proceedings, University of Missouri, Rolla.

CAMI'95: 3rd Canadian Conference on Computer Applications in the Mineral Industry
Montréal, Québec, Canada, October 22-25, 1995

Geological Computer Applications in the Uranium Industry

David J. Dyet
Haileybury School of Mines

ABSTRACT

Computer applications in the past five to seven years have become a typical and necessary practice in most modern geological offices. Manual calculations, interpretations and plotting of data can be, at times, quite tedious, inefficient and lacking in accuracy. The introduction of geostatistical and geological software can eliminate these problems.

Computer applications in the uranium industry are not new; however, they are constantly being developed. A variety of software programs, are available. Generally, these programs support most geological and geostatistical applications in uranium mines. The Eagle Point mine in northern Saskatchewan as a high grade mine, is one such case. Computer applications at the Eagle Point mine have been a mainstay in the geology department, since the mine's collaring in 1991.

This paper presents a discussion on descriptions of programs, operations and applications of computers. It also explains and describes the radiometric equipment used at Eagle Point. This paper will demonstrate how, by using computer systems, mine site information flows reliably with the involvement of computers.

RESUME

Dans la plupart des bureaux géologiques, depuis les dernières cinq a sept années, l'application de l'ordinateur est devenu typique et nécessaire, sans mentionner très pratique. Le calcul manuel et l'interprétation de relevés informatiques peuvent parfois devenir ennuyeux, inefficaces et pauvres en exactitude. L'introduction du software géostatistique et géologique peu permettre d'éliminer ces problèmes.

L'application d'ordinateurs dans l'industrie de l'uranium n'est pas nouvelle. Par contre, elle est constamment en état dévelopement. Une variété de programmes sont en effet disponibles pour supporter la plupart des applications géologiques et géostatistiques dans les mines d'uranium. Prenons par exemple la mine Eagle Point du nord de Saskatchewan. L'application d'ordinateurs au département géologique demeure toujours un soutien principal et ce depuis l'ouverture de cette mine, en 1991.

Ce document tente donc de discuter de l'opération et de l'application de l'ordinateur et de l'équipement radiométrique utilisée par Eagle Point. Il démontre aussi la sûreté du passage d'information d'un site minier grâce à l'implication de l'ordinateur.

INTRODUCTION

This paper will discuss computer applications for geological functions at Eagle Point mine in northern Saskatchewan. Focus will be placed on descriptions of computer equipment and show how the data is incorporated into daily mining activities.

This paper was chosen for two sets of criteria: one is to fulfil requirements for the co-op education guidelines and another is to pursue the author's appreciation for the geological sciences. The author spent a cumulative of 12 months, on a week in - week out basis, as a Senior Geological Technician while spending normally between three to eight hours a day underground.

The plan of presentation will start with a general synopsis of the Collins Bay area and Eagle Point Geology. It will be followed with the description and purpose of equipment that is presently being used on surface and underground, and then proceed to the applications.

COLLINS BAY AREA

Located 805km from Saskatoon in northern Saskatchewan, is one of the world leaders in uranium mining - The Rabbit Lake Operation. The Rabbit Lake Operation is situated between Collins Bay and Ivision Bay near Wollaston Lake, about 180km south of the 60th parallel. The original Rabbit Lake deposit was discovered in 1968 by Gulf Minerals Canada Limited (GMCL).

Collins Bay (commonly referred to as "The Rabbit Lake Area") has several deposits associated with it. These deposits are composed of: Rabbit Lake, A- zone, B-zone, D-zone and Eagle Point. Rabbit Lake and B-zone are mined out. A and D zones are future open pits. Eagle Point is the current operation and will be the main focus of this report.

The Rabbit Lake operation produced approximately 75 million pounds of triuranium octoxide(U_3O_8) between 1975 to 1993 for use in nuclear generated electricity. In 1993 production was approximately 6 million pounds (U_3O_8). Forecast production from the Eagle Point mine is approximately 64 million pounds at 1.5% U_3O_8.

REGIONAL GEOLOGY

The Eagle Point uranium deposits occur along the eastern edge of the Athabasca Basin, near the western shores of Wollaston Lake. The area is in the Churchill province of the Canadian Shield, which lies within the Wollaston Lithostructural Domain (See Fig. 1).

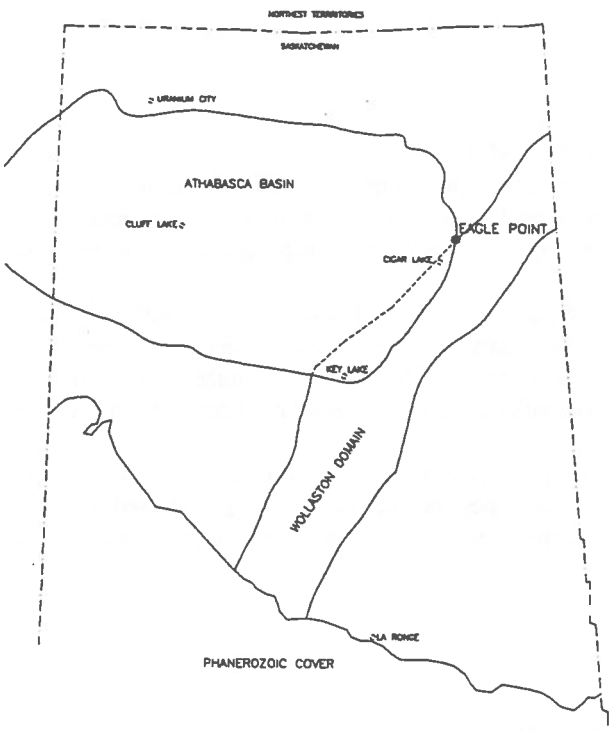

Figure 1. Geological Map of Saskatchewan

EAGLE POINT GEOLOGY

The uranium deposits occur within the Wollaston Group of metasedimentary composition of early Aphebian age, and altered quartz sandstones and conglomerates within the Athabasca Group of Paleohelikan age. These two units unconformably overlie granitoid gneiss dispersed with metasediments and minor graphitic seams all of Archean age (See Fig. 2).

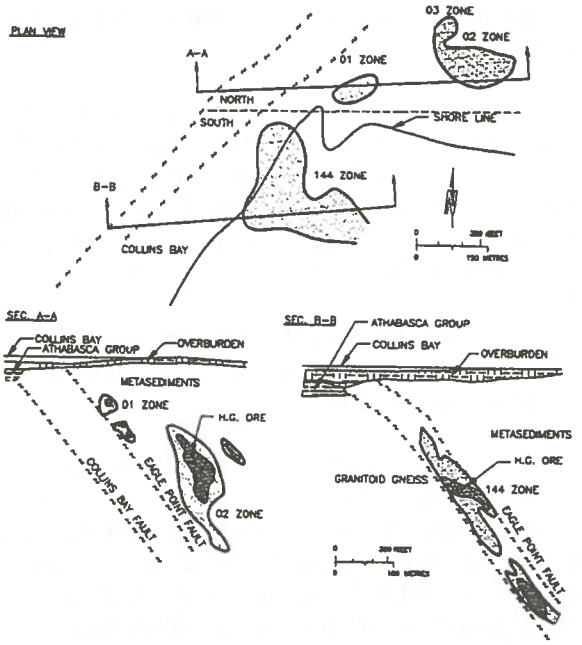

Figure 2. Geological Plan and Sections of Eagle Point

The regolith is overlain at the unconformity which is described as well-developed and lateritic in character.

Amphibolite assemblages of metamorphic origin typify the Wollaston Domain. Coarse-grained to pegmatitic segregations commonly occur within most lithologies.

The structural features consist of a thrust-faulted area, with two well defined faults (Collins Bay fault and Eagle Point fault). Both are parallel to each other, striking northeast and dipping at 45° southeast.

The uranium mineralization occurs in a series of lenses, rods and veins that are concordant and discordant to the stratigraphy, and distributed through the Wollaston Group to a depth of 1000ft.

COMPUTER EQUIPMENT

Computers are used as an efficient tool for storing, manipulating and interpreting geological, structural and radiometric measurements. End results can be produced efficiently and accurately for daily mining activities.

The equipment consists of high end, high performance computers to process the data. Various pieces of radiometric equipment are used as data collectors to obtain raw data.

Office Equipment

Two workstations are used in the geology department. One is used for the mine production and the other for the exploration program. They are both 486 DX66 with a 210Mb hard drive and 16 Mb of RAM. The printers consist of a NEC dot matrix and a Hewlett Packard laser jet, with the latter being most widely used. A Hewlett-Packard DesignJet 650C continous feed plotter is used for drawings. One workstation has a Summa-Sketch digitizing tablet for AutoCAD applications.

Computer Programs, Four main programs are used; Sermine, AutoCAD, Wordperfect and Lotus 123. Various utility programs are used for managing the hard drive (XTREE and DOSSHELL).

Sermine ver.11, Sermine is a specialized geological and geostatistical software package. It is a multi versatile program which can be used and adapted to any mining environment.

The optimal system requirements for running Sermine are: a DOS operating system, 386 processor with math co-processor chip, 4 Mb RAM and a 70 Mb hard drive.

Sermine is used for manipulating, interpreting and plotting results of data obtained by radiometric equipment. It performs many functions: converts radiometric (ie. gamma radiation) readings into readable computer files in the ASCII format, performs grade calculations, plots cross-sections, plans and graphs . This program, being so versatile, is widely used in this environment.

AutoCAD ver.12, is available on computer terminals, but is not used as much as Sermine for geological data presentation. Sermine performs all the necessary drawings without the aid of an additional CAD package. When needed, Sermine files are easily translatable into working AutoCAD files using Cadvert.

Wordperfect ver5.1, Wordperfect is used in most office environments, and also used here for all word processing work

Lotus 123 ver3.4, Lotus is used for several applications; underground and surface results from daily

mine production and exploration drilling are entered on the program. The following is a list of spreadsheets that are maintained: 1) Daily U/G and surface production data 2) Milling head grade optimization 3) Stockpile tracking and reconciliation 4) Exploration drilling statistics .

Radiometric Equipment

The radiometric equipment is used for the detection and retrieval of gamma radiation from mineralization.

The equipment consists of data collecting apparatus. In the past, normal radiometric detectors such as scintillators were used to obtain readings. This method had limited accuracy and low efficiency. With the introduction of the data collectors and apparatus, accuracy has been increased tremendously.

Data Collectors, These are used to detect and store radiometric measurements. They range in size from a cigarette-package-sized cartridge to a suit-case-sized box (See Fig. 3).

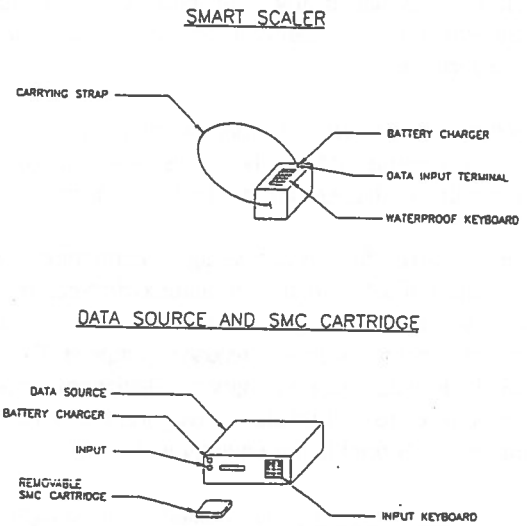

Figure 3. SMART Scaler and SMC Cartridge with Data Source

Smart Scaler (portable pulse-counting instrument) stores the natural gamma-rays emanating from the mineralization. Different probes can be utilized for detecting gamma radiation either down drill holes or by scanning rockfaces. The scaler has numbered buttons on the face for programmable data entry and a L.E.D. readout window for observing entries. The scaler is preloaded with several programs for various probing applications such as exploration and blastholes. Different parameters can be entered in the programs (i.e. different thresholds or cutoffs).

SMC (Static Memory Cartridge) is a black, hard plastic cassette-sized cartridge; this is used to store data. The SMC saves only the data; it needs a data source for retrieval of the measurements. This data source is a suit-case-sized box which reads the analog signal, coming from the scanning heads, and places it on the SMC.

The SMC is inserted into a slot in the data source (See Fig. 3). This data source is normally stationary and the SMC is transported instead of the entire unit.

Data Collecting Apparatus, These are parts that make up the retrieval of the data possible. They consist of: probes, coilers, scanning blocks and scanning arms. Probes and coilers are used in drill holes where the uranium is confined. The scanning blocks and the scanning arms are for open and exposed uranium such as mine faces or muckpiles, or individual rocks.

Probes, are light weight stainless steel metal tubes containing two Geiger-Mueller detectors and the necessary electronics to convert the readings of the detectors into a readable analog signal (See Fig. 4). For proper operation, the radioactive source in the rod needs to be calibrated first before it can be used. When radiometrics are received in the probe, the analog signal then proceeds up through the coiler to data source (either SMART scaler or SMC).

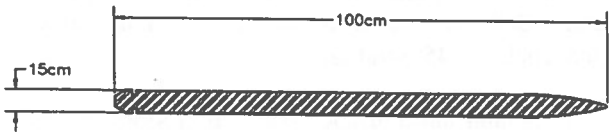

Figure 4. Standard Probe

Coiler, is a fibreglass reinforced co-axial cable wound on a portable steel carriage on wheels (See Fig. 5).

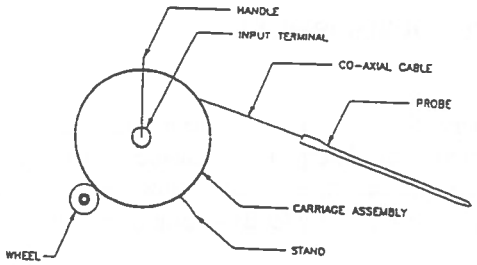

Figure 5. Coiler Set-Up

At one end of the coiler, the probe is screwed on, and at the other end is a terminal in the middle of the carriage to which the SMART scaler is hooked-up. After the signal from the probe it is sent through the coiler, it then is transferred to the SMART scaler for storage.

Scanning Brick, is used for measuring open and exposed radiation; it can be used underground or on surface (See Fig. 6). The purpose of the brick is relatively the same as that of a scintillator. The brick detects gamma-rays, converts to an analog signal, and sends that signal, to the SMART scaler for storage.

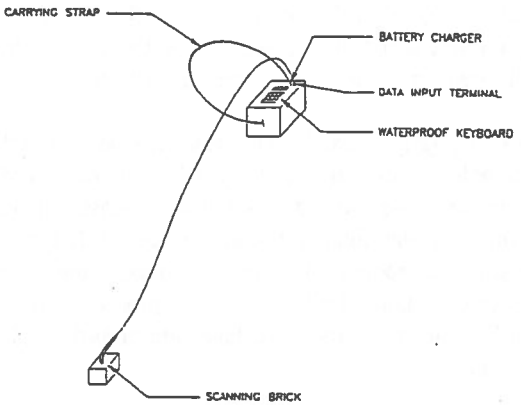

Figure 6. Scanning Brick Set-Up

Scanning Arms, are used in the underground scanner bay to measure radiation emanating from the haulage vehicles (See Fig. 7). There are six retractable arms located on the drift back, and a PEIS cesium iodide scintillating crystal is used for detection of the gamma-rays. A signal then is sent to the data source, which then stores the measurements on the SMC cartridge.

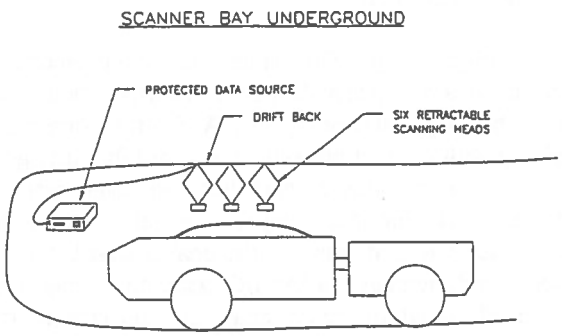

Figure 7. Underground Scanner Bay

APPLICATIONS

Underground Exploration

Currently, exploration drilling objectives are to better define the ore body and other potential structures. Drilling has to be constantly initiated because of the veining nature of the ore deposit. Drilling methods consist primarily of diamond and percussion (See Fig. 8).

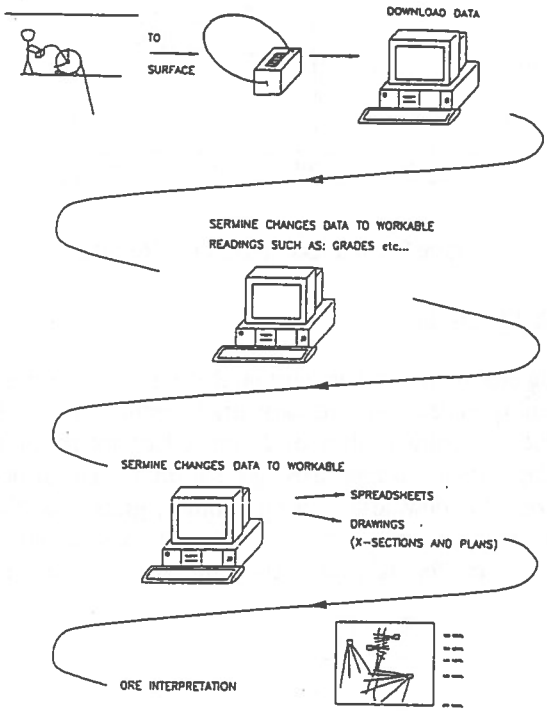

Figure 8. Underground Exploration

Diamond/Percussion Drilling, After the hole has been collared and drilled, it is measured for radiometrics. A preset program specifically for diamond and percussion holes is used. As the first reading is taken, the coiler is manually released, and this is done every half meter. If the gamma-rays start to increase, a smaller increment of ten centimeters is used. After the hole is finished the SMART scaler is taken to surface and downloaded into the Sermine software. Sermine takes the raw counts and converts them to a ASCII file.

The file now can be used for any application in Sermine such as determining grade calculations and plotting of holes. A plot of the hole (cross-section and plan view) is

made, along with radiometric peaks (See Fig. 9). The geologist then does an interpretation of the veins, by hand, to better define the vein or structure.

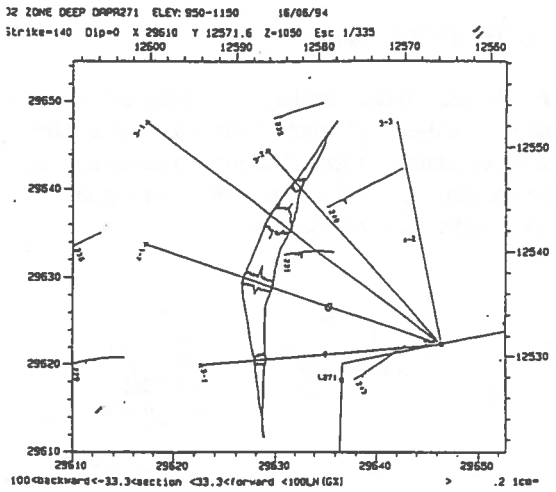

Figure 9. Cross-Section of Data Results

Mine Production

Computer applications in mine production are involved in: scanning underground haulage trucks before they go to surface, weighing haulage trucks on surface and scanning haulage trucks before they go the mill. Information recovered is downloaded using Sermine; grade ($\%U_3O_8$) and tonnage results are then obtained. Results go to spreadsheets for daily production information (See Fig. 10).

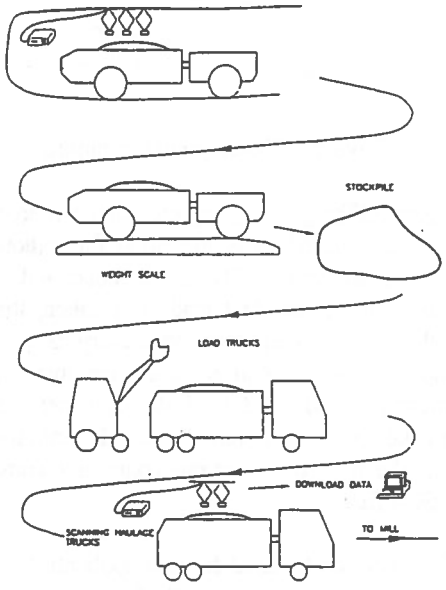

Figure 10. Mine Production

Underground Scanner Bay, The underground scanner bay is made up of a SMART Scaler and a PEIS cesium iodide scintillation crystal to detect and record the gamma radiation coming from the trucks.
First, the haulage vehicle is loaded with muck (ore/waste); it then proceeds to the 80 level where the scanner bay is located (See Fig. 7).

A haulage truck backs up into the bay which is at one side of the decline. By ways of a remote control the truck driver points a remote control at a billboard size L.E.D. readout. The truck driver enters a set of numbers corresponding to the location of where the muck came from. The scanning arms come down and read the truck, which takes 10 seconds. A signal is then carried to the SMC where it is analysed and saved. The result will tell the truck driver one of three results: if it is ore, special waste or waste.

Longole Radiometric When a stope has been drilled off by longhole methods, the blast holes then can be probed by a technician. The method of obtaining measurements is the same as the diamond and percussion holes. The purpose of the probing is to update and modify ore outlines for blasting plans. Drill holes are probed using the SMART scaler and probe. All holes are probed at 20 cm increments.

Stope Development When a undercut or overcut for a stope is developed there is a possible chance for radiation in the heading. To avoid this expected problem, sometimes probing of the hole is necessary, to see at what location the ore is located.

Weight Scale, After the haulage vehicle comes from underground, it then proceeds to the weight scale which measures gross and tare, and calculates and records net weight of the muck. The results are entered into spreadsheets. The purpose of the weight scale is to check and confirm accuracy of tonnage calculations derived from the underground scanner.

Surface Scanner Ore hauled from underground is deposited in a stockpile at the portal . Transportation to the mill is then required (See Fig. 10). A 30 ton haulage truck loads up with ore and proceeds to the mill, but first goes under a scanner. This scanner has two non-retractable scanning bricks for measuring. The signal is sent to the data source where it converts the analog signal, then it sends the information to a SMART scaler for storage. Ore is then classified by grade range and directed to the appropriate stockpile. The SMART scaler is again downloaded into Sermine.

CONCLUSION

The purpose of presenting this discussion is to show that positive flow efficiency and accuracy can be obtained with computer applications. Computers, in collaboration with radiometric equipment, can process large amounts of data, allowing for accurate geological and informed decisions to be made. Although Sermine is widely used at Eagle Point and locally in Saskatchewan, other geostatistical and geological software are available. ASCII text files from Sermine can used with other software packages such as Gemcom and Borsurv.

Our dependence with computers today and in the future will enhance the uranium industry. Computers in the uranium industry will show ever-increasing developments in the software and how it will be manipulated, making the processing and interpreting of data much easier.

ACKNOWLEDGEMENTS

This paper could not have been presented without financial support of Northern College - Haileybury School of Mines. Appreciation is also expressed to Professor Paul Bateman for his collaboration. and Professor Viswasundara Rao (KV) Kunduri for his inspiration. Cameco Corporation is also thanked for their helpful comments, as is Mélenie Levésque for her translation of the resume.

REFERENCES

CAMECO CORPORATION, 1993
Eagle Point Project 180-515 Test Stope Summary Report, Saskatoon, Saskatchewan.

CLARK, G.W., Dec 1989
Rabbit Lake Project - Mining and Development, CIM Bulletin.

ELDORADO RESOURCES LTD., Nov. 1986.
Eagle Point Uranium Deposits, Economic Minerals of Saskatchewan Conference.

HEINE, T.H., 1986.
The Geology of the Rabbit Lake Uranium Deposits of Canada, CIM Special Volume.

JONES, B.E., June 1980.
The Geology of the Collins Bay Uranium Deposit, Saskatchewan, CIM Bulletin.

WARD, D.M., Dec 1989.
Rabbit Lake Project - History and General Geology, CIM Bulletin.

CAMI'95:3rd Canadian Conference on Computer Applications in the Mineral Industry
Montréal, Québec, Canada, October 22-25, 1995

Safety Assessment Software for Spontaneous Combustion in the Valea Jiului Coal Basin

Ion Matei, Gabriel Băbuţ, Roland Moraru and Cristian Hanna
Technical University of Petroşani, Str. Universităţii, 20, 2675-Petroşani, Romania

Translated by: Gabriela Dumbravă
Technical University of Petroşani, Str. Universităţii, 20, 2675-Petroşani,Romania

ABSTRACT:

Starting from the analysis of gas balance in sealed mines, the paper presents the results of research at the T.U.of Petroşani for the elaboration of an operative method to allow the safe re-opening of isolated areas by reducing the impact on the underground environment in these situations. In order to facilitate the application of this method the FOCUS software was elaborated. The achievement of this program was possible by using the object-oriented programming.

RÉSUMÉ:

En partant de l'analyse de l'équilibre des gaz dans les mines de charbon fermées, l'ouvrage présente les résultats des recherches effectuées à l'Université Technique de Petroşani pour l'élaboration d'une méthode opérative qui permettent la reouverture dans des conditions de sécurite des zones isolées, en réduisant ainsi l'impact sur l'environnement du fond. Pour faciliter l'application de la méthode on a élaboré le programme FOCUS. Pour la réalisation du programme on a employé la technique de programmation orientée vers des objects.

INTRODUCTION

Valea Jiului is the main Romanian coal basin (13 mines, 45 000 employees). The mining object is hard coal, which, due to its predisposition to self-ignition, can generate spontaneous combustion, especially in the case of mining thick seams (80% of the coal deposits in the basin). Statistic data reveal the fact that, during the past 10 years, 39% of the total number of spontaneous combustions are reactivations of older combustions, being caused by the re-opening of isolated areas.Taking into account the above-mentioned, it was necessary to elaborate an assessment method for the safe re-opening of areas previously sealed because of spontaneous combustion. The elaboration of this method started from the studies of the U.S.Bureau of Mines (Litton D.C, 1986) and from the conditions specific to the Valea Jiului coal basin. The studies mentioned above point out that it is possible for certain mines (areas) to be re-opened even if CO concentration is very high, whereas for others, re-opening can be hazardous even if CO concentrations are very low. Consequently, indices based on the determination of CO concentrations are not valid for any coal mine, as specific conditions involve a degree of uncertainty.The reduction of this degree of uncertainty can be achieved by estimating normal conditions on grounds of measurements made before re-opening the mine/area-which is, unfortunately, not the case of Romanian mines. Another possibility of diminishing the degree of uncertainty would be to assess the extent to which normal conditions are attained.We shall present a simple methodology for determining the normal conditions within the sealed area in which a safe re-opening would be possible. The methodology relies on the monitoring of gas concentrations in sealed areas.

GAS BALANCE IN SEALED AREAS

The atmosphere in a sealed area can be considered to contain the following basic elements: air, methane, ethane and residual gas.
For a gas sample collected from a sealed area we consider residual gas R_g the volume percentage of gas left in the sample after removing the air, the methane and the ethane. The 'atmospheric air' element (A.a) can be determined starting from the oxygen concentration in the sample, by using the following relation:

$$A.a. = \alpha \cdot O_2 \quad [\%] \qquad (1)$$

The residual gas contains nitrogen in excess (in comparison with the nitrogen of atmospheric origin) combustion products (CO, CO_2, H_2, hydrocarbons) as well as other gaseous elements resulting from chemical reactions which are not directly related to the combustion process. The concentration of residual gas in a sample can be determined by the following relation:

$$R_g = 100 - \alpha \cdot O_2 - CH_4 - C_2H_4 \quad [\%] \qquad (2)$$

As the determination of ethane concentration is more difficult and for values ranging between 0-500ppm error in the determination of residual gas concentration does not exceed 0.2% equation (2) can be written:

$$R_g = 100 - \alpha \cdot O_2 - CH_4 \quad [\%] \qquad (2')$$

Each component of the residual gas (which contains all gases except O_2, CH_4 and atmospheric N_2) can be expressed by its concentration with respect to the total concentration of residual gas.

As a particular case, CO concentration in the residual gas can be determined by the relation:

$$(CO)_{R_g} = \frac{(CO)_s}{R_g} \cdot 100 \quad [\%] \qquad (3)$$

where: $(CO)_s$-carbon monoxide concentration in the sample, ppm.

Starting from the previous relation, an index R_i can be defined as it follows:

$$R_i = \frac{1}{R_g} \cdot (CO)_{R_g} = \left[\frac{(CO)_s}{R_g^2} \right] \cdot 100 \qquad (4)$$

If R_i remains constant one of the following situations may occur: sustained low-temperature combustion, or a sustained low rate of ambient CO production.

If combustion is taking place, the average R_i value will be higher than if ambient CO production is occurring, because CO production increases with temperature.

In deriving a ratio, the actual measured R_i is referred to as $(R_i)_{act.}$ A second R_i, known as the maximum equilibrium value $(R_i)_{eq}$, is also obtained:

$$(R_i)_{eq} = 2 \cdot a \left(\frac{R_g}{O_2} \right)^2 \qquad (5)$$

where: $(R_i)_{eq}$ represent the maximum equilibrium value of the R_i-Index for a gas sample, if only ambient temperature processes are responsible for CO production.

The application of this assessment method is conditioned by a previous determination of coefficients a and b for each mine or coal basin. For this purpose, relation (5) is liniarized and least-squares method is applied.

The data subjected to statistical analysis can be obtained in two ways: by laboratory or 'in situ' measurements.

For the conditions specific to the Valea Jiului coal basin, measurements made up to now lead to the following: a=137,b=-0.43 (r^2=0.94)-for Vulcan mine;a=129,b=-0.38 (r^2=0.87)-for Paroşeni mine (MATEI I. and BĂBUŢ G., 1995). The complex tectonic structure involves a great variety of deposit conditions which leads to the necessity of determining the values of coefficients a and b for each mine.

If data for the determination of coefficients a and b are not available, the data provided by scientific bibliography can be used, but in the latter case the accuracy of the application of this method is conditioned by the extent to which the conditions for which these values were determined coincide with the ones existing in the area or mine in question.

An equation, refferred to as RATIO (R) has been created to determine the state of a sealed area:

$$R = \frac{(R_i)_{ef}}{(R_i)_{eq}} = \frac{50}{a} \cdot CO \cdot R_g^{-(b+2)} \cdot O_2^b \qquad (6)$$

Values of R>1 clearly indicate the failure in achieving the safety conditions imposed by the re-opening of a sealed area.

Values of R<1 indicate a certain stability which can be attained if the RATIO is stabilized at a value <1.

It is important to remember that as long as the RATIO decreases from one sample to another (even if values are <1), equilibrium conditions at a normal temperature are not achieved. This stage is reached only if the

RATIO is stabilized at a subunit value within a time range of minimally 30 days.

If at a certain moment the RATIO (for one sample) becomes higher that 1 and then drops again below 1, another 30-day period is necessary.

Specifications regarding the use of the method

a.The previously presented analysis is valid for all the cases when O_2>1%. If not so, the maximal equilibrium value of R_i is given by the relation:

$$(R_i)_{max}=2\cdot a\cdot (R_g)^{-\frac{1}{2}}\cdot O_2^{-1} \qquad (7)$$

and the expression of the RATIO becomes:

$$R=\frac{1}{3}\cdot CO\cdot (R_g)^{-\frac{3}{2}}\cdot O_2 \qquad (8)$$

This situation may occur especially in mines with high gas emissions, where methane concentrations can lead to the dilution of all the other gases until they reach low concentrations.

Substantial methane emissions also contribute to the acceleration of oxidation processes, as a result of the extension of free surfaces during oxidation.

b.The values of R_i depend not only on the coal type, but also on the local conditions, humidity playing a very important part. Generally, the values of R_i are lower for the types of coal with a high moisture degree. With coals having a low moisture degree, the free surface resulting from oxidation is larger and consequently, there will be a higher CO production and higher values of R_i.

FOCUS SOFTWARE

In order to facilitate the application of an operative method the FOCUS software was elaborated. The achievement of this software was possible by using the object-oriented programming and the TURBO PASCAL 6.0 language (the object library TURBO VISION).

The use of a high level language provides the following facilities:

-the sofware can be used by specialists with minimal knowledge of computer processing due to the presence of pull-down menus (fig. 1);

-the software can be handled rapidly and comfortably by using a mouse;

-the software also manages files containing output and input data;

-output data can be presented optionally,tabular or graphical (fig.2 and fig.3);

-the user is assisted in decision making; so, the software also has the features of an expert system (fig.4);

-by using an interface, the software can process and analyze data provided by a telemeasuring system.

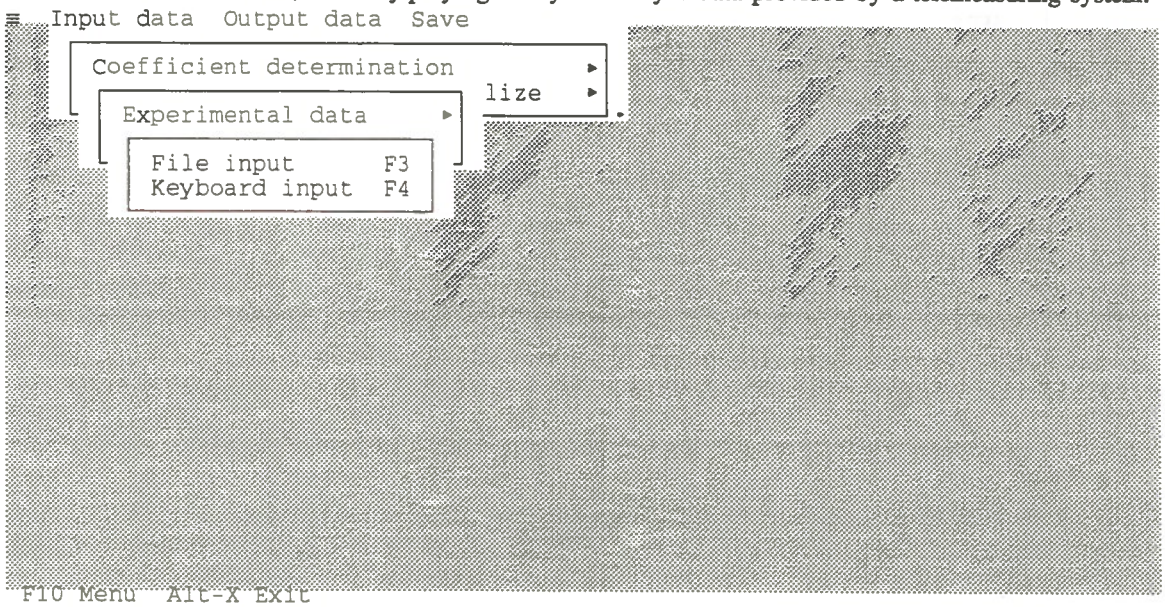

Figure 1

Measurement	CO	O2	CH4	R
0	(ppm)	(%)	(%)	
1	5291.00	18.7000	2.5000	[illegible]
2	4315.00	18.5000	2.6500	[illegible]
3	2987.00	18.5000	3.1000	[illegible]
4	2504.00	18.2000	2.9000	[illegible]
5	2706.00	18.0000	3.0000	[illegible]
6	1907.00	17.8000	3.2000	[illegible]
7	2315.00	17.8000	3.2000	[illegible]
8	1858.00	17.5000	3.5000	[illegible]
9	1600.00	17.2000	3.7000	[illegible]
10	2120.00	17.1000	3.8000	[illegible]
11	2400.00	17.0000	3.8000	[illegible]
12	2267.00	16.7000	4.1000	[illegible]
13	1858.00	16.6000	4.2000	[illegible]
14	1963.00	16.6000	4.3000	[illegible]
15	1670.00	16.4000	4.5000	[illegible]
16	2120.00	16.1000	4.6000	[illegible]
17	2004.00	16.0000	4.6000	[illegible]
18	1503.00	15.8000	4.9000	[illegible]
19	1706.00	15.7000	5.0000	[illegible]
20	1435.00	15.5000	5.0000	[illegible]
21	1510.00	15.4000	5.1000	[illegible]
22	1208.00	15.4000	5.2000	[illegible]
23	981.00	15.2000	5.2000	0.8528
24	1034.00	14.9000	5.3000	0.8275
25	903.00	14.7000	5.4000	0.6873
26	736.00	14.4000	5.6000	0.5232
27	811.00	14.1000	5.7000	0.5373
28	602.00	13.8000	5.7000	0.3711
29	575.00	13.4000	5.8000	0.3258
30	406.00	13.0000	5.9000	0.2128
31	509.00	12.8000	6.0000	0.2576
32	489.00	12.7000	6.0000	0.2428

Press any key to continue . . .

Figure 2

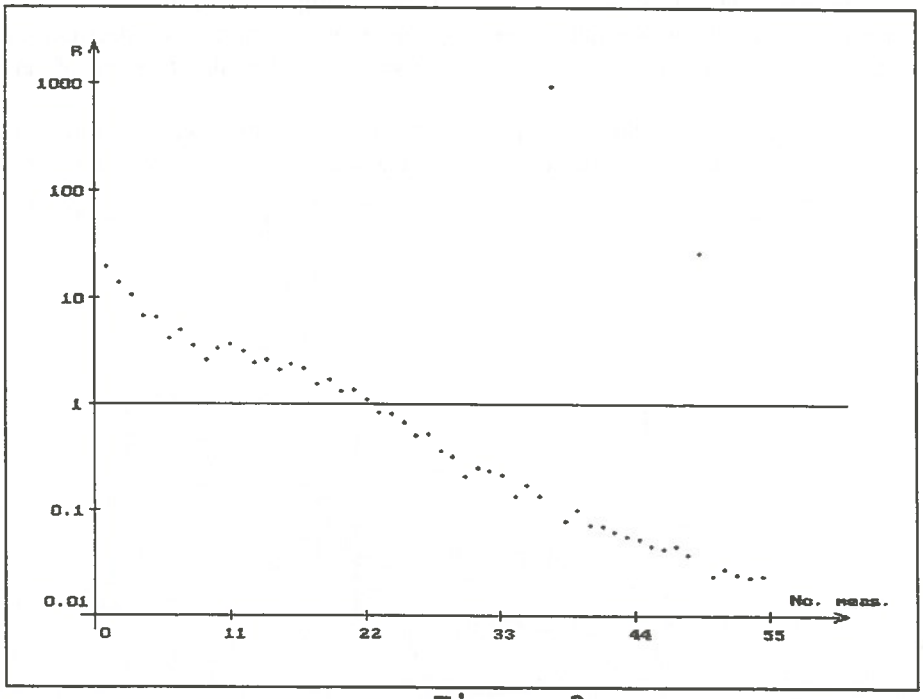

Figure 3

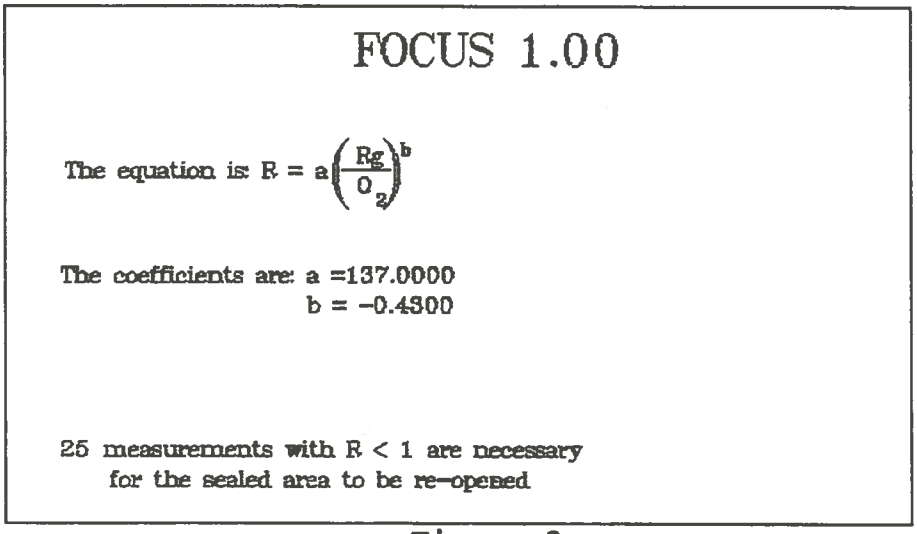

Figure 3

The FOCUS software, together with a user's guide, are available at the Technical University of Petroşani.

CONCLUSIONS

Starting from the analysis of gas balance in mines/sealed areas, the paper presents a simple methodology based on the measurement of the concentration of a minimal number of gases (CO, CH_4, O_2), which allows the safe re-opening of sealed areas and reduces the impact on the environment in such situations. The analysis is simplified by the use of the FOCUS sofware, especially conceived for this purpose. By using an interface, this sofware can process and analyze data provided by a telemeasuring system.

The method is recommended as an extra tool for the monitoring of the evolution of spontaneous combustions in mines/sealed areas as it is a means of considerably increasing safety in re-opening operations.

REFERENCES

LITTON, D.C., 1986.
Gas equilibrium in sealed coal mines. U.S. Bureau of Mines, R.I.-9031.

MATEI,I. and BĂBUŢ G., 1995.
Operative method for the assessment of safety conditions in re-opening areas previously sealed because of spontaneous combustion. The Scientific Papers of the Technical University of Petroşani, 27(2), pp.157-163.

12.

mineral processing
traitement du minerai

CAMI'95: 3rd Canadian Conference on Computer Applications in the Mineral Industry
Montréal, Québec, Canada, October 22-25, 1995

Application of Knowledge-Based Systems Technology in Optimization of Mineral Grinding Circuits

Akbar Farzanegan
Department of Mining and Metallurgical Engineering, McGill University, Montréal, Québec, Canada

André R. Laplante
Department of Mining and Metallurgical Engineering, McGill University, Montréal, Québec, Canada

David A. Lowther
Department of Electrical Engineering, McGill University, Montréal, Québec, Canada

ABSTRACT

For more than three decades, there has been continued efforts to provide mineral processors with efficient computer-based tools for the optimization of grinding circuits. This resulted in the development of steady-state and dynamic simulators based on process unit models which can successfully predict grinding circuit performance. Simulators are normally used to mimic the behaviour of the grinding circuits under different operating conditions for the purpose of designing new plants or optimizing of existing ones. This paper describes the concepts of building grinding simulators employing the knowledge-based approach, highlighting differences and similarities between knowledge-based and procedural implementation methods. Experiences with developing a prototype system using the CLIPS expert system shell will also be demonstrated.

RÉSUMÉ

Depuis trente ans, d'importants efforts ont été faits pour procurer aux minéralurgistes des outils informatiques efficaces pour l'optimisation des circuits de broyages. Ces efforts ont conduit au développement de simulateurs statiques et dynamiques qui peuvent prédire le comportement des circuits de broyage, dans certains cas avec beaucoup de précision. Ces simulateurs sont normalement utilisés pour fins de conception ou optimisation. Cet article décrit certains concepts servant à la conception de tels simulateurs à partir d'une approche de systèmes à base de connaissances (SBC), également appelés systèmes-experts. Nous efforçons de mettre en évidence les différences et les similarités probables entre l'approche SBC et l'approche conventionnelle. Nous décrivons certains aspects du développement d'un prototype de système expert utilisant la coquille CLIPS.

INTRODUCTION

Computer-aided grinding optimization has been an active research area in mineral processing field over the past several years [Sastry and Little, 1992]. The ultimate goal of developing and applying optimization techniques is to make a plant more profitable. This can be accomplished through process improvement, better understanding of the underlying process, optimal flowsheet design and modifications and development of new and more efficient control systems [Mular, 1972]. Computer simulation of grinding, which is basically one of the most important optimization tools, enables improved circuit design, diagnosis and control. Deriving general mathematical models of the different units used in comminution circuits was the primary step in

order to develop circuit simulators. The history of these grinding models and their status have been illustrated elsewhere in detail [Napier-Munn and Lynch, 1992]. However, the emergence of artificial intelligence (AI) technologies, e.g. knowledge-based systems (KBSs) and neural networks (NNs), has affected newly developed software, particularly in control applications. For instance, rule-based expert control systems have been successfully installed in several grinding plants in recent years [Herbst et. al. 1989; Flintoff et. al. 1988].

This paper discusses grinding optimization as a problem domain for the KBS technology and how the knowledge-based approach can be applied to this domain in order to construct more effective tools for grinding optimization. At the end, the specifications of a prototyped system developed using the C language and the CLIPS (C Language Integrated Production System) KBS shell will be described.

GRINDING OPTIMIZATION

Optimization considerations must be taken into account at both the design and operational stages of a grinding circuit. The selection of the best circuit configuration (e.g., the type and the numbers of physical units, series or parallel linkage, design variables such as the milling rate and equipment dimensions) is normally considered as optimization at the design stage. On the other hand, minor modifications to circuit flowsheet, such as changing grinding media size or shape, would be thought as optimization at the operational stage. It can be implemented either off-line or on-line, depending on whether a valid process model is available or not [Mular, 1972].

Mathematical Process Unit Models

Unit models form the building blocks of any grinding simulator. For example, mathematical models can be employed to simulate the individual operation of mills or classifiers. However, if the intention is to simulate a full grinding circuit, then, a main program should be written to call the unit models as sub-routine programs. When there are recycled streams such as circulating loads in closed-wet grinding circuits, an iterative approach is normally used to calculate recycle stream variables. Ball mills and hydrocyclones are commonly used devices in grinding plants for which models varying widely in complexity have been proposed.

Simulation of ball milling as a single unit operation is based on population balance modelling (PBM), a common approach for the analysis of particulate systems. Considering grinding as a rate process and material balance constraints has led to the derivation of the classical batch grinding equation. The batch grinding model has been extended by introducing residence time distribution (RTD) functions to simulate continuous operation. For hydrocyclones, two empirical models have been developed and are widely accepted [Plitt, 1976; Lynch and Rao, 1975].

Circuit Simulation

Steady-state grinding simulators were found to have useful applications for design and circuit analysis (diagnostics). On the other hand, dynamic grinding simulators have been used successfully for developing and testing new control system strategies. Although considerable work has been done on developing unit operation models, a few grinding simulators have been developed according to software engineering standards which ensure their acceptability by the targeted end users, i.e. mineral process engineers. Simulating a real grinding plant requires much effort which begins with model building for each physical unit of the circuit. Then, validated unit models are connected together to simulate whole circuits. The sequential modular approach is widely used to simulate grinding circuits which include mathematical models to represent processing units, Figure 1. An executive program monitors the information flow among the unit models and therefore links the unit models.

In grinding circuits closed with classification systems, recycle calculations (circulating load) are of importance in terms of computing efficiency. Simulation of recycled streams is mainly based on the stream tearing and system decomposition theory which is very common in process flowsheet analysis [Upadhye and Grens, 1975]. As in most cases an iteration technique is employed to solve the recycles, then computation speed would be critical to achieve a steady-state according to a predefined convergence criterion.

Knowledge-Based Approach to Grinding Simulation

The knowledge-based approach could be considered as a new methodology for constructing grinding simulators. This recently standardized methodology adds new

dimensions to the way software is usually developed, i.e, by employing conventional tools such as

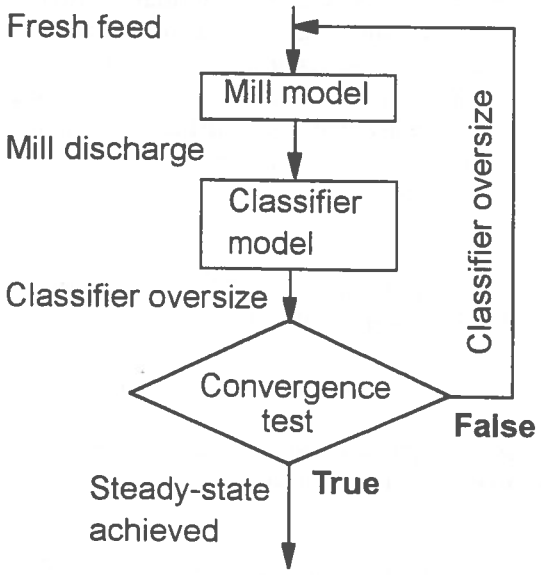

Figure 1. Simulation of a closed grinding circuit

C or FORTRAN. One of the main advantages of KBS tools is their capability to accommodate the heuristic (rule of thumb) knowledge of the domain more efficiently. Conventional languages use a procedural way of knowledge representation which often suits the programming of algorithms for mathematical calculations. In the context of grinding simulation, it is noteworthy that the numerical procedures, e.g. an algorithm to calculate a ball mill discharge size distribution, still need to be implemented in procedural languages.

KNOWLEDGE-BASED SYSTEMS

Generally defined, a KBS uses knowledge or expertise about a specific domain to solve problems of that domain [Gonzalez and Dankel, 1993]. Expertise means the problem solving knowledge held by a person (i.e. expert) which he has accumulated during years of experience in his specialty. The most noticeable differences between KBSs and conventional algorithmic programs are: the separation of knowledge from control, the use of highly specific domain knowledge, and the use of heuristics (rules of thumb) and reasoning with symbols [Durkin, 1994; Gonzalez and Dankel, 1993]. Knowledge acquisition, knowledge representation, reasoning or inference methods and uncertainty management are among the most important research topics in knowledge engineering. A KBS has several components as shown in Figure 2. Often, due to the necessity of integration to other software, industrial KBSs are more complicated than what is depicted in Figure 2.

Knowledge Representation

Knowledge representation defines the method used to structure and encode the acquired knowledge. For instance, rules and frames are the most common methods supported by commercial software. In hybrid

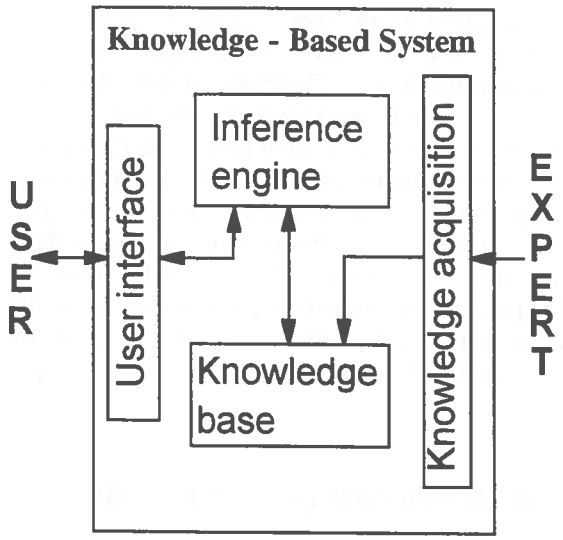

Figure 2. General structure of a typical KBS

systems, the knowledge-based system name may refer to its major type of representation method, e.g. rule-based or frame-based systems.

Briefly, rules are structures which connect a piece or a cluster of known information (facts) to other information. Then, if the known information (antecedents) are believed to exist, the other part of information (consequent) is logically inferred to be true. Frames are considered as structures which hold the stereotypical knowledge about an object. It should be noted that the knowledge representation(s) method supported by a specific KBS shell is a critical factor in its selection as the development tool.

Reasoning and Inference Techniques

Several reasoning methods are commonly used in KBSs to draw conclusions based on facts and knowledge represented to the system. These include deductive, inductive, abductive, analogical, common-sense and

non-monotonic reasoning [Durkin, 1994]. Inference, however, refers to the mechanism or the process of applying a reasoning method, which is done by a module called the inference engine. Forward and backward chaining form the two basic inference techniques supported by most KBS development shells.

Uncertainty Management in KBSs

This is of much importance in the knowledge engineering field. In reality, there are usually some uncertainties attached to the known facts about the problem, e.g. data given by the user, and the problem solving knowledge, e.g. rules given by the expert, encoded in the knowledge base. Therefore, a KBS has to be designed so that it can represent uncertain rules and also continue problem solving process using uncertain data. This requirement for KBSs has given rise to the development of theories related to reasoning under uncertainty and inexact information, such as certainty factors and fuzzy logic. Available KBS shells and development tools support some types of uncertainty management schemes which should be taken into account during their selection.

FRAME-BASED GRINDING SIMULATION

The concepts of using object-oriented design in grinding simulation and real time process control have been discussed by Sastry and Little [1992] and Ynchausti, Hales and Smith [1992]. This type of software design resembles frame-based systems in AI. Nowadays, both terminologies interchangeably refer to the same thing [Durkin, 1994]. The main idea is to establish a hierarchy of different physical objects which make up a grinding circuit such as mills, classifiers, material handling equipment and streams. The notion of objects is not restricted exclusively to physical entities and can be extended to conceptual subjects. For instance, the concepts of breakage function and selection function can be represented as objects.

The areas of frame-based design and object-oriented programming share many features which make them very similar [Durkin, 1994]. A frame-based approach is natural for simulation and control problems [Durkin, 1994]. Grinding circuit simulation using a frame-based (or object oriented) expert system shell should be considered as a new approach in contrast to those of traditional packages which use only a single (procedural) knowledge representation.

After creating classes (frames) and instances (frames), two mechanisms can be used to manipulate the knowledge contained in the frames, i.e., pattern matching rules and object communication. Using the former approach, after defining BALLMILL as a class, we need only one rule to calculate the size distribution of all instances of that class:

```
IF
    ball mill feed data are available
    ball mill model is defined
THEN
    calculate ballmill output size distribution
```

in the second approach, however, a message is sent to each instance of the BALLMILL class:

```
IF
    ball mill feed data is available
    ball mill model is defined
THEN
    SendMessage(ballmill1, CalculateOutputSize)
```

After rule execution, a message is sent to ballmill1 to generate the ball mill output size distribution. It is assumed that we have already defined a procedure attached to the class frame BALLMILL which intercepts the message and calculates the size distribution of the product accordingly. In this example, the message was sent from the right hand side (RHS) of a rule. Messages can be sent also from an object (defined in its class frame) to another object.

PROTOTYPED SYSTEM: AN OVERVIEW

A prototype system was developed for Windows™ as a test bed to try applications of KBSs concepts in grinding optimization domain. The software has been designed as an off-line steady-state grinding simulator and also a decision support for choosing the optimum circuit configuration and operating variables.

The program consists of two main components. The first, written in the C language, includes all functions related to grinding simulation such as the sub-routine which calculates ball mill discharge size distributions and the sub-routine which estimates selection functions. The second is a knowledge base written in CLIPS. Integration of these two components is of importance if

the embedding of CLIPS in a simulation package is the purpose of software development.

Grinding Simulation Module

CLIPS provides a mechanism which allows programmers to use a class of predefined mathematical functions for numerical calculations in the RHS of rules. Nevertheless, it is not possible to perform number crunching computations efficiently in the RHS of rules, a requirement in grinding simulation. For this reason, all complex calculations should be done in functions which are external to CLIPS.

Simulation of ball milling is based on the classical size-discretized population balance model of the grinding process assuming a first order kinetics. The model for the batch grinding can be represented in a matrix form as follows:

$$d\underline{M}/dt = (B-I)S\underline{M}$$

where $\underline{M}$ is a column vector showing the size distribution of the mill hold-up; B is the breakage function matrix and S is the selection function matrix. The solution to the above differential equation is:

$$\underline{M} = T\exp(-St)T^{-1}\underline{M}(0)$$

where $\underline{M}(0)$ is the initial (feed) size distribution; t is grinding time and T is transformation matrix whose [Luckie and Austin, 1972] elements are:

$$T(i,j) = 0, \qquad i<j$$

$$T(i,j) = s_j, \qquad i=j$$

$$T(i,j) = \frac{1}{s_i - s_j}\sum_{k=1}^{i-1} b_{ik}s_k T(k,j), \qquad i>j$$

To simulate continuous grinding, the transport of material through the mill should also be modelled and incorporated into the batch grinding equation. Assuming that transport is particle size independent, it can be effectively described with a residence time distribution (RTD). A tank-in-series model proposed by Weller [1980] is used here, that incorporates one plug flow reactor, two identical perfect mixers and a third, larger, perfect mixer. These units have mean retention times of τ_{pf}, τ_s and τ_l, respectively. This yields:

$$\underline{M} = T[I+S\tau_s]^{-2}[I+S\tau_l]^{-1}\exp[-S\tau_{pf}]T^{-1}\underline{M}(0)$$

A sub-routine program has been included in the simulation package for the estimation of the selection function for all particle size classes, which can also serve as a diagnostic tool to investigate the efficiency of the grinding kinetics. Given the size distribution of ball mill feed and discharge, the breakage function data and the RTD parameters, the algorithm does a binary search to find an acceptable value of the selection function for each size class.

CLIPS: KBS Development Tool and Shell

CLIPS, a software product by NASA, was used as the knowledge-based system shell. It is a forward-chaining system which supports several knowledge representation schemes such as rules, procedural, and objects. In addition, CLIPS provides some tools for editing, debugging and verification of the knowledge base. Details of CLIPS 6.0 have been documented in the CLIPS Reference Manual [1993].

Grinding Knowledge-Base

The current grinding knowledge base was developed in the CLIPS language format using a set of 25 grinding rules. Besides the rules which define grinding knowledge, the knowledge-base contains some rules and constructs for user interface and query the user. CLIPS has provided a construct called DEFMODULE which allows a knowledge base to be partitioned to modules. The knowledge base consists of three modules concerning the grinding domain: ball mills, hydrocyclones and circuits. There are also some modules for utility purposes such as menu, query and printing results. All rules are composed of two parts, i.e. Left Hand Side (LHS) and Right Hand Side (RHS) which represent conditional elements and conclusions of the rule, respectively. Some of the grinding rules of the system knowledge base are as follows:

Rule 1:
IF
    no hump exists in the selection function curve
    ball mill feed does not get much coarser
THEN
    ball size must be decreased

Rule 2:
IF
    ball size must be decreased
    ball size is greater than or equal to 1.5"
THEN
    decrease ball size by 0.5"

Rule 3:
IF

ball size must be decreased
ball size is less than 1.5"
THEN
decrease ball size by 0.25"

Rules 1, 2 and 3 constitute an inference chain which results in different conclusions concerning a new ball size to be used. The final conclusion depends on the knowledge about the selection function curve, the ball mill feed size distribution and the grinding media size.

The shape of a selection function curve must be obtained by the user through a multi-stage process including sampling, size analysis and parameter estimation calculations. The latter step is performed by the sub-routine included in the simulation package. The user then draws the selection function curve to examine its shape. Determining that the curve has a hump or not is not a clear-cut decision which requires heuristic judgment by the user, Figure 3.

In terms of the knowledge base verification, the current system is working well. However, the knowledge base covers a limited area of expertise concerning wet industrial grinding which requires more knowledge acquisition efforts and system maintenance by adding newly extracted knowledge encoded in chains of rules. It was found that the knowledge coverage by the grinding KBS has a strong impact on its validity and final acceptance as well as its effectiveness in solving

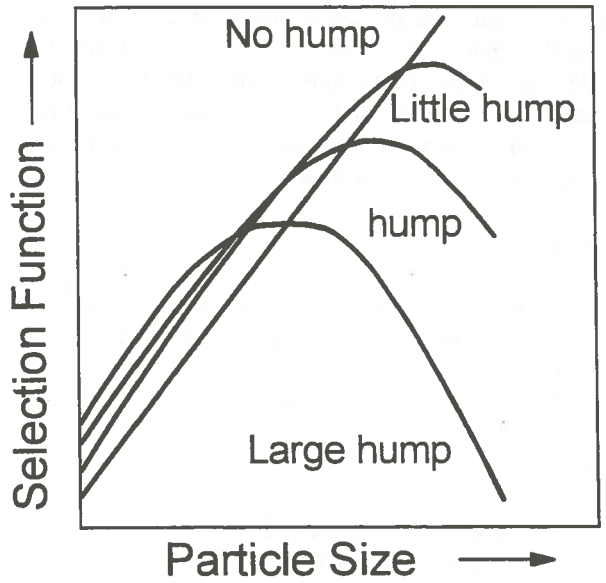

Figure 3. The shape of the selection function curve can help to diagnose the grinding efficiency for the range of particle size classes

expected problems in grinding optimization.

System input and output

The program was intended to be a user-friendly software using pull-down menus, dialog boxes for data entry and other features commonly found in graphical user interfaces. Figure 4 shows an example view of the program interface.

The system user can begin a consultation session by running CLIPS. Currently, the user interface directly supported by CLIPS is only text input and output. The user should answer the system's questions by typing appropriate answers. However, in larger commercial systems, this type of user interface is not desirable, as it causes errors due to user's typing mistakes. Graphical user interfaces (GUI) reduce user errors and increase system usability.

Figure 5 shows a consultation session with the grinding

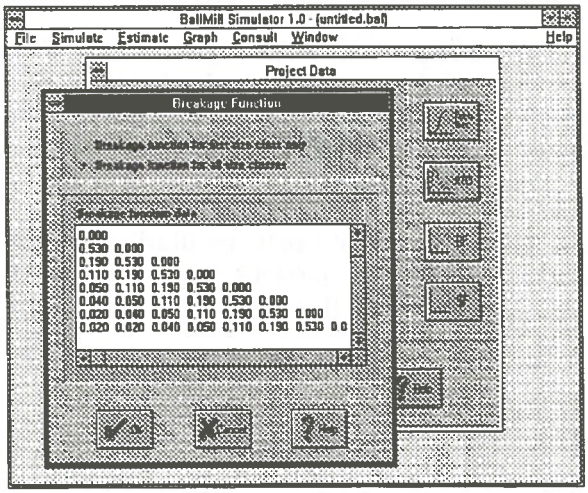

Figure 4. A view of the program user interface showing dialog boxes for data input

expert system. Each session is composed of two parts. In the first part, the system queries the user about underlying problems. Then, based on the answers given by the user, a possible conclusion(s) is offered by the expert system. For each conclusion, the last rule which led to the current result is identified, which might help the user to find an explanation for the basis of such a conclusion.

Linkage of Grinding Simulator and CLIPS

One of the features of CLIPS is its capability to be integrated with external languages, e.g., C and

FORTRAN [CLIPS Reference Manual, 1993]. This

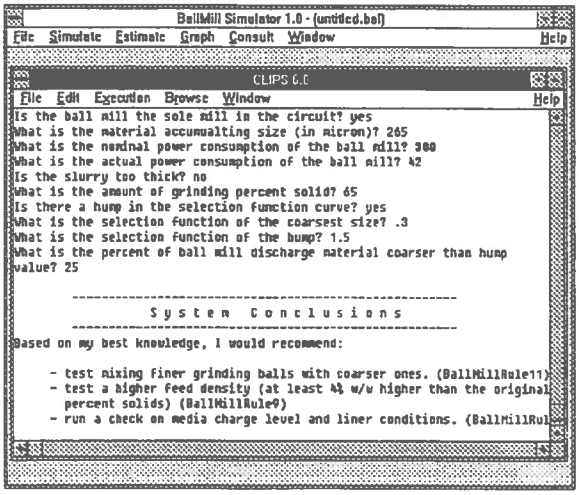

Figure 5. A typical consultation session with the grinding expert system

means that functions written in either of these languages can be called by CLIPS as a consequence of rule firing. Grinding simulation requires numerical calculations which can be done effectively by writing functions in procedural languages. As previously mentioned, in conventional simulators, the control of execution is done sequentially through a monitor or executive program which calls necessary modules such as ball mill or hydrocyclone models to calculate product size distributions. In a rule-based grinding simulator, however, the monitor or executive program is replaced by a number of rules so that modules will be called from the RHS of these rules.

CONCLUSIONS

The general concepts of knowledge-based approach as a new software development methodology and its application to the grinding optimization domain has been reviewed. Adding the capabilities of rule-based and frame-based systems to off-line grinding simulators should make it possible to incorporate human expertise more effectively. Current simulators lack this feature. A system was developed as a prototype to investigate the applicability and benefits of using the knowledge-based approach in grinding optimization. Preliminary results showed that heuristic grinding knowledge can be easily added to the conventional simulators which then may be consulted by the user for decision support purposes. However, it was observed that a rule-based representation is insufficient to accommodate the diversity of the knowledge in the grinding domain. Developing certainty factors for grinding heuristics is not an easy task which makes handling uncertainty very difficult. It is evident that frames are more efficient than rules in terms of structuring the knowledge of about processing units (particularly, the physical specifications of equipment used in a grinding circuit)required for circuit simulation.

ACKNOWLEDGEMENTS

The first author gratefully appreciate the financial supports provided by the Ministry of Culture and Higher Education of Iran.

REFERENCES

CLIPS Reference Manual, 1993
Software Technology Branch of NASA, Lyndon B. Johnson Space Center, Vol. 1, pp. 1-25

Durkin, J., 1994
Expert Systems: Design and Development, McMillan Publishing Company, New York, pp. 437-487

Flintoff, B.C., Edwards, R.P. and Neale, A.J., 1988
Real-Time Expert Systems in Process Control preprint of Proc. of Ann. CMP Meeting, Vancouver, Canada, Dec. 9, pp. 1-19

Gonzalez, A.J. and Dankel, D.D., 1993
The Engineering of Knowledge-Based Systems: Theory and Practice, Prentice Hall, Englewood Cliffs, New Jersey, pp. 1-47

Herbst, J.A., Hales, L.B., Pate, W.T. and Sepulveda, J.E., 1989
Reports on Actual Benefits Arising from The Application of Expert Control Systems in Industrial Semi-Autogenous Grinding Circuits Proc. of IFAC, Buenos Aires, Argentina, 4-8 Sept., pp. 53-60

Lynch, A.J. and Rao, T.C., 1975
Modelling and Scale-Up of Hydrocyclone

Classifier, 11th Int. Miner. Process. Congr., Cagliari, Italy, 20-26 April, pp. 245-269

Luckie, P.T. and Austin, L.G., 1972
A Review Introduction to The Solution of The Grinding Equations by Digital Computation, Minerals Sci. Engng, Vol. 4, No. 2, April, pp. 24-51

Mular, A.L., 1972
Empirical Modelling And Optimization of Mineral Processes, Minerals Sci. Engng. Vol. 4, No. 3, pp. 30-42

Napier-Munn, T.J. and Lynch, A.J., 1992
The Modelling And Computer Simulation of Mineral Treatment Processes- Current Status And Future Trends, Minerals Engineering, Vol. 5, No.2, pp. 143-167

Plitt, L.R., 1976
A Mathematical Model of The Hydrocyclone Classifier, CIM Bulletin, PP. 114-123

Sastry, Kal V.S. and Little S.N., 1992
Fundamental And Practical Aspects of An Advanced Simulator for Comminution in Comminution-Theory and Practice, S. Komar Kawatra, Editor, SME Inc., Littleton, CO., pp. 307-316

Ynchausti, R.A., Hales, L.B. and Smith, R., 1992
Real-Time Process Control Using Object Oriented Expert Systems in Comminution-Theory and Practice, S. Komar Kawatra, Editor, SME Inc., Littleton, CO., pp. 575-582

Weller, K.R., 1980
Hold-Up and Residence Time Characteristics of Full Scale Grinding Circuits, Third Symp. of IM3P of IFAC, Montreal, 18-20 August, pp. 303-309

CAMI'95: 3rd Canadian Conference on Computer Applications in the Mineral Industry
Montréal, Québec, Canada, October 22-25, 1995

Measurement of Bubble Swarm Buoyancy Velocity in Three-Phase System

G.Shen, H.Nawfal, J.Watson and J.A.Finch
Department of Mining and Metallurgical Engineering
McGill University, Montreal, Quebec

S.Banisi
Shahid Bahonar University, Kerman, Iran

ABSTRACT

Using a new technique based on conductivity, the bubble swarm buoyancy velocity was measured in a column in a three-phase system. Previous work on a flotation column had shown that the gas holdup decreased (by up to 40% relative) in the presence of solids. One hypothesis was that the solids caused an increase in the rise velocity of the bubble swarm (Banisi et al., 1995b). In this work, it is established that one measure of swarm velocity, the buoyancy velocity, is increased in the presence of solids.

RÉSUMÉ

L'utilisation d'une nouvelle technique basée sur la conductivité a permi de mesurer la vélocité de la flottabilité des bulles dans une colonne contenant un système à trois phases. Un travail précédent avec une colonne de flotation a demontré que le gaz emmagasiné avait diminué (jusqu'a 40%) lors de la présence de solides. On peut supposé que la présence de solides amène une augmentation dans l'élévation de la vélocité des bulles (Banisi et al., 1995b). Dans ce travail, nous avons établi qu'une mesure de la vélocité des bulles, la flottabilité de la vélocité, augmente en présence de solides.

INTRODUCTION

In three-phase reactor design, the effect of solids on gas holdup has been the focus in many studies. However, the results of these studies were often contradictory: both increasing and decreasing effects have been reported (Sada et al., 1986; Hidaka et al., 1992; Ostergaard, 1971, 1978; Ying et al., 1980; Clark, 1990).

Under simulated flotation conditions, the gas holdup in air-water and air-water-solid systems was determined in a continuously operating column by Banisi et al. (1995a). The effect of concentration, size and type of solid particles on gas holdup was examined. In all cases examined, the presence of solids significantly decreased the gas holdup (Figure 1). Several mechanisms were explored (Banisi et al., 1995b). One hypothesis was that solids increased the rise velocity of bubbles due to stabilization of the bubble wake. To test the hypothesis, a novel technique based on conductivity used to measure bubble swarm velocity in air-water systems and described at CAMI'91 (Shen et al., 1991) could, it was felt, be adapted.

In this technique, a step change in gas rate causes an interface to form between regions of different gas holdup. This interface is readily detected and tracked by the difference in conductivities across the interface resulting from the difference in gas holdup. In the case when the gas flow is terminated, above the interface the gas holdup, ε_g, is that prior to the termination while below the interface $\varepsilon_g = 0$. By definition (Nicklin, 1962), the velocity of this rising interface is the buoyancy velocity of the bubble swarm, u_0. The u_0 is a characteristic of the system and is proportional to the bubble swarm velocity.

The conductivity technique was used here to measure the buoyancy velocity in the air-water-silica system. The results illustrate that the presence of the solids does cause an increase of the buoyancy velocity of the bubble swarm.

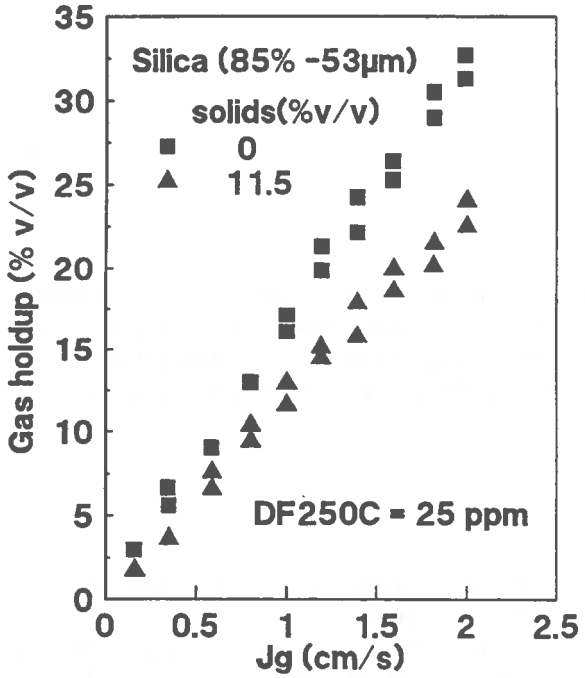

Figure 1 Example of presence of solids decreasing gas holdup (after Banisi et al. 1995a).

APPARATUS AND TECHNIQUE

The general set-up is shown in Figure 2. The flotation column, made of Plexiglas, was 4.47 m in height and 10.18 cm in diameter. Bubble generation was through a porous (~10 μm diameter holes) cylindrical stainless steel sparger at the bottom of the column. A calibrated gas mass flowmeter (Tylan model FM-380) and MIC 2000 controller were used to measure and display the air flowrate. Masterflex pumps (model 720-33) were used to feed and discharge the column. A stirrer was used in the reservoir to mix the slurry and keep the solids in suspension.

Two grid electrodes (Uribe-Salas et al., 1994) separated 74 cm were installed inside the column, which were linked to a custom-made fast response conductivity meter (Shen et al., 1991). A computer (IBM PS/2 Model 60) equipped with a 12-bit A/D board (μDAS-8 PGA) was used to record the output of the conductivity meter. For each experiment, data were saved as a file for analysis.

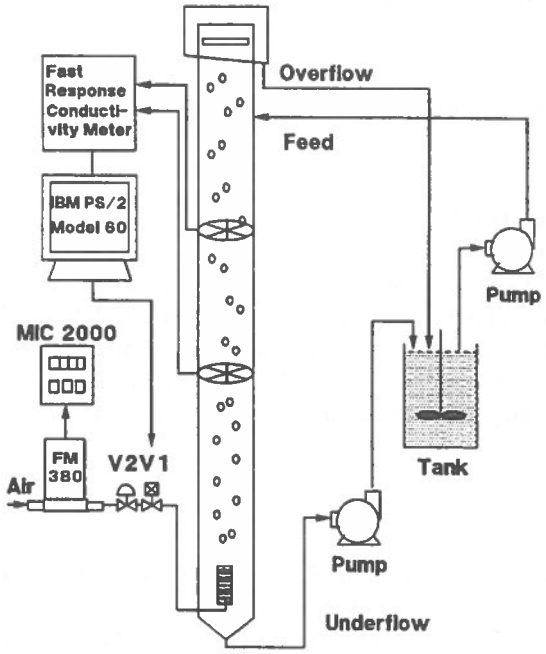

Figure 2 Schematic illustration of experimental set-up.

The air flow was controlled by two valves: a manual valve V2 and solenoid valve V1. The manual valve was used to vary the air flowrate and the solenoid valve, used for switching the air on or off, was controlled by the computer.

The experiment was initiated by terminating the air flow. The procedure, controlled by the computer, was:

(a) open Valve 1 (V1) and adjust Valve 2 (V2) to set the superficial gas velocity, J_g;
(b) wait for steady state conditions in the column (judged by stability of conductivity readings);
(c) start data acquisition;
(d) close V1;
(e) after the interface leaves the upper electrode, stop data acquisition.

Fine silica particles (90% -325μm) were used in

concentrations of 10% and 20% (v/v), and the frother, DF250C, was used in 5 ppm and 20 ppm. This fine silica was readily held in suspension by the flow of bubbles.

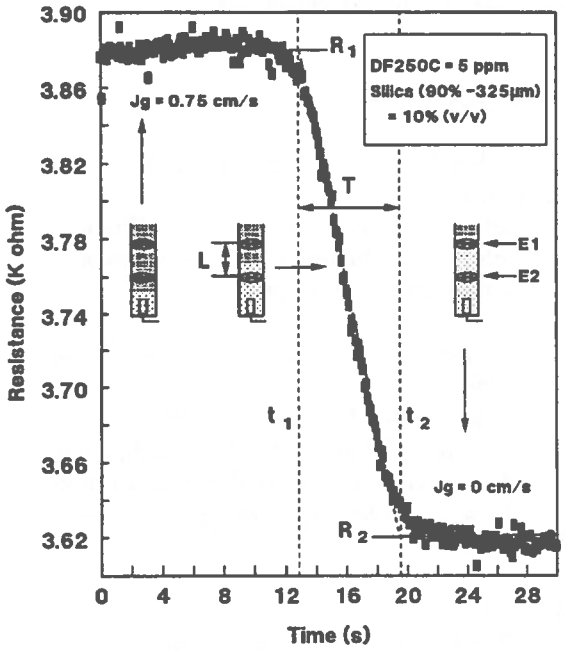

Figure 3 Resistance (i.e. inverse of conductance) versus time between two electrodes.

RESULTS

Figure 3 illustrates the resistance (between two electrodes) versus time at J_g = 0.75 cm/s, DF250C = 5 ppm and silica = 10% (v/v). Before the rising interface reaches E2 (Electrode 2), the resistance of the air-water-silica mixture, R_1, is constant. As the interface rises from E2 to E1, the resistance decreases. After the interface leaves E1, the resistance (of the water-silica mixture), R_2, is again constant. The buoyancy velocity, u_0, is calculated from

$$u_0 = \frac{L}{t_2 - t_1} = \frac{L}{T} \qquad (1)$$

where L is the distance between E1 and E2 (74 cm), and T is the time for the interface to move from E2 to E1. In Figure 3, it can be seen that during the period T the resistance R is a function of time t, i.e.

$$R = A + B\,t \qquad (2)$$

where A is the intercept, and B is the slope of the line. By substituting R_1 and R_2 into Equation 2, t_1 and t_2 are obtained. Therefore, the buoyancy velocity, u_0, can also be calculated from

$$u_0 = L\,\frac{B}{R_2 - R_1} \qquad (3)$$

Figures 4 and 5 show that u_0 increases in the presence of the solids, and Figure 5 also illustrates that u_0 increases as the solids concentration increases. This result supports the hypothesis of Banisi et al. (1995b) that the presence of solids increases the bubble swarm

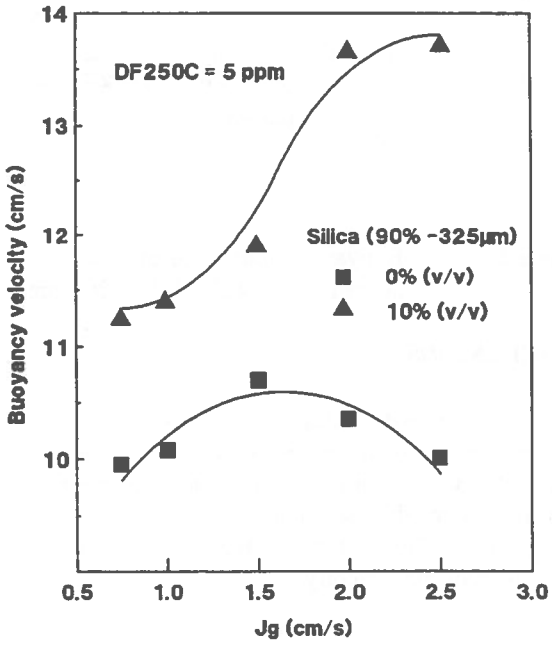

Figure 4 Buoyancy velocity of bubble swarm, u_0, at DF250C = 5 ppm.

velocity. (Although it is specifically the buoyancy velocity that has been measured, its known relationshipwith swarm velocity permits this

conclusion.) The magnitude of the increase upon addition of solids is of the under expected to produce up to 40% reduction in gas holdup as reported by Banisi et al.

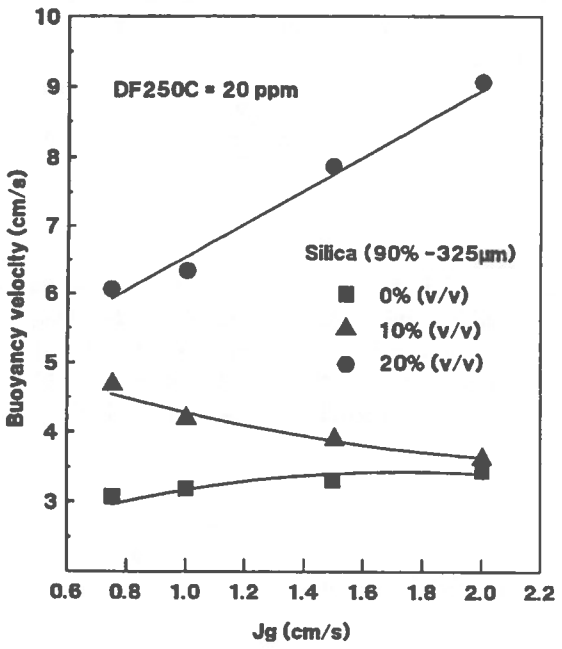

Figure 5 Buoyancy velocity of bubble swarm, u_0, at DF250C = 20 ppm.

CONCLUSIONS

Using a conductivity technique, the buoyancy velocity of a bubble swarm in the air-water-silica system was measured in a column. The results support the hypothesis that the presence of solids reduces gas holdup in the three phase system by increasing the bubble swarm rise velocity.

NOMENCLATURE

- J_g superficial gas velocity, cm/s
- L distance between Electrodes 1 and 2, 74 cm
- R_1 resistance of mixture of air bubbles, water and silica particles, ohm
- R_2 resistance of mixture of water and silica particles, ohm
- t time, second
- t_1 time that interface reaches E1, second
- t_2 time that interface leaves E2, second
- T time for the interface to move from E2 to E1, second
- u_0 buoyancy velocity of bubbles in columns, cm/s
- ε_g gas holdup, dimensionless

REFERENCES

Banisi, S, Finch, J.A., Laplante, A.R., and Weber, M.E., 1995a
Effect of Solid Particles on Gas Holdup in Flotation Columns. Part I: Measurement; *Chem. Eng. Sci.* in press.

Banisi, S, Finch, J.A., Laplante, A.R., and Weber, M.E., 1995b
Effect of Solid Particles on Gas Holdup in Flotation Columns. Part II: Investigation of Mechanisms of Gas Holdup Reduction in Presence of Solids; *Chem. Eng. Sci.* in press.

Clark, K.N., 1990
The Effect of High Pressure and Temperature on Phase Distributions in a Bubble Column; *Chem. Eng. Sci.*, Vol.45, 8, pp2301-2307

Hidaka, N., Ontitani, M., Matsumato, T., and Morooka, S., 1992
Axial Mixing Segregation of Multicomponent Coarse Particles Fluidized by Concurrent Gas-Liquid Flow; *Chem. Eng. Sci.*, Vol.47, 13/14, pp3427-3434

Nicklin, D.J., 1962
Two-Phase Bubble Flow; *Chem. Eng. Sci.*, Vol.17, pp693-702

Ostergaard, K., 1971
Three-Phase Fluidization; Chap. 18 in *Fluidization*, Harrison, D., Ed., Academic Press, New York

Ostergaard, K., 1978
Hold-Up Mass Transfer and Mixing in Three-Phase Fluidization; *AIChE Symp. Series*, Vol.74, 176, pp82-86

Sada, E., Kumazawa, H., and Lee, C.H., 1986
Influence of Suspended Fine Particles on Gas Holdup and Mass Transfer Characteristics in a Slurry Bubble Column; *AIChE Journal*, Vol.32, 5, pp853-856

Shen, G., Uribe-Salas, A., Ahmed, N. and Finch, J.A., 1991
Measurement of Dynamic Gas Holdup in a Bubble Column; in *Computer Applications in the Mineral Industry*, vol.2 (eds. Poulin, R., Pakalnis, R.C.T., and Mular, A.L.), Proceedings of the Second Canadian Conference on Computer Applications in the Mineral Industry, Vancouver, Canada, Sept. 15-18, 1991, pp.287-298

Ying, D.H., Givens, E.N., and Weimer, R.F., 1980
Gas Holdup in Gas-Liquid-Solid Flow Reactors; *Ind. Eng. Chem. Process Des. Dev.*, Vol.19, pp635-638

Uribe-Salas, A., Gomez, C.O., and Finch, J.A., 1994
Conductivity Technique for Gas and Solids Holdup Determination in Three-Phase Reactors; *Chem. Eng. Sci.*, Vol.49, 1, pp1-10

CAMI'95: 3rd Canadian Conference on Computer Applications in the Mineral Industry
Montréal, Québec, Canada, October 22-25, 1995

Computer Simulation Applied to the Design of Mineral Processing Plants

Mary Goldman
Royal Oak Mines, NWT Division

ABSTRACT:

Computer simulation has become a versatile tool for the Design Engineer in a wide range of applications. Metallurgical circuits may range from a few unit operations and a limited number of streams to very complex flowsheets containing over forty unit operations. Once a computer simulation model is built, it can be used to investigate any number of processing strategies. It can also be quickly modified to simulate alternative processing flowsheets.

Steady state computer simulation models were built to simulate refractory gold ore processing flowsheets using the Metsim® software package. The models can be calibrated with actual plant data or using pilot plant testwork results. Operating and simulated results for Barrick Goldstrike Mines Inc.'s pressure oxidation circuit are presented.

RÉSUMÉ:

La simulation par ordinateur est devenue un outil versatile pour l'ingénieur de conception dans une grande gamme d'applications. Les circuits métallurgiques peuvent varier d'à peine quelques opérations unitaires à de très complexes organigrammes contenant plus de quarante opérations uniaires. Lorsqu'un modèle de simulation par ordinateur est mis sur pied, il peut être utilisé pour étudier toute stratégie de traitement. Il peut également être modifié rapidement pour simuler des organigrammes de traitement alternatifs.

Des modèles de simulation continue ont été développés pour simuler les étapes de traitement de mineral d'or réfractaire en utilisant le progiciel Metsim®. Les modèles peuvent être calibrés avec des données réelles provenant de l'usine, ou en utilisant les résultats d'essais menés en usine-pilote.

Des résultats d'opération et de simulation provenant du circuit d'oxydation sous pression de Barrick Goldstrike Mines Inc. sont présentés.

INTRODUCTION

Throughout history gold has been recovered by different methods: gravity concentration, amalgamation, cyanidation (leaching, CIP and CIL), roasting, pressure oxidation and bioleaching.

Pressure oxidation was introduced in the 1980's as a pretreatment of refractory gold ores prior to the leaching stage (Thomas, 1991). This process uses oxygen, high temperature and pressure to oxidize sulfides, in autoclave vessels, and liberate the gold that would otherwise be unavailable for cyanidation.

Modelling and computer simulation of autoclaves has received considerable attention in recent years (Pieterse, 1993; Baldwin, 1993; Papangelakis, 1992; Conway, 1990).

In addition to autoclaves, pressure oxidation circuits generally include several unit operations. The performance of each unit operation is closely associated with the performance of the others. For this reason computer models were built including all unit operations of the pressure oxidation circuit to be simulated, in order to conduct the required heat and mass balances.

BUILDING A MODEL

Metsim®, a proprietary computer program marketed by Proware, was used to build models to simulate the operation of refractory gold ore processing circuits.

The program includes a thermodynamic database of chemical compounds and elements. The flowsheet and the chemical reactions are specified by the user.

Metsim® is a very flexible package allowing the user to simulate different flowsheets. When building a model, a step by step approach is recommended. At first, a model may contain one single unit operation. Additional unit operations are then added, one at a time. Chemical reactions and process controls are added as required. Models containing over 40 unit operations and over 100 process streams were built using this approach.

The simulated flowsheets included acidulation and neutralization tanks, autoclaves, flash tanks, slurry heater vessels, heat exchangers and CIL tanks. Table 1 provides a list of unit operations and their corresponding Metsim® unit operation.

TABLE 1 Metsim® unit operations used in refractory gold flowsheets

Unit Operation	Metsim® Unit Operation
Acidulation Tank	TNK - Tank, Plain
Slurry Heater Vessel	SPP - Splitter, Phase
Autoclave	AUT - Autoclave
Flash Tank	FLA - Flash Separator
Slurry Cooler Surge Tank	FLA - Flash Separator
Venturi Scrubber	SPP - Splitter, Phase
Slurry Cooler	HTX - Heat Exchanger
Neutralization Tank	TNK - Tank, Plain
Carbon-in-leach Tank	CIP - CIP/CIL

Output from the program includes:

- mass and volumetric flowrates
- %solids and specific gravity
- temperature for all streams
- composition of all streams

ACIDULATION CIRCUIT

If carbonates contained in the ore have to be destroyed prior to pressure oxidation, the flowsheet will include an acidulation circuit (Figure 1).

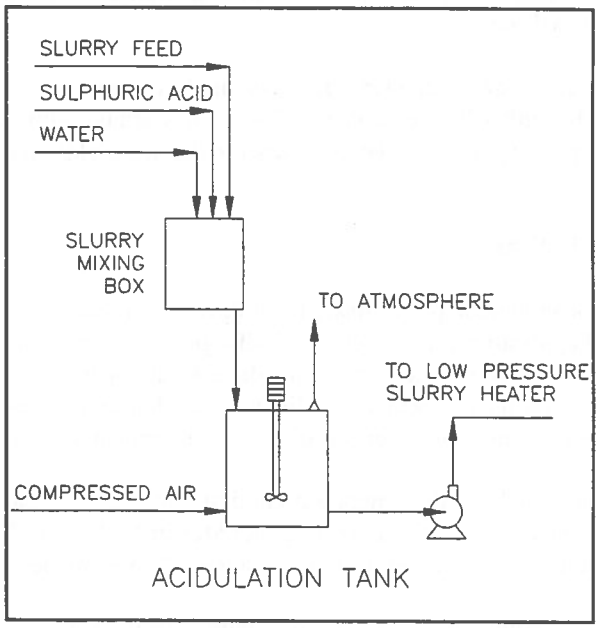

Figure 1 Acidulation Circuit

Ore slurry and sulphuric acid are fed to the acidulation tank and react according to the chemical reactions listed below.

$$CaCO_3 + H_2SO_4 + H_2O = CaSO_4.2H_2O + CO_2$$

$$CaMg(CO_3)_2 + 2\ H_2SO_4 = 2\ CO_2 + CaSO_4.2H_2O + MgSO_4$$

The model may include process controls set to perform the following tasks:

- Set sulphuric acid addition to achieve a certain concentration of free acid at the autoclave discharge.
- Set the water vapour pressure in the acidulation tank off-gas at the Steam Table value.

AUTOCLAVE

Figure 2 presents an autoclave circuit consisting of autoclave vessel, low pressure and high pressure slurry heater vessels, low pressure and high pressure flash tanks, discharge pumpbox and surge tank.

Some of the chemical reactions included in the autoclave unit operation are:

$$20\ FeS_2 + 75\ O_2 + 13\ H_2O = 9\ Fe_2(SO_4)_3 + Fe_2O_3 + 13\ H_2SO_4$$

$$As_2S_3 + Fe_2(SO_4)_3 + 7\ O_2 + 10\ H_2O = 2\ FeAsO_4.2H_2O + 6\ H_2SO_4$$

$$2\ FeAsS + 7\ O_2 + 6\ H_2O = 2\ FeAsO_4.2H_2O + 2\ H_2SO_4$$

$$3\ Fe_2(SO_4)_3 + 14\ H_2O = 2\ (H_3O)Fe_3(SO_4)_2(OH)_6 + 5\ H_2SO_4$$

$$CaMg(CO_3)_2 + 2\ H_2SO_4 = 2\ CO_2 + CaSO_4 + MgSO_4 + 2\ H_2O$$

$$CaCO_3 + H_2SO_4 = CaSO_4 + CO_2 + H_2O$$

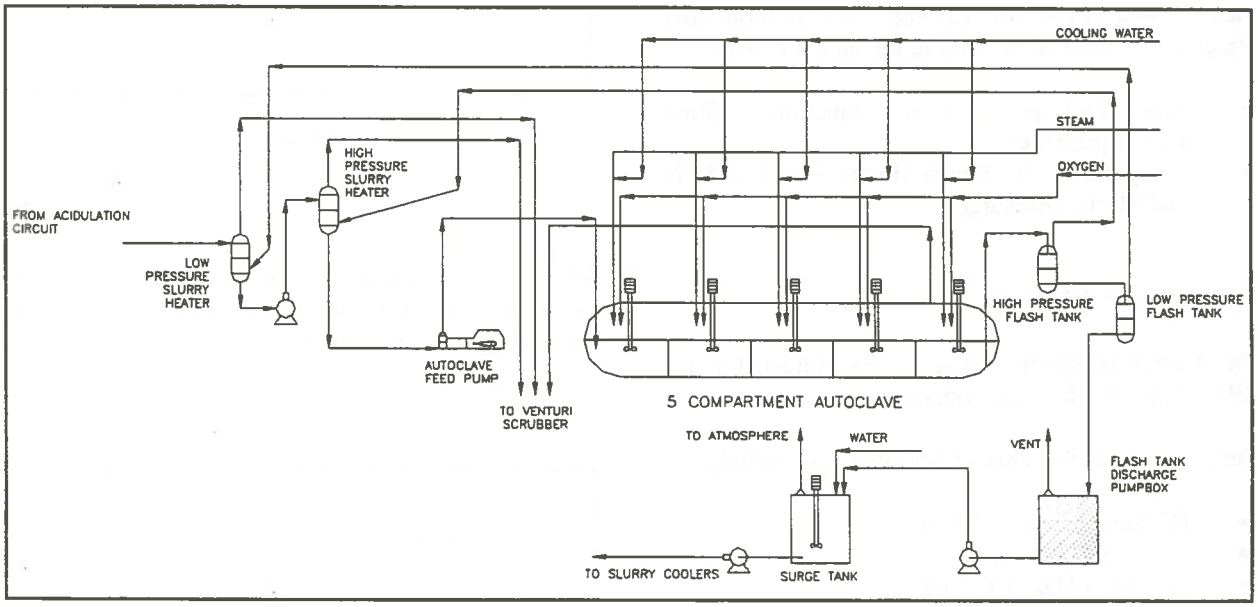

Figure 2 Autoclave Circuit

The autoclave is a horizontal multi-compartment vessel, operating at high temperature and pressure. Steam and water are supplied to each compartment as required for temperature control. Metsim® calculates the steam or water required to maintain the temperature specified by the user for each autoclave compartment. Metsim® also calculates the oxygen flowrate to each compartment based on the requirements of the oxidation reactions, taking into account the oxygen utilization specified by the user.

Models may include process controls to:

- Set extent of chemical reactions in each compartment as a function of residence time
- Set oxygen utilization as a function of sulfur grade in the feed

SLURRY HEATERS AND FLASH TANKS

Flash tanks and slurry heater vessels may be included in pressure oxidation circuits to recover heat from the autoclave slurry discharge and use it to pre-heat the autoclave feed.

In the circuit shown in Figure 2 the autoclave slurry discharge is fed to the High Pressure (HP) Flash Tank. Steam is released in the flash tank cooling down the ore slurry. Slurry discharges from the flash tank at the temperature corresponding to the tank pressure, in the Steam Tables. The slurry is further cooled in the Low Pressure (LP) Flash Tank, with additional release of steam.

Ore slurry discharged from the acidulation circuit is pre-heated in the LP and HP Slurry Heater Vessels with steam released in the low and high pressure flash tanks. Process controls can be used in the model to set :

- Flash Tank pressures as a function of Slurry Heater pressures
- Temperature of Slurry Heater Vessel Off Gas and Slurry Discharge

VENTURI SCRUBBER

The Venturi Scrubber (Figure 3) was simulated by two SPP - Splitter, Phase unit operations.

Feed streams to the Venturi Scrubber may include:

- HP Slurry Heater Off gas
- Autoclave Off gas
- LP Slurry Heater Off gas
- Flash Tank Discharge Pumpbox vent

Models may include process controls to perform the following tasks:

- Set water flowrate to Venturi Scrubber as a function of gas feedrate
- Set temperature of the discharge water

CIL SLURRY COOLERS

The slurry discharge from the autoclave circuit is further cooled by tube and shell heat exchangers (Figure 4), before being fed to the neutralization tanks.

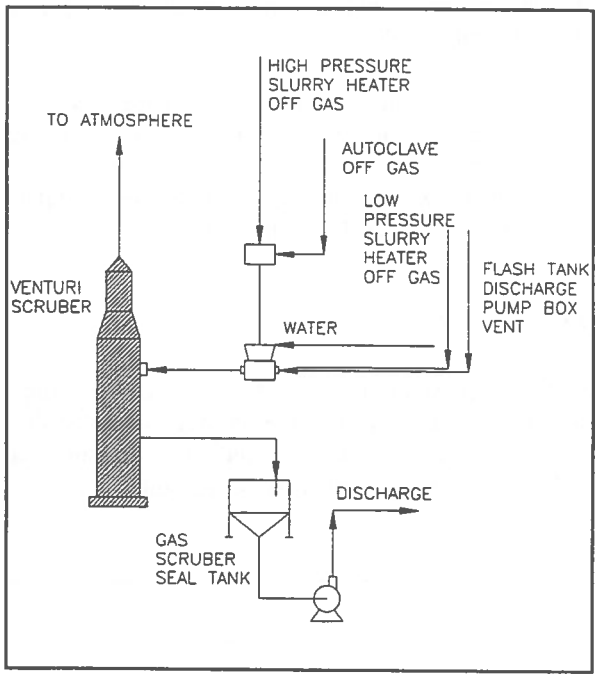

Figure 3 Venturi Scrubber

The model may include a process control to calculate the cooling water flowrate required to achieve a certain slurry discharge temperature.

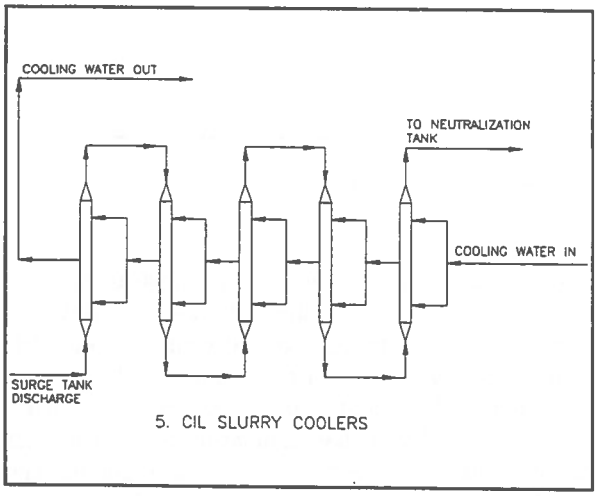

Figure 4 CIL Slurry Coolers

NEUTRALIZATION TANKS

Figure 5 presents a neutralization circuit consisting of three neutralization tanks, pump and pumpbox. Slaked lime is used in the neutralization tanks to precipitate impurities and raise the pH.

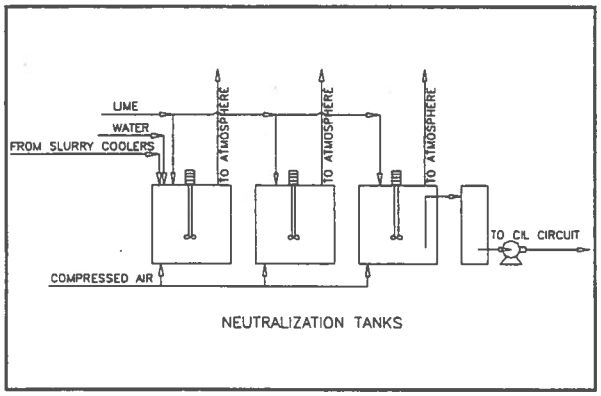

Figure 5 Neutralization Circuit

Some of the chemical reactions included in the model are:

$$Fe_2(SO_4)_3 + 2\ H_3AsO_4 + 3\ Ca(OH)_2 + 4\ H_2O = 2\ FeAsO_4.2H_2O + 3\ CaSO_4.2H_2O$$

$$Fe_2(SO_4)_3 + 3\ Ca(OH)_2 + 6\ H_2O = 2\ Fe(OH)_3 + 3\ CaSO_4.2H_2O$$

$$FeSO_4 + Ca(OH)_2 + 2\ H_2O = Fe(OH)_2 + CaSO_4.2H_2O$$

$$H_2SO_4 + Ca(OH)_2 = CaSO_4.2H_2O$$

Models may include process controls to perform the following tasks:

- Set lime flowrate to the neutralization tanks, taking into account the requirements to precipitate all impurities and raise the pH
- Set the flowrate of steam in the neutralization tank off gas at the Steam Table value

CARBON-IN-LEACH CIRCUIT

The neutralization circuit discharge is fed to the CIL circuit. The circuit shown in Figure 6 includes 6 CIL tanks, trash screen, loaded carbon screen, carbon safety screens and pumps.

Reactions included in CIL unit operations are as follows.

$$Au_{(solid)} = Au_{(solution)}$$

$$Au_{(solution)} = Au_{(adsorbed)}$$

$$CN_{(solution)} = CN_{(degraded)}$$

Process controls may be included in the model with the following objectives:

- Set cyanide addition to achieve a certain cyanide level in the tanks
- Set the extent of cyanide degradation in the tanks

SIMULATION OF BARRICK GOLDSTRIKE MINES' PRESSURE OXIDATION CIRCUIT

Barrick Goldstrike Mines Inc. (Goldstrike) is located in Nevada, USA. The majority of its ore reserves are refractory in nature, mainly due to pyrite and marcasite encapsulation of the gold (Pieterse, 1993).

Computer models were built using Metsim® software package to simulate the operation of Goldstrike's pressure oxidation circuit, as part of a project to predict steam requirements for a projected plant expansion to 15 900 t/day (17,500 STPD).

The computer models included a five compartment autoclave, LP and HP flash tanks, LP and HP splash vessels (slurry heaters). The models were calibrated using the following procedure:

- Plant data was used to set the value of the variables listed below

  %solids and feedrate to the LP Splash Tank
  %S and $\%CO_3$ in autoclave feed
  autoclave pressure
  total sulfur oxidation in autoclave

- Oxygen utilization was calculated based on theoretical and actual oxygen consumptions
- Splash Tanks pressures were initially set at plant value

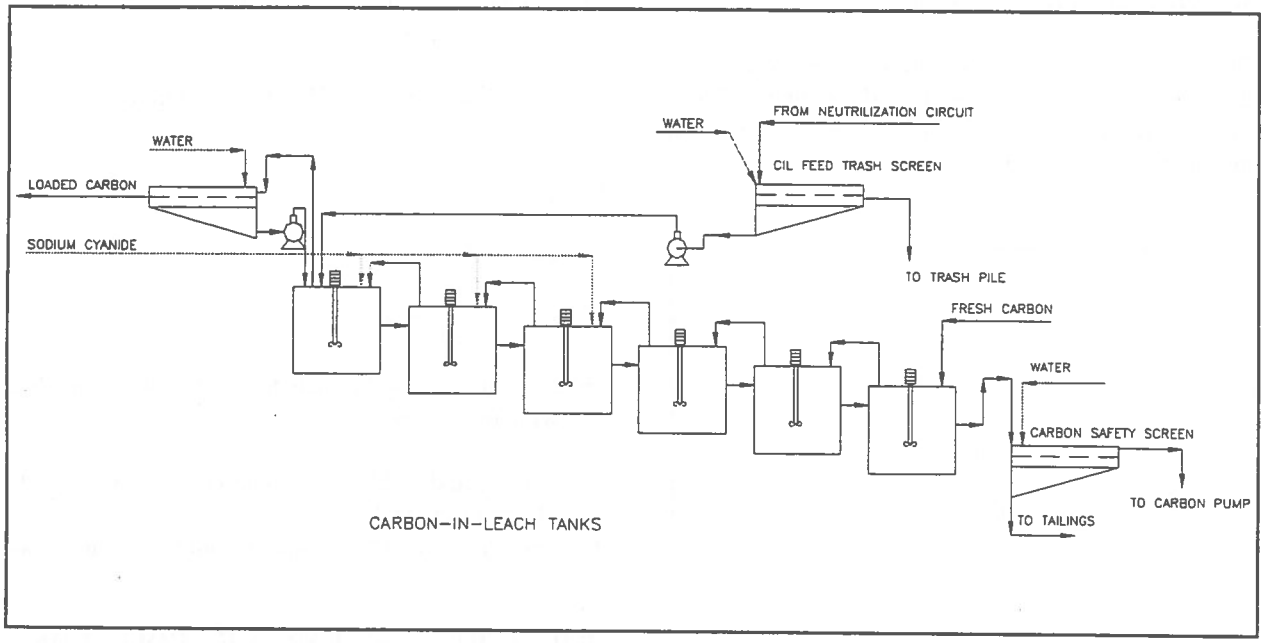

Figure 6 CIL Circuit

- The autoclave temperature profile was initially set at plant value
- A sulfur oxidation profile was arbitrarily chosen
- The simulation was run and the calculated steam consumption was compared to the actual steam consumption
- Values for the variables listed below were adjusted until the difference between actual and calculated steam consumption was lower than 5%

  LP Splash Tank pressure
  HP Splash Tank pressure
  Autoclave Temperature profile
  Autoclave Sulfur Oxidation profile

A comparison of operating and simulated results for three sets of plant data is provided on Tables 2, 3 and 4 below. In all cases the computer model was able to 'mimic' very closely plant performance with respect to process temperatures, pressures, steam and oxygen consumptions, with the exception of the pressures associated with the LP Splash Vessel, which are lower than those observed in plant practice, for all models. This discrepancy may be attributed to errors in the measurement of this data.

CONCLUSION

Steady state computer models were built to simulate refractory gold ore processing flowsheets, using Metsim® software package.

Due to the flexibility of the package the models can be quickly changed to simulate alternative flowsheets and processing strategies.

Three models were built to simulate the operation of Goldstrike's pressure oxidation circuit. The models were calibrated using actual plant data and were able to 'mimic' very closely plant performance with respect to process temperatures, pressures, steam and oxygen consumptions.

ACKNOWLEDGEMENTS

The author wishes to thank Barrick Gold for the permission to present Barrick Goldstrike Mines Inc. plant data in this paper.

Table 2 Operating and simulated results for Barrick Goldstrike Mines Inc. Pressure Oxidation Circuit

Plant Data: Circuit #6, 22 March 1994, Shift 1

Operating parameter		Plant	Simul.
LP Splash			
Flow	m^3/h	191.7	191.7
Feed Density	wt%	50	50
Feed Temp.	C		32
Pressure (gage)	kPa	82.74	0
Slurry Temp.	C	88	88
HP Splash			
Pressure (gage)	kPa	820.5	813.6
Slurry Temp.	C	144	144
Off gas Flowrate	t/h		0.55
Autoclave			
Autoclave Feed			
$S^=$	%	2.68	2.68
CO_3	%	1.90	1.90
S oxidation	%	94.3	94.3
Pressure (gage)	kPa	2895.8	2895.8
Comp #1 Temp.	C	200	200
Comp #2 Temp.	C	216	216
Comp #3 Temp.	C	222	222
Comp #4 Temp.	C	224	224
Comp #5 Temp.	C	223	224
Cooling Water	m^3/h	0	0
Oxygen flowrate	t/h	8.6	8.6
Steam flowrate	t/h	14.5	14.1
LP Flash			
Temperature	C	95	97
Free Acid	g/L	16	22.8
HP Flash			
Temperature	C	175	176

Table 3 Operating and simulated results for Barrick Goldstrike Mines Inc. Pressure Oxidation Circuit

Plant Data: Circuit #6, 23 March 1994, Shift 2

Operating parameter		Plant	Simul.
LP Splash			
Flow	m^3/h	199.9	199.9
Feed Density	wt%	50	50
Feed Temp.	C		32
Pressure (gage)	kPa	82.74	0
Slurry Temp.	C	89	89
HP Splash			
Pressure (gage)	kPa	820.5	813.6
Slurry Temp.	C	157	143
Off gas Flowrate	t/h		0.65
Autoclave			
Autoclave Feed			
$S^=$	%	2.39	2.39
CO_3	%	1.60	1.60
S oxidation	%	92.6	92.6
Pressure (gage)	kPa	2895.8	2895.8
Comp #1 Temp.	C	196	196
Comp #2 Temp.	C	214	214
Comp #3 Temp.	C	220	220
Comp #4 Temp.	C	222	222
Comp #5 Temp.	C	222	222
Cooling Water	m^3/h	0	0
Oxygen flowrate	t/h	7.71	7.71
Steam flowrate	t/h	15.4	15.0
LP Flash			
Temperature	C	95	97
Free Acid	g/L	16.4	20.5
HP Flash			
Temperature	C	176	176

Table 4 Operating and simulated results for Barrick Goldstrike Mines Inc. Pressure Oxidation Circuit

Plant Data: Circuit #6, 29 March 1994, Shift 1

Operating parameter		Plant	Simul.
LP Splash			
Flow	m^3/h	219.9	219.9
Feed Density	wt%	50	50
Feed Temp.	C		32
Pressure (gage)	kPa	89.6	0
Slurry Temp.	C	96	92
HP Splash			
Pressure (gage)	kPa	827.4	813.6
Slurry Temp.	C	146	142
Off gas Flowrate	t/h		0.58
Autoclave			
Autoclave Feed			
$S^=$	%	2.24	2.24
CO_3	%	1.90	1.90
S oxidation	%	92.4	92.4
Pressure (gage)	kPa	2895.8	2895.8
Comp #1 Temp.	C	194	194
Comp #2 Temp.	C	211	211
Comp #3 Temp.	C	216	216
Comp #4 Temp.	C	218	218
Comp #5 Temp.	C	217	218
Cooling Water	m^3/h	0	0
Oxygen flowrate	t/h	9.5	9.5
Steam flowrate	t/h	17.7	17.3
LP Flash			
Temperature	C	96	97
Free Acid	g/L	14	13.4
HP Flash			
Temperature	C	176	176

REFERENCES

Baldwin, S.A., Demopoulos, G.P. and Papangelakis, V.G., 1993
Computer simulation and analysis of pressure oxidation autoclaves using REACTSIM. Proceedings, International Symposium on Modelling, Simulation and Control of Hydrometallurgical Processes, pp. 123-142.

Conway, M.H. and Gale, D.C., 1990
Sulfur's Impact on the size of pressure oxidation autoclaves. JOM, Vol. 42, n. 9, pp. 19-22.

Papangelakis, V.G. and Demopoulos, G.P., 1992
Reactor models for a series of continuous stirred tank reactors with a gas-liquid-solid leaching system: Part III. Model application. Metallurgical Transactions B, volume 23B, pp. 865-877.

Pieterse, H.J.H and Thomas, K.G., 1993
Barrick Goldstrike pressure oxidation modelling. Proceedings, International Symposium on Modelling, Simulation and Control of Hydrometallurgical Processes, pp. 145-158.

Thomas, K.G., 1991
Economics of treating gold ores, CIM Bulletin, Vol. 84, n. 953, pp. 33-37.

CAMI'95: 3rd Canadian Conference on Computer Applications in the Mineral Industry
Montréal, Québec, Canada, October 22-25, 1995

Automation Possibilities for Sample Prep in Mining Laboratories

Gerd A. Schroth
Herzog Automation Corp. - Cleveland, Ohio

Most US Mining Companies are using in their laboratories highly sophisticated analytical instruments. However, with a few exceptions, these same companies are still using manual procedures for sample preparation. Since a large amount of the overall analytical error is attributable to inconsistent sample preparation (the largest contributing factor is the sample taking itself) a considerable number of companies is modernizing their lab operations through mechanizing and automation. This will result in obtaining more accurate and better reproducible analytical results in a very timely manner. In addition, this will also improve efficiency of the work force, will lower the over cost and last but not least will increase the workplace safety and industrial hygiene significantly. A series of examples will be given outlining the actual laboratory modernization programs of companies in the US, Canada and Australia using either the "everything at once" or the "step by step" approach. Actual investment figures for different approaches will be discussed.

1. Introduction:

Accurate and repeatable analytical results obtained in laboratories depend on various factors. The most important ones are the applied analytical principles and instruments, the procedures used to prepare the samples and, of course, the way the sample is obtained in the plant or mine. The approximate error contribution of each of these factors is shown in Fig.1. This indicates clearly that most laboratories use state of the art analytical methods and instruments, but that the sampling process and the sample prep procedures could be vastly improved.

This paper will deal only with sample prep procedures and will not deal with the question of whether a particular sample received in the lab has actually been taken in accordance with certain basic rules, such as ASTM or ISO standard or other generally accepted industry procedures concerning the proper sample amount depending on particle size and geology of the sample.

2. Description of Equipment

The typical steps for preparing mine run samples are shown in Fig. 2 beginning with the drying of the received sample, its registration, its weighing, crushing, splitting and pulverizing. After the pulverizing, the samples are either used for fire assay or AA analysis, or in some cases, pressed into pellets and then analyzed in an XRF instrument. In some cases other analytical methods using fusion or solution might be applicable. All of these steps can be mechanized and/or automated, however, the most cost effective areas are crushing, splitting and pulverizing. The applicable equipment for these tasks is a sequence of two modular machines which will consistently produce the same amount of a finely ground powder sample from large coarse samples independent of the weight of the initial sample.

All of these tasks can be accomplished by integrated machines using an internal robot for sample transfer or by a series of modular machines using an interconnected internal linear conveying system. The machines described below are of the modular design.

2.1 Automatic Weighing/Crushing and Splitting

A sample prep machine combining one or two crushers and an adjustable splitter is shown on Fig. 3 and its working principle is shown in Fig. 4. The large and coarse primary sample is loaded into the machine, its weight is determined and the splitter ratio automatically selected to obtain the desired final sample weight, such as 250 grams for a fire assay. After weighing, the sample is lifted up and emptied into the jaw crusher, which in some cases is followed by a roll crusher. The crushed material is conveyed via gravity or via a vibrating feeder into the splitter and from the splitter into a waiting sample cup.

A dust tight seal between the discharge hose and sample cup prevents any spillage of material. The sample cup is then lifted up again and discharged from the unit. The excess material is collected from the bottom of the splitter and can either be kept for further use or discarded. After each sample, all parts of the machine that have been in contact with the sample material will be cleaned with compressed air.

There is a defined relationship between the maximum particle size and the weight of the final sample applicable to each splitting operation as shown in Fig. 5. Therefore, and as shown in Fig. 6, it might become necessary to install a roll crusher between the jaw crusher and the splitter to further reduce the particle size, to obtain a smaller final sample amount.

Of the various splitting methods presently used, a rotary cone splitter is the most accurate and reliable device. The working principle of such a rotary cone splitter is schematically shown in the same Fig. 6. The principle of the adjustable splitting ratio is illustrated in Fig. 7. The material enters the splitter from the top through a rapidly rotating tube. The sample material is then discharged from the rotating tube against the conical housing of the splitter. The splitter housing is provided with one or several openings or an adjustable opening, depending on the application. The height and also the width of this opening must be at least three to four times the largest diameter of the material fed into the splitter to avoid clogging of the splitter opening. Obviously, by varying the length of the opening, the splitter ratio can be adjusted. For instance, if the opening equals 36° of the circumference a splitting ratio of 1 to 10 will be obtained; if the opening is only 3.6°, then a splitting ratio of 1 to 100 will be obtained.

The following series of pictures show some specific design features of this unit. The primary coarse sample is entered into the system in a container and immediately weighed (Fig. 8). The desired specific weighing, crushing and splitting program is selected at the integrated control panel (Fig. 9) and the automatic process is started. The sample container is lifted and discharged via a chute into a jaw crusher equipped with dual fly wheels (Fig. 10). The crushed material is then conveyed directly into the adjustable splitter (Fig. 11), and the final sample material is collected through the splitter opening and conveyed via a flexible tube into the waiting sample cup (Fig. 11). The excess material is discharged through the bottom of the splitter. To assure a dust free environment, the sample cup is pressed against the splitter discharge hose throughout the entire discharge time. After the sample has been collected, the sample cup is elevated to the discharge level and leaves the unit via an internal conveying system. All parts of the machine which have been in contact with the sample material are cleaned by compressed air.

2.2 Automatic Pulverizing Mill

The crushed and split sample obtained from the automatic crusher/splitter (secondary sample) is then conveyed automatically and directly into a pulverizing mill (Fig. 12), which automatically performs all of the following functions:

- feed sample into grinding vessel
- dispense grinding aid
- pulverize sample
- transport sample cup to discharge position
- discharge sample into same cup
- return sample and sample cup to discharge position opposite feed position
- clean grinding system with compressed air, or
- clean grinding system with water, alcohol and compressed air, or
- clean grinding system with inert material

All operating parameters such as grinding time, amount of grinding aid, cleaning method, cleaning time, etc., can be selected and/or changed at the integrated control panel in accordance with various programs stored in the internal control system.

In case of fire assays, the final pulverized sample (secondary sample) can be emptied directly and automatically into crucibles, whereas, in case of preparation of pellets for x-ray analysis, the finely ground sample will be conveyed to an automatic pellet press (Fig.13).

2.3 Automatic Pellet Press

The automatic pellet press, as shown in Fig. 13, can operate as a stand alone unit or can be part of an automatic prep system and will perform all of the following functions:

- input of sample into the dosing station
- volumetric dosing of sample in one or several steps
- pressing of pellet using 5 - 40 metric tons of pressure and pressure holding times of 1 - 99 seconds

- discharge of pressed pellet by the internal transport system
- cleaning of all parts which have been in contact with the sample material by brushes and compressed air
- removal of excess material by external dust collection system
- receive steel ring with pellet from XRF instrument after completion of analysis, discard pellet, clean steel ring and position steel ring for another pressing cycle

Similar to the previously described automatic pulverizing mill all operating parameters, such as, sample amount to be fed into the press tool, desired pressure and pressure holding time can be selected or changed according to various programs stored in the internal control system. These programs can very easily be changed by the operator to adopt to changing conditions.

3. Case Studies

Using four actual laboratory modernization projects including installations, which are presently implemented, the practical use of these machines will be demonstrated.

3.1 Project C - Execution of a Project in Phases

One of the most important steps to assure the technical and financial feasibility of a laboratory modernization project is defining the actual present practices and anticipated future needs (Fig. 14). Thereafter, a flowsheet showing the sample flow for the new lab, including future requirements should be developed (Fig. 15). At that point, it also should be decided which portion of the lab should be automated, based on technical and financial feasibility, and which portion should remain manual. The new lab is designed to have bar coded sample registration and will use one (1) automatic weighing/crushing/splitting machine, two (2) automatic pulverizers, one (1) automatic press and one (1) XRF/XRD instrument with automatic feed. In the case of this project the implementation has to be done over a two (2) year period due to budgetary constraint. Consequently, Phase 1 consists of the new analytical instrument (XRF/XRD) and one (1) of the two (2) automatic pulverizers (Fig. 16). In Phase 2 the remaining equipment and connecting transport systems will be installed (Fig. 17).

The final layout of the laboratory is determined already during Phase 1 (Fig. 18). This will assure that sufficient space is available to accommodate all the present and future equipment and that underfloor channels for electrical cables and other required utilities are installed in the appropriate location relative to all machines installed in both Phases 1 and 2.

3.2 Project SA-Defining the Technically Correct and Financially Justifiable Project Scope.

During the early stages of this project, the operator of a new mine expressed the broad desire to automate all aspects of sampling, sample transport and sample preparation. Starting with a primary coarse sample of up to 10 kg with particle sizes between 8 mesh and ¼", one (1) final sample of 10 g at -150 mesh for AA analysis and one (1) of 90 g at -150 mesh as reserve had to be obtained from each primary sample. Since there were only two over a period of time, two alternatives were developed.

Alternative 1 was a central lab, which would receive from the two (2) sampling points samples via a pneumatic tube system. All samples would then be prepared and analyzed by AA (Fig. 19) at this centralized lab.

Alternative 2 considered two (2) satellite labs at the mine site adjacent to the sampling points deleting the pneumatic tube system, but duplicating some prep equipment. This reduced the capital expenditure considerably. However, due to the relatively small number of samples per day even this solution could not be justified financially (Fig. 20).

The final solution presently being built deleted several steps such as the automatic drying of the primary coarse sample, the automatic pneumatic transport of the secondary sample from the mine to the lab and also the automatic dividing of the final sample in portions for analysis and reserve sample. This approach concentrates on automating just the most important, but very time consuming and rather labor intensive part of the sample prep process (Fig. 21).

The incoming coarse primary samples are manually dried in laboratory ovens and then emptied into large sample containers of a 30 position feed magazine. The samples are then automatically weighed, crushed and split from up to 5 kg to a sample of consistently 100 g, pulverized to -150 mesh and

discharged in stainless steel sample cups into a 30 position magazine.

The actual equipment cost for this final solution was only 25% of the cost for the originally specified scope.

Depending on the actual grinding time in the pulverizer, these machines will produce a prepared sample every 3 - 4 minutes. This translates into a period of 90 - 120 minutes, during which the operator is free for other duties in the laboratory after he has emptied 30 sample bags into the containers of the feed magazine and started the automatic process.

Due to the large size of the incoming primary sample the feed magazine, of course, becomes quite large. Fig. 22 shows the overall space requirements for such a sequence of modular machines. This design is the least expensive solution, however, in case of space limitations, more compact but also more expensive designs may need to be used.

3.3 Project "AU" Connection of Sample Prep Machines to LIMS

The task to be solved and the equipment used is very similar to Project SA. However, in this case an immediate feedback to the LIMS has been designed by the client. The client also designed special magazines for the sample containers and developed all the required special software.

The flowsheet (Fig. 23), again shows the automated steps of weighing, crushing, splitting and pulverizing. All sample containers for the incoming primary samples are bar coded. All sample cups, which receive the crushed and split sample are also bar coded (Fig. 24). The incoming primary sample ID (bar code of large sample containers) is transferred to the bar code of the sample cups at the discharge of the splitter and then remains with the sample until it reaches the AA analysis.

3.4 Project A Simultaneous Sample Prep for AA and XRF

In this case the laboratory is required to prepare final samples for AA and XRF from the same incoming initial sample, as shown on Fig. 25. The task is to receive an initial primary sample varying between 2.5 and 6.0 kg and to produce two final samples, one of 90 g, -200 mesh for AA analysis and another one of 10 g, -200 mesh pressed into a steel ring for XRF analysis. The required machinery is an automatic weighing, crushing and splitting unit combined with an automatic pulverizing, dosing and pelletizing unit. The internal sample transport is accomplished by a linear robot. The space requirements for such an integrated unit are shown on Fig. 26.

In case the requirement for simultaneous preparation of samples for two different types of analytical processes can be deleted the integrated machine using an internal robot can be replaced by three (3) modular machines and the capital cost can be reduced by approximately 20%. This indicates again the tremendous importance of a detailed and correct definition of the actual requirement at present and of the anticipated future needs. The space requirements for these modular machines are very similar to the integrated unit (Fig. 26).

4. Summary

A recently developed line of modular automated sample prep equipment (Fig. 27) is addressing the most time consuming and labor intensive part of sample preparation, such as crushing, splitting, pulverizing (and in some cases, pellet pressing). This new line reduces the capital cost requirements considerably as compared to previously used integrated sample prep machines and very importantly allows a lab modernization in Phases in case of budget constraints.

A series of case studies show how individual, automated, modular machines or a sequence of these automated modular machines can reduce the overall analytical error, improve workplace safety and hygiene, speed up sample prep time and assist laboratory personnel to handle ever increasing workloads.

To arrive at the technically correct and financially most attractive solution, each investment into automated sample prep should be preceded by a detailed assessment not only of present requirements, but even more importantly, of all anticipated future requirements.

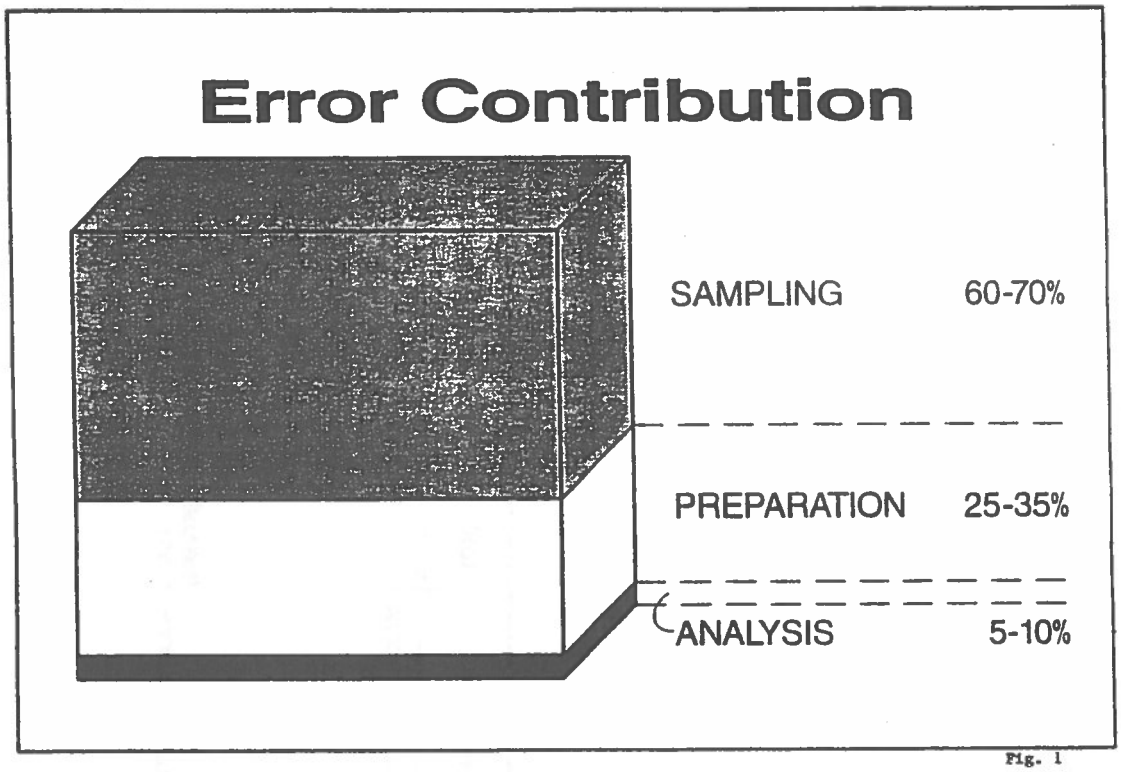

Fig. 1

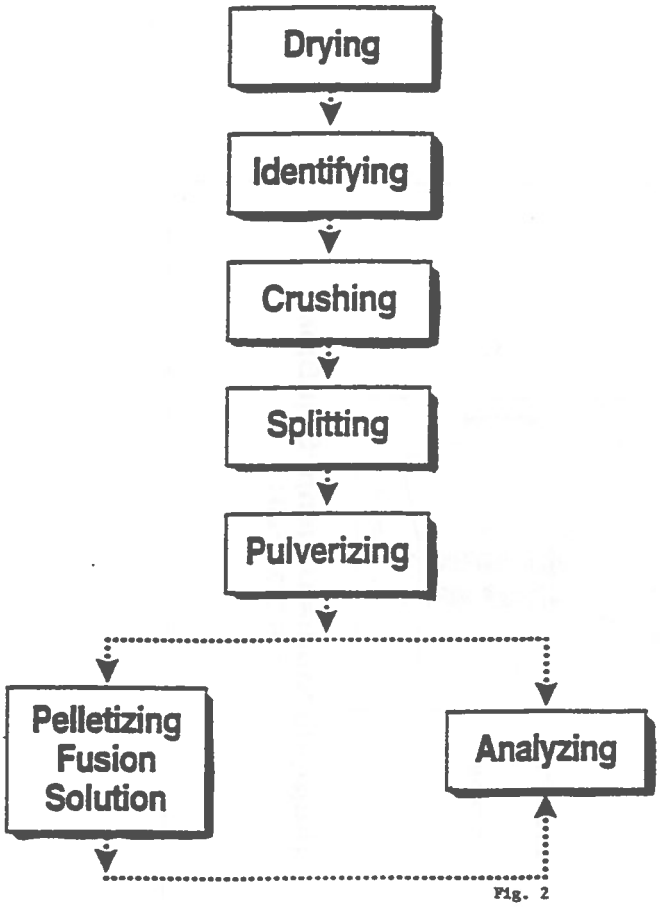

Fig. 2

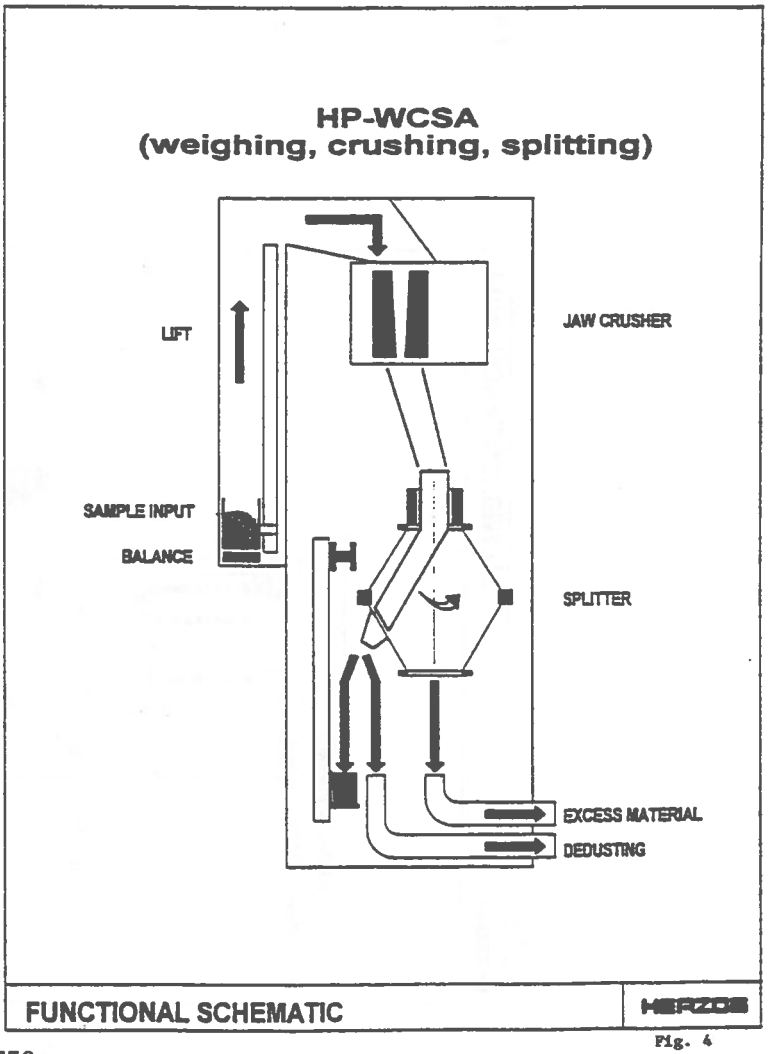

Fig. 4

MINIMUM SAMPLE SIZE

(ISO 1988 - 1975; ISO 2203 - 1980)

1) LESS THAN 150 MM

$$\underset{(KG)}{\text{MINIMUM SAMPLE WEIGHT}} = \underset{(KG/MM)}{0.06} \times \underset{(MM)}{\text{MAXIMUM PARTICLE SIZE}}$$

2) MORE THAN 150 MM

$$\underset{(KG)}{\text{MINIMUM SAMPLE WEIGHT}} = \underset{(KG)}{6} \times \left(\frac{\text{MAXIMUM PARTICLE SIZE}}{\underset{(MM / MM)}{150}} \right)^3$$

Fig. 5

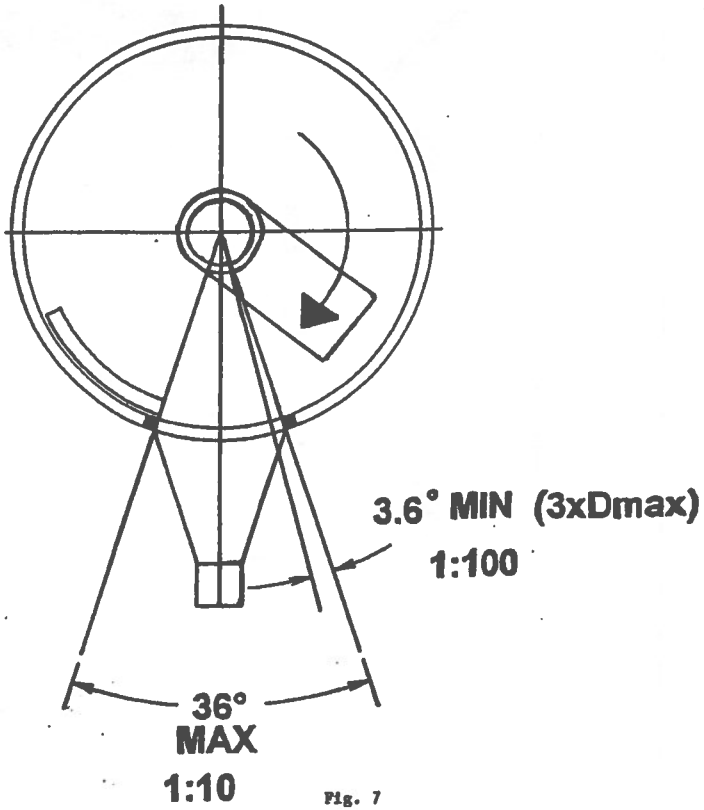

Fig. 7

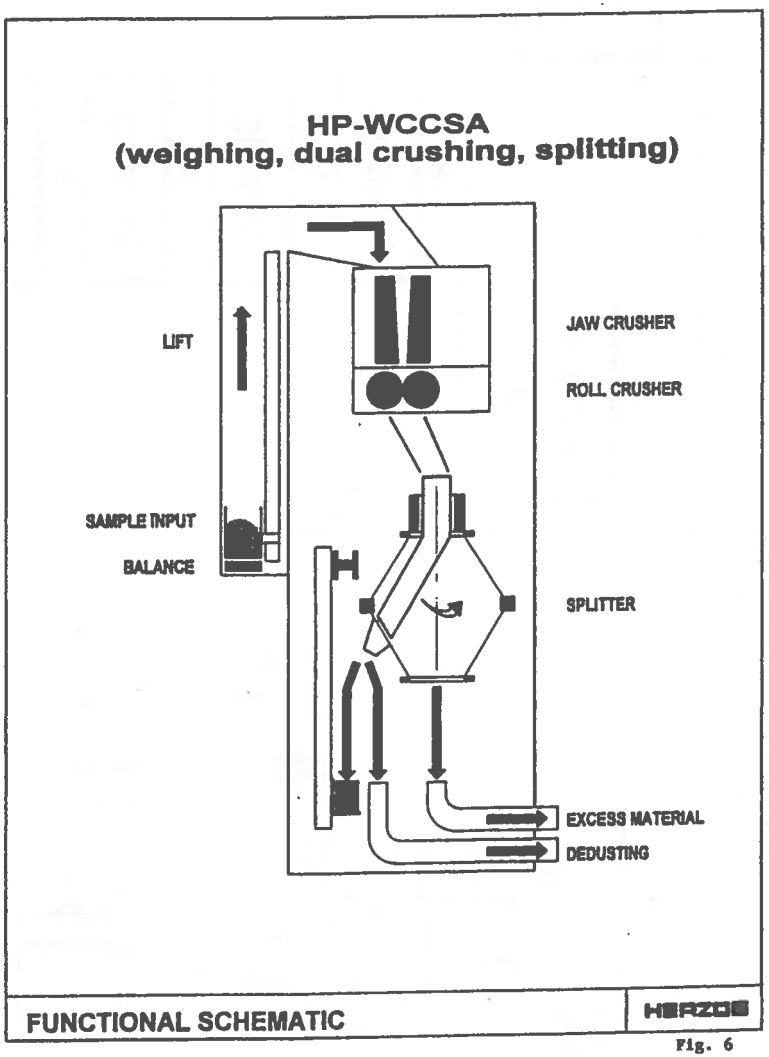

Fig. 6

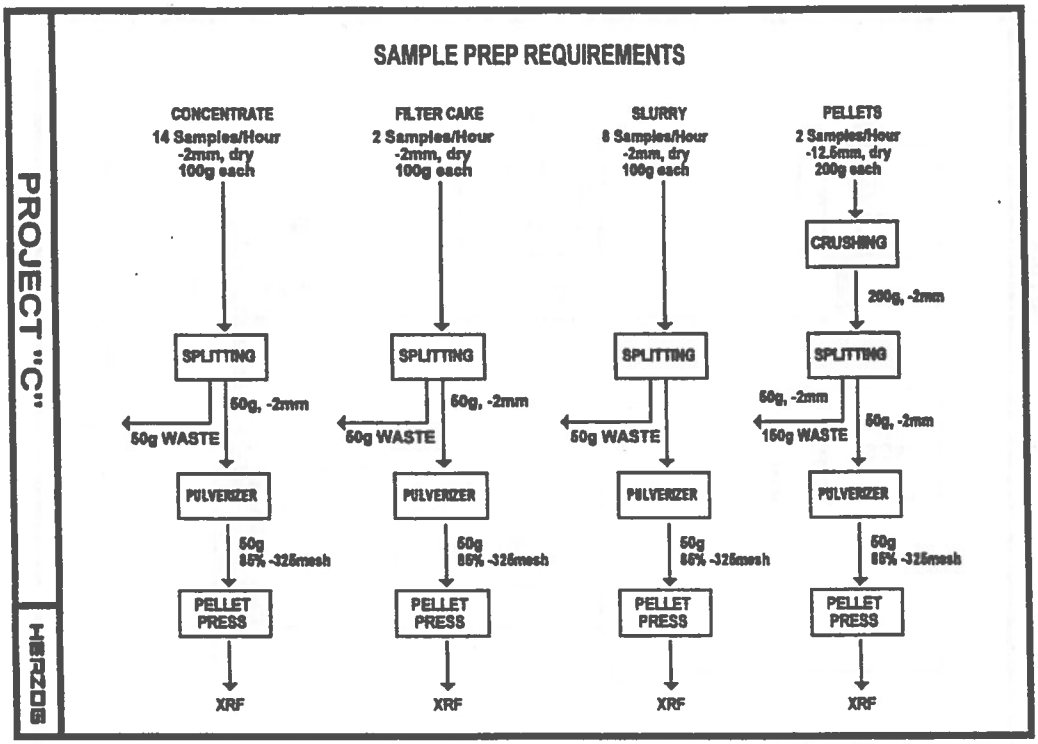

Fig. 14

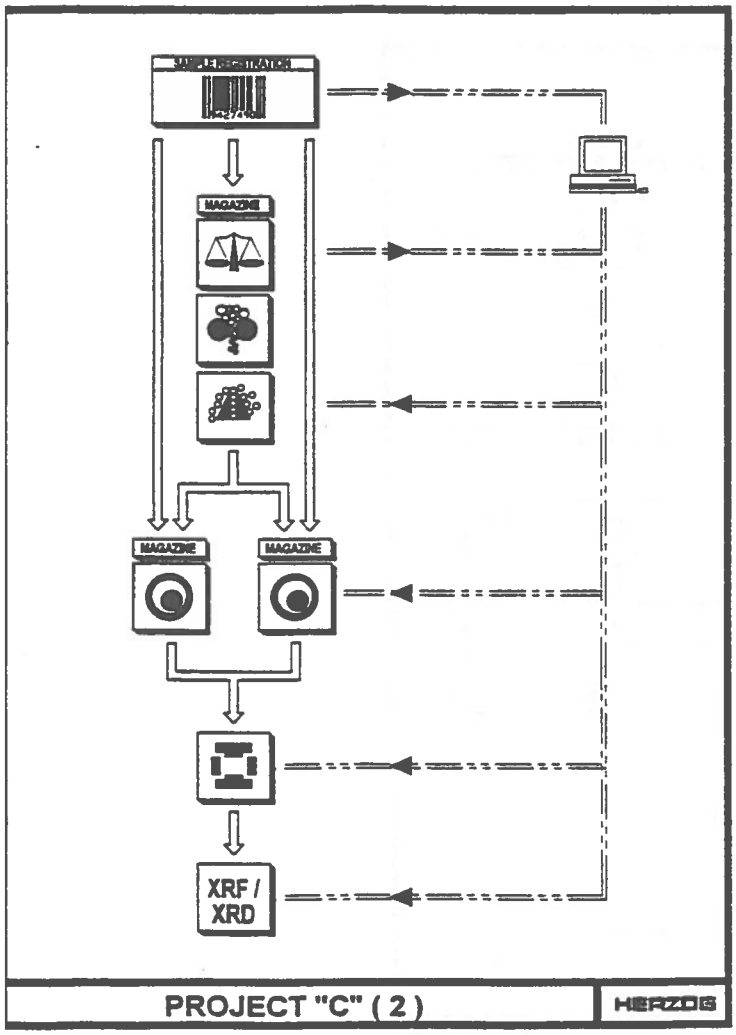

Fig. 15

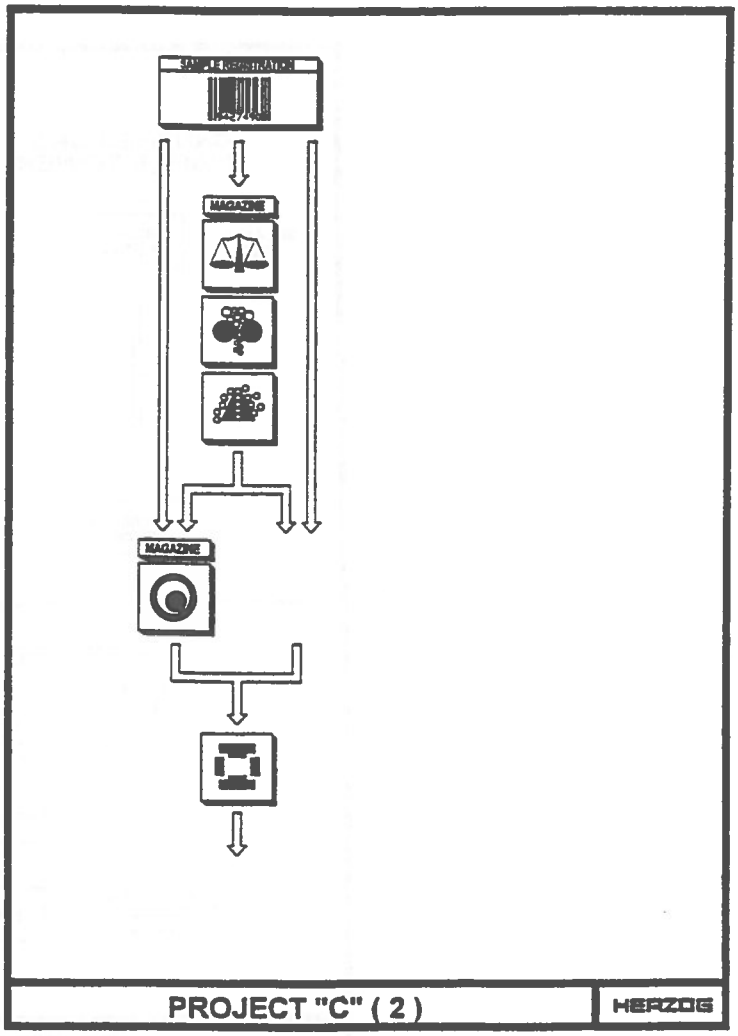

Fig. 17

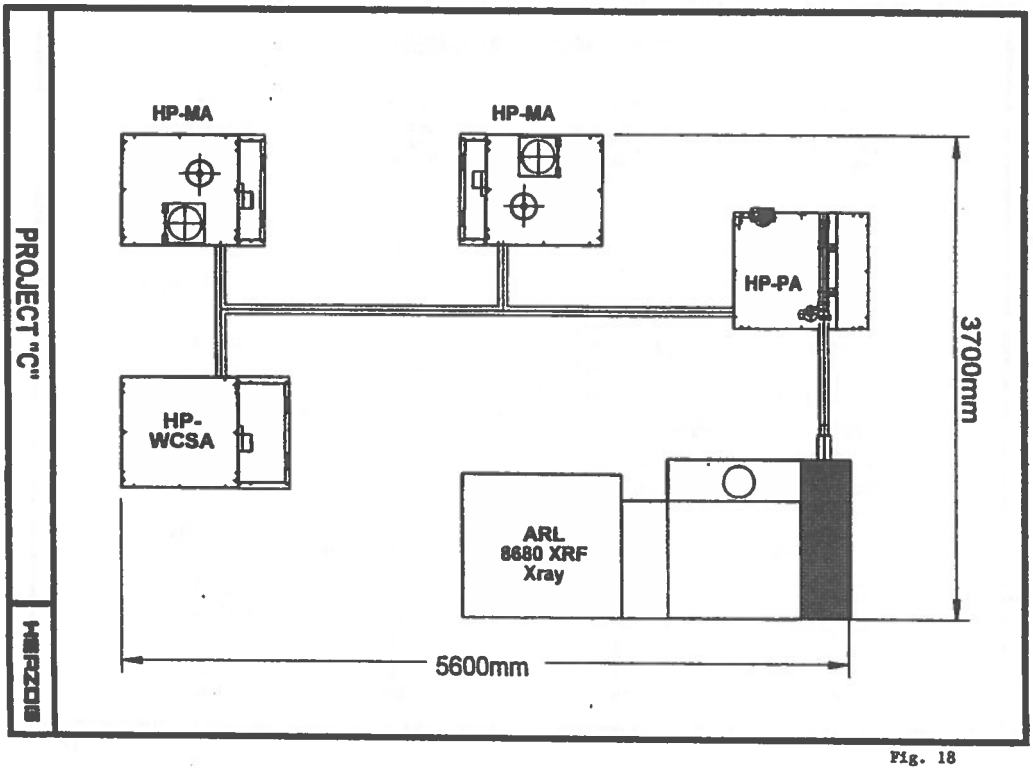
HP-MA
HP-MA
HP-PA
HP-
WCSA
ARL
8680 XRF
Xray
3700mm
5600mm
PROJECT "C"
HERZOG

Fig. 18

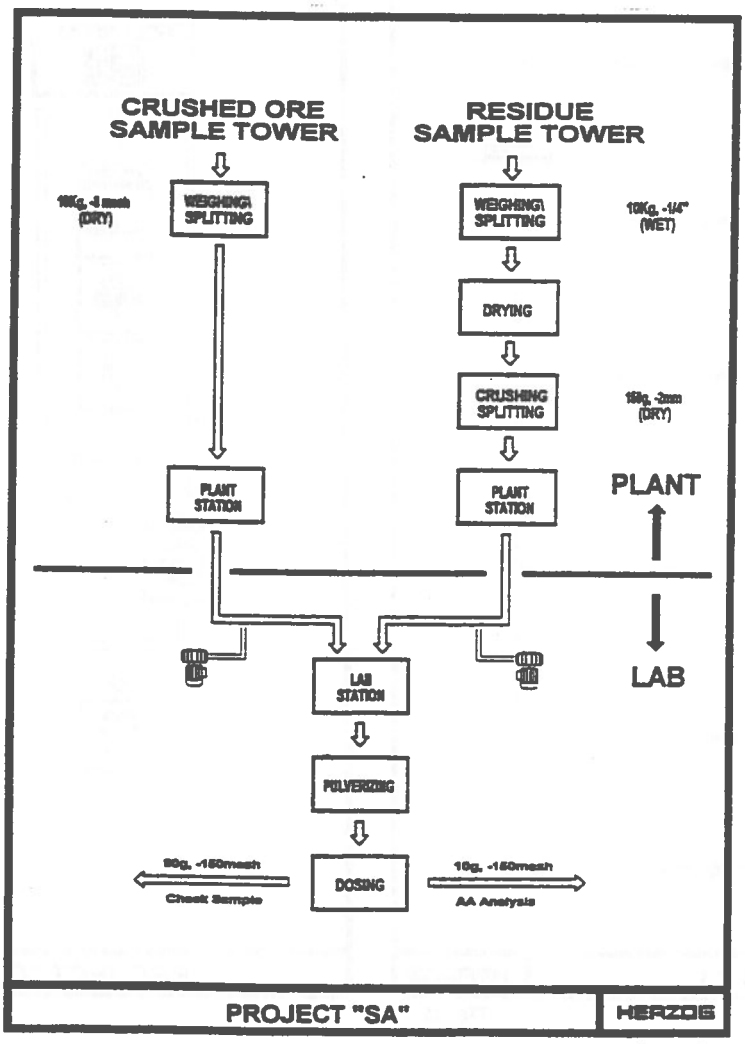
CRUSHED ORE
SAMPLE TOWER
RESIDUE
SAMPLE TOWER
WEIGHING\
SPLITTING
WEIGHING\
SPLITTING
DRYING
CRUSHING
SPLITTING
PLANT
STATION
PLANT
STATION
PLANT
LAB
LAB
STATION
PULVERIZING
DOSING
Check Sample
AA Analysis
PROJECT "SA"
HERZOG

Fig. 19

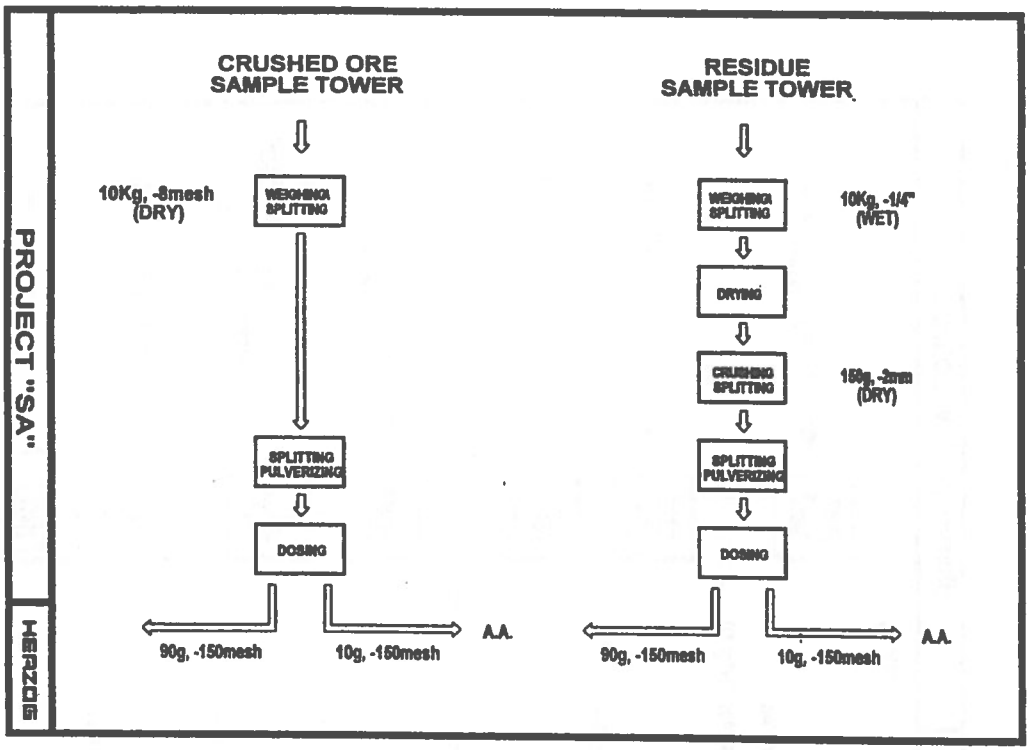

Fig. 20

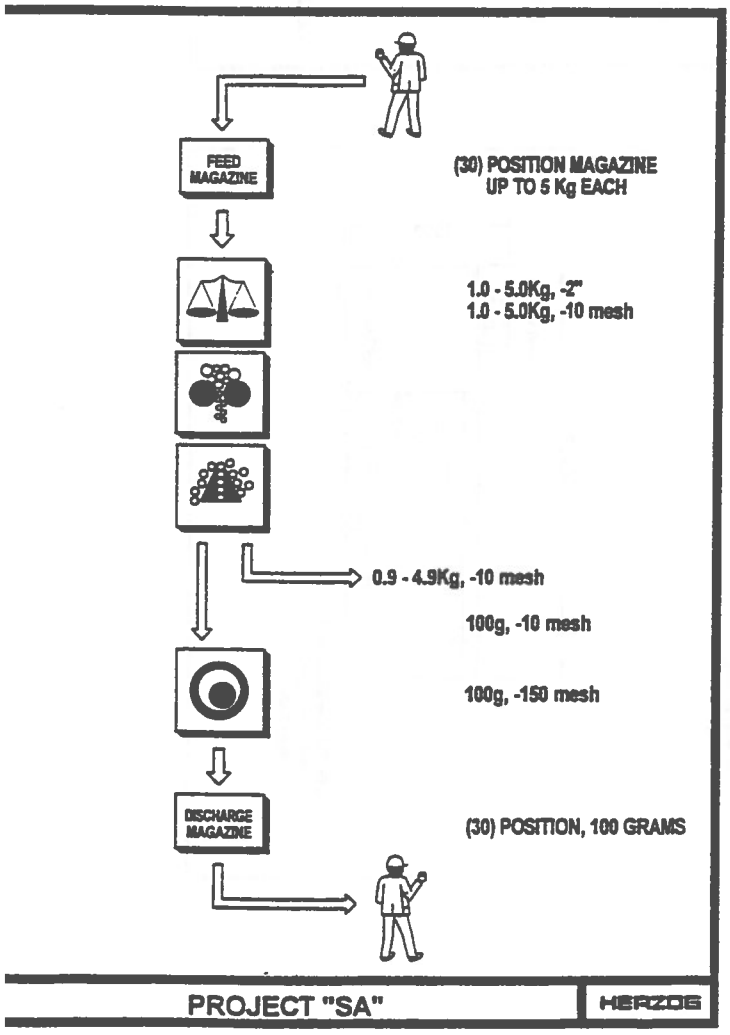

Fig. 21

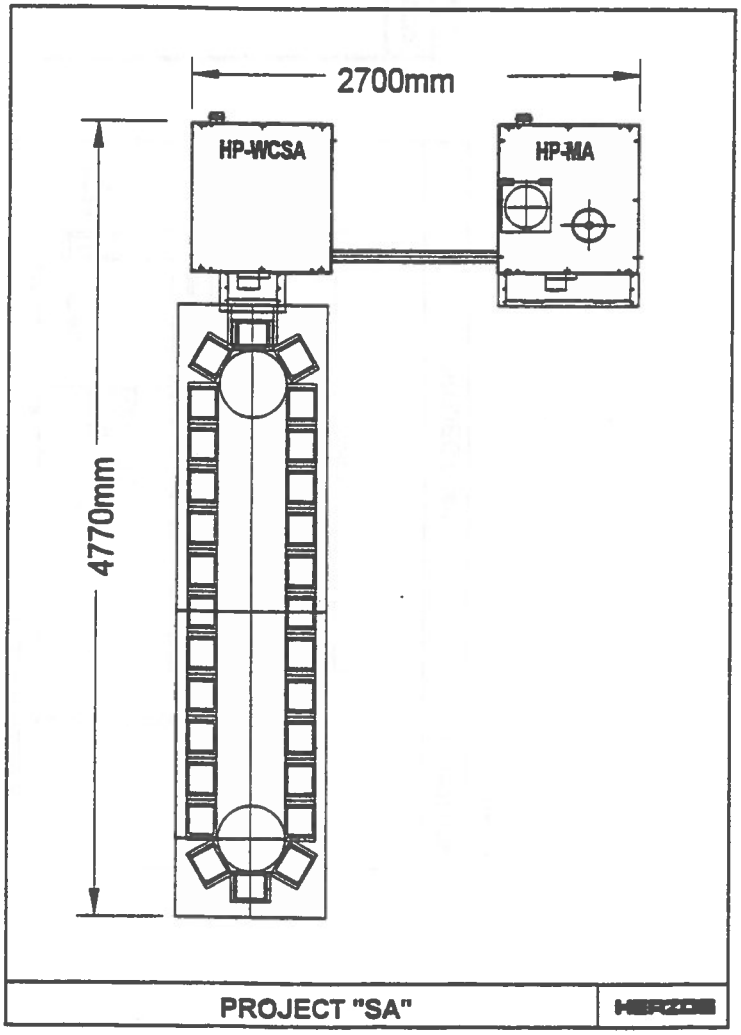

Fig. 22

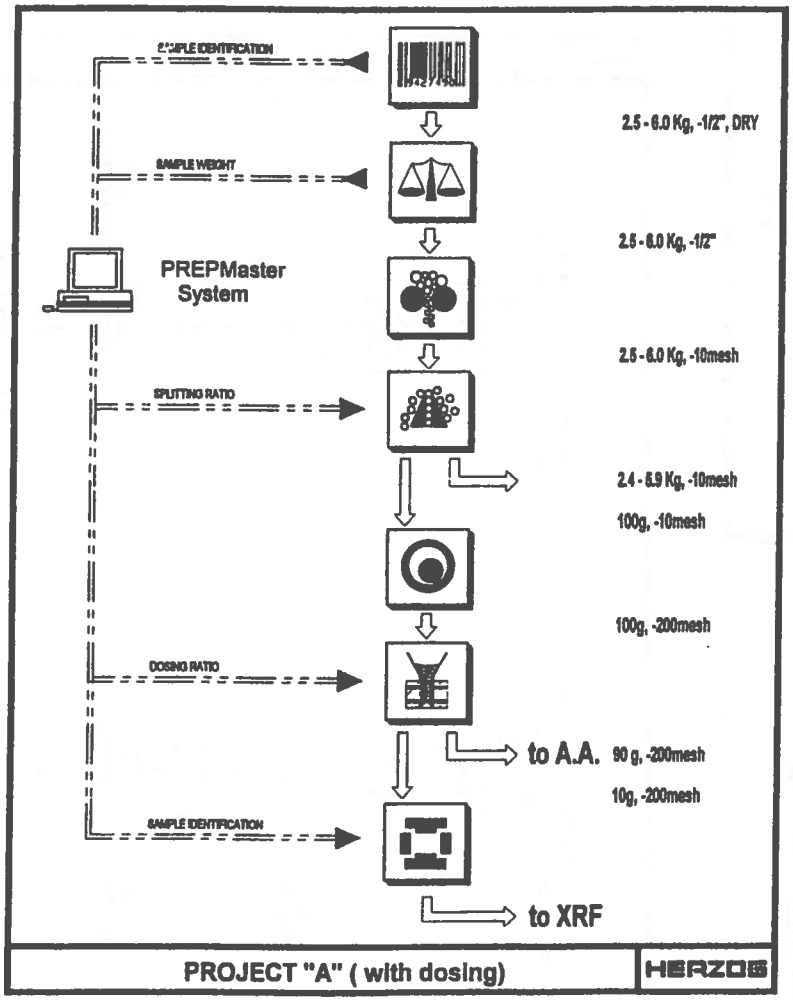
SAMPLE IDENTIFICATION
SAMPLE WEIGHT
PREPMaster System
SPLITTING RATIO
DOSING RATIO
SAMPLE IDENTIFICATION
2.5 - 6.0 Kg, -1/2", DRY
2.5 - 6.0 Kg, -1/2"
2.5 - 6.0 Kg, -10mesh
2.4 - 5.9 Kg, -10mesh
100g, -10mesh
100g, -200mesh
to A.A. 90 g, -200mesh
10g, -200mesh
to XRF
PROJECT "A" (with dosing)
HERZOG

Fig. 25

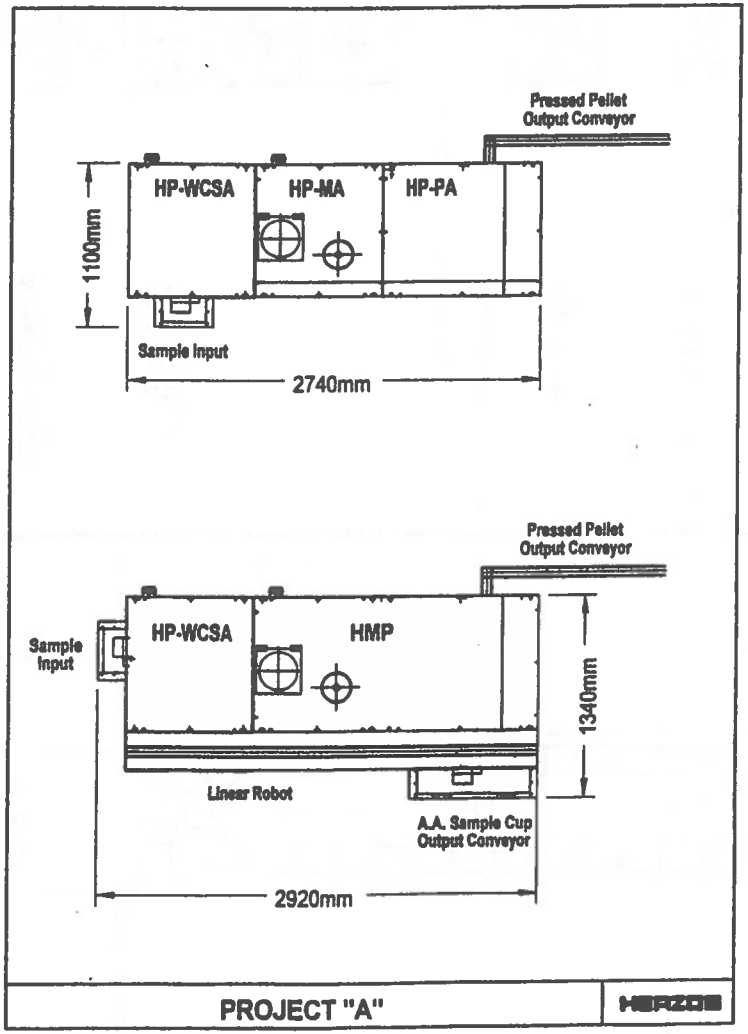
Pressed Pellet Output Conveyor
HP-WCSA
HP-MA
HP-PA
1100mm
Sample Input
2740mm
Pressed Pellet Output Conveyor
Sample Input
HP-WCSA
HMP
1340mm
Linear Robot
A.A. Sample Cup Output Conveyor
2920mm
PROJECT "A"
HERZOG

Fig. 26

CAMI'95: 3rd Canadian Conference on Computer Applications in the Mineral Industry
Montréal, Québec, Canada, October 22-25, 1995

An Assessment of the Effects of Recirculating Loads on the Dynamic Performance of Simple Flotation Circuit Structures

B.C. Blakey, D. Hodouin, C. Bazin
GRAIIM, Département de mines et métallurgie, l'Université Laval

ABSTRACT:

As asserted by many authors, the impact of recycling streams on the dynamics of continuous processes is not well understood at this time. In the case of flotation, research into this area is particularly timely in view of the current trend in flow sheet configuration philosophy exhibited by a significant number of Canadian minerals processors: elimination of recirculating loads where possible. The objective of the present work is to clarify the consequences of recirculation in flotation systems. To this end, general effects of materials recycle on process operability are briefly summarised. On a more practical level, the effects of recirculating loads in simple flotation flow sheet structures are evaluated by use of mathematical models. It is demonstrated that significantly higher grade – recovery relationships are possible for rougher – scavenger circuit designs that incorporate circulating loads. However, such systems are more sensitive to high frequency disturbances due to steady state considerations, while, in contrast, possess elevated overall settling times. Generally the magnitudes of disturbance gains are either unaffected or lowered by the presence of recycle.

RÉSUMÉ:

Plusieurs chercheurs l'ont affirmé: les effets des charges circulantes sur la dynamique des procédés continus ne sont pas bien compris actuellement. Pour le cas de la flottation, la recherche dans ce domaine intéresse particulièrement certaines compagnies minières canadiennes afin d'optimiser leurs usines de concentration. L'objectif de cet article est de clarifier les effets des flux de recyclage. Après un resumé des observations générales faites dans la littérature sur le comportement des systèmes à recyclage, on propose un modèle mathématique d'un circuit de flottation simple pour quantifier ces comportements. Il est demontré que les bancs d'ébauchage – épuisage avec recyclage procurent des teneurs de concentré plus élevées à rendement métal égal en comparaison des circuits sans recyclage. Cependant ces systèmes sont plus sensibles aux perturbations hautes fréquences de l'alimentation, bien que les constantes de temps soient plus élevées et les gains statiques en perturbation légèrement inferieurs.

INTRODUCTION

Imagine if it were possible to significantly increase the residence time of valuable minerals in a flotation circuit relative to that of the gangue with but a negligible capital cost. Such an innovation would most certainly gain the attention of minerals producers who continuously search for means of increasing their separation efficiencies. However, a technique to

achieve this type of enhancement has been employed in concentrators for nearly as long as there have been flotation plants, namely; recirculation. But curiously, a recent trend in Canadian mineral processing flow sheet design has been the reduction of the number of recirculating loads. This philosophy appears to have resulted from difficulties observed in day-to-day plant operability, which is largely an issue of dynamics.

Previously published works have revealed that (1.) the dynamical effects of recycle are largely unknown, and (2.) problems currently attributed to recycling in flotation systems have not been well defined. The following subsections provide a summary of this material.

Recycle Systems "in General"

In the first of a series of papers, Luyben (1993) summarises most of the limited number of published materials concerning chemical processes with recycle. Much of this work has been based on examinations of the linear dynamics of simple reactor/distillation column systems. Recycling loops such as these have been demonstrated to be mathematically equivalent to a *positive* feedback control loop. Note that under this analogy the terms "closed-loop" and "open-loop" can refer to systems with recycle and without recycle (respectively) in addition to their conventional meanings of controlled and uncontrolled (respectively), as is frequently done in the minerals industry. Note further that this absolutely does not imply that systems with recycle are unstable by nature. Rather, the recycle system will have a propensity for the following behaviour in comparison to its forward path-only counterpart (all other things being approximately equal):

1. the steady state operating point of the system will be different (obviously).
2. larger steady state gains. [Kapoor, *et al.* (1986)]
3. larger overall time constants (sluggish response). [Gilliland, *et al.* (1964)]
4. possibility of under-damped behaviour (if some input change impinges on the system, the output may now oscillate around the new steady state value, but it will dampen out). [Verykios and Luyben (1978)]
5. increased sensitivity to low frequency disturbances. [Denn and Lavie (1982)]

Obviously, the degree to which recycling streams influence the magnitude of each of these differences is dependant upon the amount of material recycled relative to that of the incoming feed, as well as the specific configuration and operating state of the circuit.

Importantly, the above results suggest that the estimation of the dynamic behaviour of an integrated circuit in which recycle is present should not be based on considerations of the behaviour of its unit operations alone. The work of Papadourakis and co-workers (1987) has indeed shown that Bristol's relative gain array for isolated units "cannot be relied upon to give a correct measure of even the steady-state interactions" if they are to be placed within a recycling circuit structure.

Recycle in Flotation Systems

Recently, Stowe (1992) and Edwards and Flintoff (1994) discussed the effects of recycle in flotation circuits and referred to several case studies in which process improvement campaigns that included circuit simplification proved profitable. The results led these authors to attribute recirculating loads to the following operational problems:

1. decreased understanding of the circuit. This impedes an operator's determination of how to achieve target operating points and problem identification.
2. decreased responsiveness and increased sensitivity to disturbances and, therefore, lower amenability to process control.

While the potential for the above effects of recycle cannot be contested, it should be pointed out that the campaigns referred to involved changes in equipment type and configuration, and, doubtless, other changes in operating philosophy, *etc.*, in addition to the reduction of the number of recycling streams. Thus, it has not been rigorously proven that recirculation in flotation plants alone is, at best, a necessary evil required to satisfy steady state recovery targets.

Consider further that point one's validity is, in part, dependant upon the level of automation in the plant. As the number of rudimentary plant elements automatically controlled is increased (which is the current trend), or, inversely, as the operator is freed to

allocate his attention to more global plant issues, the problem becomes less relevant. Secondly, this issue is negated if the dynamic effects of recycle are well understood. While this is not evident in the engineering community as yet, it may be possible for an experienced operator who has developed an intuitive feel for his process to use recirculating loads to their intended advantage.

Point two introduces the notion of the inherent operability of a specified flow sheet configuration. This particular point will be examined in this and future studies. In doing so, it is believed that an increased understanding of this issue will develop, and thus provide answers for questions generated by point one.

Present Objectives

The purpose of the present exercise is to investigate the disturbance rejection properties of recycling elements in flotation circuits. The thesis is that plants that include features possessing good disturbance rejection properties will be easier to control, and, ultimately, are more economical; all other things being effectively equal.* A simple way of determining these properties is through the study of linear mathematical models of the effects of typical disturbances on important measured outputs without specification of the manipulated variables. The following section presents a flexible linear model suitable for this purpose.

A GENERIC ROUGHER – SCAVENGER CIRCUIT

A Single, Generic Cell

Consider the following non-specific model of a flotation cell:

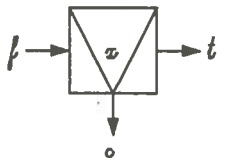

where f is the vector of mass flows of components (classified in terms of particle sizes, or flotation characteristics, or mineralogy, *etc.*, or a combination thereof) in the head feed, x is likewise the vector of mass fractions in the cell pulp, t is the tailings stream mass flows, and o is the mass flow of components exiting the cell by flotation and/or entrainment.

Appropriate relationships between these variables are required to complete the model; the most important of which describe the mixing regime, flotation/ entrainment kinetics, and tailings transfer. Given these one may construct the (nearly always) non-linear disturbance model

$$\mathbf{dx}/\mathbf{dt} = \mathbf{f}(\mathbf{x}, \mathbf{d}) \qquad (1)$$

where $\mathbf{x}$ is the vector of state variables (which include x) and $\mathbf{d}$ is the vector of disturbances (including f). In order to use the techniques provided by linear mathematics, equation (1) must be linearized around an operating point of choice (which is most conveniently the steady state) yielding, say

$$\mathrm{Lin}(\mathbf{f}) = \mathbf{Ax} + \mathbf{Ed} \qquad (2)^{**}$$

whose behaviour is hopefully close to that of the original equation. If equations (1) and (2) are sufficiently similar the system may be described in the Laplace domain as

$$\begin{aligned}\mathbf{x} &= (s\mathbf{I} - \mathbf{A})^{-1}\mathbf{Ed} \\ &= \mathbf{G}_x\mathbf{d}\end{aligned} \qquad (3)$$

if $\mathbf{G}_x \equiv (s\mathbf{I} - \mathbf{A})^{-1}\mathbf{E}$.

Of particular interest are the effects of the impinging disturbance(s) $\mathbf{d}$ on the compositions of the concentrate and tailings streams. Upon linearization of the definitions of these quantities, one may finally say for a single flotation cell

* It is recognised that the effects of recycle on manipulated variables necessary to correct disturbances are also highly important. However, an investigation concerning this subject would require that significant assumptions be made. This will be the subject of future studies.

** From hereon all vector variables are expressed in deviation terms with respect to their steady states.

$$o = G_o d \tag{4}$$

$$t = G_t d \tag{5}$$

where the matrices G_o and G_t are functions of the definitions of the output streams and G_x.

Note that now flotation circuits can be mathematically constructed simply by using transfer function algebra involving equations (4) and (5), given the appropriate steady state data for each cell. The following subsection details such a construction used in the present examination.

Rougher – Scavenger Banks

Consider the general representation of a rougher – scavenger depicted in Figure 1a. As one is most interested in the properties of the bank concentrate o with respect to incoming disturbances (which may all be described by changes in the feed rate/composition vector f), the general equation is to be developed. Using the same notation developed in the previous subsection, matrix algebra yields the dynamics of the circulating load o' by beginning as follows:

$$o' = \left(\sum_{k=N-R+1}^{N} \left(G_o^k \cdot \prod_{l=1}^{k-1} G_t^l \right) \right) f' \tag{6}$$

where Σ denotes element by element addition and Π denotes left side (dot) matrix multiplication. For brevity, the resulting matrix to the left of f' in equation (6) may be called H_R, where the subscript R is used to imply that this matrix characterises the dynamics of the recycle path in Figure 1a. Noting that $f' = (o' + f)$, one may obtain

$$o' = (I - H_R)^{-1} H_R f \tag{7}.$$

Now, the forward path dynamics are

$$o = \left(\sum_{k=1}^{N-R} \left(G_o^k \cdot \prod_{l=1}^{k-1} G_t^l \right) \right) f' \tag{8}$$

and again the resulting matrix to the left of f' in this equation is defined as H_F (F = forward path). The above relations may now be assembled into the equation

$$o = H_F f + H_F (I - H_R)^{-1} H_R f \tag{9}$$

which will be discussed subsequently.

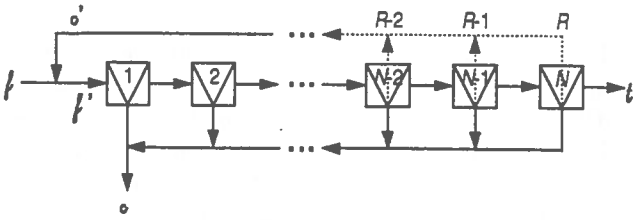

Figure 1a. Generalised representation of a rougher – scavenger of N cells with R cells recycling back to the feed.

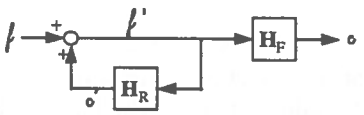

Figure 1b. Block diagram representation of the process in Figure 1a as modelled by equation (9).

General Considerations of the Effects of Circulating Loads

Equation (9) may be represented by block diagram form as given in Figure 1b. This graphic allows some general predictions of the effect of circulating loads to be made. Firstly, it is easily seen that the total dynamics of the system may be broken down into distinct forward and recycle paths.

Consider a single line of rougher cells with feed to concentrate dynamics described by the matrix H_F (*i.e.*, no circulating load: $R = 0$). Returning to Figure 1a, it may be inferred that the initial dynamic behaviour of the total bank concentrate when submitted to a disturbance in feed is determined by the first few rougher cells. That is to say, the contribution of a single cell to the initial (*i.e.*, high frequency) dynamics of the system is diminished the further it is down the bank (1.) because the disturbance dynamics are damped by the previous cells and (2.) because its effect is delayed due to the transport time of material to that cell.

Now, what would happen if the concentrates from R cells at the end of the bank were then recycled back to the feed? If the dynamics of the concentrates of these end cells are described by $\mathbf{H}_R$ the situation may be depicted in Figure 1b. Here, it is seen that disturbances in the feed are transmitted to the concentrate launder (1.) directly through the forward path dynamics $\mathbf{H}_F$, and (2.) to the recycle dynamics, $\mathbf{H}_R$, "positively fed back" to $\mathbf{H}_R$, and then passed to the final concentrate launder via $\mathbf{H}_F$. Since $\mathbf{H}_R$ primarily describes the dynamics of the last R cells in the bank, it is expected from the discussion in the previous paragraph that the effects of the disturbances are damped and delayed relative to those impinging on the initial cells in the forward path. Thus, this recycle element will serve to increase the system settling time (time to new steady state) due to the slower dynamics of $\mathbf{H}_R$ and its positive feed back loop. Additionally, it is expected to alter the magnitude of the steady state gain of the system (either up or down).

Note that the above discussion requires that both the open-loop and closed-loop circuit cases have similar operating points. In reality, the implementation of circulating load can significantly influence the choice of the steady state operating point, particularly when given capital constraints. This statement holds, it will be seen, even if the important external operating variables (*e.g.*, grade and recovery) are similar between different circuit configuration cases. Thus, the dynamics of circulating loads are inextricably linked to their influence on the steady state operation. The next section gives an examination of these issues through simple examples.

A SIMPLE EXAMPLE OF ROUGHER – SCAVENGER RECYCLE

For these studies, relatively elementary circuit structures containing a limited number of cells (to a maximum of six) have been selected. This has been done in order to facilitate understanding of the rather complicated dynamic behaviour exhibited by this process. The simple modelling approach used is the global kinetic description of the complex rate phenomena advocated by Lynch *et al.* (1981). Industrial validation of this model is found in the famous study by Fewings and co-workers (1979) on the dynamic behaviour of the chalcopyrite circuit at Mount Isa Mines in Australia. Important aspects of this model with respect to the present work follow.

In this particular approach, one can imagine a three component system: water, valuables, and gangue. The latter two are each divided into two classes of kinetic entities: fast and slow floating/entraining, represented by a set of two rate constants. Thus, the "floatability" of these solids classes can be described by the fraction of slow floating material ϕ_s. This parameter is intended to represent the combined effects of changes in the (practically) non-measurable variables of mineralogical composition, degree of oxidation, size distribution, surface modifications, and water chemistry. The rate constants refer to the overall rate of transfer from the pulp body to the concentrate launder (*i.e.*, includes the rates of particle – bubble attachment, rising to pulp – froth interface, transfer to froth phase, transfer to concentrate launder, in addition to the reverse processes).

The model also allows description of the behaviour of the flotation circuit as a function of collection air flow rate through the parameter "a", which is essentially a kinetic rate constant multiplication factor. For the present purpose, this value will be called a_{con} if it pertains to the air flow rate in cells whose concentrates will exit the bank, and a_{rec} for cells whose concentrates will be recycled back to the feed. The minimum value for this variable is zero, implying no air flow, while a maximum of two has been arbitrarily set, above which it is no longer effective (due to, say, excessive bubble coalescence, high turbidity, *etc.*). The intermediate value ($a = 1$) is intended to serve as a base case.

The flotation machines used at Mount Isa are assumed to be similar to Agitair 120 × 500's. Given a total pulp plus air cell volume of 14.2 m^3, one may imagine that the total pulp volume only is 13.5 m^3. From non-linear simulations studies, it was observed that approximately 65% of the mass of the pulp is water under all conditions of interest thoughout all cells in the rougher – scavenger line. Given, then, that the density of the pulp is approximately 1.34 t m^{-3} at all times, a total target cell mass hold-up of about (13.5 × 1.34) t = 18 t may be assumed. Working with these values, one finds an average cell residence time of 2 min for a reasonable throughput of about 3 t min^{-1} solids. Table 1 summarises the relevant assumptions made during the construction of this model.

Table 1. Important rougher-scavenger model assumptions.

Assumption	Validity supported by ...
1. two-rate constant approach	Lynch *et al.* (1981)
2. approximate perfect pulp mixing behaviour	SME Mineral Processing Handbook (1985)
3. (nearly) constant pulp density*	non-linear dynamic simulation
4. (nearly) constant mass hold-up*	non-linear dynamic simulation
5. (nearly) constant froth height	validity of 3. and 4.
6. negligible transport time between banks**	depends on cell/circuit design

* at all times, under given input changes.

** relative to dynamic responses to given input changes.

Steady State Grade – Recovery Performance

Figure 2a shows the influence of circuit structure on grade – recovery performance at constant operating conditions. Here, it is seen that increasing the number of cells producing concentrate in a bank has the logical consequence of increasing recovery at the expense of overall concentrate grade. Note that as the total number of concentrate-producing cells is increased this effect is reduced. The same figure also shows that increasing the number of recycling cells increases both grade and recovery. Again, this effect is diminished as the total number of recycling cells increases.

These points serve to illustrate the trade-offs associated between grade – recovery objectives and capital costs. However, the present example ignores the fact that when structural changes are made to circuits there are necessary changes to be made in the operating conditions in order to optimise separation. This point is developed subsequently.

The steady state behaviour of one cell as a function of air collection rate is given in Figure 2b. Here, it is noted that a single cell, or equivalently the first cell in a bank, is characterised by high grade output, but at low recovery. It is for this reason that many plants send the first (or the first few) cell concentrate(s) directly to the final concentrate stream. Note, however, that the range of operation given by adjusting a_{con} is rather limited, and, alone, is certainly not sufficient to achieve economical recoveries. As the number of cells in the bank is increased, Figure 2b shows that higher grade – recovery curves are possible and that the range of operation is significantly expanded. Noting that a bank of six rougher cells gives good performance at the base case $a_{con} = 1$ (yielding 16.9 %Cu at 95 % recovery), the discussion proceeds to the steady state effects of a circulating load using this circuit as the reference open-loop case.

If there existed a rougher bank in which only these six cells were available (representing a capital cost constraint), it would be of interest to determine if higher metallurgical performances could be achieved by changing the circuit configuration. Figure 2b indeed shows that recycling the last three of the six-cell bank produces higher grade – recovery curves. Now consider the three curves representing the characteristics of the three recycling cases (in which the air flow factor for the recycled concentrate, a_{rec}, is 1, 1.5, and 2) together with the bank of three cells only (which can represent the case where $a_{rec} = 0$). This exercise shows that increasing the air collection rate (or, equivalently, the circulating load) results in increasing the operating grade – recovery curve level. This effect diminishes as a_{rec} and a_{con} approach their maximum.

Consider again the reference bank of six cells operating at unit air factor with 95 % recovery. Suppose that this is the recovery level selected on economic grounds. If the plant configuration is then changed to incorporate the recirculation of the last three cell concentrates in order to be able to operate on a higher grade - recovery curve, one is obliged to operate the first three cells at about $a_{con} > 1.7$ (if $a_{rec} = 1$*) in order to achieve the same recovery. Assume, however, that the most economical closed-loop case is found at $a_{con} = 1.8$, where both the grade and recovery are higher than the reference bank: 18.2 %Cu at 96.4 % recovery, respectively.

* While slightly higher grades and recoveries are available at $a_{rec} > 1$, this value will be maintained for the purposes of the subsequent discussion on the effects of the magnitude of the circulating load on dynamic performance.

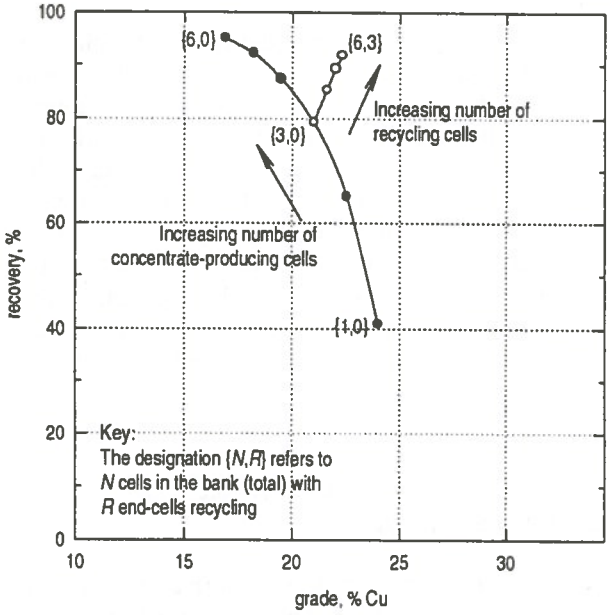

Figure 2a. Grade – recovery relationships for different rougher – scavenger configurations as functions of total number of cells, N, and number of recirculating cells, R. All operating conditions are constant (*i.e.*, $a_{con} = a_{rec} = 1$).

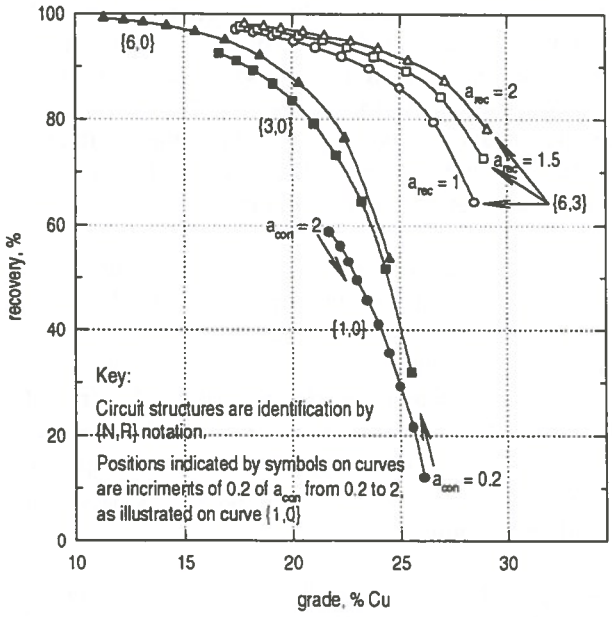

Figure 2b. Grade – recovery relationships for different rougher – scavenger configurations as functions of concentrate "air factor" a_{con}.

While a discussion of what happens to the steady state grade – recovery performance under changes in circuit configuration has been given to this point, an investigation of why the system behaves in this manner has not been performed. The following compares the internal (*i.e.*, cell-by-cell) behaviour of the most economical open-loop and closed-loop cases in order to develop an improved understanding.

A closer look at the steady state consequences of circulating loads: The internal steady state behaviour of the open-loop and closed-loop cases are represented in Figures 3a and b, respectively. From Figure 3a, it is seen that the concentrate grade and solids mass production decrease in a near-linear fashion as one goes down the bank in the tailings direction. Thus, if it were possible to take the concentrate of, say, the first three cells it is to be expected that the grade would be increased significantly on the one hand, and that the total production of concentrate (which relates to recovery) would decrease by an amount equal to the output of the last three. Figure 2b shows that this situation would yield a 21 %Cu concentrate grade at 79 % recovery. Since the rate of recovery for just the first three cells can be seen as far too low for rougher flotation, one may wish to attempt to recover the valuable material of the last three cells by recirculating this stream back to the feed. Doing this, an increase in recovery might now be expected because the residence time of the valuable mineral in the first three cells is "artificially" increased due to the recirculating load. At the same time, since in the present case the grade of the recycling material from the last three cells is higher than the head feed (see Figure 3a), the first three cells of the bank are now fed material that is richer in valuable mineral than in the open-loop case. And indeed, Figure 2b shows an elevated operating point yielding about 22 %Cu at 90 % recovery.

The recovery of valuable material is most important at the rougher – scavenger stage [Herbst *et al.* (1986)]. While to this point the concentrate grade has been elevated substantially, the recovery level is still low. From Figure 2b, it is seen that increasing the air flow factor of the exit concentrate cells, a_{con}, is extremely effective in increasing rougher - scavenger recovery levels. By doing so, the situation in Figure 3b is observed, where a_{con} has been elevated to 1.8. In comparison to the system represented by Figure 3a, it is seen that concentrate grade levels of all cell concentrates in the recycle case have significantly

decreased. This has occurred due to the increase in a_{con} in the first three cells required to achieve superior recoveries (*i.e.*, a slide up and to the left on the grade – recovery curve), which, in turn, affects the concentrate grade of the last three cells by decreasing the grade of the feed to these units.

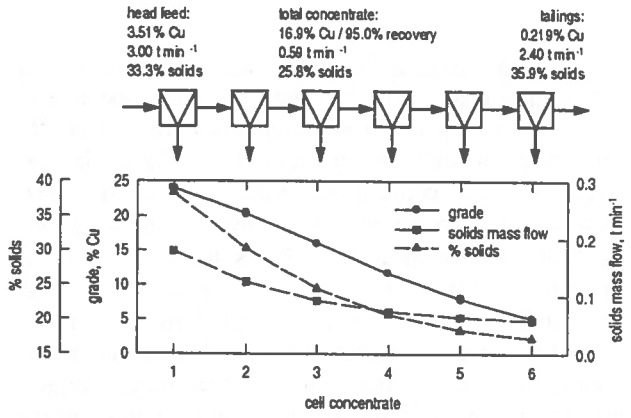

Figure 3a. Steady state characteristics of an open-loop line of rougher/scavengers.

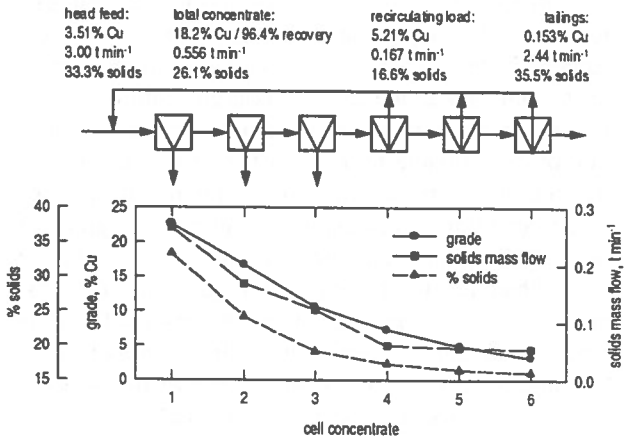

Figure 3b. Steady state characteristics of a closed-loop (with recycle) line of rougher/scavengers (a_{con} = 1.8).

Linkage between steady state and dynamic performance: It has been seen that "higher" grade – recovery curves are possible when recycle is incorporated into a rougher – scavenger flow sheet. This has also been implied by the simulation studies of King (1975 and 1976) and by the large number of plants that still employ this feature. However, the complaints coming out of industry at present appear to concern the day-to-day "operability" of the plant, as discussed in the introduction. This is an issue of plant dynamics; the key element of which, it may be argued, is the ability of the system to reject disturbances impinging on the system. A flotation plant that possesses good characteristics in this respect will most likely experience improved metallurgy resulting from its ability to achieve its objectives more consistently, and reagent conservation, as dosing becomes more accurate. The following section examines these issues for the above systems already described in the steady state.

Dynamic Consequences of Circulating Loads on Rougher – Scavengers

Assume that there exists a disturbance d on an important plant output y that may be described by

$$y / d = G_d = k_d / (1 + \tau_d s) \qquad (10)$$

a first order transfer function in the Laplace domain. For a flotation circuit, it may be assumed that all disturbances are caused by changes in solids mass flow and composition, and unknown changes in pulp chemistry in the head feed coming into the plant. Thus, for a given mineral body and a specified production capacity, the vector of all disturbances **d** are dependant on the way in which they influence outputs **y** only through $\mathbf{G}_d$, that is to say, the configuration and operating conditions of the plant.

Now, if a plant response to a disturbance is approximately represented by equation (10), one would wish that k_d would be as low as possible, and that τ_d be as high as possible in order to facilitate disturbance rejection via feedback control. Indeed, Waller *et al.* (1988) have found a correlation between the parameter k_d/τ_d with the disturbance rejection properties for various configurations of closed-loop distillation columns.

The dynamic version of the present mathematical model has been used in an investigation of the effects of disturbances in floatability, head grade, and mass flow fluctuations on those controlled variables commonly used in industrial practice: concentrate grade, concentrate solids mass flow, and tailings grade [Herbst et al., (1986)]. As the floatability parameter is particularly nebulous, and is truly a non-measurable

variable that can only be mitigated by feedback control, for the purposes of brevity only the effect of this parameter on concentrate grade (perhaps the most important output variable) is considered in detail. General conclusions given at the end of this article are made from observations of the results of the complete model.

Open-loop roughers: Table 2 gives the cell-by-cell response of the open-loop bank of six cell compartments to a step down in valuables' floatability. In the first cell concentrate launder, it is seen that the response is approximately first order in the decrease of grade and production of concentrate. Moving to cells further down the bank, it is obvious that two opposing forces are at work: (1.) the decreased floatability of material entering the cell, and (2.) an elevation in the amount of valuable material that is transferred to subsequent cells. For an alternative view of this situation, consider that if there is a decrease in the ability of a mineral to float, it would require a longer residence time to appear in a concentrate launder. In this case, this effect actually results in an elevation of the concentrate grade for the cells at the end of the bank. Note from the response of the end cells' concentrate production, however, that this effect on the overall concentrate is reduced. Furthermore, because the response of cells further down the bank is delayed due to the transport time, it may be assumed that the first few cells of the bank determine the initial dynamic response (or, equivalently, the high frequency characteristics) of the system, confirming the prediction made in the general discussion given in the previous section.

Summing the concentrates represented in Table 2, it is easily seen that the bank's behaviour, given in terms of total concentrate grade, is that represented by the thicker curve in Figure 5a.

Closed-loop rougher/scavenger comparison: The thinner lines in Figure 5a provide a comparison of the open-loop and closed-loop banks described previously. The closed-loop example is divided into cases of different circulating loads. This has been done by changing the air flow rate, here represented by a_{rec}, for cells producing circulating concentrate, as is frequently the case in industrial practice [SME *MPH* (1985)]. Table 3 gives complete information on the steady state characteristics of the circulating load as a function of the air parameter.

It is evident that the quicker initial response in the recycle case is due to (1.) the reduced number of cells contributing to the dynamics, and (2.) the higher velocity of the concentrate exiting the cell due to an elevated a_{con}. These factors suggest that the effect of changing operating conditions to accommodate a circulating load, under constant equipment constrains and similar grade – recovery requirements, generally result in increased high frequency disturbance sensitivity. Indeed, this assertion is verified by Figure 5b, which shows the Bode magnitude and phase angle plots of the system considered in Figure 5a.

Table 2. Responses of concentrates of each cell launder in the open-loop bank to a step change down in valuables' "floatability" (ϕ, increases 0.1).

Con. No.:	1	2	3	4	5	6
Change in Grade[1]	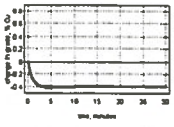	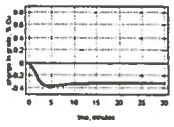	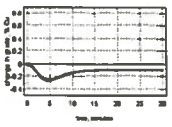	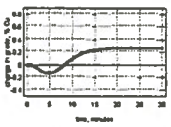	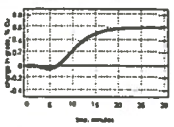	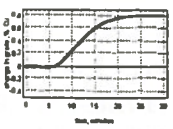
Change in Solids Mass Flow rate (SMF)[2]	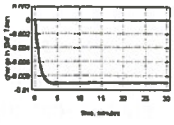	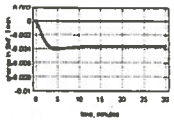	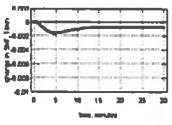	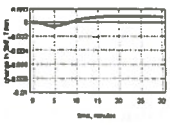	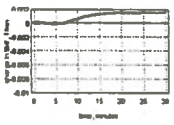	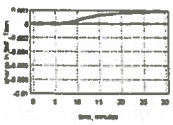

Abscissae: "time, minutes" from 0 to 30.
Ordinates: [1] "change in grade, % Cu" from -0.4 to 1
[2] "change in SMF, t/min" from -0.01 to 0.002

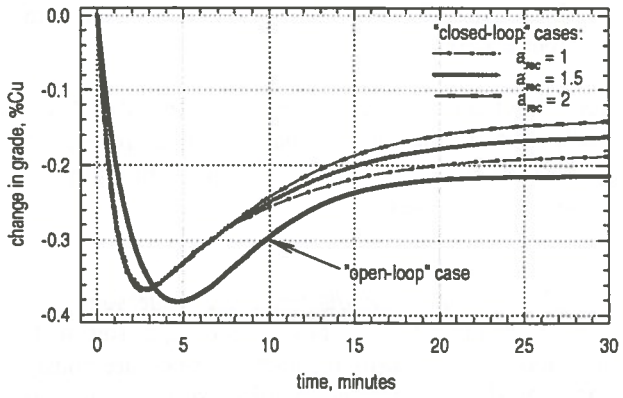

Figure 5a. Responses of concentrate grade to a step change down in valuables' "floatability" (ϕ_v increases 0.1) for an open-loop rougher and closed-loop rougher – scavengers operating at various circulating loads.

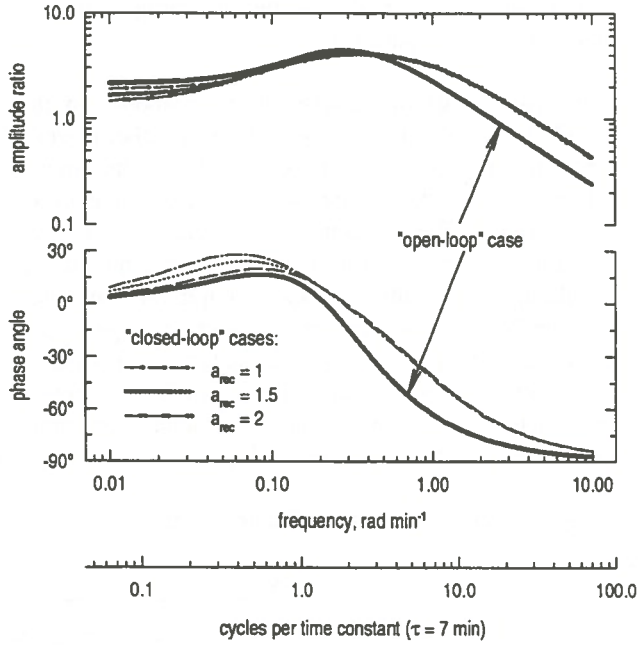

Figure 5b. Frequency responses of concentrate grade to valuables' "floatability" for an open-loop rougher and closed-loop rougher – scavengers operating at various circulating loads.

These figures also allow consideration of the dynamical effects due to the circulating load as it is elevated from 5 to 10.5 % of head feed (*i.e.*, as a_{rec} goes from 1 to 2). Here, it is obvious that the initial dynamical response is unaffected. This is to be expected from the discussion provided in the previous subsection concerning the importance of the first few cells of the bank in determining the initial/high frequency system dynamics. It may be assumed, however, that the high frequency dynamics would be affected in a positive manner if higher circulating loads were possible, resulting in increased total throughput, and, thus, decreased cell residence times.

On the other hand, in Figure 5a it is observed that the settling time of the system is increased with increasing circulating loads. This is a natural characteristic of recycle, as discussed in the introduction. Furthermore, the steady state gain of the system is shown to decrease with increased circulating load. This phenomena is a consequence of the fact that the floatability response of the last few cell concentrates (*i.e.*, the concentrates that are recycled) is opposite to the cells along the forward path, as discussed in the previous subsection. These factors contribute to decreased sensitivity of the system to low frequency disturbances, as indicated in Figures 5a and 5b.

Table 3. Characterisation of the circulating load as a function of the air flow rate factor.

a_{rec}	grade, %Cu	solids mass flow t min^{-1}	circulating load (% head)
1	5.21	0.167	5.6
1.5	4.54	0.243	8.1
2	4.12	0.316	10.5

CONCLUSIONS AND RECOMMENDATIONS

The main conclusions resulting from this exercise are:

1. significantly higher grade – recovery relationships are possible for flotation plant designs that incorporate circulating loads.
2. steady state economic considerations, under a constant equipment constraint, tend to place the operating point of a rougher – scavenger circuit in a region more susceptible to disturbances at high input frequencies.
3. higher circulating loads tend to lower the low frequency sensitivity.

4. higher circulating loads tend to increase the overall settling time of the system with respect to disturbances.
5. there is no significant impact from changing circulating loads on disturbance sensitivities at higher frequencies, unless the circulating load is so large that it significantly affects the residence time in the cells.

Finally, since system dynamics are significantly affected by the choice of the operating point in the present case, it is believed that an investigation on the ways in which the manipulated variable dynamics are changed should be conducted.

ACKNOWLEDGEMENTS

The authors wish to thank the consortium of Canadian mining companies under the MITEC umbrella for making work such as this possible, and the Natural Sciences and Engineering Council of Canada for its post graduate scholarship support. Thanks is also due to Dr. Daryll T. Fogal, formerly of McMaster University, for his kind assistance during the literature survey.

REFERENCES

Denn, M.M., Lavie, R., 1982
Dynamics of Plants with Recycle, Chem. Eng. J., 24, pp. 55-9

Edwards, R.P., Flintoff, B.C., 1994
Process Engineering of Flotation Circuits, CMP Conference, Ottawa

Fewings, J.H., Slaughter, P.J., Manlapig, E.V., Lynch, A.J., 1979
The Dynamic Behaviour and Automatic Control of the Chalcopyrite Flotation Circuit at Mount Isa Mines Limited, 13th International Mineral Processing Congress, Warsaw, pp. 1541-73

Gilliland, E.R., Gould, L.A., Boyle, T.J., 1964
Dynamic Effects of Material Recycle, JACC, Stanford, California, pp. 140-6

Herbst, J.A., Hales, L.B., Zaragoza, R., 1986
Strategies for the Control of Flotation Plants, in Design and Installation of Concentration and Dewatering Circuits, Mular, A.L., Anderson, M.A., *eds.*, SME, Littleton, Colorado, pp. 548-569

Kapoor, N., McAvoy, T.J., Marlin, T.E., 1986
Effect of Recycle Structure on Distillation Tower Time Constants, AIChE J., 32, 3, pp. 411-8

King, R.P., 1975
Simulation of Flotation Plants, Society of Mining Engineers, AIME, Transactions, 258, pp. 286-293

King, R.P., 1976
The Use of Simulation in the Design and Modification of Flotation Plants, in Flotation, Fuerstenau, M.C., *ed.*, AIME, New York, vol. 2

Lynch, A.J., Johnson, N.W., Manlapig, E.V., Thorne, C.G., 1981
Mineral and Coal Flotation Circuits: Their Simulation and Control, Elsevier Scientific Publishing Company, New York

Luyben, W.L., 1993
Dynamics and Control of Recycle Systems, 1., Simple Open-Loop and Closed-Loop Systems, Ind. Eng. Chem. Res., 32, pp. 466-75

Papadourakis, A., Doherty, M.F., Douglas, J.M., 1987
Relative Gain Array for Units in Plants with Recycle, Ind. Eng. Chem. Res., 26, pp. 1259-62

SME Mineral Processing Handbook, 1985
Norman L. Weiss, *ed.*, SME, New York

Stowe, K.G., 1992
Noranda's Approach to Complex Ores – Present and Future, AMIRA Annual Technical Meeting

Verykios, X., Luyben, W.L., 1978
Steadystate Sensitivity and Dynamics of a Reactor/Distillation Column System with Recycle, ISA Trans., 17, p. 49

Waller, K.V., Haggblom, K.E., Sandelin, P.M., Finnerman, D.H.,
Disturbance Sensitivity of Distillation Control Structures, AIChE J., 34, 5, pp. 853-858

CAMI'95: 3rd Canadian Conference on Computer Applications in the Mineral Industry
Montréal, Québec, Canada, October 22-25, 1995

Remote Communication for Sensor Testing and Tune-Up

C.O. Gomez, E. Chnyrenkov, J.A. Finch
Department of Mining and Metallurgical Engineering
McGill University, Montréal, Québec

F. Falvo
Central Mills, Process Technology
INCO Limited, Copper Cliff, Ontario

ABSTRACT:

One of the major difficulties in the transfer of technology from universities to industry is the cost involved in plant testing of new ideas for equipment or instrumentation. In the case of the minerals industry, this is a critical factor because most of the industrial operations are located in remote areas away from universities and research centres. For the past several years, McGill has been developing sensors for the mineral processing industry based on the measurement of the electrical conductivity of dispersions. Several of these sensors, which are driven by a computer, have been successfully tested in laboratory installations. The testing and tune-up of industrial prototypes has been greatly simplified by attaching a modem to the sensor computer. By allowing daily monitoring of the sensor output, this device makes it possible for university researchers to check sensor performance and to modify software to cover unpredicted situations, and at the same time, to work with plant personnel in the development of operating practices based on the variable being measured. The advantages of using remote communication are illustrated through the installation, tune-up and utilization of a mud line sensor for a concentrate thickener.

RÉSUMÉ:

Les coûts associés aux essais en usine de nouvelles idées ainsi qu'à l'installation et la mise au point d'équipement et d'instrumentation sont un problème majeur lors du transfert de technologies entre les universités et l'industrie. Ceci devient un facteur critique pour l'industrie minière puisque la plupart des ces installations industrielles sont situées dans des endroits éloignés des universités et centres de recherche. Au cours des dernières années, McGill a mis au point, pour le traitement des minéraux, des détecteurs utilisant la mesure de la conductivité électrique des dispersions. Plusieurs détecteurs, reliés à un ordinateur, ont été mis à l'épreuve avec succès dans des laboratoires. L'essai et la mise au point des prototypes industriels ont été grandement simplifiés par l'ajout d'un modem à l'ordinateur du détecteur. Par une surveillance quotidienne des données provenant du détecteur, cet appareil permet aux chercheurs universitaires de vérifier le fonctionnement du détecteur et d'en modifier le logiciel pour compenser certains changements imprévus. De même, il rend possible une collaboration avec le personnel de l'usine quand à la mise en pratique de techniques de travail basés sur les résultats obtenus. Dans un épaississeur à concentré, l'installation, la mise au point et l'utilisation d'un détecteur de l'interface des boues démontrent bien les avantages de cette technique.

INTRODUCTION

One of the most important factors limiting the transfer of technology from universities to industry is the high cost of having personnel on-site during the period in which equipment or instrumentation developed in laboratories is adapted to plant conditions. This is particularly true in the case of the minerals industry, as most operations are remote from universities and research centres. The Mineral Processing group at McGill University has been faced with this problem when trying to test industrial prototypes of new sensors at different plants in Canada. These sensors, which measure the electrical conductivity of dispersions, have been successfully tested in laboratory installations. However, their use and acceptance by plant personnel is not immediate as they provide measurements which were not available before. Fortunately, the testing and tune-up of industrial prototypes has been made easier by adding a modem to the system driving the sensor. This device allows daily monitoring of the sensor output without the need of being on-site; therefore, it is possible for university researchers to react quickly to unpredicted situations by adapting hardware and/or software. The disturbance to plant personnel in this process is minimum and they can continue performing their duties while commissioning and testing is in progress. The successful use of this technology is illustrated through the installation and tune-up of a mud-line sensor for a concentrate thickener located at INCO Limited, Copper Cliff, Ontario.

MUD LINE DETECTION IN THICKENERS USING CONDUCTIVITY

Thickening is one of the basic unit operations in mineral processing and hydrometallurgy and it is used to separate suspended solid particles from a solid-liquid dispersion by gravity settling. As the dispersion enters the thickener, the solids settle to the bottom and clarified water overflows the top. A thickener, which may be continuous or batch, is basically a large vertical cylindrical tank provided with devices to feed the dispersion and to remove the settled solids. The tank provides residence time for the particles to settle. The dispersion enters the thickener through the feedwell whose function is to dissipate the momentum of the feed stream and to create relatively quiescent conditions around the entering point. Rotating rake arms move the settled solids towards the discharge point located at the bottom center of the tank.

There are normally three distinct zones in a thickener: a top layer of clear water, a middle layer called a sedimenting zone in which particles are settling, and a bottom layer called a compression zone in which particles are pressed together as a consequence of the weight of settled particles. The proper operation of a thickener requires two simultaneous conditions: no solids in the water overflowing the top and the correct solids content in the underflow pulp. To achieve these conditions is difficult because sensors for detecting the sediment line (interface between clear water and sedimenting zone) and the mud line (top of the compression zone) are not commercially available.

For the past several years, sensors based on the measurement of the electrical conductivity of mineral dispersions have been developed at McGill. One of these sensors was a probe designed to detect the interface between the froth and collection zones in flotation columns (Gomez et al., 1989) as well as in mechanical cells (Uribe-Salas et al., 1991). The working principle of this probe, collection of a conductance profile around the interface, also applies in the detection of the sediment and mud lines in a thickener. Tests run with a prototype demonstrated that the different zones present in a thickener can be clearly identified (Xu et al., 1994). Using the rings at the top of the thickener to give an estimate of the solids-free conductivity a solids content profile can be determined utilizing Maxwell's model (Uribe-Salas et al., 1993). This makes possible the estimation of the solids inventory.

MUD-LINE PROBE CHARACTERISTICS

The probe has the appearance of a long plastic cylinder with a series of equally-spaced metallic rings (Figure 1). Its construction is based on a basic module formed by a non-conducting PVC cylinder shaped to support a SS ring that acts as an electrode (Figure 2). This module was designed so that a probe can be assembled by mounting a series of them around a SS pipe; the dimensions and number of modules used define the detection length of the probe as well as the accuracy with which the mud-line is detected. The central pipe

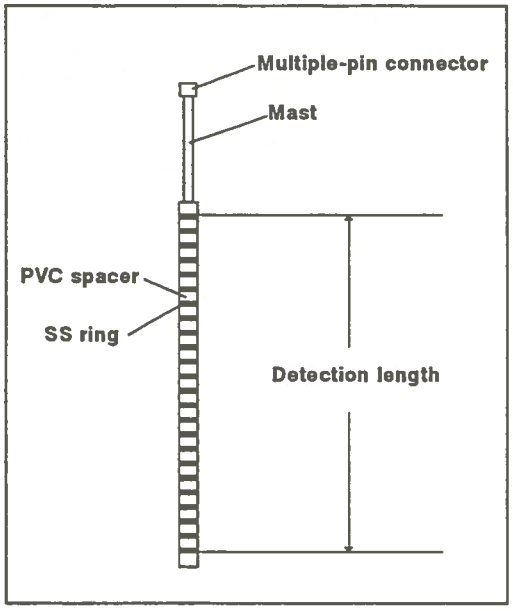

Fig. 1 Schematic of mud-line sensor.

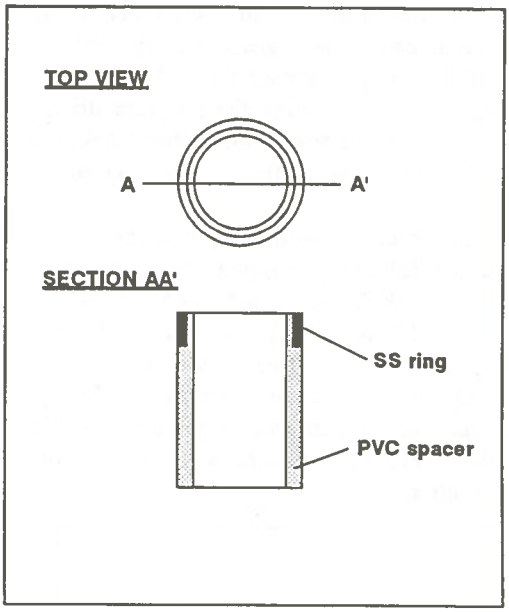

Fig. 2 Details of probe construction module.

is longer than the detection length of the probe leaving a mast which is used to install the probe in its working position. Each ring electrode is wired on its internal face with the wire going into the central pipe and ending in a multiple-pin connector installed at the top of the mast. The probe installed at INCO (Sudbury, Ontario) has a total length of 4.0 m, with a detection length of 3.1 m (32 ring electrodes separated 0.1 m). To avoid the rake, the probe is mounted on a vertical SS tube which in addition to maintaining the probe in its working position, is pivoted at the top through a hinged mounting bracket attached to the catwalk structure. Every time one of the rake arms passes, it pushes this supporting tube (and the probe with it) out of its vertical position, which is retaken after the rake arm passes.

The probe functions by means of computer-driven electronics. By using a multiple-wire cable, each ring electrode is connected to a switch relay installed on a computer board. Outputs of even and odd relays are connected to different terminals of the conductivity meter. Digital and analog I/O boards are installed in an IBM-compatible computer and used, respectively, to activate switch relays and to read the output of the conductivity meter. When two neighbouring electrodes are simultaneously connected, an electric circuit is closed, and the conductance between the two electrodes is measured. The two electrodes constitute a conductivity "cell."

A computer program automates the collection of a conductance profile along the thickener by sequentially connecting two neighbouring rings, from top to bottom, to the conductivity meter. The same program stores and processes the information contained in the conductance profile and, for example, calculates the location of the mud line and the solids inventory. Control signals proportional to the value of these variables are then delivered to the control room.

Experience has shown that every installation is unique, therefore, a different combination of algorithms is necessary in each case to process the information. Furthermore, conditions in a thickener frequently change as the plant experiences up-stream operating changes; the magnitude and quickness of these changes cannot be predicted. Therefore, a tune-up period after the probe has been installed is inevitable. The effort and cost of tuning-up the instrument to meet the conditions and operating practices of a particular installation can be dramatically reduced by remote communication, which makes possible software modifications from a distance. By incorporating a modem to the computer driving the probe, the system can be linked to a second computer (located at McGill in this case).

A commercial software package (pc ANYWHERE, Norton) was used for communication purposes. The use of this package is incidental and does not constitute

endorsement of this product. In fact, most of the software communication packages currently available have the capability of performing the tasks this work requires: stopping and restarting the program driving the probe, retrieval of data files from the hard disk, and reloading modified versions of the driving program.

The electronics associated with the probe installed at Sudbury had the following components: a computer (IBM compatible, 386SX/40, 1 MB RAM, 1.44 MB floppy drive, 80 MB hard disk), an analog I/O board (Metrabyte, DAS8/AO), two 16-relay boards (Metrabyte, REL-16), a conductivity meter (Bailey, model 440), and an internal modem (Zoltrix, 14.4k, mod V32 bis). Figure 3 illustrates the interactions between these units.

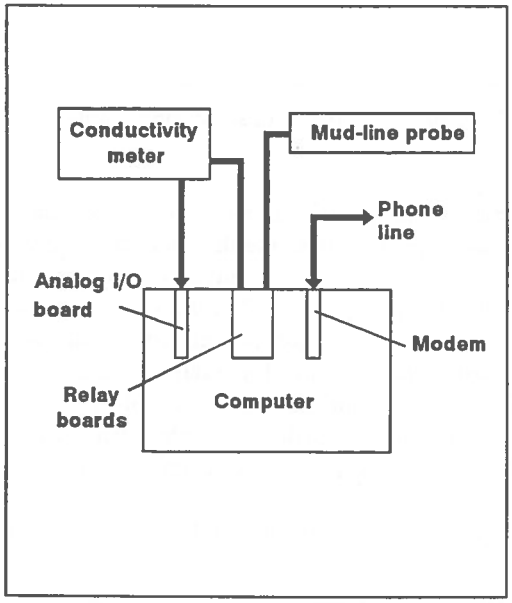

Fig. 3 Schematization of electronics associated with mud-line probe.

COMMISSIONING AND TUNE-UP

The probe was commissioned in October 1994. Figure 4 shows a profile collected on October 8 after just a few hours operation. To calculate solids content from conductance, the conductivity of the solids-free liquid is required, which was to be obtained in the case of a thickener from the conductance readings reported by those cells located near the top of the thickener. The profile displayed in Figure 4 shows features not found in the profiles collected by Xu et al., namely the low conductance values reported by the top two cells as a result of the presence of a froth layer. Therefore, an immediate correction was necessary in the selection of the cells used to estimate the conductivity of the solids-free liquid (the original algorithm considered it as an average of the values calculated from the top five cells). The algorithm was modified to use the average of the third, fourth and fifth cells (counting from the top).

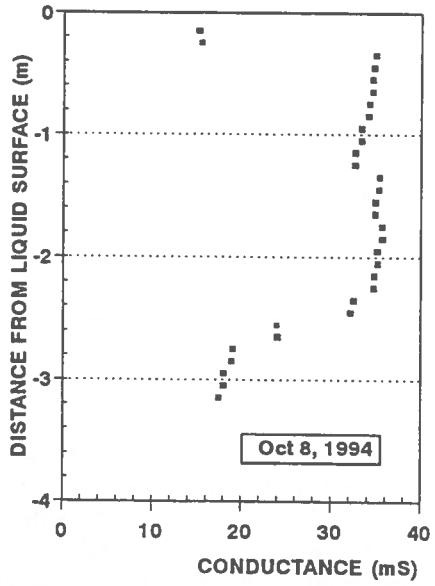

Fig. 4 Conductance profile after installation (low values at the top are associated with a froth layer on the top of the thickener).

Analysis of data over subsequent days revealed another problem: the conductance decreased at given depth as the probe was being used although there were no solids at that depth. This is illustrated in Figure 5 which shows the top portion of profiles collected on October 8, 12, and 17. These results also showed that the presence of the froth layer was not permanent.

It was found that these reducing conductance values near the top of the probe were the result of deposition of some material on the ring electrodes. A probe inspection by plant personnel reported that the rings were not covered by a layer of solids, as anticipated, but instead by a thin layer of a yellowish oily material. An observation that may help to determine the source and nature of the material being deposited is that the cells affected are those that move from the clear liquid into the froth layer as the rake passes. This deposition

decreases the cell constant, therefore, a lower conductance is measured. Figure 6 presents conductance values of two of the cells affected by the deposition. The rings of one of these cells were cleaned at about 2:00 pm; this resulted in an immediate increase in conductance for the cleaned cell while the other reported a fairly constant value. The trace for the cleaned cell also shows a steady decline suggesting deposition restarts almost immediately.

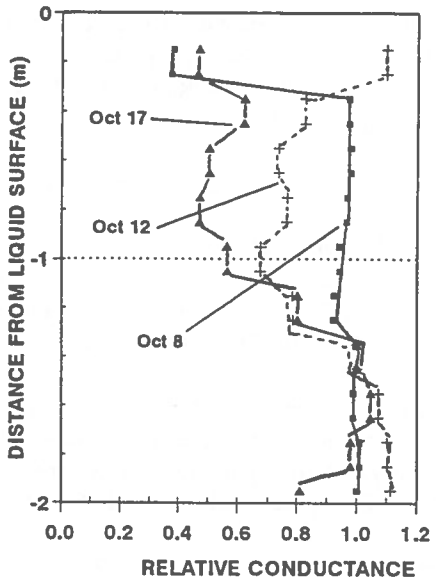

Fig. 5 Conductance profiles on different dates.

Unusual conductance profiles began to be collected on December 20, as illustrated in Figure 7; values reported for the top four cells were very low. Seeing this, personnel at McGill suggested those cells were permanently out of the liquid as a consequence of a frozen froth layer trapping the probe at an angle. Inspection by plant personnel demonstrated that was the case. Provisions were taken for maintaining the probe in normal operation for the rest of the winter.

A close examination of the profile shown in Figure 7 reveals that an electronic problem was present because the occurrence of two consecutive cells reporting the same conductance was too frequent. We referred to this as "pairing." After several tests were done from a distance, it was concluded that the ground used for the electronic system was the same as the ground of the power network. It was decided to isolate the ground of the electronic system and a McGill engineer travelled to Sudbury for this purpose. The problem was solved in less than one hour and subsequent profiles were free from pairing, as illustrated in Figure 8.

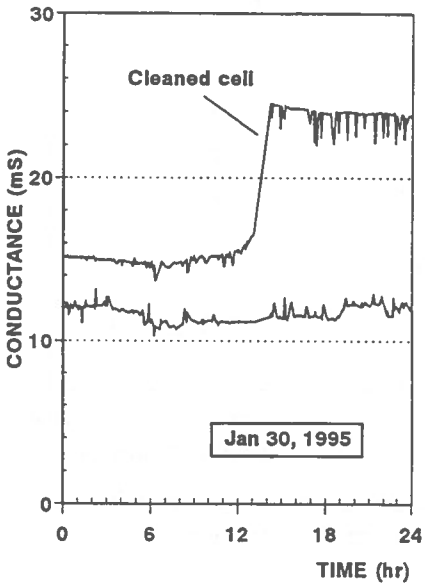

Fig.6 Effect of removing material deposition from ring electrodes: rings of one cell (the upper trace) were cleaned, the other was left.

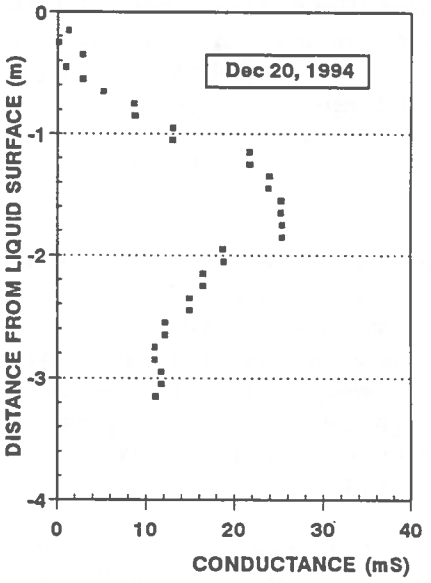

Fig. 7 Conductance profile with probe stuck on top of frozen froth layer; also, note "pairing" (see text).

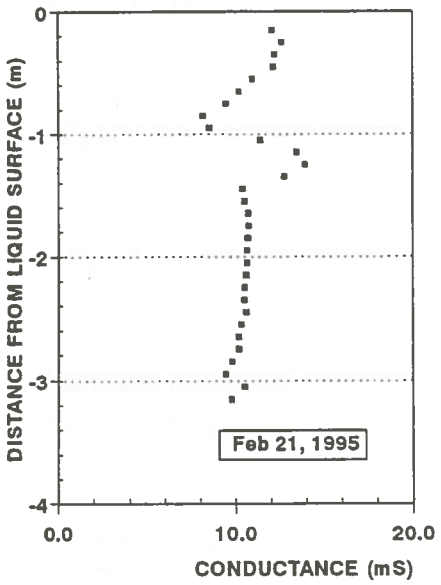

Fig.8 Conductance profile showing the pairing problem was overcome.

CONCLUSIONS

Remote communication has been instrumental in facilitating technology transfer between McGill and INCO Limited (Central Mills, Copper Cliff, Ontario). The problems arising during the commissioning and tune-up of a conductivity probe for measuring the mud line in thickeners were solved with minimum inconvenience to plant personnel. Cooperation between plant personnel and McGill researchers rapidly developed.

As a result, the installation and testing of the probe was considered highly successful. This success and the close cooperation developed led McGill and INCO to collaborate on further work in this area. Work is in progress to develop operating practices based on the information provided by the mud-line sensor. Remote communication is also playing an important role in this phase of the work.

The success of this experience is promoting within McGill the use of remote communication in the development of other sensors. Companies, specially those with operations spread across a large geographic area, can readily take advantage of this technology.

REFERENCES

Gomez, C.O., Uribe-Salas, A., Finch, J.A. and Huls, B.J., 1989.
A level detection probe for industrial flotation columns, in Processing of Complex Ores (eds., Dobby, G.S. and Rao, R.S.), Pergamon Press, pp 325-334.

Uribe-Salas, A., Leroux, M., Gomez, C.O., Finch J.A., and Huls, B.J., 1991.
A conductivity technique for level detection in flotation cells. Copper '91, Vol. II (eds., Dobby, G.S., Argyropoulos, S.A. and Rao, R.S.), Pergamon Press, pp. 261-275.

Uribe-Salas, A., Vermet F., and Finch, J.A., 1993.
Apparatus and technique to measure settling velocity and holdup of solids in water slurries. Chem. Engng Sci., 48, 4, pp. 815-819.

Xu, M., Probst, A. and Finch, J.A., 1994.
Level and solids profile detection in thickeners using conductivity, CIM Bulletin, 87, 985, pp. 46-52.

CAMI'95: 3rd Canadian Conference on Computer Applications in the Mineral Industry
Montréal, Québec, Canada, October 22-25, 1995

External Reflection Infrared Spectroscopy of Collector Monolayers on Mineral Surfaces: A Computer Simulation Approach

Zhenghe Xu
Department of Mining and Metallurgical Engineering
McGill University, Montreal, Quebec, H3A 2A7

ABSTRACT

A computer simulation approach is presented in this communication to enable a further understanding of external reflection spectroscopy as applied to mineral flotation. The simulation is based on modern optical theory using a planar stratified medium model. The spectra of cuprous ethyl xanthate on copper in the *ex situ* and *in situ* experimental arrangements are calculated. The experimental parameters and their uncertainty are examined using the simulation approach. The substrate effect on spectral features is elucidated using copper, copper sulphide and lead sulphide. Other potential applications of the approach are discussed.

RÉSUMÉ

Dans ce document, une simultation par ordinateur nous est présentée afin de mieux comprendre le principe de spectroscopie par réflexion extèrne lorsqu'appliqué à la flotation des minéraux. La simulation, basée sur la théorie optique moderne, utilise comme modèle un médium stratifié par plan.Le spectre des arrangements expérimentaux *ex situ* et *in situ* du éthyl xanthate cuivreux sur le cuivre sont calculés. Les paramètres expérimentaux ainsi que leur incertitude sont examinés utilisant cette simulation. L'effet de la couche adjacente à la surface sur les bandes spectrales est élucidé en utilisant du cuivre, du sulfide de cuivre et du sulfide de plomb. D'autres applications possible de cette approche y sont discutées.

INTRODUCTION

Selective collector adsorption on targeted minerals plays a crucial role in mineral separation using flotation. This has led to great interest in studying interactions between collectors and mineral surfaces and also in determining the amount of collector adsorbed on mineral surfaces. Infrared spectroscopy has found its way to this important practical application, especially following the development of Fourier transform infrared spectroscopy (FTIR). One of the advantages of using infrared compared with other surface analytical techniques is that the *in-situ* study in real time space can be conducted. As a result, the information obtained is more relevant to the practical problems commonly encountered in mineral processing.

The difficulty associated with the use of this versatile technique in flotation systems remains its sensitivity and the interpretation of the spectrum. A band shift is often observed when a collector is present as a metal ion precipitate (transmission spectrum) compared with that present on mineral surface. The relative intensity of the bands associated with a given collector-metal compound also varies with the substrate. This may be caused by optical effects, which makes the direct comparison between the standard spectrum obtained with bulk

precipitates and that from adsorbed or deposited collectors on mineral surfaces less straightforward. Therefore, a knowledge of the change of spectral features due to optical effects is required before relating the observed spectral variations to the changes in molecular structures and chemical bonding.

Computer simulation based on modern optics of electromagnetic wave propagation has shown great potential in isolating the optical effect from the structural changes in infrared spectra. This approach was previously used by Allara and Nuzzo (1985) in studying the orientation of organized molecular assemblies on oxidized aluminum surfaces. The calculation of the spectrum aided the determination of molecular orientation of species assembled on aluminum oxide surface. The approach was subsequently used by Dluhy (1986) who studied the quantitative difference between the external reflection infrared spectrum of an insoluble monolayer on water and metal substrates. He identified an optimal incident angle of 0-40° for the investigation of a monolayer on water rather than a grazing angle greater than 80° for the same monolayer on a metal substrate. It was also shown that the absorbance of monolayer on water is about 60% of the value for the same monolayer on metal substrate. Recently, Mielczarski (1993) applied the same approach to the study of collector monolayers on various substrates (including metallic, semiconductor and nonmetallic). By comparing the experimental spectrum with those calculated, he was able to distinguish the optical effect from those due to molecular orientation to account for the observed spectral differences. In addition, computer simulation provides a useful tool for optimizing the conditions of spectral acquisition, such as the incident angles.

In the present communication, computer simulation is used to show the effect of the substrate on the bands appearance of the spectrum. Furthermore, the effect of experimental uncertainty in spectrum acquisition on spectral features is illustrated. Finally, the angle dependence of spectral sensitivity in *in situ* and *ex situ* experiments is examined.

OPTICAL MODEL AND THEORY

External reflectance spectroscopy of adsorbed collector layer in the form of *ex situ* (Fig. 1a) or *in situ* (Fig. 1b) experiment can be simulated using a stacking multi-layer model. As shown in Fig. 1, incident infrared radiation beam is directed towards the surface at a given angle (ϕ), propagating through the stratified medium. Part of the energy is reflected after interacting with the medium. The reflectivity is defined as the ratio of the intensity of the electric field reflected from the surface (measured experimentally by the infrared detector) against that of the incident beam. To determine the absorbance (or reflectance) of infrared radiation by planar films, the intensity of the electric field of the reflected beam with respect to the incident beam needs to be known in the absence and presence (Fig. 1) of adsorbed collector. The relationships for such calculation have been thoroughly established from boundary layer solutions to Maxwell equations (Hansen, 1968; Allara and Nuzzo, 1985; Dluhy, 1986).

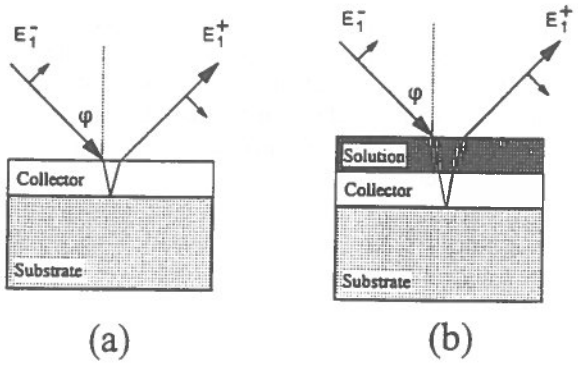

Fig. 1 Schematic illustration of interaction between infrared radiation and adsorbed collector as in *ex situ* (a) and *in situ* (b) experiments

For the systems considered in this communication (Fig. 1), the reflected electric field of a given polarization is related to the electric field of polarized incident beam by the Jones matrix M (Fowles, 1968; and Hansen, 1968), which is characteristic of the stratified medium.

$$\begin{bmatrix} E_1^- \\ H_1^- \end{bmatrix} = M \begin{bmatrix} E_{N-1}^+ \\ H_{N-1}^+ \end{bmatrix} \qquad [1]$$

where E and H are the magnitudes of tangential components of electrical and magnetic fields, respectively; the subscript identifies the phase boundary; and the superscripts - and + represent incident and reflected beams (Heavens, 1991). In the above equation,

$M = M_2 M_3 .. M_{N-1}$ where M_j is a 2 by 2 matrix whose elements are determined by the optical constants (n_j) and film thickness (d_j) of the j^{th} phase, and incident angle (ϕ). It should be noted that Eq. [1] is valid for planarly polarized radiation only. For a parallel polarized (p-polarization) incident beam (defined in Fig. 1) considered in this communication, the Jones matrix for phase j is given by:

$$M_j = \begin{bmatrix} \cos\beta_j & \frac{-i}{q_j}\sin\beta_j \\ -iq_j\sin\beta_j & \cos\beta_j \end{bmatrix} \qquad [2]$$

in which $q_j = \xi_j/n_j^2$ and $\beta_j = 2\pi(d_j/\lambda)\xi_j$, where λ is the wavelength of the incident infrared beam and $\xi_j = n_j\cos\phi_j = (n_j^2 - n_1^2\sin^2\phi)^{1/2}$. The matrix elements of each phase in a stratified medium can be readily calculated if the optical constants and film thickness are known.

The Fresnel reflection coefficient defined as E_1^+/E_1^- for the experimental set-up shown in Fig. 1 is given by:

$$r = \frac{(m_{11} + m_{12}q_N)q_1 - (m_{21} + m_{22}q_N)}{(m_{11} + m_{12}q_N)q_1 + (m_{21} + m_{22}q_N)} \qquad [3]$$

where m_{ij} is the elements of overall matrix M. The reflectance of the stratified medium is therefore given by the magnitude of the reflectance coefficient, i.e. $R = |E_1^+|^2/|E_1^-|^2 = |r|^2$. The absorbance as often used in spectral representation is then calculated using:

$$A = -\log(R/R_o) \qquad [4]$$

where R and R_o are the reflectance of the stratified medium in the presence and absence of adsorbed collector layers, respectively.

The theoretical infrared spectrum can be calculated with known optical constants for each of the phases of a stratified medium using Eqs. [2-4]. In the present communication, the optical constant of cuprous ethyl xanthate obtained by Mielczarski et al. (1992) was used. The optical constants for the substrates (copper, copper sulphide and lead sulphide) and water are taken from the Handbook of Optical Constants of Solids (Guizzetti and Borghesi, 1985; Lynch and Hunter, 1985; Querry Wieliczka, 1991). A curve fitting procedure was necessary in extrapolating the optical constants over the infrared region considered in this communication. The optical constants or the equations used in calculating optical constants of the materials are summarized in Table 1. An incident angle of 55° and copper substrate are used in all calculations, unless otherwise specified. The calculation is limited to parallel polarization only, but can be readily extended to perpendicular polarization.

Table 1. Summary of the optical constants or the equations for calculating optical constants used in spectral simulation (wavenumber ν is in cm^{-1})

Material	n	k
Cu	$35.024 - 3.17\times10^{-2}\nu + 8.173\times10^{-6}\nu^2$	$93.940 - 0.0562\nu + 1.135\times10^{-5}\nu^2$
CuS	6.27	0.19
PbS	$3.7848 + 2.3\times10^{-4}\nu$	$7.94\times10^{-2} - 1.204\times10^{-4}\nu + 4.750\times10^{-8}\nu^2$
H_2O	$-4.3 + 1.5\times10^{-2}\nu - 1.5\times10^{-5}\nu^2 + 6.6\times10^{-9}\nu^3 - 1.06\times10^{-12}\nu^4$	$16.3 - 5.5\times10^{-2}\nu + 6.9\times10^{-5}\nu^2 - 3.9\times10^{-8}\nu^3 - 8.1\times10^{-12}\nu^4$

RESULTS AND DISCUSSION

Simulation vs Measurement The calculated external reflection infrared spectrum for a 1 nm thick cuprous ethyl xanthate on copper surface is given in Fig. 2a. The spectrum shows five distinct bands at 1204, 1126, 1050, 1040 and 1010 cm^{-1}, respectively. These bands are assigned to the molecular stretching vibrations of C-O-C (1204 and 1126 cm^{-1}) and O-CS_2 (1050, 1040 and 1010

cm^{-1}) groups. An excellent match of the bands (including relative band intensity) is shown between simulated (Fig. 2a) and experimentally measured (Fig. 2b) spectra, confirming the computer simulation approach.

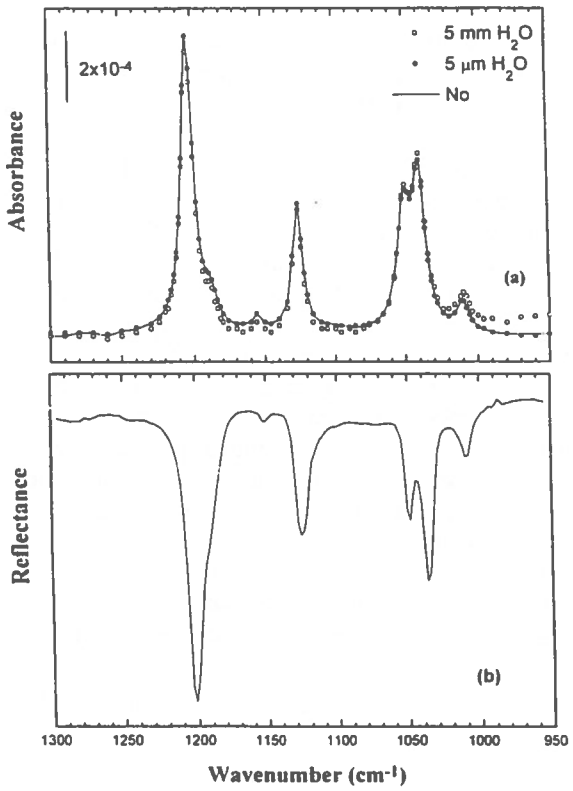

Fig. 2 External reflection infrared spectra of cuprous ethyl xanthate on copper surface obtained by simulation (a) and experiment (b). Spectrum in (b) was obtained using Bruker IFS-66 Fourier Transfer Infrared Spectrometer with SpectraTech baseline external reflectance accessory and Harrik wire polarizer.

Ex Situ vs *In Situ* Spectra: A criticism often made to *ex situ* surface characterization techniques is that the environment of the adsorbed collector is not preserved. As a result, the information derived from *ex situ* measurement is open to questioning. To obtain more relevant information requires the *in situ* characterization with which the conditions commonly encountered in processing practice are maintained and replicated during the course of the experiment. Infrared is one of the most commonly used *in situ* characterization methods. The principal difference between an *ex situ* and an *in situ* measurement is that a thin layer of liquid (often an aqueous solution containing reagents of interest) is present in the *in situ* measurement.

The *in situ* experiment can be readily simulated by including a layer of water on substrate (R_o) and adsorbed collector (R) (Fig. 1b) using the present approach. The infrared spectrum of cuprous xanthate on a copper substrate in the presence of a thin layer of water (5 μm to 5 mm) is calculated is also shown in Fig. 2a. It is interesting to note that the spectral features are essentially the same with or without liquid film being present. The absolute absorbance value varies slightly. This finding suggests that even in the presence of a 5 mm thick water layer, the acquisition of an *in situ* external reflectance infrared spectrum should not theoretically impose any experimental difficulty in the spectral range of interest here. However, if the spectrum is presented in reflectance instead of absorbance modes, it is clear that the presence of 5 μm water film decreased the calculated reflectance value significantly from 0.97 to 0.45 as shown in Figs. 3a and 3b, indicating that about 50% of input radiation energy is dissipated indiscriminately. This reduces the energy throughput of the infrared beam. As a result, a spectrometer with an intense infrared radiation source (large throughput) would be required to detect weak signal for good quality spectrum of adsorbed sub-monolayer collector as shown in Fig. 2a.

An additional advantage of using a computer to calculate the infrared spectrum is to provide the insight of spectral signals. As an example, the calculated reflection spectrum of a stratified medium with (solid line) and without (dotted line) an adsorbed collector layer is given in Fig 3a. This figure clearly shows that the variation in reflectance is marginal (0.2% at maximum). This finding suggests that a dedicated instrument with stable infrared radiation source, as well as a stable and sensitive detector has to be used to obtain high quality spectra. If a layer of an absorbing medium such as water is present, the contribution of the absorbance from adsorbed collector layer is even smaller as shown in Fig. 3b. However, a good quality instrument such as computer simulator will give the same quality spectrum as in the absence of the absorbing layer (symbols in Fig 2a).

Optimizing Operating Parameters: Another important application of computer simulation outlined in this communication is to optimize the instrumental parameters for spectral acquisition. As an example, the effect of incident angle on spectral signal of adsorbed species is simulated and the results are given in Figs. 4a (*ex situ*) and 4b (*in situ*). Fig. 5a shows that the band

intensity due to adsorbed cuprous xanthate increases with increasing incident angle. This finding suggests that to achieve high sensitivity, the use of greater incident angles approaching grazing angle is beneficial. It is worth mentioning, however, that with increasing incident angle, the energy throughput decreases. In order to obtain the improved sensitivity by increasing incident angle, good quality infrared instruments are necessary.

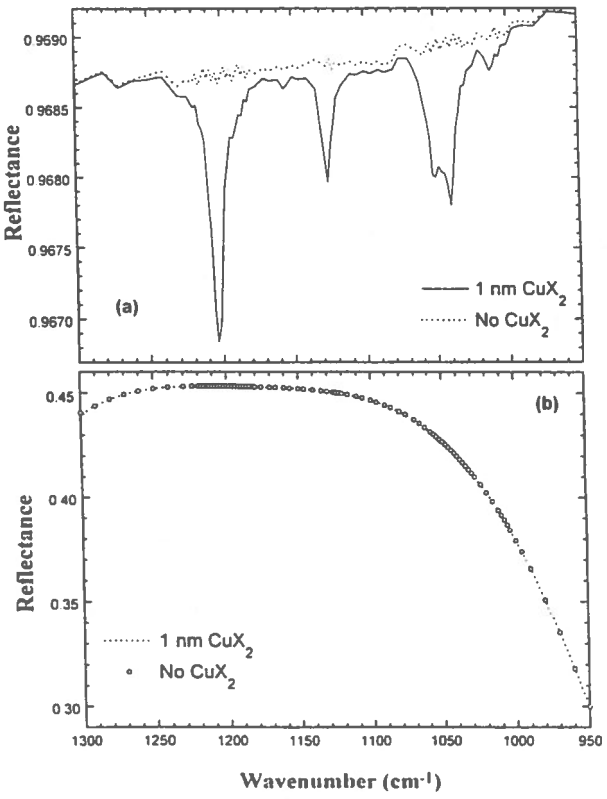

Fig. 3 Calculated reflectance of cuprous ethyl xanthate on copper surface as in *ex situ* (a) and *in situ* (b) experimental set-up: incident angle is 55°

In the *in situ* experiment (Fig. 4b), on the other hand, band signal increases initially with increasing incident angle up to 80°, after which a further increase in incident angle reduces the band intensity. This observation may be related to the penetration depth of infrared radiation into sample. It is likely that at the incident angle of 80°, the infrared radiation just penetrates deep enough to sample the whole thickness of the adsorbed collector layer. A further increase of incident angle beyond 80° would allow infrared radiation to interact effectively with only part of the adsorbed collector layer. It is therefore expected that the optimal incident angle depends on the thickness of water layer remaining on collector layer.

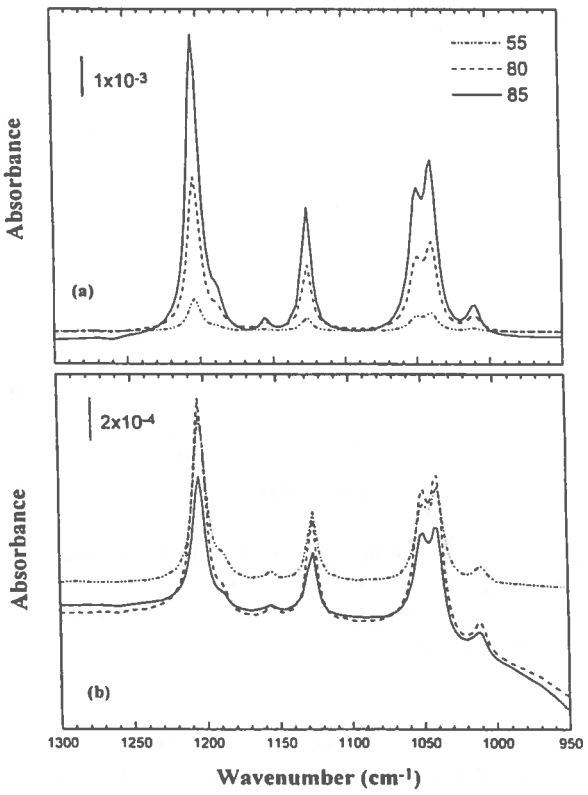

Fig. 4 Angle dependence of external reflection infrared spectrum of cuprous ethyl xanthate on copper surface as in *ex situ* (a) and *in situ* (b) experimental set-up.

Experimental Uncertainty: One of the difficulties encountered using *in situ* infrared spectroscopy is to maintain the constant thickness of liquid layer between background and sample spectral acquisition, since the variation in water film thickness will change the absorbance. The effect of variation in water layer thickness on the infrared spectrum was simulated and the calculated spectrum is shown in Fig. 5. In the calculation, the water layer thickness on adsorbed collector is fixed at 1 μm while those on substrate varies from 0.99 to 1.01 μm. As shown, the absolute value of absorbance varies significantly with water layer thickness, while the spectral features (i.e. band positions and relative intensity) are essentially the same. If proper baseline correction is applied to the spectrum, this experimental uncertainty can be eliminated in quantitative

analysis. It is worthwhile mentioning that the simulation also shows the linear relationship between the band intensity and the adsorbed layer thickness, confirming the feasibility of quantitative analysis using external reflectance infrared spectroscopy.

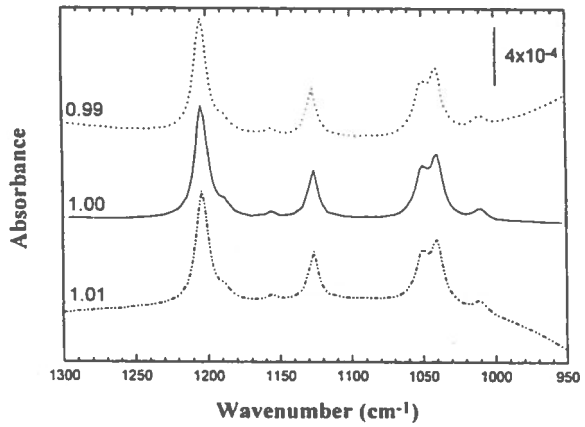

Fig. 5 Variations of *in situ* external reflection infrared spectrum of cuprous ethyl xanthate on copper surface with experimental uncertainty in water film thickness.

Another experimental uncertainty often encountered is the reproducibility of positioning the sample with respect to incident angle between background and sample spectral acquisitions. This uncertainty is also simulated, and the calculated spectra are given in Fig. 6. In this set of calculations, the incident angle when the collector layer was present was fixed at 55° while it varied by ±1° during background calculation. As shown in Fig. 6, variation in incident angle by ±1° caused significant variation in the absolute value of absorbance, but the spectral features remained the same. Only base line correction is required for quantitative analysis.

Substrate Effect: Finally, the effect of the substrate on the spectral shift can be readily studied with computer simulation. Fig. 7 shows the simulated spectra of cuprous ethyl xanthate on copper, copper sulphide and lead sulphide. As can be seen in this figure, substrate has significant impact on the spectrum of a given compound. When cuprous xanthate is deposited on copper sulphide, a negative absorption band at 1035 cm^{-1} appeared while other characteristic bands of cuprous xanthate remained. The negative band at a similar wavelength was experimentally observed (Mielczarski and Yoon, 1989).

When the calculation was carried out on lead sulphide (galena) substrate, three additional negative absorbance bands (at 1205, 1125 and 1040 cm^{-1}) appeared and two original bands (1185 and 1010 cm^{-1}) changed the sign and shift slightly in band positions. For the bands at 1050 and 1040 cm^{-1}, the relative intensity of the two bands changed for cuprous xanthate deposited either on copper or lead sulphide It is important not to assign these spectral variations to the changes in orientation of collector molecules or to the variations of binding environment between xanthate molecules and substrate. These spectral changes are due to optical effects.

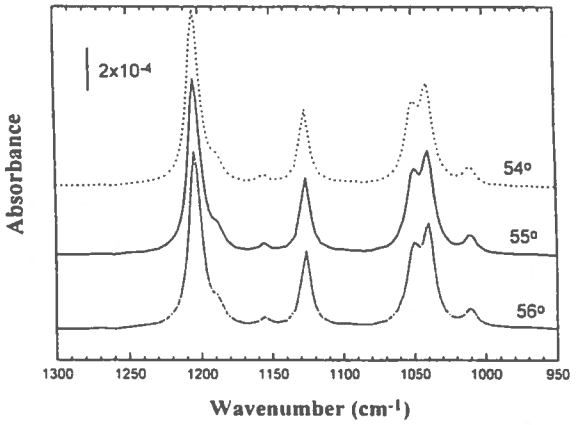

Fig. 6 Variation of *in situ* external reflection infrared spectrum of cuprous ethyl xanthate on copper surface with experimental uncertainty in incident angle.

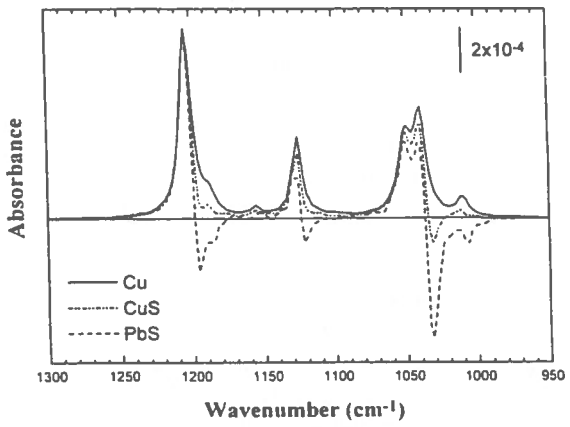

Fig. 7 Calculated external reflection infrared spectra of cuprous ethyl xanthate on copper, copper sulphide and lead sulphide surface.

Fig. 7 also shows that the relative intensity as well as the

absolute value of the intensity of absorbance bands change with substrate. The presence of a collector on highly reflective surfaces (e.g. copper) shows stronger absorbance bands, in particular at lower wavenumber. Therefore, in comparing the amount of xanthate adsorbed on various substrates using band intensity or area, the substrate effect has to be considered. The example given here clearly demonstrates the importance of computer simulation in spectral interpretation.

General Comments: It is worth mentioning that in the present communication, the simulation is restricted to the parallel polarized radiation. Comparison between experimental and theoretical spectra can be readily made by conducting the measurement with a polarized radiation source. In most experiments, however, non-polarized radiation is often used to obtain the maximum throughput of the instrument for characterizing the sub-monolayer collector. To transfer the absorbance of polarized radiation to a non-polarized case, a new formulation relating polarized absorbance (both parallel and perpendicular polarizations) to nonpolarized absorbance is required and this work is under development.

It was also assumed in the present communication that the adsorbed collector layer is uniformly distributed and isotropic with a layer thickness being the length of fully extended collector molecules (1 nm). In reality, the adsorbed collector may form domains and unlikely to be isotropic. The non-uniformity of adsorbed molecules can be readily simulated by including a surface coverage in the model. To simulate adsorbed collector layer of anisotropic nature, the optical constant and the sizes of head group and tails have to be known. This can be modelled by using small size molecules of the same functional group to simulate the head group and the alkane of the same length to simulate the tails. With these optical constants, the spectrum of collector molecules on various minerals can be readily calculated. The information on molecular orientation, the surface coverage or adsorbed layer thickness and nature of the binding between functional head group and solid surfaces can be derived readily.

Computer simulation can be very useful for studying adsorbed collector layers of more than one species. It has been found that the principal surface speciation of activated pyrrhotite by copper is dixanthogen rather than copper xanthate. It may well be possible that the copper xanthate is "buried" underneath the dixanthogen. This can be confirmed by simulating the spectrum of stratified medium incorporating a layer of varying thickness dixanthogen on copper xanthate.

SUMMARY

The present communication clearly demonstrates the application of computer simulation in understanding the spectral changes of a given collector in mineral flotation systems and in optimizing the instrumental and spectral acquisition parameters. Based on the simulations conducted in this communication, the optical properties of substrate have significant effect on spectral features. The optical effects can be readily eliminated in spectral interpretation to enable molecular orientation as well as the binding environment of adsorbed collectors to be elucidated. The optimal experimental conditions have been found to be system dependent. An incident angle of greater than 85° would be beneficial for *ex situ* experimental set-up, while an angle of about 80° should be used for the optimal sensitivity in *in situ* experiments.

ACKNOWLEDGEMENT

The author wishes to thank Professor J.A. Finch for stimulating the writing up of this communication. The constructive discussions with Professor M. Andrews and Dr. S. Brienne are greatly acknowledged. Thanks are also due to Mr. V. Bozkurt for his experimental contributions (Fig. 2b). This work was partially supported by Formation de Chercheurs et l'Aide á la Recherche (FCAR): Établissement de Nouveaux Chercheurs program.

REFERENCES

Allara, D.L. and Nuzzo, R.G., 1985
Spontaneously organized molecular assemblies: 1. Formation, dynamics and physical properties of n-alkanoic acids adsorbed from solution on an oxidized aluminum surface. *Langmuir*, Vol. 1, pp. 52-66

Dluhy, R.A., 1986
Quantitative external reflection infrared spectroscopic analysis of insoluble monolayers spread at the air-water interface. *J. Phys. Chem.*, Vol. 90, pp. 1373-1379

Fowles, G.R., 1968
Introduction to modern optics (2nd edition), Dover Publications, Inc., New York

Guizzetti, G. and Borghesi, A., 1985
Lead sulfide (PbS). In *Handbook of optical constants of solids* (ed. by Palik, E.D.), Academic Press, Inc., New York, pp. 525-533

Hansen, W.N., 1968
Electric Fields produced by the propagation of plane coherent electromagnetic radiation in a stratified medium. *J. Opt. Soc. Am.*, Vol. 58, pp. 380-390

Heavens, O.S., 1991
Optical properties of thin solid films, Dover Publications, Inc., New York

Lynch, D.W. and Hunter, W.R., 1985
Optical constants of metals. In *Handbook of optical constants of solids* (ed. by Palik, E.D.), Academic Press, Inc., New York, pp. 280-289

Mielczarski, J.A., 1993
External reflection infrared spectroscopy at metallic, semiconductor, and nonmetallic substrates: 1. Monolayer films. *J. Phys. Chem.*, Vol. 97, pp. 2649-2663

Mielczarski, J.A., Milosevic, M. and Berets, S.L., 1992
Optical properties of strongly absorbing media determined by external reflection spectroscopy. *Applied Spectroscopy*, Vol. 46, pp. 1040-1044

Mielczarski, J.A. and Yoon, R.H., 1989
Orientation of thiol collectors on chalcocite. In *Processing of complex ores* (ed. by Dobby, G.S. and Rao, S.R.), Pergamon Press, New York, pp.29-40

Querry, M.R. and Wieliczka, D.M., 1991
Water (H_2O). In *Handbook of optical constants of solids II* (ed. by Palik, E.D.), Academic Press, Inc., New York, pp. 1059-1077

CAMI'95: 3rd Canadian Conference on Computer Applications in the Mineral Industry
Montréal, Québec, Canada, October 22-25, 1995

Surface Complexation Modelling

Q. Zhang, Z. Xu and J. A. Finch
McGill University, Montreal, Quebec

ABSTRACT

Chemical modelling of the mineral/water interface is a major step towards modelling and controlling flotation chemistry. A new computational procedure is described which is both simple and robust. Results on the sphalerite-Fe ion-water system illustrate the procedure.

RÉSUMÉ

La modèlisation chimique de l'interface minéral/eau est une étape majeure vers la modèlisation et le contrôle de la chimie de flotatio". Une nouvelle méthode informatisée de alcul á la fois simple et robuste est décrite. Les résultats sur le système sphalerite-Fe ion-eau, illustre celle-ci.

INTRODUCTION

In recent years there has been a remarkable increase in the number of studies devoted to chemical modelling of the interfacial region between a mineral solid and an aqueous solution. In large measure, these studies have led to quantitative models of both cation and anion adsorption phenomena by exploiting the fertile combination of concepts from co-ordination chemistry and the theory of the electrical double layer. The quantitative success of this approach, which is collectively termed the *surface complexation model*, has been amply documented in a series of recent reviews. A general weakness, however, is that several different surface complexation models can represent the same set of adsorption data equally well, with the corresponding chemical parameters taking on quite different values (Sale et al., 1988 and Linthurst et al., 1986).

An examination of the literature reveals that most of the surface complexation models pay in-sufficient attention to the relationship with chemical thermodynamics and statistical mechanics. For example, what are the Standard States on which the various equilibrium constants introduced in the models are based are often not mentioned, and the same applies to the relationship between the conditional equilibrium constants in the models and conventional thermodynamic activity coefficients. Perhaps more serious is the fact that a clear distinction has not been made between the thermodynamic and the statistical mechanical aspects of the models, with the result that their common, macroscopic (and, therefore, model-independent) features have not been exposed clearly, and their strictly molecular features have been mistakenly accorded thermodynamic significance (Van and Storey, 1990). These kinds of difficulties can contribute to confusion in any attempt to evaluate the models on the basis of their chemical foundations, especially when their quantitative successes are parallel.

Although these models may be expressed with similar mass law and material balance equations, they involve different descriptions of the electrical double layer. In this paper we discuss a general method for the mathematical formulation of these models, which will allow us to compare in a systematic way not only the physical picture which the models represent but also the performance of the models in reproducing experimental data. The objective of this paper is to create a new computational package for surface complexation modelling which is simple and mathematically stable, and to extend the established modelling for oxide/water systems to sulphide/water systems. The models lie at the heart of modelling flotation chemistry.

METHODS

Triple Layer Model. The conceptual model of surface complexation reactions developed Davis et al. (1978) partitioned the electrical double layer into two constant-capacitance layers and an outer diffuse layer. The 0 plane of a solid, containing only potential determining ions, is characterized by a charge density, σ_0, and potential, ψ_0. Charged surface sites at the innermost plane lead to specific ion adsorption in the second (β) plane with characteristic charge and potential σ_β and ψ_β, respectively. In addition, adsorption of the supporting electrolyte occurs in the β-plane.

For sulphide minerals, e.g. sphalerite, the acid/base properties are described as follows:

$$|SZn + 2\,H^+ = |SH_2 + Zn^{2+} \quad (1)$$

$$|SZn + H_2O = |SZnOH^- + H^+ \quad (2)$$

$$|ZnS + H^+ = |ZnSH^+ \quad (3)$$

where | denotes a structural metal ion of the mineral surface; and, $|ZnSH^+$, $|SH_2$ and $|SZnOH^-$ are the protonated, neutral and deprotonated surface species, respectively. The concentration of protons within the electrical double layer is related to the bulk aqueous proton concentration by the Boltzmann distribution. The resulting mass action expressions for eqs 1 and 2 in terms of aqueous activity of the hydrogen ion become

$$K_1 = \frac{[|SH_2][Zn^{2+}]_s}{[|SZn][H^+]_s^2} = \frac{[|SH_2][Zn^{2+}]}{[|SZn][H^+]^2} \quad (4)$$

where $[Zn^{2+}]_s = [Zn^{2+}]\exp(-2e\psi_0/kT)$

and $[H^+]_s = [H^+]\exp(-e\psi_0/kT)$

$$K_2 = \frac{[|SZnOH^-][H^+]_s}{[|SZn][H_2O]} = \frac{[|SZnOH^-][H^+]}{[|SZn]}\exp(-e\psi_0/kT) \quad (5)$$

$$K_3 = \frac{[|ZnSH^+]}{[|ZnS][H^+]_s} = \frac{[|ZnSH^+]}{[|ZnS][H^+]}\exp(e\psi_0/kT) \quad (6)$$

The formation of surface complexes readjusts the equilibrium and affects the proton balance. The surface charge defined from the proton balance, s_0, represents the net number of protons released or consumed by all surface reactions including ion-binding reactions as well as ionization of the surface to form the surface species. Those surface species are distributed among the total number of sites available.

The computer program uses a powerful mathematical package MATLAB as the basis for solving the set of equations. The complete set includes the site-binding model describing the electrical double layer at the solid-aqueous solution interface. (A detailed description is given in elsewhere (Zhang, Xu and Finch, 1995). Broyden-Fletcher-Goldfarb-Shanno (BFGS), an updated quasi-Newton algorithm with a mixed quadratic and cubic line search procedure (Bazaraa, Sherali and Shetty, 1993), was used to solve the four matrices: the concentration matrix, physical constant matrix, equilibrium constant matrix, and local charge variable matrix.

The calculation begins with the reading of the experimental data and some physical constants. The initial values of the variables, and the program

termination options are given before the running of the main program. The program will accept data from any number of experiments for a given system and the constants are then adjusted to fit all points simultaneously. For each experiment the initial conditions are read in, followed by the zeta potential values. The computer then combines the data for individual experiments and subsequently the data for all experiments are treated together, Finally, the computer trains itself to find the solution according to the termination option .

After reading the data and carrying out preliminary calculations, the computer begins to determine for each experimental point the residuals and differential terms required for the solution of the least-squares equations. Initial estimates are first required for each free metal ion and surface species concentration. These approximations are then improved iteratively according to the BFGS subroutine until they are satisfactory roots to the simultaneous equations for total metal ions, surface species concentrations, and zeta potentials. The equilibrium constants obtained in this manner are used to calculate the concentration of other species and the double layer parameters for each experimental point. Progressing through each experimental point, the lease-squares equations are built-up, and are solved by matrix inversion to yield new estimates of the constant. together with the estimated standard deviation. This cycle is repeated until the defined termination option is met. On completion, a table is printed showing, for each experimental point, the pH, the zeta potential, the surface charge density, the residual, and the total concentrations of each metal ion and species.

A number of additional features aid the running of the program. If the increment specified in the input data for use in the numerical differentiation was too small, it is successively increased until the differential term becomes significant. The term is then calculated, and the increment is returned to its input value. In the case of non-convergence in subroutine BFGS, the residual for the relevant point is set at zero and the calculation is continued. If this occurs more times than the option value set at the beginning, the calculation is

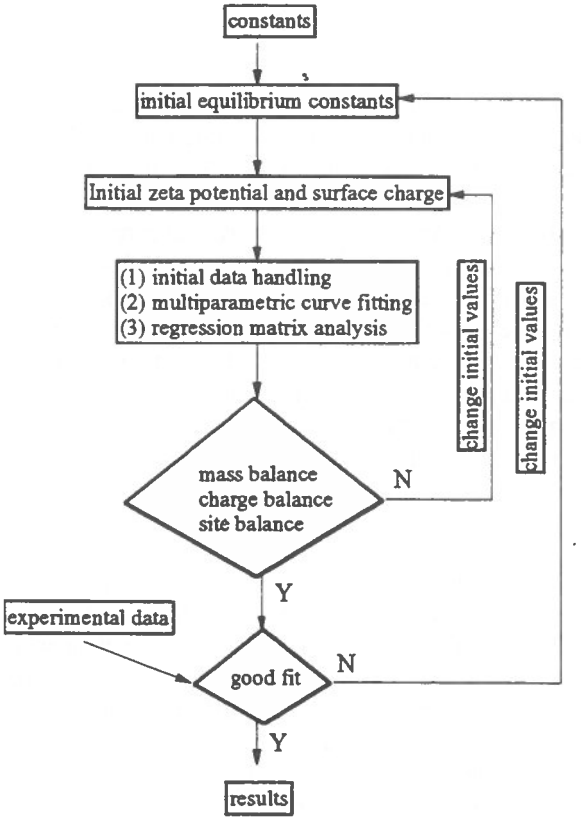

Figure 1. Strategy of the fitting routine

abandoned and the computer proceeds to the next set of data.

When the adjustments to the constants have been calculated, the computer checks them and reduces any which are excessively large (2 times value). Also a check is made that the sum of the squares of the residuals is in fact less after adjustment of the constants than at the start of the cycle. If this is not so then the adjustments have been too large and they are divided by 2 and applied again.

The strategy of the fitting is shown in Figure 1. The whole program is listed elsewhere (Zhang, 1994). It could be used for a system of any number of metal ions and surface species.

A notable improvement in the surface species calculations over the usual approach (MINEQL developed by Westall etc al. (1992), modified and used by most researchers (Sun, 1991, Wood, et al., 1990) is that only *one* set of experimental results (i.e., zeta potential) is required to solve the whole set of equations describing the solid-aqueous system. By simultaneously fitting the experimental data over the whole experimental range, the characteristics of the zeta potential, surface charge density, and species distribution both on the solid surface and in solution, can be derived (Zhang, Xu and Finch, 1995).

Another advantage of our computational approach is that all calculations are performed as the matrices. It is much easier to form the equation sets here than with the other fitting programs. Only two matrics (the initial value matrix, and the variable matrix) need to be changed for all the different conditions and environments. Consequently, this program can be easily expanded to very complex multiphase equilibria.

The use of BFGS guarantees finding the global minimum point rather than any local minima. This computing method can handle ill-conditioned real-number problems. This simplifies Park's procedure (1976) which manipulates the stoichiometry of the reactions to transfer ill-conditioned numerical problems of equation solving into well-conditioned forms. The concept behind Park's approach is based on electrical network theory applied to chemical reactions. The computational approach used in BFGS manipulates the initial values to make sure the values are well-conditioned before putting them into the calculations and checks the values whenever a new step is completed. Our approach reduces the need for manual intervention with the experimental data and simplifies the preparation for the computing procedure.

TABLE 1. Best-Fit parameters for the surface-charge and zeta potential calculation of sphalerite using the computational method with MATLAB software (Zhang, et al., 1995)

Electrolyte conc. (M)	pK_1	pK_2	pK_3	pK_4	pK_5	pK_6	C_1 (F/m^2)
0.1	-1.45	4.53	-1.16	-3.25	-3.51	-3.05	0.7
0.01	-1.45	4.52	-1.15	-3.24	-3.49	-3.05	0.68
0.001	-1.43	4.5	-1.13	-3.23	-3.49	-3.05	0.68
0.0001	-1.43	4.51	-1.14	-3.22	-3.48	-3.06	0.67
0.000001	-1.44	4.5	-1.13	-3.24	-3.48	-3.05	0.66

The program was successful in fitting zeta potential of sphalerite alone and sphalerite in the presence of ferrous ions under different conditions. The results are summarized in Tables 1 and 2. From the results it is clear that the surface equilibrium constants obtained with this computing approach agree for all the conditions.

TABLE 2. Best-Fit parameters for the surface-charge and zeta potential calculation of sphalerite treated with ferrous ions using the computational method with MATLAB software (Zhang, et al., 1995)

pK_1	pK_2	pK_3	pK_4	pK_5
-1.4	4.523	-1.15	-3.252	-3.489
pK_6	pK_7	pK_8	pK_9	C_1 (F/m^2)
-3.049	-3.269	-3.401	-0.54	0.65

CONCLUSIONS

A new computational procedure, based on MATLAB, is described for solving the set of equation describing the chemical equlibria at the mineral/water interface. The success was illustrated using data for the sphalerite-Fe ion-water system.

ACKNOWLEDGEMENTS

The authors gratefully acknowledge financial support from the Mining Industry Technology Council of Canada (representing in the project: INCO, Falconbridge, Cominco, Noranda, Teck and Hudson Bay Mining & Smelting) and the Natural Sciences and Engineering Research Council of Canada under the Research Partnerships Program.

REFERENCES

Baxaraa M.S., Sherali H.D. and Shetty C.M., 1993, Nonlinear programming: Theory and algorithms, Second edition, Charity Robey (Editor), John Wiley & Sons Inc.

Davis J., James R.O. and Leckie J.O., 1978a, Surface ionization and complexation at the oxide/water interafce I. Computation of electrical double layer properties in simple electrolytes, J. Colloid Interface Sci., Vol. 63, No. 3, .480-499.

Davis J. and Leckie J.O., 1978b, Surface ionization and complexation at the oxide/water interface II. Surface properties of amorphous iron oxyhydroxide and adsorption of metal ions, J. Colloid Interface Sci., Vol. 67, No. 1, p.90-107.

Linthurst R. A., Landers D.H., Eilers J.M., Brakke D.E., Overton W.S., Merier E.P. and Crowe R., 1986, Characteristics of lakes in the eastern United States. Volume 1: Population descriptions and physico-chemical relationships (EPA/660/4-86/007a). Washington, D.C.: U.S. Environmental Protection Agency.

Park D.J.M., 1976, J. Chem. Phys., Vol. 65, p3085.

Sale M.J., Kaufmann P.R., Jager H.I., Coe J.M., Cougan K.A., Kinney A.J., Mitch M.E., and Overton W.S. (1988), Chemical characteristics of streams in the mid-atlantic and southeastern United States. Volume II: Streams samples, descriptive statistics and compendium of physical and chemical data (EPA/600/3-88/021b). Washington, D.C.: U.S. Environmental Protection Agency.

Schecher W.D., 1992, Mineql+: A software environment for chemical equilibrium modeling, Comput. Environ. and Urban Systems, Vol. 16, p.65-76.

Sun Z, 1991, Surface reactions in aqueous and metal sulfide systems, Ph. D. thesis, Division of Inorganic Chemistry, Luleå University of Technology, Luleå, Sweden.

Van Zeggeren F. and Storey S.H., 1990, The computation equilibrium of chemical equilibria. London: Cambridge University Press.

Wood R., Fornasiero D. and Ralston J., 1990, Electrochemistry of the boehmite-water interface, Colloid and Surface, Vol. 51, p389-403.

Zhang Q, 1994, Sphalerite Activation in the Presence of Iron ions, Ph. D. thesis. McGill Unviersity, Canada.

Zhang Q., Xu Z. and Finch J.A., 1995, Surface Ionization and Complexation at the Sphalerite/water Inerface I. Computation of Electrical Double-Layer Properties of Sphalerite in Simple Electrolyte. J. Colloid and Interface Sci., Vol. 169, p414-421.

Zhang Q., Xu Z. and Finch J.A., 1995, Surface Ionization and Complexation at the Sphalerite/water Inerface II. Computation of Electrical Double-Layer Properties of Sphalerite in the Presence of Ferrous Ions., accepted by J. Collloid and Interface Sci..

CAMI'95: 3rd Canadian Conference on Computer Applications in the Mineral Industry
Montréal, Québec, Canada, October 22-25, 1995

Multivariable Receding Horizon Predictive Control of a Grinding Circuit with Constraints and Maximisation of Ore Throughput

Richard Lestage, André Pomerleau and
Daniel Hodouin.

Groupe de Recherche sur les Applications de l'Informatique à l'Industrie Minérale (GRAIIM),
Département de Mines et Métallurgie, Université Laval, Sainte-Foy, Québec, Canada, G1K 7P4

ABSTRACT:

The objective of this study is to develop and apply a quadratic controller that regulates some output variables while maximising or minimizing some other variables. The added objective of optimizing manipulated variables brings the process to its constraints. If the variable is related to a cost (like the energy consumption), it is advantageous to minimise its value. Similarly, if it is related to a product quantity, it is advantageous to maximise its value. A particular attention is devoted to the steady state value of the process when constraints are active. This technique is applied to a simulated grinding process where particle size distribution is regulated while the ore throughput is maximised.

RÉSUMÉ:

Le but de cet article est d'illustrer comment, en présence de contraintes, il est possible de modifier les objectifs traditionnels de la commande prédictive de façon à pouvoir maximiser certaines variables. Les objectifs complémentaires sont alors de maximiser ou de minimiser les variables manipulées de façon à amener le procédé à la limite de ses contraintes. Si la variable manipulée est associée à un coût, il est avantageux de minimiser sa valeur. Si au contraire, elle est associée à une quantité de production, il est profitable de maximiser cette valeur. Une attention particulière est portée à la solution en régime permanent lorsque certaines contraintes sont actives. La technique est appliquée à un simulateur de procédé de broyage sur lequel une régulation de la granulométrie est effectuée tout en maximisant le débit de minerai.

INTRODUCTION

The main advantage of receding horizon predictive controllers is their ability to handle hard constraints on the manipulated variables and the outputs. Output constraints may be associated or not to setpoints. Auxiliary outputs without setpoints must rest within a safety range limited by a upper and lower bound. Exemples of predictives controllers are the GPC (Clarke *et al.* 1987), the DMC (Cutler and Ramaker 1980) and the MPC (Richalet *et al.* 1978). Here an internal model controller with a state-space model representation is used.

Gauthier and Bornard have published in 1977 an article about constrained predictive control but it was only in the late '80 that this technique emerged with industrial applications of the DMC controller by Cutler (Cutler and Ramaker 1987, Van Hood *et al.* 1989). These applications were very interesting since in addition to the respect of setpoints, some variables related to the cost were minimized while ones related to performance were maximised until constraints were reached. Few informations were available about the implementation tools. However, in more fundamental study, the constrained multivariable GPC give details about the mathematical form of the control law and the implementation (Wilkinson *et al.* 1990, Wilkinson *et al.* 1991, Mutha and Shah 1991, Dion *et al.* 1991 and Camacho 1993). These publications however never made references to the strategy used by Cutler to maximize or minimize variables in order to bring the

process to its constraints limits. Only Dion discussed a method to minimize control energy when some freedom is available on manipulated variables.

The first part of this article explains the internal model receding horizon controller with maximization of manipulated variables. The steady state behaviour of the process is studied with and without maximization. For comparison, the two strategies are then applied to a grinding circuit process.

I. INTERNAL MODEL RECEDING HORIZON CONTROLLER WITH MAXIMIZATION

The usual control objectives of an internal model receding horizon controller is to minimize over the horizon the quadratic sum of the setpoints deviation while minimizing the quadratic sum of variations of the actions. This calculus is made on the predicted trajectory of the process model over the dictated horizon. The control horizon NU may be different from the prediction horizon NY. It is assumed that after NU, the manipulated variables are held constant. Diagonal matrices Q and R weight the relative cost of setpoint deviations and input variations.

In order to optimize the performance of the process operation, a supervisory controller usually calculates setpoints. This calculation is often based on a linear steady-state optimization. The innovative part of this study is the introduction of the T matrix which weights the amplitude of the manipulated variables. This permits to solve simultaneously the quadratic control and the linear optimization problems. By minimizing actions cost (T positive) or maximizing process feed (T negative), the process is then driven to a point where a constraint is reached. The criterion to minimize is the following:

$$J_i = \sum_{k=i-1}^{i+NY} [\underline{y_d}(k)-\underline{y_m}(k)]^T \cdot Q \cdot [\underline{y_d}(k)-\underline{y_m}(k)] + \sum_{k=i-1}^{i+NU} [\underline{u}(k-1)-\underline{u}(k-2)]^T \cdot R \cdot [\underline{u}(k-1)-\underline{u}(k-2)] + 2 \cdot \sum_{k=i-1}^{i+NU} T \cdot \underline{u}(k-1) \quad (1)$$

The constant two before the third term is arbitrary and will be simplified later.

Diagonal matrices Q and R permit to have a pseudo dynamic decoupling of the controlled process and weight the relative cost of deviations of setpoint and input variations. The R matrix is used to make a compromise between the dynamic response speed and the robustness of the controller. It also fixes the relative amplitude of the manipulated variable variation. . When all setpoints cannot be reached, the Q matrix determines the relative steady-state errors between outputs. During the transient response, the combined effect of T and R causes constant rise of the manipulated variables until constraints are reached. On steady-state, a compromise is made between the maximization caused by T and the setpoints errors minimized by the Q matrix. This compromise will create deviations to setpoints in order to provide an increased manipulated variable. The setpoint errors can be as small as wished by using a small value for T but will cause a slower maximization. To prevent a slow maximization, one can also use smaller R but the robustness of the controller will be reduced. A compromise has to be made between robustness, setpoint dynamics, setpoint errors and manipulated variable maximization speed.

Modifications to the criterion in order to maximize or minimize outputs variables are also possible but are not treated in this article.

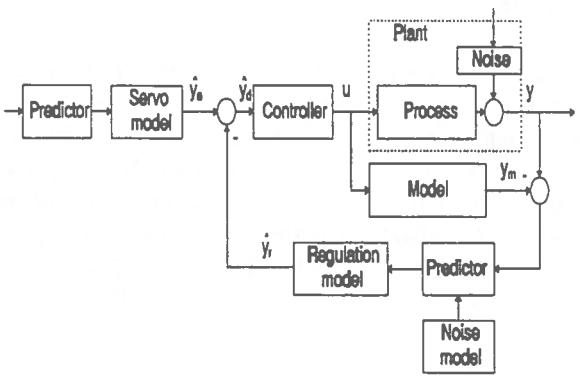

Figure 1: Internal model controller structure.

Figure 1 shows the diagram of the system. The prediction of the process output comes from the sum of a deterministic part $\hat{\underline{y}}_m$ and a stochastic part. The deterministic part is predicted from a discrete state-space model. The stochastic part is estimated by a predictor from the difference between the real process and the model. The stochastic part takes into account perturbation and modelisation errors. A second predictor estimates the future value of the setpoint. A servo reference model gives the desired trajectory in tracking $\hat{\underline{y}}_s$ and a regulation reference model gives the trajectory in regulation $\hat{\underline{y}}_r$. The future desired trajectory $\hat{\underline{y}}_d$ for the process model is calculated from the diffence between the two predictions.

II. VECTORIAL FORM OF THE CONTROLLER

Knowing the actual state vector $x_m(i)$ of the the process model and expressing the predicted outputs $\hat{y}_m(i)$ and the optimal inputs $\hat{u}(i)$ in a vector form, one has

$$\underline{\hat{y}_m}(i) = \begin{bmatrix} \underline{y_m}(i+1) \\ \underline{y_m}(i+2) \\ \cdots \\ \underline{y_m}(i+NY) \end{bmatrix} \qquad \underline{\hat{u}}(i) = \begin{bmatrix} \underline{u}(i+1) \\ \underline{u}(i+2) \\ \cdots \\ \underline{u}(i+NU) \end{bmatrix} \tag{2}$$

$$\underline{\hat{y}_m}(i) = \Gamma \cdot \underline{x_m}(i) + \Psi \cdot \underline{\hat{u}}(i) \tag{3}$$

where

$$\Gamma = \begin{bmatrix} C \cdot A \\ C \cdot A^2 \\ \cdots \\ C \cdot A^{NY} \end{bmatrix} \tag{4a}$$

$$\Psi = \begin{bmatrix} C \cdot B & 0 & \cdots & 0 \\ C \cdot A \cdot B & C \cdot B & \cdots & 0 \\ \cdots & \cdots & \cdots & \cdots \\ C \cdot A^{NU} \cdot B & C \cdot A^{NU-1} \cdot B & \cdots & C \cdot B \\ C \cdot A^{NU-1} \cdot B & C \cdot A^{NU} \cdot B & \cdots & C \cdot B + C \cdot A \cdot B \\ \cdots & \cdots & \cdots & \cdots \\ C \cdot A^{NY} \cdot B & C \cdot A^{NY-1} \cdot B & \cdots & \sum_{i=0}^{NY-NU} C \cdot A^i \cdot B \end{bmatrix} \tag{4b}$$

The matrices A, B and C represent the state space process model.

By substitution of equation (3) into (1), the criterion that has to be minimized is given by (Foulard *et al.* 1987):

$$J(i) = \underline{\hat{u}}(i)^T \cdot FU \cdot \underline{\hat{u}}(i) + 2 \cdot \underline{\hat{u}}(i) \cdot FO(i) + cte \tag{5}$$

where

$$FO(i) = FOX \cdot \underline{x_m}(i) - FOYD \cdot \underline{y_d}(i) - FOU \cdot \underline{u}(i-1)) + FOT$$

and

$$FU = \Psi^T \cdot \hat{Q} \cdot \Psi + \hat{R}$$

$$FOX = \Psi^T \cdot \hat{Q} \cdot \Gamma \qquad FOU = \begin{bmatrix} R \\ 0 \\ \cdots \\ 0 \end{bmatrix} \quad (r \cdot NU \times NU) \tag{6}$$

$$FOYD = \Psi^T \cdot \hat{Q}$$

$$FOT = \begin{bmatrix} T & T & \cdots & T \end{bmatrix} \quad (1 \times r \cdot NU)$$

$$\hat{Q} = \begin{bmatrix} Q & & & \\ & Q & & \\ & & \ddots & \\ & & & Q \end{bmatrix} \qquad \hat{R} = \begin{bmatrix} 2R & -R & \cdots & 0 \\ -R & 2R & \cdots & 0 \\ 0 & \cdots & 2R & R \\ 0 & \cdots & -R & R \end{bmatrix} \tag{7}$$

$(m \cdot NY \times m \cdot NY)$ $\qquad$ $(r \cdot NU \times r \cdot NU)$

r and m are respectively the number of inputs and the number of outputs of the system.

The optimal solution is obtain by finding the actions vector $\underline{\hat{u}}(i)$ which minimizes equation (5) with respect to the constraints.

III. CONSTRAINTS FORMULATION

Constraints are defined here as the maximum bounds of the outputs, inputs and of the variation of the inputs. Constraints on outputs variations may also exist.

The general expression for the contraints is

$$G \cdot \underline{\hat{u}}(i) \leq \underline{h} \tag{8}$$

Where the matrix G and the vector $\underline{h}$ corresponds to the desired constraints.

A. Constraints on the amplitude of the manipulated variables.

The minimum and maximum values of the inputs at time i are chosen as:

$$\underline{\alpha_u}(i) \leq \underline{u}(i) \leq \underline{\beta_u}(i) \tag{9}$$

Extremum values for the complete horizon can be defined by vectors:

$$\underline{\hat{\alpha}_u}(i) \leq \underline{\hat{u}}(i) \leq \underline{\hat{\beta}_u}(i) \tag{10}$$

where

$$\underline{\hat{\alpha}_u}(i) = \begin{bmatrix} \underline{\alpha_u}(i) \\ \underline{\alpha_u}(i+1) \\ \cdots \\ \underline{\alpha_u}(i+NU) \end{bmatrix} \quad \underline{\hat{\beta}_u}(i) = \begin{bmatrix} \underline{\beta_u}(i) \\ \underline{\beta_u}(i+1) \\ \cdots \\ \underline{\beta_u}(i+NU) \end{bmatrix} \tag{11}$$

Inputs constraints can then be written in a form compatible with equation (8):

$$\begin{bmatrix} -I_{r\cdot NU} \\ I_{r\cdot NU} \end{bmatrix} \cdot \underline{\hat{u}}(i) \le \begin{bmatrix} -\underline{\hat{\alpha}_u}(i) \\ \underline{\hat{\beta}_u}(i) \end{bmatrix} \tag{12}$$

where $I_{r,NU}$ is the unitary matrix of size $r \cdot NU$ and r is the number of inputs of the process. One then has:

$$G_u = \begin{bmatrix} -I_{r\cdot NU} \\ I_{r\cdot NU} \end{bmatrix} \qquad \underline{h_u} = \begin{bmatrix} -\underline{\hat{\alpha}_u}(i) \\ \underline{\hat{\beta}_u}(i) \end{bmatrix} \tag{13}$$

B. Constraints on the variation of the manipulated variables.

The maximum values of the variations of the inputs at the time i are defined as:

$$| \underline{u}(i) - \underline{u}(i-1) | \le \underline{\Delta_u}(i) \tag{14}$$

In a form compatible with Equation (8), constraints are given by:

$$G_{\Delta u} = \begin{bmatrix} I_r & 0 & \cdots & 0 & 0 \\ -I_r & I_r & \cdots & 0 & 0 \\ \cdots & \cdots & \cdots & \cdots & \cdots \\ 0 & 0 & \cdots & -I_r & I_r \\ -I_r & 0 & \cdots & 0 & 0 \\ I_r & -I_r & \cdots & 0 & 0 \\ \cdots & \cdots & \cdots & \cdots & \cdots \\ 0 & 0 & \cdots & I_r & -I_r \end{bmatrix} \quad \underline{h_{\Delta u}}(i) = \begin{bmatrix} \underline{u}(i-1)+\underline{\Delta_u}(i) \\ \underline{\Delta_u}(i+1) \\ \cdots \\ \underline{\Delta_u}(i+NU) \\ -\underline{u}(i-1)+\underline{\Delta_u}(i) \\ \underline{\Delta_u}(i+1) \\ \cdots \\ \underline{\Delta_u}(i+NU) \end{bmatrix} \tag{15}$$

where I_r is the unitary matrix of size r, and r the number of input variables.

C. Constraints on the process outputs.

The outputs of the process are predicted by equation (3). If their extremum values at time i are:

$$\underline{\alpha_y}(i) \le \underline{y}(i) \le \underline{\beta_y}(i) \tag{16}$$

The vector of the constraints over the horizon NY are given by:

$$\underline{\hat{\alpha}_y}(i) = \begin{bmatrix} \underline{\alpha_y}(i) \\ \underline{\alpha_y}(i+1) \\ \cdots \\ \underline{\alpha_y}(i+NY) \end{bmatrix} \quad \underline{\hat{\beta}_y}(u) = \begin{bmatrix} \underline{\beta_y}(i) \\ \underline{\beta_y}(i+1) \\ \cdots \\ \underline{\beta_y}(i+NY) \end{bmatrix} \tag{17}$$

Equation (16) leads to:

$$\underline{\hat{\alpha}_y}(i) \le \underline{\hat{y}_p}(i) \le \underline{\hat{\beta}_y}(i) \tag{18}$$

where

$$\underline{\hat{y}_p}(i) = \underline{\hat{y}_m}(i) + \underline{\hat{y}_r}(i) \tag{19}$$

$$\underline{\hat{y}_m}(i) = \Gamma \cdot \underline{x_m}(i) + \Psi \cdot \underline{\hat{u}}(i)$$

and $\hat{y}_r$ is the predicted output of the regulation model.

Matrices G and $\underline{h}$ of the constraint equation (8) can then be written:

$$G_y = \begin{bmatrix} -\Psi \\ \Psi \end{bmatrix} \qquad \underline{h_y}(i) = \begin{bmatrix} -\underline{\hat{\alpha}_y}(i) + \Gamma \cdot \underline{x_m} + \underline{\hat{y}_r}(i) \\ \underline{\hat{\beta}_y}(i) - \Gamma \cdot \underline{x_m} - \underline{\hat{y}_r}(i) \end{bmatrix} \tag{21}$$

If delays are present in the process, some rows of the G_y matrix may be empty. These rows does not correspond to constraints and can be removed them with their associated rows in the $\underline{h}$ vector.

When constraints are put on auxiliairy outputs, they can be expressed in two ways. First, these ouputs can be included in the process model and a null value is given to their components in the Q matrix. We can also use a separate constrained model and define other matrices Γ_c and Ψ_c which will be used in the constraint formulation. This last solution is simpler since the auxiliary outputs are not defined in the control criterion. Time varying constraints are allowed but may leads to unfeasible situations. This problem may occur when an active amplitude constraint changes faster than it is allowed by the constraint on variation. In this case, both constraints cannot be satisfied simultaneously. Variations of output constraints must be compatible with the process dynamics. If the process contains a delay or a non-minimum phase behaviour, constraints must

satisfy these behaviours.

D. Solution of the constrained optimization problem.
To simultaneously satisfy all constraints, the following matrices are defined:

$$G = \begin{bmatrix} G_u \\ G_{\Delta u} \\ G_y \end{bmatrix} \qquad \underline{h}(i) = \begin{bmatrix} \underline{h_u}(i) \\ \underline{h_{\Delta u}}(i) \\ \underline{h_y}(i) \end{bmatrix} \tag{22}$$

The constrained optimisation problem to be solved is then to minimized:

$$\min J(i) = \min \left\{ \underline{\hat{u}}(i)^T \cdot FU \cdot \underline{\hat{u}}(i) + 2 \cdot \underline{\hat{u}}(i) \cdot FO(i) \right\} \tag{23}$$

subject to the following constraints:

$$C \cdot \underline{\hat{u}}(i) \leq \underline{h} \tag{24}$$

This problem is called a quadratic programming problem. For simulation purpose, the "qp" fonction of the "matlab optimization toolbox" software (Grace 1992) has been used to solve the constrained minimisation problem. Other authors had used other commercial tools (Mutha and Shah 1991, Dion *et al.* 1991) or had proposed their own solution (Heath 1994, Rossiter and Kouvaritakis 1993, Camacho 1993, Wilkinson *et al.* 1990, Wilkinson *et al.* 1991, Gill *et al.* 1981).

IV. RECEDING HORIZON CONTROLLER WITHOUT MAXIMIZATION OF THE MANIPULATED VARIABLES: STEADY-STATE UNDER CONSTRAINTS

A controller without constraints can satistify setpoints when the number of manipulated variables is equal or greater than the number of setpoint. When constraints are active, degrees of freedom are lost. All setpoint values can not be simultaneously satisfied. A two input, two output system with two or more constrained outputs is studied below. Depending on the number of active constraints, the following situation may happen:

- No constraints are active, setpoints are obtained.
- Two constraints are active, setpoints are completly ignored. The two inputs are used to respect the constraints.
- More than two constraints are violated, there is no solution. The use of a robust algorithm is necessary to handle these situations. The constraint violations can be minimised or contraints can be respected according to priority rules set by the operator.
- One constraint is active, it is impossible to simultaneously obtain both setpoints. Setpoint errors are distributed according to the weight of the Q matrix as explained below in the steady-state case.

Model gains are defined by:

$$\begin{bmatrix} \Delta y_1 \\ \Delta y_2 \end{bmatrix} = \begin{bmatrix} k_{11} & k_{21} \\ k_{12} & k_{22} \end{bmatrix} \begin{bmatrix} \Delta u_1 \\ \Delta u_2 \end{bmatrix} \tag{25}$$

and constrained outputs have the following gains:

$$\Delta y_C = \begin{bmatrix} k_{1C} & k_{2C} \end{bmatrix} \cdot \begin{bmatrix} \Delta u_1 \\ \Delta u_2 \end{bmatrix} \tag{26}$$

The constraint on y_C prescribes $\Delta y_C = 0$ and a dependance between Δu_1 and Δu_2 is obtained such that one degree of freedom is lost:

$$\Delta u_2 = -\frac{k_{1C}}{k_{2C}} \cdot \Delta u_1 \tag{27}$$

If outputs are expressed with respect to the remaining input, the following relative gains are obtained:

$$\left.\frac{\Delta y_1}{\Delta u_1}\right|_{\Delta y_C = 0} = k_{11} - k_{21}\frac{k_{1C}}{k_{2C}} = k'_{11}$$
$$\left.\frac{\Delta y_2}{\Delta u_1}\right|_{\Delta y_C = 0} = k_{12} - k_{22}\frac{k_{1C}}{k_{2C}} = k'_{12} \tag{28}$$

In steady-state, the solution of the optimal criterion reduces to the minimization of

$$\min J = \min \left\{ \varepsilon_1^2 \cdot Q_1 \cdot NY + \varepsilon_2^2 \cdot Q_2 \cdot NY \right\} \tag{29}$$

where $\varepsilon = y - y_{csg}$ is the setpoint error.

Without loss of generality, it is assumed that setpoints and operation points are zero. In order to have a non-trivial solution, it is assumed that a disturbance p has occured on y_1. The expression of the input-output relation is then:

$$\varepsilon_1 = k'_{11} \cdot \Delta u_1 + p$$
$$\varepsilon_2 = k'_{12} \cdot \Delta u_1 \tag{30}$$

Dropping the constant factor NY, the criterion is expressed as:

$$\min J = \min\left\{(k'_{11}\cdot u_1 + p)^2\cdot Q_1 + (k'_{12}\cdot u_1)^2\cdot Q_2\right\} \quad (31)$$

Its minimum is found by deriving J relative to u_1 and setting the result equal to zero:

$$\frac{1}{2}\frac{\partial J}{\partial u_1} = (k'^2_{11}\cdot Q_1 + k'^2_{12}\cdot Q_2)\cdot u_1 + k'_{11}\cdot p\cdot Q_1 = 0 \quad (32)$$

$$u_1 = -\frac{k'_{11}\cdot p\cdot Q_1}{k'^2_{11}\cdot Q_1 + k'^2_{12}\cdot Q_2} \quad (33)$$

It can be shown that the ratio of setpoints errors is:

$$\frac{\varepsilon_1}{\varepsilon_2} = -\frac{k'_{12}}{k'_{22}}\frac{Q_2}{Q_1} = -\frac{Q_2}{Q_1}\frac{\left\{\left.\frac{\Delta y_2}{\Delta u_1}\right|_{\Delta y_c=0}\right\}}{\left\{\left.\frac{\Delta y_1}{\Delta u_1}\right|_{\Delta y_c=0}\right\}} \quad (34)$$

The next two expressions are also true:

$$\frac{\varepsilon_1}{\varepsilon_2} = -\frac{Q_2}{Q_1}\frac{\left\{\left.\frac{\Delta y_2}{\Delta u_2}\right|_{\Delta y_c=0}\right\}}{\left\{\left.\frac{\Delta y_1}{\Delta u_2}\right|_{\Delta y_c=0}\right\}} = -\frac{Q_2}{Q_1}\left\{\left.\frac{\Delta y_2}{\Delta y_1}\right|_{\Delta y_c=0}\right\} \quad (35)$$

This ratio is independant of the disturbance p. The error ratio is derived from the model gains and is therefore independant of modelling errors since they are embedded in the disturbances. It may happen that $\left.\frac{\Delta y}{\Delta u}\right|_{\Delta y_c=0}$ is zero (when a regulated output y is constrained. i.e. when y and y_C are the same). In this case, the y setpoint is neglected since uncontrollable. Usually, errors are shared between outputs according to Q_1 and Q_2 and depending on contraint which is active since different constraints produce distinct k_{1C} and k_{2C} and then other values of k'_{12} and k'_{11}.

V. RECEDING HORIZON CONTROLLER WITH MAXIMIZATION OF MANIPULATED VARIABLES: STEADY-STATE.

In this example, a receding horizon controller will be studied for a two-input process with one setpoint on an output y. In addition, a manipulated variable u_1 is to be maximized. The maximum of u_1 is reached when the auxiliary output y_C reaches its constraint.

The steady state criterion to optimize is then:

$$\min J = \min\left\{\varepsilon^2\cdot Q\cdot NY + 2\cdot T\cdot NU\cdot u_1\right\} \quad (36)$$

with the constraint $\Delta y_C = 0$.

The following steady state relations are known:

$$\begin{aligned}\Delta y &= k_{11}\cdot\Delta u_1 + k_{21}\cdot\Delta u_2\\ \Delta y_C &= k_{1C}\cdot\Delta u_1 + k_{2C}\cdot\Delta u_2 = 0\end{aligned} \quad (37)$$

Since the constraint on y_C is active, there is a dependance between u_1 and u_2:

$$\Delta u_2 = -\frac{k_{1C}}{k_{2C}}\cdot\Delta u_1 \quad (38)$$

The substitution of the value of u_2 into the expression of y gives

$$\left.\frac{\Delta y}{\Delta u_1}\right|_{\Delta y_c=0} = k_{11} - k_{21}\cdot\frac{k_{1C}}{k_{2C}} = k' \quad (39)$$

Without loss of generality, zero values are given to the setpoint and operation point. Then, since $\varepsilon = y$ and $u_1 = \frac{y}{k'} = \frac{\varepsilon}{k'}$, the criterion to be minimized is:

$$\min J = \min\left\{\varepsilon^2\cdot Q\cdot NY + 2\cdot T\cdot NU\cdot\frac{\varepsilon}{k'}\right\} \quad (40)$$

Its minimum is obtained when:

$$\frac{\partial J}{\partial \varepsilon} = 2\cdot Q\cdot\varepsilon\cdot NY + 2\frac{T}{k'}\cdot NU = 0 \quad (41)$$

The steady-state error is then given by:

$$\varepsilon = -\frac{T\cdot NU}{Q\cdot NY\cdot k'} = \frac{-T\cdot NU}{Q\cdot NY}\left\{\left.\frac{\Delta u}{\Delta y}\right|_{\Delta y_c=0}\right\} \quad (42)$$

VI. SIMULATION: GRINDING CIRCUIT

A. Process description

Grinding is used in mineral processing in order to reduce particle size for the liberation of valuable ore. The resulting product is used into the next separation stages.

The grinding circuit used in this study is composed of an open-loop rod-mill which unloads into a sump. A constant speed pump feeds a group of hydrocyclone classifiers. Cyclone overflow is the finished product used in the flotation stage. Cyclone underflow product is recycled to the sump box by a ball-mill (Figure 2).

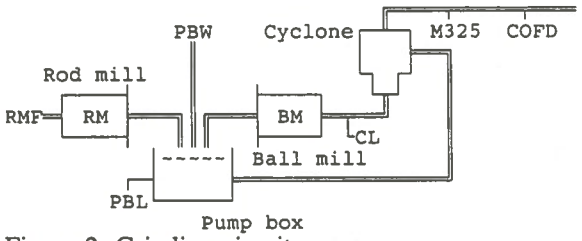

Figure 2: Grinding circuit

One of the control objective is to get a specified particle size distribution (M325) at the cyclones overflow. It is defined as the fraction of particles which are smaller than 325 mesh. The second objective is to maximize the ore throughput. Manipulated variables are the rod-mill feed (RMF) and pump box water addition (PBW). The number of hydrocyclones in operation is an important parameter which can also be manipulated.

Constraints on auxiliary outputs limit the possible production. The circulating load (CL) throught the ball-mill must not exceed a given value otherwise the mill is overloaded and the efficency is low. The cyclone overflow density (COFD) must not be too high to prevent sedimentation problems. It must not be too low to prevent dilution of the product. The pump box (PBLevel) must not overflow or be empty.

The process is simulated using the software DYNAFRAG (FLAMENT *et al.* 1991 and DESBIENS *et al.* 1994). It is a simulator calibrated on industrial data. DYNAFRAG is a phenomenological simulator programmed in APL which runs on its own computer. This computer is linked to the control computer by analog signals. Transfer fonctions linearized around the operating point are shown in Table 1. The sampling period is 300 seconds.

From this linear model, a feasability zone bounded by constraints may be established. In the M325-RMF space, this zone is given by figure 3. The upper constraint on the pump box level is nearly parallel to the constraint on the circulating load. These two variables have the same behaviour and often, when no sensor are available, the circulating load is estimated by the pump box level. However, these two outputs must be observed since perturbations as change of ore hardness may move these two contraints. The exact feasability zone is shown in figure 4 for different states: 5 or 6 hydrocylones with a normal ore and 6 hydrocyclones with a hard ore.

TABLE 1: Linearized transfer function of the process

	PWB	RMF
PBL	$\frac{1.962\ \frac{\%}{m^3/h}}{1+4700s}$	$\frac{5.749\ \frac{\%}{t/h}}{(1+5500s)(1+210s)}$
COFD	$\frac{-0.14(1+4050s)\ \frac{\%}{m^3/h}}{(1+3200s)(1+60s)}$	$\frac{0.0255(1-5600s)e^{-600s}}{(1+5300s)(1+750s)}$
M325	$\frac{0.012(1+39500s)\ \frac{\%}{m^3/h}}{(1+4400s)(1+50s)}$	$\frac{-0.2(1-900s)\ \frac{\%}{t/h}}{(1+5200s)(1+750s)}$
CL	$\frac{4.2(1-700s)\ \frac{t}{m^3}}{(1+5000s)(1+5s)}$	$\frac{13.8}{(1+5700s)(1+400s)}$

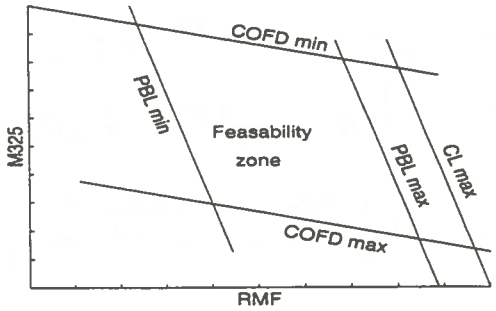

Figure 3: Feasability zone

From these figures, the following statements can be made:

- At constant size distribution, maximum feed is obtained when the circulating load is maximum or when the pump box level is maximum.
- If the constraint on the minimum COFD is reached, it is better to decrease the number of cyclones in operation since at constant particle size, the maximum feed is greater.

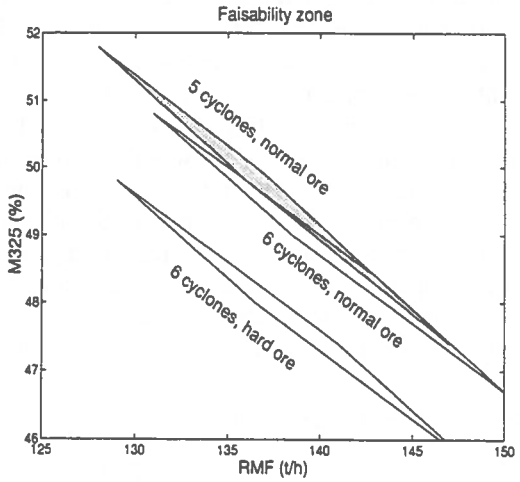

Figure 4: Feasability zone

- If the constraint on the maximum COFD is reached, it is better to increase the number of cyclones in operation.

B. Simulation parameters

In the next simulations, prediction and control horizon have been set to $NU = NY = 6$ samples. These values are high enough to ensure stability while limiting the computing effort.

Regulation reference models used are:

$$M325: \frac{1}{1+500s} \qquad CL: \frac{1}{1+1000s}$$

$$PBL: \frac{1}{1+1000s} \qquad COFD: \frac{1}{1+1000s}$$

When a setpoint is present on an output, the servo reference models are chosen equal to the regulation models.

C. First strategy: Setpoint on particle size and circulating load.

During normal operation, the limiting factor for the production is the circulating load (CL). In this case, if we keep the circulating load setpoint at its maximum, the throughtput is maximum. The strategy is then to regulate M325 and CL. The CL setpoint has been kept to 820 t/h for all the simulations. The choice of the weighting matrices and the applied constraints are:

$$Q_{M325}=2500$$
$$Q_{CL}=10$$
$$R_{PBW}=10$$
$$R_{RMF}=100$$

$$15\% \le PBL \le 85\%$$

$$48\% \le COFD \le 52\%$$

For these parameters, using equation (28) and (35), the relative setpoint errors when constraints are active can be evaluated. Results are shown in table 2.

TABLE 2: Setpoint errors under constraints

Active constraint	relative gain $\Delta CL/\Delta M325$	Setpoint error ratio $\varepsilon_{M325}/\varepsilon_{CL}$
PBL	-6.35	0.0254
COFD	-73.63	0.2945

When the COFD contraint is active, the error ratio is twelve times higher than when the PBL constraint is active.

The control law calculation requires the solution a quadratic programming problem with 12 independant variables and 24 constraints.

D. Second strategy: Setpoint on granulometry and maximisation of the ore feed.

From the steady-state gains of the process model and Equation (39), the ratio of the rod-mill feed variation to the particle size variation may be calculated. If a steay-state error of less than 0.2% on M325 is requested, the Equation (42) is used to find the proper value of Q and T. A summary of these calculations is shown in Table 3.

TABLE 3: Setpoint error in fonction of the active constraint

Active constraint	gain ratio $\Delta RMF/\Delta M325$	Setpoint error $\varepsilon_{M325}(\%)$
CL	-4.18	-0.167
PBL	-4.25	-0.170
COFD	-4.40	-0.176

The chosen weighting parameters are the following:

$$T_{RMF} = -100$$
$$Q_{M325} = 2500$$
$$R_{PBW} = 10$$
$$R_{RMF} = 100$$

The applied constraints are:

$$CL \leq 820\ t/h$$

$$15\% \leq PBL \leq 85\%$$

$$48\% \leq COFD \leq 52\%$$

The control law calculation requires the solution a quadratic programming problem with 12 independant variables and 30 constraints.

E. Simulation and Results

The sequence of events of the simulation are shown in table 4. The simulation results are shown in Figures 5 and 6 for the two control strategies.

TABLE 4: Simulation event sequence

Time	Event
0h	Granulometry setpoint: M325=48%, normal ore hardness, 6 cylones operating.
5h	Ore hardness perturbation, ore is now harder.
10h	Change of the number of operating cyclones, 5 cyclones are now operating.
15h	Setpoint change: M325=47%.

In Figure 5, one can observe that the two setpoints are reached for the first five hours. When the ore hardness perturbation occurs, the lower constraint on COFD is reached. This causes setpoint deviation on both M325 and CL but the error on M325 is of greater importance. At 10h, the change of the number of cyclones rises COFD to its upper constraint and also rises PBL at its upper bound. Since there is two active constraints, setpoints are totally ignored: The setpoint change at 15h has no effect.

For figure 6, the setpoint on M325 is reached with the predicted -0.167% error and the RMF is rised until the circulating load (CL) constraint is active. When the ore harness change occurs, two constraints (CL max andCOFD min) are active. Setpoints are then totally neglected. It has been concluded previously that it is advantageous to decrease the number of operating

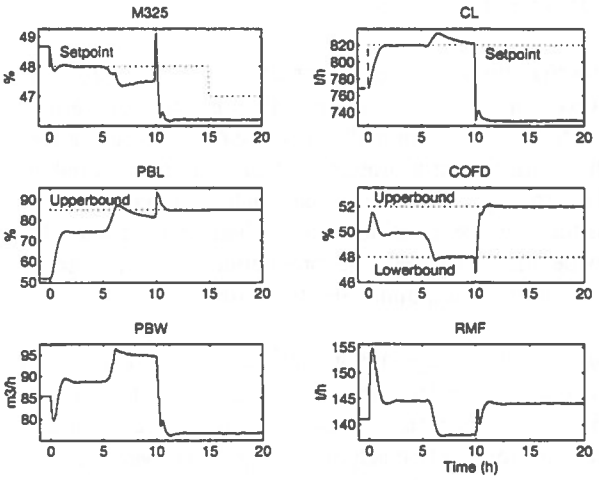

Figure 5: Granulometry (M325) and circulating load (CL) setpoints

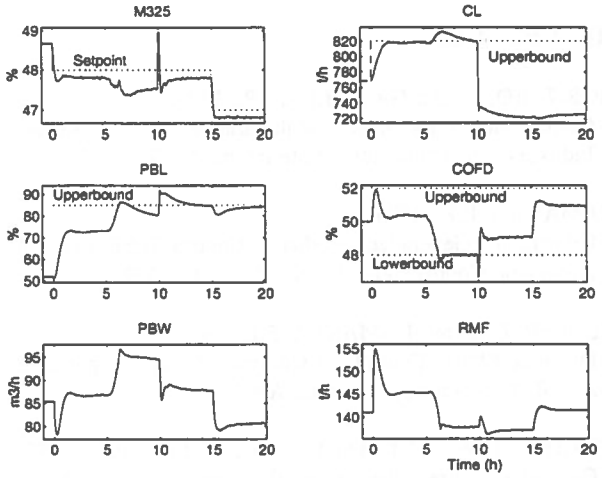

Figure 6: Granulometry (M325) setpoint and rod-mill feed (RMF) maximisation

cyclones when the lower COFD bound is reached. This change at 10h liberates a degree of freedom so that M325 can now be controlled. In this case, the limiting constraint is the upper pump box level. The setpoint change at 15h is efficiently done.

From these simulations we can conclude that with the two setpoints stategy, when constraints are present, the controller does not statisfy the particle size setpoint. Even a change in the number of cylones in operation cannot allow to reach this setpoint. By opposition, a control strategy with a setpoint on particle size and maximization of the rod mill feed is more representative of the true operating objectives. In this case, when two constraints are active, it is easy to change the number of cylones in operation to get the desired objectives.

VII. CONCLUSION

Internal model receding horizon process control with constraints is very efficient to control multivariable processes. In addition, the presence of constraints allows the utilisation of a strategy that can maximize variables. This strategy has shown to be much more representative of the true operating objectives when a compromise had to be made between the production quality, which is expressed as setpoints, and the throughput.

Simulations on a grinding circuit process with a setpoint on the particle size and maximization of the ore feed gives constant results whatever is the active constraint. In opposition, a two setpoint stategy gives very variable setpoint errors when a constraint is active. This can cause severe degradation of particle size distribution.

REFERENCES

BORNARD, G. and GAUTHIER, J.P., 1977.
Commande Dynamique Multivariable des Systèmes Industriels de Production, Note interne LAG no. 77-29.

CAMACHO, E.F., 1993.
Constrained Generalized Predictive Control, IEEE trans. on Automatic Control, Vol. 38, No. 2, pp. 327-332.

CUTLER, C.R. and RAMAKER, B.L., 1980.
Dynamic Matrix Control - A Computer Control Algorithm, AIChE 86th National Meeting, April.

CLARKE, D.W., MOTHADI C. and TUFFS, P.S., 1987. Generalized Predictive Control - part I: The Basic Algorithme; Part II: extensions and interpretation. Automatica, Vol. 23, pp. 137-160

DESBIENS, A., POMERLEAU, A. and NAJIM K., 1994. Adaptive Predictive Control of a Grinding Circuit, Int. journal of Mineral Processing, Vol. 41, pp.17-31.

DION, J.M., DUGARD, L., FRANCO, A., NGUYEN MINH TRI and REY, D., 1991. MIMO Adaptative Constrained Predictive Control Case Study: An Environment Test Chamber, Automatica, Vol. 27, No. 4, pp. 611-626.

FLAMENT, F., DEL VILLAR, R. and LANTHIER, R., 1991. Computer aided design of a control strategy for an industrial grinding circuit. In: R. Poulin, R.C.T. Pakalnis and A.L. Mular (Editor), Proc. of the 2nd Can. Conf. on Computer Applications in the Mineral Industry, Vol. I, pp.337-348.

FOULARD, C. GENTIL, S. and SANDRAZ, J.P., 1987. Commande et régulation par calculateur numérique, théorie aux applications, Éd. Eyrolles, Paris, 573 p.

GAUTHIER, J.P. and BORNARD, G., 1983.
Commande Multivariable en Présence de Contraintes de Type inégalité, R.A.I.R.O. Aut. Syst. Anal. Control, Vol. 17, No. 3, p. 205 à 222.

GILL, P.E., MURRAY, W., WRIGHT, M.H., 1981.
Practical Optimization, Academic Press, London, Toronto, 401 p.

GRACE, A., 1992.
Optimization toolbox for use with Matlab, Mathworks.

HAWKINS, R.B. and CUTLER, C.R., 1987.
Constrained Multivariable Control of a Hydrocracker Reactor, Proc. of the 1987 American Control Conference, Minneapolis, June 10-12, pp. 1014-1020.

HEATH, W.P., 1994.
Correspondance: Constrained Stable Generalised Predictive Control, IEE Proc.-Control Theory Appl., Vol. 141, No. 4, pp. 274-276.

MUTHA, R.K. and SHAH, S.L., 1991.
Constrained Long Range Predictive Control of a Heavy Oil Fractionator, Proc. of the 1991 American Control Conference, pp. 779-784.

RICHALET, J., RAULT, J.A., TESTUD, J.P. and PAPON, J., 1978. Model Predictive Heuristic Control, Application to Industrial Processes, Automatica, Vol. 14, pp. 413.

ROSSITER, J.A. and KOUVARITAKIS, B., 1993.
Constrained Stable Generalised Predictive Control, IEE Proc.-Control Theory Appl., Vol. 140, No. 4, pp. 243-254.

TREIBER, S., De TREMBLAY, M. and BELL, M., 1992. Multivariable Constraint Control of a Polyethylene Reaction Process, ISA/92 Canada General Program, Toronto, Ontario, pp. 251-260.

VAN HOOD, A.H., CUTLER, C.R. and FINLAYSON, S.G., 1989.
Application of a Constrained Multi-variable Controller to a Hydrogen Plant, Proc. of the 1989 American Control Conference, Pittsburgh, PA, pp. 1555-1560.

WILKINSON, D.J., MORRIS, A.J. and THAM, M.T., 1990. Multivariable Constrained Generalised Predictive Control A comparison with QDMC, Proc. of the 1990 American Control Conference, San Diego, CA, pp. 1620-1625.

WILKINSON, D.J., THAM, M.T. and MORRIS, A.J., 1991. High Performance Distillation - Case Studies in Constrained Predictive Control, Advanced Control of Chemical Processes : ADCHEM'91 : Selected Papers form the IFAC Symposium, Toulouse, France, pp. 121-126.

CAMI'95: 3rd Canadian Conference on Computer Applications in the Mineral Industry
Montréal, Québec, Canada, October 22-25, 1995

AUTOSTOP: A Unified Software for Simulation of Automatic Stochastic Optimal Predictive Control Loops

Daniel Hodouin, Éric Gagnon, André Pomerleau
GRAIIM (Groupe de Recherche sur les Applications de l'Informatique à l'Industrie Minérale)
Université Laval, Québec

ABSTRACT

AUTOSTOP is designed to help teaching and development of model-based predictive process controllers. It simulates linear control loops of processes modelled by discrete transfer functions. It provides, in a unified internal model structure, tools for simulation and design of setpoint tracking controller, and unmeasured and measured disturbances rejection controllers.

RÉSUMÉ

AUTOSTOP est un logiciel conçu pour faciliter l'enseignement de la commande prédictive et la conception de systèmes automatiques. Il permet la simulation d'une boucle de commande linéaire pour un procédé modélisé par des fonctions de transfert. Il offre dans une structure à modèle interne unifiée les possibilités de simuler la poursuite de consigne et la compensation des perturbations mesurables et non mesurables.

INTRODUCTION

The software AUTOSTOP was developed as part of the KBAC project (Knowledge-Based Automatic Control of mineral processing plants). The KBAC objectives were to screen advanced methods of control and assess their performances when applied to mineral processes. In the last two decades a wide range of control techniques have been developed, however it appeared, during the first survey of the literature in this field, that, behind the variations of the vocabulary used to name the methods and the diversity of the mathematical formulations of the controllers, there was a common objective and many similarities in the proposed algorithms. The objective of developing AUTOSTOP was to put in a single structure most of the linear control methods, in order to synthetize and clarify the field of applied linear control. AUTOSTOP has been designed for training purposes, mainly in order to accelerate the process of learning and implementation of advanced control methods by mineral process engineers.

AUTOSTOP makes use of a structure (the internal model control structure (Garcia and Morari, 1982)), a controller design criterion (the predictive least-squares objective function (Garcia et al., 1989)), a formulation of the desired specifications through reference models (Irving et al., 1986), and, finally, a stochastic prediction of the measured and unmeasured disturbances (Box and Jenkins, 1976). It is programmed in a user friendly environment based on the MATLAB/WINDOWS software.

AUTOSTOP incorporates in a single structure most of the advanced control techniques such as the pole placement controller (Åström and Wittenmark, 1990), the minimum variance controller (Åström and Wittenmark, 1990), the extended horizon controller (Ydstie et al., 1985), the generalized predictive controller (Clarke et al., 1987) and the partial-state predictive controller (Irving et al., 1986; M'Saad, 1991). The software is presented in the monovariable case, however the same structure can also be used for multivariable processes. The paper first presents the control algorithm and its relation to other controllers.

Then the software is presented, and finally an example is given.

PROCESS MODEL

As advanced control methods are based on a prior knowledge of a mathematical model of the process, and as measurements and control actions are handled by computers, this first section will briefly introduce the concept of discrete process modelling.

When a process is controlled by a computer, the variation of the manipulated variable is performed only one time per time interval T. Between the changes made by the computer, the manipulated variable is hold at its last value. The signal used by the sensor is also sampled once per time interval T. This sampling process must be preceded by analog filtering of the signal in order to avoid the generation of fictitious low frequencies is the discretized signal. For the purpose of this paper the process will be in fact the chain of Figure 1. The discretized process input and output are noted $u(t)$ and $y(t)$ in the followings. The dynamic variations of $u(t)$ and $y(t)$ are represented using the ***backshift operator*** z^{-1}, which is defined by

$$z^{-k} x(t) = x(t-k) \qquad (1)$$

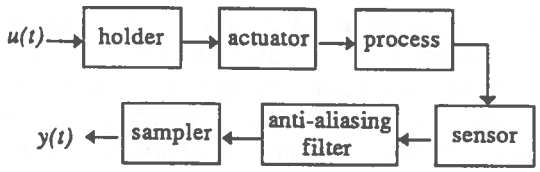

Figure 1: Equivalent discretized process.

Various forms of process models for predictive control can be proposed: step response (Cutler and Ramaker, 1980), frequency response, discrete transfer function (Clarke et al., 1987), state-space representation (Foulard et al., 1987). Since this paper is limited to single-input-single-output process, ***discrete transfer functions*** are used. The most general form of the model is presented in Figure 2 where the process output y is modelled as a sum of the effects of the manipulated variable u, the measured disturbance p and the unmeasured disturbance δ. ξ_p and ξ_δ are purely random variables (white noises) which generates the disturbance p and δ (Box and Jenkins, 1976).

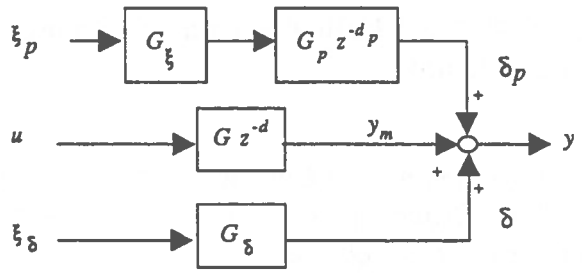

Figure 2: Model for process simulation or controller design.

Any of the transfer functions G of Figure 2 is a ratio of two z^{-1} ***polynomials:***

$$G = \frac{B(z^{-1})}{A(z^{-1})} \qquad (2)$$

which expresses a dynamic relationship between the transfer function input $I(t)$ and output $O(t)$ of the recursive form:

$$O(t) = -a_1 O(t-1) - a_2 O(t-2) \ldots + b_0 I(t) + b_1 I(t-1) \ldots \qquad (3)$$

where a_k and b_k are the coefficients of the polynomials $A(z^{-1})$ and $B(z^{-1})$.

In the transfer functions G and G_p, the pure delay parts (z^{-d} and z^{-d_p}) have been factorized. Because of the presence of G_δ and G_ξ the model allows the design of ***stochastic controllers***. The model of a process can be more or less complex depending of the objective, however the minimum part of the model which is required for controller design is $G\,z^{-d}$, the output of which is called the ***model output.***

It happens frequently that the model $G\,z^{-d}$ must be factorized to obtain ***realizable and stable*** controllers (Åström and Wittenmark, 1990). The factorization consists in defining an internal process variable x, called sometimes a ***partial state*** (Irving et al., 1986), which will be controlled instead of y_m. Figure 3 shows the following decomposition:

$$G\,z^{-d} = \underline{G}\,\overline{G}\,z^{-d} \qquad (4)$$

where $\underline{G}$ contains the ***unstable zeros*** (z roots of the G numerator which have a real part larger than 1) or the

oscillatory zeros (roots which have a real part between -1 and 0), and has a unit gain.

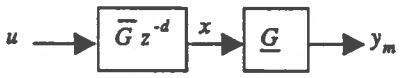

Figure 3: Model output and partial state.

The model structure of Figure 2 is used to simulate the process as well as to design the controller of the process. The model of any process is inherently inaccurate, so that there is no reason why the process models for ***simulation*** and ***control*** should be identical. AUTOSTOP is organized in such a way that different transfer functions G, G_p, G_ξ and G_δ can be used for simulating the process and designing the controller.

CONTROLLER DESIGN PRINCIPLES

Model-based linear controllers are designed to control the model output y_m or the model partial state x and not the process itself since its true model is, by definition, unknown. There are essentially two ways to design a controller, algebraically or optimally. An ***algebraic controller*** is an algorithm which exactly calculates the control action $u(t)$ to be applied at time t such that:

$$y_m(t+d) = \hat{r}(t+d/t) \qquad (5a)$$

or

$$x(t+d) = \hat{r}(t+d/t) \qquad (5b)$$

subject to:

$$y_m(t+d) = G\,u(t) \qquad (6a)$$

or

$$x(t+d) = \bar{G}\,u(t) \qquad (6b)$$

and where $\hat{r}(t+d/t)$ is the predicted value at time $t+d$, calculated at time t, of the reference trajectory that should be followed by the model output or the partial state.

The resolution of (5a) and (6a) or (5b) and (6b) leads to $u(t)$. The design criterion of this algebraic controller involves only the model output. Since there is no constraint on the control action $u(t)$, this controller frequently leads to very demanding control actions.

Optimal control is an alternative controller design which consists in simultaneously specifying desired properties of y_m (or x) and u by defining an optimal compromise between u and y_m (or x). For instance in the ***d-step ahead predictive controller***, the following criterion is minimized with respect to $u(t)$

$$J[u(t)] = [y_m(t+d) - \hat{r}(t+d/t)]^2 + \lambda[u(t) - u(t-1)]^2 \qquad (7)$$

subject to

$$y_m(t+d) = G\,u(t) \qquad (8)$$

or the equivalent criterion with $x(t+d)$ instead of $y_m(t+d)$, subject to $x(t+d) = \bar{G}\,u(t)$.

The second term in Equation (7) penalizes the squared variation of $u(t)$ in such a way to avoid a too large control action. Obviously the first term in Equation (7) cannot be exactly equal to zero as it was in the algebraic design. The trade-off between a desired smooth control action and a desired output at a reference value is handled by the λ coefficient. The larger it is, the lower is the control cost, but the farther is the model output from its reference trajectory. For $\lambda = 0$, the problem defined by Equations (7) and (8) degenerates into the algebraic design.

To generalize the above optimally designed controller one can extend the prediction horizon by minimizing the following criterion instead of the one of Equation (7):

$$J[u(t) \ldots u(t+h_c-1)] = \sum_{i=d}^{h_p} [y_m(t+i) - \hat{r}(t+i/t)]^2 + \lambda \sum_{i=0}^{h_c-1} [u(t+1) - u(t+i-1)]^2 \qquad (9)$$

An alternative similar criterion can be defined for x instead of y. In criterion (9), h_p is the ***prediction horizon*** and h_c the ***control horizon***. The control horizon h_c must be lower than h_p-d+1, since control actions at any time k influences only y(or x) values at time $\geq k+d$. The controller which minimizes (Eq.9) subject to the process model is called ***a long-range predictive controller***. It contains obviously the

algebraic and the *d*-step ahead optimal controllers as particular cases.

The next step in the design of a controller consists in defining the reference trajectory $\hat{r}(t+1/t)$. This reference trajectory will depend on the type of control objective (setpoint tracking, measured disturbance rejection or unmeasured disturbance rejection), on the desired dynamic behaviour of the controlled process and on the nature of the process model (deterministic or stochastic).

SETPOINT TRACKING

For setpoint tracking one ideally wants the model output to track the setpoint so that:

$$\hat{r}(t+i/t) = y_{sp}(t+i) \qquad (10)$$

where y_{sp} is the setpoint. Usually future values of the setpoints are not known, so that it is simply assumed that

$$\hat{r}(t+i/t) = y_{sp}(t), \ \forall\, i \qquad (11)$$

The resolution of the system of Equations (5a), (6a) and (11) then gives:

$$u(t) = \overline{G}^{-1}\, y_{sp}(t) \qquad (12)$$

a control algorithm which is known as the ***dead-beat setpoint tracking controller.***

Most of the time, a smoother response to setpoint change than the one described by Equation (9) is desired. In that case the reference trajectory is defined by:

$$\hat{r}(t+1/t) = F(z^{-1})\, y_{sp}(t+1) \qquad (13)$$

where $F(z^{-1})$ is a filter (a transfer function) which defines exactly the dynamic behaviour required for the controlled process. It has a unit gain and may have a finite time response (only a numerator) or an infinite time response (a numerator and a denominator). It is usually selected as a first or second order transfer function. The controller is in this case:

$$u(t) = \overline{G}^{-1}\, F\, y_{sp}(t) \qquad (14)$$

Instead of an algebraic design, an optimal design can be used leading, in the *d*-step ahead case, to the following controller

$$u(t) = \frac{F}{\overline{G} + \lambda\, \overline{G}^{-1}(0)\ (1-z^{-1})}\, y_{sp}(t) \qquad (15)$$

where the process model inverse of Equation (14) is replaced by a ***pseudo-inverse*** which depends on the tuning parameter λ. The prediction horizon can be extended leading to a controller which is more difficult to express by a simple equation, but which has a similar behaviour to the above optimal controller with two additional tuning parameters h_p and h_c.

Figure 4 shows the setpoint tracking controller structure where C is either $\overline{G}$ or the pseudo inverse or the long-range predictive controller depending on the selection of λ, h_p and h_c. $P_H(h_p)$ stands for the operation of assuming that future values of the setpoint are identical to the present one. This operator is called a ***predictor-holder***, since it blocks the h_p future values of y_{sp} at the value $y_{sp}(t)$. A double line has been drawn between P_H and C, in order to visualize that when $h_p \neq d$ the output of the predictor-holder and the input to the controller are vectors of predicted values. The controller output is only the value $u(t)$ even when $h_c > 1$, since only the first value of the calculated u vector is applied to the process, the next value being recalculated at the next sampling period.

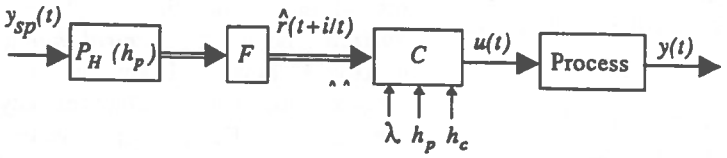

Figure 4: Setpoint tracking control.

MEASURED DISTURBANCE REJECTION

When the input disturbance $p(t)$ is measured, it is possible to predict its effect $\delta_p(t+1)$ at the process output if $G_p\, z^{-d_p}$ is known. If the model of $p(t)$, $G_\xi(t)$, is also known, the predicted effect δ_p can be improved. Defining the future value of δ_p by:

$$\delta_p(t+i/t)$$

the reference trajectory for the model output should be:

$$\hat{r}(t+i/t) = -\delta_p(t+i/t) \qquad (16)$$

in which case the effect of the disturbance will be compensated since the model output will cancel the predicted effect of the input disturbance, leaving only the prediction error as uncompensated disturbance. In the deadbeat algebraic case, the problem is to find $u(t)$ such that:

$$y_m(t+d) = -\delta_p(t+d/t) \qquad (17)$$

The controller is then

$$u(t) = -G^{-1}\,\delta_p(t+d/t) \qquad (18)$$

where it is clear that the controller is the same as the setpoint tracking controller driven by the opposite value of the predicted output disturbance. When G is not invertible, it is factorized and x is controlled instead of y_m, leading to $\bar{G}^{-1}$ instead of G^{-1} in Equation (18).

As in the case of setpoint tracking, instead of deadbeat performance, a smoother dynamic behaviour of the controlled may be obtained by filtering $\delta_p(t+d/t)$, leading to the controller

$$u(t) = F\,G^{-1}\,\delta_p(t+d/t) \qquad (19)$$

The problem of measured disturbance rejection is then a problem of prediction of δ_p. At time $t+i$, δ_p is

$$\begin{aligned}\delta_p(t+i) &= G_p\, z^{-d_p}\, p(t+i) \\ &= G_p\, p(t+i-d_p)\end{aligned} \qquad (20)$$

Then

$$\delta(t+i/t) = G_p\, \hat{p}(t+i-d_p/t) \qquad (21)$$

with

$$\hat{p}(t+i-d_p/t) = G_\xi\, \xi_p(t+i-d_p/t) \qquad (22)$$

When $i \le d_p$, $\hat{p}(t+i-d_p/t)$ depends only on past and present values of ξ_p which can be calculated recursively from the model G_ξ and the measured values $p(t)$. When $i > d_p$ one has to estimate future values of ξ_p. Since ξ_p is a centered white noise, the best predicted value is zero. This predictor is a ***minimum variance predictor***, is that sense that it minimizes the variance of the prediction error. Let $P(h_p)$ be the operator which predicts $\hat{p}(t+i/t)$ from $i = 1$ to $i = h_p$ according to the above procedure. Then the general long-range predictive controller for measured disturbance rejection can be represented as in Figure 5.

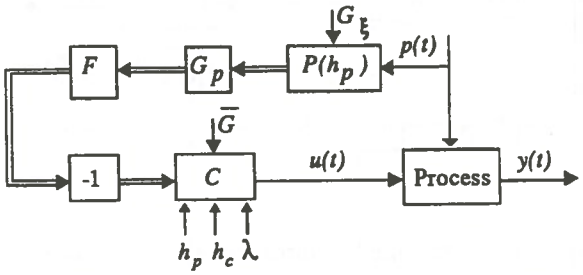

Figure 5: Measured disturbance rejection controller.

UNMEASURED DISTURBANCE REJECTION

The two above controllers are ***feedforward*** controllers. The ***feedback*** controller will be now defined to reject the unmeasured disturbances. The controller which cancels the unmeasured disturbance δ can be derived exactly as the previous one. The algebraic deadbeat controller is obtained by calculating $u(t)$ such that:

$$y_m(t+d) = -\delta(t+d/t) \qquad (23)$$

Again it is identical to the setpoint tracking controller driven by the opposite of the predicted disturbance. A filter can be used to specify the desired disturbance rejection dynamic, and the problem can be solved also by the optimal design method.

The problem of designing an unmeasured disturbance rejection controller is to design a predictor of $\delta(t+i/t)$.

For that purpose an estimator of $\delta(t)$ is first constructed, then the prediction of δ is made using the stochastic model of δ and the procedure explained in the previous section for predicting $p(t+i)$. It must be emphasized here that $\delta(t)$ includes all the output disturbance, i.e. the unmeasured disturbances, the modelling errors (differences between $G\,z^{-d}$ for simulating the process and $G\,z^{-d}$ for controlling the process), and the effect of input disturbances when they are not measured and not compensated by a feedforward controller. The model generating $\delta(t)$ must be identified accordingly. As a consequence of this definition of $\delta(t)$, it is estimated as the difference between the process output (which must be measured), and the model output, leading to the control scheme of Figure 6 which represents the feedback ***long-range predictive controller*** for unmeasured disturbance rejection.

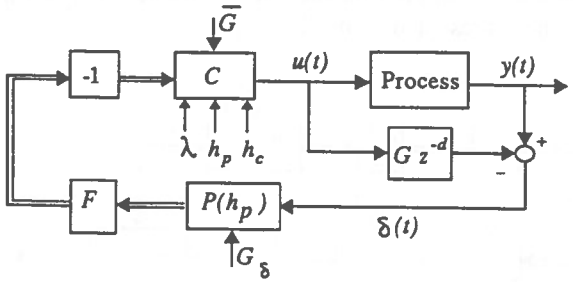

Figure 6: Unmeasured disturbance rejection controller.

MULTIPURPOSE PREDICTIVE CONTROLLER

To obtain a linear controller which performs simultaneously the three actions (setpoint tracking, measured and unmeasured disturbance rejection), the control action applied to the process is simply obtained by algebraically summing the three control actions calculated by the three controllers. The corresponding scheme is given in Figure 7. It must be noted in Figure 7 that $\delta(t)$ is estimated by subtracting to the measured process output the model output $y_m(t)$ as well as the model output $\delta_p(t)$, since input disturbances are assumed to be measured and rejected.

AUTOSTOP is designed assuming that the three controllers have the same tuning parameters λ, h_p and h_c, thus leading to:

$$C = C_p = C_\delta = C_{sp} \qquad (24)$$

The controller C can be put after the algebraic summator of the reference trajectories as shown in Figure 8.

SOFTWARE AUTOSTOP

AUTOSTOP implements the control strategies described above on a process simulated by transfer functions. The MATLAB/WINDOWS environment is used for programming the controller and simulating the process.

The control-loop flowsheet is interactively displayed on the screen by selecting the various control configurations. The basic loop automatically displayed on the screen is the open control loop of Figure 4. Four different arrangements of the control loop can be obtained by activating push-buttons "FEEDFORWARD" or "NO FEEDFORWARD" and "OPEN-LOOP" or "CLOSED LOOP". When "FEEDFORWARD" is on, the rejection of measured disturbances is active. When "CLOSED LOOP" is on, the rejection of unmeasured disturbance is active. In all cases setpoint tracking is active.

For each control-loop configuration, the controller can be selected as algebraic or optimal, by activating a push-button. Algebraic controllers can be obtained also through the optimal design option by selecting $\lambda = 0$, $h_p = d$, $h_c = 1$. In the algebraic mode the user must define himself or herself the transfer function of the

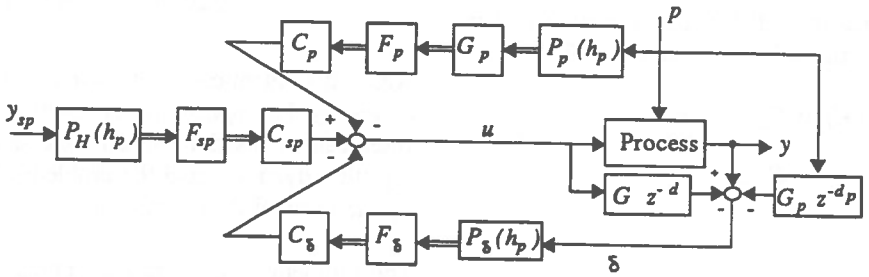

Figure 7: Generic long-range predictive controller.

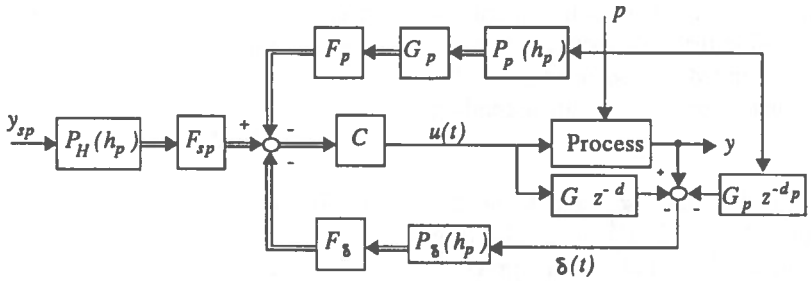

Figure 8: Control structure programmed in AUTOSTOP.

controller, while in the optimal mode the control action is calculated by the criterion minimization.

By using the options available in the window "BLOCS" the user can add to the control loop:

- ***reference models*** for setpoint tracking and/or unmeasured disturbance feedback rejection and/or measured disturbance feedforward rejection.
- ***predictors*** of measured and/or unmeasured disturbances for stochastic control.

The most complete control structure is the one depicted in Figure 8 and appearing on the screen as shown in Figure 9.

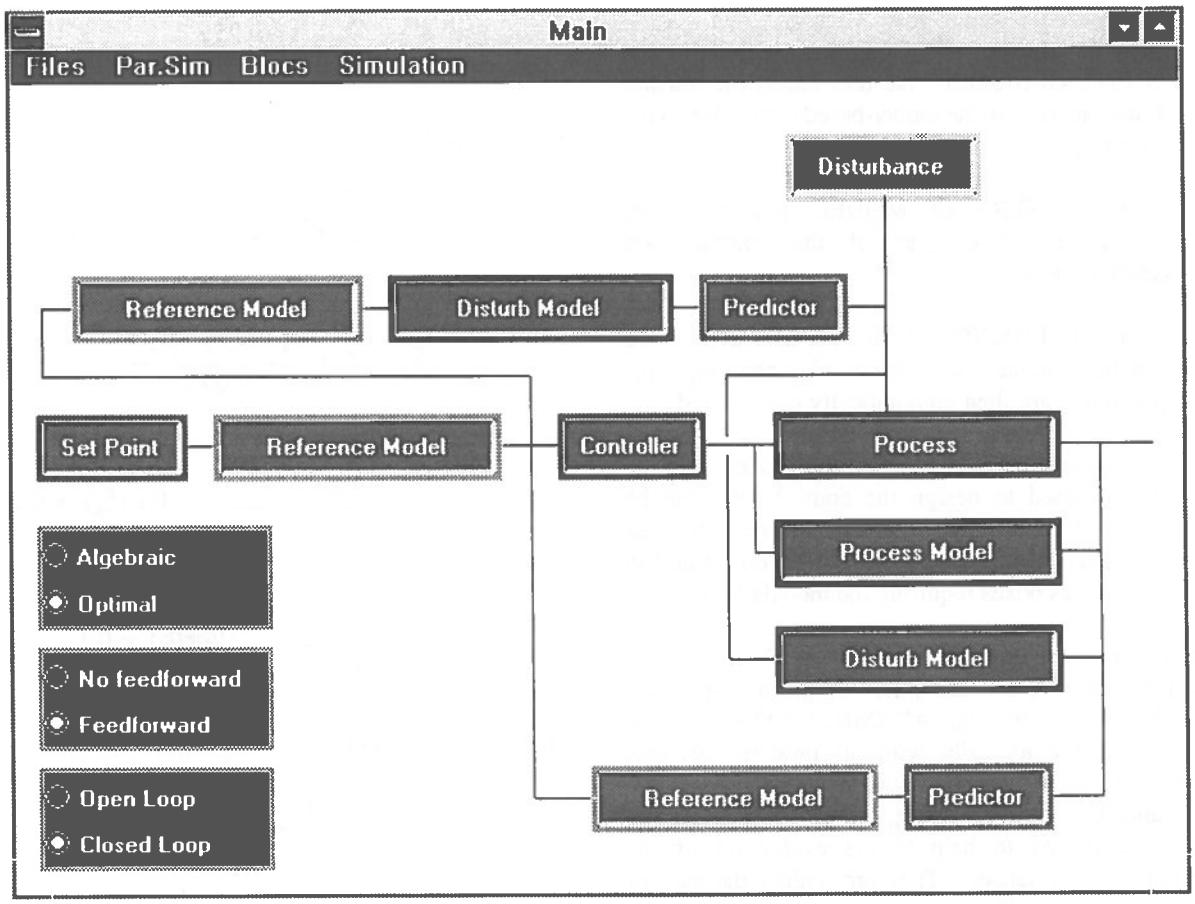

Figure 9: Screen of the selected controller when all the possible options have been activated through the push-buttons or the "BLOCS" window.

By clicking in the various boxes of the selected control structure the user can define the corresponding transfer functions. They are entered as sequences of the numerator and denominator coefficients in ascending power of z^{-1}:

- In the "PROCESS" box the user can define the transfer functions $G\,z^{-d}$, $G_p\,z^{-d_p}$ and G_δ (see Figure 2) of the model for simulating the process. Clicking in the "INPUT" box of the "PROCESS" box, ξ_δ can be defined by its variance or, alternatively, a step function can be defined by its amplitude.

- In the "DISTURBANCE" box the transfer function G_ξ is defined for simulating the process disturbance and the internal "INPUT" box is used to define ξ_p.

- The "CONTROLLER" box is used to enter the controller tuning parameters h_p, h_c and λ or the control transfer function when in algebraic mode.

- In the boxes "PROCESS MODEL" and "DISTURB MODEL" the user enters the transfer functions used in the model-based controller, in the factorized form.

- In the "REFERENCE MODEL" boxes the user defines the filter part of the control loop specifications.

- In the "PREDICTOR" boxes the user defines the ARIMA model describing G_δ and G_ξ, the predictors are then automatically constructed.

- The models used to simulate the process and the models used to design the control loop can be made different by entering different transfer functions in the process simulation boxes and in the various boxes requiring the models for control.

When the simulation parameters have been defined (sampling interval and simulation time), the user starts the calculation by clicking on "SIMULATION". Results are presented graphically with all process variables either in the same graph or in two different graphs (one for u and one for y, y_m and y_{sp}). Statistical indicators can be displayed to help to the evaluation of the controller performances. They are mainly the sum of squares of the deviation to the setpoint along the trajectory and the sum of the squared variations of the control action.

ONE EXAMPLE

The following process is selected:

$$G\,z^{-d} = \frac{z^{-2} + 1.2\,z^{-3} - 0.45\,z^{-4}}{1 - 1.8\,z^{-1} + 0.96\,z^{-2} - 0.13\,z^{-3}}$$

$$G_p\,z^{-d_p} = \frac{z^{-1} - 1.6\,z^{-2}}{1 - 0.85\,z^{-1}}$$

$$G_\delta = \frac{1 + 0.8\,z^{-1}}{1 - 1.5\,z^{-1} + 0.5\,z^{-2}}$$

$$G_\xi = \frac{1}{1 - 0.95\,z^{-1}}$$

It is modelled by

$$\overline{G}\,z^{-d} = \frac{2\,z^{-2}}{(1 - 0.85\,z^{-1})^2}\;;\quad \underline{G} = \frac{1 + 1.6\,z^{-1}}{2.6}$$

$$G_p\,z^{-d_p} = \frac{(1 - 1.5\,z^{-1})\,z^{-1}}{1 - 0.8\,z^{-1}}$$

$$G_\delta = \frac{1 + 0.6\,z^{-1}}{(1 - z^{-1})\,(1 - 0.4\,z^{-1})}\;;\quad Var(\xi_\delta) = 0.1$$

$$G_\xi = \frac{1}{1 - 0.9\,z^{-1}}\;;\quad Var(\xi) = 0.1$$

The controller tunings are:

$$h_p = 8$$
$$h_u = 2$$
$$\lambda = 0.1$$

and the filters of the model references:

$$F_\delta = F_p = \frac{0.6}{1 - 0.4\,z^{-1}}$$

$$F_{sp} = \frac{1}{3}\left(1 + z^{-1} + z^{-2}\right)$$

Both predictors are activated. Figures 10 show the results for 100 sampling periods. A setpoint change has been activated at time index 50.

The control loop structure is implemented in a user-friendly software which simulates the dynamic behaviour of a controlled process. It is extremely useful for teaching advanced process control and for designing control systems for the mineral processing industry.

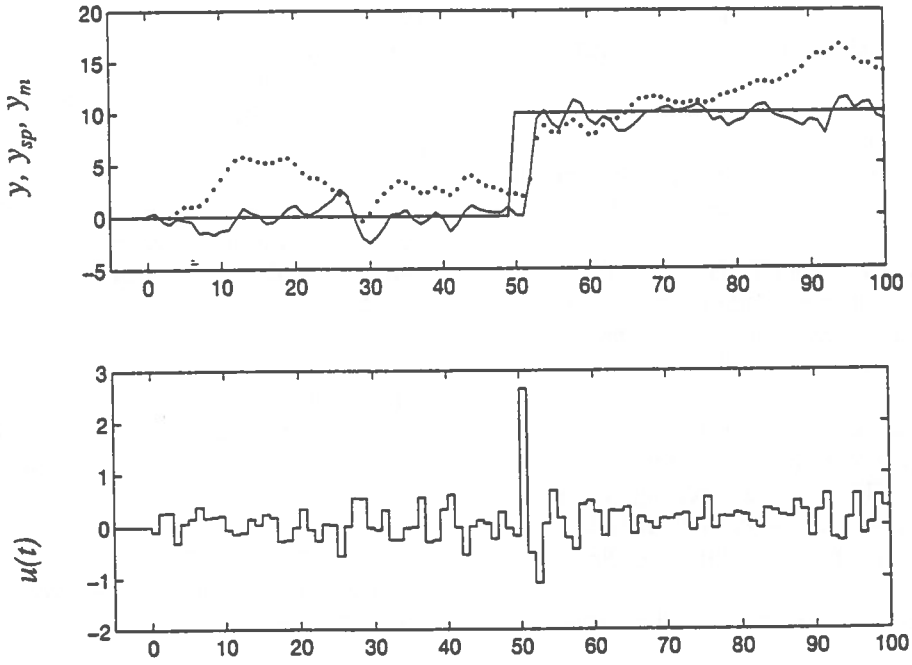

Figure 10: Graphs produced by AUTOSTOP
(in top figure are represented the process setpoint y_{sp},
the process output y, and the model output y_m in dotted line).

CONCLUSION

A control loop structure has been proposed which incorporates most of the traditional or advanced control techniques such as the Dahlin's and Kalman's algorithms, the Smith predictor (Ash), the minimum variance controller, the constrained and generalized minimum variance controllers, the extended horizon controllers, the pole-placement controller, the generalized predictive controller, the partial state predictive controller, and the feedforward predictive controller.

The software presented in this paper is developed for the single-input-single-output case, however it has also been developed in the multi-input-multi-output case, but the software is not yet user-friendly because of the greater complexity of the control loop in the multivariable case. Predictive control has been evaluated with this software and other programs including adaptive ones for grinding and flotation systems (Hodouin et al., 1991; Hodouin et al., 1993; Desbiens et al., 1994a and b).

ACKNOWLEDGEMENTS

The authors would like to thank a consortium of eight mining companies under the umbrella of MITEC, as well as the NSERC, the Centre de recherches minérales and CANMET of respectively Natural Resources Québec and Canada, for their support of the KBAC research program.

REFERENCES

Åström, K.J. and Wittenmark, B., 1990
Computer-Controlled Systems Theory and Design. Prentice-Hall.

Box, G.E.P. and Jenkinx, G.M., 1976
Times series analysis forecasting and control holden-day. San Francisco, California, 574 p.

Clarke, D.W., Mohtadi, C. and Tuffs P.S., 1987
Generalized predictive control, Part I. Basic algorithm, Part II. Extensions and interpretations. Automatica Vol.23, pp.137-160.

Cutler, C.R. and Ramaker, B.L., 1979
Dynamic matrix control – a computer control algorithm. AIChE National Meeting, Houston, Texas, 1979; also Proc. Joint Automatic Control Conference, San Francisco, California, 1980.

Desbiens, A., Hodouin, D., Najim, K. and Flament, F., 1994a
Long-range predictive control of a rougher flotation unit. Minerals Engineering Vol.7 no.1, pp.21-37.

Desbiens, A., Pomerleau, A. and Najim K., 1994b
Adaptive predictive control of a grinding circuit. Int. J. Min. Proc. (In press).

Foulard, C., Gentil, S. and Sandraz, J.P., 1987
Commande et régulation par calculateur numérique: de la théorie aux applications", Eyrolles, 573 pages.

Garcia, E.C., Prett, D.M. and Morara, M., 1989
Model predictive control: theory and practice - a survey. Automatica, Vol.25, p.335.

Garcia, C. and Morari, M., 1982
Internal model control 1: a unifying review and some new results. Industrial Engineering Chemical Proc. Des. Dev., Vol.21, pp.308–323.

Hodouin, D., Flament, F. and Bazin, C., 1993
Predictive control of flotation plants. Proceedings of the SME Symposium "Emerging Computer Techniques for the Mineral Industry", Reno, Nevada, February 1993.

Hodouin, D., Marcotte, Y., Pomerleau, A. and Flament, F., 1991
Predictive control of grinding circuits – an evaluation by dynamic simulation. Mineral Processing and Process Control, Copper'91, Pergamon Press, Vol.2, pp.377–394.

Irving, E., Falinower C.M. and Fonte C., 1986
Adaptive generalized predictive control with multiple references model. Proceedings of the 2nd IFAC Workshop on Adaptive Systems and Signal Processing, Lund, Sweden.

M'Saad M., 1991
Adaptive control: an overview. Proceedings of ADCHEM 91, IFAC Symp., Toulouse, France, octobre 1991.

Seborg, D.E., Edgard, T.F. and Shah, S.L., 1986
Adaptive control stragegies for process control: a survey. AIChE J., Vol.32, p.881.

Ydstie, B.E., Kershenbaum, L.S. and Sargent R.W.H., 1985
Theory and application of an extended horizon self-tuning controller. AIChE J., Vol.31, No.11, p.1771.

CAMI'95:3rd Canadian Conference on Computer Applications in the Mineral Industry
Montréal, Québec, Canada, October 22-25, 1995

Application of time series analysis to the control and optimization of ilmenite reduction furnaces

Claude Bazin,
Department of Mining and Metallurgy, Laval University, P.Q.

Bruno Girard,
Quebec Iron and Titanium, Sorel, P.Q.

ABSTRACT:

Data collected during the normal operation of ilmenite reduction furnaces of the Quebec Iron and Titanium smelter (Canada) was analyzed using time series techniques. Results show a predictable behaviour in the quality of the titanium slag produced by two furnaces for three different periods of time. The data is currently used to review and standardize the operator practices for the control of the furnaces.

RÉSUMÉ:

Les techniques d'analyse des séries temporelles (suite d'observations prises séquentiellement dans le temps) sont appliquées sur des séries de données prélevées au cours de l'opération normale des fours de réduction de la compagnie QIT-Fer et Titane Inc., située à Tracy (Canada). L'analyse des séries temporelles montre une tendance prévisible de la qualité de la scorie de titane produite par trois fours au cours de trois différentes périodes de temps. Les données sont également utilisées pour réviser et uniformiser la procédure suivie par les opérateurs pour le contrôle des fours.

INTRODUCTION

A time series is a set of observations of a variable taken sequentially in time. Techniques for the analysis of time series make the link between the statistician, the production engineer and the process control engineer. This link has been even more highlighted by the introduction of quality based management in the North American industry since the mid 1980's (Pyzdek, 1989). Box and Jenkins(1976) were probably the first authors to bring time series techniques to the engineer's level. In the early 70's Astrom(1970) introduced the concept of stochastic control that is strongly related to time series analysis.

Pyrometallurgical operations have strongly evolved in the last 20 years. Process control (Verhelst and Prevost, 1993) and Statistical Process Control (Delvecchio,1988) has been introduced in many operations as well as new technologies (Sohn, 1991). On the other hand there have been few reported applications of process analysis by statistical methods to pyrometallurgical plants (Saxén, 1994). This paper examines the potential of applying time series techniques to smelter operation. The variation of the titanium slag chemistry produced by the direct reduction of an ilmenite concentrate was analyzed using time series techniques. The univariate analysis show that potential improvement can be achieved by improving the control strategy for the furnaces. The bivariate time series analysis of the data provided ground to start reviewing training practices.

TIME SERIES ANALYSIS TECHNIQUES

A time series is a sequence of observations of a random variable. The random variable could be daily temperature measurements, weekly average of stock market index, daily LME copper prices....

Theoretically, consecutive observations should be separated by a constant time interval or sampling period. Techniques for the analysis of time series belong to two groups, those of the time domain (Box and Jenkins, 1976; Ljund and Soderstrom, 1983) and those of the frequency domain (Jenkins and Watt, 1968). This paper is concerned with the analysis of time series in the time domain. Commercial softwares such as MATLAB (1989) are now available to perform the type of analysis presented in this paper.

The basic tool for the analysis of a time series is the autocorrelation function (ACRF) used for the detection of trends. The ACRF is a measure of the correlation between observations of a time series separated by one or more sampling intervals. An estimate of the ACRF for observations separated by k sampling intervals, $r_{xx}(k)$, is given by:

$$r_{xx}(k) = \sum_{i=1}^{N-k}[x(i)-x][x(i+k)-x] / \sum_{i=1}^{N}[x(i)-x]^2 \qquad (1)$$
$$k = 0,1,2,3...N/15$$

where x(i) is the i^{th} observation of the time series X(i), N the number of observations in the series and x the average value given by:

$$x = \sum_{i=1}^{N} x(i) \; / \; N \qquad (2)$$

The autocorrelation function is usually presented as a graph of the $r_{xx}(k)$ as a function of the lag k. Figure 1 shows the ACRFs of a white noise (Fig. 1a), for which observations are independent, of an autoregressive process (AR), for which the observations are correlated for an extended period of time (Fig. 1b), and of a moving average process (MA) for which the correlation between observations rapidly vanishes with increasing time between observations (Fig. 1c). The ACRF is used to detect trends in a time series, and as a tool to assess tuning of controllers (Harris, 1989).

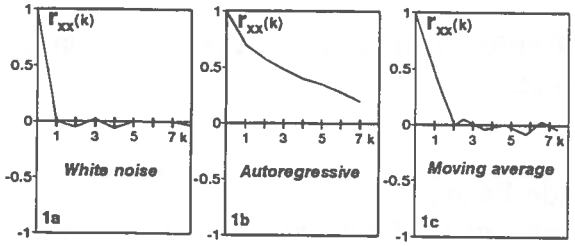

Figure 1. Typical behaviour of autocorrelation functions.

If a time series exhibits correlation between measurements it is possible to model its behavior using an autoregressive moving average (ARMA) model given by:

$$\hat{x}(i) = c_1\hat{x}(i-1)+c_2\hat{x}(i-2)+..+c_p\hat{x}(i-p)+\hat{a}(i) \qquad (3)$$
$$+d_1\hat{a}(i-1)+..+d_q\hat{a}(i-q)$$

where $\hat{x}(i)$ is the modelled value for x(i), the c's and d's are the ARMA model parameters of orders p and q, and $\hat{a}(i)$ a purely random sequence from which the time series is generated. A detailed discussion of the calibration methodology for ARMA models is given by Box and Jenkins(1976). Specialized softwares provide the required calibration routines. Once a model is calibrated on a time series, it can be used to forecast the behaviour of the time series (Box and Jenkins, 1976). Forecasting is extensively used in stochastic controllers (Astrom, 1970).

The crosscorrelation function (CCRF) is used to assess the degree of time correlation between input and output variables. The CCRF at lag k between an input variable U(t) and the output variable Y(t) is estimated using:

$$r_{uy}(k) = (1/N) \sum_{i=1}^{N-k}[u(i)-u][y(i+k)-y] / s_u s_y \qquad (4)$$
$$k = 0,1,2,3...N/15$$

$$r_{yu}(k) = (1/N) \sum_{i=1}^{N-k}[y(i)-y][u(i+k)-u] / s_u s_y \qquad (5)$$
$$k = 0,1,2,3...N/15$$

with u,y and s_u,s_y are respectively the average and standard deviation values for the input and output time series. The $r_{uy}(k)$ measures the correlation between the current value of the input and future values of the output, while $r_{yu}(k)$ measures the correlation between current output values and future input values. This last correlation is used to detect or confirm the presence of a feedback from the output to the input variable.

In the presence of significant correlation between the input and output variables a discrete transfer function (DTF) can be calibrated on the data. The general structure of a DTF is:

$$y_m(i) = a_1 y_m(i-1) + \ldots + a_n y_m(i-n) + b_0 u(i-d) + \ldots + b_m u(i-m-d) \quad (6)$$

where $y_m(i)$ is the modelled output for y(i), a_j and b_j the parameters for the DTF's and d the pure delay in sampling intervals, which is larger or equal to zero. The process gain, or the ratio of change in the output variable following a change in the input variable is given by:

$$g = (b_0 + b_1 + \ldots + b_m)/(1 - a_1 - a_2 - \ldots a_n) \quad (7)$$

where g is the gain. A positive gain indicates that the process output increases or decreases with the input, while negative gain corresponds to an opposite behaviour of the variables. The calibration of the a_j and b_j parameters on an actual input-output system is well described by Box and Jenkins(1976). The ratio of the explained variation by the model to the total variation of the measured variable given by:

$$R^2 = \sum_{i=1}^{N} y_m(i)^2 \; / \; \sum_{i=1}^{N} y(i)^2 \quad (8)$$

could be used as an indication of the ability of the model to represent the total variation of the output variable. Calibrated models can subsequently be implemented in process control strategies (Hodouin and Najim, 1992).

APPLICATION TO ELECTRIC ARC FURNACES

Quebec Iron and Titanium

Techniques for time series analysis have been applied to data collected during normal operation of two ilmenite reduction furnaces at the Quebec Iron and Titanium (QIT) Company in Sorel, PQ, Canada. QIT processes ilmenite ($FeO.TiO_2$) to produce titanium oxide slag, high purity pig iron, steel billets, and iron and steel powders. Ore is mined at the Lac Tio open pit near Havre St-Pierre, PQ and shipped to Sorel where it is enriched by gravity and magnetic separations (Thomas, 1977). The concentrate is mixed with coal and processed in electric arc furnaces to produce metallic iron and titanium slag. Both slag and iron are tapped intermittently. Slag is cooled, crushed and shipped to customers. The molten iron co-product is recarburized, desulphurized, transferred then either to QIT's steel billet plant, metal powder plant, or cast into pig iron destined for the ductile iron foundry industry (Chao, Grau, 1994).

The reduction process of the electric arc furnaces is controlled to maintain a target iron content (Fe) of the slag. The manipulated variables are the coal dosage, noted C factor in the following, and the concentrate feed rate, called the F factor. Slag composition is obtained at each tap. If the iron content is above the target, the operator increases the C factor or/and reduces the F factor. The opposite action is taken when the iron content is below target. Operators manipulate the C and F factors according to their experience of the process but within limits established in the operating norms.

Data collection

Operating data for the furnaces was collected during 1992 and 1993 from production records of furnaces 1 and 5. The records represent three two-month operation periods of about 250 to 450 points per time series. Figure 2 shows the collected time series, expressed as degrees of variation for purposes of confidentiality (as requested by the company). An obstacle to processing this data with time series techniques is related to the non-constant slag sampling period mainly caused by iron taps. Major deviations from the average sampling period were observed during unusual operation such as addition of electrodes, short emergency shut-downs and start-ups. Slag iron content for these periods were replaced

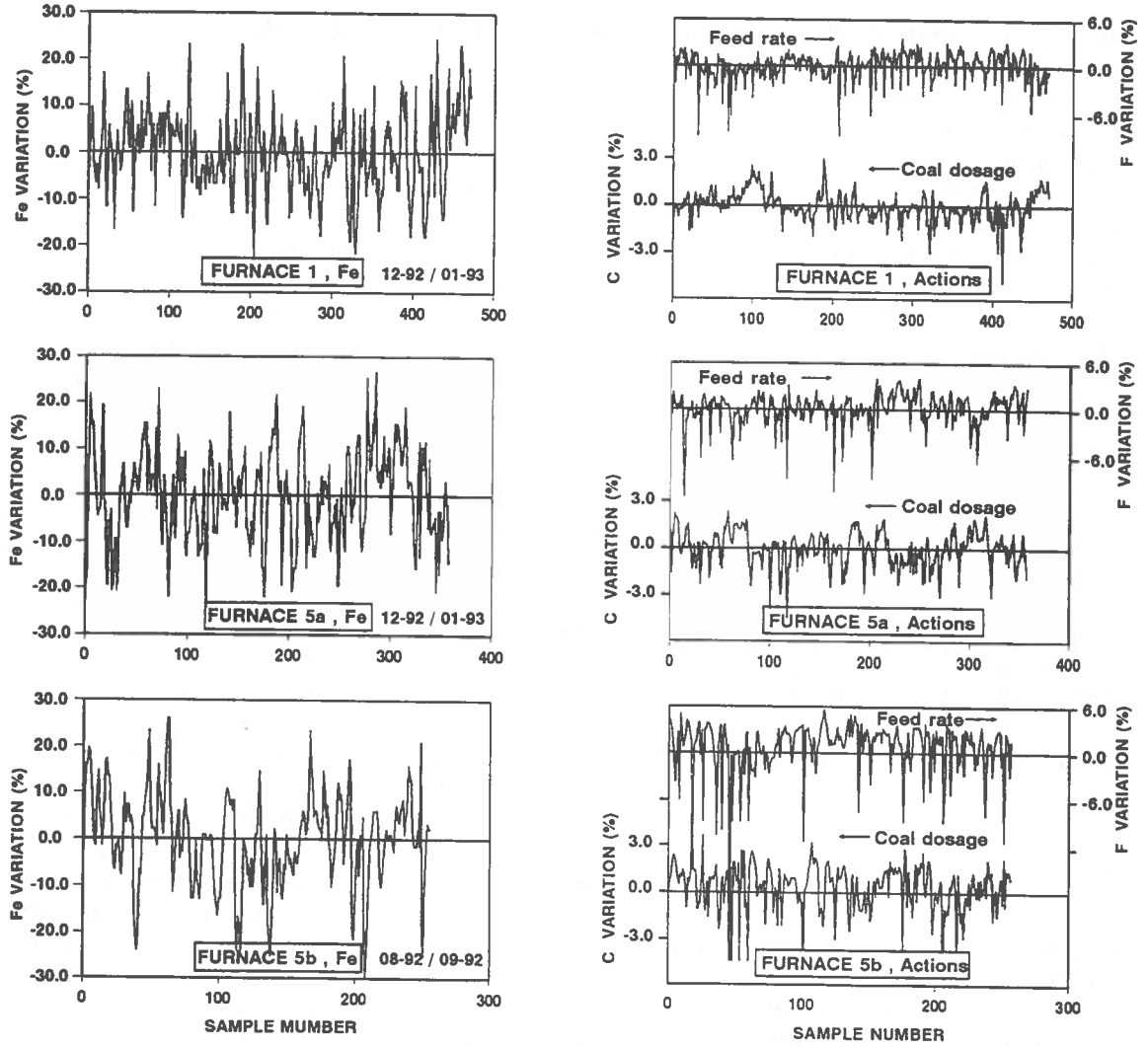

Figure 2. Collected time series. [Variation = 100 (Value-Average)/Average]

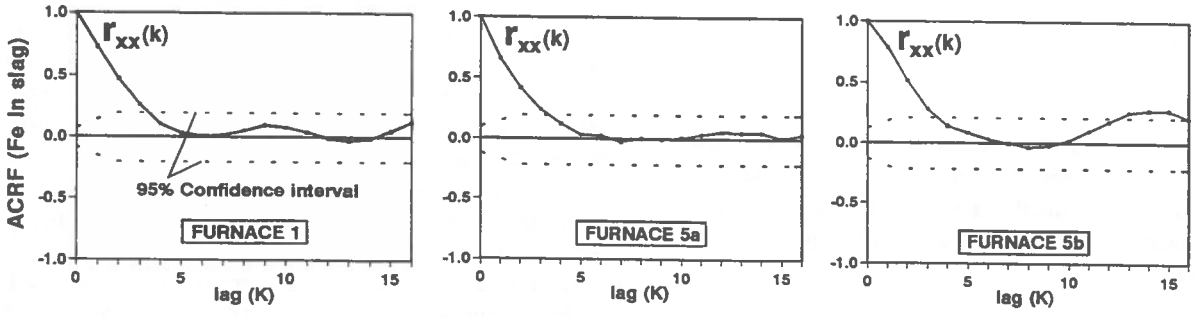

Figure 3. ACRF's for the slag composition.

using a cubic spline interpolation.

Univariate analysis

Figure 3 shows the autocorrelation functions for the slag composition of the series of Figure 2. Although data is obtained from different furnaces and time periods, results show a similar autoregressive pattern. Such behaviour is impossible to detect by a visual inspection of the series in Figure 2. The presence of coloration in the series is an indication that control of the furnace operation can be improved to reduce the variation about the target iron content of the slag (Harris, 1989).

Table 1 gives the calibrated ARMA models for the considered time series of slag composition. An example of reconstructed series is shown in Figure 4 for a portion of slag composition time series for furnace 5, collected during August and September, 1992. For the three sets of data, an autoregressive model of order 2 was found to adequately model the behaviour of the time series. This similitude in the results for two different furnaces and three different periods is indicative of a consistent trend in the operation of the furnaces. Results indicate that 53% of the variation is predictable and can probably be reduced by an adequate automatic control strategy or by improving the operators's training.

Bivariate analysis

To develop the model-based control strategy that was expected to reduce the variation of slag composition, it was attempted to find relationships between input and output variables of the furnace operation. The crosscorrelation functions (CCRF) between current output values (Fe) and future input values (C,F) are shown in Figure 5. The CCRF are calculated from eq. 5 and give the *correlation between current output and future input*. Results for the Fe-C system show a positive correlation for the three data sets. For the Fe-F system the correlation is negative and weaker than for the Fe-C system. The positive correlation between the coal addition and the iron content of the slag indicates that as Fe increases the C factor also increases. On the other hand the negative correlation between the concentrate feed rate factor and the iron content, means that as Fe increases the F factor decreases. In both cases the sign of the correlation is consistent with the plant operating rules. Actions on C or/and F factors are taken according to the slag iron content. This behavior is due to the feedback control action performed by the operators.

The presence of feedback in the data makes the model calibration very difficult unless special calibration techniques are used for data collected from systems operating in close loop (Box and MacGregor, 1974), which is not the case for the actual study. At that stage it was decided to model the operator's behaviour and compare the results to the basic control strategy for the operation of the furnaces. Table 2 gives the calibrated models relating the R and E factors to the iron content of the slag.

An internal study relative to the thermodynamics has demonstrated that the average models of Table 2 are valid (Girard, 1995). The average model relating the C factor to the iron content is given by:

$$C(i) = 0.08Fe(i) + 0.54C(i-1) \qquad (8)$$

which indicates that operators make the adjustment according to the deviation from the iron content target, Fe(i), of the slag and the previous coal dosage adjustment, C(i-1). The presence of the C(i-1) term in eq. (8) transduces an integral action similar to the one carried out by a Proportional and Integral (PI) controller. The parameter values do not change significantly from one data set to another one, which indicates a consistent average behaviour of the operators in the time and from one furnace to another one. There is a rotation of four operators per furnace. However the model explains only 43% of the total C factor variation as it is illustrated in Figure 6 for a portion of the furnace 5 time series. The poor prediction is an indication that actions on the C factor are sometimes significantly away from the average behaviour. Some operators may react strongly to change in iron content while other operators may take smaller actions or prefer to act on the F factor or on both the F and C factors to correct a situation.

The negative gain for the Fe-F process is consistent with plant practice of decreasing the F factor as the iron content increases. The proportion of the F factor variation explained by the model is rather low at 22%, which indicates significant deviations from the average control strategy. The deviation between actual and predicted actions was

TABLE 1. Results of the calibration of ARMA models.

Series	Model	R^2 %
Furnace 1	Fe(i) = 0.86Fe(i-1) - 0.16Fe(i-2) + a(i)	56
Furnace 5a	Fe(i) = 0.72Fe(i-1) - 0.04Fe(i-2) + a(i)	48
Furnace 5b	Fe(i) = 0.88Fe(i-1) - 0.21Fe(i-2) + a(i)	54
Average	Fe(i) = 0.82Fe(i-l) - 0.14Fe(i-2) + a(i)	53

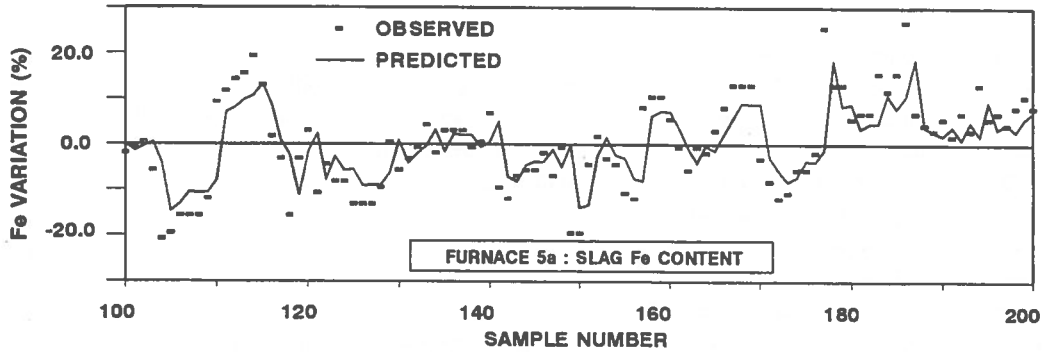

Figure 4. Reconstructed slag composition series (Furnace 5a)
[Variation = 100 (Value - Average) / Average]

TABLE 2. Models for operators control strategy.

Identification	Model	Gain	R^2(%)
Coal dosage adjustment as a function of slag composition			
Furnace 1	C(i) = 0.08Fe(i) + 0.50C(i-1)	0.16	45
Furnace 5a	C(i) = 0.08Fe(i) + 0.49C(i-1)	0.16	34
Furnace 5b	C(i) = 0.08Fe(i) + 0.63C(i-1)	0.22	41
Average	C(i) = 0.08Fe(i) + 0.54C(i-l)	0.18	40
Feed rate adjustment as a function of slag composition			
Furnace 1	F(i) = -0.0074Fe(i) + 0.65F(i-1)	-0.021	18
Furnace 5a	F(i) = -0.0048Fe(i) + 0.75F(i-1)	-0.019	20
Furnace 5b	F(i) = -0.0070Fe(i) + 0.75F(i-1)	-0.018	21
Average	F(i) = -0.0064Fe(i) + 0.72F(i-1)	-0.023	20

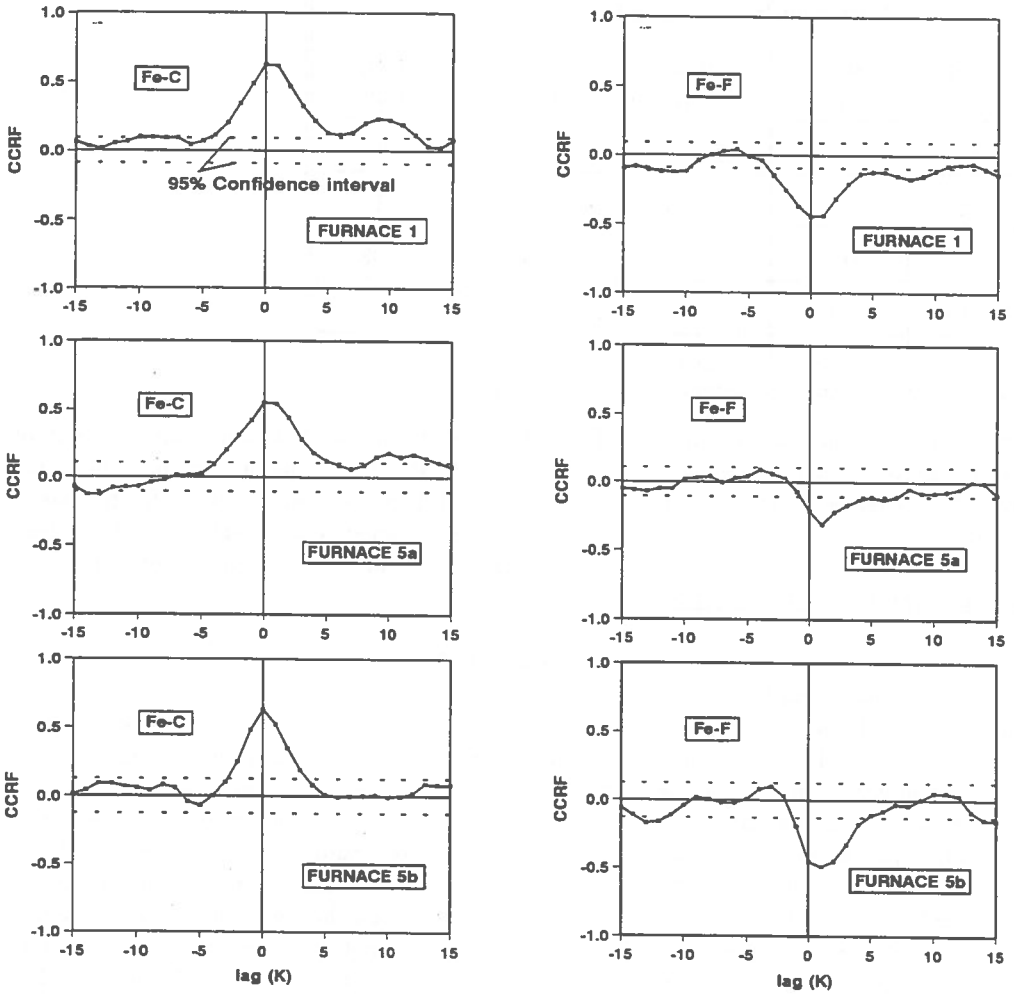

Figure 5. Crosscorrelation functions for the analyzed data sets.

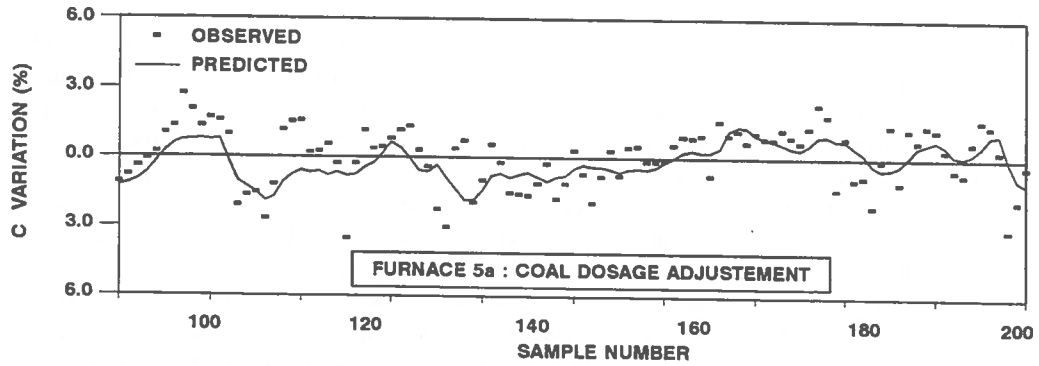

Figure 6. Predicted and actual adjustment of coal dosage (Furnace 5a)
[Variation = 100 (Value - Average) / Average]

TABLE 3. Operating tables for the coal dosage adjustment.

Previous adjustment C(i-1)	Deviation from targeted iron content				
	-1.25; -0.75	-0.75; -0.25	-0.25; 0.25	0.25; 0.75	0.75; 1.25
0.25;0.15	0.03	0.07	0.11	0.15	0.19
0.15;0.05	-0.03	0.01	0.05	0.09	0.13
0.05;-0.05	-0.08	-0.04	0.00	0.04	0.08
-0.05;-0.15	-0.13	-0.09	-0.05	-0.01	-0.03
-0.15;-0.25	-0.19	-0.15	-0.11	-0.07	-0.03

related to insufficient follow-up in the training program, which suggests the need for further operator training or the eventual implementation of an automatic control strategy.

Applications to training and development of process control strategies

The calibrated models (Table 2) were used to prepare operating tables similar to that of Table 3, which give the coal dosage adjustment carried out by the operators according to the slag composition and the previous coal dosage adjustment. A similar table was constructed for the feed-rate adjustment. The two tables were discussed in several meetings with the operators. The discussion led to revised tables which account for operating problems that are not taken into account by the models of Table 2. The revised operating tables were recently implemented for the manual control of Furnace #3 at Quebec Iron and Titanium. Following the implementation of the revised strategy, it was observed that the standard deviation of the slag composition dropped from 1.1% to 0.9% Fe, which confirms that the proposed approach can successfully be applied to the evaluation and improvement of training rules (Girard, 1995). The implementation of the revised training also led to a reduction of electrode consumption with a better thermal and coal efficiency of the furnaces. The next step in the revision of the control strategy will be the forecasting of the slag chemistry using an ARMA model (Table 1). For instance a one step ahead forecast for the slag composition can be calculated using:

$$Fe(i+1|i) = 0.82Fe(i) + 0.14Fe(i-1) \qquad (9)$$

The combined utilization of the constructed operating tables and forecasting equation should allow the operator to optimize its control action. Such strategy may avoid over or under compensation, that can lead to unnecessary variation of the slag composition.

CONCLUSION

Time series analysis was applied to data collected from normal operation of electric arc furnaces. The autocorrelation function of the collected series was used to demonstrate the presence of a well predictable pattern in the variation of slag composition. The presence of this deterministic pattern is an indication that the control strategy could be improved to reduce the variation of slag composition. The calibration of ARMA models showed that a 50% reduction of variation in the slag composition can probably be achieved through efficient process control. Although it was not possible to develop a model based control strategy, a model of the operator strategy was calibrated and used to revise and improve the training program for the plant operators. The model can also be used to initiate the development of an automatic control strategy or the construction of an expert system for process control. Recent results following the implementation on furnace #3 of the operating tables show significant cost savings and a 20% reduction of the variability of one of the furnace product. This last result confirmed the potential of the time series techniques for the training of plant operators. The revised strategy should subsequently be upgraded by the addition of a slag composition forecast using an time series ARMA model.

ACKNOWLEDGEMENTS

The authors wish to acknowledge Quebec Iron and Titanium company for its permission to publish this paper. The project is also funded by the Natural Sciences and Engineering Research Council (NSERC) of Canada.

REFERENCES

ASTROM, K.J., 1970.
Introduction to stochastic control theory, Academic Press, New-York.

BOX, G.E.P. and MACGREGOR, J.F., 1974.
The analysis of closed-loop dynamic stochastic systems, Technometrics, 16, pp. 391-396.

BOX, G.E.P.and JENKINS, G.M., 1976.
Time series analysis: Forecasting and control, Holden-Day, 2nd edition, San-Francisco.

CHAO, J.T., GRAU, A.E., 1994.
Upgrading processes for titanium bearing ores, 33rd annual Conference of metallurgists of CIM, art. 28.5, August 21-25, 1994, Toronto.

DELVECCHIO, O., 1988.
Proceedings of the International Symposium on SPC in the non-ferrous and mineral process industry, CIM General Meeting, August 28-31, Montreal.

GIRARD, B., 1995.
Application de l'analyse des séries temporelles à l'optimisation de fours de réduction d'ilménite, Master Thesis, Laval University, Ste-Foy, PQ, Canada.

HARRIS, T., 1989.
The assessment of control loop performance, Can. J. Chem. Engr., 67, pp.856-861.

HODOUIN, D. and NAJIM, K., 1992.
Adaptive control in mineral processing, CIM Bull., 85(965), 70.

JENKINS, G.M. and WATTS, D.J., 1968.
Spectral analysis and its applications, Holden-Day, San-Francisco.

LJUND, L. and SODERSTROM, T., 1983.
Theory and practice of recursive identification, The MIT Press, Cambridge, Massachussetts.

MATLAB, 1989.
The Math Work, Inc, 21 Eliot Street, South Natick, MA, 01760.

PYZDEK, T., 1989.
What every engineer should know about Quality Control, Marcek Dekker, New-York.

SAXÉN, H., 1994.
Short-term prediction of silicon content in pig iron, Canadian Metallurgical Quarterly, 33,4,pp. 319-326.

SOHN, H.Y., 1991.
The coming-of-age of process engineering in extractive metallurgy, Metallurgical Trans. B, 22B, pp. 737-754.

THOMAS, R., 1977.
QIT-innovative, aggressive, a leader in ilmenite smelting, E/MJ Operating handbook of mineral processing, McGraw-Hill, Inc., New-York, pp. 269-270.

VERHELST, D. and PREVOST, Y., 1993.
Computer-assisted control of the Noranda Process, CIM Bull., 86(969), 94.

13.

mine waste management
aménagement des résidus miniers

CAMI'95: 3rd Canadian Conference on Computer Applications in the Mineral Industry
Montréal, Québec, Canada, October 22-25, 1995

A Conceptual Model for the Flow of Brine Through Salt Backfill

E. De Souza and R.S. Winsor
Department of Mining Engineering
Queen's University

ABSTRACT

The presence and movement of inflow brine in backfilled panels can critically impact the performance of the salt fill, and have a detrimental effect on the overall mechanics and safety of the mining process. This paper describes the development of conceptual models which may be used to predict the flow behaviour of brine in salt tailings backfill material. The developed models involve the solution of 1-D and 2-D transient, saturated, flow equations encompassing both non-Darcy and Darcy flow behaviour, Richards model and the advective-dispersive transport model. Model validation based on laboratory simulation studies indicates that this flow problem is very similar to saturated, subsurface groundwater resource problems.

1. INTRODUCTION

A few potash mines in Canada utilize backfill as an integral component of mining. However, recent environmental and governmental directives have motivated other mines into looking at the possibility of placing salt tailings underground. Research efforts on the part of the potash mining industry have shown that new mining methods involving the use of backfill offer the potential to increase productivity while minimizing ground control and subsidence problems. The presence of inflow brine in backfilled panels can, however, critically impact the performance of the fill. This is due to the physical and chemical interactions that can occur between the brine and the tailings product. An understanding of the phenomenon of brine flow through salt tailings backfill would assist operators in evaluating the operational risks associated with inflow in backfilled panels.

In this paper, conceptual models are used to investigate the flow behaviour of brine in salt tailings backfill material. In this approach, such complex transport physical system, the mathematical treatment of which is quite complex, is replaced by a simpler - yet practical - system, which can be treated mathematically. The mathematical treatment, in this case, involves numerical coefficients which can only be determined experimentally.

Two models have been devised to describe the movement of inflow brine through salt tailings backfill in underground potash mines typical of Saskatchewan (Winsor, 1995): through a bulkhead in a heading designed to isolate areas of inflow from active mine workings (Figure 1) and, through large areas of backfilled panels where backfill may be placed to provide additional ground support in a high extraction mine design scenario (Figure 2). In both these models it may be possible for the brine to inflow directly into the bulk of the tailings backfill structure from a crack in the back, walls or floor. It may also inflow through a crack in an open unbackfilled area and then impinge or seep into the

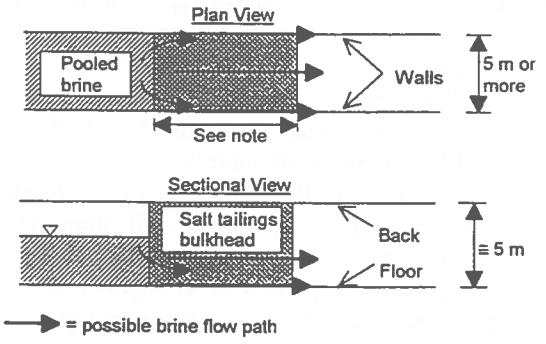

Note: This dimension to be determined by static stability analysis.

Figure 1. Brine flow through salt bulkhead

bulk of the tailings backfill structure as it ponds in the vicinity of the interface between the open space and the backfill. In cases of extreme inflow, the brine may quickly fill the open area and become pressurized, subjecting the bulkhead structure to very high wash out forces.

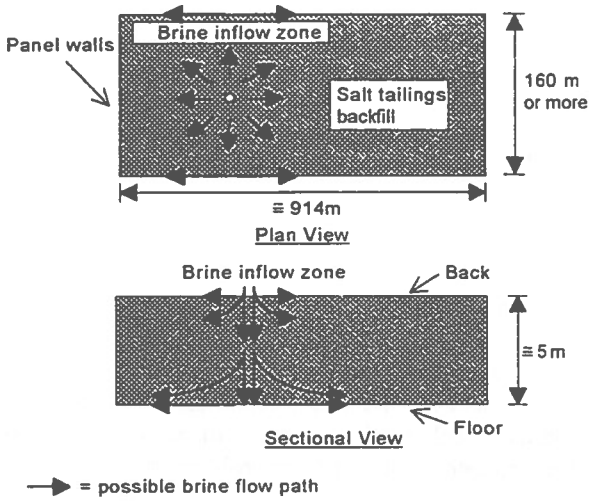

Figure 2. Brine flow through backfill in a high extraction panel

The vertical boundaries of a panel constitute solid salt strata and horizontal boundaries constitute extensions of the solid potash seam. Since these boundaries have low permeability they can be considered as quasi no flow boundaries, capable of vertically and horizontally isolating the bulkhead or backfilled panel. It is common in potash mines for these boundaries to be laced with clay seams which may considerably increase their permeability when roof sagging or floor heave occur. High brine pressures may easily force large quantities of brine through the clay material. It is also important to note that the existence of any gaps between the bulk of the backfill and its boundaries may create preferential flow pathways for brine. These gaps, due to backfill shrinkage, may have a critical impact on the ability of the fill structure to act as a flow barrier.

Since the backfill may be placed with an appreciable brine content it is understood that this brine will be present in the pore space of the tailings during placement and for some time after placement. During consolidation of the salt backfill there will be a time and compression stress dependent release of brine from the backfilled area at regions of lower hydraulic head. These areas may be along the open or exposed face of the tailings backfill pile, where the last of the tailings was placed or where the backfilling process was halted. This brine will have to be dealt with and the maximum quantities of brine released can be estimated with knowledge of the backfill placement tonnage and its brine content.

Flow of brine through salt tailings is further complicated by the fact that brine has the ability to dissolve the solid salt tailings. The brine contains considerable dissolved solids and the reverse reaction can also occur, in which brine liberates or precipitates solid salt crystals. The net effect of salt tailings dissolution and brine precipitation is perceived to be a respective increase or decrease in backfill porosity, which in turn may respectively lead to an increase or decrease in backfill's ability to transmit brine. Also, because very large energy potential discontinuities can occur at the point of inflow, the flow rates will be such that Darcy's law cannot be used to describe flow in the vicinity of the inflow source.

An experimental program has been developed to describe the above models and to determine most parameters important to the phenomenon of brine flow through salt backfill.

2. MODELS OF BRINE FLOW THROUGH POROUS MEDIA

The description of brine flow through backfill involves the solution of transient, saturated, flow equations encompassing both non-Darcy and Darcy flow behaviour. Flow behaviour in close vicinity to an inflow zone may have very high energy potential (20.68 MPa) and thus may be characterized as high flux non-Darcy flow. Flow progressing further from the inflow zone will show a marked decrease in energy potential and thus may be characterized as lower flux Darcy flow. Two other models are presented to describe flow of brine through backfill, Richards model and the advective-dispersive transport model. Richards model, although of less importance in describing brine flow in salt tailings backfill, can be used to describe the physical processes associated with unsaturated flow and transport. The advective-dispersive transport model can be used to incorporate changes in brine concentration, due to chemical interactions, as it travels through the backfill.

2.1 Darcy model

Darcy's law shows that the volume flux of fluid, q (m/s) - defined as the volume of fluid per unit area perpendicular to flow per unit time - is proportional to the cross sectional area, A (m^2), of the medium

through which the flow is occurring, proportional to the difference in the fluid level elevations in the intake and exit of the medium, ∇h (m), and inversely proportional to the medium length, L (m),

$$q = -K.\nabla h = -K.dh/dL \qquad (1)$$

where, K is the hydraulic conductivity (m/s), and $\nabla h = dh/dL$ is the change in fluid head over a length L. The hydraulic head, h, in a groundwater system is,

$$h = z + P/\rho g \qquad (2)$$

where, z is the elevation head (m), P is the fluid pressure (Pa), and ρ is the fluid mass density (kg/m^3).

Darcy's law can thus be expressed in 'pressure' form as,

$$q = - (\partial P/\partial L + \rho.g.\partial z/\partial L).k/\mu \qquad (3)$$

where, k is the intrinsic permeability (m^2) defined as, $k = K.\rho.g/\mu$, and μ is the absolute viscosity of the fluid ($N.s/m^2$).

Darcy's law can only be used to describe a flow phenomenon if the flow is steady state, the Reynolds number, defined as $R_e = q.\rho.D/\mu$, is in the range of 1 to 10, and if the medium is saturated.

The hydraulic conductivity, K, which indicates the ability of a porous medium to conduct fluid under the influence of hydraulic head variations or gradients, may be written as,

$$K = c.d^2.\rho.g/\mu \qquad (4)$$

where, c is some dimensionless coefficient, and d is the mean grain diameter D_{50} of the medium (m).

Salt backfill can be considered as a homogeneous medium with respect to K, that is, its K values are the same, in the same directions, at any point. Time has also a strong influence in determining whether or not the backfill medium could be isotropic or anisotropic. If the K values at a specific point are the same regardless of direction, the porous medium can be considered to be isotropic at that point. Otherwise the porous medium is said to be anisotropic. Anisotropy in groundwater flow problems is usually attributed to nature and stress which may flatten and elongate the individual particles of a porous medium over time. Preferential pathways may also form in aquifers over time due to leaching, chemical and diagenetic processes. With time, similar processes may affect salt tailings. Dissolution and precipitation can form pathways and block pores in the matrix making the directional determination of K a prerequisite for the numerical modelling of any flow problem involving salt tailings. For the purposes of numerically modelling this flow problem, the medium may be considered to have two components of hydraulic conductivity in the horizontal x-y plane. The vertical z dimension may be considered redundant because the production panels in Saskatchewan have very small heights of only 3 or 4 m, while the x and y dimensions of the flow domain may be 1000's of meters. For all practical purposes any developed numerical model would be concerned with the flow of brine in the horizontal plane only.

Since the flow is considered to occur only in the horizontal plane it is highly likely that the flow problem will be isotropic with respect to K, since the tailings material is homogeneous and the hydrostatic stress which compresses the material is normal to both the x and y coordinate directions with the same magnitude in these directions. It is however possible that after long periods of time the backfill could acquire heterogeneous tendencies.

A 2-D form of Darcy law, for an anisotropic medium ($K_x \neq K_y$), is as follows,

$$q = (-K_{xx}.\partial h/\partial x - K_{xy}.\partial h/\partial y) + (-K_{yx}.\partial h/\partial x - K_{yy}.\partial h/\partial y) \qquad (5)$$

and a 2-D transient flow equation to describe brine transport is as follows,

$$\partial(K_{xx}.\partial h/\partial x + K_{xy}.\partial h/\partial y)/\partial x + \partial(K_{yx}.\partial h/\partial x - K_{yy}.\partial h/\partial y)/\partial y = S_s.\partial h/\partial t \qquad (6)$$

or,

$$\partial(K_{ij}.\partial h/\partial x_j)/\partial x_i = S_s.\partial h/\partial t \qquad i,j = x,y \qquad (7)$$

where, S_s is the specific storage (1/m). The specific storage is defined as the volume of fluid that a unit volume of aquifer releases from storage under a unit decline in hydraulic head, given as,

$$S_s = \rho.g(\alpha + \phi.\beta) \qquad (8)$$

where, α is the compressibility of the porous medium (N/m^2), β is the compressibility of the fluid (N/m^2), and ϕ is the porosity.

The term $S_s.\partial h/\partial t$ in equation 6 defines the reduction in medium volume due to compression of the fluid and compression and packing of the grains associated with changes in effective stress.

For an isotropic and heterogenous medium, equation

7 can be written as,

$$\partial(K.\partial h/\partial x_j)/\partial x_i = S_s.\partial h/\partial t \qquad i,j = x,y \qquad (9)$$

and, for an isotropic and homogenous medium, equation 7 can be written as (diffusion equation),

$$\partial^2 h/\partial x_i^2 = (S_s/K).\partial h/\partial t \qquad i,j = x,y \qquad (10)$$

In order to solve the various forms of the flow equation, the boundary conditions must be determined. Typically, a fixed head or Dirichlet boundary condition, or a constant flux or Neumann boundary condition are considered in flow studies.

Model validation based on laboratory simulation studies has indicated that Darcy's model can be used to objectively describe the flow of brine through salt backfill.

2.2 Richards model

The Richards equation, can be used to describe flow of brine in an unsaturated porous medium. It can be derived from the equation of continuity and Darcy's law as,

$$\partial\theta/\partial t = \nabla.(K.\nabla h) + \partial K/\partial z \qquad (11)$$

or,

$$C(h).\partial h/\partial t = \partial[K(h).\partial h/\partial z]/\partial z + \partial K(h)/\partial z \qquad (12)$$

where, t is time, z is the vertical position coordinate, and the hydraulic conductivity, K, may be expressed as a function of the volumetric fluid content, θ (equal to porosity in a saturated medium), or the pressure head, h. C(h) is the specific fluid capacity, defined as,

$$C(h) = \partial\theta(h)/\partial t \qquad (13)$$

A finite difference program can be developed to solve Richards using an approach developed by Whisler and Watson (1968), as follows. The condition of zero flux at the upper boundary is expressed as,

$$-K(h)[\partial h/\partial z + 1]_{z=0} = 0 \qquad t>0 \qquad (14)$$

and the condition of a fluid at atmospheric pressure at the lower boundary is,

$$h(z,t)_{z=-L} = 0 \qquad t>0 \qquad (15)$$

The initial condition is,

$$h(z,0) = h_o(z) \qquad -L<z<0 \qquad (16)$$

where h_o is the initial distribution of the pressure head in the column.

To solve equation 12 numerically, a grid is superimposed on the region $t\geq 0$, $-L\leq z\leq 0$ and the z axis is divided into N intervals, so the mesh points can be defined by, $t_m = m.\Delta t$; $z_n = -(N-n+1).\Delta z$; $\Delta z = L/N$ and m = 0,1,2... and n = 1,2,...N+1.

The partial derivatives in equation 12 may be approximated as follows, with m and n subscripts denoting time steps and depth increments, respectively,

$$\partial(K(h).\partial h/\partial z)/\partial t \approx [K_{n+\frac{1}{2},m-\frac{1}{2}}(h_{n+1,m} + h_{n+1,m-1} - h_{n,m} - h_{n,m-1}) - K_{n-\frac{1}{2},m-\frac{1}{2}}(h_{n,m} + h_{n,m-1} - h_{n-1,m} - h_{n-1,m-1})]/2(\Delta z)^2 \qquad (17)$$

$$\partial h/\partial t \approx (h_{n,m} - h_{n,m-1})/\Delta t \qquad (18)$$

$$\partial K(h)/\partial z \approx (K_{n+\frac{1}{2},m-\frac{1}{2}} - K_{n-\frac{1}{2},m-\frac{1}{2}})/\Delta z \qquad (19)$$

where, arbitrarily,

$$K_{n+\frac{1}{2},m-\frac{1}{2}} = (K_{n,m-1} + K_{n+1,m-1} + K_{n+1,m} + K_{n,m})/4 \qquad (20)$$

and a similar definition holds for $K_{n-\frac{1}{2},m-\frac{1}{2}}$.

The finite difference approximations of 17 through 20 are then substituted into 12, giving,

$$E_n h_{n-1,m} - F_2 h_{2,m} + G_2 h_{3,m} = H_2 \qquad (21)$$

where,

$E_n = K_{n-\frac{1}{2},m-\frac{1}{2}}$; $F_n = 2C_{n,m-\frac{1}{2}}/r + E_n + G_n$; $G_n = K_{n+\frac{1}{2},m-\frac{1}{2}}$; $H_n = G_n(h_{n+1,m-1} - h_{n,m-1}) - E_n(h_{n,m-1} - h_{n-1,m-1}) + 2\Delta z(G_n - E_n) + 2C_{n,m-\frac{1}{2}}.h_{n,m-1}/r$; $C_{n,m-\frac{1}{2}} = (C_{n,m-1} + C_{n,m})/2$; and $r = \Delta t/(\Delta z)^2$.

When equation 21 is applied at n = 2 invoking the boundary condition given by 15, results in,

$$-F_2 h_{2,m} + G_2 h_{3,m} = H_2 \qquad (22)$$

and at n = N, with boundary condition 14, invokes,

$$E_n h_{N-1,m} - (F_N - G_N)h_{N,m} = -(H_N - G_N \Delta z) \qquad (23)$$

Equations 21, 22 and 23 constitute a set of N-1 equations in N-1 unknowns. The solution proceeds in steps of Δt along the t axis. The initial conditions are

used as the first set of $h_{n,m-1}$ values, and as the initial estimate of $h_{n,m}$. The values of E_n, F_n, G_n and H_n are calculated, and the resulting simultaneous equations can be solved by Gaussian elimination for improved values of $h_{n,m}$. The process is then repeated until the change in the h values is smaller than an arbitrary limit. These values are then accepted for the first step and used as the first estimate for the next step. At the end of each time step, the pressure head at the top of the column is calculated from $h_{N+1} = h_N - \Delta z$. Cumulative outflow is calculated by converting the pressure heads into moisture contents, and integrating numerically between the initial and current moisture content distributions. A finite difference program can be easily implemented using the above solution.

2.3 The advective-dispersive transport model

If chemical interactions occur between the brine and salt tailings such that the concentration of brine changes in space and time domains, advection, dispersion, diffusion and adsorption mechanisms must be incorporated into the model. The advective-dispersive equation is the most common means of describing transport of a contaminant in porous media, given in its most general form as,

$$\partial\theta C/\partial t = -\nabla.(\theta qC - \theta D.\nabla C) - \rho_b.\partial S/\partial t \pm \Sigma R_i \qquad (24)$$

or as,

$$\frac{\partial(\theta C)}{\partial t} = \frac{\partial}{\partial z}(qC) - \frac{\partial}{\partial z}\left(\theta D \frac{\partial C}{\partial z}\right) - \rho_b.\frac{\partial S}{\partial t} \pm \Sigma R_i \qquad (25)$$

where, C and S are the solute concentrations associated with the solution and the solid phase of the medium, θ is the volumetric fluid content, t is time, q is the interstitial fluid velocity or Darcy flux, ρ_b is the bulk density of the medium, D is the coefficient of hydrodynamic dispersion, and R_i is the rate of solute production/consumption during fluid-medium reactions.

Hydrodynamic dispersion is a mixing process by which a transition zone develops in the moving solute front, widening with the distance travelled by the front. Across this transition zone, the concentration of the solute varies from that of contaminant liquid to that of the original pore fluid. This mixing is due to the combined action of two distinct phenomena, mechanical dispersion and molecular dispersion. Mechanical dispersion is a result of velocity variations in the flow domain. The degree of mixing due to this effect is a function of the fluid velocity and the configuration of pores in the backfill, which is quantified as the dispersivity. Molecular diffusion is caused by concentration gradients, and so results in a flux of solute even in the absence of fluid motion.

Although the variations of D and θ have long been recognized, a satisfactory means of describing these variations in a general mathematical model has yet to be formulated. The variation of q in the adaptation of Darcy's law to the unsaturated case may be expressed as,

$$q = K(\theta).\partial(P - Z)/\partial z \qquad (26)$$

where, Z is the elevation head, and P is the pressure head. The variation of K with θ is complex, and although difficult to define, it has been experimentally established for brine and salt backfill in this paper. As well, P varies with θ in a nonlinear and nonunique manner.

The mathematical problems caused by nonlinearities, combined with the difficulty in defining values for most of the hydraulic parameters, render the advective-dispersive equation (equation 25) practically unsolvable by computer modelling. Because of these difficulties, physical models have been developed to experimentally address this problem.

3. LABORATORY MODELLING

In order to model the flow of brine through consolidated salt tailings backfill during inflow a Flow Test Apparatus, shown in Figure 3, was designed and fabricated for use in two MTS machines. The system consisted of a tailings compression cell, mounted on a 5000 kN MTS loading frame, used to control backfill compression and creep, and a brine pressurization cell, mounted on a 890 kN MTS loading frame, used to simulate brine inflow. Typical model parameters controlled in each test included compression stress, stress rate, time, total porosity, brine injection volume, rate, and head.

Using samples of brine and tailings procured from an operating mine in Saskatchewan, approximately 2 kg of salt tailings with a brine content of 16% by mass was compacted in the tailings compression cell to develop a constant height of 142.24 cm with a dry density of 1.5 g/cc. After placement the sample was slowly loaded to a target stress of 6.89, 13.79 or 20.68 MPa and compressed for a period of 3, 18 or 87.5 hours. At the end of the compression period

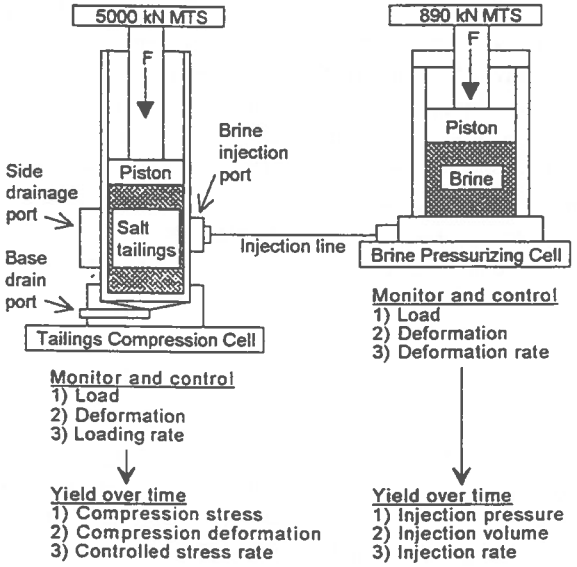

Figure 3. Flow Test Apparatus

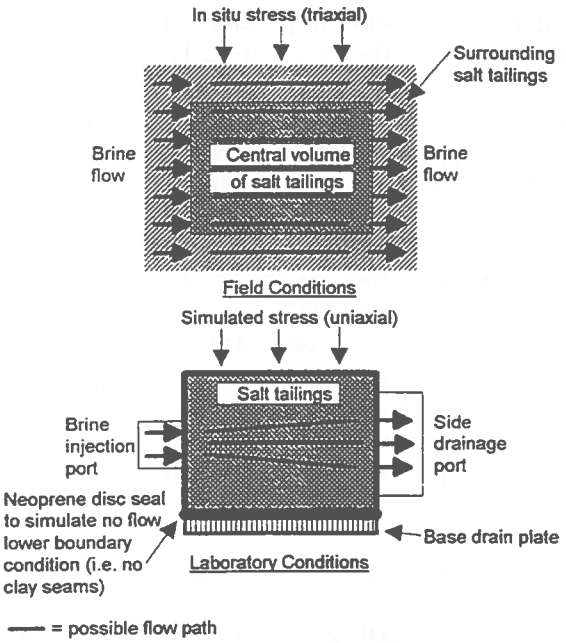

Figure 4. Simulation of flow through backfilled in a high extraction panel

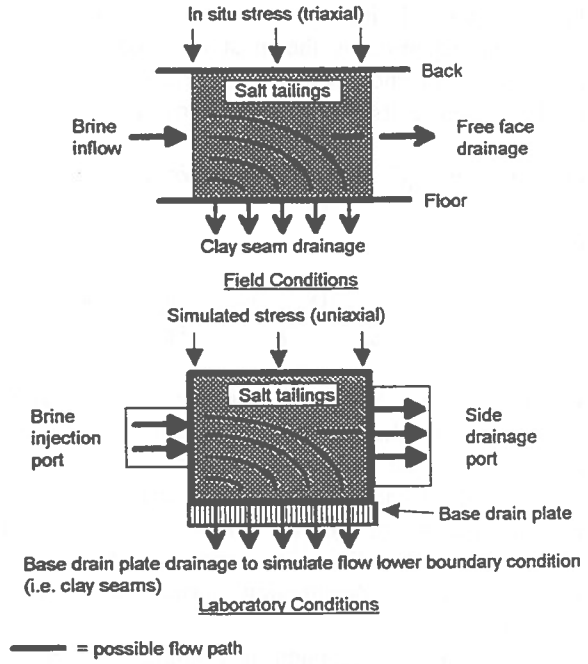

Figure 5. Simulation of flow through a tailings bulkhead in a panel with clay seams in the floor

approximately 1600 mL of brine (4.4 original pore volumes) was injected at constant flow rates of 3.80, 7.60, 15.20 and 30.40 mL/s, into the compressed tailings sample which was still being held at the target stress level. At the end of the injection period the compressed core was extruded from the tailings compression cell and divided into 3 horizontal layers which were then subsequently divided into 9 sections, respectively. Brine content for each of the resulting 27 sections was determined to spatially verify areas in which the injected (inflow) brine was present.

A critical part of the design of the testing apparatus is the accurate representation of the actual field conditions illustrated in Figures 1 and 2, from which three scenarios of brine flow through salt tailings are recognized. The first scenario, derived from Figure 2, involves the flow of brine through a central volume of tailings, as modelled in Figure 4. In this situation brine flow is considered to be primarily horizontal and, although Figure 2 suggests some component of vertical flow in situ, it is considered insignificant, because the vertical dimensions of the panel are so small in comparison to the horizontal. This horizontal state of flow was created by sealing the base drain plate of the tailings compression cell with a neoprene disc and creating a quasi no flow lower boundary condition.

The second and third scenarios, derived from Figure 1, involve both vertical and horizontal or purely horizontal brine flow through a bulkhead, as modelled in Figures 5 and 6, respectively. Figure 5 simulates the situation in which the bulkhead is placed in a panel with clay seams in the floor, which may create leakage of brine through the floor and into other areas of the mine. In this case the clay seams are simulated with an open base drain plate which creates a quasi flow lower boundary condition in the tailings compression cell. Figure 6 simulates the situation in

which a bulkhead is placed in a panel with no clay seams in the floor, which suggests that there be no leakage of brine into the floor of the panel. In the laboratory, this condition was created by sealing the base drain plate with a neoprene disc in the same way as described in the first scenario.

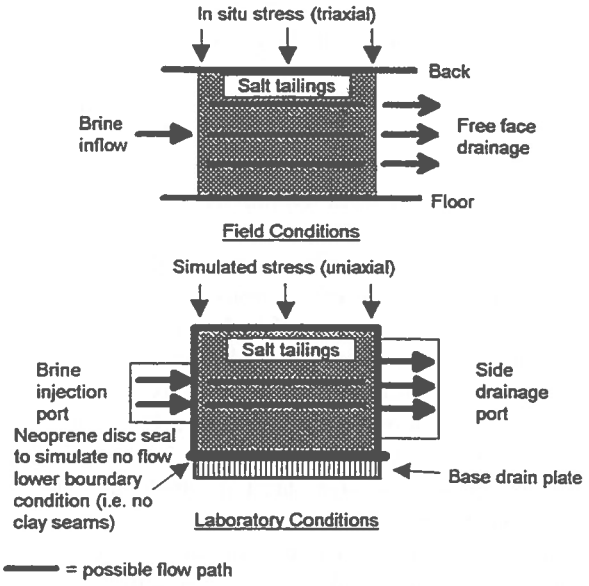

Figure 6. Simulation of flow through a tailings bulkhead in a panel with no clay seams in the floor

4. RESULTS AND DISCUSSION

4.1. Backfill axial strain

Figures 7 and 8 show backfill axial strain (%) versus time (minutes) histories for 8 different models. These relationships were generated as engineering strain, dividing the cumulative change in sample height by the original sample height. These figures reveal that a backfill subjected to brine flow early after placement (i.e. 3 hours) may easily liquefy and possibly fail as a ground support and that at times long after placement (i.e. 87.5 hours) the backfill's support ability is excellent, during and after brine inflow. The initial behaviour of the backfill is attributed to the lubricating and leaching effects that the brine has on the backfill and the change in behaviour over time is attributed to the decrease in permeability of the backfill. This change in permeability, which is time and stress dependent, is a result of grain reorientation and deformation, and the formation of solid crystals in the pore spaces. The general trends in all models also revealed that time has a bigger impact on increasing backfill stability and injection performance than stress. It is also apparent from these figures that the support performance of the fill is greatly reduced in a panel with no clay seams and that at times long after placement the effect of clay seams is less significant.

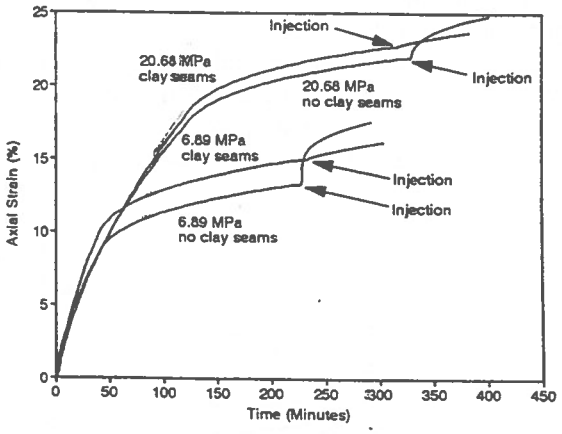

Figure 7. Axial strain vs. time, 3 hours

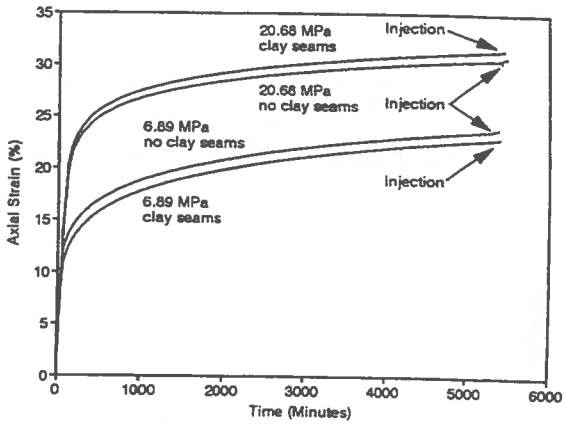

Figure 8. Axial strain vs. time, 87.5 hours

4.2. Backfill total porosity

Porosity is one of the most important parameters in any flow through porous media problem, and in particular to the advective-dispersive transport model. Total porosity is the combination of the dead end and the interconnected porosities. Dead end porosity refers to the volume of pore space in a porous medium that is incapable of transmitting flow of a fluid. In a granular medium such as salt backfill, it may be thought of as a pore area that is partially enclosed or totally enclosed by closely packed media grains. Interconnected porosity is most important to fluid transmission or flow, and it may be thought of as fractures extending through the entire flow domain.

Total porosity (n_t) was calculated from,

$$n_t = (V_T - V_S)/V_T \quad (26)$$

where V_T (cm^3) is the total volume of the sample and V_S (cm^3) is the volume of solids in the sample. Total porosity at the start of each test, was set at approximately 31%.

Figures 9 and 10 show the total porosity (%) versus time (minutes) histories for 6 different models. These plots indicate that total porosity is inversely proportional to time and stress. Typical values of total

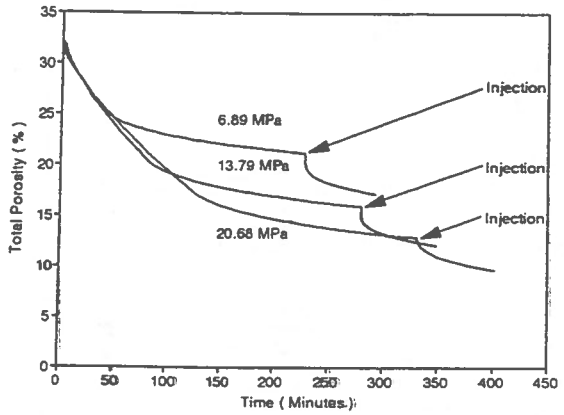

Figure 9. Total porosity vs. time, 3 hours, no clay seams

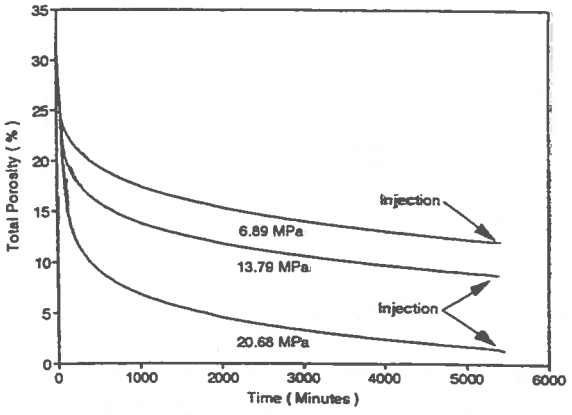

Figure 10. Total porosity vs. time, 87.5 hours, clay seams

porosity at injection for models compressed for 87.5 hours at 20.68 MPa were as low as 2 or 3%, and for models compressed at 6.89 MPa for 3 hours values of total porosity at injection were in the range of 22 or 23%. For a compression stress of 20.68 MPa maintained for 87.5 hours, the total porosity of the tailings sample can decrease by approximately 90% and a stress of 6.89 MPa maintained for 3 hours can result in a decrease in total porosity of 34%.

It is important to note that total porosity calculations reflect only the change in sample volume due to axial strain and do not take into account the possibility of brine precipitate forming between the grains of the salt tailings which would have the effect of further decreasing the total porosity. The formation of this precipitate is believed to be affected mostly by time, backfill drying and the amount of brine present in the backfill to liberate the solid precipitate.

4.3. Backfill hydraulic conductivity

As previously described, hydraulic conductivity indicates the ability of a porous medium to conduct fluid under the influence of hydraulic head variations or gradients. This study provides estimates for K by using the 1-D form of Darcy's law, given by equation 1. In this equation, q = Q/A, where Q was the flow rate of the brine being injected into the tailings sample, A was the area through which the flow was observed to occur which was set at 5.07 cm^2 for all tests, dh was the difference in hydraulic head across the sample, calculated from the measured values of brine injection pressure, and dL was the length of the flow path which was set at 5.08 cm for models simulating clay seams and 10.16 for those simulating flow with no clay seams.

Trends observed in the injection behaviour of the models gave rise to the evaluation of two injection pressures, breakthrough pressure and residual pressure. A typical plot of injection pressure for 3 models is shown in Figure 11. Breakthrough pressure is considered to be the highest pressure recorded during injection, corresponding to the peak of the curve and residual pressure is the arithmetic mean of

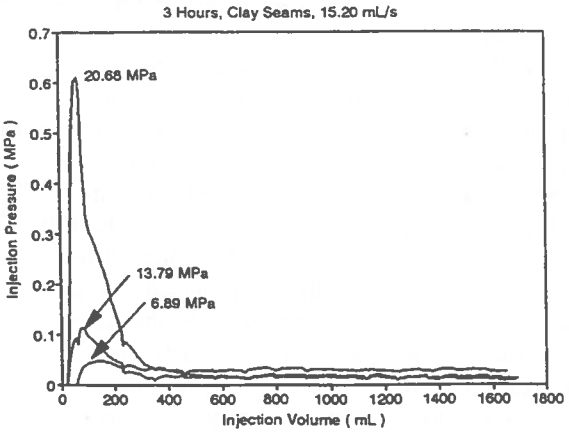

Figure 11. Typical brine injection pressure vs. injection volume relationship

the breakthrough pressure and all the pressures recorded after breakthrough. As a result, breakthrough and residual pressure were used in Darcy's law to calculate estimated minimum and residual hydraulic conductivity, ESTKmin and ESTKres, respectively.

4.3.1. The effect of time and stress on permeability

The measured variations of ESTKmin and ESTKres with time and stress are illustrated in Figures 12 and 13. Trends show that ESTKmin decreases consistently with time and stress. Larger decreases in ESTKmin are noted between the 3 and 18 hour compression intervals with respect to the 18 and 87.5 hour intervals. This difference is attributed to a decrease in tailings compression activity with increasing compression time, and suggests that a fill compressed for less than 18 hours has very little application as a brine flow preventer. Values of ESTKres are consistently 4 to 7 times higher than ESTKmin due to the fact that after breakthrough extensive flow paths were formed from fracturing and dissolution of the tailings solids. Their higher degree of scatter is attributed to the random nature of these occurrences.

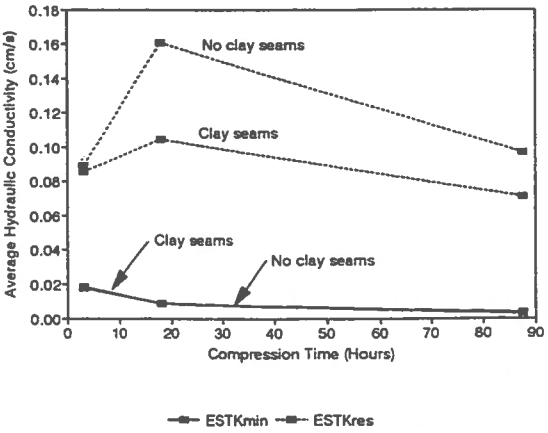

Figure 12. Average K vs. compression time

4.3.2. Total porosity and permeability

Figures 14 and 15 show ESTKmin and ESTKres versus total porosity at injection for nine models. In each of these figures the line of best fit to data is plotted. This line may be used to predict tailings hydraulic conductivity before and after breakthrough. With estimates of backfill total porosity or dry density it may be possible to determine the hydraulic conductivity of the backfill. These values of K can

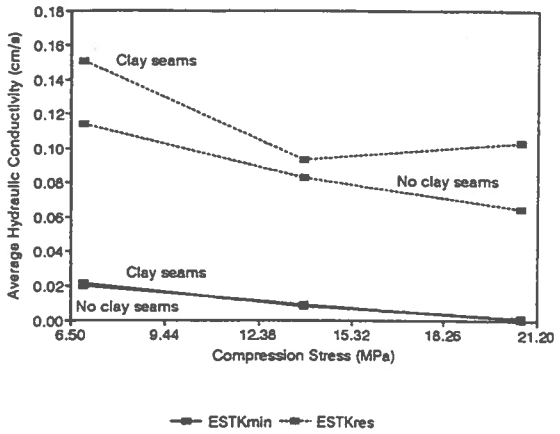

Figure 13. Average K vs. compression stress

then be used to determine the outcome of a brine inflow and possibly even the outflow rates of brine from backfilled panels experiencing inflow.

All plots show clearly that K decreases with increasing backfill density or decreasing backfill total porosity. This is attributed to closer packing of backfill grains, creep compression, and the precipitation of solids from the brine which has the effect of filling pores and reducing preferential flow pathways. Values of ESTKmin ranged from 7.05×10^{-5} to 3.69×10^{-2} cm/s, spanning 4 orders of magnitude with the lowest orders of magnitude appearing on the tailings samples that were compressed at high stress for long time periods. There is more scatter or randomness in the values of ESTKres compared to those of ESTKmin. Again, this may be attributed to the extensive fracturing and leaching processes that occur during and after breakthrough which can be very random in nature. Values of ESTKres ranged from 6.73×10^{-4} to 2.21×10^{-1} cm/s. These values of ESTKres are consistently 1 or 2 orders of magnitude

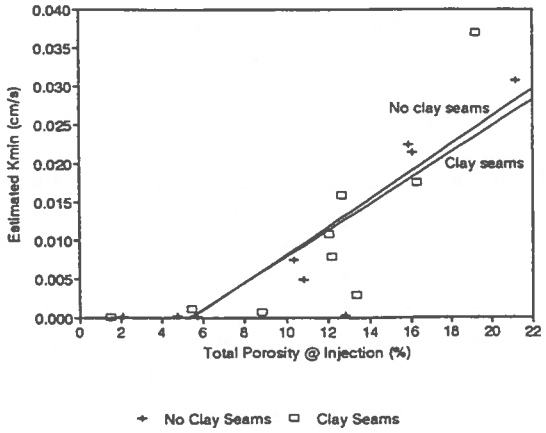

Figure 14. ESTKmin vs. total porosity

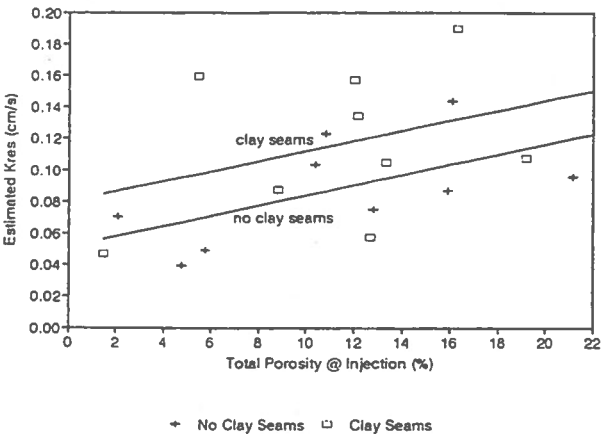

Figure 15. ESTKres vs. total porosity

higher than ESTKmin values. Typical values of hydraulic conductivity for some natural soils obtained from other researchers indicate that the tailings has achieved a hydraulic conductivity at breakthrough similar to that of a silt, very fine sand, and a fine sand (Strack, 1989). This suggests that there is room for further decrease in conductivity with high stress longer term compression simulations. Results also show that backfill with a total porosity of 2% exhibits very good performance as a flow barrier with no measurable hydraulic conductivity.

4.3.3. The effect of injection rate on permeability

Figures 16 and 17 show ESTKmin and ESTKres versus injection rate for 18 hours of compression at 20.68 MPa. In general, these plots show no real trends of increasing or decreasing K with injection rate. K can be considered approximately constant within the same order of magnitude for the flow rates used, which indicates the validity of Darcy's model to describe the flow of brine through salt backfill.

CONCLUSIONS

This paper introduced models and a laboratory procedure capable of describing the flow of brine through consolidated salt tailings backfill, and established relationships and parameters important to the phenomenon of brine movement through backfilled panels. An assessment of the movement of brine through salt tailings backfill and an evaluation of the fill's ability to act as "control barrier" for inflow brine have indicated that salt tailings backfill can be engineered for use as a brine flow preventer while still maintaining value as ground support.

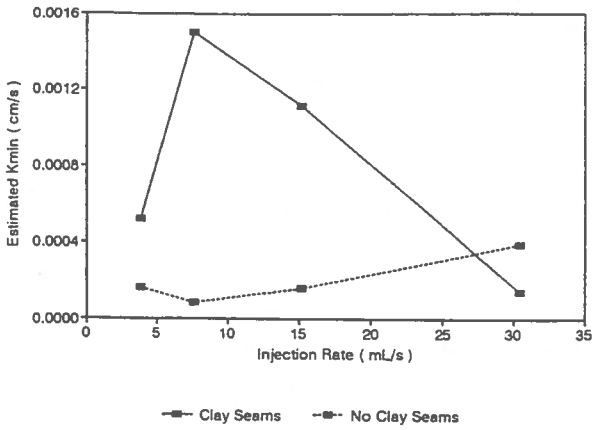

Figure 16. ESTKmin vs. injection rate

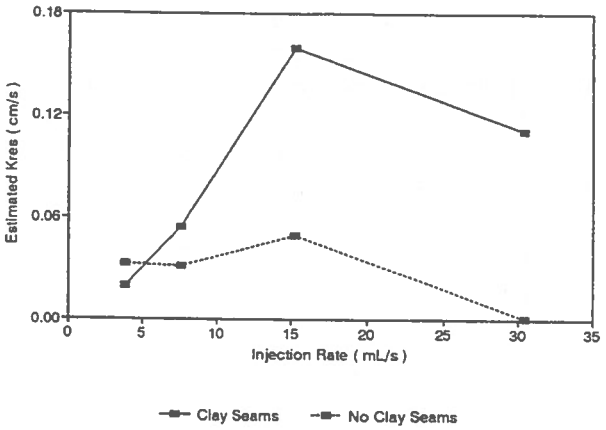

Figure 17. ESTKres vs. injection rate

ACKNOWLEDGEMENTS

Financial assistance was provided by the Natural Sciences and Engineering Research Council of Canada, for which the authors are greatly indebted.

REFERENCES

Strack, O.D.L. (1989) *Groundwater Mechanics*, Prentice Hall Inc., Englewood Cliffs, New Jersey.

Whisler, F.D. and Watson, K.K. (1968) 'One-dimensional gravity drainage of uniform columns of porous material' *Journal of Hydrology*, 6:277-296.

Winsor, R.S. (1995) *The Effect of Brine on the Hydro-Geotechnical Behaviour of Salt Tailings*, M.Sc. Thesis, Queen's University.

Databases for Acid Rock Drainage Prediction and Monitoring

Richard W. Lawrence and Elizabeth J. Sherlock
Department of Mining and Mineral Process Engineering
University of British Columbia, Vancouver, B.C.

ABSTRACT

Acid rock drainage (ARD) is a major environmental challenge facing the mining industry. Proponents of new mining operations and operators of existing mines are required to predict the occurrence and impact of ARD in support of permit applications and closure plan submissions. Prediction of ARD, including the development of models to assess the generation, transport and water quality of acidic drainage, can be aided by the availability of prediction test data produced for other mines and by the data obtained during the monitoring of water quality and other parameters at operating mines. Although large quantities of these data exist, they are not easily accessed since they are largely contained in reports stored in government agency offices across the country. Two databases have been developed to assist researchers, regulators and others involved in prediction and modeling to access relevant data. The first, known by its acronym DBARD, has been restructured to operate in Paradox for Windows and provides detailed data generated in ARD prediction test programs. The second database, WASTEdb provides information on data available from monitoring data obtained form mine waste dump sites. This paper provides a review of these databases and their utility.

RÉSUMÉ

Le drainage minier acide (DMA) est un défi majeur dont fait face l'industrie minière. Les proposeurs de nouvelles opérations minières et les opérateurs de mines existantes sont requis de prédire la présence et l'impact du DMA pour procéder à l'application d'un permis et à la soumission d'un plan de fermeture. La prédiction du DMA, incluant le développement d'un modèle pour évaluer la production, le transport et la qualité de l'eau de drainage acide, peut être facilitée par la disponibilité de données d'essais de prédiction produites pour d'autres mines et de données de contrôle de qualité et autres paramètres de mines en opération. Même si de grandes quantités de données existent, elles ne sont pas facile d'accès puisqu'elles sont contenues dans des rapports déposés dans des bureaux gouvernementaux à travers le pays. Deux bases de données ont été developpées pour assister les chercheurs, régulateurs et autres personnes impliquées dans la prédiction et la modélisation à accéder à des données pertinentes. La première, désignée par son acronyme DBARD, est structurée pour opérer avec Paradox pour Windows et fourni des données de détail générées lors de programmes d'essais de prédiction de DMA. La deuxième banque de données, WASTEdb fournie des informations sur les données disponibles provenants du contrôle de haldes de stérile. Cette article présente une revue de ces bases de données et leur utilité.

INTRODUCTION

Acid rock drainage (ARD) is a widely recognized environmental concern at many mine sites around the world. The oxidation of sulfide minerals in mine rock, ore, tailings and mine walls can generate acidic conditions with correspondingly high levels of contaminant metals. The development of effective closure plans for both new mines and existing mines, where acidic drainage might already be present, depends on the ability to predict with confidence the behaviour of the various mine components when stored in or exposed to the environment during operations and after mine closure. Prediction is a major challenge facing the industry and regulators since, for new mines, the understanding of the long term behaviour of waste materials has to be based to a large degree on the data gained from test programs conducted in the short term. For existing operations, prediction of the ongoing behaviour of wastes is attempted by carrying similarly short term tests and through interpretation of water quality and other monitoring data. In many cases, however, monitoring programs provide only a snapshot in time and might not have included all parameters which are required for a reasonable analysis. Interpretation is not, therefore, straightforward.

Prediction of the occurrence, magnitude and temporal continuity of acidic drainage at a specific site might be facilitated if additional prediction and monitoring data from other operations were available. Data from past studies might provide an indication of future conditions for a proposed mine with similar geographical location, mineralogy, and waste management plan. In some cases, the sum of relevant past work may exceed the work conducted at a proposed mine site and may thus represent a significant component of acidic drainage prediction by pointing to critical information such as ranges in the rates of sulfide oxidation, the relationship between the acid producing and acid consuming components of a waste, and water chemistry. Detailed studies of acidic drainage and metal leaching at proposed mine sites to predict the potential for acidic drainage as well the monitoring of operating waste facilities have been conducted but in many cases the testwork and data are available only in original company reports, making retrieval and re-interpretation difficult and time consuming.

To address these interests and concerns, two databases related to acid rock drainage prediction and monitoring have been developed in the past three years. The first, known by its acronym *DBARD*, the Database for Acid Rock Drainage, was developed through the initiative of the British Columbia Acid Mine Drainage Task Force to accept, store, and retrieve relevant data from acid drainage prediction testwork, including data from one-time or repetitive laboratory experiments and field tests. The second database, *WASTEdb*, the Database for Acid Rock Drainage Research and Monitoring on Waste Rock Dumps, was designed to provide information on the type and availability of data on waste rock dump monitoring, particular for researchers developing mathematical models to predict the quality of drainage from waste dumps. This paper provides information on the structure, operation and function of these two databases which are run using the software program Paradox for Windows.

ACID ROCK DRAINAGE PREDICTION AND MONITORING

Prediction and monitoring are two essential components for the successful management of acid rock drainage and which also includes prevention, control and treatment. An effective prediction strategy is an iterative process involving initially the characterization of waste rock, tailings, pit walls, ore stockpiles and other components which might give rise to acidic drainage upon exposure to air and water. The characterization attempts to provide an understanding of the way in which the various components will behave in the context of a large number of site specific features including lithology, mineralogy, meteorology, hydrogeology and hydrology. An understanding of the behaviour of the components will allow further prediction of the quality of groundwater, surface runoff and seepages which can be affected by numerous physical, chemical, physiochemical and biological controls along the flowpath. If it is deemed necessary to employ ARD prevention and control measures such as underwater disposal of waste rock and tailings, the flooding of open pits, or the application of cover systems over waste materials, the outcome of these proposed measures must also be predicted.

The scope of prediction studies and amount of testwork required to satisfy regulatory requirements for permit application for a new project or a closure plan in Canada can be extensive. A typical prediction assessment will involve the development of a rigorous sampling program; elemental and mineralogical

analysis of samples; leaching tests to determine short term contaminant release; so-called static geochemical tests to determine theoretical acid producing potential; kinetic tests to predict the rates of acid production and contaminant release; development of ARD prevention and control strategies as required; further kinetic tests to determine the efficacy of prevention and control strategies; and the final development of a waste management plan.

Usually the largest volume of data is generated from the static and kinetic tests. Current practice can involve the subjection of up to hundreds of samples to static testing which attempts to determine the balance between acid producing components, principally the sulfide minerals pyrite and pyrrhotite, and acid consuming components such as carbonate and some silicate minerals. Regulators in Canada and many other jurisdictions place significant emphasis on the results of static tests, with values of the arithmetic difference or ratio of the acid potential and neutralization potential used to define mine components which may be safely disposed or which require further evaluation to determine control requirement. Further evaluation is carried out using kinetic testing which, although usually conducted on a fewer number of samples, can generate very large quantities of water quality data.

Monitoring is carried out at, and in the vicinity of, a mine site to determine the effect of mining activities both locally and regionally. Initially carried out to define baseline conditions, monitoring identifies the changes taking place during and after mining. Although monitoring is a requirement of nearly all operating permits to ensure regulatory compliance, most mining companies carry out additional programs to provide early detection of ARD or developing contaminant migration. In addition, monitoring facilitates decisions regarding remediation and reclamation and allows the determination of the effectiveness of ARD control measures.

With respect to ARD, monitoring of surface runoffs and seepages in underground and open pit workings, tailings and waste rock piles is carried out to assess water quality. In addition to the monitoring of chemical characteristics, a monitoring program will also include meteorological data; physical processes such as surface and subsurface water flows and geotechnical stability; and biological response and impact assessment. As with prediction programs, therefore, monitoring programs can generate very large quantities of data over the life of a mining operation and post closure.

Although many of the data generated from prediction and monitoring programs are public domain, in practice such information is not readily available. Many data can be obtained from provincial government departments responsible for the issuing of mining permits, inspection and compliance and from federal agencies such as Environment Canada. Other data are stored in internal company reports. Further details on the technical aspects of prediction and monitoring can be obtained in the proceedings of many conferences held in the past few years or in the reports of the MEND (Mine Environment Neutral Drainage) Program administered by Natural Resources Canada. MEND is a collaborative effort between industry, provincial and federal government agencies, universities and research groups across Canada who donate financial support and time to solving the many facets of the acid rock drainage problem.

CHOICE OF A DATABASE PLATFORM FOR PREDICTION AND MONITORING DATA

Paradox for Windows Version 1.0 was originally selected as the preferred platform the monitoring database, WASTEdb. Based on the favourable experience of this development, Paradox was selected again for the conversion of the prediction database, DBARD. Current versions of DBARD and WASTEdb are programmed to run in Paradox for Windows 5.0.

An initial informal survey of potential users of the databases indicated an equal interest in a database that could be used in either a PC environment or accessed directly via Internet. In the former case, users would be able to access the data using the chosen database platform or by obtaining the data in a .dbf or equivalent format on disk or by computer file transfer. In the latter case, users would be able to browse the database, perform non-Boolean searches, and execute text file transfers via the Internet. Although research into possible formats indicated that both interests could be satisfied within the development budget, the focus became the production of a PC-based product for greater simplicity and lower cost. Following a review of software for PC applications, Paradox for Windows was selected on the basis of relatively low cost, availability, the ability to create database files that can

be used in a variety of software formats, ease of learning and use, design capability, and the availability of local programming expertise. Other popular commercially-available database software such as FoxPro, Superbase, and Access could have been selected and would have likely been as effective as Paradox.

Paradox is a full-featured relational database that can be used either as a standalone system or as a multi-user system on a network. A powerful feature of the software is the application language programming capability for more complex procedures and allows customization of the desired application. Reporting capability is significant, with provision to include graphs and crosstabs for visual impact. The software satisfies the criterion of allowing the creation of the database files in readily usable formats by other software programs. Users of the databases are therefore able to exercise considerable choice in database or spreadsheet selection for manipulating files.

DBARD: THE DATABASE FOR ACID ROCK DRAINAGE

Development History

The original DBARD, developed by Morwijk Enterprises Ltd. of Vancouver, British Columbia, in 1992 was a series of programs written in the dBASE III Plus programming language. As part of the development, ARD prediction data were entered for several proposed and operating mines in British Columbia. Subsequently, the bulk of data acquisition and entry was carried out under the auspices of the Chair of Mining and the Environment at the University of British Columbia. Updated program and database files, together with a user's manual, was released in January 1994 (Lawrence, 1994).

To improve data entry, report generation, and overall ease of operation, the objective of the most recent stage of DBARD development was the conversion of the original DOS-based program to a Window's platform (Lawrence and Harries, 1995). As discussed above, Paradox for Windows was selected for the new format. The change in software platform and its design also allowed the addition of new fields to the database to improve the extent of data, their quality and cross referencing capability. Additional data from British Columbia mines has been entered using the new format. Data acquisition and entry is ongoing.

Organization and Capabilities of DBARD

The general structure of the previous DOS version of DBARD was largely retained. The database can accept, edit and store the information obtained during the testing of various mine components as part of evaluations carried out for waste management planning and permitting. Information is stored on mines (including location, operators, deposit type, general geology, production rate, mining and milling method), identification and description of mine components samples (including, ore, waste rock, tailings, underground walls, open pit walls) and detailed test data (geology, metal analysis, leaching tests, static tests, kinetic tests).

Figure 1 is a schematic of DBARD for Paradox to show the organization of the database and the relationship of the various data entry/edit forms that can be accessed from the main menu form. Each of the forms, designed to facilitate easy viewing, entry and editing of data, is coupled to its corresponding data table which is not accessed during normal operation. An additional table contains information for all of the samples stored in the database.

Technical Overview

The data in DBARD are stored in eight tables: *mindat.db, geology.db, analysis.db, leaching.db, static.db, cycle.db* (part of the kinetic data), *kinetic.db,* and *sample.db*. Over 150 fields are contained in the eight tables. Two tables are global to the rest of the DBARD system, *mindat.db and sample.db*. Each *mindat.db* record has a minekey field which uniquely identifies that mine throughout the DBARD system. The *sample.db* table has two key fields: the minekey and the sample key. These two keys provide a unique way to identify the sample record and link it to its mine.

For the six test data tables *geology.db, analysis.db, leaching.db, static.db, kinetic.db,* and *cycle.db,* each sample record with its accompanying data entered into the test table is linked in two ways to other data:

1) the mine key links the sample directly with the *mindat.db* table

2) the sample key (automatically created every time a new sample record is entered) links the sample to the *sample.db* table which also contains the mine key.

An additional data table to store specific kinetic test details, *kinetic.db*, is accessed from the kinetic form.

A secondary table, called the *drivetab.db* table, links the data tables. Every time a user selects a mine and/or a new component, the *drivetab.db* table is updated to reflect the current choice. This table completes the linkages between all the tables by enabling the user to view how many samples have been entered into a test table for the currently chosen mine and component combination.

Operation and Use of DBARD

Being a Windows-based application, using DBARD for Paradox is essentially self evident for any user familiar with such applications. A detailed user's manual for the database is therefore not essential and most questions regarding its use can be answered by consulting the Paradox manuals. When DBARD is opened within Paradox, the main menu form (see figure 1) is displayed and from which all other forms can be accessed for data browsing, entry and editing.

DBARD for Paradox offers a variety of methods for manipulating, viewing, and printing data, including a tool to convert data to a spreadsheet-type structure. Depending on the complexity of the task at hand, users may utilize one or more methods employing the default methods offered by Paradox 5.0 or by customizing these methods. There are many possibilities, therefore, for the reporting of the DBARD data according the user's requirements and objectives. The current version provides for the attaching of customized reports to buttons on the main form. Design and delivery of such reports can be easily accomplished by accessing the tables of data linked to each entry form. DBARD tables can be exported to other software, for example Excel or Lotus, with the Export tool. This enables users who may be more comfortable using a spreadsheet format to view and manipulate the data. Instructions on the operation of DBARD is provided in the user's manual (Lawrence and Harries, 1995).

Given the broad spectra of individuals who might wish to use DBARD and their specific objectives, the use and manipulation of the data is highly variable and a complete discussion of possibilities is beyond the scope of this paper. However, the following examples, using the static prediction data, highlight some of the possible uses. For these examples, the data was extracted from DBARD using Paradox query formats and then exported to Excel for Windows for further manipulation and graphing.

Figure 2 represents a simple extraction of static prediction data from one mine site. Such graphs are commonly used to interpret the acid potential (AP) and neutralization potential (NP) values determined from static prediction tests. In British Columbia, current criteria used to evaluate these data collected at individual sites include the guideline that the ARD potential will be considered uncertain for materials with an NP:AP ratio of less than 4:1. In such cases, additional testing would be required. Figure 2 shows that, for this particular mine site, there is a broad range of AP and NP values. More importantly, those samples that fall above the 4:1 line would be interpreted to have an uncertain ARD potential, while those below the line have little potential for ARD.

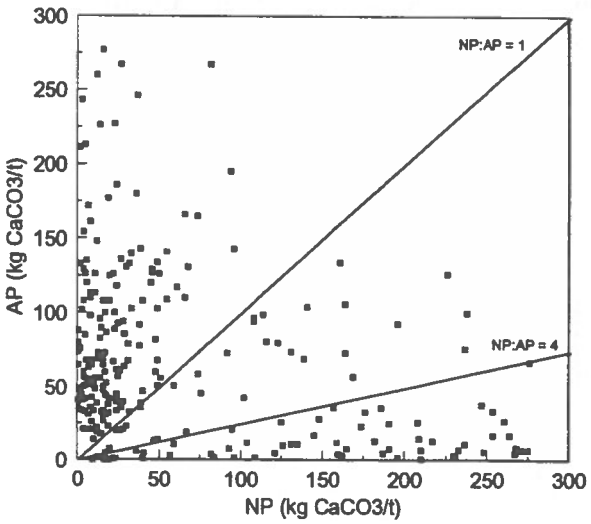

Figure 2. Relationship between NP and AP for a B.C. mine site

Another example of static prediction data use is based on the comparison of sites. This comparison might be useful for new sites in order to use the experience gained at other sites that have, for example, similar geology or be in close proximity. Fields within DBARD allow for the extraction of data to complete such comparisons and, as an example, Figure 3 shows

AP and NP data from two adjacent sites. This figure demonstrates that the two sites, despite their proximity have very different AP and NP values and would have correspondingly different in interpretations. Mine 1 has a very high potential for ARD while Mine 2 has uncertain to no potential.

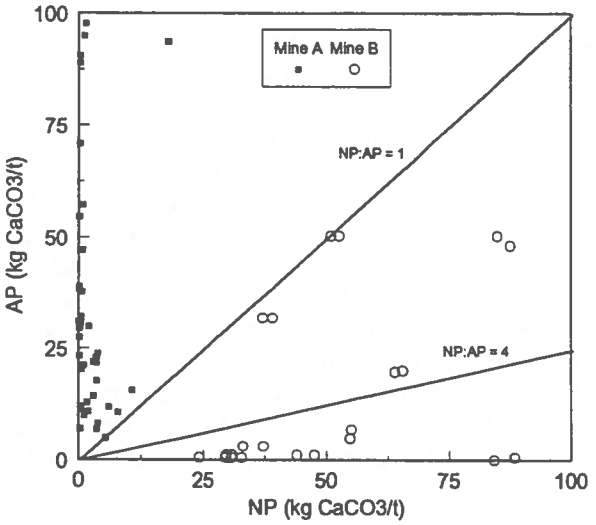

Figure 3. Comparison of NP and AP data for two adjacent B.C. mine sites

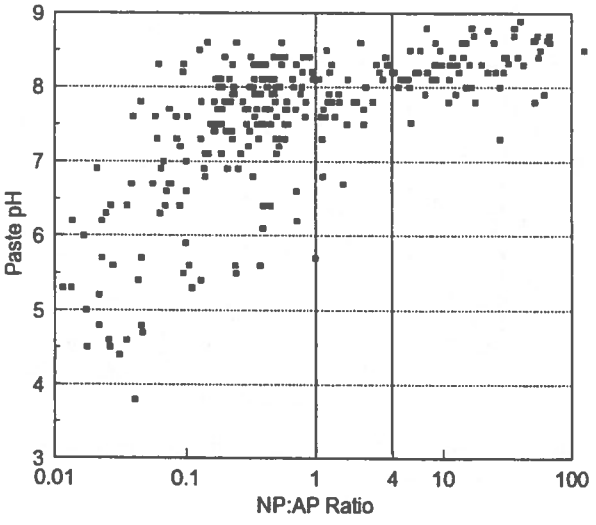

Figure 4. Relationship between paste pH and NP:AP ratio for a proposed B.C. mine development

As a third example of static prediction data, Figure 4 shows the paste pH and NP:AP data for one mine site. Paste pH is a common, easy screening tool for ARD prediction that can be measured in the field. Previous experience has shown that for some sites, a relationship exists between paste pH and NP:AP ratio. Figure 4 indicates that at this particular mine site, paste pH values below 7.0 suggest a NP:AP ratio of less then 4:1. Such correlations can be significant to mine operators since they allows for a quick, relatively inexpensive technique to approximate the NP:AP ratio based on paste pH measurements.

The examples presented here are limited to static test data. However, given the significant number of fields and tables within DBARD, the possible data use and manipulation is essentially unlimited.

WASTEdb: WASTE ROCK MONITORING DATABASE

Development History

An important part of ARD prediction strategies has been the development of modeling techniques to predict the generation, transport and water quality of acidic drainage from mine waste rock. A workshop hosted by MEND was held in 1992 to focus research and development of modeling capabilities and to identify presently available international expertise in this area (MEND, 1992). Since ARD is a problem common to mining operations throughout the world, many international experts participated in the workshop.

It was concluded that a usable water rock model should incorporate: oxygen and heat transport; solute transport and hydrology; geochemistry; and microbiology. Since the prediction of effluent quality from waste rock is not solely a mathematical exercise, the need for applicable field measurements is evident. Monitoring at mine sites and waste dumps is therefore an essential part of the modeling exercise. Two issues with regard to monitoring were identified: what measurements are needed to enable model validation; and what measurements are needed to understand and monitor what is happening at a waste rock dump site over the long-term. Specific requirements for models that could be addressed by evaluating monitoring programs include: identification of significant parameters; location and frequency of measurements; disposal site evaluation; methods of measurement and instrumentation; characterization of waste materials; effect of waste dump design; variations of parameters over time (rates of acid generation and neutralization, contaminant release and loadings, downstream

loadings); hydrology, assessment of control measures, climatic conditions and geographic variations.

It was proposed, therefore, that a database of ongoing studies in waste rock be developed to make best use of all available information to the ARD prediction modeling effort. As with the prediction data described above, monitoring data are not generally available. A monitoring database would therefore provide modeling researchers and others involved in ARD regulation and management a valuable means of determining what data exist and where to find them A contract for the development of this database was initiated in 1993 and completed in 1994 at which time data from 36 mines and 55 associated waste dumps had been entered (Lawrence, 1994). Since the completion of the development contract, additional data have been added.

Organization and Capabilities of WASTEdb

The waste rock monitoring database contains information on monitoring data obtained from waste rock piles in Canada, the United States, Australia and Sweden. The database does not contain the actual monitoring data but rather information on what kind of data are available from different mine sites and how to access them. Information is stored in groupings and includes mine sites (type of mine, operators, location, precipitation, temperatures, hydrology) dump characterization (dump type, method of construction, tonnage, dimensions, geometry, dumping rate, ARD control measures), dump material characterization (geologic materials, composition, mineralogy, static and kinetic prediction data), monitoring program details (program outline, parameters measured, methods and instrumentation, data analysis and modeling) and data access information (contact persons, report names and dates).

The structure of WASTEdb is shown schematically in Figure 5 and indicates the organization and relationship of the various data entry/edit forms that can be accessed from the main menu form. As with DBARD, the tables in which data are stored are not accessed during normal data entry and editing but can be utilized for customized reporting. The entry forms allow easy viewing and data entry and are coupled to their corresponding data tables.

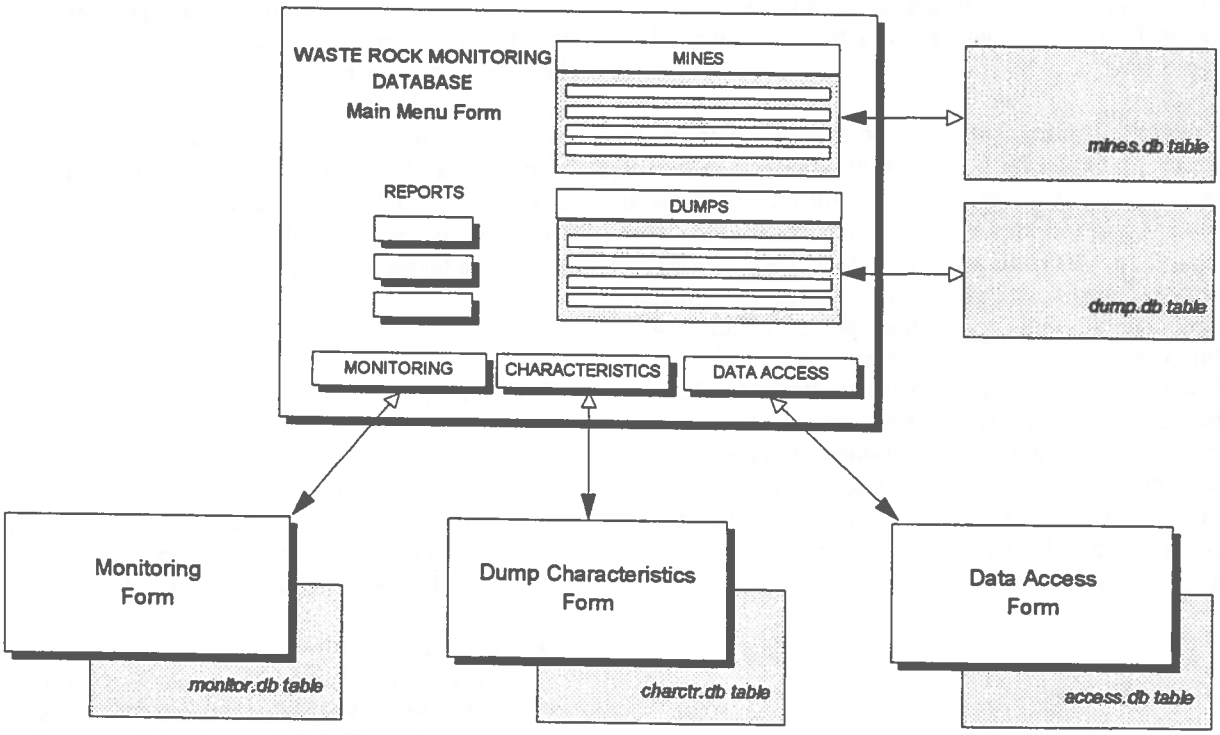

Figure 5. Structure of WASTEdb for Paradox

Technical Overview

The data in WASTEdb are stored in five tables: *mines.db*, *dump.db*, *monitor.db*, *charctr.db* and *access.db*. Nearly 100 fields are contained in the tables. Two tables, *mines.db* and *dump.db* are global to the rest of the database. These tables have a mine key and dump key respectively to identify a specific mine - dump combination throughout the system

Operation and Use of WASTEdb

As with DBARD, operation of the database is very straightforward. When WASTEdb is opened within Paradox, the main menu form (see figure 5) is displayed. The other forms can then be easily accessed for data browsing, entry and editing.

Information for the database was mainly acquired by using a questionnaire sent to persons in the mining industry and researchers in several countries. Operation of the database allows a user to determine what data exists for the monitoring of a specific waste dump site. Detailed information on the mine setting, general dump characteristics, dump material characteristics, and monitoring programs exist for many of the entries. For each dump entered, information on who to contact to obtain further information and actual monitoring data is provided.

Reporting requirements are not anticipated to be as varied as for DBARD. However, the possibilities of reporting for individual users are still too numerous to have considered providing fixed report formats. Two reports are available as part of the current version: a detailed report of one single record of interest, providing all field information for a specific waste dump; and a report containing an output of the entire database. These report formats are attached to buttons on the main menu form. Other customized reports can be similarly attached to additional buttons to suit individual requirements. The reader is referred to the section on DBARD for general comments regarding the use of Paradox for reporting and exporting of data to other software.

CONCLUSIONS

Two databases which store data and information related to the prediction and monitoring of acid rock drainage have been described. Both databases run using the commercially-available database software program Paradox for Windows Version 5.0. The quantity of data related to ARD prediction and monitoring is substantial and not easily accessed in the literature. These databases are intended to provide ready access to these data for mine operators, regulators and researchers concerned with the management, control and regulation of this important mining environmental challenge in Canada and elsewhere in the world. Development of the databases using a Windows-based platform has allowed for easy data entry and editing. Furthermore, the reporting capability of the software provides users considerable flexibility and power to report and manipulate data in a variety of text and graphical formats.

ACKNOWLEDGMENTS

Funding for the development of DBARD and WASTEdb was provided by the Canada/British Columbia Mineral Development Agreement, Energy Mines and Resources Canada, the B.C. Ministry of Energy, Mines, and Petroleum Resources and Environment Canada. Numerous people assisted with bringing the projects to fruition and the development of the databases, notably Bill Price, Grant Feasby, Marcia Blanchette, Henry Steger, Bruce Downing, Peri Mehling, Rob McCandless, Chuck Edwards, Kevin Morin, Nora Hutt, Errol van Huyssteen, Ralph Sayle, Lisa Harries and Sherry Corvalan. We gratefully acknowledge the contribution of these persons and all others who helped to bring the databases to fruition.

REFERENCES

Lawrence, R.W., 1994.
DBARD - The Database for Acid Rock Drainage, MEND Project No. 1.12.1a and BC AMD Task Force Project No. 1.20.

Lawrence, R.W., 1994.
Database For ARD Research And Monitoring On Waste Rock Dumps. MEND Project No. 1.41.2., DSS Contract No. 23440-3-9011/01-SQ.

Lawrence, R.W. and Harries, L.M., 1995.
DBARD for Paradox: Developments in DBARD - the Database for Acid Rock Drainage. MEND Report Project 1.12.1b.

MEND, 1992.
Proceedings of an international workshop on waste rock modeling, Toronto, Canada, September 29 - October 1, 1992, Mend Secretariat, CANMET, Ottawa.

CAMI'95:3rd Canadian Conference on Computer Applications in the Mineral Industry
Montréal, Québec, Canada, October 22-25, 1995

Selected Modelling Approaches to Assess Sulphide Mineral Oxidation in Mine Wastes

R.V. Nicholson
Department of Earth Sciences
University of Waterloo
Waterloo, Ontario

J.M. Scharer
Department of Chemical Engineering
University of Waterloo
Waterloo, Ontario

B. Elberling
Department of Earth Sciences
University of Aarhus, Denmark

E.C.M. Kwong
Department of Chemical Engineering
University of Waterloo
Waterloo, Ontario

ABSTRACT:

The oxidation and leaching of sulphide minerals in mine wastes can lead to water quality problems that require long-term treatment of capital-intensive rehabilitation. Selecting appropriate waste-management alternatives requires some understanding of the outcomes of selected control strategies. Sulphide oxidation and acid generation involve complex physical and chemical interactions that generally require computer simulation.

A series of algorithms and computer codes have been developed over the past few years to i) understand the limits of acid generation and water quality extremes that can develop in sulphide mine wastes, ii) determine the critical controls on sulphide mineral oxidation rates in different waste types and settings and iii) compare pollutant loadings for various rehabilitation strategies, including moist porous-covers and underwater disposal. We have learned that comprehensive models are useful to study complex interactions and to simulate concentrations of trace constituents such as metals in space and time. Simpler models can be useful to interpret the controlling factors on oxidation rates. Diffusion of oxygen has been shown to control this process in tailings whereas diffusion may or may not control rates in waste rock. The latest modelling efforts combine chemical interactions and hydrologic transport, allowing comparison of loadings for selected management scenarios for tailings. The model results provide a focus for decision making but require further evaluation with appropriate field measurements to increase the level of confidence in the predicted behaviour.

INTRODUCTION

Mathematical modelling has become an important tool to assess management options for acid mine drainage. A number of modelling studies have been conducted to investigate the factors contributing to acidic drainage from sulphide-bearing tailings and waste rock (Jaynes et al., 1984; Scharer et al., 1991; Davies and Ritchie, 1986; Elberling et al., 1994; Scharer et al., 1994; Nicholson et al., 1995). Acid drainage results from the reaction between atmospheric oxygen and sulphide minerals in the presence of water. Water quality resulting from sulphide oxidation is generally characterized by elevated levels of dissolved sulphate, iron and other metals and by depressed or acidic pH levels. Many complex processes contribute to the final effluent quality that enters the environment around mine wastes and reliable and precise predictions of contaminant levels targeted by regulators may not be feasible. However, models can be used to couple processes such as chemical and biological kinetics of sulphide oxidation, water flow and chemical transport, gas diffusion and flow that all contribute to the final effluent quality. In this way, we can gain a better understanding of the order-of-magnitude effects of the various contributing processes. It is also possible to study the effects of rehabilitation strategies to provide decision makers with data needed for cost-benefit analysis. The objective of this paper is to illustrate several modelling approaches that have been taken to develop a better understanding of the important processes controlling sulphide oxidation in tailings and to quantify time-dependent trends in these wastes. Each of the models were developed to address specific issues and ask specific questions related to sulphide oxidation and the generation of acidic drainage. Development of the models follow an evolution that highlights a strategy for including essential physical-chemical processes that provide a reasonable representation of the natural system without the extreme complexity of representing all processes in minute detail.

DESCRIPTION OF MODELS

Three models were selected to illustrate the evolution of model development and application. The models are described in more detail elsewhere (Elberling et al., 1994; Scharer et al., 1994; Nicholson et al., 1995). At the centre of all models in the coupling between oxygen diffusion in the gas-filled pore spaces and the reaction kinetics that control the rate of oxidation at the sulphide-mineral surface. The oxygen transport and oxidation reaction are modelled as a one-dimensional problem because of the simple physical boundary conditions that exist in tailings. The fundamental controlling equation is:

$$D_e \frac{\partial^2 C}{\partial z^2} - k f(C) = \frac{\partial C}{\partial t} \qquad (1)$$

where C is the concentration of oxygen, z is depth, t is time and k is the surface-reaction rate constant for sulphide oxidation. Laboratory measurements and model calculations have shown that steady-state is generally attained within days so that for times of weeks to months, the time-dependent behaviour can be ignored. This allows individual time steps of one month to be treated as asymptotic approximations to steady-state and allow time-dependent processes to be calculated through specified time-steps.

The models differ in the treatment of hydrology, chemical components and spatial scale. A brief description of the models follows.

Model I - One-Dimensional/No Chemistry/No Hydrology

This model was developed to investigate the rate of oxidation in a tailings profile with time as sulphide is depleted near-surface. The model is based on gas diffusion except for the first-order reaction-rate shown in equation 1 above (Figure 1). Sulphide minerals are assumed to have an initially-uniform grain size and mass balance is maintained over monthly time steps.

Model II - One-Dimensional/Mixing Cell/Transport/Aqueous and Solids Chemistry

This model incorporates the components of Model I and, in addition, includes simple hydrology and transport through mixing cells along with aqueous and secondary solids chemistry for the key components that control water quality in acidic drainage (Figure 2). The

model was developed to study the effect of important variables on water quality in the oxidation zone of tailings. The goal of the modelling exercise was to identify a critical subset of physical and chemical processes that could adequately describe the generation and modification of acidic drainage in sulphide tailings systems.

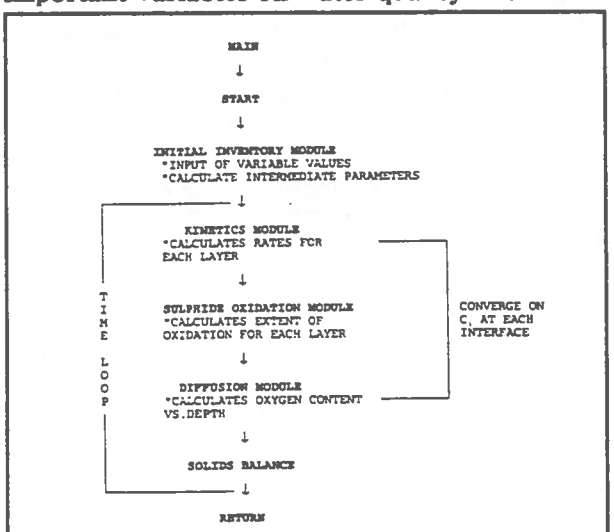

Figure 1: Algorithm for Model I

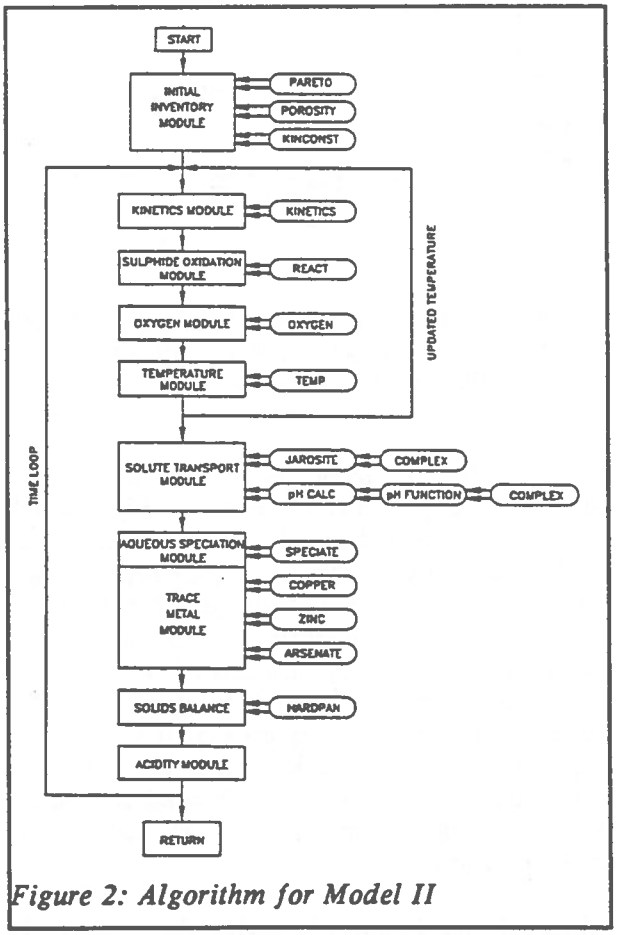

Figure 2: Algorithm for Model II

Model III - Control Volume Reactors/Dispersed Transport/Water Balance/Aqueous and Solids Chemistry

The purpose of this model was to provide a tool to evaluate water quality of the effluent discharged from a tailings basin to the environment. This model incorporates the critical components of Model II for the production of acid drainage in the zone of oxidation above the water table as well as secondary neutralization reactions within and beyond the tailings. In contrast to the One-Dimensional approach taken previously, the model incorporates surface and subsurface flow and solute transport between compartments of the tailings that are judged to have relatively homogeneous conditions for diffusion properties and chemistry among others. The model can be applied to different management scenarios so that various options such as moist soil covers and water covers can be compared. The model allows the application of such management options at special times after the tailings become inactive. In this manner, the effects of history of oxidation prior to rehabilitation can be examined. A schematic of the model processes is given in Figure 3.

RESULTS

Model I

The following results and discussion are based solely on the computer simulations. Initially, the tailings are unoxidized. At early times, an oxidation front is established that extends from ground surface to a depth that depends on the effective diffusion coefficient for a specified rate constant value k. With time, the oxidation front moves downward, resulting in lower concentrations of oxygen available for oxidation and a greater diffusion distance. As a result, the rate of diffusion and oxidation will decrease

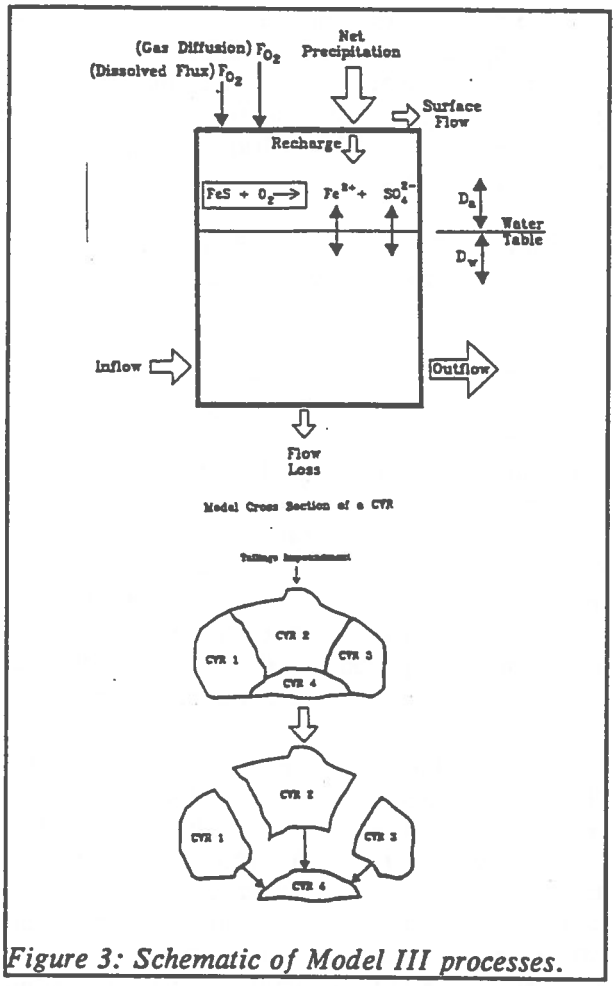

Figure 3: Schematic of Model III processes.

with time. It may be noted that the overall oxidation rate is largely independent of the particle size (silt to sand), and the pyrite content (5-15%) after 100 months of oxidation. Highest oxidation rates were noted initially for fine-grained pyrite, but after a few years the effects disappear. The sensitivity of the oxidation rate to the particle diameter decreases for small particles. The overall oxidation rate is highly dependent on the effective diffusion coefficient; highest rate values correspond to high effective diffusion coefficients. The effect is reduced with the passage of time, however, it is still significant after 30 years of oxidation.

The downward rate of movement of the oxidation front decreases as time passes (Figure 4). The boundary separating the depleted zone from the partially oxidized zone of the tailings moves faster than the boundary separating the partially oxidized zone from the non-oxidized zone. This results in a sharper oxidation front with time. Highest oxidation rates and the sharpest oxidation fronts were noted for the smallest particle size; the differences in the oxidation profile increase significantly with time. The mass of pyrite oxidized monthly at various depths is closely related to the change in pyrite content with depth and time).

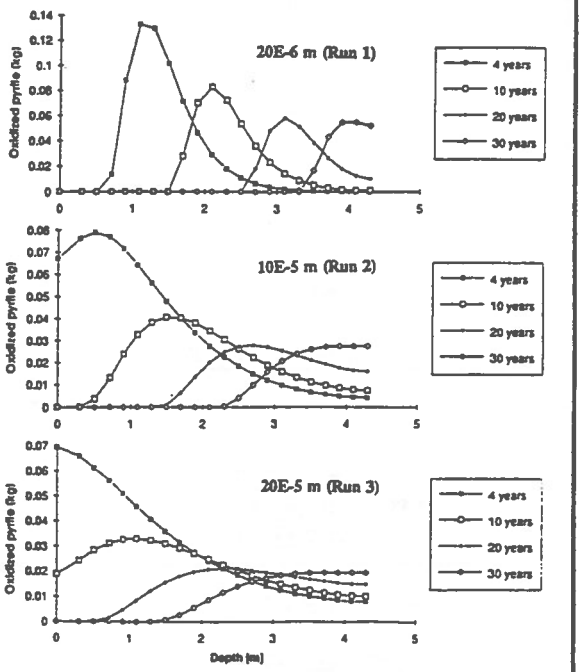

Figure 4: Mass of pyrite oxidized per month as a function of tailings depth for initial particle sizes of 20, 100 and 200 microns.

The effective diffusion coefficients considered in this study ranged from a high value representing well-drained tailings conditions (1 x 10^{-6} m^2 s^{-1}) to a very low value representing nearly flooded tailings conditions (5 x 10^{-11} m^2 s^{-1}). Under well-drained conditions, the oxidation front moves more than 3 m in 4 years compared with nearly flooded condition where the oxidation front moves less than 0.5 m over 30 years (Figure 5). The thickness of the oxidation zone varies from 0.3 m under flooded conditions to greater than 4.2 m after 4 years under well-drained conditions.

Although oxidation of pyrite does occur in abiotic environments represented by the rate constant used here, chemolithotrophic bacteria

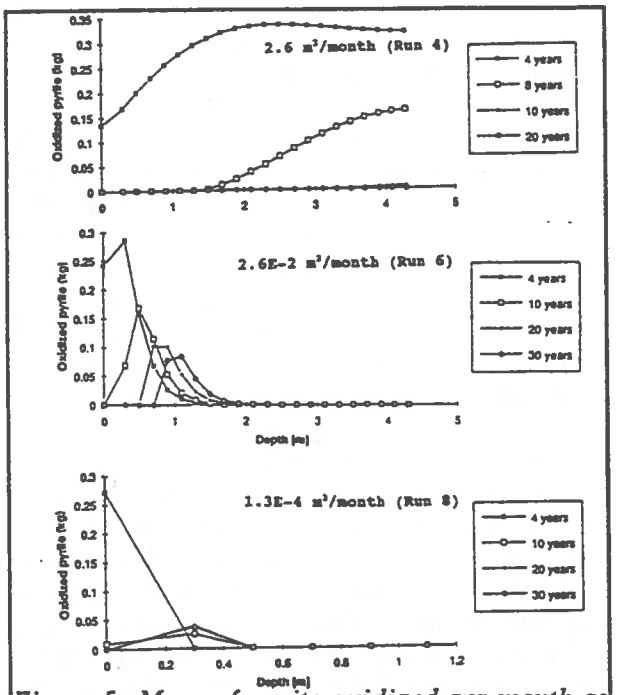

Figure 5: Mass of pyrite oxidized per month as a function of tailings depth for effective diffusion coefficients of 2.6, 0.026 and 1.3×10^{-4} m^2 $month^{-1}$.

can accelerate the intrinsic oxidation rate by a factor of 50 or more. As a result of the ultimate diffusion control with these high rates, a very narrow oxidation front will be observed and diffusion control will dominate.

Model II

In this paper, model simulations are reported for the Nordic tailings management area near Elliott Lake, Ontario. The Nordic tailings cover approximately 100 hectares and contain 12 million metric tons of pyritic tailings. The deposition of tailings in this basin was halted in 1968. The reactive mineral content of the tailings at the cessation of mill operations is estimated to be 6% pyrite (10% in coarse tailings), 5% gypsum, 0.5% calcite, 0.4% ferric hydroxide, 0.2% aluminum hydroxide, and 13.6% sericite. Smyth (1981) collected extensive field data on the site. The data selected for comparison are from two sampling sites (designated as T3 and T5) approximately 0.75 km apart. Location T5 comprises coarse tailings (sands) adjacent to the old tailings discharge pipe. The depth to the water table is 4.0 to 4.5 m. At location T3, the tailings consist of fine material (slimes) and the water table is 6.0 to 6.5 m below the surface.

Conditions for 1968 were used as initial conditions and the simulation was run for 13 years. The model output after 13 years of simulation is compared with field data collected in 1981. There was no parameter adjustment between year zero (1968) and year 13 (1981). The measured and predicted gaseous oxygen concentrations with depth are shown in Figure 6 (location T5).

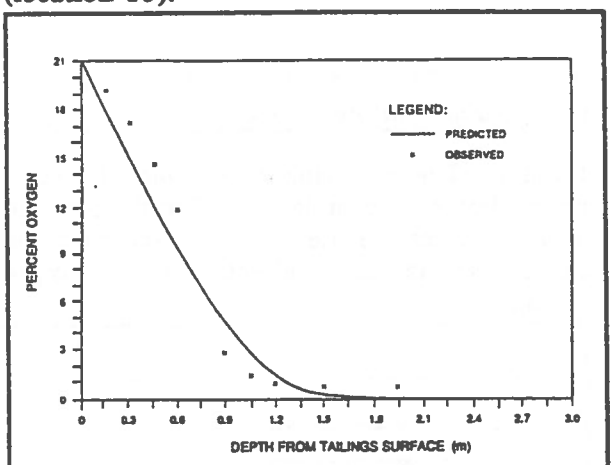

Figure 6: Observed and simulated oxygen gas concentrations at location T5.

The pH simulations for the porewaters at T3 are shown in Figure 7. The predicted pH values are within 1 pH unit of observations, which is reasonable in view of the ionic imbalance noted in the field data. The stepwise profile of the simulations reflect the presence of buffering minerals. Both the measured and simulated pH values were lower in coarse tailings indicating greater depletion of solid buffers under higher acid flux. This is consistent with the higher gaseous porosity, hence higher rate of oxygen transport in coarse tailings.

The residual pyrite content after 13 years of oxidation is shown in Figure 8. The oxidizing front (pyrite depletion) at T3 is sharper, which is consistent with the higher moisture content and higher oxygen gradient in the fine-grained

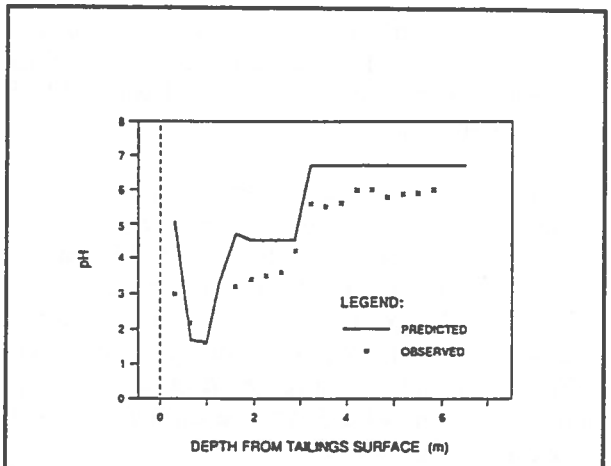

Figure 7: Observed and simulated pH in the fine-grained tailings at location T3.

tailings. The oxidizing zone after 13 years is approximately 1.5 m deep at T3 and 2.5 m deep at T5. The greater depth of the oxidizing zone in coarse tailings reflects higher oxygen transport.

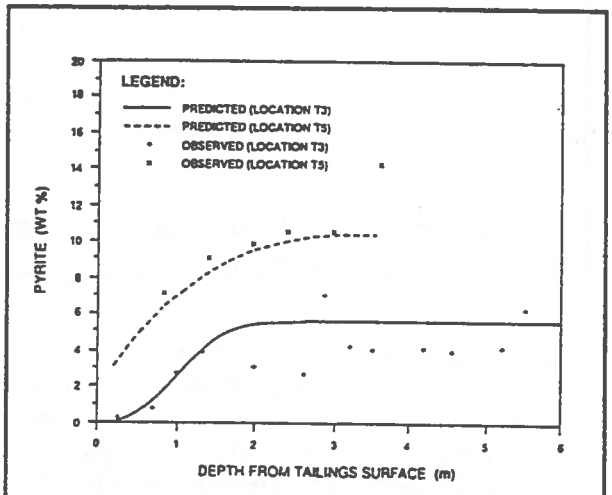

Figure 8: Pyrite content in vertical profiles at T3 and T5 after 13 years simulation.

Model III

An existing pyrrhotite tailings impoundment was studied to assess the effects of flooding and cover construction nine years after the tailings became inactive. The study site is located at the Falconbridge Ltd New tailings pond, Northeast of Sudbury, Ontario. Pyrrhotite tailings were deposited from 1978 to 1986 to a maximum depth of 7.5 m and up to 10% pyrrhotite by weight. A map of the site with model compartments is shown in Figure 9. The tailings deposit consists of relatively homogeneous medium sand- to silt-sized tailings. The tailings pore water generally had pH values greater than 6 below the water table. Pore water in the tailings contained elevated levels of sulphate (up to 5000 mg/L) and iron (up to 500 mg/L). Higher concentrations of sulphate and iron with pH values as low as 3 were observed in pore waters above the water table. The depth of the water table across the tailings varies from 0 m at the edge of existing ponds (CVR-3 and CVR-5) to 1.2 m in the vicinity of the beach (CVR-7) and 2.5 m near Dam #1 (CVR-8). Water flow is generally from Southwest to Northeast where tailings drainage flows into the tailings pond (CVR-2). A more detailed description of the site can be found in Elberling et al., 1993 and David and Nicholson (1995). This site was selected because it had a relatively short history of oxidation with a shallow water table and short subsurface flow paths as well as having areas that were crudely covered by low-sulphur slimes (CVR-5, CVR-6, CVR-8) before becoming inactive. Each CVR was given individual characteristics. Details of the model parameters can be seen in Nicholson et al., 1995.

Falconbridge Ltd was considering action to reduce the long-term release of oxidation products in the effluent from the existing tailings pond. Two management strategies were studied. The first management scenario involves flooding of the entire surface of the tailings in 1995, nine years after becoming inactive. The second management strategy involves the construction of a moderately conservative cover on the currently exposed tailings surface. This cover would have characteristics similar to a 30 to 50 cm thick fine sand or silt as an oxygen barrier that would be covered by a 20 cm layer of coarse gravel to prevent evaporation from the fine-grained layer.

The model was used to evaluate the concentrations and loadings of sulphate and iron in the tailings effluent for 1) the Status Quo, 2)

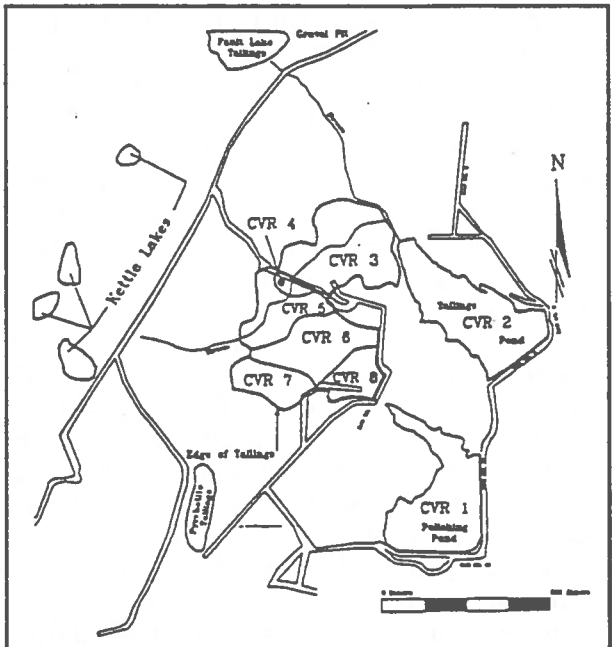

Figure 9: A map of the new tailings site with control volumes shown. Water flow was from CVR7 to CVR2. Scale bar is 800 m.

Flooding the entire surface and 3) covering with a fine-grained Cover Layer (designed as an oxygen barrier). The results of preliminary modelling suggested that both the flooding and the cover could provide significant improvement in the effluent quality from the tailings pond if a significant portion of the sulphide minerals in the tailings above the water table remained unoxidized prior to covering. The results showed that delayed flooding of the pyrrhotite tailings may not provide as significant a reduction of loadings if a large proportion of sulphide was depleted at the time of flooding. The actual proportion of sulphide solids oxidized above the water table over time is very sensitive to the diffusion coefficient of the near-surface tailings and similarly, the calculated rate of oxidation in the model is sensitive to the selected diffusion coefficient for the CVR's. The results of the solids sampling showed that the maximum depth of depletion of sulphide across the tailings was about 0.4 m. The maximum depth occurred near the "beach" in CVR-7, as expected. Little depletion occurred in wet areas near the upper pond above the road dam (CVR-5). Sulphide depletion in CVR-3 above the tailings pond appeared to be less than 0.15 m. The field measurements show that less than 50% of the available pyrrhotite above the water table has been oxidized in well drained areas and far less oxidation has occurred in areas that have wetter layers near the surface or that have shallower water table conditions.

The modelling results show that when the tailings are either flooded or covered at a time of nine years after becoming inactive (1995), that oxidation rates are significantly reduced in those areas, such as CVR-7, that were well drained. Wetter areas (CVR-5) that have lower diffusion coefficients for oxygen at the surface exhibit less dramatic decreases in the oxidation rates as a result of cover application or flooding. These effects are visible in Figure 1- in which the calculated sulphide content of the tailings is plotted against time for the two control volumes. The rate of oxidation is represented by the magnitude of the slopes on these plots. The results for CVR-7 (upper plot) indicate the significant decrease in oxidation rate caused by the management options.

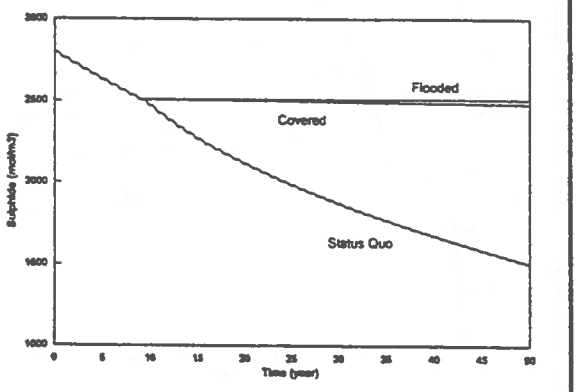

Figure 10: Calculated sulphide content of tailings silids with time for (top) a well-drained tailings and (bottom) a wetter area with a shallow water table.

The effects of rehabilitation are less dramatic in the effluent concentrations leaving the tailings pond (CVR-2). Figure 11 shows the concentrations of sulphate in the tailings pond over time for the three scenarios considered. The

Status Quo scenario suggests that concentrations in the tailings pond attain maximum values of about $2.7x10^{-3}$ mol/L (260 mg L^{-1}) at about 20 years. Calculated concentrations of sulphate in the tailings pond decrease to about $2x10^{-3}$ mol/L (150 mg L^{-1}) after 50 years. Flooding of the tailings results in apparent higher concentrations of sulphate in the tailings pond at 10 years with a rapid decrease to values approaching $1.3x10^{-3}$ mol/L (120 mg L^{-1}) after 30 years. Calculated sulphate concentrations for the cover scenario are intermediate between the Status Quo and the flooded option. The cumulative sulphate loadings for the Status Quo scenario over the 50 year period was estimated to be almost 8 million kg. After either flooding or covering, the cumulative loadings after 50 years do not appear to be significantly reduced but the slopes or rates of increase of sulphate released are much lower than in the case of the Status Quo. The major advantage of flooding is the rapid decrease in the effluent concentrations to long-term steady levels within a time frame of 15 years after flooding or at about 25 years after becoming inactive (time=0 refers to 1986).

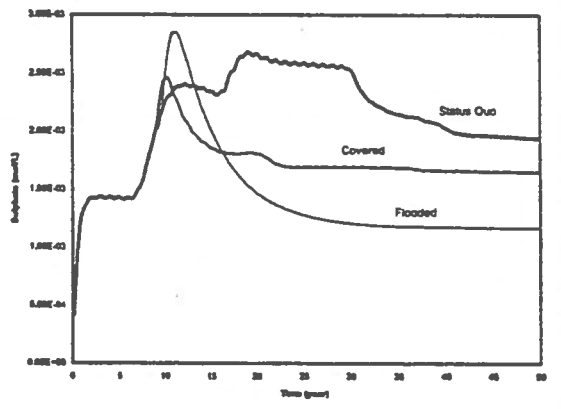

Figure 11: Calculated sulphate concentrations in the tailings pond (CVR2) over a fifty year period.

The trends of the sulphate concentrations and loadings with time can be explained by the various processes acting to control oxidation rates combined with processes controlling transport of dissolved species to the tailings pond. The rates of oxidation are expected to have maximum values soon after tailings discharge ceases when fresh unoxidized sulphide minerals are exposed at the tailings surface. These rates decrease as the sulphide is depleted and longer diffusion paths occur at any specified location. The sulphate concentrations in the effluent, however, do not reach a maximum value immediately because the high sulphate waters must migrate, primarily through subsurface pathways in this case, to the pond. The migration rates and hence the time to observe the arrival of the sulphate depends on the flow rates and travel distances involved. The main reason for the observed peak in effluent concentrations in the flooded scenario is the presence of high concentrations in the near-surface zones and back diffusion of pore water solutes across the entire tailings into the overlying pond . Because the ponded water effectively halts the oxidation process, the concentration of sulphate in the effluent decreases rapidly as upstream and infiltration water washes out the pulse of high sulphate concentrations that results from flooding. The simulations of the cover scenario do not show a similar peak in effluent concentrations because much of the flow system remains as it was before covering with a significant component of downward migration. In this case it is assumed that the cover does not decrease the infiltration of water from rain and snowmelt but it maintains a high moisture content.

The major advantage to management of the tailings either by flooding or the application of a cover is the decrease in the future oxidation of sulphide minerals that remain above the water table at time of intervention. For example, the total quantity of sulphide available above the water table in CVR-3 oxidized in about 20 years with the Status Quo, more than 30 million kg of pyrrhotite. Flooding at year 9 effectively halts the oxidation of sulphide and the total pyrrhotite consumed was about 13 million kg or less than half of the available quantity. Pyrrhotite oxidation continues but at a very slow rate indicated by the almost horizontal slopes of the lines after 10 years, as shown in Figure 10. The cover scenario produced similar results to the flooding option. It is evident that areas with deeper water table conditions, will benefit more from delayed management intervention than areas with shallow water table conditions. When

the total loadings from each of the oxidizing compartments is compared for each of the management options to the Status Quo, it is estimated that flooding or covering will prevent oxidation of 50 to 60% of the available pyrrhotite. These calculations show that the Status Quo produces the equivalent of 82 million kg of sulphate over a 50 year period compared to 30 and 35 million kg for the flooded and covered scenarios respectively.

CONCLUSIONS

Computer models provide tools to investigate processes that control and behaviour resulting from oxidation of sulphide mine wastes. Different models with differing levels of detail and sophistication can be used to address a variety of questions related to fundamental processes to application of waste management strategies. Modelling efforts to date have focused on developing a better understanding of controlling processes and quantification of temporal trends for acid production rates and effluent quality. Model applications allow comparisons of various management scenarios to provide a basis for cost-benefit analysis. Currently and in the foreseeable future, these models and others will not be capable of providing precise predictions of trace metal concentrations that are targeted by regulators. Rather, the models can provide reasonable ranges for loadings of oxidation products, including some trace metals. Loadings are not as sensitive to the natural variations in flow rates, especially surface flow, that tend to decrease confidence in forecasting concentrations even if all of the chemical and physical processes are well described in a model.

Modelling exercises, such as those described in this paper, increase our knowledge about sulphide waste behaviour and the potential influence on the receiving environment. It is important that we apply such tools judiciously to appropriate problems so that our conclusions are reasonable and appropriate for a specific waste management objectives.

REFERENCES

David, D.J. and Nicholson, R.V., 1995. Field measurements for determining rates of sulphide oxidation. Proc., Sudbury '95 Conference on Mining and the Environment, Sudbury, Ontario, May 28-June 1.

Davis, G.B. and Ritchie, A.I.M., 1986. A model of oxidation in pyritic mine waste: Part 1: Equations and approximate solution. Appl. Math. Model., 10:314-322.

Elberling, B., Nicholson, R.V. and Scharer, J.M., 1994. A combined kinetic and diffusion model for pyrite oxidation in tailings: A change in controls with time. J. Hydrol., 157:47-60.

Elberling, B., Nicholson, R.V. and David, D.J., 1993. Field evaluation of sulphide oxidation rates. Nordic Hydrology, 24:323-338.

Halbert, B.E., Scharer, J.M., Knapp, R.A. and Gorber, D.M., 1983. Determination of acid generation rates in pyritic mine tailings. Paper from the 56th Annual Conference of the Water Pollution Control Federation, Atlanta, GA.

Jaynes, D.B., Rogowski, A.S. and Pionke, H.B., 1984a. Acid mine drainage reclaimed coal strip mines 1. Model description. Water Resour. Res., 20:233-242.

Nicholson, R.V., Scharer, J.M., Kwong, E., Annable, W. and Williams, G., 1995. An application of the WATAIL model to develop a management strategy for a pyrrhotite tailings impoundment. Proc., Sudbury '95 Conference on Mining and the Environment, Sudbury, Ontario, May 28-June 1.

Nicholson, R.V., Elberling, B. and Williams, G., 1995. A new oxygen consumption technique to provide rapid assessment of tailings reactivity in the field and laboratory. Proc., Sudbury '95 Conference on Mining and the Environment, Sudbury, Ontario, May 28-June 1.

Scharer, J.M., Nicholson, R.V, Halbert, B. and Snodgrass, W.J., 1993. A computer program to assess acid generation in pyrite tailings. Environmental Geochemistry of Sulphide

Oxidation, Alpers, C.N. and Blowes, D.W. (eds.), ACS Symposium Series 550, 132-152.

Scharer, J.M., Garga, V., Smith, R. and Halbert, B., 1991. Use of steady state models for assessing acid generation in pyritic mine tailings. In: Proc. 2nd Int. Conf. on the Abatement of Acidic Drainage, Montreal. Vol. 2, pp. 211-230.

CAMI'95: 3rd Canadian Conference on Computer Applications in the Mineral Industry
Montréal, Québec, Canada, October 22-25, 1995

Components in the Design of Engineered Soil Cover Systems for Acid Generating Mine Waste

D.A. Swanson
PTI Environmental Services, Boulder, Colorado, U.S.A.

S.L. Barbour, G.W. Wilson, and M. O'Kane,
Unsaturated Soils Group, Department of Civil Engineering, University of Saskatchewan, Saskatoon, Sask., Canada

ABSTRACT:

Closure options for the decommissioning of acid generating mine waste often include soil cover systems. The development of a methodology for the design of an engineered soil cover system requires an understanding of the theoretical framework and behavior of unsaturated soil systems. This paper describes a methodology for the design of engineered soil covers which consists of three components. The first component involves laboratory characterization of potential cover materials. The second component utilizes computer modelling techniques to select the most effective cover design. The third component includes the development of field test plots to evaluate and improve model predictions to allow for confident selection of an optimum cover design.

This paper focuses on a computer modelling methodology for the design of an engineered soil cover system. Computer modelling includes the transient simulation of water (liquid and vapor) and heat transport within the soil-cover system coupled to the atmospheric demand imposed on the system (precipitation and evapotranspiration). The computer modelling methodology is divided into three stages. The first stage involves preliminary modelling to select cover designs to be incorporated in field test plots. The second stage, referred to as field response modelling, involves comparison of the computed and measured responses for the field test covers. For example, measured and computed soil suction profiles are compared as well as changes in moisture content, percolation through the cover, and surface runoff. Calibration of the numerical model is carried out in this stage to improve the accuracy for long term predictions. Predictive modelling is the third and final stage of the numerical modelling methodology and involves the use of the calibrated models to make long-term predictions for selected cover designs. An optimal design can then be selected from the calibrated simulations.

INTRODUCTION

The containment of acid mine drainage from waste rock piles and tailings facilities left over from the mining and milling stages has been described as the largest environmental problem facing the mining industry today (The Financial Post, 1992).

Acid rock drainage (ARD) results from the exposure of sulphide bearing waste rock and tailings to air and water. The oxidation of sulfide bearing rocks and tailings through exposure to air, combined with infiltration due to rain and snow melt results in drainage that is low in pH and high in heavy metals. The extent of the potential environmental impacts are put into perspective upon realization that waste rock piles approaching hundreds of millions of tonnes exist at many open pit mining operations.

An engineered soil cover is often used to reduce the extent of acid rock drainage by limiting the influx of precipitation and oxygen to the sulphide bearing material. Waste material deposited in humid regions can take advantage of the benefits of a compacted clay based cover design. Infiltrating waters are kept to a minimum by the low hydraulic conductivity of the cover material while oxygen influx is minimized by maintaining a high degree of water saturation in the cover. A clay cover is not always practical for waste material deposited in arid climates due to the high potential for desiccation of the cover. Cover materials with the capacity to store infiltrating waters for extended periods are used as

an alternative. The potential then exists for evaporation and plant transpiration to extract the stored moisture before infiltration into the waste occurs.

The ability to predict how a cover system will perform with respect to limiting infiltration and oxygen influx is critical as owners of waste facilities must develop effective and economical decommissioning strategies. Furthermore, regulatory agencies must be able to assess these decommissioning strategies to determine their effectiveness and acceptability.

COVER DESIGN METHODOLOGY

The design methodology for engineered soil covers is comprised of three components. These include material characterization, computer modelling, and instrumentation of field test plots. The relevant soil properties of potential cover and waste materials must be characterized to provide an initial screening of cover designs and to provide the necessary input for numerical modelling efforts. Numerical modelling is performed first to identify feasible cover

The design methodology is illustrated in chronological fashion in Figure 1. The following sections elaborate on the components outlined in Figure 1 with an emphasis on the computer modelling component.

Identification and Characterization of Potential Cover Materials

Potential cover materials are collected and tested for hydraulic and moisture retention properties. The objective of the laboratory program is to identify potential cover materials for use in layered soil cover systems. Choice of optimal cover materials depends several factors. These include: on site climate conditions (i.e. arid/semi-arid or humid), suitability of layering different soils in order to take advantage of capillary breaks, and physical integrity of the soil cover system in terms of slope stability and erosion. Naturally occurring local material is probably the most economic. However, local material may not possess the required characteristics and alternative materials and/or cover designs must be identified.

design options for incorporation into field test plots, and secondly to select an optimal design based on simulations calibrated to field conditions.

An understanding of the behavior of unsaturated soils is essential in dealing with the three design components. Fredlund and Rahardjo (1993) present a framework which describes the theory, measurement and application of the fundamental properties of an unsaturated soil (i.e., hydraulic conductivity, shear strength, and volume change indices). This provides the bases to adequately characterize soil cover systems. The computer modelling component is carried out using SoilCover (MEND, 1993), a finite element water and heat flow model developed at the University of Saskatchewan to simulate the movement of moisture and heat within saturated and unsaturated cover systems. The model which was originally developed by Wilson (1990) is coupled to atmospheric supply and demand (i.e., precipitation and evapotranspiration) to allow for the description of cover performance based on a continuous natural soil system (i.e., soil to the atmosphere).

In general, the laboratory test program includes grain size analysis, consolidation - permeameter testing, and moisture retention characteristics testing. The most important component of the laboratory program is the accurate measurement of the relationship between soil suction and water content for each potential cover material. Each component of the laboratory program should account for potential variations in field conditions. For example, the effect on the moisture retention characteristics of a compacted till sample, due to varying the moulding water should be evaluated since quality assurance and control in the field is often difficult.

The laboratory program should also include the measurement of the coefficient of diffusion of oxygen in order to predict oxygen flux across the soil cover system. Finally, the hydraulic properties of the waste material should also be measured. The laboratory characterization of tailings is relatively simple due to its relatively fine and uniform texture. However, measuring the hydraulic properties of waste rock is a significantly more difficult task.

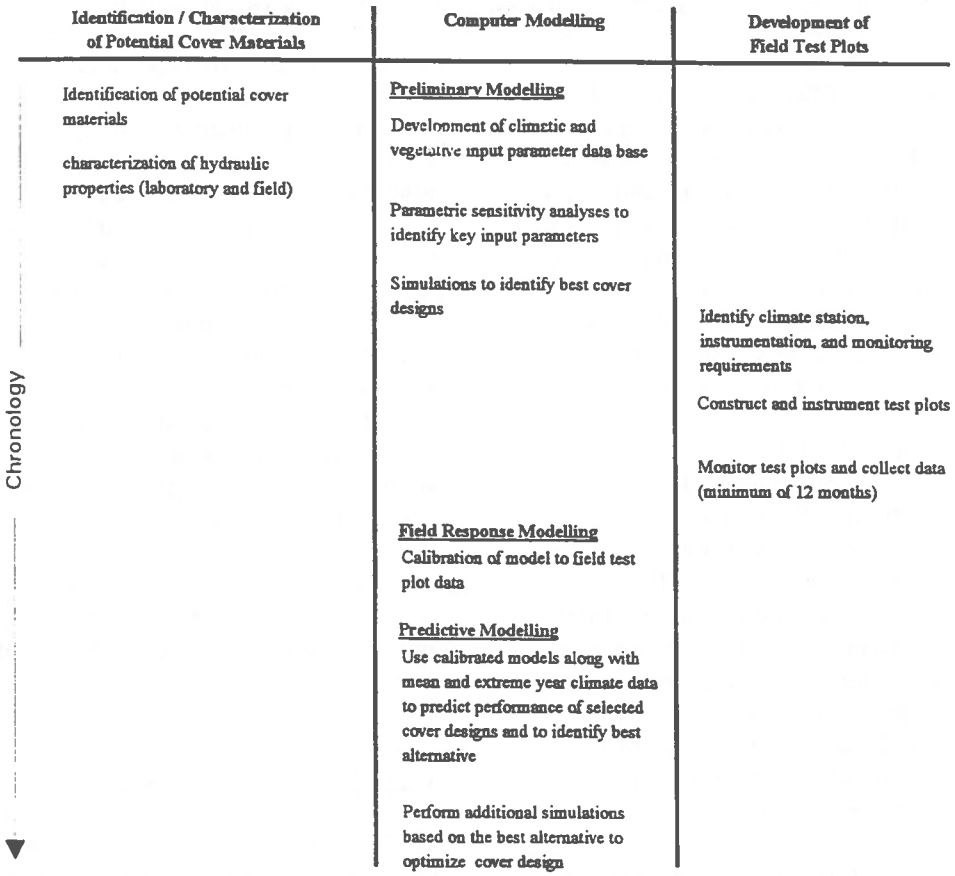

Figure 1 Cover design methodology

Computer Modelling

The objective of the computer modelling component is to select an optimal cover design. Computer modelling predicts the performance of various cover options in terms of the ability of the cover system to limit the influx of moisture and oxygen into the waste material. The modelling is used to first select a limited number of cover options and second, to select an optimal cover design through calibration on prototype field test plots.

Accurate quantification of the water balance components for a saturated/unsaturated profile is required to predict the performance of various cover designs. This includes the partitioning of precipitation into evaporation, transpiration, and surface runoff and the simulation of internal moisture movement (liquid and vapor). A natural soil system can be described by three main zones, namely: the saturated zone, the unsaturated zone, and the soil-atmosphere interface (Figure 2).

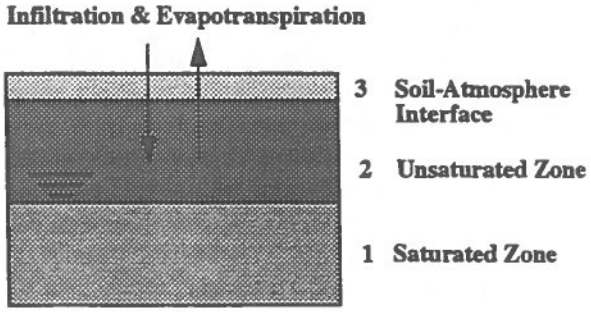

Figure 2 Components of a natural soil system

In the saturated zone, the soil pores are completely filled with water and hydraulic conductivity is relatively constant. In the unsaturated zone, the soil pores are only partially filled with water and the hydraulic conductivity is a function of the soil matric suction. The movement of moisture in the unsaturated zone can occur in both the liquid and vapor phases. That part of the unsaturated zone which is exposed to the atmosphere is referred to as the soil-atmosphere interface. The soil-atmosphere interface is a dynamic zone where soil moisture moves in both the liquid and vapor phases in response to precipitation and evapotranspiration.

The software utilized to simulate moisture movement in soil cover systems in this paper is based on the SoilCover model (MEND, 1993) developed at the University of Saskatchewan. SoilCover is a one-dimensional heat and water transfer (liquid and vapour) model which uses a physically based method for predicting the exchange of moisture between the atmosphere and a soil surface. The theory is based on the well known principles of Darcy's, Fick's and Fourier's laws which are used to describe the movement of liquid water, water vapour, and heat respectively, within the soil profile.

The water and heat flow equations were developed by Wilson (1990) within the framework of continuum mechanics as put forth by Fredlund and Dakshanamurthy (1982). The flow equations are solved using the finite element formulation developed by Joshi (1993). The coupling of the soil profile to the atmosphere is accomplished using a modified Penman formulation developed by Wilson (1990) and implemented by Machibroda (1994) which allows for the calculation of evaporation from a saturated or an unsaturated soil surface. The extraction of water from plant roots is quantified using methods described by Tratch (1995). The development of the program for use on a personal computer was carried out by Cook (1994). The SoilCover model was extended by Swanson (1995) to provide a simple estimation of potential oxygen flux through a cover layer (i.e., 100% oxygen consumption at the base of the cover) using Fick's law and assuming steady state conditions.

The SoilCover model provides a daily simulation of moisture and heat movement within the soil profile coupled to the surface water balance components of infiltration, evaporation, and runoff. Daily climatic information (i.e., maximum and minimum air temperature, maximum and minimum relative humidity, average wind speed, and net radiation) is required for the calculation of potential evaporation. Air temperature, relative humidity, and net radiation are distributed in a sinusoidal fashion to represent variations that occur throughout the day. The hydraulic and thermal properties of each soil layer are required for the analysis and include the soil-water characteristic curve, hydraulic conductivity versus matric suction function, the thermal conductivity versus gravimetric water content, and the specific heat versus gravimetric water content functions. In addition, parameters that describe the oxygen diffusion coefficient versus degree of saturation function are also required for the daily estimation of potential oxygen influx.

The following sections describe a three stage modelling methodology for the selection of an optimal cover design for acid generating mine waste.

Stage 1: Preliminary modelling:

The first stage consists of a preliminary modelling stage which has the objective of identifying cover design(s) to be incorporated in field test plots. The preliminary modelling stage involves the development of the model input parameter data base, parametric sensitivity analyses, and cover system simulations.

Development of the model input parameter data base should begin at the onset of the laboratory testing program to make the most efficient use of time so that simulations can be run as soon as material properties are available. A historical climatic data base for the site needs to be compiled which includes precipitation, net radiation, air temperature, relative humidity, and wind speed. Most importantly is daily precipitation data; however, as much site-specific data should be compiled as possible. A historical data base of at least 50 years should be compiled from the closest weather station to the site. Care needs to be taken in the selection of the weather station as the closest station may not necessarily be the most representative of site conditions due to micro-climatic variations caused by regional topographic conditions characteristic of mountainous regions. An extreme wet, extreme dry, and a mean

year should be identified from the historical data base to be used in the preliminary modelling simulations. Mean monthly values for air temperature, relative humidity, and wind speed obtained from 30 year climate normal summaries are adequate for numerical simulations in some cases. Mean monthly values for net radiation are seldom available for most locations but can be determined indirectly from mean monthly sunshine hours or global solar radiation using methods described by Maidment (1993). Information describing the vegetative parameter inputs (i.e., root depth, leaf area indices, and growing season) must also be researched and compiled.

A parametric sensitivity analyses is performed on selected cover designs to establish a hierarchy of importance for the model input parameters and to ensure that computed responses of the cover system are adequately understood. This analysis can provide valuable information for field test plot instrumentation and monitoring requirements and for additional model input data required for model calibration. Figure 3 illustrates the identification of a hierarchy of importance for the climatic model input required for the calculation of potential evaporation. The plot shown in Figure 3 is referred to as a tornado sensitivity plot (from Swanson, 1995) and describes the possible variation in a specific model output due to an expected variation in a specific model input parameter. The figure illustrates the importance of net radiation and wind speed in the calculation of surface evaporation. Analyses such as this are also used to identify the accuracy to which lower boundary conditions need to be delineated and to assess the adequacy of the soil property data.

Simulations for various cover design options can be performed when soil property data becomes available and climatic and vegetative data have been compiled. Cover designs selected at this stage will consist of various layering schemes and thicknesses for the potential cover materials. An extreme wet, dry and a mean year simulation is performed for each cover design. The most promising cover designs are selected based on analysis of cumulative water and oxygen flux through the cover system for the extreme and mean years. One or two designs are then incorporated in field test plots to provide a means of calibrating model predictions and to provide a direct evaluation of cover performance. The development of field test plots are described as the third component of the design methodology and may include more than one design option depending on the site conditions.

Stage 2: Field response modelling:

The objective of the field response modelling stage is to provide calibration of the model which will be used to make long term predictions of cover performance. Calibration to field test plots is required due to the differences in laboratory and insitu soil properties, and due to the site specific nature of climatic and vegetative parameter input. The laboratory soil water characteristic curve is calibrated to field conditions using field measured matric suction and moisture content data. Figure 4 illustrates the calibration of the soil water characteristics curves for an in-place waste rock soil cover system consisting of a compacted glacial till cover overlain with a loose glacial till layer. The compacted cover layer was calibrated based on field porosity determined from moisture content data and field densities. A field curve was constructed for the loose till layer using soil matric suction data obtained from thermal conductivity sensors installed in the cover and from moisture contents measured by neutron probe.

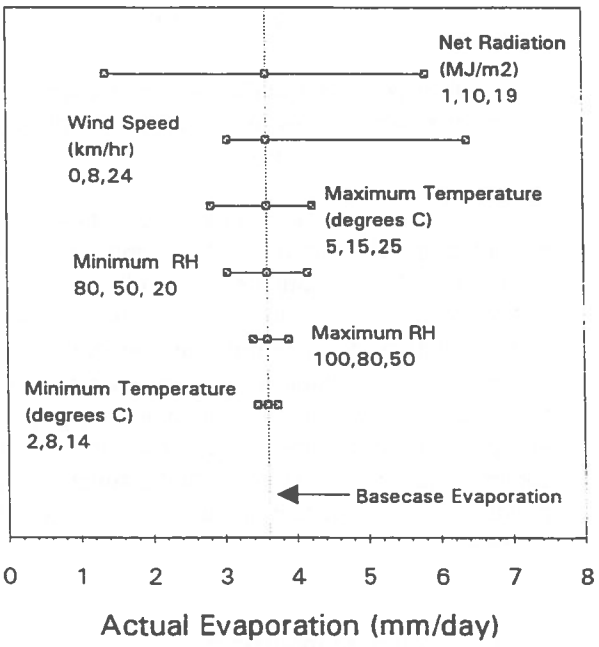

Figure 3 Tornado sensitivity plot illustrating the hierarchy of importance of input parameters on calculated evaporation under wet conditions

Simulations of field responses for the test plot cover systems are then performed using daily values of climatic parameters obtained from the site climate station along with measured lower boundary condition data (i.e., soil matric suction an/or water content). The saturated hydraulic conductivity of the cover materials can be calibrated by comparing the computed soil matric suctions within the cover and the water fluxes through the cover to the values measured in the test plots using matric suction sensors and percolation lysimeters.

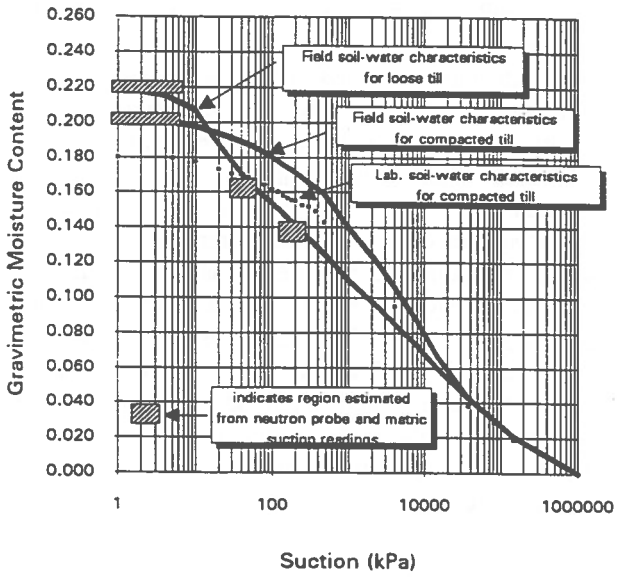

Figure 4 Field calibrated soil water characteristics curves for a glacial till soil cover system

Figure 5 shows the comparison of computed and measured matric suction at two depths for a five month period. The saturated hydraulic conductivity was calibrated to result in similar high peaks in matric suction as measured in the field. The calibration was evaluated through comparison of computed and measured moisture content profiles for the cover system. Figure 6 shows the moisture content comparisons revealing that simulations were providing an adequate prediction of the field responses.

Stage 3: Predictive modelling

The calibrated model can be used along with the mean and extreme year climate input parameters to make confident predictions of the long term performance of the cover systems. These predictions represent verification and improvement of the simulations performed as part of the preliminary modelling stage and provide more confident results from which to base the selection of an optimal cover design.

Results of mean-year calibrated predictions for the in-place glacial till cover system described previously are shown in Figure 7 to illustrate a typical output from the predictive simulations. Included in the results are cumulative water and potential oxygen flux through the cover, cumulative water balance components, and the variation in the degree of saturation and oxygen diffusion coefficient throughout the non-winter months. Results such as these can be used to assess the performance of the selected cover designs and to select the best design. Simulations can then be performed to refine the design (i.e., increased or decreased thickness) to identify an optimal cover design.

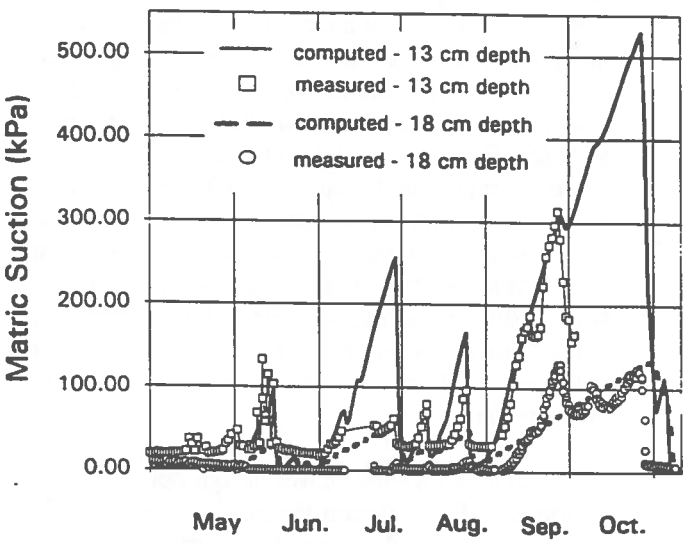

Figure 5 Comparison of computed matric suction from Swanson (1995) and measured matric suction from O'Kane (1995) for two depths in a glacial till cover system

Development of Field Test Plots

Reduction of oxygen diffusion coefficients and the associative reduction in oxygen flux is a primary factor for minimiqing acid generation. This factor,

together with controlling water flux is the objective sought when engineered soil cover systems are placed over sulphidic waste material.

Engineered soil cover systems take advantage of the capillary barriers which are formed at the interface of layered coarse and fine textured soils. The concept involves the principles of unsaturated flow between layered soils of different texture.

The conceptual design of field test plots will include the objectives of the closure plan with respect to control of acid rock drainage and physical integrity of the cover system. The design will also include the effect of placing the soil cover system in an arid or humid climate.

The design of an instrumentation program will depend on the climate conditions and soil types used in the cover system. However, the general objective is to evaluate the flux boundary conditions at the soil-atmosphere interface with respect to heat and water transfer. Therefore, measurement of daily climate and soil conditions are required. Accurate site information for precipitation, air temperature, relative humidity, wind speed, and net radiation is required for accurate field response modelling. In general, daily precipitation measurements are most important although this may change for a particular site.

The suction, temperature, and water content conditions within each layer of the soil cover system are essential to accurate field response modelling. Measurement of soil suction is most important since changes in hydraulic conductivity, water content, degree of saturation, and therefore oxygen flux are a function of the soil suction. In addition the actual evaporation from an unsaturated soil is a function of not only the atmosphere above but also the soil suction within the profile. Instrumentation of the cover layer incorporating the soil atmosphere interface is most important since the greatest dynamic change and response to climate conditions will occur near the surface.

Field responses of the soil cover system can be defined as changes in soil suction, temperature, and water content within the cover due to the atmospheric conditions above the soil-atmosphere interface. In addition, field responses include both potential and actual evaporation rates, infiltration, runoff, and plant transpiration. Therefore, the cover instrumentation program should include the ability to monitor these responses in order properly calibrate the SoilCover model as a basis for predictive modelling.

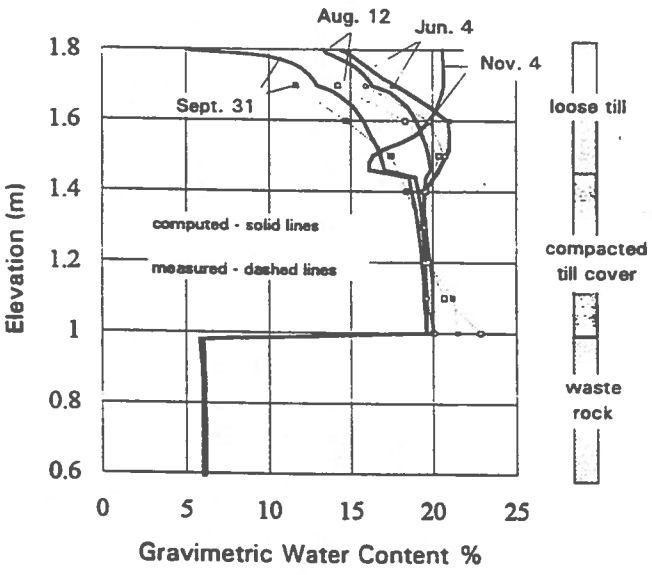

Figure 6 Comparison of computed moisture content profiles from Swanson (1995) and measured moisture content profiles from O'Kane (1995) for a glacial till cover system

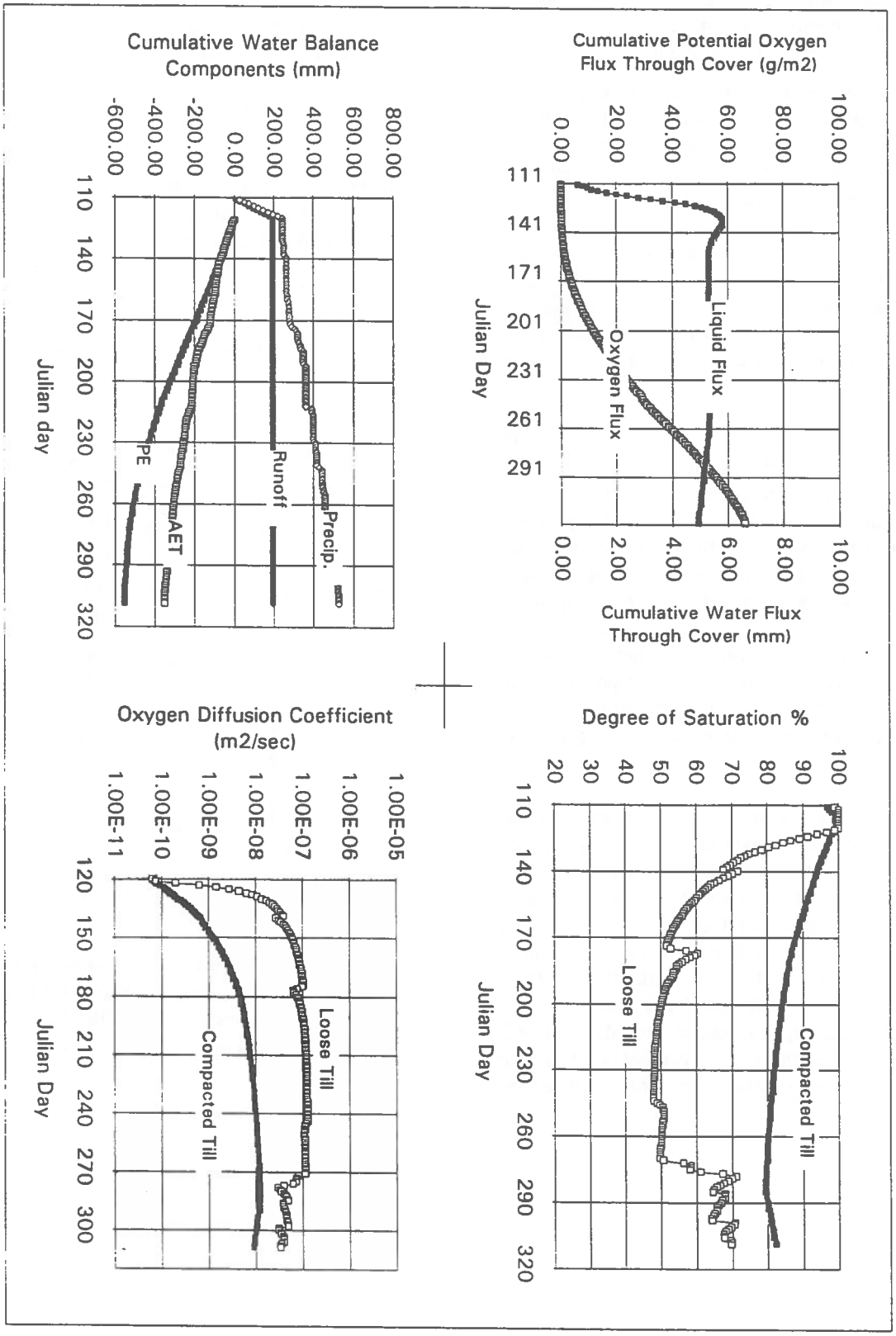

Figure 7 Results of mean-year predictive modelling for a glacial till cover system

SUMMARY AND DISCUSSION

A methodology for the design of engineered soil covers for acid generating mine waste was presented which consists of three components: laboratory characterization of potential cover materials, computer modelling, and the development of field test plots.

This paper focusses on computer modelling which consists of a three stage process. First, preliminary modelling is required to select cover designs to incorporate into field test plots. This is followed by field response modelling to calibrate model predictions to field conditions. Finally, predictive modelling allows for confident predictions using calibrated models for the selection of an optimal cover design.

ACKNOWLEDGEMENTS

The authors would like to thank Placer Dome Canada Ltd. and the Natural Sciences and Engineering Research Council for their continued support of the research described in this paper.

REFERENCES

Bruch, P. 1993. Evaporative Fluxes in Homogeneous and Layered Soils. M.Sc. Thesis, Department of Civil Engineering, University of Saskatchewan, Saskatoon, Saskatchewan.

Cook, D., 1994. Modification of a Finite Element Soil-Atmosphere Model. B.Sc. Undergraduate Thesis, Department of Civil Engineering. University of Saskatchewan, Saskatoon, Saskatchewan, Canada.

Fredlund, D. G. and Rahardjo, H., 1993. Soil Mechanics for Unsaturated Soils. John Wiley and Son's, Inc., New York.

Fredlund, D.G., and Dakshanamurthy, V., 1982. Predicting Moisture Flow and Related Swelling or Shrinking in Unsaturated Soils. Geotechnical Engineering, Vol. 13, p 15 - 49.

Joshi, B., 1993. A Finite Element Model for the Coupled Flow of Moisture and Heat in Soils Under Atmospheric Forcing. M.Sc. Thesis, Department of Civil Engineering, University of Saskatchewan, Saskatoon, Saskatchewan, Canada.

Machibroda, R.T., 1994. Evaluation of Evaporative Fluxes from Mine Tailings Using the Modified Penman Formulation. M.Sc. Thesis, Department of Civil Engineering, University of Saskatchewan, Saskatoon, Saskatchewan, Canada.

Maidment, D.R., 1993. HandBook of Hydrology. McGraw-Hill Inc.

MEND, 1993. SoilCover: User's Manual for an Evaporative Flux Model. University of Saskatchewan, .Saskatoon, Saskatchewan, Canada.

O'Kane, M., 1995. Instrumentation and Monitoring of Engineered Soil Covers for Acid Generating Mine Waste. M.Sc. Thesis, In Progress. Department of Civil Engineering, University of Saskatchewan, Saskatoon, Saskatchewan, Canada.

Swanson, D.A., 1995. The Modelling of Moisture Movement in Engineered Soil Covers for Acid Generating Mine Waste. M.Sc. Thesis, Department of Civil Engineering, University of Saskatchewan, Saskatoon, Saskatchewan, Canada.

The Financial Post, 1992. Cost of Closing Mines Grows Hazardous. September 7th Issue.

Tratch, D., 1995. Moisture Uptake Within the Root Zone. M.Sc. Thesis, In progress, Department of Civil Engineering, University of Saskatchewan, Saskatoon, Saskatchewan, Canada.

Wilson, G.W., 1990. Soil Evaporative Fluxes for Geotechnical Engineering Problems. Ph.D Thesis, University of Saskatchewan, Saskatoon, Saskatchewan, Canada.

CAMI'95: 3rd Canadian Conference on Computer Applications in the Mineral Industry
Montréal, Québec, Canada, October 22-25, 1995

Unsaturated Flow Modeling of Covers for Reactive Tailings

Bruno Bussière
Unité de recherche et de service en technologie minérale (URSTM), Rouyn-Noranda, Québec

Michel Aubertin, Mostafa Aachib, Robert P. Chapuis, Rodolfo J. Crespo
Department of Mineral Engineering
École Polytechnique de Montréal, Montréal, Québec

ABSTRACT:

The installation of a cover is one of the main techniques to control the production of acid mine drainage by sulfide tailings. Such so called "dry covers" are used to restrict the flow of water and oxygen. A capillary barrier effect is usually created within covers to reach these objectives. Numerical simulations were done to evaluate the hydrogeological behavior of different types of cover with two and three layers. The results show that the main factors affecting the hydrogeological behavior are the suction properties contrast between the different materials and the thickness of the base layer that creates the capillary break. The simulations also show the large influence of the constitutive model used to evaluate the unsaturated hydraulic conductivity function.

RESUME:

L'installation de barrières de recouvrement constitue l'une des principales méthodes pour empêcher la génération de drainage minier acide de parcs à résidus miniers sulfureux. Ces recouvrements, appelés "barrières sèches", sont installés dans le but d'isoler les résidus de la migration de l'eau et de l'oxygène. Un effet de bris capillaire est habituellement créé dans le recouvrement pour atteindre ces objectifs. Des simulations numériques ont été réalisées afin d'évaluer le comportement hydrogéologique de recouvrements comprenant deux et trois couches. Les résultats obtenus démontrent que les principaux facteurs qui affectent le comportement hydrogéologique sont le contraste des propriétés de succion entre les différents matériaux et l'épaisseur de la couche grossière du bas qui créé le bris capillaire. Les simulations montrent également la grande influence qu'a le choix du modèle constitutif utilisé pour prédire la conductivité hydraulique non saturée.

INTRODUCTION

The most serious environmental problem facing the Canadian mining industry is the production of acid mine drainage (AMD) by sulfide tailings. The main methods used to prevent the production of AMD essentially aim at eliminating the interactions between the constitutive elements of the reactions, which are iron sulfides, water and oxygen. One of the most interesting way to do so is to use dry covers installed over reactive tailings in order to restrict the oxygen flow (SRK, 1989).

This paper deals with capillary effects created in covers to limit the oxygen and the water flow. A capillary barrier can exist when unsaturated flow occurs through a fine grained soil overlying a coarse grained soil. The paper also shows how numerical methods can be used to evaluate the performance of such capillary barriers. The formulation of the mathematical equations used by the numerical model SEEP/W are presented. Then, simulations with different types of material and different configurations are analyzed and briefly discussed.

CAPILLARY BARRIERS

General description

Most covers used to isolate municipal and industrial wastes are constructed with natural (clay, till) and/or industrial (geosynthetics) materials. In the former case, the fine grain layer in the cover has to maintain a high degree of saturation in order to avoid cracking due to wet-dry cycles and to limit gas migration through the air filled pores. To maintain this high degree of saturation, a capillary barrier effect can be artificially created in the cover system.

Figure 1 shows a typical layered cover system. In such system, capillary barrier effect is created when a fine grain layer overlies a coarse grain layer, as for layers D and E in Figure 1. In this case, the water that infiltrates the surface flows through layer E (considered initially dry) only when the capillary tension in layer D is close zero, that is when it is nearly saturated. A similar effect can be created when a coarse material is placed over a fine material, as for layers C and D in Figure 1. Such configuration prevents rising of the water by capillary forces, from the fine to the coarse material.

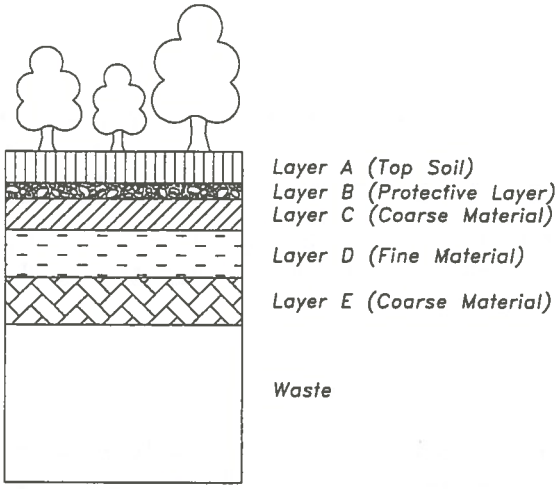

Figure 1. Typical configuration of a multi-layered cover (after Aubertin et al., 1993)

The cover system showed in Figure 1 thus includes a double capillary barrier effect, one on both sides of the fine layer. In this case, drainage of layers C and E inhibits the flow of water from the fine material layer and helps to maintain a high degree of saturation in layer D. More details on the description of capillary barrier effects have been presented by Morel-Seytoux (1992), Chiu and Shackelford (1994) and Aubertin et al. (1995).

Unsaturated flow

As previously mentioned, a capillary barrier effect results when unsaturated flow occurs through a relatively fine-grained soil overlying a relatively coarse-grained soil. When a soil is not saturated ($S_r < 100\%$, where S_r is the degree of saturation), air (or other gas) fills a fraction of the pores. The flux of water is then reduced in comparison with the one observed under saturated conditions (for a given hydraulic gradient).

It is not the objective of this paper to give a detailed presentation on the theory of unsaturated flow. It is nevertheless necessary to introduce the basic concepts in order to understand the principles involved in the modeling of covers. More details on this theory can be found elsewhere (e.g. Hillel, 1980; Kovács, 1981; Mualem, 1986; Fredlund et Rahardjo, 1993).

The flow of water through a porous media can be estimated with the Darcy's law (presented here in a scalar form):

$$v = k\frac{\delta h}{\delta x} \qquad (1)$$

where v is de Darcy's velocity, k is the hydraulic conductivity and $\delta h / \delta x$ is the hydraulic gradient commonly identified as i.

It is usually considered that Darcy's law is valid for both saturated and unsaturated conditions. In saturated conditions, the pore pressure is positive and the k value can be considered as a constant for a specific material. In unsaturated conditions, the water is maintained in the pores by capillary forces associated to the surface tension created at the water-air interface. Because the capillary forces depend on the radius of curvature of the surface at the water-air interface, small pores generates a larger capillary tension. Thus, fine materials will retain more water than coarse materials for a given pore pressure.

In unsaturated media, pore pressure changes with the degree of saturation (or the volumetric water content). The relationship between negative pore pressure (or suction) and volumetric water content (often called soil-water characteristic curve or ψ-θ relationship) can be used to estimate the unsaturated condition. Several mathematical models exist in order to describe (e.g. van Genuchten et al., 1991; Fredlund et Xing, 1994) or predict (e.g. Kovács, 1981; Aubertin et al., 1995b) the soil-water characteristic curve.

The hydraulic conductivity k of an unsaturated soil is not a constant. It depends on the volumetric water content θ, which, in turn, depends upon the soil suction ψ. Several functions have been developed over the years to relate permeability function (ψ-k relationship) to soil-water characteristic curve. These models can be empirical (e.g. Brooks and Corey, 1964) or statistical (e.g. Green and Corey, 1971; Mualem, 1976).

NUMERICAL MODELING

Numerical methods are used to solve mathematical models, which can be defined as a set of mathematical equations describing the physical process involved in

the real system. For a proper use of numerical methods, it is important that the resolution method used and the mathematical equations involved are known and understood.

The software used in this study is SEEP/W, from GEO-SLOPE International. This software uses the Finite Element Method (FEM) to solve the differential equations of the mathematical model. SEEP/W analyses the movement of water through porous media as soils and rock mass. Different types of problems can be simulated, including saturated and unsaturated flow analysis, steady-state and transient conditions, two dimensional and axisymetric configurations.

The fundamental differential equation used by the software can be presented as follows (GEOSLOPE International, 1994):

$$\frac{\partial}{\partial x}\left[k_x \frac{\partial H}{\partial x}\right]+\frac{\partial}{\partial y}\left[k_y \frac{\partial H}{\partial y}\right]+Q=\frac{\partial \theta}{\partial t} \qquad (2)$$

where H is the total head, k_x is the hydraulic conductivity in the x-direction, k_y is the hydraulic conductivity in the y-direction, Q is the applied boundary flux, θ is the volumetric water content and t is the time. More details on the fundamental aspects behind the software can be found elsewhere (GEOSLOPE International, 1994; Huyakorn and Pinder, 1983; Bathe, 1982; Zienkiewicz, 1977). The main characteristics of SEEP/W are presented in Table 1.

TABLE 1. General characteristics of SEEP/W

Type of elements	• Quadrilateral with or without secondary nodes (integration order 9 or 4) • Triangular with or without secondary nodes (integration order 3 or 1)
Interpolating functions	• Bathe's interpolating functions (Bathe, 1982)
Finite element equations	• Galerkin method
Time integration	• Backward difference method
Numerical integration	• Gauss numerical integration
Equation solver	• Gauss elimination techniques
Convergence	• Euclidean norm of the pressure head vector

The output files created by the software include: head file, velocity file, material properties, flux, convergence and initial head. With these files, it is possible to determine the water content profile, the pressure profile developed in the materials, the flux through a section and the permeability conditions.

NUMERICAL CALCULATIONS

In order to evaluate the hydrogeological behavior of layered covers, column tests were simulated. Similar calculations were performed by Akindunni et al. (1991). A comparison of calculated and measured conditions in column tests were also done by Yanful and Aubé (1993), Barbour and Yanful (1994) and Aubertin et al. (1995b) for different configurations of soils. Only the calculation results are presented here. The model is based on columns of 25 cm in diameter and of various height. The phreatic surface is initially placed at the top of the cover and gradually (3 600 s) lowered to the bottom of the column; such time function relaxes the constraint on the numerical model caused by a large and sudden change in the boundary conditions. Free drainage is allowed at the bottom. No function was used to simulate the effect of evaporation. The type of elements used for the generation of the finite element mesh was rectangular quadratic elements of the Lagrange family. The height of these elements were 0,25 and 0,5 cm with an integration order of 9. The iteration process stops if the difference of the vector norm between two successive iterations is less than 0,01%. The vector norm is a measure of the size of the pressure head vector.

Material Properties

The soil-water characteristic curves of the different materials studied are presented in Figure 2. Materials 1 and 2 are a sand (Crab Creek sand) and a silt (Touchet silt), which were taken from Akindunni et al. (1991). The characteristics of materials 3 and 4 (fine and coarse tailings) were evaluated by Bussière et al. (1994). The curves presented in Figure 2 were obtained with the van Genuchten model (van Genuchten, 1980); this commonly used model is different from the well-known Brooks and Corey model (1964), which can be expressed as follows:

$$\theta_e = \left(\frac{\psi_a}{\psi}\right)^{\lambda} \qquad (3)$$

Where

$$\theta_e = \frac{\theta - \theta_r}{\theta_s - \theta_r} \quad (4)$$

θ_e is the volumetric water content in its normalized form, θ_s is the saturated volumetric water content, θ_r is the residual water content, ψ is the suction applied, ψ_a is the air entry value and λ is the pore-size distribution index. The equation of the van Genuchten model can be written as follows (van Genuchten, 1980):

$$\theta_e = \left[\frac{1}{1+(\alpha\psi)^n}\right]^m \quad (5)$$

In equation (5) α, n and m are three different soil parameters, Model parameters for different types of soils are presented in van Genuchten and Nielsen (1985). In this case, parameter m is equal to 1 - 1/n and parameters n and α are fitted to experimental data. The relevant hydraulic parameters for the selected materials are presented in Table 2.

TABLE 2. Summary of the hydraulic and curve-fitting parameters for the selected materials

Materials	AEV (cm)	θ_r	θ_s	k_s (cm/s)	α (cm^{-1})	n
Crab Creek sand	24,0	0,141	0,448	$7{,}18 \times 10^{-3}$	0,029	10,21
Touchet silt	165,0	0,180	0,485	$5{,}83 \times 10^{-4}$	0,004	7,05
Coarse tailings	50,0	0,010	0.460	$3{,}00 \times 10^{-3}$	0,012	2,91
Fine tailings	140,0	0,054	0,430	$3{,}15 \times 10^{-4}$	0,0036	2,88

The permeability function (ψ-k relationship) must be specified for the numerical simulations. In this study, the permeability functions have been predicted using the soil-water characteristic curves. Two methods were used to evaluate the ψ-k relationship; the Mualem method (Mualem, 1976) and the Green and Corey method (Green and Corey, 1971).

The Green and Corey method is already included in SEEP/W, so one can directly calculate the permeability function from the soil-water characteristic. The Green and Corey equation can be expressed as (Green and Corey, 1971; GEOSLOPE International, 1994):

$$k(\theta)_i = \frac{k_s}{k_{sc}} \cdot \frac{30T^2}{\mu g \eta} \cdot \frac{\xi^p}{n^2} \cdot \sum_{j=i}^{M}\left[(2j+1-2i)h_i^{-2}\right] \quad (6)$$

where $k(\theta)_i$ is the calculated hydraulic conductivity for a specified water content or negative pore-water pressure, k_s is the measured saturated conductivity, k_{sc} is the calculated saturated conductivity, i is the last water content class on the wet end, h_i is the negative pore-water pressure head for a given class of water filled pores, n is the total number of pore classes between the residual water content and the saturated water content, M is the pore class corresponding to the saturated water content, θ is the volumetric water content, T is the surface tension of water, ξ is the water-saturated porosity, η is the viscosity of water, g is the gravitational constant, μ is the density of water and p is a parameter that accounts for the interaction of pore classes (in our simulations, p = 2).

Elzeftawy and Cartwright (1981) have compared the experimental results obtained for different types of soils and those obtained from the Green and Corey relationship and concluded that the relationship is sufficiently accurate for most field applications. Yanful and Aubé (1993) also used the Green and Corey equation in their simulations and concluded that the method is applicable to predict the hydraulic conductivity of unsaturated media in most conditions. However, they also noted that the model seems inadequate for a sand at water contents close to the residual water content.

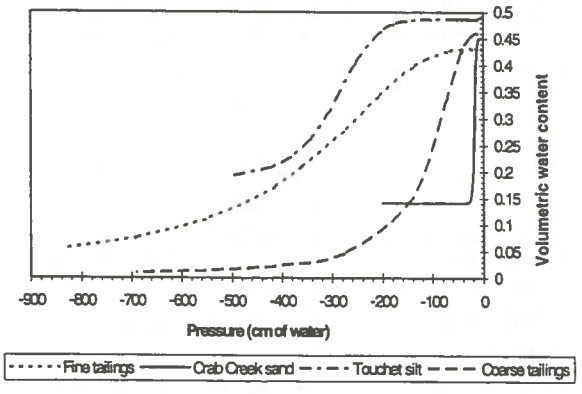

Figure 2. Soil-water characteristic curves for the selected materials

The Mualem equation, on the other hand, has become the most commonly used equation for predicting the permeability function using the soil-water characteristic curve (e.g. Wise et al., 1994; Yeh et al., 1994, Chiu and Shakelford, 1994; Marion et al., 1994; Akindunni et al.,

1991; Mishra and Parker, 1990). The software used in this study to evaluate the ψ-k relationship with the Mualem equation is the RETC program written by van Genuchten et al. (1991). Based on the Mualem equation, the relation between water content and hydraulic conductivity is given by (van Genuchten, 1980):

$$k(\theta) = k_s \left\{ 1 - \left[1 - \theta_e^{(1/m)} \right]^m \right\}^2 \theta_e^{\lambda} \qquad (7)$$

where k_s is the saturated hydraulic conductivity and θ_e. is the volumetric water content in its normalized form. The parameters needed by the software are: data from a suction test (ψ-θ), the residual water content θ_r, the saturated water content θ_s (= n), the saturated hydraulic conductivity k_s and the curve fitting parameters (α and n, evaluated with $\lambda = 1/2$ and $m = 2/3$ as proposed by van Genuchten et al., 1991). With these values, the software fits a curve where the error between the experimental values and fitted values is minimized. It is this fitted curve, in the form θ vs ψ, that is inserted in the SEEP/W for the simulations.

Figure 3 shows the permeability functions of the different materials used in this study. The curves obtained by the RETC program are identified with the letters V-G while the Green and Corey curves are identified with the letters G-C. It can be seen that the Green and Corey equation gives, for Touchet silt, a greater value of k than the Mualem equation, especially at low pressure. For the Crab Creek sand, a relatively large difference exists between the two equations at the residual water content (k_r). For the Green and Corey equation, k_r is approximately 1 x 10^{-6} cm/s. instead of 6 x 10^{-9}cm/s with the Mualem equation. Finally, it is important to note that, for the two tailings studied, only the Mualem equation is used in the following to evaluate the permeability function.

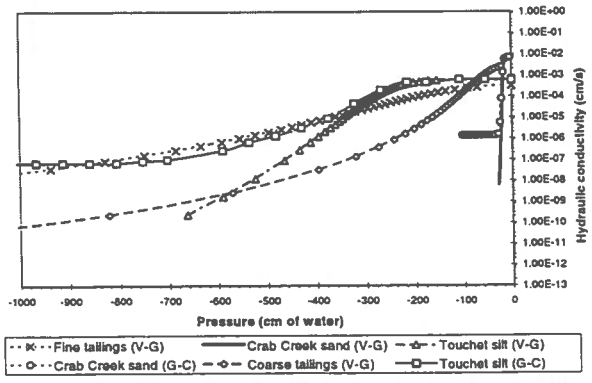

Figure 3. Permeability function curves for the selected materials

Modeling of bi-layered covers

Numerical simulation 1, The first simulation is similar to the one performed by Akindunni et al. (1991), which is 2,5 m of sand (Crab Creek sand) overlain by 1 m of silt (Touchet silt), with the use of the van Genuchten and Mualem models for the determination of the θ-k and ψ-k relationships. One of the objectives of this simulation is to validate the calculations. The system is initially saturated, and then allowed to drain.

One can see in Figure 4 that the degree of saturation goes down rapidly in the sand layer and reaches an equilibrium around the 14th day at 35% of saturation. During that time, the silt layer remains fully saturated over it's entire thickness, for the total duration of the simulation. Figure 5 shows that a pressure equilibrium is reached after 14 days. It is also important to note that this equilibrium is not the hydraulic equilibrium (or static equilibrium) which would show a constant slope. The results obtained in this first simulation are very similar to those presented by Akindunni et al. (1991).

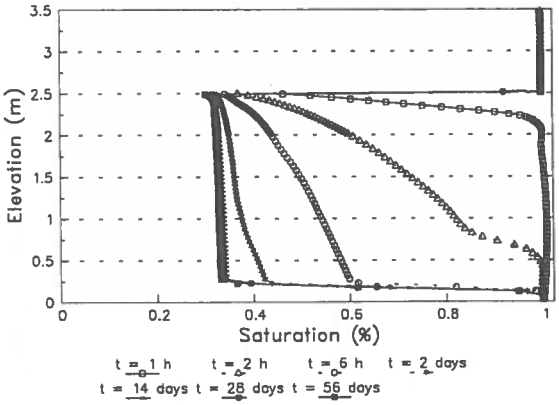

Figure 4. Variation in saturation with elevation at selected times for Numerical simulation 1

Numerical simulation 2, The second simulation evaluates the effect of using the Green and Corey model for the sand and silt instead of the Mualem model. In this simulation, the residual water content (θ_r) of the two soils was not fixed at a unique value (see Table 1). Rather, it is considered that the water content decreases progressively toward zero at a value of ψ of about 10^6 kPa as proposed by Fredlund and Xing (1994). Other parameters of this numerical simulation are identical to those used in the first simulation.

Figure 6 shows that the saturation profile is different of the one obtained for the Numerical simulation 1. The degree of saturation in the coarse layer goes down below the equilibrium value observed in Figure 4, which was about 35%. After 56 days, Figure 6 shows

that the top of the coarse layer is at a degree of saturation of approximately 17%. This is due to the fact that the residual water content is continues to decrease and, consequently, the shape of the soil-water characteristic and the permeability function are different at high pressure. Also, the degree of saturation of the fine layer decreases at the top of the layer to about 96%. The pressure applied at the top of this layer is - 20 kPa compared to - 14 kPa for Numerical simulation 1.

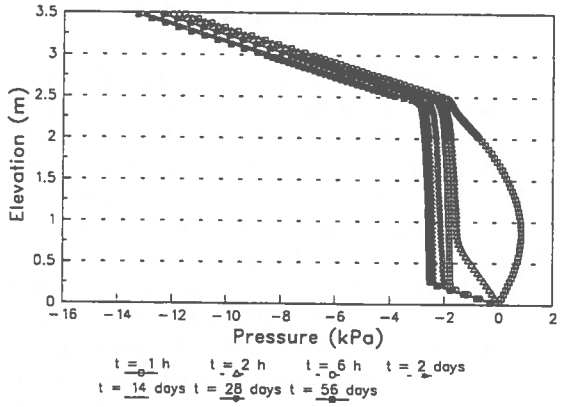

Figure 5. Variation in pressure with elevation at selected times for Numerical simulation 1

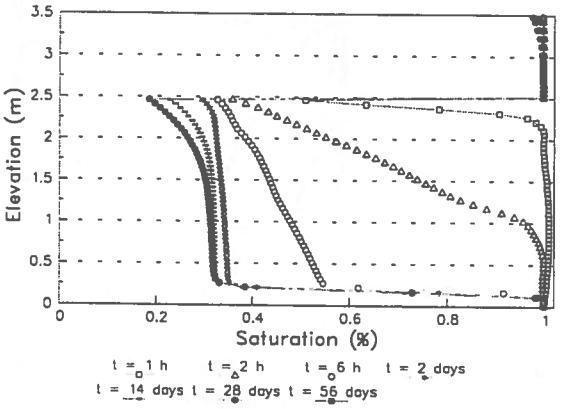

Figure 6. Variation in saturation with elevation at selected times for Numerical simulation 2

Numerical simulation 3, The objective of the third simulation is to evaluate the impact of reducing the thickness of the sand layer (to 1 m) on the global behavior of the cover. The permeability function used in this simulation is the one calculated with the Mualem function. The thickness of the fine layer is still the same, that is 1 m.

As it is the case with the results of Numerical simulation 1, the sand layer drains rapidly and reaches an equilibrium by the 14th day (at 35% of saturation) and the silt remains fully saturated over it's entire thickness for the total duration of the simulation (see Figure 7). In terms of pressure (not shown), the profile and the values in the fine layer are similar to the ones obtained in Numerical simulation 1.

From this simulation, it can be said that the thickness of the sand layer can be reduced to 1 m without reducing the degree of saturation of the fine layer.

Numerical simulation 4, As shown in the previous simulation, the thickness of the coarse layer can be reduced to 1 m without affecting the behavior of the capillary barrier (in terms of water content in the fine layer). In Numerical simulation 4, the thickness is further reduced to 0,3 m; a value which is not much larger than the AEV of the sand. Others parameters are similar to the Numerical simulation 3.

The Figure 8 shows that the capillary break is still present, but that it could not be developed if the thickness was reduced below about 20 to 30 cm. The equilibrium is reached rapidly in the coarse layer (after 2 days). The fine layer remains fully saturated for the total duration of the simulation.

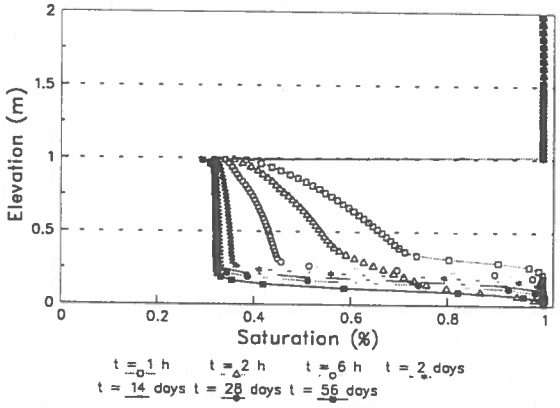

Figure 7. Variation in saturation with elevation at selected times for Numerical simulation 3

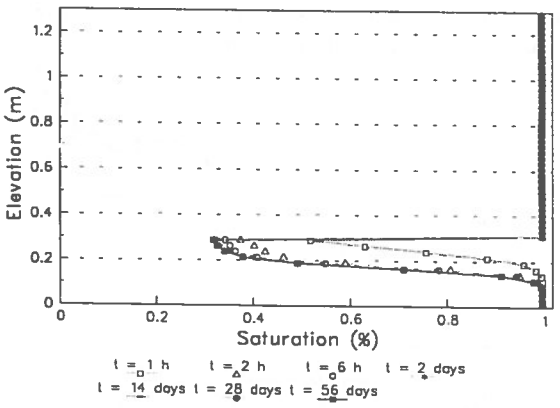

Figure 8. Variation in saturation with elevation at selected times for Numerical simulation 4

Numerical simulation 5, For all the numerical simulations presented above, free drainage was allowed at the bottom of the column by considering that the water table was located at elevation zero. In this next numerical simulation, a negative pressure is applied at the bottom of the column in order to evaluate the impact of placing the phreatic line 2 m below the bottom of the column. Other parameters are identical to those used in Numerical simulation 4.

The main difference between this simulation and the Numerical simulation 4 is that the degree of saturation of the coarse layer quickly reaches a constant value (approximately 35%) for the entire thickness. For the Numerical simulation 4, the bottom of the coarse layer has a degree of saturation of about 100%. Figure 9 also shows that, even if the phreatic line is located 2 m below the bottom of the column, the fine layer stays fully saturated. Again, the coarse sand layer act as a capillary barrier.

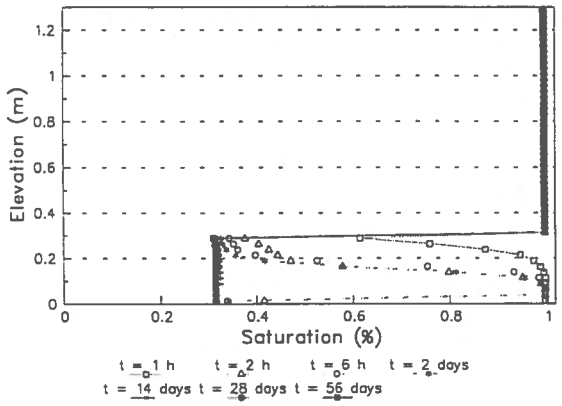

Figure 9. Variation in saturation with elevation at selected times for Numerical simulation 5

Modeling of three-layered covers

Numerical simulation 6, The main objective of this simulation is to evaluate the behavior of a cover made of three layers. The coarse layer at the bottom is made of 1 m of coarse tailings. The fine layer is 0,6 m thick, and is made of fine tailings. Finally, the coarse layer on top is made with the same material as the bottom layer, with a thickness of 0,4 m. The ψ-k relationship and ψ-θ relationship of these two materials are presented in Figures 2 and 3. Once again, the ψ-k relationships were evaluated with the Mualem equation.

One can see in Figure 10 that the degree of saturation of the three layers reaches an equilibrium by the 14th day. For the coarse layer on top, the final degree of saturation reaches about 20%; for the fine layer, it remains around 90%; it is about 55% for the coarse layer of the bottom. To inhibit the oxygen diffusion, the degree of saturation should remain greater than about 90% (Aubertin et al., 1993), so the objective is attained (but the margin of safety is small).

The pressure profile of the layered cover is presented in Figure 11. It can be observed that an equilibrium is reached by 14th day and that it is close to the static equilibrium.

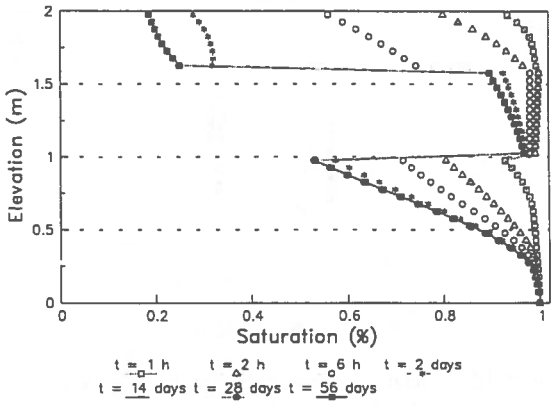

Figure 10. Variation in saturation with elevation at selected times for Numerical simulation 6

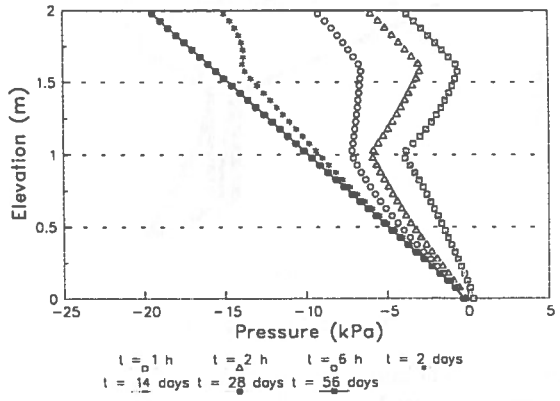

Figure 11. Variation in pressure with elevation at selected times for Numerical simulation 6

Numerical simulation 7, In order to improve the efficiency of the barrier system shown in Figure 11, the contrast in capillary properties between the fine and the coarse material layers is increased in the Numerical simulation 7. To do so, the authors have used Crab Creek sand instead of coarse tailings as the constituent of the coarse layers. As in Numerical simulation 6, the fine layer is fine tailings and the equation used to evaluate the permeability function is the Mualem equation.

One can see in Figure 12 that the end degree of saturation of the two coarse layers drops to approximately 35%, which represents the residual value, and the degree of saturation of the fine layer is over 95%. It seems evident that the increase of suction contrast has improved the effectiveness of the capillary barrier. This confirms the findings of Morel-Seytoux (1992).

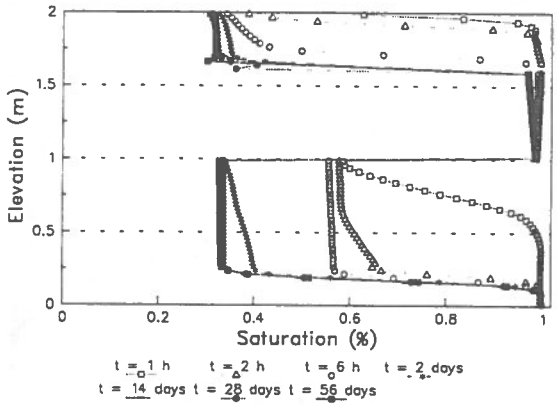

Figure 12. Variation in saturation with elevation at selected times for Numerical simulation 7

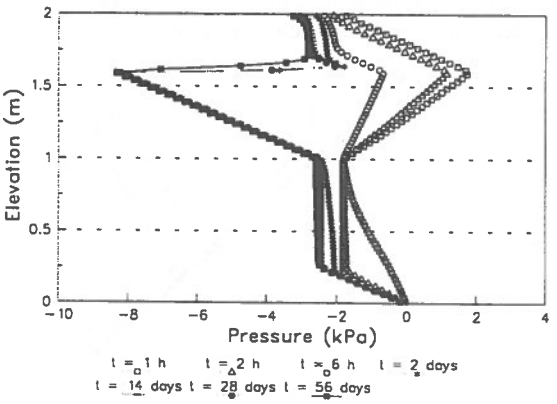

Figure 13. Variation in pressure with elevation at selected times for Numerical simulation 7

On the other hand, Figure 13 shows that the pressure in the fine layer is less in this simulation than in the Numerical simulation 6. This is shows that the capillary break is more effective in this case.

CONCLUSION

The following conclusions can be deduced from the numerical simulations:

1. The model used for the determination of the permeability function from the soil-water characteristic curve can have a large influence on the results obtained from the numerical simulation. In that regards, the value of the permeability function at high negative pressure has to be further investigated.
2. The thickness of the bottom coarse layer is an important parameter for the design of capillary barriers. The optimization of the thickness of this layer is highly dependent on the soil-water characteristic and the permeability function.
3. The suction contrast between the coarse layer and the fine layer is another important parameter for the efficiency of a capillary barrier.
4. The phreatic line position is not a critical parameter on the behavior of covers (in terms of water content in the fine layer) if the capillary break is well developed.

For a better understanding of the behavior of covers, numerical modeling can be used as a predictive tool. Nevertheless, some more work has to be done to better evaluate the practical significance of these results. Comparison between measured and predicted values in column tests (currently underway) is something that has to be investigate. The influence of slope (2 D and 3 D) and of *in situ* conditions will be also looked at in the near future.

REFERENCES

AKINDUNNI, F.F., GILLHAM, R.W. and NICHOLSON, R.V. 1991.
Numerical simulations to investigate moisture-retention characteristics in the design of oxygen-limiting covers for reactive mine tailings. Canadian Geotechnical Journal, 28 :446-451.

AUBERTIN, M., CHAPUIS, R.P., BUSSIÈRE, B. and AACHIB, M. 1993.
Propriétés des résidus miniers utilisés comme matériau de recouvrement pour limiter le drainage minier acide (DMA). Geoconfine 93, Arnould, Barrès and Côme (eds), Balkema, 299-308.

AUBERTIN, M., RICARD, J.F. and CHAPUIS, R.P. 1995a.
A study of capillary properties of mine tailings: measurements and modeling. Proceedings of the 48th Canadian Geotechnical Conference, Vancouver (to be published).

AUBERTIN, M., CHAPUIS, R.P., AACHIB, M., BUSSIÈRE, B., RICARD, J.F. and TREMBLAY, L. 1995b.
Évaluation en laboratoire de barrières sèches construites à partir de résidus miniers. Final Report (Draft version), Prepared for CANMET, Report C.D.T. P1622, École Polytechnique de Montréal, 202 p.

BARBOUR, S.L. and YANFUL, E.K. 1994.
A column study of static nonequilibrium fluid pressures in sand during prolonged drainage. Canadian Geotechnical Journal, 31 :299-303.

BATHE, K-J. 1982.
Finite Element Procedures in Engineering Analysis. Prentice-Hall, 282 p.

BROOKS, R.H. and COREY, J.C., 1964.
Hydraulic properties of porous medium. Colorado State University (Fort Collins), Hydrology Paper 3.

BUSSIÈRE, B., LELIÈVRE, J., OUELLET, J. and BOIS, D. 1994.
Valorisation des résidus miniers : une approche intégrée. Rapport final soumis au Ministère des Ressources naturelles dans le cadre du volet Mines écologiques de l'Entente Auxiliaire du Développement Minéral, 194 p.

CHIU, T-F. and SHACKELFORD, C.D.. 1994.
Practical aspects of the capillary barrier effect for landfills. Presented at the 17th International Madison Waste Conference, Septembre 21-22, 1994, 357-375.

ELZEFTAWY, A. and CARTWRIGHT, K. 1981.
Evaluating the saturated and unsaturated hydraulic conductivity of soils. Permeability and Groundwater Contaminant Transport, ASTM STP, T.F. Zimmie and C.D. Riggs (eds), 168-181.

FREDLUND, D.G. and XING, A. 1994.
Equations for the soil-water characteristic curve. Canadian Geotechnical Journal, 31: 521-532.

FREDLUND, D.G. and RAHARDJO, H. 1993.
Soil Mechanics for Unsaturated Soils. John Wiley & Sons, inc., New York, 517 p.

GEOSLOPE International, 1994.
SEEP/W User's Guide, Version 3.

GREEN, R.E. and COREY, J.C. 1971.
Calculation of hydraulic conductivity : A further evaluation of some predictive methods. Soil Science Society of America Proceedings, 35: 3-8.

HILLEL, D. 1980.
Fundamentals of Soil Physics, Academic Press, 413p.

HUYAKORN, P.S. and PINDER, G.F. 1983.
Computational Methods in Subsurface Flow. Academic Press inc., San Diego, USA, 473 p.

KOVÀCS, G. 1981
Seepage Hydraulics, Elsevier Scientific Pub.

MARION, J.M., OR, D. ROLSTON, D.E., KAVVAS, M.L. and BIGGAR, J.W. 1994.
Evaluation of methods for determining soil-water retentivity and unsaturated hydraulic conductivity. Soil Science, Vol 158, 1: 1-13.

MISHRA, S. and PARKER, J.C. 1990.
On the relation between saturated conductivity and capillary retention characteristics. Ground Water, Vol. 28, 5: 775-777.

MOREL-SEYTOUX, H.J. 1992.
The capillary barrier effect at the interface of two soil layers with some contrast in properties. HYDROWAR Report 92.4, Hydrology Days Publications, 57 Shelby Lane, Atherton, CA 94027-3926, 109 p.

MUALEM, Y. 1976.
A new model for predicting the hydraulic conductivity of unsaturated porous media. Water Resources Research, 12 : 513-522.

MUALEM, Y. 1986.
Hydraulic conductivity of unsaturated soils : Prediction and formulas. In A. Klute (ed.). Methods of Soil Analysis. Part 1. Physical and Mineralogical Methods. Agron. Monogr. 9 (2nd ed.). American Society of Agronomy, Madison, Wisconsin, 799-823.

SHACKELFORD, C.D., CHANG, C.K. and CHIU, T.F. 1994.
The capillary barrier effect in unsaturated flow through soil barriers. Proceedings of the First International Congress on Environmental Geotechnics, Edmonton, ISSMFE/CGS, 789-793.

SHOUSE, P.J., RUSSELL, W.B., BURDEN, D.S., SELIM, H.M., SISSON, J.B. and van GENUCHTEN, M.Th. 1995.
Spatial variability of soil water retention functions in a silt loam soil. Soil Science, Vol. 159,1: 1-12

SRK (Steffen, Robertson and Kirsten). 1989.
Draft Acid Rock Technical Guide. BC AMD Task Force, Vol. 1.

van GENUCHTEN, M.Th., LEIJ, F.J. and YATES, S.R. 1991.
The RETC code for quantifying the hydraulic functions of unsaturated soils. Environmental Protection Agency, EPA/600/2-91/065.

van GENUCHTEN, M.Th and NIELSEN, D.R. 1985
On Describing and predicting the hydraulic properties of unsaturated soils. Annales Geophysicae, 3: 615-628.

van GENUCHTEN, M.Th. 1980.
A closed-form equation for predicting the hydraulic conductivity of unsaturated soils. Soil Science Society of America Journal, 44: 892-898.

YANFUL, E.K. and AUBÉ, B. 1993.
Modelling moisture-retaining soil covers. Proceedings of the Joint CSCE-ASCE National Conference on Environmental Engineering, Montreal, Vol. 1, 373-380.

YEH, T.-C. J, GUZMAN, A., SRIVASTAVA, R. and GAGNARD, P.E. 1994.
Numerical simulation of the wicking effect in liner systems. Ground Water, Vol. 32, 1:. 2-11.

WISE, W.R., CLEMENT, T.P. and MOLZ, F.J. 1994.
Variably saturated modeling of transient drainage : sensitivity to soil properties. Journal of Hydrology, 161 : 91-108.

ZIENKIEWICZ, O.C. 1977. The Finite Element Method. McGraw-Hill Book Company (UK) Ltd, Maidenhead, England, 787 p.

CAMI'95: 3rd Canadian Conference on Computer Applications in the Mineral Industry
Montréal, Québec, Canada, October 22-25, 1995

Conventional and New Methods For Treating Acid Mine Drainage

Nural Kuyucak
Water and Earth Sciences Associates Ltd.

ABSTRACT: The oxidation of sulphide minerals from tailings deposits, waste rock piles and mine workings results in formation of acid mine drainage (AMD) which is characterized by high acidity and elevated concentrations of sulphates and dissolved metals. AMD is treated to eliminate acidity, precipitate heavy metals and remove suspended solids. Lime neutralization is the most common and successful method of increasing alkalinity and reducing heavy metal concentrations in acidic metal-contaminated effluents. Sludge compaction and chemical stability are major concerns in the lime neutralization/precipitation process. Sludge dewatering and disposal costs can be reduced by improving process parameters. Several other methods and neutralizing reagents such as $Mg(OH)_2$, Na_2S, NH_3, NaOH and $CaCO_3$ are also used for treating AMD and for reducing the volume of the sludge. Ion exchange appears to be an alternative method to reduce difficult metals such as Mo, Hg, Se, to very low concentrations. Recently, possible application of membrane processes (reverse osmosis, ultrafiltration, microfiltration) for treating AMD have been investigated. Significant research efforts have also been made in developing passive treatment processes (e.g. wetlands, biosorbents and anoxic limestone beds). The use of biological sulphate reduction method in open pits and flooded mines has also been studied. Cyanide destruction can be achieved through SO_2, alkaline chlorination or hydrogen peroxide. Removal of NH_3 and NO_3 is difficult to achieve; some techniques are under investigation including biological nitrification and denitrification, chlorination, hydrogen peroxide oxidation and ion exchange.

RÉSUMÉ: Récents développements des méthodes de traitement conventionnelles, ce qui inclut la neutralisation par la chaux, l'oxidation par aération et les différentes techniques de densification des boues sont expliquées, ainsi que l'utilisation de neutralisants alternatifs.

INTRODUCTION

Mining and metallurgical operations generate several types of acidic and toxic effluents which are treated before their discharge to the environment. These effluents include mill tailings excess decant (or reclaim tailings water), acid mine drainage (AMD) and seepages, and process acid streams. Reclaim tailings waters are neutral to high pH containing <20 mg/L total dissolved metals and usually polishing with lime is sufficient to comply with regulatory limits. Process acid streams originate the use or generation of acids during metallurgical processes such as barren solutions, spent electrolyte and weak acids, and recycle process waters. Natural oxidation of sulphide minerals present in mine wastes, tailings and waste rocks, at mine sites results in occurrence of AMD. AMD is characterized as low pH, high acidity effluents containing heavy metals and sulphate. Regulations and guidelines for the mining industry are determined by federal and/or provincial agencies and, can be site specific and vary from site to site.

Control of AMD generation resulting from mining activities is not yet possible. Consequently, treatment of AMD is necessary to meet regulated water quality standards. Several processes investigated to treat AMD including neutralization, biological treatment, reverse osmosis, electrodialysis, crystallization, ion exchange and distillation (Yeh and Jenkins, 1971; Wilmoth et al., 1978; Ritcey, 1989; Kuyucak, et al., 1995; Borek et al., 1995; Riveros, 1995; Robertson and Rohrs, 1995). Results of extensive investigations indicated that ion exchange, reverse osmosis, distillation and electrodialysis are uneconomic due to power and chemical reagent costs. The most conventional treatment to neutralize AMD uses lime. Other alkalis such as NaOH form soluble salts at neutral pH that can lead to further environmental problems (Du Pont, 1987). The AMD characteristics profoundly affect system performance, final effluent quality and sludge characteristics.

To improve final effluent quality and to minimize sludge disposal issues, several other neutralizing reagents such as $Mg(OH)_2$, Na_2S, NH_3, NaOH and $CaCO_3$ are also used for treating AMD. Biological processes such as wetlands, sulphate reduction in reactors or in trenches and anoxic lime drains have recently received attention as cost-effective alternatives to conventional methods and their development is underway (Borek et al., 1995; Fyson et al., 1995; Kuyucak and St-Germain, 1994). However, lime (as CaO or $Ca(OH)_2$) is the most commonly used neutralizing reagent for treating AMD and other acid process waters because of its high reactivity, availability and relatively low cost. Chemical neutralization processes, in particular lime, are

considered as conventional processes and other methods considered as new ("emerging") technologies. In this communication, the emphasis will be given to lime neutralization techniques and parameters critical to the process performance. Alternative neutralization processes for acid waters will be briefly discussed as well as other technologies for removing cyanides and nitrogen compounds from process and mine effluents.

CONVENTIONAL PROCESSES

Lime Neutralization

In lime neutralization processes, acid is neutralized and metals, such as Fe $^{(2+/3+)}$, Zn, Cu, Al, and Pb, are precipitated in the form of metal hydroxides. The mixture of $CaSO_4$ (gypsum) and metal hydroxides is called "sludge". The principal reaction in lime neutralization can be expressed as follows (Eq. 1):

$$Ca(OH)_2 + Me^{2+}/Me^{3+} + H_2SO_4 <-> Me(OH)_2/Me(OH)_3 + CaSO_4 + H_2O \quad (1)$$

Air is frequently used to oxidize the ferrous to ferric iron during precipitation. The sludge produced is allowed to settle in clarifiers/thickeners. When the solid content is less than 1 mg/L sand bed filters are employed for polishing, to meet the required level of suspended solids in the final effluent (Kuyucak and Payant, 1995). The supernatant is then discharged to receiving stream and the settled sludge is disposed of in specifically designed ponds. Depending on site factors, lime neutralization facilities can vary greatly in degree of sophistication. They range from the simple addition of lime to the tailings pipe lines to plants consisting of reactors, clarifiers, and sludge dewatering equipment as depicted in Figure 1. The sludge densities vary from 1-30% solids, depending on the metal concentration of the water and the sophistication of treatment process. The formation of a voluminous sludge is an undesirable side effect of the process. Therefore, many recent studies in the field of lime neutralization of AMD have been directed toward generating denser sludges.

The current state-of-the-art lime neutralization process for treating AMD and other acidic waters is called the "High Density Sludge (HDS)" process and is capable of producing more compacted sludges than traditional methods of liming (Herman, 1983; Herman et al, 1984). In the HDS process, more than one reactor is used to perform the neutralization (Figure 1). A mixture of sludge, recycled from the clarifier underflow, and lime is used as the alkaline reagent in the first reactor. Both reactors are aerated to oxidize Fe^{2+} and pH is continuously monitored. The neutralized AMD with metal precipitates is then flocculated with a polymer and a clarifier/ thickener is used to facilitate S/L separation. The solid content in the resulting sludge is significantly higher (e.g. 10-30%) as opposed to the case not involving sludge recycle (Kuyucak et al., 1991).

A two-step lime neutralization ("NTC") process was developed by the Noranda Technology Centre to produce denser and less voluminous sludges (Kuyucak and Sheremate, 1992; Kuyucak et al., 1995). In this process, pH of the influent is raised to 4-5 with recycled sludge in the first reactor and, in the second reactor, pH is set to 9-10 and aeration is provided (Figure 2). Three pilot studies at three different mine sites were conducted. In all cases, sludge density and settling rates were improved by 30-50% as opposed to sludges generated by the high density sludge (HDS) process. The implementation of this process to Geco Mines is underway.

Critical Lime Neutralization Process Parameters

Rate of Neutralization: By fast neutralization of AMD with lime, the ferric iron is insolubilized in form of amorphous, gelatinous, hydrated ferric oxide ($Fe_2O_3.xH_2O$), that results in voluminous sludge (Burkhart and Voigt, 1986). The sludge generated in this way contains 1 to 1.7 percent solids. In case of HDS process. A controlled amount of the settled sludge is recycled, mixed with lime slurry that normally would be used in the neutralizer, and this sludge-lime slurry was then added to the neutralizer. OH^- ions are adsorbed on the recycled sludge which are gradually released into the water providing a control over the rate of neutralization.

Rate of Oxidation/Ferrous Iron Oxidation: It is preferred to remove iron as ferric hydroxide because it remains insoluble over a very broad pH range while ferrous hydroxide rapidly resolubilizes at pH values less than 11 (Rice and Herman, 1986). At a pH of 9 or more, the precipitated ferrous iron continues to oxidize, usually by air, resulting ferric iron precipitates and proton acidity (H^+).

Mixing Rate and Retention Time : Rapid mixing has a detrimental effect on sludge density (Bosman 1974). Good results were obtained when the peripheral velocity of the mechanical stirrer was between 1.3 and 4 m/s. The retention time required for mixing the recycled sludge did not increase substantially when the original retention time was 20 min or more.

Effect of Fe^{2+}/Fe^{3+} Ratio: Kostenbader and Haines (1970) found that the max attainable sludge density was

Figure 1 Types of lime neutralization processes

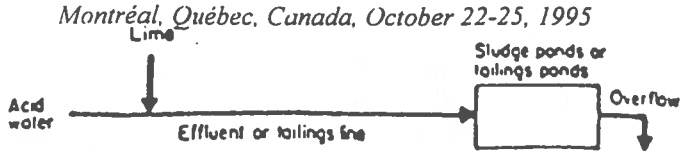

Type 1. Lime addition to effluent or tailings lines.

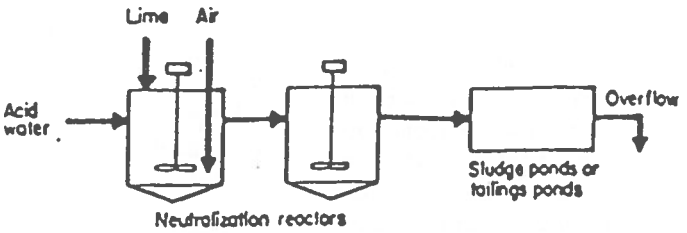

Type 2. Lime addition to neutralization reactors. Solid/liquid separation in ponds.

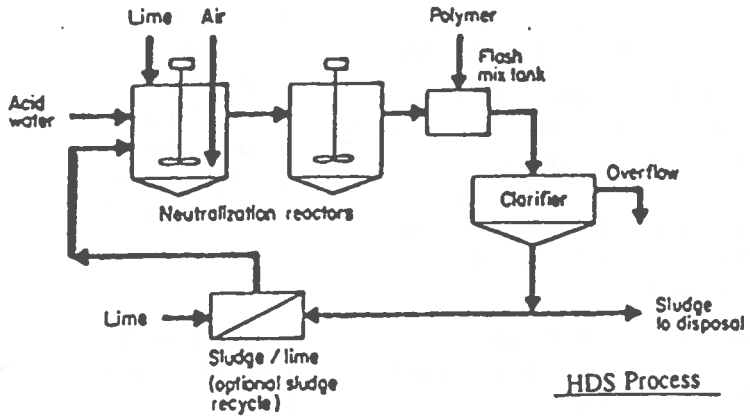

Type 3. Lime addition to neutralization reactors. Solid/liquid separation in clarifiers.

Figure 2 Two-step NTC Process Flowsheet.

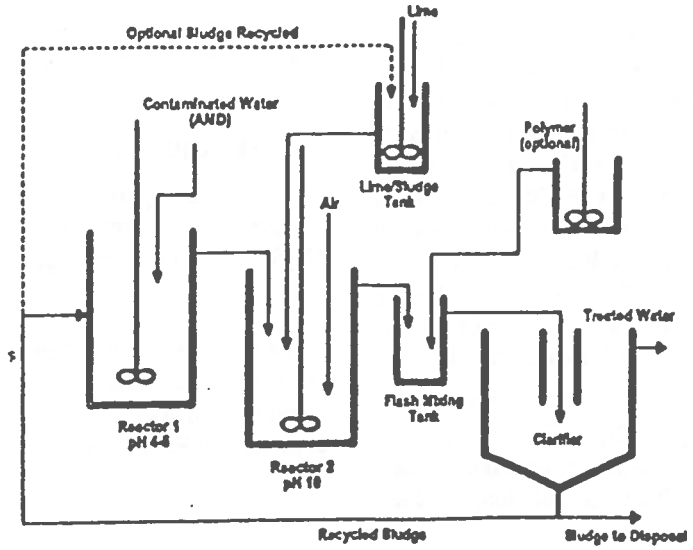

very dependent on Fe^{2+}/Fe^{3+} ratio. Bosman (1974) reported that higher sludge densities resulted from acid water having higher proportion of Fe^{2+}. Betlehem Steel researchers (Herman et al., 1984) also indicated the importance of ferrous iron stating that 15 to 40% solids could be achieved depending on the ratio of Fe^{2+}/Fe^{3+}. It is explained that adsorption of ferrous iron onto ferric iron leads to the generation of denser sludges.

Recycling of Settled Sludge: Recycling of sludge has been attempted to produce denser sludges. Birch (1970) noted that the settling time was reduced by about 50%. Larger and heavier flocs were produced when the precipitated sludge was recycled. Improved solids content reduces thickener requirements and final sludge volume (Kuit, 1980). Many investigators reported that by recycling the sludge to the raw AMD, lime requirements for the treatment may be reduced up to 30% (Kuyucak et al., 1995; Keefer and Sack, 1983).

The other process variables of major importance were stated to be recycle ratio, pH, point of lime slurry addition, temperature, and crystallization. The best neutralization pH was found to be 7.2-7.7 for iron. At low pH values, the oxidation rate of ferrous iron was too slow and at high pH values, thickener operating problems were encountered.

Aging Effect: Sludge solids content may be increased by aging. In the study conducted on lime sludges of Canadian Mineral Industry, fresh and aged sludge samples from the same locations indicated similar characteristics except the total solids content. The mechanism of sludge compaction by aging can be explained by hydrolysis and condensation reactions that take place.

Metal Removal Efficiency: Lime neutralization is efficient for treatment of common heavy metals. However, complete precipitation of all metals cannot be expected at the same pH in AMD containing a combination of metals such as Cu, Zn, Ni, Cd, Pb, and Fe. As illustrated in Figure 3, for metal hydroxides, there exist an optimum point where solubility limit is achieved and metal hydroxides precipitate out of solution. At pH 9 to 10, Cu and Zn can be reduced to levels of < 0.1 mg/L while Pb and Fe^{3+} are reduced to µg/L (Monhernius, 1986). Levels of Cd and Ni below 1 mg/L can be achieved with pH adjustment above 10 unless the water contains high levels of iron. Cr can be lowered to levels of <0.5 µg/L at pH 7-8, following reduction of Cr^{6+} to Cr^{3+}. Mn removal requires strong oxidation followed by liming at pH greater than 10.

Other contaminants such as As, Sb, Mo and Se require additional chemicals (H_2O_2, $FeCl_3$ or $Fe_2(SO_4)_3$, Na_2S, CO_2) as adjuncts to lime process. A common method for removing Hg is by sulphide precipitation, resulting in an effluent of 10-20 µg/L. Co-precipitation with iron lowers Mo from 4 mg/L to 0.5 mg/L. Ion exchange appears to be an alternative method to achieve low Hg and Mo levels, 1 to 5 µg/L and 2 mg/L, respectively. Oxidation of As^{3+} to As^{5+} is necessary to remove As from effluent prior to lime and ferric iron precipitation. For removal of less common metals, such as As^{3+}, As^{5+}, Ba, Cr^{6+}, Hg, Se^{4+} and Se^{6+} from effluents, in some cases, pH adjustment is ineffective, or not quite effective. Therefore, other emerging technologies (ion exchange, membrane separation, solvent extraction, etc.) should be considered to meet the required standards.

Stringent final effluent limits for controlling dissolved level of Cd and Mn have been met by addition of sulphide (Na_2S) during lime treatment at pH 10.5 into the first reactor (Kuyucak and Payant, 1995). The process developed by Spira and Kuyucak (1989) was implemented at full-scale at Samatosum Site, Kamloops, British Columbia. Dynasand filters were installed to separate solids and produce an final effluent quality with low turbidity and containing metals below 0.1 mg/L total for each of the heavy metals (i.e. Zn, Pb, Mn, Cd).

In-Line Lime Treatment: Neutralization and aeration were combined into single step by injecting a caustic reagent into the port of a jet pump (Ackman and Kleinmann, 1984). Oxidation of Fe^{2+} occurred in a few seconds indicating that combining neutralization and aeration optimized reaction rates. Overall cost of the process including capital, operating and maintenance was also found to be much lower than the conventional mechanical aerators. However, for higher concentration of Fe^{2+} (>200 mg/L), in-line lime treatment was inefficient; the conventional neutralization process was found to be more feasible. The in-line method was recommended to neutralize low strength AMD containing Fe, Zn, Cu, Pb, Mg (43, 38, 0.96, 0.4, 17 mg/L, respectively).

Alternative Neutralizers

As has been reported by several investigators, denser sludges can be obtained when $CaCO_3$, $Mg(OH)_2$, or Na_2S (or CaS) is used as the neutralizing agent.

Limestone ($CaCO_3$) Neutralization: Limestone can remove acidity and precipitate iron Svanks, 1973). Limestone in AMD dissociates and CO_2 gas evolves as expressed in Eq.s 2 and 3.

$$CaCO_{3(s)} + H_2SO_{4(aq)} <---> CaSO_{4(s)} + H_2O + CO_2(g) \quad (2)$$

$$CaCO_{3(s)} + Fe_2(SO_{4(aq)})_3 + 3H_2O <---> 3CaSO_{4(s)} + 2Fe(OH)_{3(s)} + 3CO_{2(g)} \quad (3)$$

The slower oxidation rate of ferrous iron favours the formation of the crystalline precipitates (goethite) resulting a high density sludge. However, limestone neutralization may offer some disadvantages. Due to CO_2 gas release, carbonate ion is formed. Carbonate ion acts as a buffer and sets an upper limit on pH (max pH 6.5) and also affects the rate and amount of lime consumption. Ferrous iron remains in solution as suspended solids at the pH of 6.5 (Ackman, 1982). Ferrous iron should, therefore, be oxidized to ferric before the neutralization process. Powdered limestone used in a well-mixed system where surface of limestone is continuously scoured. The precipitates may settle very slowly because of their small particle size. Removal of broad range of metals cannot be achieved since they require higher pH levels than 6.5.

A combination of limestone-lime treatment process was suggested by Svanks (1973). The Dowa Mining Co. (Japan) has developed a two step process where ferrous iron is biologically converted to ferric iron followed by limestone neutralization (Imaizumi, 1986). The process was resulted in a savings of up to 66% of total process cost as compared with the previous method in which elevated temperatures and nitric acid were used to oxidize iron before neutralization.

Magnesium Hydroxide ($Mg(OH)_2$): $Mg(OH)_2$ can result in a lower volume and more dense metal hydroxide sludge when it is properly applied in the neutralization system. $MgSO_4$, which is more soluble than $CaSO_4$, forms in the process and $Mg(OH)_2$ can also remove metals through surface adsorption (Teringo, 1987). However, the rate of neutralization is slow and depends on several conditions beyond the usual kinetic effects of increased temperature and agitation. The concentration of acid being neutralized has an inverse effect on the rate of neutralization as well as the concentration and type of other metals present. The buffering capability of $Mg(OH)_2$ prevents the pH from exceeding 9. Depending on the pH requirements, it can be used in conjunction with NaOH. Due to its slow kinetics requiring hours to react and its relatively high cost, $Mg(OH)_2$ and dolomites are less commonly used in treating AMD. $Mg(OH)_2$ is usually employed in treatment plants, such as Canadian Copper Refinery (CCR) in Montreal east, where the disposal cost of sludges generated is high, in order to reduce sludge disposal costs.

Sulphides: Sulphide precipitation (Na_2S) has been used to treat wastewaters from metal finishing industries; it is not routinely used to treat AMD. Solubilities of metal sulphides are usually several orders of magnitude less than metal hydroxides (Figure 3). Na_2S, FeS, $(NH_4)_2S$, BaS or H_2S can be used as reagents. Sulphide precipitation results in better metal removal in effluents which contain phosphate, ammonia, organics, surfactants, chelators and Cr^{6+} (US EPA, 1980). Removal of Hg, As and Cd by sulphide precipitation can be achieved at pH 5.5-6.5. The sludge volumes produced are less than those resulting from hydroxide precipitation and the metals precipitate as sulphides at lower pH. The H_2S evolution from the system and, fine and colloidal metal precipitate formation which are difficult to settle and separate have been found to be potential problems. These problems can be alleviated by the addition of Fe^{2+} as $FeSO_4$ to scavenge the excess H_2S and by filtering the resulting solution.

The mine water occurring in the Laisvall mine of Boliden Mineral AB, Sweden has been treated with Na_2S to remove Pb (0.5 mg/L) and Zn (0.7 mg/L). The full-scale process involves precipitation of Pb and Zn with Na_2S, flocculation with a cationic polymer and sludge separation in sand filters which are intermittently backwashed. A small addition of Na_2S (e.g. 5 mg/L) in lime neutralization at pH 10.5 was suggested to lower Cd less than 0.01 mg/L in the treated tailings water of Samatosum (Spira and Kuyucak, 1989).

Sodium Hydroxide (NaOH): It has high reactivity and results in less voluminous sludge. But, it is not commonly used because, the resulting sludge does not settle well and in most cases requires filtering and it is expensive.

Ammonia (NH_3): It is preferred by coal mining industries due to its high solubility and resulting less sludge properties. It is usually injected near the bottom of ponds or inlet water as gaseous anhydrous ammonia (Phipps, et al., 1991). Some hazards are associated with handling of ammonia as well as some uncertainty concerning potential biological reactions. However, the use of ammonia has been suggested to be a feasible alternative to lime for neutralizing low flows containing low acidity.

Others (Waste/By-Products of Industries): Some waste or by-products of industries such as power plants, crude oil combustion and gasification processes have potential as a lime substitute for the treatment of AMD.

For example, fly ash from power stations which use alkaline dry scrubbing holds some potential as neutralizing reagents. However, metal contaminants present in fly ash may raise some concerns and its reaction rate may be slow as compared to lime.

Coagulation/Flocculation For Better Solid/Liquid Separation

Following neutralization, the fine particles (precipitates) in suspension need to be aggregated for satisfactory solid/liquid (S/L) separation or sedimentation in clarifiers (Degremont, 1973). Agglomerated material usually contines to dewater with time (Smelley, 1980). Some advantages can also be taken from this property by storing the sludge on a bed of coarse material (i.e. sand) for further compaction. Aggregation is a formation of a group of particles held together in any manner; furthermore, coagulation is a specific type of aggregation which leads to formation of aggregates called flocs that are compact (Somasundaran, 1980). Floc formation is initiated by the addition of a coagulant to discharge or destabilize the electronegative colloids and bridge the neutral particles (Benefield, et al., 1982). A coagulant can be either from inorganic or organic origin. The salts of Al^{3+} and Fe^{3+} are commonly used as coagulants (inorganic) in water and wastewater treatment. Organic coagulants called "polymers" are broadly classified into natural or synthetic origin, the latter type predominating in water treatment applications due to its relative low cost

Polymer performance in coagulation, flocculation, sedimentation, filtration and sludge conditioning is usually evaluated by screening available polymer types in jar tests (Dentel, et al., 1988). In this way, a potential polymer is selected and optimum doses for water treatment applications are determined. It was found that fish gills are negatively charged and can easily accumulate positively charged materials causing suffocation of fish (Gron, 1991). The use of mixture of cationic and anionic polymers can alleviate the problem. The temperature of the system, viscosity and chemical characteristics of the pulp, and external stirring are important parameters in the flocculation process.

pH Adjustment In Final Effluent

Often regulations require to have the pH between 6.5 and 9 in the final effluent. The pH is adjusted to the desired level with either sulphuric acid or CO_2. If an increase in SO_4 levels is not a concern, sulphuric acid is preferred. Otherwise, CO_2 is used (Kuyucak and Payant, 1995; Bartlett and Payant, 1991).

Sludge Dewatering Options

Lime treatment plants generally utilize one basin for the dual purpose of effluent clarification and sludge thickening. Dewatering via filters has not been widely practised in mining industries and has been considered as a very site specific application. However, sludges containing less moisture can be sent to recovery operations (i.e. smelter) or high sludge disposal costs can be reduced with an appropriate dewatering method (Cushnie, 1984).

The technique of freeze-dewatering has been investigated as an efficient alternative. Streeter et al. (1971) reported that the volume of sludge generated from coal mine drainage can be reduced by 90% with a single freeze-thaw cycle. X-ray diffraction analysis on lime sludges revealed that freezing helped to build crystalline gypsum components, forcing particles into more tightly compacted solids pocket (Kuyucak, et al., 1991). Iron compounds were not affected by the freeze-thaw process. Some investigators also noted that the sludge must be frozen at low rate (Martel, 1989; Vesilind and Martel, 1990). A feasible rate of freezing can be obtained by manipulating the depth of the sludge.

Sludge Stability and fixation

During storage of the sludge, heavy metals may become solubilized and released in the water in the sludge pond. Overtime, those metals may migrate into ground and surface waters. Possibility of metal mobilization is determined by a "leaching test" (e.g. EPA's TCLP, Menviq, etc.). Depending on sludge characteristics and site specific requirements, sludge is stabilized by mixing with cement and/or lime prior to its disposal.

EMERGING TREATMENT PROCESSES

In order to reduce drawbacks, such as high capital and operating costs, production of large volume of sludges, meeting stringent final effluent quality requirements (e.g. reduced metals, SO_4 and total suspended solids), associated with the conventional processes, new technologies are sought. Emerging technologies are mainly based on either physico-chemical (ion exchange, membrane processes) or biological (e.g. wetlands, sulphate reduction) principals. Ion exchange and membrane processes (i.e. reverse osmosis, ultrafiltration, microfiltation, etc.) could be employed for very site specific applications because, these methods are still not technically and economically feasible for treating AMD. Passive processes have received attention as alternatives to conventional methods for treating AMD, particularly for replacing

common collection and treatment practices which would be unaffordable for low flow streams and seepages (Kuyucak and St-Germain, 1993; Kuyucak and St-Germain, 1994a,b). Major passive processes investigated to date include: Wetlands, Sulphate Reduction/The use of Sulphate Reducing Bacteria (SRB), Anoxic Limestone Drains (ALD), Biosorbents. They all have been found to be suitable for the treatment of low flow and low strength AMD situations. However, ALD have been practised widely in the United States for restoration of abandoned mine sites and for pretreating AMD before routing to a constructed wetland (Brodie et al., 1992).

Wetlands: A wetland usually composed of two distinct zones: Oxidation, where is vegetated with aquatic plants, and Reducing, where is the sedimentation zone rich in SRB, denitrifying and Mn reducing bacteria. Organic and inorganic compounds, and suspended solids can be removed. Plants play a filter role, take up metals and help for oxidation processes to occur while bacteria act as catalyzers for chemical reactions.

Sulphate Reduction (The use of Sulphate Reducing Bacteria "SRB"): SRB convert SO_4 in AMD to H_2S, and carbonic nutrients to bicarbonates. Thus, the reaction products play an important role in removing metals as sulphides and increasing alkalinity (pH). Organic materials, such as straw, sawdust, wood shavings, manure, are added into the system to provide a slow release nutrients to bacteria. Sometimes, limestone and soil are also added into the nutrient mixture to increase alkalinity and, subsequently, enhance the activity of SRB.

The use of SRB in controlled reactors has been implemented by Budelco, The Neitherland, at full-scale to remove metals and SO_4 from underground mine water (Scheeren et al., 1992). Parameters critical to the success of the process are: Temperature, nutrients, alkalinity, retention time, bacterial population, contaminants present in AMD and loading rates (flow, acidity and metals).

Anoxic Limestone Drains (ALD)

An ALD system generally consist of an excavated seepage interception trench backfilled with crushed limestone and covered with plastic and clay-soil to keep air out (Brodie, et al., 1992). ALD basically provides an increase in alkalinity. Oxidation of Fe^{2+} and formation of ferric oxyhydroxides, which armour the limestone and prevent decrease in alkalinity, are thus avoided. Designs of ALD are reported to be site-specific (Hedin and Nairn, 1992). Usually, an ALD system is followed by a wetland for oxidation and precipitation of iron and other contaminants.

Biosorbents

Biological materials such as sawdust, sphagnum moss or algae can be used as adsorbents (or biosorbents) in treating AMD. A bed of biosorbents can be placed where the seepage occurs. When it is saturated by metals, the proponents suggest it can either be disposed of (with tailings or recycled to a smelter), or washed with an appropriate eluate for recovery of metals (Kuyucak and St-Germain, 1993).

CYANIDE DESTRUCTION AND REMOVAL OF NITROGEN COMPOUNDS

The widely used method for removal of cyanides and ammonia is natural degradation in holding ponds. Cyanides are oxidized giving ammonia and carbon dioxide (Kilborn, 1991; Ritcey, 1989). Then, natural degradation of ammonia involves the transpiration of dissolved ammonia gas from the wastewater. The removal is enhanced by increasing pond area, increasing pH and by allowing for more contact with air. A biological process unique to Homestake Mining in South Dakota decomposes metal-cyanide complexes and efficiently oxidizes cyanides to ammonia which is further oxidized by bacteria ("nitrification") to nitrate. Base metal cyanide complexes are selectively oxidized to cyanate by mixture of SO_2 and air, in the presence of copper as a catalist, in controlled pH range. This is a proven process and is known as Inco Method. Similarly to the Inco process, hydrogen peroxide can oxidize cyanides to cyanates. The peroxide method is also used at a number of operations. Hemlo Gold (Noranda) adds the premixed $CuSO_4/FeSO_4$ reagent to the mill solution, in which the pH is controlled at 9.5 and cyanide is removed with cuprous ions. Other methods such as: air stripping, steam stripping, alkaline chlorination with hypochlorite at pH 10-11, engineered wetlands, acidification/volatilization, adsorbents and ion exchange resins for removal of cyanides and ammonia have limited use.

The potential processes for removal of nitrates and nitrites include: biological denitrification where nitrates/nitrites are reduced to nitrogen gas, ion exchange and reverse osmosis where nitrates/nitrites are removed from the water and are obtained in a very concentrated form requiring further disposal methods. Wetland filtration has a limited use.

References

Ackman, T.E., 1982. Sludge Disposal from AMD Treatment. USBM Report of Investigations, RI: 8672.

Ackman, T.E., and R.L.P. Kleinmann, 1984. In-line Aeration and Treatment of Acid Mine Drainage. USBM Reports of Investigations, RI:8868.

Bartlett, D., and S. Payant. 1991. Noranda Minerals Inc Review of Effluent Treatment Plants 1991 Update. Research Report, Env. & Min. Lab. Centre de technologie Noranda.

Benefield, L.D., J.F. Judkins, and B.L. Weand. 1982. Process Chemistry for Water and Wastewater Treatment. Prentice Hall, N.J.

Birch, J.T., 1970. "Application of Mine Drainage Control Methods", 2nd Symp. on Coal Mine Drainage Res., Mellon Inst., Pittsburgh, P.A.

Borek, S.L., D.H. Dvorak, and H.M. Edenborn, 1995. Ability of Cheese Whey to Support Bacterial Sulfate Reduction in Mine Water Treatment Systems. In the proceedings of *Sudbury '95 Mine Environment Conf.*, Sudbury, Ont, May 28-31, 1995. Ed.s: T.P. Hynes and M.C. Blanchette. p. 879-885.

Bosman, D.J. 1974. The Improved Densification of Sludge from Neutralized AMD. J. of South African Inst. Min. Met., April'74.

Boyd, J.L., and D.A. Dahlstrom, 1975. Heavy Metal Removal for Water Reuse and Effluent Treatment, AIME Annual Meeting, 16-20 February 1975, New York, N.Y.

Brodie, G.A., Britt, C.R., Tomaszewski, T.M., and Taylor, H.N., 1992. Anoxic Lime Drains to Enhance Performance of Aerobic Acid Drainage Treatment Weltands, Presented at the 1992 West Virginia Surface Mine Drainage Task Force Symp. April, Morgantown, West Virginia.

Burkhart, L. and J. Voigt, 1986. Aqueous Precipitation in Hydrometallurgy, Hydrometallurgical Reactor Design and Kinetics, SME-AIME Symp. Eds: R.G. Bautista, R.J. Wesely, G.W. Warren, March 2-6, 1986, New Orleans, Louisiana. The Metal. Soc. Inc. Publ.

Chusnie, G.C., 1984. Removal of Metals from Wastewaters. "Neutralization and Precipitation". Pollution Technol. Review, No. 107. Noyes Publ., N.J., U.S.A.

Degremont, G., 1973. Coagulation, Flossulation, Sedimentation. Water Treatment Handbook. 4:111-141.

Du Pont, A., Lime Treatment of Liquid Waste Containing Heavy Metals. Pollution Eng., 19: 84-88.

Environment Canada, 1975. Mine and Mill Wastewater Treatment, EPS 3-WP-75-5.

Freedman and Shannon, 1973. Modern Alkaline Cooling Water Treatment. Industrial Wastewater Engineering, Jan-Feb., 1973. p. 31.

Gron, P., 1991. Samatosum Treatment Plant, Minnova Inc.

Fyson, A., M. Kalin, and M.P. Smith, 1995. Microbially-Mediated Metal Removal from Acid Mine Drainage. In the proceedings of *Sudbury '95 Mine Environment Conf.*, Sudbury, Ontario, May 28-31, 1995. Ed.s: T.P. Hynes and M.C. Blanchette. p. 459-466.

Hedin, R.S., and Nairn, R.W., 1992. Designing and Sizing Passive Mine Drainage Treatment Systems. Presented at the 1992 West Virginia Surface Mine Drainage Task Force Symp., April, Morgantown, West Virginia.

Herman, S.T., J.B. Pfeiffer, R.T. Sewaird, and C.J. Stoner. 1984. Treatment Of Industrial Wastewaters, U.S. Patent No. 4, 465597.

Herman, S.T. 1983. The High Density Sludge Process: An Improved Technology for Hydroxide Precipitation of Heavy Metals. EPA/AISI Symp. on Iron and Steel Pollution. Abatement Technolog. Chicago, OH.

Imaizumi, T., 1986. Some Industrial Applications of Inorganic Microbial Oxidation in Japan. Biotechnol, Bioeng. Symp. No. 16, p. 363-71.

Keefer, G.B., and W.A. Sack, 1983. Sludge Recycle and Reuse in Acid Mine Drainage Treatment, Y. WPCF, 55:278-284.

Kilburn, Inc., 1991. Ministry of Environment, Metal Mining Sector. Best Available Pollution Control Technologies, Dec. 91.

Kim, B.M., 1981. Treatment of Metal Containing Wastewater with Calcium Sulphide. AIChE Sym. Series; Water, Vol. 77, No: 209.

Kostenbader, P.D., and Haines, G.F. 1970. "High Density Sludge Process for Treating AMD". 3rd Symp. on Coal Mine Drainage Research, Pittsburgh, PA.

Kuyucak, N., T.M. Sheremata, and K.G. Wheeland, 1991. Evaluation of Improved Lime

Neutralization Processes, Part I: Lime Sludge Generation and Stability. 2nd Int. Conf. on the Abatement of Acidic Drainage, September '91, Montreal, Canada. Vol. 2, p 1-14.

Kuyucak, N., R.J. Mikula, and K.G. Wheeland, 1991. Evaluation of Improved Lime Neutralization Processes, Part III: Interpretation of Properties of Lime Sludge Generated by Different Processes. 2nd Int. Conf. on the Abatement of Acidic Drainage, September '91, Montreal, Canada. Vol 3.

Kuyucak, N. and S. Payant, 1995. Lime neutralization methods for improving sludge density and final effluent quality. In the proceedings of *CIM, 2nd Int. Symp. on Waste Processing and Recycling,* Vancouver, BC, August 19-23, 1995.

Kuyucak, N., S. Payant, and T. Sheremata, 1995. An improved lime neutralization process. In the proceedings of *Sudbury '95 Mine Environment Conf.,* Sudbury, Ontario, May 28-31, 1995. Ed.s: T.P. Hynes and M.C. Blanchette.

Kuyucak, N. and P. St-Germain, 1994,a. Possible options for in-situ treatment of acid mine drainage seepages. *Int. Land Reclamation and Mine Drainage Conf. and 3rd Int. Conf. on Abatement of Acid Drainage,* Pittsburg, PA, April 26-29, 1994.

Kuyucak, N. and P. St-Germain, 1994,b. In-situ treatment of acid mine drainage by sulphate reducing bacteria in open pits: scale-up experiences. *Int. Land Reclamation and Mine Drainage Conf. and 3rd Int. Conf. on Abatement of Acid Drainage,* Pittsburg, PA, April 26-29, 1994.

Kuyucak, N., and T. Sheremata. 1992. Improved Lime Neutralization Process. U.S. and Canada Patent Pending, Case no. 336.

Martel, J.C., 1989. Lime Substitutes for the Treatment of AMD, Min. Eng. J., Jan. 87, p. 33-36.

Monhemius, A.J., 1986. Precipitation Diagrams for Metal Hydroxides, Sulphides, Arsenates and Phosphates. Trans. IMM, C202-C206.

Phipps, T.T., W.A. Fiske, and J.G. Skousen, 1991. A Methodology for Evaluating the Costs of Alternative AMD Treatment System. 12th Annual West Virginia Surface Mining Drainage Task Force Symposium, Morgantown, WV, April 3-4, 1991.

Rice, M.A., and S.T. Herman, 1986. Removal of Complexed Zinc-Cyanide from Wastewater with Improved Sludge Stability. US Patent No. 4 606 829.

Ritcey, G.M., 1989. Tailings Management, Problems and Solutions in the Mining Industry. Process Met. 6, Elsevier Publ.

Riveros, P.A., 1995. Application of Ion Exchanges to the Treatment of Acid Mine Drainage. In the proceedings of *Sudbury '95 Mine Environment Conf.,* Sudbury, Ontario, May 28-31, 1995. Ed.s: T.P. Hynes and M.C. Blanchette. p.441-449.

Robertson,A.M.,andR.G. Rohrs,1995. Sulfate Removal of Acid Mine DrainageWaterAfter Lime Treatment. In the proceedings of *Sudbury '95 Mine Environment Conf.,* Sudbury,Ontario, May 28-31, 1995. Ed.s: K. Mailhort and T.Hynes. p. 575-685.

Scheeren, P.J.H., R.O. Koch, C.J.N. Buism,an, L.J. Barnes and J.H. Versteegh, 1992. New Biological Treatment Plant for Heavy-Metal Contaminated Groundwater. *Trans. Instu. Min. Metall* 101: C190-C199.

Singer, P.C., and W. Stumm, 1969. Oxygenation of Ferrous Iron; the Rate-Determining Step in the Formation of Acidic Mine Drainage. US EPA, Report No DAST-29, 1401006/69.

Smelley, A.G., B.J. Scheiner, and J.R. Zatko, 1980. "Dewatering of Industrial Clay Wastes". USBM. Res., RI 8498.

Somasundaran, P., 1980. Principles of Flocculation, Dispersion, and Selective Flocculation. Fine Particle Processing AIME Sym. NY. 2:947-76.

Spira, P., and N. Kuyucak, 1989. Treatment of Samatosum Tailings Water, Research Report, Noranda Technology Centre, RR N-8821-5C: RR 89-1.

Streeter, R.C., R.K. Young, and R.A. Glen, 1971. Studies on Densification of Coal Mine Drainage Sludge, NTIS Publ., PB 203 189, BCR Inc., Pennsylvania.

Stumm, W., and J.J. Morgan, 1981. Aquatic Chemistry, 2nd Ed., Wiley Sci. Inc., NY

Svanks, K., 1973. "Factors Controlling Sludge Density during Acid Mine Drainage Neutralization". Ohio State University, PB-226615.

US EPA Technology Transfer Report, 1980. Control and Treatment Technology for the Metal Finishing Industry, Sulphide Precipitation. EPA 625/8-80-003.

Vesiland, P.A., and C.J. Martel, 1990. Freezing of Water and Wastewater Sludges. J. Env. Eng., Vol. 116, No. 5, p. 854-862.

Wilmoth, R.C., T.L. Baugh, and D.W. Decker, 1978. Removal of Selected Trace Elements from AMD Using Existing Technology, 33rd Ind. Waste Conf. Purdue Univ., p. 886-94.

Yeh, S.J., and C.R. Jenkins, 1971. Disposal of Sludge from AMD Neutralization, J. of WPCF, p. 679-88.

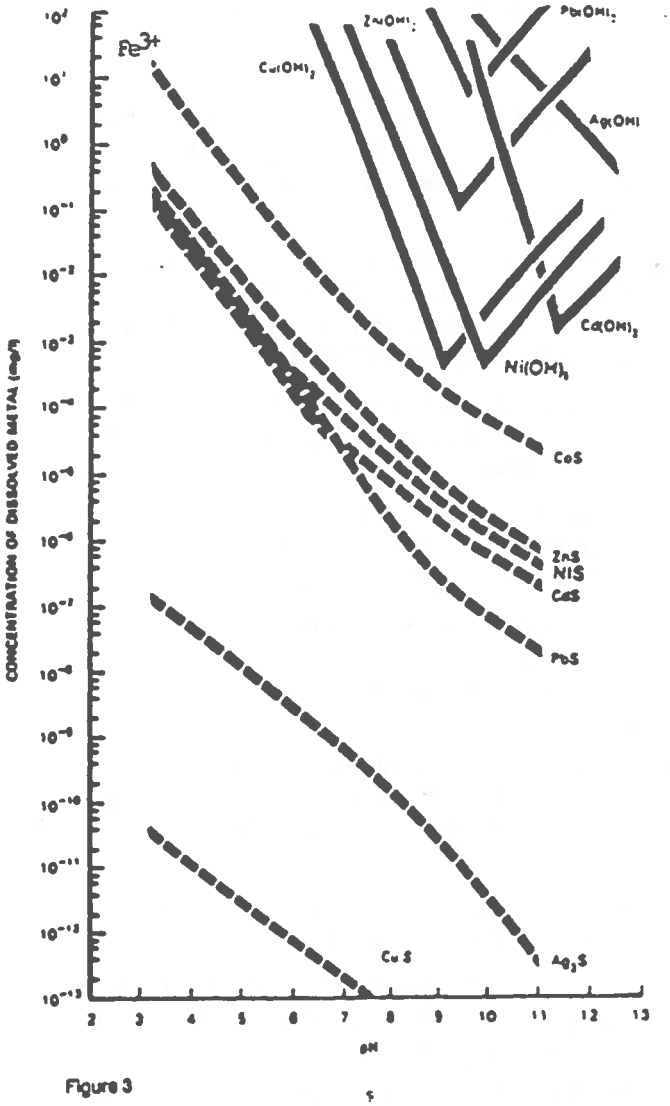

Figure 3

Comparison of Solubilities of Metal Hydroxides and Sulphides as a Function of pH (adapted from Kim, 1981; Freedman and Shannon, 1973).

CAMI'95: 3rd Canadian Conference on Computer Applications in the Mineral Industry
Montréal, Québec, Canada, October 22-25, 1995

Applications of Finite Element Techniques in the Analyses of the Stresses and Deformations of Tailings Dams

Hani M. Keira
Groupe AXOR, Montreal, PQ

Caius Priscu
McGill University, Montreal, PQ

Bachir Touileb
Hydro Quebec, Montreal, PQ

ABSTRACT:

The nature of tailings dams makes them sensitive to liquefaction. To evaluate properly the liquefaction potential, the stress distribution should be properly evaluated. One approach is to use the finite element method for that purpose. To define properly the modelling requirements, the paper reviews types of tailings dams, their composition and general geometry, engineering characteristics of tailings and impacts of methods of tailing deposition on dam behaviour.

Different constitutive laws which represent soil behaviour are presented, with summary of methods of obtaining their parameters and discussions on their limitations.

Available finite element stress and deformation models are reviewed along with the advantages and limitations of each model, in dealing with the analyses of tailings dams and recommendations for future studies.

RÉSUMÉ

Par la nature des stériles de mine, les barrages en stériles sont très susceptibles de se liquéfier. Avant d'évaluer leur potentiel de liquéfaction, la distribution des contraintes devra être connue.

Une façon d'aborder ce problème est d'utiliser la méthode des éléments finis. En vue de bien définir les éléments nécessaires pour la modélisation, cet article présente une revue des différents types de barrages en stériles, leur composition, leur géométrie et les caractéristiques des stériles de mine. L'impact de la mise en place (séquence de construction) des stériles est aussi discutée.

Différentes méthodes de modélisation du matériel (lois constitutives) sont présentées, ainsi que les méthodes pour obtenir les paramètres impliqués, et leurs limitations.

Finalement, différents programmes existants d'analyse par la méthode des éléments finis sont présentés, avec leurs avantages et leurs limitations quant à l'analyse numérique des barrages en stériles. Des recommandations pour des études futures sont proposées.

1.0 CHARACTERISTICS OF TAILINGS DAMS

1.1 Processing of Ore and Tailings Development

The process of ore includes: (a) Primary and secondary crushing and grinding of ore. (b) Separation of concentrate from tailing by : (b-1) **Gravity separation**, where sluices and/or classifiers (with water) are used to collect the lighter or the heavier particles leaving the remaining particles as tailings.(b-2) **Magnetic separation**, where magnetic particles are collected and nonmagnetic particles remain as tailings. (b-3) **Forth flotation**, where mineral bearing particles are made water repellent and receptive to attachment to air bubbles, particles with higher mineral content rise to the surface and is skimmed and the remaining particles become tailings. Other methods of processing, which may be used to supplement or replace concentration, are leaching and heating. (c) Part of the water is then removed from the slurry (pulp) following separation using thickeners, hydro-cyclones, drum, disc and belt filters. Tailings are transported in slurry form to the tailings impoundment. (d) The tailings are then deposited behind tailings dam by either single point discharge or spigotting.

1.2 Tailings Depositional Characteristics

Physical Characteristics: Tailings are deposited hydraulically, accordingly, coarser tailings particles tend to settle near the point of discharge. Finer and colloidal particles are carried further to the ponded water or the decant pond, where they eventually sediment in standing water. This results with (a) above water **tailings beach** with average slope grade of 0.5 - 2.0 % in the first few 100 meters (steeper slopes resulted from higher pulp density and/or coarse gradation). At a longer distance slope may flatten to 0.1%. (b) **Slimes** zone associated with the settlement of colloidal particles when they reach still water of the decant pond.

The hydraulic deposition results with heterogeneous deposits in the vertical direction in layered system. The variation of fines % in the deposit is 10 - 20% for closely spaced discharge points and may reach 50% for large spaced ones. Horizontal variation takes place also with coarser particles settling closer to the discharge point. Particles segregation is influenced by gradation characteristics and pulp density of discharged slurry.

The minimum density of the sand tailing ranges between 1.2 to 1.58 t/m^3 with voids ratio e = 0.72 to 1.32. **The maximum density** is ranging between 1.58 to 2.06 t/m^3 with e = 0.51 to 0.68. Average **in-place relative density** of sand tailings is ranging between 10 to 50% and it may reach up to 68% (cycloned copper sand). **The specific gravity** ranges between 2.6 and 3.3, except for coal which can be as low as 1.4.

Engineering Characteristics: Due to the nature of hydraulic deposition and the stratification, considerable variation between k_h and k_v permeability was found. Ratio k_h/k_v in the range 2 - 10 for uniform beach sand deposits or under water deposited slimes. Ratio $k_h/k_v >$ 100 were reported for zones of uncontrolled discharge with sand-slime inter-layering. Zone of high permeability sand are found near the point of discharge, while low permeability is found in the slimes zone. The relative width of each zone depends on the relative proportion of sand to slimes and the location of ponded water relative to the discharge point. The permeability varies between 10^{-2} to $5x10^{-4}$ cm/s for sands and 10^{-4} - 10^{-8} cm/s for slimes.

Sand and slimes tailings are more compressible than natural soils due to (a) loose deposition state (b) high angularity (c) grading characteristics. Over-consolidation may be produced by desiccation or capillary suction on exposed above water slime deposits.

The compression index C_c of slimes (0.20 - 0.30) is about 3 to 4 times than that of sand (0.05 - 0.1). Density at deposition or initial voids ratio has major impact on compressibility. The looser the initial state, the higher the compressibility.

Bauxite slimes and gypsum tailings exhibit time-dependent deformation characteristics due to inter-particle bonding and/or creep of the individual grains.

The primary consolidation governs the rate of pore pressure dissipation under constant load. In sand tailings it takes place very fast. For beach sand deposits, **the coefficient of consolidation** c_v varies between 5×10^{-1} to 10^2 cm^2 /sec. For slimes tailings, the coefficient of consolidation c_v varies between 5×10^{-2} to 10^{-4} cm^2 /sec. In natural clays, c_v increases with increase in void ratio. In slimes it increases, decreases, stay constant, or has no trend depending on the origin of rock. Trends between permeability (or stress/strain) and coefficient of compressibility also differ.

The secondary consolidation produces continuing deformation under constant load even after pore pressure dissipation and the end of primary consolidation. It is caused by particles rearrangement and grain to grain slippage under load. It is usually small and relatively insignificant compared to primary consolidation. Gypsum tailing is exceptional since creep is very significant.

The drained (effective stress) shear strength is high (about 3 to 5 degrees higher than similar natural soils) due to their high degree of particle angularity inspite there loose state. Tailings normally have zero effective cohesion since they are cohesionless. Shear strength is measured using either consolidated drained (CD) triaxial or direct shear tests or consolidated undrained (CU) triaxial test with pore pressure measurements.

The angle of internal friction for tailings decreases with the increase of vertical stress levels due to particle crushing (41° at 0 stress and 29° at 145 kPa). Stresses above 275 kPa does not affect very much the shear strength. At that level all the crushing is completed. Typical values are in the range of 33-37° for sands and 28-37° for slimes. There is a little variation between the drained shear strength of sand and slime tailings except for fine coal defuse, which may have highly plastic clay.

The undrained shear strength is required for rapid application of shear stresses. Can be determined by consolidated undrained (CU) triaxial tests to produce Φ_T (total stress friction angle) and C_T (total stress cohesion). Undrained direct shear tests or field vane can be also used. Strength values (normally measured at initial void ratios) has Φ_T in the range of 14-24° which is about 15° less than that for similar natural soils. Cohesion is about 70 kPa. Little variation exists between the strength of sands and slimes. Void ratio has small effect on Φ_T, but influences C_T.

The Stress-strain characteristics of tailings are similar to loose and medium natural soil of similar gradation. Failure normally takes place at 5-10% strain with little or no reduction in post failure strength and without well defined peak. Pore pressure has a tendency to reach a peak value then remain constant or decrease slightly.

The cyclic strength is affected by the relative density, grain size distribution, method of deposition, aging effects and seismic history. Cyclic strain of 10% is used as a strain related failure criteria which normally coincides with initial liquefaction for many tailings.

1.3 Types of Tailings Dams

The two main categories of tailings dams are the following:

The water retention dams are conventional dams constructed to their full height prior to impoundment using natural soils. The design is according to conventional earth dam design. The upstream slopes do not experience rapid draw-down and accordingly they are steeper than conventional water storage dams. They are well suited to tailing impoundments with high water storage requirements (large storm run-off or limited recirculation of ponded water)

The raised embankments main difference from water-retention dams is the staging over the life time of impoundment. Construction begins with starter dike and sized initially for about 2 to 3 years mill tailings plus allowance for flood inflows. Subsequent raises are made to keep the pace with the rising of tailings elevations and flood allowances. This type of dams requires more planning effort and attention to scheduling since they are constructed as part of the mining operation.
The embankment material may be: natural soils, pit mine waste rock, underground excavation muck, hydraulically deposited tailings and cycloned sand tailings.

The advantages of raised embankments are: (a) Lower initial project cost. (b) Construction costs are distributed over the life of the impoundment, resulting in cash flow benefits. (c) More flexibility in selection of acceptable materials required for the different dam zones by storing it when available to be used when required. (d) Using of mine waste rock if economical.

There are three types of raised embankments and their names designate the direction in which the embankment crest moves with regard to the initial starter dike as they are raised. The three types are the following:

The upstream method has the following sequence of operation: (a) Starter dike is constructed. (b) The tailings are discharged peripherally from its crest to form a beach. (c) The beach becomes a foundation for a second perimeter dike, and so on. This method is not suitable in high flood zones and areas of high seismic potential. Rapid raise of embankment can produce excess pore pressures within the deposit particulary in slimes zones. Excess pore pressure in slimes will result when rates exceeds 5 - 10 m/year, while failure due to excess pore pressures in clean sand tailings is associated with rates of 50 m/year.

Major advantages of this method are: (a) low cost and simplicity of construction. (b) Minimum volume of mechanically placed fill is required for starter dike.

The downstream method has the following sequence of operation: (a) Initially starter dike is constructed.
(b) After tailings reaches close to crest of first level, subsequent raises are constructed by placing embankment fill on the downstream slope of the previous raise. This allows construction of internal elements such as core, internal drains, etc. (c) The use of well controlled tailings beach can improve phreatic surface control and reduce or eliminate the need for internal impervious zones

This method require careful planning since the dam toe keeps progressing outward with raising. It may be of higher cost than the upstream method.

Major advantages are: (a) Well suited to conditions where significant storage of water along the tailings is necessary. (b) Method is liquefaction resistant due to lower water table and embankment can be compacted. (c) No limits on raising rates since dam is independent from tailing.(d) Equivalent to water-retention type dams.

The centreline method has the following sequence of operation: (a) Starter dike is constructed. (b) Tailings are deposited until the crest level of starter dike is reached. (c) Subsequent raises are constructed by placing fill above the beach and above the downstream slope of the previous raise.

This method can't be used for permanent storage of large depths of water. However, water can be allowed to rise temporarily during floods. The overall raising rate is not restricted. The method has generally good seismic resistance. In general it is a compromise between the upstream and downstream methods.

Some of the factors which influence the choice of the embankment type are: (a) Type of tailings and their engineering characteristics. (b) Mill output of tailings and liquid effluent. (c) Site related factors (d) Level of seismicity. (e) Flood control and water handling requirements. (f) Construction materials.

1.4 Tailings Embankment Design

Control of phreatic surface is very important since it governs the overall stability under static and seismic conditions. It should be controlled to avoid seepage - induced failures. The objective is to keep phreatic surface as low as possible close to the embankment downstream face. The general rule is that downstream of the impervious zone, the permeability of various internal zones should increase in the direction of seepage flow. As the permeability increases, the phreatic surface is progressively lowered.

Low permeability **core** is used in downstream or centreline methods. The core is mandatory where water will stand directly upstream of embankment. Inclined cores are more suitable for downstream method. Central cores are more suitable for centreline method. Downstream shell material should be more pervious in comparison with the core material to insure good phreatic control.

Drainage zones are used as a supplement to cores. They could be one of the following types: (a) Chimney drains. (b) Blanket drains. (c) Combined blanket and chimney drains. (d) Strip drains (individual drains that are discontinuous in the direction parallel to the embankment centreline).

Material Selection : Tailings can be used for embankment construction. Sands are cycloned on the embankment crest and slimes are discharged through pipes extending further to form two separate permeability zones. In this case storage of water is not permitted unless a core is made. and a wide beach is required at all times. The characteristics of the produced cycloned sand tailing can be adjusted for the design requirements. Using cycloned sand will reduce impoundment storage requirements and accordingly reduces the cost of the whole operation. Compaction is desirable to reduce pore pressure built-up during shear and the possibility of flow slides. Compaction is important in controlling the susceptibility of saturated embankment sand to seismic liquefaction.

Mine waste may be used if its schedule is compatible with fill quantity requirements schedule. Maximum use of stripping waste (overburden or weathered rock) should be made if found economical. This material is always available at the start of operation when needed most for starter embankment. Some of the limitations for using mine waste are: (a) Large hauling unites produces very thick lifts which are difficult to compact. It also causes segregation due to end dumping. (b) Fragmentation is controlled by mining operation and not by embankment requirement.

The use of natural soils should be very limited in mining operations. Natural soils can be used fully or in combination with mine waste or cycloned tailings.
If clays are available, this may dictate designing internal core embankments. If sands and gravels are available, this will dictate design of embankment with internal drainage zone.

Influence of foundation conditions: Weak materials such as normally consolidated or soft clays present major problems. Embankment slopes should be flattened or the weak material should be removed. Analysis of pore water pressure dissipation and strength gain characteristics of foundation considering the rate of embankment construction should be considered in the design.

Compressibility may cause considerable embankment settlements. Cracking of fill due to severe settlement may cause damage to the impervious zones which increase the seepage. Crossing conduits passing through or under the embankment can be severely damaged by excessive foundation settlements and the collapse of the pipe can cause embankment failure.

The cases to be studied in the stability and the stress and deformation analyses of tailing dams are: (a) **End of construction**. This method applies for starter dike on soft foundation or centreline raises on fine tailings. The strength parameters to be used are undrained strength and $\Phi = 0$ analysis. (b) **Staged construction**. This methods applies for embankment of any type on soft foundation. Incremental analysis should be used to account for changes in excess and static pore pressure as a function of time. Strength parameters to be use are Φ_T or S_u/σ'_c to account for pore pressure during shear.
(c) **Long term**. This applies for maximum height embankment where raises are constructed slowly or for maximum height embankment where rapid changes in loading of loose material may occur. Effective stress analysis using Φ' and steady seepage phreatic surface may be used or total stress analysis accounting for pore pressure during shear, usually using Φ_T. (d)

Design in cold regions: Many minerals deposits are located in areas where permafrost are found. The thermal regime will be disrupted by tailing impoundments and embankment design must account for settlement, strength, seepage, and piping related problems that can develop by thawing and freezing of foundations. The impoundment may cause lowering of permafrost table resulting in foundation thawing or raising it and producing frozen condition within the embankment. Thermal profile can be predicted by numerical solutions.

Ice rich permafrost beneath embankment can be excavated and removed. This is a very expensive operation. Foundation may be allowed to thaw during the impoundment with consideration of reduction in foundation strength. Vertical sand drains may be used to accelerate consolidation of soils containing high percent of ice lenses. The starter dike fill may freeze to a depth 3.5-4.5 m below the face which affects its performance specially the drainage zones. For this reason, drainage zones must be located within the central portion of the embankment where freezing is unlikely. Heated pipes may be used to collect seepage water. Drains may be located below the zone of seasonal freezing. Creeping of frozen foundation should be considered for sloping sites.

2.0 CONSTITUTIVE LAWS

2.1 General

In order to analyze dam behaviour using finite element method, the relations between stress, strain and time should be described. These are known as "constitutive relations" or "constitutive laws", and they must be established for each type of material involved in the analysis. Constitutive relations define the stiffness of the (soil) element and how it changes under various loading conditions. Soils generally present a non-linear behaviour. The vast majority of the above mentioned relationships for geomechanical media fall into one of the following groups:

1. Nonlinear elastic. This group includes bi-linear and multi-linear models, hyperbolic models, simulation of a set of stress-strain data by using spline functions, high order polynomials and high order elasticity models (strain-energy functions). **2. Plastic.** This group includes simple perfect plasticity (non-frictional and frictional) models, and the so-called capped yield models (Cam-Clay, Modified Cam-Clay, Ohta-Sekiguci elasto-plastic, etc.). **3. Viscous.** Models included in this group were developed in the last 15 years. It includes visco-plastic and elasto-visco-plastic models that take into account time effects such as creep.

From the multitude of constitutive relations, the hyperbolic model (from the first group) and the Modified Cam-Clay model (from the second group) are the most commonly used in geotechnical engineering. These two

models will be briefly discussed, together with the method of determining the parameters involved, and their limitations.

2.2 The Hyperbolic model.

This widely used function for simulation of stress-strain curves in finite element analysis was formulated by Duncan and Chang using Kondner's finding that the plot of stress vs. strain in a triaxial compression test is very nearly a hyperbola, as seen in Figure 1, which can be stated in equation form:

$$(\sigma_1 - \sigma_3) = \frac{\epsilon}{a + b\epsilon}$$

where: σ_1, σ_3 - the major and minor principal stresses
ϵ - the axial strain
a, b - constants to be determined experimentally

The asymptotic value may be related to the compressive strength by means of a factor R_f as shown by equation:

$$(\sigma_1 - \sigma_3)_f = R_f\,(\sigma_1 - \sigma_3)_{ult}$$

where: $(\sigma_1-\sigma_3)_f$ - compressive strength, or stress difference at failure
$(\sigma_1-\sigma_3)_{ult}$ - asymptotic value of the stress difference
R_f - failure ratio, always less than 1.0

The relationship between initial tangent modulus and confining pressure may be expressed as:

$$E_i = k\,p_a\,(\frac{\sigma_3}{p_a})^n$$

where: E_i - initial tangent modulus
σ_3 - minor principal stress
p_a - atm. pressure (same units as E_i and σ_3)
k - modulus number
n - exponent determining the rate of variation of E_i with σ_3

In terms of Mohr-Coulomb failure criterion, the relationship between compressive strength and confining pressure may be expressed as:

$$(\sigma_1 - \sigma_3)_f = \frac{2c\,\cos\phi + 2\sigma_3\,\sin\phi}{1 - \sin\phi}$$

The tangent modulus becomes:

$$E_t = [1 - \frac{R_f(1-\sin\phi)(\sigma_1-\sigma_3)}{2c\,\cos\phi + 2\sigma_3\sin\phi}]^2\, kp_a\,(\frac{\sigma_3}{p_a})^n$$

This expression for tangent modulus may be employed very conveniently in incremental stress analyses. It may be employed in either effective stress or total stress analyses.

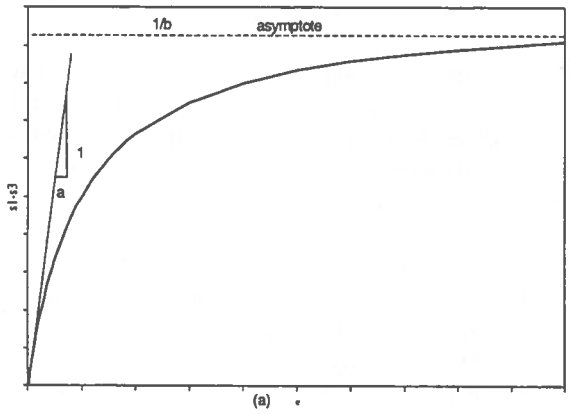

Fig.1. Hyperbolic model for nonlinear material

The simplicity of the relationship described by these equations relies on two facts: **1.** Because E_t is expressed in terms of stresses only, it may be employed in any problem involving initial stress conditions. **2.** The parameters **k**, **n**, $\mathbf{R_f}$ involved can be easily determined from triaxial laboratory tests, the same tests needed to determine "**c**" and "**Φ**" parameters. And using them with any combination of principal stresses defining a state of stress, values of tangent modulus for that particular material can be calculated

The way of approximating nonlinear stress-dependent stress-strain behaviour in f.e. analysis is by assigning different modulus values to each of the elements into which the soil is subdivided; this is done based on stress or strain level in each element. One technique used to approximate nonlinear stress analyses is described below.

The incremental procedure is based on analyzing the change in loading in a series of steps. Therefore, at the beginning of each new step (increment), an appropriate value of the modulus is selected for each element on the basis of stress and strain values in that element. Using this procedure one can easily take into account an initial stress value (initial stress conditions). The main limitation of the iterative procedure is that it is not capable to account for a decrease in the value of stress, after a peak value for the strain.

Many applications in f.e. modelling of the soil use this model, mainly for its simplicity and ease to determine the parameters involved.

2.3 The Modified Cam-Clay model.

The original Cam-Clay Model, as developed at Cambridge University, is an elasto-plastic stress-strain relationship with stress-dependent stiffness and strength characteristics. The relationships are formulated in terms of the stress invariants **p'** (the mean normal effective stress) and **q** (a generalized deviatoric stress).

The model can be described in terms of three principal elements (see also Fig.2.):
a) **The failure surface** (or strength envelope) is a straight line in the p'-q plane with a slope **M** to horizontal, described by the equation $q_f = M \times p'$, where q_f is q at failure.
b) **The yield surface** defines the directions of the plastic strain increments. The yield surface is elliptical, having the equation:

$$(1 + \frac{\eta^2}{M^2}) * p' - (p')_0 = 0$$

where $\eta = q/p'$ and p'_0 = the value of p' when the ellipse intersects the p' axis.
c) **Stress-strain relationship**, in which the total strain is the sum of both elastic and plastic components, dependent on ν (Poisson's ratio), k and λ (parameters of the compression curve).

Various authors have proposed different ways to modify the original Cam-Clay Model. Some of them modified all the three elements mentioned above: the failure surface to represent behaviour of soils which have a cohesion intercept, the yield surface which takes into account stress dependency of the volumetric strain and the elastic behaviour where the value of Poisson's ratio varies with p'. Other authors have also incorporated dilatancy and rheological effects.

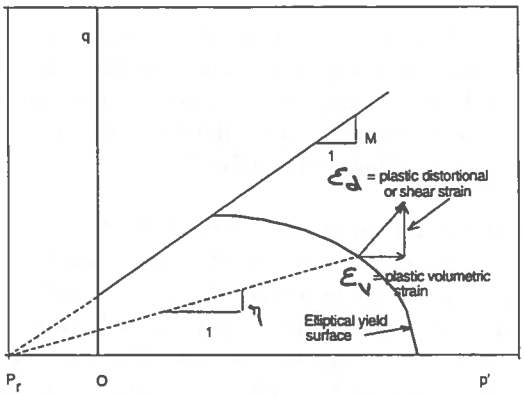

Fig.2. Yield surface for Modified Cam-Clay Model

The parameters can all be determined from the normal range of laboratory tests that are performed on soils. In situ testing techniques are desirable in addition to high quality lab tests on undisturbed samples.

Triaxial tests on isotropically consolidated samples can be used to obtain the frictional constant **M**. The value of **M** becomes $\mathbf{M = 6 * \sin\phi' / (3+\sin\phi')}$. Parameters λ and **k** (slopes of the normal consolidation and swelling lines) can be obtained from oedometer tests or from triaxial tests on samples either isotropically or with K_0 normally consolidated.

In situ parameters (σ_v', σ_h', u_0, p_c') have to be carefully evaluated, as the stiffness matrix of a finite element in an elasto-plastic analysis will be dependent on the initial state of stress within the element.

3.0 FINITE ELEMENT PACKAGES FOR STRESS AND DEFORMATION ANALYSIS

Accurate evaluation of the state of stress in tailings dams plays an extremely important role in the evaluation of their stability under static and dynamic loading and their liquefaction potential (static or dynamic).

Available finite element programs for stress and deformation analysis of soil structures offer a variety of capabilities: choice of material modelling, element types, loading conditions, coupling with other programs, pre- and post-processor for fast and effective input/output

data processing, etc. Review was made for the features of some of the most widely used finite element programs in geotechnical engineering in order to determine which ones are most suitable for the tailing dams analyses.

In Table 1, a review of selected programs is presented, summarising the important features of these programs. Although the list may not be complete, it provides the reader with the important relevant features of these programs to tailings dam analyses.

The first column of the table presents the list of the main features for each program. They are classified in 8 groups. As it can be observed, many of the features found in some programs are not available with others, and vice-versa. It may be concluded that there's a need for further development for one of these programs to bring it up to a level which can satisfy the tailing dams analyses requirements.

The program should be developed on a PC environment, should have powerful and easy to use pre- and post-processors, being more user-friendly and saving lots of precious time in manipulating data.

4.0 PROPOSED MODEL FOR TAILINGS DAMS

Since most of the available programs are powerful, it may be more efficient to use an existing program that is best fit to perform such analyses, after improving its capabilities in order to have a final product that will be both performant and user friendly. Based on the above mentioned tailings dam requirements, it was concluded that the CON2D program features has a large group of computational capabilities that are needed in such analyses. In addition to these capabilities, some features have to be added in order to satisfy the user. The following list summarises the proposed modifications needed to meet the tailings dam requirements.

4.1 Main program

- The program should include the hyperbolic model, besides the existing Modified Cam-Clay; in this way the user has the flexibility in using various available parameters.
- Provide procedure for material parameters evaluation; this applies mainly when some of the parameters are not available, therefore they have to be evaluated.
- Compatibility with seepage programs or have coupling feature for seepage/stress analyses is one of the most important features; as described in previous sections, the control of the phreatic surface is a key factor in ensuring the overall stability under static or dynamic conditions.
- The program should be compatible with dynamic analyses programs so that it will make it easy to transfer information between the stress program and the dynamic analysis program; this is very important in the case of these, as they are very sensitive to liquefaction .
- At any stage of the construction, excavation or loading, the material properties can be changed at the user's choice; this is crucial as the tailings dams behave differently in time, depending on the tailings properties and the sequence of placing them, as described earlier.
- Different failure criteria should be incorporated; these criteria shall be used to evaluate the factor of safety at different points and to identify zones of critical condition or failure.

4.2 Preprocessor

- The program should be interactive to create the input data file. The user should have an option to present the data in a batch file directly or through the interactive approach.
- The user should be able to modify the parameters either interactively or by direct change in the input file.
- The input file should be created such that an identification shall be given to each line (card) so that quick verification by visual inspection can be made. Some immediate checks should be made by the interactive program to warn the user of possible errors in the data.
- The preprocessor should include a mesh generator routine which will read the input file, create the mesh and verify and warn for any possible errors. The routine will also provide graphic presentation of the mesh showing different options such as:
  - Material distribution.
  - Excavation / construction sequence.
  - Element / Node numbers.
  - Zoom in/ Zoom out feature.
  - Text editing for printing.
- Interactive method should be used for the modification of the grid and input.
- The program should be easy to use in terms of changing the loading conditions such as :
  - -Change of reservoir levels (for both stress analyses and seepage analyses)
  - -Pore pressure
  - -Earthquake loading (Quasi static).

TABLE 1 STATIC ANALYSES OF STRESS AND DEFORMATION, FINITE ELEMENT PROGRAMS

	MAIN PROGRAM FEATURES	CON2D	CRISP	FEADAM	FLEX	SOILSTRUCT	TELSTA	PLEXIS	NLSSIP	SOILSTRESS	GEFDYN	FLAC	SIGMAW	ABAQUS
1	GENERAL													
1.1	Source	VIRGINIA P	Cambridge	Berkeley	Weidlinger	Virginia Tech	TAGA En	T U DELF	U.B.C.	U.B.C	COYNE&BE	P.CUNDAL	GEOSLOP	MKC INC
1.2	Language	FORTRAN	FORTRAN	FORTRA	FORTRAN	MS FORTRA	FORTRAN77		FORT I	FORT IV				
1.3	Computer type	PC	PC & MF	PC	PC, WS, M	PC	PC		MF	MF	WS&MF	PC	PC	WS,MF
1.4	Last update	1991	1987	1991	1991	1990	1990	1989	1979	1989				
1.5	Method of analyses	FE	FE	FE	FE	FE	FE	FE	FE	FE	FE	FD	FE	FE
1.6	User friendly	N	Y					Y	N	N			Y	Y
1.8	Source code available	Y	Y	Y	Y	Y	Y		Y	Y	N		N	N
2	TYPE OF ANALYSES													
2.1	# dimensions	2-D	2-D	2-D	2 & 3-D	2 - D	2 - D	2D	2D	2D	2&3D	2D	2D	2&3D
2.2	Plane stress	N	Y	N		Y						Y	N	Y
2.3	Plane strain	Y	Y	Y		Y	Y	Y	Y	Y	Y	Y	Y	Y
2.4	Axisymmetric	N	Y	N				Y	N	Y	Y	Y	Y	Y
2.5	Static analysis	Y	Y	Y	Y	Y	Y	Y	Y	Y	Y	Y	Y	Y
2.6	Dynamic analysis	N	N	N	Y	N	N	N	N	Y(QS)	Y	Y	N	Y
2.7	Coupling with fluid flow	Y					development		N		Y	Y		Y
3	TYPES OF ELEMENTS													
3.1	Elements & nodes	Qu,Tr 4-8	Tr 6-15	Quad 4	Quad 4 &8	Quad 4	Quad 4	Qu&Tr 15	QU 4	QU, TR	QU9,T7		QU8,T6	QU8
3.2	Beam elements	Y	N	N	Y	Y	developme	Y	Y		Y	Y	@Y	Y
3.3	Bar elements	Y							Y		Y	Y	NO	Y
3.4	Interface elements	Y	N	N	Y	Y	Y				Y	Y	@Y	Y
3.5	Slideline & faults	N	N	N	Y		Y				Y		@Y	Y
4	LOADING CONDITIONS													
4.1	Total Stress	Y	Y					Y	Y	Y	Y	Y	Y	Y
4.2	Effective stress	Y	Y					Y	Y	Y	Y	Y	Y	Y
4.3	Undrained problems	Y	Y							Y	Y	Y	Y	
4.4	Drained problems	Y	Y							Y	Y	Y	Y	Y
4.5	Consolidation problems	Y	Y								Y	Y	Y	Y
4.6	Pre existing elements	Y						Y	Y	Y	Y		Y	Y
4.7	Incremental construction	Y	Y	Y		Y	Y		Y	Y	Y		@Y	Y
4.8	Excavation sequance	Y	Y			Y	Y	Y			Y		@Y	Y
4.9	Tension redistribution	N	N	N	N	N	Y						N	Y
5	MATERIAL MODELING													
5.1	Non linear	Y	Y	Y	Y	Y	Y	Y	Y	Y	Y	Y	Y	Y
5.2	Soil Hyperbolic model	N	N	Y		Y	Y	Y	Y	Y	@Y	Y	N	
5.3	Modified Cam clay model	Y	Y						N	N			Y	
5.4	Anisotropic material	N	Y	N	Y		Y						Y	Y
5.5	Partly saturated soil	Y	N	N	N	N	N				Y		N	
5.6	Creep or viscoplastic	N	N	N	Y						Y		N	Y
5.7	Simulate compaction on saturation	N					Y				Y		N	
5.8	Dilatance								Y	Y	Y		Y	Y
5.9	Drop from peak to residual	N					Y					Y	Y	
5.10	Change of property	N						Y				Y	Y	Y
5.11	Rate dependent concrete model	N	N	N	Y						Y		N	Y
5.12	Choosing failure Crieteria										Y		Y	Y
5.13	Jointed rock simulation	N	N	N	Y						Y		N	
6	TYPE OF LOAD													
6.1	Force load	Y	Y	Y	Y		Y		Y	Y	Y		Y	Y
6.2	Stress load	Y	Y		Y		Y	Y	Y	Y	Y		Y	Y
6.3	Displacement load	N	Y	N	Y			Y						Y
6.4	Pore pressure load	Y	Y	N				Y	Y				Y	Y
6.5	Reservoir load	Y	?	?			Y				Y			Y
7	PREPROCESSOR													
7.1	Method of data entering	BATCH	SIMPLE		Y	Y		BATCH	BATCH	BATCH		BATCH	SIMPLE	BATCH
7.2	Grid generation	N	Y	Y			Y	Y	N	Y	Y	Y	Y	Y
7.3	Changing of the grid	MANUAL	EASY						MANUA	MANUAL			Y	MANUAL
7.4	Changing the loading condition	MANUAL	EASY						MANUA	MANUAL			Y	MANUAL
7.5	Lab data analyses for parameters	N	N	Y	N	N	N		N	N	Y			Y
8	POSTPROCESSOR													
8.1	Finite element grid	Y	LIMITED	Y	Y	Y	Y			Y			Y	Y
8.2	Deformed grid	Y					Y	Y			Y		Y	Y
8.3	General cross section	Y		Y									Y	Y
8.4	Material zones												Y	Y
8.5	Stress	Y		V & C	Y	Y	Y	Y			Y		Y	V&C
8.6	strain	Y		V & C				Y			Y			V&C
8.7	Displacement	Y		V & C			Y	Y					V	V&C
8.8	Pore Pressure										Y		Y	Y
8.9	Identify critical zones							Y					Y	

LEGEND:

@	Approximate	FE	Finite element	Qu 4	Quadrilateral element with 4 nodes
2D	Two dimensions	MF	Main frame computer	Tr 6	Triangular element with 6 nodes
3D	Three dimensions	N	No	V	Vectorial presentation
C	Contour presentation	PC	Personal Computer	WS	Work station computer
FD	Finite difference	QS	Quasi Static	Y	Yes

- A subroutine should be developed for the analyses of lab tests for the Hyperbolic model and the modified Cam-Clay parameters (optional use).

4.3 Postprocessor

- The Postprocessor should produce contour lines for the pore pressure data, the major and minor principal stress and critical zones based on specific acceptance criteria for the stresses, deformations, seepage and pore pressures.
- Tracing of the Mohr circle for any specified element and the corresponding failure criteria.
- The program, pre- and post-processors should be able to simulate different types of instruments used and their readings. Simplifying input data manipulation will make it easy to calibrate the model using instrumentation readings.
- Simplify the choice of the parts of the output file required by the user. A summary report of the main features of the case under-consideration should be at the choice of the user.

A research program is under consideration at McGill University in order to develop this program. This will be an extension of a research program conducted by AXOR and Hydro Quebec applicable to embankment dams in hydroelectric developments.

References

BRITTO,A.M. and GUNN,M.J.,1987.
Critical state soil mechanics via finite elements. Ellis Horwood Ltd. Publishers, Chichester, England.

CHANG,C.S. and DUNCAN,J.M., 1977.
"Analysis of consolidation of earth and rockfill dams", Report No. TE 77-3, Univ. of California Berkeley, Vol I, 127 p and Vol. II , 87 p.

CHRISTIAN,J.T. and DESAI,C.S.,1977
Constitutive laws for geologic media. Numerical Methods in Geotechnical Engineering, Desai and Christian ed.,McGraw Hill, pg.65-115

CLOUGH,G.W. and DUNCAN,J.M., 1969.
Finite Element Analyses of Port Allen and Old River Locks, (Program LOCK), U.S. Army Engineering Waterways Experiment Station.

DESAI,C.S.,1977
Constitutive modelling and soil-structure interaction. Proceedings, Numerical Methods in Geomechanics, NATO Advanced Study Inst., Vimeiro, Portugal, D.Reidel Publishing Co.

D'ORAZIO,T.B., SUNAMI,S., DUNCAN,J.M.,1991.
CON2D90: A finite element computer program for analysis of consolidation. Virginia Polytechnic Institute, Blacksburg,VA.

DUNCAN,J.M., BYRNE,P., WONG,K.S. and MABRY,P., 1980.
Strength, Stress -Strain and Bulk Modulus Parameters for Finite Element Analyses of Stresses and Movements in Soil Masses, Report No. UCB/GT/80-01, Univ. of California Berkeley.

DUNCAN,J.M. and CHANG,C-Y.,1970.
Nonlinear analysis of stress and strain in soils.J.of Soil Mech. and Foundations. ASCE Division, vol.96, sept.

DUNCAN,J.M., D'ORAZIO,T.B., CHANG,C.S., WONG,K.S. and NAMIQ,L.I. 1981.
CON2D: A Finite Element Computer Program for Analysis of consolidation, Report No. UCB/GT/81-01, Univ. of California Berkeley.

DUNCAN,J.M., WONG,K.S. and OZAWA,Y. 1980.
FEDAM: A Computer Program for Finite Element Analysis of Dams, Report No. UCB/GT/80-02, Univ. of California Berkeley.

KEIRA,H., 1992
Mining Waste Management Techniques, Course notes, Course #306-638A, Dept. of Mining and Metallurgical Engineering, McGill University.

KRISHNAYA,A.V.G., 1973.
"Finite Element Non-Linear Analysis for Two Dimensional Problems (Program FENA2D)", Dept of Civil Eng., University of Alberta.

KULHAWY,F.H.,1977.
Embankments and excavations. Numerical Methods in Geotechnical Engineering, Desai and Christian ed.,McGraw Hill, pg.528-554.

KULHAWY,F.H., DUNCAN,J.M. and SEED,H.B., 1969.
"Finite Element Analyses of Stresses and Movements in Embankments During Construction (Program LSBUILD)", U.S. Army Engineering Waterways Experiment Station.

NOBARI,E.S. and DUNCAN,J.M., 1972.
"Effect of Reservoir Filling on Stresses and Movements, in Earth and Rockfill Dams", Geotechnical Engineering Report, University of California, Berkeley.

OZAWA,Y. and DUNCAN,J.M., 1973.
"ISBILD: A Computer Program for Analysis of Static Stresses and Movements in Embankments, Report No. TE-73-4, Univ. of California Berkeley.

CAMI'95: 3rd Canadian Conference on Computer Applications in the Mineral Industry
Montréal, Québec, Canada, October 22-25, 1995

Hybrid Simulation of Hydrocyclone Separation for Oil-Solids-Water

Robert M. Changirwa
Maria C. Rockwell
Department of Mining and Metallurgical Engineering
Technical University of Nova Scotia, Halifax, Nova Scotia

ABSTRACT

It is pivotal in the mining industry and allied industries to concurrently decrease the levels of solids and oil in contaminated water before its reuse or disposal. Immoderate oil and oil-coated solids levels have jeopardous environmental effects. The current research attempts to solve this impediment by hybridization of two hydrocyclones designed for solid-liquid and liquid-liquid separation. Through computer simulation the hybrid hydrocyclone design has demonstrated promising performance in separating oil-solids-water in a single-stage operation. The resultant hybrid hydrocyclone design is hydrodynamically incorporated with a transverse aperture for solids dismissal which enables concurrent three phase separation of liquid-solid-liquid.

INTRODUCTION

Through theoretical, computer simulation and experimental modelling, solid-liquid separation hydrocyclones (Changirwa and Rockwell, 1993), (Kelsall, 1952) and (Periculous, 1987) and liquid-liquid separation hydrocyclones (Colman, 1981) and (Meldrum, 1987) have been developed. However, little attention has been given to concurrent three-phase hydrocyclone separation in a single-stage operation.

The feasibility of the three-phase separation by a hydrocyclone was investigated and some of the operating constraints identified (Changirwa and Rockwell, 1994) and (Changirwa, 1994). The simulation model developed in this paper hybridizes two two-phase hydrocyclones producing a hybrid three-phase hydrocyclone. The hybrid is used to separate droplets and particles of oil and solids respectively dispersed in contaminated water. Using the mathematical development (Changirwa and Rockwell, 1994) the model touches on the internal flow thus giving the oil and solids droplets/particles velocity profiles.

HYBRIDIZATION PROCESS

Though individual simulations of two-phase separation hydrocyclones offer optimum liquid-liquid and solid-liquid separations, a composite simulation yields a hybrid hydrocyclone for concurrent three-phase separation, liquid-solid-liquid, as shown in Fig. 1.

The hybrid simulation involves hybridization mechanism which consists of four stages as shown in Fig. 2. Stage I consists of a series connection of a liquid-liquid hydrocyclone on the underflow by a solid-liquid hydrocyclone. Stage II consists of the union of the two hydrocyclones with the vortex finder of the second hydrocyclone eliminated since it is associated with promotion of short-circuits and eddies.
Stage III makes the underflow of the first hydrocyclone co-axial with the overflow of the second hydrocyclone. At this stage the four apertures are very clear. The underflow of the first hydrocyclone is orthogonal to the underflow of the second hydrocyclone. This underflow and swirl chamber of the second hydrocyclone form a fourth aperture of the hybrid.

In Stage IV since aperture size is critical to separation efficiency, the fourth aperture is constricted in proportion to other apertures and moved to the intersection of the last cone and cylindrical section of the first hydrocyclone. A transverse aperture is made at this intersection.

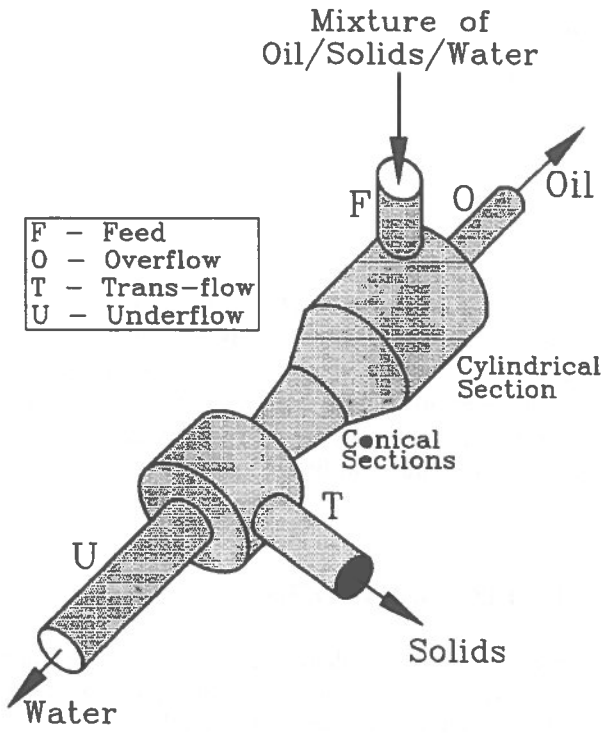

Fig. 1: Schematic of Concurrent Three-phase Hydrocyclone.

Hydrodynamically, the inlet velocities for liquid-liquid separation in a double-cone hydrocyclone should not exceed 8m/s, and that for a single-cone hydrocyclone for solid-liquid (Changirwa and Rockwell, 1993) separation should not exceed 16m/s. The hybridization is equivalent to the union of liquid-liquid and solid-liquid hydrocyclones as illustrated in Fig. 3.

The evaluation of both liquid-liquid and solid-liquid hydrocyclone shows that the former requires very low inlet velocities for optimum separation whereas the latter requires high inlet velocities for the same. To separate solids in the liquid-liquid hydrocyclone at the very low inlet velocities, medium-angled multiple-cones are stacked on the hydrocyclone (see Fig. 1).

At the same time good efficiencies for liquid-liquid separation are maintained.

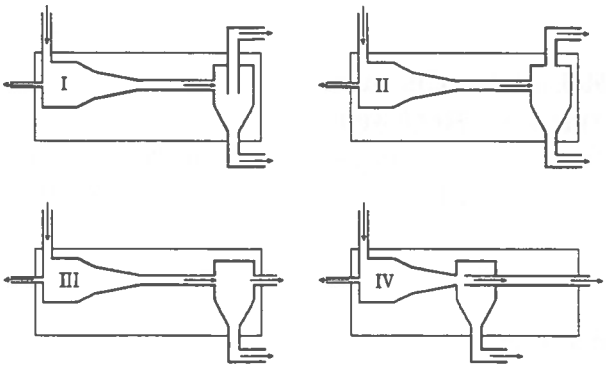

Fig. 2: Stages of Three-Phase Geometrical Hybridization.

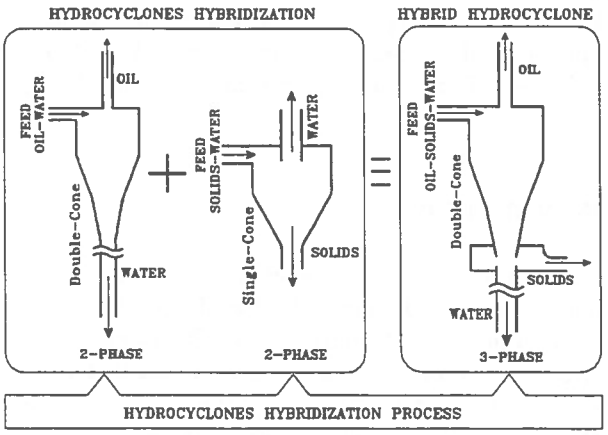

Fig. 3: Two-Phase Hydrocyclones Hybridization for Three-Phase Separation.

For a strong vortex capable of separating both the oil droplets and solids from water the hybrid inlet velocity, v_i, should be the maximum inlet velocity for the liquid-liquid hydrocyclone. Both the oil and solids must be subjected to centrifugal field so that 1) the oil can fully participate in the reversal flow forming an inner vortex coaxial with the hydrocyclone axis towards the overflow orifice and hence exit from the hydrocyclone, 2) the solids can participate in the outer vortex and be pushed to the boundary layer prior to smuggling through the transverse orifice (exit) and the underflow. The left side hydrocyclones shown in Fig. 3 will separate two phases liquid-liquid and solid-liquid.

The hybrid multiple-cone on the right side will separate concurrently three phases since it is incorporated with a transverse aperture for dismissal of solids. It should be noted that the hybrid design has a duality of operation, i.e., two-phase mode when the transverse aperture is closed and three-phase mode when it is open as shown Fig. 1. This type of hybridization of two hydrocyclones enables concurrent three-phase separation of oil-solids-water in oily-water systems in a single-stage operation of the hybrid hydrocyclone.

Conceptual three-phase separation of oil-solids-water can be expressed as a circuit diagram of two vortices - outer vortex carrying most of the influent dispersions and inner vortex carrying mostly oil. This is depicted in Fig. 4.

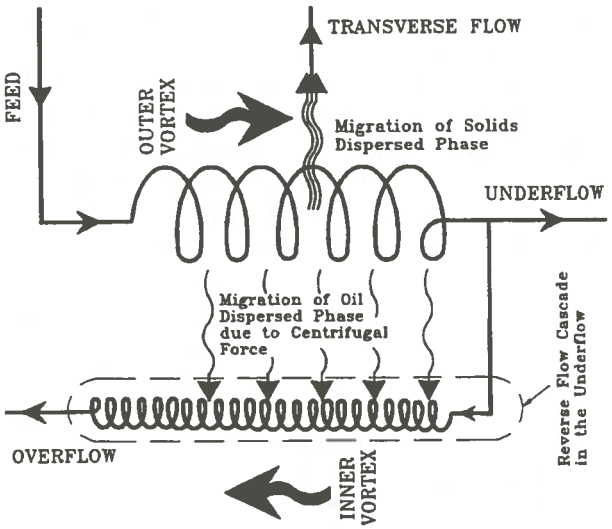

Fig. 4: Conceptual Schematic for Three-Phase Hydrocyclone Separation.

HYBRID VELOCITY PROFILES

In the three-phase hydrocyclone the three phases namely oil, solids and water separate in the radial direction with the coarse solids being pushed to the wall - boundary layer from which the sedimenting solids are conveyed through the circumferential transverse aperture. At the same time the fine oil particles or droplets migrate to the axis and out to the overflow. The effects of gravity and turbulence are assumed insignificant in the following theory.

The relative velocities of the oil and solids can be evaluated by consideration of the forces acting on a particle/droplet in equilibrium. By balancing the centrifugal force against the radial drag force;

$$(\rho_s-\rho_w)\frac{u_\tau^2}{r}V_s = \frac{1}{2}\rho_w v_r^2 \frac{\pi d_s^2}{4} C_D \quad \ldots (1)$$

Eq. 1 can be solved for radial drag slip velocity:

$$v_r^2 = \frac{4d_s}{3C_D}\left(\frac{\rho_s-\rho_w}{\rho_w}\right)\frac{u_\tau^2}{r} \quad \ldots\ldots (2)$$

where

V_s = Volume of solid particle = $\pi d_s^3/6$
ρ_w = density of water
ρ_s = density of solid particles
C_D = drag coefficient

Where C_D, quoted from (Periculous, 1987), is given by:

$$C_D = \begin{cases} \frac{24}{Re} & \text{for } Re \le 64 \\ 0.42 & \text{for } Re \ge 64 \end{cases} \quad \ldots\ldots (3)$$

While the value Re is determined as:

$$Re = \frac{\rho_w v_r d_s}{\mu} \quad \ldots\ldots\ldots (4)$$

Applying Stokes law for particle drag on a sphere; Rearranging Eqs. 1, 2, 3 and 4 get:

$$v_r = \frac{d_s^2}{18\mu}(\rho_s-\rho_w)\frac{u_\tau^2}{r} \quad \ldots\ldots\ldots (5)$$

The tangential velocities (Colman, 1981) are given as:
$0 \le r \le r_\tau$

$$u_\tau = m\left(\frac{r_c^n}{r_\tau^{n+1}}\right)v_i r \quad \ldots\ldots\ldots (6)$$

$r_\tau \le r \le r_w$

$$u_\tau = m r_c^n v_i \frac{1}{r^n} \quad \ldots\ldots\ldots (7)$$

(Kelsall, 1952) and (Colman, 1981) have discussed the values of m, n, and r_r. For solid-liquid separation m and n vary from 0.4 - 0.6. To account for the decay of angular momentum which occurs in the characteristic long liquid-liquid hydrocyclones due to wall friction, a low value of m and n of 0.5 will be used in this research. The value of r_r was found to be a half the radius of the largest withdrawal orifice which in this case the underflow radius - $r_r = r_c = \frac{1}{4}D_u$.

HYBRID RUNS AND RESULTS

To enable computer runs of the hybrid simulation model a computer language adopting C-code and Eqs. 1-7 was used. Parameters incorporated into the model are presented in Table 1 and Fig. 5. Fig. 6 shows the proposed facilities for experimental testing.

TABLE 1: Properties of Materials For the Model.

Density of water	ρ_w	1000kg/m^3
Density of medium crude oil	ρ_o	830kg/m^3
Density of quartz sand	ρ_s	2650kg/m^3
Viscosity	μ	10^{-3}Nsm^{-2}
Inlet velocity	v_i	8m/s
Droplet/Particle size	d_s	10-150μm

The Figs. 7-10 show representative radial velocity profiles for varying wall radii from the axis and droplet/particle size. Simulated droplet/particle sizes range from 30 - 150 μm. Linear velocity profiles exist from the axis to a radius of 5mm which is a transition from forced vortex (see shaded area) to free vortex. From the transition radius the slip velocities vary inversely to the square of the radius. It should be noted that inlet velocities have the effect of lowering the velocities as can be seen in the graphs depicted with flowrates from 130 -150 L/min.

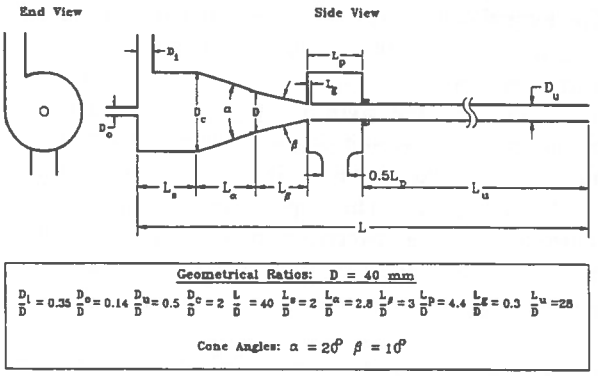

Fig. 5: A Three-Phase Hydrocyclone Geometry.

The radial velocities of the oil and solids for droplet/particle size of 100 - 150 microns are plotted in Figs. 11 - 14 to show the concurrent velocity profiles for the same particle size and inlet velocity. The low oil velocity profile region has been zoomed in each plot so that its profiles are readable. The profiles are found to be in good agreement with the researchers (Kelsall, 1952), (Periculous, 1987) and (Colman, 1981). The hybrid model has a limitation in that it neglects the effect of turbulence in the hybrid design.

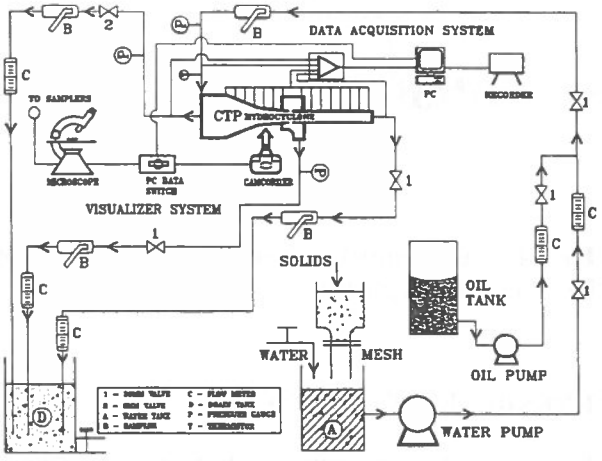

Fig. 6: Proposed Three-Phase Hydrocyclone Test Facilities.

CONCLUSIONS

The simulation model has demonstrated the industrial potential for concurrent separation of three phases, oil-solids-water. In addition, its duality of operation i.e., in two and three phase modes enables it to double-function as a liquid-liquid and liquid-solid-liquid separator. The modelling also revealed that:

- the concurrent separation of oil-solids-water is dependent on droplet/particle size. The bigger the size the better the separation performance.
- the velocity profiles undergo a transition - are linear in forced-vortex zone and asymptotic to the radial distance from the hydrocyclone axis in the free-vortex zone.

NOMENCLATURE

d_s	Particle/droplet size, m
D_i	Hydrocyclone inlet diameter, m
D_o	Hydrocyclone overflow orifice diameter, m
D_u	Hydrocyclone underflow orifice diameter, m
D_c	Hydrocyclone nominal diameter, m
L	Hydrocyclone length, m
L_s	Hydrocyclone swirl chamber length, m
L_α	Hydrocyclone length of 1st taper section, m
L_β	Hydrocyclone length of 2nd taper section, m
L_u	Hydrocyclone cylindrical underflow section, m
r_c	Radius of the swirl chamber
r_w	Cone wall radius
r_r	Transition radius at forced to free vortices
α	Angle included by first cone
β	Angle included by the second cone
ρ_w	Density of the continuous phase (water), kg/m^3
ρ_o	Density of the oil-dispersed phase, kg/m^3
ρ_s	Density of the solids-dispersed phase, kg/m^3
u_r	Tangential velocity (continuous phase), m/s
v_i	Inlet velocity to hydrocyclone, m/s
v_r	Radial droplet/particle slip velocity, m/s

REFERENCES

CHANGIRWA, R.M. and ROCKWELL, M.C., 1993. An Optimization Model for a Multiple Hydrocyclones Separation System, Paper WD3.1, Proc. 35th Conf. of the Canadian Operational Research Society (CORS), Halifax, May 25-27.

CHANGIRWA, R.M. and ROCKWELL, M.C., 1994. A Mathematical Model for a Multiple-Cone Hydrocyclone Concurrent Three-Phase (CTP) Separation System, the Petroleum Society of CIM 45th Annual Technical Meeting and AOSTRA Annual Technical Conference, Calgary, Alberta, June 12-15.

CHANGIRWA, R.M., 1994. Modelling of a Three-Phase Separation Hydrocyclone, M.A.Sc. Thesis, Department of Mining and Metallurgical Engineering, Technical University of Nova Scotia, Halifax, Nova Scotia, 134p.

COLMAN, D.A., 1981. The Hydrocyclone for Separating Light Dispersions, Ph.D. Dissertation, Department of Mechanical Engineering, Southampton University, UK, 165p.

KELSALL, D.F., 1952. A Study of the Motion of Solid Particles in a Hydraulic Cyclone. Trans. Inst. Chem. Eng. 30: p87-104.

MELDRUM, N., 1987. Hydrocyclones: A Solution to Produced Water Treatment, Proc. 19th Annual Offshore Technology Conference, OTC 5594, Houston, April 27-30.

PERICULOUS, K.A., 1987. Mathematical Simulation of Hydrocyclones, App. Math. Modelling, Vol. 11, p242.

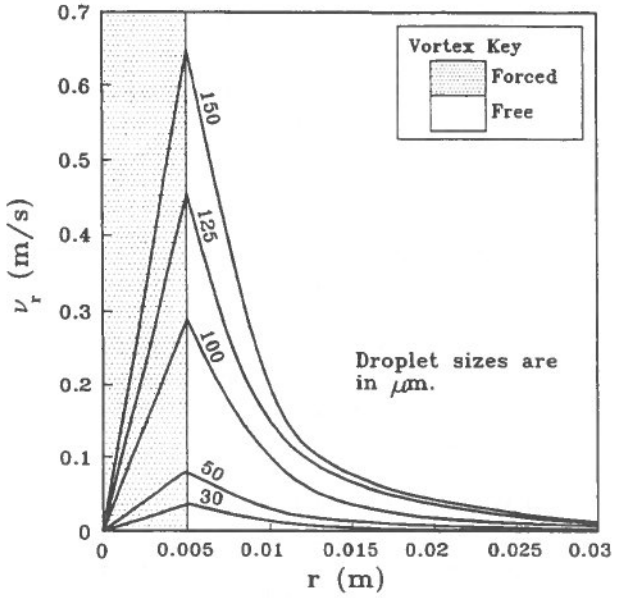

Fig. 7: Radial velocity profiles for oil droplets simulated at Q=150 l/min.

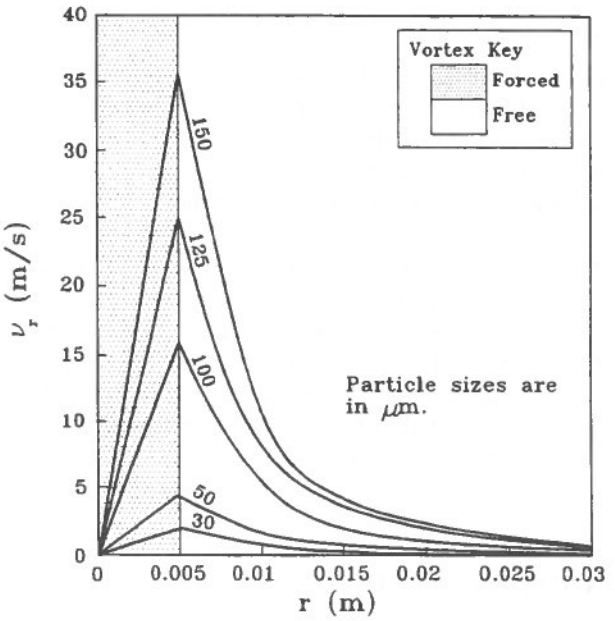

Fig. 8: Radial velocity profiles for sand particles simulated at Q=150 l/min.

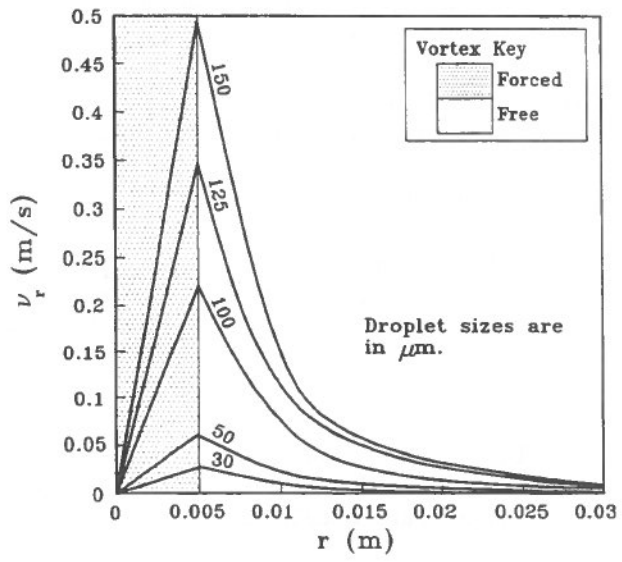

Fig. 9: Radial velocity profiles for oil droplets simulated at Q=130 l/min.

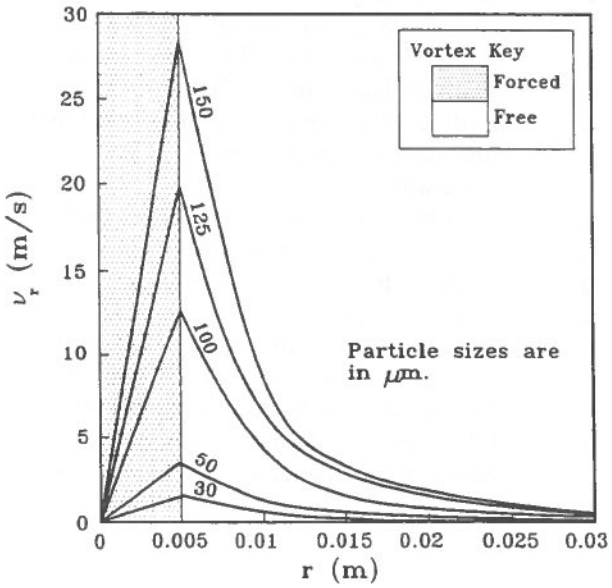

Fig. 10: Radial velocity profiles for sand particles simulated at Q=130 l/min.

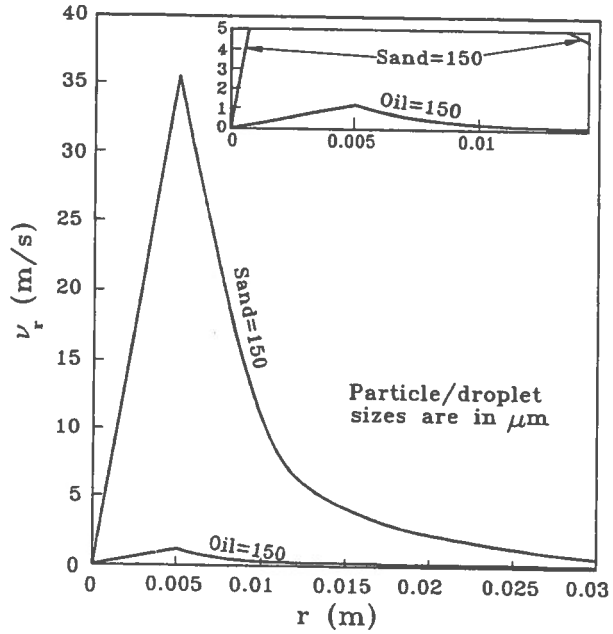

Fig. 11: Concurrently simulated oil and sand velocities at Q=150 and d_s=150μm.

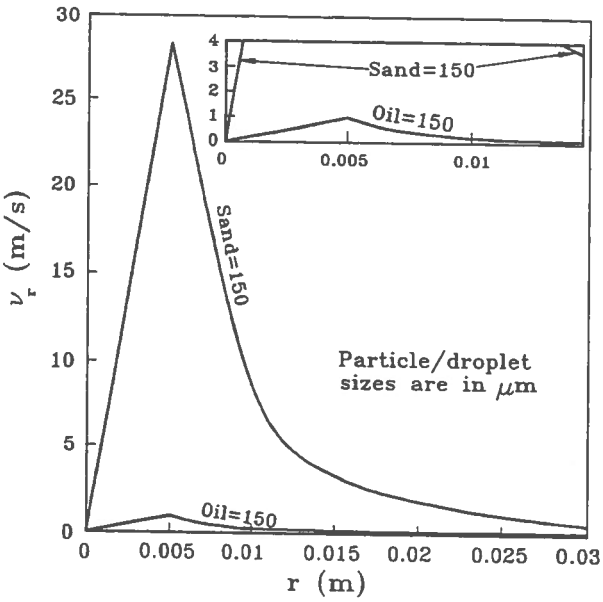

Fig. 12: Concurrently simulated oil and sand velocities at Q=130 and d_s=150μm.

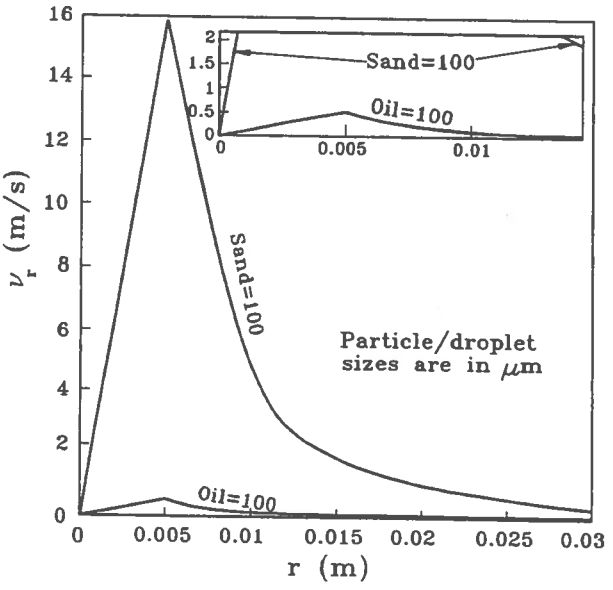

Fig. 13: Concurrently simulated oil and sand velocities at Q=150 and d_s=100μm.

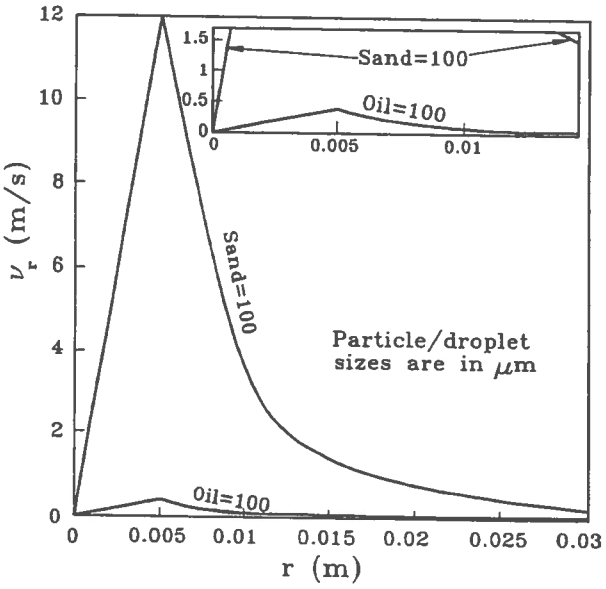

Fig. 14: Concurrently simulated oil and sand velocities at Q=130 and d_s=100μm.